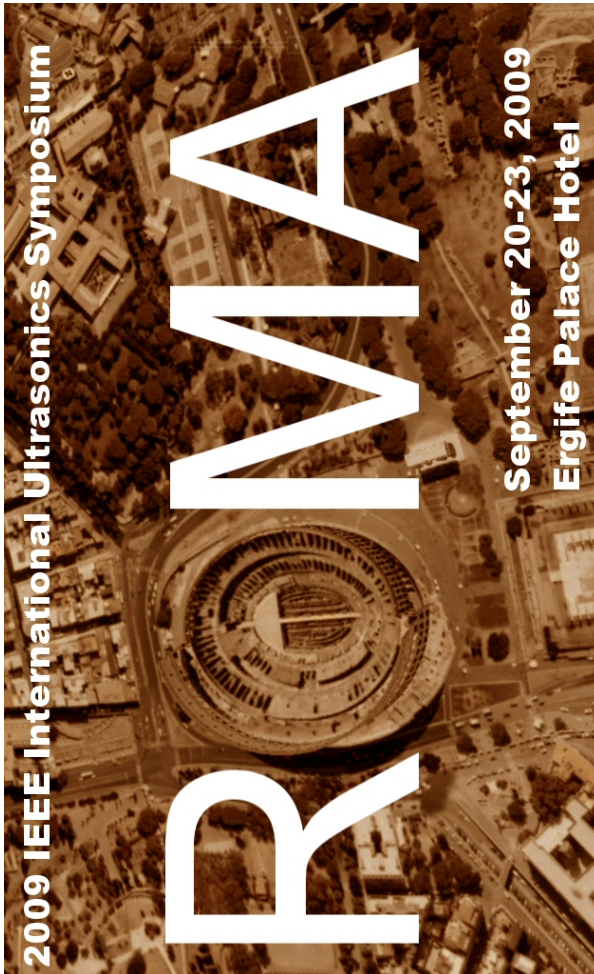


**2009 IEEE INTERNATIONAL
ULTRASONICS SYMPOSIUM
AND SHORT COURSES**



**Sponsored by the IEEE Ultrasonics,
Ferroelectrics, and Frequency Control Society
Under the aegis of the Presidency of the Italian Republic**

Table of Contents

Welcome from the General Chair	5
Venue	6
Registration	7
Local Transportation	8
Exhibitors	10
Industrial Forum	11
Plenary Session	11
Student Lunch	14
Awards Reception	14
Guest Program	14
Shopping & Food	16
Message Board	22
Wireless Access & Printing	22
IEEE and UFFC-S Enrollment	22
Proceedings	23
UFFC CD Archive	23
Message from the Technical Chair	24
Speakers Room	25
Policy on Photography	25
Short Courses	25
Invited Speakers	29
Clinical Session	34
Student Paper Finalists	34
Organizing Committee	39
Technical Program Committee	40
Conference Management	44
Special Thanks	45
Future Ultrasonics Symposia	45
Technical Session Schedule	46
Session Chairs	805
Author Index	807
Floor Plans	830
Posters Layout	831
Condensed Program	833

Oral Sessions, Monday, September 21, 2009:

Session 1A: Targeted Contrast Agents	47
Session 2A: Ultrasound Systems and Devices	51
Session 3A: Ferroelectrets and Other Transducer Materials	57
Session 4A: Microfluidic Manipulation	62
Session 5A: SAW Applications	68
Session 6A: Phononic Crystals-Fundamentals	73
Session 1B: Contrast Agents and Sonoporation	78
Session 2B: Therapy Monitoring, Control, and Quality Assurance	82
Session 3B: Transducers & Ultrasound Modeling	87
Session 4B: Advances in NDE	92

Session 5B:	SAW Modeling	96
Session 6B:	Visualization Interferometry	101
Session 1C:	New Methods and High Frequency Ultrasound for Tissue Characterization	106
Session 2C:	Therapeutic In-Vivo Studies	110
Session 3C:	CMUT Modeling	115
Session 4C:	Acoustic Wave Sensors	119
Session 5C:	BAW I	125
Session 6C:	Novel Ultrasonic Motors I	130

Poster Sessions, Monday, September 21, 2009, 10:00 am – 11:30 am:

Session P-S:	Student Finalist Poster Session	125
Session P1-A:	Contrast Agents: Behavior and Imaging	151
Session P1-B:	Contrast Agents Applications	161
Session P1-C:	Therapeutic Applications	171
Session P1-D:	Beamforming Systems and Hardware	177
Session P1-E:	Blood flow I	184
Session P1-F:	Blood Flow II	190
Session P1-G:	Myocardial Imaging	196
Session P1-H:	Quantitative Elasticity Methods	205
Session P1-I:	Acoustic Imaging	213
Session P1-J:	Guided Waves and Microscopy	219
Session P1-K:	Signal Processing and Imaging	228
Session P1-L:	Phononic Crystals-Band Structure and Propagation	234
Session P1-M:	Materials Characterization	240
Session P1-N:	Physical Acoustics: Modeling & Simulation	245
Session P1-O:	Thin Films-Growth and Characterization	254
Session P1-P:	Actuators and Pumps	258
Session P1-Q:	Measurement & Yields	266
Session P1-R:	Device Modeling	270
Session P1-S:	High Temperature Materials and Propagation	275
Session P1-T:	Tags and Sensors	279
Session P1-U:	Transducer Materials and Characterization	283

Oral Sessions, Tuesday, September 22, 2009:

Session 1D:	Clinical Ultrasound	299
Session 2D:	High Frequency Ultrasound and its Applications	301
Session 3D:	Elastography	307
Session 4D:	Flow Sensing	312
Session 5D:	Oscillators and Temperature Compensation	317
Session 6D:	Bulk Wave Effects and Devices	321
Session 1E:	Therapeutic Arrays	326
Session 2E:	Microbubbles: Characterization and Modeling	331
Session 3E:	Elastography Methods	336
Session 4E:	Array Imaging	341
Session 5E:	BAW II	346
Session 6E:	Ultrasonic Linear Motors	351
Session 1F:	Therapeutic Applications	356

Session 2F:	Contrast Agent Imaging	361
Session 3F:	Cardiac Imaging	366
Session 4F:	NDE Signal Processing	371
Session 5F:	SAW Device Design	377
Session 6F:	Phononic Crystals-Propagation	381
Session 1G:	Therapy Microbubbles	386
Session 2G:	Tissue Characterization	391
Session 3G:	Cancer Imaging	396
Session 4G:	Nanoscale Acoustic Sensing	401
Session 5G:	Novel SAW Materials and Structures	405
Session 6G:	High Frequency Transducers & Arrays	410

Poster Sessions, Tuesday, September 22, 2009, 10:00 am – 11:30 am:

Session P2-A:	Therapy: Monitoring, Control and Quality Assurance	415
Session P2-B:	Therapy Microbubbles	426
Session P2-C:	Contrast Agents: Characterization and Modeling	433
Session P2-D:	Ultrasound Systems and Devices	440
Session P2-E:	Acoustic Radiation Force Imaging	446
Session P2-F:	Hard Tissue and Bone	453
Session P2-G:	Cardiac, Vascular and General Tissue Characterization	464
Session P2-H:	Wave Propagation and Energy Harvesting	472
Session P2-I:	Ultrasonic Signal Processing	480
Session P2-J:	Bulk Wave Effects	485
Session P2-K:	Laser Interactions	492
Session P2-L:	Bubbles and Beads	498
Session P2-M:	High Intensity Ultrasound Application	503
Session P2-N:	Device Modeling	511
Session P2-O:	MEMS and Sensors	516
Session P2-P:	BAW Materials	524
Session P2-Q:	Sensors, High Frequency, CMUTs & Micromachining	529
Session P2-R:	Various Transducer Topics	538

Oral Sessions, Wednesday, September 23, 2009:

Session 1H:	Optical and Photoacoustic Imaging	543
Session 2H:	Medical Imaging	547
Session 3H:	Bone I	553
Session 4H:	Acoustic Imaging and Characterization	558
Session 5H:	Novel Devices & Systems	564
Session 6H:	Phononic Crystals-Devices, Filters, Couplers	568
Session 1I:	Elasticity and Thermal Effects	573
Session 2I:	Beamforming	578
Session 3I:	New Developments in Blood Flow Imaging	584
Session 4I:	Energy Harvesting	589
Session 5I:	Piezoelectric Transducer Materials	593
Session 6I:	Acoustic Propagation	597
Session 1J:	Cardiovascular Elastography	602
Session 2J:	Bioeffects	607
Session 3J:	Bone II	612

Session 4J:	Ultrasound in Air	617
Session 5J:	Micromachined Ultrasonic Transducers	622
Session 6J:	RF MEMS	627
Session 1K:	Dynamic Elastography	632
Session 2K:	Signal Processing	637
Session 3K:	Surgical Automation	643
Session 4K:	Material and Defect Characterization	648
Session 5K:	Medical Imaging and Therapeutic Transducers	654
Session 6K:	Industrial Ultrasonics	659

Poster Sessions, Wednesday, September 23, 2009, 10:00 am – 11:30 am:

Session P3-A:	Tissue Characterization	664
Session P3-B:	Imaging Methods	674
Session P3-C:	Beamforming	687
Session P3-D:	Signal Processing	697
Session P3-E:	Elasticity Methods: Clinical Applications	708
Session P3-F:	Motion Tracking and Elasticity Imaging	712
Session P3-G:	Vascular Elastography	717
Session P3-H:	Ultrasound Segmentation	722
Session P3-I:	Acoustic Sensors	727
Session P3-J:	Defects and Characterization	739
Session P3-K:	Thin Films-Characterization	748
Session P3-L:	Lamb Waves	752
Session P3-M:	Optical Interactions	758
Session P3-N:	Novel Ultrasonic Motors II	764
Session P3-O:	Air-Coupled Ultrasonics	771
Session P3-P:	Acoustic Materials and Structures	775
Session P3-Q:	Device Design	780
Session P3-R:	Device Modeling (SAW)	785
Session P3-S:	Medical Imaging Transducers	789
Session P3-T:	Transducer Modeling	797

Welcome from the General Chair



Massimo Pappalardo
University Roma Tre
General Chair

Welcome to Roma!

I am pleased to welcome you to the 2009 IEEE International Ultrasonics Symposium in Rome from September 20 to 23 at the Ergife Palace Hotel.

It is a great honor and a great pleasure to have had the opportunity to organize the International Ultrasonic Symposium in Rome. In this city, shortly after the end of the second World War and a few years before the birth of our Society, was held one of the first international congresses on Ultrasounds ([International Congress on Ultracoustics](#), Rome June 14-17, 1950). After 59 years the international scientific community, engaged in the by now numerous and important applications of ultrasounds, meet again in this historical and beautiful city. From the date of that first post-war conference till today the technical and technological progress has indeed been great and astonishing even to experts in the field. Our Society has given an important contribution, particularly in sensors, devices for telecommunications, non destructive testing, and medical diagnostics. The symposium is by now the window to observe what is really new in these fields, and I am sure that this venue in Italy will stimulate young researchers to a new and profitable interest both in this country and, I hope, in all the world.

I am sure that you will enjoy your visit to Rome, which is rightly known

as one of the most beautiful and interesting cities in the world. It is a city of culture and history, packed with the remains of well over two thousand years on inhabitation.

Founded around the middle of the 8th cent. BC, for almost 1000 years Rome was the largest, richest, and politically most important city in the Western World. Today you can still admire the majestic monuments of the ancient Roman Empire: the Forum, the Coliseum, and the Pantheon just to mention a few. But, besides being the city of the Emperors, Rome is also the city of the Popes, who from the very beginning established Rome as the center of Christianity, and the city remained the cultural center of the Western World attracting the greatest artists and architects creating masterpieces of painting and sculpture and an endless number of grand, beautiful churches and palaces.

I look forward to meeting you in Rome.

[Massimo Pappalardo](#)

2009 IEEE Ultrasonics Symposium General Chair

Venue



Ergife Hotel

Via Aurelia, 619 - 00165 ROME - Italy

Tel. +39 06 66441

Fax +39 06 6632689

E-mail: info@ergifepalacehotel.com

Registration

The registration desk is located in Volubilis Room.
The hours for the registration desk are:

Saturday September 19	6pm-9pm
Sunday September 20	7am-6pm
Monday September 21	7am-6pm
Tuesday September 22	7am-6pm
Wednesday September 23	7am-1pm

Registration and fees

	Gala Dinner	Before Sept 4th	After Sept 4th
IEEE Member	Included	\$525	\$650
Non-IEEE Member	Included	\$730	\$855
Student/Retiree	Included	\$150	\$150
IEEE Life Member	\$35	\$0	\$0
One-day Registration	\$35	\$350	\$350
Guest	\$35/each	\$35/each	\$35/each
Short Courses: Member/Non-member Student/Retiree		\$150/each \$50/each	\$200/each \$75/each

Notes:

- Full Registration (IEEE Member, Non-IEEE Member, Student, Retiree) will include one DVD conference proceedings and admission to the Gala Dinner Awards Reception Monday September 21st.
- Life Member is defined by IEEE as at least 65-year old and the age plus years of IEEE membership should be equal or greater than 100. Life members should show their IEEE Life Member card or evidence of Life Membership when getting registration materials.
- One-Day Registration includes event tickets for the day of registration only.

- Guest Registration includes two evening guest refreshments Sunday and Tuesday. Guests must register for the guest program in order to be allowed to register for the banquet. Guests are NOT allowed to attend any technical sessions except for the Monday morning plenary session.
- Short course attendees must register for the conference (at least a one day registration) in order to be able to register for the short courses.
- Students are required to show their valid identifications (IDs) to the registration desks to qualify for the student rates and get any registration materials.

Local Transportation

Transportation to/from the Ergife Hotel

From/to the airports - day time

[Fiumicino and Ciampino airports](#) are both about 30 Km from the centre of Rome and are both well linked with the two principal railway stations (Termini station and Tiburtina station) by trains.

From/to Fiumicino International Airport (FCO)

Rome's main airport is well-connected to the center during the day by a direct train. The direct train between Fiumicino and Termini costs € 11,00 and takes approximately 30 minutes. Tickets can be purchased at vending machines, ticket offices and other vendors at both Termini and Fiumicino.

schedule: every 30 minutes

Fiumicino - Roma Termini from 6.37am until 11.37pm

Roma Termini - Fiumicino from 5.52am until 10.52pm

When you are in Roma Termini (the principal railway station in Roma), you can use the follow [route](#) calculation that use only **public means** to reach the Ergife area.

- Departure from Roma "Stazione Termini"
- Walk 50 meters
- Go to stop **Termini METRO A**
- Take Line METRO A (direction **BATTISTINI**) to 10 stops (METRO A every 3 min.)

- Get off at stop **Cornelia**
- Walk 100 meters
- Go to bus stop **C.NE CORNELIA/AURELIA** (you are 1000 mt. away from the Ergife Hotel)
- Take Line Bus **246 (MALAGROTTA)** to 3 stops (line 246 every 12 min.)
- Get off at stop **AURELIA/DA ROSATE**
- Walk 150 meters to via Aurelia 619, the Ergife Venue

From/to Ciampino International Airport (CIA)

A smaller airport dealing mainly with charter flights and budget airlines. It is connected to **Line A** metro station **Anagnina** by **Cotral** buses; ticket costs € 1,03.

Buses leave the airport every 30-60 minutes.

Take Line Metro A (direction **Battistini**) and get off at stop **Cornelia**. You can take the line bus **246 (Malagrotta)** to 3 stops and get off at stop **Aurelia/Da Rosate**, or you can walk from Cornelia stop to the Ergife (about 1000 mt.)

From/to the airports - night time

Fiumicino

For arrivals and departures between 11.30pm and 5am, a night bus connects Fiumicino with Tiburtina station, stopping also at Termini Station.

From Fiumicino: 1.15am - 2.15am - 3.30am - 5.00am

From Tiburtina: 0.30am - 1.15am - 2.30am - 3.45am

The 40N bus connects Tiburtina and Termini during the night.

Ciampino

Buses connecting Ciampino airport with the centre of Rome stop running at 11pm, so the only way to get into town late at night is by taxi.

Taxi from/for airport

The price for a ride from **Leonardo da Vinci (Fiumicino) Airport** to the city centre (within the Aurelian Walls) is about Euro 40,00-50,00.

The price for a ride from **Ciampino Airport** to the city centre (within the Aurelian Walls) is about Euro 30,00-40,00.

You may be approached by illegal taxi drivers in the station and at the airport. If you need a taxi, look for the official white taxis which have meters. There are taxi stands at both Fiumicino, Ciampino, and Termini.
Info: tel. +39 060606 or +39 06 671070844

Exhibitors

An exhibitors breakfast will be held Wednesday Sept 23rd from 7-8am in the Moesia Room (Coffee, tea, pastries).

Exhibits will be in Sala 3. Companies will display their products and representatives will be there to meet conference attendees. The exhibitors will be in place on the following dates and times:

Monday-Tuesday 8:30-5pm and Wednesday 8:30-1pm

Registered Exhibitors: (as of 7/2/2009)

1. LECOEUR ELECTRONIQUE
www.lecoeur-electronique.com
2. POLYTEC GmbH (+BPS)
www.polytec.de
3. BPS s.r.l. (co-exhibitor of POLYTECH)
www.bpsweb.it
4. Sonora Medical Systems
www.4sonora.com
5. IMASONIC
www.imasonic.fr
6. DASEL
www.daselsistemas.com
7. Ferroperm Piezoceramics A/S
www.ferroperm-piezo.com
www.ferroperm.net
8. kiberio GmbH
www.kiberio.com
9. Sound Technology, Inc.
www.sti-ultrasound.com
10. Valpey Fisher Corporation
www.valpeyfisher.com
11. Electronics & Innovation, Ltd.

www.electronic sandinnovation.com;

www.eandiltd.com/

12. The Piezoinstitute c/o Ferroperm Piezoceramics A/S

www.piezoinstitute.com

13. Weidlinger Associates

www.wai.com

14. Ultrasonix Medical Corporation

www.ultrasonix.com

15. Precision Acoustics Ltd.

www.acoustics.co.uk

16. Onda Corporation

www.ondacorp.com

Industrial Forum

Moesia Room Wednesday September 23rd 1-2:30pm

Industrial forum is intended to give the Exhibitors the opportunity to present recent developments or applications of their products or technology.

Plenary Session

Date, Time, and Location:

- 8:00 a.m. – 9:30 a.m.
- Monday, September 21, 2009
- Room: Leptis Magna

Agenda:

Welcome:

- *Massimo Pappalardo* , Ph.D., General Chair, 2009 IEEE International Ultrasonics Symposium (IUS)
- *Mauricio Pereira da Cunha* , Ph.D., Vice President of the IEEE Ultrasonics, Ferroelectrics, and Frequency Control Society (UFFC-S) for Ultrasonics

- **Donald Yuhas**, Ph.D., Technical Program Committee (TPC) Chair, 2009 IEEE IUS
- **Susan Trolier-McKinstry**, Ph.D., President of the UFFC-S

Awards and Recognitions Presenter: **Helmut Ermert**, Ph.D., Awards Chair of the UFFC-S

Plenary presentation: **Prof. G. Parisi**, University of Rome "La Sapienza"

A new approach to the study of Heart Sounds

Heart Sounds have a fundamental role in cardiac semiotics. However, a deterministic and unambiguous association between noises in cardiac dynamics has yet to be accomplished due to the many and different overlapping events which contribute to the acoustic emission. The current computer-based capabilities in signal processing enabled us to move beyond the standard cardiac auscultation. Its improved form, like hi-tech phonocardiograms, allow us to pay attention to unexplored characteristics of heart-related sounds: their spatial distribution on the chest surface and their time evolution. In this presentation, we will describe results obtained using new instrumentation and a new sound visualization technique designed to enable the association of the spatial distribution of the heart acoustic emission with physiological and pathological patient condition.



prof. Giorgio Parisi

Biography Plenary Speaker

Giorgio Parisi was born 8/4/48 in Rome, Italy. He graduated from Rome University in 1970, his thesis supervisor being Nicola Cabibbo. He has worked as researcher at the Laboratori Nazionali di Frascati from 1971 to 1981. In this period he has been on leave of absence from Frascati at Columbia University, New York (1973-1974), at the Institute des Hautes Etudes Scientifiques (1976-1977) and at the Ecole Normale Supérieure, Paris (1977-1978). He became full professor in 1981. From 1981 to 1992 he was full professor of Theoretical Physics at the University of Rome II (Tor Vergata), becoming later professor of Quantum Theories at the University of Rome I (La Sapienza). He received the Feltrinelli prize for physics from the Accademia dei Lincei in 1986, the Boltzmann medal in 1992, the Italgas prize in 1993, the Dirac medal and prize in 1999, the Enrico Fermi Prize in 2003, the David Heinmann Prize in 2005, the Galileo Prize in 2006 and the Microsoft European Science prize in 2007. He became correspondent fellow of the Accademia dei Lincei in 1987 and fellow in 1992; he is also fellow of the French Academy from 1993, of the Accademia dei Quaranta from 2001 and of the US Academy of Science from 2004.

Awards and Recognitions:**IEEE Awards:**

IEEE Fellow Award 2009

IEEE UFFC Society Awards:

Achievement Award 2009

Distinguished Service Award 2009

Outstanding Paper Award 2008

2009-2010 Distinguished Lecturer Award

Ultrasonics Award:

Rayleigh Award 2009

Note: The order of presentation of awards is to be determined

Student Lunch

All students attending the Conference are invited to attend a complimentary standing buffet lunch from 1:00-2:30pm Monday September 21 in the Moesia Room.

Awards Reception

The Gala Dinner Awards Reception is included in the full conference registration: The reception will be held Monday September 21st at the restaurant Le Quattro Stagioni (inside Ergife Hotel) from 8pm to 11pm. Tickets to this event are included in full registration. Life members, one day registrants and guests may purchase tickets at a cost of \$35.00 per person.

Guest Program

We encourage guests of conference attendees to register. The registration fee of \$35 US Dollars permits you to attend the evening guest refreshments Sunday September 20th and Tuesday September 22nd from 4:00 pm – 6:00 pm. The evening guest refreshments will provide an opportunity to meet fellow guests and coordinate daily excursions and activities. The Gala dinner awards reception Monday September 21st is not included in guest registration but can be added at an addition charge of \$35 US Dollars per guest. Guest registration is required in order to register for the Gala dinner awards reception.

Guests should register with their accompanying conference attendees on the conference registration form. Guests are not allowed to attend any technical sessions except for the Monday morning plenary session.

Five individually priced guest tours have also been arranged, see below. We are pleased to announce that there is no minimum registration requirement for the guest tours this year, so there is no risk of a tour being cancelled due to too few registrants. There is an English tour guide on the tours.

Guest refreshments include coffee, tea and pastries on Sunday and Tuesday evening from 4:00 pm – 6:00 pm in the Moesia room or outdoors (weather permitting). The Ergife Palace Hotel will also be the departing and return points for the guest tours.

Note: The guest Refreshments are for registered guests only.

- Guest Tour 1 – Classic Rome, Monday morning, Sept. 21
- Guest Tour 2 – Imperial Rome, Monday afternoon, Sept. 21
- Guest Tour 3 – Vatican Museums, Tuesday morning, Sept. 22
- Guest Tour 4 – Papal Audience, Wednesday morning, Sept. 23
- Guest Tour 5 – Christian Rome, Wednesday afternoon, Sept. 23

POST CONFERENCE TOURS

The IUS 2009 Committee has organized two individually priced tours for the attendees after the 2009 IEEE International Ultrasonics Symposium. We are pleased to announce that there is no minimum registration requirement for the tour this year, so there is no risk of a tour being cancelled due to too few registrants. There is an English tour guide on every tour.

PC-Tour 1 - FIRENZE

3 days (2 nights in a First Class hotel, 1 meal and 2 breakfasts)

From September 24 to September 26, 2009

Florence, the cradle of the Renaissance period, where you breathe art in its Medieval streets, the craftsmens' workshops and the Renaissance Palaces. Here, the memories of the Medici family are linked with the splendor of the works of renowned artists like Michelangelo, Leonardo da Vinci, and Botticelli.

PC-Tour 2 - NAPOLI, POMPEI, SORRENTO, CAPRI

*3 days (2 nights in a First Class hotel, 4 meals and 2 breakfasts)
From September 24 to September 26, 2009*

Three days to discover not only the excavations of the ancient city of Pompeii but also to see the breathtaking coastline of the Sorrento Peninsula and Capri, the jewel of the Mediterranean sea. This is a journey to discover art, history, folklore and archaeology in the most beautiful region of southern Italy.

Shopping and Food

Shopping and Food near the Ergife palace Hotel

Choosing the venue for a congress is never easy. The success of a congress often depends on aspects that are apparently of secondary importance: organizational ability and efficiency, technological facilities, the elegance of the venue and quality of the accommodation and its amenities.

However what counts above all else is the prestige of the location. In this sense, Rome is ideal, with its fascinating and uniquely special setting, abounding in history. The city's historical, archaeological and architectural heritage is breathtaking; in addition, the pleasures of excellent cuisine are always offered, and a trip to the shops is essential.

We would like to suggest some shopping & food around the Ergife Palace Hotel (*within 500 m*), to simplify the congressman's life!

See the map, to choose your downtime!

FOOD



- 1) Chinese Resturant - **Xian Du**, via Aurelia 611-613 - phone 0666418808 - 100 seats - 5/20 €
- 2) Pizza - **Mille Pizze E ...**, via Aurelia 601 - phone 0666415457 - closed on Sunday - 50 seats
- 3) Bar, coffee, breakfast - **Matrix Bar**, via Aurelia 558 - phone 0645448323
- 3) **Pharmacy** - Medicine shop
- 3) **Cigarettes** and tobacco
- 4) Bar, coffee, breakfast, ice-creams - **Bar Bonsignori**, via Aurelia 591 - phone 06469950587
- 5) Restaurant & Pizza - **Postodivino**, via Aurelia 528/a phone 0666410456 - closed on Tuesdays, 70 seats
- 6) Restaurant - **Osteria Romana**, via Aurelia 553 phone 066623302 - 25/30€ - 90 seats
- 7) Restaurant, bar - **Benedetto**, via Aurelia 666/b phone 0666415004 - 20/30€ -150 seats
- 8) Restaurant & Pizza - **Il Postiglione**, via Aurelia 664 phone 0666541012 - 20/30€ - 170 seats
- 9) Bar & Pizza - **Festival**, via Aurelia 570 phone 0666512572 - 3/10€ - 50 seats
- 10) **McDonald's** - P.zza Giovanni Battista De La Salle 9 phone 0666017165

11) **Mercato Irnerio** - A typical Rome corner market

**It is possible to use the restaurant facilities of the Ergife:
Buffet Lunch/Dinner (seated): € 35,00 per person, per service.
Buffet Lunch/Dinner (standing): € 32,00 per person, per service.**

You can also have a lunch/dinner à la carte.

SHOPPING

For shopping, we suggest to move into the centre of the city.

Rome, the eternal city, rich in history, art and culture but also a cosmopolitan city and important landmark in fashion and new trends.

Arriving in Rome with the intention to follow a very fashionable route, therefore, you have only the embarrassment of choice.

Starting point for this unusual, but no less fascinating tour of the city can only be the elegant and famous Via Condotti, one of the favorites for foreigners to purchase in Roman ateliers, from the most important Italian and international fashion designers such as Valentino, Armani, Gucci, Dolce & Gabbana and Dior, to name a few.



Via Condotti

Of note, again in Via Condotti, the precious jewels of Bulgari, Cartier and Federico Buccellati.

Equally glamorous and elegant Via Frattina which is, together with Via Borgognona and Via Bocca di Leone, home to some major world-renowned brands such as, it is worth to mention, the Trussardi store, the elegant shops of Cesare Paciotti and the refined Pal Zileri atelier.



Via Borgognona

Leaving the area near the Spanish Steps along via della Mercede you can arrive in Via del Corso, one of the main arteries of the city. Partially closed to traffic, it houses shops of various types, capable to meet different needs: from the clothing for women and for men, to underwear, accessories, footwear, and young and trendy fashion megastores.

To see, walking along Via del Corso, the charming and characteristic Galleria Colonna (now Galleria Alberto Sordi) with many shops in complete peace and in shelter from rain and cold. Here it is just to choose

between the modern and captivating "Jam", the alternative "Pinko", and the elegant Calvin Klein boutique.



Via del Corso

Walking in Campo de Fiori, you must not miss Via dei Giubbonari. While you are moving towards Piazza Venezia, you cannot do without a walk along Via Nazionale, full of shops and boutiques. In the area of the Vatican, finally, another must-stop is in Via Cola di Rienzo, where you can range from the classic and elegant boutiques as Luisa Spagnoli, Max Mara, Cerruti and David Saddler to large chains of fashion and glamour as Mango, Miss Sixty, Ethic, Fornarina, Onix, Benetton and Sisley, for a shopping at 360-degrees.



Campo dei Fiori



Via Cola di Rienzo

Message Board

There will be four video-message boards (40" LCD TV) for the attendees in some points of the congress-venue. The use of the message board will be available for all both leaving a message in the computer room, and by internet, using a web page of the official web site.

Wireless Access & Printing

The entire area of the congress (lobby, common areas, session rooms) will have free WiFi. The information on the setup will be available to the congress.

There is an additional charge for Internet use in the guest rooms of the Ergife Palace Hotel and an IP cable is needed.

In the computer room (Gerasa) and in the registration room (Volubilis) will be available a laser printer.

IEEE and UFFC-S Enrollment

Join IEEE-UFFC Society

The Ultrasonics, Ferroelectrics, and Frequency Control ([UFFC](#)) Society of the Institute of Electrical and Electronics Engineers ([IEEE](#)) covers areas of ultrasonics, ferroelectrics, and frequency control among others. It will be very beneficial to join this excellent Society for your future professional careers. You will be able to interact with other members and contribute to the growth of the IEEE UFFC society. You will also be eligible for consideration to receive travel supports to various IEEE UFFC national and international conferences. The future of the society is in your hands. Please click on the [link](#) to join today and you will also be able to access the IEEE Transactions on Ultrasonics, Ferroelectrics, and Frequency Control ([TUUFFC](#)) journal among other publications that will benefit your entire professional life. A discount membership fee is available for students.

Proceedings

The 2009 IEEE IUS Symposium Proceedings (DVD format) will be available in December 2009. To ensure a timely delivery of the Proceedings, no papers will be accepted after 8:00 A.M. *Rome time*.

(For details on paper submission please see:

http://ewh.ieee.org/conf/ius_2009/). Please note that only those papers presented in the Symposium will be included in the Proceedings.

The DVD copy of the proceedings will be mailed to all paid registrants except guests and one-day registrants. A printed version of the Proceedings can be ordered from IEEE Shop: Conference Proceeding after the Symposium.

UFFC DVD Archive

The Digital Archive is available on DVD. The entire set is available to UFFC members for \$100. Yearly updates will be available free of charge to current UFFC members. Please use the online form (<http://www.ieee-uffc.org/main/publications.asp>) to request updates or purchase the entire set.

If you have received DVD updates but did not get all DVDs 1-5, you may need to download the indices for the DVD structure. Use this link (ftp://Indices:y3m0n5skmXQE@ftp.ieee-uffc.org/DVD_Indices.zip) to download these indices. Please note that this zip file is quite large, and will take at least 1.5 hours to download. Once the download is complete, unzip the file. Open this file and move all of its contents into your UFFC Digital Archive folder. Once this is completed, you should see the ARCINDEX (2-5) folders and ARCINDEX (2-5).PDX files in your UFFC Digital Archive folder. Then proceed to initialize the search engine as described in the instructions on the DVD.

Message from the Technical Program Chair



Donald E. Yuhas
Industrial Measurement Systems, Inc.
Technical Chair

On behalf of the Technical Program Committee (TPC), I am thrilled to invite you to the 2009 IEEE International Ultrasonics Symposium to be held September 20-23, 2009, at the Ergife Palace Hotel in Roma. The outstanding work of the IEEE Ultrasonics TPC group has established our Symposium as the major international forum for Ultrasonics innovation. In 2009 we will highlight 21 invited presentations covering the 5 major technical sub-groups: 1) Medical Ultrasonics, 2) Sensors, NDE & Industrial Applications, 3) Physical Acoustics, 4) Microacoustics – SAW, FBAR, MEMS, and 5) Transducers & Transducer Materials. Keeping the successful traditional events, the first day of the conference is reserved to top quality short courses featuring expert instructors, followed by the three days of technical sessions, which include the student paper competition. The posters of the student finalists will be on display in a specially designated area for the duration of the conference. Roma, as a venue, provides all the excitement of one of the greatest cosmopolitan areas in the world! We have confidence that our outstanding technical program and your technical contribution are a great match to the sites and charm of Roma. I hope we all share the same excitement! All roads lead to Roma, I am looking forward to seeing you there in 2009!

[Donald E. Yuhas](#)

2009 IEEE International Ultrasonics Symposium Technical Chair

Policy on Photography

Photography or Recording:

To respect the privacy of presenters and minimize interruptions to the conference, photography and sound recording are not allowed in any technical sessions (both oral and poster) except for the plenary session.

Speaker's Ready Room

Facilities will be available for presenters to review their presentations. Speaker Ready Room (Gerasa) will be open from 7:00 am to 6:00 pm Sunday-Wednesday.

Short Courses

Short Courses will be held in rooms and times according to timetable which follows the listing.

Short Courses TIMETABLE

Sunday, September 20 2009 (room)		
8:00am - 12.00am	1:00pm - 5.00pm	6.00pm - 10.00pm
1A (Hama)	1B (Hama)	1C (Merida)
2A (Efeso)	2B (Spalato)	2C (Spalato)
3A (Merida)	3B (Merida)	3C (Efeso)
4A (Pola)	4B (Pola)	4C (Pola)
5A (Cesarea)	5B (Efeso)	5C (Hama)
6A (Spalato)	6B (Cesarea)	6C (Cesarea)

Tutorials and Short Courses

Course 1A

Film Bulk Acoustic Resonator (FBAR)

Richard Ruby and John Larson

Avago Technologies

U.S.A.

Course 2A

Materials for Acoustic Wave Devices

Manfred Weihnacht

IFW Dresden

Germany

Course 3A

Microwave Acoustic Sensors

Enrico Verona

O.M. Corbino Institute of Acoustics - National Research Council (CNR)

Italy

Course 4A

Seattle Therapeutic Ultrasound

Lawrence A. Crum, Joo Ha Hwang, and Michael R. Balley

Applied Physics Lab., University of Washington

, U.S.A.

Course 5A

Ultrasonic NDE and Industrial Process Diagnostics at High Temperatures

Jean-Pierre Monchalin and Cheng-Juei Jen

National Research Council Canada

Canada

Course 6A

Estimation and Imaging of Blood Flow Velocity

Hans Torp and Lasse Løvstakken

Norwegian University of Science and Technology

Norway

Course 1B

SAW Modeling Techniques

*Victor Plessky
GVR Trade SA
Switzerland*

Course 2B

Piezoelectric Ultrasound Transducer Fundamentals - Materials, Structure, Behavior, and Analysis

Sandy Cochran¹ and Paul Reynolds²

¹*Institute for Medical Science and Technology, University of Dundee, UK*

²*Weilinger Associates Inc., Mountain View, U.S.A.*

Course 3B

Quantitative Acoustic Microscopy - Fundamentals and New Applications from Cells to Airplanes

Roman Gr. Maev¹, Naohiro Hozumi², Kazuto Kobayashi³, Yoshifumi Sajio⁴

¹*Centre for Imaging Research and Advanced Materials Characterization, University of Windsor; Ontario, Canada*

²*Dept. of Electrical and Electronics Engineering, Aichi Institute of Technology; Aichi, Japan*

³*Honda Electronics Co. Ltd., Aichi, Japan*

⁴*Tohoku University, Sendai, Japan*

Course 4B

Ultrasound Imaging Systems: from Principles to Implementation

*Kai E. Thomenius
General Electric Global Research
Nishayuna, NY, USA*

Course 5B

Passive UHF RFID Tags, Systems, and Applications

*Leonhard Reindl, Jochen Eßel, Robert Weigel
University of Freiburg and University of Erlangen-Nuremberg
Germany*

Course 6B

Ultrasonic Signal Processing for Detection, Estimation, and Imaging

*Jafar Saniie, Ramazan Demirli, Erfal Oruklu
Illinois Institute of Technology*

Chicago, IL

Course 1C

Time Reversal Acoustics

Mathias Fink

Ecole Supérieure de Physique et de Chimie Industrielles de la Ville de Paris (ESPCI)

Paris, France

Course 2C

Ultrasound Contrast Agents: Theory and Experiment

Nico de Jong and Michel Versluis

Erasmus MC and University of Twente

Rotterdam and Enschede, Netherlands

Course 3C

Zooming into the Near Field

Alireza Baghai-Wadji

RMIT University

Melbourne, Australia

Course 4C

CMUTs: Theory, Technology, and Applications

B.T. Khuri-Yakub, O. Oralkan, and M. Kupnik

E.L. Ginzton Lab., Stanford University

Stanford, USA

Course 5C

Guided SH-SAW Devices for Liquid-Phase Biochemical Sensors

Fabien J. Josse

Dept. of Electrical and Comp. Eng., Marquette University

Milwaukee, WI, USA

Course 6C

Elasticity Imaging: Dynamic Approaches

Kathy Nightingale and Mark Palmeri

Duke University

USA

Invited Speakers

Group I : Medical Ultrasonics

Jan D’hooge, Vice-Chairman

Session 1J. Cardiovascular Elastography(abstract 1422)

Room: Sala 1 Wednesday 3:30-4:00 p.m

Title: Acoustic Radiation Force Imaging

Author/ Speaker: Greg Trahey

Affiliation: Department of Biomedical Engineering Duke University, Durham, N.C. US

E-mail: gregg.trahey@duke.edu

Session 1A. Targeted Contrast Agents (abstract 1198)

Room: Sala 1 Monday 11:30-12:00 a.m

Title: Molecular Imaging using Contrast Ultrasound

Author/Speaker: Alexander Klibanov

Affiliation: Cardiovascular Division, Department of Medicine, University of Virginia

Email: sklib1@gmail.com

Session 1B. Contrast Agents and Sonoporation (abstract 1354)

Room: Sala 1 Monday 3:30-4:00 p.m.

Title: Ultrasound-based imaging of nanoparticles: from molecular and cellular imaging to therapy guidance

Author/Speaker: Stanislav Emelianov

Affiliation: Department of Biomedical Engineering, University of Texas at Austin

E-mail: emelian@mail.utexas.edu

Session 1G. Therapy Microbubbles (abstract 1499)

Room: Sala 1 Tuesday 5:00-5:30 p.m

Title: Enhancement of ultrasonic heating with microbubbles and their location in target tissues

Author/Speaker: Shin-ichiro Umemura

Affiliation: Department of Information and Intelligent Systems, Graduate School of Biomedical Engineering

Tohoku University, Aoba 6-6-05, Aramaki, Aoba-ku, Sendai 980-8579, Japan

Email: sumemura@ecei.tohoku.ac.jp

Session 1H. Optical and Photoacoustic Imaging (abstract 1498)

Room: Sala 1 **Wednesday 9:00-9:30 a.m**

Topic: Optical coherence tomography: recent technical developments and the impact on clinical utility

Author/Speaker: Melissa J. Suter

Affiliation: Massachusetts General Hospital and Harvard Medical School

E-mail: msuter@partners.org

Session 1C. New Methods and High Frequency Ultrasound for Tissue Characterization (abstract 915)

Room: Sala 1 **Monday 4:30-5:00 p.m**

Topic: Acoustic Microscopy – Beyond High Resolution Imaging

Author/ Speaker: Yoshifumi Saijo

Affiliation: Biomedical Imaging Laboratory, Graduate School of Biomedical Engineering

Tohoku University, 4-1 Seiryomachi, Aoba-ku, Sendai 980-8575, Japan

E-mail: saijo@idac.tohoku.ac.jp

Group II: Sensors, NDE, and Industrial Application Jafar Saniie, Vice-Chairman

Session 4I. Energy Harvesting (abstract 957)

Room: Tarragona **Wednesday 11:30-12:00 a.m**

Title: Energy conversion improvement in ferroelectrics: application to energy harvesting and self-powered systems.

Author/Speaker: [D. Guyomar](mailto:daniel.guyomar@insa-lyon.fr), M Lallart

Affiliation: LGEF (Electrical engineering lab), INSA Lyon, Lyon University

INSA Lyon, LGEF, Bât Gustave Ferrié, 8 rue de la physique, 69621 Villeurbanne CEDEX France

Email: daniel.guyomar@insa-lyon.fr

Session 4B. Advances in NDE(abstract 681)

Room: Tarragona **Monday 2:30-3:00 p.m**

Title: Electromagnetic Transducers and their Potential for Modern Non-Destructive Evaluation - State of the Art and Latest Applications

Author/Speaker: Hans-Juergen Salzburger,

Affiliation: Fraunhofer-Institute for Non-Destructive Testing Campus E 3.1

D-66123 Saarbruecken

Germany

E-mail: salzburger@izfp.fhg.de

Session 4E. Array Imaging (abstract 788)

Room: Tarragona **Tuesday 12:00-12:30 p.m**

Title: Echographic Imaging Plates

Author/Speaker : [F. Montero de Espinosa](#), O. Martínez, Y. Gómez-Ullate, L. Gómez-Ullate.

Affiliation: Applied Acoustics Institute, CSIC, Serrano 144, Madrid, Spain

Contact Person/Address: F. Montero de Espinosa Freijo
Vicepresidente Adjunto de Relaciones Institucionales,CSIC
Serrano 117, 28006 Madrid, Spain

Email: pmontero@orgc.csic.es

Session 4G. Nano-scale Acoustic Testing (abstract 613)

Room: Tarragona **Tuesday 4:30-5:00 p.m**

Title: Recent advances in carbon nanotubes for application to chemical and biological sensors

Author/ Speaker: F. Xavier Ruis

Mailing address: Faculty of Chemistry. Campus Sescelades. University Rovira

i Virgili. 43007 Tarragona. Spain

Email: fxavier.rius@urv.cat

Group III: Physical Acoustics

Yook-Kong Yong, Vice-Chairman

Session 6E. Ultrasonic Linear Motors (abstract 1113)

Room: Baalbek **Tuesday 11:30-12:00 p.m**

Title: Ultrasonic Motors

Authors: Minoru Kurosawa

Affiliation: Tokyo Institute of Technology, Japan

Email: mkur@ae.titech.ac.jp

Session 6A. Phononic Crystals-Fundamentals (abstract 126)

Room: Baalbek **Monday 12:30-1:00 p.m**

Title: Phononics

Authors: Vincent Laude

Affiliations: Directeur de recherche CNRS, Institut FEMTO-ST, France

Email: vincent.laude@femto-st.fr

Session 6B. Visualization Interferometry (abstract 1190)

Room: Baalbek **Monday 3:00-3:30 p.m**

Title: Laser interferometers in physical acoustics

Authors: Kimmo Kokkonen

Affiliation: Helsinki University, Finland

Email: kimkok@cc.hut.fi

Session 6I. Acoustic Propagation (abstract 1350)

Room: Baalbek **Wednesday 12:30-1:00 p.m**

Title: Fundamentals of acoustics - conditions of existence of acoustic waves in crystals with surfaces and interfaces

Authors: V.I. Alshits

Affiliation: Institute of Crystallography RAS, Moscow, Russia

Email: alshits@ns.crys.ras.ru

Group IV: Microacoustics - SAW, FBAW, MEMS Clemmens Ruppel, Vice-Chairman

Session 5D. Oscillators and Temperature Compensation (abstract 66)

Room: Pergamo **Tuesday 8:00-8:30 a.m**

Title: Comparison of Quartz and MEMS Resonators and Oscillators

Author/ Speaker: Bernd Neubig

Affiliation: AXTAL CONSULTING

Email: BNeubig@axtal.com

Session 5C. BAW I (abstract 1491)

Room: Pergamo **Monday 5:00-5:30 p.m**

Title: The role of high Q bulk acoustic wave resonators in low power IC design

Author/ Speaker Brian Otis

Affiliation: University of Washington

Email: botis@u.washington.edu

Session 6J. RF MEMS (abstract 55)

Room: Baalbek **Wednesday 2:30-3:00 p.m.**

Title: RF MEMS: Focusing on the Next Step

Author/ Speaker: Takeo Oita

Affiliation: Nihon Dempa Kogyo

Email: oita@ndk.com

Session 5F. SAW Device Design (abstract 579)

Room: Pergamo **Tuesday 2:30-3:00 p.m**

Title: High Performance Microwave Acoustic Components for Mobile Radios

Author/ Speaker: M. Pitschi, et al

Affiliation: EPCOS AG, Univ. of Erlangen-Nuremberg

Email: maximilian.pitschi@epcos.com

Group V: Transducers and Transducer Materials Scott Smith, Vice-Chairman

Session 5H. Novel Devices & Systems (abstract 1492)

Room: Pergamo **Wednesday 8:00-8:30 p. m.**

Title: Biologically Inspired Ultrasound - its applications in NDE

Author/ Speaker: Gordon Hayward

Affiliation: University of Strathclyde

Email: g.hayward@eee.strath.ac.uk

Session 3A. Ferroelectrets and Other Transducer Materials (abstract 614)

Room: Sala 4 **Monday 12:00-12:30 p.m**

Title: Broadband Ferroelectret Transducers

Author/ Speaker: Gerhard Sessler

Affiliation: Darmstadt TU

Email: g.sessler@nt.tu-darmstadt.de

Session 3C. CMUT Modeling (abstract 790)

Room: Sala 4 **Monday 5:30-6:00 p.m**

Title: CMUTs, achievements and limitations

Author/ Speaker: Arne Ronnekleiv

Affiliation: NTNU, NUST Room 473 Besøksadresse: Elektrobygget, O.S. Bragstads plass 2a, 7034 Trondheim, Norway

Email: arne.ronnekleiv@iet.ntnu.no

Session 5I. Piezoelectric Transducer Materials (abstract 496)

Room: Pergamo **Wednesday 12:00-12:30 p.m**

Title: Growth, Properties and Applications of PMN-PT based Giant-Piezoelectric Crystals

Author/ Speaker: Pengdi Han

Affiliation: HC Materials, 479 Quadrangle Dr. Suite-E, Bolingbrook, Illinois 60440

Email: han@hcmat.com

Clinical Session

Session 1D. Clinical Ultrasound

Room: Sala 1 **Tuesday**

Time: 8-8:30am

Title: Recent Advances in Clinical Ultrasound (**abstract 1481**)

Author/ Speaker: David Cosgrove

Affiliation: Imperial College

Time: 8:30-9:00a.m.

Title: Cardiovascular Ultrasound (abstract 1501)

Author/ Speaker: Lars-Ake Brodin

Time: 9:00-9:30a.m.

Title: Current Sonographic Imaging in Obstetrics & Gynaecology (abstract 1409)

Author/ Speaker: Juriy Wladimiroff

Affiliation: Dept of Ob&Gyn, Erasmus University Medical Centre

Student Paper Finalists

Posters are required for all student finalists and will be displayed in a special section, PS, in the first poster session on Monday. These posters will remain on display until the final poster session on Wednesday.

This is the 9th year of the student paper competition. 19 finalists were selected at the Technical Program Committee Meeting held in Chicago,

IL June 13-14th 2009. Posters will be displayed Monday-Wednesday in Sala Orange.

GROUP 1 - Medical Ultrasonics (6 finalists)

Finalist #1.1 *Adam D. Maxwell, *Tzu-Yin Wang, *Charles A. Cain, *J. Brian Fowlkes, **Oleg A. Sapozhnikov, **Michael R. Bailey, *Zhen Xu

“The role of compressional pressure in formation of dense bubble clouds in histotripsy” *Biomedical Engineering, University of Michigan, Ann Arbor, MI, USA, **Applied Physics Laboratory, University of Washington (abstract 527)

Finalist #1.2 *Amin Nikoozadeh, *Omer Oralkan, **Kai Thomenius, **Aaron Dentinger, **Douglas Wildes, ***Kalyanam Shivkumar, ***Aman Mahajan, ****Douglas N. Stephens, *****Matthew O’Donnell, *****David Sahn, *Pierre T. Khuri-Yakub

“Forward-Looking Volumetric Intracardiac Imaging Using a Fully Integrated CMUT Ring Array” *Stanford University, Palo Alto, CA, USA, **General Electric Corporate Research & Development, ***University of California, Los Angeles, ****University of California, Davis, *****University of Washington, *****Oregon Health and Science University (abstract 1181)

Finalist #1.3 *Nikita Reznik, **Ross Williams, *Peter N. Burns

“Optical and Acoustic Characterization of Vapourized Perfluorocarbon Droplets as Ultrasound Contrast Agents” *Department of Medical Biophysics, University of Toronto, Canada, **Sunnybrook Health Sciences Centre (abstract 969)

Finalist #1.4 *David Thomas, **Marcia Emmer, **Hendrik Vos, *Vassilis Sboros, **Nico de Jong

“Optical observations of microbubble oscillation in small tubes” *Medical Physics, University of Edinburgh, **Thorax Center, Biomedical Engineering, Erasmus Medical Center (abstract 495)

Finalist #1.5 Skylar Marvel, Elizabeth Loba, Paul A. Dayton

“Applications of Low Intensity Pulsed Ultrasound for Functional Bone Tissue Engineering using Adult Stem Cells” Joint Dept of Biomedical Engineering, University of North Carolina-North Carolina State University (abstract 1273)

Finalist #1.6 Ivan Nenadic, Matthew W. Urban, James F. Greenleaf
“Ex Vivo Measurements of Mechanical Properties of Myocardium
Using Lamb and Rayleigh Wave Dispersion Velocities”
Mayo Clinic College of Medicine (abstract 1285)

GROUP 2 - Sensors, NDE & Industrial Applications (3 finalists)

Finalist #2.1 *Jeanne-Louise Shih, **Makiko Kobayashi, **Cheng-
Kuei Jen
“Flexible Ultrasonic Transducers for Structural Health Monitoring
of Pipes at High Temperatures”
*McGill University, **Industrial Materials Institute National Research
Council Canada (abstract 511)

Finalist #2.2 *Venkata Chivukula, **Daumantas Ciplys, *Michael
Shur, ***Jinwei Yang, ***Remis Gaska
“Surface Acoustic Wave Interdigital Transducers Response to Deep
UV Illumination in AlGa_N/Sapphire”
*Center for Integrated Electronics, Rensselaer Polytechnic Institute,
Department of Radiophysics, Vilnius University, *Sensor Electronic
Technology, Inc. (abstract 825)

Finalist #2.3 Atsushi Miyamoto, Mami Matsukawa
“Measurement of three-dimensional distribution of crack tips by low
power pulsed laser”
Doshisha University (abstract 1256)

GROUP 3 - Physical Acoustics (3 finalists)

Finalist #3.1 *Dana Gallimore, **Thomas Moonlight, *Mauricio
Pereira da Cunha
“Extraction of Pt/Rh/ZrO₂ High Temperature Elastic Constants”
*Electrical and Computer Engineering / Laboratory of Surface Science
and Technology, University of Maine, **University of Maine (abstract
513)

Finalist #3.2 *Mirza Pasovic, *Mike Danilouchkine, *Paul van Neer,
*Antonius van der Steen, **Olivier Basset, **Christian Cachard, *Nico
de Jong

“Angular spectrum method for the estimation of pressure fields in the super harmonic band”

*Biomedical Engineering, ErasmusMC, **CREATIS-LRMN, Univeriste de Lyon, INSA Lyon (abstract 306)

Finalist #3.3 *Hengky Chandralim, *Sunil Bhawe, **Christian Rembe, **Sebastian Boedecker, ***Ronald Polcawich, ***Jeff Pulskamp

“Heterodyne laser-doppler interferometric characterization of contour-mode resonators above 1 GHz”

*Electrical and Computer Engineering, Cornell University, **Polytec, ***US Army Research Laboratory (abstract 1467)

GROUP 4 - Microacoustics – SAW, FBAR, MEMS (4 finalists)

Finalist #4.1 Florian Thalmayr, Ken-ya Hashimoto, Tatsuya Omori, Masatsune Yamaguchi

“Fast Evaluation of Lamb Wave Scattering by Time Harmonic FEM simulation”

Graduate School of Engineering, Chiba University (abstract 113)

Finalist #4.2 *Mohamed Abd Allah, **Jyrki Kaitila, **Robert Thalhammer, **Werner Weber, *Doris Schmitt-Landsiedel

“Temperature Compensated Solidly Mounted BAW Resonators with Thin SiO₂ Layers”

*Lehrstuhl für Technische Elektronik, Technische Universität München, **Infineon Technologies (abstract 191)

Finalist #4.3 *Eduard Rocas, *Carlos Collado, **Enrique Iborra, ***Robert Aigner

“Unified model for nonlinear effects in BAW resonators”

*Signal Theory and Communications, Universitat Politècnica de Catalunya, **Grupo de Microsistemas y Materiales Electrónicos, Universidad Politécnica de Madrid, ***R&D Acoustic Technologies, Triquint Semiconductor (abstract 703)

Finalist #4.4 Bennett Meulendyk, Mauricio Pereira da Cunha

“Suppression of transverse waveguide modes for SAW resonators with Pt and Pt/Rh/ZrO₂ electrodes”

Electrical and Computer Engineering, University of Maine (abstract 1015)

GROUP 5 - Transducers & Transducer Materials

Finalist #5.1 *Alper Sisman, **Jaime Zahorian, **Gokce Gurun,
*Mustafa Karaman, **Mujdat Balantekin, **F. Levent Degertekin,
**Paul Hasler

“Evaluation of CMUT Annular Arrays for Side-looking IVUS”
*Isik University, Electronics Eng. Dep., **Georgia Institute of
Technology (abstract 1218)

Finalist #5.2 Matthew Eames, John Hossack

**“Selectable Frequency CMUT with Membrane Stand-Off
Structures”**
University of Virginia (abstract 1186)

Finalist #5.3 Joseph Kilroy, Linsey C. Phillips, Abhay V. Patil, John
Hossack

“Ultrasound Cather for Microbubble Based Drug Delivery”
Biomedical Engineering, University of Virginia (abstract 920)

Organizing Committee

Finance Chair



Jackie Hines
Applied Sensor Research
jhines@ieee.org
Exhibit/Sponsor Chairs



Clemens Ruppel
EPCOS AG
c.c.ruppel@ieee.org



Georg Schmidt
GEROTRON COMMUNICATION GmbH
georg.schmidt@gerotron.com

Short Course Chair



Mauricio Pereira da Cunha
University of Maine
mdacunha@ecee.maine.edu

Editorial Chair



Marjorie Passini Yuhas
Industrial Measurement Systems Inc.
myuhas@imsysinc.com
A-V Chair & WebMaster



Nicola Lamberti
University of Salerno
nlamberti@unisa.it
Student Arrangements



Roman Gr. Maev
University of Windsor
maev@uwindsor.ca
Local Arrangements Chair



Giosuè Caliano
University of Roma Tre
caliano@ieee.org

Technical Program Committee

Group I: Medical Ultrasonics

Vice Chair of TPC:

Jan D'hooge

*Katholieke Universiteit Leuven
Leuven, Belgium*

Members:

Olivier Basset, CREATIS, Lyon, France
Ayache Bouakaz, INSERM, Tours, France
Charles Cain, Univ. of Michigan, USA
Jean-Yves Chapelon, INSERM, Lyon, France
Greg Clement, Harvard Medical School, USA
Paul Dayton, Univ. North Carolina/NCSU, USA
Emad Ebbini, Univ. of Minnesota, USA
Stanislav Emelianov, Univ. of Texas at Austin, USA
David Evans, Univ. of Leicester, UK
Kathy Ferrara, Univ. of California Davis, USA
Stuart Foster, Univ. of Toronto, Canada
James Greenleaf, Mayo Clinic, USA
Anne Hall, GE medical systems, USA
Christopher Hall, Philips Research, USA
Peter Hoskins, Univ. of Edinburgh, UK
John Hossack, Univ. of Virginia, USA
Kullervo Hynynen, Univ. of Toronto, Canada
Jorgen Jensen, Technical Univ. of Denmark, Denmark
Chris de Korte, Catholic Univ. of Nijmegen, the Netherlands
Nico de Jong, Erasmus Medical Centre, the Netherlands
Jeff Ketterling, RiversideNew York, USA
Michael Kolios, Ryerson University, Canada
Hiroshi Kanai, Tohoku University, Japan
Nobuki Kudo, Hokkaido University, Japan
Pai-chi Li, National Taiwan University, Taiwan
Jian-yu Lu, Univ. of Toledo, USA
Tom Matula, Univ. of Washington, USA
Leonardo Masotti, Univ. Of Firenze, Italy
James G. Miller, Washington University, USA
Kathy Nightingale, Duke University, USA

Svetoslav Nikolov, BK Medical, Denmark
William O'Brien, Univ. of Illinois at Urbana-Cham., USA
Georg Schmitz, Ruhr-Universität Bochum, Germany
Ralf Seip, Philips Research, USA
Mickael Tanter, University Paris VII, France
Tom Thomas, Boston Scientific, USA
Kai Thomenius, GE's corporate R&D, USA
Hans Torp, Univ. of Science&Technology, Norway
Piero Tortoli, Univ. of Firenze, Italy
Ton van der Steen, Erasmus Medical Centre, the Netherlands
Kendall Waters, Silicon Valley Med. Instruments, USA
Keith Wear, Food and Drug Administration, USA

Group II: Sensors, NDE, and Industrial Application

Vice Chair of TPC:

Jafar Saniie, Ph.D.

*Illinois Institute of Technology
Chicago, Illinois, U.S.A.*

Members:

Robert C. Addison: Rockwell Science Center, USA
Walter Arnold: Fraunhofer Institute for Nondestructive Testing,
Germany
Michal Bezdek: Endress+Hauser Flowtec AG, Switzerland
Ramazan Demirli: Canfield Scientific, USA
Eric S. Furgason: Purdue University, USA
David Greve: Carnegie Mellon University, USA
Edward Haeggstrom: University of Helsinki, Finland
Mitsutaka Hikita: Kogakuin University, Japan
Jacqueline Hines: Applied Sensor Research and Development
Corporation, USA
Fabien J. Josse: Marquette University, USA
Lawrence W. Kessler: Sonoscan Inc., USA
Pierre T. Khuri-Yakub: Stanford University, USA
Mario Kupnik: Stanford University, USA
Jun-ishi Kushibike: Tohoku University, Japan
Roman Maev: University of Windsor, Canada
Kentaro Nakamura: Tokyo Institute of Technology
Massimo Pappalardo: University Roma Tre, Italy
Tony Sinclair: University of Toronto, Canada
Bernhard Tittman: Pennsylvania State University, USA

Jiromaru Tsujino: Kanagawa University, Japan

John F. Vetelino: University of Maine, USA

Paul Wilcox: University of Bristol, UK

Donald E. Yuhas: Industrial Measurement Systems, Inc., USA

Group III: Physical Acoustics

Vice Chair of TPC:

Yook-Kong Yong, Ph.D.

Rutgers University Piscataway, New Jersey, U.S.A.

Members:

Robert Aigner: TriQuint Semiconductor, USA

Art Ballato: U.S. Army, USA

Jan Brown: JB Consulting, USA

Weiqiu Chen: Zhejiang University, China

David Hecht: DLH Consulting, USA

Fred Hickernell: Retired from Motorola, USA

Yonkee Kim: U.S. Army, USA

Amit Lal: Cornell University, USA

C.S. Lam: Epson Electronics America, Inc., USA

John Larson: Avago Technologies, USA

Moises Levy: Department of Physics, Naples, Florida, USA

George Mansfeld: Russian Academy of Sciences, Russia

Vitold Poghar: Scientific and Technological Center of Unique

Instrumentation of Russian Academy of Science, Russia

Valeri Proklov: Institute of Radio Engineering & Electricity, Russia

Edgar Schmidhammer: EPCOS, Germany

Susan Schneider: Marquette University, USA

Bikash Sinha: Schlumberger-Doll Research, USA

Ji Wang: Ningbo University, China

Qing-Ming Wang: University of Pittsburgh, USA

Group IV: Microacoustics - SAW, FBAW, MEMS

Vice Chair of TPC:

Clemmens Ruppel, Ph.D.

EPCOS AG - SAW RD SAM
Germany

Members:

Ben Abbott: Triquint, USA

Robert Aigner: Triquint, USA

Sylvain Ballandras: FEMTO-ST, France

Kushal Bhattacharjee: RF Micro Devices, USA

Sunil Bhawe: Cornell University, USA

Sergey Biryukov: IFW Dresden, Germany

Paul Bradley: Avago, USA

Jidong Dai: RF Monolithics, USA

Omar Elmazria: Nancy Université - CNRS, France

Gernot Fattinger: Triquint, USA

Ken-ya Hashimoto: Chiba University, Japan

Daniel Hauden: FEMTO-ST, France

Shitang He: IACAS, China

Chunyun Jian: Huawei Technologies Canada Co., Ltd., Canada

Michio Kadota, Murata, Japan

Jyrki Kaitila: Avago, Germany

Jan Kuypers: Sand 9, Inc., USA

Ken Lakin: Consultant, USA

Don Malocha: University of Central Florida, USA

David Morgan: Impulse Consulting, UK

Hiroyuki Odagawa: Tohoku University, Japan

Pensala Tuoma: VTT, Finland

Mauricio Pereira da Cunha: University of Maine, USA

Viktor Plessky: GVR Trade SA, Switzerland

Bob Potter: Vectron International, USA

Leonard Reindl: Albert-Ludwigs-University Freiburg, Germany

Richard Ruby: Avago, USA

Takahiro Sato: Fujitsu Media Devices, Japan

Peter Smith: McMaster University, Canada

Marc Solal: Triquint, USA

Karl Wagner: EPCOS AG, Germany

Robert Weigel: Friedrich-Alexander University, Germany

Sergei Zhgoon: Moscow Power Engineering Institute, Russia

Group V: Transducers and Transducer Materials

Vice Chair of TPC:

Scott Smith, Ph.D.

GE Global Research

Niskayuna, New York, U.S.A.

Members:

Sandy Cochran: University of Dundee, UK

Christopher Daft: Siemens Medical Solutions, USA

Levent Degertekin: Georgia Institute of Technology, USA

Charles Emery: Mirabilis Medica, USA

John Fraser: Philips Healthcare, USA

Jean-Francois Gelly: GE Healthcare, France

Reinhard Lerch: Friedrich-Alexander-Universität Erlangen-Nuremberg,
Germany

Geoff Lockwood: Queen's University, Canada

Clyde Oakley: W. L. Gore, USA

Omer Oralkan: Stanford University, USA

Paul Reynolds: Weidlinger Associates, USA

Yongrae Roh: Kyungpook National University, Korea

Ahmad Safari: Rutgers University, USA

Mark Schafer: Sonic Tech Inc., USA

Thomas ShROUT: Pennsylvania State University, USA

Kirk Shung: University of Southern California, USA

Stephen Smith: Duke University, USA

Wallace Smith: Office of Naval Research, USA

Yasuhito Takeuchi: Kagoshima University, Japan

Jian Yuan: Boston Scientific, USA

Qiming Zhang: Pennsylvania State University, USA

Qifa Zhou: University of Southern California, USA

Conference Management

The 2009 IEEE International Ultrasonics Symposium (IUS) acknowledges the support from the following organizations:

Other companies:

Mira Digital Publishing, St. Louis, Missouri, USA- for technical programs (abstract submission, review, conference program meeting planner, Technical Program Committee meeting support.

Yes Events, Baltimore Maryland, USA- for online conference registration

Hyatt Regency O'Hare- Rosemont, Illinois, USA June 13-14, 2009 for the 3rd TPC meeting of the 2009 IEEE IUS in Chicago, IL

Industrial Measurement Systems, Inc. Aurora, Illinois, USA, president, Donald E. Yuhas and staff for sending blast emails for publicity and calls for papers, TPC meeting arrangements.

Special Thanks

Numerous members of the organizing committee have contributed to this program and program book. A special thanks to Ms Loretta Oleksak and Ms. Carol L. Vorres for their valuable contributions.

Future Ultrasonics Symposia

2010 IEEE International Ultrasonics Symposium San Diego, CA USA October 11-14, 2010

General Chair: Bob Potter;E-mail: bpotter@vectron.com

Technical Session Schedules

The technical program is arranged as follows:

- Oral Sessions, Monday, September 21, 2009
- Poster Sessions, Monday, September 21, 2009
- Oral Sessions, Tuesday, September 22, 2009
- Poster Sessions, Tuesday, September 22, 2009
- Oral Sessions, Wednesday, September 23, 2009
- Poster Sessions, Wednesday, September 23, 2009

Monday Oral Sessions

1A. Targeted Contrast Agents

Sala 1

Monday, September 21, 2009, 11:30 am - 1:00 pm

Chair: **Tom Matula**
Univ. of Washington

1A-1

11:30 AM Molecular Imaging using Contrast Ultrasound

Alexander L. Klibanov¹, Talent Shevchenko², Sunil Unnikrishnan², Muzaffer Celebi², Annemieke van Wamel³, Joshua Rychak^{2,4}, Christopher Anderson⁴, Balasundar Raju⁵, Chien Ting Chin⁵, Michael Lawrence², John Hossack², Klaus Ley^{6,1} *Cardiovascular Division, University of Virginia, Charlottesville, VA, USA, ²University of Virginia, USA, ³Erasmus Medical Center, Rotterdam, Netherlands, ⁴Targeson Inc, USA, ⁵Philips Research, USA, ⁶La Jolla Institute of Allergy and Immunology, USA*

Background, Motivation and Objective

Ultrasound imaging is performed in real time with inexpensive portable equipment. This imaging modality is popular; it does not use ionizing radiation. Ultrasound is used for imaging anatomical structures, guidance of biopsies and therapeutic (ablation) procedures; however, imaging of physiological processes and molecular/cellular events requires the use of ultrasound contrast agents.

Statement of Contribution/Methods

Gas-filled particles, such as microbubble materials are the best ultrasound contrast agents, because of the excellent particle compressibility. Microbubbles are several micrometers in size, and consist of a perfluorocarbon gas core, coated with a thin shell (e.g., a lipid monolayer). As the size of microbubbles is smaller than the diameter of the capillaries, microbubbles circulate in the bloodstream. Typically, microbubble lifetime in the bloodstream does not exceed several minutes; they eventually deflate and gas is exhaled through the lungs. An individual microbubble particle, with a picogram mass, can be observed in the bloodstream by a clinical ultrasound imaging system. Multipulse imaging techniques, such as phase inversion and amplitude modulation, allow detection of microbubbles with complete suppression of the tissue background signal. Microbubbles are used in the clinical setting as blood pool agents. Microbubble agents are actively investigated in animal models for molecular and cellular imaging.

Results

Molecular imaging with microbubbles is achieved by attaching specific targeting ligands (antibodies, peptides/mimetics, or carbohydrates) onto the microbubble shell. The use of an extended spacer arm for ligand attachment improves targeting efficacy. Because microbubbles stay intravascular, they can be only targeted to the receptors on the surface of vascular endothelium: markers of inflammation or angiogenesis, such as P- and E-selectin, ICAM-1, VCAM-1, VEGFR2. Specialized ligands, such as sialyl Lewis oligosaccharides, that are used to arrest leukocytes on activate endothelium, allow targeting in the conditions of fast flow. Combination of two ligands on the microbubble surface also mimics leukocyte adhesion to activated endothelium.

Discussion and Conclusions

Ultrasound imaging of targeted microbubbles can successfully delineate the areas of inflammation, and characterize receptor pattern on the vascular endothelium in the neovasculature. Because microbubble circulation time is short, and targeted microbubbles can be destroyed by high-MI ultrasound, repeated injections of different microbubble preparations targeted towards various receptors can be performed within minutes of each other, to provide information on the vascular endothelium biomarkers in a rapid and noninvasive fashion. Microbubble-based particles can be loaded with drugs, and ultrasound can release the drug in the desired area of the body, expanding the use of ultrasound contrast from molecular imaging to targeted therapy.

1A-2

12:00 PM Intravascular Ultrasound Detection and Delivery of Molecularly Targeted Microbubbles for Gene Delivery

Linsey C. Phillips¹, Alexander L. Klibanov¹, Brian R. Wamhoff¹, John A. Hossack^{1,2} *University of Virginia, Charlottesville, VA, USA*

Background, Motivation and Objective

Current treatment for millions of patients with stenotic atherosclerotic arteries relies on balloon angioplasty followed by stent placement. Localized drug delivery is often required to prevent restenosis. Due to the risk of thrombosis with drug eluting stents, we have investigated microbubble based targeted delivery and combined intravascular ultrasound (IVUS) imaging. Although IVUS imaging is often used for visualizing arterial lumens it has recently been shown by our group to achieve gene delivery under non-clinical ultrasound conditions. The goals of these studies were to determine whether IVUS could be used to detect targeted microbubbles and enhance drug/gene delivery through targeting.

Statement of Contribution/Methods

Vascular cell adhesion molecule-1 (VCAM-1) is an inflammatory cell surface marker present in atherosclerotic and injured smooth muscle cells. Fluorescent (DiI) microbubbles (d = 1-3 μm) composed of a phosphatidylcholine lipid shell with biotinylated polyethylene glycol spacers were molecularly targeted through streptavidin conjugation with biotinylated VCAM-1 antibodies. Inflamed vascular smooth muscle cells were cultured in acoustically transparent Opticell flasks and injected with control or targeted bubbles (1.5e7/ml) with CMV-GFP plasmid (3 $\mu\text{g/ml}$). Gene delivery was performed by emitting Gaussian 1.5 MHz ultrasound pulses from a fabricated, 1mm wide, single element transducer at a PRF of 8 kHz for ~5 seconds per cell.

A commercially available intravascular ultrasound catheter transducer was used for imaging at 40 MHz (Boston Scientific Atlantis). Image intensity was assessed with and without microbubble delivery. Cylindrical flow chambers 2.5mm wide were constructed in PDMS (silicone) with a thin polystyrene membrane at one edge of the chamber wall to allow for optical inspection under flow. To simulate inflamed vasculature VCAM-1 coated membranes were for in vitro verification of targeted microbubble adhesion.

Results

Molecularly targeted microbubbles remained adherent to the inflamed cells (an average of 25 bubbles per cell) under 10 dynes/cm² flow. Targeted microbubbles resulted in a 50% increase in gene transfection over non targeted bubbles. At an equivalent density of 3x10e4 bubbles/mm², IVUS image intensity increased 4.3 fold over that of non bubble coated surfaces. No difference in image intensity was observed with control bubbles on either plain or VCAM-1 coated membranes, but with targeted bubbles IVUS imaging revealed a 4.1 fold increase in intensity on VCAM-1 surfaces. Rupture of microbubbles from the single element transducer resulted in a 53% reduction in image intensity.

Discussion and Conclusions

Taken together, these results indicate IVUS may be used to detect targeted microbubbles to inflamed vasculature and subsequently deliver a gene/drug. Enhanced echoes from microbubbles targeted to VCAM-1 have clinical potential for early atherosclerosis detection.

1A-3

12:15 PM Nanoparticle-Loaded Perfluorocarbon Droplets for Imaging and Therapy

Naomi Matsuura¹, Ross Williams¹, Nikita Reznik², Ivan Gorelikov¹, Joydeep Chaudhuri¹, John Rowlands^{1,2}, Kullervo Hynynen^{1,2}, Stuart Foster^{1,2}, Peter Burns^{1,2} *Sunnybrook Health Sciences Centre, Canada, ²University of Toronto, Canada*

Background, Motivation and Objective

Nanoscale particles for therapeutic and diagnostic applications in ultrasound are a rapidly developing area of research. Perfluorocarbon droplets that are in the liquid phase at physiological temperatures, but which can be converted to gas using ultrasound, can be used as a contrast agent for the detection and therapy of solid tumours. Because of the enhanced permeability of tumour vascular endothelium, particles with diameters from 100-300 nm can preferentially extravasate into tumours, remaining present for extended periods of time once the contrast agent has been cleared from the systemic circulation. Furthermore, nanoparticles can be encapsulated within the droplets, providing a novel way to extend the functionality of perfluorocarbon droplets to other imaging and therapy modalities, while constraining the biophysical interactions to those determined by the properties of the encapsulating droplet.

Statement of Contribution/Methods

In this work, we report on the interaction of ultrasound with droplet emulsions composed of various perfluorocarbons (PFP, PFH, PFOB) encapsulated with a fluorosurfactant, and on a novel method to solubilize nanoparticles and incorporate them within the perfluorocarbon droplets, demonstrated using quantum dots and gold nanorods. The droplet diameters ranged from 100-300 nm as measured by dynamic light scattering. Ultrasound experiments to measure droplet cavitation at low frequency were performed at 1 MHz using a single-element transducer with passive detection at 500 kHz; high frequency experiments to detect droplet vaporization were performed with a high-power flash mode in conjunction with pulse-echo detection at 18 MHz using a VisualSonics 2100 linear array transducer.

Results

Experiments were conducted to demonstrate that: 1) the cavitation and vaporization pressure thresholds could be manipulated by varying droplet composition so that phase conversion is obtained at $MI=1-2$; 2) the incorporation of nanoparticles lowered the inertial cavitation threshold at 1 MHz by 20% and enhanced the efficacy of mixed cavitation and HIFU therapy, demonstrated using a macrophage cell line in conjunction with perfluorohexane droplets; 3) that low-boiling point perfluoropentane droplets can be converted to gas and imaged at high frequency in hepatomas in mice, using brief high pressure flashes to achieve the conversion; and 4) that optically fluorescent quantum dots can be used to trace the biodistribution of droplets within rabbits and mice using fluorescence histology, demonstrating little toxicity but enhanced accumulation in the liver and spleen.

Discussion and Conclusions

This work demonstrates that perfluorocarbon droplets are a promising agent for both therapeutic and diagnostic applications of ultrasound over a wide range of frequencies. Practical issues and requirements for further droplet development will be discussed.

1A-4

12:30 PM Radiation force-enhanced targeted imaging using a dual-frequency high-resolution transducer

Ryan Gessner¹, Mike Lee², Marc Lukacs², F. Stuart Foster², Paul Dayton¹; ¹Biomedical Engineering, University of North Carolina at Chapel Hill/North Carolina State University, USA; ²University of Toronto, Canada

Background, Motivation and Objective

Recently, there has been an interest in the application of radiation force (RF) to enhance both diagnostic and therapeutic ultrasound (US) imaging studies. RF pulses have shown to enhance adhesion of targeted microbubble contrast agents (MCAs), thus improving their signal to noise ratio, while it has also been shown effective in concentrating therapeutic delivery vehicles at desired locations. These abilities are of particular interest for small animal studies, where much of the work in US molecular imaging and therapeutic delivery is being tested. The magnitude of RF on MCAs is maximized when generated near their resonance frequency. Traditional high frequency imaging transducers are therefore not optimized to produce RF on most MCAs. Our goal was to test a dual frequency high resolution US probe for its suitability in RF enhanced targeted imaging in small animal studies.

Statement of Contribution/Methods

Our team has supplemented a standard VisualSonics 30 MHz imaging transducer with a second, confocal, low-frequency element. This adaptation has enabled us to produce radiation force simultaneously with high-resolution imaging, generating RF pulses in the range of 2-4 MHz with imaging at 30 MHz. We present preliminary RF enhanced targeting data in vitro. Biotinylated MCAs were injected through a 200 μ m cellulose tube coated with avidin. RF pulses lasting 10 s were delivered to the tube and the efficiency of this targeting was verified optically. Scattered US signals from free and targeted contrast agents were delineated by applying slow time filters to the radio frequency data. Additionally, the image intensities in the B-Mode images were compared in regions with and without the RF pulses.

Results

We have verified optically that the probe is capable of pushing a polydisperse distribution of MCAs moving with a linear flow velocity of 44 mm/s a distance of 200 μ m perpendicular to their direction of motion and against buoyancy in 10 ms. Using a 10 second RF pulse, the probe has proven capable of improving the binding efficiency of freely flowing targeted MCAs in a localized area. Signal processing on the radio frequency data confirms a localized region of enhanced signal intensity from increased adhesion of targeted contrast agents in the region of RF application. Signal processing of stationary echo signals from RF data allows display of targeted contrast agent signal overlaid with B-mode image data.

Discussion and Conclusions

The ability to enhance targeting efficiency via the application of short RF pulses to quickly flowing MCAs has been demonstrated in-vitro. Extending this ability with the confocal high frequency probe to in-vivo studies will allow for improved signal to noise ratios in diagnostic US applications as well as enhanced accumulation of therapeutic-bearing MCAs at specific locations.

1A-5

12:45 PM The effect of radiation force on binding efficiency and specificity of target-specific contrast-agent microbubbles

Peter Frinking¹, Isabelle Tardy¹, Martine Theraulaz¹, Sibylle Pochon¹, Jeffrey Powers², Marcel Arditi^{1,2}/Bracco Research S.A., Geneva, Switzerland, ²Philips Medical Systems Inc., Bothell, WA, USA

Background, Motivation and Objective

Target-specific microbubbles are showing a great potential in ultrasound molecular imaging applications. Binding efficiency of these microbubbles may, however, be limited due to hemodynamic factors preventing adhesion to target molecules present on the vascular endothelium. Radiation force has been suggested to improve bubble binding by pushing the bubbles towards the endothelium of the vessel wall. However, nonspecific binding in normal tissue may also be promoted by radiation force and could reduce binding specificity. In this work, the effect of radiation force on binding efficiency and specificity of target-specific microbubbles was investigated.

Statement of Contribution/Methods

BR55 microbubbles, a phospholipid-based contrast agent functionalized with a heterodimeric peptide specific for VEGFR2 (KDR/Flk-1), were injected in Copenhagen rats in which adenocarcinoma cells (G Dunning R-3327) were implanted in one lobe of the ventral prostate. Radiation force was applied to bubbles in the prostate during 2 min following injection using a linear array probe (L9-3) connected to a Philips iU22 ultrasound scanner. A specific scanning protocol was implemented to generate high duty-cycle (98%) radiation force pulses (3.5 MHz, 38 kPa) effectively exposing the entire prostate (approx. 2 cm in width). This allowed comparing the effects of radiation force on binding in tumor (specific) and normal (nonspecific) tissue at the same time. Bubble binding was determined by imaging targeted bubbles using Power Modulation (4.0 MHz, 180 kPa) 10 min after agent injection (i.e. 8 min following radiation force application) using the same probe and ultrasound system. Different agent concentrations (0.2-0.8 $\mu\text{L gas/kg}$) were used. As a reference, bubble binding without radiation force at the highest concentration (0.8 $\mu\text{L gas/kg}$) was determined. Data obtained from different animals were analyzed off-line, and mean echo power values calculated in tumor and normal tissue of the same prostate were compared.

Results

Compared to the reference, radiation force improved bubble binding efficiency in tumor tissue by a factor of 3-10, depending on agent concentration. However, at the highest concentration, increased binding was also observed in normal tissue (by a factor 3) resulting in reduced specificity. This increase in nonspecific binding was not observed at lower concentrations. For an optimal concentration (0.4 $\mu\text{L gas/kg}$), the net effect of radiation force resulted in a 3-4 fold improvement in binding specificity compared to the reference.

Discussion and Conclusions

Radiation force improves binding efficiency of target-specific microbubbles in pathological tissue, but it may reduce binding specificity at too-high agent concentrations. Therefore, optimal exploitation of radiation force, resulting in improved binding efficiency and specificity of target-specific microbubbles, requires careful considerations concerning agent concentration.

2A. Ultrasound Systems and Devices

Sala 2

Monday, September 21, 2009, 11:30 am - 1:00 pm

Chair: **Piero Tortoli**
Univ. of Firenze

2A-1

11:30 AM **Estimation of Skin Elasticity by Measuring Surface Wave Velocity under Impulse Stimulus**

Bo Qiang¹, Xiaoming Zhang¹, James Greenleaf¹; ¹*Department of Physiology and Biomedical Engineering, Mayo Clinic College of Medicine, Rochester, MN, USA*

Background, Motivation and Objective

Skin viscoelasticity provides valuable information for medical diagnosis like skin cancer and understanding physiological phenomena like aging. Medical devices such as Magnetic Resonance Elastography (MRE), vibro-acoustography and Optical Coherence Elastography (OCE) have been actively researched for measuring tissue elasticity by tracking the shear wave propagation inside tissue. On the other hand, surface Raleigh waves on skin can be measured conveniently with non-contact methods. This paper presents a compact system designed for evaluating skin elasticity by measuring surface wave velocity.

Statement of Contribution/Methods

A novel system targeted for clinical usage is prototyped and tested on a rubber-based phantom. The system includes an electromagnetic shaker, a function generator and a multi-channel laser displacement sensor device. The shaker delivers 1 ms duration pulses to the testing surface and the surface waves are recorded at multiple points along the propagation direction with the laser. Akaike Information Criterion (AIC) function is used to resolve the arrival times of the wave front. Then, Young's modulus is calculated based on the wave velocity. The impulse method is much less affected by boundary conditions than Continuous Wave (CW) method because measurements can be made before reflections occur.

Results

The surface wave velocity can be related to the Young's modulus as $cs = \sqrt{E/3\rho}/1.05$, Where cs is the surface wave velocity, E is Young's modulus and ρ is mass density of the material.

On the phantom, the group velocity is 12.61 m/s; therefore Young's modulus is 526 kPa. This result is consistent with the estimate obtained by CW excitation (549 kPa, X. Zhang et al., J. Acoust. Soc. Am., vol. 122, 2522-2525, 2007). Systematic and random noises are modeled in order to understand the source of error and improve the accuracy of the predictions.

Discussion and Conclusions

In this study, we demonstrated a novel system for tissue elasticity measurements. This method measures the surface wave propagation and features convenience, simplicity and compact size. The preliminary testing results on a tissue simulating phantom are consistent with our previous study. Design issues and error analysis are also presented.

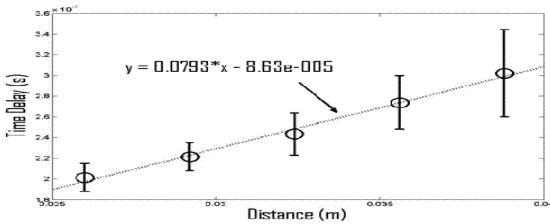


Figure 1. Time delay calculated by AIC picker as a function of sensor-to-sensor distance. Group velocity is reciprocal of the slope.

2A-2

11:45 AM GPU-Based Reconstruction and Display for 4D Ultrasound Data

Abubakr Aelsebai¹, Ahmed Nokrashy², Elhassan Mohamed¹, Yasser Kadah¹; ¹Nile University, Egypt, ²IBE Tech, Egypt

Background, Motivation and Objective

Due to the required computational effort of 4D ultrasound imaging, such systems depend on low complexity techniques like nearest neighbor interpolation, which affects volume quality. Moreover, more accurate techniques like normalized convolution, backward trilinear interpolation, and forward spherical and ellipsoidal Gaussian kernel, are avoided in real-time imaging because of the tight reconstruction time. The goal of this work is to utilize recent commercial graphics hardware technology of graphics processing unit (GPU) to speed up the reconstruction time while increasing the quality of displayed volume.

Statement of Contribution/Methods

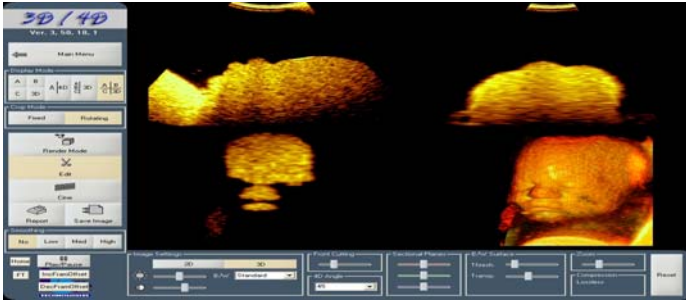
This work presents a hybrid reconstruction method for 4D ultrasound implemented on the GPU. We used forward reconstruction with interpolation based on normalized convolution optimization. Image registration using direct pixel nearest neighborhood is used. Then, an interpolation and hole-filling stage is done using resizable ellipsoidal kernel with Gaussian weighted values. The upsampling step is combined with normalized convolution optimization. The proposed methods are designed and implemented in such a way to take advantage of the GPU environment to gain maximum hardware acceleration and multiprocessor utilization.

Results

Test data were acquired using 3D mechanical transducer (Prosonic, inc.) interfaced to a Tetrad Sonata ultrasound imaging system and a fetal ultrasound training Phantom (CIRS, inc.). Volume size was 256×492×87, fan angle of 86 deg, and scan depth of 160 mm. The implementation of the proposed method was done using C++ under Qt ver. 4, OpenGL and CUDA (NVIDIA, inc.). A personal computer with Intel Core 2 Quad CPU with 8 GB RAM, and an NVIDIA GeForce 9600 graphics card with GPU was used under Windows XP operating system. The initial prototype of our algorithm was able to achieve an average volume reconstruction and display frame rate of more than 40 frames/s. A sample screen shot of the developed system is shown in Fig. 1 where 3 perpendicular slices as well as the reconstructed volume are all displayed in real time.

Discussion and Conclusions

A new low-cost 4D ultrasound reconstruction and display system is introduced. The new system takes advantage of the recent advances in computer graphics card GPU technology to reconstruct high quality volumes at high frame rates.



2A-3

12:00 PM **Accurate assessment of middle ear effusion by monitoring ultrasound reflections from a tympanic membrane**

Junho Song¹, Kullervo Hynynen^{1,†} *Sunnybrook Health Science Centre and Department of Medical Biophysics, University of Toronto, Toronto, ON, Canada*

Background, Motivation and Objective

Middle ear with effusion (MEE) is a common bacterial disease in children. Detection of the presence of MEE in early stage prevents from the risk of temporarily or long-term hearing loss in young children. Commonly, the determination between a healthy and diseased middle ear is relied on the physician's skill and experience by visually examining the tympanic membrane using an otoscope. However, diagnosing MEE is considerably challenging in infants or young children due to the lack of cooperation.

In this paper we have developed a simple, disposable, and inexpensive ultrasound transducer to detect middle ear with effusion by monitoring the presence of fluid in the middle ear. The accurate diagnosis is achieved by analyzing the amplitude of reflected signals from the tympanic membrane. The transducer transmits high frequency ultrasound signals and receives reflections from the tympanic membrane through a low-pressure water jet generated from the transducer to the membrane.

Statement of Contribution/Methods

An ultrasound transducer was fabricated from a 2.5 mm in diameter, 300 um thick PZT-4 ceramic. It was attached on the tip of a 3 mm in diameter brass tubing. A mixture of a PZT/epoxy backing material was filled in the brass tubing. A 1 ml syringe (OD=5 mm) was used as a transducer outer casing, and the transducer was attached in front of the plunger. A 0.5 mm in diameter PET tubing was attached to the plunger to provide enough pressure to generate a straight water jet through an orifice at the open end of the syringe. A 25 um thick Mylar film with a thin water layer (0.2 ~ 1 mm thick) was used to simulate the abnormality of a middle ear with effusion in the experiments. The film was placed at 10 ~ 30 mm from the transducer.

Results

The system generated a low-pressure, straight water jet up to 30 mm using less than 0.2 ml. When there was no fluid present in behind the membrane, only one strong echo was received. In case of fluid behind the membrane, two echoes were received, one from the membrane and the other at the back wall of the fluid filled chamber simulating middle ear. The reflection from the membrane without fluid behind was approximately three times higher than when fluid was behind the membrane. The time interval between the first and last echoes was used to estimate the thickness of a fluid layer. Therefore, the conditions of the middle ear, such as a healthy/infected middle ear and thickness of a fluid layer, could be accurately diagnosed by evaluating signal amplitude or counting the number of peaks.

Discussion and Conclusions

A novel idea of using ultrasound beam and an instantaneous water jet for the detection of fluid in the middle ear was shown by constructing a simple and inexpensive ultrasound transducer. Since the transducer sends and receives ultrasound beam through a water jet, it is not sensitive to the excessive background noise such as crying and does not require significant co-operation from the patient.

12:15 PM **SURF imaging – A real time dual-frequency band ultrasound system**

Svein-Erik Masoy¹, Jochen M. Deibele¹, Thor Andreas Tangen¹, Sven Peter Nasholm¹, Oyvind Standal¹, Tommi F. Johansen¹, Rune Hansen^{1,2}, Bjorn Angelsen¹; ¹Department of Circulation and Medical Imaging, Norwegian University of Science and Technology, Trondheim, Norway, ²Department of Medical Technology, SINTEF Health Research, Trondheim, Norway

Background, Motivation and Objective

This group has developed a method named Second-order Ultrasound Field imaging, abbreviated SURF imaging. The SURF imaging technique is based on transmission of dual-frequency band pulses using a low-frequency (LF) manipulation pulse and a high-frequency (HF) imaging pulse, typically having a frequency separation of greater than 1:7. The two pulses are wide band, usually with a length less than 4 periods. The purpose of the LF pulse is to manipulate the scattering and propagation of the HF imaging pulse, and is only transmitted and not received. The HF imaging pulse is then used to image tissue or nonlinear scatterers under the influence of the manipulation pulse. Here, a real time ultrasound imaging system capable of transmitting dual-frequency band pulses is presented.

Statement of Contribution/Methods

The system is a modified version of the Ultrasonix RP platform (Ultrasonix Medical Corporation, Vancouver, Canada). The modification consist of constructing new probes capable of transmitting dual-frequency pulses, adding a pulser for the LF pulse, a new connector for these probes, and software for post-processing of data.

Three probes capable of transmitting dual-frequency pulses using the same acoustic surface, have been designed and manufactured (Vermon, France) for various imaging purposes. A linear array with 1.25/10 MHz center frequencies, an endo-rectal curved linear array with 1.25/10 MHz center frequencies, and a linear array with 0.9/7 MHz center frequencies. All the probes have 64/192 acoustic elements arranged in a bi-layer piezo-electric stack.

The LF pulser has 64*2 channels with a sampling rate of 10-80 Mhz.

The connector has 360 pins, 192 allocated for the HF, and 104 for the LF. A multiplexer is also built onto the connector to multiplex the 128 transmit channels of the Ultrasonix RP system to the 192 HF channels on the dual-frequency probes. The pulser with control software, and connector was produced by Norbit AS, Trondheim, Norway.

Software has been written in-house to perform post-processing on the received HF echoes.

With the aid of Ultrasonix Medical Corporation, an interface to the LF software/hardware and the in-house written post-processing software has been created, allowing for real-time adjustment of the LF beamforming and parameters for post-processing.

Results

Images from the development of the system are presented. Water tank measurements recorded with a hydrophone demonstrate the function of the dual-frequency band probes as well as the simultaneous real-time beamforming control of both the LF and HF pulses. Real-time images of in vitro contrast agent detection at 10 MHz in a tissue mimicking phantom is also presented, demonstrating SURF imaging as a method for high-frequency contrast agent detection.

Discussion and Conclusions

A real-time system capable of transmitting dual-frequency band pulses has been constructed and demonstrated to work as intended.

12:30 PM **Real-Time Imaging with the Sonic Window: A Pocket-Sized, C-Scan, Medical Ultrasound Device**

Michael Fuller^{1,2}, Kevin Owen^{1,3}, Travis Blalock^{1,2}, John Hossack^{1,3}, William Walker^{1,3}; ¹PocketSonics, Inc., Charlottesville, VA, USA, ²Dept. of Electrical and Computer Engineering, University of Virginia, Charlottesville, VA, USA, ³Dept. of Biomedical Engineering, University of Virginia, Charlottesville, VA, USA

Background, Motivation and Objective

The Sonic Window is a pocket-sized, C-scan ultrasound device designed to expand ultrasound into clinical settings and applications that have yet to benefit from its utility. The low component cost, compact form factor with integrated 2D transducer array, and an intuitive C-scan image format displayed directly over the anatomy of interest are what distinguish the Sonic Window from conventional ultrasound systems. Initially conceived for guiding vascular access procedures, the technology at the core of the Sonic Window is a potential platform for

developing other devices for general clinical use or for niche applications such as foreign body identification, sports medicine, veterinary medicine, long-term monitoring, or IVUS.

Statement of Contribution/Methods

A prototype of the Sonic Window was designed and constructed consisting of a fully sampled 60x60 transducer array, custom integrated circuits (ICs) containing 3,600 front-end receive channels, a high-voltage transmit circuit, an off-the-shelf digital signal processor (DSP), and a liquid crystal display. The 2D transducer array was fabricated on one side of a 2-layer PCB and the front-end ICs were attached onto the other side using a flip-chip process. The front-end ICs acquire the data for one C-scan slice per transmit event and send digital data to the DSP, which uses the Direct-Sampled In-phase Quadrature (DSIQ) method for beamforming. The prototype fits in a 6-cm x 15-cm enclosure containing a 1500 mAh rechargeable battery.

Results

The Sonic Window prototype device is currently forming real-time C-scan images at 5 FPS and has a battery life of over 1.5 hours while imaging. Lateral resolution is approx. 900 microns and cystic contrast is approx. 20 dB. Phantom target and in vivo images are presented to demonstrate the imaging capability of the device.

Discussion and Conclusions

This work demonstrates for the first time a fully integrated prototype of the Sonic Window imaging in real-time. Characterization and refinement of device performance is ongoing, but initial results indicate the device performs adequately for its intended application in guiding vascular access procedures. Further development will incorporate clinical feedback in tailoring performance, image quality and ergonomics toward the needs of the clinician.



2A-6

12:45 PM **Fiber Optic Broadband Ultrasonic Probe for Virtual Biopsy: Technological Solutions**

Stefano Cerbai¹, Luca Belsito², Elena Biagi¹, Alberto Roncaglia², Niccolò Speciale³, Guido Masetti³, Leonardo Masotti¹; ¹Electronics and Tlc, University of Florence, Florence, FI, Italy, ²CNR IMM Bologna, Bologna, BO, Italy, ³DEIS, University of Bologna, Bologna, BO, Italy

Background, Motivation and Objective

Our group proposed the design and realization of an ultrasonic source based on opto-acoustic effect in 1996, with a metal layer over the fiber optic tip as absorbing target. In 2001 we improved the opto-acoustic conversion by replacing the metal absorbing target with a graphite one. Two years later, in 2003, we proposed a complete opto-acoustic and acousto-optic setup for a fully fiber optic ultrasonic probe.

The proposed probe consists of two optical fibers: one generating ultrasounds by opto-acoustic conversion, the second one, based on acousto-optic effect, used to detect ultrasounds.

The intrinsic high frequency and wide band associated both to the opto-acoustic source and to the interferometric acousto-optic element could open a way towards a "virtual biopsy".

"Virtual biopsy" is perspective to provide the physicians the possibility of studying the nature and health condition of small portions of living tissue "in situ" by using ultrasounds.

Statement of Contribution/Methods

A Micro-Opto-Mechanical-System (MOMS) approach is proposed to realize miniaturized opto-acoustic probes on optical fibres, in which the optical emitters and receivers are realized on micromachined frames that can be subsequently mounted on the fibre tip in a self-aligned way.

For the ultrasound emitter, a carbonization procedure has been adopted on photoresist patterns to obtain amorphous carbon layers suitable for optoacoustic emission. For the receiver, Fabry-Perot interferometers composed by two thin metal layers (evaporated Al) and a SU-8 spacer have been realized using different thicknesses of the individual layers. The carbon, SU-8 and Al layers have been characterized with Raman, Fourier Transform Infrared (FTIR) and optical spectroscopy to determine their optical properties and in particular the spectral reflectivity of the SU-8 interferometers. Ultrasound emission of the carbon layers and the Fabry-Perot response has been evaluated.

Results

We present our technological achievements in the development of the first all fiber optic probe and novel images of simple test objects, obtained with a complete opto-acoustic setup.

Discussion and Conclusions

Prototypes realized with different solutions, both for the transmitting and receiving element, are presented and discussed. It is demonstrated that the generated ultrasonic power is sufficient to be revealed by an interferometric acousto-optic fiber receiver.

It is also demonstrated how graphite-like amorphous carbon thin layers, suitable for opto-acoustic generation, are obtainable with thickness around 1 μm and average tolerance of about 5% on a 4 inch wafer while 10 μm thick SU-8 interferometers on silicon substrates have been successfully realized providing a reflectance sensitivity around 13 μm^{-1} with respect to the spacer thickness.

3A. Ferroelectrets and Other Transducer Materials

Sala 4

Monday, September 21, 2009, 11:30 am - 1:00 pm

Chair: **Reinhard Lerch**
Friedrich-Alexander University

3A-1

11:30 AM High Temperature Piezoelectric Properties of $\text{CaBi}_2\text{Ta}_2\text{O}_9$ Ceramics

Tadashi Takenaka¹, Toji Tokutsu¹, Yuji Hiruma¹, Hajime Nagata¹, ¹*Tokyo University of Science, Japan*

Background, Motivation and Objective

The industrial and scientific communities have expressed the need for sensing over a broad temperature range. The maximum operation temperature of piezoelectric materials for sensors is limited by the Curie temperature, T_C , combined with the level of sensitivity determined by the piezoelectric voltage constant, g_{ij} . Bismuth layer-structured ferroelectrics (BLSFs) are attractive from the viewpoint of sensor applications, because BLSFs are characterized by their low dielectric constant, ϵ_s , high T_C , and large anisotropy in the electromechanical coupling factor, k_{33}/k_{31} . One of BLSF, $\text{CaBi}_2\text{Ta}_2\text{O}_9$ (CBT), is expected to be a candidate material for high temperature sensors due to its high- T_C , approximately 900°C. However, there are few reports about piezoelectric properties for CBT-based ceramics. The reason is that it is very difficult to evaluate piezoelectric properties because of a difficulty in poling from a large coercive field. In this study, their electrical properties and piezoelectric properties of CBT-based ceramics were investigated by using the specimen poled in silicone oil at high temperature of 280°C. Also, the high temperature piezoelectric properties were examined.

Statement of Contribution/Methods

CBT ceramics were prepared by a conventional ceramic fabrication technique. Piezoelectric properties were measured by the resonance-antiresonance method. For thermal depoling behavior measurements, a poled sample was heated at high temperature for 1 h, and then, cooled it to room temperature and measured their piezoelectric properties.

Results

From the temperature dependence of dielectric constant ϵ_s and loss tangent $\tan\delta$ for the CBT ceramics, the T_C was at 923°C. Poling treatment at high temperature of 280°C was very effective to move the domain walls, and piezoelectric properties such as electromechanical coupling factor, k_{33} , and piezoelectric g constant, g_{33} , were improved to 0.085 and 8.4×10^{-3} V m/N at room temperature, respectively. The thermal depoling test indicated that the k_{33} and g_{33} for the CBT ceramics after keeping at 890°C for 1h, were 0.082 and 8.2×10^{-3} V m/N, respectively. This results indicated that piezoelectric properties of CBT ceramic were maintained close to the T_C . Furthermore, in-situ measurement of piezoelectric properties in (33) mode indicated stable piezoelectric properties up to 400°C.

Discussion and Conclusions

From above results, the CBT ceramic seems to be a candidate for high temperature sensors because of its high- T_C and good high temperature piezoelectric stability.

3A-2

11:45 AM Testing of High Temperature Bismuth Titanate Ultrasonic Transducers Fabricated by Using a Modified Sol-gel Spray Deposition Technique

Cliff Searfass¹, Bernhard Tittmann¹, Dinesh Agrawal^{1,2} *Department of Engineering Science and Mechanics, Pennsylvania State University, University Park, Pa, USA*

Background, Motivation and Objective

Ultrasonic non-destructive evaluation is a powerful means of preventing system failure in many real world applications. In order to reduce system down time for structural evaluation it is necessary to develop means of monitoring in-situ. This is particularly challenging when operating in extreme conditions where temperatures

exceed 500 °C because of needs for suitable couplants, difficulty maintaining structural contact, and the limited amount of materials capable of generating ultrasound at these temperatures. Examples of structures requiring NDE in these conditions include cannon barrels, turbine blades in the aerospace and power industries, and furnaces. The overall objective of this work is to develop means of performing in-situ ultrasonic NDE at elevated temperatures.

Statement of Contribution/Methods

In order to overcome design obstacles associated with the use of ultrasound at high temperatures, the sol-gel spray deposition technique of thick film piezoelectric bismuth titanate transducers has been adapted and modified. In this method, the piezoelectric material can be deposited directly onto the structure in question. Therefore high temperature couplants and means of maintaining structural contact are eliminated. In this paper new processing techniques that have greatly reduced fabrication time and our sensor performance are introduced. One modification is replacing the ball milling stage with high intensity ultrasound. This has reduced our mixing times by a factor of ten and has eliminated chances of accidental contamination. In place of using conventional furnaces for sintering, a multimode microwave furnace was used to sinter at temperatures over 800 °C in atmospheric gas conditions. The entire sintering process, from heating to cooling, takes only 2 hours with the microwave furnace; whereas with conventional furnaces the process could take 22 hours or more. Our sensors fabricated with these modifications displayed better electromechanical properties and substrate adhesion.

Results

Tested sensors were capable of generating longitudinal waves in stainless steel at temperatures exceeding 600 °C. Sensors were also fabricated for the generation of ultrasonic guided waves in stainless steel rectangular bars and plates at elevated temperatures. These sensors were capable of generating ultrasound at temperatures in excess of 600 °C and recorded signals show that the mode shapes are quite sensitive to temperature changes less than 50 °C.

Discussion and Conclusions

The use of high intensity ultrasound and microwave sintering technologies have been employed in order to increase our sensor performance as well as to reduce fabrication time. Sensors are capable of generating multiple types ultrasonic waves at temperatures exceeding 600 °C. Changes in mode shapes of guided waves at elevated temperatures indicate a priori knowledge of a system may be necessary such that proper wave modes can be generated at target temperatures.

3A-3

12:00 PM Broadband ferroelectret transducers

Gerhard M. Sessler¹, Joachim Hillenbrand^{1,1} *Institute for Communications Technology, Darmstadt University of Technology, Darmstadt, Germany*

Background, Motivation and Objective

Ferroelectrets (or piezoelectrets) are a new group of piezoelectric materials consisting of a cellular polymer such as polypropylene (PP). The voids in the polymer are all positively charged on one side and negatively on the other side. Major advantages of ferroelectrets, as compared to other piezoelectric polymers, are the high piezoelectric d_{33} -coefficient of about 500 pC/N, which is 20 times higher than that of PVDF, availability in large areas, simplicity of transducer design and low material cost. Ferroelectrets may be used to generate and detect sonic and ultrasonic signals in air and water up to the resonance frequency of the cellular film which is typically at a few hundred kHz.

Statement of Contribution/Methods

Major new developments include the improvement of the d_{33} -coefficient and the enhancement of the thermal stability of the piezoelectric effect by application of an additional dc-voltage [J. Hillenbrand and G. M. Sessler, J. Appl. Phys. 103, 074103 (2008)]. Another promising approach to increased thermal stability is the use of layered fluoropolymere films, which have superior charge-storage properties. Ferroelectret transducers consist essentially only of a thin piezoelectric film plus additional housing and contacts. Transducers with stacked films are being used to further increase the sensitivity.

Results

The sensitivities of ferroelectret transducers are proportional to the piezoelectric d_{33} -coefficient. This coefficient, measured interferometrically for various external dc-voltages, is shown in Fig. 1 as a function of frequency. In the near ultrasonic range, transmitters utilizing such ferroelectrets generate sound pressure levels in excess of 120 dB while sensors have sensitivities of about 10 mV/Pa. Directional transducers based on the interference principle and

transducer arrays with high directivity have also been studied. Thermal stability of d_{33} and thus of the transducer sensitivity have been extended up to about 90°C.

Discussion and Conclusions

Ferroelectret transducers are well suited for the generation and detection of airborne ultrasonic signals. Improvements in their sensitivity and thermal stability together with their simplicity of design have made them of interest for a variety of applications in this frequency range.

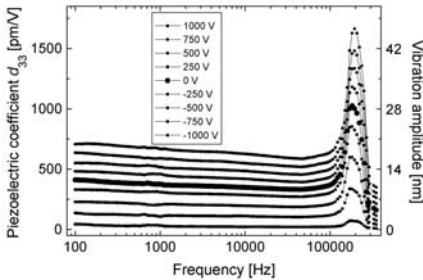


Fig. 1: Frequency response of the d_{33} -coefficient for various external dc-voltages

3A-4

12:30 PM Ferroelectret Sensor Array for Characterization of Cavitation Effects in Ultrasonic Cleaning

Stefan Rupitsch¹, Alexander Sutor¹, Reinhard Lerch¹; ¹Department of Sensor Technology, Friedrich-Alexander-University Erlangen-Nuremberg, Germany

Background, Motivation and Objective

In industrial manufacturing the process of ultrasonic cleaning has to meet the demand for a continuously increasing cleaning efficiency. Until now, cleaning systems are mostly designed empirically and there are no sufficient methods and tools for a defined planning and control of cleaning processes. Based on these requirements, the objective is the development of a sensor for characterization of cavitation effects which are the most important mechanisms of cleaning impact.

Statement of Contribution/Methods

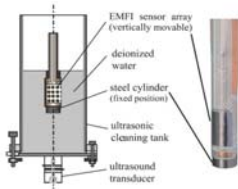
As an advancement of the state of the art a new piezoelectric sensor for cavitation measurement is developed, which can be applied directly on the surface of components. This sensor enables the examination of the specific cavitation effects near a wall and the impact of the component to be cleaned on the resulting sound field. The cavitation measurement is based on the assessment of specific components in the acoustic spectrum which result from cavitation bubble dynamics. The sensor consists of a thin electromechanical film (EMFi) sheet with electrodes on top determining locally spaced elements forming a transducer array. Due to its flexible structure, this film material can be directly attached to surfaces of the parts to be cleaned even when they are of curved shape. The acoustic spectrum is compared to cavitation erosion experiments using a new test layer.

Results

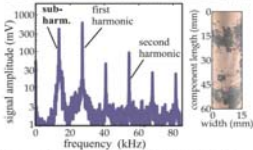
The sensor array was designed by using appropriate finite element simulation. Several prototypes have been characterized by diverse experiments. The obtained sensor features, for instance the directional pattern, the signal-to-noise-ratio and the cross-talk, prove the applicability of the sensor. In a practical test, the sensor array was fixed on a component surface (Fig. 1). Figure 2 shows subharmonic components in the sensed acoustic spectrum (left) and cavitation erosion of the test layer (right). We found a correlation between the cavitation activity (determined by the spectrum) and the cleaning effect.

Discussion and Conclusions

The new EMFi sensor array provides locally resolved cavitation measurements directly on component surfaces. Thus, it now enables the component specific design of cleaning tanks and the optimization of process parameters and can be used for process control.



(a) Figure 1: EMF sensor array applied to a component (right) and positioning in ultrasonic cleaning tank (left).



(b) Figure 2: Acoustic spectrum in circulating fluid (left) and zones of cavitation erosion in test layer (right).

3A-5

12:45 PM CMOS-Compatible AlN Piezoelectric Micromachined Ultrasonic Transducers

Stefon Shelton¹, Mei-Lin Chan¹, Hyunkyu Park¹, Bernhard Boser², Igor Izyumin², Richard Przybyla², Tim Frey³, Michael Judy³, Kieran Nunan³, Firas Sammoura³, Ken Yang³, David Horsley¹.¹Mechanical Engineering, University of California, Davis, Davis, CA, USA, ²University of California, Berkeley, USA, ³Analog Devices Inc., USA

Background, Motivation and Objective

Aluminum Nitride (AlN) is a piezoelectric material that is now widely used for film bulk acoustic resonators (FBARs) and has attractive properties including compatibility with standard CMOS fabrication methods. Here, we describe AlN piezoelectric micromachined ultrasonic transducers (pMUTs). The relatively low dielectric constant of AlN results in pMUTs that have a coupling efficiency similar to that demonstrated in the best PZT pMUTs, while AlN devices have the important advantage that they may be monolithically integrated with CMOS circuitry. However, the capacitance of the AlN pMUT is roughly two orders of magnitude smaller than a comparably sized PZT device. As a result, the effect of parasitic capacitance is greatly increased, leading to reduced coupling efficiency when the detection electronics are not integrated with the transducers.

Statement of Contribution/Methods

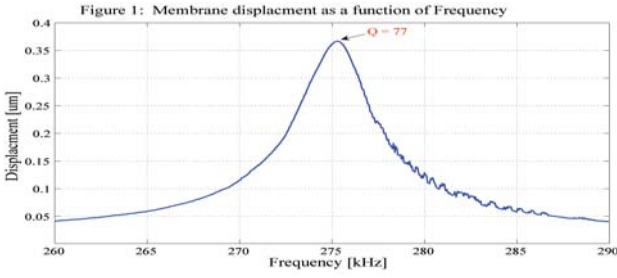
AlN films were sputtered using a low-temperature process that allows deposition on fully metalized CMOS wafers. pMUTs had a bimorph construction consisting of a 1 μm low-stress CVD SiO₂ layer, a Ti/W/Pt bottom electrode, followed by a 1 μm AlN layer and a Cr/Au top electrode. After lithography and patterning of the films on the top surface, wafers were thinned to 300 μm and bimorph membranes with diameters ranging from 300 to 400 μm were fabricated using silicon DRIE.

Results

Devices were tested using a Laser Doppler Vibrometer (LDV) to measure membrane deflection (shown in figure 1) and a LCR meter to measure the impedance as a function of frequency. The resonant frequency for a 350 μm membrane with a 225 μm dia. top electrode was found to be 275.3 kHz with a quality factor (Q) of 77. The measured natural frequency compares well to the 217 kHz value predicted using an analytical model. The coupling coefficient k^2 was calculated to be 2.7% based on the measured resonance and anti-resonance frequencies.

Discussion and Conclusions

AlN pMUTs have been successfully fabricated and characterized. The residual stress in the SiO₂ and AlN layers leads to a slight increase in the measured natural frequency compared to the analytical value. For these prototype devices, the relatively high parasitic capacitance (~8 pF) in comparison to the pMUT capacitance (~4 pF) degrades the measured value of k^2 ; coupling coefficients that are approximately 2-3x higher are possible if the parasitic capacitance can be reduced by future CMOS integration



4A. Microfluidic Manipulation

Tarragona

Monday, September 21, 2009, 11:30 am - 1:00 pm

Chair: **Edward Haeggstrom**
University of Helsinki

4A-1

11:30 AM **A novel integrated system of sensor and actuator for droplets on sensor plate/matching layer/piezoelectric substrate structure**

Jun Kondoh¹, Noriyuki Yasuda², Mitsunori Sugimoto³; ¹*Graduate School of Science and Technology, Shizuoka University, Hamamatsu-shi, Shizuoka, Japan*, ²*Graduate School of Engineering, Shizuoka University, Hamamatsu-shi, Shizuoka, Japan*, ³*Research Institute of Electronics, Shizuoka University, Hamamatsu-shi, Shizuoka, Japan*

Background, Motivation and Objective

Microfluidic systems are widely applied to drug development systems, cell analysis, immunoreaction measurements, etc. Normally, samples are mixed in buffer solution and continuously flowed using an electrophoresis and a micro pump. Recently, digital microfluidic systems are also proposed for manipulating droplet. In those systems, and electrowetting method is used for controlling droplet. Droplet can be manipulated using a surface acoustic wave (SAW). As the advantage to use SAW is simple configuration, digital microfluidic systems will be realized with a SAW device. However, disposable system is required for measuring biomolecules. Therefore, we propose novel integrated system of sensor and actuator for droplets. The system consists of glass plate/matching layer/piezoelectric substrate. Using three-layer structure, droplets are manipulated and mixed by SAW and measured by a sensor on the glass plate. μm

Statement of Contribution/Methods

In this paper, distilled water is used as matching layer and 128YX-LiNbO₃ is for the piezoelectric substrate. An interdigital electrode (IDT) is fabricated on a 128YX-LiNbO₃. The SAW generated the IDT radiates a longitudinal wave into the matching layer. Then, an acoustic wave (AW) is induced on the glass plate. Using the AW, droplets on the glass plate are manipulated. Fabricated sensor on the glass plate, which is an interdigital electrode (IDE) sensor, has the same structure with the IDT. The IDE sensor is used for measuring liquid impedance.

Results

Manipulation of droplet on the glass plate was demonstrated. In the same way of droplet manipulation on the piezoelectric substrate, droplet on the glass plate was manipulated and controlled by the SAW, which was generated on the 128YX-LiNbO₃. However, large applied power was needed for manipulating on the glass plate. For 7 μl water droplet, applied power was 2.25W. Flow in the droplet was observed and the same acoustic streaming on a piezoelectric substrate was confirmed. Then the IDE sensor was fabricated on the glass plate. Two droplets were placed on the glass plate. One droplet was manipulated and mixed with the other on the IDE sensor. Potassium chloride aqueous solutions with different concentrations were selected as sample liquids. The impedance of mixed droplet was measured and compared with theory. As both values agree well, we concluded uniform mixture was realized on the glass plate.

Discussion and Conclusions

Novel application of a SAW device, disposable digital microfluidic system, was demonstrated. We named the system as micro-laboratory. The experimental results strongly suggest that the proposed system can be applied for digital microfluidic system. Using the micro-laboratory, a small amount of sample liquid was transported, mixed and measured. In the future, we will apply the micro-laboratory to the measurement of immunoreactions. Theoretical calculation of the propagating wave is necessary for the optimization of the structure.

4A-2

11:45 AM **Ultrafast Surface Acoustic Wave Driven Microcentrifugation**Leslie Yeo¹, James Friend¹; ¹*Mechanical & Aerospace Engineering, Monash University, Clayton, VIC, Australia***Background, Motivation and Objective**

The dominance of surface forces over body forces makes it extremely difficult to drive microfluidic flow. Whilst considerable progress has been made to develop devices for microfluidic actuation and manipulation, there is still a need for faster and efficient devices. An area that remains elusive is microcentrifugation: to date, the proposed devices are not only large but also requires bulk rotation of the entire disk (the so-called lab-on-a-disk), which is cumbersome and also makes fluid connection difficult.

Statement of Contribution/Methods

We demonstrate a novel method to drive fast centrifugation flows in a microdevice using focused surface acoustic waves (SAW). Concentric single-phase unidirectional transducers are fabricated on a 128° rotated y -cut x -propagating lithium niobate piezoelectric substrate to generate the focused SAW. Azimuthal acoustic streaming is then induced within a millimeter dimension fluid drop placed asymmetrically on the substrate in the propagation pathway of the focused SAW (Fig 1).

Results

Fig 2 shows the concentration of a dispersion of 500 nm fluorescent particles in a 0.5 μ l water drop in under 1 s. The particle concentration arises due to the fast azimuthal streaming flow in the drop induced by the asymmetric leakage of acoustic energy into the drop. The azimuthal flow, with 1 cm/s order linear velocities, then generates a strong microcentrifugation effect which convects the particles in a helical trajectory to a central point at the bottom of the drop.

Discussion and Conclusions

We have thus demonstrated that focused SAWs are a viable method for driving rapid microcentrifugation for particle concentration (e.g., separation of blood cells from plasma for diagnostic applications) or mixing (for lab-on-a-chip applications) at the microscale.

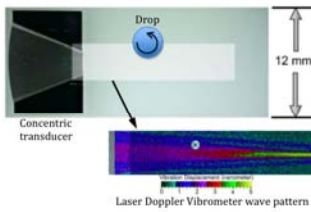


Figure 1

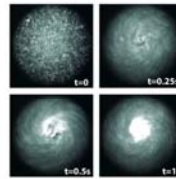


Figure 2

4A-3

12:00 PM **Inducing Rapid Fluid Flows In Microchannels with Surface Acoustic Waves**Ming Tan¹, Leslie Yeo¹, James Friend¹; ¹*MicroNanophysics Research Laboratory, Monash University, Clayton, VIC, Australia***Background, Motivation and Objective**

The difficulty in pumping fluids in microfluidics devices against viscous and surface friction forces is a critical problem in their adoption for many potential applications in chemistry, biotechnology and medicine. Inducing droplet motion with surface acoustic waves is familiar, but only recently has such an approach been tried in closed channels more appropriate for microfluidics.

Statement of Contribution/Methods

We experimentally and theoretically examine the interaction of SAW with particulate-carrying fluids in microchannels. Using microparticle image and scanning laser Doppler velocimetry for tracking the wave and fluid propagation, and comparing with our custom finite-difference time-domain code with piezoelectric coupling, compressibility, viscosity and fluid free surfaces, we provide for the first time a complete picture of SAW microfluidics phenomena.

Results

We induce a 20-50 MHz SAW parallel in lithium niobate to a smooth 50×100 micron rectangular microchannel cut into the substrate. The vibration energy carried along the sides and bottom of the channel is diffracted into it, imparting momentum to the fluid via Sclifcting and Eckart acoustic streaming. The flow moves at up to 2 cm/s, two orders of magnitude faster than any other method. Further, transitions to chaotic mixing and particle motion and collection are discovered and explained, such as the relationship between the channel width and the wavelength of sound in the fluid determining the mixing phenomena.

Discussion and Conclusions

The experimental and numerical work presented in this study permit us to explain the peculiarities of fluid flow in microchannels and the ways such phenomena may be applied to cell sorting, flocculation, fluid pumping and other applications critical to the future use of microfluidics technology.

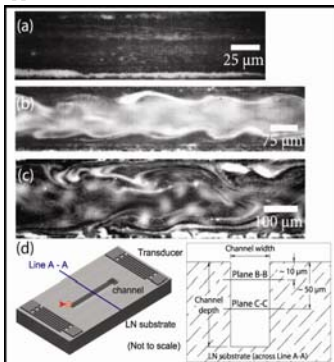


Fig 1: The (a-c) flow of water in a microchannel at (d) plane C-C as viewed from the top with Rayleigh SAW radiating along the channel left-to-right from one straight IDT to another at 20 MHz. As the channel grows beyond the wavelength of sound (80 microns) in water, the (a) uniform flow grows (b) undulatory with a 75-micron wide channel to become completely mixing with a 125-micron wide channel. Such phenomena points to the possibility of changing frequencies to switch between mixing and pumping fluids in microchannels. Particles are PS 1 μ m.

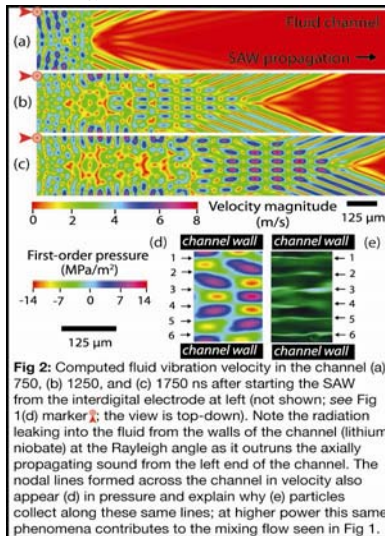


Fig 2: Computed fluid vibration velocity in the channel (a) 750, (b) 1250, and (c) 1750 ns after starting the SAW from the interdigital electrode at left (not shown; see Fig 1(d) marker \uparrow ; the view is top-down). Note the radiation leaking into the fluid from the walls of the channel (lithium niobate) at the Rayleigh angle as it outruns the axially propagating sound from the left end of the channel. The nodal lines formed across the channel in velocity also appear (d) in pressure and explain why (e) particles collect along these same lines; at higher power this same phenomena contributes to the mixing flow seen in Fig 1.

4A-4

12:15 PM The alignment of micron-scale particles in fluidic systems using surface acoustic waves

Richard O'Rourke¹, John Cunningham¹, Christopher Wood¹, Christoph Walti¹, Alexander Davies¹, Stephen Evans², Edmund Linfield¹, Sevan Harput¹, Stephen Freear¹, ¹School of Electronic and Electrical Engineering, University of Leeds, Leeds, United Kingdom, ²School of Physics and Astronomy, University of Leeds, Leeds, United Kingdom

Background, Motivation and Objective

Surface acoustic waves (SAWs) are most commonly used in electronic devices to form bandpass filters. They have, though, also recently been studied for microfluidic applications. The periodic mechanical displacement of a SAW propagating in a piezoelectric solid can be coupled into an adjacent fluid in contact with the solid's surface. We have recently shown that a SAW standing wave, created using two opposing SAWs, can be used for the controlled positioning of particles suspended in a fluid – lines of particles form in the standing wave nodes, with a spacing governed by the SAW wavelength [1] (Fig. 1a). Furthermore, by exciting a second orthogonal SAW standing wave, we can form a two-dimensional array of particles coalesced from the liquid [2] (Fig. 1b). The objective of

our work here is to investigate and optimise the dynamics of this alignment, for potential integration into biological sensor arrays.

Statement of Contribution/Methods

Interdigitated transducers were fabricated on 128° Y-cut lithium niobate crystals with a half-wavelength spacing corresponding to a 30 MHz frequency. Microfluidic channels were defined between the piezoelectric substrate and a glass superstrate, between the two acoustic transducers. Suspended fluorescent latex beads of 1 μm diameter were used to image the alignment properties of the resulting standing SAW; images of the system were captured during array formation at 25 frames per second, allowing a detailed analysis of the alignment process for a range of capillary thicknesses and acoustic powers.

Results

The spacing of nodes and antinodes in the SAW induced array is set by the SAW wavelength, allowing array formation to be changed by varying either the phase of the applied signal or the SAW frequency. The rate of formation of the array increases with acoustic power, until the threshold for acoustic streaming is reached. At this point, the array is disturbed by bulk fluid flow.

Discussion and Conclusions

We interpret our experimental results with a two-dimensional time-dependent model developed using the commercial package PZFlex (Weidinger Associates, Inc., Mountain View, CA) – the nodes and antinodes of the liquid pressure wave responsible for particle alignment spontaneously appear when the opposed SAWs have a sufficient interaction.

References:

- [1] C. D. Wood et al, Appl. Phys. Lett. 92, 044104 (2008).
 [2] C. D. Wood et al, Appl. Phys. Lett. 94, 054101 (2009).

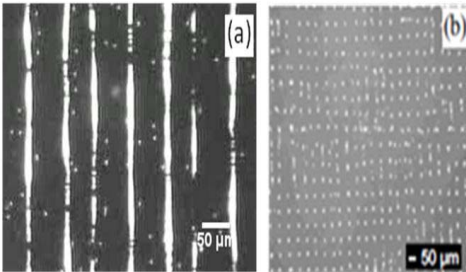


Figure 1

Alignment of latex beads into: a) lines using two opposing SAWs at 30.6 MHz and b) an array using four SAWs at 32.5 MHz.

4A-5

12:30 PM Development of an ultrasonic particle trap incorporating 3-dimensional geometric features

Adam Hughes¹, Jamie Hill¹, Thomas Purchase¹, Robert Jones¹, Martyn Hill¹, **Rosie Boltryk¹**, Michael Gedge¹, Peter Glynn-Jones¹; ¹University of Southampton, Southampton, Hampshire, United Kingdom

Background, Motivation and Objective

Here we describe the development of a device designed to collect a concentrate of cells for environmental monitoring and bio-hazard detection using ultrasonic radiation forces. The practicalities of a flow-through design are challenging, therefore it is proposed to use batch trapping, periodically diverting the trapped cells through a high concentration outlet. Trapping against the flow is possible if acoustic radiation forces oppose fluid drag forces, but the challenge is to generate these strong lateral forces.

Statement of Contribution/Methods

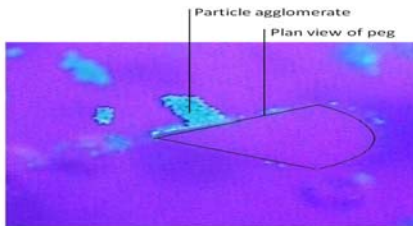
Here we report on a device that uses a series of machined pegs which we propose promote lateral variations within the acoustic field, thus generating lateral forces. Pegs were incorporated into a planar resonator designed using an impedance transfer model. This design was fabricated in a glass ceramic (macor) using a micro-mill and fluid chamber encapsulated using a glass slide. Both experiment and modelling (finite element analysis) were used to evaluate the design.

Results

During experiment it was shown that 20 and 1 μm diameter polystyrene beads can be trapped against a flow (figure) and then eluted in order to collect a concentrate of the particles. By periodically monitoring the outlet concentration using a haemocytometer, it was shown that after a period of trapping and by switching off the power to release the trapped beads a 10 times increase in the outlet concentration can be achieved.

Discussion and Conclusions

Finite element analysis (ANSYS) of the device suggests that strong lateral acoustic pressure variations exist within the fluid chamber and are comparable in magnitude with axial variations. These give rise to lateral trapping forces generated by a combination of enclosure and structural modes, especially of the pegs themselves. The fabrication method allows a large number of geometries to be explored and therefore there is much scope to optimise peg design and position. Additionally we expect greater outlet concentrations to be achieved by switching the channel through which the trapped beads are eluted. In summary, the concept of this device (geometric design and operation) represents a practical advance for sample processing in sensor instruments.



4A-6

12:45 PM Interface Acoustic Wave Based Particle Manipulation in Microfluidic Channels

Ventsislav Yantchev¹, Johannes Enlund¹, Ilija Katardjiev¹, Stefan Johansson², Linda Johansson², ¹*Solid State Electronics, Uppsala University, Uppsala, Sweden*, ²*Uppsala University, Sweden*

Background, Motivation and Objective

Acoustic wave microfluidic particle manipulation has been studied in view of practical utilization in biological and biochemical applications. Recently, the use of acoustic wave manipulation has been successfully demonstrated in a number of cell sorting/trapping applications. Two basic approaches regarding acoustic manipulation are currently exploited. The first one utilizes bulk acoustic waves (BAW) operating in the 1 – 10 MHz frequency range, while the other utilizes surface acoustic waves (SAW).

Statement of Contribution/Methods

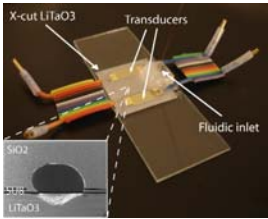
Particle manipulation utilizing surface acoustic waves has been recently demonstrated. In the proposed structure, a 40 MHz standing SAW has been excited on 128° Y-cut LiNbO₃ by means of interdigital transducers (IDT) symmetrically placed on both sides of a microfluidic channel formed at the PDMS/LiNbO₃ interface. It is noted that SAWs do exist on the load free 128° Y-cut LiNbO₃ surface only. When subsequently the SAW enters into the relatively long PDMS/LiNbO₃ interface, the wavenumber preservation results in a strong coupling to BAWs into the PDMS. Therefore, the acoustic wave radiates into the lossy PDMS substrate, which in turn reduces the amount of energy entering the microfluidic channel. Accordingly the overall efficiency of the particle manipulation system is low. In this work high frequency particle manipulation based on the utilization of interface acoustic waves (Stoneley waves) is proposed. The Stoneley wave has been used to efficiently transfer the acoustic wave power into a microfluidic channel micromachined in the fused silica glass.

Results

In here, a particle manipulation system (see fig. 1) utilizing Stoneley waves is proposed. In this system, a 34 MHz SAW propagating in the Z direction on the surface of a X-cut LiTaO₃ is excited by means of IDTs and subsequently coupled to a Stoneley wave propagating in the X-cut LiTaO₃/Fused Silica interface. Efficient alignment of 0.5 μm polystyrene beads is successfully demonstrated at different flow rates.

Discussion and Conclusions

Particle manipulation utilizing interface acoustic waves is demonstrated in a proof of principle study. Streaming and spurious alignments are found to be suppressed in the proposed system. Efficient particle manipulation is successfully demonstrated on a submicron level.



5A. SAW Applications

Pergamo

Monday, September 21, 2009, 11:30 am - 1:00 pm

Chair: **Clemens Ruppel**
EPCOS AG

5A-1

11:30 AM **Rayleigh-mode Spurious Analysis for Non-flat SiO₂/Al/LiNbO₃ Structure by using FEM/SDA**

Hiroyuki Nakamura¹, Rei Goto¹, Hidekazu Nakanishi¹, Koji Seo¹, Ken-ya Hashimoto², Matsune Yamaguchi²;
¹Panasonic Electronic Devices Co., Ltd., Kadoma City, Osaka, Japan, ²Chiba University, Chiba City, Chiba, Japan

Background, Motivation and Objective

The UMTS Band I system has a wide frequency interval between transmitting (Tx) and receiving (Rx) bands. When developing a small-sized SAW duplexer for this application, one needs a substrate with a large electromechanical coupling factor (K^2) and good temperature coefficient of frequency (TCF). Although an SiO₂/Al/LiNbO₃ structure meets these two requirements, it also supports a certain number of unwanted spurious responses. As the authors have previously discussed, the Rayleigh-mode spurious can be suppressed by controlling the cross-sectional shape of an SiO₂ overlay deposited on resonator electrodes [1]. Here, we analyzed the Rayleigh-mode spurious behavior for the non-flat SiO₂/Al/LiNbO₃ structure by using FEM/SDA [2].

Statement of Contribution/Methods

The FEM/SDA is a combination method; the finite element method (FEM) is applied to the grating region, and the spectrum domain analysis (SDA) to the substrate. In this study, we applied the extended FEM/SDA to the non-flat SiO₂/Al/LiNbO₃ structure.

The SiO₂ structure has a trapezoidal shape on the resonator electrodes, which we developed for UMTS Band I duplexer with small-sized and high performances. We evaluated the Rayleigh-mode spurious dependences of SiO₂ shapes in the analysis and the experiment. In the shape A, the upper base width of the trapezoidal region is almost the same as the electrode width, and the lower base width is larger than the electrode width. In the shape B, the upper base width is narrower than the electrode width. In the shape C, on the other hand, both the upper and lower widths are narrower than the electrode width. Here, thicknesses of SiO₂ and Al are 0.20 λ and 0.08 λ , and the cut angle of the LiNbO₃ substrate is 5°.

Results

The analysis indicates that the spurious level due to the Rayleigh-mode spurious decreases with a decrease in the average width of the trapezoidal region, namely, in the order of the shape A, B and C. The spurious really gets almost zero for the shape C. And, The resonator has high K^2 of 15% and good TCF of -30 ppm/°C in the experiments. Furthermore, the analysis has good agreements with the experiments for the Rayleigh-mode spurious and the resonator responses.

Discussion and Conclusions

We have analyzed behavior of the Rayleigh-mode spurious on the non-flat SiO₂/Al/LiNbO₃ structure. It was shown how the spurious level changes with both the shape and mass of SiO₂ on the resonator electrodes. And, the results indicated that the analysis could expect the behavior for the Rayleigh-mode spurious.

References

- [1] H. Nakamura, et al., Jpn. J. Appl. Phys. 47 (2008) pp.4052.
- [2] K. Hashimoto, et al., Proc. IEEE Ultrasonic Symp., 2007, pp.711.

5A-2

11:45 AM **Voltage tunable SAW phase shifter on AlGaIn/GaN**

Jorge Pedrós¹, Fernando Calle¹, Jesús Grajal², Zahia Bougrioua³, ¹*Instituto de Sistemas Optoelectrónicos y Microtecnología and Dpto. Ingeniería Electrónica, Universidad Politécnica de Madrid, Madrid, Spain,* ²*Dpto. Señales, Sistemas y Radiocomunicaciones, Universidad Politécnica de Madrid, Madrid, Spain,* ³*CRHEA-Valbonne and IEMN, CNRS & Lille University, Villeneuve d'Ascq, France*

Background, Motivation and Objective

The AlGaIn/GaN high electron mobility transistor technology is developing rapidly into monolithic microwave integrated circuits for a wide range of signal processing and frequency control applications, in which surface acoustic wave (SAW) devices may have an outstanding role. Interesting properties arise when a SAW interacts with the two dimensional electron gas (2DEG) created at the AlGaIn/GaN heterojunction. The electric fields accompanying the SAW couple to the mobile carriers in the semiconductor, modifying the wave propagation properties. Furthermore, the piezoelectric transduction itself is affected by the conductivity of the nitride layer. Therefore, the appropriate control of such effects on the acoustic response is not only required for the integration of SAW devices with the electronics but also offers novel capabilities and functionalities for the acoustic devices.

Statement of Contribution/Methods

In this paper, we report the development of voltage tunable SAW phase shifters on 2DEG AlGaIn/GaN heterostructures. The phase shift is controlled through a voltage applied to a metal-insulator-semiconductor (MIS) structure inserted between the input and output interdigital transducers (IDT) of a SAW delay line, which depletes the 2DEG in the acoustic propagation path. The modulation of the acoustoelectric interaction is shown to effectively tune the propagation velocity of the SAW modifying the delay with almost no additional loss.

Results

In particular, a phase shift of 30° with less than 2 dB of attenuation has been achieved with a voltage of 60 V in a 1.175 mm-long MIS structure and an IDT period of 8 μm. Since the phase shift is proportional to the electromechanical coupling coefficient and inversely proportional to the wavelength, the phase shift can be easily enhanced by reducing the IDT period without increasing the length of the MIS structure.

Discussion and Conclusions

In addition, the independent DC bias applied to the IDTs to deplete the 2DEG and allow the piezoelectric transduction can be used to simultaneously tune the gain of the system. In particular, a modulation of 6 dB has been achieved for DC voltages varying from 10 to 30 V (well above the threshold voltage of the heterostructure) without affecting the SAW phase shift. This mechanism can be employed as the loop gain control element for the fabrication of a voltage-controlled SAW oscillator (VCSO) with near-class-A operation

5A-3

12:00 PM **CDMA and FMCW Surface Acoustic Wave Temperature Sensors for Wireless Operation at High Temperatures**

Alberto Canabal¹, Evan Dudzik², George Harris³, Donald Hummels⁴, **Mauricio Pereira da Cunha**^{2,1}*LASST, University of Maine, Orono, ME, USA,* ²*ECE, University of Maine, USA,* ³*LASST, University of Maine, University of Maine, Orono, ME, USA,* ⁴*Dept of Electric and Comp. Eng., University of Maine, Orono, Maine, USA*

Background, Motivation and Objective

High temperature sensors, capable of operation at temperatures up to 1000C, are desirable in applications such as industrial process or combustion engine monitoring. Moreover, both wireless and multiple device access capabilities are of great interest in general, and a required feature when direct physical connections are not an easy alternative. Examples are rotating shafts, such as those for torque or jet engine monitoring.

Statement of Contribution/Methods

In this paper we present two surface acoustic wave (SAW) devices fabricated on langasite (LGS) using 100 nm thick Pt/Rh/ZrO₂ electrodes, which can withstand temperatures up to 1000C. The devices under study are a 15-bit code division multiple access (CDMA) sensor and a frequency modulated continuous wave (FMCW) multi-track reflective delay line. Both devices are designed to operate as wireless temperature sensors. The inter-digital transducers (IDTs) of such devices have been designed using a FEM/BEM simulation package which includes the LGS and Pt/Rh/ZrO₂ properties.

Results

Device results at room temperature are presented in Figures 1 and 2. Figure 1 shows the time domain response of the LGS CDMA sensor to the 15-bit coded input sequence, and Figure 2 depicts the two reflected pulses from the two-track FMCW radar device. These devices are now being characterized both wirelessly and as a function of temperature.

Discussion and Conclusions

Devices performance and wireless tests up to 750C will be reported and discussed in the paper.

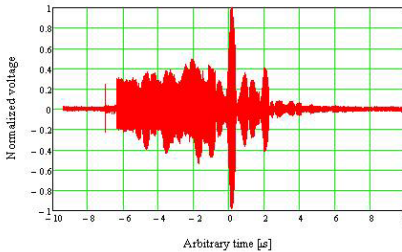


Figure 1: CDMA sensor response in time domain.

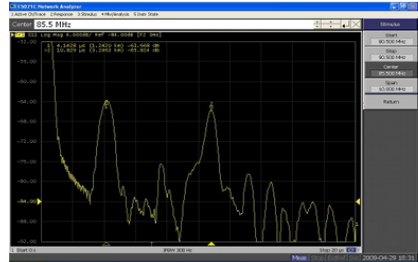


Figure 2: FMCW sensor response in time domain.

5A-4

12:15 PM Unraveling Interfacial Jetting Phenomena Induced by Focused Surface Acoustic Waves

James Friend¹, Leslie Yeo¹, Ming Tan¹; ¹MicroNanophysics Research Laboratory, Department of Mechanical and Aerospace Engineering, Monash University, Melbourne, VIC, Australia

Background, Motivation and Objective

We examine in detail the physical phenomena of surface-acoustic wave jetting first discovered by Shiokawa. Such liquid jets form beyond a critical Weber number when sufficient inertia is driven into a droplet, overcoming restoring capillary interfacial stresses. Such jets may prove useful for a wide variety of printing and atomization applications (Eggers 2008).

Statement of Contribution/Methods

We use a novel electrode-width-controlled, single-phase unidirectional transducer pair (Fig 1) expressly designed to induce fluid jetting, and use a scanning laser Doppler vibrometer and high-speed microvideography to precisely measure the input power and resulting motion of the ejected fluid. By forming simple equations via scaling laws for the droplet and jet geometry and the fluid properties, we are able to completely describe the nature of the ejection phenomena.

Results

Regardless of the newtonian fluid chosen, our simple model describes the ejection of the droplet (Fig 2). By accounting for the Weber and acoustic Reynolds number in a dynamic momentum balance between the acoustic, gravitational, surface tension, and viscous forces, we derive an expression for the jet length and its breakup pattern. Furthermore, we see the influence of the acoustic wave propagating in the fluid jet with internal reflections appearing in the jet over centimetre length scales, and demonstrate the ability to steer the jet with precision over about 45 degrees.

Discussion and Conclusions

Our study provides a complete physical basis for understanding the phenomena of SAW-driven jetting sufficient for using it in actual applications. Our device, employing a matched pair of EWC-SPUDTs, is an illustration of the potential use of the technology in microprinting not only inks but metals and other materials for rapid prototyping.

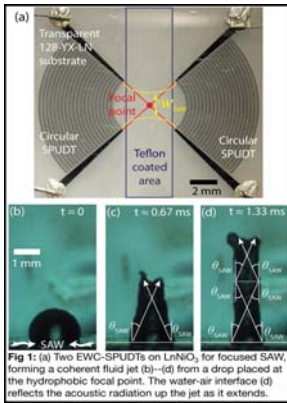


Fig 1: (a) Two EWG-SPUDTs on LiNbO₃ for focused SAW, forming a coherent fluid jet (b)–(d) from a drop placed at the hydrophobic focal point. The water-air interface (d) reflects the acoustic radiation up the jet as it extends.

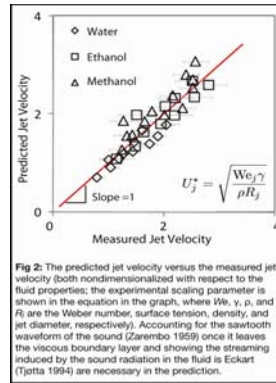


Fig 2: The predicted jet velocity versus the measured jet velocity (both nondimensionalized with respect to the fluid properties; the experimental scaling parameter is shown in the graph, where We_j , γ , ρ , and R_j are the Weber number, surface tension, density, and jet diameter, respectively). Accounting for the sawtooth waveform of the sound (Zaremba 1959) once it leaves the viscous boundary layer and showing the streaming induced by the sound radiation in the fluid is Eckart (Tjotta 1994) are necessary in the prediction.

5A-5

12:30 PM Effect of surface acoustic waves on low temperature curing of polyimide films

Ching-Chung Yin¹, I-Han Chang², Kang-Che Huang^{2,1} *Department of Mechanical Engineering, National Chiao Tung University, Hsinchu, Taiwan, ²National Chiao Tung University, Taiwan*

Background, Motivation and Objective

The application of surface acoustic waves and other guided acoustic modes in realignment of nematic liquid crystal molecules has received attention for many years. However, the need for relatively large actuating area limits its industrial applications. On the other hand, liquid crystal based flexible display is built on a variety of plastics. Most fabrication processes commonly used for flat panel displays can not be transferred to flexible devices. This paper reports the effect of acoustic reorientation of polyamic acids on ring closures to polyimide alignment layer for the flexible liquid crystal display.

Statement of Contribution/Methods

In experiment, three interdigitated transducers (IDTs) made on a 128-deg-rotated Y-cut lithium niobate wafer were used to launch surface acoustic waves propagating along the X direction. Two of the IDTs were located on both ends of the glass plate coated with polyamic acids. The surface acoustic waves with 20 micron or less wavelength were launched in the opposite direction to form a standing wave. The surface acoustic wave mediated alignment could assist ring closure proceeded by dehydration in polyamic acids to yield polyimide. The third IDT was used to generate a chirped, traveling surface acoustic wave perpendicular to the standing waves. Elliptical motion at substrate surface induces an influence like mechanical rubbing process.

Results

The FTIR spectrum of the pre-baked polyimide film after treatment by surface acoustic waves indicates that dehydration and ring closure reaction of polyamic-acid have been achieved. The conversion of polyamic-acids to polyimides has been influenced by the standing surface acoustic waves in low temperature environment. The effects of acoustic realignment on polyamic acids cured in different low temperatures were investigated and compared. The chirped, propagating surface acoustic waves induces a pretilt angle effect on the liquid crystals. Liquid crystal response time can be significantly reduced by the surface treatment of the substrates.

Discussion and Conclusions

The polyimide film can be formed in lower temperature than usual by the alignment process of polyamic acids using surface acoustic waves. The alignment is feasible for large area flexible substrates. It provides good liquid crystal properties and mechanical stability for the flexible liquid crystal displays. The chirped traveling surface acoustic wave treatment can further induce a pretilt angle effect and reduce the liquid crystal response time.

12:45 PM **Very Low Amplitude Ripple SAW Filter For Infrastructure Systems Using 41°Y-X and 15°Y-X Lithium Niobate: Full FEM/BEM Design Approach.**

Stephane Chamaly¹, Xavier Perois², Hoi Yan Fong¹, Markus Mayer³; ¹Research and Development, EPCOS PTE LTD, Singapore, Singapore, ²EPCOS SAS, Sophia-Antipolis, France, ³EPCOS AG, Munich, Germany

Background, Motivation and Objective

In demand of high data rate communication devices, wide band filters are necessary. In infrastructure systems like Base Transceiver Stations and microwave Radio-Links, such filtering function was carried out by ceramic filter technology. They were preferred for their low in-band ripple and VSWR necessary for low EVM and amplifier linearity. We have developed a design technique allowing SAW devices to advantageously replace ceramic filters in many systems.

Statement of Contribution/Methods

One important parameter that determines the performance of a piezoelectric device is the electromechanical coupling coefficient. RF filters designed on widely used 42°Y-X LiTaO₃ are not meeting the stringent specification requested by infrastructure systems. To increase the width of the bandwidth and reduce the in-band ripple, a material with high electromechanical coupling coefficient is needed. This paper describes the search for the optimal working point using a full FEM/BEM approach and proposes a new design technique on 41°Y-X and 15°Y-X LiNbO₃.

Results

On 41°Y-X LiNbO₃, bandwidths larger than 8% at 3dB attenuation are achieved leading to very low amplitude ripple. A GSM Rx filter for base station at 1747.5MHz will be demonstrated. Filter bandwidth is 140MHz leading to ripple in 1710MHz – 1785MHz lower than 0.2dB nominal and 1dB over temperature and total 6 sigma manufacturing. Insertion loss is 2.5dB while image rejection is better than 45dB. Size is 3x3mm² in a high reliability ceramic cavity package. Finally, a very wide band filter built on 15°Y-X LiNbO₃ with standard electrode material will be demonstrated.

Discussion and Conclusions

The close correspondence between simulation and measurement demonstrates the ability of our methodology to design SAW devices rapidly and accurately on virtually any material. The filters designed by this technique on 41°Y-X LiNbO₃ and 15°Y-X LiNbO₃ are demonstrating a wide band and very low in-band ripple perfectly matching the infrastructure systems requirement.

6A. Phononic Crystals-Fundamentals

Baalbek

Monday, September 21, 2009, 11:30 am - 1:00 pm

Chair: **Abdelkrim Khelif**
CNRS/Georgia Tech

6A-1

11:30 AM **Elastic waves in a 3D unconsolidated granular phononic crystal with rotating particles**

Aurélien Merkle¹, Vitaliy Gusev², Vincent Tournat^{1,1} *LAUM, Université du Maine, Le Mans, France*, ²*LPEC, Université du Maine, Le Mans, France*

Background, Motivation and Objective

Ordered unconsolidated structure of monodisperse spherical beads constitutes a granular phononic crystal. The behavior of a granular phononic crystal at the macroscopic scale is induced by the local contacts between the beads at the microscopic scale. The local contact between two beads is described by the Hertz-Mindlin law and shows strong nonlinearities.

Nevertheless, the macroscopic mechanical behavior of unconsolidated granular media is poorly understood. The complexity of mechanical phenomena comes partially from the disorder character of granular assemblies at the microscopic level.

Existing theoretical formulas have not been developed to the level necessary to understand wave propagation in a 3D unconsolidated granular crystal and comparison with experiments does not exist.

Statement of Contribution/Methods

The bulk modes of an unconsolidated packing of monodisperse beads, considered as rigid masses connected with springs, arranged in the hexagonal close packed structure are theoretically evaluated. The calculation of the dispersion relations in particular directions allows to estimate the resonance frequencies in a crystal of finite size which are compared to experimental results.

Because of friction, the contacts between spheres are modelled by two springs, one for normal interaction and one for transverse interaction. The existence of the transverse interaction requires to take in account the rotational degrees of freedom of the beads and leads to predict the existence of rotational waves.

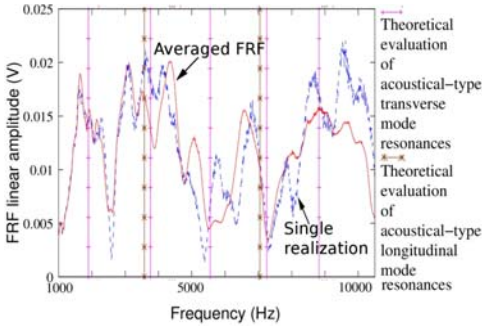
Results

Theoretical results predict, in the direction perpendicular to the layers plane, the existence of an elastic acoustical-type longitudinal mode, an elastic optical-type longitudinal mode, pure elastic rotational modes and coupled transverse-rotational modes.

The frequency response function of a hcp crystal of beads is measured, with an averaging over one hundred distributions of contact force in order to minimize the effects of disorder, as shown in Fig.1.

Discussion and Conclusions

Theoretical results show that there exist optical-type modes in a hcp crystal, which are absent of the previous theories on granular crystals, and that the rotational degrees of freedom have an important contribution on the dispersion of the transverse waves. The evaluated resonance frequencies are identified on the measurements which is a step before including nonlinear effects.



6A-2

11:45 AM **Elastic Band Gaps of Two-dimensional Phononic Crystals Tuned by Material Parameters**

Xiao-Zhou Zhou¹, Yue-Sheng Wang¹, **Chuanzeng Zhang**^{2,1} *Beijing Jiao-Tong University, China, People's Republic of, ²University of Siegen, Germany*

Background, Motivation and Objective

Since the pioneer work of Kushwaha (Phys. Rev. Lett., 1993, 71: 2022), a great deal of attention has been focused on the so-called phononic crystals - the artificial periodic elastic structures based on the traditional natural crystals and photonic crystals. A physical character of the phononic crystals is the existence of phononic band gaps (PBGs) in which the sound and elastic waves are all forbidden. Phononic crystals have numerous potential engineering applications, on the most of which the basis depends on the existence of PBGs. So it is essential to find out the way how to tune the available PBGs.

PBGs are dominated by some factors, including structural parameters and material parameters. Compared with a great many researches of the structural parameters, there are limited investigations on the material ones. The material parameters include the elastic constants, mass density, wave velocity, and acoustic impedance, etc. So far, most of the investigations are based on the calculation of band structures for the systems with particular material combinations, and the conclusions are non-universal.

Statement of Contribution/Methods

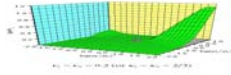
In this paper, we will begin with the basic wave equations and derive the material parameters directly determining band gaps for two-dimensional cases. Then the effects of these parameters on phononic band gaps are discussed in details with different filling fractions and lattice forms for in-plane wave modes. The present analysis can be applied to artificially design or control phononic band gaps.

Results

For the in-plane wave mode, the band gap determined by the third and fourth lowest bands is considered. This is the second but the most applicable potential band gap for most phononic crystals. Figure 1 shows the normalized gap width as a function of the mass density ratio and of the contrast of elastic constants in square lattice.

Discussion and Conclusions

The result shows the material parameters determining band gaps of two-dimensional phononic crystals include the mass density ratio, the shear modulus ratio, and Poisson's ratios of the two component materials. The band gaps easily appear at both large mass density ratio and shear modulus ratio and become wider with both of these two parameters increasing. For the in-plane mode both the mass density ratio and the shear modulus ratio may play equally important roles in controlling the band gaps.



6A-3

12:00 PM Characterization of evanescent ultrasonic waves in a band gap of a 1D phononic crystal.

Maxime Bavencoffe¹, Morvan Bruno¹, Anne-Christine Hladky-Hennion², Jean-Louis Izbicki³; ¹Groupe Ondes Acoustiques, LOMC FRE CNRS 3102, Le Havre, France, ²Groupe Acoustique, IEMN UMR CNRS 8520, Lille, France, ³FANO FR CNRS 3110, Le Havre, France

Background, Motivation and Objective

This work deals with the propagation of Lamb waves on a plate engraved by a 1D periodic grating. As the propagation takes place in a periodic medium, the dispersion curves of the modes exhibit pass bands and stop bands related to the geometry of the waveguide. The presence of a stop band implies a coupling between different modes inside the Brillouin zone. A part of the energy of the incident wave is transmitted in other modes and this coupling is maximum at the central frequency of the gap. Considering a limited periodic grating, the attenuation of the propagating waves is linked to a conversion phenomenon. Therefore, in the frequency range of a stop band, some waves propagate with attenuation. The aim of this work is to establish a link between the attenuation of the ultrasonic waves observed in the case of a limited grating and the values of the imaginary part of the wave number in a stop band.

Statement of Contribution/Methods

The band structure of a 1D phononic crystal is computed with the finite element method (ATILA[®] code). The complex branches of the dispersion curves are obtained by combining Bloch-Floquet's theorem with well-known transfer matrix techniques.

In the frequency range of a stop band, only complex wave numbers $k = k' + jk''$ exist. The imaginary part of the wave number k'' involves an attenuation of the corresponding mode in the direction of propagation through a limited periodic grating. This attenuation is estimated by performing harmonic analyses.

Results

A parametric study of the complex band structure of the 1D phononic crystal has revealed that the maximum value of the imaginary part of the wave number k'' occurs at the central frequency of the gap. This statement is in agreement with the results of the harmonic analyses considering a wave propagating through a limited grating.

Moreover, considering a limited periodic grating, the decay of the amplitude of the propagating waves along the wave guide is approximated by a decreasing exponential function $\exp(-k''x)$, where k'' is the imaginary part of the wave number given in the complex band structure of the 1D phononic crystal and x the distance of propagation. Experiments confirm the theoretical observations.

Discussion and Conclusions

The real and imaginary parts of the wave number of the evanescent modes in a stop band of a 1D phononic crystal have been computed. Parametric studies have shown the influence of the dimensions of the periodicity of the grating on the real and imaginary parts of the wave number. In addition, the influence of this imaginary part has been linked to the decay of the amplitude of the propagating waves through a limited periodic grating.

6A-4

12:15 PM **Study of plane periodic multilayered viscoelastic media: Experiment and simulation**

Olivier Lenoir¹, Pierre Maréchal¹:¹LOMC FRE CNRS 3102, FANO FR CNRS 3110, Université du Havre, Le Havre, France

Background, Motivation and Objective

Phononic crystals or periodic media are widely studied because of their very interesting properties such as exhibiting absolute or local band gaps in their dispersion curves, namely frequency domains in which no transmission of acoustic waves is possible. The breaking of periodicity by inserting defects in the structure enables to open very thin pass bands in those band gaps. The possible applications are to obtain very selective filters or wave guides according to the locations or features of these pass bands compared to those of the perfect periodic media. This preliminary work deals with plane multilayers composed of 2 and 3 elementary periods. The aim of this study is to compare experiments and modeling results where the plates and periods are supposed perfectly bonded.

Statement of Contribution/Methods

The studied period is composed of aluminum and polyethylene. These materials were chosen for their contrasting acoustic impedance, resulting in highly reflecting structure. For simplicity's sake, attenuation is only considered in the polyethylene plate. The reflection at normal incidence is analyzed in case of 1, 2 and 3 periods. Simulations are based on the stiffness matrix method developed by Rokhlin et al. [1], proved to be stable numerically. Experiments are performed either in water at 2.25 MHz or in air at 2.25 and 15 MHz.

Results

When immersed in water on both sides, the multilayer reflection coefficient exhibits wide minimums linked with Lamb waves in aluminum. In the cases of 2 and 3 periods, stop bands where the reflection coefficient is unity are also observed. These stop bands are separated by very thin transitions. If no attenuation is taken into account, the reflection coefficients are identical whatever the incidence side. On the contrary, if attenuation is considered in polyethylene, the reflection coefficients are different and attenuation of the whole multilayer structure could be deduced. Similar simulation data are observed when the structure is loaded with water on one side and air on the other side. Experiments in immersion and contact are in good agreement with those modeling results.

Discussion and Conclusions

Simulation results show the sensitivity of the constitutive layer properties, particularly attenuation. The influence of surrounding media is discussed and confirmed with measurement results. In order to compare efficiently experiments and simulations, a good estimate of the attenuation in polyethylene is required. Pulse-echo measurements have been performed to obtain the longitudinal attenuation in the polyethylene layer. Using as a guess the estimated attenuation, the simulated reflection coefficient is fitted to the experimental data. As a perspective, the inclusion of a defect between two periods would add pass bands in the reflection spectrum.

[1] Rokhlin S.I. and Wang L., "Stable recursive algorithm for elastic wave propagation in layered anisotropic media: Stiffness matrix method", *J. Acoust. Soc. Am.*, 112(3), 822-834, 2002.

6A-5

12:30 PM **Phononics, phononic crystals, and beyond**

Vincent Laude¹:¹Institut FEMTO-ST, Centre National de la Recherche Scientifique, Besancon, France

Background, Motivation and Objective

The objective of this invited paper is to present a review of the domain of phononics. A general aim is to attract new researchers to this growing field that has strong connections with ultrasonics. Along this talk, I will try and provide answers to a number of basic questions, such as: What is phononics, Who is presently involved in phononics? What is new and what is not? Why switch to phononics? What is still to be done? Are there any applications?

Statement of Contribution/Methods

Phononics can be defined as the science of designing artificial acoustic materials with tailored dispersion properties. Of special interest are phononic crystals, two- or three-dimensional periodically structured materials that show a number of amazing properties - but only if properly designed. For instance, strong confinement of wave energy can be obtained inside complete band gaps, i.e. frequency ranges within which no wave propagation

is allowed, whatever the incidence and the polarization. Outside band gaps, the periodic structure leads to very strong spatial dispersion, resulting in properties unavailable with usual homogeneous materials. A basic tool is the so-called band structure that summarizes the dispersion relations of all waves propagating in a phononic crystal. Some simple hints to understand band structures will be given.

Results

I will then highlight recent achievements in the field of phononics and use them to emphasize that much remains to be achieved. For instance, although the theory of band gaps is quite advanced, experimental demonstrations have not been that many, and technical difficulties still stand ahead. Confinement by defects has been shown to lead to efficient energy storage in cavities, to wave guiding in very narrow spaces, and more generally to simple phononic circuits; however, the practical achievement of true phononic circuits or filters is still an unsolved challenge. It is highly desirable to design phononic crystals for surface acoustic waves, and initial demonstrations have been performed, but there is still a major bottleneck to their development: efficient structural technologies for piezoelectric materials have to be obtained. The spatial dispersion properties of finite phononic crystals have been employed to design acoustic lenses, through the use of positive or negative refraction; but these lenses have shown limited efficiency, and limited frequency range.

Discussion and Conclusions

The geometrical dimensions of phononic crystals ultimately dictate the frequency ranges inside which band gaps appear. I will give a summary of achievements that have been obtained for bulk waves, surface waves, phononic plates, phononic layers-on-a-substrate, and true 3D phononic structures. It will be seen that the frequency range of operation has generally been limited by available transducers for acoustic or elastic waves. As one possible answer to that, I will discuss the use of phononics to improve transducers or dramatically change their design.

1B. Contrast Agents and Sonoporation

Sala 1

Monday, September 21, 2009, 2:30 pm - 4:00 pm

Chair: **Paul Dayton**
Univ. North Carolina/NCSU

1B-1

2:30 PM **Sonoporation of endothelial cells with CD31-targeted microbubbles at low acoustic pressures**

Klazina Kooiman¹, Miranda Foppen-Harteveld¹, Nico de Jong^{1,2}, *Biomedical Engineering, Erasmus MC, Rotterdam, Zuid-Holland, Netherlands,* ²*Applied Physics, Physics of Fluids, University of Twente, Netherlands*

Background, Motivation and Objective

To enhance drug uptake by cells, the membrane permeability can be increased by ultrasound in combination with contrast agents. With this method, termed sonoporation, oscillating or jetting microbubbles induce transient cell membrane pores so that extracellular therapeutics can enter the cell. So far, only non-targeted microbubbles have been used to induce sonoporation [1,2]. However, in an in vivo situation this may be challenging since there may not be sufficient microbubble-cell contact due to the blood flow. A microbubble targeted to the cell membrane may overcome this, but it is not known whether sonoporation can still be induced. This study focuses on inducing sonoporation with CD31-targeted microbubbles in endothelial cells. CD31 was chosen since this adhesion molecule is expressed constitutively on the surface of endothelial cells [3].

Statement of Contribution/Methods

Lipid coated microbubbles (composition in mol %: DSPC 59.4; PEG-40 stearate 35.7; DSPE-PEG(2000) 4.1, DSPE-PEG(2000)-biotin 0.8) with a C4F10 gas core were made by sonication [4]. CD31 antibody was conjugated via avidin-biotin bridging [5]. Human umbilical vein endothelial cells (HUVEC) were grown to confluence in an Opticell. Microbubbles were added to HUVECs and allowed to adhere. The Opticell was mounted in the set-up such that the bound microbubbles were on top of the cells. At 37°C, microbubble-cell behavior upon insonification at 1 MHz (10 cycle sine-wave bursts) was studied with the Brandaris 128 high-speed camera. Microbubble diameter (D) – time curves were extracted from the recordings and $D_{max} - D_{min}$ (ΔD) normalized to the resting diameter D_0 were determined. The cell-impermeable propidium iodide (PI; 25 $\mu\text{g/ml}$) was used as indicator for increased cell membrane permeability due to sonoporation, and studied using a fluorescence microscope onto which a CCD camera (LCL-90 2K, Watec) was mounted.

Results

On average, ~ 1 microbubble bound to each cell. At 80 kPa peak negative acoustic pressure (P_-), the targeted bubbles ($D_0 = 3-4 \mu\text{m}$) oscillated spherically, shrank by $\sim 20\%$ but were not destroyed. $\Delta D/D_0$ was 0.1. Although cell deformation was not detectable, PI was taken up locally in the area surrounding the bubble (area $\sim 4x$ the bubble D_0). Sonoporation was also studied when targeted bubbles were insonified at a higher P_- of 200 kPa. At this P_- , bubble oscillation was violent, non-spherical, and jets were observed. $\Delta D/D_0$ was 1.4. Cell deformation of $1 \mu\text{m}$ was detected and PI was taken up and was found to be distributed throughout the entire cell.

Discussion and Conclusions

This study reveals that targeted microbubbles, which adhered to the endothelial cell membrane, can induce sonoporation. This feature may now be used in molecular imaging, thereby combining diagnosis and drug delivery.

- 1 van Wamel et al, J Control Rel 2006
- 2 Schneider, J Endourol 2008
- 3 DeLisser et al, Immunol Today 1994
- 4 Klibanov et al, Invest Radiol 2004
- 5 Lindner et al, Circulation 2001

1B-2**2:45 PM Ultrasound-mediated endothelial cell permeability changes with targeted contrast agents**

Pavlos Anastasiadis¹, John S. Allen¹; ¹*Mechanical Engineering, University of Hawaii at Manoa, Honolulu, HI, USA*

Background, Motivation and Objective

Advances in molecular imaging and drug delivery with ultrasound have followed from the development of site-targeted ultrasound contrast agents (UCAs), gas-filled microbubbles which are conjugated with targeting ligands on their surface for the detection and evaluation of intravascular pathology. Targeted microbubbles in combination with low-frequency ultrasound can have a direct effect on the cell membrane in terms of increases in the permeability or absorption of drugs into cells and tissues, though the underlying mechanisms are currently not well understood. Since endothelial cell monolayers form the main barrier to the passage of macromolecules and circulating cells from blood to tissues, understanding endothelial permeability mechanisms is of the utmost importance for the diagnosis and treatment of cardiovascular diseases.

Statement of Contribution/Methods

Endothelial permeability studies in combination with ultrasound and UCAs have been observed, but the effects have not been directly quantified in terms of changes in the cell spacing. Furthermore, we evaluate alterations in the endothelial barrier function by rigorously quantifying ultrasound-mediated changes in endothelial cell permeability in real-time with a novel electrical impedance method. Endothelial cell monolayers were studied by employing low-frequency ultrasound under physiological conditions without the use of staining or other molecular interventions. Human Coronary Artery Endothelial Cells (HCAECs) were grown on collagen IV coated cell culture dishes equipped with gold microelectrodes. The endothelial cell-to-cell and cell-to-substrate gaps were measured in real-time with the electric cell-substrate impedance sensing system (ECIS, Applied BioPhysics, Troy, NY) while subject to ultrasound.

Results

HCAECs show an increase in permeability by employing non-targeted microbubbles in combination with ultrasound at 1 MHz. For targeted ultrasound contrast agents conjugated with different ligand antibodies and cyclic analogs of the arginine-glycine-aspartic acid (RGD) ligand, the permeability changes observed are significantly greater when compared to the non-targeted case.

Discussion and Conclusions

Targeted UCAs in general, and in conjunction with RGDs, ligand antibodies and low-frequency ultrasound, in particular, alter the permeability of endothelial cell membranes in vitro. Furthermore, the results suggest that the cell membrane permeability changes are temporary and these changes can be quantified with respect to the electrical cell impedance sensing system parameters which relate directly to changes at the cellular level.

1B-3**3:00 PM Evaluation of Subharmonic Emission from Encapsulated Microbubbles as an Indicator for Sonoporation of Cell Monolayers**

Karin Hensel¹, Abdelouahid Maghnooui², Stephan A. Hahn², Georg Schmitz¹; ¹*Institute of Medical Engineering, Ruhr-University Bochum, Germany*, ²*Molecular GI-Oncology, Ruhr-University Bochum, Germany*

Background, Motivation and Objective

Sonoporation is the ultrasound induced transient opening of cell membranes. Large scale oscillation of nearby microbubbles (MBs) is considered to be the primary effect in sonoporation whereas MB destruction correlates with lower sonoporation rate and increased cell damage. The scale of MB oscillation in a cloud can be determined by monitoring subharmonic power emission. This effect is enhanced by exciting MBs at twice their resonance frequency.

The subharmonic to fundamental ratio (SFR) has the potential to be employed as a monitoring parameter to identify MB behavior during therapy. In this study, backscattered SFR is measured during therapy of cell monolayers and evaluated as an indicator for sonoporation.

Statement of Contribution/Methods

293T cells are grown in Opticell containers, which are filled with a medium containing SonoVue MBs and Propidium Iodide (PI). Each container is placed in water in the focus of a single element transducer emitting 5

cycles sine-bursts at 3.3 MHz repeated 50 times. This excitation frequency equals twice the resonance frequency of the employed MBs (1.5-1.75 MHz). The peak negative pressure (PNP) is varied from 0.06 to 1.41 MPa. Backscattered signals are recorded by the therapy transducer to monitor SFR during therapy. A fluorescence microscope is focused on the therapy region to quantify MB destruction and to monitor PI fluorescence in the cells during and after acoustic excitation. PI cannot overcome intact cell membranes and changes fluorescence properties when bound to intracellular fluid. A cell is considered sonoporated, if PI enters the cell during insonication and is released again afterwards. That results in a sharp rise of fluorescence intensity and a subsequent decrease for several minutes. A cell is considered permanently stained, if fluorescence is concentrated at the cell nucleus and rises to a plateau. A high speed camera is coupled to the microscope to verify MB oscillation.

Results

With increasing PNP, the percentage of sonoporated cells significantly rises to a maximum of 1.9% at 0.81 MPa and decreases for higher PNP. The same holds true for the SFR, which significantly rises to a maximum at 0.81 MPa, too. The percentages of permanently stained cells and destructed MBs, on the other hand, depict their maximum at maximal PNP being 84% and 100% respectively. Optical monitoring further reveals that those MBs which sonoporate cells disrupt, coalesce or dissolve afterwards.

Discussion and Conclusions

The correlation of sonoporation rate and SFR reveals that subharmonic emission from encapsulated microbubbles can be used to optimize sonoporation of cell monolayers. This further supports the hypothesis, that large scale oscillating MBs are responsible for sonoporation. The overall low sonoporation rate results from the fact, that permanently stained cells might still be viable (sonoporated) but are not able to release PI once it has reached the nucleus.

1B-4

3:15 PM Observations of bubble-vessel interactions in ultrasound fields

Hong Chen¹, Andrew A. Brayman¹, Michael R. Bailey¹, Thomas J. Matula¹; ¹Center for Industrial and Medical Ultrasound, Applied Physics Laboratory, University of Washington, Seattle, WA, USA

Background, Motivation and Objective

Interactions between bubbles and nearby boundaries have been studied for some time; however, the direct interactions between bubbles and tissue boundaries, especially blood vessel walls, have not been studied to a large extent. In this work high-speed microscopy was used to study the dynamical interaction between microbubbles and microvessels of *ex vivo* rat mesentery subjected to a single pulse of ultrasound.

Statement of Contribution/Methods

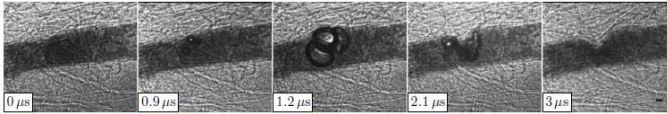
Ultrasound contrast agent microbubbles were injected into the blood vessels of rat mesentery subsequent to having the blood flushed out. India ink was used to increase the contrast between microvessels and surrounding tissues. Tissue samples were aligned at the focus of both an ultrasound transducer with a center frequency of 1 MHz and an inverted microscope coupled to a high speed camera. Fourteen high-speed microphotographic images were acquired for each experiment using 50 ns shutter speeds.

Results

Observations of the coupled dynamics between bubbles and vessels ranging from 9.4 μm to 100 μm diameter suggest that the vessel wall dilates during bubble expansion, and invaginates during bubble contraction. The phase of vessel dilation/invagination follows closely the phase of bubble expansion/contraction, except for conditions approaching inertial collapse. For such cases the tissue remains invaginated at least 10 μs after the passing of the ultrasound pulse. The degree of dilation and invagination depends on vessel size, as well as maximum bubble expansion. The ratio of invagination to dilation is usually >1 . Furthermore, in agreement with our previous studies, invagination appears to be a more stressful condition for vessel walls, as local strains appear to be much greater for invaginated vessels than for dilated vessels. In the following figure, the maximum local radial strain during vessel invagination is estimated to be over 10 times greater than the maximum strain during vessel dilation (initial vessel diameter=46 μm).

Discussion and Conclusions

The coupled dynamics between the vessel wall and bubble oscillation shows that the vessel responds on microsecond timescales. We also observe that vessel invagination can be significantly greater than dilation, and may be a dominant mechanism for microbubble-induced damage to microvessels. Work supported by NIH (5R01EB000350 and 5R01AR053652).

**1B-5****3:30 PM Ultrasound-based imaging of nanoparticles: from molecular and cellular imaging to therapy guidance**Stanislav Emelianov¹; ¹Department of Biomedical Engineering, University of Texas at Austin, USA**Background, Motivation and Objective**

The effectiveness of an imaging technique is often based on the ability to image quantitatively both morphological and physiological functions of the tissue.

Statement of Contribution/Methods

We have developed several ultrasound-based imaging techniques capable of visualizing both structural and functional properties of living tissue. Each imaging system utilizes custom-made targeted nanoparticles developed to probe specific molecular events and, therefore, the images display the molecular processes in the body. Furthermore, the molecular contrast agents can also be used for molecular therapy.

Results

For each imaging system, the basic physics will be described to introduce the principles of each approach. We will then discuss experimental aspects of each imaging system including fabrication of integrated imaging probe and associated imaging hardware, development of signal and image processing algorithms, and design of targeted contrast agents. Finally, we will demonstrate and discuss biomedical and clinical applications of the developed imaging approaches ranging from microscopic to macroscopic imaging of pathology, cardiovascular diseases, cancer detection, diagnosis, therapy and therapy monitoring, etc.

Discussion and Conclusions

The nanoparticle-augmented ultrasound-based methods for imaging and therapy are feasible and practical. These methods may become an important clinical tool of sufficient sensitivity and specificity for diagnosing the pathology or disease, selecting appropriate therapy, initiating or guiding therapy, and even monitoring therapeutic outcome.

Partial support from National Institutes of Health under EB 008101, HL 084076 and EB008821 grants is acknowledged.

2B. Therapy Monitoring, Control, and Quality Assurance

Sala 2

Monday, September 21, 2009, 2:30 pm - 4:00 pm

Chair: **Emad Ebbini**
Univ. of Minnesota

2B-1

2:30 PM **MR guidance, monitoring and control of Brain HIFU therapy in small animals: In vivo demonstration in rats at 7T**

Benoît Larrat¹, Mathieu Pernot¹, Elvis Dervishi², Abdel Souilah¹, Danielle Seilhean³, Yannick Marie⁴, Anne-Laure Boch², Jean-François Aubry¹, Mathias Fink¹, Mickael Tanter¹; ¹*Institut Langevin - ESPCI Paristech, Univ Paris 7, CNRS UMR 7587, Paris, Paris, France*, ²*Department of neurosurgery, Groupe Hospitalier Pitié-Salpêtrière, France*, ³*Department of neuropathology, Groupe Hospitalier Pitié-Salpêtrière, France*, ⁴*CNRS UMR 71, Groupe Hospitalier Pitié-Salpêtrière, France*

Background, Motivation and Objective

In the framework of HIFU transcranial brain therapy it is mandatory to develop imaging techniques capable of assessing the focusing quality and location before the treatment. Monitoring heat deposition in real time as well as verifying the extension of the treated area are also important steps. The objective of this study was to develop a complete MR-guided HIFU protocol for small animals experiments in a high field MRI scanner. Three complementary MR sequences are proposed to non invasively:

- locate the US radiation force induced displacement in tissues and quantify the acoustical pressure at focus prior to HIFU;
- monitor the temperature rise during HIFU;
- assess the changes in elasticity in the heated area.

Statement of Contribution/Methods

A 7T Bruker MRI scanner was equipped with a stereotactic frame for rats and a single element focused US transducer working at 1.5MHz. Rats were kept under gas anesthesia (Isoflurane 2% v/v) and their heads were shaved.

A motion sensitized spin echo MR sequence was optimized to measure the radiation force induced displacement in the brain. Once localized, the maximum displacement was measured and linked to the acoustical pressure at focus by means of a calibration procedure. The measured pressures in vivo ranged from 0 to 3.5MPa. An MR-Thermometry sequence allowed mapping the temperature rise every 500ms in the focal plane with 0.5°C accuracy and an in plane resolution of 0.7mm. MR-Elastography datasets were acquired before and after HIFU. Standard T2 and T1 (with and without Gadolinium) images were also recorded. Wave propagation and bioheat equation were simulated using 3D finite differences schemes in order to maximize heat deposit at focus while minimizing skull heating.

Results

The proposed protocol was successfully tested on 10 rats with and without injected tumors. Three tumor models were tested: C6, 9L and RG2. Three MR sequences all based on phase contrast imaging were validated.

The accurate localization of the US focal point prior to HIFU was demonstrated in vivo through the skull without any tissue damage, as confirmed by histology. It was achieved with the same material and in the final position for HIFU. Furthermore, the acoustical pressure was estimated in situ, allowing more accurate simulations of the heat deposition at focus. This enabled to optimize the parameters for the HIFU treatment (electrical power, duration). The temperature measurements were in good accordance with the predicted curves. The elasticity maps showed significant changes after treatment which could be followed for two weeks. In particular, the inflammatory response appeared to decrease the elasticity.

Discussion and Conclusions

Radiation force, temperature and elasticity MR-imaging were combined and successfully implemented in a MR-guided HIFU setup and evaluated on 10 rats. In the perspective of human therapy at 1MHz, this small animal protocol seems adequate and all sequences should be implemented on clinical systems.

2B-2

2:45 PM Realtime Two-Dimensional Temperature Imaging Using Ultrasound

Dalong Liu¹, Emad Ebbini²; ¹Biomedical Engineering, University of Minnesota, Minneapolis, MN, USA, ²Electrical and Computer Engineering, University of Minnesota, Minneapolis, MN, USA

Background, Motivation and Objective

Noninvasive temperature estimation continues to attract attention as a means of monitoring and guidance for minimally-invasive thermotherapy. Currently, minimally-invasive RF ablation is the most commonly used form of thermal therapy, but other techniques are being used or investigated. For example, high-intensity focused ultrasound (HIFU) is being evaluated clinically as a form of noninvasive thermal therapy. Successful implementation of real-time noninvasive temperature estimation will be a boon for thermal therapy as it becomes less invasive and as the heating sources become more sophisticated.

Statement of Contribution/Methods

We present first results from a realtime system for 2D imaging of temperature change using pulse-echo ultrasound. The frontend of the system is a commercially available scanner equipped with a research interface, which allows the control of imaging sequence and access to the RF data in realtime. The 2D RF data is then streamlined to the backend of the system, where a 2D temperature imaging algorithm based on speckle tracking is implemented on a graphics processing unit (GPU). The resulting images of temperature change match the spatial and temporal resolution of the imaging system, i.e. temperature change data is produced at every pixel in the RF data set.

Results

Verification of the algorithm was performed by monitoring localized HIFU-induced heating of a tissue-mimicking elastography phantom. The acoustic, thermal, and elastic properties of the phantom were carefully measured to provide calibrated values of the temperature coefficient. A HIFU transducer was used to produce subtherapeutic localized, short-duration heating in the phantom while being monitored by the diagnostic scanner. Realtime images of temperature change were produced at 500 fps using 10 scanlines per frame with an axial extent of 40 mm. The pulsed HIFU source was synchronized with the scanner to allow for acquisition of the frame data while briefly silencing the HIFU driver. The pHIFU driving signal was set such that the temperature rise in the phantom is below 3°C for 1.5-second shot (i.e. subtherapeutic). The experiment was repeated 8 times at 30-second intervals to allow the temperature to cool down to baseline. Similar experiments were also performed multiple times *in vitro* porcine heart tissue before and after HIFU-induced lesions were formed.

Discussion and Conclusions

The realtime temperature imaging results clearly demonstrate the repeatability and sensitivity of the algorithm. The standard deviation in maximum estimated temperature change from 8 runs was 0.04°C. Furthermore, *in vitro* results demonstrating the possible use of this algorithm in imaging changes in tissue parameters in HIFU-induced lesions are presented. These results clearly demonstrate the value of the realtime data streaming and processing in monitoring and guidance of minimally-invasive thermal therapeutic procedures.

2B-3

3:00 PM Dosimetry Optimization for Controllable Lesion Size in High Intensity Focused Ultrasound Therapy

Ria Sutedia¹, Xinliang Zheng¹, Shahram Vaezy¹; ¹Bioengineering, University of Washington, Seattle, WA, USA

Background, Motivation and Objective

HIFU treatment has been proved to be a potential procedure for tumor ablation. However, the treatment of tumors with large sizes has been a challenge for HIFU therapy. The problem comes from the fact that the focus of a HIFU transducer is usually on the scale of millimeters while the volume of the tumor can be several centimeters. Therefore multiple HIFU exposures are needed to cover the whole volume, leading to long treatment time and, more importantly, possible pre-focal damage to the healthy tissue surrounding the tumor.

Statement of Contribution/Methods

To prevent the damages due to excessive HIFU exposure, a solution using low total energy level is proposed. The energy was applied in pulses that had high peak intensity with a short duty ratio. In this way, while thermal and cavitation mechanisms for tissue ablation are utilized optimally during the HIFU treatment, the time interval between every two pulses would provide a cooling period to effectively reduce the pre-focal damage. Ex-vivo experiments on chicken tissue were performed to study the effect of duty ratio on the size of a necrotic lesion. For each series of experiments, the total energy was kept at the same level between 10000 - 20000 J, while the duty ratio was varied between 10% and 96%. The spatial peak intensity level was therefore between 104.17 W/cm² and 1666.67 W/cm² and the exposure time was between 30 s and 120 s. After each exposure, the tissue was sliced laterally into slices with the thickness of 1.75 mm and the volume of the lesion was calculated by integrating the area of the lesion in each slice over the axial dimension.

Results

Results showed that with the same total energy level, the volume of the lesion would increase when the duty ratio was shortened. The lesion volume, increased approximately linearly as the decrease in duty ratio, was up to 20 times larger than that at the highest ratio. It was also found that for the same exposure time at 120 s, if the duty ratio and peak intensity level were carefully designed, lower total energy of 10000 J could even produce lesions 4 times larger than those produced with a total energy of 15000 J. Furthermore, with less total deposited energy, the problem of pre-focal damage was reduced.

Discussion and Conclusions

The findings in this study have the potential to be used in treatment planning by helping to determine a suitable treatment regime for each specific patient. By choosing the optimal exposure parameters, the efficacy and safety of the treatment can be greatly improved.

2B-4**3:15 PM Cavitational Anti-tumor Effects with Phase-change Nano Droplet and Ultrasound**

Ken-ichi Kawabata¹, Rei Asami¹, Takashi Azuma¹, Shin-ichiro Umemura², ¹Life Science Research Center, Central Research Laboratory, Hitachi, Ltd., Kokubunji, Tokyo, Japan, ²Department of Electrical and Communication Engineering, Tohoku University, Sendai, Japan

Background, Motivation and Objective

Although HIFU therapy is well established as a minimally invasive cancer treatment, there is a great demand for an improved throughput on total operation time. One of approaches for improving the throughput is using microbubbles as sensitizers for coagulating larger volumes with each shot of HIFU. We further propose the use of nano-sized precursor of microbubbles instead of microbubbles for a controlled distribution of bubbles inside body[1]. The precursor is designed to convert into bubbles upon ultrasound pulses, thus microbubbles are generated only at the focus of the pulse. In this paper, preliminary *in vivo* results on anti-tumor effects will be presented with the exposure of relatively low frequency ultrasound (around 1 MHz) in the presence of the microbubble precursors.

Statement of Contribution/Methods

The nano sized microbubble precursor was prepared by high-pressure (20 MPa) homozinizing of the mixture of phospholipids liposome and volatile perfluorocarbons (phase-change nano droplet, PCND). Focused ultrasound transducer (frequency: 1.1 MHz, diameter: 40 mm, F number: 1.2) was used as the source for the activation of the precursor and exposure for therapy. The exposure time was set to 1 ms for the activation of PCND and 20 sec for therapy. *In vivo* effect of the ultrasound exposure was investigated with tumor-bearing mice while monitoring with medical ultrasound scanner. PCND was injected intravenously.

Results

The effect of the combination of PCND and ultrasound (0.5 kW/cm²) on tumor growth was investigated. When both PCND and ultrasound were applied, the tumor size was reduced to less than measurable limit (< 1 mm³) 4 days after treatment, while ultrasound alone showed almost no effect on the tumor growth. Furthermore, it was suggested that the therapy process can be ultrasonically monitored. The echo intensities at the focus of therapeutic ultrasound increased when exposure was started and kept about the same value, though, suddenly decreased to pre-treatment level when tissues were destroyed.

Discussion and Conclusions

Our results suggested that the combination of PCND and 1-MHz ultrasound can provide an energy-efficient ultrasound therapy compared to ultrasound alone. It was also suggested that the combinational therapy can monitor the therapeutic process with the aid of diagnostic ultrasound scanner. Such a therapeutic modality would provide a safe and high-throughput cancer treatment.

Reference

[1] K. Kawabata, *et al.*; Jpn. J. Appl. Phys. **44** 4548 (2005)

Acknowledgement

Part of this work was supported by the New Energy and Industrial Technology Development Organization of Japan.

2B-5

3:30 PM Active protection in pulsed cavitation ultrasound therapy (histotripsy)

Tzu-Yin Wang¹, Zhen Xu¹, J Brian Fowlkes², William Roberts¹, Charles Cain¹; ¹*Biomedical Engineering Department, University of Michigan, USA*, ²*Radiology Department, University of Michigan, USA*

Background, Motivation and Objective

The goal of this study is to develop strategies for producing precise lesions during a histotripsy treatment while actively "protecting" selected adjacent zones. The cavitation damage threshold in the pre-selected zone may be raised by destabilizing cavitation nuclei using appropriate protection pulses. We investigate spatial-temporal pulsing strategies for active protection.

Statement of Contribution/Methods

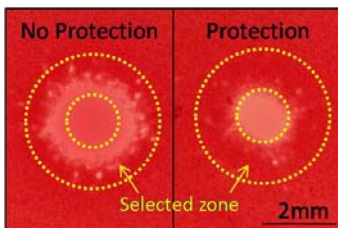
A 1-MHz 512-channel therapeutic array was used to deliver both the protection and the therapy pulses. The therapy pulses consisted of 10-cycle 1-MHz pulses delivered at 15-MPa peak negative pressure and 100-Hz pulse repetition frequency. A ring area with a 1.4-mm inner diameter and a 3.5-mm outer diameter was selected to be "protected." This area was scanned with a 1-MHz 20-cycle ultrasound pulse at 4-MPa peak negative pressure using a rotational multi-foci pattern 30 μ s prior to each therapy pulse. To study effects of the protection pulses on bubble clouds, high speed imaging of the bubble clouds generated with and without protection pulses was conducted. The histotripsy treatments were performed in red blood cell-gel phantoms, where cavitation damage was clearly indicated by the color change resulting from local cell lysis. The total area of damage in the selected zone, and the diameter of the overall lesion, was compared between lesions induced with and without active protection.

Results

High speed imaging showed a substantial decrease in the number of bubbles in the selected zone when the protection pulses were applied. The cloud width was narrowed from 2.5 ± 0.3 mm (N=8) to 1.1 ± 0.5 mm (N=8) using active protection. Results from 27 histotripsy treatments in red blood cell-gel phantoms showed that the damage area was reduced by 70 \pm 10% in the protected zone. The lesion diameter decreased from 2.2 ± 0.4 mm (N=14) to 1.6 ± 0.1 mm (N=13) with active protection. Example lesions produced with and without active protection are shown in Figure 1 (damaged area shown in white).

Discussion and Conclusions

Active protection of selected zones adjacent to histotripsy therapy zones is feasible using destabilizing bubbles. The active protection strategy may reduce damage in selected adjacent zones, allowing precise treatment of target tissues while protecting critical structures.



3:45 PM **Nonlinear Derating Method For High Intensity Focused Ultrasound (HIFU) Fields**

Olga V. Bessonova¹, Vera A. Khokhlova², Michael S. Canney², Michael R. Bailey², Lawrence A. Crum²; ¹Dept. of Acoustics, Physics Faculty, Moscow State University, 119991 Moscow, Russian Federation, ²Center for Industrial and Medical Ultrasound, Applied Physics Laboratory, University of Washington, Seattle, WA 98105, USA

Background, Motivation and Objective

Current methods of determining high intensity focused ultrasound (HIFU) fields in tissue rely on extrapolation of measurements in water assuming linear wave propagation both in water and in tissue. Neglecting nonlinear propagation effects in the derating process can result in significant errors. In this work, a new method is introduced that can be used to estimate focal parameters of nonlinear HIFU fields in tissue with greater accuracy. The hypothesis is that increasing the source output to overcome linear attenuation in the tissue path will result in the same peak pressure and focal waveform in tissue as in water at the initial output.

Statement of Contribution/Methods

A derating method was first tested using numerical simulations of the KZK-type equation and then validated experimentally. Simulations were performed over a wide range of source outputs and geometries ranging from diagnostic sources, with focusing gains of 5-10, to sources used in high intensity focused ultrasound, where the focusing gains were 40-60. Focal waveforms calculated in water and in tissue were compared not for the same source pressures as it is usually done in existing derating techniques, but for the same focal pressures equalized by scaling the source outputs. The scaling factor accounted for losses over the prefocal path in tissue and was approximated by the linear attenuation at the source frequency. Experiments were performed in water, absorptive tissue phantom, and *ex vivo* tissue. A 2 MHz HIFU source of 44 mm aperture and focal length was operated at various excitation levels at which *in situ* intensities reached 25 kW/cm² and large amplitude shocks formed at the focus. A fiber-optic hydrophone of 100 μ m size and 100 MHz bandwidth was used in the pressure measurements.

Results

Good agreement was demonstrated between focal waveforms obtained in direct simulations in tissue and those calculated in water for lower outputs that were scaled using the proposed method. The derating technique worked well for both slightly distorted and shocked focal waveforms. The accuracy of the method to predict focal intensity and peak positive pressure increased from 35% for weakly focused diagnostic transducers having a linear gain of 5-10 to 5% for strongly focused therapeutic transducers having linear gain of 40-60. Peak negative pressure was derated with the accuracy of 5% for both low and high gain sources. The measurements in water and behind absorptive phantom and tissue with scaling the source amplitudes also gave similar waveforms.

Discussion and Conclusions

A derating method for nonlinear HIFU fields was proposed and validated. Simulations and experimental data demonstrate that for HIFU sources with high focusing gains, the focal field parameters in tissue can be determined from the results of modeling or measurements in water even in the presence of shocks. [Work was supported in parts by NIH EB007643, NSBRI SMST01601, and RFBR 09-02-01530 grants.]

3B. Transducers & Ultrasound Modeling

Sala 4

Monday, September 21, 2009, 2:30 pm - 4:00 pm

Chair: **Yongrae Roh**
Kyungpook University

3B-1

2:30 PM Design of a High Intensity Focused Ultrasound multi-element phased array transducer for transcatheter treatment of liver tumours

Pierre Gelat¹, Ian Rivens², Gail ter Haar^{2,1} ¹Quality of Life Division, National Physical Laboratory, Teddington, United Kingdom, ²Joint Department of Physics, Institute of Cancer Research, Sutton, United Kingdom

Background, Motivation and Objective

The efficacy of high intensity focused ultrasound (HIFU) for the non-invasive treatment of cancer has been demonstrated for a range of cancers including those of the liver, prostate and breast. As a non-invasive focused therapy, HIFU offers considerable advantages over other interventions such as chemotherapy and surgical resection, in terms of invasiveness and harmful side effects. Despite its advantages, there are a number of significant challenges currently hindering its widespread clinical application. One of these challenges is the need to transmit sufficient energy through the rib cage to induce targeted tissue necrosis whilst minimising the formation of unwanted side lobes.

Statement of Contribution/Methods

This study involved the design and modelling of a randomly distributed 256-element bowl-shaped phased array transducer. Each element consisted of a PZT ceramic cylinder with a quarter-wavelength matching layer, modelled using the finite element method. The full piezo-elastic properties were included in the model. This represents a step forward from many HIFU transducer models in the literature, which usually assimilate each element to a rigidly vibrating plane circular piston. Operation in water under linear propagation conditions was assumed. A sensitivity analysis on the array design parameters was carried out and the ultrasonic field computed using boundary element techniques at required field positions. Shadowing representing the presence of ribs, was imposed on the pressure field at selected locations, and the field forward propagated to locations close to the geometric focus using the angular spectrum approach. Optimisation was then used to determine the values of the magnitude and phase of the voltage across each element's electrodes required to achieve a local maximum at the required treatment region.

Results

This analysis shows that, using a random multi-element phased array transducer, it is possible to achieve a focused beam through a shadowed array representing the ribs and to electronically steer the beam centimetres from the geometric focus without generation of substantial side lobes.

Discussion and Conclusions

This model represents a useful design tool for determining the specifications of a prototype device for transcatheter HIFU therapy for liver (and perhaps kidney and pancreatic) tumours. With the aid of distributed computing methods, it is hoped that accounting for the dynamic properties of the ribcage in three dimensions, as well as effects of nonlinear propagation, will be possible in the near future.

3B-2

2:45 PM Aperiodic and Deterministic 2D Phased Array Structures for Ultrasonic Imaging

Andrew Tweedie^{1,2}, Gordon Hayward², Victor Murray¹; ¹Alba Ultrasound, Glasgow, Lanarkshire, United Kingdom, ²Centre for Ultrasonic Engineering, University of Strathclyde, Glasgow, Lanarkshire, United Kingdom

Background, Motivation and Objective

Many ultrasonic imaging applications require ultrasonic phased arrays capable of rapid volumetric steering, and to do so, some form of two-dimensional (2D) array is necessary. However, such devices have typically required a

large increase in the number of active array elements, with inevitable constraints on performance and cost effective manufacture. We propose a new, flexible design approach, which allows the array to be closely tailored to a given application. This allows a reduction in the number of elements needed to achieve a specified beam shape, when compared to more traditional sparse 2D array designs.

Statement of Contribution/Methods

Conventional sparse 2D arrays have been restricted to grids, rings, simple repeating structures, and random distributions. These offer limited flexibility in terms of sidelobe levels, beam shapes and the number of elements required to achieve a specific design goal. Our process, which is based on evolutionary structures that are encountered routinely in the natural world, allows the designer to choose an apodization function, which determines the beam shape and sidelobe structure. In addition, the overall apodisation created by the layout of the array's elements can be used to create a naturally collimated beam, without the need for electrical transmit apodisation. The designer specifies the number of active elements to be used, and the desired aperture. Mathematical optimization is then used to modify the parameters of a deterministic array structure in order to minimize the worst case sidelobe level. A variety of structures have been investigated, and are aimed at achieving rotational symmetry and low side lobe levels in the beam structure. The aperiodicity of the structures avoids aliasing, suppressing grating lobes in the beam. Rotational symmetry smooths the sidelobe floor, avoiding peaks.

Results

The simulated beam profiles of these novel arrays are presented, and compared to that of more traditional array structures. It is shown that the new designs have lower sidelobes under both CW and pulsed excitation. Sidelobe levels were reduced by 6 dB over an equivalent periodic grid, and 3 dB over a random design. A range of apodization functions are shown to demonstrate that the beam shape can be adjusted to meet the design specification. Finally, experimental results are presented to show that these novel arrays offer functional imaging performance, while using significantly fewer elements than standard designs. A 127 element array, with a circular aperture of 16λ was used to image flat bottom holes in an aluminum block. A traditional $\lambda/2$ spaced grid would require over 800 elements.

Discussion and Conclusions

This design approach makes it possible to construct high resolution 2D arrays, without incurring the costs of purchasing large array controllers, with many hundreds of channels. This makes these arrays well suited for applications where cost, power consumption, and weight must all be kept to a minimum.

3B-3

3:00 PM Calibration of Acoustic Trapping Forces by Fluid Drag Forces

Jungwoo Lee¹, K. Kirk Shung^{1,2} *Biomedical Engineering, University of Southern California, Los Angeles, CA, USA*

Background, Motivation and Objective

Forces applied on micron-sized particles must be calibrated to reliably characterize acoustic tweezers, a device that can be used to non-invasively control the particle motions. It was proposed that an acoustic trap can be formed by a sharp intensity gradient near the focus, and the particle size greater than the ultrasonic wavelength. Given a Gaussian intensity distribution, the maximum trapping forces applied by the tweezer, using the numerical method in the previous studies, can be calculated in the ray acoustics regime and later balanced with viscous drag forces. This paper then analyzes the particle or escape velocity using viscous drag forces, to estimate the applied forces on trapped particles and to help design the experimental configuration for the force calibration.

Statement of Contribution/Methods

Viscous drag forces exerted by fluid flows have commonly been used to calibrate forces. It is assumed that a lipid particle of 125 μm in diameter is trapped underneath an acoustically transparent mylar film, when a 36 MHz ultrasonic transducer excited by sinusoidal bursts. To find the escape velocity, the maximum trapping forces are computed and then balanced with drag forces by Stokes' law. Note that inertial forces are negligible due to low Reynolds numbers for microparticles. The drag effect, however, can be larger when the distance between the particle and the film becomes comparable to the particle radius (Faxen's law). So the drag forces must be corrected by Happel's method before the calibration.

Results

The estimated maximum trapping force was 35 nN for the peak intensity of 141 W/cm² at the focus of 3 mm. The corresponding escape velocity was calculated to be 9.6 mm/s, and its TI and MI were 0.17 and 0.22, respectively.

Prior to the correction the escape velocity was 29.7 mm/s, higher than the corrected one. This implies that the lower velocity is needed to calibrate the trapping force in the current version of acoustic tweezers than otherwise.

Discussion and Conclusions

The calibration method using viscous drag forces was demonstrated for stationary particles to estimate the applied trapping forces in the order of tens of nano-Newtons. In contrast to optical tweezers where only relatively small escape velocities ($\sim 20 \mu\text{m/s}$) could be measured, the resultant escape velocity indicated that the acoustic trapping of micron-sized particles was capable of producing much faster particle motions or larger forces than its optical counterpart. The drag effect of fluid flows near the film must be corrected because the calibration results may considerably differ from otherwise.

3B-4

3:15 PM Estimation of Material Parameters for Piezoelectric Actuators Using Electrical and Mechanical Quantities

Stefan Rupitsch¹, Felix Wolf¹, Alexander Sutor¹, **Reinhard Lerch¹**; ¹*Department of Sensor Technology, Friedrich-Alexander-University Erlangen-Nuremberg, Germany*

Background, Motivation and Objective

By means of numerical simulations the efforts for the development of piezoceramic actuators and sensors including piezo-composite transducers can be considerably decreased. However, the reliability of these simulations depends on the accuracy of the required material parameters. The common approaches to determine these parameters are based on the IEEE or CENELEC standard, for which well-defined geometries of the investigated piezoceramic material are mandatory. It is obvious that such approaches are not applicable for a variety of transducers, e.g. piezo-composites. Hence, there is a great demand for an alternative method concerning parameter determination, which does not require different sample geometries.

Statement of Contribution/Methods

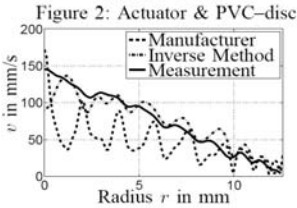
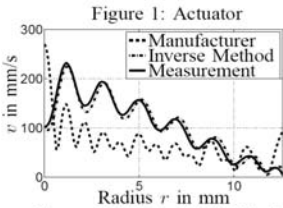
Our research is concentrated on Finite Element (FE) based Inverse Methods in order to determine the non vanishing entries of the material tensors for the investigated piezoceramics. So far, we used the frequency resolved electrical impedance as input quantity of the Inverse Method. Although the resulting material parameters provide a better matching of simulations and measurements, the occurring deviations in the mechanical displacements are remarkable. On account of this fact, we extended the Inverse Method. The novel method considers both, the frequency resolved electrical impedance as well as the spatially resolved mechanical displacement (or surface normal velocity).

Results

Figure 1 shows the measurement and simulation results of the spatially resolved surface normal velocity for an investigated piezoceramic disc (diameter 25.2 mm; thickness 2.0 mm; material Pz27). In contrast to the manufacturer's material parameters, the novel Inverse Method yields parameters which can be used for reliable FE simulations. In addition, the estimated parameters were used to determine the surface normal velocity of a transducer (Fig. 2), which is composed of the piezoceramic disc and a disc made of polyvinyl chloride (PVC). Again, the parameters of the Inverse Method provide reliable simulation results, while against that, the manufacturer's material parameters are not suitable to describe the behavior of the investigated transducer.

Discussion and Conclusions

The results clearly show that the Inverse Method is applicable for material parameter estimation. Currently, the novel method is applied for different actuator shapes.



3B-5

3:30 PM **Parameter sensitivity study of a Field II multilayer transducer model on a convex transducer**

David Bæk¹, Jørgen Arendt Jensen¹, Morten Willatzen²; ¹Department of Electrical Engineering, Technical University of Denmark, Kgs. Lyngby, Denmark, ²Mads Clausen Institute for Product Innovation, University of Southern Denmark, Sønderborg, Denmark

Background, Motivation and Objective

A multilayer transducer model for predicting a transducer impulse response has in earlier works been developed and combined with the Field II software. This development was tested on current, voltage, and intensity measurements on piezoceramic discs (Bæk et al. IUS 2008) and a convex 128 element ultrasound imaging transducer (Bæk et al. ICU 2009). The model benefits from its 1D simplicity and has shown to give an amplitude error around 1.7-2 dB. However, any prediction of amplitude, phase, and attenuation of pulses relies on the accuracy of manufacturer supplied material characteristics, which may be inaccurate estimates. The previous test cases have assumed the simulation parameters to be exact as received from the manufacturer. In this paper the influence of a deviation in the accuracy of the different parameters is studied by comparing simulation and measurement. The objective is a quantitative calibrated model for a complete ultrasound system. This includes a sensitivity study as presented here.

Statement of Contribution/Methods

The study alters 35 different model parameters which describe a 128 element convex transducer from BK Medical Aps. The changes are within $\pm 20\%$ of the values supplied by the manufacturer, which are considered the zero reference (ZR). Simulations of a system consisting of a transmit unit, a five material layer transducer, and the Field II predicted pressure are performed by altering in turn the value of a single parameter in steps of 2%. The remaining simulation parameters are held fixed at the ZR. The influence of the parameter change is determined by calculating the pressure and the intensity at a distance of 112 mm on an element's center axis and comparing it with hydrophone measurements. These are performed with a water bath hydrophone setup using an Agilent MSO6014A oscilloscope that is set to average consecutive pulses 48 times for noise reduction of the hydrophone output. A commercial transmitter unit is used to drive the transducer with a 10 cycle tone burst at a frequency of 4.0 MHz and a maximum excitation amplitude of 31 volt.

Results

Predictions using the ZR give a pressure pulse error (PPE) and an intensity error (IE) of 32% and 23%, respectively, relative to the measured response. Altering the piezoelectric permittivity +12% from ZR decreases the PPE to 30% and the IE to 2% relative to the measured. Changing the stiffness constant of the lens -4% from ZR increases the PPE and the IE with 6% and 1%, respectively. Performing the same with the ceramic stiffness the PPE is lowered 1.5% and the IE is lowered 12%.

Discussion and Conclusions

PPEs are found mainly to be sensitive to lens properties and piezoceramic properties, but minor sensitive to changes in matching layers. IEs are mainly sensitive to the piezoceramic properties. The study shows that minor changes can improve predictions significantly.

3B-6

3:45 PM A triangle-cut piezocomposite structure for application in hexagonal-shaped 2D Ultrasonic array for NDE Applications

Jerzy Dziejewicz¹, Anthony Gachagan¹, Richard L. O'Leary¹, Nishal S. Ramadas¹, Gordon Hayward¹; ¹Centre for Ultrasonic Engineering, University of Strathclyde, United Kingdom

Background, Motivation and Objective

Present 2D ultrasonic arrays for NDE applications suffer from low SNR and limited steering capabilities. Yet, there is a great desire to increase the operational frequency, in order to enhance their imaging resolution. State-of-the-art arrays use orthogonal matrix of rectangular elements, as this is a natural step forward from the conventional 1D array structure. The objective of this work is to evaluate properties of 1-3 connectivity piezoelectric composites wherein the ceramic phase comprises triangular prismatic pillars, rather than more typical parallelepiped pillars. The triangular prismatic pillars are arranged such that a hexagonal-element 2D array structure will result.

Statement of Contribution/Methods

The hexagonal array element offers advantages of increase aperture, low element pitch and enhanced volumetric coverage, when compared to the more typical orthogonal array structure. Additionally, the triangular prism pillar offers improved mechanical robustness, a significant advantage in the manufacture of high-frequency arrays.

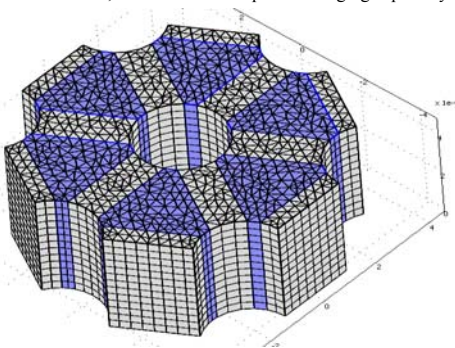
A combination of PZFlex and COMSOL models has been utilized to predict behaviour of the hexagonal array structure, finding acceptable levels of inter-element cross-coupling.

Results

2.25MHz and 3MHz prototype devices, both orthogonal and the new hexagonal substructure, have been manufactured. The measured mechanical cross-coupling level is -18dB between neighbouring elements and excellent corroboration between measured and FE modelled device behaviour is demonstrated. Finally, a drilled version of the microstructure (Figure 1) has been simulated using COMSOL. This modified structure is predicted to further improve device sensitivity and mechanical cross-talk in the hexagonal structure.

Discussion and Conclusions

It is argued that hexagonal microstructure piezocomposite offers significant advantages over orthogonal microstructure, which result in improved imaging capability of resulting 2D ultrasonic array.



4B. Advances in NDE

Tarragona

Monday, September 21, 2009, 2:30 pm - 4:00 pm

Chair: **David Greve**
Carnegie Mellon University

4B-1

2:30 PM EMAT's and its potential for modern NDE – State of the art and latest applications

Hans-Juergen Salzburger¹; ¹Fraunhofer IZfP, Saarbruecken, Saarland, Germany

Background, Motivation and Objective

Electro Magnetic Acoustic Transducers (EMAT) are a well known type of ultrasonic probes used for non-destructive evaluation (NDE) of electrically conductive materials.

Ultrasonic Testing (UT) is mostly performed by longitudinal waves and mode converted shear-waves generated by piezoelectric probes. EMAT's are broadening the range of usable wave modes by the direct conversion of polarized shear waves with normal and angle beams and the selective generation and detection of nearly all types of guided waves. Despite their limitations (low efficiency, lift-off sensitivity, limited frequency range etc.) they have the big advantage to perform UT without couplants. The dry coupling allows UT at elevated temperatures, in media which do not tolerate liquids (e.g. natural-gas pipelines), on sensitive or coated surfaces of blanks used for car bodies in the automotive industry etc.

NDE is not only related to defect detection but more and more to material state and condition analysis and monitoring. To this end, polarization, dispersion, propagation velocity, and mode conversion are physical parameters usable for improved and high sophisticated non-destructive measurements.

Statement of Contribution/Methods

The contribution will put special emphasis on the unique capability of EMAT's for generation and detection of polarized shear waves as well as angled beams of horizontally polarized shear (SH)-waves as straight beams of linearly or radially polarized shear waves. Guided modes of SH-waves in plates and tubes - not yet widely used for UT due to the lack of availability of appropriate probes and equipments - are a further topic of the presentation.

Results

New solutions for UT by polarized Shear waves and guided waves are presented: For the in-line inspection for defects and weld geometry of butt welds, for crack inspection in gas pipelines, for screening of hidden corrosion in tubular goods, for long range inspection of pipes and for the inspection of multilayered aircraft components.

The latest developments of the probe design are reported in brief. The equipments and their integration in production lines as well for in-service application are shown together with examples of inspection results during their practical applications.

Discussion and Conclusions

4B-2

3:00 PM High-Frequency Focusing Poly(Vinylidene fluoride-trifluoroethylene) Transducers and Measurements of Elastic Constants of Thin Layers

Yung-Chun Lee¹, Cheng-Hsien Chung¹; ¹Mechanical Engineering, National Cheng Kung University, Tainan, Taiwan, Taiwan

Background, Motivation and Objective

PVDF and its copolymer such as P(VDF-TrFE) films have been widely used in making ultrasound transducers. There are two approaches: to permanently deform a piezoelectric polymer film into a concave shape or to form a piezoelectric polymer film by spin-coating on a concave surface. The latter is favorable in achieving focusing transducers with higher operating frequency and wider aperture angle, and both are important in the so-called

lensless acoustic microscopy and $V(f,z)$ measurements. In this work, we proposed a new approach in making high-frequency PVDF-based focusing transducers. The fabricated transducers are then used for accurate determination of dispersion curves of thin plates or layered medium, with the goal of accurate determination of their elastic constants.

Statement of Contribution/Methods

We have successfully integrated three key elements, namely, the high-speed spinning, pneumatic air-pressuring, and infrared thermal heating, into a transducer fabrication system which allows high-quality [P(VDF-TrFE)] copolymer films being uniformly coated on either spherical or cylindrical concave surface of a substrate. The ferroelectric hysteresis loops of the spin-coated P(VDF-TrFE) films are measured to establish the best fabrication parameters. The fabricated transducers are used for high-frequency wave velocity measurements from few MHz up to 120 MHz, and for non-destructive determination of elastic constants of thin plates and coatings.

Results

Several point-focused and line-focused P(VDF-TrFE) transducers are successfully fabricated. The radius of curvature ranges from 1 mm to 15 mm, and the full aperture angle covers from 30 to 100 degrees. The film thickness is from few to few tens of micrometers and is uniformly distributed along the full aperture. The central frequency of transducer varies from few MHz up to 70 MHz, and typical -6 dB bandwidth around 80% to 120%. Based on these transducers, defocusing measurement system and $V(f,z)$ waveform processing method are developed and implemented. Both surface waves and Lamb waves with frequency up to 120 MHz are accurately determined and multiple modes of dispersion curves are measured, which are then inversely used for calculating the elastic constants of samples under investigation. Good results are obtained with an estimated error less than 5%.

Discussion and Conclusions

A modified spin coating process is successfully developed to fabricate P(VDF-TrFE) copolymer ultrasound transducers. Ferroelectric hysteresis loops of the spin-coated P(VDF-TrFE) copolymer films are measured for determining the best fabrication parameters and conditions. The fabricated transducers are used for non-destructive determination of elastic constants of thin plates and coatings. The test results show good agreement with the reported materials data provided by the manufacturers.

4B-3

3:15 PM Ultrasonic Probes Simultaneously Producing One Longitudinal and Two Shear Waves and Their Potential Applications

K.-T. Wu¹, M. Kobayashi², C.-K. Jen², L. Zhao³; ¹Electrical and Computer Engineering, McGill University, Canada, ²Industrial Materials Institute, National Research Council Canada, Canada, ³The State Key Laboratory of Polymer Materials Engineering, Sichuan University, China, People's Republic of

Background, Motivation and Objective

The Young's modulus, shear modulus, Poisson's ratio, texture, stress and thickness of materials or manufactured parts may be measured concurrently at elevated temperatures by using an ultrasonic probe which can generate and receive simultaneously one longitudinal (L) and two orthogonally polarized shear waves (S_V and S_H). One objective of this research is to develop such probes. Another objective is to use such probes to perform NDE of materials and real-time non-invasive monitoring of polymer injection molding process at high temperatures so that the desired part properties can be obtained on-line.

Statement of Contribution/Methods

Piezoelectric integrated ultrasonic transducers (IUTs) directly coated onto probes and mold inserts made of steels have been made and used to excite and detect L, S_V and S_H simultaneously in pulse-echo modes using proper mode conversion angles. The coating was done by a sol-gel spray technology. They can operate at temperatures above 150°C. This may be the first time such probe is made and used for the on-line polymer injection molding. The theories explaining the capabilities of these probes to measure simultaneously the above mentioned material and part properties will be provided.

Results

Piezoelectric lead-zirconate-titanate thick (~75 μm) composite films have been deposited onto side edges perpendicular to each other at the top of steel rods as IUTs. One of them generates and receives both L and S_V waves and another S_H . The signal-to-noise ratios (SNRs) of the echoes obtained in pulse echo mode are higher than 23 dB and have a center frequency around 15 MHz. Such sensors have been also fabricated onto special mode inserts of a 150-ton Injection Molding machine and real-time non-invasive ultrasonic polymer injection molding process monitoring was carried out. All ultrasonic measurements were performed by a two-channel system.

Discussion and Conclusions

L , S_V and S_H waves can be simultaneously generated and received at high temperatures with piezoelectric miniature IUTs. Such probes may be used to measure thickness of a sample accurately together with a correction of texture including texture coefficients such as W_{400} and W_{420} . The stress applied to the probe may be also measured. Because they can sustain high temperatures, on-line ultrasonic measurements of Young's modulus, Shear modulus and anisotropy of the molded or casted parts during polymer injection molding and light weight metal die casting may be achieved.

4B-4

3:30 PM Nondestructive Characterization of Radially Oriented Hydride in Zircaloy Cladding Tubes with a Laser Ultrasound Technique

Cheng-Hung Yeh¹, Che-Hua Yang¹; ¹Institute of Manufacturing Technology, National Taipei University of Technology, Taipei, Taiwan

Background, Motivation and Objective

Degradation of mechanical properties in Zircaloy cladding tubes commonly used in nuclear fuel are well known to be related to the concentration of precipitated hydrides. The fuel integrity can be threatened while the hydrides concentration reaches a critical value. Besides concentration, the hydride orientation is recently found out to be another key factor influencing the mechanical integrity; hydrides orientated in the radial direction (Fig. 1) reduce the fracture toughness much more than the circumferentially orientated ones.

Statement of Contribution/Methods

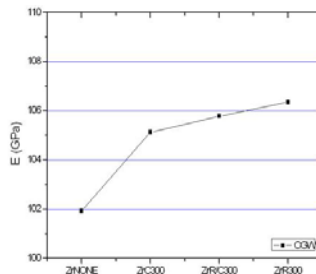
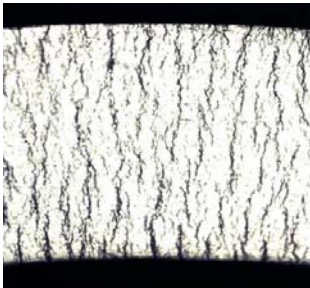
This research is focused on characterizing Zircaloy cladding tubes with different concentration ratios between radially(R) orientated hydrides and circumferentially(C) ones. A procedure corporate with an experimental technique and an inversion algorithm is used to investigate the effects of R/C ratio on the dispersion spectra of guided waves (GW) propagating in the tubes. A laser ultrasound technique (LUT) is used to measure the dispersions of circumferential guided waves (CGW) propagating along the circumferential direction of the cladding tubes. An inversion algorithm based on simplex method is used to extract interested properties from the measured GW dispersion spectra.

Results

With good measurement accuracy, the measured CGW dispersion spectra is able to be distinguish different levels of hydrogen concentration in the cladding tubes. In the meanwhile, as shown in Fig. 2, this procedure is able to distinguish the R/C ratio in a quantitative way. It is also observed that the bulk elastic modulus increases as the R/C ratio increases.

Discussion and Conclusions

This method is potentially useful to probe the hydrogen concentration and the associated R/C value in a remote and nondestructive way which is desired in nuclear power industry.



4B-5

3:45 PM **Railway Wheel-Tread Inspection by Ultrasonic Techniques**

Jose Brizuela¹, Alberto Ibañez¹, Carlos Fritsch¹; ¹*Instituto de Automática Industrial, La Poveda - Arganda del Rey, Madrid, Spain*

Background, Motivation and Objective

Nowadays, high speed trains represent a real technology challenge to cover long distances in the less time possible. Transport security and quality require a proper and effective maintenance system to avoid related risks and to prevent incidents and accidents. Wheels are the critical part of the train and must be watched very closely. Typical wheel tread damages are flat, shelling, spalling and cracks. Infrastructure and rolling stock get worse through vibrations and noise caused by irregular rail-wheel contact. Moreover, wheel tread damages found at early stage can help to keep the passengers safe and the train in service.

Many NDT inspection systems are used today such as Eddy current and ultrasounds. However, most of them are off-line methods and poorly time-efficient during maintenance processes. This work proposes a different approach, a new inspection system for railway wheels using a dynamic ultrasonic technique. This method can be applied to trains moving at low speed (10-15 Km/h typical) and allows all wheelsets mounted to be inspected within a few seconds.

Statement of Contribution/Methods

The proposed system determines wheel tread damages while the train moves at a low speed over a measuring rail. The special rail is used to propagate Rayleigh wave pulses at regular intervals. Echoes produced by the rail-wheel contact, while the train is moving, are recorded by a piezoelectric transducer. Time of flight measurements are used for a) tracking the wheel movement and b) determining the rail-wheel contact condition. Damages on the wheel tread can be also sized.

Results

The method described is able to detect different tread irregularities, such as flat, shelling and spalling. The system is a dynamic technique that allows checking the railway wheels while the train is in movement within speed limits (1 and 3m/s). The suggested technique allows determining length irregularities with 4mm resolution.

Discussion and Conclusions

The system represents an innovation for NDT by ultrasound field where defects are considered as static reflectors. The system can be placed at the entrance of repairs shops where routine inspections are carried out in order to reduce time for maintenance schedules. Tread damage detection does not consider wheel impact loads nor uses optical systems. Moreover, moving parts are not required by the online inspection method described. As a conclusion, a reliable flat detection on wheels can be performed in a minimum time, guaranteeing a commensurate cost-profit ratio for railway companies.

5B. SAW Modelling

Pergamo

Monday, September 21, 2009, 2:30 pm - 4:00 pm

Chair: **Karl Wagner**
EPCOS AG

5B-1

2:30 PM SAW Strain Sensitivity of Selected Rayleigh Wave Crystal Cuts

Gudrun Bruckner¹, Gernot Stampf¹, Georg Franz¹, Robert Hauser², Rene Fachberger¹; ¹Carinthian Tech Research AG, Villach, Austria, ²Carinthian University of Applied Sciences, Villach, Austria

Background, Motivation and Objective

Given its high pressure sensitivity and superior temperature compensation, standard quartz (ST-quartz) is the common substrate for wireless SAW pressure respectively force sensors. Drawbacks are its frequency limitations and poor coupling coefficient. In particular for medical applications, either for implants into the human body or integration into medical devices like external fixators, the operation temperature is obviously limited. Hence good signal coupling and higher frequencies may trump the temperature effects and thus, also other piezoelectric crystals with fair temperature dependencies are of practical interest. Yet, the force / strain sensitivity of such alternatives has rarely been investigated, limiting the options in sensor designs. This paper presents investigations to overcome this limitation.

Statement of Contribution/Methods

Of the available choices, Languisite LGS_138.5 with Euler angles of (0°|138.5°|26.6°) was selected for its low temperature coefficients of frequency and lithium tantalate LT_112.2 (x-cut, 112.2° y-direction) for its high frequency applicability. The measurements were referenced against ST-quartz (45°), using a differential delay line layout and measuring the impulse responses versus varying mechanical loads. A dedicated bending beam geometry test stand was designed for that and the actual mechanical loads were measured. The strain distributions in the SAW elements were calculated using advanced FEM methods considering anisotropic elasticity. The changes in delay times characterize the sensitivities of the substrate. Both values, the sensitivity to force and the calculated sensitivity to strain are used as evaluation criteria.

Results

For the given geometry the investigated change in delay time was caused by the elongation of the propagation path as well as by the change of the wave velocity. By calculating the strain the two effects could be separated. All three substrates exhibited linear behavior, correlating to the force and strain values. In comparison, quartz still shows the highest sensitivities; LGS_138.5 is weaker to an extent, that could be countered by the better coupling efficiency. LT_112.2, showing still weaker sensitivities, appears to be less suitable.

Discussion and Conclusions

While this study confirms the qualification of ST-quartz for pressure and force sensing applications, LGS_138.5 could be a viable alternative. While the actual force respectively strain sensitivity is lower, the factor 3.5 higher Rayleigh wave coupling coefficient makes this material interesting for special sensor applications. LT_112.2, finally, exhibits a sensitivity that is too low to be adequate for a practical pressure sensor.

5B-2

2:45 PM SAW Device Design using the Nelder-Mead Minimisation Algorithm

David Morgan¹; ¹Impulse Consulting, Northampton, Northants, United Kingdom

Background, Motivation and Objective

Most SAW bandpass filters need to be designed to satisfy demanding requirements on the frequency response, taking account of specified tolerances. In general the response is a very complex function of the design parameters, and it is necessary to take account of second-order phenomena such as multiple-transit signals, circuit

effects, diffraction and waveguiding. The discrepancy between the calculated response and the requirement can be expressed as an 'error' function which needs to be minimised. A global design algorithm is needed, minimising this complex function of a large number of variables (the design parameters), without having explicit information on the device analysis. By modifying the parameter values, the algorithm is required to progressively reduce the error, which eventually becomes small enough for the response to satisfy the specification. However, the complexity of the problem is such that the error is not monotonically reduced - at times, it needs to be allowed to increase.

Algorithms which do this include simulated annealing, the genetic algorithm and sequential quadratic programming. These are widely applicable to complex non-linear minimisation problems, and the latter two have been applied to SAW LCR design [1, 2]

1. J. Meltaus et al. 'Genetic Optimization Algorithms in the design of coupled SAW filters'. IEEE Ultrasonics Symp., 2004, pp. 1901-1904
2. R. Peach and Z. Xu. 'Design of LCR filters using non-linear optimization applied to simplified Green function models'. *ibid.*, 2006, p.78-81

Statement of Contribution/Methods

This paper describes use of the Nelder-Mead algorithm, which is a downhill simplex method [3]. Software has been developed for design of DART and LCR filters. It is shown that the algorithm is effective in design of DART and LCR filters. The algorithm is very versatile. It is capable of minimising an error function which is a very non-linear function of the design parameters, and can include step functions. It does not need differentials to be evaluated. The author's experience is that this method is very reliable and rapid in execution.

3. W.H. Press et al. 'Numerical Recipes', Cambridge Univ. Press, 1989.

Results

Design results show that the Nelder-Mead algorithm is very effective for design of DART and LCR filters, and examples are shown. The error to be minimised is a very non-linear function of the design parameters, including step functions.

The method is simple to programme and operates rapidly and reliably.

Discussion and Conclusions

The Nelder-Mead algorithm is applicable to a wide class of non-linear optimisation problems since the algorithm itself operates independently from the actual device analysis. It can cope with very non-linear functions, and it does not require evaluation of differentials.

5B-3

3:00 PM Performance Simulation of SAW Ring Waveguide Resonator by 3D FEM

Sergey Biryukov¹, Hagen Schmidt¹, Manfred Weinhacht¹; ¹*IFW Dresden, Dresden, Germany*

Background, Motivation and Objective

The ring waveguide resonator (RWR) as a new electrode structure for SAW devices has been proposed recently in [1]. Its behavior has been approximately estimated using the 2D scalar wave equation in polar coordinates [2]. The structure consists of an IDT in the form of a closed ring placed on the Z-cut of a hexagonal piezoelectric crystal like AlN. Thereby the IDT itself creates a waveguide effect on the substrate, which is isotropic in plane. It was shown that due to the structure regularity the electrical admittance of RWR does not have sidelobes and all possible angular modes besides the main one are completely suppressed. The main mode resonance has a high quality factor Q depending on the radiating loss into the surrounding region. The properties of such promising structure have to be investigated more carefully than in the frame of used 2D formulation. The objective of this work is a 3D simulation of the RWR.

Statement of Contribution/Methods

Because of the angular periodicity a single periodic cell of RWR is considered by the 3D FEM for all four components of the field. The periodic cell contains two electrodes and two busbars of finite thickness, which are placed on a cylindrical sector of the substrate. The substrate is restricted in depth and along the radius by an absorbing medium to suppress parasitic wave reflections from the external boundaries. In angular direction the periodic boundary conditions are imposed. So the formulation of the boundary-value problem corresponds to a real structure and the problem solution in fact is a numerical experiment for the RWR.

Results

The RWR has been calculated for one-degree angular period. It corresponds to 360 electrode pairs in the whole ring. The middle radius of RWR is 1060 microns and the RWR aperture with busbars is 120 microns. Material parameters for Al electrodes and AlN substrate are used. The frequency dependence of the RWR electrical admittance has five distinct narrow peaks at 294.9, 302.6, 308.2, 313 and 317.6 MHz with Q-factors 12900, 9200, 5000, 3600, and 5200, respectively. There are no sidelobes between the peaks. These peaks correspond to five transverse modes with mechanical displacement profiles containing from one to five oscillating loops along the aperture, respectively. The displacement field of the first mode is concentrated near the external ring radius and the field of following modes expands towards the internal radius.

Discussion and Conclusions

The first numerical experiment for the RWR demonstrates the excellent structure performance, which is outstanding for SAW devices. This means that such advantages of bulk acoustic wave devices as high selectivity and a large Q-factor are probably also achievable by SAW devices without losing their inherent simplicity of manufacturing. Obviously, the RWR structures can be attractive also for sensor applications.

[1] S. V. Biryukov, G. Martin, and M. Wehnacht, APL, 173503, 2007.

[2] S.V. Biryukov, H. Schmidt, and M. Wehnacht, Proc. 2008 IEEE Ultrason. Symp., 284-287.

5B-4

3:15 PM Characterization of Electrode Material Parameters

Ben Abbott¹, Alan Chen¹, Tim Daniel¹, Kevin Gamble¹, Julien Gratier¹, Taeho Kook¹, Natalya Naumenko^{2,1} *TriQuint Semiconductor, Apopka, FL, USA, ²Moscow Steel and Alloys, Russian Federation*

Background, Motivation and Objective

Rigorous methods to the analyses of SAW devices, such as FEM/SDA, rely upon the accurate characterization of the elastic moduli and mass density for both the piezoelectric substrate as well as the materials comprising the devices' thin film electrodes.

As the values for the moduli and density of thin films are different than those for bulk materials, and depend upon the process by which they are deposited, a means to characterize the values for these parameters for thin film materials is needed.

Statement of Contribution/Methods

To accomplish the goal of characterizing the moduli and mass density for a thin film metallization, an approach has been devised which is sensitive to the longitudinal and shear modulus, the thin film's mass density, as well as the geometry of the SAW device's electrodes.

In short; (1) a piezoelectric substrate supporting both a Rayleigh type SAW mode and a Shear Horizontal type SAW mode is selected. (2) One-port resonators, with varied periods and metallization ratios, are fabricated with the thin film metallization to be characterized. (3) The mean and standard deviation of the fabricated devices' resonant frequencies are measured. (4) The elastic moduli and density for the thin film are determined by applying nonlinear optimization to minimize the error between the numerical and measured values for the devices' resonant frequencies.

Results

Using the summarized approach, the elastic moduli and mass density for a thin film, proportionally composed of Copper, have been characterized.

The resulting RMS error between the mean of the measured resonant frequencies and the numerical results was found to be less than that of the standard deviation of the measurements. Which is an indication that the variation in the devices' physical geometry is of a greater significance as compared to the errors in the characterized elastic moduli and mass density.

Discussion and Conclusions

To validate the goal of characterizing the thin film's moduli and mass density for the accurate simulation of SAW devices, a comparison is made between measured experiments and numerical results obtained by using published bulk material values and the newly characterized values.

The characterized values are found to reduce the error between the measured and predicted resonant frequencies by about 50 times.

5B-5

3:30 PM Improved SHSAW Transduction Efficiency using Gratings and Uniform Electrode Guiding

Thomas Pollard¹, Mauricio Pereira da Cunha^{1,1} *Electrical and Computer Engineering, University of Maine, USA*

Background, Motivation and Objective

Pure shear horizontal surface acoustic wave (SHSAW) devices have been increasingly considered for liquid phase and bio-sensing applications due to their sensitivity to mass, stiffness, viscosity, and electrical surface perturbations, and ability to operate under liquid loaded conditions. The SHSAW is typically weakly guided or not even exists under a free surface boundary, e.g. ST-90 quartz. As a result strong excitation of spurious bulk acoustic wave (BAW) by the interdigital transducer (IDT) is typical. Alternatively, dense or thick electrodes in periodic or uniform configurations must be placed between IDTs in delay line devices to increase the ratio of SHSAW power to input power, η_{SH} . The degree of η_{SH} improvement depends on the structure metallization thickness, composition, and geometry.

Statement of Contribution/Methods

In previous work, the authors discussed η_{SH} using finite and boundary element method (FEM/BEM) models limited to cases of free or finite thickness periodic electrodes surrounding surfaces. This work extends the analysis to the important case of uniform semi-infinite electrode guiding, used in most liquid-phase and biosensor application. The far field SHSAW power generated by an IDT surrounded by uniform finite thickness guiding electrodes is determined based on the simulation of a truncated finite device which incorporates an acoustic matching electrode. This matching electrode makes the overall structure appear infinite, thus allowing the far-field behavior to be predicted.

Results

The η_{SH} is computed with both periodic and uniform electrode guiding on quartz ST-90 with Au metallization for varying number of IDT electrodes and film thicknesses. For 18 and 318 electrode split-finger IDTs surrounded by guiding gratings, for instance, η_{SH} goes from 25% to 90% for the Au film thickness relative to the wavelength ($h/l=0.234\%$). For the 318 electrode IDT, for instance, η_{SH} varies from 90% to 100% when the h/l is increased from 0.234% to 1.875%. For the case of uniform guiding electrodes, η_{SH} goes from 64% to 83% for $h/l=0.234\%$. For the 318 electrode IDT, η_{SH} goes from 83% to 92% when the h/l is increased from 0.234% to 1.875%. To verify the model an IDT with uniform guiding structures was simulated and compared to a fabricated device. The simulations predicted 9 dB directivity which was experimentally confirmed to within 1 dB.

Discussion and Conclusions

For the first time η_{SH} has been characterized for finite length IDTs with finite film thickness uniform guiding electrodes. The modeling technique created allows the evaluation of SHSAW transduction efficiency based on the sensor platform design parameters, such as film thickness, materials, and IDT geometry. The tool was experimentally verified and is useful in the design and development of SHSAW devices in order to exhibit improved transmission response and reduced BAW excitation, both for communication and sensor applications.

5B-6

3:45 PM **Introduction and Creation of Computational Nodes in Multilayered Micro-acoustic Device FEM Modelling**

Murat Muradoglu¹, Alireza Baghai-Wadji¹, Markus Mayer²; ¹*School of Electrical and Computer Engineering, RMIT University, Melbourne, Victoria, Australia*, ²*EPCOS AG, Munich, Germany*

Background, Motivation and Objective

Consider a Surface Acoustic Wave (SAW) or a Bulk Acoustic Wave (BAW) device that comprises a number of ideally-conductive massive metallic electrodes loaded by a sequence of elastic/piezoelectric layers of non-uniform cross-section. Current Finite Element Method (FEM) simulations of realistic device models result in a large system of equations which need to be re-calculated for any design modifications that may merely affect a small section of the device. Such design alterations may consist of only the re-arrangement of the position of layers and/or choice of the layer-, or substrate material. An accurate, flexible and fast simulation tool has to be developed to respond to this need.

Statement of Contribution/Methods

The proposed method involves the logical partitioning of the entire device structure into small non-overlapping physical subregions (computational nodes) that can be designed individually, solved independently and stored and retrieved effectively. Thereby, a key idea is our formulation and implementation of a generalized Impedance Boundary Condition (IBC) for arbitrary subregion geometry which will be presented for the first time. The IBC has been devised in order to accommodate fixed displacement, stress free, or arbitrary interface conditions in a unified form. This abstraction permits viewing any of physical subregions as a computational node. The proposed scheme has been designed to enable a further key feature which is the low data communications overhead between the computational nodes. The introduction of our IBC along with the low data communication overhead make this method highly suitable for parallel computation.

Results

Preliminary test runs for realistic SAW devices are encouraging and show acceleration of the computations by up to one order of magnitude, while assuring high accuracy. Comparisons with experimental data, and with alternative simulations will be presented.

Discussion and Conclusions

Given a complex physical layout of microacoustic devices, the proposed method allows flexible modification of the design parameters without necessitating the re-calculation of the entire device structure. The method achieves a high degree of accuracy, while substantially decreasing simulation cycles.

6B. Visualization Interferometry

Baalbek

Monday, September 21, 2009, 2:30 pm - 4:00 pm

Chair: **John D. Larson**
Avago Technologies

6B-1

2:30 PM Imaging surface acoustic waves on phononic crystal devices

Paul Otsuka¹, Sorasak Danworaphong², Motonobu Tomoda¹, Oliver Wright¹, Osamu Matsuda¹, Dieter Profunser¹, Yukihiro Tanaka¹, Abdelkrim Khetif³, Vincent Laude³, Sarah Benchabane³, ¹*Graduate School of Engineering, Hokkaido University, Japan*, ²*School of Science, Walailak University, Thailand*, ³*FEMTO-ST, Besancon, France*

Background, Motivation and Objective

Surface acoustic wave devices based on one-dimensional (1D) periodic structures have found extensive application in high-frequency signal processing. 2D phononic crystals exhibit interesting physical properties that have the potential to improve on and expand the range of these devices. Optical generation and detection of surface waves has proved effective in visualising their propagation in real time. Here we present results of real-time imaging of laser-induced surface acoustic waves at frequencies up to ~1 GHz in various phononic crystal structures.

Statement of Contribution/Methods

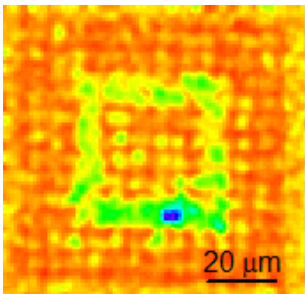
We use a Ti:sapphire laser to generate optical pulses of duration ~200 fs, wavelength 830 nm and repetition rate 76 MHz. A 415 nm pump beam derived from this laser excites surface acoustic waves in various crystal structures. The 830 nm beam is used to probe the sample after being delayed relative to the pump beam. The beams are focused to a spot of about 2 μm diameter. The probe beam is scanned across the sample to generate images, which are obtained at various times by adjusting the probe delay.

Results

We obtained images of the propagation of surface acoustic waves in phononic crystals that include structures such as waveguides, cavities, slabs and prisms. The dispersion relations and the acoustic fields in two dimensions at individual frequencies are extracted by spatio-temporal Fourier transforms. Time-resolved images reveal effects such as diffraction, refraction, reflection, resonance and waveguiding. The figure shows the field amplitude at 380 MHz of waves confined to a square cavity (made of four linear sections) in a phononic crystal made up of a square lattice of circular holes in Si (100) of radius 6.5 μm and filling fraction 70%.

Discussion and Conclusions

We have obtained real-time images of surface acoustic waves on various crystal structures using an optical pump and probe technique. Such research should be invaluable for the evaluation of future surface acoustic wave devices and for revealing the physics of the interaction of surface waves with phononic crystals.



2:45 PM Real-time simulations and experiments on ultrahigh frequency surface acoustic waves in microstructured phononic crystals

Istvan A. Veres¹, Dieter M. Profunser², Oliver B. Wright², Osamu Matsuda²; ¹Department of Electronic & Electrical Engineering, University of Strathclyde, Glasgow, United Kingdom, ²Graduate School of Engineering, Hokkaido University, Japan

Background, Motivation and Objective

Periodic elastic structures, or phononic crystals, promise diverse applications in the control of propagating sound. These acoustic metamaterials possess stop bands where the elastic waves are heavily damped. The most prevalent examples are one-dimensional (1D) phononic crystals that take the form of interdigital transducers for generating and detecting surface acoustic waves. The promise of acoustic filtering and sound control has also stimulated work on surface acoustic waves in 2D phononic crystals consisting of arrays of cylinders or holes.

Statement of Contribution/Methods

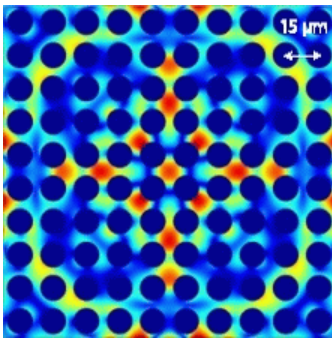
We investigate numerically and experimentally the interaction between ultra-high frequency surface acoustic waves and periodic microstructured patterns. We performed real-time finite element (FEM) simulations of the propagating ultra-high frequency surface waves in 1D and 2D phononic crystals, allowing the investigation of surface acoustic wave scattering in the same geometries as real fabricated phononic crystals or devices. We image surface acoustic waves with frequency components up to 1.3 GHz by means of ultrashort pulsed optical excitation and interferometric detection with picosecond temporal and micron spatial resolutions. We use microfabricated 1D phononic crystals made of copper lines embedded in silicon-oxide, as well as 2D phononic crystals consisting of air-filled holes etched in silicon (100) in a square lattice.

Results

We first present real-time animations of surface acoustic waves scattered by the 1D and 2D microstructured phononic crystals. Movies of the scattered surface acoustic wave in real-time simulation and experiment are treated by spatiotemporal Fourier transforms to reveal the band structure. Eigenmode spatial distributions at each frequency are derived from the temporal Fourier transforms. The figure shows the simulated amplitude of the acoustic field in the 2D phononic crystal at 195 MHz.

Discussion and Conclusions

In conclusion, we have probed the dispersion relation for surface wave propagation in 1D and 2D phononic crystals. The numerical and experimental dispersion relations are in good agreement, and show evidence for phononic stop bands. Further investigations are required to elucidate the effect of the hole depth and to better understand the form of the constant frequency surfaces.



3:00 PM **Laser Interferometers in Physical Acoustics**Kimmo Kokkonen^{1,2}*Helsinki University of Technology, Espoo, Finland***Background, Motivation and Objective**

Need to understand the physics of wave motion in materials and ongoing interest in developing microacoustic components for, e.g., signal processing applications, have created a demand for versatile characterization methods. In many cases, components whose operation is based on mechanical vibrations, such as surface acoustic and bulk acoustic wave (SAW and BAW) devices, as well as, e.g., microelectromechanical (MEMS) resonators, are studied in electrically excited test structures or in real device configurations. Therefore, much of the characterization relies on measuring the electrical response of the structure and comparing that to simulations. Although these methods are well established, they provide only secondary information of the wave motion and the underlying device physics.

On the other hand, optical probing enables direct measurement of the vibration fields within the sample structure without disturbing the device operation. The ability to measure the vibration fields yields primary information of the wave physics and on the device performance.

Statement of Contribution/Methods

Optical probing has been in use for a long time as a research tool to deepen the understanding of the wave physics in various materials, their combinations and in different device configurations. Due to the extensive history and successful application of laser interferometers for characterization of microacoustic devices, there is a number of research groups utilizing an interferometer as an important part of their research facilities.

Results

Laser interferometric techniques are well suited, e.g., to image the wave field amplitude distributions in SAW devices, revealing possible sources of losses and unwanted responses, such as excitation of transverse modes in resonators, escaping acoustic beams, acoustic crosstalk in filters, etc. In the case of BAW research, the wave dispersion properties derived from vibration field measurements play an important role in device design and characterization, especially in the case of solidly mounted resonators. Also the recent progress in the research of phononic crystals, acoustic metamaterials, is expected to benefit from laser interferometric measurements.

Discussion and Conclusions

This paper focuses on the role of laser interferometers in physical acoustics, reviewing several different published setups, their capabilities, and recent progress in the field. Examples of recent research results on SAW, BAW and MEMS devices are presented and discussed.

6B-43:30 PM **Heterodyne laser-doppler interferometric characterization of contour-mode resonators above 1 GHz**Hengky Chandralim¹, Sunil Bhawe¹, Christian Rembe², Sebastian Boedecker², Ronald Polcawich³, Jeff Pulskamp³;
¹*Electrical and Computer Engineering, Cornell University, Ithaca, New York, USA*, ²*Polytec, Germany*, ³*US Army Research Laboratory, USA***Background, Motivation and Objective**

AFM has been used to image and characterize vibrations of MEMS resonators [1]. Characterization of MEMS resonators using heterodyne interferometer is of interest because it provides accurate measurement of resonances and broadband vibrations [2,3] without contacting the surface of the resonators.

Statement of Contribution/Methods

We report a special technique to measure frequencies and vibrations of contour-mode resonators (Fig. 1a) up to 1.2 GHz using only a 618 MHz carrier frequency (f_c). The detector signal of the vibrometer is digitized by a fast oscilloscope and demodulated off-line in a computer (Fig. 1b). This method enabled us to realize an algorithm to extend the measurement bandwidth by a factor of 2. The algorithm takes only the frequency components of the detector signal into account which are higher than f_c to construct an IQ-(in-phase, quadrature) signal from a virtual carrier signal with $2x$ the original frequency. The Rohde & Schwarz SMBV100A broadband Vector Signal Generator has been used to excite the specimen with a periodic chirp signal [4]. We set the spacing of the periodic-chirp frequencies to the resolution bandwidth of the measurement and adjusted the evaluated frequencies to the center of the FFT lines of the demodulated spectrum to determine the vibration amplitudes without leakage. In addition, the energy is distributed equally to all frequency components.

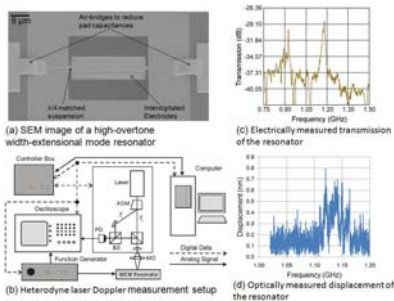
Results

A PZT transduced high-overtone width-extensional mode resonator was first characterized electrically on an RF probe station. Frequency response in air at room temperature is recorded in Fig. 1c. Optical measurement using a heterodyne interferometer technique was performed. Resonator's displacement as a function of frequency was plotted in Fig. 1d.

Discussion and Conclusions

A novel characterization technique of MEMS resonators above 1 GHz using heterodyne interferometer was performed. By measuring modes of vibrations optically, misalignment in lithography that leads to parasitic modes and unexpected resonance peaks can be identified without contacting the surface of the resonators.

[1] San Paulo et al, Microelectronic Engineering, pp. 1354-1357 (2007).
 [2] Rembe et al, SPIE 7098, pp. 70980A-70980A-12 (2008).
 [3] Stoffels et al, to be published at Transducers '09.
 [4] Schüssler et al, SPIE 4072, pp. 354-360 (2000).



6B-5

3:45 PM Measuring the frequency response of photodetectors used in ultrasonic applications by a heterodyne system with difference-frequency servo control

Christian Koch¹; ¹Physikalisch-Technische Bundesanstalt, Braunschweig, Germany

Background, Motivation and Objective

One of the important quantities describing the properties of photodetectors is the frequency response which can be defined as the voltage at the detector's output in response to a constant or well-defined optical input signal versus frequency. Photodetectors in ultrasonic applications are applied in very different optical configurations and during a calibration of the photodetector these conditions should be reconstructed to ensure that the frequency response obtained matches the application conditions. For traceable optical measurements it is advisable to have an in-house calibration set-up which is adapted to the ultrasound application requirements. Since sophisticated and costly optical equipment is usually not present in a laboratory dealing with ultrasonic applications, a set-up had to be constructed which used only simple components available in a standard optical laboratory.

Statement of Contribution/Methods

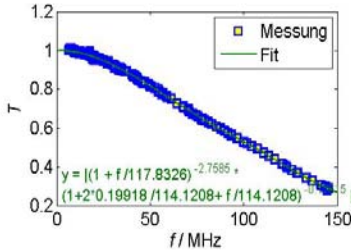
A heterodyne system was realized using two commercially available DFB lasers, and the required frequency stability and resolution was ensured by a difference-frequency servo control scheme. The frequency-sensitive element generating the error signal for the servo loop comprised a delay-line discriminator constructed from electronic elements which converts a frequency deviation into an amplitude deviation. The output signal is used as an error signal for a servo loop controlling the emission frequency of one laser via the driving current.

Results

Measurements were carried out up to 450 MHz and as an example the frequency response of a photodetector used in a multilayer optical hydrophone system is depicted in Fig. 1. The uncertainties of about 4% (k=2) can be further reduced without losing the feature of using only simple elements by improved rf power measurement.

Discussion and Conclusions

High-quality optical measurements in ultrasound require calibrated equipment traceable to a national standard. The presented method allows the wide-frequency determination of the frequency response of photodetectors under conditions occurring in ultrasonic applications and it improves the metrological basis of ultrasound measurement.



1C. New Methods and High Frequency Ultrasound for Tissue Characterization

Sala 1

Monday, September 21, 2009, 4:30 pm - 6:00 pm

Chair: **Georg Schmitz**
Ruhr-Universität Bochum

1C-1

4:30 PM Acoustic Microscopy – Beyond High Resolution Imaging

Yoshifumi Saijo¹:¹*Graduate School of Biomedical Engineering, Tohoku University, Sendai, Miyagi, Japan*

Background, Motivation and Objective

The year 2009 is the 60th anniversary of acoustic microscopy because the concept of "ultrasound microscope" to visualize opaque media was first proposed in 1949. As the wavelength of 3-GHz ultrasound in water is the same as the wavelength of green light in air, acoustic microscopy has been developed to catch up the resolution of optical microscopy. Today, acoustic microscopy using lower frequency ultrasound than expected at that period provides important information beyond high resolution imaging. There are three major objectives of acoustic microscopy in medicine and biology; 1) rapid examination of histopathology without staining or slicing, 2) search for the origin of echo in clinical ultrasound imaging and 3) novel approach to the pathophysiology from biomechanical point of view.

Statement of Contribution/Methods

The most important originality of our acoustic microscopy laid on the quantitative measurement of sound speed in the tissue. Varying the central frequency of the burst waves, the frequency dependent amplitude and phase characteristics were analyzed to determine the tissue thickness and sound speed. The algorithm has become more sophisticated in the 21st century to equip a frequency-domain analysis of a single pulse. Thin slicing of the fresh biological specimen has been the biggest limitation for practical use of acoustic microscopy in clinical settings. Ultrasound impedance microscopy was developed to visualize surface morphology of the fresh tissue by just touching the tissue surface with the ultrasound probe which is made of a thin plastic plate, coupling medium and a mechanical transducer. The reflection from the interface between tissue and plastic plate is obtained and compared with the reflection from a material with known specific acoustic impedance such as saline to measure specific acoustic impedance of the tissue. The design of our newest acoustic microscopy is flexible to realize multimode ultrasound microscope with conventional C-mode, surface impedance mode, B-mode and reconstructed 3D mode.

Results

Measurements of microscopic acoustic properties in gastric cancer, renal cancer, myocardial infarction, atherosclerosis, tendon, cartilage and brain have provided useful information not limited in the field of medical ultrasound but also in the field of biomechanics especially in cardiology and orthopedic surgery. Spectral analysis of the radio-frequency signal for B-mode image has realized automatic classification and segmentation of skin and regenerated skin model.

Discussion and Conclusions

The resolution of acoustic microscopy applied in medicine and biology is still inferior to that of optical microscopy. The continuous effort to fabricate 3-GHz transducer with newest technologies of material science will realize such resolution. However, passions of biomedical researchers to find the new horizons in pathophysiology are more important for future progression of acoustic microscopy.

1C-2

5:00 PM **Acoustic nonlinearity parameter of tissue on echo mode: review and evaluation of the different approaches for B/A imaging**

François Varray¹, Mirza Pasovic¹, Christian Cachard¹, Piero Tortoli², Olivier Basset¹; ¹CREATIS LRMN, Université de Lyon, INSA-Lyon, Université Lyon 1, CNRS UMR 5220, Inserm U630, France, ²Microelectronics Systems Design Laboratory, Università di Firenze, Italy

Background, Motivation and Objective

In nonlinear imaging applications such as tissue characterization, harmonic or contrast imaging, the nonlinear parameter B/A plays the main role in the generation of harmonics during ultrasound wave propagation. Many efforts have been so far addressed to evaluate this parameter, either theoretically and experimentally, in transmission mode. The proposed methods generally provide a global B/A value for a homogenous medium. The final objective of our work is to map the B/A parameter through echo mode imaging. The present paper extends the use of previously described approaches to B/A imaging and compares the related performance.

Statement of Contribution/Methods

The potential existing methods for B/A imaging can be grouped in four categories: methods based on the second harmonic increase [1], insertion-comparative [2], dual frequencies waves [3] and pumping wave [4] methods. They have been implemented using an existing propagation simulator based on the Burger or the KZK equations. For a given transmitted pulse, the resulting pressure at any point on the propagation axis is computed taking into account the attenuation, the nonlinearity effect and the diffraction of the beam. The evolution of the fundamental and the nth harmonic are deduced from the resulting pressure. The above approaches, initially proposed for transmission mode, have here been adapted to echo mode imaging to evaluate different B/A values along the propagation direction. The simulation results are presented with and without considering the diffraction effect of the probe. Our approach, based on the insertion-comparative method, has been first implemented on an Ultrasonix SONIX RP scanner and evaluated using a phantom including different media.

Results

The values used in the simulator are based on the characteristics of an experimental ultrasound probe (128 elements, transmit focus at 7.1 cm, frequency between 1 and 6 MHz) and on a B/A range between 3 and 10. When the chosen probe parameters yield low diffraction effects, the accuracy on estimated B/A values results generally better than 5 %. The insertion-comparative method adapted to echo mode is the most robust with respect to diffraction effects. Its application to the experimental RF echo-signals provided by the Ultrasonix scanner, have produced maps which clearly distinguish the different B/A regions of the phantom.

Discussion and Conclusions

Preliminary results with insertion-comparative methods show interesting potentialities for nonlinear parameter imaging. The other methods require further adjustments of related models, which do not take into account the diffraction effects and have been developed for single element transducers.

1. Law et al., *Ultrasound Med. Bio.*, 1985, 11 (2)
2. Gong et al., *J. Acoust. Soc. Am.*, 1996, 116 (3)
3. Nakagawa et al., *IEEE Ultrasonics Symposium*, 1986
4. Fukukita et al., *J. Acoust. Soc. Am.*, 1996, 99(6)

1C-3

5:15 PM **Three-Dimensional High-frequency Characterization of Excised Human Lymph Nodes**

Jonathan Mamou¹, Alain Coron², Masaki Hata³, Junji Machi³, Eugene Yanagihara³, Pascal Laugier², Ernest J. Felleppa¹; F. L. Lizzi Center for Biomedical Engineering, Riverside Research Institute, New York, NY, USA, ²UMR 7623, Laboratoire d'Imagerie Paramétrique, UPMC Univ Paris 06, Paris, France, ³University of Hawaii and Kuakini Medical Center, Honolulu, HI, USA

Background, Motivation and Objective

High-frequency ultrasound (HFU, >20 MHz) offers a means of investigating biological tissue at the microscopic level because the short wavelengths (<75 μm) and small focal-zone beam diameters of HFU transducers provide fine-resolution images (<100 μm). Most human lymph nodes have sizes ranging from 2 to 8 mm and readily can be imaged with HFU. The objective of this study was to develop 3D quantitative-ultrasound (QUS) methods to detect metastases from freshly-dissected lymph nodes of cancer patients. Detection of metastases is critically important for staging and treatment planning.

Statement of Contribution/Methods

3D radio-frequency (RF) data were acquired by scanning dissected lymph nodes using a 26-MHz center-frequency transducer. Adjacent A-lines and B-planes were 25 μm apart and scanning time was <5 minutes. A 3D segmentation algorithm based on the watershed transform was used to segment saline, residual fat, and nodal tissue in the 3D RF data. Overlapping cylindrical regions-of-interest (ROIs, 1-mm diameter, 1-mm deep) were processed to yield four QUS estimates. Spectral intercept (I) and spectral slope (S) were computed using a straight-line model and scatterer size (D) and acoustic concentration (CQ^2) were estimated using a Gaussian scattering model. An SNR-estimation method was used to derive an ROI-dependent optimization bandwidth to fit either model to the system-corrected attenuation-compensated ROI power spectra. 3D QUS images were generated by expressing QUS estimates as color-encoded pixels and overlaying them on conventional, 3D, B-mode images.

Results

QUS estimates were obtained for 46 lymph nodes from 27 patients diagnosed with colon cancer. Table I displays estimates for metastatic and cancer-free nodes and indicates statistically-significant differences between cancer-containing and cancer-free nodes for all QUS estimates except CQ^2 . Furthermore, areas under the ROC were greater than 0.95 for D or I alone and greater than 0.99 when linear discriminant analysis was used with I and S or with D and CQ^2 .

Discussion and Conclusions

Excellent classification performance was obtained using 3D QUS methods on this representative set of lymph nodes. Therefore, these initial results suggest these methods may provide a clinically important means of identifying small metastatic foci that might not be detected using standard pathology procedures.

Table 1

Average QUS estimates (means \pm standard deviations) for the non-metastatic and metastatic nodes. (The symbol "*" indicates statistical significance based on ANOVA results giving $p < 0.005$.)

Node	D (μm)	CQ^2 (dB mm^{-3})	I (dB)	S (dB/MHz)
Non metastatic (N=37)	21.6 \pm 4.80*	8.39 \pm 6.39	-63.0 \pm 3.92*	0.58 \pm 0.15*
Metastatic (N=9)	31.7 \pm 3.54*	5.70 \pm 4.37	-53.5 \pm 3.22*	0.39 \pm 0.14*

1C-4**5:30 PM Quantifying ultrasonic properties of cells during apoptosis using time resolved acoustic microscopy**

Eric Strohm¹, Michael Kolios¹; ¹Department of Physics, Ryerson University, Toronto, Ontario, Canada

Background, Motivation and Objective

Scanning acoustic microscopy (SAM) is an imaging modality that uses ultra high frequency focused ultrasound (100+ MHz) to create high mechanical contrast images of micrometer sized structures and living cells. SAM can also be used to quantitatively measure the ultrasonic properties of cells. The pulse echoes from the cell can be used to calculate the thickness, speed of sound, acoustic impedance, density, bulk modulus and attenuation within the cell. The objective of our research is to study the effects of chemotherapeutic drugs on cancer cells and how the mechanical properties change as a function of time after cytotoxic exposure.

Statement of Contribution/Methods

The acoustic microscope used in these studies is equipped for simultaneous optical and acoustic measurements, which allows for precise alignment and comparison of acoustic and optical images. Time resolved SAM was used to measure the mechanical properties of MCF7 breast cancer cells at 375 MHz using 7 ns pulses. The time and amplitude of the ultrasound echoes from the cell surface and the cell-substrate interface were used to calculate the mechanical properties. The technique was previously validated using 9 μm PVDF with known properties. Cells were treated with paclitaxel for 15 hours and then the effect of the chemotherapeutic agent was investigated by measuring the ultrasonic properties during the structural changes of the cells as they undergo apoptosis. Optical movies of cells undergoing apoptosis were recorded and compared to acoustic data.

Results

Untreated and treated cells before apoptotic collapse (a hallmark feature of apoptosis) showed minimal backscatter variations and variations in ultrasonic properties as a function of time. During and after apoptotic collapse, rapid

structural changes observed optically were correlated to large transient variations of the ultrasound backscatter within the cell. The attenuation within the center of the cell increased by 30% after collapse, and the attenuation around the periphery of the cell (mainly the cytoplasm) increased by over 100%. In our preliminary experiments, a comparison of the nucleus to the cytoplasm after apoptotic collapse showed a decrease in the speed of sound from 1583 ± 9 to 1547 ± 15 m/s, an increase in the density from 992 ± 6 to 1015 ± 10 kg/m³ and a decrease in the bulk modulus from 2.49 ± 0.01 to 2.42 ± 0.02 GPa.

Discussion and Conclusions

For the first time, the mechanical properties of cells undergoing apoptosis induced by chemotherapeutic treatment are reported as a function of time. The rapid variations in the ultrasound backscatter after cellular collapse indicate extensive activity within the cell, which correlates well with optical observations. After cellular collapse, the attenuation within the entire cell increased, but was greater around the cell periphery. The density around the periphery also increased. This corroborates the morphological observation that the cell becomes denser when it collapses due to apoptosis.

1C-5

5:45 PM High-Resolution Ultrasonic Monitoring of Cellular Differentiation in an Ex Vivo Produced Oral Mucosal Equivalent (EVPOME)

F. Winterroth¹, J. B. Fowlkes², S. Kuo³, K. Izumi³, S. E. Feinberg⁴, S. J. Hollister¹, Kyle Hollman¹; ¹Biomedical Engineering, University of Michigan, Ann Arbor, MI, USA, ²Biomedical Engineering & Radiology, University of Michigan, Ann Arbor, MI, USA, ³Oral and Maxillofacial Surgery, University of Michigan, Ann Arbor, MI, USA, ⁴Biomedical Engineering & Oral and Maxillofacial Surgery, University of Michigan, Ann Arbor, MI, USA

Background, Motivation and Objective

This study examines the use of high-resolution ultrasound to monitor an ex vivo produced oral mucosal equivalent (EVPOME) as it develops from oral keratinocytes being seeded on a dermal cadaveric scaffold, with surface variations, into a stratified uniform cellular layer. Ultrasonic profilometry should be able to detect filling and smoothing of surface irregularities as seeded cells proliferate. As these tissue-engineered structures develop, seeded cells stratify from their differentiation in which they produce a keratinized protective upper layer. These cells change in shape and composition, lose water content, and accumulate proteins (keratins) - transformations which could alter ultrasonic backscatter. If non-invasive ultrasonic monitoring could be developed then tissue cultivation could be adjusted in-process to account for variations in the development of the stratified cellular layer.

Statement of Contribution/Methods

To create an EVPOME specimen, oral mucosa keratinocytes were dissociated from human oral tissue samples and then seeded onto a scaffold of acellular cadaveric dermis. EVPOME's were cultured submerged for 4 days to form a continuous epithelial monolayer and then raised to an air-liquid interface for another 7-10 days. At specific intervals (1, 2, 4, and 7 days) specimens were imaged with an ultrasound acoustic microscope that consists of a single-element transducer (61 MHz center frequency, 32 MHz bandwidth, 1.52 f#) with a three-axis stepper-motor-controlled positioning system. Lateral step size was 15 μ m, about half of the 37 μ m resolution. Ultrasonic images were created using confocal image reconstruction. Tissue surfaces were determined by thresholding the magnitude of the signal at the first axial incidence of a value safely above noise. Roughness was measured with root-mean-squared (RMS) surface height. Echogenicity was measured using apparent integrated backscatter (AIBS) with respect to a fused silica flat. AIBS was calculated over bandwidth after gating the signal with a window centered at the specimen surface.

Results

There was no considerable change in measured roughness (20 to 22 μ m) from unseeded scaffold through day 4 after seeding. Between days 4 and 7 RMS heights decreased from 22 μ m to 13 μ m. AIBS first changed between days 1 and 2 when it dropped from -30 dB to -41 dB. Echogenicity increased again from days 4 to 7 from -40 dB to -29 dB.

Discussion and Conclusions

Ultrasonic profilometry did not detect seeded cells filling in scaffold irregularities until cells had sufficiently stratified and differentiated by day 7. The initial drop in AIBS on day 2 may be due to undifferentiated seeded cells attenuating but not scattering ultrasound at that layer. More maturely differentiated cells, present at day 7, show brighter echogenicity possibly due to cellular changes. These initial results show that ultrasonic characterization may have potential to monitor EVPOME development during its manufacturing process.

2C. Therapeutic In-Vivo Studies

Sala 2

Monday, September 21, 2009, 4:30 pm - 6:00 pm

Chair: **Elisa Konofagou**
Columbia Univ.

2C-1

4:30 PM **In-vivo study of non-invasive thrombolysis by histotripsy in a porcine model**

Adam D. Maxwell¹, Gabe Owens², Hitinder S. Gurm³, Charles A. Cain¹, Zhen Xu¹; ¹Department of Biomedical Engineering, University of Michigan, Ann Arbor, MI, USA, ²Department of Pediatric Cardiology, University of Michigan, Ann Arbor, MI, USA, ³Department of Internal Medicine, University of Michigan, Ann Arbor, MI, USA

Background, Motivation and Objective

Current treatments for thrombolysis involve either drugs or catheter-based procedures, both of which have drawbacks including risk of bleeding. We demonstrated previously that histotripsy can break down in-vitro clots into fragments smaller than red blood cells. This paper is the first study to evaluate the feasibility of histotripsy for non-invasive thrombolysis in-vivo.

Statement of Contribution/Methods

Experiments were performed in 35 kg pigs. Clots were formed in the femoral veins by vessel occlusion and thrombin injection through a catheter. After one hour, a water bath was placed on the leg to provide acoustic coupling of the therapy transducer to the subject. A focused 1 MHz transducer was used as to generate cavitation. An ultrasound imaging probe guided the alignment of the therapy focus with the clot based on a hyperechoic bubble cloud induced by histotripsy. The treatment used 5 cycle pulses delivered at a rate of 1 kHz and peak negative pressure of 12-14 MPa. Treatment outcome was evaluated by B-Mode ultrasound and restoration of blood flow on Doppler images.

Results

In four experiments performed to date, blood clots between 1.5 and 2.5 cm length were formed in the femoral vein. The clots were apparent on B-Mode images as areas of increased echogenicity in the vein. Veins with clots showed obstruction or complete elimination of flow on Doppler images. Guided by ultrasound imaging, histotripsy pulses generated a bubble cloud of 2-4 mm diameter on the clot in the 6-7mm diameter vein. Within 10 seconds, areas where the bubble cloud was generated became hypoechoic, indicating clot disintegration. Using pre-programmed mechanical scanning, the bubble cloud was moved along the clot. In two experiments, the clot was entirely eliminated after 5-13 min of sonication. The clot was no longer visible on the B-Mode image (Fig. 1), and Doppler showed increased flow through the vessel. In two other cases, the clot was partially eliminated as shown by a region of reduced echogenicity, but flow was not restored.

Discussion and Conclusions

Guided by ultrasound imaging, we were able to successfully target and disintegrate clots in-vivo using histotripsy alone. Small bubble clouds can be generated inside the vessel lumen and scanned along the clot without cavitating outside the lumen. This work is the first in-vivo study of histotripsy's potential as a non-invasive ultrasonic technique for thrombolysis.



2C-2

4:45 PM Brain region and microbubble-size dependence of the focused ultrasound-induced blood-brain barrier opening in mice in vivo

James Choi¹, Jameel Feshitan², Babak Baseri¹, Shougang Wang³, Yao-Sheng Tung¹, Mark Borden², Elisa Konofagou^{1,3}, ¹Department of Biomedical Engineering, Columbia University, New York, NY, USA, ²Department of Chemical Engineering, Columbia University, New York, NY, USA, ³Department of Radiology, Columbia University, New York, NY, USA

Background, Motivation and Objective

Currently, the major impediment to the treatment of brain diseases is the inability of therapeutic agents to bypass the interface that lines the cerebral capillaries: the blood-brain barrier (BBB). Previous studies have shown that systemic administration of bubbles in an acoustic field temporarily opens the BBB. Most reported studies utilized bubbles polydispersed in size (1-10 μm in diameter). However, cerebral capillaries are 4-8 μm in diameter, and, thus, smaller (i.e., 1-2 μm in diameter) or larger bubbles (i.e., 4-5 μm in diameter) may have different acoustic pressure thresholds of BBB opening. In addition, the capillary density and geometry varies in different brain regions and may influence the amount of drugs delivered. The purpose of this study was to investigate the dependence of the FUS-induced BBB opening on microbubble size, acoustic pressure, and location of the targeted brain region.

Statement of Contribution/Methods

Lipid-shelled microbubbles were manufactured in-house and size-isolated using differential centrifugation. Twenty eight mice were each injected with bubbles of either 1-2 or 4-5 μm in diameter. The left hippocampus of each mouse was then sonicated using focused ultrasound (1.5 MHz frequency; 20 ms pulse length; 10 Hz pulse repetition frequency) while the right hippocampus served as the control. Each mouse was sonicated at a specific acoustic peak-rarefactional pressure ranging between 0.15 and 0.61 MPa in order to identify the threshold of BBB opening. Approximately 10 min after sonication, 3 kDa Texas Red®-tagged dextrans were systemically administered and allowed to circulate for 20 min prior to animal sacrifice. BBB opening was then determined by an increase in fluorescence signal in the left relative to the right hippocampus.

Results

The BBB opening pressure threshold was identified to lie between 0.30 and 0.46 MPa in the case of the 1-2 μm bubbles and between 0.15 and 0.30 MPa in the 4-5 μm case. At every acoustic pressure studied, the fluorescence was greater with the 4-5 μm bubbles than with the 1-2 μm bubbles. At 0.61 MPa, in the 1-2 μm bubble case, the amount and area of fluorescence were both greater in the thalamus than in the hippocampus.

Discussion and Conclusions

The 4-5 μm bubbles required a lower pressure to induce BBB opening than the 1-2 μm bubbles. This may be due to the fact that the 4-5 μm bubbles are closer in size to the capillary diameter and thus may not require as high of an acoustic pressure to induce BBB opening as the 1-2 μm bubbles. The greater fluorescence signal observed in the thalamus compared to the hippocampus may be due to its larger capillary density, which may imply a greater number of opened capillaries. This is being further investigated in ongoing studies. However, it was clearly determined that FUS-induced BBB opening was dependent on both the size distribution of the injected microbubbles and the brain region targeted.

2C-3

5:00 PM In vivo thermal ablation of liver tumors in rabbits using a HIFU toroidal transducer

David Melodelima¹, William N'Djin¹, Amélie Battais¹, Michel Rivoire², Jean-Yves Chapelon¹, ¹Unit 556 - Therapeutic Applications of Ultrasound, INSERM, Lyon, France, ²Institute of experimental surgery, Centre Leon Berard, Lyon, France

Background, Motivation and Objective

To demonstrate in a rabbit liver tumor model that high intensity focused ultrasound (HIFU) produced with toroidal-shaped emitters may have a role in treating colorectal liver metastases.

Statement of Contribution/Methods

Eight ultrasound emitters were created by sectioning a single toroidal piezocomposite transducer. Each of the eight emitters was divided into 32 transducers operating at a frequency of 3 MHz. The toroidal transducer has a diameter of 70 mm and a radius of curvature of 70 mm. A 7.5 MHz ultrasound imaging probe (Vermon, Tours, France) was

placed in the centre of the device. Using this transducer single lesions of 7 cm³ were created in 40 seconds. Juxtaposition of single lesions was performed under ultrasound guidance. VX2 tumor segments (25 mg) were implanted into right lateral liver lobes of 45 New Zealand white rabbits. Fifteen rabbits were treated with toroidal HIFU ablation (Group 1). Fifteen rabbits were resected (Group 2). Fifteen rabbits were not treated and formed a control group (Group 3). Group 1 and 3 were compared to evaluate treatment efficacy. Group 1 and 2 were compared to evaluate if the toroidal HIFU treatment increases the risk of tumor dissemination. Total hepatectomy took place 11 days after treatment. The therapeutic response was evaluated with follow-up ultrasound imaging and the corresponding gross pathology and histology.

Results

HIFU ablation produced using the toroidal transducer allowed fast and homogeneous tumor treatments. Ablations were visible on sonograms. The VX2 tumors were completely coagulated and were surrounded by ablated liver tissue without secondary thermal lesions in surrounding organs. In the control group tumor volume was 225% higher at the time of autopsy when compared to the volume at the day of the treatment. Tumor dissemination was lower in the HIFU group (25%) compared with resected (67%) and control (38%) groups. Findings of ultrasound imaging, gross pathology and histology supported these outcomes.

Discussion and Conclusions

Successful rabbit liver tumor ablation can be achieved using a toroidal HIFU transducer under ultrasound imaging guidance and therefore could be an effective treatment of localized tumors. There was no complication related to the HIFU procedure. Its clinical usefulness has to be further proven.

2C-4

5:15 PM Non-invasive Fetal Sheep Surgery using Histotripsy

Yohan Kim¹, Carlen Gomez Fifer², Sarah Gelehrter², Jennifer Williams³, Jimmy Lu², Charles Cain¹, Zhen Xu^{1,4}:¹Dept. of Biomedical Engineering, University of Michigan-Ann Arbor, Ann Arbor, MI, USA, ²Dept. of Pediatric Cardiology, Medical School, University of Michigan-Ann Arbor, Ann Arbor, MI, USA, ³Dept. of Obstetrics and Gynecology, Medical School, University of Michigan-Ann Arbor, Ann Arbor, MI, USA

Background, Motivation and Objective

Previous experiments have shown that mechanical tissue fractionation can be achieved using pulsed cavitation ultrasound ("histotripsy"). The goal of this study is to investigate the feasibility of using histotripsy for non-invasive fetal therapy in an in vivo fetal sheep model.

Statement of Contribution/Methods

Experiments involved four sheep at 100-120 days into gestation (full gestation period: 150 days). Histotripsy therapy was applied by a focused 1 MHz transducer positioned in a water bolus coupled to the maternal abdominal wall. The fetal heart, kidney and liver were exposed to ultrasound pulses (<10µs) at a 1 kHz pulse repetition rate and 10-16 MPa peak negative pressure. The entire procedure was guided by real-time ultrasound imaging through a 3 MHz imaging probe mounted in the center hole of the therapy transducer.

Results

Hyperechoic cavitating bubble clouds were successfully generated in the targeted fetal organs, located beneath up to 8 cm of overlying tissue and fetal bones. Ultrasound imaging provided real-time targeting guidance and monitoring of treatment initiation, progress and completion. In the fetal heart, erosions were created in the ventricular septum (VS) by 30s - 1min exposures. Figure 1 shows a treated fetal heart sample, in which two areas of erosion were generated in the VS, each with 3mm in diameter and 10mm apart. In the fetal kidney and liver, 0.3-1 cm³ cube-shaped lesions were created in 5-10 min by mechanically scanning the transducer focus. Post mortem morphology confirmed lesions with location, size and shape corresponding to regions in which cavitation was monitored. Histologic inspection indicated complete cellular fractionation within the therapeutic ultrasound exposure zones with no discernible damage to overlying tissue.

Discussion and Conclusions

Preliminary results show that histotripsy can generate precise tissue fractionation at targets within the fetal chest cavity at depths of up to 8 cm, without damaging the overlying fetal and maternal tissue. To our knowledge, no existing non-invasive surgery modality has achieved such accuracy in treating fetal organs under similar conditions. These results, coupled with real-time ultrasound imaging feedback, suggest that histotripsy has potential in non-invasive fetal surgery applications such as treatment for hypoplastic heart syndrome.

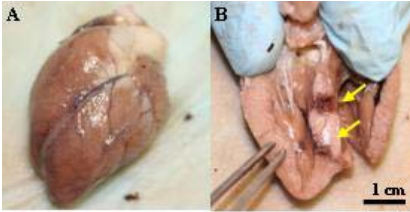


Fig. 1: A) Normal view of intact fetal heart. B) Cross sectional view showing eroded VS (as indicated by arrows).

2C-5

5:30 PM Microbubble and Ultrasound Enhancement of Radiation-Induced Tumour Cell Death in Vivo

Gregory Czarnota^{1,2}, Raffi Karshafian³, Azza Al Mahrouki¹, Anoja Giles¹⁻³ Radiation Oncology, and Imaging Research, Sunnybrook Health Sciences Centre, Toronto, Ontario, Canada, ²Radiation Oncology, and Medical Biophysics, University of Toronto, Toronto, Ontario, Canada, ³Physics, Ryerson University, Toronto, Ontario, Canada

Background, Motivation and Objective

It is now appreciated that radiation not only damages the DNA inside tumour cells in vivo but may act by damaging the endothelial cells of the vasculature. In this study we tested the hypothesis that microbubble agents in vivo may be used a priori to cause endothelial cell perturbations thus causing "radiosensitization" of tumours.

Statement of Contribution/Methods

Human prostate cancer xenograft-bearing mice (120 animals) were exposed to combinations of ultrasound, activated-microbubbles, and radiation (8 animals per group). For ultrasound treatments, animals were exposed to 16 cycles tone burst at 500kHz center frequency 570kPa peak negative pressure with a 3 kHz pulse repetition frequency for 5 minutes. For treatments involving bubbles, Definity bubbles (Bristol Myers-Squibb) were first administered and for radiation treatments 160 kVp X-rays were used at doses of 2 and 8 Gy. Representative tumour sections were examined using immunohistochemistry. Clonogenic assays and growth delay studies were also carried out. Separate experiments were carried out using endothelial cells in vitro to identify the biochemical mechanism of cell death activation due to microbubbles.

Results

Analyses indicated a synergistic increase in tumour cell kill due to vascular disruption caused by the combined therapies that increased when microbubbles were used in conjunction with radiation with increases of cell kill from 5% to over 50% with combined single treatments. Immunohistochemistry indicated endothelial cell apoptosis and activation of the ceramide cell-death pathway to be caused by microbubbles. Effects from parallel in vivo experiments using cultured endothelial cells indicated production of ceramide after exposure to microbubbles and an upregulation of key genes involved in membrane repair and cell death.

Discussion and Conclusions

Radiation effects were synergistically enhanced by using microbubbles to perturb tumour vasculature prior to the administration of radiotherapy. Analyses indicated activation of ceramide-mediated apoptotic cell death in endothelial cells leading to vascular disruption in tumours. This led to profoundly enhanced tumour cell death even after one combined treatment using a 2 Gy radiation dose. This work forms the basis for ultrasound-induced spatial targeting of radiotherapy enhancement.

5:45 PM **Harmonic Motion Imaging (HMI) for Focused Ultrasound (HMIFU): Initial in vivo results**

Caroline Maleke¹, Elisa Konofagou¹; ¹*Biomedical Engineering, Columbia University, USA*

Background, Motivation and Objective

The capability of HMIFU for real-time monitoring of tissue stiffness changes during thermal therapy was previously demonstrated ex vivo[1]. Here, initial feasibility of the HMIFU for thermal ablation generation and monitoring is shown in a transgenic mouse model of breast cancer in vivo.

Statement of Contribution/Methods

A focused ultrasound (FUS) transducer with a center frequency of 4.5 MHz was used to generate an oscillatory radiation force at the tumor region. The FUS transducer was driven by an amplitude-modulated (AM) signal at 15 Hz. The focus was set at a depth of 45 ± 2 mm and the acoustic intensity was equal to 1050 W/cm² at the focus. A 3.3-MHz phased-array was used to image the relative tissue stiffness changes during application of the oscillatory radiation force. A digital low-pass filter removed the spectrum of the FUS beam and its harmonics from the acquired RF signals prior to displacement estimation. 1D cross-correlation (window size = 1 mm and 85% overlap) was performed to estimate the resulting tissue axial displacement. The peak-to-peak displacement amplitude was monitored throughout the entire treatment. Two transgenic mice were used with 8 lesions formed in each mouse (16 lesions total). The mammary tumors were invasive adenocarcinomas and typically grew to 3 to 10 mm in diameter.

Results

Grayscale B-mode and M-mode images overlaid with color-coded HMI displacements during heating were used to simultaneously provide functional and anatomical visualization. The average HMI displacement amplitude around the focal region shows that it could follow the lesion formation due to the relative tissue stiffness changes throughout the entire duration of the thermal treatment. The average peak-to-peak displacement amplitude was found to be equal to 17.34 ± 1.34 μ m and 10.98 ± 1.82 μ m, before and after lesion formation, respectively. Comparison of the displacement amplitude before and after lesions were formed using a pair t-test exhibited a statistically-significant difference (p-value < 0.001). The lesion formation was also identified by a 30% decrease in displacement amplitude. Cell death in the tumor area was confirmed by H&E histology.

Discussion and Conclusions

HMIFU was shown capable of monitoring and localizing thermal ablation of tumors in vivo. The color-coded harmonic displacement offers complementary tissue stiffening information to the B-mode or M-mode imaging's anatomical view. HMI can thus be used as a guidance tool for visualization of the targeted region and monitoring of the relative tissue stiffness changes during thermal treatment so that the treatment procedure can be performed in both a cost- and time-efficient manner.

1. C Maleke and EE Konofagou, Phys. Med. Biol., 53, 1773-1793, 2008.

3C. CMUT Modeling

Sala 4

Monday, September 21, 2009, 4:30 pm - 6:00 pm

Chair: **Jian Yuan**
Boston Scientific

3C-1

4:30 PM **Non-linear dynamic response of cMUTs population: modeling and characterization**

Nicolas S en egond¹, Franck Teston¹, Cyril Meynier², Fr ed eric Patat¹, Dominique Certon^{1,1} *UMR Universit e Fran cois Rabelais de Tours INSERM U930 CNRS ERL3106, TOURS, France, ²VERMON S.A, TOURS, France*

Background, Motivation and Objective

The understanding of temporal cMUT behavior is a key aspect for optimization and fabrication of transducers. Depending on applications, several driving modes exist. For reception, the conventional mode is based on membranes polarized with DC voltage superimposed by a low amplitude dynamic voltage. For therapeutic applications and echographic imaging in transmit mode, high voltage excitations are rather used but produced some undesired non-linear effects. This paper proposes to investigate the dynamic collective behavior of membranes, loaded with fluid medium and coupled for different excitations. For that, a time domain model is presented and compared with heterodyne interferometer measurements.

Statement of Contribution/Methods

The motion of membrane immersed in oil is measured with a homemade interferometer. This device is based on a double-passing of the laser beam through the Bragg cell in order that the ultrasonic frequency carrier moves from 70 MHz to 140 MHz with a laser spot around 3 μm in fluid. For modeling the time response of cMUTs population, each membrane is replaced by an equivalent "fluid loaded piston" which parameters are extracted and fitted from harmonic displacement measured with laser interferometer and network analyzer. Each equivalent piston is coupled each other through acoustic mutual coupling expressed in time domain. To this end, the diffraction impulse response theory is used. Electric and acoustic degrees of freedom are grouped to express time domain equations of cMUTs population in a matrix form. Displacement at each sampling time is obtained through finite difference scheme.

Results

Responses of 20*20 μm^2 and 25*25 μm^2 membranes are studied for different excitation magnitudes and frequencies (from 200 kHz to 10 MHz). Analysis of non-linear response is conducted through the displacement vs. input voltage curve. cMUT behavior can be divided in several domains. At low frequencies, membrane motion is driven by the membrane elasticity and is strongly non-linear. Indeed, for high voltage excitation, the displacement vs. input voltage curve reminds static hysteretic cycle with presence of collapse and snapback phenomena. For high frequencies, inertial effects due to fluid loading control the membrane response which becomes linear. Between these two domains, both effects drive the membrane. The impulse response of membrane is also studied for different levels of excitation and impacts on bandwidth are studied.

Discussion and Conclusions

Model and measurements are compared and present good agreements: the displacement vs. input voltage curves are similar. Theoretical hysteretic cycle points out same collapse and snapback voltage values than extracted ones from experimental cycles. The impulse responses of cMUTs are well predicted. Finally, we show how taking advantage of cMUT non-linearity to enlarge the emitted ultrasound bandwidth and how controlling the pressure radiated pulse shape in a large frequency range.

3C-2

4:45 PM Minimizing the bottom reflections in Ultrasonic CMUT transducer backing using low profile structuring

Kamal Chapagain¹, Arne Ronnekleiv²; ¹*Electronics and Telecommunication, NTNU, Trondheim, Trondheim, Norway,*
²*Electronics and Telecommunication, NTNU, Trondheim, Norway*

Background, Motivation and Objective

Ultrasonic CMUT transducers need a supporting structure with a high acoustic impedance which will not absorb energy from the transducer. The CMUTs are usually made on silicon, which has to be backed to absorb any acoustic signals from the transducer so that they are not reflected back into the transducer and create false echoes. Such a backing is conveniently made from epoxy filled with tungsten powder, to make it lossy with matching impedance.

In many cases there is little space available under the transducer where it is difficult to accommodate a sufficiently thick layer of material with realistic propagation losses to avoid echoes. Irregular structures of the bottom surface are customary used to scatter the waves, but they also take up some space. Here we suggest a low profile structure to scatter the waves. It is similar to that proposed by Khuri Yakub et al.(US patent 7321181B2,2008)

Statement of Contribution/Methods

The structure proposed by Khuri-Yakub consists of parallel rectangular grooves with equal width and spacing of the grooves, which, in principle, gives cancellation of specular reflection of waves when the groove depth is 1/4 of the acoustic wavelength at broadside. This structure scatters the waves into waves with significantly changed transverse wave vectors, giving long propagation paths back to the transducer. It may also convert longitudinal waves into shear waves which normally have much higher propagation losses than longitudinal waves. Khuri-Yakub discuss scattering in a narrow band. We will show that the scattering can be extended to a broader frequency range by superimposing grooves with different depths and different directions or different periodicities. The principle is to provide sets of reflecting surfaces with equal areas but different depths that may be grouped in pairs such that the depths differ by a quarter of a wavelength at a set of frequencies; grouping is different at different frequencies. Cancellation of specular reflection at two independent frequencies requires 4 different depths; at three frequencies it requires 8 different depths. We also discuss other ways of implementing the structure. One may use a checker board pattern where the white and the black fields have different depths; or a pattern of rectangles split in two triangles where the two triangles have different depths.

Simple versions of the structure will also be analyzed by FEM methods, and the FEM results will be compared with the results using the analysis based only on delay differences.

Results

By using the proposed structure, we can reduce the specular reflection up to 20dB over a range of 1 to 10 in frequency, as evaluated by a simple time delay difference model for signals reflected at 16 different depths.

Discussion and Conclusions

The proposed structure is expected to make it easier to form well damped backing layers for CMUT array transducers in cases where little space is available under the CMUT array, as for instance in equipment for intravascular ultrasound imaging.

3C-3

5:00 PM Acoustic Characteristics of CMUT with Rectangular Membranes Caused by Higher Order Modes

Hiroki Tanaka¹, Shuntaro Machida¹, Kunio Hashiba¹, Takashi Kobayashi¹; ¹*Central research laboratory, Hitachi, Ltd., Kokubunji, Tokyo, Japan*

Background, Motivation and Objective

One of the most important issues involved in improving the performance of capacitive micro-machined ultrasonic transducers (CMUTs) is the trade-off between sensitivity and output pressure. Several pieces of previous research show that the rectangular membranes improve the fill factor and the performance of CMUTs compared with circular or square ones [1]. However, a finite aspect ratio of the rectangular membranes causes higher order modes. The effect of these higher order modes on the acoustic characteristics of CMUTs has not yet been comprehensively understood.

Statement of Contribution/Methods

The three-dimensional (3D) nature of a membrane shape is an essential principle in this work. We used PZFlex™ software to create 3D simulation models of the rectangular membranes. We calculated the impedance and analyzed the mode shape of the rectangular membranes in air as a function of dimension and the aspect ratio. We also fabricated test element groups (TEGs) of rectangular and hexagonal CMUT cells, and used an impedance analyzer and laser interferometer to measure the impedances and the static and dynamic deformation shapes when DC and AC voltage was applied. The output pressure waves in a water tank were also measured by hydrophone.

Results

Typical mode shapes of the rectangular membrane with aspect ratio of 1 to 4 measured in air by a laser interferometer are shown in Figure 1. The mode frequencies of the rectangular membranes agree with theoretical and simulation results. Simulation results of the frequency spectrum in a water tank excited by impulse voltage are also shown in Figure 2. Several dips are found in the frequency spectrum by using a calculation based on a 3D model, while this characteristic phenomenon is not obtained by using a 2D model in the calculation.

Discussion and Conclusions

We found that higher modes affect the acoustic characteristics of CMUT, e.g., there were several dips in the frequency spectrum. A rectangular CMUT with a finite aspect ratio generates higher order modes. The frequency and mode shape of these higher modes are calculated by previous theoretical works. We show the relationship between the dip frequency and the parameters of the CMUT design parameters. We also discuss the essential mechanism that generates these dips.

[1] Y. Huang, et al., Optimized membrane configuration improves CMUT performance, in *Proc. IEEE Ultrasonics Symp.*, 2004.

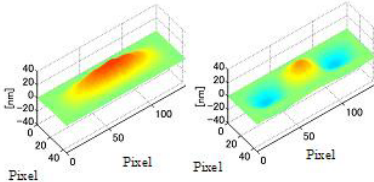


Figure 1

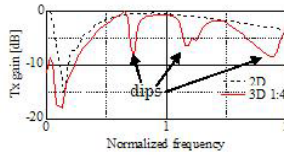


Figure 2

3C-4

5:15 PM Trade Off Between Bandwidth and Noise in Airborne cMUTs

Muhammed N. Senlik¹, Selim Olcum¹, Vahdettin Tas¹, Hayrettin Köymen¹, Abdullah Atalar¹; ¹Department of Electrical and Electronics Engineering, Bilkent University, Turkey

Background, Motivation and Objective

Capacitive micromachined ultrasonic transducers (cMUTs) offer relatively large bandwidth compared to their piezoelectric alternatives due to the lower impedance mismatch between the air and the transducer. There are various methods to increase the bandwidth of the cMUTs. For example, using thinner membranes decreases the membrane impedance and hence reduces the quality factor. On the other hand, increasing the radiation resistance also helps, since it improves the loading on the cells. Introducing lossy elements to the electrical terminals of the device may also work at the expense of reduced efficiency and sensitivity. In this work, we try to optimize the bandwidth of the cMUTs operating in air while keeping the noise figure of the overall system as small as possible. The noise figure includes the contributions of the receiver circuitry.

Statement of Contribution/Methods

In a recent work [1], the radiation impedance of a single cMUT cell and an array element is calculated. It is shown that when ka is around 3.85, the radiation resistance is maximized, where k is the wavenumber and a is the radius of a single cell. However, the choice of this ka value does not permit the use of the thinner membranes, which also improves the bandwidth. In order to increase the radiation resistance for lower ka values, we changed the distance between the cells to get a sparse arrangement of the cells. We found that as the distance between the cells increases, the ka value where the radiation resistance is maximized occurs at a lower value. We investigated the change of the radiation resistance for various array shapes and the number of the cells in an array. We calculated the bandwidth of the transducer with respect to the cell size, assuming that the cMUTs operate at 100 kHz in the air.

Results

The sparse arrangement of the cells increases the radiation resistance at lower ka values, whereas it decreases the receiver sensitivity of the transducer. To determine the receiver sensitivity we calculated the signal-to-noise ratio (SNR), at the output of the receiver circuitry for a given incident plane wave field. We calculated the SNR for the closely packed and the sparse arrays. We show that SNR is proportional to the number of the cells in the array. We use a state-of-the-art low noise opamp in the receiver circuitry. We calculate the optimum resistance that must be seen by the opamp to minimize the noise figure of the overall system at the operating frequency. We used Mason's equivalent circuit to model the cMUT. Both the deflection under the atmospheric pressure and the stress stiffening effects are included, which are critical for the thin membranes.

Discussion and Conclusions

[1] M. N. Senlik, S. Olcum, H. Koymen, and A. Atalar, "Radiation impedance of array of circular clamped membranes," IEEE Trans. Ultrason., Ferroelect., Freq. Contr., submitted for publication.

3C-5

5:30 PM Design Modeling of CMUT's for Medical Imaging

Arne Ronnekleiv¹; ¹Department of Electronics and Telecommunications, Norwegian University of Science and Technology, Trondheim, Norway

Background, Motivation and Objective

We want to develop scalable models to design CMUT's that will meet the requirements in medical imaging. The fact that CMUT transducers have not yet made it into commercial products indicates that this has so far not happened. This is probably mainly due to low sensitivity for the available arrays.

Statement of Contribution/Methods

Two slightly different equivalent circuits for CMUT arrays will be presented. Both describes coupling to grating lobes if the element size is large compared to the wavelength. They may include effects of finite viscosity in the fluid outside the array, and also lossy uniform layers on top of the CMUT membranes, and coupling to waves in the backing.

For a CMUT that mainly couples to one specific acoustic vibration mode of the membrane, the Mason equivalent circuit applies. It is well known that for this equivalent there is a link between the relative bandwidth of the transduction of the CMUT array and the transduction gain, such that low loss and high relative bandwidth requires high coupling. The basic consequences will be shortly reviewed, and also the requirements to the CMUT if it is to maintain a high electromechanical coupling over a wide range in applied DC-voltages.

Coupling to slow non radiating waves along the array surface, which is often referred to as neighbor coupling, will be discussed in terms of the product of frequency and the shear viscosity of the fluid outside the array, using the equivalents.

Results

It is verified that the effects on the array response of the neighbor coupling through the fluid is highly dependent on the shear viscosity of the fluid, but also on losses in a possible top layer and on other losses in the CMUT's. The effects of the coupling on the transducer response may be offset by using low impedance transmission or reception amplifiers. If the amplifiers in reception are based on field effect transistors, they may still offer good signal to noise ratio. But the acoustic reflection suppression of the array will suffer compared to what is commonly obtained with PZT-transducers with impedance matched amplifiers.

In the range of high coupling the properties of most CMUT's are shown to vary fast with DC-voltage. An exception to this is CMUT's in collapsed mode. Due to material problems this has not yet been a success. Hence stability and uniformity of high coupling CMUT arrays seems to be a continuing problem.

Discussion and Conclusions

So far presented arrays seem to have had problems with combining stability and uniformity over the array with high sensitivity and high bandwidth. Low sensitivity has been quoted as a reason for not using them. This may be due to too high weight on bandwidth which gives problems for good sensitivity. Proper packaging for high frequency 2D application and integration with electronics seems still to require some improvements, but may be coming. This is probably the imaging applications where the PZT-solutions have the largest problems, and where CMUT's might make a breakthrough in imaging.

4C. Acoustic Wave Sensors

Tarragona

Monday, September 21, 2009, 4:30 pm - 6:00 pm

Chair: **Donald McCann**
University of Maine

4C-1

4:30 PM Young's modulus characterisation of mesoporous titania films using Love wave sensors

laurianne blanc¹, gregory tortissier¹, angelique tetelin¹, cedric boissiere², clement sanchez², corinne dejous¹, dominique rebriere²; ¹IMS Laboratory, Universite Bordeaux I, Talence, France, ²LCMCP Laboratory, France

Background, Motivation and Objective

The Young modulus (E) of thin mesoporous films is usually derived from the measurement of gas adsorption isotherms through ellipsometric porosimetry (EP) [1]. This method calculates the expected Young Modulus for the "dry" film, before gas sorption. For chemical sensing applications and modelling, the "dry E" is not relevant because it is assumed to vary during sorption. In this work, Love wave sensors are associated to EP for real time measurement of the Young modulus variation of mesoporous films during humidity sorption.

Statement of Contribution/Methods

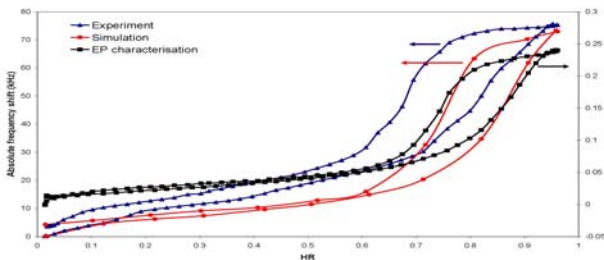
Current work is focused on showing the ability of the Love wave sensor to correctly record the water sorption-adsorption cycle through frequency shift measurements. The refractive index is recorded by ellipsometry, at the same time as the frequency shift of the sensor, thanks to a dedicated experimental set-up. For further comparison, a previously developed numerical model of the sensor was used to calculate the frequency shift that should be expected from the sensor, feeding the software with parameters derived from the ellipsometric characterisation: the thickness of the film, its density and its Young modulus.

Results

Figure 1 compares the water adsorption-desorption cycle recorded with EP and with the Love wave sensor at 18°C. It also shows the simulation of the frequency shift as described in the previous section. Both methods provide isotherms of similar shapes with quite the same capillarity condensation threshold of 70%RH.

Discussion and Conclusions

At the end of the cycle, EP extracted a Young's modulus of 8 GPa using the modified Kelvin equation [1]. This value fed the simulation software. The difference between the measurements and the simulation is explained by the fact that the Young modulus is likely to change in accordance with the humidity level. Thus, the ability of the Love wave sensor to record sorption cycles tend to be demonstrated. Future work will focus on the real-time recording of Young's modulus change in the nanostructured layer with the presented method. Further investigations with different porosity and pore size will also aim at improving the understanding of the mechanical mesoporous thin films at the nanometric scale.



4:45 PM **Measurement of methanol solutions using Love mode liquid sensor**

Yuan-Feng Chiang¹, Chia-Chi Sung¹, Ruyen Ro², Ruyue Lee², Sean Wu³, Cheng-Chiao Tu¹, Chih-Yung Huang¹:¹National Taiwan University, Taiwan, ²I-Shou University, Taiwan, ³Tung-Fang Institute of Technology, Taiwan

Background, Motivation and Objective

The Direct methanol fuel cell (DMFC) is a promisingly alternative energy owing to the merits of ease of refueling, harmless storage, and high power density. Over the operation situation, controlling the methanol concentration in the inlet of the fuel flow at anode side or in the mixing tank of DMFC is very important to maintain the high efficiency as well as the better stability. In this study, Love mode sensor based on SiO₂/ST-cut Y-propagation quartz was employed for measuring methanol concentration.

Statement of Contribution/Methods

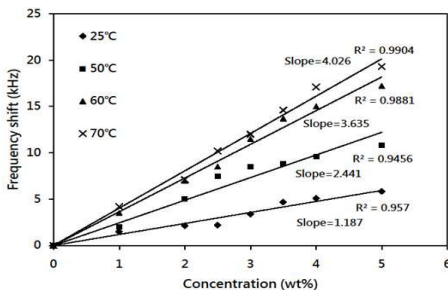
The immersed-type Love mode sensor based on SiO₂/ST-cut Y-propagation quartz was fabricated using the MicroElectroMechanical Systems (MEMS). A temperature controlled measurement system consisting of a spectrum analyzer and an oscillator circuit was employed to characterize the methanol solutions with different weight concentrations at different temperatures. A theoretical prediction of the phase velocity change for the methanol solutions with different weight concentrations was also performed for comparison.

Results

The measured center frequency and the associated insertion loss of the Love mode sensor are 37 MHz and 15.96 dB. Measurement results at different temperatures illustrate the average temperature coefficient of frequency (TCF) of the sensor is around 54 ppm/°C. The results of methanol solutions with different weight concentrations at different temperatures show that the amount of the frequency shift is approximately linearly proportional to the weight concentration, and the proportional rate increases as the temperature increases. The attached figure shows the measured frequency shift versus different weight concentrations of methanol solutions at various temperatures, the corresponding slopes and the correlation coefficients are indicated in figure. By calculating the slopes of results, the concentration resolutions were 1.1876 and 0.2484 %/kHz by weight at 25°C and 70°C.

Discussion and Conclusions

In this study, the immersed-type Love mode sensor was employed to measure the weight concentration of methanol solutions. An approximately linear relation is observed between the frequency shift and the weight concentration. This result implies that the Love mode sensor is applicable for practical methanol detection in the DMFC system.

5:00 PM **Microbead dynamics on Quartz Crystal Microbalance at elevated amplitudes**

Sourav Ghosh¹, Victor Ostani², Ashwin Seshia¹:¹Engineering, University of Cambridge, Cambridge, United Kingdom, ²Chemistry, University of Cambridge, Cambridge, United Kingdom

Background, Motivation and Objective

The Quartz Crystal Microbalance (QCM) has been utilised as a platform for biochemical sensing. The modulation of thickness shear mode quartz oscillations by bound analyte at elevated amplitudes has received sporadic attention. This study presents preliminary results for QCM-analyte interaction that provides insight into the

dynamics involved at the surface. In particular, interactions of the QCM with polystyrene microbeads physisorbed on its surface via self-assembled monolayer (SAM) are described.

Statement of Contribution/Methods

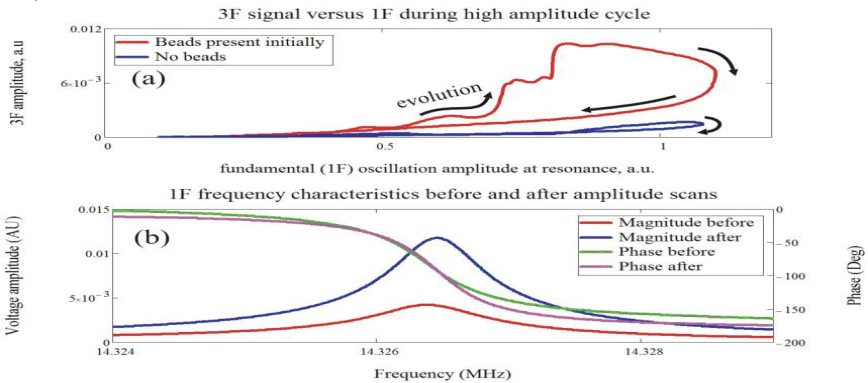
The QCM is driven at varying amplitudes at the fundamental mode (1F) frequency and the amplitude and phase of the response at the first and third harmonic (3F) are recorded. Simultaneously, video of physisorbed microbeads moving on the QCM surface is captured. The 1F frequency characteristics are measured before and after the voltage ramp at the fundamental mode frequency. Additionally, the temperature increase on the sensor surface is measured using a thermal imaging camera. These results are compared with a model of microbead dynamics on a piezoelectric disc.

Results

The video demonstrates microbeads sliding and aggregating together before finally being dispelled from the field of view at high amplitudes. This behaviour matches the kinetics estimated by the model. The 3F current rises abruptly as the 1F drive amplitude is increased and reduces sharply for reducing amplitude, describing a nonlinear response clearly different from the classical nonlinearity of quartz. The amplitude of the 3F current plotted against the 1F current exhibits large hysteresis, which is absent in similar scans for the bare QCM (Fig 1a). This 3F response also matches with the results predicted by the model. The 1F frequency characteristics taken after amplitude scan show a dramatic increase in quality factor with no significant change in the resonant frequency (Fig. 1b).

Discussion and Conclusions

The third harmonic response observed is due to the motion of beads on the surface and the nonlinearity reduces as the beads are dispelled from the surface. This model may be extended to study dynamics of chemisorbed species on QCM surface.



4C-4

5:15 PM Acoustic Mode Behavior in Lateral Field Excited Sensors

Jason McGann¹, Christian Peters², Kristopher Sgambato¹, John Vetelino¹; ¹Laboratory for Surface Science and Technology, University of Maine Orono, USA, ²Institute of Micro and Sensor Systems, University of Magdeburg, Magdeburg, Germany

Background, Motivation and Objective

Lateral Field Excited (LFE) sensors have been shown to have several very attractive features[1], the most important of which is the bare sensing surface. In contrast to the standard Quartz Crystal Monitor, the LFE sensor surface allows one to sensitively monitor both mechanical and electrical property changes in adjacent media or analyte selective biological or chemical films. Although LFE sensors have been shown to function very efficiently in liquid media[2,3], LFE sensor operation in gaseous environments has been plagued by spurious mode responses. It is the purpose of this work to study sensor curvature and selective surface etching in order to rid the LFE sensor of the spurious modes and enhance the fundamental resonant mode used in LFE gaseous sensor applications.

Statement of Contribution/Methods

The acoustic mode response spectra of AT-cut Quartz and Lithium Tantalate (LTO) LFE sensors under various boundary conditions have been investigated. In particular, the effects of mesa structures and surface contouring on the sensor response have been studied in detail.

Results

The present work examined a large number of AT-cut quartz and (YXw1)-16.5° LTO samples in which the applied lateral electric field couples only to the resonant transverse shear mode (TSM). The sample surfaces, which ranged from plano-plano to plano-convex, were selectively etched to create mesa structures. It was experimentally shown through a combination of surface contouring and selective etching that the TSM was trapped in the mesa structure and spurious modes were eliminated.

Discussion and Conclusions

Proper convex contouring of the sensor surface and selective surface etching have resulted in AT-cut quartz and LTO LFE sensors with a strong fundamental TSM and no appreciable spurious modes. These sensors have been shown to be capable of operating in a gaseous environment and will have applications ranging from thin film monitoring in vacuum deposition systems to the detection of a wide variety of air-borne gases.

1. "A Lateral Field Excited Liquid Wave Sensor," IEEE Transactions on Ultrasonics, Ferroelectrics, and Frequency Control, Vol. 51, No 11, pp.1373-1380, 2004. (Y. Hu, L.A. French, K. Radecky, M.P. DaCunha, P. Millard and J.F. Vetelino)
2. "Pesticide Detection Using Lateral Field Acoustic Wave Sensor," Sensors and Actuators B Chemical 109, pp 910-916, 2005. (W. Pinkham, D. Frankel, L. French, Y. Hu and J.F. Vetelino)
3. "A Lateral-Field-Excited LiTaO3 High-Frequency Bulk Acoustic Wave Sensor" IEEE Transactions on Ultrasonics, Ferroelectrics, and Frequency Control, Vol. 56, No 4, pp779 – p787, 2009. (D. McCann, J. McGann, J. Parks, D. Frankel, M.P. DaCunha, and J.F. Vetelino).

4C-5

5:30 PM Improved Substrate Selection for Lateral Field TSM Sensors

Jeffrey Andle¹, Reichl Haskell², Maly Chap³, Daniel Stevens⁴, ¹SenGenuity, Vectron, Hudson, NH, USA, ²SenGenuity, Vectron, USA, ³SenGenuity, Vectron, USA, ⁴Vectron, Hudson, NH, USA

Background, Motivation and Objective

In recent years there have been several motivations away from thickness field excitation and toward lateral field excitation for thickness shear mode (TSM) fluid phase sensors. Lateral field excitation offers an unmetallized sensor surface for electrical interactions and also provides for hermetic packaging of the driven electrodes.

Historical substrate selections have supported both thickness field and lateral field excitation incurring a shift in operating mode and a significant issue with spurious signals. While the effect has been fertile ground for papers, it is not conducive to a commercially viable, mass producible sensor.

The objectives of this paper are to present a ground up analysis of the ideal symmetry properties for lateral field excitation and to recommend classes of materials and proper orientations through which to obtain low-spurious lateral field excitation.

Statement of Contribution/Methods

The paper examines the fundamental structure of the piezoelectric tensors and the modes of vibration that will be excited by a driving electric field vector. The symmetry conditions provide insight into substrate symmetry groups and orientations in which thickness field coupling ceases to exist and in which lateral fields couple to the target TSM modes.

Lateral field and thickness field cases are examined on a "traditional" orientation, Y-cut langasite, and a recommended orientation, Z-cut langasite. Experimental results are presented.

It is noteworthy that lateral field excitation provides lower piezoelectric coupling strength. In fluid phase sensing this limits the range of fluid viscosity or of polymer coatings to which the sensor is suitable.

A further analysis of inter-mode coupling is performed and the properties of preferred materials are deduced.

Results

It is found that symmetry groups 32, 422, 622, (isotropic)2, and 6-bar offer the requisite symmetry. Candidate materials from symmetry groups 32 and 622 are evaluated in terms of the expected intermode coupling.

It is shown through experimental examples on several traditionally oriented substrates that altering the electrical boundary condition on the opposing (sensing) surface alters the nature of the acoustic modes whereas, on the suggested substrates, the nature of the modes is significantly less impacted by the changing electrical properties of the sensing surface.

The impact of using lateral field excitation on sensor packaging is presented as are several interesting sensor integrations that may be performed as a consequence of using lateral field coupling.

The impact of lateral field excitation on the level of viscoelastic damping that may be sustained in a given instrumentation system is also evaluated.

Discussion and Conclusions

Prior reports of lateral field excitation were not ideal due to spurious modes and inefficient coupling. The present paper offers a ground-up treatment of the substrate selection. Theoretic predictions are experimentally verified.

4C-6

5:45 PM Pseudo-LFE sensors with different electrode configurations on X-cut LiNbO₃

Zhitian Zhang¹, Chao Zhang², Tingfeng Ma¹, Wenyan Wang¹, Guanping Feng¹; ¹*Precision Instruments and Mechanology, Tsinghua University, Beijing, Beijing, China, People's Republic of.* ²*Research Institute of Tsinghua University, Shenzhen, Guangdong, China, People's Republic of*

Background, Motivation and Objective

Previous studies on (yx1)-58 μ lithium niobate LFE devices with different electrode configurations have found that these devices had different frequency shift when exposed from water to 0.06wt% NaCl solution. Recent study has found that (yx1) -58 μ lithium niobate LFE devices were working on pure-LFE mode. The sensitivities of pseudo-LFE sensors with different electrode configurations to the change of electrical properties (such as permittivity, conductivities, and so on) have not been studied. In this study, the sensitivity of X-cut lithium niobate LFE devices with different electrode configurations was investigated.

Statement of Contribution/Methods

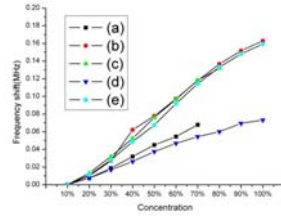
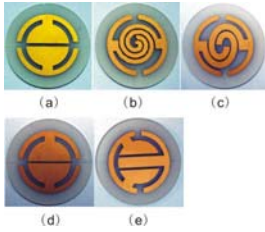
Several 4MHz LFE lithium niobate devices with different electrode configurations were fabricated on X-cut LiNbO₃, including the 1mm single gap electrode, two-turn symmetric spiral electrode, single-turn Archimedes spiral electrode, 0.5mm single gap electrode, split-parallel-gap electrode, which was in turn shown in Fig.1(a), (b), (c), (d) and (e). The sensitivities of these devices were tested.

Results

These devices were tested in isopropanol water solutions and the result is shown in Fig.2. It is found that the devices with two-turn symmetric spiral electrode, single-turn Archimedes spiral electrode and split-parallel-gap electrode have similar frequency changes, and the devices with 1mm single gap electrode and 0.5mm single gap electrode also have similar frequency changes; but the frequency changes of the three former devices are much higher than the other two.

Discussion and Conclusions

The LFE devices with two-turn symmetric spiral electrode, single-turn Archimedes spiral electrode and split-parallel-gap electrode are more sensitive than the single gap electrode. Theoretical analysis is presented.



5C. BAW I

Pergamo

Monday, September 21, 2009, 4:30 pm - 6:00 pm

Chair: **Ken Lakin**
Consultant

5C-1

4:30 PM **A Family of 2.0 x 2.5 mm² UMTS FBAR Duplexers Based on 8-pole Near-Elliptic Filters**

Paul Bradley¹, Shen Ye¹, Jeesu Kim¹, Jung-Hoon Kim², Kun Wang¹, Herb Ko¹, Yuan Xie¹; ¹*Avago Technologies, Inc., USA.* ²*Avago Technologies, Inc., Korea, Republic of*

Background, Motivation and Objective

UMTS antenna duplexers for handsets require high levels of wide-band rejection while still achieving high-isolation, low insertion loss, and good return loss in-band. Several of the UMTS duplexers also require the sharpest possible roll-offs due to a very small guardband between transmit and receive frequency bands (Band 2 and Band 8 guardband is ~1% of center frequency). Without sizeable inductors to stretch the bandwidth, this demands a higher effective coupling coefficient and near-ideal placement of a large number of poles and zeroes to achieve fast roll-off while maintaining acceptable insertion loss with so many resonators.

Statement of Contribution/Methods

Recently, FBARs with Q's of several thousand have become available which allow us to dispense with the fairly large (and tight tolerance) inductors used to achieve a better trade-off between in-band insertion loss (I.L.) and rejection. This allows us to use a low Q, low-tolerance substrate with physically much smaller size than in the past to comply with the industry-standard 2.0 x 2.5 mm² duplexer footprint. In effect, the FBARs do more work so the substrate may do less.

We propose such a design in which all resonators have the same coupling coefficient (a severe design constraint needed for a simpler manufacturing process) and small cross-coupling elements are used to shift some of the zeroes.

The larger number of resonators with small external shunt inductance also provides much better wide-band rejection than in past designs. An 8-resonator ladder filter with a cross-coupled capacitor for the Tx filter or a cross-coupling common ground inductance for the Rx filter shifts one of the zeroes from the bottom of the guardband roll-off to the middle of the rejection band without significantly degrading I.L. These zeroes together with the three zeroes remaining in the guardband near the rejection band and the one on the far-side of the rejection band produced by the presence of the other filter produce near equi-ripple filter rejection. The use of four different resonator frequencies for each filter permits fine-tuning the poles in the passband to achieve near equi-ripple response here.

Results

Duplexers were designed to achieve a typical isolation of ~60 dB in the Tx band and ~55 dB in the Rx band. Total die area grew as the need for more resonators and higher effective coupling coefficient forced the AlN thickness, hence, resonator areas to be larger than in earlier designs. I.L. for Band 2 is about 3.0 dB (Tx) and 3.5 dB (Rx).

Discussion and Conclusions

The duplexers designed with these 8-pole cross-coupled filters achieve adequate in-band isolation and out-of-band rejection to permit elimination of both the transmit and receive interstage filters (and associated matching and the need for the signal going off and back onto the transceiver chip) while maintaining similar insertion loss and return loss to the more conventional, larger, duplexers with lower levels of rejection and isolation.

5C-2

4:45 PM **An electrically-driven acoustic resonator imaged with an ultrafast optical technique**

Oliver Wright¹, Takashi Fujikura¹, Osamu Matsuda¹, Dieter Profunser¹, Jeremy Masson², Sylvain Ballandras^{2,3} *Graduate School of Engineering, Hokkaido University, Japan, ²FEMTO-ST, Besancon, France*

Background, Motivation and Objective

Thin-film bulk acoustic resonators (BAWs) driven by piezoelectric films are showing promise in the wireless communications industry to filter electromagnetic waves at ~ 1 GHz. Frequency domain imaging techniques for the acoustic field based on optical interferometry or atomic force microscopy have previously been used to directly monitor device operation and acoustic wave leakage. Here we demonstrate a new hybrid optical-electrical time-domain method up to ~ 2 GHz on a BAW resonator, and derive the acoustic dispersion relation by means of spatiotemporal Fourier transforms.

Statement of Contribution/Methods

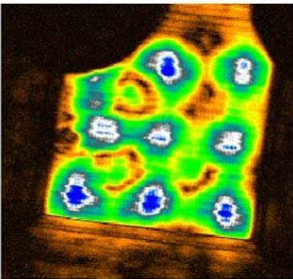
Optical pulses of duration ~ 200 fs, wavelength 830 nm and repetition rate 76 MHz from a Ti:sapphire laser are used for the dual purpose of generating electrical pulses to excite a BAW resonator and for the detection of the resulting surface motion. The rest of the laser beam - the probe light - passes through an optical delay line and then a common-path Sagnac interferometer. The beam is then focused to a ~ 2 μm diameter scanned spot on the sample. The surface velocity normal to the plane of the device is imaged as a function of the time with picosecond time resolution.

Results

Time-resolved surface vibration images reveal complex patterns within the active area of the device arising from mode conversion from longitudinal waves to in-plane guided modes such as generalized-Rayleigh, Lamb or Sezawa waves. Temporal and spatial Fourier transforms reveal the mode patterns (see 220 μm square figure for a frequency of 1368 MHz) and dispersion relations. The phase allows one to distinguish standing and travelling waves.

Discussion and Conclusions

In conclusion, we have obtained real-time and (from temporal Fourier transforms) single-frequency vibrational images of a BAW resonator up to ~ 2 GHz with a hybrid electrical-excitation and ultrashort-optical-detection technique. Improvements in the photodetector response would allow higher frequency BAW or SAW devices to be probed, potentially up to frequencies >100 GHz.



5C-3

5:00 PM **The role of high Q bulk acoustic wave resonators in low power IC design**

Brian Otis¹; ¹University of Washington, Seattle, WA, USA

Background, Motivation and Objective

The demands placed on radio integrated circuit (IC) designers are becoming increasingly severe. Portable devices must integrate multiple wireless transceivers in the same handset and, increasingly, on the same chip. In addition to being power efficient, these radios must co-exist peacefully on the same platform without significant interference. Miniaturization and power concerns, already important considerations in portable radio design, are amplified in

emerging wireless sensor applications. Additionally, there are several applications on the horizon that will demand completely thin-film integration of RF transceivers, prohibiting surface-mount components of any kind. This talk will explore three IC metrics that can greatly benefit from the use of high Q RF resonators: power, performance, and size. Several case studies will be described, and measured results will be presented.

Statement of Contribution/Methods

Results

Discussion and Conclusions

First, high Q resonators can significantly reduce the power dissipation of RF circuit blocks. The general strategy here is to use the properties of passive resonators to relax the performance specifications (and, thus, power dissipation) of active circuit blocks. Furthermore, utilizing high Q resonators can allow the realization of novel transceiver architectures. Passive impedance transformers, high-Q amplifiers, and deep notch filters providing high image rejection ratios can be realized. We will show some examples and discuss how these techniques can benefit ultra-low power RF transceivers.

Second, these resonators can be used to realize very efficient high performance circuit blocks. For example, the high Q nature of bulk resonators allows the realization of very low phase-noise RF oscillators. This allows the possibility of clean low power clock sources for RF transceivers, data interfaces, and high speed ADC sampling clocks. We introduce design methodologies for a very low-jitter PLL design that leverages high Q resonators to reduce phase noise. Test chip results will be presented and numerous challenges (tuning range, system integration, temperature stability) will be explored.

A third motivation of using RF resonators is the possibility of extreme system miniaturization. Bulk resonators manufactured using IC fabrication processes allow the potential of completely thin-film integration of RF circuits and systems. Frequency stabilization is one of the main challenges here. Replacement of the ubiquitous quartz resonator would be a significant step towards an ultra-thin transceiver. Recent efforts towards this end will be presented.

5C-4

5:30 PM Laterally Coupled Solidly Mounted BAW Resonators at 1.9 GHz

Johanna Meltaus¹, Kimmo Kokkonen², Tuomas Pensala¹, Andre Jansman^{3,1}VTT Technical Research Centre of Finland, Espoo, Espoo, Finland, ²Helsinki University of Technology, Espoo, Finland, ³NXP Semiconductors, Eindhoven, Netherlands

Background, Motivation and Objective

Lateral acoustical coupling between bulk acoustic wave (BAW) resonators has been used in quartz devices to make narrow-band filters. Acoustic even and odd resonance modes create a bandpass response. The effect has also been studied in membrane-type resonators on piezoelectric ZnO or AlN thin films.

Extending the concept to modern RF devices requiring a wide frequency band and GHz-range operation frequencies could offer a compact device with larger critical dimensions at high frequencies than surface acoustic wave filters.

Statement of Contribution/Methods

Laterally coupled solidly-mounted resonators (SMRs) are fabricated onto an acoustic mirror comprising two W-SiO₂ pairs. Thin-film AlN is used as the piezoelectric material with Mo bottom electrode and Al top electrode. Structures consist of acoustically coupled electrode fingers 2 to 8 μm wide and 300 μm long, with gaps of 4 μm in-between. Bottom electrode and AlN layer are not patterned. Electrical frequency responses are presented and compared to simulations. Mechanical vibrations are studied with a laser interferometer.

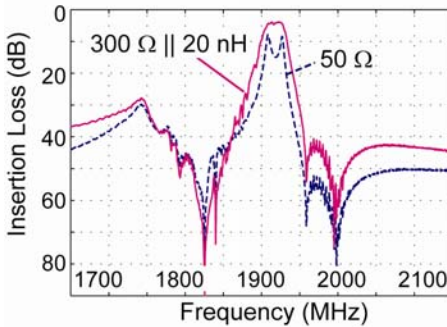
Results

Passband (PB) responses are achieved with all topologies. In 50-Ohm environment, devices are sub-optimally matched and responses have strong peaks at even and odd resonance mode frequencies, as shown in the figure for structure with 2 coupled fingers. Adding post-measurement matching results in a flat PB with minimum insertion loss of 3.92 dB, relative 3-dB bandwidth of 28 MHz (1.45% of center frequency), and out-of-band suppression of >30 dB.

Imaging acoustical vibration fields allows to connect features of electrical response to acoustical operation in the device. Resonance in the contact pad area is seen to create a notch in the electrical response, whereas higher order resonances in pads create spurious ripple below the PB. A loss mechanism in the form of escaping acoustic waves is identified within and near the PB.

Discussion and Conclusions

The achieved electrical frequency response of a 2-finger device shows that laterally coupled SMRs are promising for filter applications. In a 2-finger design, frequencies of resonance modes are close to each other, resulting in a narrow PB. A larger number of fingers and appropriate matching can be used to obtain a wider band. Deducing from the vibration field images, losses can be reduced by re-designing so that acoustic energy cannot escape the device.



5C-5

5:45 PM Study of Thin Film Bulk Acoustic Resonator Filters in Several Ten GHz Band

Motoaki Hara¹, Tsuyoshi Yokoyama¹, Takeshi Sakashita¹, Masanori Ueda¹, Yoshio Satoh^{1,†}*Fujitsu LIMITED, Japan*

Background, Motivation and Objective

A conventional frequency band is very crowded. A market of a mobile phone is expanding, and many new specifications of communication are proposed. Discussion of a wireless system using several ten GHz band can become important to use the frequency band efficiently today.

A filtering is a key in such high frequencies. A thin film bulk acoustic resonator (FBAR) gives a good solution for this purpose. The FBAR has high potential above several GHz band, and is attractive to achieve a small and low-cost system. However, FBAR filters operating above K-band have not been reported.

Statement of Contribution/Methods

In this paper, the first 24 GHz and 30 GHz band acoustic filters of the world using FBARs are introduced, and then the effect of parasitics in the FBAR filters are theoretically and experimentally described.

Results

Figure 1 shows characteristics of 24 GHz and 30 GHz band FBAR filters. A fractional bandwidth, a minimum insertion loss and a suppression in out-band were 3.0%, -3.4 dB and -13 dB in the 24 GHz band filter, and were 3.4%, -3.8 dB and -11 dB in the 30 GHz band filter, respectively. Obtained resonant Q, anti-resonant Q and k_{eff}^2 in 24 GHz FBAR were 285, 291 and 6.0%, respectively.

In several ten GHz band, it becomes impossible to disregard the parasitics. Characteristics which were measured and calculated using conventional MBVD equivalent circuit model were not corresponding due to the influence of parasitics. Although the parasitics can be calculated precisely using a numerical electro-magnetic (EM) simulation, this method spends long time and is not flexible.

It was paid attention in this study that the capacitance which parasites to the FBAR in parallel is dominant in the parasitics and is proportional to the capacitance of the FBAR. Dotted line in Fig. 1 (a) indicates the simulated characteristic using the MBVD equivalent circuit model including the capacitance. It was confirmed that the attenuation levels of pass-band and out-band were corresponding well.

Discussion and Conclusions

The first 24 and 30 GHz band acoustic filters of the world using FBARs were fabricated and analyzed using the MBVD equivalent circuit including parasitics. Obtained resonant Q, anti-resonant Q and k_{eff}^2 in 24 GHz FBAR were 285, 291 and 6.0%, respectively. An insertion loss and a fractional bandwidth were -3.4 dB and 3.0% in the 24GHz band filter, and -3.8 dB and 3.4% in the 30 GHz band filter, respectively.

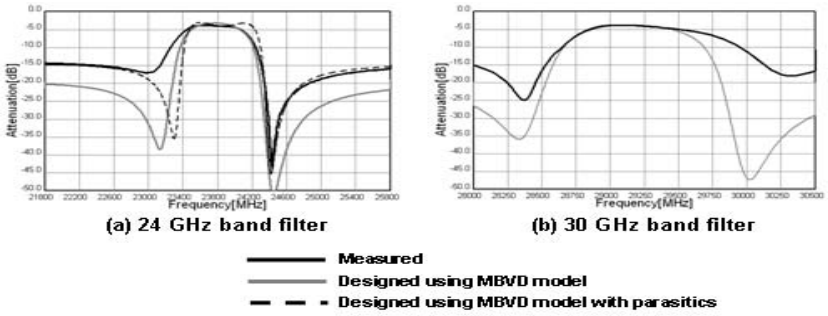


Figure 1. characteristics of 24 GHz and 30 GHz band filter

6C. Novel Ultrasonic Motors I

Baalbek

Monday, September 21, 2009, 4:30 pm - 6:00 pm

Chair: **Eun Sok Kim**
University of Southern California

6C-1

4:30 PM Increase in torque of screw-shaped ultrasonic motor

Atsuyuki Suzuki¹, Kentaro Izumi², Jiromaru Tsujino^{3,1}*Mechanical and Electrical Engineering, Tokuyama College of Technology, Shunan, Yamaguchi, Japan, ²Tokuyama College of Technology, Japan, ³Kanagawa University, Japan*

Background, Motivation and Objective

Ultrasonic motors have unique characteristics such as high torque at low speed, silent motion, and freedom from any magnetic influence. However, their use is limited, e.g., to autofocus mechanisms of cameras.

Ultrasonic motors are expected to be open to utilization in various ways after their torque is improved. They are also expected to be used in high-torque applications such as a robot arm.

We previously devised a screw-shaped ultrasonic motor comprising bolt-clamped Langevin-type longitudinal vibration transducers (BLTs). BLTs were connected to a BLT connector to form a screw shape in order to produce complex vibration. However, the driving frequency did not match the resonant frequency of the BLT. Therefore, the motor did not generate sufficient power. In this study, we devised a new screw-shaped ultrasonic motor with better torque.

Statement of Contribution/Methods

We devised a screw-shaped ultrasonic motor comprising three separate BLTs (15 mm in diameter). The figure shows the photograph of the devised ultrasonic motor. The three BLTs were driven simultaneously. The motor has free ends that are parallel to the emitting parts of BLTs. Therefore, it would be easy to match the resonant frequencies of the motor and the BLTs. Further, conical horns are installed in the motor in order to increase the vibration amplitude. Vibration and load characteristics of the motor were measured.

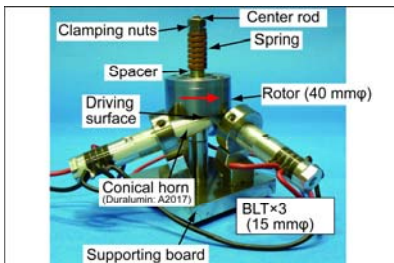
Results

Vibration distributions and loci were measured. The resonant frequency of the motor matched that of the BLT. Further, elliptical vibration loci were observed at driving surfaces of the motor.

In addition, load characteristics of the motor were measured. The maximum torque, revolution speed, and efficiency of the ultrasonic motor were 1.13 Nm, 506 rpm, and 3.53%, respectively.

Discussion and Conclusions

In order to develop a high-torque motor, we devised a separate-type screw-shaped ultrasonic motor. Its maximum torque, revolution speed, and efficiency were 1.13 Nm, 506 rpm, and 3.53%, respectively. The corresponding values of the previously devised one-piece-type motor were 0.41 Nm, 104 rpm, and 0.55%, respectively. This indicates an improvement in the characteristics of the screw-shaped ultrasonic motor. The performance of the ultrasonic motor can be improved further by matching the vibration distributions of all three BLTs.



6C-2

4:45 PM **Micro Ultrasonic Motor with Ultrasonically Assembled Micro-Mirrors**Steven Tin¹, Serhan Ardanuc¹, Amit Lal¹; ¹*School of Electrical and Computer Engineering, Cornell University, USA***Background, Motivation and Objective**

We demonstrate an ultrasonically-driven surface-micromachined micromotor with optical reflector plates integrated directly on the rotor, proving ultrasonic motors can be used to realize compact rotating platform carrying stages for micro-optics, etc. As the rotor starts to rotate, reflectors are self-assembled to be perpendicular to the rotor sono-thermokinetic force. This paper shows an ultra-compact ultrasonically driven optical beam steering sub-system realizes CMOS-compatible actuation and sensing. With potential applications in directional sensing and communications, surface-microfabricated rotating stage is easily integrated with other MEMS optical or bio devices to realize lab-on-a-chip applications. With multi-layer polysilicon fabrication process and < 5V operation, the rotating stage has low cost, low power consumption, and high integrate-ability with other MEMS devices.

Statement of Contribution/Methods

The surface-micromachined parametrically driven ultrasonic motors were previously reported by our group [1] [2]. In this paper, integrated with microfabricated reflectors, the motor is for the first time used as a rotating stage for directional communication applications. Fabricated using the SUMMiT V polycrystalline silicon surface micromachining process, the thickness and diameter of the stator and rotor are 2 μ m, 580 μ m and 2.5 μ m, 980 μ m respectively with the reflector dimension of 150 μ m long, 75 μ m wide and 2 μ m thick. After released, a rectangular PZT-4 plate is bonded to the back of the die.

Results

The PZT plate is excited with a single frequency signal at 530 kHz, while stator and motor motion are measured with a laser interferometer. As the excitation voltage increases, nonlinear parametric vibrations on the stator generate whispering-gallery traveling waves along the outer-edge. At two frequencies near 260 kHz the sum equals the drive frequency, which are whispering gallery modes. This wave couples motion into rotor through contact and acoustic streaming resulting in 100-200 rpm. The kinetic energy from the rotor impacts the hinged micro mirrors that are ratcheted into a locked vertical position, and has been used to modulate an incident laser beam.

Discussion and Conclusions

Integration of hinged micromirrors and travelling-wave ultrasonic motor has been demonstrated on a commercially available micromachining process. The integration of both an ultrasonic motor and reflecting mirrors on a micro-platform, driven by CMOS compatible voltages, enables pathways to implement closed-loop control of motor position by optical feedback, and other integrated capacitive electrodes around the rotor.

[1] Kaajakari, V., Rodgers, S., Lal, A., "Ultrasonically driven surface micromachined motor", MEMS 2000, Miyazaki, Japan, January 23-27, 2000 pp. 40-45

[2] Nayfeh, T.A., Vakakis, A. F. "Subharmonic travelling waves in a geometrically non-linear circular plate". Int. J. Non Lin, Mech, v 29, n 2, Mar, 1994, pp. 233-245

6C-3

5:00 PM **Novel Ultrasonic motor using torsional/ longitudinal vibration**

Samarth Bhargava¹, David Greve², Irving Oppenheim^{3,1}Department of Electrical and Computer Engineering, Carnegie Mellon University, Pittsburgh, PA, USA, ²Dept. Electrical and Computer Engrg., Carnegie Mellon University, Pittsburgh, PA, USA, ³Dept. Civil and Environmental Engrg., Carnegie Mellon University, Pittsburgh, PA, USA

Background, Motivation and Objective

Longitudinal-torsional converters [J. Tsujino et al., Proc. IUS 1996, p. 377; D. Wajchman et al., IEEE UFFC-55, p. 832 (2008)] have greatly simplified the structure of ultrasonic motors using a combined torsional/ longitudinal vibration, making miniaturization more practical. In this paper, we report the use of wafer-type actuators leading to further reduction in the required volume of piezoelectric material.

Statement of Contribution/Methods

Wajchman et al. used a multilayer piezoelectric actuator (MLPA) 20 mm in height to actuate a twisted beam that acted as a longitudinal-torsional mode converter. MLPAs use a large volume of piezoelectric material and also present a substantial reactive load to the driving circuit. In contrast, we have used two piezoelectric wafers

mounted on opposite sides of a flat portion of the beam. The actuating voltage V is applied across the thickness t of the wafers, causing a longitudinal displacement $d31VL/t$, where L is the length of the wafer. The wafers thus behave similarly to symmetrically excited wafers used to launch Lamb waves in plate-like structures.

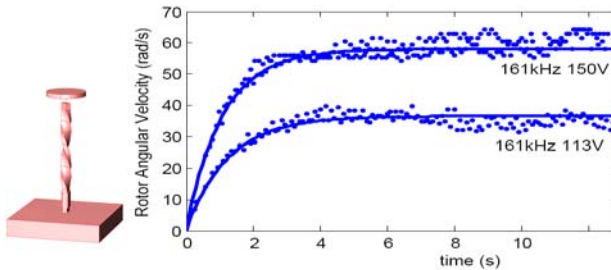
Several motors were constructed using PZT-7A material 0.64 mm in thickness, 9.4 mm long, and 6.5 wide, cemented to the wider surface of the beam. The twisted beams were fabricated from plexiglas 3.18 mm in thickness and with varying widths ranging from 4.8 to 7.5 mm. The helices had approximately two turns of twist over a length of about 47 mm. A circular brass disk 2.6 gm in mass with a 0.9 mm diameter axle was used as the rotor. The motors were driven with sinusoidal excitation at voltage amplitudes ranging up to 150 V peak. The rotational velocity was measured using an optical emitter and detector to count revolutions of the rotor.

Results

Rotation was observed for several frequencies in the range from 10-200 kHz with both CW and CCW rotation occurring at different frequencies. We will report on measurements of the maximum rotational velocity, stall torque, and the effect of varying the excitation frequency around the optimum frequency. Finally we will report on the relationship between structure in the electrical admittance measured at the motor terminals and the frequencies of rotation.

Discussion and Conclusions

The results show that this geometry effectively actuates the vibrations needed in an ultrasonic motor. This simple construction is attractive for miniaturized motors.



6C-4

5:15 PM A Ring-type Piezoelectric Actuator for Rotating a Sphere with Multi-Degree of Freedom

Shine-Tzong Ho¹, Yu-Ting Lin^{1,†} *Department of Mechanical Engineering, Kaohsiung University of Applied Sciences, Kaohsiung, Taiwan*

Background, Motivation and Objective

This study proposed a piezoelectric actuator for rotating a sphere with multi-degree-of-freedom (multi-DOF). The actuator can also be called as a multi-DOF ultrasonic motor. So far, multi-DOF actuators have become more useful in the field of robotics. The general features of ultrasonic motors are suitable for constructing a direct-drive multi-DOF actuator.

Statement of Contribution/Methods

In this study, we develop a multi-DOF ultrasonic motor composed of a spherical rotor and extremely compact piezoelectric stators, as shown in Fig.1. In this actuator, three vibration modes of a piezoelectric ring are chosen to produce three elliptical trajectories, which are orthogonal to each other. Fig.2 shows the three vibration modes. To drive the actuator, three sine voltage signals with phase difference are necessary to apply on the electrodes of the piezoelectric actuator for rotating a sphere. In analysis, a commercial software ANSYS is used to simulate the vibration modes and displacement distributions of the actuator. In experiments, a frequency response analyzer and a laser Doppler vibrometer are used to measure the stator.

Results

A prototype ultrasonic motor was fabricated for verification. The stator with outer diameter 40mm, inner diameter 7.5mm, and thickness 2mm was bonded a piezoelectric ring. In the measurement, the vibration modes, the input impedance curves and the displacement responses are obtained from the experiments. Also, a discussion about how the adhesive affect the performance of the actuator is described when bond a piezoelectric ring to a metal.

Discussion and Conclusions

The multi-DOF ultrasonic motor for rotating a sphere is presented. A rotary motion of the sphere can be induced via friction forces from the stator. The characteristics of the stator are discussed in the paper.

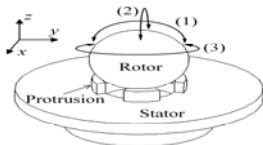


Fig.1 A ring-type piezoelectric actuator

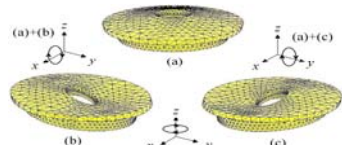


Fig.2 Three orthogonal vibration modes

6C-5

5:30 PM Modes and tip motions in ultrasonic motors using torsional/ longitudinal vibration

David Greve^{1,2}, Irving Oppenheim^{2,3}, ¹Dept. Electrical and Computer Engrg., Carnegie Mellon University, Pittsburgh, PA, USA, ²National Energy and Technology Laboratory, Pittsburgh, PA, USA, ³Dept. Civil and Environmental Engrg., Carnegie Mellon University, Pittsburgh, PA, USA

Background, Motivation and Objective

Ultrasonic motors using combined torsional/ longitudinal vibration rotate at frequencies where the stator tip has a large rotational velocity when the axial tip acceleration is high. Frictional contact with the rotor imparts a torque impulse to the rotor. Various geometries have been proposed that produce the required combination of torsional and longitudinal vibration. The resulting stator tip motions are complex and it is not obvious which frequencies will yield effective operation.

Statement of Contribution/Methods

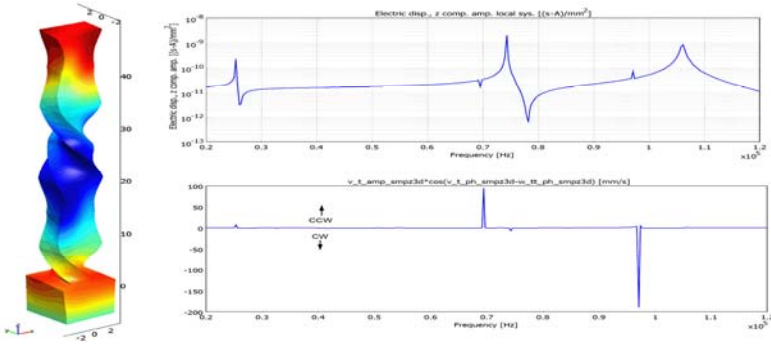
We have used COMSOL 3.4a in the piezo solid 3d mode to investigate motions in torsional/ longitudinal converters. We have focused on the spiral beam converter recently reported [D. Wajchman et al., IEEE UFFC-55, p. 832 (2008)]. The spiral was modeled as an isotropic material; piezoelectric elements attached to the spiral were driven by a sinusoidal exciting voltage with frequencies ranging from 20 kHz to 120 kHz. Sinusoidal steady state calculations every 3 kHz yield velocities and accelerations at all locations in the spiral and electric displacement throughout the piezoelectric elements.

Results

In post-processing we determine the magnitude and direction of the torque impulse exerted on the rotor from the magnitudes and phases of the relevant velocity and acceleration components. By evaluating this torque impulse for the rotor- stator contact point we can determine the frequencies where strong rotation should occur and also the direction of rotation. The electric displacement axial component provides a measure of the current drawn by the piezoelectric elements.

Discussion and Conclusions

Calculations have been performed for several motor geometries with a spiral beam and a multi-layer piezoelectric actuator. We have also simulated a related design with wafer-type piezoelectric elements attached to the sides of the beam. The results show a small number of sharply defined frequencies where the required motions are predicted to occur. We will report on the correlation between simulations and experiments, including frequencies corresponding to strong rotation and the electrical admittance at the actuator terminals.



6C-6

5:45 PM **A Cylindrical Ultrasonic Motor for NMR Sample Spinning in High Magnetic Field**

Hiraku Maeda¹, Akihito Kobayashi¹, Takefumi Kanda¹, Koichi Suzumori¹, Kiyonori Takegoshi², Takashi Mizuno³,
¹Okayama University, Okayama, Japan, ²Kyoto University, Kyoto, Japan, ³JEOL limited, Tokyo, Japan

Background, Motivation and Objective

Recently, in the medical, chemical, and biological fields, the demand for instruments which use high magnetic fields has increased. A high-resolution solid-state nuclear magnetic resonance (solid-state NMR) analysis system is one of such instruments. As for the solid-state NMR analysis, samples are required to spin at high speed. Therefore the solid-state NMR needs actuators which are used for sample spinning at high speed with accuracy under the high magnetic field. This research aims to develop an actuator for the solid-state NMR with low interference against the magnetic field.

Statement of Contribution/Methods

Currently, micro air turbines are used for sample spinning of the solid-state NMR. Although these actuators are available in the high magnetic field, it is too difficult to be used in high pressure or ultralow temperature. Generally, ultrasonic motors have low electromagnetic interference, and they are easily downsized. Thus ultrasonic motors are advantageous to the high magnetic field. Furthermore it will be easy to use ultrasonic motors in high pressure because of its advantage in downsizing. We have designed an ultrasonic motor for sample spinning of the solid-state NMR. The motor has to consist of nonmagnetic materials in order to be used in the high magnetic field. We have applied a cylindrical micro ultrasonic motor to the NMR motor. To realize high speed spinning, a transducer consists of a cylindrical metal stator with a disk piezoelectric element. The diameter and the height of the NMR motor are 11 mm and 47.9 mm including sample case. The stator of the NMR motor, which has 3 mm in outer diameter and 15 mm in height, was made of brass. We have evaluated driving performances about this NMR motor.

Results

The revolution speed was measured in changing magnetic field from 0 T to 7 T. There was no influence of the magnetic field to drive the NMR motor. The revolution speed of NMR motor and the starting torque were 3.7×10^3 rpm and 9.6×10^{-2} mNm when applied voltage, the driving frequency, the preload, and the magnetic field were 280 V_{p-p}, 34.4 kHz, 0.01 N, and 7 T, respectively. The revolution speed of NMR motor was controlled in the magnetic field. Then the error of revolution speed was less than or equal to 5 % when the speed was 3000 rpm. From these results, the NMR motor has achieved a stable spinning in the high magnetic field. Additionally, ¹H-NMR analysis of H₂O was conducted. We have succeeded in obtaining the signals of H₂O by using NMR motor.

Discussion and Conclusions

In this paper, we have designed the NMR motor and have succeeded in driving the NMR motor with no influence of the magnetic field. Additionally, because ¹H-NMR signals of H₂O have been obtained, this NMR motor is available for sample spinning of the solid-state NMR.

Monday Poster Sessions

P-S. Student Finalist Poster Session

Sala Orange

Monday, September 21, 2009, 10:00 am - 11:30 am

Chair: **Donald E. Yuhas**
Industrial Measurement Systems, Inc.

P-S-1

The role of compressional pressure in formation of dense bubble clouds in histotripsy

Adam D. Maxwell¹, Tzu-Yin Wang¹, Charles A. Cain¹, J. Brian Fowlkes¹, Oleg A. Sapozhnikov², Michael R. Bailey², Zhen Xu^{1,1} *Biomedical Engineering, University of Michigan, Ann Arbor, MI, USA,* ²*Applied Physics Laboratory, University of Washington, Seattle, WA, USA*

Background, Motivation and Objective

The onset of tissue fractionation by histotripsy pulses has been shown to coincide with initiation of a dense cavitating bubble cloud. Histotripsy pulses are short (<20 cycles) and highly non-linear, with high peak rarefactional pressures (>10MPa) and compressional pressures (>30MPa). How a histotripsy pulse forms a dense cloud in tissue is not clearly understood. Using high-speed imaging, we studied bubble cloud formation induced by a histotripsy pulse and the role of the positive pressure phase in cloud formation.

Statement of Contribution/Methods

Bubble clouds were generated in a gelatin tissue phantom using histotripsy pulses. A focused, 1-MHz transducer (aperture = 10 cm, $f\# = 0.9$) was used to apply single 15-cycle pulses with peak negative/positive pressures of 19/70 MPa. Shadowgraphic images of pulse propagation and bubble cloud formation were recorded with a high-speed camera at 0.1-10 million fps. To assess the importance of the compression phases of the pulse in forming bubble clouds, an 80-um thickness steel foil was placed between the transducer and focus to reflect the high frequency components found in the positive shock. As a result, the transmitted positive pressure was reduced by 48%, while peak negative pressure remained unchanged.

Results

High speed images show that in the first 3-5 cycles of the ultrasound pulse, a sparse field of single cavitation bubbles with maximum radii of 50 – 120 um was formed within 5 mm of the focal region. During subsequent cycles, a dense cavitation cloud erupted from one of the single bubbles at the focus, and grew in length opposite the direction of ultrasound propagation until all 15 cycles passed the focus. After the pulse ended, the cloud ceased growth and collapsed. Images suggest that the cavitation cloud started to form directly after incidence of the shock front on the single bubble. When the positive pressure at the focus was reduced, single bubbles still formed, but a bubble cloud was never observed.

Discussion and Conclusions

Bubble clouds nucleate from the location of a single cavitation bubble. After single bubbles are generated, a high compression component of the ultrasound cycle is necessary to induce cavitation clouds. Based on these results, we hypothesize that the backscattered shock from a single cavitation bubble is inverted, resulting in extremely high rarefactional pressure, which is responsible cloud formation.

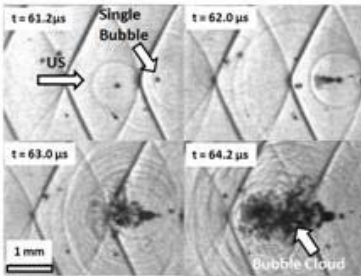


Fig. 1 – Bubble cloud forming from single bubble during 3 cycles of a histotripsy pulse

P-S-2

Forward-Looking Volumetric Intracardiac Imaging Using a Fully Integrated CMUT Ring Array

Amin Nikoozadeh¹, Omer Oralkan¹, Kai Thomenius², Aaron Dentinger², Douglas Wildes², Kalyanam Shivkumar³, Aman Mahajan³, Douglas N. Stephens⁴, Matthew O'Donnell⁵, David Sahn⁶, Pierre T. Khuri-Yakub¹: ¹Stanford University, Stanford, CA, USA, ²General Electric Corporate Research & Development, Niskayuna, NY, USA, ³University of California, Los Angeles, Los Angeles, CA, USA, ⁴University of California, Davis, Davis, CA, USA, ⁵University of Washington, Seattle, WA, USA, ⁶Oregon Health and Science University, Portland, OR, USA

Background, Motivation and Objective

Atrial fibrillation is the most common type of cardiac arrhythmia that now affects over 2.2 million adults in the United States alone. Currently fluoroscopy is the most common method for guiding interventional electrophysiological procedures.

We are developing a 9-F forward-looking intracardiac ultrasound catheter for real-time volumetric imaging. This catheter not only improves visualization and ultimately procedural success but also reduces the undesirable use of fluoroscopy.

Statement of Contribution/Methods

We designed and fabricated a 64-element 10-MHz CMUT ring array with through-wafer via interconnects. The outside and inside diameters of the ring measure 2.6 mm and 1.6 mm, respectively. The central opening of the ring can potentially be utilized to deliver a variety of devices such as HIFU transducers, RF ablation electrodes, and optical fibers for photo-acoustic imaging.

We also designed custom front-end electronics to be closely integrated with the CMUT array at the tip of the catheter for improved SNR. This integrated circuit (IC) is composed of preamplifiers and protection circuitry, and can directly interface a standard imaging system. This multi-channel IC is designed in a high-voltage process and is capable of passing up to ± 50 V bipolar pulses. Every channel in this IC is composed of two separate paths that meet at both the input and output of the channel: the transmit path, which is only composed of diode expanders, and the receive path, which contains a transimpedance amplifier and a buffer. Both the amplifier input and buffer output are protected from high voltage pulses using diode limiters.

An 8-channel front-end IC was fabricated based on this circuit topology. Additionally, a flexible PCB (flex) was designed that is composed of 8 long and narrow legs that intersect at the center of the flex. The ring array is flip-chip bonded to the center of the flex and one IC is flip-chip bonded to each leg to address a total of 64 channels. The flex legs are then folded around the ring array for final integration with the catheter.

Results

The IC was wire-bonded to a ring array for bench-top testing. We successfully applied up to ± 50 V bipolar pulses to the IC and measured an amplifier recovery time of less than 300 ns. We performed a pulse-echo experiment with the ring array immersed in oil. The CMUT array was biased at negative 70 V and a 2-burst ± 45 V sine wave was applied to an element. We measured a SNR of about 30 dB for the echo from the oil-air interface that was about 5.2 mm away. In another experiment, with the array biased at negative 60 V and a ± 45 V 8-MHz tone burst input, we measured an acoustic pressure of 1.4 MPa_{r-p} at the face of the array element.

Discussion and Conclusions

The presented experimental results demonstrate the performance of the main components of our forward-looking volumetric intracardiac imaging approach. We are currently working on the final catheter integration and backend imaging system development.

Supported by the NIH under grant HL67647.

P-S-3

Applications of Low Intensity Pulsed Ultrasound for Functional Bone Tissue Engineering using Adult Stem Cells

Skylar Marvel¹, Elizabeth Loba¹, Paul A. Dayton¹; ¹Joint Dept of Biomedical Engineering, University of North Carolina-North Carolina State University, USA

Background, Motivation and Objective

Low intensity pulsed ultrasound (LIPUS) has been used to accelerate fracture healing for over a decade. In 1994 the FDA approved a LIPUS device for fracture healing and in 2000 for nonunions. Despite this, there is still a lack of understanding the effects of ultrasound (US) parameters on cell growth. There are very few published studies that examine US pulse repetition frequency (PRF), a crucial parameter in US dose. Also, most studies are limited to the parameter ranges available within the capabilities of commercially made systems, such as a 1 MHz sine wave, 30 mW/cm² intensity applied for 20 min. per day, pulsed for 200 μ s with a PRF of 1 kHz, giving a 20% duty cycle.

Statement of Contribution/Methods

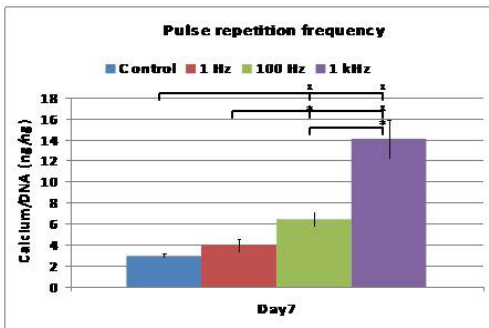
We combine expertise in tissue engineering and US physics to study the effects of LIPUS parameters on stem cell differentiation for both human bone marrow derived (hMSC) and adipose derived (hASC) adult stem cells. We have built a custom LIPUS system, which has extreme flexibility over parameter selection, in order to determine separate optimal parameter settings that will increase calcium production while also decreasing adipose production for each cell type.

Results

In recent preliminary studies, our group has discovered significant effects of LIPUS on the differentiation of stem cells. Specifically, we have found that application of LIPUS to hMSCs is capable of increasing the calcium production per cell ($p < 0.05$ control/1 kHz, 100 Hz/1 kHz) while significantly decreasing adipogenic differentiation ($p < 0.05$ control/100 Hz, control/1 kHz, 1 Hz/1 kHz). The application of LIPUS to hASCs also significantly increases calcium accretion per cell (Figure 1, $p < 0.01$ control/100 Hz, control/1 kHz, 1 Hz/1 kHz; $p < 0.05$ 1 Hz/100 Hz, 100 Hz/1 kHz).

Discussion and Conclusions

Clearly more research needs to be done exploring the effects of LIPUS on stem cells. These two cell types can be used for creating bone constructs to fill critical bone defects. Our results are particularly exciting because hASCs are understudied and have only recently begun to gain interest to researchers since they are readily available, easily obtained and new lineage potentials are continually being discovered. One of the significant factors for LIPUS has been determined to be the PRF. Once proper parameters have been found, LIPUS can be incorporated into modern bioreactors as an additional stimulus to produce a desired differentiation.



Flexible Ultrasonic Transducers for Structural Health Monitoring of Pipes at High Temperatures

Jeanne-Louise Shih¹, Makiko Kobayashi², Cheng-Kuei Jen^{2,1} *McGill University, Canada, ²Industrial Materials Institute National Research Council Canada, Canada*

Background, Motivation and Objective

Structural health monitoring (SHM) and non destructive evaluation (NDE) of pipes in power, chemical and petroleum plants and other structures have become increasingly important in the improvement of safety and in the extension of these structures' lifespans. In these applications, ultrasonic transducers (UTs) may need to be conformed to structures that have surfaces with different curvatures and may need to be operated at elevated temperatures. Conventional piezoelectric UTs having rigid flat end surfaces may not be convenient for such type of inspections due to poor signal to noise ratio (SNR) in the pulse-echo mode. The main goal of this research is to develop a simple and an economical on-site sensor fabrication approach. One objective is to develop piezoelectric flexible ultrasonic transducers (FUTs) including those formed in array configurations that can be made in the lab. Another objective is to develop an on-site bonding technique such as brazing to bond FUTs onto pipes to achieve excellent bonding for permanent SHM and NDE purposes.

Statement of Contribution/Methods

The sol-gel fabricated thick piezoelectric films coated directly onto 75 μm thick steel or titanium membranes serving as FUTs have been developed with a rapid thermal treatment and a poling under ultraviolet light technique. Top electrodes, electrical wire, conductive bonding and connectors were also developed for operation at up to 500°C. Array configurations in 1D and 2D were made by varying the arrangements of the top electrode layouts. Special induction heating techniques were developed to braze such FUTs directly onto steel pipes, where the brazing material between the FUT and the external surface of the pipe served as a permanent high temperature couplant for SHM and NDE applications.

Results

At room temperature, the ultrasonic signal strengths of the developed FUTs made of PZT composite films were the same as those of the commercially broadband UTs centered at 5 – 10 MHz. Such FUTs centered at around 11 MHz and brazed onto steel pipes with a 26.6 mm outer diameter and a 2.5 mm pipe thickness showed ultrasonic echoes with a signal-to-noise ratio (SNR) of at least 26 dB at 150°C in pulse-echo mode. FUTs made of bismuth titanate composite films and centered around 12 MHz were also made and brazed onto steel pipes and their operation temperature reached up to 500°C. Individual ultrasonic performance of the 16-element 1D and 2D FUT arrays also showed to be similar.

Discussion and Conclusions

FUTs and arrays are small, lightweight and have a high level of sensitivity that is comparable to commercially available broadband UTs at room temperature. They can be conformed to pipes and this ensures high SNR during pulse-echo measurements. Since FUTs together with all necessary electrical connections can operate at up to 500°C and can be fabricated on-site, they are excellent candidates for the purposes of SHM and NDE of pipes.

Temperature Compensated Solidly Mounted BAW Resonators with Thin SiO₂ Layers

Mohamed Abd Allah¹, Jyrki Kaitila^{2,3}, Robert Thalhammer^{2,3}, Werner Weber², Doris Schmitt-Landsiedel^{1,1} *Lehrstuhl für Technische Elektronik, Technische Universität München, Munich, Germany, ²Infinion Technologies, Munich, Germany, ³currently at Avago Technologies GmbH, Munich, Germany*

Background, Motivation and Objective

Temperature compensation is becoming more and more a high demand for RF filters in order to successfully meet the tightening specifications over a wide range of temperatures. In BAW resonators SiO₂ has been the material of choice for compensation due to its unique positive temperature coefficient of elasticity which is opposite to that of AlN and the metal electrodes. This work investigates adding thin SiO₂ compensation layers at high stress regions inside the resonators, examining their effect on the resonators Temperature Coefficient of Frequency (TCF) and extracts an accurate value of the temperature coefficient of elasticity of SiO₂.

Statement of Contribution/Methods

SiO₂ thin film layers ranging from 20-60 *nms* were placed inside the resonator, in the middle of the AlN piezoelectric layer where the stress at this location is orders of magnitude higher than that around the electrodes. In this setup the resonator TCF is very sensitive to the variation of thickness of SiO₂, and hence, it is possible to compensate resonators with a minimum amount of SiO₂ inside the resonator. With this high TCF sensitivity to the oxide thickness, it is possible to extract with high degree of accuracy the temperature coefficient of elasticity TC₃₃ of the thin film SiO₂.

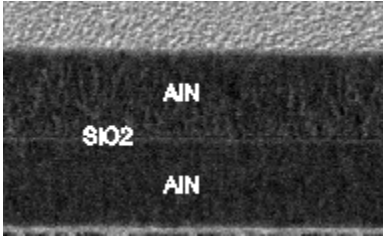
Results

Solidly mounted BAW resonators working around 2.47-2.65GHz have been manufactured with TCF ranging from -11ppm/°C till +12ppm/°C.

The extracted temperature coefficient of elasticity TC₃₃ of SiO₂ is found to be +110ppm/°C which is significantly different from that of the bulk value of +237ppm/°C

Discussion and Conclusions

Fully compensated solidly mounted BAW resonators utilizing very thin SiO₂ layers have been manufactured. The temperature coefficient of elasticity TC₃₃ of the thin film SiO₂ is different from the bulk value used in literature.



P-S-6

Unified model for nonlinear effects in BAW resonators

Eduard Rocas¹, Carlos Collado¹, Enrique Iborra², Robert Aigner³; ¹Signal Theory and Communications, Universitat Politècnica de Catalunya, Barcelona, Spain, ²Grupo de Microsistemas y Materiales Electrónicos, Universidad Politécnica de Madrid, Madrid, Spain, ³R&D Acoustic Technologies, Triquint Semiconductor, Apopka, Florida, USA

Background, Motivation and Objective

A complete physical model for intermodulation distortion and harmonics prediction is presented for thin film BAW resonators. The model consists on an extension of the Nonlinear Distributed KLM one that includes the significant role of thermal effects on material properties, which lead to IMD and harmonics generation

Statement of Contribution/Methods

Integrated physical circuit model.

The nonlinear effects are modeled with a stress and temperature dependent elasticity.

The material layers, thermally represented as a cascade of series thermal resistances and shunt heat capacitances, are coupled to the acoustic domain by dissipation and self-heating effects (Fig.1). The materials stack configuration and the packaging set the thermal dynamic response. The unified model allows to know the temperature distribution along the device, which depends on the slow time-varying instantaneous dissipated power.

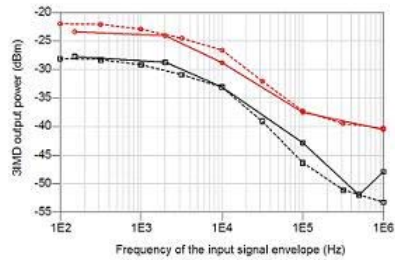
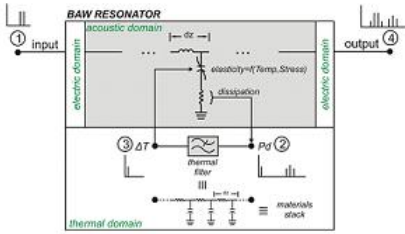
Third order IMD (3IMD) results from the contribution of both the stress dependent elasticity and the thermal effects.

Results

Simulation results show good agreement with measurements of second harmonics and 3IMD performed on BAW resonators of different areas. Figure 2 shows the simulated results (dotted lines) and measured (continuous lines) 3IMD output power at 2f1-f2 for two resonators (circles and squares). The 3IMD power depends on the input signal envelope because of the existence of thermal effects.

Discussion and Conclusions

The importance of having a unified model that accounts for the electric, mechanic and thermal domains is key to predict the nonlinear behavior of BAW resonators. The accurate modeling of the IMD generation mechanism is a significant step towards more linear designs of BAW filters for high power applications.



Monday Poster

P-S-7

Ultrasound Catheter for Microbubble Based Drug Delivery

Joseph Kilroy¹, Linsey C. Phillips¹, Abhay V. Patil¹, John Hossack¹, ¹Biomedical Engineering, University of Virginia, Charlottesville, Virginia, USA

Background, Motivation and Objective

Atherosclerosis is the leading cause of death in the developed world. Current methods of treating atherosclerotic occluded blood vessels include angioplasty followed by stent placement. Unfortunately, the potential for re-occlusion often requires the use of anti-proliferative agents. An intravascular ultrasound (IVUS) catheter that delivers drug coated microbubbles through radiation force and bursts the bubbles has been simulated and fabricated. The novel component of this device is the use of IVUS for combined radiation force for translation of bubbles into position followed by bubble breaking for drug delivery.

Statement of Contribution/Methods

Finite Element Analysis (FEA - PZFlex, WAI) was used to model the acoustic performance of an IVUS transducer for radiation force and destruction modes of operation. Microbubble translation was simulated with bubble diameters of 2, 2.5, and 4 microns based on minimum, maximum, and mean sizes for bubbles used in a flow phantom experiment. A custom IVUS transducer was designed to operate at 1.5MHz with 80 kPa and 170 kPa PNP for translation and destruction, respectively. Transducer acoustic performance was tested using a hydrophone in water when excited by a 1.5 MHz Gaussian ramped pulse.

Capacity to deliver drugs or genes was tested by breaking microbubbles carrying a red fluorescent reporter gene in proximity to rat smooth muscle cells in vitro with a -170 kPa PNP, 1.5 MHz Gaussian Pulse at a PRF of 1 kHz.

IVUS radiation was tested in a flow phantom with 4.5 mm diameter vessels coated with streptavidin to anchor bubbles once they contact the vessel surface. A solution of 2.5 micron mean diameter biotin bubbles concentrated at 4.1×10^6 bubbles/ml was flowed at 30 ml/min for 26 seconds. During flow the bubbles were exposed to a 1.5 MHz 80 kPa PNP Gaussian ramped pulse at 8 kHz PRF. The accumulation of bubbles along the vessel wall was measured in terms of image intensity by transcutaneously scanning with an Ultrasonix Research Platform Scanner and bubble specific real time imaging software developed in our laboratory.

Results

The FEA of the transducer design compared with measured acoustic output of the transducer has a correlation coefficient of 0.98. Translation model results show 2, 2.5, and 4 micron bubbles move at mean velocities of 0.4, 1, and 3 cm/s respectively. The change in image intensity on the targeted wall of the vessel was 12.5 dB. In vitro gene transfection, as a surrogate for drug delivery, of rat smooth muscle cells was achieved with the new transducer.

Discussion and Conclusions

In this paper an IVUS catheter for microbubble based drug delivery was simulated, assembled, and tested. The IVUS catheter translated microbubbles across a flow phantom vessel using radiation force in accordance with the

simulation results. Gene transfection was achieved using burst sequences. To the authors' knowledge this is the first demonstration of IVUS-mediated radiation force delivery of microbubbles to a simulated vessel wall.

P-S-8

Evaluation of CMUT Annular Arrays for Side-looking IVUS

Alper SISMAN¹, Jaime Zahorian², Gokce Gurun², Mustafa KARAMAN¹, Mujdat Balantekin², F. Levent Degertekin², Paul Hasler²; ¹Isik University, Electronics Eng. Dep., Turkey; ²Georgia Institute of Technology, USA

Background, Motivation and Objective

Side-looking (SL) IVUS probes are extensively used for management of cardiovascular diseases. Probes with single rotating piezoelectric transducer have simple front-end, but have fixed focused operation, and suffers from motion artifacts. Solid state SL-IVUS imaging probes use piezoelectric transducer arrays and electronic beamforming, and hence do not suffer from motion artifacts. Synthetic phased array processing of signals detected with small-sized array elements limits the SNR achievable with these probes. In this study, we explore, through experiments and simulations, a SL-IVUS probe architecture employing rotating phased annular CMUT array with integrated front-end microelectronic circuits for both low-cost, low-profile, and advanced IVUS probes.

Statement of Contribution/Methods

We designed and fabricated 840- μm diameter, 8 element CMUT annular arrays operating around 50-MHz using a low temperature process. The elements are discretized with 18- μm wide rings and arranged to have roughly equal area. We characterized the imaging performance of these arrays using wire target phantoms in water tank and verified our simulation methods for fixed and dynamic receive focusing arrays. We also produced simulated PSFs of rotating probe employing a fixed-focus transducer (at $f\#$ 2) and a solid-state array probe with a 64-element ring array. We compared the simulated PSFs of the CMUT annular array with these two existing probe architectures.

Results

We performed imaging experiments with the CMUT annular arrays in water. The measured axial/ lateral resolution provided by 50-MHz arrays is 35 μm /120 μm , respectively for a target at $f\#$ of 3.8 using dynamic receive focusing. The array with parylene coating shows approximately 40% fractional bandwidth measured in water limited by the cross talk as predicted by FEA. The simulation results show that the proposed annular array produces better beam quality in different depths than the fixed-focus single transducer and solid-state linear array. For example the beam widths at $f/3$ of the simulated PSFs of these three schemes are 4.4, 4.9 and 8.7 degrees respectively.

Discussion and Conclusions

CMUT based high frequency annular arrays with dynamic receive focusing provide significant improvement over single element fixed focus transducers as well as existing solid state SL-IVUS arrays. The crosstalk in CMUT arrays needs to be explored further to improve the axial resolution.

P-S-9

Heterodyne laser-doppler interferometric characterization of contour-mode resonators above 1 GHz

Hengky Chandrahilim¹, Sunil Bhawe¹, Christian Rembe², Sebastian Boedecker², Ronald Polcawich³, Jeff Pulskamp³; ¹Electrical and Computer Engineering, Cornell University, Ithaca, New York, USA, ²Polytec, Germany, ³US Army Research Laboratory, USA

Background, Motivation and Objective

AFM has been used to image and characterize vibrations of MEMS resonators [1]. Characterization of MEMS resonators using heterodyne interferometer is of interest because it provides accurate measurement of resonances and broadband vibrations [2,3] without contacting the surface of the resonators.

Statement of Contribution/Methods

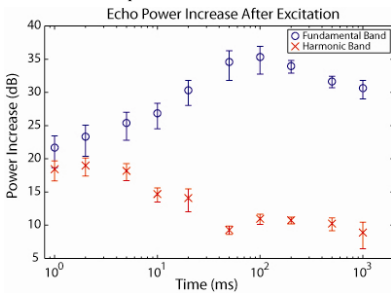
We report a special technique to measure frequencies and vibrations of contour-mode resonators (Fig. 1a) up to 1.2 GHz using only a 618 MHz carrier frequency (f_c). The detector signal of the vibrometer is digitized by a fast oscilloscope and demodulated off-line in a computer (Fig. 1b). This method enabled us to realize an algorithm to extend the measurement bandwidth by a factor of 2. The algorithm takes only the frequency components of the detector signal into account which are higher than f_c to construct an IQ-(in-phase, quadrature) signal from a virtual carrier signal with 2x the original frequency. The Rohde & Schwarz SMBV100A broadband Vector Signal

Results

Echoes from droplets excited at sufficiently high PNP (above 1.7 MPa) had a significant increase in power at both the fundamental (1.75MHz) and second harmonic (3.5MHz) bands 1ms after excitation, indicating phase conversion and subsequent resonant oscillation. In the first 100ms the fundamental signal was shown to further increase while the harmonic signal decreased prior to stabilizing for a time interval of at least 1s. Vapourized droplets were successfully detected with pulse inversion imaging. Optically, converted droplets were shown to grow in size over approximately the first 100ms, from $1.79 \pm 0.67 \mu\text{m}$ in diameter to $6.43 \pm 1.80 \mu\text{m}$, and were then stable over the next 900ms.

Discussion and Conclusions

Gas bubbles formed from excited droplets undergo increase in size in the first ~100ms, attributed to the uptake of dissolved gases from the host liquid. Following initial expansion, the bubbles stabilize in size for at least 1s, sufficient for diagnostic detection. Bubble size dynamics are also reflected in nonlinear acoustic scatter. The simultaneous power increase in the fundamental band and decrease in the harmonic band suggest that bubbles grow through their resonant size. Such characteristic behavior may serve as a basis for converted droplet specific detection techniques in-vivo.



P-S-11

Optical observations of microbubble oscillation in small tubes

David Thomas¹, Marcia Emmer², Hendrik Vos², Vassilis Sboros¹, Nico de Jong²; ¹Medical Physics, University of Edinburgh, United Kingdom, ²Thorax Center, Biomedical Engineering, Erasmus Medical Center, Netherlands

Background, Motivation and Objective

In diagnostic medicine, microbubbles (MBs) are used as contrast agents to image blood flow. Over 50% of the blood volume is contained within vessels of diameters under 25 μm . Previous theoretical predictions show a decrease in both magnitude of MB oscillation and resonance frequency due to the restriction from a tube with a diameter of the same order of magnitude as the microbubble. Since microbubble oscillation in vivo will be constrained in this manner, studies of microbubble oscillations in such tubes are needed to further understand this effect.

Statement of Contribution/Methods

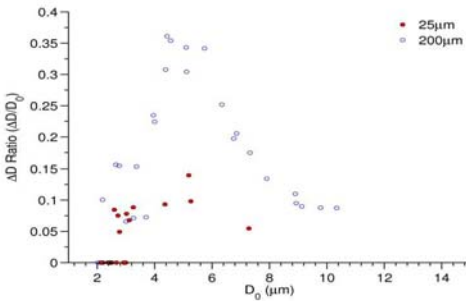
We studied the difference in the oscillation of Definity (Lantheus Imaging) MBs in tubes with inner diameter of 25 μm and 200 μm . Using the ultrahigh speed Brandaris 128 camera, the radial motion of oscillation was captured at ~12 million frames per second. MBs were insonified with six cycle pulses of 1.7 MHz and the acoustic pressure varied between 50 – 600 kPa. An MB spectroscopy technique, with the applied frequency scanned from 1.0 to 6.0 MHz, was also used to calculate the resonance frequency of MBs at 50kPa in both tubes.

Results

A significant reduction in oscillation was observed for MBs in the smaller 25 μm tube, when compared to those in a 200 μm tube. A difference was observed at all pressures (Fig. 1 shows results at 50kPa). In the 25 μm tube, at 50kPa an increased incidence of MBs which did not oscillate above the noise level of the system was observed (56% of MBs compared to 8% in the 200 μm tube), indicating an increased oscillation damping. Unlike theoretical predictions no difference was observed between the resonance frequency curves calculated for MBs in 25 μm and 200 μm tubes.

Discussion and Conclusions

While previous investigators have shown the effect of microvessels on MB oscillation at high ultrasound pressures, the present study provides the first optical images of low amplitude microbubble oscillations in small tubes. These results show significant influence of a small tube on the damping of the oscillation of phospholipid-coated microbubbles at clinically relevant acoustic pressures, but no significant shifts of resonance.



P-S-12

Ex Vivo Measurements of Mechanical Properties of Myocardium Using Lamb and Rayleigh Wave Dispersion Velocities

Ivan Nenadic¹, Matthew W. Urban¹, James F. Greenleaf¹; ¹Mayo Clinic College of Medicine, USA

Background, Motivation and Objective

Decreased elasticity of left ventricular (LV) myocardium causes a decrease in LV relaxation and reduced passive filling which could lead to heart failure. Shearwave Dispersion Ultrasound Vibrometry (SDUV) is a noninvasive method for quantifying mechanical properties of soft tissue using radiation force to excite harmonic shear waves and a pulse echo ultrasound transducer to estimate shear wave velocity [1]. We investigated the feasibility of using Rayleigh and Lamb waves to quantify viscoelasticity of excised myocardium.

Statement of Contribution/Methods

A dissected porcine LV myocardium samples were embedded in gelatin in a container and mounted on a stand inside a water tank. A glass rod coupled to a mechanical actuator was used to excite harmonic shear waves at different frequencies in the range 40 – 500 Hz and a pulse-echo transducer to detect tissue motion. In order to excite Lamb waves, the glass rod was glued to a hole bored through the thickness of the myocardium. Rayleigh waves were excited by placing a ball point rod on the surface of the sample and coupling the rod to the mechanical actuator. Amplitude and phase of the motion at different depths of the sample were analyzed to obtain dispersion curves in four orthogonal directions. Lamb wave dispersion curves were fitted by an anti-symmetric Lamb wave model [2]. An equation for Rayleigh wave dispersion was derived by modeling the excised myocardium with a homogeneous Voigt material slab immersed in a nonviscous fluid. Boundary conditions and wave potential functions were solved for the surface wave velocity.

Results

Estimated dispersion speeds of Lamb and Rayleigh waves in four orthogonal directions were within one standard deviation for all excitation frequencies. Shear elasticity and viscosity of the myocardium sample estimated from the Lamb wave dispersion curves were 9.50 ± 1.30 kPa and 9.25 ± 0.50 Pa*s. Shear elasticity and viscosity estimated from the Rayleigh wave dispersion curves were 11.25 ± 1.50 kPa and 8.13 ± 1.31 Pa*s. Mathematical expressions for Lamb and Rayleigh wave dispersion converge analytically in the frequency range above 100 Hz.

Discussion and Conclusions

Estimated values of elasticity and viscosity obtained by fitting Lamb and Rayleigh wave dispersion curves were similar in four orthogonal directions. This study suggests that material properties of the myocardium can be obtained using SDUV by exciting shear waves on either the epicardial surface or throughout the thickness of the myocardium.

- [1] S. Chen, M. W. Urban, C. Pislaru, R. Kinnick, Y. Zheng, A. Yao, J. F. Greenleaf. Shearwave dispersion ultrasound vibrometry (SDUV) for measuring tissue elasticity and viscosity. *IEEE Trans Ultrason Ferroelectr Freq Control*. 2009 Jan; 56(1):55-62.
- [2] H. Kanai. Propagation of Spontaneously Actuated Pulsive Vibration in Human Heart Wall and In Vivo Viscoelasticity Estimation. *IEEE Transactions on Ultrasonics, Ferroelectrics, and Frequency Control*, vol. 52, no. 11, Nov 2005.

P-S-13

Surface Acoustic Wave Interdigital Transducers Response to Deep UV Illumination in AlGaN/Sapphire

Venkata Chivukula¹, Daumantas Ciplys², Michael Shur¹, Jinwei Yang³, Remis Gaska^{2,1}, ¹Center for Integrated Electronics, Rensselaer Polytechnic Institute, Troy, New York, USA, ²Department of Radiophysics, Vilnius University, Vilnius, Lithuania, ³Sensor Electronic Technology, Inc., Columbia, South Carolina, USA

Background, Motivation and Objective

Aluminum-gallium nitride (AlGaN) alloys are promising materials for wavelength-tunable solar-blind SAW UV sensors. Despite recent developments in making sensitive AlGaN based delay line oscillators for deep UV applications, the physical origin of SAW frequency/phase change under UV is not completely understood. The objective of our work is to study the impact of UV illumination on performance of SAW interdigital transducers (IDT) deposited on AlGaN surface. These results are important for design and development of efficient SAW devices for UV sensing and high performance filters with tunable frequency response for signal processing applications.

Statement of Contribution/Methods

We have investigated the impact of UV illumination on admittance of IDT deposited on AlGaN - sapphire structure. The 2 μm thick AlGaN layer with Al molar fraction of 0.4 was deposited on (0001) surface of sapphire substrate by MEMOCVD technique. The IDT period was 16 μm corresponding to the SAW frequency of 335 MHz. The IDT admittance in a wide frequency range was extracted from S11 measurements with a vector network analyzer. Light emitting diodes (LEDs) with wavelengths from 280 nm to 375 nm were used as a UV source.

Results

We have observed the strong impact of UV illumination on both the real and imaginary parts of IDT admittance over entire frequency range investigated. This is illustrated by Fig. 1 for real part of admittance at frequencies in the vicinity of the SAW excitation. We perform the analysis of impact on SAW excitation of UV-induced changes in electrical properties of the IDT.

Discussion and Conclusions

We demonstrate, for the first time, that the SAW excitation in AlGaN/sapphire can be affected by the UV-induced changes in electrical properties of the IDT. In particular, these changes might be important mechanism responsible for the change in phase/frequency and insertion loss in AlGaN/sapphire based SAW UV sensors.

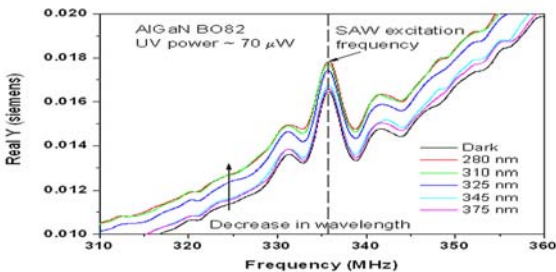


Figure 1: Dependence of IDT conductance on frequency for different UV wavelengths at constant UV power.

Measurement of three-dimensional distribution of crack tips by low power pulsed laser

Atsushi Miyamoto¹, Mami Matsukawa¹; ¹Doshisha University, Kyotanabe-shi, Kyoto, Japan

Background, Motivation and Objective

One recent solution to detect cracks in solid materials is nonlinear approach, which still has a problem of spatial resolution. We then propose a simple method to detect cracks with good spatial resolution, making use of two different techniques, laser induced pulse waves and the two-layered transducer. In this transducer, a PZT layer transmits longitudinal waves to fluctuate the crack tips. The other PVDF layer detects laser induced pulse waves, which gives us the information of crack positions. By scanning the irradiation points of laser on the sample surface, we have obtained three-dimensional distribution image of the crack tips.

Statement of Contribution/Methods

An acrylic resin sample with a plane crack was used. As shown in Fig.1, both top and bottom PVDF transducers received the transmitted and reflected waves in the sample. The PZT transducer transmitted continuous large amplitude longitudinal waves at 500 kHz. Low power laser pulses (Spectra Physics R2-VSS-104Q, 1047 nm, 80 micro J, pulse width 5 ns, repetition time 1 ms, irradiation area 0.6 mm in diameter) irradiated the top PVDF transducer, where pulse waves were induced.

The phase adjustment of continuous wave made the pulse waves passing through the opening or closing crack tips. The pulse waves were then extracted from the output of bottom PVDF receiver and analyzed. We repeated this measurement, scanning the laser irradiation area on the sample surface.

Results

We have compared the observed pulse waves which passed through the opening (P) and closing (N) cracks. The normalized spectra, $P(f) / N(f)$ of these waves showed peaks around 22 MHz. The spatial distribution of these peaks gave us the map of crack tips in the X-Y plane. The spatial resolution of this map was around 3 mm, which depended on the directivity of induced pulse waves. The top PVDF transducer received the reflected waves from the large crack area. From the time delay of the reflected waves, we obtained the depth (Z) profile of the crack. However, we could not obtain the reflected waves near the crack tips.

Discussion and Conclusions

The depth profile of the crack was in good agreement of X-ray CT data of this sample. By extrapolating the depth profile of the crack, we estimated the depth near the crack tips and combined it with the distribution of crack tips in the X-Y plane. This procedure successfully brought us a three-dimensional distribution image of the crack tips.

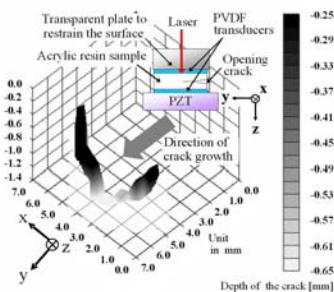


Fig.1 Three-dimensional distribution image of the crack tips.

Extraction of Pt/Rh/ZrO₂ High Temperature Elastic Constants

Dana Gallimore¹, Thomas Moonlight², Mauricio Pereira da Cunha³:¹Electrical and Computer Engineering / Laboratory of Surface Science and Technology, University of Maine, Orono, Maine, USA, ²University of Maine, USA, ³Electrical and Computer Engineering / Laboratory of Surface Science and Technology, University of Maine, USA

Background, Motivation and Objective

Filters, signal processing elements, and sensors capable of operating at temperatures up to 1000°C are needed for applications including jet engine and aerospace structure monitoring, industrial processes, and oil exploration. Acoustic wave devices have the potential for use in these environments due to the existence of piezoelectric crystals, notably gallium orthophosphate and langasite (LGS), which retain piezoelectricity up to 930°C and 1470°C, respectively. Temperature limitations are imposed by the thin film electrode material. Standard metal films used for device patterning (such as gold and platinum) experience de-wetting above 700°C, leading to loss of conductivity and signal transduction. A recently developed thin Pt/Rh/ZrO₂ film [1] has been used to pattern acoustic wave devices with successful transduction up to 1000°C. The elastic properties of the Pt/Rh/ZrO₂ film are required for modeling and design of high temperature acoustic wave devices.

Statement of Contribution/Methods

A method for extracting the thin film Pt/Rh/ZrO₂ elastic constants using surface acoustic wave (SAW) measurements is investigated on quartz and LGS. Quartz, due to its well known mechanical properties, is employed for the extraction of Pt/Rh/ZrO₂ elastic constants at room temperature. SAW measurements on LGS are necessary to allow for Pt/Rh/ZrO₂ film annealing, which is performed up to 850°C. SAW delay lines are fabricated with varying substrate orientations and delay paths metalized with Pt/Rh/ZrO₂, which is assumed to be isotropic and non-viscous. The measured SAW phase velocities are input into the matrix method for SAWs to determine independent elastic constants c₁₁ and c₄₄.

Results

Figure 1 shows the c₁₁ vs. c₄₄ curves extracted from Pt/Rh/ZrO₂ measurements on ST-X and ST-40° quartz at room temperature. Figure axes have been normalized to the elastic constants of a reference platinum film. The orientations selected provide comparable piezoelectric coupling and zero power flow angle. The intersection point of the two curves denotes c₁₁ and c₄₄ for the Pt/Rh/ZrO₂ thin film.

Discussion and Conclusions

The values of c₁₁ and c₄₄ differ by 53% and 22%, respectively, when compared to the platinum film constants. These results reveal the importance of characterizing this new film in order to apply it in the design of high temperature acoustic wave devices.

[1] IEEE 2008 Ultr. Symp, pg 205-208

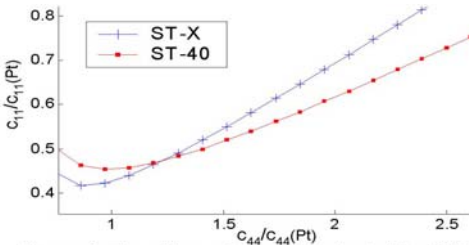


Figure 1: The c₄₄ vs. c₁₁ curves extracted for Pt/Rh/ZrO₂ film based on quartz ST-X and ST-40° measurements.

Angular spectrum method for the estimation of pressure fields in the super harmonic band

Mirza Pasovic¹, Mike Danilouchkine¹, Paul van Neer¹, Antonius van der Steen¹, Olivier Basset², Christian Cachard², Nico de Jong^{1,3}:¹Biomedical Engineering, ErasmusMC, Rotterdam, Zuid-Holland, Netherlands, ²CREATIS-LRMN, Univeriste de Lyon, INSA Lyon, Universite Lyon 1, CNRS UMR 5220, INSERM U630, Lyon, Rhone-Alp, France

Background, Motivation and Objective

Nonlinear propagation is an important physical phenomenon, which is exploited in ultrasound harmonic imaging. Second harmonic imaging is most often used in clinical practice. By using higher harmonics image quality and tissue characterization may be further improved. There is a clear need to model and understand the ultrasound field of the higher harmonics. Numerical simulations, often based on KZK equation, for studying nonlinear wave propagation are time consuming. In this paper, we present a close-form solution of the higher harmonics pressure fields and propose a light-weighted procedure, based on the angular spectrum method (ASM), to compute them.

Statement of Contribution/Methods

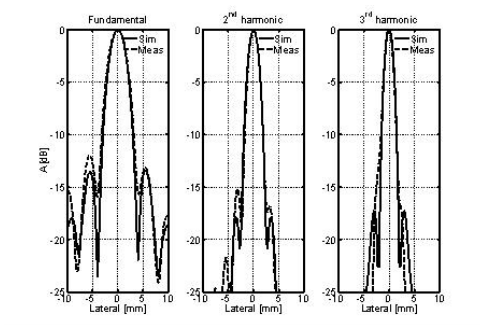
Using the successive approximation method, we have derived an analytical expression, which predicts the change of the shape of the transmitted signal during propagation in a lossless medium. The generated harmonics are described using a set of coupled nonlinear wave equations. The nonlinear term, is a properly scaled second order temporal derivative of the product between the lower harmonic and the fundamental pressure field. The pressure distribution in the plane orthogonal to the direction of the wave propagation can be efficiently computed using the ASM method.

Results

The theoretical findings were corroborated on the lateral beam profiles of a phased-array ultrasound transducer. The computed (solid line) and experimentally measured (dotted line) profiles up to 3rd harmonic, shown in Fig.1, exhibit a striking resemblance. The relative difference in the main lobe width between measurement and simulations at -6dB was 5.5%, 6.5%, and 2.9% for 1st, 2nd, and 3rd harmonic, respectively. The same parameter at -10dB was of the same order of magnitude, with the exception of the 3rd harmonic difference being 0.7%. The simulation time of the ultrasound field, based on KZK equation, is usually 50 minutes. Using the ASM method for the calculation of the higher harmonics decreases the time of the simulation to less than a minute.

Discussion and Conclusions

In this study we focus on similarities of beam profile up to 3rd harmonic. However, the validation can be easily extended to higher harmonics. We demonstrated that the ultrasound pressure fields in the super harmonic band can be reliably computed using an analytical solution in a combination with the ASM method.



P-S-17

Fast Evaluation of Lamb Wave Scattering by Time Harmonic FEM simulation

Florian Thalmayr¹, Ken-ya Hashimoto¹, Tatsuya Omori¹, Masatsune Yamaguchi¹, ¹Graduate School of Engineering, Chiba University, Japan

Background, Motivation and Objective

The evaluation of Lamb wave scattering behavior at geometry irregularities in planar waveguides draws attention for various applications. Numerical methods like Finite Element Method (FEM) are effective to analyze complex structures including multiple layers and/or interfaces.

A common technique is application of the two-dimensional fast Fourier transform (2D FFT) to the Lamb wave field calculated by FEM in the time domain. Drawback of this method is the necessity of FEM for a large number of time steps, consuming a lot of calculation time.

Statement of Contribution/Methods

This paper describes a novel method to evaluate the scattering behavior of Lamb waves in a planar waveguide at an arbitrary reflective geometry by the means of a conventional time harmonic FEM. The evaluation is carried out by applying a simple 1D FFT to the calculated surface displacements for each frequency. Thus necessary computation time is small.

An impedance matching and damping mechanism is inserted between the waveguide and the wave source, which excites one waveguide mode selectively. This is aimed at suppressing unnecessary reflection, mode-conversion and interference at the wave source to an acceptable level.

Results

First, we apply the proposed technique to the evaluation of scattering properties of S0 and S1 Lamb modes at the straight edge of an AlN planar waveguide. We also detail how the damping mechanism should be setup and the simulation is carried out. It should be noted that the design of the mechanism is not arbitrary but has to be adjusted according to waveguide geometry, material and incident mode.

It is shown that the scattering characteristic changes dramatically near the cut-off frequency of the S1 mode corresponding to the thickness extensional resonance frequency. Namely, incident S0 (or S1) mode is back-scattered into the S1 (or S0) mode efficiently below the S1 cut-off frequency, while the mode conversion diminishes above the cut-off frequency.

Secondly we apply the proposed technique for the evaluation of Lamb wave back scattering at the joint of symmetric and asymmetric stepped waveguides, and discuss how the scattering characteristic changes with the ratio of the waveguide thicknesses. Although being below the S1 (or A1) cut-off frequency in the thinner part of the stepped waveguide, we show that the power reflection coefficient of these modes is very dependent on the thickness ratio and becomes significantly smaller than unity due to mode conversion to A0 and/or S0 mode.

Discussion and Conclusions

Because of short execution time, the proposed technique is applicable to the analysis of more complex structures such as practical film bulk acoustic resonators (FBARs). This practice will allow us to characterize energy leakage of these devices through the periphery. Moreover, regarding the border region scattering behavior in FBAR design is a promising approach to improve the device performance further.

P-S-18

Suppression of transverse waveguide modes for SAW resonators with Pt and Pt/Rh/ZrO₂ electrodes

Bennett Meulendyk¹, Mauricio Pereira da Cunha¹, *Electrical and Computer Engineering, University of Maine, USA*

Background, Motivation and Objective

Transverse waveguide modes can appear as spurious resonances in the frequency response of a surface acoustic wave (SAW) resonator. For sensor applications, distinct modes normally respond differently to measurands. For this reason, spurious modes compromise the operation of the main mode by degrading the Q factor, distorting the resonant peak, and ultimately obscuring the sensor response. Additionally, spurious modes can cause unexpected frequency jumping if the resonator is implemented in an oscillator circuit. Transverse waveguide resonances can sometimes be eliminated by choosing the aperture of the device sufficiently small such that the modes are cut-off. However, this technique limits the design flexibility of the device and makes impedance matching difficult. Alternatively, suppression of transverse waveguide resonances can be accomplished through transducer apodization in the transverse direction or by the insertion of dummy electrodes between the active area and the bus bars.

Statement of Contribution/Methods

In this work, spurious transverse waveguide modes were suppressed from the frequency responses of Pt electrode resonators on ST-X quartz [0°, 132.75°, 0°] and Pt and Pt/Rh/ZrO₂ electrode resonators on LGS [0°, 144°, 24°] through careful design of the reflectors, aperture, and transducers' dummy electrodes. In particular, conventional shorted reflectors cannot be used with Pt or Pt/Rh/ZrO₂ electrodes, since the velocity discontinuity between the grating and the bus bar leaks energy from the active area. Additionally, scalar potential theory was utilized to adjust the ratio of the transducer's active area to the total aperture, such that higher-order transverse waveguide resonances are filtered from the frequency response. The stiffness parameters of the co-deposited Pt/Rh/ZrO₂ electrodes determined through SAW delay line measurements in conjunction with the matrix method for SAWs was used for the extraction of the SAW grating velocity.

Results

The Pt electrode resonator design, including the dummy electrodes, along ST-X quartz resulted in an 11% increase in measured Q factor and improved the experimentally observed suppression of a spurious transverse waveguide resonance, 80 kHz above the main resonance, from -8 dBc to -25 dBc. Similarly, the measured response of the Pt/Rh/ZrO₂ electrode resonators on LGS were improved, resulting in a Q factor of 1550 and >10 dBc spurious rejection.

Discussion and Conclusions

Spurious transverse waveguide resonances were successfully suppressed by utilizing scalar potential theory, implementation of dummy electrodes, and proper design of resonators for Pt and Pt/Rh/ZrO₂ electrodes on quartz and LGS. These progresses are relevant, since the co-deposited Pt/Rh/ZrO₂ electrodes on LGS are necessary for their high temperature SAW operation up to 1000 °C and Pt electrodes on quartz are required for their corrosion resistance in gaseous HF sensor applications.

P-S-19

Selectable Frequency CMUT with Membrane Stand-Off Structures

Matthew Eames¹, John Hossack^{1,2} *University of Virginia, USA*

Background, Motivation and Objective

Microbubbles are currently used to enhance ultrasound image contrast and are being considered for use in therapeutic applications such as drug delivery. These functions drive the desire to produce ultrasound transducers that are capable of both high-frequency, high-sensitivity operation for imaging and low-frequency, high-intensity output for bubble-related therapy. Designing a single device to operate at these disparate frequencies – as low as 1MHz to excite bubbles and as high as 40MHz to permit high resolution Intravascular Ultrasound (IVUS)-based imaging – presents a significant challenge.

Research in the area of capacitive micromachined ultrasonic transducers (CMUTs) has demonstrated a membrane-collapse mode of operation that allows a collapsed membrane to operate at approximately double its non-collapse frequency. Through the use of validated finite element analysis (FEA) simulations, we demonstrate the feasibility of implementing partial-height stand-off structures within the device vacuum-gap that divide the device membrane into smaller, higher-frequency sub-membrane structures on membrane collapse in order to produce higher-order shifts in frequency than have been previously reported.

Statement of Contribution/Methods

Extending the proven concept of collapse-mode operation of CMUT devices in this manner contributes to the state of the art in MEMS-based ultrasound and allows the standard operation mode and collapse mode resonances to be designed independently. Simulations were verified against a CMUT fabricated at the University of Virginia Microfabrication Laboratory (UVML) with a correlation coefficient of 0.92 and an amplitude error of 4.1%. Fabrication procedures closely followed previously published techniques. Each CMUT membrane within the device measured 50µm by 250µm, was 2.2µm thick, and was suspended 0.30µm above an insulated substrate electrode.

The proposed stand-off configuration, consisting of three stand-off structures, was modeled using PZFlex (Weidlinger Associates, Inc., Mountain View, CA). An optimization was performed to eliminate out-of-phase motion of the collapsed membrane structures by accounting for the dynamics of the collapsed membrane.

Results

The optimum spans for each of the four sub-membranes as a percent of the total span are 31.8% for the central sub-membranes and 18.2% for the lateral sub-membranes. A hybrid device designed to operate at both 1.5MHz and 40MHz has been shown in simulation to possess comparable bandwidth to each of two single-frequency CMUTs operating at 1.5MHz and 40MHz, respectively, suffering a reduction in output intensity of only 4.0dB and 4.5dB, respectively.

Discussion and Conclusions

These results suggest the feasibility of the selectable-frequency CMUT with minimal impact on performance. Future work involves fabrication of the proposed devices, already underway at the UVML. Fabricated devices will be characterized and these data will be used to validate the FEA.

P1-A. Contrast Agents: Behavior and Imaging

Sala Orange

Monday, September 21, 2009, 10:00 am - 11:30 am

Chair: **Jeff Ketterling**
Riverside New York

P1-A-01

Exploration of shear stress generated by oscillating microbubbles on the cell membrane in the context of sonoporation

Alexander Doinikov¹, Peggy Palanchon¹, Kadija Kaddur¹, Ayache Bouakaz^{1,2} *INSERM U930 CNRS ERL 3106, Université François Rabelais, Tours, France*

Background, Motivation and Objective

The subject of this study is shear stress exerted on the cell membrane by acoustic microstreaming generated by a contrast microbubble pulsating nearby a cell. This effect is presumed to play a major role in the sonoporation process. However, the analytical formula currently used for estimating the shear stress has been derived assuming that the microbubble is hemispherical and resting on the cell membrane.

Statement of Contribution/Methods

The aim of this study is to propose a refined theory to estimate shear stress generated by an oscillating contrast microbubble located at different distances from a cell. The model was evaluated for different acoustic pressures (0.2–1 MPa), frequencies (1–3 MHz), bubble concentrations, and distances between the bubble and the cell wall. Besides, using the same excitation parameters, sonoporation experiments were carried out on a suspension of U-87MG cells using GFP plasmid DNA as a marker and BR14 microbubbles (Bracco research, Geneva).

Results

Simulations reveal that the shear stress created on the cell membrane by an adjacent contrast microbubble is zero at the point which is the projection of the bubble center on the cell surface, then it increases, being directed away from the bubble, reaches a maximum, decreases down to zero, and changes sign, getting directed to the bubble. As a result, the maximum of the shear stress on the cell surface occurs along a circle whose radius is about $0.287d$, where d is the distance between the bubble and the cell surface. Simulations, made for different acoustic pressures (0.2–1 MPa) and frequencies (1–3 MHz), show that a bubble with a radius of $R_0 = 1.5 \mu\text{m}$, insonified with a 2.0 MHz, 200 kPa acoustic pulse, produces a maximum shear stress on the order of 400 Pa when it is in contact with the cell surface. However, as the separation distance between the bubble and the cell increases, the shear stress rapidly decreases reaching a value of 12 Pa at $d = 2R_0$. Moreover the simulations point out a decrease of the shear stress as the bubble concentration increases. These numerical data are corroborated by the experimental results. The transfection rate according to the shear stress derived from our model shows similar dependencies. Transfection rate increases with acoustic pressure and decreases with bubble concentration.

Discussion and Conclusions

This theoretical and experimental study shows the possible correlation between shear stress generated by oscillating microbubbles on the cell membrane and sonoporation rate. Additional exploration is still required to elucidate further mechanisms involved in the sonoporation process.

Monday
Poster

Comparison of pulse subtraction Doppler and pulse inversion Doppler

Veronique Mahue¹, Jean Martial Mari¹, Robert Eckersley², Meng-Xing Tang¹; ¹Bioengineering, Imperial College London, London, United Kingdom, ²Imaging Sciences Department, Faculty of Medicine, Imperial College London, London, United Kingdom

Background, Motivation and Objective

A challenge in molecular imaging is the development of methods able to distinguish adherent targeted contrast agents from freely circulating agents and tissue. One potential detection method, pulse inversion Doppler (PID) [1], is able to distinguish linear from nonlinear moving scatterers. In this paper, a new Doppler technique based on pulse subtraction imaging [2] (PSD) is compared with PID.

Statement of Contribution/Methods

PSD is based on a short pulse p_1 , followed by a longer pulse p_2 , made of the combination of time-shifted copies of p_1 . A "virtual" echo, E_3 , is constructed using $E\{p_1\}$ according to the generation of p_2 so that for a linear system the echo $E\{p_2\}$ will be the same as E_3 .

Simulation

The response, at 2 MHz, to PSD (32 pulses, 2-cycle/4-cycle, $0.01 < MI < 0.2$) and PID (32 pulses, 4-cycle, $0.01 < MI < 0.2$) sequences was modelled for two systems: a bubble (radius 3 μm) via the Rayleigh-Plesset equation, and a linear scatterer. The parameters chosen ensured that for the linear control experiment, the echo pairs arising from PSD and PID contained the same energy. The amplitude of the nonlinear part of the Doppler spectrum, indicative of bubble scattering was computed for PSD and PID.

Experiment

A bulk suspension of SonoVue microbubbles was insonated with PSD and PID pulses for the same parameters as in the simulation. The bubbles were contained in a thin latex tube (diameter 9 mm) at the focus of a pulse echo system made of two single element 3.5 MHz transducers.

Results

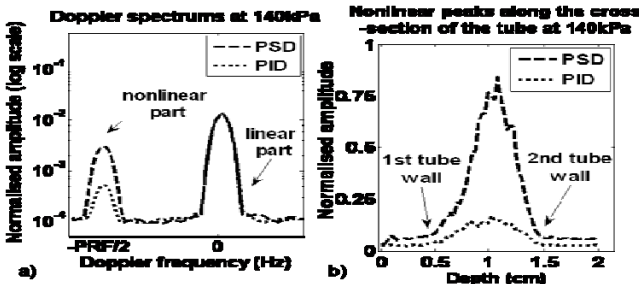
For the range of MIs tested, the nonlinear amplitudes in PSD were on average 6.4 times better than PID in simulations and 4.6 ± 1 times better in the experiments. The figure illustrates this for simulation (a) and experiment (b) at a peak negative insonation pressure of 140 kPa.

Discussion and Conclusions

For the parameters investigated in this work, PSD provides improved sensitivity to non-linear echoes compared to PID. A trade-off between resolution and Doppler sensitivity needs to be found.

References:

- [1] D.H. Simpson, C.T. Chen and P.N. Burns, IEEE Trans Ultrason Ferroelect, Freq Contr 46 (1999), pp. 372–382
- [2] J. Borsboom, Ph.D. dissertation, University of Rotterdam, Rotterdam, Netherlands, 2005



Monday Poster

P1-A-03

Exploitation of multi-frequency excitation for contrast agent imaging

Anthony Novell¹, Ayache Bouakaz¹; ¹Inserm UMR 930, CNRS ERL 3106 and Université F. Rabelais, Tours, France

Background, Motivation and Objective

A lasting challenge of ultrasound contrast agent (UCA) imaging consists in the improvement of contrast to tissue ratio. We propose in this study a contrast agent detection method based on a multi-frequency excitation. The frequency dependency of microbubbles linear scattering is known to differ significantly from the one of tissue. While ultrasound scattering increases as a function of frequency for tissue, it exhibits a different profile for UCA and shows decay as function of frequency above the resonance.

We explore in this study a multi-frequency excitation scheme to take advantage of this frequency dependency for UCA detection.

Statement of Contribution/Methods

In vitro measurements were performed using a 3.5 MHz single element transducer. Gaussian pulses at 2.5 MHz, 4 MHz and 6 MHz were transmitted simultaneously with amplitudes ranging from 220 kPa to 700 kPa. The number of cycles of each component was adapted to avoid frequency overlapping. Responses from a linear reflector (tissue) were obtained using a copper wire with a diameter of 50 μm . Contrast agent responses were measured by injecting a 1/2000 diluted solution of SonoVue or BR14 (Bracco Research, Geneva) microbubbles in a water tank. The method was also evaluated using an open scanner with analog transmitters and a 128-element linear probe centered at 3.5 MHz. A flow phantom containing a 4 mm diameter tube was used in which UCA was circulating. Transmit parameters as used with the single element transducer were reproduced and RF scans were recorded.

Results

In order to compare to contrast scattering, the amplitude of each transmitted frequency component was chosen such as the scattered power from tissue was the same for the 3 transmitted frequencies. Single element transducer measurements using SonoVue showed a maximal response at 2.5 MHz, while it was 8 and 14 dB lower at 4 MHz and 6 MHz respectively using a transmit pressure of 700 kPa. Similar trend was seen for BR14 microbubbles where responses at 4 MHz and 6 MHz were respectively 9 dB and 11 dB below the response at 2.5 MHz. These results were confirmed with the linear probe connected to the open scanner. SonoVue and BR14 responses were the highest at 2.5 MHz. They decayed with 8 and 15 dB for SonoVue and 6.5 and 13 dB for BR14 at 4 MHz and 6 MHz respectively. Lower transmit pressures did not influence significantly the difference between the 3 frequency responses for both UCAs.

Discussion and Conclusions

The results demonstrate that multi-frequency excitation scheme can be exploited further to discriminate between the response of contrast agent from the tissue response.

P1-A-04

Fractional Fourier Transform with Pulse Inversion for Second Harmonic Pulse Compression

Muhammad Arif¹, Steven Freear²; ¹Ultrasound Group, School of Electronic and Electrical Engineering, University of Leeds, Leeds, United Kingdom, ²University of Leeds, Leeds, United Kingdom

Background, Motivation and Objective

In ultrasound harmonic imaging with coded excitation, harmonic matched filter (HMF) is used in the receiving side to perform pulse compression to recover axial resolution. In the compressed waveform, the sidelobe levels grow under overlap harmonic or mismatched condition. In this paper, fractional Fourier transform (FrFT) with pulse inversion is proposed for the extraction and compression of the nonlinear second harmonic component.

Statement of Contribution/Methods

Linear FM chirp signals were used as an excitation. The pulse inversion method provides the extraction of second harmonic component from the nonlinear received signals. The extracted second harmonic chirp component was then compressed using the FrFT and HMF. The FrFT was computed with a transform angle α matched to the chirp rate of the second harmonic component of the received signal (twice the chirp rate of the excitation signal). Scaling was performed in the FrFT domain for direct comparison with the time domain HMF waveforms. The HMF was made with a centre frequency and the bandwidth was double the excitation signal. The compression performance of FrFT and HMF were assessed by three quality parameters namely: mainlobe width (MLW), peak sidelobe level

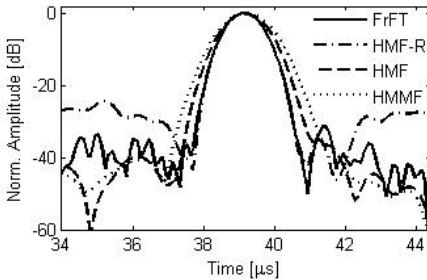
(PSL) and integrated sidelobe level (ISL). Comparisons were also made with the harmonic mismatched filter (HMMF) by applying additional tapering window on HMF.

Results

Experiments were conducted in order to validate the proposed method. A single element transducer and hydrophone were mounted coaxially in a pitch-catch configuration in a water tank. Linear FM chirp signals having a central frequency of 2.25 MHz, duration of 10 μ s and a bandwidth of 1 MHz were used as an excitation signal. The results indicate that FrFT and HMF with rectangular window (HMF-R) provide similar axial resolution but HMF-R has 7.6 dB higher sidelobe levels. Similarly, compared to HMF and HMMF, FrFT provides improved axial resolution with comparable sidelobe levels as visible in the enclosed figure.

Discussion and Conclusions

The combination of FrFT with pulse inversion, when used with chirp coded excitation, is shown to achieve pulse compression similar to HMF with improved axial resolution and comparable sidelobe levels.



Monday Poster

P1-A-05

Phase-Dependent Dual-Frequency Contrast Imaging

Chih-Hao Cheng¹, Che-Chou Shen², Chih-Kuang Yeh^{1,1}:*Department of Biomedical Engineering and Environmental Sciences, National Tsing Hua University, Hsinchu, Taiwan, ²Department of Electrical Engineering, National Taiwan University of Science and Technology, Taipei, Taiwan*

Background, Motivation and Objective

Subharmonic imaging technique has been shown to provide high contrast-to-tissue ratio (CTR) at the cost of relatively low signal intensity from microbubbles. In this study, we propose a method of dual-frequency excitation to enhance the subharmonic component. It is also verified that the phase of dual-frequency excitation pulse can be optimized for the efficiency of contrast detection.

Statement of Contribution/Methods

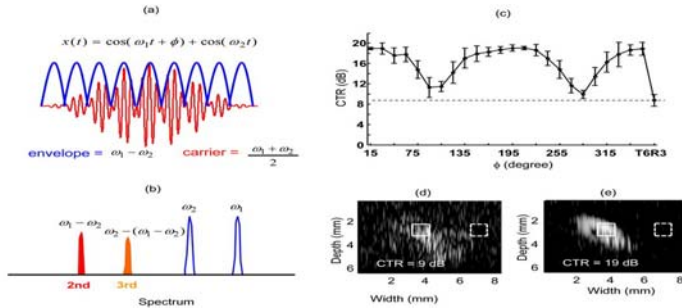
Dual-frequency pulse consists of two sinusoids (Fig. (a)), providing dynamic radiation force from the resultant envelope to induce the nonlinear oscillation of microbubbles (Fig. (b)). Therefore, the bubble's spectral component at the subharmonic frequency is not only from the subharmonic response to the single-frequency tone burst but also from the high-order nonlinearity to the dual-frequency excitation. Consequently, the 3-MHz subharmonic of the fundamental tone burst at 6 MHz (ω_2) can be elevated by transmitting an additional enhancing component at 9 MHz (ω_1). We further optimize the subharmonic generation by tuning the phase (ϕ) between fundamental and enhancing component.

Results

The enhancing ability between different phase of dual-frequency excitation pulses (6MHz+9MHz) and traditional subharmonic imaging (transmitting 6 MHz and receiving 3 MHz, T6R3) were demonstrated by imaging speckle flow phantom containing the SonoVue microbubbles. Figure (c) shows that the CTR of dual-frequency insonation changes periodically with the phase, leading to a difference up to 10 dB between the maximal and minimal CTR. Under the same acoustic pressure, all the dual-frequency insonations with different phases have better CTRs than T6R3 method does. Figure (d) and (e) are the B-mode images acquired by T6R3 and dual-frequency insonation with 180-degree phase, respectively.

Discussion and Conclusions

The results show that the phase optimization is an important factor in subharmonic imaging with dual-frequency excitation. The echo produced from the envelope component seems to be specific for microbubbles, so the proposed method has the potential in improving SNR and CTR of traditional subharmonic imaging.



P1-A-06

Investigation of chirp coded excitation with dual-frequency transmit for ultrasonic harmonic contrast detection

Che-Chou Shen¹, Yi-Yuan Chiu¹, ¹National Taiwan University of Science and Technology, Taiwan

Background, Motivation and Objective

Tissue background suppression is essential for harmonic detection of ultrasonic contrast microbubbles. To reduce the tissue harmonic amplitude for improvement of contrast-to-tissue ratio (CTR), the method of third harmonic ($3f_0$) transmit phasing utilizes dual-frequency transmit at both fundamental (f_0) and $3f_0$ frequencies to provide self cancellation of tissue harmonic signal. Nevertheless, to avoid bubble destruction, the signal-to-noise ratio (SNR) in harmonic imaging becomes limited due to the constraint on transmit pressure amplitude. This study focuses on the design of dual-frequency chirp excitation to improve the SNR together with effective suppression of tissue harmonic signal.

Statement of Contribution/Methods

In $3f_0$ transmit phasing, the frequency-sum component (i.e. f_0+f_0) and the frequency-difference component (i.e. $3f_0-f_0$) must be temporally and spectrally matched for mutual cancellation between them. Nevertheless, with the conventional chirp conversion of the transmit waveform, the resultant frequency-difference component is a single-frequency sinusoid while the frequency-sum component remains a chirp signal. The mismatch between the cancellation pair leads to marked harmonic residue in the tissue background and compromise the CTR improvement. Therefore, instead, we proposed a chirp waveform suitable for the $3f_0$ transmit phasing, the different-bandwidth (DB) chirp signal. With the DB chirp waveform, the frequency-difference component of tissue harmonic signal also becomes a chirp signal similar to its frequency-sum counterpart.

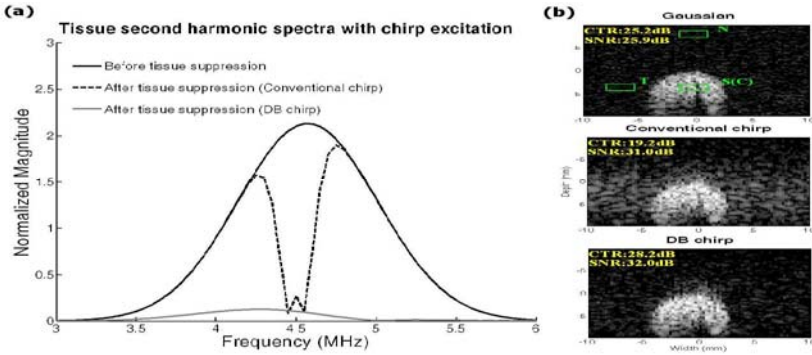
Results

Results in Fig.(a) indicate that, as compared to the conventional chirp waveform, the combination of the DB chirp waveform with the $3f_0$ transmit phasing can markedly suppress the tissue harmonic amplitude over the entire second harmonic band for CTR improvement. The observation is also in agreement with the B-mode images in Fig.(b). It is also illustrated that, when the Gaussian transmit is switched to the chirp transmit in $3f_0$ transmit phasing, the DB chirp waveform can provide 6-dB improvement of SNR together with a CTR increase of 3 dB.

Discussion and Conclusions

This study verifies the efficacy of the DB chirp waveform in $3f_0$ transmit phasing for both SNR and CTR improvements. The design of the DB chirp waveform is also applicable to other dual-frequency imaging techniques which rely on the harmonic generation at the difference frequency.

Monday
Poster



P1-A-07

Temperature dependent behaviour of ultrasound contrast agents

Helen Mulvana¹, Eleanor Stride², Robert Eckersley¹: ¹Imaging Sciences, Imperial College, London, United Kingdom, ²Mechanical Engineering, University College, London, United Kingdom

Background, Motivation and Objective

Accurate characterisation of ultrasound contrast agents (USCA) is of increasing importance as their use for quantitative imaging and therapeutic application is explored. In the laboratory such investigations are frequently undertaken in a water bath at room temperature. The effect of temperature on single bubbles has previously been demonstrated [1]. However, the effect on the acoustic properties of bulk suspensions is not presented in the literature.

Statement of Contribution/Methods

A bulk suspension (154 µl/l) of SonoVue (Bracco, Milan) held in a water bath within an acoustically transparent vessel was investigated over a range of temperatures (20-45°C). In each case, the suspension was insonated using a focussed transducer excited with a 2 cycle Gaussian pulse, centre frequency 4 MHz, with peak negative pressures from 20 kPa to 280 kPa. The propagated signals were detected with a needle hydrophone placed in the far field on the opposite side of the vessel to the transducer. These data were used to calculate the frequency dependent attenuation of ultrasound in the USCA suspension. Field measurements conducted at each temperature prior to the investigation were used to ensure instruments were accurately positioned to allow valid comparisons to be made.

Results

USCA characteristics were significantly affected by temperature over the range 20-45°C, resulting in a marked alteration in the magnitude of signal attenuation and the frequency at which a maximum (f_a) was observed. The effect was greatest over the range 20 - 40°C, for example at an insonation pressure of 100 kPa, signal attenuation increased from -1.5dB to -2.5 dB. Above 40°C signal attenuation decreased to values similar to those observed at 20°C.

The frequency spectra revealed a decrease in f_a from >6 MHz at 20°C to approximately 1.6 MHz at 35°C, suggesting that increased attenuation results from an increase in bubble diameter. Above 35°C, f_a increased, implying that bubbles increased to a critical diameter and were destroyed, resulting in a decrease in signal attenuation. This effect was most clearly observed at 45°C.

Discussion and Conclusions

It has been shown that the acoustic characteristics of the USCA SonoVue are significantly influenced by temperature. The results suggest that measurements made at room temperature require careful interpretation before conclusions can be drawn regarding contrast agent behaviour *in vivo*. It may further be speculated that similar effects may be expected for other gas-filled microbubble contrast agents.

[1] "Oscillation of single microbubbles at room temperature versus body temperature", Vos H.J., Emmer, M., de Jong, N., 2008 IEEE Ultrasonics Symposium Proceedings.

P1-A-08

Effect of Bubble Interaction on Contrast Agent Destruction Behaviour Under Repeated Insonation

Monica Siepmann¹, Georg Schmitz¹; ¹Ruhr-Universität Bochum, Germany

Background, Motivation and Objective

The controllable destruction of ultrasound contrast agents plays an important role in quantitative molecular imaging, perfusion estimation and drug delivery applications. In general, repeated insonation is required to destroy all microbubbles (MB) present. To ensure complete destruction or quantify the bubbles present it is thus of interest to determine the destruction rate over multiple pulses. The destruction behaviour of single microbubbles has been studied intensively. However, it can be expected that MB destruction mechanisms will depend on MB concentration due to MB interaction and different attenuation. While attenuation is expected to reduce destruction rates for high concentrations, microbubble interaction may lead to the destruction of more bubbles in one shot. Therefore, we investigate the dependency of the rate of destruction events on the concentration of hard shelled MBs to analyze the influence of microbubble interaction.

Statement of Contribution/Methods

To ensure the repeated insonation of each bubble at the same position, microbubbles were embedded in gelatine. Cyanoacrylate microbubbles (supplied by F. Kiessling, recipe given in [1]) were diluted in semi fluid gelatine which was refrigerated until solid. Three phantoms with concentrations of $5 \cdot 10^4$, $5 \cdot 10^5$ and 10^6 MB/ml were imaged with a Vevo770 system with RMV704 scanhead (Visualsonics) in Power Doppler mode. Destruction events of stationary bubbles can be visualized in Doppler images. This allows us to determine the number of destruction events for every frame. In each of 20 different non-overlapping regions of each phantom 7 frames were acquired. The number of destruction events was calculated from the total number of colored pixels around the transducer's focal zone. These were then normalized to the number of events in the first frame of each sequence. Alternatively, an exponential $e^{B(n-1)}$ and a power law decay function n^{-a} were fitted to the averaged results for each concentration, with n being the frame number starting from one.

Results

The power functions provide a better fit for all concentrations (mean squared error $MSE < 2.5 \cdot 10^{-4}$) than the exponential decay ($MSE < 10^{-3}$). The estimated exponents for the three concentrations are $\alpha=3.10$ for the highest, 2.32 for the medium and 1.65 for the lowest concentration. The exponents show that the relative decrease of destruction events is slower for lower concentrations.

Discussion and Conclusions

High attenuation however would slow the destruction process. Thus the results indicate that bubble interaction plays an important role and that for high concentrations destroyed MB seem to assist the destruction of neighbouring bubbles. Also, the better fit for the power law also supports the importance of interaction: a fixed percentage of destroyed microbubbles per frame would result in an exponential decay.

[1] M. Palmowski, et al., Mol Cancer Ther, vol. 7, p. 101, 2008.

P1-A-09

Improvement of the power response in contrast imaging with transmit frequency optimization

Sébastien Ménigot¹, Anthony Novell¹, Ayache Bouakaz¹, Jean-Marc Girault^{1,2}; ¹UMR Université François Rabelais de Tours, Inserm U930, CNRS ERL 3106, Tours, France, Metropolitan

Background, Motivation and Objective

The US contrast imaging domain is in effervescence. Currently the scientific community of this field seeks US excitations which should make possible the optimization of the acoustic contrast. We tackled the problem in a simple way by proposing an adaptive imaging technique which seeks the emitting frequency which maximizes the acoustic contrast. The use of an adaptive technique is justified by the fact that

- 1) during the clinical examination, the insonified medium perfused by the microbubbles is a nonstationary medium (the number of bubbles changes...),
- 2) the pressure level is unknown because of the diffraction and attenuation effects which vary from one patient to another,

3) the size and the distribution of the microbubbles of the contrast agent are not precisely known and can differ from one sample to another.

To overcome these problems, that is to disregard these unknown factors it seemed more adequate judicious to propose an US excitation whose frequency is selected in an adaptive way using the gradient's technique.

Statement of Contribution/Methods

Simulations are carried out for encapsulated microbubbles of 2 microns by considering the modified Rayleigh-Plesset equation for a 2.25MHz transmitted frequency and for various pressure levels (20 kPa up to 420kPa).

In vitro, experiments are carried out by using two transducers a transducers which were placed perpendicularly. The signal was transmitted to a 2.25 MHz transducer. Responses of a 1/2000 water-diluted solution of SonoVue™ were measured by a 3.5 MHz transducer. Each experiment has been realized with three pressure nivels (127, 244 and 370 kPa).

Results

We show through simulations and through *in vitro* experiments that our adaptive imaging technique gives

- 1) in case of simulations a gain which can reach 9 dB compared to the traditional technique and
- 2) in *in vitro* experiments a gain which can reach 14 dB. There is a non negligible discrepancy between simulations and experiments.

Discussion and Conclusions

By proposing a close loop system whose frequency adapt itself with the perfused media, throughout the examination, the optimization system adapt itself to the remaining bubbles population thus allowing an increase of the 30% examination duration. There is a non negligible discrepancy between simulations and experiments. These differences are certainly due to the fact that our simulations do not take into account the transducers imperfections, the attenuation, the diffraction and the propagation effects. However, these results are really encouraging and suggest that we should continue with this way.

P1-A-10

Registration of Ultrasound Contrast Images for Perfusion Analysis

Radim Kolar¹, Radovan Jirik¹, Kim Nylund², Odd Helge Gilja²; ¹Department of Biomedical Engineering, Brno University of Technology, Czech Republic, ²Institute of Medicine, University of Bergen, Norway

Background, Motivation and Objective

Contrast enhanced ultrasound (CEUS) imaging in medical ultrasonography has recently been used not only for better detection of tissue structure geometry, but also for assessment of the micro-vasculature and for perfusion measurements in various tissues. These CEUS techniques provides two time sets of images – first and second harmonic images after applying the bolus of ultrasound agent. For the perfusion analysis the image registration needs to be performed to provide an identical region of interest (ROI) for each B-mode image. The main aim of this study is the CEUS image registration for application in perfusion analysis.

Statement of Contribution/Methods

The registration approach of CEUS images is based on the utilization of the first harmonic images, where lower brightness variation in time can be seen during contrast measurement in comparison to the second harmonic images. The ROI-based normalized mutual information was employed as a registration criterion: $C = 2.H(x,y)/(H(x)+ H(y))$, where $H(.)$ and $H(x,y)$ states for marginal and joint entropy, respectively. This criterion has been successfully used in many multimodal image registration frameworks. Only geometrical translation has been used for image registration. The corresponding two shift parameters were obtained by searching through bounded parametric space to ensure that the global minimum is found. The optimal shift was consequently used for transformation of the second harmonic images.

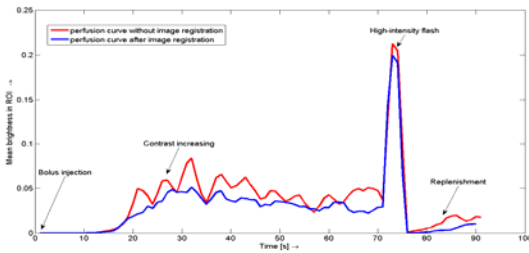
Results

This approach has been applied to CEUS sequence of tumorous pancreatic tissue after application of bolus of contrast agent (2.4 ml of SonoVue™). Due to breathing, the movement of ROI causes high brightness variability not connected to perfusion. These two perfusion curves are depicted on Fig. 1.

Discussion and Conclusions

The perfusion curves can serve as a method for evaluation of the image registration technique in CEUS sequences. The probe or tissue movement appears as unpredictable variations in mean brightness, which is high without image

registration (see the red perfusion curve) and may affect the estimation of perfusion parameters. The image registration helps to decrease this influence (blue perfusion curve).



P1-A-11

Effects of phase transition of lipid bilayer on dynamics of Bubble liposomes

Nobuki Kudo¹, Katsuji Sakaguchi¹, Ryo Suzuki², Kazuo Maruyama²; ¹Graduate School of Information Science and Technology, Hokkaido University, Sapporo, Hokkaido, Japan, ²Department of Biopharmaceutics, School of Pharmaceutical Science, Teikyo University, Sagamihara, Kanagawa, Japan

Background, Motivation and Objective

Bubble liposomes (BLs), gas-encapsulated liposomes of several hundreds of nanometers in diameter, enable modification of the physical property of lipid bilayer shell and thus modification of bubble dynamics. In this study, we investigated the effects of phase transition of a lipid bilayer on bubble dynamics.

Statement of Contribution/Methods

Four types of liposomes with different phase transition temperatures (BL55, DSPC (55°C):DSPE-PEG-OMe = 94:6; BL23, DMPC (23°C):DSPE-PEG-OMe=94:6; BL-3, POPC (-3°C):DSPE-PEG-OMe = 94:6; BL-22, DOPC (-22°C):DSPE-PEG-OMe = 94:6) were synthesized. BLs were then produced by sonication of liposome suspensions by 42-kHz CW ultrasound. Stability of bubbles under static pressure was evaluated by observation of the turbidity of suspensions because turbidity is increased by bubble formation and decreased by their destruction. Stability of bubbles under dynamic pressure was evaluated by measurement of pressure-dependent transmission of wideband ultrasound pulse of 10 MHz in center frequency (K. Sakaguchi et al. IEEE Ultrasonics Symp. Proc. 2008: 1675-1678).

Results

Unless otherwise stated, experiments were carried out at room temperature (20°C). The turbidities of BL-3 and BL-22 disappeared within 10 minutes after sonication, but turbidities of BL23 and BL55 were maintained for several hours. BL23 was also used for measurement of pressure-dependent transmission below and above its phase transition temperature. As shown in Fig. 1, (a) transmittance of ultrasound pulse decreased with increase in pulse pressure at 20°C, but (b) transmittance increased with increase in pulse pressure at 28°C. These results show that bubbles undergo stable oscillation of pressure-dependent amplitude under repetitive exposure to pulsed ultrasound only below the transition temperature.

Discussion and Conclusions

Turbidity measurements shows that the lipid bilayer shell in liquid crystal phase cannot prevent encapsulated gas from diffusion even in a static condition. Measurement of ultrasound transmittance shows that the lipid bilayer shell in gel phase can restore the intact shell immediately after bubble expansion though the shell does not cover the entire surface of the expanded bubble. The methods used in this study can provide important information on design of contrast agent bubbles.

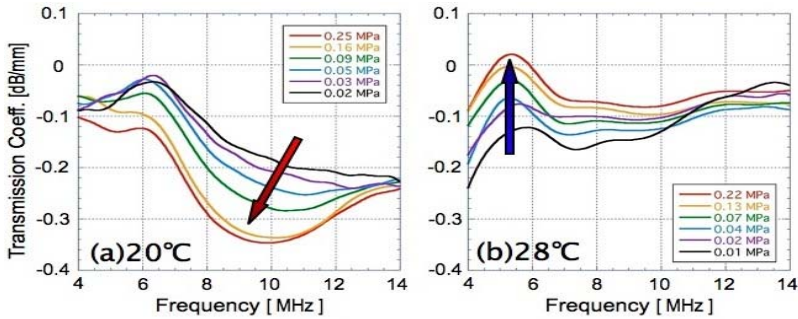


Figure 1. Pressure-dependent transmission of BL23 suspensions.

P1-A-12

Survival of single microbubbles insonated in solution and in narrow tubes

Mairead Butler¹, Aris Dermitzakis², David Thomas¹, Stephen Pye³, Vassilis Sboros¹; ¹Medical Physics, University of Edinburgh, United Kingdom, ²Medical Physics, University of Patras, Greece, ³Medical Physics, NHS Lothian, United Kingdom

Background, Motivation and Objective

To optimise the use of contrast agents clinically, it is necessary to have a thorough understanding of their behaviour. To date, observations of microbubbles in tubes of large diameter, of the order of hundreds of microns, assume the tube has no effect on the microbubble behaviour. We test this hypothesis comparing the acoustic response of biSphere™ microbubbles in both free and 200µm rigid tube environments.

Statement of Contribution/Methods

An experimental system utilising a Philips research scanner Sonos 5500, previously described, has been used for the assessment of the acoustic response of microbubble contrast agent in solution. More recently a version of this system which enabled the investigation of the acoustic response of single microbubbles in tubes from 200µm to 12µm diameter has been designed. BiSphere™ microbubbles were insonated with 7 identical consecutive pulses, at 1ms intervals, using a 6-cycle, 1.6MHz ultrasound pulse for peak negative acoustic pressures ranging 160-1000 kPa. The tubes used for the data described below were 200µm cellulose tubes with a gravity feed inducing the flow.

Results

For biSphere™, data for 800 single bubbles in tubes and 800 free single bubbles has been analysed by decomposing the calibrated backscattered RF signal into fundamental and harmonic components. At acoustic pressures below 300 kPa there was no significant difference in the acoustic response of the free and tubed microbubbles.

With microbubble destruction assumed when the acoustic signal was below noise, 7% (112) of free microbubbles and 33% (142) of tubed microbubbles were destroyed after 550kPa insonation. For 800kPa after 7 insonations, for free microbubbles 66% (215) were destroyed and for tube 86% (236). The rate of destruction was faster in the tube i.e. by the third pulse, 44% of tubed microbubble were destroyed compared with 16% of free. In addition, at 800kPa, the RMS backscattered pressure from surviving microbubbles separated into two clusters, both with higher fundamental component than harmonic. The fundamental RMS backscatter from free microbubbles was generally higher than from tubed microbubbles.

Discussion and Conclusions

Previously, microbubbles in 200µm tubes have been observed to respond in the same way as free, unrestricted microbubbles when in the centre of the tube. The microbubbles studied here are assumed to follow the fastest flow through the centre of the vertical tube. For rigid shelled biSphere microbubbles, more destruction was observed in tubed microbubbles than in free. The presence of the tube is not thought to have a significant effect on the incident acoustic field. The behaviours of free microbubbles and microbubbles in 200µm tubes are not identical and this should be addressed theoretically. Future work will collect data from a range of tube diameters to determine microbubble behaviour at the range of vessel diameters encountered in vivo.

P1-B. Contrast Agents Applications

Sala Orange

Monday, September 21, 2009, 10:00 am - 11:30 am

Chair: **Vassilis Sboros**
Univ. of Edinburgh

P1-B-01

Strength of Attachment of a Targeted, In-house, Microbubble, Lipid-based Ultrasound Contrast Agent

Adele Edgeworth¹, Jim Ross², Tom Anderson¹, Mairead Butler¹, Norman McDicken¹, Carmel Moran¹; ¹Medical Physics, University of Edinburgh, Edinburgh, United Kingdom, ²Tissue Injury and Repair Group, University of Edinburgh, Edinburgh, United Kingdom

Background, Motivation and Objective

A targeted, in-house, lipid-based, high-frequency, microbubble ultrasound contrast agent (UCA) is currently under development. The UCA will be targeted to vulnerable atherosclerotic plaques in the assessment of coronary heart disease with intravascular ultrasound (IVUS). The agent has previously been shown to remain attached to an agar surface via an avidin-biotin mechanism under wall shear stress (WSS) of up to 3.4Pa. The objective of this study was to compare the strength of attachment of an electrostatic attachment mechanism to an avidin-biotin mechanism under very high WSS.

Statement of Contribution/Methods

A flow chamber has been designed and calibrated to 50Pa WSS. In order to assess the electrostatic attachment mechanism an agar strip was manufactured to fit within the flow chamber and coated in the biotinylated in-house UCA. After 2 hours the agar strip was rinsed and placed within the flow chamber and the WSS was incrementally increased to 50Pa. IVUS images and radio frequency (RF) data of the attached microbubbles was collected from two positions along the flow channel as the WSS was increased. The experiment was repeated with a streptavidin coated agar strip to assess the strength of the avidin-biotin attachment mechanism. The agar was coated with streptavidin and, after 24 hours, 1ml of biotinylated in-house UCA was placed on the streptavidin coated agar. After 2 hours the agar was rinsed and placed in the flow chamber and the investigation repeated.

The RF data was analyzed to quantify the mean backscatter from the bubbles attached to the agar surface under the two different attachment mechanisms.

Results

Under the electrostatic attachment mechanism initial backscatter from the attached bubbles was -23.21 ± 1.43 dB compared to a mean backscatter from agar at -34.63 ± 1.23 dB. The mean backscatter from the attached bubbles decreased rapidly and at 0.66Pa WSS the mean backscatter from the agar surface was -30.34 ± 3.41 dB. This suggests that microbubbles are washed off the agar surface under increasing WSS. Beyond 0.66Pa WSS the mean backscatter from the bubbles is indistinguishable from the plain agar surface. Under the avidin-biotin attachment mechanism the initial mean backscatter was -22.57 ± 3.71 dB. Increasing WSS decreased the mean backscatter values however, at 50Pa the mean backscatter was -33.41 ± 3.97 dB, which was still significantly higher than the backscatter from plain agar, suggesting that microbubbles remain attached at 50Pa WSS.

Discussion and Conclusions

The in-house UCA has been shown to remain attached to agar via an avidin-biotin mechanism up to a WSS of 50Pa. In addition the UCA has been shown to rapidly detach from agar in the absence of an avidin-biotin bond. In conclusion the UCA, under an avidin-biotin attachment mechanism, would be suitable for use in human coronary arteries under an expected WSS of 3.5Pa and in addition is suitable for use in small animal studies where peak WSS can reach 40Pa.

Monday
Poster

Evaluation of the binding force between a biotinylated microbubble and an avidin-coated surface by ultrasound radiation

Toshihiko Sugiura¹, Klazina Kooiman¹, Marcia Emmer¹, Hendrik J. Vos¹, Nico de Jong^{1,2}, Annemieke van Wamel¹.¹Biomedical Engineering, Erasmus MC, Rotterdam, Netherlands, ²Interuniversity Cardiology Institute of the Netherlands, Utrecht, Netherlands

Background, Motivation and Objective

Recently, targeted microbubbles are under investigation to be used for molecular imaging and drug delivery. For such applications, the strength of adhesion between a bubble and a cell surface should be evaluated. This research focuses on the evaluation of the binding force between lipid coated biotinylated microbubbles and a streptavidin-coated surface, which mimics a cell surface. Controlled ultrasound radiation force is used for this evaluation by detaching microbubbles bound to the surface.

Statement of Contribution/Methods

Lipid coated microbubbles (composition in mol %: DSPC 59.1; PEG-40 stearate 35.7; DSPE-PEG(2000) 4.1, DSPE-PEG(2000)-biotin 0.8; TexasRed DHPE 0.3) with a C₄F₁₀ gas core were made by sonication [1]. The back of an Opticell membrane was coated with the fluorescent streptavidin Oregon Green (5 µg/ml), followed by washing, blocking and washing. Microbubbles were allowed to adhere to the coated membrane by flotation. After washing, the Opticell was mounted in the set-up such that the bound microbubbles were on top of the membrane. Microbubbles were insonified at 15 MHz. This frequency was higher than the resonant frequency of the microbubbles (5 MHz), allowing to insonify microbubbles without causing large oscillations that can lead to shrinkage or breakage. The experiment was performed at 37 °C. A linearized equation for radiation force was used for calculating the strength of the radiation force for detaching microbubbles.

Results

Detachment of microbubbles with radius 1.23 µm from the surface was observed if the peak negative acoustic pressure was 1.6 MPa. The radiation force required for detaching one microbubble in this experiment was ~50 nN. The contact area of 1 microbubble with the streptavidin-coated surface can be estimated as 0.08 µm², assuming that the contact area is defined as the area where the distance between the microbubble and the surface is less than 10 nm. According to [2] and taking our microbubble composition into consideration, the amount of biotin-streptavidin bonds in this area is ~160. From these assumptions, the binding force per bond in our study can be evaluated as ~300 pN. This is comparable to the reported unbinding force of one bond, 257±25 pN [3].

Discussion and Conclusions

Detachment of biotinylated microbubbles from a streptavidin-coated surface was successfully achieved by transmitting ultrasound with a frequency higher than the resonant frequency. From calculating the radiation force, the binding force was evaluated as ~50 nN/bubble or ~300 pN/bond. This method will be useful to assess binding forces of newly developed targeted ultrasound contrast agents.

- [1]Klibanov et al, Invest Radiol 39:187, 2004
- [2]Takalkar et al, J Control Rel 96:473, 2004
- [3]Moy et al, Science 266:257, 1994

Molecular Imaging of Angiogenesis with BR55: a KDR-targeted Contrast Agent

Sibylle Pochon¹, Philippe Bussat¹, Thierry Bettinger¹, Isabelle Tardy¹, Radhakrishna Pillai², Nathalie Biolluz¹, Sylvie Pagnod-Rossiaux¹, Michel Schneider¹.¹Bracco Research SA, Geneva, Switzerland, ²Bracco Research USA, Princeton, NJ, USA

Background, Motivation and Objective

Targeted-microbubble-enhanced ultrasonography is emerging as a powerful and convenient modality for molecular imaging. Various pathological conditions induce major changes in the pattern of receptors expressed by endothelial cells. The growth of new blood vessels is a prerequisite of tumor development and among the specific molecular markers of angiogenesis, the vascular endothelial growth factor receptor (VEGFR2) is recognized as a major player. In this work, we evaluated BR55, a KDR-specific ultrasound contrast-agent for its capacity to specifically recognize the human (KDR) and mouse (Flk-1) receptors.

Statement of Contribution/Methods

BR55 is a phospholipid-based contrast-agent functionalized with a heterodimeric peptide specific for VEGFR2 (KDR/Flk-1). In contrast with previously published studies using VEGFR2-targeted microbubbles, BR55 doesn't require an antibody for binding nor use a biotin/streptavidin coupling strategy. Experiments were performed to demonstrate the binding capacities of BR55 microbubbles on recombinant proteins and on various cells expressing VEGFR2. Competition experiments were designed to assess the specificity of the interaction using an excess of either VEGF, the free KDR-binder or a VEGFR2-specific antibody. BR55 was then tested in rodent tumor models to perform molecular imaging of VEGFR2 using non destructive, contrast-specific echography ten minutes after microbubbles injection.

Results

Strong binding of BR55 microbubbles was observed on a coating of recombinant receptor as well as on cells expressing VEGFR2. BR55 binding to endothelial cells was displaced by an excess of free ligand, VEGF or KDR-specific antibody so demonstrating the specificity of the interaction. The capacity to recognize the mouse receptor was confirmed using a mouse endothelial cell line. In vivo, BR55 microbubbles accumulated in the neovasculature of tumors grown in rodents and this allowed the early detection of the lesion a few minutes after injection. Good expression of VEGFR2 in the tumoral endothelium was confirmed by immunohistochemistry staining.

Discussion and Conclusions

BR55, a KDR-targeted contrast agent, was shown to specifically recognize the marker of angiogenesis and to be able to highlight malignant lesions by specific accumulation on the tumoral endothelium. The information provided by molecular imaging combined with the assessment of tumor perfusion may also be of primary interest for characterizing tumor phenotype and monitoring tumor response to therapy.

The use of targeted ultrasound contrast agents such as BR55 opens a new era in medical imaging. In addition to the information provided by ultrasound blood pool agents such as SonoVue, targeted microbubbles will allow the detection of disease-associated receptors in the vascular compartment, to follow their level of expression over time or after drug therapy which may be useful for finding the optimal time window and dosing of drugs.

P1-B-04

Effect of pre-trapping of micro bubbles on mechanical damage enhancement in bubble cavitation

Yoshiki Yamakoshi¹, Takashi Miwa¹, Yuji Takahashi¹, Hiroaki Inoguchi¹; ¹Faculty of Engineering, Gunma University, Kiryu-shi, Gunma, Japan

Background, Motivation and Objective

Sonoporation, which makes small pores through cell membrane, is an effective method in order to increase efficacy in drug/gene delivery system. However, neither precise mechanism of sonoporation nor optimum sequence of insonation has been clarified. In this paper, effects of pre-trapping of micro bubbles to the target wall, which is carried out by pumping ultrasonic wave before insonation using high intensity ultrasonic wave, is evaluated by N-isopropylacrylamide (NIPA) gel flow phantom. Amount of trapped bubbles on the wall during pre-trapping and density of micro hollows on the wall after insonation using high intensity ultrasonic wave are observed by changing the modulation sequence of the pumping ultrasonic wave.

Statement of Contribution/Methods

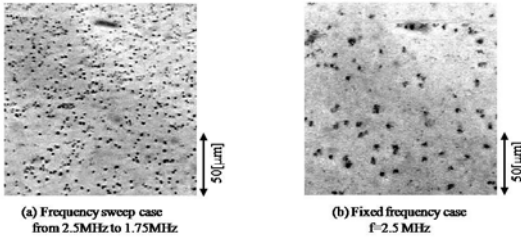
Micro bubbles are trapped by pumping ultrasonic wave (pre-trapping of micro bubbles) followed by insonation using burst ultrasonic wave (frequency: 2.5 MHz, sound pressure: 1.5 MPa) to cause bubble cavitation. An ultrasonic wave contrast agent (Levovist) is adopted as micro bubbles. Flow channel with the diameter of 2 mm is molded in NIPA gel. Sound speed of the gel is 1539 m/sec. and the density is 1.025 g/cm³, which are similar to those of soft tissue. Since the gel is optically transparent, both pre-trapped bubbles and mechanical damage of the wall are observed in-situ with microscope. 3-D image reconstruction is adopted to observe the entire wall.

Results

Figure shows an example of mechanical damage produced on the wall of NIPA gel flow channel. Fig.(a) is a result when frequency of pumping ultrasonic wave is modulated (from 2.5 MHz to 1.75 MHz followed by quick return to the start frequency). Fig.(b) is a result when frequency of pumping ultrasonic wave keeps constant (2.5 MHz). Sound pressure is set to 50 kPa. Mean flow velocity is 0.6 mm/sec. A lot of micro hollows with the diameter of a few micrometers are observed in two cases, however, density of the micro hollows in the frequency modulation case is much larger than that of the fixed frequency case.

Discussion and Conclusions

In-situ observation using NIPA gel flow phantom is an effective tool in evaluation of mechanical damage by bubble cavitation. Using the method, it is observed that pre-trapping of micro bubbles to the target wall by pumping ultrasonic wave enhances the production of micro hollows on the target wall after insonation of high intensity ultrasonic wave.



(a) Frequency sweep case from 2.5MHz to 1.75MHz

(b) Fixed frequency case f=2.5 MHz

Monday
Poster

P1-B-05

Multimodality Contrast Agent: Synthesis and Applications of ¹⁸F-labelled Microbubbles for MicroUS and MicroPET

Ai-Ho Liao¹, Shih-Yen Wu², Hsin-Ell Wang², Pai-Chi Li¹, ¹National Taiwan University, Taiwan, ²National Yang-Ming University, Taiwan

Background, Motivation and Objective

Ultrasound contrast agent with albumin shell has been widely used for ultrasound contrast imaging and molecular imaging. However, the biodistribution of such contrast agents remains undescribed. In this study, albumin-based microbubbles (MBs) was labeled with ¹⁸F using N-succinimidyl-4-[¹⁸F] fluorobenzoate (¹⁸F-SFB) and it can be used for determining biodistribution by dynamic microPET. NG4TL4 sarcoma bearing mice were used in this study.

Statement of Contribution/Methods

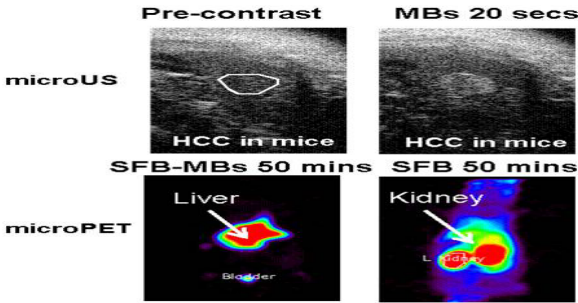
The radiofluorination agent ¹⁸F-SFB was prepared and dissolved in 50 μl dimethyl sulfoxide. The homemade albumin-based MBs were produced by sonication of 10-mL solution containing 0.1M borate buffer, 6.6% human serum albumin and perfluorocarbon (C₃F₈) gas. The ¹⁸F-SFB was added to the homemade MBs and reacted for 30 min at room temperature. The ¹⁸F-labeled MBs were centrifuged and the wash procedure was repeated three times to assure the free ¹⁸F-SFB was removed. MicroPET imaging was performed in tumor bearing mice. Data acquisition was started immediately after intravenous injection of 26.4 μ Ci (contained 3.3x10⁸ MBs) ¹⁸F-labeled MBs or ¹⁸F-SFB.

Results

Contrast enhanced ultrasound imaging with the albumin shelled MBs in hepatocellular carcinoma (HCC) bearing mice was performed. For microPET imaging, ¹⁸F labeled MBs were cleared from the blood circulation and accumulated mainly in the liver (42% injected dose [ID]/g ± 6.9) and lung (20.8% ID/g ± 4.6) at 50 minutes. However, ¹⁸F-SFB was cleared through kidneys (13.9% ID/g ± 5.6 at 50 minutes) directly. At 50 minutes, the accumulation of ¹⁸F-SFB in liver was only 3.3% ID/g± 0.9.

Discussion and Conclusions

MicroUS/microPET multimodality contrast agent demonstrates enhanced contrast of the liver in both microUS and microPET, and it can be used to assess biodistribution of ultrasound contrast agent.



P1-B-06

Targeting microbubbles with Shiga-Toxin B-subunit

Olivier Couture^{1,2}, Estelle Dransart³, Ludger Johannes³, Mathias Fink¹, Mickael Tanter^{1,4,1} *Institut Langevin - Ondes et Images, ESPCI ParisTech, Paris, France, ²Fondation Pierre-Gilles de Gennes, France, ³Institut Curie, France, ⁴INSERM, France*

Background, Motivation and Objective

The targeting moiety (B-subunit) of the Shiga toxin (STxB) is a very potent ligand for the glycolipid Gb3, which is expressed in ovarian, colorectal and breast carcinomas. It is also present on endothelial cells of tumor neovascularization. STxB binds with high apparent affinity to the plasma membrane of Gb3 expressing cells, and is efficiently internalized. Moreover, STxB has low immunogenicity. This study demonstrates the use of STxB for targeting microbubbles onto cancerous cells.

Statement of Contribution/Methods

Alexa488-tagged and biotinylated STxB was incubated at saturating concentrations with avidin-functionalized microbubbles (Bracco Research). After washing, the presence of the ligand on the microbubbles was shown by FACS analysis. Colorectal carcinoma HT29 cells were grown in Opticell culture plates. STxB-functionalized microbubbles and biotinylated controls were incubated with the cells for 30 minutes. After 3 washes, the culture plates were observed by fluorescence microscopy. The plates were then installed in a water-bath under a 8 MHz 128-element transducer array. Six B-mode images, exploiting fundamental and disruption contrast mechanisms, were obtained on each plates by moving the array.

Results

FACS analysis demonstrated that STxB was stably associated with the microbubbles. It also showed that STxB-functionalized microbubbles adhered favorably to the Gb3 expressing cells, as compared to cells in which Gb3 expression was inhibited. Efficient labeling was detected on Gb3 expressing cells by fluorescence microscopy, while only a weak unspecific labeling was observed on the Gb3-negative control cells. Conventional ultrasonography of the culture plates showed a 14 dB difference in average backscatter intensity of the surface of Gb3 expressing cells, compared to Gb3-negative cells. The difference was 11 dB for the images exploiting the disruption of microbubbles as a contrast mechanism. An intensity difference of 5 dB was also observed between cells that were incubated with STxB-functionalized-microbubbles, as compared to unspecific microbubbles.

Discussion and Conclusions

These in vitro experiments showed that STxB-functionalized microbubbles bind specifically to cells expressing the Gb3 glycolipid. This specific targeting of microbubbles to tumor cells is detectable by ultrasound imaging. The targeting moieties of toxins are a new group of ligands for microbubbles and have several advantages compared to antibodies and small peptides. In vivo experiments on Gb3-expressing tumors are currently being initiated.

Dual-mode imaging of acute cardiac ischemia and reperfusion using contrast echocardiography and fluorescence imaging

Matthew Kay^{1,2}, Luther Swift², Vesna Zderic¹; ¹Department of Electrical and Computer Engineering, George Washington University, Washington, DC, USA, ²Department of Pharmacology and Physiology, George Washington University, Washington, DC, USA

Background, Motivation and Objective

Changes in cardiac function that occur immediately after a coronary occlusion are important for understanding mechanisms of lethal arrhythmias. Our objective is to study such changes during acute local ischemia and reperfusion by combining contrast echocardiography and fluorescence imaging of NADH. While echocardiography studies have provided a wealth of information regarding the time course of reduced contractile function and structural remodeling of infarcted tissue, echocardiography has not often been used to study sudden effects of acute ischemia and reperfusion. Furthermore, the combination of NADH imaging with echocardiography provides synchronized assessment of metabolism and contraction, two fundamentally linked processes.

Statement of Contribution/Methods

Excised Langendorff-perfused rat hearts (n=4) were used to study sudden changes in myocardial function caused by the interruption of local coronary flow. An HPLC pump delivered a precise level of flow to the microannula, placed in a coronary artery (LAD). Three flow conditions were studied: normal flow, no-flow (local ischemia), and low-flow reperfusion (LFRP). The right atrium was removed to slow heart rate. Hearts were submerged in a chamber of Tyrodes solution that had a front glass window for fluorescence imaging and a rear latex window for echocardiography. Changes in metabolism were recorded by imaging the epicardial fluorescence of NADH (fNADH) using a CCD camera system. Contrast echocardiography (linear probe, 13-6MHz, and contrast agent Definity® diluted 20:1) was used to identify transmural ischemic borders and measure changes in wall thickness. Frame-by-frame changes in wall thickness for ischemic and normoxic tissue were measured using custom image processing software.

Results

Transmural borders of flow around the ischemic zone (IZ) were clearly revealed after adding the contrast agent to the coronary perfusate. This dramatically improved analysis of IZ function. When flow to the LAD was stopped, IZ wall thickness reduced 20% and IZ wall thickness changes during contraction (ie, contraction amplitude) reduced 70%. The shape of the IZ was clearly revealed by fNADH, which increased 40% during ischemia. Metabolic heterogeneity was measured as the average spatial gradient of fNADH, which increased 150% during ischemia. When LAD flow was resumed at 10% of control (0.2 mL/min, LFRP) IZ wall thickness increased 35% (from ischemia) and contraction amplitude reduced 30%. The latter was attributed to arrhythmias caused by LFRP. During LFRP, fNADH did not increase from ischemia but its gradient increased 90%, indicating increased metabolic heterogeneity during LFRP.

Discussion and Conclusions

Contrast ultrasound and fNADH imaging of excised contracting hearts provide high-contrast images for measuring heterogeneities of flow, contractile function, and metabolism caused by acute changes in coronary flow.

Parametric Imaging of Dynamic Vascular Patterns of Focal Liver Lesions in Contrast-Enhanced Ultrasound

Nicolas Rognin¹, Laurent Mercier¹, Peter Frinking¹, Marcel Arditi¹, Anass Anaye², Geneviève Perrenoud², Jean-Yves Meuwly²; ¹Bracco Research SA, Geneva, Switzerland, ²University Hospital, Lausanne, Switzerland

Background, Motivation and Objective

Statement of Contribution/Methods

Results

Discussion and Conclusions

P1-B-09

Preliminary investigations of post-excitation signals indicating inertial cavitation for microbubbles against a vessel-like wall

Mathieu Santin¹, Josquin Foiret¹, Sylvain Hauptert¹, Sara Jafari¹, Daniel King², William O'Brien², Lori Bridal¹;
¹Université Pierre et Marie Curie, Laboratoire d'Imagerie Paramétrique UMR 7623, Paris, France, ²Department of Electrical and Computer Engineering, University of Illinois, Bioacoustics Research Laboratory, Urbana, IL, USA

Background, Motivation and Objective

It is well recognized that this microbubbles flowing in small capillaries present reduced acoustic response. It has also been demonstrated that signals detected with passive cavitation detection from isolated microbubbles after insonification (post-excitation signals) are linked to acoustic destruction with inertial cavitation.

Statement of Contribution/Methods

This study investigates the post-excitation response from microbubbles in a vessel-like tube with controlled flow. When flow is stopped, microbubbles rise toward the surface and rest against the cellulose wall. At rapid flow, bubbles should be carried through the central region of the tube by the rapid flow and not come into contact with the cellulose tube.

The passive cavitation detector used in this work consisted of a 2.25MHz transmitter and a 5.0 or 13.0 MHz receiver focally aligned on a cellulose tube (inner diameter 180 μm). Insonification was performed with 2.25 MHz, 5-cycle pulse for all experiments. The insonified zone of the capillary tube was observed through a microscope. Flow rates and pulse repetition rates were such that microbubbles in the insonified volume were renewed between measurements.

Results

In a first set of experiments, microbubbles (BR14, Bracco Research Inc.) were isolated visually and positioned within the acoustic field. The acoustic response (13 MHz receiver) of microbubbles so positioned, insonified with 0.4 to 1.8 MPa peak negative pressure did not present post-excitation signals even when destruction was confirmed by microscopic imaging (N = 5).

Peak-to-peak voltage (5 MHz receiver) was then measured with insonification at a peak rarefactional pressure of 0.6 MPa of solutions of BR14 and Definity microbubbles with flow rate varying from 5 to 400 mm/s (N \geq 100 measurements at each flow rate). Peak-to-peak voltage presented a relatively constant maximum value from microbubbles at flow rates above 100 mm/s. The response decreased rapidly with decreasing flow rate by as much as 19 dB for Definity and 9 dB below for BR14 (Lowest values observed at 5 mm/s).

Finally, signals acquired from single microbubbles in highly diluted solutions of Definity and BR14 were acquired with the 13.0 MHz receiver (insonication at 0.6 MPa peak negative pressure, flow rate varied from 5 to 200 mm/s; $N \geq 10$ microbubble response at each flow rate). Each signal was examined visually for detection of post-excitation signals. The percentage of signals observed with post-excitation emissions increased as a function of flow rate.

Discussion and Conclusions

Under low-flow or no-flow conditions in the capillary tube not only was the peak-to-peak amplitude of the contrast microbubble response reduced but a smaller percentage of events presented post-excitation signals. The fact that, post-excitation signals were observed more often when microbubbles were freely flowing but less under low or no-flow conditions may indicate that inertial cavitation is reduced in slowly flowing capillary networks.

P1-B-10

Delta projection imaging of tumor vasculature by contrast-enhanced ultrasound

Chandra Sehgal¹, Theodore Cary², Peter Arger², Susan Schultz², Andrew Wood.^{2,1}*Radiology, University Of Pennsylvania, Philadelphia, PA, USA, ²University of Pennsylvania, USA*

Background, Motivation and Objective

As vascular targeting has evolved into a viable technique for cancer therapy, there is a growing need to assess changes in tumor vascularity quantitatively in response to treatment. In this study we propose an image processing technique, delta-projection imaging, performed on contrast-enhanced grayscale images to visualize and assay tumor vascularity.

Statement of Contribution/Methods

In contrast-enhanced imaging, an image sequence is acquired as a function of time during the transit of contrast agent through a fixed plane. The corresponding delta projection image sequence is constructed by computing the running maximum at each pixel location of the difference between the pixels' values over time and their baseline values at the start time.

Significant pixel changes are coded in color and superimposed on the baseline image so that the sequence of delta-projection images can be played back in real time, showing the evolution of blood vessels as they are enhanced by the incoming contrast agent. For each image in the series of projection images, the extent of vascularity (ratio of the perfused area to the tumor area) can be determined by taking the percent ratio of colored pixels enhanced by contrast agent to the total number of pixels in the tumor cross-section.

Twenty-five mice with implanted subcutaneous K1735 melanomas were imaged with delta-projection imaging to evaluate the evolution of tumor vascularity during enhancement. The same mice were also imaged with contrast-enhanced power Doppler imaging. The extent of vascularity for each tumor was determined quantitatively from delta-projection images and compared using linear regression analysis with the extent of vascularity determined from the contrast-enhanced power Doppler images.

Results

Delta-projection allowed dynamic visualization of individual blood vessels as they filled in real time. Initially, the larger blood vessels ($>250 \mu\text{m}$ in diameter) with a faster flow rate were revealed, and then the smaller diameter vessels (estimated from the images to be $<250 \mu\text{m}$ diameter), presumably with slower flow rate, became visible. As the contrast filled more blood vessels, the density of the vessel network in the images increased, and the aggregate of blood vessels appeared as regions of perfusion. The area of the tumor perfused by the contrast agent increased with time and then leveled off after the maximum perfusion was achieved. The vascularity measurements correlated linearly with power Doppler measurements (slope = 0.95, $R^2 = 0.88$).

Discussion and Conclusions

Delta-projection provides dynamic visualization of tumor network blood vessels and allows qualitative and quantitative assessment of the tumor area perfused by the contrast agent.

Effect of Anesthesia Carrier Gas on Imaging Lifetime of Ultrasound Microbubble Contrast Agents in Rats

Lee Mullin¹, Ryan Gessner¹, Paul A. Dayton¹; ¹Joint Department of Biomedical Engineering, University of North Carolina at Chapel Hill and North Carolina State University, USA

Background, Motivation and Objective

Ultrasound microbubble contrast agents (CAs) are currently implemented in many imaging studies to provide enhanced resolution of a vascular network and act as vehicles for therapeutic applications. However, the circulation lifetime of CAs is relatively short, limiting the time window for imaging or therapeutic application. Improvements are being made on the composition of the bubble to increase lifetime, but little research has been done on the in-vivo environment of the CA.

The purpose of this study was to examine the relationship between anesthesia carrier gas and microbubble CA lifetime in rats. It was hypothesized that using medical air as the carrier gas would increase the in-vivo CA lifetime compared to using pure oxygen.

Statement of Contribution/Methods

Four female Sprague-Dawley rats (Harlan; Indianapolis, IN) were imaged in this study. Animals were anesthetized with an isoflurane gas mixture and CAs were administered through a tail vein catheter. Perfluorocarbon lipid shelled CAs were prepared similar to a previously described method. After a bolus injection of CAs, images of the kidney were obtained using a Visualsonics - Vevo 770 system (Toronto ON) with a 25 MHz transducer. Video data collection started prior to injection of CAs, and continued for at least 10 minutes. A region of interest (ROI) within the kidney was selected offline and the mean pixel intensity within this ROI was calculated.

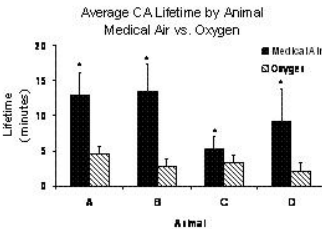
Multiple imaging sequences were obtained of each animal. Each sequence included the collection of two runs of data, each beginning with an injection of CAs. After the completion of the first imaging sequence, the anesthesia carrier gas was changed, and the animal was given ten minutes to acclimate to the new carrier gas.

Results

A statistically significant relationship ($p < 0.05$) was observed between inhaled anesthesia carrier gas type and injected microbubble CA lifetimes in all animals. Medical air as the carrier gas was shown to improve the in-vivo lifetime of CAs from an average of 3 ± 1.1 minutes with oxygen to an average of 10 ± 3.8 minutes.

Discussion and Conclusions

Increasing the circulation lifetime of microbubble CAs would improve the efficacy of current contrast imaging techniques in both diagnostic and therapeutic applications. Changing the anesthesia carrier gas demonstrates a simple yet effective means of prolonging CA circulation time in the rat model.



Fluorocarbon Droplets as Next Generation Contrast Agents - Their Behavior under 1-3 MHz Ultrasound

Rei Asami¹, Takashi Azuma¹, Kenichi Kawabata¹; ¹Central Research Laboratory, Hitachi, Ltd., Kokubunji, Tokyo, Japan

Background, Motivation and Objective

Microbubbles are the most widely used contrast agent for ultrasound and recent study expands its application beyond mere diagnostics such as high-intensity focused ultrasound (HIFU) therapy sensitizer. Despite their high echogenicity, microbubbles face one major shortcoming that their use is strictly limited to blood vessels. We propose tissue permeable contrast agent called phase change nano-droplets (PCND), nano-sized fluorocarbon droplets that can vaporize into microbubbles upon application of ultrasound pulses. Previously we have explored

PCND application such as molecular imaging and HIFU enhancer. While promising results are obtained in those studies, much of droplets' basic behavior is still to be discovered. In this paper, relationship between droplets thermal stability and ultrasound sensitivity is studied in order to discover contributing mechanism of phase changing phenomena at lower frequencies used for therapy.

Statement of Contribution/Methods

PCND is prepared as follows. Perfluorocarbon is mixed with phospholipids and emulsified at high pressure (20 MPa), resulting in 200 nm droplets. Their thermal stability is measured by acoustic monitoring of bubble generation as temperature is raised quasi-statically. Polyacrylamide gel prepared with PCND is placed in degassed water bath at 37 °C and phase change pulse is applied at frequency of 1.1, 2.2 and 3.4 MHz. Phase change was monitored acoustically on B-mode image and with a focused hydrophone.

Results

In this series of experiments, higher boiling point perfluorohexane (PFC6) is mixed with perfluoropentane (PFC5) to control physical property of droplets. Indeed, it was found that increase in PFC6 concentration resulted in increase in overall thermal stability of PCND. This confirms our previous study that thermally stabilized droplets exhibits higher phase change threshold. In the case of 1-3 MHz, PFC6 also affects ultrasound sensitivity of droplets, as droplets' phase change threshold of PFC5 and 6 mixture is above that of PFC5 alone and below that of PFC6 alone. Interestingly, only in cases of 1.1 and 2.2 MHz the proportion of PFC6 added to PFC5/6 mixture does not influence phase change threshold. It is also noted that at any perfluorocarbon contents, phase change threshold is lower at lower frequency.

Discussion and Conclusions

These results suggest that at lower frequencies, ultrasound sensitivity is less affected by degree of thermal stability graded by PFC6, which implies that different mechanisms may dominate phase change phenomena at different frequency range. In case of lower frequency range studied in this paper, cavitation effect could be the dominant factor as ultrasound intensity threshold decreases as frequency lowers.

Part of this work was supported by the New Energy and Industrial Technology Development Organization, Japan.

P1-C. Therapeutic Applications

Sala Orange

Monday, September 21, 2009, 10:00 am - 11:30 am

Chair: **Cheri Deng**
Univ. of Michigan

P1-C-01

Design and evaluations of a phased ultrasound array for transesophageal cardiac ablation

Nadine Smith¹, Jacob Werner², Eun-Joo Park³, Devina Jaiswal⁴, Author Hattel⁵, David Francischelli^{6,1} *Graduate Program in Acoustics, The Pennsylvania State University, University Park, PA, USA,* ²*Animal Resource Program and Department of Dairy and Animal Science, The Pennsylvania State University, University Park, PA, USA,* ³*Bioengineering, The Pennsylvania State University, University Park, PA, USA,* ⁴*Bioengineering, The Pennsylvania State University, University Park, PA, USA,* ⁵*Veterinary and Biomedical Science, The Pennsylvania State University, University Park, PA, USA,* ⁶*Cardiac Surgery Technologies, Medtronic, Inc, Minneapolis, MN, USA*

Background, Motivation and Objective

As one effective treatment, cardiac ablation shows a high rate of success in treating paroxysmal atrial fibrillation. A prevailing modality for this treatment is catheter ablation using radiofrequency. However, there is measurable morbidity and significant costs and time associated with this invasive procedure. To address these issues, a transesophageal ultrasound applicator for noninvasive cardiac ablation has been developed and evaluated in this research. Since the esophagus is close to the posterior of the left atrium, its position makes it attractive for the incision-less surgery of the selected area of the heart using ultrasound. The purpose of this research is to create electrically isolating lesions in myocardial tissue by effectively delivering ultrasound energy without moving the array.

Statement of Contribution/Methods

Based on multiple factors from the simulation results of transducer arrays, current transesophageal medical devices, and throat anatomy, a focused ultrasound transducer that can be inserted into the esophagus has been designed. In this research, a two-dimensional sparse phased array with flat tapered elements as a transesophageal ultrasound applicator was fabricated and evaluated in *in vivo* experiments. With this array, noninvasive cardiac ablation was performed on five pigs. The array was operated at 1.6 MHz for 8 ~ 15 minutes to create single or multiple lesions on atrial and ventricular myocardium.

Results

From the comparison of the exosimetry measurements of the probe to the simulation of the ultrasound field, the experimental and theoretical values were matched at their peak values. The conversion efficiency of the array from electrical power to acoustic power, calculated from the results of exosimetry, was 41%. After ultrasound exposure, multiple lesions were created in the left ventricle and the left atrium. The average size of lesions were 5.1 ± 2.1 mm in width and 7.8 ± 2.5 mm in length.

Discussion and Conclusions

Based on the experimental results, it was demonstrated that the array can focus and steer the beam inside the tissue. Also, the array can deliver sufficient power to the focal point to produce ablation while not damaging nearby tissue outside the target area. The results demonstrate a potential application of the ultrasound applicator to transesophageal cardiac surgery in atrial fibrillation treatment.

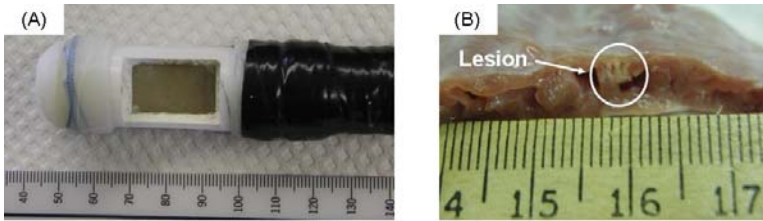


Figure 1. (A) Photograph of the constructed transesophageal ultrasound probe. The magnetic resonance-compatible probe head housing is 19 mm in diameter. (B) The cross-section of lesion on the myocardium on the left atrium. The size of lesion was 2.8 ± 0.3 mm in diameter and 2.4 ± 0.2 mm in length.

P1-C-02

Ultrasonic analysis of precision-engineered acoustically active lipospheres produced by microfluidics

Kanaka Hettiarachchi¹, Steven Feingold², Abraham P. Lee¹, Paul A. Dayton^{2,1}Biomedical Engineering, University of California, Irvine, USA, ²Joint Dept. of Biomedical Engineering, University of North Carolina–North Carolina State University, Chapel Hill, NC, USA

Background, Motivation and Objective

The development of a “magic bullet” that could carry a therapeutic dose of drug to a target organ or tumor with high specificity is the ideal goal of targeted drug delivery. Acoustically active drug carriers must possess a layer with drug-carrying capacity, similar to a liposome, yet at the same time, they must have a core with significantly different density and compressibility than the surrounding media – such as a gas. Factors such as consistent response to acoustic pulses and consistent loading per particle are important characteristics for reliable delivery. Here, we utilize microfluidic technology to precision engineer acoustically-active drug delivery vehicles. Microfluidic multi-layer flow focusing enables production of acoustically active lipospheres (AALs) with nearly identical diameter. We perform ultrasonic interrogation of these multi-layer vehicles as they are produced to determine their acoustic activity and diameter consistency.

Statement of Contribution/Methods

Gas-filled dual-layer lipospheres were produced in microfluidic flow-focusing channels molded out of polydimethylsiloxane (PDMS). A central stream of nitrogen gas was focused by two (lipid and oil) double-sided liquid sheath flows through a narrow 15 micron orifice. After production, lipospheres were pumped down an acoustically-transparent 200 micron cellulose tube. Vehicles were excited with a 1 cycle, 2.25 MHz acoustic pulse at approximately 200 kPa using a spherically focused ultrasound transducer energized with an arbitrary waveform generator and amplifier. Echo signatures for each AAL were received using a second 2.25 MHz transducer, amplified by 40dB and then recorded using a 14-bit, 100 MHz digitizer through a LabView interface. Offline processing in Matlab was used to calculate the average correlation between echoes.

Results

AALs could be formulated to carry doxorubicin in the oil layer, which was released with heating. The acoustic response AALs produced by multi-layer microfluidic flow focusing was measured as they were pumped at individual-particle concentration through a 200 micron acoustically-translucent tube. Average correlation from particle to particle was measured to be approximately 0.97, indicating that the echo signatures were nearly identical. This is in contrast to previous measurements of commercially-available polydisperse contrast agents, which exhibit echo correlations on the order of 0.7.

Discussion and Conclusions

Acoustic response from lipospheres was measured to be on the same order of magnitude as responses from thin-wall lipid shelled contrast agents, indicating the oil layer did not produce notable damping effects on the acoustic scattering. We hypothesize that based on nearly identical echo signatures, that it will be easier to optimize ultrasound radiation-force mediated concentration and acoustically-mediated drug-release to affect all AALs similarly.

P1-C-03

In vivo Sonothrombolysis of ear marginal vein and retinal vein of rabbits

Dong-Guk Paeng¹, Ruimin Chen², Naoki Matsuoka³, Walid Abdallah³, Amani Fawzi³, Qifa Zhou², Mark Humayun³, K. Kirk Shung²; ¹Ocean System Engineering, Jeju National University, Jeju, Jeju, Korea, Republic of, ²Biomedical Engineering, University of Southern California, USA, ³Doheny Eye Institute, University of Southern California, USA

Background, Motivation and Objective

Ultrasound (US) is known to enhance thrombolysis when it is used in combination with microbubbles and thrombolytic agents. However, the mechanisms of sonothrombolysis are not yet fully known. Most studies of US-enhanced thrombolysis have been performed with a thrombolytic drug, but the drug may also result in severe bleeding. In this research, US was applied only with microbubbles excluding any thrombolytic drug to investigate the sonothrombolysis in rabbit vessels in vivo.

Statement of Contribution/Methods

A Sonitron 2000 system (Artison Corp., Inola, OK, USA) was used to generate US for clot dissolution in rabbit vessels in vivo. The system was set to a frequency of 1 MHz, 7 W/cm² of intensity, and 30 % of duty cycle. US insonated an occlusion site for 10 minutes after 0.3–0.6 cc of Artison microbubbles with concentration of 13*10⁸ bubble/ml and mean diameter of 2.4 μm was injected through the other ear vein. US insonation with the injection of microbubbles was repeated 3 times. Marginal ear vein or retinal vein was occluded by laser or thrombin in 5 rabbits. Blood flow speeds in occlusion site and up- and down-stream were measured using a 40 MHz ultrasonic Doppler system with a needle transducer and Fluorescein Angiography (FA) was done before and after US application in order to confirm the opening of occlusion. All procedures related to animals were carried out in accordance with the Association for Research in Vision and Ophthalmology Statement for the Use of Animals in Ophthalmic and Vision Research and with the Institutional Animal Care and Use Committee of University of Southern California.

Results

The marginal veins of 4 rabbits occluded by either laser or thrombin were opened by US insonation with microbubbles. The Doppler speed was found to recover at the occlusion site after US insonation and FA confirmed the opening of occlusion. One occluded retinal vein showed irregular blood flow visualized by a microscope during US insonation, but the opening of the occlusion was inconclusive.

Discussion and Conclusions

Sonothrombolysis of rabbit veins was studied in vivo with only microbubbles but no thrombolytic drug. Occlusion sites induced by both laser and thrombin were opened in ear marginal vein after US insonation. These results demonstrate US may be a promising approach for treating central retinal vein occlusion in the eye which is severe disease and may cause blindness.

P1-C-04

Computational model of phased array for an image guided pediatric cardiac treatment

Nadine Smith¹, Ryan Mosse¹, Eun-Joo Park², Richard J. Meyer Jr.³; ¹Graduate Program in Acoustics, The Pennsylvania State University, University Park, PA, USA, ²Bioengineering, The Pennsylvania State University, University Park, PA, USA, ³Materials Science and Engineering, The Pennsylvania State University, University Park, PA, USA

Background, Motivation and Objective

Congenital heart diseases are a leading cause of death and chronic illness in infants and children. Although most congenital heart diseases can be palliated or corrected by cardiac surgery or percutaneous therapeutic cardiac catheterization, these invasive procedures are associated with low mortality but significant morbidities. For a noninvasive, safe and effective alternative strategy, this research is to design and evaluate an image guided noninvasive focused ultrasound system for the treatment of patent ductus arteriosus and atrial septal defects.

Statement of Contribution/Methods

Based on the metrics of a atrial septal defect as well as the metrics of isolated patent ductus arteriosus in consecutive human neonates, a first iteration of an array design has been performed. A random-sparse array configuration was used to reduce side-lobes and grating lobes (Fig 1a). To avoid the scattering and reflecting effects of ribs, the transducer is configured to fit in the gaps between the ribs. Using an average gap separation of 5mm and rib spacing of 7.5 mm, three separate random sparse arrays, 4.5mm in width, are separated by 3mm. The

three arrays are phased as if they are part of one large rectangular array. Each array contains 45 elements (3x15), with every third element active (45 total). The transducer will be driven at 1.2 MHz. At this ultrasonic frequency a small enough focal area can be created to avoid high intensities beyond the treatment area.

Results

The computational results of the linear intensity field has an input focal point at a depth of 25mm and axial beam steer of 5mm in the positive y-direction (Fig 1b). The artifacts around the focal area are caused by the relatively large gap between the arrays and beam steering. However, their intensities are much lower than the focal area.

Discussion and Conclusions

The ductus arteriosus has an average length of 3.9 mm. By steering the focal area of ultrasound, the entire ductus arteriosus can be treated without moving the ultrasound system. A higher frequency would yield a smaller focal area allowing for higher precision, but the transmission loss to the focal area would increase, requiring more power at the transducer face to deliver the same intensity to the focal region. Based on the computations, the phased array will be constructed and fully evaluated for an image guided noninvasive treatment of patent ductus arteriosus and atrial septal defects.

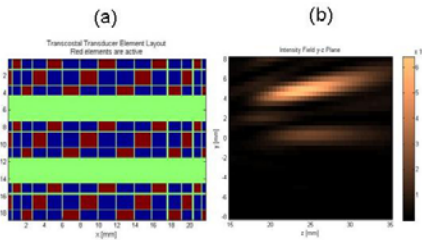


Figure 1. (a) With ASD and PDA metrics, a first iteration of an array design has been designed using a random-sparse array configuration to reduce side-lobes and grating lobes. (b) Calculated focal area within the tissue.

Monday
Poster

P1-C-05

Continuous VS Pulse Ultrasound Therapy on the Flexibility of Short Hamstring Muscles

azadeh shadmehr¹, hasan nadimi astaneh¹; ¹tehran university of medical sciences, tehran, Iran

Background, Motivation and Objective

Ultrasound has been a widely used and well-accepted physical therapy modality for the management of musculoskeletal conditions. However, there is a lack of scientific evidence on its effectiveness. We studied the effect of two different modes of ultrasound (continuous vs pulse) in reducing the shortening of hamstrings.

Statement of Contribution/Methods

Thirty non-impaired men aged 20 to 30 years (mean 23.84 years) were included in this study. They were randomly divided into two groups. Group 1 was composed of 15 subjects who underwent 10 sessions of continuous ultrasound (2W/cm2 , 1MHz, 5 min) and group 2 was composed of 15 subjects who underwent 10 sessions of pulsed ultrasound (200 microsecond burst of 1MHz sine waves repeated at 1 KHz, 0.5W/cm2 , 5 min). Ultrasound applied over their short hamstrings. Hamstring flexibility was evaluated by passive knee extension test at the base line and following interventions.

Results

Both methods of treatment were capable of significantly improving the flexibility of hamstring muscles (P<0.01). The hamstring flexibility were significantly improved in the continuous ultrasound group compared to pulsed ultrasound group (P<0.001).

Discussion and Conclusions

It seems that heating effects of continuous ultrasound may be more effective than non-thermal properties of pulsed ultrasound for increasing the flexibility of shorted hamstring.

P1-C-06

Comparative study of the effects of respiratory motion on in-vivo HIFU treatments in the liver

David Melodelima¹, William N'Djin¹, Naomi Miller², Jeffrey Bamber², Jean-Yves Chapelon¹; ¹Unit 556 - Therapeutic Applications of Ultrasound, INSERM, Lyon, France, ²Physics Department, Royal Marsden NHS trust and Institute of Cancer Research, Sutton, United Kingdom

Background, Motivation and Objective

Current development of HIFU strategies for the treatment of localized abdominal tumors are limited by organ motion during respiration. In preliminary studies, a numerical model simulated the effects of in-vivo movements on HIFU treatments in the liver. It was shown that a HIFU treatment performed during respiration with juxtaposition of millimetric lesions is modified in shape and homogeneity. Here, we report recent results from a comparative study which evaluated in simulation and in in-vivo experiments, the interest of using, during respiration, a toroidal-shaped HIFU device developed for the treatment of Liver Metastases from Colorectal Cancer.

Statement of Contribution/Methods

These experiments were performed during an open procedure, on 9 pigs divided into 3 groups. On the first group, a spherical HIFU transducer was used to juxtapose 49 millimetric lesions in the liver during respiration. The second group was treated during respiration with a 3 MHz toroidal-shaped HIFU transducer. The last group (control) was treated during apnea. For each animal, sequences of ultrasound images were acquired in the liver. Then, a combined method of modeling based on ultrasound speckle tracking and BHTE equation resolution, was used to quantify liver motion and to simulate HIFU treatments during breathing.

Results

Liver motions were mainly encountered in the cranial-caudal direction with a frequency comparable to the respiratory frequency ($f = 0.2$ Hz). Magnitude of the motion was 8.2-10.0 mm. Results of the modeling were well fitted to the observations made on in-vivo gross samples. In vivo lesions created with the spherical device were stretched by 64% and then were split in the tissues. The toroidal-shaped HIFU strategy allowed the generation of homogeneous lesions (12% stretching).

Discussion and Conclusions

These results provide a preliminary validation of the method for modeling liver motion effects. This method was used to demonstrate the effectiveness of a new HIFU device which shows promise for HIFU therapy during respiration.

P1-C-07

Enhancing Effects Of Microbubble Contrast Agent On High-Intensity Focused Ultrasound Ablation In Goat Liver In Vivo

Faqi Li¹; ¹Institute of Ultrasound Engineering in Medicine, Departmente of Biomedical Engineering, Chongqing Medical University, China, People's Republic of

Background, Motivation and Objective

To investigate the enhancing biological effect of different dosages of microbubble contrast agent on High-Intensity Focused Ultrasound (HIFU) ablation in goat livers in vivo.

Statement of Contribution/Methods

Twenty goats were divided into 4 groups randomly. Animals in group 1, 2 and 3 were bolus-injected with 0.01ml/kg/dot, 0.03ml/kg/dot and 0.05ml/kg/dot of SonoVue (Bracco SpA, Milan, Italy) intravenously respectively before HIFU exposure; and those in group 4 were not given injections as control. The livers were ablated using HIFU performed in the manner of a single dot using a clinical device. The frequency of HIFU was 0.8MHz; the intensity of HIFU was 19000W/cm². The distance from skin to the target liver tissue was 30mm. The exposure time was set at 15S for all animals. All animals were euthanized 7 days after HIFU, and volumes of coagulated necrosis were measured. Pathological examinations were performed to determine whether there were residual intact tissues within the exposure regions.

Results

Coagulated volumes in group 1, 2, 3 were larger than those in group 4, with significant difference ($p < 0.05$). The coagulated volumes increased gradually from group 1 to group 3, with significant difference ($p < 0.05$). Pathological examinations confirmed that there were no residual unaffected tissues within the exposed volume. Two remarkable changes occurred in one goat in group 3 seven days after HIFU: The surrounding adjacent tissues outside the reactive zone were necrotized, and the overlying liver tissues were destroyed.

Discussion and Conclusions

These findings showed that the enhancing effect of microbubble contrast agent in HIFU ablation was related with the dosage of the microbubble contrast agent SonoVue. The higher the dosage, the larger the volume destroyed in the target tissue. However, when exceeding a certain dosage level, SonoVue would give a negative impact on HIFU ablation, which awaits further study in future. (This work were funded by the National Natural Science Foundation of China (30830040) and the Natural Science Fundation Project of CSTC (CSTC2006BA5020).

**Monday
Poster**

P1-D. Beamforming Systems and Hardware

Sala Orange

Monday, September 21, 2009, 10:00 am - 11:30 am

Chair: **Jian-yu Lu**
Univ. of Toledo

P1-D-01

A High-Frequency Beamformer Design based on Variable PMN-PT SAW delays

Rob Adamson¹, Zahra Torbatian¹, Manohar Bance², **Jeremy Brown¹**; ¹Biomedical Engineering, Dalhousie University, Halifax, Nova Scotia, Canada, ²Surgery, Dalhousie University, Halifax, Nova Scotia, Canada

Background, Motivation and Objective

High-frequency beamformers require extremely accurate, dynamically changing timing delays to be applied to the individual elements in a receiving array. The large number of digital channels, high sampling resolution, and speed of signal processing are the primary reasons that high-frequency ultrasound beamformers are extremely expensive and not readily available. We have designed a high-frequency analog beamformer that can generate the necessary delays using carefully controlled surface acoustic wave (SAW) devices based on PMN-PT single crystal substrates. This greatly reduces the number of required electronic components and could allow high-frequency beamformers to be produced for a fraction of the cost.

Statement of Contribution/Methods

SAW delays are based on piezoelectric substrates and consist of two sets of inter-digital surface electrodes at opposite ends of the substrate. Ultrasonic surface waves are sent and received between these sets of electrodes with a delay time proportional to the distance between them. By fabricating a second set of plate electrodes on the top and bottom of the substrate in between the SAW electrodes, the physical length and speed of sound between the two sets of electrodes or "delay time" can be changed by applying an electric field. Figure 1 shows the general arrangement of the variable SAW delay beamformer.

Results

PMN-PT is an ideal candidate for a SAW delay since it is broadband with a high electromechanical coupling factor. It is also ideal for a 'variable' SAW delay due to the large d_{31} coefficient and the inherent decrease in elasticity with strain (i.e. speed of sound delay and strain delay are additive). We have designed a variable PMN-PT SAW beamformer for a 50MHz linear array, which requires a maximum delay range of ± 40 ns. By taking into consideration the change in delay due to the path length and change in velocity, a practical design for the substrate dimensions (30 mm long, 150 μ m thick) and plate voltage (± 140 V) was developed. Laser Doppler measurements have also been performed on prototype devices in order to verify that we are able to achieve our desired delay range with a reasonable voltage.

Discussion and Conclusions

This beamformer design has the potential to reduce the number of A/D channels (i.e. cost/complexity) to just one, by accurately controlling the receiving delays in a high-frequency array. Good agreement was found with theory.

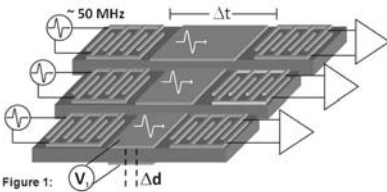


Figure 1: V_i Δd

A Digital Scan Conversion Algorithm Using Fourier Transform

Dong-Ki Ahn¹, Mok-Kun Jeong¹, Sung-Jae Kwon¹, Moo-Ho Bae²; ¹Daejin University, Korea, Republic of, ²Hallym University, Korea, Republic of

Background, Motivation and Objective

In clinical ultrasound scanners, the echo data from phased or convex arrays are acquired in the polar coordinates but need to be displayed in the Cartesian coordinates. This requires a coordinate conversion process. In this paper, the performance of spatial and frequency domain scan conversion algorithms is compared. We show that the frequency domain method produces B-scan images comparable to the bilinear method.

Statement of Contribution/Methods

Even if the echo data obtained in the polar coordinates are mapped onto the Cartesian coordinates through digital scan conversion, the spatial frequency spectra of the polar coordinate data and the Cartesian coordinate data should be essentially the same except for the relevant Fourier transform expressions. Therefore, it is possible to obtain digital scan converted image by taking the spatial Fourier transform of the polar coordinate data in the polar coordinate variables and sampling the resulting spectrum at Cartesian grid points followed by inverse Fourier transform. This method is advantageous in that various signal processing techniques can be employed in the frequency domain to improve image quality.

Results

We used many different image patterns to test the performance of the scan conversion methods. It was found that the bilinear method produced the best image quality with a minimum of computations. However, the Fourier transform method with Kaiser filtering also yielded comparable results albeit at the expense of more computation time.

Discussion and Conclusions

Considering that some synthetic aperture focusing or high frame rate imaging methods that reconstruct B-mode images in the frequency domain require the use of Fourier transform, scan conversion based on the Fourier transform method lends itself to image reconstruction and scan conversion. With further improvement of computation speed and image quality, the Fourier transform method with Kaiser filtering can be employed in digital scan converters.

Co-array Optimization of CMUT Arrays for Forward-Looking IVUS

Coskun Tekes¹, Mustafa Karaman¹, F. Levent Degertekin²; ¹Isik University, Istanbul, Turkey, ²Mechanical Engineering, Georgia Institute of Technology, Atlanta, USA

Background, Motivation and Objective

The ring annular array structure is a preferred configuration for implementing Forward-Looking IVUS (FL-IVUS) catheters as it allows for volumetric imaging as well as use of a guidewire at the center. In order to avoid grating lobes in radiation pattern and to have wide viewing angle, the FL-IVUS transducer array elements need to be small in both radial and lateral dimensions. CMUT technology is promising for these arrays especially with the flexibility of locating array elements on the circular donut area efficiently, and optimizing each transducer element independently for transmit or receive operation. To take advantage of this flexibility, in this study, we introduce a new co-array sampling strategy that improves imaging performance while keeping the number of firings at a level suitable for real-time imaging.

Statement of Contribution/Methods

We introduce a new co-array sampling strategy based on the idea of adjusting the element density of the co-array rings in radial direction to suppress side lobes. In non-uniform sampling of the co-array with a given number of firings, the inter-element distances are adjusted both in radial and angular direction from inner ring to outer ring to fit a given apodization function. Use of the closest elements in obtaining a reduced set of Tx-Rx firing pairs requires spatial quantization of element locations which results in undesired beam patterns. To handle this, we perform inverse mapping of the co-array elements back to Tx and Rx elements within a donut-shaped region between the guide wire and the catheter boundary.

Results

To test the imaging performance, we performed numerical simulations of the co-array with non-uniform sampling fitting to the raised-cosine apodization. The simulated array has 64 transmit and 48 receive elements. In the simulations, we used single element responses experimentally obtained on dual-ring CMUT FL-IVUS arrays which were fabricated and tested previously. We performed non-steered 2-D PSFs on r - θ plane and obtain averaged 1-D PSF over θ -axis. For a test case of 350 firings simulation results show nearly 10-dB improvement in maximum near side lobe levels when compared with the uniformly sampled co-array.

Discussion and Conclusions

The simulation results shows that side lobe level can be reduced/controlled by using non-uniform co-array sampling which realizes aperture apodization by adjusting the sample density. This approach does use uniform weighting of all Tx and Rx elements in beamforming, and hence does not cause any SNR loss for apodization. Our experimental response based simulations demonstrate the viability of the dual-ring CMUT arrays with the co-array optimization for real-time FL-IVUS imaging.

P1-D-04

PC-Based Modular Digital Ultrasound Imaging System

Yasser Kadah^{1,2}, Mawia Hassan², Amr Hendy³, ¹Nile University, Egypt, ²Cairo University, Egypt, ³IBE Tech, Egypt

Background, Motivation and Objective

With the availability of high-end integrated analog front-ends, distinction between different digital ultrasound systems is determined almost exclusively by their software component. Efficient digital ultrasound systems rely on embedded digital signal processing on FPGA with data conversion from oversampled 1-bit delta-sigma ADC to minimize the number of lines going into the FPGA. However, using LVDS interface protocol allows a serial output with drivers on FPGA to recover the parallel data. This alleviates the need for designing the sampling and the signal recovery filters while maintaining an optimal performance at significantly lower power consumption. Moreover, PC-based implementations for sophisticated medical imaging technologies have emerged where powerful multi-core computational ability replace expensive embedded systems. The objective of this work is to develop a modular low-cost PC-based digital ultrasound imaging system that has almost all of its processing done on the PC side.

Statement of Contribution/Methods

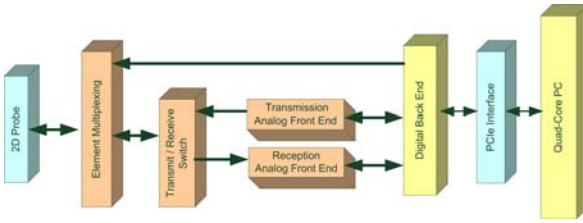
The goal is to move almost all know-how related software components into the PC. The block diagram for a 32-channel module is shown in Fig. 1 where the data are collected and interfaced to the PC via a PCI-express bus through a Virtex-5 FPGA (Xilinx, Inc.). The use of several of these modules is possible through the use of multiple lanes of this interface bus.

Results

PCI-express interface bandwidth did not allow real-time raw data transfer. Hence, a small embedded software part was added that uses a combination of Hilbert transformation FIR filter and a decimation block to lower the data rate based on probe bandwidth characteristics. Once the data were in the PC memory, reconstruction of final image was done using spatially variant filtration of the received line data implemented using look-up table. This allows the utilization of the parallel programming offered by the quad-core processor used in the system. Real-time reconstruction frame rates were achievable on the preliminary version of this system.

Discussion and Conclusions

A technique that expands the utility of current high-performance PCs to replace the high-cost embedded processing in digital ultrasound systems is introduced. The new system has the potential to lower the cost and speed up the development, thus offering new opportunities for more cost-effective systems.



P1-D-05

Using GPUs for beamforming acceleration in SAFT imaging

David Romero¹, Oscar Martinez¹, Carlos J. Martin¹, Ricardo T. Higu², Alberto Octavio³, ¹Inst. Automatica Industrial (C.S.I.C.), Arganda del Rey, Madrid, Spain, ²Universidade Estadual Paulista - Campus Ilha Solteira, Ilha Solteira, Sao Paulo, Brazil, ³Inst. Acustica (C.S.I.C.), Madrid, Madrid, Spain

Background, Motivation and Objective

The use of synthetic aperture techniques to reduce the number of electronic channels in array imaging systems has been a topic profusely studied in several application areas, such as radar, sonar or ultrasonic imaging. These techniques are based on the sequential activation of subapertures of array elements in emission and in reception, and the postprocessing of all the received signals to compose the image. Then the system can be divided into two stages: an excitation and acquisition stage, where the signals received by each element or group of elements are stored; and the beamforming stage, where the signals are processed to compose the final image. The beamforming algorithm usually includes different functions such as focusing in emission and in reception, band-pass filtering, spatial filtering, envelope detection, etc. The complexity of the algorithms, the high number of signals and of image points, justify that the processing stage can result too slow when a typical PC-based system is used.

The evolution of graphics processors over the past few years has driven the development of General Purpose computing on Graphics Processing Units (GPGPU). Nowadays GPUs are fully programmable and have a high level of parallelism which provides a great power of computing for parallel and computationally intensive applications with a good relation between price and computing capacity.

Statement of Contribution/Methods

One of the characteristics of the imaging process is the high degree of parallelism, as it needs applying a set of processing algorithms to a great amount of digitized signals, and for a dense grid of spatial points. The goal of this work is exploring GPU parallelism in order to reduce processing time during the beamforming process.

Results

In the example we use a SAFT system based on a 128-elements array, with two channels in reception and one channel in emission (2R-SAFT), while the beamforming stage has been implemented in GPU (NVIDIA cuda enable processor). For instance, we have computed the image of 300*300 points, applying the beamforming algorithm to 255 signals, and the frame rate has increased from 0.5 images/s, using CPU facilities, to more than 50 images/s, using GPUs parallelism.

Discussion and Conclusions

One of the main advantages of shifting the beamforming process from CPU to GPU is the reduction of the computational time and therefore the increment of the frame rate in image reconstruction. GPUs parallelization constitutes an excellent method of accelerating the imaging formation at very low cost and complexity.

Design of a Micro-beamformer for a 2D Piezoelectric Ultrasound Transducer

S. Blaak¹, Z. Yu², G.C.M. Meijer², C.T. Lancée¹, J.G. Bosch¹, N. de Jong¹ / *ErasmusMC, Rotterdam, Netherlands, ²Delft University of Technology, Delft, Netherlands*

Background, Motivation and Objective

Our research project is to design a transesophageal probe using a matrix ultrasonic transducer for 3D echocardiography. To obtain images with sufficient resolution, several thousand elements are required. Therefore, it is necessary to include electronics close to the transducer and use smart signal processing for data reduction.

Statement of Contribution/Methods

Our matrix transducer consists of ~2000 elements with a pitch of 200 μ m. The elements are arranged in groups and pre-steering is applied within a group, by delaying the elements relative to each other. This reduces the number of signal lines from ~2000 to ~200. To simplify the required electronics, all the groups have the same delay configuration. For a correct design, delay steps and the maximum delay are of importance. Furthermore, the delay should be programmable for each direction. Simulations in Field II [1, 2] are performed to investigate the effect of grouping and pre-steering on the received field. The delay and sum operations are realized by an integrated circuit.

Results

Fig.1 shows the received pressure field with and without pre-steering. Without pre-steering all elements within one group have the same delay. For pre-steering, the simulations show a decreased grating lobe level relative to the main lobe and an increase of the main lobe by ~5dB. Simulations on the maximum acceptable grating lobe level, -20dB below the main lobe, resulted in a delay step size of 40ns. An analog delay line is designed using sample-and-hold structure and digital control circuit, which can provide programmable delays from 40ns to 280ns, with a step size of 40ns. The distribution of the delay time among the elements in a group is calculated and an optimized delay line topology is used to keep a low system complexity.

Discussion and Conclusions

The pre-steering approach for the micro-beamformer of a 2D matrix transducer is an effective method to reduce the channel count, while maintaining a usable receive field.

[1] J.A. Jensen: Field: A Program for Simulating Ultrasound Systems, 10th Nordic-Baltic Conference on Biomedical Imaging Published in Medical & Biological Engineering & Computing, pp. 351-353, Vol. 34, Supp. 1, Part 1, 1996.

[2] J.A. Jensen and N. B. Svendsen: Calculation of pressure fields from arbitrarily shaped, apodized, and excited ultrasound transducers, IEEE Trans. Ultrason., Ferroelec., Freq. Contr., 39, pp. 262-267, 1992.

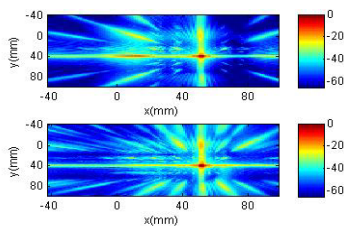


Fig. 1: The received pressure field (dB) for a matrix with focus at 60mm, 15° elevation and 25° azimuth without (top) and with pre-steering (bottom).

Real-time specific beamforming applied to motion trajectory estimation in ultrasound imaging

Guillaume Zahnd¹, Adrian Basarab¹, Hervé Liebgott¹, Olivier Basset¹, Philippe Delachartre¹; ¹CREATIS-LRMN, Lyon, France

Background, Motivation and Objective

Elasticity imaging is often based on strain computation of image pairs to discriminate tissue stiffness. Two innovations are proposed here:

- A real-time beamforming strategy, instead of the current post-processing, to acquire RF2D signals presenting lateral oscillations and providing phase images to estimate subpixel motion vector.
- A multi-frame phase-based trajectory estimation method to analyze free-hand compression/decompression cycles in elastography aiming to consider Lagrangian deformations.

Statement of Contribution/Methods

Firstly, the real-time beamforming strategy was implemented on the RP500 Ultrasonix scanner to generate real-time RF2D images and phase images dedicated to motion vector estimation. The phase images are thereby generated from two single-orthant analytic signals.

Secondly, a Lagrangian-based novel multi-frame motion estimation method was introduced and applied to a local region of the image. The first step is a spatio-temporal prediction based on the p previous estimations, assuming a constant velocity of the ROI. Then the residual displacement is estimated with a specific analytical estimator based on phase image differences. In order to overcome the speckle decorrelation between the ROI and the reference frame along the sequence, an evolution scheme of the reference frame, based on a similarity criterion (NCC), was also introduced.

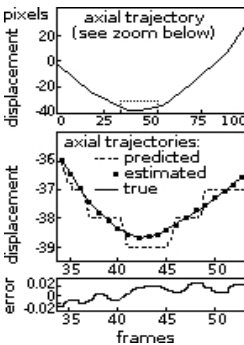
Results

A real-time RF2D image acquisition and the corresponding phase images were processed on a breast phantom (acquisition depth: 5cm, frame rate: 80 fps).

Then the trajectory estimation method was performed on an experimental phase image sequence of a reference (ground truth) displacement: a compression/decompression cycle was applied to the phantom. The ROI (6.3x0.3 mm²) was tracked along a sequence of 100 frames ($p = 5$ frames and NCC = 0.75). The maximum displacement amplitude was 70 pixels. The reference frame was updated 8 times. The figure shows that the trajectory vector estimation is very accurate, providing very low errors (not larger than 0.05 pixels) in both axial and lateral directions.

Discussion and Conclusions

This paper deals with multi-frame phase-based motion estimation using specific RF2D images acquired in real-time. In elastography, trajectory estimation opens a new perspective to control the free-hand compression and to discriminate tissue stiffness.



Monday Poster

A New ASIC Architecture for Ultrasonic Synthetic Aperture Imaging System

Moo-Ho Bae¹, Jeong-Ho Ham², Ra-Young Yoon², Han-Woo Lee², Mok-Kun Jeong³; ¹*Hallym University, Korea, Republic of*, ²*Medison co. LTD, Korea, Republic of*, ³*Daejin University, Korea, Republic of*

Background, Motivation and Objective

Previously we reported "A new architectural design of Full aperture, Full frame-rate synthetic aperture Beamforming ASIC" in 2007 IEEE Ultrasonics Symposium. This architecture is appropriate for full aperture system. However, for low cost system - limited by material cost so that number of Rx channel is smaller than number of probe element - it is not quite optimum. The reason is, for example, as follows: If a single ASIC covers 8 channels and 8 scanline(SC)s and we want to build a system with 16 channels and 128 SCs, then 16 ASIC chips are needed to meet SC requirement. Total number of input channel of these ASIC chips is 128, however, only 16 of these inputs are used and others are just wasted.

We will propose new ASIC architecture, which will have not only a very little overhead to embody conventional full aperture, full frame-rate system but also a very efficient way to embody low-cost system with a small channel number.

Statement of Contribution/Methods

Basic concept of newly proposed method is that one scanline accumulator(SC-ACC) handles multiple SC data sequentially. This concept requires trade-off between number of increased SC and decreased number of Tx synthesis accumulation. An example of this method is as follows: Assume that single chip has 8 SC-ACC, and two chips are used to cover 32 SCs. Location of the SC-ACC 0 in Chip 0 synthesizes SC 0 in 0th~15th Tx interval, and synthesizes SC 16 in 1st~16th Tx interval. And SC-ACC 1 in Chip 0 synthesizes SC 1 in 1st~16th Tx interval, and synthesizes SC 17 in 17th~32th Tx interval.

However, this basic concept has serious problem if we want to apply this concept to previously proposed architecture. In that architecture, the chip area of focusing delay and apodization data generation block can be drastically reduced by assigning adjacent SCs to a chip and by limiting the ratio between SC spacing and probe element spacing to integer. But, in the above example, at 16th Tx, SC-ACC 0 synthesizes SC 16, while SC-ACC 1 synthesizes SC 1.

A new architecture to solve this problem is proposed. After every pre-defined number of transmission, partially accumulated SC data in SC-ACC is read, moved to adjacent SC-ACC and accumulated at the same time. All SC data in the SC-ACC are moved to adjacent SC-ACC simultaneously. This movement of data is done between chips also. This movement allows that each chip always handles adjacent SC data.

Results

Proposed new architecture makes it possible that SC-ACC with limited number can handle much larger number of SC by moving partially accumulated SC data without significant overhead.

However, there's a trade-off between number of SC and Tx synthesis accumulation count.

Discussion and Conclusions

This architecture can provide the best performance for full aperture high end system, in addition, can reduce material cost for low-cost system with small channel number. Currently, a new beamformer ASIC based on the proposed architecture is being designed using 0.13um process.

P1-E. Blood flow I

Sala Orange

Monday, September 21, 2009, 10:00 am - 11:30 am

Chair: **Hans Torp**
NTNU, Norway

P1-E-01

Hematocrit Evaluation Based on Ultrasonic Estimations of Shear Rate and Viscosity in Blood Flow

Naotaka Nitta¹, Hiroshi Masuda²; ¹Institute for Human Science and Biomedical Engineering, National Institute of Advanced Industrial Science and Technology (AIST), Tsukuba, Ibaraki, Japan, ²UNEX Corporation, Nagoya, Aichi, Japan

Background, Motivation and Objective

Blood viscosity is expected as an index for detecting the blood abnormality such as thrombosis because the viscosity is highly correlated with hematocrit (HCT) and increases due to local aggregation of erythrocyte. However, since the whole blood is the non-Newtonian fluid, apparent viscosity also varies according to the magnitude of shear rate. On the other hand, the shear rate-viscosity (SV) curve is uniquely formed by the HCT. In this study, the HCT is evaluated noninvasively based on the ultrasonic estimation of SV curve, as part of blood characterization.

Statement of Contribution/Methods

At the beginning of this method, the 2-D velocity vector distribution including the lateral (x-axis) and beam-axis (y-axis) velocity components in the blood flow is estimated by using the ultrasonic Doppler measurement and the incompressible condition. After dividing the velocity vector distribution into several ROIs, the viscosity coefficient (μ) is obtained by using a previously-proposed method based on Navier-Stokes equations (Nitta, 2005), in each ROI. At the same time, the shear rate (e) is also obtained by differentiating the velocity vector distribution. The above processing results in the viscosity distribution ($\mu(x,y)$) and the shear rate distribution ($e(x,y)$), and then the SV curve (e, μ) is obtained by consolidating ROIs. Here, the consolidated ROIs can reflect the non-Newtonian property of whole blood. Therefore, the SV curve exhibits higher value for lower shear rate and lower value for higher shear rate. In HCT evaluation, the SV curve model is prepared as a mathematical function of HCT. By searching the HCT that minimize the residual error between the estimated SV curve and that model, the most likely HCT is determined.

Results

After investigating the accuracy of this method, in vivo measurements for the brachial artery of healthy men subjects were conducted. RF signals (10 MHz) for Doppler measurement were acquired on the longitudinal cross section of the artery, by using an ultrasonic diagnosis equipment (UNEX, EF18G). Based on the above-mentioned method, the shear rate $e(x,y)$ was estimated in the 78 to 264 s^{-1} range and the viscosity $\mu(x,y)$ was estimated in the 2.9 to 9.2 mPa·s range, at the time phase of maximum velocity. On the other hand, SV curve model for HCT evaluation was defined as $\mu = \alpha e^\beta$ based on the literature data (Brooks, 1970), where α and β are the functions of only HCT. As the result of HCT evaluation, the HCT of the subjects were estimated as 46.3 ± 1.8 % ($n=3$), and the repeatability was high.

Discussion and Conclusions

In the above result, although the HCT value was estimated directly, if the SV curve template of healthy subject is adopted, the residual error between the estimated SV curve and the template also becomes an useful index for diagnosing the blood abnormality. In future work, feasibility study in clinical use will be conducted by increasing the number of cases.

A High-Precision Gravity Intravenous Infusion Rate Meter Using CMUT Arrays

Mengli Wang¹, Jingkuang Chen¹: *Electrical and Computer Engineering, University of New Mexico, Albuquerque, NM, USA*

Background, Motivation and Objective

Gravity intravenous infusion (IV) administration set is widely used with its advantages of affordability, easy operation and portability. Despite of its popularity, the current IV administration sets suffer from inadequate accuracy in measuring the infusion rate. This inadequacy results in a relatively poor dose control.

Many of the commercial IV administration meters monitor the average flow rate by counting the number of drips in given time. Since this indirect method requires continuous counting of dripping, it is difficult to get an accurate and continuous infusion rate when a total or partial blockage of the needle happens. Especially, when the patient is moving around with an IV pole, infusion rate is almost impossible to monitor. A tool, which can monitor the infusion rate with a high accuracy, is badly needed.

Statement of Contribution/Methods

We have developed a high-precision miniature infusion rate meter by measuring both the flow velocity and the tube diameter simultaneously in real time using two face-to-face capacitive micromachined ultrasonic transducer (CMUT) arrays as shown in Fig.A. This CMUT flow meter is designed for clipping on the flow tube as a portable device. The meter consists of a rubber chamber coated with Vaseline, and a clamp used for securing the IV tube. Inside the chamber, there are two parallel 5.0 MHz CMUT linear arrays used for ultrasound transmission and reception. The flow tube diameter D was measured through the time flight echo delays between near and far wall reflections. The infusion velocity v , was detected using the pulse ultrasound Doppler by comparing the demodulated echo ultrasound with the incident ultrasound. Combining the measurement of tube diameter and the fluid's velocity, the volumetric flow rate can be accurately calculated.

Results

Eight different commercial PVC IV tubes were tested in this IV administration system. The tube diameter was measured from time flight of the ultrasound pulse echo as shown in Fig.B with a resolution of 0.1mm. A 0.05 ml/min flow rate resolution was achieved with the combinational measurement of tube diameter and the flow velocity.

Discussion and Conclusions

A CMUT infusion rate meter was developed and preliminary drug dispense rate experiments were conducted. This tool is useful for closed-loop infusion rate control for a high precision drug dispense system.

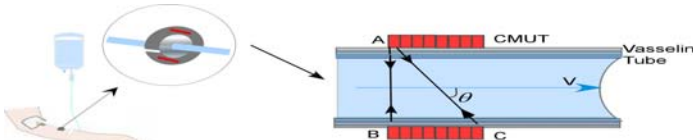


Fig. A. Schematic of a CMUT Intravenous Infusion Rate Meter. Path AB is used to measure the tube diameter using pulse-echo time differences. Path AC is used to measure the flow velocity using ultrasound Doppler shift.

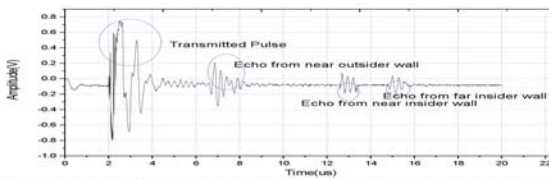


Fig. B. Pulse-echo ultrasound signal used in PVC tube diameter measurement.

Qualitative Validation Study of Fast Spectral Estimators Using *In-vivo* Data

Kristoffer L. Hansen¹, Fredrik Gran², Mads M. Pedersen¹, Iben K. Holfort³, Jørgen A. Jensen³, Michael B. Nielsen¹
¹Department of Radiology, Rigshospitalet, Copenhagen, Denmark, ²GN Resound, Ballerup, Denmark, ³Department of Electrical Engineering, Technical University of Denmark, Lyngby, Denmark

Background, Motivation and Objective

The conventional spectral Doppler method in medical ultrasound is the Welch's method (WM). WM requires a long observation window (OW) of up to 256 emissions per estimate to achieve sufficient spectral resolution and contrast. Two adaptive filterbank methods have been suggested to reduce the OW: Blood spectral Power Capon (BPC) and Blood Amplitude and Phase Estimation (BAPES) method. A preliminary *in-vivo* study with a single observer indicated that BPC and BAPES performed better than WM. In this paper the *in-vivo* performances of BPC, BAPES and WM were evaluated by nine observers and the results treated statistically.

Statement of Contribution/Methods

Ten volunteers were scanned over the carotid artery using the experimental ultrasound scanner RASMUS and a B-K Medical 7 MHz linear array transducer. Four approaches (WM with a Hanning window (W.HAN), WM with a boxcar window (W.BOX), BPC and BAPES) and seven OWs (128, 64, 32, 16, 8, 4 and 2) were combined. Thus, from each data set, 28 spectrograms were produced. All the 280 spectrograms were presented in randomised order to nine radiologists blinded to method and OW for visual evaluation: useful or not useful. Tests for multiple comparisons were performed along with kappa statistics for intra- and inter-observer variability.

Results

At OW 128 and 64, BAPES, BPC and W.HAN performed equally well ($p>0.05$) while W.BOX scored less ($p<0.05$). At OW 32, BAPES and BPC performed better than W.HAN and W.BOX ($p<0.0001$). BAPES was significantly superior to BPC at OW 16 ($p=0.0002$) and 8 ($p<0.0001$). BPC at OW 32 performed as well as BPC at OW 128 ($p=0.29$) and BAPES at OW 16 performed as well as BAPES at OW 128 ($p=0.55$). W.HAN and W.BOX at OW 16 and 8 failed as all four methods at OW 4 and 2. The intra-observer variability for three radiologists evaluating the same 280 spectrograms with >14 days apart showed good agreement (86%, $\kappa=0.72$). Inter-observer variability showed moderate agreement (78%, $\kappa=0.57$).

Discussion and Conclusions

The adaptive methods were scored useful for shorter OWs than WM and the results indicated that OW can be reduced to 32 using BPC and to 16 using BAPES without reducing the usefulness of the spectrogram. The inter-observer agreement was moderate indicating some variation and base-line differences in judgments among the radiologists. The intra-observer agreement was good. BPC and BAPES can potentially bring improvements to spectral velocity estimation: as an increase of the temporal resolution of the spectrogram or as an increase of the frame rate for the interleaved B-mode image.

Adaptive Clutter Rejection for Ultrasound Color Doppler Imaging of Lower Extremity Blood Flow: Preliminary Results

Sangwon Kim¹, Jaesok Yu², Tai-Kyong Song², Yang Mo Yoo³; ¹Interdisciplinary Program in Biofusion Technology, Sogang Univ., Seoul, Korea, Republic of; ²Dept. of Electronic Engineering, Sogang Univ., Seoul, Korea, Republic of; ³Dept. of Electronic Engineering & Interdisciplinary Program in Biofusion Technology, Sogang Univ., Seoul, Korea, Republic of

Background, Motivation and Objective

Deep venous thrombosis (DVT) is a common lower extremity vascular disease. For the assessment of patients with suspected DVT, noninvasive compression ultrasound based on B-mode is a primary procedure. However, it would be technically difficult to achieve compression ultrasound of the entire proximal deep vein system for patients with tense and swollen extremities. Thus, color Doppler imaging capable of visualizing lower extremity blood flow would be an alternative approach. However, excess flash artifacts from tissue motions are introduced during DVT scanning due to low pulse repetition frequency (PRF) and transducer movement.

Statement of Contribution/Methods

In this paper, the adaptive clutter rejection (ACR) method, in which an optimum filter is dynamically selected at each location based on clutter power and instantaneous velocities, is applied to effectively remove flash artifacts during lower extremity scanning. To evaluate the ACR method, the 80 frames of complex baseband data were

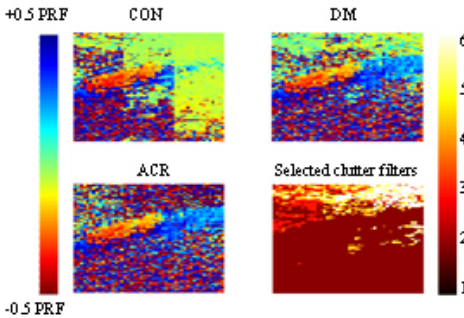
acquired from an ultrasound machine (HiVision 5500, Hitachi Medical Systems America, Twinsburg, OH, USA) by moving a 9-MHz linear array probe distally along the popliteal vein of a volunteer. The ACR method was compared with the conventional static clutter rejection (CON) and down-mixing (DM) methods in terms of flow-signal-to-clutter ratio (SCR).

Results

Figure 1 shows the color Doppler images with velocity estimates obtained from a subject by applying the CON, DM and ACR methods before applying scan conversion and thresholding to clearly visualize residual clutter (greenish colors). The dynamically-selected clutter filter in the ACR is also shown in Fig. 1. Compared to CON and DM, the ACR method shows higher clutter suppression since the higher order clutter filters are selected in the regions with accelerated tissue motions. The measured flow SCR after clutter rejection is also consistent with visual assessment (i.e., 16.0+/-7.1 dB vs. 7.5+/-10.6 dB and 4.6+/-12.7 dB for ACR, DM and CON, respectively).

Discussion and Conclusions

In this paper, we presented the adaptive clutter rejection method to effectively suppress flash artifacts introduced during lower extremity vascular scanning. From a preliminary in vivo experiment, the proposed method shows a statistically significant improvement in clutter rejection compared to the static clutter rejection methods.



P1-E-06

High frame rate quantitative Doppler imaging over a wide field of view

Ron Daigle¹, Lauren Pflugrath¹, John Flynn¹, Ken Linkhart¹, Peter Kaczowski^{1,2,1} Verasonics Inc., Redmond, WA, USA, ²Applied Physics Lab, University of Washington, Seattle, WA, USA

Background, Motivation and Objective

Color flow (CF) Doppler imaging is useful to locate flow in a region of interest (ROI), but quantitative estimates of flow (e.g., spectral Doppler) essential to clinical diagnosis require substantially longer transmit-receive ensembles. Conventional medical ultrasound systems use a focused transmit beam to probe along a line in the ROI, and can thus produce a time series of quantitative Doppler information at one or more points along that line. Comparison of flow data from points on different scanlines usually results in unacceptably low frame rates, thus requiring use of data collected over different heart cycles, and often with different system settings.

The Verasonics ultrasound system architecture provides great flexibility in event sequence programming and data processing, enabling straightforward implementation and evaluation of new ultrasound modalities. Here, the objective is to use unfocused transmit beams to collect and process very high frame rate data for both CF imaging and quantitative flow estimation over a wide ROI. We seek to demonstrate that clinical metrics (e.g., spectral parameters, velocity ratios) can be simultaneously provided for several arbitrary points anywhere in the ROI. In addition, Vector Doppler processing can be used to provide automatic angle correction for the CF display, and completely new parametric displays of flow can be produced in post-processing.

Statement of Contribution/Methods

A 128 transmit / 64 receive channel Verasonics system with an L7-4 linear array was used to image and record element-level RF data from the carotid artery of a volunteer, using interleaved Doppler and echo transmit-receive sequences. Flat-focus transmit beams at several different angles were used in continuous acquisition with a PRF between 8 and 12 kHz.

Results

A subset of the acquired frames was processed in real-time to illustrate several new Doppler imaging modes, including CF with simultaneous spectral displays at several arbitrary locations, and Vector Doppler imaging of flow direction and velocity magnitude within the ROI. Several seconds of recorded data were post-processed in a real-time playback mode for different spectral locations, and displayed in a slow-motion mode using all acquired frames. New types of parametric flow images were generated for each cardiac cycle, including angle-corrected peak velocities, and velocity ratio images for a given reference flow location or given reference time. Finally, novel cinelooop movies of selected spectral Doppler parameters (peak and mean velocity, power, bandwidth) were produced to visualize dynamic flow over several cardiac cycles.

Discussion and Conclusions

The flexibility of the Verasonics ultrasound architecture permits implementation of new modes of Doppler imaging that take advantage of the high frame rates made possible by broad beam transmission. Further study of newly developed parametric flow imaging methods must be performed to evaluate their diagnostic potential.

P1-E-07

Reducing Color Flow Artifacts caused by Parallel Beamforming

Torbjørn Hergum¹, Tore Grtner Bjåstad¹, Lasse Løvstakken¹, Kjell Kristoffersen², Hans Torp¹; ¹Norwegian University of Science and Technology, Trondheim, Norway, ²GE Vingmed Ultrasound, Horten, Norway

Background, Motivation and Objective

In color flow imaging (CFI), the inherent trade-off between frame rate and image quality may often lead to suboptimal images for medical diagnosis. This is especially the case in real-time 3D imaging, where stitching of data from several cardiac cycles based on ECG triggering is currently needed. In order to help overcome this problem, parallel receive beamforming is used. We have found that a difference in curvature of transmit and receive beams gives a bias in the Doppler velocity estimates which varies significantly within one group of parallel beams. This causes a discontinuity in the velocity estimates between groups of beams from different transmit events. Color flow also suffers from the parallel beam artifacts found in B-mode imaging. The net result of these artifacts shows up as vertical lines in the images, and a high number of parallel receive beams is therefore not used without substantial spatial smoothing. A method to correct for parallel beam artifacts named synthetic transmit beams (STB) was previously introduced, based on coherent interpolation between overlapping receive beams from neighboring transmit events. The method effectively generates synthetic transmit beams that are aligned with the received beams within a group of parallel beams. The method has previously been shown to work well for B-mode images. However, phase cancellation may occur due to an additional time lag between neighboring beams for Doppler packet acquisition.

Statement of Contribution/Methods

In this work a revision of the STB approach is presented that is applicable for CFI, correcting for all of these artifacts. As an alternative to coherent STB, an option is to use STB interpolation incoherently on the autocorrelation function. Since the autocorrelation function varies slower than the phase of the IQ data this allows for a combination of beams from significantly different times, for instance across interleaving groups or across scan planes in a 3D scan.

Results

Through simulations and *in vivo* recordings results showed 1) that coherent STB may still work in vascular imaging when beam interleaved acquisition is used, reducing the time between neighboring beams significantly, and 2) incoherent STB on the autocorrelation function proved to perform equally well in restoring the correlation phase angle estimates, and further also showed good results for larger time gaps such as between interleave regions. We used a GE Vingmed E9 with a M12L probe and 8 parallel beams to record images of the carotid artery. The Doppler bias was reduced from 17.2 ± 7.9 % (mean \pm std) for regular parallel beam acquisition to 3.0 ± 3.3 % for coherent STB and 2.1 ± 2.5 % for incoherent STB on the auto-correlation function.

Discussion and Conclusions

With STB used in color flow imaging we can maintain a high frame rate with parallel beam acquisition without compromising image quality.

P1-E-08

New Clutter Rejection Method using Time-domain Averaging for Ultrasound Color Doppler Imaging

JaeJin Lee¹, Jeong Cho¹, Yang Mo Yoo², Tai-kyong Song^{1,1}; ¹Electronic engineering, Sogang University, Seoul, Korea, Republic of, ²Sogang University, Seoul, Korea, Republic of

Background, Motivation and Objective

In ultrasound color Doppler imaging, effective rejection of clutter is important to improve the sensitivity in visualizing the blood flow. To adequately remove clutter, high pass filters, such as initialized infinite impulse

response (IIR), are utilized. In this paper, we present a new clutter rejection method which can provide comparable clutter rejection to projection-initialized IIR(PI-IIR) filtering while significantly reducing hardware complexity.

Statement of Contribution/Methods

In the proposed clutter rejection method based on time-domain averaging (TDA, clutter is first estimated, and then it is subtracted from receive Doppler signal. Specifically, the weighted 1st-order approximation is applied to three adjacent ensembles for modeling clutter in Doppler signal. To evaluate the proposed method, simulation and in vivo experiments were conducted. In simulations, the flow frequency in Doppler signal was adjusted from -0.45 pulse repetition frequency (PRF) to 0.45 PRF while the clutter frequency was fixed at 0.05 PRF. The in vivo data were captured from the liver of a volunteer using an ultrasound machine (HiVision 5500, Hitachi Medical Systems America, Twinsburg, OH, USA).

Results

Figure 1(a) shows the simulation results where the estimated flow frequency is plotted against the input flow frequency for the conventional high-pass filtering and proposed time-domain averaging methods. As shown in Fig. 1(a), the proposed TDA method shows similar results as the 3rd-order PI-IIR filter. From the liver in vivo data, under visual assessment, we obtained the comparable results as shown in Figs. 1(b) and 1(c). To evaluate hardware complexity, the proposed TDA method was implemented on a FPGA (Virtex 4, Xilinx, San Jose, CA, USA). It was found that the TDA requires 31,930 gates compared to 203,998 gates from the projection-initialized IIR filter.

Discussion and Conclusions

In this paper, the new efficient clutter rejection method was proposed where time-domain averaging is used. From simulation and in vivo experiments, the proposed method shows comparable results to a conventional high-pass clutter filtering method while significantly reducing hardware complexity (i.e., 85%). This result indicates that the proposed TDA method would be more useful for a hand-held ultrasound machine where the reduction in hardware complexity is critical in miniaturization.

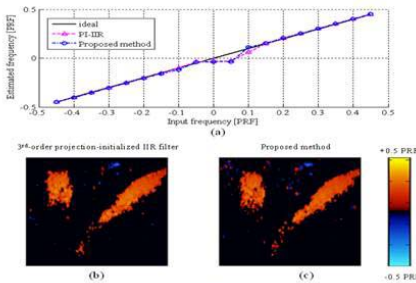


Figure 1.

P1-F. Blood Flow II

Sala Orange

Monday, September 21, 2009, 10:00 am - 11:30 am

Chair: **David Evans**
University of Leicester

P1-F-01

Performance of the Transverse Oscillation Method using Beamformed Data from a Commercial Scanner

Michael Johannes Pihl¹, Svetoslav Ivanov Nikolov², Per Haugaard², Martin Christian Hemmsen^{1,2}, Jørgen Arendt Jensen^{1,2} *Center for Fast Ultrasound Imaging, Department of Electrical Engineering, Technical University of Denmark, Kgs. Lyngby, Denmark, ²BK Medical ApS, Herlev, Denmark*

Background, Motivation and Objective

Blood velocity estimates using conventional color flow mapping (CFM) or Doppler techniques are angle dependent. One of the proposed techniques to overcome this limitation is the Transverse Oscillation (TO) method, which also estimates the lateral velocity components. Beamformed (BF) data is acquired using a commercial scanner as opposed to the previously reported results obtained with the experimental scanner RASMUS, and compared to those.

Statement of Contribution/Methods

The TO method is based on creating a double oscillating field by using special apodization profiles (APs) in receive (RCV). Two lines with a lateral displacement of $\lambda_x/4$, and a center line (for traditional axial estimation) are BF simultaneously in RCV. After echo canceling, a special phase shift estimator is used to estimate the lateral and axial velocity components. The TO AP is kept constant, leading to an increasing λ_x over depth. First stage BF data is acquired using a BK Medical (Herlev, Denmark) 2202 ProFocus scanner, a BK8812 transducer, and a BK UA2227 research interface connected to a standard PC through a DALSA (Waterloo, ON, Canada) X64-CL Express camera link. Only minor changes to the conventional CFM setup, hereunder adjusting the APs and delay profiles in RCV, are necessary to obtain the required data. The method is evaluated on a circulating flow rig with $r = 5.7$ mm, a blood mimicking fluid, a Cole-Parmer (Vernon Hills, IL) 75211-60 centrifugal pump, and a Danfoss (Sønderborg, Denmark) MAG 3000 magnetic volume flow meter. The performance is investigated by calculating the mean relative standard deviation, σ_r , and mean relative bias, B_r , of the velocity components.

Results

To increase the robustness of the TO method, the estimator averages over a number of samples. With $N = 20$ profiles, the lowest σ_r (14%) and B_r (14%) are obtained when averaging over two times the pulse length for a specific setup: CFM $f_0 = 3.75$ MHz, $f_{\text{prf}} = 1.30$ kHz, $v_0 = 0.215$ m/s, flow angle = 75° , focus at 15 mm, 16 shots per estimate, 6 cycles per pulse, and 6.6 mm between apodization peaks corresponding to $\lambda_x = 1.9$ mm at center of vessel (at 16.2 mm). For this setup, $\sigma_{r_{vx}}$ decreases {23, 17, 14, 8.2, and 7.0}% as the number of shots per estimate increases {4, 8, 16, 32, and 64}. Moving the transmit focus to 20 or 25 mm, increasing the center frequency, or lowering the number of transmit cycles reduces $\sigma_{r_{vx}}$. At 90° $\sigma_{r_{vx}}$ is 11% and the bias 38%.

Discussion and Conclusions

The present performance is comparable with the results from the experimental scanner and the simulations, and obtained with only few changes to the conventional CFM setup. This illustrates the feasibility of implementing the TO method on a commercial platform for real-time estimation.

A simulation setup to optimize particle flow velocimetry

Hang Gao¹, Florence Kremer¹, Hon Fai Choi¹, Jens-Uwe Voigt¹, Piet Claus¹, Jan D'hooge^{1,†}*Katholieke Universiteit Leuven, Belgium*

Background, Motivation and Objective

Particle Flow Velocimetry (PFV) has been introduced as a new ultrasound methodology to measure two-dimensional intraventricular flow patterns. It can potentially provide important new information on cardiac hemodynamics and function but how to optimize the method (frame rate; line density; contrast concentration; etc.) is still not clear.

As for any new ultrasound methodology, the further optimization and development of data acquisition and processing for PFV requires flexible and easy generation of ultrasound data under controlled conditions while having the ground truth flow field available. The aim of this study was therefore to build such a simulation environment by combining computational fluid dynamics (CFD) and ultrasound simulations.

Statement of Contribution/Methods

A 3D model of the left ventricular (LV) geometry was generated and meshed (Gambit 2.4, ANSYS) in order to be used as input to commercially available CFD software (Fluent 6.3, ANSYS). An analytic description of a typical ventricular inflow velocity profile (showing an early and atrial filling phase) was used as a boundary condition at the inlet of the LV model and the dynamic flow field was simulated. Point scatterers were subsequently put at random positions within the model and their positions were updated over time based on the simulated flow field. From this dynamic scatterer field, ultrasound data could subsequently be obtained using a convolution-based model previously introduced by our lab (COLE).

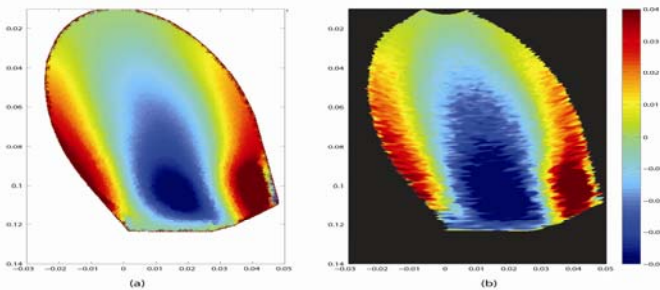
In order to test the simulation setup, RF signals from both a PW Doppler acquisition in the inlet portion of the model ($f_T=3.2\text{MHz}$; $f_S=50\text{MHz}$; $\text{PRF}=8\text{kHz}$) and a 2D color Doppler image sequence ($f_T=2.5\text{MHz}$; 120 lines; 90 degrees opening angle, 4kHz PRF) were simulated. From the former data set, the spectrogram was estimated and compared to the velocity measurement from Fluent. The latter data set was used to estimate the velocity vector field and qualitatively compared with the ground truth flow field.

Results

For the PW Doppler spectrogram, the normalized RMSE of the estimated PW velocities relative to the CFD reference was 10.94%. Moreover, good agreement was found between CFD and color Doppler measurement as show in Fig. 1 for a time point in diastasis.

Discussion and Conclusions

A simulation setup was constructed and shown to work correctly. This setup will be useful for optimizing PFV in echocardiography.



Resolving the lateral blood flow velocity component using change in correlation length of speckle due to scan direction and speed

Tiantian Xu¹, Greg Bashford^{1,1} *Biological Systems Engineering, University of Nebraska-Lincoln, Lincoln, Nebraska, USA*

Background, Motivation and Objective

The lateral array scan direction has a significant effect on the speckle from moving scatterers in the lateral direction (Fig. 1). Namely, the lateral speckle size is increased as the velocity of the blood approaches the "velocity" of the scanner. The scanner velocity is the rate and direction individual A-lines are collected to form an image. The situation is analogous to camera movement during image capture, causing variable "stretch" of the subject. We hypothesize the lateral correlation length of speckle is related to the difference between fluid velocity and scanner velocity.

Statement of Contribution/Methods

A blood flow phantom and 6 MHz transducer of an ultrasound machine was used to test a theoretically derived relationship between the scanner velocity, fluid velocity, and speckle size (relative "stretch"). The scanner was equipped with an interface allowing data capture immediately after beamformation. Two scanner velocities were used (64.8 and 37.4 cm/s). B-mode images of the phantom with varying velocities (10 to 40 cm/s) were collected. The lateral autocovariance of speckle data corresponding to flow was used to measure speckle size.

Results

Fig. 2 shows the actual versus theoretical stretch factor/velocity measurements, showing good agreement with theory. For the scan velocities of 64.8 cm/s and 37.4 cm/s, the average estimation error is 1.74 ± 1.48 cm/s and 0.65 ± 0.45 cm/s respectively. In both cases the average error is only a few percent of the theoretical values.

Discussion and Conclusions

Lateral speckle size changes with scanner velocity, providing a method of lateral blood flow velocity measurement. For the two scanner velocities used in our experiments, results were in good agreement with theory. The method potentially enables an estimate of lateral blood velocity in only one frame of data.

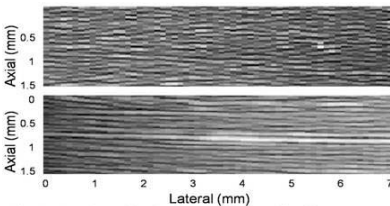


Fig. 1. Lateral speckle size change with scan direction. Top, flow against direction of scan. Bottom, flow with direction of scan. Note increased lateral speckle size (increased lateral correlation length) when flow is in direction of scan.

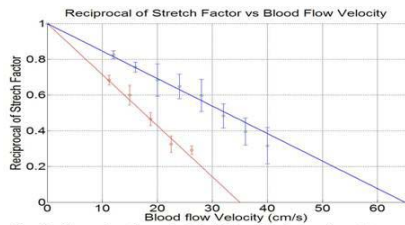


Fig. 2. Comparing theoretical (solid lines) and experimental results. Red, scan speed of 64.8 cm/s; Blue, scan speed of 37.4 cm/s. Error bars show +/- 1 SD.

A Least-Squares Vector Flow Estimator for Synthetic Aperture Imaging

Ivan K. H. Tsang¹, Billy Y. S. Yiu¹, Alfred C. H. Yu^{1,1} *Medical Engineering Program, The University of Hong Kong, Pokfulam, Hong Kong*

Background, Motivation and Objective

In synthetic aperture (SA) imaging, it is challenging to perform velocity estimation consistently using low-resolution images (LRIs) because their coarse point spread function would lead to Doppler spectral broadening. In this work, we aim to address such a challenge by developing a least-squares (LS) vector flow estimator that minimizes its mean-squared error based on frequency estimates obtained from multiple LRI-Doppler ensembles.

Statement of Contribution/Methods

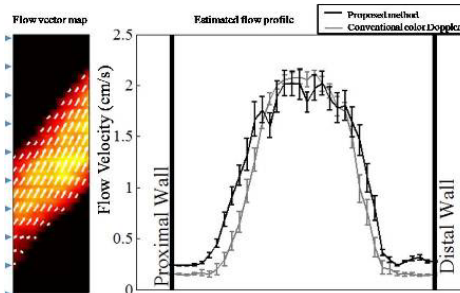
Our proposed flow estimator is intended to work with the SA data corresponding to a group of point sources. It essentially involves a two-stage estimation process. First, for each point source, we obtain LRI-Doppler ensembles and use them to compute a frequency estimate (via the lag-one autocorrelator) for every image pixel. Subsequently, by exploiting the fact that each point source deviates in beam-flow angle, we estimate flow vectors through creating a set of Doppler equations with two unknowns (i.e. axial and lateral velocities) from the frequency estimates and solving this equation set as an over-determined LS problem. As a performance analysis, Field II simulations were performed for a scenario with a 5mm-diameter steady flow tube angled at 45° (center velocity: 2.5cm/s). For these simulations, a 5.5MHz linear array with 128 elements was used; pre-beamform data were acquired for 97 virtual point sources (0.3mm spacing), and 8 two-cycle pulses were fired through each point source (PRF: 5kHz). Prior to LS estimation with the acquired data, we applied a mean-subtraction filter to each LRI-Doppler ensemble to suppress clutter arising from the tube wall (20dB more echogenic than blood). To facilitate comparison, we also performed estimation using conventional color Doppler.

Results

The figure shows a vector flow map and the cross-sectional flow profile (mean over 30 trials) obtained from a LS estimator involving LRI-Doppler estimates from point sources covering a 20° angle span. These vector flow estimates resembled the tube's flow profile, and their magnitudes are close to those found using conventional color Doppler with 45° as the nominal angle. In general, we found that the LS estimator's efficacy improved when it covered an angle span $>20^\circ$.

Discussion and Conclusions

The LS estimator showed potential in obtaining vector flow estimates from LRIs, thereby offering another way of performing SA vector flow imaging.



P1-F-05

Characterization of 3-D flow structures in the stenosed carotid bifurcation with plaque ulceration

Emily Wong¹, Jaques Milner¹, David Steinman², Tamie Poepping³, David Holdsworth¹; ¹Robarts Research Institute, Canada, ²University of Toronto, Canada, ³University of Western Ontario, Canada

Background, Motivation and Objective

Carotid plaque ulceration is a strong independent predictor of ischemic stroke. It has been shown recently that carotid plaque ulcerations can produce significant elevations in distal flow fluctuations, as characterized by the spectral parameter turbulence intensity (TI), based on velocity measurements from Doppler ultrasound (DUS). However, the nature of the flow fluctuations is not yet understood. Computational fluid dynamics (CFD) can predict the local time-varying 3-D flow field in vascular geometries, allowing for the investigation of the underlying flow patterns and the associated effect of Doppler settings.

Statement of Contribution/Methods

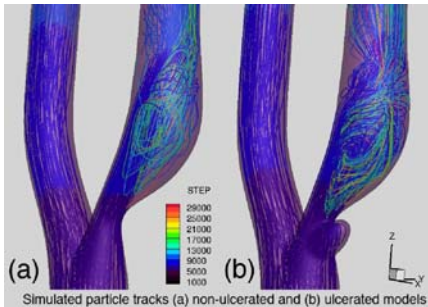
We performed CFD analyses on a stenosed carotid bifurcation geometry, with and without the presence of ulceration. CFD analysis of each model was performed with a spatial finite element discretization of over 150,000 quadratic tetrahedral elements and a temporal discretization of 4800 timesteps per cardiac cycle, to adequately resolve the flow field and pulsatile flow, respectively. Pulsatile flow simulations were iterated for 15 cardiac cycles to allow for cycle-to-cycle analysis of at least ten cycles.

Results

Similar to our DUS results, higher levels of TI were observed in the post-stenotic region of the ulcerated CFD model than in the non-ulcerated. The extent and magnitude of TI were comparable to DUS experimental results, after modeling for sample volume effects and applying a high pass filter. Regions of maximum TI were located off-center with respect to the longitudinal plane in the distal internal carotid artery bulb, producing an effect of sample volume size and location on TI. The presence of coherent structures may indicate why TI is lower when calculated from consecutive cardiac cycles. Although off-centre fluctuations occurred in both models - due to complex interactions of the oscillatory high-velocity jet with the recirculation zones - they were exacerbated in the ulcerated model due to enhanced out-of-plane recirculation and helical flow. Particle tracking results indicate that out-of-plane recirculation is induced by the deflection of flow exiting from the ulcer upon reentry into the high-velocity stenotic jet.

Discussion and Conclusions

Knowledge of the underlying 3-D flow structures may help to understand the effect of Doppler settings for the assessment of TI in the distal carotid artery.



P1-F-06

The ultrasound brain helmet for 3D transcranial doppler imaging

Brooks Lindsey¹, Nikolas Ivancevich¹, Edward Light¹, Stephen Smith^{1,1} *Biomedical Engineering, Duke University, Durham, NC, USA*

Background, Motivation and Objective

Considering the high global prevalence of neurovascular disease and the time-sensitive nature of its treatment, our goal is to provide emergency medical personnel with a rapid, low-cost diagnostic tool capable of producing real-time images of cerebral arterial flow. We previously described the first real time 3D scans of the cerebrovasculature (Fig. 1) as well as 3D aberration correction of the human skull using speckle targets.

Statement of Contribution/Methods

After modifying hardware and software, our 3D scanner (VMI) simultaneously acquires two 2.5 MHz, $63^\circ \times 63^\circ$ volumes, with 3D color flow, from opposing temporal acoustic windows. A typical 3D rendering of a blood vessel within a skull phantom simultaneously scanned from both transducers is shown in Fig. 2. We now seek to enhance image SNR by limiting transducer cable losses; a standard 2.5 m probe cable was replaced with 0.4 m MicroFlat ribbon cable. PiezoCad simulations predict SNR gains of 16.4 dB.

Results

Water tank experiments showed an improvement in summed RF signal of 14 dB in the shortened cable probe relative to the control.

Finally, we used one 3D transducer as a far-field correction beacon for the second 3D transducer positioned at opposing temporal windows. Each matrix array transducer corrected its counterpart's 100 ns RMS electronic aberrator yielding an increase in target brightness of 34% using this two-way pitch-catch phase correction.

Discussion and Conclusions

We will develop new custom transducers on short flexible circuits which interface directly with the scanner front end, thus realizing the increased SNR while maintaining our ability to position the transducers for imaging of the cerebral arterial circle and pitch-catch phase aberration correction.



Monday
Poster

P1-G. Myocardial Imaging

Sala Orange

Monday, September 21, 2009, 10:00 am - 11:30 am

Chair: **Jan D'hooge**
Catholic Univ. of Leuven

P1-G-01

QRS detection and cardiac cycle separation without ECG

Svein Arne Aase¹, Sten Roar Snare¹, Ole Christian Mjølstad¹, Håvard Dalen¹, Fredrik Orderud², Hans Torp¹,¹*Circulation and Medical Imaging, NTNU, Trondheim, Norway*, ²*GE Vingmed Ultrasound, Oslo, Norway*

Background, Motivation and Objective

Automatic detection of the QRS complex on ECG is used on most cardiac ultrasound scanners to separate recorded ultrasound data into cardiac cycles for continuous playback and storage. On small hand-held scanners it is unpractical to connect ECG cables. We aim to do automatic cardiac cycle separation and detect the start-point of a cardiac cycle corresponding to QRS on ECG using only B-mode ultrasound data.

Statement of Contribution/Methods

A deformable non uniform rational B-spline (NURB) curve is fitted to apical 2D B-mode data using an extended Kalman filter framework. The state vector of the filter is modeled as a combination of model pose parameters and positions of control points. The model is updated using a combination of edge detection and speckle tracking measurements. The resulting displacement of the atrioventricular (AV) plane of the left ventricle is extracted from the model.

The displacement curve is then processed by a rule-based curve analysis algorithm determining whether the curve has the shape of a typical AV plane displacement curve. If it does, the first time point of maximum distance from the apex/probe is detected. This event occurs close to the QRS complex of ECG. A section of the displacement curve before and after this maximum is extracted and compared to the rest of the curve by a sum of absolute differentiated differences (SADD) algorithm. The minimum of the SADD function then represents the time point at which the shape of the displacement curve repeats itself, the cycle length.

The parameters and rules of the algorithm were trained using a data set of 36 apical B-mode images with 3 cardiac cycles and ECG. Testing the algorithm against ECG cycle start and cycle length was done on a separate data set of 45 apical images with 3 cardiac cycles. Mean frame rate was 54 fps. Both data sets were pre-selected from a large normal material (HUNT3) to exclude non-standard views and images with poor image quality (35% of original images manually excluded). Images were recorded using an M3S probe on a GE Vivid 7. To emulate a real-time situation, several test cases with different start point during the first cardiac cycle were run for each recording.

Results

Totally, 1215 test cases were run. In 136 cases (11%), the curve shape was not accepted by the curve analysis rules. In remaining cases (89%), mean \pm SD difference of cycle start against corresponding QRS trig point was -18 ± 164 ms. Cycle length detection was only tried in these 1079 cases. In 71 cases, the resulting cycle lengths were automatically discarded by additional curve analysis rules. Thus, the cycle length was detected in 1008 cases (83% of total). Mean \pm SD difference against corresponding cycle lengths by ECG was 11 ± 75 ms. Mean running time of one test case in Matlab was 114 ms.

Discussion and Conclusions

Automatic detection of cardiac cycle lengths and time points near QRS of ECG is feasible based on B-mode only. However, accuracy should be improved.

Performance optimization of block matching in 3D echocardiography

Gabriel Kiss¹, Espen Nielsen², Fredrik Orderud², Hans Torp^{3,1} *Medical Imaging Laboratory, Norwegian University of Science and Technology, Trondheim, Norway;* ²*Computer Science Department, Norwegian University of Science and Technology, Trondheim, Norway;* ³*Department of Circulation and Medical Imaging, Norwegian University of Science and Technology, Trondheim, Norway*

Background, Motivation and Objective

Speckle tracking in 2D ultrasound (US) has already become a useful tool for assessing left ventricular function. The introduction of real time 3D US, allows for deformation tracking in three dimensions, without the limitations of 2D methods. Given an initial rectangular mesh, speckle tracking can be performed by block-matching. The displacement of a material point is found as the displacement of a region of interest around the point in the source frame that results in the best match within a target frame. The process is repeated for all the points in the mesh.

The aim of the study was to optimize the performance of 3D block matching by using a Single Instruction Multiple Data (SIMD) model, a technique employed to achieve data level parallelism.

Statement of Contribution/Methods

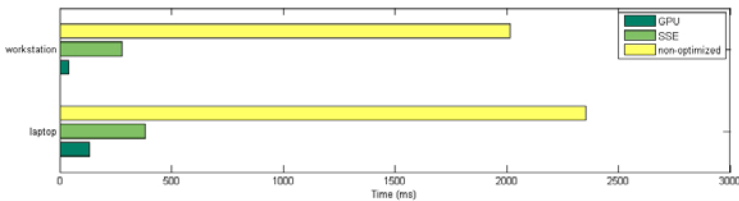
Two implementations of SIMD have been tested, in order to compute the minimum value of the sum of absolute differences (SAD). The first is based on Streaming SIMD Extensions (SSE), a SIMD model developed initially by Intel and which is nowadays integrated in both Intel and AMD processors. The second uses CUDA, a SIMD architecture proposed by NVIDIA, which is available on several graphics cards.

Results

The proposed implementations were compared against a non-optimized version of SAD on both a Dell Latitude 830 laptop: NVIDIA Quadro NVS 135M, Intel Core2 Duo T7500, 2GB RAM and on a high-end graphics system: NVIDIA GeForce GTX 285, Intel Core i7 920 Quad Core Processor, 3GB RAM. The synthetic data employed has a volume of interest (VOI) of 13x13x5 voxels and a search volume (SV) of 25x25x7 voxels. The initial rectangular mesh consists of 600 points. The figure shows average computation times (over 100 runs).

Discussion and Conclusions

With the use of SIMD architecture, the overall processing time is significantly reduced (up to 7x for SSE and up to 49x for CUDA), thus making 3D speckle tracking feasible in a clinical setting. Other matching criteria (e.g. sum of squared differences, normalized cross correlation) can be implemented efficiently (especially on the GPU) thus further improving the accuracy of the block matching process.



Bandwidth Doppler Tissue Imaging (BDTI) in the Myocardium

Norman McDicken¹, Michael Bennett¹, Carmel Moran¹, Audrey White¹, Tom Anderson¹; ¹*Medical Physics, University of Edinburgh, United Kingdom*

Background, Motivation and Objective

Heart wall comprises three muscle layers which move relative to each other in three dimensions. With ultrasound there are two approaches to studying myocardial motion namely Doppler Tissue Imaging (DTI) and Tracking of B-mode echoes. DTI produces images of one velocity component along the beam and Tracking is established in 2D. There is need for angle-independent real-time imaging in 3D. The potential of Doppler bandwidth is reported.

Statement of Contribution/Methods

Doppler techniques can measure speed of blood flow using the bandwidth of the velocity spectrum. They exhibit some insensitivity to ultrasound beam/flow angle. They appear to be sensitive to velocity gradients in the sample volume. Tissue measurements are less likely to be affected by velocity gradients. The research presented investigates Bandwidth Doppler Tissue Imaging (BDTI) in tissue mimicking material phantoms (TMM), humans and mice from the points of view of signal quality, angle dependence and temporal resolution.

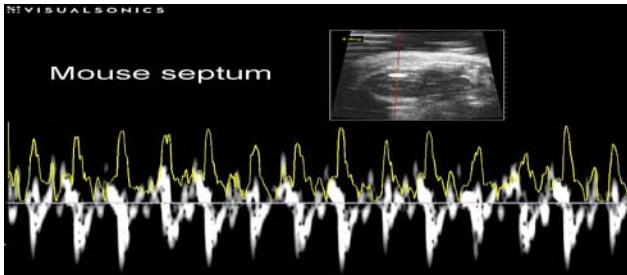
Results

A linear relationship between spectral bandwidth and TMM speed was measured up to 50 cm/s with Philips Sonos 5500 and Visualsonics Vevo 770 scanners. Angle-independent bandwidth for TMM viewed from 60° to 90° in 2D has been observed, a range of angles problematic for DTI. The Figure demonstrates placement of the sample volume at a selected location in the mouse ventricular septum and extraction of bandwidth. Measurement of bandwidth is also possible at locations where it is difficult to image with B-mode such as the apex of the human heart.

Discussion and Conclusions

Doppler techniques provide good S/N signals from the myocardium allowing accurate measurement of tissue speed. Angle-independent results in 2D appear to confirm theory. Spherical sample volumes have been proposed for angle-independent measurement in 3D (1). A more versatile test phantom has been designed to permit study over the full 0° to 90° in 3D as encountered in cardiology. The temporal resolution of BDTI is around 5 to 10ms as required for timing cardiac events. Increasing the number of sample volumes should make possible a clinical imaging tool.

(1)Yeung K-W. IEEE Trans Ultrasons Ferroelect Freq Contrl 1998; 45: 574-580.



P1-G-04

An in-vivo study on the difference between principal and cardiac strains

Daniel Barbosa¹, Piet Claus¹, Hon Fai Choi¹, Krasimira Hristova¹, Dirk Loeckx¹, Jan D'hooge^{1,2}. *U. Leuven, Belgium*

Background, Motivation and Objective

: Regional myocardial deformation is an important parameter for the assessment of regional myocardial function. As such, ultrasound methods have been proposed to estimate myocardial strain non-invasively in one, two or – more recently – in three dimensions. Although strain is most often reported in a cardiac coordinate system (radial, longitudinal, circumferential), its calculation implies that these directions are known. As this typically requires (manual) segmentation of the myocardium, authors sometimes report on the principal strains instead as they can simply be obtained through diagonalization of the strain tensor. The assumption made is that the normal cardiac strain components are close to the principal strains but this has not explicitly been tested.

The aim of this study was therefore to quantify the difference in strain values obtained in both the principal and cardiac coordinate systems and to define the average position of both coordinate system with respect to each other in an in-vivo setting.

Statement of Contribution/Methods

Volumetric ultrasound data was recorded in 10 healthy volunteers at a frame rate of 27.4±3.4Hz at 2.5MHz using a GE Vivid7 dimensions (GE Vingmed, Horten, Norway). Three-dimensional motion and deformation between

Monday
Poster

subsequent image volumes was estimated using a B-spline transformation based elastic registration method previously introduced (splineMIRIT). All data sets were manually contoured at end-diastole (using custom software – SPEQLE3D) from which the R,L,C axes could be unique defined for all LV segments. Subsequently, this contour was automatically tracked through the complete cardiac cycle based on the 3D estimated motion field. As such, the (Cartesian) strain tensor was known in all myocardial points from which both the RLC-strains and the principal strains could be derived. Moreover, the angle between the principal axes and the closest RLC axis was calculated.

Results

The cardiac peak strains, at end-systole (ES), were $49.6 \pm 22.0\%$, $10.8 \pm 1.6\%$ and $11.2 \pm 1.6\%$, for the RLC orientations, while the peak principal strains were $55.8 \pm 23.2\%$, $-14.6 \pm 1.1\%$ and $-13.1 \pm 1.8\%$ for the respective closest principal axis P1, P2 and P3. The average difference between the cardiac axis peak strain and the closest principal axis peak strain, was $-5.7 \pm 1.3\%$, $3.7 \pm 1.1\%$ and $1.9 \pm 1.0\%$ for the radial, longitudinal and circumferential directions. The angles between the between the principal axes and the closest RLC axis were $20.3 \pm 3.1^\circ$, $28.5 \pm 1.28^\circ$ and $26.8 \pm 2.0^\circ$, for P1, P2 and P3.

Discussion and Conclusions

As expected, the absolute values of the peak systolic principal strains were larger than the corresponding strains in the RLC system. However, in these normal hearts, the difference showed to be relative small. The angle between both coordinate systems is similarly small. The use of principal strains instead of cardiac strains seems to be acceptable and could thus help in automating strain estimation.

P1-G-05

A High Performance Spatio-Temporal Displacement Smoothing Method for Myocardial Strain Imaging

Shuhui Bu¹, Tsuyoshi Shiina¹, Makoto Yamakawa²; ¹Graduate School of Medicine, Kyoto University, Kyoto, Japan, ²Advanced Biomedical Engineering Research Unit, Kyoto University, Kyoto, Japan

Background, Motivation and Objective

Accurately assessing local myocardial strain is important for diagnosing ischemic heart diseases because decreased myocardial motion often appears in the early stage. The abnormal contraction motion can be visualized by myocardial strain images, but the strain calculation is very sensitive to noise. In our previous research, we proposed an adaptive dynamic grid-interpolation (ADGI) method for overcoming the limitation of the trade-off between spatial resolution and accuracy in traditional moving-average filters. Here, we extend the proposed method with the ability to process two or more frames' data for improving the SNR of myocardial strain imaging.

Statement of Contribution/Methods

Multi-frame RF data are acquired and stored for processing. The displacement vectors for each sampling point are calculated by a weighted phase-gradient method combined with an autocorrelation method. In the spatial domain, the ADGI method is used for fitting the displacement data by applying virtual springs attached at each mesh node in radial and circumferential directions. The virtual springs' pseudo-elasticity parameters, which are decided by a displacement error function, control the revision. Revising displacements are introduced, and a global error evaluation function is defined. Minimizing the function yields optimally revised displacements, and revised displacements are calculated by combining detected and revised displacements at each mesh node. In the temporal domain, the displacements are tracked and smoothed by a Kalman filter.

Results

The performance of this method was evaluated by numerically simulating the short-axis imaging of a 3-D myocardial model. A deformable model is used to simulate the strain distribution in the myocardium. The maximum radial strain is set to 15% in a normal wall and 5% in an infarcted wall. The total number of scanned frames is 30. Echo signals were generated by considering the parameters of a typical ultrasonic scanner with a center frequency of 3.75MHz. The signal-to-noise ratio is set to 10 to 30dB. The optimized pseudo-elasticity parameters that control smoothing are set in the range of 20 to 2800 in the radial direction and 20 to 800 in the shear direction.

For example, in a model with the infarcted region located around 1 to 3 o'clock, the RMS error is decreased from 60.27% to 33.50% without degrading spatial resolution compared to that generated by using median and moving averaging filters, even for a low SNR (20dB).

Discussion and Conclusions

The smoothing can be automatically adjusted based on the noise level in the spatial domain and further smoothed by a Kalman filter in the temporal domain. We can therefore see from the results that the strain generated by our proposed method is more accurate and robust and that the spatial resolution is retained. Therefore, the abnormal myocardial contraction region can be clearly identified.

P1-G-06

Sources and Characterization of Clutter in Cardiac B-mode Images

Muyinatu Lediju¹, Brett Byram¹, Gregg Trahey^{1,1} *Biomedical Engineering, Duke University, Durham, NC, USA*

Background, Motivation and Objective

In echocardiography, clutter is one of the most problematic image artifacts, often obscuring ventricular borders and introducing stationary noise in blood flow measurements. Clutter in transthoracic cardiac images is widely understood to originate from reverberations in the chest wall and off-axis echoes from structures such as the ribcage, lungs, and the heart itself. The objective of this work is to investigate the sources of clutter in cardiac images and their relative contributions.

Statement of Contribution/Methods

Raw echo data from real-time 3D cardiac images of the left ventricle (short-axis view) were acquired at a volumetric frame rate of 1 kHz, utilizing a Siemens Medical Systems SC2000 cardiac scanner with a matrix array. Three-dimensional speckle tracking was applied to the images to determine the motion characteristics of clutter and adjacent myocardium. The relationships among 3D displacement patterns through the cardiac cycle from several regions in the myocardium and within the ventricles were correlated and assessed for similarity using correlation analysis. In addition, principal component analysis (PCA) was applied to regions of the raw echo data to identify principal components with the most variability throughout the cardiac cycle. The resulting eigenvectors were used to isolate various motion patterns in selected regions of the cardiac data.

Results

When clutter adjacent to the myocardial wall was tracked, the clutter and adjacent myocardium had similar displacements. For example, during systolic contraction, axial displacements of the proximal myocardium and adjacent clutter region in the ventricle differed by approximately 5 μm , while that of the distal myocardium and adjacent clutter region differed by approximately 10 μm . However, when clutter farther from the myocardial wall was tracked, displacements were temporally and spatially complex and did not correlate well with any portion of the myocardium. The chest wall region was relatively stationary throughout the cardiac cycle. PCA of the cardiac data revealed a stationary component in the proximal myocardium, as well as in the chest wall region. Principal components with cyclic motion were also seen in the proximal myocardium. Principal components with cyclic motion were dominant in the clutter regions adjacent to the proximal and distal myocardium and in the distal myocardium.

Discussion and Conclusions

Similar displacements and cyclic principal components in regions of the ventricle and adjacent myocardium suggest that clutter in the ventricle arises from adjacent cardiac tissue. The stationary principal component observed in the proximal myocardium is most likely associated with stationary clutter. These results support the hypothesis that echoes from stationary structures, such as the ribcage and chest wall, are contributors to stationary clutter noise, while the myocardium is a dominant source of nonstationary clutter.

P1-G-07

Anisotropy in Three-Dimensional Propagation of Electric Excitation in Human Heart

Hiroshi Kanai^{1,1} *Electronic Engineering, Tohoku University, Sendai, Miyagi, Japan*

Background, Motivation and Objective

We have previously found that pulsed vibration occurs just after electrical stimulation of the extracted papillary muscle of a rat [Acoust Sci & Tech 2003; 24:17]. Based on the fact, by applying a novel ultrasound-based method to human hearts, we were able to successfully measure the proximate response of the myocardium to electrical excitation [UMB in press], and its propagation was visualized in 3D space [IEEE US Sympo 2008]. In the present study, we show that the anisotropy in 3D propagation of electric excitation in human heart can be detected.

Statement of Contribution/Methods

By controlling a stepping motor with reference to the electrocardiogram (ECG), the ultrasound probe on the chest wall was rotated intermittently by 7.2 degrees in each relaxation period during several successive heartbeats, and the RF reflective wave was acquired on each of several 2D planes obtained by slicing the left ventricle (LV). The number of directions of transmission in each plane was restricted to 16 to maintain a high frame rate (500 Hz), and thus minute velocity could be measured as waveforms. At all of about 10,000 points in the heart wall, the velocity waveforms toward the ultrasonic probe on each fan-shaped plane were simultaneously obtained, and their instantaneous phases of 40-Hz components were color-coded. By adjusting the times $\{T_R\}$ of the R-wave of the ECG in the several heartbeats, the instantaneous 3D distribution of the phase was reconstructed at every 2 ms, precisely revealing the propagation of the velocity waves in the LV, where the accuracy in the adjustment of the times $\{T_R\}$ was 0.2 ms. This novel method was applied to three healthy subjects.

Results

For healthy subjects, the results were obtained consecutively from 50 ms prior to the time of the Q-wave of the ECG. The changes in LV states were different among the subjects. For typical case, (a) a velocity component (myocardial response to the action potential) was generated at the apical side of the anterior wall, which was close to the root of the musculus papillaris posterior, and propagated counterclockwise to the whole LV at a speed of 0.7 m/s. However, the apparent propagation speed along the LV longitudinal axis was about 0.4 m/s. (b) From the radiation time of the first heart sound, another component (shear wave) was generated at the apical side of the IVS and propagated upward to the base side along the IVS at a speed of 0.6 m/s. (c) Finally, the first component became dominant again in the whole LV except at the root of the papillary muscle. This final time was close to the S-wave of the ECG and then the substantial contraction started.

Discussion and Conclusions

The subtle dynamic response of the myocardium to the arrival of the electrical stimulation demonstrated by the novel echocardiography developed in the present study with a high temporal resolution shows great potential for noninvasive assessment of myocardial tissue damage due to heart failure and desynchronization due to fibrillation.

P1-G-08

An Adaptive Estimator for Ultrasonic Myocardial Strain Imaging

Lingyun Huang¹, Congxian Jia², Sheng-Wen Huang¹, Chi Hyung Seo¹, Matthew O'Donnell¹; ¹Bioengineering, University of Washington, Seattle, WA, USA, ²Biomedical Engineering, University of Michigan, USA

Background, Motivation and Objective

In in-vivo myocardial strain imaging, decorrelation-induced peak hopping during peak systole greatly reduces both the accuracy and precision of estimated strains during this critical cardiac period. To improve performance at the large interframe strains encountered in systole, we have developed an algorithm combining a multi-scale Viterbi search with phase rotated correlation coefficient filtering.

Statement of Contribution/Methods

Data were acquired from a paced rabbit heart in a Langendorff preparation using a linear probe (5MHz central frequency, 40 MHz sampling frequency and 0.3mm pitch, Sonix RP, Ultrasonix, BC, Canada). Real RF signals were transformed to analytical signals, and cross-correlation was performed with kernels extending one speckle spot. Integer displacements along a scan line were estimated by Viterbi processing directly on correlation coefficients along the same scan line over 6 iterations. For each iteration, the Viterbi kernel was extended from one speckle spot to six (6) by one spot per step. Estimated integer displacements of the nearest neighbor were assigned to kernels not retrieved in iterations 2 to 6. Subpixel displacements were further estimated and refined using a phase rotated correlation coefficient filter with phase zero-crossing detection. The optimal displacement of a specific kernel was selected from one of the six estimates having minimum summed squared difference with neighboring kernels' displacements. The procedure was repeated across all scan lines to acquire a displacement image. The strain was further estimated using least squares fitting with a 2 mm window in both axial and lateral directions. Areas of frequent peak hopping were used to quantify improvements in strain estimates.

Results

The proposed algorithm successfully reduced peak hopping artifacts and improved strain SNR. Peak hopping in estimated strain was reduced by 86.1% for the regions highlighted in the figure. Remaining peak hopping artifacts correspond to regions with less than 0.5 correlation coefficient magnitude and are marked low-confidence regions for further processing.

Discussion and Conclusions

Multi-scale Viterbi search maximizes continuity in displacement estimation and improves the SNR of strain estimates. It is shown that this processing is most appropriate for myocardial applications with large interframe strains.

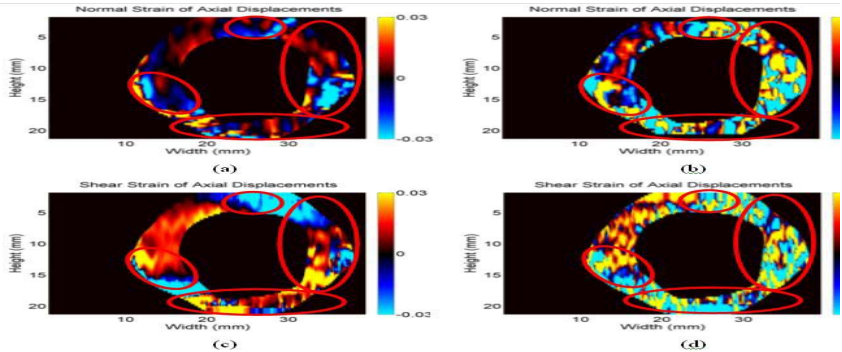


Figure 5. (a) axial derivative of axial displacement (axial strain) using multiscale Viterbi + phase correlation coefficient filter (b) axial strain using speckle tracking without Viterbi + phase correlation coefficient filter. The circled parts are peak hopping regions; (c) lateral derivative of displacement (axial component of shear strain) using multiscale Viterbi + phase rotated correlation filter; (d) axial component of shear strain using speckle tracking method without Viterbi rotated correlation coefficient filter.

P1-G-09

Increased Left Ventricular Twist - Short-Term Effect of Doxorubicin Cardiotoxicity

Noa Bachner¹, Yossi Tsadok¹, Dan Adam¹; ¹Biomedical Engineering, Technion, Haifa, Israel

Background, Motivation and Objective

Doxorubicin is a commonly used chemotherapeutic agent, but it may cause cardiomyopathy that often deteriorates to heart failure. Thus, its clinical usefulness is limited by dose dependant cardiac damage. Early detection of the remodeling process caused by doxorubicin cardiotoxicity is thus critical, before nonreversible processes occur. The aim of this study was to detect by ultrasound Doxorubicin-related cardiomyopathy at its early stages, before it is expressed in global echocardiographic parameters. To do so, a new layer-specific 2D Strain imaging analysis software was used, as a more sensitive measure of cardiac function than the standard global echocardiographic parameters.

Statement of Contribution/Methods

10 rats were used in this study. Doxorubicin was administered intraperitoneally 5 times a week at a dose of 1 mg/kg/d over four weeks, in 8 Wistar rats. 2 Wistar rats were used as controls, in which equivalent volume of Saline was administered intraperitoneally. Each week of treatment the rats were anesthetized, shaved and scanned by a VIVIDi ultrasound system, at 3 short-axis levels. The apical short-axis scans were analyzed by a high resolution 2D Strain program, based on speckle tracking, which enables segmental and layer-specific assessment of myocardial function.

Results

Out of 8 Doxorubicin treated rats only 4 survived the full treatment. In these 4 Doxorubicin treated rats there was a significant increase of the peak endocardial rotation ($P=0.006$), at the apical short axis level, after 4-5 weeks of treatment (25.1 ± 3.7 deg), versus the value of rotation at baseline and of the controls (8.0 ± 2.8 deg). Ejection fraction remained within the range of the normal values ($78.5 \pm 3.5\%$). A month after termination of the treatment, the peak rotation values returned back to normal (8.4 ± 6.8 deg). Two rats that were treated by Saline maintained normal values of rotation, versus their baseline values, during the whole experiment.

Discussion and Conclusions

Increasing the spatial resolution of 2D speckle tracking imaging allows layer-specific assessment of myocardial function, which may be useful in detecting cardiomyopathy at its early stages. Here it allowed measuring localized

Monday Poster

changes - peak endocardial rotation values were tripled versus baseline values, while ejection fraction maintained normal values. Thus, layer-specific strain imaging may serve as a clinical tool for detecting cardiomyopathy at its early stages.

P1-G-10

Frame Rate Dependence of Myocardial Elastography Estimates Using a Physiologic 3D Biventricular Finite-Element Model of the Heart with Preliminary In Vivo Validation

Wei-Ning Lee¹, Katherine M. Parker², Jianwen Luo¹, Jeffrey W. Holmes², Elisa E. Konofagou^{1,3}, ¹Biomedical Engineering, Columbia University, New York, NY, USA, ²Biomedical Engineering, University of Virginia, Charlottesville, VA, USA, ³Radiology, Columbia University, New York, NY, USA

Background, Motivation and Objective

The performance of Myocardial Elastography (ME), a 2D/3D radio-frequency (RF)-based transmural strain imaging technique, has been assessed in a theoretical framework (Lee et al, TUFFC 2007), in vivo graded myocardial ischemia animal experiments (Lee et al, IEEE IUS 2008), and a clinical setting against MRI tagging in normal and pathological cases (Lee et al, UMB 2008). In this study, the effect of the frame rate on the ME strain estimates throughout the entire cardiac cycle was investigated using a physiologic, 3D biventricular finite-element (FE) model.

Statement of Contribution/Methods

A 3D canine biventricular FE model (Continuity 6.3®, <http://cmrg.ucsd.edu/>) coupled to lumped parameter systems models of the systemic and pulmonary circulation in both normal (Control) and ischemic (left-anterior descending, LAD) cases was employed. Hemodynamics and biomechanics were in agreement with experimental measures, where end-diastolic and end-systolic pressures were respectively 13 mmHg and 84 mmHg in the normal case and 18 mmHg and 76 mmHg in the ischemic case. A time step of 1 ms was utilized to simulate the biventricular deformation for the entire cardiac cycle. A 3D linear convolution model was then used to simulate RF echocardiograms at a frame rate of 1000 fps. Variable frame rates, starting from 50 fps to 1000 fps, were achieved by progressively decimating the number of RF frames in the estimation procedure of 2D transmural displacements and angle-independent strains using the Myocardial Elastography technique, encompassing RF cross-correlation (3.0 mm window size; 80% overlap), least-squares strain estimator (lateral kernel: 6.7 mm; axial kernel: 3.4 mm) and coordinate transformation.

Results

At peak systole, the correlation coefficient increased exponentially with the frame rate (0.64 at 50 fps vs. 0.98 at 1000 fps) in both normal and ischemic cases. On the other hand, the elastographic signal-to-noise ratio (SNRE) initially increased and then decreased with the frame rate; reaching a peak of 6.10 and 8.50 at 200 fps and 500 fps for the lateral and axial SNRE's, respectively.

Discussion and Conclusions

Based on the physiologic 3D finite-element model, this study showed that for good quality axial strain estimates, a two-fold higher frame rate than for the lateral strain (500 fps vs. 200 fps) was required. As a result, this finding indicated the lateral strain to be estimated at lower frame rates and the axial strain at higher frame rates. The implementation of cardiac-phase-varying frame rate may further improve the strain estimation. Preliminary in vivo validation of this frame-rate effect on the strain estimation will also be shown.

P1-G-11

Tracking the Endocardial Border in Artifact-Prone 3D Images

K Y Esther Leung¹, Mikhail Danilouchkine¹, Marijn van Stralen¹, Antonius F W van der Steen¹, Nico de Jong¹, Johan G Bosch^{1,1}, ¹Erasmus MC, Netherlands

Background, Motivation and Objective

Analysis of echocardiograms, whether visual or quantitative, has traditionally been complicated by ultrasound artifacts such as reverberations and shadowing. Here, a novel method is presented to recognize artifacts which obscure the cardiac wall, to improve the tracking of the left ventricular (LV) borders in three-dimensional (3D) images.

Statement of Contribution/Methods

Previously, we have developed a prior knowledge driven, optical-flow (OF) based method for tracking the 3D cardiac wall [1]. Knowledge of the cardiac motion was incorporated using a statistical model, to guide the OF solution. This method was suitable for estimating the global cardiac motion. In this study, we aim at improving the local accuracy of this method, by applying a data-driven OF refinement [2] selectively in regions where the myocardium is clearly visible. To distinguish between visible and artifact-obscured myocardium, the expectation-maximization algorithm is applied in a stationary and cardiac motion frame-of-reference. This algorithm assigns probabilities to the image voxels as corresponding with a stationary (artifact) and moving (cardiac) component. From these probabilities, weights are derived reflecting the visibility of the LV wall; these are then integrated with the tracking scheme. This weighed method is compared with unweighed tracking, i.e. the refinement is applied everywhere, regardless of visibility.

Results

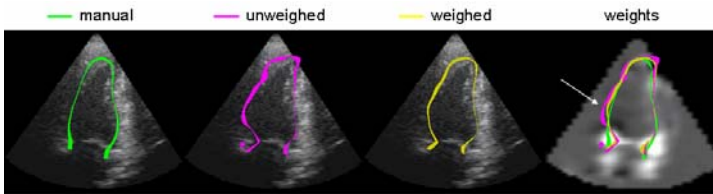
Evaluation on 35 3D clinical-quality images reveals better tracking results using this weighed tracking scheme. Point-to-surface errors decrease from 1.49 ± 0.52 to 1.19 ± 0.47 mm ($p < 0.01$). Also, smaller volume (3.9 ± 8.0 vs. 1.4 ± 6.7 ml) and ejection fraction (4.8 ± 5.5 vs. $0.9 \pm 4.8\%$) errors are found. These results compare favorably with those in the literature.

Discussion and Conclusions

The new method allows more accurate tracking, by distinguishing visible from artifact-obscured myocardium. Since in vivo images often contain ultrasound artifacts, we anticipate that this method will aid in the analysis of echocardiograms in the clinical setting.

[1] KYE Leung et al., "Tracking Left Ventricular Borders in 3D Echocardiographic Sequences using Motion-Guided Optical Flow," Proc SPIE Med Imaging 2009, 7259, 72590W

[2] BD Lucas and T Kanade, "An Iterative Image Registration Technique with an Application to Stereo Vision," Proc DARPA Image Underst Workshop 1981, 121-30



Detection of LV border (end-systole, two-chamber cross-section); arrow shows low weights for shadowed area.

Monday
Poster

P1-H. Quantitative Elasticity Methods

Sala Orange

Monday, September 21, 2009, 10:00 am - 11:30 am

Chair: **Stephen McAleavy**
Univ. of Rochester

P1-H-01

Fibroscan® in hepatology: a clinically-validated tool using vibration-controlled transient elastography

Laurent Sandrin¹, Celine Fournier¹, Sebastian Mueller², Veronique Miette^{1,1} *Echosens, Paris, France, ²University of Heidelberg, Germany*

Background, Motivation and Objective

Chronic liver diseases result in the accumulation of fibrosis inside the liver parenchyma which may eventually lead to cirrhosis. Cirrhotic liver is known to be stiffer than normal liver. Liver biopsy used to be the only gold standard for the assessment of liver fibrosis. At present, vibration-controlled transient elastography (VCTE) is more and more used for the staging of liver fibrosis. In this paper, the characteristics and performances of vibration-controlled transient elastography (VCTE) for the staging of liver fibrosis are presented.

Statement of Contribution/Methods

VCTE (Fibroscan; Echosens, Paris, France) is used in clinical practice to quantify liver stiffness non-invasively and rapidly. Liver stiffness is compared to fibrosis stage obtained using liver biopsy. In VCTE, a 50 Hz and 2 mm peak-to-peak amplitude controlled-vibration is applied at the surface of the skin and results in the propagation of an elastic shear wave through the liver. Shear wave propagation is imaged with an ultrasound transducer (2.5 MHz to 5.0 MHz) used in ultrafast pulse-echo acquisition. In a first approximation, the velocity of the shear waves is directly related to liver stiffness. Diagnostic performances are evaluated using the area under the receiver operating curve statistical approach by comparison with fibrosis staging using liver biopsy published in literature databases [1]. Effect of venous pressure [2] was studied in landrace pigs by clamping the caval vein and measuring the relationship between the hydrostatic pressure in the caval vein and liver stiffness as a function of time.

Results

Strong correlation between liver biopsy fibrosis stage and liver stiffness are reported. AUROC for the diagnosis of significant fibrosis and cirrhosis are 0.84 and 0.94, respectively. Clamping of the caval vein for 5 minutes increased liver stiffness from 3.1 kPa to 27.8 kPa.

Discussion and Conclusions

Diagnosis accuracy of liver stiffness measured by VCTE is very good for significant fibrosis and excellent for cirrhosis in a large number of liver diseases: hepatitis B and/or C, HIV, co-infection, alcoholism, etc. However liver stiffness is influenced by other hepatic conditions such as venous pressure and acute hepatitis [3] that tend to increase stiffness values as biological tissues exhibit strongly nonlinear stress-strain relationships. As a conclusion, liver stiffness is a key physical parameter for the whole liver function.

[1] Friedrich-Rust, et al. Performance of Transient Elastography for the Staging of Liver Fibrosis: A Meta-Analysis, *Gastroenterology*, 134,960-974 (2008).

[2] Millonig, et al. Venous pressure increases liver stiffness (Fibroscan®) independent of liver fibrosis, *EASL meeting, Copenhagen (2009)*.

[3] Arena, et al. Acute Viral Hepatitis Increases Liver Stiffness Values Measured by Transient Elastography, *Hepatology*, 380-384 (2008).

Validation of Ultrasound-based Transient Elastography by means of Dynamic Mechanical Analysis: Application to In vivo / In vitro Porcine Liver

Jennifer Oudry¹, Nicolas Pêrichon², Simon Chatelin², Pierre Allemann³, Luc Soler³, Rémy Willinger², Laurent Sandrin¹; ¹Research & Development, Echosens, Paris, France, ²University of Strasbourg, IMFS - CNRS, Strasbourg, France, ³Institut de Recherche contre les Cancres de l'Appareil Digestif, Strasbourg, France

Background, Motivation and Objective

It is well known in clinical medicine that palpation is an effective diagnostic tool for characterizing tissues mechanical properties. This accounts for the motivation of investigators for developing quantitative elastography techniques for noninvasively evaluating the viscoelastic properties of tissues. Comparison of a new clinical measurement technique with an established one is often needed to see whether they agree sufficiently. Dynamic Mechanical Analysis (DMA) is often considered as the reference method to characterize quantitatively mechanical properties of materials. However, DMA is an invasive technique and only in vitro mechanical properties can be estimated. In this study, a comparison between Transient Elastography (TE) and Dynamic Mechanical analysis techniques is performed on in vivo / in vitro porcine liver.

Statement of Contribution/Methods

The elastic property of porcine liver, given by the shear modulus G, was measured by both TE and DMA. Shear modulus measurements were realized on in vivo and in vitro liver to compare the TE and DMA methods and to study the influence of testing conditions (time, death of the animal) on the liver viscoelastic properties.

Results

Tests were performed on the liver of 5 female pigs. Each organ has been tested successively in vivo by TE, in vitro by TE and at least in vitro by DMA. In vitro results show that elastic properties obtained by TE and DMA are in agreement. At 50 Hz, the mean liver shear modulus measured by TE was about 2.0 ± 0.5 kPa in vivo and 1.2 ± 0.4 kPa in vitro. Furthermore, results show that the liver is homogeneous, isotropic and more elastic than viscous. Finally, it is shown in this study that viscoelastic properties obtained by TE and DMA change significantly with post mortem time.

Discussion and Conclusions

The preliminary results obtained in this study are promising. In addition to the measurement of in vivo liver tissue mechanical properties, this study demonstrates the efficiency of the TE-based method to determine in vivo liver properties. In addition to the validation of the in vitro use of the TE experimental device, this study shows a significant decrease of the liver tissue elasticity obtained by TE between in vivo and in vitro configurations. This study has also confirmed the post-mortem time dependence of the liver tissue.

Future work will extend this study to a more significant numbers of animals. Besides, TE does not measure the viscosity independently. Measuring the viscous property of a material in TE is of a great interest. However, this study has quantitatively demonstrated the validity of the elastic assumption in TE in a first approximation.

Furthermore, this work shows that TE could be the new "gold standard" method for quantitatively assessing in vivo tissue elastic properties.

In vivo assessment of fibrosis in murine liver using transient microelastography: A feasibility study

Cécile Bastard¹, Matteo Bosio², Meriem Yorgov³, Hélène Gilgenkrantz³, Laurent Sandrin⁴; ¹UMRS INSERM U930 / CNRS ERL3106 / Université de Tours, Tours, France, ²Laboratoire d'Imagerie Paramétrique, CNRS UMR7623 / Université de Paris VI, Paris, France, ³Institut Cochin, UMRS INSERM U567 / CNRS UMR8104 / Université de Paris V, Paris, France, ⁴Research and Development Department, Echosens, Paris, France

Background, Motivation and Objective

Recently, transient elastography has been successfully applied to assess fibrosis in the liver of human patients with chronic viral hepatitis C [1]. In small animal experimentation, investigations on antifibrogenic substances often involve large cohorts of animals and require massive euthanasia for lack of non-invasive technique for monitoring the progression of the pathology. In this study, the potential of transient microelastography (TME) as a non-invasive technique to assess fibrosis stage in murine liver in vivo was investigated.

Statement of Contribution/Methods

Nine mice of the same genetical background (cluster of differentiation 1) with different ages (12 ± 6 months) were divided into three equal groups: Three untreated mice, three control mice, who received biweekly injections of sole excipient (paraffin oil), and finally experimental fibrosis mice that were obtained by intraperitoneal biweekly injections of tetrachloride (CCl₄) diluted in paraffin oil. After seven weeks (14 injections), the mice were measured using TME (10 MHz ultrasound transducer, 300 Hz low frequency vibration). Two weeks and four injections later, the mice were sacrificed and blood samples were collected for alanine transaminase (ALT) testing. The liver tissues were harvested, then fixed in 4% neutral-buffered formalin and embedded in paraffin for further histological analyses. After picosirius red staining, the samples were stained with haematoxylin and eosin for light microscopy quantitative evaluation of the fibrosis content.

Results

The results of elastographic measurements show that the Young's modulus is higher for experimental fibrosis mice ($E = 18.4 \pm 3.5$ kPa) than for untreated mice ($E = 6.8 \pm 2.2$ kPa) and control mice ($E = 3.6 \pm 1.2$ kPa). A correlation performed between the picosirius red staining extent and the Young's modulus gives a Spearman's coefficient equal to 0.88 (P -value < 0.01).

Discussion and Conclusions

The values of elasticity obtained from the control mice are close to those reported in literature [2,3]. However, elastographic measurements and histology results taken from these experiments are not directly comparable since the mice received four additional injections between the TME measurement and the sacrifice. Nevertheless the results suggest that transient elastography permits a clear detection of fibrosis at an early stage of seventh-week injection of CCl₄. TME could be a valuable non-invasive tool to assess the evolution and the treatment response of fibrosis in murine models *in vivo* without proceeding to euthanasia.

[1] Sandrin et al., *Ultrasound in Medicine & Biology*, 29, 1705-1713 (2003).

[2] Yin et al., *Magnetic Resonance in Medicine*, 58, 346-353 (2007).

[3] Salameh et al., *Journal of Magnetic Resonance Imaging*, 26, 956-962 (2007).

P1-H-04

Liver fibrosis staging using SuperSonic Shear Imaging technique: a clinical feasibility study on 150 patients.

eric bavu¹, jean-luc gennisson¹, Bruno-Félix Osmanski², jeremy bercoff², Mathias fink¹, vincent mallet³, Philippe Sogni³, anais vallet-pichard³, bertrand nalpas³, mickael tanter¹, stanilas pol¹; ¹Institut Langevin - Laboratoire Ondes et Acoustique, France, ²Supersonic Imaging, France, ³Hopital Cochin, France

Background, Motivation and Objective

Fibrosis staging can be assessed by a rough estimation of the liver stiffness averaged along an ultrasonic A-line. Providing a complete 2D map of liver stiffness would thus be of great clinical interest for the diagnosis of hepatic fibrosis and help prevent upcoming cirrhosis. However, such measurement requires both a quantitative value of shear elasticity and a great precision to discriminate between different fibrosis levels. Beyond the scope of non-invasive fibrosis quantification, it is also envisioned that quantitative elasticity imaging of liver will have potential interest for liver cancer diagnosis. In this work, the Supersonic Shear Imaging technique (SSI) is proposed to map the *in vivo* viscoelastic parameters of liver on patients with hepatitis C and derive a mean elasticity of liver tissues. The results are compared to biological tests (Fib4, Apri, Forns) and Fibroscan® measurements.

Statement of Contribution/Methods

The SSI technique is based on the radiation force induced by a conventional ultrasonic probe to generate a planar shear wave deep into tissues. The shear wave propagation throughout the medium is caught in real time thanks to an ultrafast ultrasound scanner (up to 5000 frames/s). Using modified sequences and post-processing, this technique is implemented on curved arrays in order to get a larger field of view of liver tissues. A study on 150 HCV patients with different fibrosis stages F has been conducted in order to investigate the accuracy of the technique (F in [0; 4]). Quantitative maps of liver elasticity are produced for each volunteer with a linear and a curved array.

Results

B-mode images of 120x75 mm² and corresponding elasticity maps are obtained using a 2.5 MHz curved ultrasonic probe with a good reproducibility and accuracy. The shear wave phase velocity dispersion is also calculated. This study shows a good correlation between the values obtained by SSI and the fibrosis levels diagnosed by biological tests (p -index < 10 -8) and allows a good differentiation of fibrosis level F (Youden's index $Y > 0.9$ for $F > 3$ and $Y >$

0.8 for $F > 2$). Results are also compared ($r^2 > 0.92$) to the Fibroscan® elasticity measurement by fitting the velocity dispersion curves obtained by SSI at 50 Hz.

Discussion and Conclusions

This real-time elasticity mapping using an ultrasonic curved probe offers better signal to noise ratio than linear arrays and a larger area in the patient's liver ($13.3 \pm 2.8 \text{ cm}^2$ estimation area). This gives more confidence on the accuracy of the diagnosis of the fibrosis stage. Furthermore, the elasticity parameters obtained with SSI give access to the shear wave group velocity and the phase velocity. As a consequence, the SSI assessment of liver stiffness could potentially give more information on the viscoelasticity properties of the liver.

P1-H-05

Quantitative Elasticity Measurements Reveal Intratumoral Changes in Response to Antiangiogenic Therapy – Preliminary Results

Kenneth Hoyt¹, Jason Warram¹, Karri Folks¹, Amanee Salaam¹; ¹University of Alabama at Birmingham, USA

Background, Motivation and Objective

Vascular endothelial growth factor (VEGF) driven tumor neovasculature is known to be hyperpermeable, which in turn raises tumor interstitial fluid pressure and compromises delivery of chemotherapeutic agents. Bevacizumab is an antibody to VEGF and has emerged as a promising treatment option for the management of breast cancer and other tumors. Such anti-angiogenic therapies inhibit the VEGF signaling pathway leading to increased intratumoral necrosis. Additionally, therapy allows normalization of the existing tumor vasculature network and reduction of tumor interstitial pressure, thereby, allowing improved delivery of chemotherapeutic drugs. The objective of this study was to measure changes in both tumor interstitial pressure and elasticity in response to bevacizumab therapy.

Statement of Contribution/Methods

Forty nude athymic mice were implanted with 1e6 2LMP breast cancer cells in left and right inguinal regions of the mammary fat pad (20 controls and 20 in therapy group). All mice were imaged daily using a bioluminescence imaging system (IVIS system, Xenogen Inc.) to detect firefly luciferase expression and monitor tumor growth. Three wks post cell implantation, the therapy mice group received a 0.1 mg i.p. injection of bevacizumab (Genentech, South San Francisco, CA). Using a custom waterbath setup, ultrasound imaging of four mice per group was performed at days 0.1, 1, and 3 with a Siemens S2000 system (Mountain View, CA) equipped with a 4V1 transducer. Repeated (N = 5) intratumoral elasticity measurements (i.e., shear wave speed) at a fixed depth of 3 cm were acquired using the Virtual Touch feature. Subsequently, tumor interstitial pressures were measured using a commercial needle-based system (Stryker, Kalamazoo, MI) prior to mouse sacrifice. Caliper measurements of all tumors were performed prior to experimentation.

Results

For each mouse, the tumor best defined by grayscale ultrasound, was selected for further analysis. All measurements were summarized as a percent difference between the therapy and control group for a given day. Regarding tumor volume and interstitial pressure, measurements from the therapy group were consistently lower. Conversely, elasticity measurements were found to be higher in the therapy group as compared to the control. Specifically, the difference in elasticity measurements was 1.8%, 7.3%, and 44.8% at days 0.1, 1, and 3, respectively.

Discussion and Conclusions

This study measured changes in both tumor interstitial pressure and elasticity in response to bevacizumab therapy. It is hypothesized that a lower interstitial pressure in the therapy group is attributed to vasculature normalization whereas the increase in tumor elasticity is due increased concentrations of extracellular matrix (collagen) in response to dispersed cellularity and necrosis.

P1-H-06

Shear viscosity measurement using vibration-controlled transient elastography

Cécile Bastard¹, Jean-Pierre Remenieras¹, Laurent Sandrin²; ¹UMRS INSERM U930 / CNRS ERL3106 / Université de Tours, Tours, France, ²Research and Development Department, Echosens, Paris, France

Background, Motivation and Objective

The viscoelastic properties of a biological tissue are correlated with its microstructure and tissue impairment is likely to modify both elasticity and viscosity. Vibration-controlled transient elastography (VCTE) has been

successfully applied to quantify stiffness in the liver of human patients with chronic viral hepatitis C [1]. However, this technique is based on the measurement of the shear wave group velocity and does not take advantage of the shear wave dispersion in the frequency domain which is related to the viscosity of the medium. Recently, several groups have reported the use of elastography based techniques (SDUV [2], MRE [3]) to measure soft tissue shear viscosity. In this work, we propose to measure shear viscosity using VCTE.

Statement of Contribution/Methods

As the aim of this study was not to propose an accurate modeling of biological tissues, the rheological model used to describe the viscoelastic behavior of tissues was a simple Voigt model. Experimentally, the central frequency of the excitation used in vibration-controlled transient elastography can be precisely tuned but the frequency content is wide-band and allows the investigation of the shear wave dispersion in the frequency domain (20-150 Hz). The displacements induced in a homogeneous viscoelastic soft medium by a transient excitation were simulated using a Green's function approach [4]. After taking into account the source geometrical diffraction, the displacement field was studied in the Fourier domain. The phase velocity as a function of frequency, the shear wave attenuation as a function of frequency and the evolution of the centroid as a function of depth were then computed.

Results

Simulations performed for shear wave velocities in the range of 1.0 to 5.0 m/s and shear viscosities in the range of 0.5 to 5.0 Pa.s show that using these three techniques, it is possible to recover the viscoelastic parameters injected in the simulation. The influence of the near field term is investigated and does not appear to be negligible.

Discussion and Conclusions

This work demonstrates the theoretical feasibility of shear viscosity measurement using VCTE. Contrary to other techniques which measure the viscoelastic properties on an axis perpendicular to the excitation direction, the near field coupling term has to be compensated in order to avoid bias on the viscosity estimation.

[1] Sandrin et al., *Ultrasound in Medicine & Biology*, 29, 1705-1713 (2003).

[2] Chen et al., *IEEE Transactions on Ultrasonics, Ferroelectrics and Frequency Control*, 56, 55-62 (2009).

[3] Asbach et al., *Magnetic Resonance in Medicine*, 60, 373-379 (2008).

[4] Bercoff et al., *IEEE Transactions on Ultrasonics, Ferroelectrics and Frequency Control*, 51, 1523-1536 (2004).

P1-H-07

Combined Vibro-acoustography (VA) Imaging and Shearwave Dispersion Ultrasonic Vibrometry (SDUV) for Measuring Prostate Viscoelastic Properties: An In Vitro Feasibility Study

Farid G. Mitri¹, M.W. Urban¹, S. Chen¹, J.F. Greenleaf¹, M. Fatemi¹; ¹*Physiology and Biomedical Engineering, Mayo Clinic, USA*

Background, Motivation and Objective

Improved methods for prostate guided-biopsy are required to effectively guide needle biopsy to the suspected site. In addition, tissue stiffness measurement would help identifying a suspected site to perform biopsy because stiffness has been shown to correlate with pathology. Shearwave Ultrasound Vibrometry (SDUV) provided evidence of adequate tissue characterization in vivo. For prostate applications, SDUV technique should be guided by an imaging modality leading to a better biopsy sampling and reduction of the sampling error. Here, we introduce a combined system of Vibro-acoustography (VA) and SDUV to perform "virtual biopsy" at a specific location, in which measurement of prostate shear elasticity and viscosity are obtained.

Statement of Contribution/Methods

VA uses two intersecting ultrasound beams with slightly different frequencies to produce a dynamic radiation force at the difference frequency. An acoustic emission field is thus produced which is detected by a hydrophone and used to form an image of the prostate. Then, a location of interest is selected and the transducer temporarily switches to SDUV mode to measure prostate elasticity and viscosity at the specified location. The SDUV uses repeated tone-bursts to capture a shear wave (SW) generated at the focus. SW propagating outwards from the vibration center is detected by a transducer operating in pulse-echo mode at two locations along the propagation path. Its propagation speed is estimated by tracking its phase change over the distance it had propagated. Its phase velocity is characterized at 8 frequencies to assess the dispersion of its wave velocity. The resulting SW velocity dispersion curve is fit with a Voigt model to solve for its elasticity and viscosity.

Results

An excised human prostate was fixed in formaldehyde for 1h and then embedded in a gel. The gel was placed in a water tank and scanned by VA at 50 kHz. A prostatic region was selected from the VA image in which propagation of a SW was performed at 9 locations corresponding to 8 measurements, 1 mm apart, at 50 Hz and its higher harmonics (100-400 Hz). The phase of the SW at 50-400 Hz was estimated from these vibration-time records by a Kalman filter. The SW phase changes linearly with propagation distance for all the frequencies (50-400 Hz). The fit with the Voigt model of the measured SW speeds gives a mean and standard deviation values for both elastic modulus 5.195 \pm 0.65 kPa and viscosity 2.53 \pm 0.26 Pa.s. Elasticity obtained with in vivo magnetic resonance elastography in the central and peripheral prostatic portion were 2.2 \pm 0.3 kPa and 3.3 \pm 0.5 kPa, respectively. The SDUV results showed higher elasticity values than found with MRE possibly because it was an excised prostate with no blood perfusion and slightly fixed with formaldehyde.

Discussion and Conclusions

This study shows the feasibility & provides substantial motivation for combining VA to guide SDUV shear elastic modulus and viscosity measurements for "virtual biopsy" of the prostate

P1-H-08

Measurement of Elastic Property of Breast Tissue for Elasticity Imaging

Takeshi Matsumura¹, Takeshi Umemoto², Yoko Fujihara¹, Ei Ueno², Tsuyoshi Shiina³, Tsuyoshi Mitake¹:¹Ultrasound Systems Division, Hitachi Medical Corporation, Japan, ²Department of Breast Surgery, Tsukuba Medical Center Hospital, Japan, ³Graduate School of Medicine, Kyoto University, Japan

Background, Motivation and Objective

It is necessary to investigate detailed elastic property of human tissue as a foundation for developing objective and quantitative elasticity imaging (elastography). Since soft tissue has significant non-linear elasticity which causes the change of stiffness depending on compression magnitude, Young's modulus of tissue was conventionally described as E(ϵ) with reference to strain ϵ [1]. However, Young's modulus of tissue E(σ) with indicator of stress σ is more useful to study the contrast with elastography because our static-based elastography [2] visualizes the differences of tissue strain that is obtained under relatively-uniform stress field. Thus, we try to build a tissue elasticity database that is discriminated by stress range in order to discuss future elastography for differential diagnosis.

Statement of Contribution/Methods

As samples, 5mm slices including lesion and its surrounding breast tissues are obtained after surgical resection. Our measurement system consists of materials testing machine (INSTRON 3342) and 10N load cell with ϕ 3 [mm] cylindrical indenter. Young's modulus is analyzed using the measured stress-strain curve up to the stress of 1.2 [kPa] (estimated maximum stress at practical breast exam).

Results

Measured Young's moduli of tissues are shown in Table 1.

Discussion and Conclusions

- (1) Fat and gland showed similar stress-strain curves with much larger non-linearity than diseased tissues.
- (2) IDC (invasive ductal carcinoma) and mucinous carcinoma exhibited significantly larger Young's moduli than normal tissues (fat or gland), the elasticity of IDC varied over a wide range, though.
- (3) Although DCIS (ductal carcinoma in situ) revealed larger stiffness than normal tissues under a slight stress, the magnitude relation between them changed around the stress of 1 [kPa]. In fact, it is sometimes observed that DCIS cannot be easily detected (i.e. false negative) at excessive breast compression in clinical exam on elastography, the background of which seems to be confirmed by the above result.

In addition, we will describe in this paper our approach to quantitative elastography which is being studied with a view toward the consistency with the stiffness of resected tissues.

[1]T. A. Krouskop, et al. Ultrasonic Imaging 20(1998) 260-74

[2]T. Matsumura, et al. Proc. of IEEE Ultrasonics Symp. (2004) 1484-1487

Monday
Poster

Table 1: Young's modulus of breast tissue (mean \pm standard deviation [kPa])

histological type	N (samples)	stress σ [kPa]					
		0.0-0.2	0.2-0.4	0.4-0.6	0.6-0.8	0.8-1.0	1.0-1.2
normal fat	28	0.7 \pm 0.2	2.4 \pm 0.6	5.2 \pm 1.3	8.3 \pm 2.2	12.3 \pm 3.7	17.1 \pm 4.6
normal gland	22	0.8 \pm 0.2	2.3 \pm 0.6	5.1 \pm 1.3	8.3 \pm 2.0	12.0 \pm 2.9	15.7 \pm 4.0
DCIS	3	3.0 \pm 1.6	4.5 \pm 1.2	7.0 \pm 1.4	9.8 \pm 1.7	12.5 \pm 2.2	15.3 \pm 2.6
mucinous carcinoma	2	9.2 \pm 1.7	11.7 \pm 0.7	13.0 \pm 0.4	14.9 \pm 1.0	16.7 \pm 1.4	18.9 \pm 2.3
IDC	17	11.8 \pm 8.7	13.7 \pm 7.6	16.6 \pm 7.8	19.7 \pm 8.5	23.3 \pm 8.9	27.3 \pm 9.5

P1-H-09**Ultrasound-based tool for vibration-controlled transient elastography real-time assistance: automatic liver localization and skin capsule distance measurement.**

Stéphane Audière¹, Yassine Mofid², Maurice Charbit¹, Elsa Angelini¹, Véronique Miette², Laurent Sandrin², ¹ENST, CNRS LTCI, UMR 5141, PARIS, France, ²Research and Development department, Echosens, PARIS, France

Background, Motivation and Objective

Vibration-controlled transient elastography (VCTE) based Fibroscan® device (Echosens, Paris, France) is used to assess non-invasively liver stiffness which is correlated to hepatic fibrosis.

Three probes can be used with the Fibroscan®: an S probe for children, an M probe for adults, and a new XL probe for obese patients. The probe is chosen according to the skin-capsule distance (SCD): for example, the XL probe is used for SDC > 25mm.

Today, Fibroscan® operators should pass training to conduct successful examinations. The liver is localized visually via TM and A-scan modes and the SCD is measured manually with an ultrasound scanner. Furthermore, use of an ultrasound scanner is recommended to localize easily the liver in obese patients and find the optimal measurement window.

To facilitate the examination and to get rid of the ultrasound scanner assistance, we propose to integrate new indicators in the device for an automatic liver localization and SCD measurement.

In this study, we aim to demonstrate the potential of the new indicators in helping operators to localize the liver and to measure automatically the SCD.

Statement of Contribution/Methods

The automatic localization of the liver is based on combining spatial and temporal information of the real-time 1D ultrasound acquisitions. A texture analysis was applied on the A-scan signal to detect the ultrasound signature of liver. Furthermore, RF signal modification due to patient breathing for a specific PRF was investigated to improve the localization robustness.

The breathing impact is also used to estimate the SCD for the appropriate PRF. Actually, RF signals are decorrelated inside the liver and highly correlated in the zone between the skin and the liver capsule.

In this study, algorithms were tested according the following protocol. Fibroscan® probe was placed in different locations: in front of the liver and around. The SCD was calculated only when the liver was detected and all results were verified using an ultrasound scanner investigation in the same zones.

Results

Preliminary results obtained in a pilot clinical study including a large population demonstrated a good performance of real-time liver localization in all cases. SCD estimation was close to the SCD assessed manually with the ultrasound scanner. An error of 2 mm was found due to the liver movement with breathing.

Discussion and Conclusions

This study reveals encouraging results to improve the Fibroscan® procedure with an assistance tool for automatic liver localization and SCD measurement. Furthermore, using these indicators will eventually improve the examination success rate with appropriate probe and reduce the examination time. These algorithms are currently validated in a clinical study.

Nonlinear Mechanical Behavior of Cervical Tissue with Increasing Pre-compression

Tomy Varghese¹, Ryan DeWalt², Maritza Hobson¹, Mark Kliewer³, Josephine Harter⁴, Ellen Hartenbach⁵;
¹*Department of Medical Physics, University of Wisconsin, USA,* ²*Department of Biomedical Engineering, University of Wisconsin, USA,* ³*Department of Radiology, University of Wisconsin, USA,* ⁴*Department of Pathology, University of Wisconsin, USA,* ⁵*Department of Obstetrics & Gynecology, University of Wisconsin, USA*

Background, Motivation and Objective

Tissue mechanical properties may determine tissue function. This is particularly notable in the cervix, where its mechanical properties influence the outcome of pregnancy. The cervix is easily imaged with ultrasound, and its cost and portability make elastography a good candidate to use as a clinical diagnostic tool to evaluate cervical function. However, before elastography can be used clinically, the mechanical properties of cervical tissue must be characterized. In this study, we performed dynamic testing on normal human cervix tissue at several different levels of pre-compression in order to characterize its nonlinear mechanical behavior.

Statement of Contribution/Methods

Cervical specimens were obtained from the UW Hospital Pathology Lab (n = 10) from the uteri of patients who underwent a hysterectomy. Patient consent was obtained for the mechanical testing of the excised tissue samples. Samples were approximately one cubic centimeter and stored in saline solution. Samples were dynamically tested at 1 Hz using an EnduraTEC ELF 3220 for six different pre-compression ranges (one to six percent) and three different compression amplitudes (two to four percent). This study was approved by the University of Wisconsin Institutional Review Board.

Results

Our results show an increase in the measured storage modulus with increasing pre-compression. When the results were normalized to the storage modulus at 1% pre-compression, the storage modulus at 6% pre-compression was approximately 1.4 times larger. Dynamic amplitude had little effect on the storage modulus measured at each level of pre-compression. We saw no changes in tan delta with increasing pre-compression.

Discussion and Conclusions

These results show the nonlinear elastic behavior of cervix tissue with increasing pre-compression and are consistent with previous studies. Tan delta was unchanged, suggesting that pre-compression had little effect on damping. In order for ultrasound elastography to be an effective tool to determine cervical function, the initial pre-compression must be considered when measuring the elastic modulus of the cervix.

P1-I. Acoustic Imaging

Sala Orange

Monday, September 21, 2009, 10:00 am - 11:30 am

Chair: **Jafar Saniie**
Illinois Institute of Technology

P1-I-01

Determination of Sound Velocity Distribution Using Sectional Near-field Acoustical Holography and Simulated Annealing

Takeishi Ohbuchi^{1,2}, **Tadashi Ebihara**^{1,2}, **Koichi Mizutani**¹, **Naoto Wakatsuki**¹, **Hiroyuki Masuyama**^{3,1} *Graduate School of Systems and Information Engineering, University of Tsukuba, Tsukuba, Japan,* ²*Research Fellow of the Japan Society for the Promotion of Science, Japan,* ³*Electronic Mechanical Engineering Department, Toba National College of Maritime Technology, Toba, Japan*

Background, Motivation and Objective

Currently, an ultrasonic tomography is mainly used for reconstructing of sound velocity distribution, which is used for measurement of temperature for example. However, ultrasonic tomography requires a lot of measuring points and a strictly known sound source. In this study, we propose a method for determining sound velocity distribution based on optimization.

Statement of Contribution/Methods

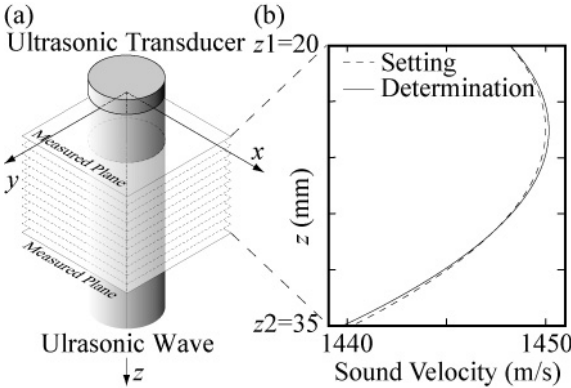
The coordinate system is shown in Fig. 1(a), and the sound velocity is assumed to only vary in the direction of z -axis. Firstly, the two-dimensional sound field at $z = z_2$ is calculated from the sound field measured at $z = z_1$ using sectional near-field acoustical holography (SNAH) in which unknown sound sources are permissible. SNAH is our proposed method; the space sandwiched between planes at z_1 and z_2 is partitioned into many parts as shown in Fig. 1(a) so that sound velocity in each part becomes approximately constant. SNAH was validated using finite element method. Secondly, the sound velocity distribution is determined using an optimization. Only sound fields at z_1 and z_2 are measured, and we set initial sound velocity distribution. The sound field at z_2 is calculated from the sound field measured at z_1 using SNAH. Then, the sound velocity distribution is optimized to minimize difference between real part of measured and calculated sound fields at z_2 . We use simulated annealing (SA) for optimization to avoid local solutions.

Results

We validated this proposed method by a simulation. In the simulation, the diameter of transducer was 6.0 mm, and ultrasonic wave was radiated into water at frequency of 1.0 MHz. In Fig. 1(b), dashed line shows the given sound velocity corresponding to water temperature. Then, two-dimensional sound fields were calculated in a region of 20×20 mm² at $z_1 = 20$ and $z_2 = 35$ mm. The space sandwiched between planes at z_1 and z_2 was partitioned into 400 parts. Sound velocities at $z = 20, 25, 30,$ and 35 (mm) were used for optimization, and the sound velocity distribution was interpolated with spline function for using SNAH. The sound velocity distribution determined using SA is shown by solid line in Fig. 1(b).

Discussion and Conclusions

The determination result well agreed with the given value, and validity of our proposed method could be established. Our technique is expected to be applicable to determine three-dimensional sound velocity with scanning transducer or transducer array.



P1-I-02

Study on the shallow underground imaging by the pulse compression method that considered frequency dependent attenuation

Tsuneyoshi Sugimoto¹, Hiraku Kawasaki²,¹Electronics and Information Engineering, Toin University of Yokohama, Yokohama, Japan, ²Inspection Technology dept., Inspection Division, IHI Inspection & Instrumentation Co., Ltd., Yokohama, Japan

Background, Motivation and Objective

The resolution improvement of shallow underground imaging using super-magnetstriction vibrator and pulse compression method has been studied.

Although the validity of the pulse compression method for resolution improvement of underground image has been confirmed, the effect of frequency dependent attenuation of chirp wave was not considered.

Statement of Contribution/Methods

Frequency dependent attenuation of chirp wave in shallow underground is measured at each frequencies and half width (axial resolution) is calculated by simulation using measurement data.

And an exploration experiment is carried out to confirm the effect of the compensation of high frequency domain(600-800Hz).

Linear up chirp wave, log up chirp wave and log down chirp wave are used for comparison with the linear down chirp wave and long duration time (200ms) is used for comparison with short duration time (100ms).

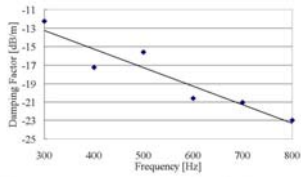
Results

From the simulation results, half width are smaller than 0.2m are obtained when Δf is more than 500Hz (800-300Hz linear down chirp, duration time 100ms).

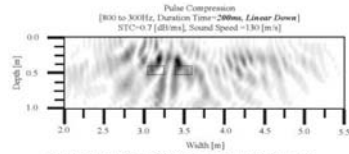
From the experimental results, compensation of high frequency domain and long duration time are effective for high resolution underground image. And linear down chirp showed the best underground image in this case.

Discussion and Conclusions

We confirmed the validity of the compensation of high frequency domain and long duration time for pulse compression image. However, the deeper a target is buried, the more difficult making underground images by using a pulse compression technique because a high frequency domain of chirp waves has strong attenuation. Therefore, examinations at increased duration in chirp waves and examinations with changing the pulse compression method according to the propagation distance will be expected to keep the best resolution at each depth.



Frequency dependent attenuation of chirp wave



An Example of Underground Image

The boundary rectangles in the images shows the buried positions. The buried objects are hollow plastic containers (about 13x12x5cm). They are buried about 20cm apart by a horizontal direction.

P1-I-03

An improved method for tomographic density imaging using a multiple frequency inverse scattering approach

Roberto Lavarello¹, Michael Oelze¹:¹University of Illinois at Urbana-Champaign, USA

Background, Motivation and Objective

Inverse scattering is one of the most robust acoustic tomography methods, allowing for the reconstruction of quantitative images of acoustic parameters. Most acoustic tomography methods neglect density variations in order to obtain speed of sound and attenuation profiles. However, density may also contain useful information or provide additional sources of image contrast. Current inverse scattering methods for density imaging have limitations that keep them from practical experimental implementations. Therefore, improved algorithms need to be developed and assessed in order to obtain density tomograms.

Statement of Contribution/Methods

In this work an improved approach, termed the multiple frequency distorted Born iterative method (MF-DBIM) algorithm, was developed for imaging density variations. The MF-DBIM approach consists of inverting the wave equation by solving for a single functional that depends on both sound speed and density variations at multiple frequencies. Density information was isolated by using a linear combination of the reconstructed single-frequency profiles. These profiles were obtained using frequency hopping in order to improve the correlation among the reconstructions at different frequencies. The results were compared to reconstructions using methods currently available in the literature, i.e., the dual frequency DBIM (DF-DBIM) and T-matrix methods.

Results

The performance of the MF-DBIM was initially assessed by reconstructing cylindrical targets of different radii, speed of sound and density contrasts. The MF-DBIM required the use of frequency hopping in order to converge to a proper solution. Useful density reconstructions, i.e., root mean square errors (RMSEs) less than 30%, were obtained even with 5% Gaussian noise in the simulated data and using frequency ranges spanning less than an order of magnitude. Therefore, the MF-DBIM approach largely outperformed both the DF-DBIM method (which had problems converging with noise even an order of magnitude smaller) and the T-matrix method (which required a ka factor close to unity in order to achieve convergence). The MF-DBIM performance degraded severely (RMSEs larger than 50%) when the angular coverage on reception was less than 180 degrees. Although the MF-DBIM performance also degraded as the frequency jump magnitude increased, the RMSEs were not largely affected when the frequency jump was smaller than 5% of the maximum frequency used for the reconstructions.

Discussion and Conclusions

In summary, the MF-DBIM approach outperformed currently available density imaging methods and required SNR levels and bandwidth ranges that are obtainable using current ultrasonic tomography scanner technology. However, the effects of non-random measurement errors (i.e., instrument calibration errors) should be taken into account for a practical, robust experimental implementation of the technique. This work was supported in part by a grant from the 3M corporation.

P1-I-04

Laser ultrasonic investigation of laminate disbonding

Alexandr Karabutov (Jr.)¹, Alexandr Karabutov², Oleg Sapozhnikov¹; ¹Physics, Moscow State University, Moscow, Russian Federation, ²International Laser Center, Moscow State University, Moscow, Russian Federation

Background, Motivation and Objective

Background, Motivation and Objective: Laminated parts are widely used in industry. They consist of thin sheets of metal or plastic glued together. Nondestructive testing (NDT) of such layered structures is of great importance because any disbonding or polymerization failures can significantly impact their service capabilities. While ultrasonic testing of laminated structures seems to be the most reliable approach, it demands the use of high-frequency ultrasound to probe laminates with thin layers. For a given frequency band, Contact Laser-Ultrasonic Evaluation (CLUE) provides significantly higher spatial resolution in comparison with traditional piezoelectric ultrasound. Consequently, exploration of the utility of CLUE for NDT of laminated structures is a topic of interest.

Statement of Contribution/Methods

In CLUE, laser pulse absorption produces a short ultrasonic pulse that propagates into the test structure and the backscattered signal is then detected by an ultra-broadband piezoelectric receiver. A laser-ultrasonic defectoscope with a probing-pulse duration shorter than 100 ns was designed and used to study laminated structures. To complement the experimental testing, finite differences were used to numerically model aspects of the technique, including optoacoustic generation as well as pressure pulse propagation in both the laminate and the contacting medium between the laminate and the optoacoustic source.

Results

Samples consisting of two or three aluminum sheets glued together with polymer layers were tested with CLUE over a frequency range from 0.1 to 6 MHz. Results of reflection-coefficient measurements agreed well with predictions from numerical simulations. Both bonded and disbonded regions were clearly distinguishable in the CLUE signals.

Discussion and Conclusions

The experimental investigation shows that CLUE can detect disbonded regions and locate their positions. The technique is simple and effective, enabling testing to proceed quickly and efficiently. The depth resolution of CLUE is determined by the probing pulse duration. The 70 ns probing pulse used here allowed a depth resolution several times higher than that for a conventional piezoelectric defectoscope with the same center frequency. In addition, CLUE provides a better capability for distinguishing the rigidity of boundaries from which signals are reflected. This capability can be very useful for the investigation of disbonding in laminate structures. Work supported by RFBR 08-02-00368 and ISTC 3691.

P1-I-05

Experimental evaluation of the moving linear array technique applied to livescan palmprinting

Antonio Iula¹, Michele De Santis¹, Giosuè Caliano², Massimo Pappalardo²; ¹D.I.F.A., University of Basilicata, Potenza, Italy, ²University Roma Tre, Italy

Background, Motivation and Objective

Biometrics can be defined as the use of physiological or behavioural characteristics to recognise or verify the claimed identity of an individual. The demand for security access control systems based on personal identification is strongly increasing and growing in many important applications. Fingerprints, Iris, Voice, Face and Palmprints are the different physiological characteristics used for identifying an individual.

Palmprint recognition systems have been developed for civilian (mainly access control) applications. These systems typically utilize low resolution (< 100 dpi) images and support full-to-full palmprint matching. Principal lines and wrinkles can be extracted from low-resolution images playing an important role in palmprint identification.

There are several different methods of capturing the initial palmprint image, the most common techniques being: optical, capacitive, thermal and ultrasonic.

Ultrasonounds have some intrinsic advantages with respect to other methods; in fact they are not sensitive to the surface contaminations, such as stain, dirt, oil, or skin wornness and they provide information not only of the skin surface but also of the under skin region.

The main explored ultrasonic technique for livescan palmprint (and fingerprint) consists in a XY mechanical scan of the palm: a high frequency (high resolution) A-Scan ultrasonic transducer scans each dots of the XY area and stores in the memory all the reflected acoustic signals from each dot. The result is a 3D image of the entire under skin volume.

Statement of Contribution/Methods

The scanning acquisition time can be reduced using an ultrasonic linear array transducer that moves in the direction perpendicular to the electronic scanning plane. This approach seems to be very promising in the next future, when high frequency (30 Mhz and up) ultrasonic linear array transducers, based on the emerging technologies like eMUT, will provide the adequate resolution and could be extended to fingerprints as well.

In the present work a first experimental evaluation of this coming up technique is carried out by using a commercial echographic machine (Esaote Technos) and of a 12 MHz 192 elements ultrasound linear array (LA523E).

The probe was tied to a motorized sledge moving along the X direction with steps of 500 im each. For each step, the B-scan image (YZ) was acquired and stored. The resulting 3D matrix was successively elaborated in MatLab environment to provide the palm C-scan at different depth inside the skin. In order to maximize the image resolution, palm skin was flattened and opportunely spaced from the probe by an acoustically transparent plate.

Results

Several experiments are carried out in different region of the palm and contaminating the surface with various polluting substances.

Discussion and Conclusions

Palmprint images obtained at different skin depths clearly show features like principal lines and wrinkles of the hand palm, demonstrating the validity of the proposed technique.

P1-I-06

Non-destructive evaluation of the 18th century ship wreck Vrouw Maria

Ari Salmi¹, Kari Steffen², Joonas Eskelinen¹, Marko Peura¹, Leone Montonen², Edward Haeggström¹:¹Department of Physics, Division of Materials Physics, University of Helsinki, Helsinki, Finland, ²Department of Applied Chemistry and Microbiology, University of Helsinki, Helsinki, Finland

Background, Motivation and Objective

Evaluating the condition of cultural heritage lying on the bottom of oceans around the world is essential for archaeologists. The decisions on whether to lift objects or to leave them in situ require knowledge of both their current and estimated future condition. We analyze the current condition of pine and oak samples recovered from a sunken, 240 years old Dutch merchant ship wreck 'Vrouw Maria' with ultrasound and other non-destructive methods.

Statement of Contribution/Methods

To evaluate the physical condition, i.e. mechanical properties, ultrasonic through-transmission sound velocity measurements at 300 kHz to 4 MHz were performed in both radial and longitudinal wood fiber directions. Presence of large discrepancies (e.g. holes created by ship worms) within the samples were probed using 2 MHz ultrasonic pulse-echo measurements. DNA-analysis was used to determine the presence of microbes, particularly fungi, in the samples. In addition, X-ray diffraction and X-ray fluorescence measurements were performed at the ESRF synchrotron facility, Grenoble, to determine both the extent of degradation at the nanometer-level in the wood cell walls and changes in the elemental composition of the samples.

Results

The ultrasonic measurements detected a layered structure in the pine sample with a thin (1-4 mm) mechanically degraded layer on top of almost intact wood (up to 60 % decay in the stiffness modulus compared to intact wood). For the oak sample, a 50% stiffness modulus reduction was detected compared to a freshly felled reference sample. DNA-analysis detected the presence of soft-rot fungi in the degraded layer and even deeper into the underlying compact wood (2 cm depth). Fungal DNA was more abundant below the heavily degraded layer indicating that fungal degradation has already moved deeper towards non-degraded parts. Differences in both the x-ray diffraction patterns and the x-ray fluorescence spectra were observed within the samples.

Discussion and Conclusions

The degraded layer in the pine sample provided insight about the temporal progression of the degradation process attacking wooden samples on the ocean bottom. The general mechanical condition of the samples was found to be fair, e.g. the modulus degradation was under 50%. Heavy degradation could be attributed to ascomycetous soft-rot fungi. The differences in both the x-ray diffraction patterns and the x-ray fluorescence spectra between the surface layer and core of the samples indicate changes of varying extent in the cell wall structure and in the elemental composition. Combining these methods offered a novel perspective into archaeological wood degradation.

P1-J. Guided Waves and Microscopy

Sala Orange

Monday, September 21, 2009, 10:00 am - 11:30 am

Chair: **Larry Kessler**
Sonoscan

P1-J-01

An Efficient Formulation for Harmonic Waves in Multilayered Cylindrical Structures

Ergun Simsek¹, **Bikash K. Sinha**²; ¹Electrical Engineering, Bahcesehir University, Besiktas, Istanbul, Turkey, ²Math and Modeling, Schlumberger-Doll Research, Cambridge, MA, USA

Background, Motivation and Objective

Sonic techniques in geophysical prospecting involve elastic wave velocity measurements that are performed by placing acoustic transmitters and receivers in a fluid-filled borehole. However, the acoustic transmitter and receivers are mounted on a logging tool that can be simulated in terms of a cylindrical column of heavy fluid with calibrated elastic moduli and mass density to account for its influence on recorded waveforms at an array of receivers. In addition, an oil and gas producing wellbore consists of a steel pipe cemented to the formation. Analyses of sonic waveforms in such multilayered structures require an efficient formulation for harmonic wave propagation that form a basis for the inversion of sonic data for formation elastic properties.

Statement of Contribution/Methods

Equations of motion for harmonic waves in multilayered cylindrical structures are given in a compact form. This compact form helps us to efficiently form a boundary condition matrix of any N-layer structure based on material parameters of all cylindrical layers. Fluid-fluid, fluid-solid, and solid-fluid boundaries are supported. The search algorithm automatically searches for zeros of a boundary-condition determinant that yields the borehole velocity dispersion for a given frequency band. We describe how to obtain radial displacements and stress amplitudes for a chosen frequency that can be useful in estimating frequency dependent radial depth of investigation for the borehole Stoneley, flexural, and quadrupole modes in the presence of a casing and tool effects on sonic data.

Results

We present an efficient way of writing equations of motion for harmonic waves in multilayered cylindrical structures. This compact form enables us to obtain modal dispersions, radial displacement and stress amplitudes in a systematic way. The accuracy of the algorithm has been validated by comparing results from a general 3D-Green's function method.

Discussion and Conclusions

This study helps in the analysis and interpretation of sonic response in open as well as cased holes in the presence of near-wellbore alteration and tool effects. Estimates of far-field formation elastic moduli in such cylindrical structures are used to identify formation lithology in terms of the compressional to shear velocity ratio which is related to the Poisson's ratio of the material. Plots of compressional to shear velocity ratio against compressional transit time help identify intervals containing limestone, dolomite, salt and quartz. Recent applications of elastic moduli of rocks in a reasonably uniform lithology are in the estimation of fluid mobility in porous rocks; formation stresses; and fracture characterization.

Piezoelectric composite film for acoustic emission detection

Walter Sakamoto¹, Ricardo Tokio Higuti², Marcelo Moreira Tiago²:¹Physics and Chemistry, University of São Paulo State - UNESP, Ilha Solteira, São Paulo, Brazil, ²Electrical Engineering, University of São Paulo State - UNESP, Ilha Solteira, São Paulo, Brazil

Background, Motivation and Objective

The continuous technological advances have required materials with properties that conventional material cannot display. Material property combinations are being the focus to the development of composite materials, which are considered a multiphase material that exhibits properties of the constituent phases. One interesting material to be studied as sensing material is the composite made of ferroelectric ceramic and polymeric matrix as a two phases composite material. In that case the combinations properties intended are the high piezo and pyroelectric activities of the dense ceramic with the impact resistant, flexibility, formability and low densities of the polymer.

Statement of Contribution/Methods

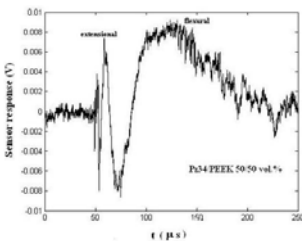
The composite studied here is made of a modified lead titanate (Pz34) ceramic and polyether-ether-ketone (PEEK) high performance polymer matrix. Using the piezoelectric property of the composite film it was used to detect acoustic emission (AE), which is a transient elastic wave generated by sudden deformation taken place in materials under stress. AE can be applied for evaluating the "health" of structures in a non-destructive way. The composite film was surface mounted on an aluminum panel and ball bearing drop and pencil lead break were used as simulating AE sources.

Results

Pz34/PEEK sensors were surface-mounted on an aluminum panel. The panel was excited using two different simulated AE sources: ball bearing drop, and pencil lead break (Pentel 2H), the so-called Hsu-Nielson source. The acoustic impedance of the sensor 50/50 vol.% is 9.0(Pas/m³) calculated using the longitudinal wave velocity of the composite films measured using the ultrasonic immersion technique.

Discussion and Conclusions

Figure 1 shows the time response of the Pz34/PEEK sensor to the lead break test. The pencil was broken on panel surface ate about 6 cm from the sensor and the signals were recorded directly by a digital storage oscilloscope (Tektronix TDS 2022) without amplification. Clearly it can be seen both plate waves modes: extensional around 55 ms and the flexural at 120 ms. The sensor composition used for this test was 50 vol.% of ceramic. It can be seen from the lead break test both modes of waves propagation (extensional and flexural) could be clearly observed without any amplification. The preliminary result indicates that the composite Pz34/PEEK can be used for non-destructive evaluation.



P1-J-03

Efficient mode conversion transducers for use in ultrasonic flow meters

Shrinivas Joshi¹, Boris Zaitsev², Iren Kuznetsova^{2,1} *Marquette University, USA, ²Institute of Radio Engineering and Electronics, Saratov, Russian Federation*

Background, Motivation and Objective

This paper is concerned with the development of miniature, high efficiency transducers for use in ultrasonic flow meters. In the transmission type of ultrasonic flow meter, two transducers are placed on opposite walls of a pipe through which the fluid is flowing. By measuring the time taken by the acoustic wave to travel from one transducer to the other, one can determine the fluid velocity and other relevant flow parameters [1]. One of the problems of currently available transducers is that they are generally large in size and protrude a considerable distance inward from the pipe wall and into the path of the flowing fluid. This causes several problems such as disturbance of flow stream resulting in erroneous flow data, fouling of transducer due to accumulation of rags, debris, etc.

Statement of Contribution/Methods

We show that a flat, planar transducer that has minimal protrusion into the pipe can be realized based on conversion of plate acoustic waves (PAWs) to bulk acoustic waves (BAWs). The transducer is essentially a thin plate of a suitable piezoelectric material on which interdigital transducers (IDTs) are fabricated to generate and detect plate acoustic waves. With proper design very efficient conversion of energy from plate waves in the piezoelectric material to bulk waves in the fluid (and vice versa) can be achieved. Prior work has used this mode conversion principle for converting energy from surface acoustic waves (SAWs) to bulk acoustic waves [2, 3]. The use of plate waves has several advantages. Since the energy of plate waves is present on both plate surfaces, the IDT can be on the surface opposite from that which is in contact with the fluid. This protects the IDT from possible damage due to the fluid and also simplifies the job of making electrical connections to the IDT. Another advantage is that one has a much wider choice of substrate materials with plate waves than is the case with SAWs.

Results

Our initial experiments have employed the fundamental anti symmetric plate wave mode (A0 mode) propagating in a Y-X lithium niobate substrate. The device fabricated on a 0.5 mm thick plate had a fundamental resonant frequency of 1.38 MHz. Total mode conversion loss (PAW to BAW and back from BAW to PAW) of less than 2.5 dB has been obtained.

Discussion and Conclusions

This paper shows that coupling between plate acoustic waves and bulk acoustic waves can be gainfully employed to realize miniature, high efficiency, wide bandwidth transducers for generating and detecting ultrasonic waves in fluids. Details of the theoretical analysis used, experimental results obtained, and potential applications will be presented.

1. L. C. Lynnworth, "Ultrasonic Measurements for Process Control," Academic Press, 1989.
2. S. G. Joshi, B. D. Zaitsev, and I. E. Kuznetsova, Proc. IEEE Ultrason. Symp., pp. 1286 – 1289, 2004.
3. S. G. Joshi, B. D. Zaitsev, and I. E. Kuznetsova, J. Appl. Phys. 105, 034501 (2009).

P1-J-04

Visualization of Sound Propagation in Solids Using Electrodynamic Probes

Uwe Völz¹, Marc Kreutzbruck¹, Heinz Mrasek¹, Klaus Matthies¹; ¹*Federal Institute for Materials Research and Testing, Germany*

Background, Motivation and Objective

When dealing in ultrasonic testing with inhomogeneous material structure such as diverse types of welds made from austenitic steel or nickel based alloys, which are currently used for modern power plants concepts, data interpretation is quite difficult. For better understanding of the complex interaction between the sound field and the component under test, the visualisation of sound propagation in solids is a substantial task to diminish the detection uncertainty of relevant defects.

Statement of Contribution/Methods

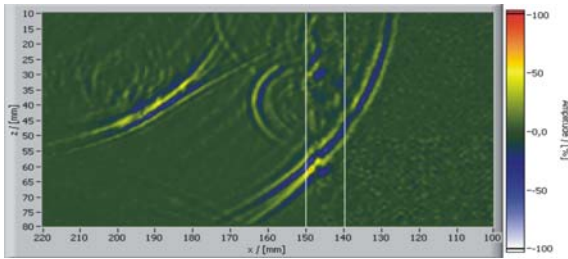
However, there exist only a small number of appropriate techniques published today, such as scanning laser interferometer, piezoelectric and optical approaches in case of transparent solids. In this work we present an electrodynamic technique providing a simple use and a high signal to noise ratio. By detecting the grazing beam with an electrodynamic probe with a size smaller than 10 mm, we measured the particle displacement as a function of time with a spatial resolution in the order of 2 mm. Adapting the electrodynamic probe and its coil alignment allows for measuring the displacement components in all three dimensions. This comprises the detection of the horizontal and vertical particle displacement with respect to the surface and thus also the transformation from longitudinal waves into transversal waves and vice versa is possible.

Results

A SNR of higher than 36 dB could be achieved within ferromagnetic and high conductive chrome steel when using a transversal wave generated by an angled beam transducer. We report on measurements of the sound field in complex weld joints. One example shows a 10 mm thick narrow gap weld joining a nickel alloy with a chrome steel with a thickness of 80 mm yielding a substantial anisotropy of the weld structure. The test system enables us to visualize the wave propagation within the weld and indicates the reflection scenario and the energy losses due to both the anisotropic structure and material defects (see figure below).

Discussion and Conclusions

The findings show that the electromagnetic approach substantially provides both a high signal-to-noise ratio and the simultaneously detection of longitudinal and transversal waves. Therefore the system can visualize wave conversion and offers a deeper insight into the interaction of the sound field with the anisotropic weld region.



P1-J-05

Guided Waves Based Approach for the Reconstruction of the Elastic Moduli of Plates

Michele Sale¹, Piervincenzo Rizzo², Alessandro Marzani^{3,1} Saipem S.p.A., Italy, ²Civil and Environmental Engineering, University of Pittsburgh, Pittsburgh, Pennsylvania, USA, ³University of Bologna, Italy

Background, Motivation and Objective

Guided ultrasonic waves (GUWs) provide a highly efficient method for the non-destructive evaluation and the structural health monitoring of waveguides. GUWs are also particular attractive to all those applications devoted to the characterization of material elastic properties for either isotropic or orthotropic materials. Typically oblique-incidence bulk waves, guided waves or leaky guided waves can be used. This paper describes an inverse technique based on simplex method to determine the elastic constants of isotropic plates. The inverse procedure minimizes the discrepancy between semi-analytical dispersion curves and experimental dispersion curves. Particularly the study focuses on the group velocity of the lower order symmetric and antisymmetric Lamb waves propagating along the plate.

Statement of Contribution/Methods

A pulsed laser and piezoelectric transducers were used respectively to generate and detect Lamb waves in an aluminium plate. Time waveforms were processed using the continuous wavelet transform to extract the time-frequency characteristics of the signals and to obtain the group velocity curve. The experimental data were compared to the theoretical predictions obtained by using a semi-analytical finite element (SAFE) algorithm. The algorithm computes the waveguide dispersion curves solving the dispersive wave equation by using standard routines for eigenvalue problems. The inverse procedure iteratively updates the plate elastic properties in the SAFE

Monday
Poster

formulation in order to minimize the discrepancy with the experimental group velocity curves. The iteration is terminated when a designed optimization function is satisfied.

Results

The inverse scheme has been demonstrated on a 2.54 mm-thick aluminum plate. Two wave propagation scenarios were studied experimentally by exciting the antisymmetric mode only and by exciting simultaneously both the symmetric and the antisymmetric modes. It was found that the inversion scheme is able to determine the properties of the aluminum by monitoring the S0 mode, the A0 mode and both modes, in the frequency range comprised between 100 kHz and 650 kHz. Better results in terms of residual error are found by monitoring both modes simultaneously.

Discussion and Conclusions

This work shows a study where a SAFE algorithm was for the first time coupled to an inverse scheme procedure to determine the elastic constant of a given material. As the SAFE modelling has been demonstrated suitable to predict the dispersive behaviour of guided waves propagating in waveguides of arbitrary cross-section, the inverse scheme proposed is general and effective to reconstruct the elastic properties of structural waveguides of complex geometry. In addition by extending the minimization of the error function to two modes simultaneously, the effectiveness of the inverse approach is achieved.

P1-J-06

High frequency guided waves in a 7 wire strand: Warped Frequency Transform for spectro-temporal characterization

Alessandro Marzani¹, Luca De Marchi², **Piervincenzo Rizzo**³, Nicolò Speciale^{2,1} *DISTART, University of Bologna, Bologna, Italy.* ²DEIS, University of Bologna, Bologna, Italy, ³Dept. of Civil & Environmental Engineering, University of Pittsburgh, Pittsburgh, USA

Background, Motivation and Objective

Methods based on guided ultrasonic waves are gaining increasing attention for the non-destructive inspection and condition monitoring of multi-wire strands used in civil structures such as prestressing tendons and cable-stay bridges. In these applications, the knowledge of the dispersive spectro-temporal structure of the propagating guided waves is required. Unfortunately, the dispersive pattern of the guided waves in multi-wire strands is not easily detectable. The main reasons are related to the complex cross-section geometry of the cable, and to the inter-wire contact force that takes place when the cable is loaded. In this work, we proposed a new signal processing tool aimed at the extraction of the guided waves' characteristics from experimentally recorded time-transient measurements.

Statement of Contribution/Methods

A pulsed laser and an interferometer are used to generate and detect broad-band guided waves signals propagating in the structure. These signals have characteristic time-frequency representations (TFRs). Unfortunately, any TFR is subject to the time-frequency uncertainty principle. This limitation prevents the capability of distinguishing multiple, closely spaced Lamb modes with spectrograms or scalograms. To this aim, we implemented a new Warped Frequency Transform (WFT) which allows for a more effective tiling of the time-frequency domain. Such tiling can be chosen to match the spectro-temporal structures of the different propagating modes by selecting an appropriate warping map to reshape the frequency axis. The described transformation is fast and invertible.

Results

An application to propagating guided waves (GWs) in a 7 wire strand is presented to show the potential of the proposed procedure. The results show that WFT limits interference patterns which appear with others TFRs and produces a sparse representation suitable for characterization purposes. The transformation is used to extract longitudinal and flexural waves dispersive velocity and frequency-dependent attenuation. In particular, the mode-frequency combinations propagating with minimal losses are identified, as they are suitable for long-range inspection of strands.

Discussion and Conclusions

This work proposes a new TFR capable to extract the dispersive behaviour of GWs that propagates in the multi-wire strand from a recorded time transient-waveform over a wide frequency range. The new tool efficiently represents the different GWs with non-linearly frequency modulated atoms. In the proposed decomposition energy peaks extraction is a simpler task and can be performed to obtain reliable mode representation and characterization.

P1-J-07

Resonant Langasite Microsensor for Scanning Microdeformation Microscopy

Gabrielle Douchet¹, Fabrice Sthal¹, Therese Leblois², Pascal Vairac², Emmanuel Bigler¹; ¹Time & Frequency, Femto-ST, France, ²MN2S, Femto-ST, France

Background, Motivation and Objective

Scanning microdeformation microscopy (SMM) is a near field microscopy in the meso-scope domain. Such a microscope has become an alternative to the high resolution acoustic microscope that operates at very high frequencies. SMM is based on a vibrating contact tip and piezoelectric detection. The lateral resolution is essentially related to the tip diameter. Classically, the SMM sensor is obtained by a complex mounting process. The tip is glued on a Si cantilever driven by a piezoelectric ceramic. Piezoelectric crystal is an alternative to get a monolithic vibrating cantilever. Quartz crystal, which is the most often used piezoelectric material, can be advantageously replaced by Langasite crystal because of:

- 1) Its higher piezoelectric coefficients
- 2) Its better temperature behaviour.

Statement of Contribution/Methods

In this paper, a theoretical comparison between quartz and Langasite crystal devices is given according to an analytical model. A new process of microfabrication to get piezoelectric cantilevers is proposed. It is based on photolithographic steps and on an anisotropic chemical etching. This batch process allows us to obtain microresonators. These devices are designed to vibrate in flexural mode in a low frequency range or in length-extensional mode. Experimental characterizations of these new devices are performed. The measurements concern the resonant frequencies, motional parameters and the temperature behaviour.

Results

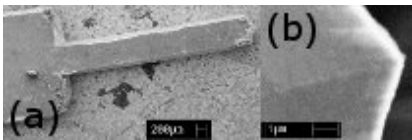
Temperature compensated orientations are given for flexural and length extensional vibrating modes. A LGS cantilever has been achieved. It consists in a 4 mm long and 500 μm wide beam. Its thickness is about 230 μm (fig. (a)).

The shape of the beam's cross-section is a consequence of the anisotropic chemical etching in an HCl solution. Moreover the beam is ended by a pointed tip, as seen in fig. (b).

Theoretical and experimental frequencies are in good agreement (about 20 kHz for flexion and 300 kHz for length extension).

Discussion and Conclusions

These devices present a great advantage in the case of length extension. Thanks to the chemical etching process, a tip is generated at the end of cantilever. Consequently, no tip gluing is necessary. This monolithic device will be tested in order to be approved for SMM.



P1-J-08

Quantitative Ultrasonic Characterization of Pharmaceutical Polymer Structures

Tom Fabritius¹, Joonas Eskelinen¹, Edward Hæggsström¹; ¹Department of Physics, University of Helsinki, Finland

Background, Motivation and Objective

Tubular layered polymer structures are used in pharmaceuticals for controlled drug release and delivery. Quality control of the manufactured items is important to ensure absence of abnormal drug release in the body, caused by structural defects or changes in the mechanical properties of the polymer. We set out to quantitatively and non-invasively measure the elasticity, layer thickness and internal layer adhesion in pharmaceutical polymer products.

Statement of Contribution/Methods

We built an acoustic microscope capable of characterize pharmaceutical layered polymer tubes at production speed. The setup consists of 50MHz immersion transducer (focal distance 12.7mm, aperture 6mm), computerized translation stage, pulser/receiver, oscilloscope and computer. The axial resolution is $\pm 10\mu\text{m}$ whereas the lateral resolution is $\pm 100\mu\text{m}$.

From surface reflections and by assuming constant density, (from sample manufacturer) we calculated sound velocity from the acoustic impedance and from it we determined the elastic modulus. We detected internal defects in the layered structure and delaminations between layers. The tubular layer thicknesses (300-400 μm range) were calculated from the velocity and the time-of-flight (TOF) of the echoes. The method also allowed monitoring dispersion and frequency dependent attenuation in the layers.

Results

We measured layer thickness with $\pm 30\mu\text{m}$ accuracy, which is sufficient for quality control purposes. Regions ($< 1\text{mm}$) of poor layer adhesion between the outer and inner layers were successfully detected in samples with suspected delaminations. We sized internal defects with $\pm 10\mu\text{m}$ accuracy. The local elastic modulus (20-50MHz range) was obtained from the measured velocity values. The obtained values were $70 \pm 30\text{MPa}$ with four control samples having different elasticity values. The results were consistent with the cross-linkage degree of the samples.

Discussion and Conclusions

We studied the feasibility of measuring thin, layered pharmaceutical polymer structures with ultrasound. The developed method can analyze the layered polymer tubes. It measures locally the layer thickness and elastic modulus as well as detects poorly adhered regions. The method could be used in laboratory analysis or be developed for on-line production quality control tool. It is sufficiently fast for current production online control.

P1-J-09

Synthetic Aperture Focusing Technique for High-Resolution Imaging of Surface Structures with High-Frequency Ultrasound

Michael Vogt¹, Jörn Opretzka¹, Helmut Ermert¹; ¹Dept. of Electrical Engineering and Information Technology, Ruhr-University Bochum, Bochum, Germany

Background, Motivation and Objective

In non-destructive evaluation (NDE), imaging of planar structures is of interest for the analysis of surfaces, for example of material samples and semiconductor chips. In this paper, a reconstruction approach for imaging surface structures using high-frequency ultrasound in the 20 MHz frequency range is presented and evaluated.

Imaging radar systems for remote sensing of the earth perform echo measurements using microwaves, which are emitted and received by one or more antennas aboard an airplane or satellite. In SLAR (side looking airborne radar), antennas are orientated perpendicularly to the moving direction of the plane and tilted towards the earth. A large area is illuminated, and the earth's surface is imaged by recording echo signal data at antenna positions along the flight path and applying synthetic focusing (SAR: synthetic aperture radar).

Statement of Contribution/Methods

The described SLAR/SAR concept has been adapted for high-resolution imaging of the surface of planar material samples with high-frequency ultrasound in the 20 MHz range. In the proposed system, a spherically focused single element transducer (6.3 mm aperture diameter, 15 mm focus length, 24° aperture angle) is mechanically scanned along a linear (1D) aperture path in a side looking orientation with respect to the object surface. Pulse echo measurements are performed, and echo signals from the object in the transducer's far field are acquired with a digitizer (400 MHz sampling frequency). Synthetic aperture focusing technique (SAFT) is applied to reconstruct 2D images of the sample's surface with respect to the scanning direction (azimuth) and the side looking direction (elevation). For the reconstruction, the focus of the transducer is considered to be a virtual point source.

Results

The proposed imaging concept has been evaluated with both, simulated echo data and measurement data from test objects like coins and other material samples. Surface structures are imaged with constant resolutions of $70\mu\text{m}$ and $200\mu\text{m}$ in elevation and azimuth, respectively, independent of the radial distance from the transducer.

Discussion and Conclusions

A synthetic aperture focusing technique has been adapted from radar technology and successfully implemented for high-resolution imaging of surface structures. Compared to the C-scan technique in acoustic microcopy, the acquisition is much faster with the proposed method because of the 1D scan concept with a large field of view in the elevational direction.

P1-J-10

Aberration Correction for Biological Acoustic Impedance Microscope

Tsutomu Uemura¹, Takaya Suzuki¹, Kunihiro Hanai¹, Sachiko Yoshida², Kazuto Kobayashi³, Seiji Yamamoto⁴, Yoshifumi Saijo⁵, Naohiro Hozumi¹; ¹Electrical Engineering, Aichi Institute of Technology, Toyota, Aichi, Japan, ²Toyohashi University of Technology, Japan, ³Honda Electronics Co. Ltd, Japan, ⁴Hamamatsu University School of Medicine, Japan, ⁵Tohoku University, Japan

Background, Motivation and Objective

We proposed an acoustic microscope for imaging cross sectional acoustic impedance of biological soft tissues. A focused pulse wave is transmitted to the object placed on the "rear surface" of a plastic substrate. The reflection is interpreted into characteristic acoustic impedance. However, this method produces significant aberration, because the sound speed of the substrate is different from water used as a coupling medium. For this reason the spatial resolution is reduced. This presentation deals with improvement of spatial resolution by using 3D deconvolution technique.

Statement of Contribution/Methods

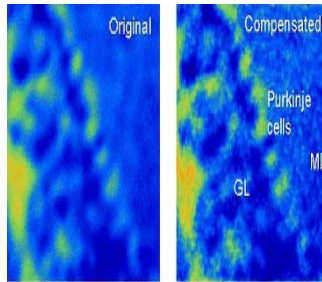
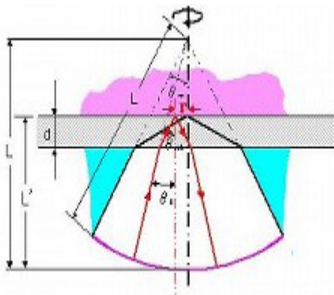
A PVDF transducer was used. The substrate was 0.8 mm thick polystyrene plate. The transmitted waves with different incident angles are reflected at different distances from the focal point (Fig. 1). In order to compensate the aberration, the impulse response of the system was calculated. Based on this impulse response, 3D deconvolution was performed.

Results

Figure 2 shows the original and compensated reflection images taken from a cerebellum tissue of rat. In the compensated image, the shape of such as Purkinje cells, with 20 micrometers in scale, are more clearly seen.

Discussion and Conclusions

It was exhibited that 3D deconvolution technique is useful for reducing the aberration. We are planning to interpret the compensated image into the acoustic impedance profile. In addition, precise sound propagation analysis will be performed.



P1-J-11

Study of global and local elastic and anelastic properties of a metallic glass obtained by atomic force acoustic microscopy and shear-wave velocity measurements

W. Arnold^{1,2}, H. Wagner³, C. Vree³, A. Kahl³, D. Bedorf³, K. Samwer³; ¹*I. Physikalisches Institut, University of Goettingen, Goettingen, Germany*, ²*Dept. Materials, Saarland University, Saarbruecken, Germany*, ³*I. Phys. Institut, University of Goettingen, Germany*

Background, Motivation and Objective

Metallic glasses show various relaxation phenomena which can be probed by mechanical spectroscopy. Here we focus on the so-called alpha- and beta- relaxations, their microscopic origin, and their relation to the plastic deformation behavior of metallic glasses. According to some recent models, the plastic deformation is related to irreversible alpha-processes involving large energy barrier crossings whereas the beta-processes describe hopping between small energy barriers within the large potential energy minimum.

Statement of Contribution/Methods

By sequential heat treatment of a Pd40Ni40P20 bulk metallic glass at different temperatures and for sufficiently short durations that alpha-relaxation is not possible, dynamic and quasi-static relaxation paths below the glass transition are identified. Following each heat treatment up to 150 °C, shear-wave velocity measurements are carried out using rf-ultrasonic pulses with a bandwidth of 100 MHz. Furthermore, we measured the local contact stiffness k^* at about 1 MHz by exploiting the contact resonances of a cantilever in atomic force acoustic microscopy (AFAM) $1/\omega$, and its imaginary part by evaluating the reciprocal quality or damping factor (Q^{-1}). We inverted these data to obtain the local indentation modulus and its imaginary part.

Results

There is a clearly observable dependence of the contact stiffness k^* and of the damping factor in the AFAM images (or C-scans) when the contact radius of the AFM tip contacting the sample surface approaches 10 nm indicating a modulus dependence on the probed volume.

Discussion and Conclusions

These data are compared to the global velocity measurements and are related to the relaxation modes of the metallic glasses which involve cooperative movements of the disordered structure of the metallic glass over different length scales in the nm range which is supported by our measurements.

/1/ M. Kopycinska-Mueller, A. Caron, S. Hirsekorn, U. Rabe, H. Natter, R. Hempelmann, R. Birringer, and W. Arnold, J. Phys.Chem. 222,471 (2008)

Monday
Poster

P1-K. Signal Processing and Imaging

Sala Orange

Monday, September 21, 2009, 10:00 am - 11:30 am

Chair: **Erdal Oruklu**
Illinois Institute of Technology

P1-K-01

A Generic Parametric Model for Ultrasonic Echo Analysis

Ramazan Demirlil¹, Jafar Saniie^{1,2} *Electrical and Computer Engineering, Illinois Institute of Technology, USA*

Background, Motivation and Objective

Parametric echo models have been widely used in recent years for ultrasonic echo analysis and parameter estimation. Several different models (e.g., Gaussian echo, Gaussian Chirplet) have been used in the context of model-based estimation and sparse signal decomposition. These models are commonly used in acoustic signal processing, mathematically tractable, and have explicit TF representations. However, most often they are not as flexible to represent complex shape ultrasonic echoes. A generic echo model that can be optimized to represent complex shape echoes is highly desirable, for example, for modeling frequency dependent attenuation and dispersion effects in a propagation path, estimating time-of-arrival of a reflector in presence of pulse-echo wavelet variance.

Statement of Contribution/Methods

In this study, we propose a generic echo model to account for complex shape ultrasonic echoes. This model is inspired from the analytic signal representation in which an ultrasonic echo is contemplated in terms of envelope and frequency components. The envelope is modeled as the sum of a number of fixed-width Gaussian Functions (GFs) whereas the frequency is modeled as a linear chirp signal. The number and bandwidth of GFs are set based upon the spectral characteristics of the transducer impulse response. Furthermore, the weights of GFs are modeled as a random vector with known mean and covariance so that the echo envelope is flexible to fit complex echoes while the echo shape (i.e., the rising and falling envelope signature) is preserved. This Gaussian mixture representation accounts for skewed shape envelopes while the linear chirp accounts for small frequency drifts in the time-support of the echo. This model generalizes the existing Gaussian and Gaussian chirp models. An optimization algorithm is developed to estimate the echo parameters. The performance of estimation is verified using simulations.

Results

Simulation results demonstrate that the parameters of the generic echo can be estimated with high fidelity in presence of White Gaussian noise. This echo-model is then used to fit complex shape pulse-echo wavelets acquired from several different transducers and measurement conditions. Finally, this echo model is embedded with a Matching Pursuit algorithm for sparse signal decomposition of ultrasonic echoes and applied to reverberation echoes measured from multiple layers. Decomposition results clearly demonstrate the advantage of the model compared to the existing alternatives.

Discussion and Conclusions

The proposed generic echo model accounts for complex shape echoes and can be useful to represent ultrasonic echoes acquired under a variety of measurement conditions. The parameters of the generic echo can be estimated accurately in the presence of measurement noise. The potential applications of this type of model are numerous: parameter estimation for NDE testing, ultrasonic deconvolution in presence of pulse variance, and feature extraction.

P1-K-02

Frequency Domain Low Time-Bandwidth Product Chirp Synthesis for Pulse Compression Side Lobe Reduction

Teemu Virolainen¹, Tom Fabritius¹, Joonas Eskelinen¹, Edward Hægström^{1,1} *Department of Physics, University of Helsinki, Finland*

Background, Motivation and Objective

Pulse compression can increase signal to noise ratio (SNR) without increasing the acoustic intensity. This is important in medical ultrasound due to safety regulations limiting the allowed peak acoustic intensity. In NDT ultrasonics the usable peak intensity is usually limited by the transducer specifications or by nonlinear saturation effects or cavitation.

Standard frequency modulated chirps exhibit cross correlation side lobes, that increase with decreasing Time-Bandwidth product (TBP). This is advantageous in NDT and medical pulse-echo ultrasonics where closely spaced multiple scatterers need to be resolved. Time domain windowing of the chirp can reduce the side lobes but trade-offs exist between the side lobe level and the correlation main lobe width. We use frequency domain generated chirp signals (FDC) with low side lobe level to reduce the side lobes while maintaining the main lobe width.

Statement of Contribution/Methods

The chirp signal synthesis comprises three steps:

- 1) The pulse is generated in time domain by multiplying a sinusoid with gaussian envelope to produce a signal with desired bandwidth. Arbitrary envelopes or pulse shapes can be used.
- 2) The actual chirp is generated in the frequency domain by applying a quadratic phase shift to the pulse as a function of frequency. This step spreads the power in time domain.
- 3) The resulting signal is transferred to time domain and is then used for pulse compression.

Adding several gaussian enveloped sinusoids with different carrier frequency was also investigated as a way to enhance the chirp bandwidth. This method allows the spectrum to be closer to an ideal square spectrum, thus giving narrower main lobe without significantly increasing the side lobes.

Results

Simulation results of pulse compression properties for various TBP values relevant to pulse-echo ultrasonics are presented. The generated FDC signals are compared to standard window functions. In general the sidelobe level of FDC was consistently low (<70dB) while the main lobe was comparable to that of an unwindowed chirp (-6dB width within 10%). The simulation results are also compared to experimental pulse echo results.

Discussion and Conclusions

FDC chirps show potential as a method for generating low TBP signals with weak side lobes and a narrow main lobe. The method allows the spectrum of the signal to be shaped without increasing the side lobe level, e.g. to enhance the impulse response of the transducer in a relevant bandwidth (spectrum shaping). Moreover, the side lobes are relatively insensitive to the signal length, which allows the chirp duration to be varied without affecting the correlation properties.

P1-K-03

Target sizing: spectral method versus wavelet-based estimator

Angel SCIPIONI¹, Pascal RISCHEFFE², Patrick SCHWEITZER³, Jérôme MATHIEU^{4,1} *Institut Jean Lamour, UMR CNRS 7198, Cosnes et Romain, France, ²MAS'Air, CReA, Salon Air, France, ³LIEN, Nancy Université, Vandoeuvre-lès-Nancy Cedex, France, ⁴IUT de Rodez, Rodez, France*

Background, Motivation and Objective

The problems tackled in this article are those of the sizing characterization of a immersed target. This wire target is insomified by an ultrasonic broadband transducer, and our goal is to compare the diameter estimation by two different methods which both rely on the analysis of the backscattered echo.

The first method of radius estimation is based on the identification of the optimal parameter which ensures the best superimposition of the spectral backscattered echo segment on the form-function. The second technique relies on a family of synthetic echoes obtained from the resonant scattering theory (RST). Those are analyzed by a wavelet transform of which the coefficients are used to establish a model identifying the experimental signals.

Statement of Contribution/Methods

In the first method, we calculate the spectrum of the windowed backscattered echo by a short time Fourier transform. The same operation is done with the backscattered echo from a block sufficiently wide to simulate an infinite plane. By combining these two spectra in the bandwidth of the transducer, we eliminate the effects of transducer directivity and other effects, as well as the attenuation of the medium. By correlating the resulting segment with the reference form-function, we obtain the estimate of the target radius.

In the second method, we perform from a well-selected wavelet a continuous wavelet transform (CWT) on different synthetic echoes. From these wavelet decompositions we construct the link between the diameter and the maximum of wavelet coefficients. By minimizing the error in the sense of least-squares of a polynomial approximation, we obtain the expression of the wavelet-based estimator. After normalization, we can apply CWT on experimental echo and submit to the estimator the maximum of the coefficients, giving thus the estimate of the target diameter.

Results

The two methods provide good estimations in term of precision and Table 1 presents the results. The relative variation of performance of the two methods increases when the diameters decrease.

Discussion and Conclusions

The two methods were tested on steel and copper targets, with diameters ranging from 0.25 mm to 1 mm. If, in comparison with the other contactless methods of small target sizing, the two methods offer good-quality results, the wavelet-based method brings a decisive performance gain.

Table 1
Comparative results of the two methods for steel and copper wires of diameter 0.25, 0.50 and 1.00 mm.

Reference diameter	Computation methods	Steel		Copper	
		SCM ¹	WM ²	SCM	WM
∅ 0,25 mm	Estimated value	0,31	0,23	0,32	0,24
	Relative error	24%	8%	28%	4%
∅ 0,50 mm	Estimated value	0,56	0,50	0,56	0,51
	Relative error	12%	0%	12%	2%
∅ 1,00 mm	Estimated value	1,08	1,02	1,12	0,92
	Relative error	8%	2%	12%	8%

¹Spectral Correlation Method, ²Wavelet Method.

P1-K-04

Enhancing Real-time Ultrasound Signatures of Molten Nugget Growth for Quality Evaluation of Resistance Spot Welds

Anthony Karloff¹, Andriy Chertov², Roman Gr. Maev^{2,1}:¹Electrical and Computer Engineering, University of Windsor, Canada, ²Institute for Diagnostic Imaging Research, University of Windsor, Canada

Background, Motivation and Objective

A state-of-the-art ultrasound transducer installed in a welding electrode has allowed real-time ultrasonic signatures to be obtained in pulse echo mode. These are now used to image the formation of the molten nugget. The main objective is to evaluate weld quality based on weld thickness, which correlates with nugget diameter. The primary challenge that arises is identifying the solid-liquid nugget interface in low signal-to-noise ratio scans due to acoustical and electric noise, the inhomogeneous and irregular weld medium, and interference and degradation of the welding electrodes.

Statement of Contribution/Methods

This article proposes a new processing algorithm for enhancing and interpreting the real-time ultrasound signatures of a spot weld by analysing the propagation of acoustic waves through the electrode and heated weld region. A new method of processing the ultrasound data is presented to remove undesired reflections in the electrode cap and enhance weak reflections at the solid-liquid interface. In addition, unknown temperature gradients are compensated for, drastically improving the accuracy of weld thickness measurements. A series of spot welds were performed to compare the results of signature analysis with physical measurement and destructive tests.

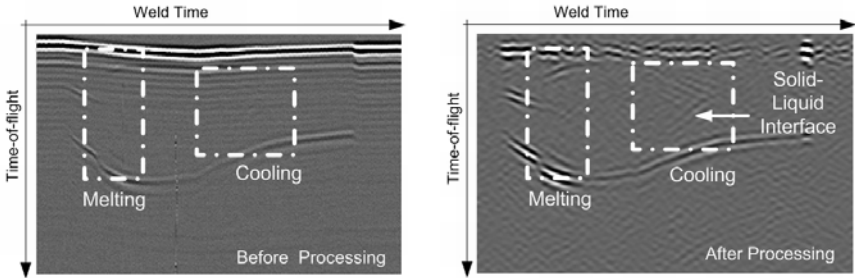
Monday
Poster

Results

The result of the proposed method is a significant qualitative improvement in identifying the solid-liquid nugget interface and a very accurate method of measuring weld thickness within 100 microns.

Discussion and Conclusions

Overall, the ability to effectively detect the solid-liquid interface in noisy signatures has permitted a significant improvement in the real-time estimation of spot weld quality, while ensuring reliable inspections over the lifetime of the electrodes.



Monday
Poster

P1-K-05

Characterization of Thin Layers in Multi-Layered Structures: On the Problem of Finding Starting Values for Numerical Solutions to Inverse Problems

Johan Carlson¹, Fredrik Hägglund¹:¹Dept. of Computer Science and Electrical Engineering, Lulea University of Technology, Lulea, Sweden

Background, Motivation and Objective

When using pulse-echo ultrasound to measure properties of thin layers within multi-layered materials, a major challenge is that the received ultrasound waveform consists of several overlapping echoes. Previous work has shown that by fitting a parametric physical model of the wave propagation to the data, estimates of reflection coefficients and times of flight through the layers can be obtained. Depending on the amount of available prior knowledge, this can then be used to compute layer densities, thicknesses, etc.

For this to work it is important to have good initial guesses of the model parameters. Sometimes this information is available, but often some manual work is required to calibrate the algorithm. For online diagnostic applications, an automated method is preferred.

Statement of Contribution/Methods

The source of the problem is that the length of the transmitted ultrasound pulse gives rise to overlapping echoes in the received waveform, making it difficult to obtain initial guesses to layer thicknesses.

The proposed method is based on the design of a deconvolution filter that tries to compress the reflected echoes into detectable peaks, followed by matched filter and envelope processing. The peaks are then used to compute initial values of the parameters to be using the full physical model. Since a perfect pulse compression is not possible, especially not in the presence of measurement noise, a regularized version is proposed, which enables a trade-off between pulse compression and resolution on the one hand numerical stability on the other.

Results

The performance of the compression technique is evaluated with simulations on three-layer materials for varying layer thicknesses and noise conditions.

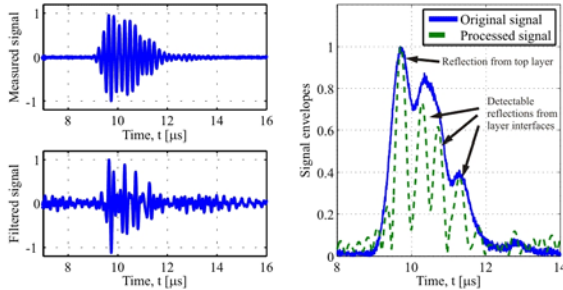
The figure shows an example of an original and a filtered signal as well as the detectable echoes.

Discussion and Conclusions

We show that the transmitted pulse shape can be compressed to the extent that it is possible to obtain estimates of the layer thicknesses, even when the echoes overlap substantially. This may be enough for some applications, but

for other cases, these estimates will serve as initial guesses for numerical solutions to a more complex physical model.

The improved performance of the full parametric model by using the proposed method is also demonstrated in the paper. Finally, some guidelines on how to implement this for various measurement scenarios are given.



Monday
Poster

P1-K-06

SAW Passive Wireless Multi Sensor System

Nikolai Kozlovski¹, Donald Malocha¹; ¹SEECs, University of Central Florida, Orlando, FL, USA

Background, Motivation and Objective

Previous work has been presented on passive wireless SAW sensors using the orthogonal frequency coding (OFC) technique [1]. Wireless operation of such sensors has been demonstrated using a network analyzer and only one sensor at a time. A technique to allow multiple sensors to operate at the same time has been developed and demonstrated using network analyzer measurements that were added together to simulate simultaneous operation within the system. NASA is sponsoring research and development of SAW wireless, passive sensors that are environmentally robust and operate in multi-sensor environment.

Statement of Contribution/Methods

This paper will present a first fully functioning 915MHz interrogation system for passive wireless OFC SAW temperature sensors. The paper will present the interrogator hardware for the SAW sensors and the analytical model and how it is used to extract the temperature data from each particular sensor. Spread spectrum techniques are demonstrated that allow operation below noise level by using processing gain techniques in a correlator synchronous receiver. The system presented has eight sensors built on YZ LiNbO₃ around 915MHz. Featured sensors consisted of wide band, eighth wavelength electrode transducer operating at 3rd harmonic and two symmetrically placed reflector banks on either side of the transducer operating on 2nd harmonic. A 45.75MHz clock is used to control the digital control of the interrogator circuit and to produce the 915MHz interrogating signal. Temperature is extracted from the sensor using an adaptive filter correlator technique.

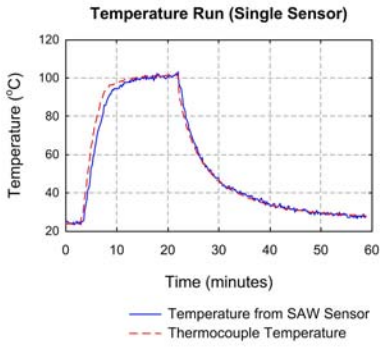
Results

Eight-sensor passive wireless system has been demonstrated. Sensors were subjected to various temperatures ranging from -200°C to 180°C. Sensors were randomly positioned within 2m radius of each other. Shown in the figure is the real free running temperature acquisition from one of the sensors on the hotplate. The 8 designed sensors showed excellent anti-collision properties crucial for multi-sensor operation.

Discussion and Conclusions

The system has demonstrated good code anti-collision properties. It is shown that the passive wireless SAW OFC sensor is a viable solution for environments where multiple sensors operate simultaneously.

[1] J. Pavlina, N. Kozlovski, B. Santos, and D. C. Malocha, "SAW Wireless, Passive Sensor Spread Spectrum Platforms", IUS, IEEE, 2008, pp 1112-1115.



Monday
Poster

P1-L. Phononic Crystals-Band Structure and Propagation

Sala Orange

Monday, September 21, 2009, 10:00 am - 11:30 am

Chair: **Roy Olsson**
Sandia National Laboratory

P1-L-01

Visualization of Negative Refraction in Phononic Crystal using Pulsed Light Source

Kojiro Nishimiya^{1,2}, Takeshi Ohbuchi^{1,2}, Naoto Wakatsuki¹, Koichi Mizutani¹, Ken Yamamoto³:¹University of Tsukuba, Japan, ²Research Fellow of the Japan Society for the Promotion of Science, Japan, ³Kansai University, Japan

Background, Motivation and Objective

The size of phononic crystal is larger than that of photonic crystal because of the relation between the wavelengths of the sound and the light. However, it is still difficult that we measure the inside behavior of the phononic crystal by using the microphone and all that. Therefore, in many cases, the inside behavior of the phononic crystal is obtained by using simulation. With that, we aim to visualize the inside of the phononic crystal and the lattice, experimentally.

In this paper, we visualize the negative refraction in phononic crystal. Negative refraction is expected to the application for the flat lens.

Statement of Contribution/Methods

The ultrasound stress is visualized with Fresnel diffraction. And visualization images are obtained using the pulsed light source synchronized to ultrasound incidence as shown in Fig. 1(left). Also, the transient response is obtained using the delay time between light emission and ultrasound incidence. The observed objects are shown in Fig. 1(a) and (b). The diameter of each lattice is 1 mm.

Results

Visualization results are shown in Fig. 2. Bright areas in the images correspond to the high stress areas. The frequency of incident ultrasound is about 1.01MHz. The visualization images were obtained that the incident ultrasound deflected with negative refraction. It was verified the two type crystals have a little differing negative refraction by changing from square lattice to rectangular lattice.

Discussion and Conclusions

In this paper, we visualized the negative refraction of phononic crystal, experimentally. As further works, we will visualize the inside of each phononic crystal and the lattice by using photoelastic.

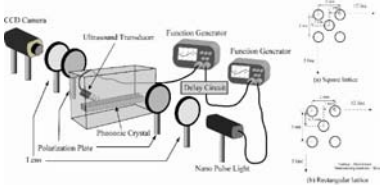
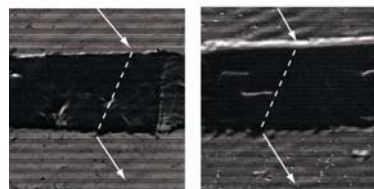


Fig. 1 : Visualization System and Objective phononic crystal



(a) Square lattice (b) Rectangular lattice

Fig. 2 Visualization results of negative refraction

Finite Element Method for Analysis of Band Structures of Phononic Crystals Slab with Archimedean-like tilings

Jianbao Li¹, Yue-Sheng Wang², Chuanzeng Zhang³, ¹Institute of Engineering Mechanics, Beijing Jiaotong University, Beijing, China, People's Republic of, ²Institute of Engineering Mechanics, Beijing Jiaotong University, China, People's Republic of, ³Department of Civil Engineering, University of Siegen, Germany

Background, Motivation and Objective

Phononic crystal is a periodic structure composed of periodic arrays of two or more material components. An important property of a phononic crystal is the existence of phononic band gaps. Due to this property, phononic crystals are expected to manipulate acoustic waves and thus have many potential applications. Phononic crystals have received extensive attention since the pioneer work of Kushwaha.

Due to the same square primitive unit cell and the first Brillouin zone, the phononic crystals slab with Archimedean-like lattices (Ladybug and Bathroom) have similar acoustic response in lower bands. Although more complicated and far less used in phononic crystals research comparing to traditional Bravais lattice, could also be very useful structures at least as an alternative or even as structures with improved the bandgap characteristics of phononic crystals.

The paper aims to evaluate the propagation of acoustic waves in the two-dimensional phononic crystals slab with Archimedean-like tilings with the help of ABAQUS code and user subroutine.

Statement of Contribution/Methods

A phononic crystal structure can be considered as successive repetition of a unit cell. Consider propagation of a harmonic wave in a phononic crystal. According to Bloch theorem, the following phase relation between the mechanical displacements u for nodes lying on the boundary of the unit cell:

$$u(x, y, z) = u(x+a, y+a, z) e^{-i(k_x a + k_y a)}$$

where k_x, k_y represent wave numbers, and a is lattice constant.

The fundamental equation for the FE simulation is:

$$([K_R] - \omega^2 [M_R])u = 0$$

where K_R is the reduced stiffness matrix; and M_R is the reduced mass matrix.

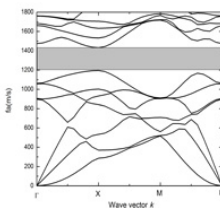
The frequencies and vibration modes of equation can be calculated by using the Lanczos iteration.

Results

Figure 1 shows Band structure of a square-lattice two-dimensional infinite phononic crystal of quartz cylinders in epoxy, computed for waves propagating in the plane of the crystal. For comparison, the results have a good agreement with literature (Khelif et al. 2006).

Discussion and Conclusions

We have extended the FE method to analyze acoustic wave propagation in 2D phononic crystals slab. The FE method has features of better convergence and fast evaluation speed. Also, the results indicate that the FEM is precise for the band structure computation of the complex Archimedean tilings phononic crystals slab.



Off-axis directional acoustic wave beaming control by an asymmetrically rubber heterostructures film deposited on steel plate in water

Feiyan Cai¹, Zhaojian He², Zhengyou Liu², Hairong Zheng^{1,1} *Key Laboratory of Biomedical informatics and Health Engineering, Chinese Academy of Science, Shenzhen Institute of Advance Technology Chinese Academy of Sciences, China, People's Republic of.* ²*Key Lab of Acoustic and Photonic materials and devices of Ministry of Education, Department of Physics, Wuhan University, China, People's Republic of*

Background, Motivation and Objective

Controlling the direction of the acoustic wave beaming can solve the problem of diffraction limit and efficiently manipulate acoustic wave. In this work, we investigate the control of directional acoustic wave beaming via surface acoustic wave (SAW) modes of a composite slab in water. As shown in Fig (a), this composite slab is made of an asymmetric rubber heterostructures film deposited on steel plate, and the rubber heterostructures is constructed by alternatively stacking rubber-1 and rubber-2 film (two kinds of rubbers with different transverse velocities).

Statement of Contribution/Methods

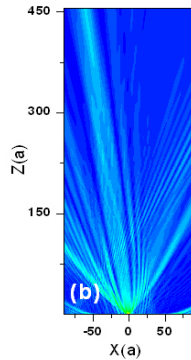
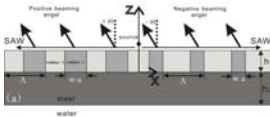
When ratio of widths on rubber-1 to rubber-2 in a periodic in left side and in right side are $(\Lambda-(W+\Delta))/(W+\Delta)$ and $(\Lambda-(W-\Delta))/(W-\Delta)$ respectively, Λ indicates the stacking period in both left side and right side, a line acoustic source is placed near the rubber heterostructures surface on the symmetric axis of the composite slab, an off-axis directional acoustic wave beaming with angle Θ can be obtained. Fig. (b) shows the calculated field intensity by the finite difference time domain (FDTD) method.

Results

The off-axis directional beaming is due to the surface acoustic wave resonances modulated by the asymmetric rubber heterostructures properties at the surface. The deviation beaming angle can be changed precisely by adjusting the width percentage of different rubbers in period asymmetrically.

Discussion and Conclusions

The directional beaming structure would be interesting for a variety of acoustic devices and elements for acoustic wave, such as mechanical filtering, non-destructive testing of materials, medical ultrasound instrumentation and etc.



Band Structures for Different Kinds of Point Defect in Phononic Crystal Thin Plates

ZONG-JIAN YAO¹, GUI-LAN YU¹, YUE-SHENG WANG^{1,1} *BEIJING JIAOTONG UNIVERSITY, China, People's Republic of*

Background, Motivation and Objective

Phononic crystals are periodic composites with frequency band gaps. If a defect is introduced into the periodic structure then defect modes can arise in band structures. The existence of band gaps and defect modes suggest wide

potential applications of phononic crystals in many fields such as noise suppressors, acoustic filters and transducer technology. The purpose of this paper is to explore theoretically the band structures for different kinds of point defect in phononic crystal thin plates for square / triangle lattice. The effects of mass density, elastic modulus, the size and geometric shape of the point defect are discussed in detail.

Statement of Contribution/Methods

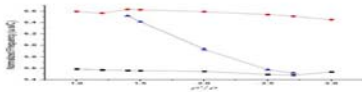
The crystal thin plate is composed of parallel cylindrical inclusion of Al₂O₃ embedded periodically in the Epoxy host. Both the square and triangle lattices are considered. The defect is created by several means such as changing the radius, the mass density, the elastic modulus, the geometric shape of one of the cylinders, etc. We choose a supercell containing 5 \times 5 unit cells. Using the improved plane wave expansion method combining with the supercell technique we can calculate the band structures for different kinds of point defect.

Results

The band structures are obtained both for square lattice and triangle lattice when the perfect phononic crystal thin plate is disordered by changing the size, the geometric shape, the mass density and the elastic modulus of one of the scatters respectively. The defect modes changing with different kinds of point defect are analyzed in detail. Figure 1 shows the effects of mass density of the point defect on the band structures for triangle lattice.

Discussion and Conclusions

The results show that the defect modes existing in the first band gap are strongly dependent on the size and the mass density of the point defect for the two lattices. While the elastic modulus and geometry shape of the defect has little influences on the defect modes. With decreasing of the size of the defect, all defect bands move from the upper edge of the first band gap towards the middle and the edges of the first band gap almost remain unchanged as the defect size varies. It can be seen from figure 1 that the defect band moves downward as the mass density increases.



P1-L-05

Phononic crystal band gaps in a polymer overlay on Lithium Niobate studied using finite element method in 3D

Lars Rindorf¹, Daniel Nilson¹, Lars Lading¹, ¹*Microtechnology and Surface Analysis, Danish Technological Institute, Taastrup, Denmark*

Background, Motivation and Objective

Phononic crystals may offer zero transmission of sound using complete phononic band gap as well as highly anomalous dispersion. We are inspired by photonic crystals which have a high index waveguide material on a low index substrate. The high index material has holes to give photonic band gaps. In acoustics this corresponds to having a low acoustic velocity (polymer) material on a high acoustic velocity (Lithium Niobate) material. A layer of polymer spun on top of Lithium Niobate can readily be fabricated and structured using UV lithography.

Statement of Contribution/Methods

We propose a phononic band gap structure which is easy to fabricate and characterize experimentally. The unit cell is rectangular with a periodicity of 2 μ m and there is a 1.4 μ m diameter cylindrical hole in the polymer layer which is 0.75 μ m thick on top of the Y-cut Lithium Niobate substrate. The structure is effectively three dimensional and we use an advanced open source finite element method (FEM) software for the challenging large computation of the Bloch diagram. 3D simulations require large number of variables and are more complex than 2D.

Results

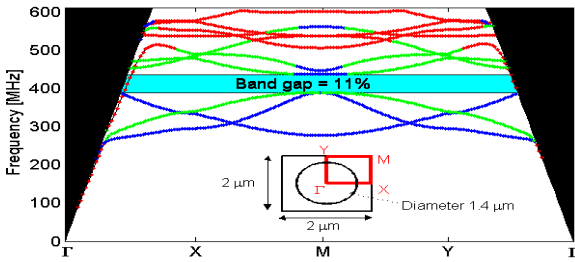
We find a large 47 MHz (11%) band gap around 412 MHz (see figure) for the shear and compressional modes in the Bloch diagram. These are well separated from the bulk modes implying that they are well guided with low loss. The colors indicate quasi-shear horizontal (blue), quasi-compressional (green), or quasi-Rayleigh (red) Bloch modes. The black areas indicate the bulk regime in which no surface guided modes exist. Inset: The rectangular unit cell, and the 1st Brillouin zone (red rectangle). A Rayleigh mode originating from the free Lithium Niobate

surface penetrates the band gap along the Gamma-X and Gamma-Y directions, so the band gap is not complete. By increasing the the polymer thickness a bandgap in this mode also appear.

Discussion and Conclusions

A layer of periodically structured polymer on Lithium Niobate gives band gaps that lend themselves to accurate experimental characterization. Experimental verification is currently in progress. The proposed structure is readily fabricated as opposed to structuring Lithium Niobate directly which is difficult and gives less guided Bloch bands.

Monday
Poster



P1-L-06

Focusing and beamforming of ultrasound beams with phononic crystals

Victor Sánchez-Morcillo¹, Kestutis Staliunas², Ester Soliveres¹, Victor Espinosa¹, Isabel Pérez-Arjona¹, Javier Redondo¹, Rubén Picó^{1,3}, *Instituto de Investigación de Gestión Integrada de Zonas Costeras, Universidad Politécnica de Valencia, Gandia, Valencia, Spain, ²ICREA/Dept. de Física i Enginyeria Nuclear, Universitat Politècnica de Catalunya, Terrassa, Barcelona, Spain*

Background, Motivation and Objective

Sonic crystals are media where the acoustic properties as density and bulk modulus are spatially modulated. They present a number of interesting features due to their celebrated temporal dispersion properties, in particular due to the existence of forbidden propagation bands or band-gaps in the dispersion curves. In addition to the peculiarities of temporal dispersion, spatially modulated materials are known also to modify the spatial dispersion, allowing to manipulate the diffraction of the waves. Many interesting effects on the beam propagation characteristics have been recently predicted, like self-collimation, super-refraction or focusing.

Statement of Contribution/Methods

We present a theoretical and experimental study of the propagation of sound beams in- and behind two- and three-dimensional sonic crystals. By a Plane Wave Expansion (PWE) we evaluate the isofrequency curves of the crystal, and identify the regimes where focusing is expected to occur. These regimes are close to the upper boundaries of the bands, where the dispersion curves are convex (corresponding to the negative diffraction regime). In the numerical study, beam propagation is simulated with the FDTD method. In the experiment we consider a sonic crystal with square geometry, consisting of a periodic array of steel cylinders with radius $r = 0.8$ mm and lattice constant $a = 5.25$ mm, resulting in a filling factor of 0.073. In such a crystal, immersed in water, the frequencies of interest correspond to the ultrasonic regime. A plane ultrasonic transducer located close to the crystal is used to generate the input beam, and its profile is measured in the whole spatial domain after the crystal.

Results

We find that the beam profile after crossing a slice of crystal is strongly influenced by the size (relative to the crystal period) and frequency of the radiating source. Narrow beams (those with broad spatial spectrum) are shown to propagate differently than broad beams. The influence on the lens-like behavior (focusing) of the sonic crystal on an incident acoustic beam is also discussed. We find that the beams can focus (collimate) behind the sonic crystal for the frequencies close to the band edge, and we analytically evaluate, numerically (FDTD) calculate, and experimentally measure the focusing properties, such as the focal distance, the width of beam waist, and the beam quality at the waist.

Discussion and Conclusions

The propagation characteristics, and in particular the focusing effect, of acoustic beams after crossing a phononic crystal, have been studied, both theoretically and experimentally. The field distribution is shown to depend strongly on the beam size and frequency, and different models for broad, intermediate and narrow beams are proposed, in the framework on the paraxial approximation. Explicit formulas for the focal distance and the beam width at the waist are proposed.

P1-M. Materials Characterization

Sala Orange

Monday, September 21, 2009, 10:00 am - 11:30 am

Chair: **John D. Larson**
Avago Technologies

P1-M-01

Evaluation of Synthetic Silica Glasses by the Ultrasonic Microspectroscopy Technology

Mototaka Arakawa¹, Hideki Shimamura¹, Jun-ichi Kushibiki¹; ¹Electrical Engineering, Tohoku University, Sendai, Japan

Background, Motivation and Objective

Ultrasonic microspectroscopy (UMS) technology was previously applied to characterization of silica glasses, and it was found that acoustic properties, viz., bulk-wave (longitudinal and shear) velocities, V_l and V_s , leaky surface acoustic wave (LSAW) velocity, V_{LSAW} , and density, ρ , are sensitive to the impurities, such as OH and Cl. In this paper, acoustic properties of synthetic silica glasses were measured to obtain relationships among fictive temperature, T_f , Cl concentration, C(Cl), OH concentration, C(OH), and acoustic properties.

Statement of Contribution/Methods

Ten specimens were prepared from commercial synthetic silica glasses. Six specimens were prepared from three different lots of ED-B and ED-C (Nippon Silica Glass Co., Ltd.) fabricated by the vapor-phase axial deposition (VAD) method. Four specimens were prepared from C-7980 (Corning Inc.), T-4040 (Toshiba Ceramics Co. Ltd.), P-10 (Shin-Etsu Quartz Products Co., Ltd.), and N-ES (Nippon Silica Glass Co., Ltd.) fabricated by the direct method. LSAW velocities and bulk-wave velocities were measured by the line-focus-beam and plane-wave ultrasonic material characterization system. Density was measured by the Archimedes method. C(OH) and C(Cl) were analyzed by infrared spectroscopy and x-ray fluorescence analysis, respectively.

Results

C(OH) of the direct-method specimens was 700-1500 wtppm, and those of the VAD specimens were zero. C(Cl) of the ED-C specimens was 1280-1740 wtppm, those of the direct-method specimens were 0-310 wtppm, and those of the ED-B specimens were zero. The maximum differences of V_l , V_s , V_{LSAW} , ρ , were 37.67 m/s, 11.75 m/s, 8.17 m/s, and 2.67 kg/m³ among the specimens, respectively. Although ED-B don't contain both Cl and OH, the maximum differences were 7.86 m/s, 3.71 m/s, 1.43 m/s, 0.45 kg/m³, respectively, among the specimens, caused by the differences of T_f . T_f of ED-B specimens were estimated from ρ using a relationship between density and T_f for silica glass [1], then relationships among velocities and T_f were obtained. C(Cl) and C(OH) dependencies of the acoustic properties were obtained by comparing the results between ED-B and ED-C and those between ED-B and direct-method specimens, respectively.

Discussion and Conclusions

Resolutions of T_f , C(Cl), and C(OH) by acoustic property measurements were estimated. V_l is most sensitive to the all properties; 0.6°C, 20 wtppm, and 3.1 wtppm, respectively. Those are much higher than the conventional evaluation methods. UMS technology is very useful for evaluation of silica glasses and their fabrication processes.

[1] H. Kakiuchida et al., J. Non-Cryst. Solids, Vol. 353, 568 (2007).

P1-M-02

Investigation of high-pressure transitions in vegetable oils by measuring phase velocity of longitudinal ultrasonic waves

Piotr Kielczynski¹, Marek Szalewski¹, Aleksander Rostocki², Maciej Zduniak², ¹Institute of Fundamental Technological Research, Polish Academy of Sciences, Warsaw, Poland, ²Warsaw Technical University, Poland

Background, Motivation and Objective

Monitoring and studying the pressure effect on liquid properties are becoming increasingly important in food, chemical, cosmetic and pharmaceutical industry as well in laboratory research. High-pressure technologies (pressures up to 1 GPa) have proved a great potential in modern bioengineering as a method of modification of biotechnological materials. The knowledge of physical properties (e.g., velocity, compressibility etc.) of treated substance is essential for understanding, design and control of the process technology. Measurement techniques for in-situ determining of physical parameters of liquids (e.g., phase velocity) under high pressure allow insight into the phenomena governing the microstructural modifications.

Statement of Contribution/Methods

The ultrasonic method for the measurement of the physical parameters of liquids under high pressure was introduced. To this end, the authors have constructed a new ultrasonic setup. This setup was especially designed to obtain a low level of parasitic ultrasonic signals. A special mounting of the transducer in the high-pressure chamber as well as a proper reflector was fabricated. The transducer was 5 MHz LiNbO₃ (Y 36 cut) plate. The phase velocity of the longitudinal ultrasonic wave was measured using a cross-correlation method to evaluate the time of flight (TOF) between first and second echoes. This assured a high accuracy of the experimental results.

Results

The measurements of the phase velocity and compressibility of vegetable oils were carried out in function of hydrostatic pressure up to 700 MPa. During the measurement we stated the phase transformation of investigated oils (e.g., soya oil). During the phase transition the increase of phase velocity was observed. After the phase transition the phase velocity has risen to the new value characteristic for the high-pressure phase of oil. The decomposition of the high-pressure phase during the decompression process has shown large hysteresis of the dependence of velocity on pressure.

Discussion and Conclusions

To the authors' knowledge, the measurement of the phase velocity of liquids under high pressure during the phase transition and during the decompression process is the novelty.

The usefulness of the constructed ultrasonic measuring setup for determining the phase velocity of oils at high-pressure has been stated. The proposed ultrasonic method can be computerized. This enables continuous (on-line) monitoring of the physical parameters of liquids, in-situ during the course of technological processes. Application of ultrasonic methods will provide real-time process monitoring and control thereby reducing down time and increasing product quality.

P1-M-03

Measurements under High Pressure of Ultrasonic Wave Velocity in Glycerol

Hassina Khelladi¹, Frédéric Plantier², Jean Luc Daridon³, Hakim Djelouah³, ¹Faculté d'Electronique et Informatique, Université des Sciences et de la Technologie Houari Boumediene, Alger, Algeria, ²Université de Pau et des Pays de l'Adour, France, ³Faculté de Physique, Université des Sciences et de la Technologie Houari Boumediene, Algeria

Background, Motivation and Objective

Glycerol is used in nature as a cryoprotectant and has been the focus of study by researchers in cryopreservation. Indeed, the cryonics is to cryopreserve humans (kidneys, brains...) so that future technology may one day restore those people to a disease free and aging free life. The means to this end is to reduce or eliminate the damage caused to tissues by freezing water. Cryoprotectants (anti-freeze agents) are the usual means to eliminate ice crystals, where high pressure is needed to assist some cryoprotectant in the cryopreservation of some tissues.

Statement of Contribution/Methods

As a lack of data concerning glycerol at elevated pressure is observed, measurements under high pressure of the ultrasonic wave velocity in glycerol and versus temperature are carried out, from which a number of important thermodynamic properties could be derived and determined as a function of pressure and temperature. A high pressure measurement cell equipped with temperature and pressure monitoring and control instrumentation is used. A time of flight method is exploited to measure, under high pressure, the ultrasonic wave velocity at different temperatures. The pressure and temperature ranges exploited in this experimental investigation of various glycerol

properties, are extended respectively from 0.1MPa to 100MPa and from 10°C to 100°C. For each isotherm, the pressure step of two consecutive measurements is 10MPa. When the isotherm is entirely covered, the temperature value is increased by 10°C step.

Results

The ultrasonic wave velocity in glycerol shows a monotonous behavior of c_0 versus (P, T) and $1741.03 \text{ m/s} < c_0 < 2153.36 \text{ m/s}$ in the investigated ranges. The ultrasonic wave velocity measurements are tainted with an inaccuracy lower than 0.2%. The experimental data of ultrasonic wave velocity in glycerol combined with measurements at atmospheric pressure, of density, specific heat and thermal expansion coefficient are used to derive density at elevated pressures. The obtained values of glycerol density are comprised between 1209.27 kg/m^3 and 1291.01 kg/m^3 . As isentropic compressibility is linked to ultrasonic wave velocity and density by means of the Newton-Laplace equation, this intrinsic physical property is easily deduced. Thus, the adiabatic compressibility coefficient in glycerol shows a monotonous behavior of χ_s versus (P, T) and $0.167 \text{ (GPa)}^{-1} < \chi_s < 0.273 \text{ (GPa)}^{-1}$ in the explored ranges.

Discussion and Conclusions

The obtained measurements of some glycerol properties, under static pressure and at various temperatures constitute a database which can provide in the future a useful tool to test liquid state theory. Future studies will concentrate on the effect of pressure on hydrogen bonding in glycerol by using molecular simulation.

P1-M-04

Electromechanical Properties of Tourmaline Single Crystals up to 1050 K

Chandra Shekhar Pandey¹, Jürgen Schreuer¹; ¹Institut fuer Geologie, Mineralogie und Geophysik, Ruhr-Universitaet Bochum, Bochum, NRW, Germany

Background, Motivation and Objective

Tourmalines are complex borosilicate minerals with favorable electromechanical properties like high ultrasound velocities in combination with low acoustic attenuation. In contrast to α -quartz, LiNbO₃ and Ca₃Ga₂Ge₄O₁₄-type crystal species, for example, the application of tourmalines up to their decomposition temperature at about 1150 K is not limited by phase transitions, electrical conductivity or strong ultrasound dissipation effects. However, because all attempts to grow large single crystals were not successful so far one has to use natural crystals with highly variable chemical composition. Unfortunately, the dependence of the relevant electromechanical properties on composition and temperature has not yet been studied in detail. Therefore, we measured in the temperature range from 150 K to 1050 K the coefficients of thermal expansion, dielectric constants, piezoelectric constants and elastic stiffnesses of natural gem-quality tourmaline crystals (point group 3m) belonging to the elbaite-schörl solid solution series.

Statement of Contribution/Methods

To this end a combination of different experimental techniques were used which includes differential scanning calorimetry, high-resolution dilatometry, and the innovative method of resonant ultrasound spectroscopy. The well-known substitution method was employed for dielectric constant measurements. The chemical composition was obtained from electron microprobe analysis, atomic absorption spectroscopy and the Karl Fischer method (determination of water content).

Results

The anisotropy of thermal expansion, dielectric constants and of elastic properties of tourmaline at room temperature correlates well with structural features. Contrary to earlier studies we observed with increasing iron content a slight decrease of the mean elastic stiffness whereas the piezoelectric constant e_{311} increases significantly. However, this behavior fits well to the compositional dependence of elastic constants reported for other iron-bearing silicates. The temperature evolution of the elastic constants is almost linear without any hint on anelastic relaxation effects. Above about 850 K small, poorly reproducible anomalies occur which are probably related to the propagation of micro-cracks. Room temperature dielectric constants k_{11} and for k_{33} are independent of frequency up to 1 MHz. Their temperature evolution is almost linear with temperature coefficients of about $5 \cdot 10^{-4} \text{ K}^{-1}$.

P1-M-05

LGS as a crystal for MEMS. Micromachining in HCl:H₂O, Anisotropy, Database and Simulations

Colette TELLIER¹, Mariam AKIL², Thérèse LEBLOIS³, ¹Frequency and Time, Institut FEMTO-ST, Besançon, France, ²FEMTO-ST, France, ³Institute FEMTO-ST, France

Background, Motivation and Objective

MEMS applications of quartz make this crystal very attractive for the development of resonant microsensors. Languisite (LGS) is considered as a crystal alternative to quartz. However up to now there is a lack of information on the wet micromachining of LGS. So this paper starts with the first complete characterization of the micromachining of 3D microstructures on LGS plates. The objective is an accurate adjustment of the database of the self elaborated simulator TENSOSIM in order to build an efficient tool for the CAD of LGS resonant structures.

Statement of Contribution/Methods

Circular and square SiO₂/Si₃N₄ masks are patterned on differently oriented LGS plates. Membranes and mesas are etched at 80 °C in a HCl solution of composition 2:1. The anisotropy of 3D shapes is studied by SEM examination. The dissolution constants that constitute the database of the simulator TENSOSIM are then determined by an iterative procedure. Simulations of 3D etching shapes are performed to validate the database and the procedure is stopped when a fair agreement is observed between simulated and experimental shapes.

Results

The anisotropy of the wet etching is found to be of type 2 as quartz rather than of type 1 as silicon. Micromachined membranes and mesas are bounded by curved facets and “square” membranes show curved contours at corners. But for some orientations in contrast with quartz mesas are partly affected by a marked convex undercutting. However the main conclusion is that a great number of differently oriented surface elements limit etched structure as for the anisotropy of type 2. Hence only a simulator based on a kinematic model such as TENSOSIM is suitable to reproduce final 3D etching shapes. The precision of the simulation depends primarily on the database construction. So the procedure outlined above is used to adjust progressively the database of the simulator. As a result the simulator with this database generates 3D etching shapes in agreement with experimental shapes. In particular the numerical precision is very satisfactory for evolving shapes at concave and convex corners.

Discussion and Conclusions

Clearly only a continuum analytical model of the chemical etching can describe the observed anisotropy of shape revealed by differently oriented LGS microstructures. Accordingly the database of the continuum simulation tool TENSOSIM must be adjusted to avoid differences between experiments and simulations. In this work we are successful in determining a consistent database. Accordingly numerical 3D etching shapes derived with the proposed database are very close to experimental shapes. Extension of our simulations to resonant microstructures such as cantilevers and beams clamped at the two ends is very promising. A future objective is thus to combine simulations of 3D shapes with FEM analysis for an efficient design of new resonant structures.

P1-M-06

Characterization of ZnO Polycrystalline Films on Silica Glass by the LFB Ultrasonic Material Characterization System

Jun-ichi Kushibiki¹, Mototaka Arakawa¹, Takanori Kondo¹, ¹Electrical Engineering, Tohoku University, Sendai, Miyagi, Japan

Background, Motivation and Objective

ZnO films have been widely used for bulk-wave ultrasonic transducers as well as SAW devices as a piezoelectric material. It is a very important research subject to have knowledge of their acoustic properties for device design and simulation. The film acoustic properties should be different from bulk acoustic properties and between single-crystalline and polycrystalline thin films, depending upon the different fabrication conditions and methods such as sputtering and chemical vapor deposition. Thin film characterization is one of the important applications of the line-focus-beam ultrasonic material characterization (LFB-UMC) system which can precisely measure the velocity of leaky surface acoustic waves (LSAWs) on a water-loaded specimen surface. Layered structure exhibits fH (product of ultrasonic frequency f and film thickness H) dependence in the LSAW propagation characteristics. In this paper, we try to make measurement procedures for a layered structure sample of ZnO film on synthetic silica (SiO₂) glass substrate.

Monday
Poster

Statement of Contribution/Methods

We prepared two specimens of ZnO film on SiO₂ substrate. Sample A was fabricated by DC sputtering ($H=0.887 \mu\text{m}$), and sample B, by RF magnetron sputtering ($H=0.807 \mu\text{m}$). Their FWHM (full width at half maximum) values in rocking curves for (002)-ZnO by X-ray analysis were 10 deg and 2 deg. We measured the fH dependences in 1-MHz steps from 100 to 300 MHz at central positions for the two specimens. We also measured line-scan results over 45 mm for the two specimens including result for SiO₂ glass substrates. The measured results were discussed in comparison with numerically calculated results using the published constants for ZnO and SiO₂.

Results

We obtained remarkable fH dependence from 3425 m/s for SiO₂ to 2673 m/s for Z-cut ZnO in numerical calculations, and compared the numerical results with the experimental result of line-scanned velocity distribution at $fH=200 \text{ Hz}\cdot\text{m}$. The velocities for sample A became minimum (3146.5 m/s) around central position, and increase by 54 m/s for 9-mm line scan toward peripheral part of the ZnO-film region (deposition area of 10 mm in diameter), while the velocities for sample B had almost constant value of 3157.5 m/s. The measured values were lower than the calculated value of 3162.4 m/s that could be due to degradation in c-axis orientation of ZnO films.

Discussion and Conclusions

The LSAW velocity distribution observed for sample A should correspond to variations in ZnO film thickness. It was estimated from the fH dependence that the film thickness decreases about 0.13 μm over 9 mm in diameter. From the above results, we can say that the LFB-UMC system is very useful for thin film characterization, having the capability of evaluating acoustic property changes by variations of acoustical physical constants that should be related to the crystal quality of c-axis orientation in polycrystalline and single-crystalline films.

P1-N. Physical Acoustics: Modeling & Simulation

Sala Orange

Monday, September 21, 2009, 10:00 am - 11:30 am

Chair: **Ji Wang**
Ningbo University

P1-N-01

Theory of SAW propagation in crystals subjected by the pure bend influence

Boris Sorokin¹, Alexander Marushyak², Sergei Burkov¹, Kirill Aleksandrov^{3,1} *Condensed Matter Physics, Siberian Federal University, Krasnoyarsk, Russian Federation,* ²*Thermotechnical Institute, Krasnoyarsk, Russian Federation,* ³*L.V.Kirensky Institute of Physics, Russian Federation*

Background, Motivation and Objective

Conditions and parameters of SAW propagation in crystals are of great interest to design new controlling acoustic devices or sensors. So it may be control the SAW parameters in the way of the mechanical boundary conditions change. In particular an external influence often has a result the non-homogeneous deformation of SAW sensor.

Statement of Contribution/Methods

SAW propagation conditions changed by crystal sample pure bend have considered. SAW propagation in crystals under the action of the bend is described by:

$$\det(\Gamma_{BA} - \rho_0 v^2 \delta_{BA}) = 0$$

where Green-Christoffel's tensor has a linearising form

$$\Gamma_{BA}(\tau) = [C_{FBAE} + (\delta_{BA} \delta_{KF} \delta_{SE} + 2C_{FBLE} S_{LAKS} + C_{FBAEPQ} S_{PQKS}) \tau_{KS}] N_F N_E.$$

Thermodynamic stresses tensor can be written as

$$\tau = C_{KSLM}^*(\eta) \eta_{LM},$$

where static finite deformation tensor

$$2\eta_{LM} = (\xi_{a,L} \xi_{a,M} - \delta_{LM}),$$

and effective elastic constants

$$C_{KSLM}^*(\eta) = C_{KSLM} + \frac{1}{2} C_{KSLMRT} \eta_{RT},$$

are the functions of finite deformation gradients

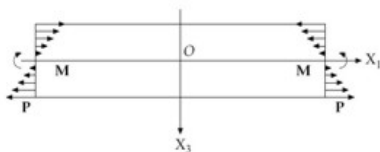
$$\xi_{a,L} = (\delta_{aL} + k \delta_{af} (S_{FRL} X_R + S_{FL11} X_3)) \quad (S_{FRL} = (S_{FR11} \delta_{3L} - S_{LR11} \delta_{3F}))$$

Results

Boundary conditions for SAW propagation on the surface of thick crystalline plate ($h \gg \lambda$) have formulated. Figure presents sample configuration and profile of loading. Computer simulation of SAW propagation under the bend influence for a lot of crystal directions and cuts has made using sillenite structure crystals as a model media. SAW velocities dependences on deform influence have obtained.

Discussion and Conclusions

In the initial approximation the non-homogeneity of crystalline plate deformation leads to change of wave velocity and wave front location. Attenuation conditions of wave partial components are changed too. Results obtained can be used to optimize the form and crystal orientation of sensor's elements.



Monday
Poster

Influence of pure bend of crystal on bulk acoustic waves propagation

Boris Sorokin¹, Alexander Marushyak², Kirill Aleksandrov³, ¹*Condensed Matter Physics, Siberian Federal University, Krasnoyarsk, Russian Federation,* ²*Thermotechnical Institute, Krasnoyarsk, Russian Federation,* ³*L.V.Kirensky Institute of Physics, Krasnoyarsk, Russian Federation*

Background, Motivation and Objective

To describe the acoustic device in which crystal element can be effected by the action of non-homogeneous deformation it is necessary to know the real deformation gradients. But the task of static finite non-homogeneous deformation for arbitrary symmetry crystal had'nt solved in common way now. It is especially important in the cases having a practical interest such as propagation of bulk acoustic waves (BAW) under the above mentioned conditions, for example BAW-sensors of force, acceleration or pressure. In this paper the model of calculation of finite deformation gradients applied to BAW propagation in anisotropic media has been introduced.

Statement of Contribution/Methods

BAW propagation in crystals under the action of bias finite stress is described by:

$$\det(\Gamma_{BA} - \rho_0 v^2 \delta_{BA}) = 0 \quad (1)$$

But Green-Christoffel's tensor has a modified form

$$\Gamma_{BA}(\tau) = [C_{LA} C_{FBLE} + \delta_{BA} \tau_{FE}] N_i N_E \quad (2)$$

Tensors of finite deformation C_{LA} , thermodynamic stresses τ_{FE} and effective elastic constants are the functions of finite deformation gradients $\xi_{\alpha,S}$. In the non-homogeneous case there is the $\xi_{\alpha,S}$ coordinate dependence.

Geometrical non-linearity factor in linear approximation was taken into account in the task of pure bending of crystal element. Non-homogeneous deformation was created by force moments applied to the ends of crystal sample. Under such condition we can obtain the exact form of deformation gradients:

$$\xi_{\alpha,L} = \delta_{\alpha L} + k \delta_{\alpha F} (S_{FRL} X_R + S_{FL1} X_3) \text{ where } S_{FRL} = (S_{FR11} \delta_{3L} - S_{LR11} \delta_{3F}) \quad (3)$$

Calculation of finite deformation tensors was produced by expressions:

$$2\eta_{LM} = (C_{LM} - \delta_{LM}), C_{LM} = \xi_{\alpha,L} \xi_{\alpha,M} \quad (4)$$

Results

Gradients (3) have been used in the numerical calculations of wave propagation in sillenite structure crystals for various crystal directions. Distribution of static deformation fields along the crystal has obtained.

Discussion and Conclusions

As a consequence of deformation's non-homogeneity effects of local dependence of velocities and wave propagation direction from coordinates values inside the crystal have raised. So the turn or distortion of wave front can exist. The results obtained can be used to solve a similar tasks for any symmetry crystals if its nonlinear elastic properties are known.

A Novel Method for Numerical Simulation of Sound Wave Propagation Using Heptic Interpolation Profile Method

Kan Okubo¹, Takao Tsuchiya², Ryo Seta¹, Norio Tagawa^{1,†} *Tokyo Metropolitan University, Japan,* ²*Doshisha University, Japan*

Background, Motivation and Objective

Numerical analyses for sound wave propagation in time domain have come to be investigated widely as a result of progress in computer technologies. Although many numerical schemes have been proposed for time domain analysis, the finite difference time domain (FDTD) method is the most popular scheme used in acoustics. However, we know that the scheme easily causes errors due to numerical dispersion. This means that the scheme is not so suitable for the analysis including rapid pressure changes. Therefore, it has become an important issue to reduce numerical dispersion error. This study presents a new numerical simulation of sound wave propagation using heptic interpolation profile (HIP) Method. This is a kind of method of characteristic (MOC), which belongs to a group of cubic-interpolated pseudoparticle (CIP) and interpolated differential operator (IDO) methods.

Statement of Contribution/Methods

Figure 1 shows the numerical grid model used in the HIP simulation for three-dimensional (3-D) sound wave propagation. This method uses the collocated grids, whereas the staggered grids are used in the FDTD method. Moreover, the method involves the use of the values of the acoustic field and their spatial derivatives at four grid points.

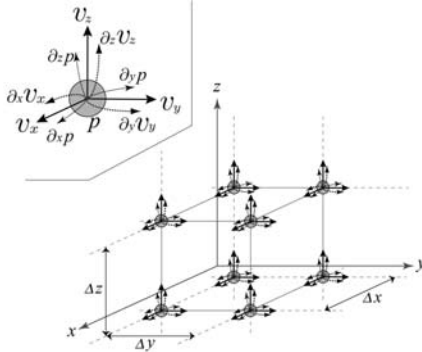
Monday Poster

Results

The results obtained by the HIP method, the FDTD method, and CIP method were compared for a 3-D acoustic field. The results indicate that HIP analysis provides much higher accuracy than other conventional methods. Numerical error of the HIP result increases little with the propagation distance. We also investigated the run-time and memory required for those methods. These results reveal the following: HIP analysis requires a little more run-time than other analyses, when equivalent discretization is used, whereas HIP analysis requires the same memory as CIP analysis. However, the calculated results indicate that the HIP analysis engenders less numerical error.

Discussion and Conclusions

We examined HIP method, which is a novel technique of numerical simulation of sound wave propagation. Results of this study demonstrate that this method can analyze wave propagation with high accuracy. Especially, it is noteworthy that the field wavefront remains uniform as it propagates. That is because HIP analysis provides higher accuracy concerning phase. We must intend to investigate a hybrid method with other method (e.g., CIP) in the near future.



P1-N-04

Numerical simulation of parametric field patterns of ultrasonic transducers arrays

Milan Cervenka¹, Michal Bednarik², Petr Koniccek²; ¹Czech Technical University in Prague, Faculty of Electrical Engineering, Prague 6, Czech Republic, ²Czech Technical University in Prague, Faculty of Electrical Engineering, Czech Republic

Background, Motivation and Objective

The paper is concerned with numerical modeling of planar 2D ultrasonic transducers arrays for highly directional transmission of audio-frequency sound in air. As it is well-known, nonlinear interactions of pre-processed audio signal modulated on intense ultrasonic carrier wave can be utilized for ensuring directivity of the transmitted low-frequency acoustic wave with preserving small radiator dimensions. If an array of many conventional relatively low-cost electrostatic transducers is used for this purpose, it is reasonable to study suitable deployment configurations of individual transducers in order to obtain optimum radiation pattern of primary and secondary acoustic fields. Such a parametric acoustic source can be subsequently utilized as a highly directional loudspeaker for many applications, e.g. acoustic diagnostics and nondestructive testing.

Statement of Contribution/Methods

As the proposed transducer arrays consisting of many circular radiators don't have radial symmetry, direct integration of the KZK equation for study of the parametric wave patterns would require huge computational demands. For this reason, a multi-Gaussian beam (MGB) model was utilized for an analytical description of the primary-wave beam, whereas method of successive approximations was used for quasi-linear evaluation of self-demodulated wave pattern using only single spatial integration. Even if the coefficients sets for the MGB decomposition of some transducer velocity distributions were previously published in literature, simple and effective algorithm based on Evolution strategies (ES) stochastic techniques was proposed for calculation of these coefficients for arbitrary transducer velocity distributions.

Results

Using proposed ES stochastic algorithm, original sets of the MG beam decomposition coefficients were calculated in order to increase efficiency/accuracy of the field calculation scheme. The numerical results show that even if the primary field patterns noticeably depend on the distribution of the ultrasonic transducers in the array (amplitudes of the off-axis side lobes), the secondary fields (self-demodulated audio waves) show similar directivity patterns. Out of the studied array configurations with 61-64 transducers (rectangular, hexagonal, rectangular/hexagonal), the

combination of rectangular/hexagonal symmetry of transducers deployment provides primary acoustic field with the least conspicuous off-axis side lobes.

Discussion and Conclusions

Method of multi-Gaussian decomposition was shown to be an efficient tool for study of parametric fields transmitted by arrays consisting of many individual transducers. Using of Evolutionary algorithms for decomposition of transducer velocity distribution into series of Gaussian functions seems to be promising, simple and efficient approach.

Monday Poster

P1-N-05

A Theoretical Potential-Well Model of Acoustic Tweezers

Shih-Tsung Kang¹, Chih-Kuang Yeh¹; ¹Department of Biomedical Engineering and Environmental Sciences, National Tsing Hua University, Hsinchu, Taiwan

Background, Motivation and Objective

Surface-modified drug vehicles have been popularly used in targeting image and local therapy. To increase the drug targeting efficiency, we propose an acoustics-vortex based trapping model of acoustic tweezers to manipulate small particles. The principle of the trapping model is similar to the phenomenon of dark hole induced by optical vortex. One multi-element ultrasound transducer is adopted to produce an acoustic-filed specific potential well and thus particles are expected to trap within the well.

Statement of Contribution/Methods

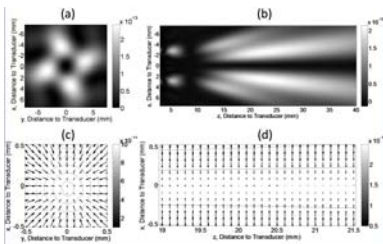
Trapping force and region in an acoustic-based potential well are assumed in Rayleigh regime. The potential well can be formed by an acoustical vortex which has corkscrew of waves transmitted by a multi-element transducer with different phases. Transmission waves with different phases would produce the constructive and destructive interference, and form a ring like acoustic field along the wave propagation direction. The results show that there is relatively low potential energy at the center of the ring, as well as potential well.

Results

A four-element planar transducer was used to transmit 1-MHz and 1-MPa sine waves at phase increment of pi/4 in the simulations. The polystyrene particles with sizes smaller than 23-um were considered as the drug vehicles. The figure (a) shows that the ring structure of the acoustical vortex produces a 2.5 mm wide potential well at the location of 20 mm from the transducer in X-Y plane; (b) shows the presence of the potential well in X-Z plane. The arrows in (c) and (d) indicate that particles inside the potential well sustain forces about 10-100 pN toward the axis. It is expected that the particles would be pushed forward and then aligned on the axis.

Discussion and Conclusions

Different phases, element configurations, and particle materials were also considered to compare the structure and strength of the potential well in the study, respectively. The volume of the potential well is expected to trap substantial vehicles. It should be noted that the effect of non-linear wave propagation should be minimized to retain the complete structure of potential well for practical application. In the future, the manipulation of microbubbles is of particular interest to assist in ultrasound targeted imaging and drug delivery.



P1-N-06

Attenuation of ultrasound pressure fields described via contrast source formulation

L. Demi¹, M.D. Verweij², J. Huijssen², N. de Jong³, K.W.A. Dongen¹: ¹Laboratory of Acoustical Imaging and Sound Control, Faculty of Applied Sciences, Delft University of Technology, Delft, Zuid-Holland, Netherlands, ²Laboratory of Electromagnetic Research, Faculty of Electrical Engineering, Mathematics and Computer Science, Delft University of Technology, Delft, Zuid-Holland, Netherlands, ³Laboratory of Experimental Echocardiography, Erasmus Medical Center, Netherlands

Background, Motivation and Objective

Experimental data reveal that attenuation is a relevant phenomenon in medical ultrasound. The phenomenon is particularly important for applications that are based on nonlinear propagation, since the higher frequency components of the pressure field generally experience greater attenuation.

Therefore a method that is able to model attenuation accurately is essential for, e.g., the design of transducers for novel ultrasound modalities.

Statement of Contribution/Methods

Attenuation can be modeled via a compliance memory function that describes how the dilatation rate, up to a particular moment, contributes to the pressure at that moment.

This model is used to define a contrast source that accounts for the attenuation. The resulting integral equation is solved using the Neumann iterative solution.

Results

For the 1D case, the present approach is compared with the method where attenuation is included in the Green's function. For a 1 MHz pressure field in liver tissue and a propagation distance of 50 mm, the relative error in the present method, after 3 iterations, compared to the method with a lossy green's function, equals 8.1×10^{-6} . Consequently the results are in close agreement with each other. The convergence of our scheme is investigated for relevant media (e.g. blood, brain, liver) and with respect to frequency, depth and attenuation parameters.

Finally, as an example, the 1D attenuative and nonlinear wave field in liver is modeled by including a loss term in the contrast source of the lossless INCS method. This method and the INCS method with an attenuative Green's function produce identical results.

Discussion and Conclusions

A method has been developed to model attenuation via a contrast source formulation. The obtained results are in excellent agreement with the approach where the attenuation is included in the Green's function.

P1-N-07

Application of Waterman-Truell and the generalized self-consistent model to the human bone case

Alejandro Villarreal¹, Miguel Molero², Lucia Medina³: ¹Biomedical Engineering, Universidad Autonoma Metropolitana, Mexico, ²Systems, Instituto de Automática Industrial, Spain, ³Acoustics, Universidad Nacional Autonoma de Mexico, Mexico

Background, Motivation and Objective

The present study is concerned with the interaction between ultrasonic radiation and human bone. The human bones are porous material may be considered as a heterogeneous media with cylindrical-shaped inclusions randomly distributed. The ultrasonic plane wave traveling in such materials is scattered due to the inclusions resulting in frequency-dependent velocity and attenuation of the scattered wave.

Statement of Contribution/Methods

The interaction between ultrasonic radiation and human bone is analyzed based on the multiple scattering theory of Waterman-Truell and the generalized self-consistent model (GSCM). The Waterman-Truell theory gives the formulation of scattering waves due to randomly distributed inhomogeneties in a material. The generalized self-consistent model allows us to determine the dynamic effective moduli of a heterogeneous material as a function of the carrier frequency and inhomogeneties concentration.

An analytical expression based on this theoretical background is applied for the human bone interacting with an ultrasonic source. In this paper the bone pores are considered infinitesimal length cylinder with a wavelength size diameter and filled with marrow. Bone pores were randomly distributed in a matrix of calcium material with no interaction between inclusions

Monday
Poster

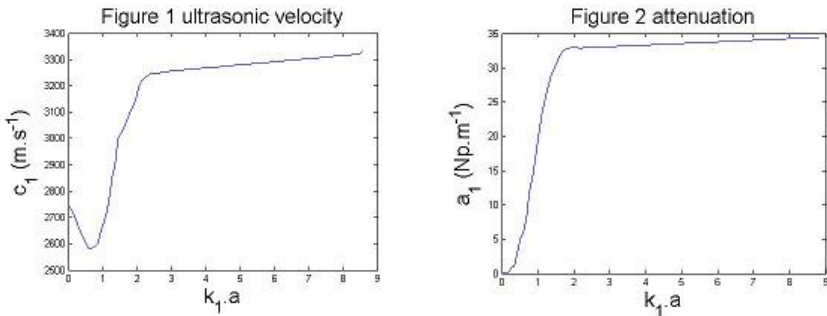
Results

The effective acoustic properties were computed for the arrangement above using the composite method proposed here. Figures 1 and 2 show theoretically acquired results of phase velocity and attenuation of the ultrasonic wave at a given concentration.

Discussion and Conclusions

Our results showed a good agreement with those published in the literature.

Monday
Poster



P1-N-08

2D Finite Impulse Response filters for surface wave identification.

Loïc Martinez¹, Nicolas Wilkie-Chancellier¹, Bart Sarens², Christ Glorieux²; ¹SATIE Université de Cergy, France, Metropolitan, ²ATF, University of Leuven, Belgium

Background, Motivation and Objective

Acoustic surface waves are widely used to sense and map the properties of the propagation media. For decreasing both the acquisition time of such signals along the region of interest (ROI) and reach useful space-time resolutions, impulse generation for wideband acquisitions are required. This is at the cost of increasing the post-signal processing complexity. Methods such as 2D and 3D Gabor analysis are powerful for localizing and identifying both transient and surface waves, as they need no prior knowledge upon the involved signals. Nevertheless, knowing which wave is observed, extracting the full bandwidth contribution of one surface wave from the others and to map it in the signal domain is also of great interest. As in the Fourier domain, the acoustic energy is concentrated along the wave-number frequency ($k-\omega$) dispersion curves, a way to extract one wave from others is to filter the signals by mean of $k-\omega$ band-pass area that keeps only the selected surface wave. The objective of the present paper is to propose 2D Finite Impulse Response (FIR) filters based on an arbitrary area shape.

Statement of Contribution/Methods

FIR filtering is based on convoluting the impulse response of the filter with the signals, so obtaining the impulse response corresponding to the desired filter function is one of the important steps. In the present work two impulse responses are investigated, they are derived from using $k-\omega$ rectangular areas (R-FIR) or elliptical areas (E-FIR). In both cases the main axis of the area is oriented along the selected surface wave dispersion curve. The advantage of such areas is to have the analytical formulas of the impulse responses, as a function of the k and ω bandwidth parameters, without the need to use Inverse Fourier transform. R-FIR impulse response is based on sinc functions, whereas E-FIR impulse response is based on Bessel functions.

Results

2D F-FIR and E-FIR filters are tested on experimental space-time signals corresponding to the propagation of Lamb waves observed by classic transducers on a cylindrical shell and by laser Doppler on a plate and generated by a pulse. R-FIR and E-FIR exhibit their potential for extracting very well Lamb modes, as their direction of propagation, even in noisy datasets. Due to their more natural round shape energy distribution in $k-\omega$ space, E-FIR filtering adds less artefact to the filtered signals. By using wide k -bandwidth and narrow ω -bandwidth E-RIF or R-FIR filters, Gabor like analysis can also be achieved. Results in terms of space-time- $k-\omega$ localisation are discussed and compared with Gabor analysis.

Discussion and Conclusions

E-FIR is a good alternative to Gabor analysis, with the ability to be more flexible. E-FIR can be extended to non-uniform sampled data and to 3D datasets.

P1-N-09

Modelling Ultrasonic Wave Propagation in Multilayered Medium of Resistance Spot Weld

Janusz Kocinski¹, Pawel Kustron¹, Andriy Chertov², Andrzej Ambroziak¹, Roman Gr. Maev^{2,1} *Mechanical, Wrocław University of Technology, Poland, ²University of Windsor, Canada*

Background, Motivation and Objective

The poster presents the results of modelling of ultrasonic waves propagation in multi-layered media. The analysis allow better understand the wave behaviours and visualize phenomena accompanying its propagation.

Statement of Contribution/Methods

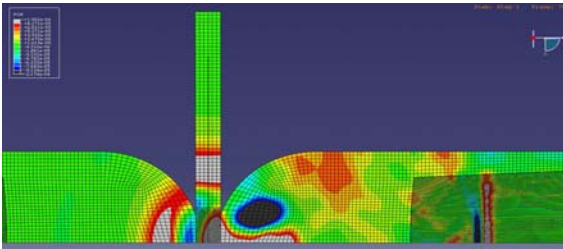
Using the Finite Element Method (FEM) a simulation of wave propagation was developed for the case of resistance spot welds. The simulation allows see factors affecting wave propagation through the structure of inhomogeneous layers. Here, inhomogeneity is generated by uneven temperature distribution within the sample causing phase transformation in some cases. FEM analysis is a good way to understand the temperature influence on such parameters as waves time of flight, amplitude dynamics. The models took into account possible geometry variations.

Results

The FEM simulation results were compared with data obtained with ultrasonic system for real-time quality characterization of spot welds. The analysis indicates high correlation with experimental data, what confirms that models were created correctly and that simplifications had no significant influence on the results.

Discussion and Conclusions

FEM is a good technique to visualize the behaviour of ultrasonic wave propagation. Using obtained results it was possible to optimize electrode cap geometry to improve efficiency of real-time testing system by reducing beam divergence and increasing signal to noise ratio.



P1-N-10

Eigenfrequency of cavity resonators at different reflection conditions

Andreas Peter¹, Lothar Zipsner^{1,1} *HTW Dresden, Germany*

Background, Motivation and Objective

The objective of this study was to investigate the influence of inhomogeneities at the termination on the eigenfrequency f_0 of cylindrical cavity ultrasonic resonators. These inhomogeneities could be small bores or particular sonically soft terminations with a limited stiffness. Often, it is not possible to assume ideal boundary conditions.

Statement of Contribution/Methods

By using the complex wall impedance Z_W of the cavities termination, it is possible to calculate the complex reflection coefficient r . Here are 3 special cases of a non-complex reflection coefficient r , which are sonically hard ($r = 1$), sonically soft ($r = -1$) and impedance matching ($r = 0$). Real terminations, for example with small bores, will cause a complex reflection coefficient r . The complex reflection coefficient r enables the computation of the continuous change of the eigenfrequency f_0 of cylindrical cavity resonators.

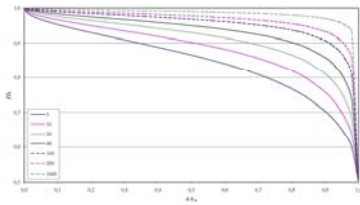
Results

We found a relation between the ratio of the area of open bores A to the area of the entire termination A_0 and the eigenfrequency f_0 of the cavity resonator. In addition, there is a possibility to predict the quality factor Q , the damping ratio ξ or the attenuation α of the cavity resonators in a real termination configuration.

Figure 1 shows the ratio of the changed eigenfrequency f to the eigenfrequency f_0 of ideal sonically hard termination as a function of the ratio of the area of bores A to the entire area A_0 of the termination. The parameter characterizes the ratio of the wall impedance Z_W to the characteristic acoustic impedance Z_0 of the gas filled cavity.

Discussion and Conclusions

A method is shown to predict the eigenfrequency f_0 of cylindrical cavity resonators. The virtual pipe extension ΔL can be computed as a function of the complex reflection coefficient r of a real termination. With the resulting virtual length L' of the pipe, it is possible to calculate the speed of sound c of the gas filled cavity resonator through measured eigenfrequencies f_0 , and by knowing the geometrical dimensions and termination characteristics.



Monday
Poster

P1-N-11

Frequency Domain Perfectly Matched Layers for Acoustic Scattering Integral Equation Problems

E.J. Alles¹, K.W.A. van Dongen^{1,†}:*Laboratory of Acoustical Imaging and Sound Control, Faculty of Applied Sciences, Delft University of Technology, Delft, Zuid-Holland, Netherlands*

Background, Motivation and Objective

In order to improve and develop novel ultrasound imaging techniques, accurate acoustical scattering simulations beyond the Born approximation are required. One technique to perform such simulations is solving, in the temporal Laplace domain, the full scatter integral equation.

In essence this is an inversion problem which involves a convolution of the Green's function with contrast source functions defined via products of the total field and the compressibility or density contrast profiles.

Difficulty arises at the boundaries of the spatial domain. Especially in situations where the inhomogeneities extend over these boundaries, unwanted additional reflections are generated which have to be suppressed.

Statement of Contribution/Methods

One possible technique to suppress these additional reflections is attenuating the scattered field within an absorbing boundary layer enclosing the computational domain. However, care has to be taken to avoid reflections off this absorbing layer.

For this reason, we derive a PML formulation for the scatter integral equation in the temporal Laplace domain by means of analytic continuation of the governing Helmholtz equation. Using this formulation, it becomes feasible to compute, for known contrast distributions and known incident field, the total field by applying a conjugate gradient (CG) inversion scheme while suppressing reflections off the boundaries. To the best of our knowledge, this PML technique has never been applied to integral equation methods. Note that the method is also applicable to e.g. electromagnetic simulations.

Results

The effectiveness and importance of the PMLs is demonstrated for various relevant three-dimensional situations. It is shown that strong attenuation is achieved, without reflections off the PML, where the absorbing layer is less than a wavelength thick. Compared to the situation without PMLs, no additional grid elements are required and the computational load of one CG-iteration is not significantly increased.

Discussion and Conclusions

In this paper, we include for the first time PMLs in an acoustic scattering integral equation formulation. We show that PMLs are effective and efficient in suppressing unwanted reflections off the computational domain boundaries. Contrasts in both density and compressibility are included.

P1-O. Thin Films-Growth and Characterization

Sala Orange

Monday, September 21, 2009, 10:00 am - 11:30 am

Chair: **Nobutomo Nakamura**
Osaka University

P1-O-01

Quasi-epitaxial growth of crystalline wurtzite AlN thin films on Si (001) by RF magnetron sputtering

Cinzia Caliendo^{1,2}, Patrizia Imperatori³, Guido Scavia³; ¹*Istituto dei Sistemi Complessi, Consiglio Nazionale delle Ricerche, Rome, Italy, Italy*, ²*ISC, CNR, Italy*, ³*ISM, CNR, Rome, Italy, Italy*

Background, Motivation and Objective

In the last few years aluminium nitride (AlN) has attracted much attention due to its wide band gap, its high chemical and thermal stability, high thermal conductivity and coefficient of thermal expansion. AlN also shows the highest surface acoustic wave among all the piezoelectric materials, good piezoelectric coupling coefficient, full compatibility with conventional silicon technologies, and high electrical breakdown voltage. All these remarkable properties lead to its application for optoelectronic and high power electronic devices.

Despite the lattice incoherency of Si(001) and AlN (20% lattice constants mismatch with the four-fold symmetry of the (100) Si plane), the wurtzite AlN film deposition on Si(001) substrates is a highly attractive goal for monolithic microwave integrated circuit technology and high frequency application.

Statement of Contribution/Methods

Piezoelectric AlN films were deposited on Si(001) substrates and the sputtering parameters were varied in order to optimize the technological process parameters. The optimization of the sputtering parameters (i.e., target-substrate distance, RF power, gas composition) resulted in the quasi-epitaxial growth of crystalline wurtzite AlN thin films. The structural, morphological and piezoelectric characteristics of the optimized films were studied with respect to the gas composition.

Results

All the AlN films present the hexagonal structure of wurtzite with a preferential orientation along the c-axis, perpendicularly to the growth plane. The full width at half maximum (FWHM) of the 002 peak ranges from 0.227 to 0.100° and in the fully 002 textured films it decreases with increasing the nitrogen amount in the gas mixture, indicating an improved crystallization.

The morphological evolution of the AlN layer was studied by AFM and a dependence of roughness and grain dimensions with the gas composition is showed. Roughness decreases reaching a minimum value of few nanometers. The increase of the nitrogen percentage leads to a gradual decrease in the grain size (150, 60 and 40nm for 50% 73% and 80-93%) and to a corresponding grain aggregation.

The piezoelectric strain constant d33 of the AlN films was measured by following the method described in ref. [1]. The evaluation and analysis of the d33 parameter revealed that the piezoelectricity of the sputtered films varies with the amount of nitrogen in the Ar/N2 mixture and it is correlated with the structural, electrical and morphological parameters. The estimated values of the d33 parameter ranged from 3.0 to 15 pC/N, the highest value being referred to the sample that shows the best crystalline quality and crystalline alignment.

Ref.1. C.K.Xu, V.N.Umashev, I.B.Yakovkin, Sov. Phys. PTE6, (1986) 192

Discussion and Conclusions

The maximum value of d33 = 15 pC/N has been found for the maximal FWHM. This value is by far larger than the bulk single crystal AlN constant would allow. Further analysis is necessary to fully understand such large d33 fluctuations.

P1-O-02

Switchable excitation of eigen acoustic modes in multilayer structures with ferroelectric films

Anatoly Mikhailov¹, Aleksandr Prudan¹, Sergei Ptashnik¹, Andrei Kozyrev¹; ¹Electronics, Saint-Petersburg State Electrotechnical University, Saint-Petersburg, Saint-Petersburg, Russian Federation

Background, Motivation and Objective

Multilayer structures, comprising thin films of barium-strontium titanate (BST) in the paraelectric (centrosymmetric) state are commonly used for frequency agile applications due to the dc bias dependent capacitance of the structure. However, if a dc bias is applied to the multilayer structure with ferroelectric film, the central symmetry of the BST crystal structure is broken due to electrostriction and piezoelectricity is induced. The multilayer structure in microwave frequency range seems like high Q-factor acoustic resonator with hypersound source, because the BST film generates bulk acoustic waves with microwave electric field frequency. Although this phenomena can be useful for development of novel class of microwave devices like tunable thin-film bulk acoustic resonators, oscillators, filters, etc., it is negative in point of the conventional microwave application of such ferroelectric capacitance structures.

Statement of Contribution/Methods

Existing to date analytical technique for this phenomena based on calculation of multilayer structure complex impedance. However, there are no data about spatial distribution pattern of eigen acoustic modes and the conditions of its excitation. Furthermore, this technique is suitable for multilayer structures with only one ferroelectric film. For structures based on two ferroelectric films the solution of electromechanical equations system with corresponding boundary conditions is needed.

Results

In present paper the variational-differential calculation of eigen acoustic modes of metal-dielectric-metal structure with both one and two thin ferroelectric films in paraelectric state is carried out. For estimation of excitation efficiency of bulk acoustic waves by ferroelectric films the system of electromechanical equations is solved and spatial distribution of mechanical displacement amplitudes along the multilayer structure is presented. Finally, the influence of the dc bias voltage both on the spatial distribution pattern of the acoustic standing wave in multilayer structure and on the resonance frequency shift is discussed. For multilayer structure with two ferroelectric films there is a possibility to apply the dc bias in opposite polarities that results in an antiphase generation of acoustic waves by ferroelectric films. Depends on the multilayer structure geometry, this phenomena leads to a cancellation of some eigen acoustic modes.

Discussion and Conclusions

The results of present work look very promising both for the microwave capacitance structures due to the suppression of additional loss mechanism and for the designing of novel switchable thin-film bulk acoustic resonators.

P1-O-03

The Magnetic Dependence of Properties of Optical Quantum Transition of ZnS and Ge of Electron- Piezoelectric Interaction System under Two Circularly Oscillating Fields

Sug Joung-Young¹, Lee Su-Ho², Choi Jun-Yong², Lee Jun-Tak³, Sa-Gong Geon³, Kim Jin-Gyou¹, Kwon Sung-Yeol⁴; ¹Kyungpook National University, Korea, Republic of; ²Kyungpook National University, Korea, Republic of; ³Dong-A University, Korea, Republic of; ⁴Pukyong University, Korea, Republic of

Background, Motivation and Objective

We have considered two systems - one is under a right circularly oscillating external fields (RCF) and the other is under a left circularly oscillating external fields (LCF). The main purpose of this work is to compare quantum transition line shapes (QTLs) and optical quantum transition line widths (QTLWs) under both directions right and left of circularly polarized oscillatory external fields.

We have applied the quantum transport theory (QTR) to the systems in the confinement of electrons by square well confinement potential. There are several methods of obtaining useful formulas for the scattering factors of the electron-background particle correlation response function. (1-15) One method is the projected Liouville equation method. Kenkre^{9,10} suggested a response formula that contains nonlinear terms and a linear term in the lowest order. The study of quantum transport theories based on the projected Liouville equation method is useful for investigating the scattering mechanism of solids. Using the projected Liouville equation method with the

equilibrium average projection scheme (EAPS), we have proposed a new quantum transport theory of the linear-nonlinear form[1]. The merit of using EAPS is that the generalized susceptibility and scattering factor can be obtained in a one-step process of expanding the quantum transport theory. The study of the dynamical behavior of electrons interacting with piezoelectric potential phonons in semiconductors has received a great deal of attention among condensed matter physicists. It is well known that wurtzite-type crystals e.g., (ZnO, CdS, CdSe, and AgI) and sphalerite-type crystals e.g., (ZnS, ZnSe, and GaAs) are piezoelectrically active. The reason we are interested in these materials is that they have excellent acoustoelectric properties and optical conductivity and thus can be used in diverse applications.

Through numerical calculation, we have analyzed the temperature and magnetic field dependences of QTLSs and QTLWs under both directions right and left of circularly polarized oscillatory external fields in various cases. The analysis of various cases is difficult using other theories because they require the calculation of absorption power to obtain QTLWs. However, we can obtain QTLWs directly using the EAPS. In order to analyze the quantum transition process, we compare the temperature and magnetic field dependences of the QTLWs and the QTLSs of two transition processes, the intra and inter-Landau level transition process.

Statement of Contribution/Methods

Results

Discussion and Conclusions

As a brief summary, the results indicate that the QTR of EAPS is a useful method to explain the resonant phenomena based on the quantum transition and scattering effect in a microscopic view. It is to be regretted that these results cannot be checked experimentally because no experimental results are available as yet. However, we expect the results in Figs. 1 and 4 to be of help in any future experimental works.

P1-O-04

The Temperature Dependence of Quantum Optical Transition Properties of GaN and GaAs in a Infinite Square Well Potential System

Lee Su-Ho¹, Sug Jung-Young¹, Choi Jun-Yong¹, Sa-Gong Geon², Lee Jun-Tak², ¹Kyungpook National University, Korea, Republic of, ²Dong-A University, Korea, Republic of

Background, Motivation and Objective

In this work, in GaN and GaAs, we investigate the optical Quantum Transition Line Shapes(QTLSs) which show the absorption power and the Quantum Transition Line Widths(QTLWs), which show the scattering effect in the electron-piezoelectric potential phonon interacting system. The reason why we are mostly interested in these materials are that they have excellent acoustoelectric property and optical conductivity and thus can be used for diverse applications including actinometers, fluorescent pigment and amplifiers for ultrasonic wave. The analysis of the temperature and the magnetic field dependence of the QTLWs are very difficult in alternative theories or experiment, because the absorption power in the various external field wavelengths is required to be calculated or observed. The QTR theory of EAPS is advantageous in this respect as it allows the QTLWs to be directly obtained, through EAPS, in the various external field wavelengths. In short the calculation of the absorption power is not required to obtain the QTLW. With the numerical calculation, we analyzed the temperature and the magnetic field dependences of the QTLWs and QTLSs in various cases. In order to analyze the quantum transition, we compare the temperature and the magnetic field dependences of the QTLWs and the QTLSs on two transition processes, namely, the phonon emission transition process and the phonon absorption transition process.

Statement of Contribution/Methods

Results

Through the numerical calculation of the theoretical result, of QTLS and of the QTLW, we analyze absorption power and line widths of Gallium-Nitride (GaN) and Gallium-Arsenide(GaAs).

In order to analyze the quantum transition process, we denote the total QTLW as γ_{total} , where, γ_{em} and γ_{ab} are the QTLW of the total phonon emission and absorption transition process, respectively.

In FIG. 1(a) the temperature dependence of QTLW is plotted. As shown in FIG. 1(a), γ_{total} increase as temperatures increase for the external field wavelengths, $\lambda = 220, 394, 513, 550$ and $550 \mu m$. In FIG. 1(b), the temperature dependence of the QTLW, $\gamma_{total}(T)$, $\gamma_{em}(T)$ and $\gamma_{ab}(T)$ of GaN for external field wavelength $\lambda = 394 \mu m$ is shown.

In FIG. 2(a) the temperature dependence of $\gamma_{total}(T)$ QTLW is plotted.

Discussion and Conclusions

In a summary, The approach to the analysis of quantum transition processes with ease is the merits of our EAPS theory. Through the analysis of this work, we found the increasing properties of QTLW and QTLS with the temperature and the magnetic fields. We also found the dominant scattering processes are the phonon emission transition process. The results of this work will help to analyze experimental the scattering mechanisms in the electron-piezoelectric potential interacting materials.

P1-O-05

Response of SAW on AlGaN/GaN Film for Ultra-violet Light Irradiation

Satoshi Oshiyama¹, Keishin Koh¹, Kohji Hohkawa^{1,2} *Kanagawa Institute of Technology, Japan*

Background, Motivation and Objective

AlGaN/GaN films have found many applications, such as in high-performance and high frequency front end integrated circuits. In addition, their piezoelectric properties have been researched extensively for developing high performance filters and semiconductor-coupled SAW devices. On the other hand, we have also interested in the ultra violet optical detector and tried to apply AlGaN/GaN film SAW device to this area.

Statement of Contribution/Methods

The AlGaN/GaN film is prepared on a (0001) Sapphire substrate and the aluminum mole fraction of AlGaN layer was nominally 0.255. The GaN layer thickness is about 2000nm. The AlGaN layer thicknesses are 20 nm. We have measured propagation properties of SAW delay devices by irradiating ultraviolet light swept from 200 nm to 380 nm. We radiated optical signal either direction from the film surface to the bottom, or vice versa (Fig. 1). In the experiment, we have also controlled 2DEG electrode existing on the interface between GaN and AlGaN by applying DC bias between 2 DEG layer and IDT electrodes.

Results

Figure 2 illustrates one of experimental results. When the wave length of light wave was reduced, the insertion loss of SAW devices has shown larger insertion loss. As is indicated by the arrow, the insertion loss curve had two stepping points corresponding to the band gap energy of GaN and AlGaN.

Discussion and Conclusions

We have measured basic ultraviolet optical properties of the AlGaN/GaN film on Sapphire substrate using a simple experiment equipment.

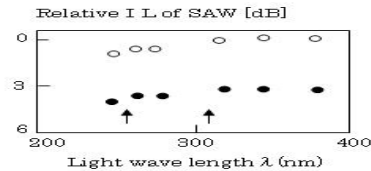
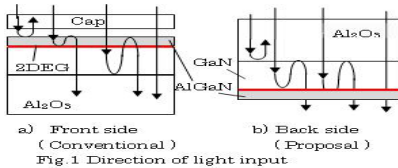


Fig.2 Wavelength dependence of relative I.L.

P1-P. Actuators and Pumps

Sala Orange

Monday, September 21, 2009, 10:00 am - 11:30 am

Chair: **Atsuyuki Suzuki**
Tokuyoma College of Technology

P1-P-01

Design and characteristics of novel type valveless micro-pump

Jin-Heon Oh¹, Jong-Nam Lim¹, Kee-Joe Lim¹, Hyun-Hoo Kim²; ¹Chungbuk National University, Cheongju, Chungbuk, Korea, Republic of, ²Doowon Institute of Technology, Paju, Gyeonggi, Korea, Republic of

Background, Motivation and Objective

Most of pumps consist of a chamber to be created by the deformation of actuator and the check valves to take an on/off role of input and output. But these valves have some problems such as abrasion, fatigue and clogging condition. In order to eliminate the critical problems, we apply the operation principle of traveling wave ultrasonic motor to the basis for a pumping mechanism of micro-pump that transfers fluids. We propose a simple and novel design of piezoelectric micro-pump which is driven peristaltically by piezoelectric actuators.

Statement of Contribution/Methods

In this pump, the extensional vibration mode due to the traveling wave excited in PZT ring is used as a volume displacing mechanism. Reviewing the operation principle of the traveling wave rotary type ultrasonic motor, it is easy to see the formation of multiple spaces due to the crests of the traveling wave. These spaces offer a platform for the transportation of capture fluid along the direction of the wave propagation. The greatest feature of this pump is not required the valves because the peristaltic action produces to the tightly closed space. As the voltage is turned off, the chamber formed by vibrator stops the flow of liquids, and then produces automatically self-locking action as the operation of conventional valves.

Results

Finite element analysis about the proposed pump model was carried out by commercial software to verify its operation principle. And, to ratify the concept of the pump and to make valid the simulation result, components of prototype pump were made, erected and tested.

Discussion and Conclusions

Using extensional vibration mode of PZT ring, a valveless micro-pump is successfully made. This pump takes a noticeable operation into the simple volume displacing mechanism using peristaltic motion without the physical moving parts.

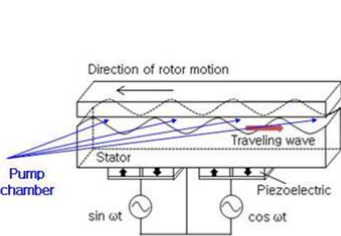


Fig.1. Operation principle of traveling wave rotary type ultrasonic motor

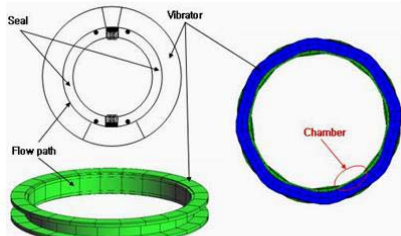


Fig.2. Entire shape and chamber formation of proposed micro-pump model

P1-P-02

Pneumatic Flow Control Valve Using Particle Excitation by PZT Transducer

Daisuke Hirooka¹, Koichi Suzumori¹, Takefumi Kanda¹; ¹Okayama University, Okayama, Japan

Background, Motivation and Objective

Pneumatic actuators such as pneumatic cylinders are widely used in the automation machine equipments because they are simple, lightweight, and high compliant. In general, pneumatic actuators need speed controllers to avoid the stopping shock at the stroke ends. But conventional speed controllers cannot smoothly control the airflow rate and this makes pneumatic actuators difficult to drive at high speed without shock at the stroke ends. This study develops a new tiny flow control valve driven by PZT transducer. This flow control valve solves all these problems while retaining the advantages of pneumatic actuators.

Statement of Contribution/Methods

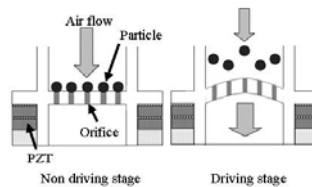
A PZT transducer has been used for controlling flow rate in this study. The flow control valve in this report consists of an orifice plate which has 13 orifices, a PZT transducer which is fixed on the orifice plate with the bolt, and the iron particles of 0.8mm diameter. The orifice plate is made of stainless steel and it is 10mm in diameter, 9mm in height and 0.8mm in plate thickness. The orifice aperture diameter is 0.5 mm and the orifices are circularly arranged with the intervals of 0.9mm on the orifice plate. The mass of the flow control valve is only 2.5 g. The valve is normally closed, because air flow carries the particles onto the orifice and the particles seal the air flow. Because the orifice plate excitation by the transducer works to make the particles away from the orifice plate, the air flows through the orifices.

Results

From the experiments of flowing quantity evaluation, this flow control valve achieves a maximum flow rate of 62.65 L/min under applying voltage of 79.9 V_{pp} and air pressure of 0.70 MPa.

Discussion and Conclusions

The results show that the ratio of the flow capacity /valve weight is about ten times larger than that of typical commercial valves.



P1-P-03

SAW Excitation by Using Pulse Wave

Ryo Tamon¹, Hiroyuki Kotani¹, Masaya Takasaki¹, Takeshi Mizuno¹; ¹Saitama University, Japan

Background, Motivation and Objective

Previously an active type surface acoustic wave (SAW) tactile display has been proposed. Using the SAW tactile display, we can feel tactile sensation like roughness or smoothness. Switching SAW, tactile sensation can be indicated. For expanding of the indication area of the display, the size of the SAW transducer must be expanded too. Property of the piezoelectric substrate had prevented the expansion. Indirect SAW excitation on a glass substrate has been proposed for the expansion. To realize a large size tactile display, array of the excitation can be applied.

However, in this method, the SAW has been excited by a bursted sinusoidal wave. For the arrayed indirect transducers, one high-frequency generator will be equipped for each transducer. To reduce the redundancy of the driving circuit, this paper proposes a new method for the SAW excitation using pulse wave. In this proposal, driving circuit can be simplified. Arranging a number of SAW transducer and driving individually, it is possible to focus the SAW on one point and increase the amplitude there. A large-area SAW tactile display can be realized.

Statement of Contribution/Methods

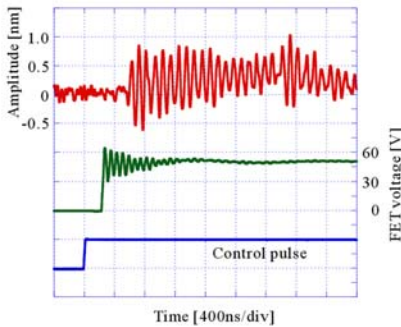
The conventional SAW exciting method used a bursted sinusoidal wave by a high-frequency function generator and a high-frequency amplifier. Proposed SAW excitation method uses much lower frequency square-wave pulse by low-cost pulse generator and FET driving circuit.

Results

Using the proposed method, 20 waves of the SAW were excited by rising edge of the square wave successfully (Fig.1). The wave number of the SAW is equal to the finger number of the interdigital transducer (IDT).

Discussion and Conclusions

Applying a high-voltage pulse wave to IDT, the SAW, whose wave number equals to the finger number of the IDT, was excited at the rising edge and the trailing edge. Arranging a number of SAW transducer and driving individually, a number of SAW propagate with lags. With the controlled lags, the SAW can be focused on one point and the amplitude can be increased there. It is expected that our proposal can be applied to the SAW tactile display.



P1-P-04

An actuator, based on a Langevin-type transducer, able to excite large bending vibrations in thin foils

Nicola Lamberti¹; ¹D.I.I.I.E., University of Salerno, Fisciano, Italy

Background, Motivation and Objective

In dermatological aesthetics piezoelectric actuators have many applications; the skin treatment is obtained by the bending vibration, along the length, of a steel foil of about 0.5 mm in thickness; the vibration frequency is ultrasonic, to avoid annoying noise. In this paper a piezoelectric actuator able to excite a bending motion in the steel foil is described; the active part of the actuator is a piezoelectric Langevin-type transducer soliciting the foil at one edge; the objective is to obtain a system with high efficiency, low losses and high mechanical stiffness.

Statement of Contribution/Methods

First of all we analyzed the resonance modes of the foil in order to identify bending modes at an ultrasonic resonance frequency; the modal analysis was performed by ANSYS. Due to the foil length (45 mm) a bending resonance mode is approximately located at 26 kHz. The second step was the design of a Langevin transducer with the same resonance frequency. By means of analytical models we computed the thickness of the front and back masses of a transducer composed by 4 piezoceramic rings, electrically connected in parallel, imposing that the resonance frequency is 26 kHz. In order to amplify the displacements on the Langevin front face we inserted a displacement amplifier realized by using a classical stepped horn ultrasonic concentrator with both sections one-quarter wavelength long; the amplification factor is equal to the ratio between the areas of the two end sections. Finally, the connection between the foil and the displacement amplifier is realized by means of an ad hoc prismatic steel “support”.

Monday
Poster

Results

The proposed actuator is therefore composed by a Langevin transducer, a stepped horn displacement amplifier, a support and the bending foil. In order to optimize the design we analyzed the actuator behaviour by ANSYS, with the purpose to maximize the bending displacement at the free edge of the foil, to minimize the stresses on the piezoceramics and the deformations at the interface between various components. The FEM let us to analyze the whole actuator and to take into account elements that are neglected in analytical models, like the electrodes between the piezoceramic rings, the bolt connecting the front and back masses, the pre-stress etc. The obtained results show that the proposed actuator is able of large displacements ($\approx 100 \mu\text{m}$) with a reasonable low ($\approx 200 \text{ V}$) voltage supply; the stresses on the piezoceramics are 100 times below the depolarization limit, while the deformations at the interfaces are 40 times below the breaking limit.

Discussion and Conclusions

In this paper a piezoelectric actuator, based on a Langevin transducer, able to excite a large bending motion in a steel foil is described; the actuator is analyzed and designed by means of ANSYS. The simulation results show very promising performances; next step will be the realization of a prototype, in order to experimentally verify the device performances and to refine its design.

P1-P-05

Minute Object Support Mechanism by Using Ultrasonic Vibration

Yasuhiro Kato¹, Daisuke Terada¹, Yuji Ishino¹, Masaya Takasaki¹, Takeshi Mizuno¹; ¹Saitama University, Japan

Background, Motivation and Objective

Recently, the demand of non-contact transportation of electric components and optical components has risen. The application of non-contact transportation using acoustic levitation for liquid crystal glass substrate and silicon wafer has been proposed. In near-field acoustic levitation, it is well known that such planar objects can be levitated vertically upward above the vibrating surface of an ultrasonic transducer. On the other hand, the downward ultrasonic suspension in the air has been proposed and achieved the non-contact suspension of a small planar object downward the vibration surface. In this phenomenon, it seems that the pressure acting on the object is negative at the certain gap. In this paper, an object with curvature was focused as the suspended object. The small plastic lens was used as the object. Suspension of the lens was investigated experimentally.

Statement of Contribution/Methods

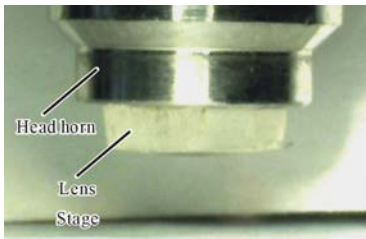
A Langevin transducer with a horn block that enlarges the vibration amplitude at the suspension part was used. The head of the horn block was concave approximately in parallel with the curvature of the lens.

Results

A Langevin transducer with diameter of 30 mm was used as the ultrasonic transducer. The diameter of vibration surface was 8.0 mm. The lens whose diameter was 6.5 mm was suspended downward successfully with driving voltage of 60 Vrms and driving frequency of 24 kHz (Fig.1). The lens was easily released when the vibration was stopped.

Discussion and Conclusions

For the planar object, it has been investigated experimentally that the negative or positive force acting on the object surface depends on the gap between an object and vibration surface. According to the force, the negative or positive force is considered to act on microscopic area, because the gap was not constant due to surface accuracy. The suspension result shows that the total of the microscopical forces was attractive force. This mechanism can be applied for handling of an object with curvature. For the handling, we do not need to concentrate our attention to the surface accuracy.



Noncontact ultrasonic particle manipulation for a long distance in air using a bending vibrator and a reflector

Daisuke Koyama¹, Yu Ito¹, Kentaro Nakamura^{1,2}:*Precision and Intelligence Laboratory, Tokyo Institute of Technology, Yokohama, Kanagawa, Japan*

Background, Motivation and Objective

Ultrasonic manipulation of small particles including a liquid droplet for a long distance is discussed. It is well known that a particle, which is much smaller than a wavelength of acoustic standing wave, can be trapped at the node points. Several groups have reported the particle manipulation techniques using the ultrasonic standing wave. However, the manipulation for a long distance over 1 m and the noncontact transportation of liquid in air have not been reported. A noncontact manipulation technique for a long distance of small particles such as electronic parts and liquid droplets will be attractive in a field of manufacturing industry.

Statement of Contribution/Methods

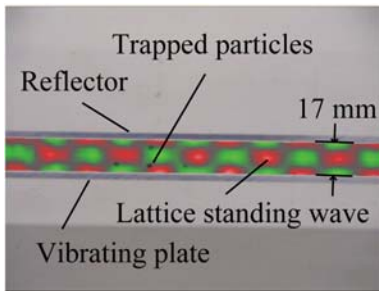
The experimental setup consists of a 3-mm-thick and 605-mm-long duralumin bending plate and a reflector. Two bolt-clamped Langevin type transducers with horns were attached on the both side of the plate to generate the flexural vibration along the plate. The plane reflector with the same dimensions as the vibrating plate is installed parallel to the plate with the distance of approximately 17 mm to generate an ultrasonic standing wave between them and trap the small particles at the node lines. The acoustic field between the plate and reflector was calculated through finite element analysis (FEA) to predict the trapped position of the particles. The sound pressure distribution was measured experimentally by using a scanning laser Doppler vibrometer via a change in the refractive index of air. By controlling the driving phase difference between the two transducers, the flexural traveling wave can be generated along the plate, and the node points of standing wave and the trapped particles can be moved.

Results

The flexural wave was excited in air along the vibrator at 22.5 kHz. The lattice standing wave with the wavelength of 36 mm in the length direction could be excited between the vibrator and reflector, and foam polystyrene particles with the radii of several mm could be trapped at the node lines of standing wave (Fig. 1). The experimental and calculated results showed a good agreement.

Discussion and Conclusions

The noncontact transportation of the trapped particles for a long distance could be achieved by changing the driving phase difference: the trapped position of particles can be controlled as 0.046 mm/deg. An ethanol droplet could be also trapped and moved.



Analysis of Exponentially Tapered Piezoelectric Bimorph Actuator

Moojoon Kim¹, Jungsoon Kim²:¹*Physics, Pukyong National University, Korea, Republic of,* ²*Multimedia, Tongmyong, Korea, Republic of*

Background, Motivation and Objective

Piezoelectric bimorph has been widely used as sensors and actuators in industry. However, it is not easy to design the various resonant modes with given length of the rectangular type.

To give the variety of the resonant frequency, a piezoelectric bimorph with exponentially decreasing width along the length was analyzed.

Statement of Contribution/Methods

By selecting the exponential function of length as the decreasing width, the general solution was derived from the equation of motion for the piezoelectric bimorph. The electromechanical coupling coefficient of each resonant mode was calculated. Three different shapes of exponentially tapered piezoelectric bimorphs were manufactured. They have same length of 63.9mm, maximum width of 13.5mm, and the thickness of a piezoelectric plate is 0.44mm.

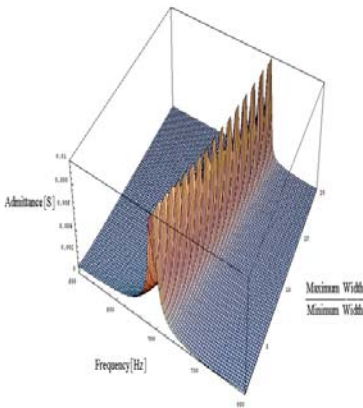
To verify the calculation method, the experimental results were compared with the theoretical results.

Results

As one of the results, the figure shows the variation of the fundamental resonant frequency according to the ratio of the widths of both ends. The resonant frequency moves to higher side as the ratio increases, and its admittance value is varied according to the ratio.

Discussion and Conclusions

The number of resonant modes was increased as the width was decreased rapidly along the length when the boundary condition was free-free ends. In fixed-free ends condition, the resonant modes have the tendency moving to high frequency range. It was confirmed that the wide frequency band width could be obtained by combination of the different shaped bimorph actuator. From these results, it is expected that the electroacoustic characteristics analysis will be useful to design the frequency band width of piezoelectric bimorph.



P1-P-08

Experimental consideration of high frequency ultrasonic atomization using SAW devices

Jun Kondoh¹; ¹Graduate School of Science and Technology, Shizuoka University, Hamamatsu-shi, Shizuoka, Japan

Background, Motivation and Objective

A liquid actuator is realized using a surface acoustic wave (SAW) device. A longitudinal wave is radiated into a liquid when the liquid is placed on a surface acoustic wave (SAW) propagating surface. Nonlinear phenomena are caused by a radiated longitudinal wave and are called SAW streaming. Several applications of liquid actuators using SAW streaming are reported. Atomization is one of them. In this paper, mechanism of the atomization is discussed. First, an elliptical displacement at water/128YX-LiNbO₃ interface was calculated using Campbell and Jones method. Then, mechanism of the atomization is discussed using observation results. Finally, for practical application, long time atomization is examined.

Statement of Contribution/Methods

Two SAW generation systems were used. One consists of signal generator, function synthesizer, and RF-power amplifier. The other consists of FM transceiver with a pulse circuit. Atomization was observed using a high-speed camera.

Results

From the calculated results, ellipse displacement was obtained at the crystal surface. Increasing the distance from the surface, it changes and becomes linear polarization, namely longitudinal wave, at 0.005 wavelengths. Polarization direction agrees with Rayleigh angle. Therefore, longitudinal wave is not directly radiated from the surface.

Thin water layer prepared on the surface and observed atomization by varying applied power. Our previous research, atomization had been occurred when applied power was larger than 2.25W. In this study, using the high-speed camera, we found that minimum applied power for generating mist was 0.042W when liquid volume was less than 0.04 μ l.

Using the transceiver system, long time atomization was demonstrated. Applied power was 3 W. The device property was evaluated using S11. The initial S11 of -23.7dB became -12.8 dB after 42 days.

Discussion and Conclusions

The atomization was observed even at low power. Loss due to attenuate longitudinal wave into thin water layer of 0.04 μ l was 1.4 dB. In other words, radiation power into the liquid was 1.4 dB. Previously, we considered that atomization was occurred by the SAW streaming force. However, it is impossible to generate mist with such low radiated power. The observed results cannot be explained on the basis of SAW streaming. Also, direction of the force agrees with the longitudinal wave radiation direction. The experimental results show that mist is generated from the whole water surface. Therefore, we conclude that mechanism of atomization is a capillary wave like a conventional ultrasonic atomization. For realization of atomization system, such as thin film deposition, detail discussions and test of device lift time are necessary.

P1-P-09

Propulsion of droplets on non-piezoelectric substrates via mode conversion of Lamb waves

Martin Schmitt¹, Gerhard Lindner¹, Sandro Krempel¹, Hendrik Faustmann¹, Ferdinand Singer^{1,2} *Institute of Sensor and Actuator Technology, University of Applied Sciences Coburg, Coburg, Bavaria, Germany*

Background, Motivation and Objective

The mode conversion of acoustic surface waves contacted by liquid droplets has been utilized for the propulsion of nanoliter droplets with respect to lab-on-a-chip applications [1]. In this case, however, a piezoelectric substrate equipped with interdigital transducers on the surface on which the droplets are moving had been used for the excitation of surface acoustic waves [2]. Our approach is aiming at the acceleration of comparably large droplets such as raindrops on non-piezoelectric substrates, e. g. glass plates.

Statement of Contribution/Methods

The propulsive action of Lamb waves has been demonstrated by Moroney et al. [3]. Following this approach, we have been excited Lamb waves on glass plates by piezoelectric interdigital transducers attached at the rear side of the substrate, which is not in contact with the liquid [4].

Results

A propulsive action on water droplets of ml size has been observed, which could be improved by hydrophobic surface coatings. With continuous wave excitation at a frequency of 1 MHz and an amplitude of 200 Vpp an acceleration of about 0,3 m/s² has been achieved so far with water droplets of 10 μ l on a 1 mm glass plate.

Fig. 1 Snapshots of water droplets on a glass plate, on which a piezoelectric interdigital transducer has been attached on the rear side, before and after Lamb wave excitation

Discussion and Conclusions

This concept allows numerous technical applications, including “intelligent” droplet removal from glass panels in combination with droplet detection via a Lamb wave transmission line established via a second interdigital transducers.

- [1] Wixforth, A.: Acoustically driven planar microfluidics, *Superlattice and Microstructures* 33 (2003) 389 – 396.
- [2] Kurosawa, M., Watanabe, T., Futami, A., Higuchi, T.: Surface acoustic wave atomizer, *Sensors and Actuators A* 50 (1995) 69 - 74.
- [3] Moroney, R. M., White, R. M., Howe, R. T.: Microtransport induced by ultrasonic Lamb waves, *Appl. Phys. Lett.* 59 (71), 1991, 774 – 776.
- [4] Lindner, G., Faustmann, H., Fischer, T., Krempel, S., Münch, M., Rothballer, S., Schmitt, M.: Acoustic Surface Wave Induced Propagation of Liquids in Open Channels, 2007 IEEE International Ultrasonic Symposium; 28.-31. October 2007 in NewYork/NY; p. 2331-2334

Monday
Poster



P1-Q. Measurement & Yields

Sala Orange

Monday, September 21, 2009, 10:00 am - 11:30 am

Chair: **Jan H. Kuypers**
Sand 9, Inc.

P1-Q-01

Compensation of Time Delay in Detection Electronics for Fast Scanning 2D SAW/BAW Laser Probe

Tatsuya Omori¹, Keisuke Kashiwa¹, Ken-ya Hashimoto¹, Masatsune Yamaguchi¹:¹Graduate School of Engineering, Chiba University, Chiba-shi, Chiba, Japan

Background, Motivation and Objective

The 2D observation of acoustic wave propagation is believed to be most effective in developing high performance SAW/BAW devices, because it offers invaluable information hardly acquired by other means. In obtaining the 2D images, time consumption should be minimised without sacrificing their spatial resolution and dynamic range.

Recently, the authors have developed a fast mechanical scanning SAW/BAW visualisation system using the Sagnac interferometer and demonstrated how it effectively works.[1]

In the system, the detection electronics determine the delay time of the signal output as well as the thermal noise level, and thus limit the attainable scanning speed. Even when the scanning speed is lower than the limit, the time delay causes the deviation of the captured output signals from the observation points, which makes it most difficult to apply the fast two-way mechanical scan to the system.

Statement of Contribution/Methods

This paper describes the enhancement of the measurement speed by compensating the time delay caused in the detection electronics.

In the present laser probe, in order to synchronise the mapped and observation points, the outputs of the detection electronics are sampled with trigger pulses generated every 40 nm by a linear encoder attached to the mechanical stage. Here it should be noted that because of the deviation in the translation speed, the pulse trains are not always periodic in terms of time. The compensation is performed by delaying trigger pulses by the delay time t_d of the detection electronics. A digital circuit was newly developed for the purpose.

A simple technique was also developed for estimating t_d with sufficient accuracy. When SAWs propagating under straight electrodes are observed by the two-way mechanical scan with incomplete compensation, they may appear as zigzag lines in the captured 2D image due to the deviation mentioned above. This means that one is able to characterise the incompleteness quantitatively by evaluating the intensity of specific spots appearing in the FFT of the captured 2D image.

Results

As a demonstration, an SAW field in a one-port resonator at 926 MHz was visualised with a size of 1,250x250 pixels (0.4 μ m step) by the developed system. It is shown that under an optimal compensation, the influence of the delay time can be dissolved, and that a high quality image is obtained even when the two-way scan is applied. The measurement was completed in about 4 min., which corresponds to the average sampling rate of 1.3 kS/s.

Discussion and Conclusions

It was shown that the fast data acquisition became possible by the introduction of the novel method for the compensation of the time delay in detection electronics. To the best of the authors' knowledge, the proposed SAW/BAW visualisation system allows much faster imaging compared to other laser-probes employing a mechanical scan.

Reference:

[1] K. Hashimoto, *et al.*: Tech. Digest, IEEE Microwave Symp. (2008) pp. 851-854.

P1-Q-02

200mm manufacturing process feasibility of BAW coupled resonator filters

Sylvain Joblot¹, Alexandre Reinhardt², Pierre Bar¹, Christophe Billard², Nicolas Buffet², Guy Parat², Jean-François Carpentier¹; ¹STMicroelectronics, Crolles, France, ²CEA-LETI, Grenoble, France

Background, Motivation and Objective

During the last 20th years, acoustic filter manufacturing for mobile phone applications have been dominated by Surface Acoustic Waves (SAW) filters. Nevertheless since few years, the Bulk Acoustic Waves technology (BAW) presents large interest and challenges SAW technology. It has been shown that BAW filters present advantages in terms of power handling, thermal behaviour and robustness of Electro-Static-Discharge (ESD). Moreover, it is compatible with the silicon mainstream technology and an appropriate candidate for high frequency application up to 5GHz-10GHz [1]. Coupled Resonator Filter (CRF) is necessary to include impedance transformation and single-ended to balanced signal conversion functionalities as achieved by SAW filter [2]. Previous studies have reported CRF realisation on solidly mounted resonator or cavity with promising performances, but impact of layers dispersion and trimming steps have not been described in details. The objective of this paper is to emphasize the keys to achieve an attractive yield on wafer in industrial environment.

Statement of Contribution/Methods

Usually to adjust final filter frequency at wafer scale, BAW technology required trimming step based on a homothetic resonator response. In this way, for CRF, dedicated top and bottom resonators would be necessary and induce heavy process with for instance multiple CMP planarisations. Consequently, to simplify processing with no dedicated top resonator, final trimming step has been directly achieved on filter response. In this paper, processing of CRF with CMOS classical materials such as W/SiO₂ for Bragg reflector and coupling layers, Mo/AlN/Mo for resonators and its thin film packaging will be detailed and discussed. Frequency sensitivities of piezo-stack and SiO₂ layers near to the both resonators will be given and layers dispersion impact on frequency response will be highlighted. Finally, we will discuss the two trimming steps on the bottom resonator and on the final filter.

Results

Experimental results of frequency, bandwidth and insertion losses will be presented with this fabrication method. The best insertion losses (IL) measured on 50Ω single-ended filters for W-CDMA application is -2dB. An attractive yield of 70% filters with central frequency comprised in +/-3MHz is measured across the wafer and validates the trimming method.

Discussion and Conclusions

In this paper, the robustness of a 200mm CRF process in silicon manufacture has been shown. By using innovative trimming methodology, processing has been relaxed. Standard thickness trimming would be discussed on SiO₂ bottom coupling layer. Then, design solution could be considered to reduce thickness sensitivities impact and still improves central frequency dispersion [3].

[1] R. Aigner et al; IEEE UFFC proceedings 2008, pp. 582.

[2] K.M. Lakin et al; IEEE UFFC proceedings 2001, pp. 833.

[3] P. Bar et al; patent pending.

P1-Q-03

Multilayer scanning of RF BAW device for focus adjustment by laser probe system

Nan Wu¹, Ken-ya Hashimoto¹, Tatsuya Omori¹, Masatsune Yamaguchi¹; ¹Graduate School of Engineering, Chiba University, chiba, chiba, Japan

Background, Motivation and Objective

The authors have developed a phase-sensitive laser probe system based on the Sagnac interferometer for the diagnosis of RF SAW/BAW devices.

High lateral resolution is achieved by an objective lens with large magnifying power. Since it also results in a shallow focal depth, the out-of-focus problem may occur partly in the captured image field when the device surface is uneven. For example, even if the change in the surface height is about 2 μm in 2 GHz RF BAW devices, this would badly affect the captured image quality when a 100x objective lens is employed.

Statement of Contribution/Methods

This paper describes a scanning method to make the whole image in focus. It is accomplished by the following procedures. First, scanning of a device surface is repeated multiple times setting an objective lens at a different height, and both the interferometric (RF) and monitor (DC) outputs of a photo detector are recorded. Then, the lens height giving the best focus at each sampling point is determined from the DC output. Finally, the RF output with the best focus height at each sampling points are extracted to compose a whole image.

Results

Using a 100x objective lens, we scanned the surface of a 2 GHz RF BAW device 8 times with lens height of 0.8 um intervals. Fig. 1 (a) shows variation of the lens height giving the maximum DC output. Fig. 1 (b) shows the amplitude image composed by the RF output with the best focus at each sampling point.

Discussion and Conclusions

Fig. 1(a) clearly shows the change in the surface height within the device as well as surface inclination. Although the impact of the present technique is not clear in Fig. 1(b), it becomes more apparent in the image shown in Fig. 2, where color map is modified into saturation. Thanks to the proposed technique, the leakage can clearly be seen; one can recognize the energy flow with small decay.

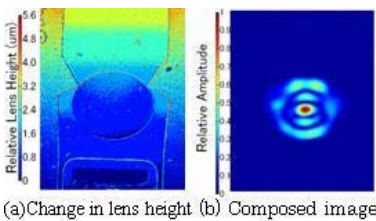


Fig. 1 Images with the best focus

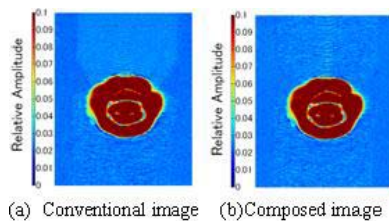


Fig. 2 Amplitude with modulated color bar

P1-Q-04

Method for Phase Sensitive Measurements of Surface Vibrations Using Homodyne Interferometry without Stabilization

Lauri Lipiäinen¹, Kimmo Kokkonen¹, Olli Holmgren¹, Matti Kaivola^{1,2}, *Applied Physics, Optics and Photonics, Helsinki University of Technology, Espoo, Finland*

Background, Motivation and Objective

We have implemented a phase sensitive absolute amplitude detection method to extend the capabilities of a homodyne scanning laser interferometer [1], originally developed for measuring relative amplitude data of surface vibrations in microacoustic devices. Absolute amplitude and phase data allow for, e.g., separation of waves propagating into different directions, analysis of acoustic reflections, and determination of dispersion curves. Furthermore, the wave motion can be animated to bring further insight to the device operation.

To enable phase and absolute amplitude measurements, homodyne interferometers have traditionally been stabilized to a single quadrature point (QP). Without stabilization, the interferometer operation point randomly drifts over several QPs. The existence of two different QP types then leads to ambiguity in determining the phase if the QP type is not known.

Statement of Contribution/Methods

The advantage of the detection scheme presented here is that no stabilization is required. In addition, this method also enables absolute amplitude measurements via normalization. The amplitude and phase of surface vibrations are measured while the interferometer operation point is swept through several QPs. The phase ambiguity issue is resolved by identifying the QP types.

A concept for measuring the phase of surface vibrations using homodyne interferometry, with no active stabilization, was recently proposed [2]. With such a method, however, the QP type should be known in order to determine the phase unambiguously, an issue not discussed in the article.

Results

The method implemented in this work has been tested by measuring vibration fields in piezo-actuated micromechanical (MEMS) square-plate resonators [3]. Amplitude and phase maps of different vibration modes are presented at selected high-Q resonance frequencies.

Discussion and Conclusions

The absolute amplitude and phase measurement method described here allows for a simple homodyne interferometer design without stabilization. The test measurements of MEMS resonators confirm that the concept works as expected. Due to a more compact size and lower power consumption, these MEMS resonators are studied as potential candidates for replacing bulky quartz reference oscillators, e.g., in wireless communication. Piezo-actuated resonators offer intriguing alternatives to capacitively coupled MEMS resonators since bias voltage and sub-100 nm gap structures are not required. Absolute amplitude and phase data enable better understanding of the underlying device physics and hence provide valuable feedback for modeling and device design.

- [1] J. V. Knuutila et al., *Opt. Lett.*, Vol. 25, No. 9, pp. 613-615, 2000.
- [2] A. Gollwitzer et al., *IEEE Int. Freq. Control Symp.*, pp. 424-427, 2006.
- [3] A. Jaakkola et al., *Proc. IEEE Ultrason. Symp.*, pp. 717-720, 2008.

P1-R. Device Modelling

Sala Orange

Monday, September 21, 2009, 10:00 am - 11:30 am

Chair: **Leo Reindl**
University of Freiburg

P1-R-01

SAW Reflection from Surface Inhomogeneities of Isotropic and Anisotropic Substrates

Alexandre Darinskii¹, Manfred Weihnacht², Hagen Schmidt³, ¹*Institute of Crystallography RAS, Moscow, Russian Federation*, ²*InnoXacs, Dippoldiswalde, Germany*, ³*IFW Dresden, Dresden, Germany*

Background, Motivation and Objective

Artificial surface inhomogeneities, e.g., grooves or strips, are used as reflectors in SAW devices. Besides, the interaction of SAW with electrodes, i.e. metallic strips, crucially affects the performance of IDTs. Analytic considerations allow one to estimate only leading terms of physical characteristics of one's concern with respect to relevant parameters even for isotropic solids. Therefore such problems require numerical studies.

Statement of Contribution/Methods

The reflection of SAW from single steps as well as single and multiple grooves, projections, and strips on half-infinite isotropic (fused quartz, FQ) and piezoelectric (lithium niobate, LN) substrates are investigated by FEM. The perfectly matched layer (PML) is used to confine the computational domain. The amplitude of the reflected SAW is found by applying FFT to the scattered field on the surface of the substrate. Special computations are carried out to validate the PML quality and the method of determining the amplitude of SAW.

Results

The dependences of the absolute values and the phases of the reflection coefficient R on the height and width of imperfections are computed. In particular, it is found out that the curves showing the width dependence of $|R|$ for a groove and a projection of identical shape (or for overlaying and buried strips) are shifted relatively each other, this shift being significant even if the thickness to wavelength ratio is small. A minimum on one curve may correspond to a maximum on the second curve. It is notable that the values of R for a groove on 128LN agree well with known experimental results. The coefficient R for steps and grooves on FQ is also computed as a function of the angle of incidence. $|R|$ goes down to a non-zero minimum at an angle whose value is estimated fairly correctly using an expression of R derived in the first approximation in height to wavelength ratio. The width dependence of R from an infinitesimally thin electrode on YZ and 128LN is computed. Numerical data are close to estimations by an analytic expression derived in the weak electromechanical coupling approximation, especially when the width is smaller than $1/3$ wavelength. In addition, the reflection coefficients from gratings comprising a finite number of grooves and electrodes are computed and compared with the predictions of COM-theory. The required COM-parameters are extracted from computations for infinite gratings.

Discussion and Conclusions

The obtained results give insight into the dependence of the reflection coefficient on the characteristics of surface imperfections useful for SAW devices. The comparison of numerical and analytic findings elucidates the contribution of higher-order terms in parameters involved as well as reveals the limits of the COM-theory. Our study also demonstrates the applicability of the FE/PML method to scattering problems in half-infinite solids.

P1-R-02

4-Wave Interaction in 2D Periodic Structures

Elena Mayer¹, Victor Plessky², Leonhard Reindl¹; ¹Department of Microsystems Engineering, University of Freiburg, Freiburg, Germany, ²GVR Trade SA, Bevaix, Switzerland

Background, Motivation and Objective

Renewed interest in wave propagation in periodic structures is observed and is associated with the popular term “phononic crystals”. It had been shown earlier that the presence of strong periodic perturbations can radically change the structure and parameters of a wave propagating in such structures [1] or can even make such propagation impossible at some frequencies. If the elements creating the periodic structure have resonance properties the behaviour can be even more interesting [2]. However in device applications, strong dispersion, multimode behaviour etc. are not necessarily advantageous features. On the other hand, the possibility to control the propagation of “normal” SAW can be attractive. Here, we theoretically study 2D periodic reflector structures on an isotropic material with the rows of elements oriented with an angle of $\pm 45^\circ$ relative to the propagation direction of the incident wave. In such a grid, 4 waves propagating along $\pm 0X$ and $\pm 0Y$ directions are coupled by said reflectors. The objective of this study is to clarify how 4 SAWs interact with a two-dimensional periodic array and to find amplitude distributions in the grid. Such structures, maybe in combination with standard reflectors, can potentially be used in SAW resonators, RACs, replace in some cases the wave couplers, etc.

Statement of Contribution/Methods

Using a perturbation technique, we derived a system of 4 Coupling-Of-Mode (COM) equations [3] describing the mutual reflections of SAW in the 2D periodic structure. The cases of mass loading and periodic surface roughness ($h/\lambda \ll 1$) are considered. The strength of perturbation can be different for reflections in $+90^\circ$ and -90° directions. Multiple reflections are included resulting also in 180° reflectivity.

Results

Each of the 4 obtained COM equations include only $\pm 90^\circ$ reflections. The SAW amplitude distribution in this structure strongly depends of the shape of the area occupied by the structure. First we find the eigenmodes of the infinite structure and then we study the case when SAW propagating on a flat surface along the $+0X$ axis is incident on a half-space ($x > 0$) occupied by a 2D grid. Contrary to the 1D reflectors, the stopband width is proportional to the square of the perturbation parameter $(h/\lambda)^2$.

Discussion and Conclusions

In most of the papers on phononic crystals the stopband gaps are determined for wave propagation in selected directions of an infinite structure. However, for practical cases of finite structures, the SAW amplitude distribution in 2D is of importance. Here we present an attempt of analysis of such interaction of 4 waves in a 2D grid of reflectors.

[1] Y. V. Gulyaev and V. P. Plesskii, Sov. Phys. Tech. Phys., 1978, 23, 266.

[2] A.-R. Baghai-Wadji, V. P. Plessky, and A. V. Simonian, Sov. Phys. Acoust., 1992, 38, 442.

[3] S. V. Biryukov, Yu. V. Gulyaev, and V. V. Krylov, Surface acoustic waves in inhomogeneous media, Springer Verlag, Berlin, 1995.

P1-R-03

Extraction of the P-Matrix Parameters Varied with Frequency for Leaky Surface Acoustic Wave

Hao Wang¹, Weibiao Wang², Jiming Lin³, Xianglong Shi¹, Haodong Wu¹, Yongan Shui^{1,2}; ¹Key Laboratory of Modern Acoustics, Institute of Acoustics, Nanjing University, Nanjing, Jiangsu, China, People's Republic of, ²Shoulder Electronics Limited, Wuxi, Jiangsu, China, People's Republic of, ³Information and Communication College, Guilin University of Electronic Technology, Guilin, Guangxi, China, People's Republic of

Background, Motivation and Objective

Extraction of COM parameters and simulation by P-matrix cascading method has been extensively used to the design of SAW devices. Traditional COM parameters are taken as frequency independent, however, within the interested frequency range, the propagation attenuation of LSAW changes dramatically, and COM parameters taken as constant will introduce a considerable error. These years, scientists and engineers tried to extract COM parameters varied with frequency for 42°LTO. Reference [1] considered the central frequency f_0 as a function of

frequency while mutual coupling parameter κ as a constant. Reference [2] considered κ as a function of frequency while f_0 as a constant. They could not obtain κ and f_0 as functions of frequency simultaneously because the infinite periodical model was used in their works. The purpose of our work is to extract precise P-matrix parameters as functions of frequency independently.

Statement of Contribution/Methods

We propose a new method to evaluate the P-matrix parameters as functions of frequency.

A periodical grating with finite length is in consideration. The finite FEM/BEM is used to calculate electric charge and stress distribution under each electrode, and the displacement and potential distribution of forward and backward LSAW within the grating could be accurately obtained by Source Regeneration Method [3]. COM model is also used to simulate the fields of forward and backward LSAW within the grating. Comparison between the field distribution of both methods above, f_0 , κ and propagation attenuation γ are evaluated by short-circuited grating and excitation coefficient α is evaluated by open-circuited grating at every frequency. The static capacitance is extracted by the periodic FEM/BEM since it is a constant parameter independent of frequency.

In our method, the length of grating is finite, so we can obtain κ and f_0 as functions of frequency simultaneously. In case the number of fingers is large enough, we can get precise results. In addition, FEM/BEM method is able to offer the bulk wave radiation information directly, which increases the independent data into consideration.

Results

As an example, all the P-matrix parameters for LSAW on 42°LTO with relative aluminum electrode thickness of 8% and metallization ratio of 0.4-0.6 are presented as functions of frequency.

Discussion and Conclusions

Using these obtained parameters, a DMS filter is simulated. The results are in good agreement with precise simulation and experiments. We can also get dispersive curve, the reflection and transmission coefficient of grating using the method in this paper.

References:

- [1]. Th. Pastureaud, 2004 IEEE IUS Proc. pp.80-84
- [2]. B. V. Sveshnikov, et al, 2003 IEEE IUS Proc. pp.715-719
- [3] W. Wang, et al, IEEE Trans-UFFC, 2007, 54(7), 1445-1453

The project is supported by Natural Science Foundation of China No. 10774073.

P1-R-04

Computation of plate wave dispersion diagrams and surface wave velocities without explicit boundary conditions

Vincent Laude¹, Badreddine M. Assouar², Zhilin Hou^{3,1}, Institut FEMTO-ST, Centre National de la Recherche Scientifique, Besancon, France, ¹Institut Jean Lamour, Nancy University - CNRS, Vandoeuvre, France, ²Department of physics, South China University of Technology, Guangzhou, Guangdong, China, People's Republic of

Background, Motivation and Objective

The evaluation of the dispersion relation of elastic waves is a numerical problem which practical difficulty strongly depends on the algebraic form of the solution. For instance, the computation of the velocity of bulk acoustic waves in an arbitrary anisotropic material can be cast in the form of an eigenvalue problem and solved easily and reliably. In contrast, in the case of surface acoustic waves (SAW) or plate (Lamb) waves, it is generally first necessary to form a determinant of the boundary conditions (BC) and then to seek its zeros as a function of the wave vector for a fixed frequency. Finding all zeros can be a numerically difficult problem and a cumbersome one for plate waves, as the number of allowed modes increases with the thickness of the plate.

Statement of Contribution/Methods

The plane wave expansion (PWE) method is used in the field of phononic crystals (PC) to formulate eigenvalue problems to compute dispersion diagrams. Historically, the PWE method was limited to compositions of two or more solid materials that are arranged periodically. Recently, it has been remarked that it can cope with solid-vacuum compositions where vacuum is represented by a solid with zero mass density and elastic constants [1].

This idea was then used to compute the dispersion of waves in two-dimensional PC in the plate geometry [2]. We discuss in this paper how the BC are included implicitly in the form of the PWE solution, thus leading to an efficient eigenvalue problem.

Results

We have implemented a PWE method to solve the plate wave problem for arbitrary anisotropic elastic materials. As a numerical trick, the plate is repeated periodically with a vacuum separation between replicas. Since in the limit of a large number of Fourier harmonics there are no elastic waves in the vacuum part, the solutions of the eigenvalue problem represent waves propagating in the plate with a given wave vector along the surface. By comparing with a classical determinant-based method, it is verified that all solutions are found with excellent accuracy. Furthermore, SAW velocities can be estimated from the slowest wave for large wave vectors.

Discussion and Conclusions

The PWE numerical algorithm we propose is fast and accurate. We will discuss the issue of convergence (the number of harmonics that have to be included in the computation) and the extension of the method to multilayered plates and to piezoelectric materials, where an additional difficulty appears because of the existence of an electromagnetic field in vacuum. We believe the method can be of value for numerical codes requiring a generic method for wave dispersion that does not require an initial guess for the solution, as opposed to zero-finding procedures.

[1] V. Laude et al., Phys. Rev. E 71, 036607 (2005).

[2] Z. Hou et al., Phys. Lett. A 372, 2091 (2008).

P1-R-05

Simulation of SAW Waveguiding on Substrates with Asymmetric Slowness and Excitation

Markus Mayer¹, Karl Wagner^{1,†}*Epcos AG, Germany*

Background, Motivation and Objective

The 2D P-matrix method is able to describe effects of waveguiding and diffraction in SAW filters with high accuracy. Recently an extension of this method to symmetric, but otherwise general, anisotropies of slowness and excitation was presented [1].

A generalization to asymmetric slownesses, however, faces the problem of mode orthogonalization of radiation modes: For each wave number in main propagation direction two solutions exist. The inner product of these two degenerated modes in general diverges.

Besides slowness and excitation also the phase shift between reflection and excitation can show strong anisotropy. As a consequence in transversally symmetric NSPUDT devices antisymmetric modes are excited [2].

In this work the 2D P-matrix method is extended to deal with asymmetry of slowness and excitation as well as anisotropy of the phase of reflection and excitation.

Statement of Contribution/Methods

It is shown that orthogonalization of the degenerate modes can be achieved if continuity of the transversal Poynting vector at the interfaces of transversal sections is required.

Anisotropy of the phase shift between reflection and excitation is achieved by introduction of an anisotropic excitation phase. This leads to a transversal shift of the excitation profile [2].

Results

For lithium tantalate (XY1)/112.2 the method to deal with asymmetric slowness and excitation is successfully demonstrated.

At the example of Quartz (YX1)/34.0 the anisotropy of reflection and excitation is simulated. As predicted in ref. [2] antisymmetric modes are excited in a geometrically symmetric transversally coupled SAW filter.

Discussion and Conclusions

The 2D P-matrix scheme was successfully generalized to treat asymmetric anisotropies of slowness and excitation as well as diffraction effects in NSPUDT devices.

[1] M.Mayer, A. Bergmann, G.Kovacs and K.Wagner "Simulation of Waveguiding in SAW Devices on Substrates with Anisotropic Slowness and Excitation" IEEE Ultrasonics Symposium, pp. 803-806, 2008

[2] C.S. Hartmann, B.P. Abbott, S. Jen and D.P. Chen "Distortion of Transverse Mode Symmetry in SAW Transversely Coupled Resonators Due to Natural SPUDT Effects", IEEE Ultrasonics Symposium, pp. 71-74, 1994

P1-R-06

Influence of mechanical pressure on bulk acoustic waves propagation in lithium tantalate single crystals

Boris Sorokin¹, Dmitry Glushkov¹, Sergei Burkov^{1,1} *Condensed Matter Physics, Siberian Federal University, Krasnoyarsk, Russian Federation*

Background, Motivation and Objective

Lithium tantalite (LTO) crystals LiTaO₃ due to its high electromechanical coupling and low acoustic loss are widely used in surface acoustic waves applications. But complete set of nonlinear material constants of LiTaO₃ is still unknown.

Statement of Contribution/Methods

Nonlinear elastic properties of LiTaO₃ are described by 14 independent components of 6-rank tensor of third order elastic constants. These constants may be calculated from bulk acoustic waves (BAW) velocities changing under the external mechanical pressure in various propagation directions. Experimental results are presented in form of controlling coefficients $\alpha^i_v = (1/V(0))(\Delta V/\Delta \tau)_{\Delta \tau \rightarrow 0}$. For example, for shear wave along [001] and uniaxial pressure applied along [100] controlling coefficient is:

$$\alpha^5_v = (2C_{44}S_{11} + C_{155}S_{11} + C_{144}S_{12} - C_{444}S_{14} + C_{344}S_{13}) / (2C_{44})$$

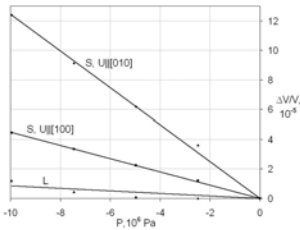
In this paper investigation of BAW propagation in LiTaO₃ under the uniaxial and hydrostatic mechanical pressure was derived by the pulse ultrasonic technique (30 MHz). Base X,Y,Z-cuts and a number of rotated X-cuts of LiTaO₃ are used. Only non-piezoeactive modes are considered.

Results

BAW velocities and its uniaxial and hydrostatic pressure dependences were measured. All dependences were close to linear ones in all range of pressure value applied. Controlling coefficients α^i_v were obtained. Example of curves is shown on the figure (propagation direction along [001], uniaxial pressure applied along [010]). Anisotropy of uniaxial mechanical pressure influence on BAW propagation was calculated.

Discussion and Conclusions

Due to better thermostability property comparing with lithium niobate LTO crystals are perspective for acoustic devices such as filters, duplexers. Results obtained may be used to choose crystal cuts with optimal combination of thermostability and acoustic wave characteristics concerned with sensitivity to external influence.



Monday
Poster

P1-S. High Temperature Materials and Propagation

Sala Orange

Monday, September 21, 2009, 10:00 am - 11:30 am

Chair: **Robert Weigel**
University of Erlangen-Nuremberg

P1-S-01

Investigation of New High Temperature SAW Metallizations Based on Platinum Group Metals

David Eisele¹, Ismail Shrena¹, René Fachberger², Gudrun Bruckner², Leonhard Reindl^{1,3} *Department of Microsystems Engineering, University of Freiburg - IMTEK, Freiburg, Germany, ²Carinthian Tech Research, Austria*

Background, Motivation and Objective

An advantage of passive wireless surface acoustic wave (SAW) sensors compared to other wireless technologies, such as semiconductors, are their ability to operate in harsh environments and high temperatures. Piezoelectric substrates for SAW devices which are stable and usable up to 1000°C are already known and available, such as langasite ($\text{La}_3\text{Ga}_5\text{SiO}_{14}$, LGS) and other members of the langasite family.

Due to effects, such as diffusion, recrystallization, oxidation, and dewetting, finding good thin film metallizations for high temperature SAW devices is challenging. Platinum is well known and commonly used in high temperature sensors, but exhibits degradation by dewetting at temperatures above 600°C. Different approaches to increase the durability of the platinum layer are published, such as building multilayer structures and co-depositioning with ZrO_2 , alloying the platinum with gold or rhodium, and also depositing a stabilizing continuous passivation layer on top of the whole structure. Through the use of these techniques long term temperature stability at 800°C and slow degradation at temperatures up to 1000°C can be achieved. However, the sheet resistivity and the applicability for UHF-SAW-devices is not yet investigated.

Statement of Contribution/Methods

In this paper, new metal combinations with platinum group metals are examined for their suitability in high temperature SAW devices and UHF. Therefore, different thin film structures, such as meander structures and delay lines with free and metallized surfaces, are fabricated on LGS. Tempering tests and measurements under different protective atmospheres up to 1000°C are performed. Processing the measurement data we evaluate sheet resistances, SAW velocities and damping of free and electrically shorted surfaces. Additionally microscopic examination of the structures are performed before and after the measurements.

Results

The interdigital transducers (IDT) of the delay lines consists of a double split finger structure, which excites four frequency bands. The first and second center frequencies are also reflection compensated. By choosing finger widths of 1.2 μm , the center frequencies are in the range of 100 MHz up to 1 GHz. The meander structures exhibit the same finger widths to ensure comparability. Similar to the differential delay lines, the meander structures have different number of fingers, enabling well defined resistance measurements of the finger structures.

Discussion and Conclusions

Alternative metallization combinations using platinum group metals are presented. In addition, the applicability for high temperature SAW applications will be discussed, based on the time-temperature trend of the evaluated parameters, along with microscopic analysis of possible degradation effects.

Study of Tantalum and Iridium as adhesion layers for Pt/LGS high temperature SAW devices

Thierry Aubert¹, Omar Elmazria¹, Badreddine Assouar¹, Laurent Bouvot¹, Zoumnone Bournebe¹, Michel Hehn¹, Sylvain Weber¹, Mourad Oudich¹, Patrick Alnot¹; ¹Institut Jean Lamour, UMR 7198, CNRS - Nancy University, France

Background, Motivation and Objective

Platinum/Langasite SAW devices are very promising for high temperature applications. An important remaining challenge is to find an adequate interdigital transducer (IDT) structure that would limit the de-wetting phenomenon of Pt thin film.

Some sophisticated solutions developed by Da Cunha et. al. based on co-deposition of Pt/Rh and ZrO₂ gave excellent results for very long-time applications. Our aim is to find a simpler IDT metals combination (platinum/adhesion layer) that can withstands an operating temperature of 1000°C for at least 30min. Up to now, zirconium gave the best results as adhesion layer but is limited to temperatures close to 800°C.

Statement of Contribution/Methods

SAW delay lines operating at 167MHz based on Pt/Ta/LGS and Pt/Ir/LGS structures were fabricated. The thicknesses of Pt and Ta/Ir adhesion layers were 100nm and 10nm respectively. Both devices were investigated before and after annealing of 30min at 1000°C by different characterizations: frequency response, thin film electrical resistivity, SEM, SIMS, EDS ...

Results

Morphological characterizations reveal an advanced degradation of IDTs in the Ir case, threatening the electrodes continuity (Fig.1b). Apart from the apparition of small crystallites at the surface of the Pt film, Pt/Ta combination shows no significant alteration after annealing (Fig.1c). Electrode continuity was confirmed by S₂₁ frequency response, which is for both cases almost unaffected by the annealing (Fig.2).

Discussion and Conclusions

Pt/Ta/LGS SAW devices operating at 1000°C during 30min were achieved. The apparition of the crystallites on IDT surface, which can induce electrode deterioration, can be attributed to diffusion phenomena occurring during annealing. More investigations are conducted in order to prevent it.

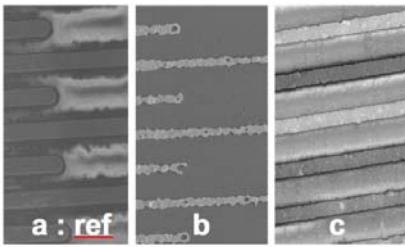


Figure 1

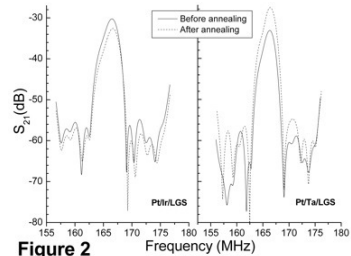


Figure 2

Material and Design Dependent Loss in Langasite Bulk Acoustic Wave Resonators at High Temperatures

Michal Schulz¹, Denny Richter¹, Holger Fritze¹; ¹TU Clausthal, Goslar, Germany

Background, Motivation and Objective

Single crystalline langasite (La₃Ga₅SiO₁₄) resonators exhibit piezoelectrically excited bulk acoustic waves up to temperatures close to its melting point at 1470 °C as shown by the relative resonance frequency in Fig. 1. The loss, expressed as the inverse Q factor in Fig 1, depends obviously on the materials properties and the resonance frequency. Anticipated operation at extremely high temperatures requires the understanding of both influences and enables tailoring of both properties to reduce the loss.

Statement of Contribution/Methods

Electrical impedance spectroscopy and diffusion runs using stable isotopes are the key methods used to study the atomistic transport processes and the electromechanical properties of langasite. Potential loss mechanisms are included in a modified one-dimensional model.

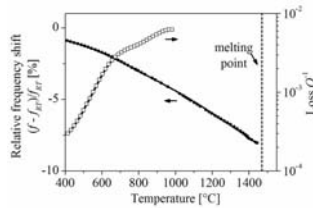
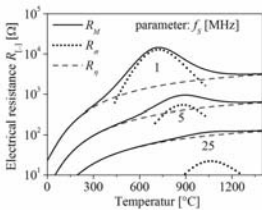
Monday Poster

Results

At elevated temperatures, electrical as well as mechanical loss contributions are found. In particular, oxygen vacancies are responsible for strong losses which can be, however, suppressed by appropriate dopants. Above 650 °C the impact of the conductivity related loss becomes pronounced. Further, the coupling of mechanical and electrical properties due to the piezoelectric effect causes a loss maximum at the dielectric relaxation frequency as shown in Fig. 2 by the resistors of the equivalent electrical circuit for such resonators. Doping of langasite modifies the electrical conductivity and shifts, thereby, the dielectric frequency. Consequently, the choice of appropriate dopants and/or of the resonance frequency far off the latter frequency minimizes the loss.

Discussion and Conclusions

The lowering of the loss by doping and/or choice of an appropriate resonance frequency is demonstrated and leads to an improved performance of resonant sensors at high temperatures.



P1-S-04

High temperature packaging for SAW transponders

Daniel Blum¹, Georg Straub¹, Rene Fachberger², ¹University of Applied Sciences Munich, Munich, Germany, ²CTR Carinthian Tech Research AG, Villach, Austria

Background, Motivation and Objective

The commercial use of passive surface acoustic wave (SAW) transponders for high temperatures (HT) is primarily limited by two reasons: The SAW metallisation and the packaging. Whereas recently developed metallisation materials show a good progress, a HT stable packaging technology for radio frequency (RF) devices is still lacking. Conventional sealing materials, wire and die bonds suffer considerable damage above 250°C. Known effects are delamination, breakage of bonds and adhesives and leakage of the package.

Statement of Contribution/Methods

We have investigated a packaging technology suitable for application of SAW transponders up to 600°C. The paper describes the package design comprising the housing, the electrical feedthroughs, the mounting of the crystal substrate, the contacting of the inter-digital transducer (IDT) and the sealing technology. The suitability of this novel packaging was examined by thermal aging. After aging, tensile shear tests of the crystal and peeling tests of the wire bonds were carried out.

Results

The geometry of the housing is based on a TO8 metal housing. The housing material is composed of a Fe-Ni-Co alloy (Kovar) matching with the thermal expansion of the substrate crystal. A glass coating and several inorganic adhesives (based on ZrO, SiO, MgO, NaSi, SiO-Al, SiO-steel and NaSi-Ag) to mount the crystal on the housing have been applied. The metal filled adhesives showed the best results. In the temperature range from 25°C up to 600°C they do not evaporate and provide an excellent potential for automation. They show good adhesion forces in combination with a certain amount of ductility, thus compensating stress caused by the different thermal expansion of crystal and housing to a certain extent. However, we have still discovered material failure after applying large temperature gradients. This limitation of use is being determined in ongoing investigations. The IDT and the electrical feedthroughs were contacted by platinum wire bonds providing a fair signal quality and an excellent temperature stability. For the electrical feedthroughs a Kovar wire enclosed by a ceramic bead was brazed into the cavities of the metallic base plate. In order to accomplish a hermetic package, the housing is sealed by a metal lid by means of projection resistance welding.

Discussion and Conclusions

The paper specifies a packaging concept for wireless SAW transponders for operating temperatures up to 600°C with reasonable production costs in order to enable commercial use. Its components are well suited for application in harsh environments, especially at high temperatures.

P1-S-05

Influence of Packaging Atmospheres on the Durability of High-Temperature SAW Sensors

Jochen Bardong¹, Gudrun Bruckner², Martin Kraft², René Fachberger^{2,1} *SAW Sensor Development, CTR AG Austria, Villach, Austria, ²CTR AG Austria, Austria*

Background, Motivation and Objective

Surface acoustic wave (SAW) devices are a technology of choice for passive, radio-interrogable sensor applications operating under extreme conditions. Suitably designed SAW devices can withstand e.g. temperatures exceeding 300°C, something that cannot be achieved with any other wireless sensing technology known. At such high temperatures (HT), thermal energies reach values corresponding to the activation energies of reactions between gas components with the SAW element's crystal substrate and the metallisation, respectively. Thus, the atmosphere in the hermetic packaging, which encloses and protects the SAW elements, becomes a crucial factor for the sensor's durability. This work investigates the influence of various potential packaging atmospheres on the durability of SAW devices.

Statement of Contribution/Methods

SAW test structures, which consist of two delay lines of different lengths, have been processed on i) langasite (LGS) and ii) lithium niobate (LN). The delay lines are made of 60 nm Pt-based thin films and are electrically coupled so they are interrogated at the same time. These SAW test devices were annealed in a tube oven equipped with a specially developed HT-stable radio frequency (RF) measurement system. The surrounding quartz glass tube was equipped with a vacuum-tight feed-through to provide different controlled atmospheres: He, Ar, Kr, N₂, O₂, air and vacuum. The measurements were carried out at temperatures rising stepwise up to 650°C. The change of insertion losses, propagation losses and time shifts over temperature were evaluated. Additionally the SAW surfaces were characterised microscopically after the exposure.

Results

Independent of the surrounding atmosphere, all devices showed degradation effects of both metallisation and chip surface, respectively. Reactive atmospheres, like O₂ and air, degraded the metallisation severely, but retained the oxidation state of the crystal materials. Of the noble gases tested, He had the smallest impact on the metallisation; the devices stayed partly functional up to 600°C. In Ar and Kr, the metallisation showed considerable dewetting, and the LN materials darkened, due to loss of oxygen. While this effect also occurred under vacuum, at ≤ 1 mbar the metallisation was hardly affected, and those devices showed the most stable signals.

Discussion and Conclusions

The protective gas used within hermetic packages is crucial for the HT durability of SAW devices. The annealing tests showed that piezoelectric substrates and metallisations would ideally require different ambient atmospheres. For practical applications, a trade-off between degradation of the substrate and the metallisation has thus to be found. At present, the best compromise is to use a vacuum preceded by an inert gas purge as SAW packaging atmosphere for HT applications.

P1-T.Tags and Sensors

Sala Orange

Monday, September 21, 2009, 10:00 am - 11:30 am

Chair: **Viktor Plesski**
GVR Trade SA

P1-T-01

Sensitivity evaluation of a SH-SAW based micro rate sensor

Wen Wang¹, **Shitang He**¹; ¹Chinese Academy of Sciences, institute of Acoustics, Beijing, Beijing, China, People's Republic of

Background, Motivation and Objective

Recently, interests for surface acoustic wave (SAW) gyroscope have greatly increased owing to its superior inherent shock robustness, low cost and simplicity. The first purpose of this paper is to establish a theoretical model on shear horizontal (SH) SAW gyroscopic effect. Another aim is to develop a novel SH-SAW micro rate sensor, which utilizes two delay-line-oscillators with opposite direction on ST-90oX quartz with gold metallization.

Statement of Contribution/Methods

Fig. 1 shows the schematic and the principle of the sensor system using a differential scheme. When the sensor is subjected to the rotation, a running wave was induced by the Coriolis force, and coupling with the carry wave, modulating the wave velocity and producing changes at the frequency output of the oscillator. The 80MHz delay line was fabricated for the feedback element using the lift-off technique with gold metallization on ST-90oX quartz, which supports a SH SAW propagation. SPUDT and combed transducers were used to structure the SAW device.

Results

Fig. 2 shows the calculated interrelations among the relative sensitivity, normalized gold thickness and rotation rate, resulting in optimal gold thickness of ~0.007, moreover, larger electromechanical coefficient (0.35%) and high velocity (4500m/s) are observed from the SH-SAW at such gold thickness. The sensor response towards to the external rotation was measured by the rate table. In the gyroscope experiment, high frequency sensitivity of ~2Hz/deg/sec was evaluated in the rate ranges of 0~2000 deg/sec.

Discussion and Conclusions

A theoretical analysis on SH-SAW gyroscopic effect was performed, the optimal design parameters was extracted. High sensitivity was observed in the gyroscope experiment by rate table setup using the fabricated SH-SAW micro rate sensor.

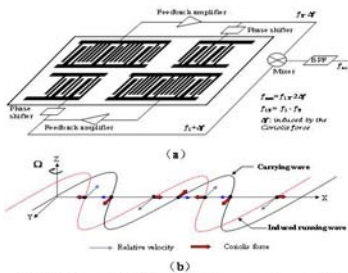


Fig.1 (a) schematic of the micro rate sensor system, (b) SH-SAW perturbed by rotation

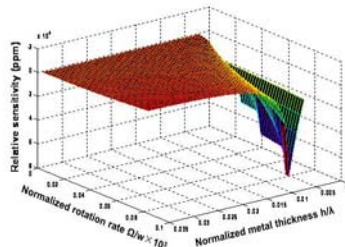


Fig 2 the interrelations among the relative sensitivity, normalized metal thickness and normalized rotation rate

Monday
Poster

Measurement of naturally collimated propagation of SAW around the Z axis cylinder of a quartz ball

Takayuki Yanagisawa¹, Tsuneo Ogi², Noritaka Nakaso¹, Kazushi Yamanaka³, ¹Toppan Printing Co. Ltd, Tohoku University, JST-CREST, Japan, ²Toppan Printing Co. Ltd, JST-CREST, Japan, ³Tohoku University, JST-CREST, Japan

Background, Motivation and Objective

We have discovered a phenomenon that surface acoustic wave (SAW) on a ball makes ultramultiple roundtrips, and by using a piezoelectric single-crystal ball with an interdigital transducer (IDT), we developed the ball SAW sensor with excellent sensitivity [1]. By moving an IDT close to each position of a quartz ball, it was found that the optimum positions where SAW makes multiple roundtrips with the smallest disturbance were distributed with a meander belt around the Z axis cylinder [2].

Statement of Contribution/Methods

In this study, we developed an orientation controlled ball SAW device with an IDT fabricated at the center of the meander belt, investigated the SAW propagation path on the quartz ball using a proximate planer IDT shown in Fig.1 (a) and measured the roundtrip signals shown in Fig.1 (b).

Results

The distributions of the amplitude at the 2nd and the 20th turns are shown in Fig.2 (a) and Fig.2 (b). They took a meander pattern with a half width of 5°, maximum deviation angle of 2.2° and a period of 120°. This pattern was almost identical to the previously observed meander belt. However, it should be noted that the width of propagation path was maintained even after 20 turns, confirming the collimation of the beam.

Discussion and Conclusions

Fabricating an IDT at a meander belt, we developed an orientation controlled ball SAW device in which roundtrip SAW signals attenuates exponentially without disturbance. By using this device, it is expected that the performance and accuracy of ball SAW sensor will be enhanced.

[1] K.Yamanaka et al., IEEE Trans. On UFFC, 53, 793-801, 2006

[2] T. Yanagisawa et al. Jpn. J. Appl. Phys.47, No.7, (2008), 4081

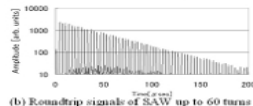
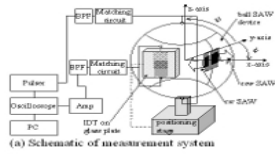


Fig.1

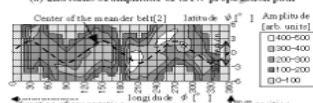
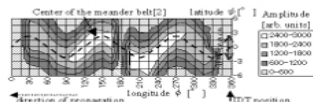


Fig.2

A Wireless Pressure Sensor Based on Surface Transverse Wave

Tao Han¹, Xiaojun Ji¹, Weibiao Wang², Hongyun Li¹, De Zhang³, ¹Shanghai Jiaotong University, China, People's Republic of, ²Shoulder Electronics Limited, Wuxi, China, People's Republic of, ³Nanjing University, China, People's Republic of

Background, Motivation and Objective

Surface acoustic wave (SAW) pressure sensors can be passive (no power required), wireless and well suited for measuring pressure in moving objects (e.g., cars or truck tyres). The SAW pressure sensor is usually composed of a clamped circular quartz membrane, where a one-port Rayleigh wave mode resonator is fabricated. However, the resolution and the measurement range of the sensor are limited by the encapsulation of sensing structure, the low

Monday Poster

pressure sensitivity of the Rayleigh wave mode, and the not high Q factor of the Rayleigh wave mode SAW resonator, which is related to the Cramer-Rao lower bound of the frequency estimation. In order to improve the reliability and the accuracy of the wireless pressure sensor, in this paper, a wireless pressure sensor based on surface transverse wave (STW) is studied.

Statement of Contribution/Methods

Combined with the perturbation theory proposed by Tiersten and the Green's function simulator, the pressure-induced frequency shifts for STW on quartz are calculated. Some optimal cut orientation on quartz with both high pressure sensitivity and delay temperature stability of STW are determined. In order to further improve the sensitivity of the sensor, a novel cantilever package is proposed. The strain distribution on the substrate is simulated by finite element method, and the performance of the pressure sensor is analyzed.

Results

The calculated results demonstrate that the cut orientation in vicinity of BT cut membrane has simultaneously both high pressure sensitivity and delay temperature stability of STW. The pressure sensitivity is over two times that of the ST-cut for SAW. In addition, the FEM analysis shows that the cantilever package can isolate the stress interference, and the stress sensitivity does not change with the position imposed by the external force.

Discussion and Conclusions

We have developed a high sensitivity STW pressure sensor with very low temperature dependence. The geometry of the sensor were determined by using a FEM software. The experimental data show that the pressure sensitivity is sufficiently high and the relative frequency shift varies linearly.

This paper is supported by Natural Science Foundation of China under Grant 60774052, 50875167, and Shanghai Rising-Star Program 08QA14037.

P1-T-04

SAW Tags Based of the Selfmatched Unidirectional Transducers

Boris Sveshnikov¹; ¹State University, Nizhny Novgorod, Russian Federation

Background, Motivation and Objective

Single-phase unidirectional transducers (SPUDTs) allow reduction of the insertion loss in SAW tags. Parasitic "double-transit" signals, caused by additional SAW reflections from a transponder, may be notably decreased there also. However, one can achieve both these goals only with external matching circuitry, increasing the tag cost. The possibility to develop self-matched unidirectional transducers (SMUDTs), which provide at the same frequency self-matching and high degree of the SAW radiation directionality on substrates with strong piezoelectricity (such as LiNbO₃), has been found in 1992 [1]. Being properly designed, SMUDT provides the maximum radiation directionality $D_{max} \gg 1$ at frequency 'fm' (which doesn't coincide with the fundamental Bragg frequency 'fo'), compensating at the same point the static capacitance 'Co' of a transducer by its motional reactance, so that the total SMUDT susceptance disappears under $f=fm$: $Im\{Y(fm)\} = Im\{Ya(fm)+i2\pi fmCo\} = 0$. Investigation of the SAW tags using similar transducers as transponders is the present report objective.

Statement of Contribution/Methods

Flexible and reliable approach, presented at the 1999 Ultrasonics Symposium and named as SEA ("Sequential Enumeration of Aplitudes"), is applied to simulate the SAW tags with arbitrary architectures. When finding (by simple algorithm in the frequency domain) the spatial distribution of SAW amplitudes within a tag, one can always verify validity of the obtained results using two fundamental principles - energy conservation law in the hypothetical absence of dissipation and the reciprocity principle in general case. The tag time-domain response to interrogating radio-frequency pulse with arbitrary duration is calculated afterwards by usual FFT technique.

Results

Setting the desired transduction loss level we find the corresponding D_{max} -value and optimal parameters of a SMUDT: its aperture, number 'N' of periods and reflectivity per one period, as well as the frequency shift $\Delta f=fm-fo$. The optimal (minimizing N-value) magnitude of the phase parameter of radiation directionality ($|\varphi|$) in SMUDT is equal to $\pi/4$ (in contrast with SPUDTs, where $|\varphi_{opt}| = \pi/2$). Under given number of the coding reflectors and known attenuation coefficient (characterizing propagation loss and depending on the substrate type and working frequency) one can synthesize the desired spatial distribution and architectures of all reflectors to provide the rather uniform amplitudes of all pulses in the time domain response of a tag.

Discussion and Conclusions

Calculations confirm efficiency of the proposed solution which simplifies the SAW tag architecture. This circumstance may facilitate considerably manufacturing of the low-cost RFID SAW systems. Substrates supporting the natural directionality effect represent the special interest with this view.

[1] B.V. Sveshnikov, Sov.Tech.Phys.Lett. 18(4), 1992, pp.210-212

P1-T-05

A High Efficiency Encoding SAW RFID at 920 MHz ISM Band

Along Kang¹, Tao Han¹, Haodong Wu², Yongan Shui^{2,1}*Shanghai Jiaotong University, China, People's Republic of*
²*Nanjing University, China, People's Republic of*

Background, Motivation and Objective

In recent years, SAW RFID provides some solutions to identify in harsh environments or where long read ranges are required, where ordinary semiconductor based RFID technologies have been failed to be deployed. However, SAW RFID tags had limited commercial success primarily because SAW tags could only implement a limited set of unique ID number. One high code capacity solution proposed by RFSAW satisfies the global RFID requirements using the international 2.45GHz ISM band with 40-80MHz bandwidth [1]. As for another ISM frequency band at about 920 MHz, which is more common for semiconductor based RFID, only a narrow bandwidth of 5 MHz is permitted in terms of the governmental mandated emission requirements. It is more difficult to obtain high code capacity for SAW RFID with such a narrow bandwidth. In this paper, a new encoding system is proposed so as to be more efficient and be suitable for the application at 920 MHz ISM band.

Statement of Contribution/Methods

According to the practical errors of RFID system, we use adequate value of the demodulation resolution so as to enlarge the code capacity greatly. The 112 degree Y-rotated LiTaO₃ is utilized as the substrate. In a not very large temperature range, the temperature calibration could be relieved, and therefore, more reflectors can be used for encoding.

Results

In case of the lengths of the chips are 6mm and 10mm, the tags are composed of a transducer and 8-12 reflectors. the code capacities are correspondingly 3×10^9 and 10^{21} . SAW RFID prototypes working at the frequency range of 917.5-922.5 MHz is designed and fabricated. The tags are identified experimentally as the designed code values.

Discussion and Conclusions

The result demonstrates that after our method, in narrow bandwidth case, even on a wafer with practical length, the code capacity is high enough to guarantee the global application, the anti-collision and error checking requirements.

Acknowledgement

This paper is supported by Natural Science Foundation of China under Grant 60774052,10774073 and Shanghai Rising-Star Program 08QA14037.

[1] C. S. Hartmann. A global SAW ID tag with large data capacity, Proceedings of the IEEE Ultrasonics Symposium, pp. 65-69, 2002.

P1-U. Transducer Materials and Characterization

Sala Orange

Monday, September 21, 2009, 10:00 am - 11:30 am

Chair: **Ahmad Safafi**
Rutgers

P1-U-01

Improvement of Subharmonic Phased Array for Crack Evaluation (SPACE) with LiNbO₃ Single Crystal Array Transmitter

Hiroaki Endo¹, Yohei Shintaku¹, Makoto Hashimoto¹, Yoshikazu Ohara¹, Kazushi Yamanaka¹; ¹Department of Materials Processing, Tohoku University, Sendai, Miyagi, Japan

Background, Motivation and Objective

Closed cracks in structures cause overlooking and underestimation. Thus we developed subharmonic phased array for crack evaluation (SPACE), and demonstrated accurate sizing of closed fatigue and stress corrosion cracks. However, previously we used a single LiNbO₃ crystal (LN) transmitter on a wedge and transmit a large amplitude ultrasound with a fixed deflection angle. Therefore we needed to move the transmitter or exchange it, in order to vary the deflection angle. Here we propose an improved approach with LN array transmitter which can steer the large amplitude ultrasound.

Statement of Contribution/Methods

To examine the area to which we can steer a large amplitude ultrasound, we measured the displacement distribution on a back surface of an aluminum specimen at several steering angles using a laser interferometer. Then, we imaged a closed fatigue crack at different steering angles.

Results

Fig. 1 shows the displacement distribution at different steering angles. Whereas the natural beam deflection by the wedge is 45°, we confirmed that the LN array transmitter can steer ultrasound of more than 20 nm amplitude to within 30° and 60°. Fig. 2 shows images of the fatigue crack. In the fundamental images (f), the crack was not observed. In the subharmonic images (f/2), a crack tip was clearly visualized at optimized steering angle of 45° and 51°.

Discussion and Conclusions

If we use a divergent wave to detect cracks in a wide area, the wave amplitude would be too small to generate subharmonics. However, we observed clear subharmonic images of closed cracks in a wide area without moving or exchanging transmitters. Therefore we conclude that the LN array transmitter significantly improves the SPACE.

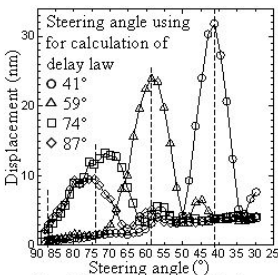


Fig. 1 Displacement distribution

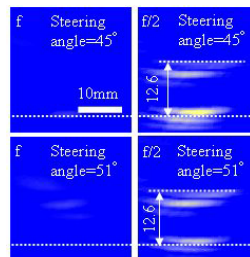


Fig. 2 Images of the fatigue crack

Nanocomposite cerium oxide hybrid polymer matching layers with adjustable acoustical impedance between 4 MRayl and 7 MRayl

Frank Tiefensee¹, Anette Jakob¹; ¹Ultrasound, Fraunhofer-Institute for Biomedical Engineering, St. Ingbert, Saarland, Germany

Background, Motivation and Objective

The positive effect of matching layers is widely known in ultrasound technology. New ultrasound applications in medical diagnosis in ophthalmology, dermatology and vascular wall diagnosis use frequencies up to 100 MHz, because high frequencies and therefore small wavelengths allow a better spatial resolution. The state of the art to produce matching layers is to mix micro scale powders in a polymer and to adjust the acoustic impedance by the content of the particulate component. The micro scale particles are the limitation of these matching layers, because they lead to strong scattering at frequencies higher than 10 MHz. The objective of the presented work was to develop a new matching layer material for high frequency applications with adjustable acoustical impedance up to 7 MRayl.

Statement of Contribution/Methods

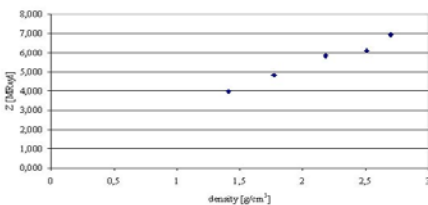
The acoustic impedance of 7 MRayl could be reached with nano particles of cerium oxide in an epoxy functionalized organic inorganic hybrid polymer, that can be cured thermally. The chosen particles are commercially available and have average diameters between 10 nm and 15 nm. To avoid agglomeration of the particles, their surface was modified prior to use. Thereafter an aqueous solution of the modified nano particles was mixed with 3-glycidoxypropyltriethoxysilane and zirconium butylate.

Results

The acoustic impedance can be varied continuously between 4 MRayl and 7 MRayl. The acoustic impedance is a linear function of the density with a slope of 2100 m/s. To prove the functionality of the new material 100 MHz ultrasound transducers were furnished with the new matching layer. The amplitudes of the signals with matching layer were about 100 % higher. The measurements also allowed to measure the attenuation factor of the material, which was 0.5 dB/μm.

Discussion and Conclusions

A new way to synthesize nano composite materials for matching layers is shown. The particles in the layer agglomerate to units of 20 nm diameter. At 100 MHz the wavelength in the material is 21 μm, so the agglomerates don't cause scattering. As the material is synthesized via a wet chemical approach, solvents can be used to adjust the viscosity. The matching layers were produced with a spin coating process and the thickness could be varied between 1 μm and 10 μm. The functionality of the material could be shown with 100 MHz transducers.



Comparison of different piezoelectric materials for acoustic microscopy transducers

Anette Jakob¹, Michael Bender¹, Frank Tiefensee¹, Robert Lemor¹, Qifa Zhou², BenPeng Zhu², K. Kirk Shung², Michael Bender³, Tobias Lehnert³, Michael Veith³; ¹Ultrasound Department, Fraunhofer IBMT, St. Ingbert, Germany, ²NIH Transducer Resource Center and Department of Biomedical Engineering, University of Southern California, Los Angeles, California, USA, ³Leibnitz Institut für Neue Materialien, Saarbrücken, Germany

Background, Motivation and Objective

Acoustic microscopy allows non-invasive investigation of biological tissues and cell imaging. The small dimensions of structures of interest require ultrasound transducers with frequencies from 50 MHz to 1 GHz to

Monday Poster

obtain the needed lateral and axial resolution. The ultrasound is generated with thin piezoelectric films with a thickness from 1 μm to 25 μm . Comparing the piezoelectric parameters of different piezoelectric materials leads to lead zirconate titanate, PZT, as the best choice as transducer material, but zinc oxide based transducers are still state of the art in acoustic microscopy because of the difficulty in fabricating high performance thin PZT films. In this work we have compared promising PZT materials fabricated with novel technologies (sol-gel PZT and MOCVD PZT) to ZnO. Their performance for applications in acoustic microscopy was evaluated.

Statement of Contribution/Methods

Piezo films of the following materials with similar aperture size, frequency and substrate materials have been realized including:

ZnO by physical vapour deposition method (PVD),

PZT by metal organic chemical vapour deposition method (MOCVD) using a novel single source precursor,

PZT by ceramic powder / sol-gel solution modified composite method (sol-gel).

The films were characterized by measuring their piezoelectric parameters. After assembly the lateral and axial resolution of transducers in an acoustic microscope were quantified.

Results

ZnO films from 1-25 μm thick on silicon and sapphire substrates were built. Reactive sputtering at 400°C led to piezoelectric films with wurtzite lattice structure. Assembled transducers showed acceptable performance in acoustic microscopy.

Crack free PZT films from 1-3 μm thick were deposited by using MOCVD method of a novel single source precursor. X-ray diffraction analysis revealed the epitaxial growth and chemical composition near the morphotropic phase boundary.

Piezoelectric thick films from 1-20 μm thick with enhanced electrical properties have been fabricated on the (111) Pt/Ti/SiO₂/Si substrate using a ceramic powder/sol-gel solution modified composite method. X-ray diffraction analysis and scanning electron microscope revealed that the film was in the well-crystallized perovskite phase and cracked free. The film exhibited good dielectric and ferroelectric properties. At 1 KHz, the dielectric constant and the loss were 1925 and 0.015, respectively. The remnant polarization was 42.0 $\mu\text{C}/\text{cm}^2$ at room temperature. The dielectric constant and the polarization of the film are much larger than those of the films reported in the literature and previous work.

Discussion and Conclusions

The precursor synthesis for PZT methods is complex whereas ZnO can easily be sputtered with commercial available targets. The new PZT films showed promising piezoelectric parameters compared to ZnO. Their availability will lead to transducers with improved performance in acoustic microscopy.

P1-U-04

A Novel Method to Determine the Electric, Piezoelectric and Elastic Coefficients of Thin Piezoceramic Fibers

Thomas Rüdig¹, Robert Dittmer¹, Andreas Schönecker^{1,1} *Dielectric Ceramics and Composites, Fraunhofer IKTS, Dresden, Germany*

Background, Motivation and Objective

PZT fibers are used in 1-3 composites to obtain high end ultrasound transducers. The advantages refer to improved and adjustable acoustic impedance, bandwidth and sensitivity. The performance of the ultrasound transducer depends on the properties of the 1-3 composite and the individual piezoelectric fibers. Consequently the electrical, mechanical and electromechanical properties of single fibers have to be determined. The brittle nature of the ceramic fibers and their high aspect ratio limit the use of known standard measurement methods applicable for piezoceramics.

Statement of Contribution/Methods

A novel non-destructive and contactless method, developed at IKTS, is based on ultrasound guided waves in solids. The piezoelectric fiber itself is used for generating and receiving ultrasound waves. Mechanical contact points and consequently source of errors between transducer and wave path are avoided. For electromechanical coupling two pairs of ring electrodes are applied. One set of the ring electrodes is placed on the end and the other set is placed in the middle of the long fiber (>100 mm). The fiber segments between the two pairs of ring electrodes are poled in parallel to the fiber direction. Applying a pulse voltage on the pairs of ring electrodes at the end of the fiber generates an ultrasound wave propagating along the fiber as a quasi longitudinal wave.

Results

The novel method requires a set of different measurements, e.g. delay time (pulser-receiver and transmission) and echo signal amplitude under different electrical boundary conditions of the poled and electrical contacted segment in the middle of the fiber. By adjusting the electrical boundary conditions the Young's Modulus Y^E and Y^D , meaning the short-circuit-conditions and open-circuit-conditions, respectively, can be determined. Applying the known piezoelectric equations the electromechanical properties k_{33} und d_{33} can be calculated. Additionally, the calculation requires the density of the fiber and the dielectric constant of the poled fiber segment, which are determined by standard measurement methods.

Discussion and Conclusions

For comparison standard electrical measurement methods are applied to 1-3 composites made of PZT fibers. A laser vibrometer measurement is used to visualize and understand the propagation of the ultrasound wave guided by the piezoelectric fiber. In parallel, an electromechanical model of single fibers under ultrasound wave loads has been developed and used for the interpretations of the measurements results. The novel characterization method is designed for single fiber measurements. The results can be used for materials development and quality control. Improved piezoelectric fibers will significantly enhance the performance of 1-3 composites as well as ultrasound transducer made of 1-3 composites.

P1-U-05

Modulation and Codification of Ultrasonic Signals with EMFi Transducers

Fernando Seco^{1,1}*Sistemas, Consejo Superior de Investigaciones Científicas - CSIC, Arganda del Rey, Madrid, Spain*

Background, Motivation and Objective

The electromechanical film (EMFi) is a thin polypropylene film with electret properties, high flexibility and large bandwidth, which makes it suitable for construction of ultrasonic transducers for air applications. The limited bandwidth of currently available transducer technology restricts the use of spread spectrum CDMA (Code Division Multiple Access) signal processing techniques and its potential benefits to many ultrasonic applications: simultaneous operation of many transducers, increased resistance to noise obtained through processing gain and higher measurement accuracy. In this research we explore experimentally the benefits of CDMA modulation and codification of ultrasonic signals with custom-built EMFi transducers.

Statement of Contribution/Methods

Our ultrasonic system consists of 20 mm x 20 mm square EMFi emitters and receivers in a direct air transmission setup, with associated electronics (arbitrary function generator, wideband power amplifier, signal amplifier and acquisition card). CDMA signals are created, acquired and processed in a PC. We have experimented with EMFi emitters/receivers consisting of one to three stacked layers, to explore different combinations of transducers bandwidth and gain.

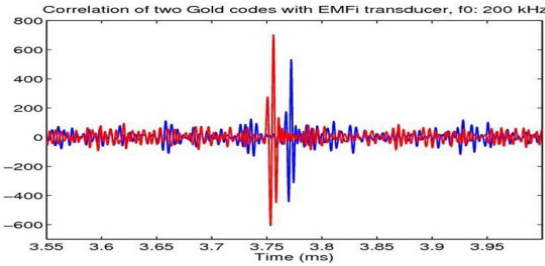
Results

The usable frequency range of a single layer EMFi transducer in air is DC to 300 kHz, with transmitting SPL of up to 95 dB at 30 cm; these characteristics can be changed by stacking several layers of the film.

In the experiment shown in the figure, we simultaneously transmitted two BPSK-modulated, 255 bits long Gold code signals with central frequency 200 kHz and 1 cycle/bit, through two EMFi transducers placed side by side. In spite of the high attenuation of ultrasound in air, the signals are easily resolved by correlation by an EMFi receiver placed 1 m away from the emitters, achieving better efficiency than other ultrasonic transducers.

Discussion and Conclusions

The performance of EMFi transducers for transmission of spread spectrum signals exceeds that of commonly used transducers (piezoelectric, capacitive and PVDF) for air applications. We are exploring modifications of the film for custom design of transducers. Results are interesting for robot navigation and exploration, local positioning systems, nondestructive testing, and medical ultrasound applications.



P1-U-06

A study of time stability of piezoelectricity in porous polypropylene electrets

Hidekazu Kodama¹, Yoshinobu Yasumo², Munehiro Date², Eiichi Fukada²; ¹Kobayasi Institute of Physical Research, Kokubunji, Tokyo, Japan, ²Kobayasi Institute of Physical Research, Kokubunji, Tokyo, Japan

Background, Motivation and Objective

Porous polymer electrets show a large piezoelectricity in a thickness mode. Time stability of piezoelectricity in porous polypropylene electrets was studied by dielectric, elastic, and piezoelectric properties.

Statement of Contribution/Methods

A porous polypropylene provided by Yupo Corporation was used. Aluminum electrodes were deposited on both surfaces of the sheet. The sample was charged by corona discharge. Frequency spectra of relative complex permittivity.

Results

Fig. 1 shows frequency spectra of real and imaginary parts of relative permittivity measured before charging, just after charging and after 2 days passed from charging. The real part at 1 kHz increased from 1.20 to 1.39 by charging and further increased to 1.44 after 2 days passed from charging. As shown in fig. 2, real and imaginary parts in charged samples show a resonance due to a thickness mode around 250 kHz. The peak of the imaginary part moved to higher frequency and its height decreased after 2 days passed from charging. The spectra gives $k_t = 0.080$, $c_{33} = 0.633$ MPa just after charging and $k_t = 0.074$, $c_{33} = 0.681$ MPa after 2 days passed from charging where k_t is the electromechanical coupling factor and c_{33} is the elastic constant. The approximate piezoelectric constant d_{33} was 350 pC/N just after charging and decreased to 317 pC/N after 2 days passed from charging.

Discussion and Conclusions

The results suggest that pores account for 67 % of a thickness before charging, decrease to 44 % by charging, and further decrease to 39 % after 2 days passed from charging. A decrease of k_t suggests a decrease of an electric charge in a sample. A decrease of d_{33} is mainly caused by both a decrease of electric charge and an increase of elastic constant.

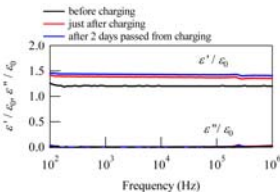


Fig. 1. Frequency Spectra of a real part ϵ'/ϵ_0 and an imaginary part ϵ''/ϵ_0 .

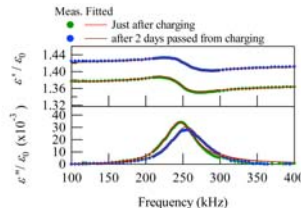


Fig. 2. A dielectric resonance of charged samples.

Characteristics of Thin Film Piezoelectric Ultrasonic Transducer Array by Chemical Solution Deposition

Jaakko Palosaari¹, Jari Juuti¹, Frode Tyholdt², Niels P. Østbo², Andreas Vogl², Erik Poppe², Sigmar Guðbjörnsson³, Erling Ringgaard⁴, Bertil Hök⁵, Per-Erik Fägerman⁶, Per Gloersen⁷, Henrik Røder⁸, Heli Jantunen¹, ¹Microelectronics and Materials Physics Lab., EMPART Research Group of Infotech, University of Oulu, Finland, ²SINTEF, Norway, ³Star-Oddi Ltd., Iceland, ⁴InSensor A/S, Denmark, ⁵Hök Instrument AB, Sweden, ⁶Mandalon Technologies AB, Sweden, ⁷Infineon Technologies SensoNor AS, Norway, ⁸Sonitor Technologies AS, Norway

Background, Motivation and Objective

Small, cost-effective and low voltage transducers are needed in wide range of modern applications. Different types of micro-electro-mechanical systems (MEMS) have been utilized in, for example, sensors, micropositioning and ultrasonic transducers. Among different designs of force and displacement productions piezoelectrics offer great advantages in terms of energy density, compactness, simplicity, operation frequency and accuracy. In this paper, thin film piezoelectric ultrasonic transducers with a two electrode design manufactured via chemical deposition (CSD) on a silicon wafer are introduced and their characteristics are measured. The aim is to realize ultrasonic transducers feasible for animal monitoring in biological research.

Statement of Contribution/Methods

The transducers were fabricated on a silicon wafer by CSD where PZT was deposited with a total thickness of ~2 µm. Afterwards, a cavity was wet etched underneath the piezoelectric layer creating a bending membrane with a total thickness of ~13 µm. Different transducers with cavity sizes from 0.056 mm² to 0.154mm² were manufactured and electrical and electromechanical properties were measured as a function of frequency with a fiber-optic laser vibrometer (OFV-5000 Polytech GmbH, Germany) and network analyzer (3577A Hewlett Packard, USA).

Results

The measured resonance frequencies for the transducers varied from ~780 kHz to ~2000 kHz and the displacements from ~100 nm to ~290 nm. These displacements resulted to effective piezoelectric coefficients from ~100 nm/V to ~290 nm/V. Q factors from 70 to 135 were obtained from the transducers resonance oscillations.

Discussion and Conclusions

Piezoelectric transducers have successfully fabricated via CSD for 1 MHz range. Simulated cavity sizes corresponded well with the measured resonance frequencies. High Q factor and low voltage operation enable long-term reliability for the transducer.

Lead-free piezoelectric thick films based on potassium sodium niobate solutions

Karsten Hansen¹, Konstantin Astafiev², ¹InSensor A/S, Kvistgaard, Denmark, ²Ferroperm Piezoceramics A/S, Kvistgaard, Denmark

Background, Motivation and Objective

Lead-based piezoelectric materials such as lead zirconate titanate (Pb(Zr_xTi_{1-x})O₃ or PZT) and lead meta-niobate (PbNb₂O₆) are the most widely used materials nowadays in the market for piezoelectric application, including recently developed thick films based devices, because of their excellent piezoelectric properties, good reproducibility, and low production cost. At the same time, the high lead toxicity, problems with the recycling and disposal of piezoelectric devices containing lead have inspired wide investigations of the lead-free piezoelectric materials. The necessity in development of biocompatible piezoelectric materials for the medical applications has additionally motivated an activity in the field of lead-free piezoelectrics.

Statement of Contribution/Methods

In present work, the processing route for (K_{0.485}Na_{0.485}Li_{0.03})(Nb_{0.8}Ta_{0.2})O₃ (KNN) based lead-free piezoelectric ceramic powder, which can be sintered at lower temperatures and therefore used for the thick film production, has been developed. The possibility of screen printing lead-free piezoelectric thick films has been demonstrated by manufacturing a number of different structures on two types of substrates: alumina substrates for showing the compatibility of KNN and the screen printing technology, and porous substrates (acoustically engineered KNN bulk ceramics) for manufacturing a lead-free thick film based high frequency transducer.

Fine powder of Li- and Ta-modified KNN, and other commercial available ingredients were used to manufacture a paste, which is compatible with the screen printing technique. The lead-free thick films were pressed in green state with a cold isostatic press (CIP) to obtain high green state density. Problems with humidity, moisture and polarisation are discussed, evaluated and a well suited solution is obtained.

Lead-free thick films prepared have been characterised using several methods. The ferroelectric activity of the piezoelectric material has been determined by the Sawyer-Tower setup. d_{33} piezo-meter, impedance analyser and pulse echo system (in case of the acoustic transducers) have been utilised in order to measure the chosen properties of the material and the test devices. Microstructure characterisation has been carried out with a scanning electron microscope.

Results

The measured (effective) d_{33} piezoelectric coefficient of the investigated lead-free KNN thick films is equal to 80 pC/N. Moreover it has been demonstrated that the developed material is fully compatible with the screen printing technology.

Discussion and Conclusions

According to the best knowledge of the authors these results are the most successful and one of the few published results on lead-free piezoelectric thick films.

P1-U-09

Ultrasound-Assisted Hydrothermal Method for piezoelectric materials

Peter Bornmann¹, Takeshi Morita², Yoichi Kadota², Ryo Ageba²; ¹University of Paderborn, Germany, ²The Univ. of Tokyo, Japan

Background, Motivation and Objective

Piezoelectric ceramics are used in many technical applications, e.g. fuel injection systems and positioning devices. Due to legislative lead free piezoelectric ceramics are requested because they are not harmful. Compared to conventional ceramics the production is more complex and takes longer times. This process, namely the hydrothermal method, can be considerably improved by ultrasound assistance. Another application for the hydrothermal method are PZT thin films.

The aim of this research topic is to build a system for the ultrasound-assisted hydrothermal method to produce lead free piezoelectric ceramics of high quality which are producible at moderate costs. Another aim is to improve the production of PZT thin films.

Statement of Contribution/Methods

The synthesis is carried out under high pressure and high temperature in a pressure vessel. For applying ultrasound directly to the solution the transducer has to be resistant against the corrosive KOH and has to be able to apply sufficient acoustic power under the mentioned conditions. Especially the high temperature is a challenge for the transducer because of depolarization effects in the piezo ceramics and because of increasing performance of the a conventionally built transducer.

Regarding these requirements a transducer from Hastelloy C-22 was designed which is resistant against KOH. Conservation of prestress was achieved using aluminium washers which compensate the prestress loss.

For withstanding higher temperatures, PIC 181 ceramics were chosen which have a Curie-temperature of 330°C and are designed for high-power acoustic applications.

To achieve high output velocity the horn of the transducer was optimized concerning amplitude magnification.

Results

First tests using the ultrasound-assisted hydrothermal method have shown that shortened reaction times were achieved while a fine-grained powder was produced what leads to ceramics and thin films of higher quality.

The improved transducer design showed good performance under load. Due to the aluminium washers the performance did not decrease by elevating the temperature up to 140°C.

Discussion and Conclusions

The advantages of the ultrasound-assisted hydrothermal method have been proven in first tests. Lead free ceramics and PZT thin films of high quality could be produced while the reaction time was shortened. The results also showed that further advancements are possible by increasing the acoustic power applied to the solution. In respect thereof the improvements in the transducers design were successful. The built transducer generates high acoustic power under load and its performance does not decrease at elevated temperatures.

For further improvements the parameters of the sound field will be optimized. Therefore simulations and measurements will be done to find out which sound field parameters are best for the process (e.g. standing waves, streaming effects and cavitations) and how these parameters can be adjusted.

Monday
Poster

P1-U-10

Transparent Ferroelectric Polymer Films for Flexible Electronics

Yoon young Choi¹, Jongin Hong², Kwangsoo No¹; ¹Department of Materials Science and Engineering, Korea Advanced Institute of Science and Technology(KAIST), Daejeon 305-701, Korea, Republic of. ²Department of Chemistry, Imperial College London, South Kensington Campus, London SW7 2AZ, United Kingdom

Background, Motivation and Objective

Great attention has been shown to ferroelectric polymers because they are cheap, lightweight, flexible and easily processed. Among them, poly(vinylidene fluoride-trifluoroethylene), [P(VDF-TrFE)] has stable ferroelectric β -phase at room temperature that exhibits strong ferroelectric properties; and may be applied to transducers, actuators, sensors and nonvolatile memory devices. Recently, organic flexible electronics are being developed for practical applications including computer displays and radio frequency identification tags. However, there is not much investigation of flexibility and transparency in [P(VDF-TrFE)] films. Therefore, we fabricated [P(VDF-TrFE)] thin films on transparent indium tin oxid (ITO)/polyethylene terephthalate (PET) substrates and thereby evaluated an effect of fabrication condition on optical and ferroelectric properties.

Statement of Contribution/Methods

We prepared different concentrations of [P(VDF-TrFE)] solutions, and polymeric films were deposited on the ITO/PET substrates by a spin-coating technique and subsequently annealed at different temperatures. The films were analyzed by Fourier Transform infrared (FTIR) spectroscopy, UV-VIS spectroscopy, atomic force microscopy (AFM) and piezoelectric force microscopy (PFM).

Results

Both concentration and annealing temperature significantly affected the optical and ferroelectric properties. Figure 1 shows surface morphology and piezoelectric response of the [P(VDF-TrFE)] film annealed at 90 °C for 2hours. We could confirm successful polarization of the box patterns on the film.

Discussion and Conclusions

More detailed results will be discussed in the conference.

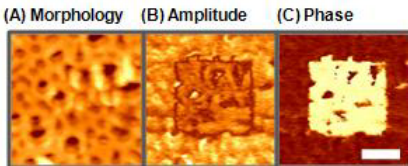


FIGURE 1. Morphology and domain switching of the P(VDF-TrFE) film annealed at 90 °C (Scale bar: 1 μ m)

P1-U-11

Processing of Fine PZT Fibers by Sol-gel Method and Preparation of Piezocomposites

Serkan Tekdas¹, Ebru Mensur Alkoy^{2,1}:¹Gebze Institute of Technology, Kocaeli, Turkey, ²Sabanci University, Istanbul, Turkey

Background, Motivation and Objective

Lead zirconate titanate is the most widely used ferroelectric material in ultrasonic transducers, non-volatile random access memory devices, microelectromechanical devices, sensor and actuator applications due to its high dielectric constant, high electromechanical coupling coefficient, and large remnant polarization. PZT in fiber form is appealing because of its increased anisotropy, improved flexibility and strength over monolithic PZT ceramics. Fiber composites have also been studied for biomedical ultrasound transducer applications. In this study, fine PZT fibers were obtained by sol-gel method and fiber/epoxy piezocomposites were prepared and characterized.

Statement of Contribution/Methods

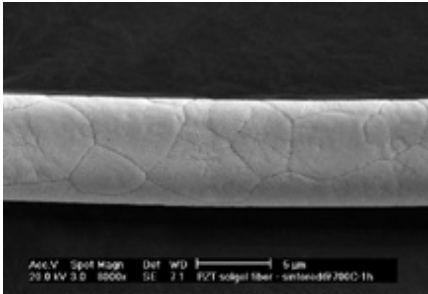
PZT sol-gel solutions were obtained from lead acetate trihydrate, titanium isopropoxide and zirconium n-butoxide in n-butanol. 2-methoxyethanol was used as the main solvent. Acetic acid and water were added to the precursor solution with various ratios to initiate the gelation process. Gelation was carried out at 80°C. Fine PZT fibers were drawn out by hand using a glass rod. Fibers were dried at room temperature and sintered at 700°C. PZT nanopowders were fabricated from the same solution and pellets were prepared by dry pressing.

Results

XRD pattern of the crashed PZT fibers exhibits a pure tetragonal perovskite phase. The effect of various gelating additives on the microstructure and electrical properties were investigated. The gelation and fiber drawing times were also determined for different solutions. The optimum gelation recipe was PZT sol:acetic acid:water ratios of 2:1:1 where longest (30-40 cm) and uniform PZT fibers with an approx. sintered diameter of 10 micrometer was drawn (Fig. 1). The viscosity of the gel was 5x10⁴cP. Piezocomposites were prepared by embedding the fibers into an epoxy matrix. Dielectric constant and loss of PZT pellets were measured as 552 and 2%, respectively. The piezoelectric d_{33} coefficient was found to be 152 pC/N. Ferroelectric, dielectric and piezoelectric measurements were done systematically for composites and pellets prepared under various conditions.

Discussion and Conclusions

The content of the gelling sol was found to be critical on the uniformity and microstructure of the fibers and their electrical properties. Fine, uniform fibers and piezocomposites were prepared and characterized successfully.



P1-U-12

Fabrication and characterization of large area 1-3 piezo-composites based on PMN-PT single crystals for transducer applications

Mai Pham Thi¹, Hung Le Khanh¹, Anne-Christine Hladky-Hennion², Didace Ekeom³, Pascal Tran-Huu-Hu⁴, Marc Lethiecq⁴, Franck Levassort⁴:¹THALES Research & Technology France, Palaiseau, France, ²IEMN-UMR CNRS 8520, Lille, France, ³Microsonics, Saint-Avertin, France, ⁴UMR Imagerie & Cerveau, Université François Rabelais, Tours, France

Background, Motivation and Objective

SONAR applications usually require both large area piezoelectric elements and high piezoelectric properties. Piezoelectric single crystals (PSCs) fulfil this second requirement, but are difficult to fabricate in large sizes while

keeping homogeneous properties. Moreover, 1-3 piezo-composites based on PSC fabricated by the « dice and fill » method (DFM) enable the electromechanical properties to be improved, but their size is often limited by that of the original bulk PSC samples. Recently, an alternative process to DFM based on a lamination technique (LMT) has been developed [F. Wang et al., *Materials Chemistry and Physics*, vol. 105, pp. 273-277, 2007]. It is well adapted to produce large area samples. The aim of this study is to apply the technique to transducers.

Statement of Contribution/Methods

1-3 piezo-composites were fabricated by DFM and LMT with two piezoelectric materials (PMN-PT ceramic and single crystal) and epoxy resin. Design of these composites was performed with finite element analysis (ATILA). Particular attention was paid to sample characterization. An original technique of electrical impedance fitting with FEA was used to determine the properties of both components in their operating conditions. Slight differences were observed between the properties of constitutive materials in a bulk form and in the composite. Moreover, the LMT led to a non perfect alignment of the piezoelectric rods in the composites and this effect was quantified by FEA in terms of electromechanical performance.

Results

The measured thickness coupling factors of the composites obtained by both methods are between 60 and 80% according to the chosen constituents. Several single element transducers with a center frequency around 1 MHz were fabricated. Their characteristics were compared and results showed that sensitivity of the 1-3 LMT piezo-composite based transducer was slightly lower than that of the DFM one, but sufficient to find applications where large area apertures are required

Discussion and Conclusions

1-3 composite transducers have been fabricated by the dice-and-file technique and by the lamination technique. Their performances confirm the utility of the new fabrication method.

P1-U-13

Microstructure of Piezoelectric AlN Films Deposited by AC Reactive Sputtering

Shawn Tanner¹, Valery Felmetsger¹,¹PVD Products Group, Tegal Corporation, San Jose, CA, USA

Background, Motivation and Objective

Piezoelectric AlN films with a high degree of c-axis texture are widely used in resonator-based applications such as BAW and FBAR filters both as the active layer and as the seed layer for metal electrodes. Crystal orientation evaluated by X-ray diffraction (XRD) rocking curves and theta-2theta scans is a critical parameter in sputter process optimization, determining the potential of a given film for application in electroacoustic devices. XRD characterization, however, provides incomplete information as this method can be insensitive to details of the grain structure and, especially, the occurrence of structural defects such as inversion domains which may influence the piezoelectric response. Therefore, in this study, we employed a combination of methods including defect selective chemical etching for comprehensive characterization of the AlN films.

Statement of Contribution/Methods

An ac (40 kHz) reactive sputtering process by a dual cathode S-gun magnetron was used to produce 1000 nm thick AlN films on low doped silicon wafers and on molybdenum (Mo) electrodes. 50 nm thick Mo films were deposited by a dc powered S-Gun on top of 25 nm thick AlN films serving as a seed layer to enhance Mo [110] texture. XRD rocking curve, texture measurements, scanning electron microscopy (SEM), and defect selective etching were employed to evaluate the suitability of a given set of process parameters for the active device layer and seed layer.

Results

Rocking curves of the AlN (0002) diffraction peak of 1000 nm films deposited at various process conditions have full width at half maximum (FWHM) in the range of 0.65 to 4.0 degrees. XRD theta-2theta scans show only [0001] oriented grains to be present regardless of the rocking curve FWHM. Defect selective etching in hot phosphoric acid reveals the presence of inversion domains which can adversely affect device performance. The inversion domain density doesn't correlate well with the FWHM measurements and processes which produce low FWHM don't necessarily produce low inversion domain density. SEM cross sections reveal changes in the grain structure as well. Films with the lowest rocking curves have larger grains, less visible grain boundaries and increased inversion domain density. Films with the lowest inversion domain density have more visible grain boundaries and narrower columnar grains.

Discussion and Conclusions

The implication of these results for the use of AlN as the active layer in piezoelectric devices is not completely clear to us at this point. For seed layer applications however, results indicate that the lowest FWHM AlN films, regardless of the inversion domain density, produce superior results for metal electrode crystal alignment which leads to superior AlN active layer alignment. Using this result, 50 nm Mo electrodes with FWHM of 2.0 degree were produced. Additionally, we have improved our AlN active layer and seed layer technology through the use of a combination of evaluation techniques.

P1-U-14

Piezoelectric Composites: Electromechanical Properties and Design Maps

T Venkatesh^{1,2} Stony Brook University, Stony Brook, New York, USA

Background, Motivation and Objective

Piezoelectric composites have been recognized for their potential towards providing an optimum combination of mechanical and piezoelectric properties in transducers, particularly for biomedical applications. While some models have been developed to study the effective properties of select classes of piezoelectric composite materials, a comprehensive study that provides a quantitative comparison of the fundamental properties and the performance characteristics of all the principal composite classes (where in the constituents exhibit zero-, one-, two- or three-dimensional spatial connectivity) is not yet available. Hence, the objective of our present study is to develop a comprehensive model to predict the complete electromechanical properties of particulate, short-fiber, long-fiber, layered, and networked piezoelectric composites.

Statement of Contribution/Methods

A unique three-dimensional finite element model has been developed to fully capture the complete electromechanical response of five types of piezoelectric composites (i.e., particulate, short-fiber, long-fiber, laminate, and networked composites) where in the constituent phases could, in general, be elastically anisotropic and piezoelectrically active. Furthermore, the effects of fiber shape, fiber distribution, poling orientations, grain-size and porosity shape, orientation and distribution have been modeled as well.

Results

Overall, it is demonstrated that the geometric connectivity of constituent phases in a composite has a significant influence on the fundamental electromechanical properties and the performance characteristics of a piezoelectric composite. Significant influence of the fiber shape on some of the piezoelectric properties of composites has been noted. The distribution of fibers tends to influence the magnitude of interfacial stresses that could develop at the fiber/matrix interface. Changes in poling directions of the matrix and the fiber phases can result in composite materials with multi-directional sensitivity. Furthermore, the orientation, shape and distribution of porosity could have a significant influence on the piezoelectric properties of the composite system as well.

Discussion and Conclusions

By constructing piezoelectric composite materials design maps, the long-fiber composites (with their highest piezoelectric coupling constants) and networked composites (with their highest piezoelectric charge coefficients) are, respectively, identified as being most suitable for ultrasonic imaging and hydrophone applications. Furthermore, grain-size modifications of the constituent phases can significantly enhance the effective piezoelectric properties of a composite such as coupling constants and charge coefficients of a composite while maintaining suitable acoustic impedance, esp., in the case of the networked composites.

P1-U-15

Tapered transmission line implementation of graded matching layers for thickness mode piezoelectric transducers

Sivaram Nishal Ramadas¹, Richard L O'Leary¹, Anthony J Mulholland², Anthony Gachagan¹, Gordon Hayward¹, Alexandre Troge², Richard A Pethrick^{3,1} Centre for Ultrasonic Engineering, University of Strathclyde, United Kingdom, ²Department of Mathematics, University of Strathclyde, United Kingdom, ³Department of Chemistry, University of Strathclyde, United Kingdom

Background, Motivation and Objective

Conventionally, in order to acoustically match thickness mode piezoelectric transducer to a load medium, multiple quarter wavelength (QW) matching layers are employed at the front face of the device. Typically a number of layers, 2-4 in number, are employed resulting in discrete impedance steps within the acoustic matching scheme.

This can result in impedance matching with limited bandwidth characteristics. This paper investigates the application of tapered transmission line filter theory to implement a graded impedance profile, through the thickness of the matching layer scheme, to solve the impedance mismatch problem whilst accounting for enhanced transducer.

Statement of Contribution/Methods

Firstly, the theory to calculate the reflection and transmission coefficients of such tapered impedance profile is presented. Examples include, but are not limited to, exponential, triangular and Chebyshev taper profiles. Simulated pulse-echo insertion loss into water, using both approximate analytical and Finite Element (FE) techniques were used to study different profile designs and the effect of filter design parameters on device bandwidth are also discussed.

Secondly, matching layers with a broad range of acoustic properties for application in piezoelectric probe assemblies are manufactured using a methodology based on photopolymerisation of epoxy resins. The photopolymerisation allows for the rapid fabrication of polymer materials by successive photocuring of thin layers of polymer. The method is elegant in implementation, since the layers can be readily deposited directly onto the front face of the transducer element, eliminating additional bond lines. Indeed, by employing different monomers and dispersing particles into the monomers prior to polymerization, a stratified structure can be produced with the desired acoustic impedance profile.

Results

Finally, results from a range of key prototypes are presented in order to demonstrate the effectiveness of this approach - device fractional bandwidths exceeding 80% are demonstrated, for a nominal 1MHz thickness mode transducer design. Comparison of various graded matching layer devices; along with conventional QW matching layers are presented.

Discussion and Conclusions

The use of tapered transmission line techniques to design matching layers has been presented. The fabrication of graded matching profile for thickness mode transducer designs to improve device bandwidth and SNR is also presented. The experimental and simulation results presented compare well and demonstrate the feasibility of the technique.

P1-U-16

Ultrasonic Extension Sensing of Piezoelectric Multilayer Actuators for Adaptive Optics

Erman Uzgur¹, Shin-Sung Kim¹, Mel Strachan², Katherine Kirk^{1,†}*School of Engineering and Science, University of the West of Scotland, Paisley, United Kingdom, ²UK Astronomy Technology Centre, Edinburgh, United Kingdom*

Background, Motivation and Objective

The technique of wavefront correction using adaptive optics has enormous potential for improving image quality in telescopes through reducing atmospheric distortion effects. Cost effective solutions to the requirements of future high order corrective compact adaptive optic systems is strongly required to maintain the development in telescope systems for obtaining every single information from light received.

We have been investigating technologies, ultrasonic extension sensing of piezoceramic multilayer actuators for deformable mirrors as an alternative to the currently available technologies. Overcoming the hysteresis issue and linearising the piezo-actuators are key factors to sense the position of the deformable mirror surface to better accuracy and more conveniently in a large array of actuators.

Statement of Contribution/Methods

Two different approaches have been investigated for the extension sensing of multilayer piezoelectric actuators: a time-domain technique using pulse-echo measurements and a frequency-domain technique using the resonance spectrum of an integrated transducer or of the actuator itself. Integration of the ultrasonic transducer has been realised by bonding the transducer on top of the actuator or by using electrically separated lamina of the actuator as a transducer.

Results

In both time domain and frequency domain techniques it was observed that an increase in the DC bias was accompanied by a non-linear increase in the acoustic velocity, with a 0.4 % increase at 150 V. The effect of increased velocity is found to be more dominant than the effect of extension in the actuator, thus leading to an

earlier echo during extension under DC bias. The phenomenon of a faster acoustic velocity in actuators under DC bias has been consistently observed both in the time domain and in the frequency domain measurements

Discussion and Conclusions

The resulting relation of the displacement and the time- / frequency-shift shows a strong hysteretic behaviour, which fact does not seem to be favourable in establishing a means of extension sensing by simply measuring the time- / frequency-shift, without pre-knowledge of the relation of velocity to DC bias in the actuator. The two most probable reasons for the hysteresis between frequency-/time- shift and extension are the extrinsic effect (domain motion) in piezoelectrics, or interaction of coupled vibrational modes in the piezoelectric under applied electric field.

Further investigation is deemed necessary to explore the possibility of using some other measurable material parameters of the actuator that have direct correspondence with the amount of extension. Establishing the sound velocity-voltage relationship and extracting the DC effect from the measurements could increase the accuracy of extension sensing. In order to understand the DC effect on actuators, more detailed analysis of the actuator resonant peaks is also required.

P1-U-17

Ceramic Piezocomposites Modeling and Fabrication

Andrey Rybyanets¹, Andrey Nasedkin², Tamara Domashenkina¹, Anastasia Rybyanets³, Maria Lugovaya³.¹Institute of Physics, South Federal University, Russian Federation, ²Faculty of mathematics, mechanics and computer science, South Federal University, Russian Federation, ³Physical Faculty, South Federal University, Russian Federation

Background, Motivation and Objective

The transducer materials presently available for the ultrasonic transducer design in NDT inspection systems are limited, considering combination of high sensitivity (efficiency) and resolution (bandwidth). Over the past years, considerable advances have been made to improve the mechanical properties of ceramics using ceramic composite approaches. Numerous technologies based on incorporating of functional ceramics into structural ones and vice-versa have been developed and the novel design idea has been applied in the field of functional ferroelectric ceramics. However, the problem of property trade-off, i.e. a deterioration of electromechanical properties remains unsolved. In this work, the development of a new family of low-Q ceramic piezocomposites is described.

Statement of Contribution/Methods

New “damped by scattering” ceramic piezocomposites were developed on the base of microstructural design concept. The original microstructural design concept (MSD), is based on controllable substitution during composite formation of separate crystallites or crystallite groups making a polycrystal by pores, crystallites with other composition and/or structure or amorphous substances, all with preliminary choice of chemically, thermally and technologically compatible components and with FEM modeling of polycrystalline composite properties. The main idea of “damping by scattering” approach is introducing scattering particles as a secondary phase into the piezoceramics matrix. Comprehensive FEM calculations based on effective moduli method and direct FEM calculations gives results that take into account real composites microstructure and well agrees with the preliminary experiments.

Results

The ceramic composites composed by the soft PZT matrix with randomly distributed dense refractory crystals with a mean particle diameter 20-200 nm and volume fraction from 9 up to 36 vol.% were fabricated and measured. Complex sets of elastic, dielectric, and piezoelectric parameters of the new piezocomposites were systematically studied using impedance spectroscopy approach and ultrasonic method.

A line of wide-band NDT ultrasonic transducers with high sensitivity and resolution was manufactured and tested. FEM was used to perform the dynamic analysis of focusing ultrasonic transducers from piezocomposite material.

Discussion and Conclusions

A new family of polymer-free ceramic piezocomposites with properties combining better parameters of PZT, PN type ceramics and 1-3 composites for wide-band NDT ultrasonic transducer applications is presented. New “damped by scattering” ceramic piezocomposites were developed based on the original microstructural design concept and characterized by previously unachievable low QM (QMt =2-3) combined with high piezoelectric (d33=250-350) and electromechanical (kt=0.45-0.5) parameters, high Curie point (340°C), low acoustic impedance (15-20 MRayl) in a wide working frequency range (0.2-12 MHz).

LGS (La3Ga5SiO14) Wet-Etching Experiments and Simulations

Guangmin Ouyang¹, He Liu¹, Zekija Ramic¹, Einar Halvorsen^{1,2} Vestfold University College, Norway

Background, Motivation and Objective

LGS is a promising piezoelectric material alternative for high temperature piezoelectric sensors because it remains piezoelectric without any phase transition all the way up to its melting temperature. It is suitable for SAW (surface acoustic wave) devices and can therefore be used for wireless passive sensors. In order to utilize the material, micro-fabrication techniques need to be developed and well characterized. In this work, the LGS wet etching of small grooves has been investigated regarding different temperatures, groove orientations and groove widths.

Statement of Contribution/Methods

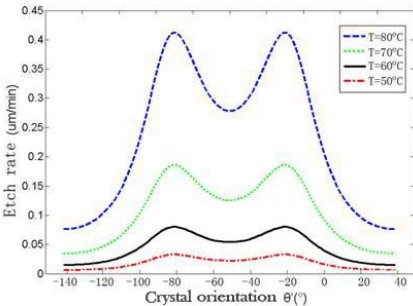
Wafers with orientation (0°, 138.5°, 26.7°), which are commonly used for SAW devices, were investigated. 85% H3PO4 was chosen as the etchant. First, several mask materials were tested to find a suitable mask material. Second, etch properties were investigated with regards to crystal orientation, temperature, activation energy and surface roughness. Finally, a 2-D simulator based on the string algorithm was constructed to investigate the mechanisms of LGS etch profile in grooves.

Results

The experiments indicated that both etch rate and surface roughness are temperature dependent. The etch rate showed good agreement with the Arrhenius equation, and the calculated activation energy for the (0°, 138.5°, 0°) plane was 0.84eV. The surface roughness increase with etch temperature. An anisotropic LGS wet etching in 85% H3PO4 was clearly observed based on different etch profile on grooves with different orientations. In the simulation, the groove etching is described by combined effect of crystallographic anisotropy and a constant lateral etch rate at the polymer/LGS interface. Experiments and simulations show fair agreement and the simulation reproduced orientation dependent anisotropic etching well.

Discussion and Conclusions

In conclusion, we have demonstrated that the profiles of grooves etched in LGS using H3PO4 and a polymer resist, are governed by the anisotropic etch rate of the material and a lateral interface etch rate. Characterisation of the etching process was performed in terms of the etch rate and surface roughness. The etch rate has an Arrhenius form temperature dependence with activation energy of 0.84eV. A 2-D simulator was built using the constructed etch rate model, and it represents the anisotropic wet etching of LGS well.



Novel Piezoelectric Ceramic-Polymer Aligned Composites via the Freeze Casting Method for High Frequency Transducer Applications

Qifa Zhou¹, Benpeng Zhu¹, K.Krik Shung¹, E. P. Gorzkowski², M. J. Pan², ¹University of Southern California, USA, ²Naval Research Laboratory, USA

Background, Motivation and Objective

Recently, there has been an increasing interest in combining piezoelectric ceramics with a passive polymer to form piezoelectric ceramic-polymer 2-2 composites which have not only the high electromechanical coupling and higher dielectric constant for array fabrication but also the low acoustic impedance. There is no report about piezoelectric

Monday
Poster

ceramic-polymer 2-2 composite formed with ice template method which is a promising way for high frequency array application.

Statement of Contribution/Methods

We report a novel approach to fabricate piezoelectric ceramic-polymer 2-2 composites with low cost ice template and a simple directional freezing technology. During directional freezing of an aqueous suspension, ice platelets growth front repels ceramic particles to form the interleaving ice/ceramic layered 2-2 microstructure. Upon freeze drying, the ice platelets sublime and leave a laminar ceramic structure with long empty channels in the direction of the temperature gradient. Subsequently the green ceramic body is sintered to form the final microstructure. Composites could be fabricated after the infiltration with the polymer under vacuum.

Results

The dielectric constant of the composites versus temperature was determined. The peak value of dielectric constant for the PZT-5H and PMN-10PT were 500 and 4000, respectively. The polarization versus field plots for the PZT-5H and the PMN-10PT aligned composite samples show an expected ferroelectric behavior for both samples. The values for the coercive field, remnant polarization, and saturation polarization of PZT-5H and PMN-10PT are 18 kV/cm, 14 $\mu\text{C}/\text{cm}^2$, 17 $\mu\text{C}/\text{cm}^2$ and 5 kV/cm, 7 $\mu\text{C}/\text{cm}^2$, 12 $\mu\text{C}/\text{cm}^2$, respectively, which are comparable to commercially available ceramic samples. of PZT-5H composite was measured to be 0.54, which is similar to that of single phase ceramic. The piezoelectric coefficient (d_{33}) of PZT-5H composite was determined to be ~ 250 pC/N.

Discussion and Conclusions

The measured pulse echo waveform and the normalized frequency spectrum of the PZT-5H aligned composite single element ultrasound transducer showed that the center frequency of the transducer was 58 MHz and the bandwidth at -6dB was around 70%.

P1-U-20

Preparation of Piezoelectric Ceramic Fibers, Springs and Hollow Shells for Transducer Applications Using a Novel Alginate Gelation Method

Sedat Alkoy¹, Cem Gol¹, Emre Tekel¹; ¹Gebze Institute of Technology, Kocaeli, Turkey

Background, Motivation and Objective

Piezoelectric fibers are used in various transducers where solid fibers are aligned parallel to poling direction. In this arrangement fibers are operated in the longitudinal d_{33} mode. Hollow fibers with inner and outer electrodes are needed that utilize the transverse d_{31} mode to increase the displacement under a lower operating voltage. Transducers with hollow shell geometries are also known to have higher d_h and lower acoustic impedance compared to bulk ceramic. In this study, fabrication of solid and hollow lead zirconate titanate (PZT) fibers, springs, and hollow shells using a novel alginate gelation process are reported.

Statement of Contribution/Methods

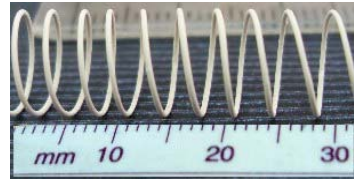
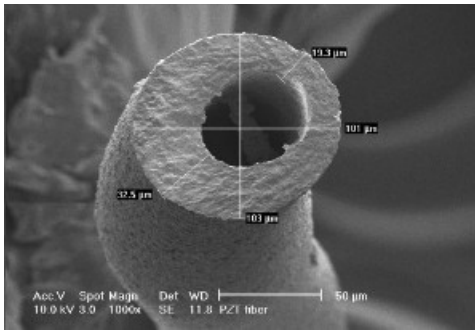
PZT powders were mixed with alginate in DI water to form a viscous slurry. Fibers were obtained by injecting the slurry into a CaCl_2 solution. The exchange of Na^+ with Ca^{2+} ions causes crosslinking of the linear polymers creating a three-dimensional network and confining ceramics particles through fast gelation to form a consolidated green body. Hollow fibers and spherical shells were obtained by dip-coating a sacrificial core with PZT slurry followed by gelation in CaCl_2 .

Results

Dense PZT fibers with solid or hollow cross-section (Fig 1) were fabricated with diameters from 100 to 500 μm . Piezosprings were fabricated (Fig 2) from both the solid and hollow green fibers and sintered in their helical shape. Hollow spherical and ellipsoidal shells were also obtained.

Discussion and Conclusions

Electrical properties indicated that alginate caused a decrease in the electrical properties due to introduction of Na and Ca ions into the perovskite structure. However, properties are still reasonably well to allow their use in transducers with unique properties.



P1-U-21

Multi-Modal and Uni-Modal Functionally Graded Piezoelectric Ultrasonic Transducers

Wilfredo Montealegre Rubio¹, Emílio C. N. Silva¹, Flavio Buiocchi^{1,1} Department of Mechatronics and Mechanical Systems Engineering, University of Sao Paulo, Sao Paulo, SP, Brazil

Background, Motivation and Objective

Usually, piezoelectric transducers are designed to have a multi-modal or uni-modal frequency response, which defines the kind of acoustic wave pulse generated (short pulse or continuous wave, respectively). Per authors' knowledge, multi-modal or uni-modal piezoelectric transducers have not been designed by applying the Functionally Graded Material (FGM) and Topology Optimization Method (TOM) concepts. FGMs are made by changing gradually the properties with position inside a material domain. When this concept is applied to design piezoelectric ultrasonic transducers, reflection waves inside the transducer are reduced, and smaller time waveform (large bandwidth) is achieved. The TOM is a generic and systematic optimization technique, which combines optimization algorithms with Finite Element Method to maximize a user-defined objective function.

Statement of Contribution/Methods

In this work, the main goal is to find the optimal material distribution of Functionally Graded Piezoelectric Ultrasonic Transducers (FGPUTs), including the following requirements: (i) the FGPUT must present one mode with a strong contribution to the response transducer, and the other modes must have resonance frequencies far from the resonance frequency of this strong mode with a weak contribution to the transducer response, thus, a narrowband transducer or a uni-modal dynamic behavior is emulated; (ii) keeping resonances, in the desired frequency band, close to each other, and with their respective modes making a strong contribution to the transducer response, hence, a broadband transducer or a multi-modal dynamic behavior is emulated. For measuring the strength of a specific mode, the Electromechanical Coupling Coefficient (EMCC) is utilized. For tracking a desirable mode, the Modal Assurance Criterion is applied; specifically, FGPUTs are required to oscillate in a thickness extensional mode or piston-like mode (aiming acoustic wave generation application). The optimization algorithm is constructed based on Sequential Linear Programming, and the concept of the Continuum Approximation of Material Distribution is considered.

Results

To illustrate the method, two FGPUTs are designed. FGPUTs are graded along thickness from PZT-5A to PZT-5H properties. For uni-modal FGPUT, the EMCC value of the piston-like mode is increased by 261% while the EMCC values of adjacent modes are decreased by 115%. For the multi-modal transducer, the EMCC value of the piston-like mode is increased by 22%, while the EMCC values of the left and right adjacent modes are increased by 14.5% and 20%, respectively.

Discussion and Conclusions

TOM and FGM concepts have shown to be useful tools for designing piezoelectric ultrasonic transducers with uni-modal and multi-modal dynamic behavior.

Tuesday Oral Sessions

1D. Clinical Ultrasound

Sala 1

Tuesday, September 22, 2009, 8:00 am - 9:30 am

Chair: **Ton van der Steen**
Erasmus Medical Centre

1D-1

8:00 AM **Recent Advances in Clinical Ultrasound**

David Cosgrove¹; *Imperial College, United Kingdom*

Background, Motivation and Objective

Recent developments in diagnostic ultrasound have improved the quality of grey-scale imaging and at the same time improved the ease-of-use of scanners, with attendant lessening of its user-dependence. The introduction of 3D probes, initially mechanical but increasingly via matrix arrays, and of 3D with real time (so-called 4D) have simplified understanding of complex anatomy, especially in the heart and the fetus. The ability to re-slice the image data set to obtain previously unavailable planes (e.g. the C-plane) have improved assessment of some types of pathology, e.g. in the breast and uterus.

Statement of Contribution/Methods

An important innovation has been the development of contrast agents for ultrasound in the form of microbubbles. They act as blood-pool agents and can even be detected in the microvasculature using multipulse techniques at low MI. As well as their importance in cardiology, they have improved the performance of liver ultrasound such that it is an alternative to contrast CT and MR. Quantification of the time intensity curves following bolus iv injection allows early assessment of the response of tumours to antiangiogenesis therapy. They are also essential tools for guiding interstitial ablation therapy in the liver. Microbubbles can be tagged with ligands and therapeutic agents; the former allows molecular imaging, for example of activated endothelium while the latter promises to allow targeted therapy.

Another innovation that seems especially promising is elastography which measures or images the stiffness of tissue as it distorts under an applied stress. An interesting way to apply the stress is to use the acoustic radiation force that a standard transducer produces. The induced tissue motion sets up a shear wave whose velocity is proportional to the tissue elasticity. Measuring the local velocity of the shear wave requires an ultrafast ultrasonic imaging system which has been achieved by using a non-focussed interrogating wave so that the entire image pane is sonicated in a single pulse. Focussing is applied on receive. It is being tested for superficial structures.

Ultrasound has long been used in therapy (physiotherapy and lithotripsy are examples) but the development of effective high intensity focussed ultrasound for non-invasive tissue ablation is an exciting innovation that has been spear headed in China.

Results

Discussion and Conclusions

Thus it can be seen that the field of medical ultrasonics remains active with several exciting developments under way. Some at least should translate into useful clinical tools.

1D-2

8:30 AM **Deformation and velocity measurements with Ultrasound.**

Prof Lars-Åke Brodin, Anna Bjällmark, Matilda Larsson, Frida Lindberg and Dennis Sturm; Royal Institute of Technology KTH Stockholm Sweden

Today can velocity measurements be performed with two different techniques, the Doppler based technique which measure velocities by looking of the phase shift of the returning signal in comparison with the transmitted signal and the reflector based speckle tracking technique. The two techniques are not giving equivalent results, because there are differences how the velocities are achieved. The Doppler method always measure the velocity in the resultant vector towards the transducer. In contrast the standard for reflector based velocities are in parallel with the long axis of the wall or in 90 degrees to the wall. None of these measurements are not completely in accordance with the mechanical work of the heart. Both methods have advantages, the reflector based method is more robust and has less inter- and intra-observers variation. The limitation of the method is the temporal resolution, which so far is limited to approx. 70 frames /sec. The Doppler based velocities can be registered with pulsed Doppler or being extracted from colour images. The first method could not be recommended due to higher values with a systematic overestimation of true motion. The recommended method should therefore be velocity extracted from colour images.

One big obstacle with both methods are protected by different patents. Different equipments from different vendors uses different algorithms. There is a big variation between velocity and deformation measurements in the same individual performed with different machines. Sometimes there is not even a correlation between results from different machines. Some of the different results is partly due to different settings of the filter functions. Today the companies do not make a declaration of the used algorithms or filter settings. There is even differences in the same machine between different software version, the declaration of such changes are very limited in the communication from the companies to the customers. A standardization most probably start from the European society of Cardiology.

There are still variables that are less dependant on machine differences and that is the duration of time events. A new approach to use time events for diagnostic purposes will be presented- the state diagrams.

The use of deformation and velocity measurements are not only limited to cardiac applications. Vascular diagnostics using wall deformations seems to be a powerful tool for cardiovascular riskstratification. We have also started to use tissue Doppler for skeletal muscle, which has given us new understanding about skeletal muscle mechanics and activation. We have also used tissue Doppler for revitalisation of elastographic measurements.

1D-3

9:00 AM Current sonographic imaging in Obstetrics & gynaecology

Jurij Wladimiroff¹; ¹Dept of Ob&Gyn, Erasmus University Medical Centre, Rotterdam, Netherlands

Background, Motivation and Objective

3-D and 4-D ultrasound technology has opened new strategies for fetal research with focus on the craniofacial area, central nervous system and heart. 3-D oblique face, flipped face and reverse face views are used to identify palate anomalies. 4-D fetal echocardiography can be carried out in real-time with matrix array transducers and off-line following acquisition of a dynamic data set with volumetric probes applying the STIC (Spatio-Temporal Image Correlation) acquisition method. An alternative rendering algorithm transforms echolucent structures like cardiac chambers into echogenic voxels. A tool for semi-automatic cardiac volume segmentation has been developed for analysis of fetal cardiac cavities and vessels. It still lacks a fully manual mode to edit volume segments and it analyses only still volumes.

Fetal volume calculations are performed using the multiplanar method or rotational method with Virtual Organ Computer-aided Analysis (VOCAL) software. There have been conflicting results in comparisons between these two methods.

3-D Power Doppler ultrasound allows assessment of a virtually reconstructed vascular tree within a volume of interest and determines its vascularization through calculation of indices using so-called Vocal software (GE Medical System). The technique is studied in the field of placental and fetal vascularization, reproductive Medicine, Pelvic Floor and Gynaecological Oncology. Questions remain regarding the clinical significance of indices like volume vascularization, flow index as well as machine settings and speed of acquisition.

Tissue Doppler imaging allows measurement of maternal myocardial tissue velocities during left ventricular systole and diastole and is relatively load independent. It may detect early signs of cardiac failure.

Another novel technique is an immersive virtual reality system, the Barco I-space. In the I-space, binocular depth perception gives the examiner a realistic 3-D illusion allowing vastly improved images of the developing embryo compared with conventional 3-D rendering in surface mode. The current set-up is still complex and cumbersome but a desk version appears to be in the making (ref: CM Verwoerd-Dikkeboom, Virtual Embryology, PhD Thesis, Erasmus University Medical School, Rotterdam, May 2009)

Statement of Contribution/Methods

Results

Discussion and Conclusions

2D. High Frequency Ultrasound and its Applications

Sala 2

Tuesday, September 22, 2009, 8:00 am - 9:30 am

Chair: **Stuart Foster**
Univ. of Toronto

2D-1

8:00 AM **Imaging the Auditory System: A New Application of High-Frequency Ultrasound**

Zahra Torbatian¹, Rene van Wijhe², Ronald Pennings³, Rob Adamson¹, Manohar Bance⁴, Jeremy Brown¹,
¹Biomedical Engineering, Dalhousie University, Canada, ²Ear & Auditory research Laboratory, Dalhousie University, Canada, ³Department of Medicine, Division of Otolaryngology, Dalhousie University, Canada, ⁴Department of Medicine, Division of Otolaryngology & Biomedical Engineering, Dalhousie University, Canada

Background, Motivation and Objective

Although hearing loss is an extremely common chronic disorder, affecting approximately 10% of the general population, there are few imaging techniques available to clinicians to diagnose the possible causes. Most hearing disorders are due to either a mechanical problem in the middle ear, or to the failure of transduction mechanisms in the cochlea (inner ear). The relevant physiological structures of the ear are too small to be adequately resolved by CT and MRI, leaving optical surface microscopy as the only imaging modality in common use. However, it provides very little information about the pathology of the ear beyond the surface of the eardrum. This work describes an ex-vivo imaging study of the auditory system using high-frequency ultrasound. Tissue structures relevant to hearing disorders were imaged using a realistic in-vivo approach and a custom built 50 MHz annular-array imaging system.

Statement of Contribution/Methods

A previously developed 50 MHz array-based imaging system was used to obtain 2D&3D high-resolution ex-vivo images of the human auditory system. The imaging system consisted of a 2 mm diameter 7-element annular-array transducer, and a FPGA-based beamformer. Images of the middle ear were generated on intact cadaveric temporal bones across the eardrum. Intra-cochlea images of the inner ear were generated across the round window membrane (RWM). Both of these approaches were intended to represent a realistic in-vivo approach. For the middle ear, a trans-tympanic saline injection was needed prior to imaging, to achieve the necessary acoustic coupling. Trans-tympanic injections are routinely used for injection of drugs into the middle ear. The most logical approach to imaging the cochlea was through the RWM, since it is otherwise surrounded by dense bone. To access the RWM in-vivo, it is necessary to pass the imaging probe through the middle ear by creating a small hole in the eardrum. This can again be achieved during a routine and minor clinical procedure. In our imaging study, the middle ear was removed prior to imaging the cochlea due to the relatively large packaging of the probe and mechanical scanning mechanism.

Results

For the images generated of the middle ear, the eardrum and middle ear ossicles could clearly be visualized. For the images generated of the cochlea, the basilar membrane separating the cochlear duct could clearly be visualized. Fenestrations were drilled "post imaging" into the side of the middle ear as well as the cochlea and the intra-structures were photographed through a microscope to confirm the anatomical accuracy of the images. Comparison of the ultrasound images with the microscopic photos showed that our system was able to capture detailed clinically relevant anatomy of the ossicles and confirmed the accuracy and positioning of the basilar membrane.

Discussion and Conclusions

We have shown that high frequency ultrasound has the potential to revolutionize diagnostics and surgical interventions in the field of otology.

Tuesday
Oral

8:15 AM High-frame-rate mouse embryo cardiac imaging using Doppler derived gating

Orlando Aristizabal¹, Mamou Jonathan², Daniel H. Turnbull¹, Jeffrey A. Ketterling², ¹Skirball Institute, NYU School of Medicine, New York, New York, USA, ²Riverside Research Institute, New York, New York, USA

Background, Motivation and Objective

Electrocardiogram (ECG)-gated ultrasound imaging has enabled high temporal resolution cardiac imaging in adult mouse models of cardiac disease. Extending these techniques to the mouse embryo will enable improved in utero analyses of congenital heart disease models. Here a technique is presented that derives gating signals from Doppler blood flow waveforms as an alternative to ECG signals, which cannot be reliably measured in multiple (8-12) embryos per mouse. This method has been validated by acquiring high-frame-rate images of the mouse embryonic heart.

Statement of Contribution/Methods

Prospective high-frame-rate imaging was accomplished by acquiring a set of 101 50- μm spaced M-modes each containing 250 lines digitized at a PRF of 500-Hz, using a 40-MHz fixed-focus transducer with 90- μm lateral, and 35- μm axial resolution. Each M-mode acquisition was initiated at the same point in the cardiac cycle as follows. With the embryonic heart placed in the center of the imaging plane, the Doppler sample volume of a separate 43-MHz CW Doppler transducer was placed over the aorta. Doppler waveforms were then digitized at 24 kHz for 10 ms, and time-frequency spectrograms were computed. The Doppler envelope was traced in real-time by detecting the highest frequency peak in each line of the spectrogram, and the envelope was monitored for the first occurrence of a local maximum above a set threshold. Once the peak was detected, breath gated M-mode data at the prescribed PRF was acquired.

Results

The Doppler envelope detection algorithm was implemented in real time (Fig1. a), demonstrating $\sim 1\%$ variation in the cycle length of the Doppler derived triggers (Fig1. a, 0.368 ± 0.004 ms). To validate the method prospective high-frame-rate images were acquired from an E11.5 mouse embryo heart. The parsed M-mode data yielded a B-mode cine loop of 0.5-s at the equivalent of 500 frames per second. Representative images of the heart in diastole (Fig1. b) and systole (Fig1. c) demonstrate accurate reconstruction of the embryonic anatomy, with ventricular fractional area shortening close to 45%.

Discussion and Conclusions

This study demonstrates a novel Doppler approach to non-invasively acquire stable triggers synchronized to the fetal mouse heart cycle, enabling prospective high-frame-rate imaging at 40-MHz. Future work will focus on reducing motion artifacts present in the reconstructed images.

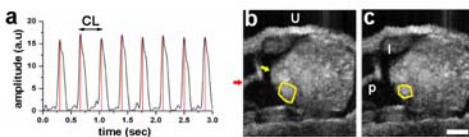


Figure 1. (a) Real-time Doppler envelope from an aorta of an E11.5 embryo. Red vertical lines indicate peaks from which cardiac triggers were derived. Average cycle length (CL) was equivalent to a heart beat of 163 bpm. Two frames from a 500 fps cine-loop visualizes the presumptive ventricle (yellow tracing) in diastole (b) and systole (c). Other anatomical features were also identified such as the atrium (yellow arrow), limb (l), vitelline vessel (p) and the uterus (U). Red arrow indicates the geometric focus of the imaging transducer. Scale bar= 1 mm

2D-3

8:30 AM **Tissue-mimicking Phantoms for Assessing Resolution of High Frequency Imagers**

Ernest Madsen¹, Gary Frank², Matthew McCormick²; ¹Medical Physics, University of Wisconsin-Madison, Madison, Wisconsin, USA, ²Medical Physics, University of Wisconsin-Madison, USA

Background, Motivation and Objective

The VisualSonics Model 770 is used in many research labs for imaging small animals e.g. mice. Single-element focused transducers range from 25 to 55 MHz. Manufacturer's specifications give single values for axial and lateral resolution and for depth of field. Line or point spread functions measured in water for estimating resolution can bias toward the high frequency end of the pulse spectrum which may not even be present at depth in tissue. Also, the combined effect of all three resolution components is not addressed. Our aim is to quantify resolution with depth treating all three components equally and accounting for frequency-dependent attenuation as in tissue.

Statement of Contribution/Methods

Tissue-mimicking (TM) anechoic spheres with frequency-dependent attenuation approximating that of blood were mass-produced in eight narrow diameter-range groups including 100-1090 μm . Each group was randomly distributed with volume fraction .07 in a $3 \times 3 \times 1 \text{ cm}^3$ TM background section with identical attenuation, but with 7 μm scatterers to simulate tissue backscatter. A reference section also exists containing no spheres. The depth range over which spheres can be detected is determined as well as the depth range over which no artifactual echoes are seen.

Results

The two resolution depth ranges for a 25 MHz (model 710) and a 55 MHz (708) transducer are shown in the table. Sphere diameters 100 and 115 μm are not shown since no detection occurred for either transducer. No detection occurred for the 200 μm spheres at 25 MHz. For 25 MHz the detection range increased from 17-14 mm = 3 mm to 8 mm with increase in diameter, and for the 55 MHz it increased from 1.8 mm to 4.8 mm.

Discussion and Conclusions

From the manufacturer's specifications, the 25 MHz axial and lateral resolutions are 70 μm and 140 μm , but the smallest sphere diameter detected was 290 μm ; for the 55 MHz case, axial and lateral resolutions are given as 30 μm and 70 μm , but the smallest sphere diameter detected with the phantom was 200 μm . The phantom allows a quick assessment of resolution capabilities. It should be clear that the smaller the sphere that can be detected, especially with no artifactual echoes, the better the delineation of objects and representation of gray levels at that depth.

We will also obtain data and present results for the new VisualSonics 2100 which uses variable focus linear arrays.

transducer freq. (MHz)	detectable or artifact-free	depth range in mm					
		200 μm	290 μm	400 μm	530 μm	825 μm	1090 μm
25	detect	---	14-17	14-18.5	13.5-18.5	12.5-19	12-20
25	art-free	---	---	14-18.5	13.5-18.5	14-17	13.5-17.5
55	detect	3.5-5.3	3.5-5.5	3.2-6.0	2.9-6.2	2-6.6	2.2-7.0
55	art-free	uncertain	3.5-5.4	3.5-5.5	3.5-5.5	3.5-6.2	3.5-6.6

2D-4

8:45 AM **In Situ Measurements of attenuation coefficient for evaluating the hardness of cataract lens by a high frequency ultrasonic needle transducer**

Huang Chih-Chung¹, Chen Ruimin², Shung K. Kirk², Tsui Po-Hsiang³, Zhou Qifa², Humayun Mark S.^{4,1}
Department of Electronic Engineering, Fu Jen Catholic University, Hsinchuang, Taipei, Taiwan, ²Department of Biomedical Engineering, University of Southern California, USA, ³Division of Mechanics, Research Center for Applied Sciences, Academia Sinica, Taiwan, ⁴Department of Ophthalmology, Keck School of Medicine, University of Southern California, USA

Background, Motivation and Objective

A cataract is a clouding of the lens in the eye that affects vision. Phacoemulsification is the mostly common surgical method for treating cataracts, and determining the optimal phacoemulsification energy is dependent on measuring the hardness of the lens. This study explored the use of an ultrasound needle transducer for in situ minimally invasive measurements of ultrasound attenuation coefficient to evaluate the hardness of cataract lens.

Statement of Contribution/Methods

A 47 MHz high frequency needle transducer with a diameter of 0.9 mm was fabricated by a polarized PMN-33%PT single crystal in the present study. The attenuation coefficients at different stages of artificial porcine cataract lens were measured using the spectral shift approach. The hardness of the cataract lens was also evaluated by mechanical measurement of its elastic properties.

Results

The results demonstrated that the ultrasonic attenuation coefficient was increased from 0.048±0.02 to 0.520±0.06 dB/mm-MHz corresponding to an increase of Young's modulus from 6 to 96 kPa as the cataract further developed. In order to evaluate the feasibility of combining needle transducer and phacoemulsification probe for real time measurement during cataract surgery, the needle transducer was mounted on the phacoemulsification probe for vibration test.

Discussion and Conclusions

The linear fit to these data showed that there was a high correlation between ultrasonic attenuation coefficient and Young's modulus: the correlation coefficient (R) value for the 95% confidence interval was 0.932. This result appears to suggest that the spectral-shift approach is sensitive and reliable for detecting the hardness of a cataract. In vibration test, the results indicated that there was no apparent damage to the tip of needle transducer and the pulse-echo test showed a good performance in sensitivity was maintained after the vibration test.

2D-5

9:00 AM **Spectral analysis of ultrasound backscatter for characterization of HIFU lesions in cardiac tissue with high-frequency imaging**

Ronald E. Kumon¹, Yun Zhou¹, Kun Yang¹, Cheri X. Deng^{1,1}
Department of Biomedical Engineering, University of Michigan, Ann Arbor, MI, USA

Background, Motivation and Objective

Reliable and effective HIFU lesion detection is important for expanded use of HIFU in a clinical context. Spectrum analysis of backscattered radio-frequency (RF) ultrasound has proven to be an effective method for identifying changes in tissue state. In this method, the spectrum from tissue in a region of interest is obtained from backscattered RF data and then calibrated to remove artifacts from system hardware. The calibrated spectrum has been shown to be related to the microstructural properties of the tissue like scatterer size and acoustic concentration. The purpose of this study was to investigate the use of spectral analysis of ultrasound backscatter as a means to characterize the temporal evolution and spatial extent of HIFU lesions.

Statement of Contribution/Methods

This study employed a prototype image-guided HIFU system consisting of HIFU transducer and an ultrasound imaging probe arranged within a water tank with porcine cardiac tissue specimens placed in the common focal plane. The therapy transducer (4.33 MHz) produced pulsed HIFU exposures at 100 Hz PRF and 80% duty cycle. The high-frequency ultrasound imaging system (Visualsonics Vevo 770 or a single element 50 MHz transducer controlled by a mechanical scanning system) was used to acquire (1) M-mode RF data (10 kHz PRF, 2 s x 7 mm) before, during, and after HIFU treatment in the center of the lesion and (2) a series of sagittal B-mode RF data (3 mm x 7 mm) at 0.1 mm intervals in the lesion for off-line analysis. The imaging transducer was calibrated by

Tuesday
Oral

measuring pulse reflection from an optically flat surface. Linear regression was performed to calculate mid-band fit, slope, and intercept of the calibrated spectra.

Results

Parametric image maps of mid-band, slope, and intercept fit were constructed based on M-mode and B-mode data revealing spatiotemporal changes in tissue induced by HIFU exposures. No significant change in any parameters was observed until ~ 0.25 s after the HIFU (1500 W/cm^2) was turned on, after which the HIFU region began to expand spatially before reaching a stable width of ~ 2 mm. In the lesion region, mid-band fit increased by more than 20 dB, intercept increased by more than 40 dB, while the slope decreased by up to 1 dB/MHz. In some cases, transient spectral broadening was observed which was suggestive of acoustic cavitation. After treatment, good agreement was seen between the lesion in the gross tissue and corresponding B-mode parametric image maps of all parameters, with the largest parameter changes observed along the lesion axis.

Discussion and Conclusions

Spectral parameters from ultrasound backscatter change significantly in lesions of porcine cardiac tissue relative to surrounding tissue and can potentially be used for monitoring the spatiotemporal evolution of HIFU lesions. The observed increase in mid-band fit and intercept and decrease in slope implies a significant increase in scatterer size resulting from the coagulative processes involved during tissue ablation.

2D-6

9:15 AM Focused Ultrasound for Early Detection of Tooth Decay

David Allan Hughes¹, John Girkin², Chris Longbottom³, Sandy Cochran⁴; ¹DTC Medical Devices, University of Strathclyde, United Kingdom, ²University of Durham, United Kingdom, ³School of Dentistry, University of Dundee, United Kingdom, ⁴IMSAT, University of Dundee, United Kingdom

Background, Motivation and Objective

Ultrasound is a well-established tool for medical imaging but it has yet to emerge in routine use in dental diagnostics. Nevertheless, it was shown in the late 1970s that ultrasound can be used to probe the internal structures of teeth, and more recently to observe surface changes due to caries and acid erosion.

Dental caries is the localised demineralisation of enamel by bacteria acidic waste-products. The disease manifests itself in its early, and reversible, stage as subsurface lesions which contain biological fluids. Current methods of detection and diagnosis in the dental surgery are limited to the subjective act of visual inspection and bite-wing X-ray. Neither method provides quantitative information about the state of the disease in the tooth for accurate diagnosis and subsequent treatment planning.

Statement of Contribution/Methods

Early caries lesions are less than $100 \mu\text{m}$ in thickness, and therefore cannot be accurately characterised by ultrasound pulse-echo techniques at conventional frequencies. However, the change in the underlying material when a lesion occurs can be used to detect the lesion by considering the attenuation and surface reflection instead. In this work we present a laboratory method for detecting early caries lesions by recording B-scans of teeth which exhibit caries lesions with high frequency ultrasound.

A selection of extracted teeth with visible caries white spot lesions were obtained and immersed individually in a water tank on a precision translation stage. A focused piezocomposite transducer with a 35 MHz centre frequency (AFM Ltd, Birmingham) was then used to record a B-scan across each lesion, determining areas of sound and demineralised enamel. The focused nature of the transducer provided a spatial resolution of $110 \mu\text{m}$. The B-scans were post-processed using signal processing algorithms in Scilab and presented as grey scale images for analysis.

Results

B-scans have been produced which show differences in the return pulse amplitude between sound and demineralised enamel because of the difference in the properties between the two types of material.

Discussion and Conclusions

Sound enamel is very hard, with a high acoustic impedance, and thus produces a large reflection at the water-enamel boundary, $R = \sim 80\%$. Demineralised enamel, while still hard produces a lower reflection coefficient, estimated as $R = 66\% \pm 5\%$. This difference also causes a larger proportion of the incident ultrasound to be transmitted into the lesion, manifest as a spreading of the pulse in time in the B-scan.

By using high frequency ultrasound, we have shown that a localised 'map' of a region of caries can be recorded. With the advent of high frequency ultrasound arrays, this gives promise to an diagnostic ultrasonic tool for the dental clinic.

**Tuesday
Oral**

3D. Elastography

Sala 4

Tuesday, September 22, 2009, 8:00 am - 9:30 am

Chair: **Timothy Hall**
Univ. of Wisconsin-Madison

3D-1

8:00 AM **A robust Real-time Speckle Tracking Algorithm for Ultrasonic Elasticity Imaging**

Jingfeng Jiang¹, Timothy Hall^{1,2} *Medical Physics, University of Wisconsin, USA*

Background, Motivation and Objective

Ultrasonic strain imaging systems are rapidly gaining attention for breast tumor differentiation, despite the fact that consistently obtaining high quality in vivo strain images is a persistent challenge. Our objective is to develop a robust speckle tracking algorithm that can be used not only for real-time strain imaging but also potentially for high-quality displacement data acquisition during elastic modulus imaging, thereby enhancing its clinical utility.

Statement of Contribution/Methods

The proposed algorithm is a novel combination of our regularized speckle tracking algorithm (UMB, 2009) and a competitive (i.e. quality-based) seeding strategy proposed by Chen et al. (Med Image Anal, 2009) as a two step process. In the first step, displacement vectors in a coarse grid (typically every half centimeter) were obtained by optimizing using a cost function combining correlation and motion continuity constraints. To solve the optimization problem with a reasonable computational load, a dynamic programming technique that does not require iterations (i.e. Viterbi Algorithm) was used. In the second step, only displacement vectors have sufficiently high correlation values in the initial search grid will be used as seeds for the subsequent predictive search for the entire region of interest with a much reduced search range (a 3 by 3 sample grid). The competitive seeding in the second step will ensure that high-quality seeds carry priority.

Results

Through processing of in vivo breast and thyroid tissue data (10 sets with different types of thyroid and breast lesions and roughly 1000 RF echo frames in total), our findings demonstrated that the new algorithm provides more consistent displacement estimates than our previous real-time algorithm (Ultrasonics Symposium, 2006) for in vivo clinical data. In particular, among five sets of thyroid lesion data with the presence of complex anatomy, the new algorithm is capable of tracking larger frame-average tissue deformation (0.5-1%) and increasing strain image consistency in a sequence of images. For instance, based on Displacement Quality Metric (DQM>0.6; Jiang et al, UFFC, 2006), a significantly longer sequence of high contrast strain images (e.g. 45 vs. 15 in one cancer dataset) could be obtained with the new algorithm compared to the our previously-reported real-time algorithm. We project that the new algorithm can achieve more than 15 frames/second with a 3 cm by 3 cm region of interest, which is sufficient to provide real-time feedback during in vivo elasticity imaging.

Discussion and Conclusions

A modified block-matching algorithm integrated with dynamic programming (Viterbi algorithm) and a competitive seeding strategy for motion tracking is presented. These preliminary results support the hypothesis that this novel algorithm may potentially make ultrasound-based elasticity imaging more easy to use by providing high quality strain imaging data in real-time.

Tuesday
Oral

3D-2

8:15 AM **BiPlane Ultrasound Strain Imaging during Induced Contraction of Skeletal Muscles**

R.G.P. Lopata¹, J.P. van Dijk², S. Pillen³, J.M. Thijssen¹, D.F. Stegeman², C.L. de Korte^{1,2} *Clinical Physics Lab, Department of Pediatrics, Radboud University Nijmegen Medical Center, Nijmegen, Netherlands.* ²*Department of Neurology, Radboud University Nijmegen Medical Center, Nijmegen, Netherlands.* ³*Department of Pediatrics, Radboud University Nijmegen Medical Center, Nijmegen, Netherlands*

Background, Motivation and Objective

In neuro-physiological research, monitoring of muscular disorders such as amyotrophic lateral sclerosis (ALS) may benefit from ultrasound strain imaging, i.e., the assessment of local deformation. Contraction of skeletal muscle can be either spontaneous or induced by electrical stimulation. Since the movement and deformation (rates) are large, a high frame rate is required for ultrasound strain imaging. BiPlane imaging is a fast semi-3D imaging technique that enables strain estimation in 2 orthogonal planes. In this study, BiPlane strain imaging of induced contracting skeletal muscle tissues is used for estimating strain in 3 orthogonal directions.

Statement of Contribution/Methods

Triggered BiPlane imaging was performed during excitation of the left tibialis anterior (TA) and the biceps femoris (BF) muscle. These muscles were chosen for their compact size and superficial position. Isometric contraction (using a force transducer) and surface EMG were measured simultaneously. In both the TA and the BF, supramaximal excitation was induced. The maximum stimulation level was found empirically for each subject by registration of the EMG. In the TA, the level of stimulation was lowered stepwise until no or only little contraction was observed. In the BF, the response to a pulse train of 10 and 20 Hz was examined. Raw ultrasound data were acquired with a Philips SONOS 7500, equipped with an X4 matrix transducer and an RF-interface. An RF-based 2D displacement estimation technique was used to estimate displacements in both planes. The muscle tissue was tracked during the contraction and relaxation phases and the vertical and horizontal strain images were computed using the accumulated displacements and a least-squares strain estimator. Cumulative strain curves were obtained for a manually segmented ROI, excluding bone and other tissue.

Results

The muscle contraction was tracked properly for all excitation levels and the strain curves revealed little hysteresis. In both muscles, vertical strains (\approx axial) were measured in a range of 10 to 30%. Large horizontal strains (\approx lateral) were measured in the direction of the muscle fibers up to -10 to -20% in the longitudinal cross-section. In the TA, an excellent correlation between electrical stimulation and maximum strain was found. For very low electrical stimulations, this correlation was weak: fewer motor units are stimulated and thus different parts of the muscle are excited. The strain curves after pulse train excitation of the BF revealed that tetanic contraction was measured.

Discussion and Conclusions

In this study, strain imaging in electrically stimulated muscles was shown to be feasible. Strain imaging has the advantage of enabling local assessment of muscle contraction, whereas the force is global. Full 3D strain imaging is necessary to account for out-of-plane motion, but only at sufficiently high imaging frame rates, since supramaximal contraction revealed relatively high strain rates.

3D-3

8:30 AM **Ultrasound-based 2D Strain Estimation of the Carotid Artery: an in-silico feasibility study**

Matilda Larsson^{1,2}, Florence Kremer², Piet Claus², Lars-Åke Brodin¹, Jan D'hooge^{2,1} *School of Technology and Health, Royal Institute of Technology, Stockholm, Sweden.* ²*Department of Cardiovascular Diseases, Catholic University of Leuven, Lab on cardiovascular imaging & dynamics, Leuven, Belgium*

Background, Motivation and Objective

Ultrasound based estimations of arterial wall properties are commonly used to assess vessel wall stiffness in studies of vascular diseases. As such, radial motion and strain of the vessel wall have commonly been used. More recently, it was shown that the longitudinal motion of the vessel during systole can be measured using speckle tracking. However, the assessment of longitudinal strain in the vessel wall has to be further investigated. The aim of the study was to test the feasibility of simultaneous assessment of radial and longitudinal strain in the carotid artery with commercially available hardware using computer simulations.

Tuesday
Oral

Statement of Contribution/Methods

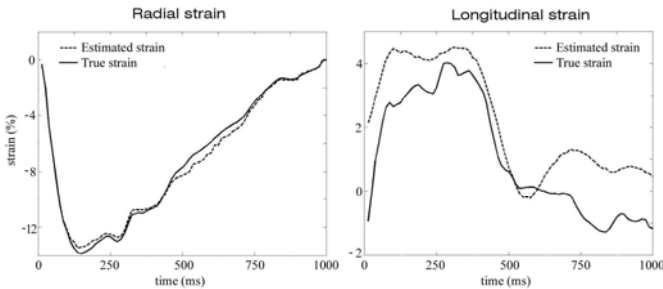
A kinematic cylindrical model of the carotid artery with realistic dimensions (radius 2.7mm; wall thickness 0.45mm) was constructed. The model was deformed radially according to temporal distention measured in-vivo while longitudinal deformation was the result of conservation of volume. Moreover, longitudinal motion was superimposed based on profiles obtained in-vivo. Point scatterers were randomly positioned within the model and subsequently moved. Ultrasound long axis images were simulated using a generalized convolution model (COLE) with realistic image properties (frequency 13MHz; bandwidth 60%; frame rate 80Hz). Four models with different scatterer distributions were built. For each of them, longitudinal (i.e. perpendicular to the beam) and radial (i.e. along the beam) motion were estimated using normalized cross-correlation with spline interpolation to detect sub-sample motion. Radial and longitudinal strains were then obtained by linear regression and subsequently temporally low-pass filtered to remove noise. The maximum of the measured systolic longitudinal and radial strain was then compared with the ground truth from the model.

Results

Figure 1 shows the true and estimated radial and longitudinal strain curves of one of the models. Radial strain was estimated as $-13.33 \pm 0.76\%$ (ground truth -13.04%) while longitudinal strain was $3.72 \pm 2.13\%$ (ground truth 4%).

Discussion and Conclusions

This study shows the feasibility of simultaneously measuring radial and longitudinal strain in the carotid artery by making use of currently available hardware. In future work, this method will be applied to in-vivo data. The clinical value of measuring longitudinal strain in vessels remains to be determined.



3D-4

8:45 AM Exploring the nonlinear elastic behavior of phantom materials for elastography

Theo Z Pavan^{1,2}, Ernest L Madsen², Antonio AO Carneiro¹, Gary L Frank², Timothy J Hall²; ¹Departamento de Física e Matemática, Universidade de São Paulo, Ribeirão Preto, SP, Brazil, ²Department of Medical Physics, University of Wisconsin, Madison, WI, USA

Background, Motivation and Objective

Most ultrasound-based strain image systems track local incremental deformations of up to about 5% (region of relatively linear behavior). However for deformations beyond this amount, most of the human tissues present nonlinear stress strain relationship. In order to study the nonlinear elastic behavior of tissues it is necessary to understand the behavior of nonlinear elastic imaging techniques, requiring the development of phantom materials with nonlinear properties which must be well understood. Agar presents a nonlinear elastic behavior, while for the gelatin it is quite linear. The main purpose of this work is to quantitatively compare the nonlinearity of plain agar and gelatin, agar/gelatin mixtures and agar/gelatin mixtures with oil emulsification methods.

Statement of Contribution/Methods

The first two gels tested in this effort were plain agar (dry weight of 2%) and plain gelatin (8%). Mixtures were created based on gelatin (8%) poured into agar (1 to 5%) using a volume fraction of 60% agar and 40% gelatin. Therefore five samples were obtained. The gelatin concentrations were the same for all samples since a phantom containing inclusion would have to have the same concentration of gelatin as the background.

The third set of samples contained gelatin (8%) poured into agar (1 to 4%) as the base material for oil dispersion with oil percentages of 0, 20 and 50% resulting in twelve samples. Dynamic mechanical tests (EnduraTEC 3200 ELF) were performed on each sample.

The Veronda-Westmann model for hyperelastic materials was adopted to fit the stress strain curves. This model is a good tradeoff between accuracy and complexity and requires estimating only two parameters (shear modulus at no strain - μ and the nonlinear parameter - γ). To obtain the stress strain curves, mechanical tests using large amplitudes of deformation (up to 25%) were performed.

Results

The nonlinear parameter of the plain agar $\gamma = 9$ was 10 times greater than for the plain gelatin. The Young's moduli obtained from the Veronda-Westmann model were compared to the storage modulus calculated by the DMA method (1% of pre deformation and 1% of amplitude). The difference found between the results obtained by the two methods was of 4.5% and 7.8% for the gelatin and the agar respectively. The nonlinear parameters for the agar/gelatin mixtures fluctuated around a value of $4.5\text{Å}\pm 0.3$. The presence of oil reduced the stiffness and the nonlinear behavior of the samples. The nonlinear parameter reduction observed for the oil in samples relative to the agar/gel with no oil was about 21% to 53% which was comparable to, and correlated with, the range of oil volume percentages (20% and 50% respectively).

Discussion and Conclusions

The results allow predicting what materials to employ to manufacture a specific phantom with target nonlinearity different than its background. Nonlinear finite elements simulations and phantom studies are methods to verify the viability of nonlinear elastography techniques.

3D-5

9:00 AM Real Time Ultrasound Elastography in Neurosurgery

Chris Uff¹, Leo Garcia¹, Jeremie Fromageau¹, Jeff Bamber¹; ¹Institute of Cancer Research, United Kingdom

Background, Motivation and Objective

A recent study by this group demonstrated the safety and feasibility of ultrasound elastography in the human brain with the aim of utilizing it intra-operatively during tumour resection surgery to guide surgical procedure and ensure that the full extent of the lesion had been removed. This study aims to continue the work of the previously described study in addition to demonstrating the intra-operative use of a recently developed 3D ultrasound elastography system.

Statement of Contribution/Methods

Real time 2D ultrasound elastograms were acquired during neurosurgical operations for brain and spinal cord tumours. In select cases where access allowed use of the 5 x 5 cm 3D probe face, 3D elastograms were acquired in the brain. Spinal cord must not be compressed and elastograms were successfully generated from vascular pulsations with a water stand off. In select cases, the resection cavity was explored for residual tumour, based on pre-resection elastogram appearances. Two scanning systems were used: Z.One (Zonare Medical Systems Inc., US) with a 12 MHz 2D transducer and Diasus (Dynamic Imaging Ltd, UK) with 5-10 MHz 2D transducer and 6-12 MHz 3D transducer in conjunction with Stradwin 3.7 (Cambridge University, UK) ultrasound elastography acquisition software.

Results

2D and 3D elastography revealed strain differentials that correlated well with the surgeon's assessment of the stiffness of the tissues. Cleavage planes were correctly identified from areas of decorrelation (correlation images) and areas of very high axial strain (elastograms). Off line axial and engineering shear strain calculation assisted in image interpretation.

Discussion and Conclusions

These results indicate that real time 2D and 3D ultrasound axial strain imaging is not only viable, but also clinically useful in the human brain and spinal cord. Axial strain images, correlation images and shear strain images (calculated off line), were useful to the surgeon in identifying and characterizing the tissue-tumour interface.

3D-6

9:15 AM **3D in vivo brain elasticity mapping in small animals using ultrasound**

Emilie Macé¹, Ivan Cohen², Jean-Luc Gennisson¹, Richard Miles², Mathias Fink¹, Mickaël Tanter¹; ¹*Institut Langevin - LOA, CNRS UMR 7587, Université Paris VII, ESPCI ParisTech, INSERM, Paris, France*, ²*Cortex et Epilepsie, INSERM EMI 0224, CHU Pitié-Salpêtrière, Université Paris VI, Paris, France*

Background, Motivation and Objective

Imaging damaged tissues in the brain in vivo is a major issue in neurology and neurosurgery. Brain elasticity imaging is a promising approach, given that the mechanical properties of neural tissues are likely to be modified when damaged. Such an imaging technique could respectively help improve clinical follow-up or diagnosis of neurodegenerative diseases and provide intra-operative localization of lesions. It would also be of great interest in the development of HIFU brain therapy that requires precise monitoring of necrosis during treatment. In this work, the ability of Ultrasound Transient Elastography to quantitatively map brain elasticity is demonstrated in vivo on rats using the Supersonic Shear Imaging technique.

Statement of Contribution/Methods

Experiments are performed on adult rats placed in a stereotaxic frame. A 15x25 mm² cranial window is opened to expose the brain. A standard high frequency (15 MHz) ultrasound linear probe is set in the coronal plane and controlled with a micromanipulator system. For coronal slices every 500 μm , shear waves induced by radiation force are imaged at very high frame rate (10 kHz) with an ultrafast ultrasound scanner. Ultrafast movies are then post-processed to reconstruct a 3D elasticity map of the brain. A high resolution ultrasonic scan of brain anatomical structures is also acquired and superposed with elasticity images. To estimate artifacts due to physiological motion such as pulsatility, 3D transient dynamics of brain vibrations are measured during a whole cardiac cycle using ultrafast imaging at a 400 Hz.

Results

The high resolution ultrasonic scan of the brain allows a clear identification of anatomical regions. The 3D map of the shear modulus shows a mean value of 3.2 ± 0.7 kPa in the cortex and the thalamus and a higher value of 18.8 ± 7.0 kPa in the corpus callosum. Mechanical waves induced by the ultrasonic radiation force exhibit higher frequencies (50 Hz - 1000 Hz) than pulsatile waves (5 - 15 Hz). The measurement of motion during a whole cardiac cycle shows a pulsatile movement peaking approximately 60 ms (30% of cycle) after systole, with a maximum amplitude of 5 to 30 μm depending on regions whereas radiation force generates smaller displacements (1-5 μm).

Discussion and Conclusions

In this study, we proved the feasibility of elasticity imaging of the brain in vivo in rats. We observed a correlation between elasticity heterogeneities and anatomical structures. Furthermore, we showed that pulsatility induces important movements in the brain which are coherent with the localization of blood vessels. Small animals were chosen for the perspective offered by existing models of neurodegenerative diseases such as Alzheimer's and Parkinson's diseases. Next experiments will focus on applying this new technique in those models to quantify the effect of damaged tissues on elasticity. Concerning transition to clinical use, this technique could be evaluated intra-operatively in the context of surgery of brain lesions.

4D. Flow Sensing

Tarragona

Tuesday, September 22, 2009, 8:00 am - 9:30 am

Chair: **Mario Kupnik**
Stanford University

4D-1

8:00 AM Transverse Flow Velocity Measurement Using A Single Circular Planar Transducer By Ultrasonic Doppler-Spectra

Juei Igarashi^{1,2}, Naoto Wakatsuki¹, Koichi Mizutani¹; ¹Graduate School of Systems and Information Engineering, University of Tsukuba, Tsukuba, Ibaraki, Japan, ²Optics and Sensors - Engineering, Schlumberger Kabushiki Kaisya, Sagamihara, Kanagawa, Japan

Background, Motivation and Objective

Doppler effect is usually known to be observed on the velocity component parallel to the wave propagation. Hence, for flow velocity measurements, it is generally required to arrange one or more transducers to generate an ultrasonic beam as the beam axis has the flow velocity component. In industry applications, that fact sometimes limits the measurement apparatus design. In this paper, a transverse flow measurement method using a simple configuration is suggested.

Statement of Contribution/Methods

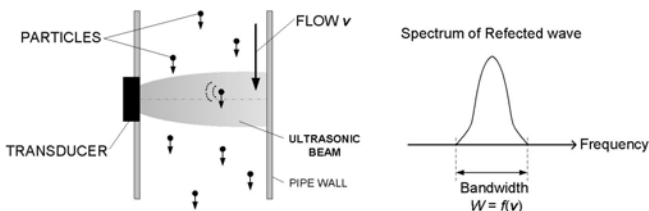
Doppler-spectra is a method for measuring velocity of an object moving across the ultrasonic beam. While an object moves across the ultrasonic field perpendicular to the axis of radiation, the bandwidth of the wave reflected from the object changes depending on the velocity. The transverse velocity measurement using an ultrasonic beam radiated from a circular planar transducer was suggested with numerical calculations and some experiments for its feasibility assuming a single moving object existing in the field, based on the time required for running through the beam. (Igarashi et al., Jpn. J. Appl. Phys. 34, 1995 and Igarashi et al. Jpn. J. Appl. Phys. 35, 1996) In this paper, the application of the method for the transverse fluid flow velocity measurement is discussed assuming the fluid contains plural number of particles which scatter ultrasonic wave. In case the divergent beam is used, compared with the case of the focused beam, the method is applicable in wider range of the location of the moving object path both for the distance between the transducer and the path and for the offset of the path from the axis of the transducer. Here we attempt numerical simulations for the case plural number of particles passing across the beam with different paths in random timing in a finite period of time. Further, we perform an experiment of the flow measurement for the fluid containing particles to confirm the feasibility of the discussion.

Results

Based on the results of numerical simulations, it was confirmed that the bandwidth of the superimposed spectrum of the reflected waves from the plural particles consistently depends on the velocity of the flow.

Discussion and Conclusions

It has been validated that the Doppler-spectra method is applicable for the measurement of the transverse fluid flow velocity passing across a divergent ultrasonic beam. This method can be applied for a simple flowmetry.



4D-2

8:15 AM **Liquid Level Torsional Acoustic Waveguide Sensor**

William Spratt¹, Lawrence Lynnworth², John Vetelino^{1,1} *University of Maine, USA*, ²*Lynnworth Technical Services, USA*

Background, Motivation and Objective

The sensing of liquid level in hostile aggressive liquids within process control systems poses significant challenges. First, the materials used in the liquid level sensor must be able to survive in the probed liquid. Secondly, the probing mechanism inherent in the sensor must be very sensitive to the liquid level and finally the excitation and reception of the signal associated with the probing mechanism should be external to the medium being probed. In contrast to common electrical probing mechanisms such as electromagnetic waves and electric current, acoustic waves offer a probing mechanism which can survive in hostile liquids. In this paper an acoustic waveguide structure which utilizes torsional acoustic waves as the probing mechanism is designed, fabricated and tested to sense liquid level.

Statement of Contribution/Methods

The acoustic waveguide is constructed of a single metallic material which consists of a lead-in zone and a sensing zone (see figure 1). The sensing zone is immersed into the medium of being probed. The cross sections of the two zones are circular and rectangular respectively. Torsional acoustic waves excited by a lead zirconium titanate (PZT) shear transducer propagate down the waveguide and reflect at the interface of the lead-in section and sensing zones, the surface of the probed liquid and the end of the sensing zone. The flight times associated with the various reflections are then used to measure the fluid level.

Results

A sensor made of 316 Stainless Steel (SS) with rectangular sensing cross section was immersed in tap water from 0 to 50.8 mm in depth. Flight times were measured from both interface and end echoes. Results showed that interface echoes recorded a 1051 ns/mm shift in flight time while the end echo flight time changed 46 ns/mm. The standard deviation in flight time measurement was approximately 1 ns resulting in a sensing resolution of +/- 0.3 mm.

Discussion and Conclusions

A method for measuring fluid level using ultrasonic torsional waves was performed. A comparison of using the interface and end echoes to perform the measurement showed that interface echo measurements have a sensitivity 20 times higher than end echoes, but have a signal to noise ratio (SNR) 8 times as low. The sensor is highly attractive to the process control industry as the design is durable in many hostile environments and can be expanded to detect multiple measurands simultaneously.

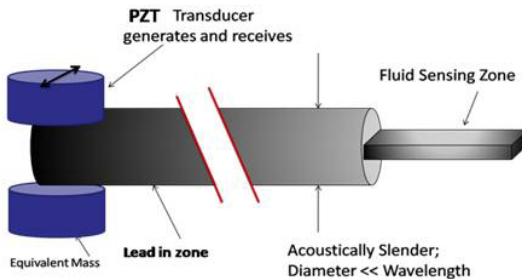


Figure 1 – Torsional Acoustic Waveguide sensor conceptual diagram

4D-3

8:30 AM Dynamic response of water droplet coated silicon MEMS resonators

Angel T-H Lin¹, Jize Yan¹, Ashwin A Seshia^{1,†} / *University of Cambridge, United Kingdom*

Background, Motivation and Objective

Silicon MEMS resonators are being explored as a potential alternative to the quartz crystal microbalance for biosensing wherein operation in contact with aqueous media is often desirable. However, fluid damping often limits much of the applicability of these devices for biosensing in solution. We demonstrate the effect of hydrophobic self assembled monolayer (SAM) for reducing viscous damping of the resonator in contact with water.

Statement of Contribution/Methods

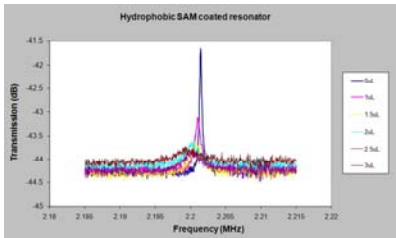
The frequency response of two single crystal silicon resonators are compared in air with various sizes of water droplets spotted on the resonator surface. One resonator is treated with hydrophobic SAM (perfluorodecyltrichlorosilane), and the other is bare silicon. Water droplets ranging from 1–4 μ L are spotted on the centre of the resonator, and the resonator response is characterized using differential electrostatic driving and piezoresistive sensing.

Results

The frequency response plots of the SAM coated resonator to varying water droplet size are shown in figure 1. The extracted quality factor and resonant frequency for the measured data is summarized in table 1.

Discussion and Conclusions

The SAM coated resonator showed a higher quality factor as compared to the plain silicon resonator, which indicates that hydrophobic SAM coating effectively enhanced the performance in a liquid environment. For the SAM coated resonator, there is a decreasing trend in resonant frequency and Q-factor with increase in water droplet size. However, for the bare silicon resonator a dramatic decrease in Q can be seen even for small water droplets on the resonator surface demonstrating the effectiveness of the SAM.



Droplet size (μ L)	Plain silicon resonator		Hydrophobic SAM coated resonator	
	Resonant frequency (Hz)	Quality factor	Resonant frequency (Hz)	Quality factor
none	2199925	7333	2201425	8388
1	2198912	167	2201012	2445
1.5	2199212	129	2200750	1197
2	2199925	148	2206187	946
2.5	***	***	2199925	553
3	***	***	2199100	178

4D-4

8:45 AM Phase shift migration for imaging layered materials and objects immersed in water

Tomas Olofsson¹, Tadeusz Stepinski¹, / *Dept. of Engineering Sciences, Uppsala University, Sweden*

Background, Motivation and Objective

The synthetic aperture focusing technique (SAFT) is in theory capable of realizing the theoretical resolution potential of ultrasonic waves and considerably improving the signal-to-noise-ratio of ultrasonic images of coarse-grained materials. SAFT has been most often implemented in time domain using delay-and-sum operations but can also be implemented in the frequency-domain offering substantial advantages in terms of performance and computational efficiency.

However, the use of SAFT for layered materials or objects immersed in water is made complicated by the refraction at layer interfaces, which makes the correct time delays difficult or time consuming to compute. Neither can the conventional frequency domain implementations of SAFT offer a simple treatment of the problems caused by refraction. The objective of the study has been to find a practical and efficient method for imaging layered structures and objects immersed in water using synthetic aperture techniques.

Tuesday Oral

Statement of Contribution/Methods

In the paper we propose the use of phase shift migration for imaging layered structures and objects immersed in water. The method that was developed in reflection seismology is a frequency domain technique that in a computationally efficient way restores images of the objects in media which are homogeneous in the lateral direction but inhomogeneous in depth.

Results

The performance of the proposed method was demonstrated using immersion test data from a block with side drilled holes and with additional scatterers present in water above the block. In this way the method's capability of simultaneous imaging scatterers present in different media and at different depths was investigated. The method was also applied to a copper block with flat bottom holes as well as to a layered aluminium structure. The results altogether verify that the proposed method is capable of producing high resolution and low noise images for layered or immersed objects.

Discussion and Conclusions

Phase shift migration is demonstrated to produce high resolution images for the inspected objects with a relatively small computational effort. Some difficulties were observed concerning inaccuracies in sound speed values used in the algorithm and this could be a topic for future investigations.

4D-5

9:00 AM Localization Methods in Ultrasonic Thermometry

Mark Mutton¹, L. J. Busse², Donald E. Yuhas¹, Joseph Lloyd³,¹Electrical Engineering, Northern Illinois University, DeKalb, IL, USA, ²LJB Development, Inc., USA, ³IMS Inc., Aurora, IL, USA

Background, Motivation and Objective

Industrial use of ultrasound to measure temperature has its origins in the late 1960's. These techniques, all based on the temperature dependence of ultrasonic velocity, have been limited to measuring average temperature in extreme operating environments in excess of 2000°C[1]. Recent developments in ultrasonic instrumentation, improved signal processing, and high speed data acquisition have rekindled interest in ultrasonic thermometry and made temperature localization feasible and economically attractive to a wider range of applications. Ultrasound-based temperature measurements offer several advantages: they are non-intrusive, have high temporal response, isolate the sensor from explosive or chemically harsh environments, and do not adversely influence thermal transport. In this research we formulate and evaluate ultrasonic thermometry techniques to non-intrusively measure local temperature and thermal gradients within solids.

Statement of Contribution/Methods

Implementation of the method requires sub-nanosecond time-of-flight (TOF) resolution demanding high speed A/D rates combined with sub-sampling index measurement precision (low phase jitter). By tracking the small TOF shifts (or phase changes) in the sequential backscattered ultrasonic frames, a direct measurement of temperature distribution and thermal time history are made.

Results

Analysis has been carried out using both structural and microstructure echoes on copper test bars subjected to controlled heating. Two processing methods have been developed. One is a time domain analysis using sophisticated echo windowing and tracking algorithms. The second method employs frequency domain analysis using phase shift in a manner similar to that which is employed in medical applications[2]. We present results comparing the two processing methods and demonstrate the ability to non-intrusively measure internal thermal gradients as small as 1 degree Centigrade/cm.

Discussion and Conclusions

Ultrasonic temperature localization methods applicable in the industrial environment will be compared to similar applications found in the medical arena. These methods do not require thermal models and the results depend only on one material parameter, the ultrasonic velocity temperature coefficient. This feature, coupled with the non-intrusive nature of the technique, is particularly important in structural health monitoring and thermal transport applications associated with hypersonic flight. The instrumentation requirements, sensitivity, and limitations of the technique will be elucidated.

[1] L.C. Lynnworth, Ultrasonic Measurements for Process Control, Academic Press Inc., San Diego, CA, pp. 369-422, 1989.

[2] Claudio Simon, Philip VanBaren and Emad S. Ebbini, "Two-Dimensional Temperature Estimation Using Diagnostic Ultrasound," IEEE Transactions on Ultrasonics, Ferroelectrics, and Frequency Control, Vol. 45, No. 4, July 1998.

4D-6

9:15 AM **Acoustoelectronic method for the detection of electrical and mechanical properties of adhering cell cultures**

Glen Guhr¹, Hagen Schmidt¹, Manfred Weihnacht¹, ¹*IFW Dresden, Germany*

Background, Motivation and Objective

In biosensor applications even living cells can be used as sensing elements. Cell based biosensors are applicable in many fields ranging from environmental monitoring over pharmaceutical drug screening to tissue engineering. Research including impedance measurements of biological systems is performed since one century. In contrast, the research using of surface acoustic wave (SAW) sensors in biological fluids was started just a few years ago. SAW are mainly affected by the mechanical properties of the surrounding media. By combining SAW measurements with impedance spectroscopy one is able to benefit from the different measurement ranges revealing different properties of the substances of interest.

Statement of Contribution/Methods

In this study, a new method of investigating SAW based sensor devices is reported. For that, SAW one port resonators with a metallization of gold were developed. These sensors allow the continuous detection of electrical and viscoelastic properties of living cell cultures in one measurement step. The growing behaviour of the cells on the sensor was observed during measurements by inverted optical microscopy. The sensors response in a wide frequency range is recorded and characterized to obtain the electric properties of the cells. For the detection of viscoelastic properties, the change of the sensors resonant frequency is monitored vs. time.

Results

The adhesion behaviour of murine fibroblast cells was investigated. The settling and adhesion process of the cells caused an increase of the resonant frequency and its impedance. During this phase the cells start to express the proteins of the extra cellular matrix (ECM) to enable cell adhesion. When the formation of the cell monolayer is finished the resonant frequency stays constant. The cells start to die when the medium is exhausted. During this phase the resonant frequency and its impedance are decreasing reaching their initial values. Considering the penetration depth of the acoustic waves, the properties of the ECM should mainly affect the SAW sensor signals. In contrast the electric field should be able to penetrate the samples in larger dimension. Therefore the changes of the absolute value of impedance detected at a broad frequency range below 10 MHz can be related to the properties of the cell bodies. During initial spreading phase an increase of impedance was observed that can be related to the increase of charge in the cell membrane.

Discussion and Conclusions

The combination of SAW measurement with impedance spectroscopy offers a new tool simultaneously to assess mechanical and electrical properties of tissue in one measurement step.

5D. Oscillators and Temperature Compensation

Pergamo

Tuesday, September 22, 2009, 8:00 am - 9:30 am

Chair: **Jan H. Kuypers**
Sand 9, Inc.

5D-1

8:00 AM **Comparison of Quartz and MEMS Resonators and Oscillators**

Bernd Neubig¹, Bernd Neubig¹; ¹Lab MOS, AXIAL CONSULTING, Mosbach, Baden-Wuerttemberg, Germany

Background, Motivation and Objective

Oscillators incorporating MEMS (Micro-Electronic Mechanical Systems) resonators are aggressively penetrating the market, which was so far a domain of quartz crystal oscillators.

MEMS oscillators are available in different technical realizations from several commercial companies like Si-Time, Discera, SiLabs, Silicon Clocks and others.

Numerous publications in trade magazines and various marketing campaigns claim that MEMS oscillators would be “the beginning of the end for quartz”.

Statement of Contribution/Methods

In our talk we will give a survey over the various technologies are used for MEMS oscillators. This will also cover other oscillators on silicon, which are marketed under the “MEMS” label.

A critical study on the performance of MEMS oscillators will be presented, which includes results of our measurements of short-term stability, phase noise, output spectrum and temperature stability of MEMS oscillators from several manufacturers.

Results

The results will be compared with the typical performance parameters of quartz crystal oscillators.

Some first results were published in [1].

[1] Neubig, Bernd: MEMS-Oszillatoren – Chancen und Grenzen; Markt & Technik Nr. 37 (12.09.2008); see http://www.axtal.com/info/MuT_37_08.pdf

Discussion and Conclusions

The presentation will show the strength and potential of MEMS-resonator based oscillators.

The performance in comparison with quartz crystal oscillators will show its advantages as well as its drawbacks for certain applications which need increased spectral purity and stability

5D-2

8:30 AM **IC-compatible Power Oscillators Using Thin Film Plate Acoustic Resonators (FPAR)**

Ivan Avramov¹, Lilia Arapan², Ilija Kataradjiev², Veselina Strashilov³, Ventsislav Yantchev²; ¹Georgy Nadjakov Institute of Solid State Physics, Bulgaria, ²Solid State Electronics, Uppsala University, Uppsala, Sweden, ³Solid State Physics and Microelectronics, University of Sofia, Sofia, Bulgaria

Background, Motivation and Objective

Current MEMS technologies allow easy integration of high-Q acoustic resonators on Si for low close-in oscillator phase noise. However, they rarely feature sufficient power handling capability to provide thermal noise levels below -175 dBc/Hz as required in high-performance integrated microwave clocks. This study presents first results from IC-compatible FPAR stabilized clocks in the 900 MHz range running at up to 27 dBm (0,5W) loop power for thermal noise levels below -180 dBc/Hz.

Tuesday
Oral

Statement of Contribution/Methods

The key to achieving high loop power in an oscillator is the ability of the stabilizing acoustic resonator to withstand that power without damage or performance degradation. We found that AlN based FPARs, supporting the high velocity, weak dispersion S0 Lamb wave (close to 11 000 m/s), can be an ideal candidate for high-power applications. In this study, we designed and fabricated discrete two-port S0 FPAR devices at 880 MHz which were tested for their power handling capabilities in a feedback-loop power oscillator circuit. The S0 Lamb waves were excited and detected by a classical two-port resonator structure, as in Rayleigh SAW (RSAW) resonators. It consists of two interdigital transducers (IDT) and two reflective gratings, deposited on the thin film AlN membrane. After wafer dicing, the discrete FPARs were contacted to special test fixtures with SMA connectors used both for electrical characterization and as building blocks for the power oscillator tests. Incident power levels up to 24 dBm (250 mW) for the FPARs were provided by a high-power sustaining amplifier in the loop.

Results

The FPAR devices demonstrate a single-mode resonance with an insertion loss of 4 dB and a loaded Q of 800. Detailed narrowband

frequency and phase responses were recorded prior to and after power-oscillator tests in which each device was operated for 24 hours at 250 mW of incident continuous power level in the test oscillator. No measurable performance degradation was observed. At power on, a 50 KHz frequency downshift occurs as a result of thermal dissipation in the IDT electrodes. This thermal transient can be reduced by at least an order of magnitude by applying proper temperature compensation to the FPAR. It is further noted that, FBARs fabricated using the same technology, exhibited irreversible degradation at powers of 250 mW, although 1W power handling is typical for commercial FBARs. The latter illustrates the great potential of the FPAR technology. Physical explanation of the demonstrated power handling capabilities will be further presented.

Discussion and Conclusions

The results from this study indicate that IC-compatible FPAR devices operating on the lowest order fast symmetric Lamb wave mode in C-oriented AlN membranes on Si can dissipate orders of magnitude higher RF-power levels than their RSAW counterparts on quartz and are well suited for integrated microwave power oscillators with thermal noise floor levels below -175 dBc/Hz.

5D-3

8:45 AM Temperature Compensated Solidly Mounted BAW Resonators with Thin SiO₂ Layers

Mohammed Abd Allah¹, Jyrki Kaitila^{2,3}, Robert Thalhammer^{2,3}, Werner Weber², Doris Schmitt-Landsiedel¹. *Lehrstuhl für Technische Elektronik, Technische Universität München, Munich, Germany, ²Infineon Technologies, Munich, Germany, ³currently at Avago Technologies GmbH, Munich, Germany*

Background, Motivation and Objective

Temperature compensation is becoming more and more a high demand for RF filters in order to successfully meet the tightening specifications over a wide range of temperatures. In BAW resonators SiO₂ has been the material of choice for compensation due to its unique positive temperature coefficient of elasticity which is opposite to that of AlN and the metal electrodes. This work investigates adding thin SiO₂ compensation layers at high stress regions inside the resonators, examining their effect on the resonators Temperature Coefficient of Frequency (TCF) and extracts an accurate value of the temperature coefficient of elasticity of SiO₂.

Statement of Contribution/Methods

SiO₂ thin film layers ranging from 20-60 nm were placed inside the resonator, in the middle of the AlN piezoelectric layer where the stress at this location is orders of magnitude higher than that around the electrodes. In this setup the resonator TCF is very sensitive to the variation of thickness of SiO₂, and hence, it is possible to compensate resonators with a minimum amount of SiO₂ inside the resonator. With this high TCF sensitivity to the oxide thickness, it is possible to extract with high degree of accuracy the temperature coefficient of elasticity TC₃₃ of the thin film SiO₂.

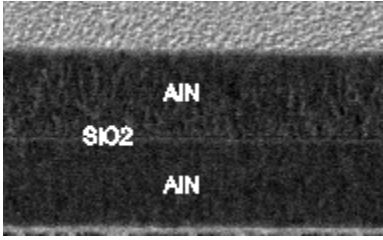
Results

Solidly mounted BAW resonators working around 2.47-2.65GHz have been manufactured with TCF ranging from -11ppm/°C till +12ppm/°C.

The extracted temperature coefficient of elasticity TC₃₃ of SiO₂ is found to be +110ppm/°C which is significantly different from that of the bulk value of +237ppm/°C

Discussion and Conclusions

Fully compensated solidly mounted BAW resonators utilizing very thin SiO₂ layers have been manufactured. The temperature coefficient of elasticity TC₃₃ of the thin film SiO₂ is different from the bulk value used in literature.



5D-4

9:00 AM Design and Fabrication of Reproducible Thermally Compensated BAW Resonator for Time Reference Applications

Pierre Bar¹, David Petit¹, Sylvain Joblot¹, Alexandre Reinhardt², Christophe Billard², Philippe Renaux², Caroline Arnaud¹, Guy Paraf¹, Jean-François Carpentier¹, ¹STMicroelectronics, France, ²CEA-LETI, France

Background, Motivation and Objective

Due to the excellent temperature stability of their resonance frequency, quartz crystals are used in many electronic products requiring very well-defined timing. To go further into integration of thermally stable oscillators into system-in-package radio devices, bulk acoustic wave (BAW) technology appears to be a promising cheap alternative to quartz. Recent works have demonstrated that stable oscillator based on a thermally compensated BAW resonator have the ability to achieve a spectral purity similar to crystal oscillator. This is the result of the high resonance frequency of BAW resonators that enable sufficient f^*Q product (>2.1012) to satisfy the requirements of Lesson's formula. The optimisation of a stable oscillator (included compensation circuit) imposes for the resonator to satisfy concurrently targeted frequency, Q factor and temperature stability. The electrical performances reachable by the designed oscillator are correlated to the dispersion of these three interrelated parameters. Hence, for time reference applications, manufacturing of surface mounted BAW resonators (S-BAW) with reproducible electrical response and thermal behaviour is the next challenge.

Statement of Contribution/Methods

Low thermal drift S-BAW resonators are fabricated taking advantage of SiO₂ material as thermal compensation layer. The requested layer thicknesses are optimized with a 1-D Mason thermal model predicting frequency drifts of resonators versus temperature. The influence of SiO₂ thickness dispersion on the electrical parameters such as resonance frequency, Q factor, electromechanical coupling and TCF is analyzed. To reduce these variations, a dedicated trimming step is used to make this crucial layer uniform. Furthermore, other effects disturbing the ideal thermal deviation of the resonator have been identified. Spurious and substrate modes contributions to the thermal stability of the resonator between resonance and anti-resonance frequencies have been studied. We demonstrate that these parasitic acoustic resonances have to be monitored in a proper way to fulfil predictions of the thermal model and to reduce TCF dispersion at wafer scale. Detailed design considerations and approach to improve performances of resonant elements and reproducibility will be discussed in the talk.

Results

Cartographic measurements for various temperatures and resonator designs are presented in this paper. A good matching between simulated and measured response versus temperature is obtained. Measured dispersions of targeted frequency, Q Factor and TCF at wafer scale will be detailed.

Discussion and Conclusions

Regarding the severe specifications required for time reference applications, detailed discussions are made on the dependence of BAW resonator characteristics versus temperature at wafer scale. Solutions to guarantee sufficient reproducibility are proposed and corroborated by measurement.

Tuesday
Oral

5D-5

9:15 AM **High precision signal processing algorithm to evaluate the SAW properties as a function of temperature**

Ismail Shrena¹, David Eisele¹, Jochen Bardong², Leonhard Reindl¹; ¹*Department of Microsystems Engineering, University of Freiburg – IMTEK, Freiburg, Germany,* ²*Carinthian Tech Research AG, Villach, Austria*

Background, Motivation and Objective

In order to measure the temperature using Surface Acoustic Wave devices, it is important to characterize the substrate material over a desired temperature range, which strongly depends on the accuracy of the analysis algorithm used.

Statement of Contribution/Methods

This paper presents a special signal processing algorithm, which accurately evaluates the desired SAW properties as functions of temperature. The investigated properties are group and phase velocity, propagation loss, and electromechanical coupling coefficient of the SAW device. To evaluate these properties, two delay lines of different lengths were designed and measured. These delay lines use IDTs with several frequency pass bands so that the material properties can be evaluated at up to four different frequencies with one measurement. The algorithm extracts the transfer function of the delay lines from the raw output signal at several temperature levels and computes the corresponding properties at these temperatures. In the first step of analysis, the algorithm determines the center frequency and obtains the delay time difference by cross correlating the signals out of the short and long delay lines. The extracted parameters are then used in a second analysis step to calculate the acoustic properties of the SAW material as a function of temperature. To validate this algorithm, its accuracy is studied. A test signal is generated from the delay line time differences and center frequencies obtained during the first step of analysis. The test is performed by applying the analysis algorithm to the generated test signal and comparing the original parameters with the recalculated parameter set.

Results

When applied, the test showed that the algorithm is very accurate and enables the group velocity to be determined within a tolerance of about ± 0.04 m/s, and the time delay within a tolerance of about ± 5 ppm.

Discussion and Conclusions

This high accuracy enables the precise evaluation of the acoustic properties of SAW materials used in temperature measurement applications.

Tuesday
Oral

6D. Bulk Wave Effects and Devices

Baalbek

Tuesday, September 22, 2009, 8:00 am - 9:30 am

Chair: **Bikash Sinha**
Schlumberger-Doll Research

6D-1

8:00 AM Measurement of electric properties in a ZnO single crystal via electromechanical coupling using Brillouin scattering method

Takahiko Yanagitani¹, Hiroyuki Sano², Mami Matsukawa^{2,1} *Graduate School of Engineering, Nagoya Institute of Technology, Nagoya, Aichi, Japan, ²Laboratory of Ultrasonic electronics, Doshisha University, Kyotanabe, Kyoto, Japan*

Background, Motivation and Objective

Wide band-gap semiconductors such as GaN, AlN, ZnO have piezoelectric effect. Therefore, electric properties of these materials can be measured via a "piezoelectric stiffening". Here, we propose local electric property measurement in the in-plane direction of the semiconductors, using electromechanical coupling. To estimate resistivity in the intrinsic crystal with less than 1 Ω-m, GHz acoustic wave measurement is necessary."

Statement of Contribution/Methods

An RIGA Brillouin scattering method allows us to measure GHz bulk acoustic wave velocities and electromechanical coupling in the in-plane direction [1]. First, we have checked the dependence of the longitudinal wave velocity on resistivity in an a-plane ZnO single crystal with 0.7 Ω-m at R. T.. During the measurement, resistivity of the sample was controlled by the temperature in -50 to 170°C.

Results

As expected, velocity values decreased by increasing temperature, namely decreasing resistivity (Fig.1). Experiment curve in 5 GHz almost corresponded to the theoretical one. Figure 2 shows distribution of longitudinal and shear wave velocity values at different nine points.

Discussion and Conclusions

Longitudinal wave velocity values at low temperature are varied drastically, whereas, the velocity at high temperature and shear wave velocity value, which should not have piezoelectric coupling, are almost constant. Large variety in longitudinal wave velocity toward c-axis direction is caused by variety of resistivity in this direction. This fact also has been confirmed by standard electrode resistivity measurement. This technique may be useful for a microscopic measurement in the wide band-gap semiconductors.

[1]T. Yanagitani, Proc. IEEE Ultrason. Symp.(2008) 1487

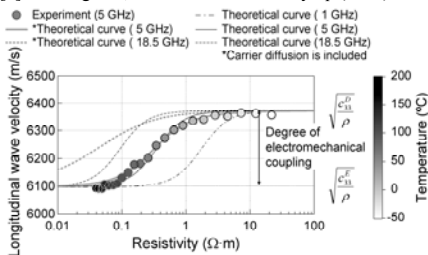


Fig. 1 Longitudinal wave velocity of the of the ZnO single crystal measured in -50~170 °C. In the estimation of carrier diffusion effect, carrier mobility is assumed to be constant in 180 cm² / V sec.

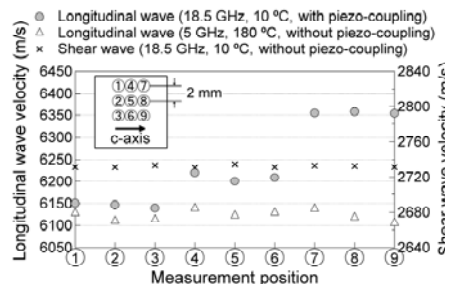


Fig. 2 Distribution of the longitudinal wave velocity in the ZnO single crystal

Tuesday
Oral

6D-2

8:15 AM **Eigen-frequency and Frequency response Calculation of Piezoelectric Resonator Parameters**

Yook-Kong Yong¹, Frank Fang², Shih Chuang²; ¹*Civil and Environmental Engineering, Rutgers University, Piscataway, NJ, USA*, ²*Statek, Inc., Orange, CA, USA*

Background, Motivation and Objective

The electrical parameters of a piezoelectric resonator are needed for the design of its oscillator circuit. These parameters are measured on network analyzers and are part of the specifications for the resonator itself. For a stable, high quality oscillator, we would want to optimize the resonator parameters for Q, capacitance ratio, and motional resistance. At present when designing resonators a frequency response analysis is the method employed to calculate the electrical parameters. The frequency response analysis however is not only time consuming but also not as useful for finding good resonator designs. An eigen-frequency analysis is usually the method employed for finding good resonator designs.

Statement of Contribution/Methods

The electrical parameters of a piezoelectric resonator are usually those of a Butterworth Van Dyke resonator with C_0 the static capacitance, C_1 motional capacitance, L_1 motional inductance, R_1 motional resistance and Q quality factor. C_0 can be calculated at 1 Hz when the resonator is essentially not vibrating. Since the other parameters C_1 , L_1 , R_1 and Q are essentially constant in the neighborhood of the resonant frequency, we could derive equations for calculating these parameters from the frequency response.

Equations for calculating the resonator parameters from eigen-frequency analysis were derived. C_1 could be calculated from the open circuit and short circuit resonant frequencies and C_0 . L_1 was obtained from the short circuit resonant frequency and C_1 . The Q could be obtained from the ratio of the imaginary eigenfrequency to the real eigenfrequency. And R_1 was calculated using the now known values of Q and C_1 .

Results

The values of C_0 , C_1 , L_1 , R_1 and Q were calculated using the derived equations, and frequency response and eigen-frequency analyses. Both sets of values from the frequency response and eigen-frequency analyses compared well the measured values of two quartz AT-cut, 12 MHz thickness shear resonators.

Discussion and Conclusions

Equations for calculating the electrical parameters from the frequency response analysis were derived. The electrical parameter values compared well with the measured values. The equations were found to be fairly stable with respect to frequency increments of the frequency response curves.

Equations for calculating the electrical parameters from the eigen-frequency analysis were derived. The electrical parameter values compared well the measured values. The equations from the eigen-frequency analysis are very useful for studying the effects of electrode and resonator geometries and the effects of mounting support structures.

6D-3

8:30 AM **Understanding Third Order Non-linear Behavior in BAW Devices**

David Feld¹; ¹WSD, AVAGO technologies, San Jose, CA, USA

Background, Motivation and Objective

Accurate modeling of the nonlinearities in BAW duplexers is important since handset manufacturers employing BAW duplexers at the handset ANT port desire low levels of 2nd harmonic emissions and intermodulation distortion. There are numerous papers describing ways in which non-linear behavior in BAW resonators can be modeled and it is generally agreed upon that it is the piezoelectric AIN that gives rise to this non-linear behavior. Little attention has been given to the generation of third order non-linear products and their impact on system performance. In this paper we discuss how these second order models in the literature can give rise not only to second order mixing products but also to third order products. We show that this can happen through a process of re-mixing in which second order mixing products are initially generated in the piezoelectric AIN, and are subsequently remixed with the applied fundamental thus generating third order products.

Tuesday
Oral

Statement of Contribution/Methods

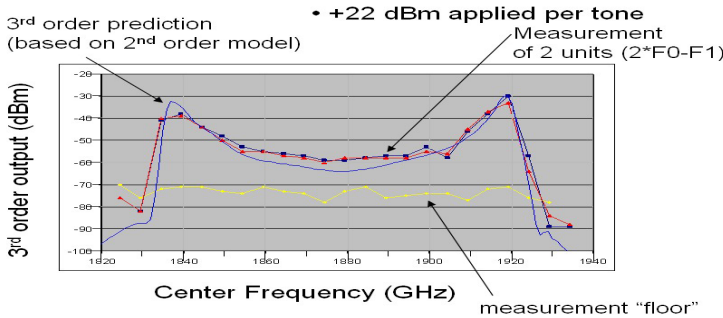
We compare measurements of third order behavior in duplexers and resonators and compare them to the 3rd order behavior that is predicted by 2nd order models found in the literature.

Results

The output power of a standard third order measurement is made in which two tones spaced 1.0 MHz apart and having a power level of +22 dBm each are injected into the Tx port of a 2GHz duplexer. Tones at $2f_0-f_1$ are measured at the duplexer ANT port as a function of the center frequency of the tones and their output power levels are plotted in Fig. 1. The output of a model containing only second order terms produces third order products at $2f_0-f_1$ through re-mixing is superimposed on the plot showing reasonable agreement with the measured data.

Discussion and Conclusions

We conclude that substantial third order products can be generated through a remixing process in a resonator model containing only 2nd order terms. This being the case we answer the question of whether or not third order terms need to be added to these models to make third order predictions. Finally it is well known that BAW resonators placed in an anti-parallel fashion are a circuit method by which to null out second harmonic generation. We will explain why this technique is useless in nulling out third order mixing products and show that as resonators become ever smaller as resonator frequencies are increased to 4 GHz and above that third order mixing may be of concern in duplexer design.



6D-4

8:45 AM Nonlinear Acoustic Waves Localized at Crystal Edges

Andreas Mayer¹, Alexey Lomonosov², Peter Hess^{3,1} *HS Offenburg, Gengenbach, Germany, ²General Physics Institute, Moscow, Russian Federation, ³Institute of Physical Chemistry, University of Heidelberg, Heidelberg, Germany*

Background, Motivation and Objective

Acoustic wedge waves have been discovered and studied mainly in isotropic elastic media. Unlike SAWs of Rayleigh type, little is known about the existence of edge waves in anisotropic media.

Because of the high degree of localization and the absence of dispersion at perfect edges, strong cumulative nonlinear effects may be expected. For symmetry reasons, waves localized at rectangular edges in the isotropic Poisson case experience nonlinearity of third order. An open question has been up to now, whether for edge modes in anisotropic media, 2nd-order nonlinearity and hence 2nd-harmonic generation occurs to an appreciable extent.

Statement of Contribution/Methods

Using an expansion of the displacement field in Laguerre functions, similar to the early studies of wedge acoustic waves in isotropic media [1], a variety of propagation geometries of crystalline wedges with wedge angles of 90° and 45° has been investigated. For several of these, pronounced edge modes have been identified, and their displacement pattern could be analyzed. In others, it has been found that no edge mode exists.

With the velocities and displacements of linear edge waves determined numerically, the 2nd-order coupling coefficients governing nonlinear waveform evolution have been quantitatively evaluated. The corresponding evolution equation for wedge waves in the presence of 2nd-order nonlinearity [2] was subsequently extended to account for dispersion of linear edge waves due to modifications of the wedge tip or coating of the surfaces. Using an iterative optimization scheme, solitary edge pulses were computed.

Results

Edge acoustic waves have been found to exist in various propagation geometries of anisotropic elastic media. For the example system of silicon with the tip of the edge and the normals of the adjacent surfaces parallel to the crystallographic axes, 2nd-order nonlinearity vanishes for symmetry reasons. For the geometry of the wedge tip being along (1 1-2) and adjacent (1 1 1) and (-1 1 0) surfaces, preliminary results reveal that the 2nd-order nonlinearity is comparable to that found for Rayleigh waves in the propagation geometry $S(1 1 1) < 1 1-2 >$, where nonlinear pulse evolution has been investigated experimentally [3].

Discussion and Conclusions

Similar to nonlinear SAW pulses, high-intensity edge pulses may be used to investigate materials properties like crack formation [3]. In the presence of weak dispersion, solitary pulses can form. Predictions are made for their three-dimensional displacement pattern.

[1] S. L. Moss, A. A. Maradudin, and S. L. Cunningham, Phys. Rev. B 8, 2999-3008 (1973).
[2] V. V. Krylov and D. F. Parker, unpublished.
[3] A. M. Lomonosov and P. Hess, Ultrasonics 48, 482-487 (2008).

Tuesday
Oral

6D-5

9:00 AM **The Nonlinear Finite Element Analysis of Quartz Crystal Resonators**

Ji Wang¹, Leping Chen¹, Jianke Du¹, Yook-Kong Yong², Lihong Wang³; ¹Mechanics and Engineering Sciences, Ningbo University, Ningbo, Zhejiang, China, People's Republic of, ²Civil and Environmental Engineering, Rutgers University, Piscataway, NJ, USA, ³Mathematics, Ningbo University, Ningbo, Zhejiang, China, People's Republic of

Background, Motivation and Objective

The finite element analysis of quartz crystal resonators has been gradually adopted in the design and product improvement due to the advantage in predicting the vibration frequency, energy trapping, and calculation of device properties. The analysis can be done with 3D theory of elasticity or piezoelectricity or the Mindlin plate theory by general purpose software or custom development, which has the advantage of reducing the size of analysis significantly for typical thickness-shear vibrations of quartz crystal plates. While linear finite element analysis is adequate for the vibration frequency and frequency-temperature relations, further analysis on important phenomena and electrical parameters require the consideration of nonlinear material properties of quartz crystal.

Statement of Contribution/Methods

The nonlinear finite element analysis is performed with the nonlinear Mindlin plate theory, which takes into consideration of material nonlinearity and higher-order strain components. The 2D nonlinear equations are implemented so the problem will have a smaller size in comparison with 3D approach. General nonlinear finite element analysis procedure based on the iterative solution procedure is implemented. The program is in parallel implementation with advanced features such as the sparse matrix handling, latest eigenvalue computing, and linear algebra library in public domain. The program is developed and tested on a Linux cluster to enable fast solution of large scale problems.

Results

With the nonlinear finite element program on top of the earlier program with linear Mindlin plate theory, the analysis of vibration frequency and frequency-temperature relations can now be performed with the consideration of nonlinear material properties and strain components. In addition to the essential results, we can extend the program to analyze the resonator behavior under driving voltage to provide many important properties like drive-level dependence and other nonlinear properties. These analytical capabilities will expand current features of finite element programs and provide efficient tools on parallel platforms.

Discussion and Conclusions

The finite element analysis of quartz crystal resonators has been making great contribution to the design and improvement facing the fast shrinkage of resonator size and elevated precision requirements. The full advantage of the finite element analysis can be taken if electrical parameters and performance behavior can be predicted with the improved analytical model and consideration of nonlinear material properties. The current approach based on the nonlinear theory will meet these objectives since the advantage of the finite element analysis on parallel platforms have been well understood and widely implemented. Our nonlinear analysis will validate the nonlinear Mindlin plate theory and provide important and essential details on the nonlinear behavior of quartz crystal resonators.

6D-6

9:15 AM Measurements of Electromechanical Coupling Constant of ZnO Films Used in HBAR's and FBAR'sGeorgy Mansfeld¹, Sergey Alekseev¹, Natalia Polzikova¹ / IRE RAS, Moscow, Russian Federation**Background, Motivation and Objective**

The knowledge of an electromechanical coupling constant K_2 of thin piezoelectric films used in transducers in FBAR's and HBAR's is very important. Traditional way of the evaluation of this parameter is based on the measurements of the difference between measured values of resonant and antiresonant frequencies. Sometimes this procedure is not correct, especially on microwaves and at high numbers of overtones when the mentioned above frequency difference strongly depends also on the losses in the resonator structures [1,2].

Statement of Contribution/Methods

In this work in order to find the value of K_2 is measured together with the difference between peculiarities on frequency dependence of the phase of the reflection coefficient of the electromagnetic signal from resonator s_{11} at the same overtone number. Both differences of the frequencies depends on K_2 and the losses in structure. Using these data and the expressions from our work [1] it is possible to calculate both K_2 and the attenuation constant of the acoustic waves excited in the resonator structures.

Results

Experimental setup provided getting of the necessary data of frequency differences in a wide frequency band from 500 up to 4000MHz. The samples under study were BAW composite resonators operating on longitudinal and shear acoustic waves. The substrates were flat parallel face plates of langatate, langasite and sapphire. ZnO films (1-8 μ m) deposited between thin Al electrode onto the surface of the plate were used in transducers. The best measured values of the electromechanical coupling of ZnO constant in structures were up to 0.07.

Discussion and Conclusions

The simple method of evaluation of electromechanical coupling constant is demonstrated. The work was supported by grants RFBR 07-02-01006

[1] G. D. Mansfel'd, S. G. Alekseev and N. I. Polzikova, Equivalent circuit of a composite acoustic resonator for microwave radioelectronic devices, Acoustical Physics, Volume 54, Number 4 / July 2008

[2] G. D. Mansfel'd, S. G. Alekseev and N. I. Polzikova Unique properties of HBAR Characteristics, 2008 IEEE International Ultrasonics Symposium, Beijing China, November 2-5, 2008, 270-271

1E. Therapeutic Arrays

Sala 1

Tuesday, September 22, 2009, 11:30 am - 1:00 pm

Chair: **Mathias Fink**
ESPCI - France

1E-1

11:30 AM **Energy based Adaptive Focusing: Optimal Ultrasonic Focusing using Radiation Force Magnetic Resonance Guidance**

Benoit Larrat¹, Mathieu Pernot¹, Gabriel Montaldo¹, Mathias Fink¹, Mickael Tanter¹; ¹*Institut Langevin - ESPCI Paristech, Univ Paris 7, CNRS UMR 7587, Paris, France*

Background, Motivation and Objective

The non invasive correction of phase aberrations is mandatory in the framework of human brain HIFU therapy at relatively high frequency (> 500 kHz). This study proposes an adaptive focusing technique based on the use of acoustic radiation force MR imaging.

The main objective is here to demonstrate experimentally the ability of acoustic radiation force MR imaging to restore a sharp focus through strong phase aberrators using a set of short US bursts.

Statement of Contribution/Methods

A 64-element linear phased array operating at 6MHz was used inside a 7T MRI scanner. A motion sensitized MR sequence was synchronized with the US emissions. The displacement field was mapped in a tissue mimicking gelatin based phantom, with a resolution of $300\mu\text{m} \times 300\mu\text{m} \times 2\text{mm}$. In a first experiment, an aberrating law with strong phase shifts was added numerically to the ideally beamformed US beam. In a second experiment a physical aberrator was placed between the array and the phantom.

A non-iterative process was applied based on the spatial decomposition of the phase aberration on the Hadamard basis. It consisted in the successive emission of ultrasonic spatial coded excitations. For each transmit, the acoustic intensity at the target location was indirectly estimated using MR imaging. This intensity was estimated while imaging tissue displacements induced by the radiation force of 400 μs US bursts. The set of time delays and amplitudes to be applied on each element of the US array for the optimal focusing was then recovered by a direct inversion of the intensity measurements.

Results

MR imaging allowed accurate estimation of the acoustical power at the focus of the array. After the complete 256 transmit experiment, the proposed method was able to recover the spatial distribution of phase aberrations up to 2pi radians for both numerical and physical phase aberrating layers. A relatively low error was found on the non invasive phase aberration estimation (standard deviation of 0.3 radians). Moreover, the acoustical power at the focus was increased by a factor of 5 after phase correction.

Discussion and Conclusions

An adaptive focusing technique based on the single knowledge of the acoustic intensity at desired focus is here demonstrated to perform optimal focusing through strongly aberrating layers using MR motion sensitive sequences. This corresponds to a first experimental evidence of extremely efficient MR guidance for US aberration correction. Beyond this proof of concept, current work focuses on applying this technique to the aberration correction through a human skull bone with a 512-element phased array operating at 1MHz in a clinical 1.5T MRI scanner. Total acquisition time should be kept reasonable for in vivo application.

1E-2

11:45 AM Adaptive Transthoracic Targeting Using Dual-Mode Ultrasound Arrays: A simulation and experimental study

Andrew Casper¹, John Ballard¹, Emad Ebbini¹; ¹Electrical and Computer Engineering, University of Minnesota, Minneapolis, MN, USA

Background, Motivation and Objective

The rib cage partially obstructs many transthoracic tumor locations e.g. liver and kidneys, during high intensity focused ultrasound (HIFU) therapy. Inhomogeneities due to the ribs and layered abdominal tissue can result in a distorted HIFU focus as well as adverse heating across the ribs, due to their increased absorption of the HIFU beam and increased reflection due to impedance mismatch. Previously, we have presented an image-based refocusing algorithm using dual-mode ultrasound arrays (DMUA) that minimizes the incident power across the ribs while maintaining a specified level of power deposition at the target location.

Statement of Contribution/Methods

We have recently developed a finite difference time domain (FDTD) simulation tool capable of characterizing the HIFU beam through inhomogeneous, attenuating medium. B-mode images obtained with the DMUA allow for registration of the tissue inhomogeneities, such as the ribs, and target location for inputs into the FDTD simulation. In addition, the transient bioheat transfer equation (tBHTE) was utilized in the simulation model to allow for the computation of the temperature rise throughout the treatment region, including the ribs.

Results

The acoustical model used in the FDTD simulation is verified experimentally with a 64-element, 1 MHz, DMUA. Hydrophone measurements were taken to verify the simulations predictive ability in calculating the transient acoustic pressure. Thermocouple measurements in an attenuating tissue mimicking phantom (~0.5 dB/cm/MHz) were used to verify the results of the tBHTE simulation at the target and rib locations. Comparisons between the adaptive image-based refocusing and phase-conjugate (time-reversal) solutions were also made. The results demonstrate that the time-reversal solution maximizes the power deposition at the target, but results in more than 2-fold increase in power deposition at the ribs compared to the adaptive refocusing solution. This result was verified experimentally and computationally in a tissue-mimicking phantom with embedded Plexiglas ribs obstructing the path of the HIFU beams.

Discussion and Conclusions

The experimental and numerical results are in good agreement and they demonstrate the feasibility of the optimization of transthoracic focusing if information about the rib locations is available. DMUAs provide this information by imaging the treatment region, including the rib structures, to identify any obstacles in the path of the HIFU beam. The inherent registration between the imaging and therapeutic coordinate systems of DMUAs allows for direct estimation of the beamforming parameters necessary for finding the optimal solution. Comparisons between the different approaches (e.g. time reversal vs. adaptive optimization) reveal important insight into the exposure to the ribs while achieving the treatment objectives at the target.

1E-3

12:00 PM Ultrasonic adaptive transrib focusing using the decomposition of the time reversal operator

Etienne Cochard¹, Claire Prada¹, Jean-François Aubry¹, Fink Mathias¹; ¹Institut Langevin, Laboratoire Ondes et Acoustique, France

Background, Motivation and Objective

Thermal ablation induced with high intensity focused ultrasound has produced promising clinical results to treat hepatocarcinoma and other liver tumors. However skin burns have been reported in many clinical studies. The energy deposition on the skin is indeed enhanced by the presence of the ribs that both reflect the wave front back to the therapeutic array and heat significantly because of the high ultrasonic absorption of bone tissues. This study proposes to use the decomposition of the time-reversal operator (DORT) method to produce an ultrasonic beam that focuses at a chosen target point while avoiding the ribs. The DORT method has been widely used in the past to focus selectively on different scatterers in a complex media. In the present study, the ribs are the dominant scatterers and the method is used in an orthogonal approach to avoid them.

Tuesday
Oral

Statement of Contribution/Methods

Three human ribs have been immersed in water in front of a 128 elements linear array of 1.5 MHz central frequency. A focusing weight vector was constructed in order to avoid energy deposition on the ribs. In a first step, the transducer array was used in pulse echo mode to measure the echoes of the ribs by the acquisition of the array response matrix $K(t)$. Then, the singular value decomposition of the frequency domain response matrix $K(\omega)$ was calculated to provide the invariants of the time reversal operator. It was verified that, as expected, the dominant singular vectors (or the invariants) are phase and amplitude laws that focus on the ribs. Finally, the weight vector which focuses on the region to treat was built in the space orthogonal to the subspace of emissions focusing on the ribs. To this end, the cylindrical wave front focusing at the chosen target point has been projected orthogonally to the dominant singular vectors. After emission of the projected signals, the resulting pressure fields have been measured with a needle-hydrophone both in the focal plane and in the plane of the ribs. For comparison, the same measurement has been done for the cylindrical focusing. The specific absorption rate (SAR) gain (ratio of the rates of absorption at the focal point and on the ribs) were calculated when using this non invasive ribs sparing technique and with a non-corrected beam (cylindrical beam). This procedure was repeated for several geometries with an intercostal space varying from 10 mm to 15 mm.

Results

Depending on the intercostal space, the mean SAR gain obtained with the projected emission was 25 to 100-fold better than with the cylindrical focusing. The corresponding pressure field at the bone location was on average 23 dB lower with the proposed focusing.

Discussion and Conclusions

An adaptive non invasive ribs sparing technique has been proposed and validated. It has been shown to significantly decrease the energy deposition on the ribs. Such a technique should benefit to transcostal ultrasonic ablation of the liver by reducing the risk of skin burns.

1E-4

12:15 PM **Treatment of Rabbit VX2 Tumor by Miniaturized Image-Ablate Ultrasound Arrays**

T. Douglas Mast¹, Peter G. Barthe², Inder Raj S. Makin², Michael H. Slayton², Chandra Priya Karunakaran¹, Mark T. Burgess¹, Amel F. Alqadah¹, Joseph F. Buell³, Steven M. Rudich⁴, ¹Biomedical Engineering, University of Cincinnati, Cincinnati, OH, USA, ²Guided Therapy Systems/Ardent Sound, Mesa, AZ, USA, ³Surgery, University of Louisville, Louisville, KY, USA, ⁴Surgery, University of Cincinnati, Cincinnati, OH, USA

Background, Motivation and Objective

Minimally-invasive bulk ultrasound ablation has promise for treatment of liver cancer and other soft tissue tumors. Advantages include superior selectivity, insensitivity to perfusion effects, and monitoring ability compared to radiofrequency ablation. This work evaluates the performance of miniaturized ultrasound arrays for imaging and ablation of VX2 tumor implanted into rabbit liver.

Statement of Contribution/Methods

Image-ablate ultrasound probes have been constructed based on an optimized design, incorporating a 20-mm aperture of 32 array elements within an 8-gauge shaft, with circulatory cooling and coupling appropriate for laparoscopic or interstitial use. Performance of these arrays for imaging and ablation was confirmed by *in vitro* experiments supplemented by analytic and numerical modeling. VX2 tumor was implanted in rabbit liver, resulting in formation of tumors 0.9±0.3 cm diameter in 11-14 days and 1.9±0.5 cm diameter in 21 days. VX2 tumors were then imaged and treated in open surgical procedures, with the image-ablate probe placed directly on the liver surface. Ablation exposures employed unfocused, 4.8 MHz continuous-wave ultrasound with *in situ* SPTA intensity 38-78 W/cm² and treatment times 20-120 s. *In vivo* ablation results were quantitatively assessed by H&E histologic and TTC vital stains.

Results

Assessment of array performance shows their capability to image VX2 tumor boundaries and detect ablation-induced tissue changes. In ablation mode, the arrays are capable of surface intensities >60 W/cm² at 3.5 or 4.8 MHz. Vital staining confirmed complete ablation of a VX2 tumor cross section in 7 of 12 trials, including all trials where the total delivered acoustic energy exceeded an empirical threshold of 747 J. Ablation zone widths measured from stained cross sections were 22.0±2.0 mm for treatments above this energy threshold. Histologic staining showed cellular changes consistent with thermal coagulative necrosis. Tissue ablation volume was proportional to the total delivered acoustic energy ($r=0.55$, $p=0.05$). The measured volumetric ablation rate of 0.83±0.34 ml/min was limited mainly by the finite rabbit liver lobe size.

Tuesday
Oral

Discussion and Conclusions

These experiments show the feasibility of performing *in vivo* ablation of liver cancer using miniaturized, image-ablate ultrasound arrays. Experimental results demonstrate the capability of these devices to achieve ablation more efficient than high-intensity focused ultrasound, with treatment selectivity and control superior to radiofrequency ablation. A therapeutic platform based on these devices has potential to improve minimally-invasive management of liver cancer in the clinical setting.

1E-5

12:30 PM **Concurrent ARFI imaging and HIFU ablation using a diagnostic transducer array and ultrasound system with custom beam sequences**

Kristin Frinkley Bing^{1,2}, Veronica Rotemberg¹, Mark Palmeri¹, Kathryn Nightingale^{1,1} *Duke University, USA,*
²*Georgia Tech Research Institute, USA*

Background, Motivation and Objective

High-intensity focused ultrasound (HIFU) has primarily been performed using a specialized ultrasound transducer for therapy and either a separate transducer for imaging or a different imaging modality. Accurate localization and monitoring of HIFU treatment, as is done for liver cancer, is important to improving the efficacy of the treatment as well as minimizing complications. The goal of this work was to demonstrate the feasibility of using a diagnostic ultrasound system to perform spot ablations in liver with concurrent Acoustic Radiation Force Impulse (ARFI) stiffness imaging in order to monitor lesion formation.

Statement of Contribution/Methods

Ex vivo samples of bovine liver were degassed, sealed in bags with an acoustic window, and immersed in 36°C water, mimicking an intra-operative liver ablation procedure. A diagnostic ultrasound system (Siemens Antares™ and CH6-2 curvilinear array) with a cooled waterbag around the transducer was used to both: 1) ablate the liver with a custom M-mode sequence and 2) to monitor the resulting tissue stiffening with 2-D ARFI imaging. The custom M-mode sequence utilized a 35-45 mm waterpath standoff and was focused at 50 mm laterally (F/1.5) and at 69 mm in elevation (F/5.75) with 20-25% system voltage, 5.6 μs pulses, 11.3 kHz PRF, 4.44 MHz center frequency, and 60 s on-time for heating per location. Ablation patterns were generated using a grid of varying numbers of heating locations.

Results

ARFI images showed irreversible liver stiffening with heating that corresponded to discolored regions in gross pathology. Images were taken before and after ablation, as well as in 5-second intervals during ablation to monitor the increase in the degree and extent of stiffening with time. Ablation lesions were generated at depths up to 15 mm from the surface of the liver. No gaseous body formation was observed during the ablations in B-mode, thus lesions were not visualized in matched B-mode images. In order to mimic the presence of a stiffer tumor, bovine muscle tissue ($\approx 2.5 \text{ cm}^3$) was inserted into a liver sample, and subtraction images (pre-post ARFI) clearly distinguished the ablated (stiffened) liver tissue from the stiffer muscle tissue; however, the sequences utilized did not clearly ablate the muscle tissue.

Discussion and Conclusions

This study demonstrated the ability of a diagnostic system using custom beam sequences to localize an ablation site, heat the site to the point of irreversible damage, and monitor the formation of the ablation lesion. Future work will involve testing this treatment system *in vivo*.

1E-6

12:45 PM **Scanned-beam assisted mild tumor heating using a dual-functional ultrasound linear array**

Chun-Yen Lai¹, Dustin Kruse¹, Charles Caskey¹, Douglas Stephens¹, Patrick Sutcliffe¹, Katherine Ferrara^{1,1} *Dept. of Biomedical Engineering, University of California, Davis, USA, Davis, CA, USA*

Background, Motivation and Objective

Image-guided tissue heating by a single ultrasound beam has been shown to create mild hyperthermia in a small region of interest (ROI). Our approach uses a modified co-linear array ultrasound transducer, which has multiple confocally-focused arrays which are combined for effective heating and imaging. The objective of this study was

to develop methods for creating and maintaining ultrasound-induced mild hyperthermia in an extended region of interest. *In vitro* and *in vivo* heating studies were performed to compare the two heating modes.

Statement of Contribution/Methods

Our system consists of a SIEMENS Antares ultrasound scanner, a custom-designed co-linear array transducer, modified system software and a real-time temperature feedback controller. The co-linear array transducer provides the dual functions of imaging and heating at 5.5 MHz and 1.54 MHz, respectively. A rectangular color-mode ROI with arbitrary size was used to guide heating, with periodic B-mode image updates during the therapy. A needle-type thermocouple was inserted into a phantom or a tumor for temperature measurement, with the measured temperature fed to a proportional-integral-derivative (PID) controller embedded in a LabVIEW program with an Ethernet-based interface. An additional anti-windup term was included in the PID controller to improve the system stability. Duty cycle and pressure can be scaled; however, the primary PID control parameter is duty cycle, controlled via the pulse repetition frequency (PRF). A 74% (w/w) syrup-based polyacrylamide phantom was used for *in vitro* experiments. Five thermocouples were placed in the phantom at a fixed focal depth and with varied azimuthal locations. The two-dimensional drug-release pattern was examined by placing fluorescent dye-encapsulated, temperature-sensitive liposomes within the phantom with single-beam and scanned-beam heating applied to the three orthogonal planes. For *in vivo* heating, a 10-mm Met-1 tumor was tested, and the heating response was compared for the two heating modes.

Results

In the *in vitro* tests with 2W total acoustic power, single-beam and scanned-beam heating achieved a 5°C temperature increase in 45 and 165 seconds, respectively. With scanned-beam heating, the spatial variation in temperature within the ROI was less than 6%. In *in vivo* tests, orthotopic breast tumors reached $42 \pm 0.2^\circ\text{C}$ within 2-6 minutes with scanned-beam heating.

Discussion and Conclusions

We have developed methods for spatially and temporally-controlled mild hyperthermia using a co-linear array transducer with two heating modes. In this presentation, we will explore weighting scanned-beam profiles in order to achieve more uniform heating. (Acknowledgement: NIH CA 103828, 1R21EB009434)

2E. Microbubbles: Characterization and Modeling

Sala 2

Tuesday, September 22, 2009, 11:30 am - 1:00 pm

Chair: **Ayache Bouakaz**
INSERM, Tours

2E-1

11:30 AM Characterization of viscoelastic properties of ultrasound contrast agents

Hélène Moreschi¹, Anthony Novell¹, Samuel Callé¹, Marielle Defontaine¹, Ayache Bouakaz¹; ¹Imagerie et Cerveau équipe 5, INSERM U930 CNRS ERL 3106 F.Rabelais University, France, Metropolitan

Background, Motivation and Objective

Ultrasound contrast agents (UCA) composed of gaseous microbubbles exhibit acoustic properties that differ from those of surrounding tissue. In order to increase the contrast to tissue ratio, it is necessary to propose a method that characterizes optimally the ultrasonic properties of UCA.

The aim of this study is to determine the viscoelastic properties of UCA using a dynamic acousto-elastic method. The approach, based on the interaction of two acoustical waves, provides non-contact and localized measurements of viscoelastic and dissipative nonlinearities of the microbubbles.

Statement of Contribution/Methods

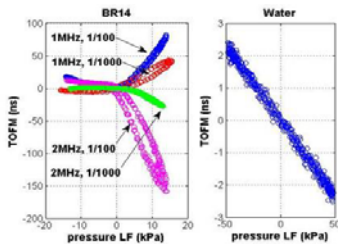
The method consists in using a low frequency (LF) wave (2.8 KHz) acting as an expansion/compression quasi-hydrostatic pressure and high frequency (HF) pulses (10 pulses/LF period, 1 or 2 MHz) that are used to extract nonlinear viscoelastic properties (Time Of Flight Modulation, TOFM) and nonlinear dissipative variations (Relative Amplitude Modulation, RAM) of UCA. SonoVue and BR14 microbubbles (Bracco research, GE) were characterized at two different frequencies (1MHz and 2 MHz) and at two dilutions (1/100 and 1/1000).

Results

The figure shows TOFM curves as a function of instantaneous LF pressure amplitude for several media. A nonlinear classical behavior is observed in pure water. As expected, the corresponding nonlinear parameter β , obtained from the slope of TOFM curve, was estimated to 5. In UCA, the TOFM curves exhibit different slopes in expansion and compression phases and an important hysteresis during compression phase. These results demonstrate the nonlinear and non classical behavior of UCA in comparison to water. Concerning the dissipative nonlinearities, a quasi total attenuation of US pulses was observed during the LF compression phases. Whereas dilution only influences the TOFM amplitude, ultrasound frequency affects significantly the UCA complex response.

Discussion and Conclusions

The results shown in this study demonstrate the originality of this experimental approach in characterizing viscoelastic properties of UCA. Such a strategy might be also suited to describe targeted microbubbles properties and thus might offer a new way for UCA characterization. A deeper analysis is necessary to understand the UCA response when using HF pulses close to UCA frequency resonance.



2E-2

11:45 AM Theoretical and experimental validation of enhanced subharmonic behavior of phospholipid-coated ultrasound contrast agent microbubbles

Jeroen Sijl¹, Benjamin Dollet², Marlies Overvelde¹, Timo Rozendal¹, Nico de Jong^{1,3}, Detlef Lohse¹, Michel Versluis¹;
¹Physics of Fluids Group, University of Twente, Enschede, Netherlands, ²Groupe de Matière Condensée et Matériaux, Université Rennes 1, France, ³Biomedical Engineering, Erasmus MC, Rotterdam, Netherlands

Background, Motivation and Objective

Coated microbubbles, unlike tissue, are able to scatter ultrasound subharmonically and can therefore greatly enhance the contrast in medical ultrasound imaging. Theoretically, a threshold amplitude of the driving pressure can be calculated above which subharmonic oscillations of microbubbles are initiated. Interestingly, earlier experimental studies on phospholipid coated microbubbles demonstrated that the measured threshold driving pressure for these bubbles is much lower than predicted by the traditional elastic shell models.

Statement of Contribution/Methods

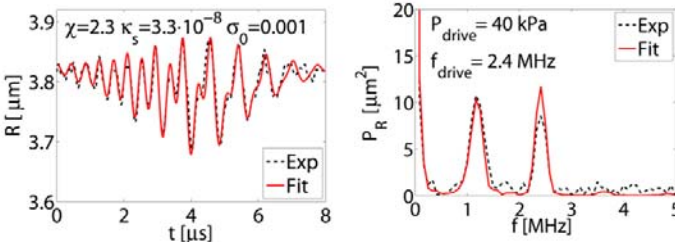
This paper presents an experimental study of the subharmonic behaviour of individual BR-14 (Bracco Research S.A., Geneva, Switzerland) coated microbubbles with resting radii between 1.6 and 4.8 micrometer. The subharmonic behaviour was studied as a function of both the amplitude and the frequency of the driving pressure. The radial response of the microbubbles was recorded with the Brandaris ultra-high-speed camera at a frame rate of 15 million frames per second.

Results

As expected from theory, the experimental study showed that the threshold pressure is minimal around a driving frequency equal to twice the resonance frequency of the bubble. Furthermore, certain bubbles showed a threshold pressure for subharmonic behavior as low as 10kPa.

Discussion and Conclusions

An explanation for the lower than expected threshold pressure for subharmonic behaviour of phospholipid coated microbubbles is provided by the model proposed by Marmottant et al.. We show that the change in the elasticity of the bubble shell as a function of the oscillation amplitude, as proposed in this model, is responsible for the enhancement of the non-linear subharmonic behaviour of phospholipid-coated Ultrasound Contrast Agent microbubbles.



2E-3

12:00 PM Quantification of the Microvascular Blood Flow of the Ovine Corpus Luteum with Contrast Ultrasound

Costas Strouthos¹, Marios Lampaskis¹, Vassilis Sboros², Joan Docherty³, Alan McNeilly³, Michalakis Averkiou¹;
¹Mechanical and Manufacturing Engineering, University of Cyprus, Cyprus, ²Medical Physics, Centre for Cardiovascular Sciences, University of Edinburgh, United Kingdom, ³Medical Research Council Human Reproductive Sciences Unit, University of Edinburgh, United Kingdom

Background, Motivation and Objective

Contrast ultrasound at low MI has been successfully used to detect blood flow at the microcirculation level in cardiology and oncology. Methods for quantification of microvascular flow are currently an active area of research aiming to assess myocardial perfusion and cancer therapy monitoring. The corpus luteum (CL) of the sheep ovary is a microvascular tissue that provides a natural angiogenic and antiangiogenic process that follows the oestrous

cycle of the ewe. Quantification of the microvascular flow of the CL from ultrasound images is possible with the aid of models based on indicator dilution theory. Our objectives are: 1) select an appropriate model, 2) extract hemodynamic parameters such as area under the curve (AUC), peak intensity (PI), mean transit time (MTT), wash-in time (WIT), and 3) measure intra- and inter-animal reproducibility and variability from 48 injections.

Statement of Contribution/Methods

Images of microvascular flow in the CL after intravenous bolus injection of SonoVue were collected with a Phillips iU22 ultrasound system with power modulation at low MI. The CL was surgically relocated close to the skin, without disturbing its normal function or vasculature, in order to allow the positioning of an ultrasound probe at an optimal and fixed position. The image data (48 loops) were from 10 different animals all at the peak (day 8-12) of the estrus cycle. Four indicator dilution models are considered: the lognormal function, the gamma variate function, the diffusion with drift models (LDRW and FPT) and the lagged normal functions. Analysis of the image loops was performed with QLAB and MATLAB, to select the most suitable model and measure the reproducibility of AUC, MTT, PI, and WIT.

Results

All animals between days 8 and 12 of the estrous cycle provided significant contrast in the 48 bolus injections performed. All contrast loops provided very low noise and high reproducibility. The diffusion with drift models and the lognormal model gave the best curve fits and the most accurate values of the hemodynamic related parameters. We chose the LDRW model whose physical basis takes into account the diffusive architecture of the CL microvascular bed. The variability of MTT, WIT, PI and AUC were 9.8%, 12.1%, 110% and 134%, respectively for the same animal, and 20.9%, 24.7%, 137% and 137%, respectively across animals.

Discussion and Conclusions

The CL of the ewe is proposed as the ideal model to allow development of methodology for angiogenesis monitoring with contrast ultrasound. The LDRW model is selected to model time intensity curves in the CL because it has the appropriate physical basis and produces high quality fits. Our intra- and inter-animal analysis showed that the MTT and WIT are reproducible with acceptable relative dispersions, hence can be used to study angiogenesis changes. Future work will address the large variabilities of PI and AUC and assess their potential for quantitative microvascular imaging.

2E-4

12:15 PM Assessing Breast Cancer Response to Bevacizumab using Contrast-Enhanced Ultrasound – Initial Results using a Murine Model

Kenneth Hoyt¹, Jason Warram¹, Heidi Umphrey¹, Lin Belt¹, Sharon Samuel¹, Karri Folks¹, Cecil Stockard¹, Mark Lockhart¹, Michelle Robbin¹, William Grizzle¹, Kurt Zinn^{1,2} *University of Alabama at Birmingham, USA*

Background, Motivation and Objective

It is currently a dilemma in cancer therapy to ascertain if and when an individual patient will respond to a therapeutic agent, becoming ever more complicated with the use of multiple drugs that have potential synergy. As molecular targeted therapies also become more prevalent, it has become increasingly desirable to monitor response in individual patients. The objective of this study was to assess changes in breast cancer vasculature in response to bevacizumab therapy using contrast-enhanced ultrasound (CEUS).

Statement of Contribution/Methods

Twenty nude athymic mice were implanted with 1e6 2LMP breast cancer cells in left and right inguinal regions of the mammary fat pad (10 controls and 10 in therapy group). All mice were imaged daily using a bioluminescence imaging system (IVIS system, Xenogen Inc.) to detect firefly luciferase expression and monitor tumor growth. Three wks post cell implantation, baseline CEUS images were acquired in all mice following a 0.03 mL i.v. bolus injection of ultrasound contrast agent (UCA) (Definity, Lantheus Medical Imaging). Subsequently, the therapy mice group received a 0.1 mg i.p. injection of bevacizumab (Genentech, South San Francisco, CA). Six days after baseline imaging, all mice were reimaged using CEUS. All scans were performed using an iU22 system (Philips Medical Systems) equipped with an L12-5 transducer. US scanning used an UCA destruction-replenishment protocol and DICOM data was processed using custom software developed using Matlab (Mathworks). For a given user selected tumor ROI, the following metrics: Area under the curve (AUC), peak intensity (I_{pk}), and time to peak intensity (T_{pk}), were derived from an average time-intensity curve. Subsequently, mice were sacrificed and tumors surgically excised. Tumor response to therapy was assessed histologically via CD31 staining and quantification of tumor microvessel density (MVD).

Results

For each mouse, the tumor exhibiting greatest intratumoral blood flow on day 6 was selected for reference to baseline data. Of the 20 mice, three controls were excluded from analysis due to inadequate CEUS baseline images. A comparison between control and therapy group US imaging-based tumor perfusion metrics revealed larger increases in AUC ($p < 0.01$), Ipk ($p < 0.01$), and Tpk ($p = 0.20$) for the therapy group whereas increases in tumor area were more pronounced in the control group ($p = 0.18$). MVD counts were significantly higher in the control versus therapy group ($p < 0.01$).

Discussion and Conclusions

This study demonstrates that CEUS imaging is a promising modality for assessing changes in breast cancer vasculature in response to bevacizumab therapy.

2E-5

12:30 PM Compression-only behavior and subharmonic scattering of phospholipid-shell microbubbles

Peter Frinking¹, Emmanuel Gaud¹, Marcel Arditi^{1,†}*Bracco Research S.A., Geneva, Switzerland*

Background, Motivation and Objective

Subharmonic scattering of phospholipid-shell microbubbles excited at very low acoustic pressure amplitudes (<30 kPa) has been associated with echo responses from compression-only bubbles. As described by the model proposed by Marmottant et al. [JASA 2005], compression-only bubbles are near a tension-free buckling state at rest and have initial surface tension values close to zero. In this work, the relation between subharmonics and compression-only behavior of phospholipid-shell microbubbles was investigated as a function of the initial surface tension of the bubbles.

Statement of Contribution/Methods

The initial surface tension was controlled by changing the hydrostatic pressure through the application of an ambient overpressure. Echo responses from a dilution of an experimental phospholipid-shell contrast agent were measured as a function of ambient overpressure with values ranging from 0 to 140 mmHg. The microbubbles were excited using a 64-cycle Hanning-apodized transmit burst with a center frequency of 4 MHz and peak negative pressure amplitude of 50 kPa. Echo-power spectra were calculated, and the subharmonic response was determined for each overpressure value. Simulations using the Marmottant model were also performed. To account for the effect of ambient overpressure, changes in bubble size and corresponding changes in initial surface tension were considered. The correlation between subharmonics present in the scattered signals and compression-only behavior was investigated by analyzing the simulated pressure-time and radius-time curves.

Results

An increase in subharmonic response was measured as a function of ambient overpressure; the subharmonic amplitude increased by 20 dB after applying 140 mmHg overpressure (for which the initial surface tension was zero). The increase in subharmonic response as a function of ambient overpressure, i.e. as a function of the initial surface tension, was predicted by the model, and simulation results were in good agreement with measurement results. Moreover, the simulations confirmed the correlation between subharmonics observed in the pressure-time curves and compression-only behavior observed in the radius-time curves for bubbles with initial surface tension values close to zero.

Discussion and Conclusions

Subharmonics present in the echo responses of phospholipid-shell microbubbles excited at very low acoustic pressure amplitudes are indeed related to the echo responses from compression-only bubbles. By applying an ambient overpressure, subharmonics appear in the scattered echo signals and bubbles become compression-only once the initial surface tension value approaches zero. In this study, an increase in subharmonic amplitude, instead of a decrease as reported by others [Shi et al., UMB 1999], was measured as a function of ambient overpressure. This observation may be exploited in a new method for noninvasive pressure measurement.

2E-6

12:45 PM Experimental verification of an image calibration method in ultrasound contrast agent imaging using a perfusion flow phantom

Daniel Finfer¹, Robert Eckersley², Mengxing Tang¹; ¹Department of Bioengineering, Imperial College, London, United Kingdom, ²Faculty of Medicine, Imperial College, London, United Kingdom

Background, Motivation and Objective

Tissue perfusion is a critical factor in diagnosing a wide variety of clinical conditions. However, physical inhomogeneities and the spatially variant transfer function of ultrasound scanners prevent accurate quantification of blood flow with ultrasound contrast agents (UCAs). Tang et al. [1] hypothesised that pulse inversion data could be used to calibrate UCA images via the “pulse inversion ratio” (PIR); the ratio of the sum quantity to the difference quantity. This paper will show that PIR can suppress shadowing artefacts and make time-varying intensity curves more consistent for different perfusion regions.

Statement of Contribution/Methods

A homogenous dialysis filter was used to simulate perfusion in tissue having a uniform flow velocity profile. Degassed water was pumped through the dialyser. A cross-section of the filter was monitored at 2.5 MHz using an Ultrasonix scanner. Sonovue bubbles were introduced into the system with bolus injections. Ultrasound data collected during flow were processed using PI, PIR, and the method of Hughes and Duck [2]. The time-varying intensity of images constructed using each of the algorithms was measured in 3 regions of interest (ROI).

Results

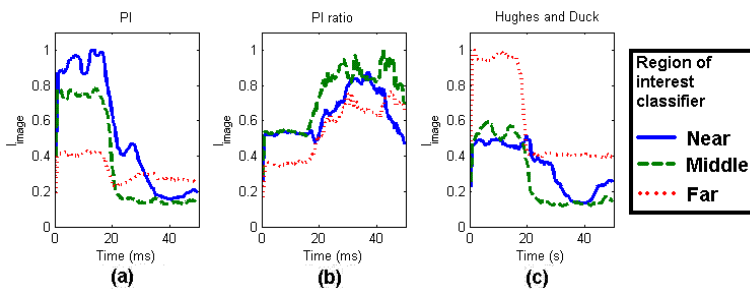
Results of the experiment are shown in the figure. Bubbles were injected into the system at 18 s, significant shadowing can be seen in both (a) and (c). It can be seen that PIR offers two significant advantages over the competing algorithms. First, the image intensity varies in proportion to bubble density independent of the location of the region of interest. Second, the image intensity inside each ROI is matched more closely in PIR than in the competing algorithms.

Discussion and Conclusions

It was shown that PIR returned an image intensity which was both more spatially consistent and more highly correlated with UCA concentration than that calculated using either basic PI or the method of Hughes and Duck. Thus PIR seems to offer a theoretically well-grounded, easy-to-implement solution to image calibration.

[1] M. X. Tang, J. M. Mari, P. N. T. Wells and R. J. Eckersley, *Ultrasound in Med. & Biol.*, vol. 34, no. 12, pp. 1998-2008, 2008.

[2] D. I. Hughes and F. A. Duck, *Ultrasound in Med. & Biol.*, vol. 23, no. 23, pp. 651-664, 1997.



3E. Elastography Methods

Sala 4

Tuesday, September 22, 2009, 11:30 am - 1:00 pm

Chair: **Mickael Tanter**
INSERM, Paris

3E-1

11:30 AM Electromechanical Wave Imaging: Non-invasive Localization and Quantification of Partial Ischemic Regions In Vivo

Jean Provost¹, Wei-Ning Lee¹, Kana Fujikura², Elisa E. Konofagou^{1,2,1} Biomedical Engineering, Columbia University, New York, NY, USA, ²Radiology, Columbia University, New York, NY, USA

Background, Motivation and Objective

Electromechanical Wave Imaging (EWI) has been shown capable of mapping the electromechanical activation sequence of the heart transmurally, in mice, dogs, and humans non-invasively in vivo. By processing radio-frequency (RF) frames acquired at very high rates, the onset of small, localized, transient deformations resulting from the early electrical activation of the heart, i.e., the electromechanical wave (EMW), can be mapped. Our group has previously shown that the EMW cannot propagate through acutely ischemic regions [1]. In this work, we demonstrate the capability of EWI to detect and quantify the extent of ischemic regions of increasing sizes.

Statement of Contribution/Methods

A non-survival canine ischemic model (n=7) was performed by steadily increasing the amount of mid-distal occlusion of the blood flow in the left-anterior descending (LAD) coronary artery, from 0% to 100% with 20% increments. After reperfusion of the LAD, pathology was performed to delineate the extent of the acutely ischemic zone.

EWI was performed at every occlusion level using an Ultrasonix RP system with a 3.3 MHz phased array, operating at up to 520 fps using a customized acquisition sequence previously developed by our group [2]. The 'motion-matching' technique was used instead of ECG-gating to reconstruct the full parasternal two- and four-chamber views at each occlusion level, which were then combined into a three-dimensional 'bi-plane' view. Incremental strains were obtained using RF cross-correlation and gradient techniques [2].

Results

When the level of occlusion of the LAD reached 60%, it was possible to observe a region where the EMW could not propagate, in the anterior and anterior-lateral walls, near the apex. As the level of occlusion increased to 80% and 100%, the size of this region increased towards the base and the lateral wall, even reaching the posterior wall near the apex, and decreased after reperfusion. The size of this region was in good agreement with the acutely ischemic region size determined in pathology.

Discussion and Conclusions

The EMW could not propagate through the ischemic region, allowing EWI to clearly detect and localize its extent, which increased in size with the level of occlusion and decreased after reperfusion, as expected. Currently, early ischemia is detected in the clinic with a stress echocardiography test, which is limited by low image quality caused by fast heart rates and potential administration of contrast agents and dobutamine. Hence, since EWI is entirely non-invasive, it could become a valuable complementary or alternative diagnostic tool to the current state-of-the-art of detection of disease at the early stages.

[1] Provost et al., Seventh International Conference on the Ultrasonic Measurement and Imaging of Tissue Elasticity, Austin, TX, 2008.

[2] Wang et al., IEEE Trans. UFFC, Vol. 55, No. 10, pp.2221-2233, 2008.

3E-2

11:45 AM **Quantitative surface wave method for measuring local viscoelasticity of lungs**

Xiaoming Zhang¹, Bo Qiang¹, Matthew Urban¹, Randall Kinnick¹, Rolf Hubmayr², James Greenleaf¹; ¹Physiology and Biomedical Engineering, Mayo Clinic, Rochester, Minnesota, USA, ²Pulmonary and Critical Care, Mayo Clinic, Rochester, Minnesota, USA

Background, Motivation and Objective

Certain lung diseases, particularly idiopathic pulmonary fibrosis, are associated with altered lung mechanical properties. While adequate techniques exist to measure the lung functions, current methods are relatively cumbersome and only provide global measurements of lung stiffness. We have developed a novel surface wave method for noninvasively measuring the viscoelasticity of lungs [X. Zhang, et al., 2008 IEEE International Ultrasonics Symposium].

Statement of Contribution/Methods

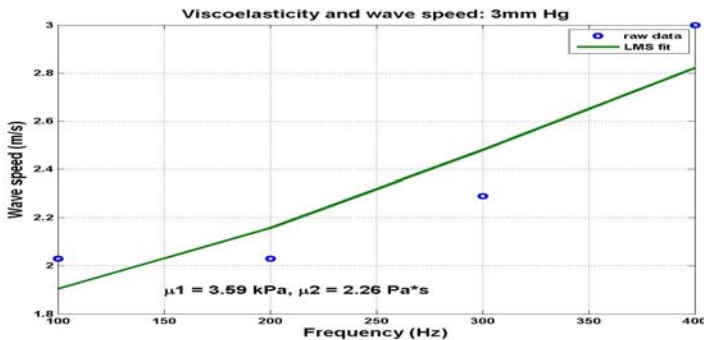
In this paper, three types of experiments were carried out on an ex vivo pig lung. The lung was pressurized through a connecting tube to its trachea. The first experiment measured the pressure-volume relation of the lung during the inspiration and expiration. The second experiment measured the surface wave speed of the lung at different pressures. The surface wave was generated by an electromechanical shaker, and the surface wave propagation on the lung surface was measured by a laser vibrometer. The third experiment was to measure the surface wave speed with an ultrasound linear array transducer.

Results

The bulk elastic modulus of the lung is analyzed by the pressure-volume curve. A four-parameter Venegas model is used to fit the pressure-volume curves. For inspiration, the bulk modulus is 321.69 Pa, 596.39 Pa and 1143.7 Pa for 3, 6 and 9 mm Hg Pressures, respectively. The local shear elasticity μ_1 and viscosity μ_2 are measured by the surface wave method. Fig. 1 shows the surface wave dispersion of the lung at 3 mm Hg pressure, from which μ_1 and μ_2 are estimated, respectively, $\mu_1=3.59$ kPa and $\mu_2=2.26$ Pa.s. The shear elasticity and viscosity are, respectively, $\mu_1=4.55$ kPa and $\mu_2=2.41$ Pa.s for 6 mm Hg pressure, and $\mu_1=5.10$ kPa and $\mu_2=2.98$ Pa.s for 9 mm Hg pressure. The ultrasound measurements of surface waves are in agreement with the laser measurements.

Discussion and Conclusions

Local shear elasticity and viscosity increase with increasing transpulmonary pressure, consistent with bulk modulus increases during pressure volume curves of the same lung. If surface waves can be produced using ultrasound radiation pressure on the surface of the lung in the intercostal spaces this method may be useful clinically.



3E-3

12:00 PM **Quantitative shear wave imaging of cancer cell cultures**

Marko Orescanin¹, Michael Insana^{2,1}; ¹Electrical and Computer Engineering, University of Illinois at Urbana-Champaign, Urbana, IL, USA, ²Bioengineering, University of Illinois at Urbana-Champaign, Urbana, IL, USA

 Tuesday
 Oral

Background, Motivation and Objective

Collagen scaffold volumes populated by epithelial and mesenchymal breast cells are now standard culture media for exploring cancer mechanobiology. Deformation exhibits fluidic and solid-matrix mechanical responses typical of breast stroma, and embedded cells respond to biochemical signaling to promote proliferation and matrix stiffening. They are ideal media for discovering biological sources of elasticity image contrast. Although assays for biomarkers can define the relevant cell biology, there is no reliable method for accurately measuring viscoelastic properties under sterile conditions. A Doppler-based shear-wave imaging technique for estimating the complex shear modulus ($\mu+i\omega\eta$) of 3D collagen hydrogels at shear-wave frequencies between 50 and 450 Hz is described.

Statement of Contribution/Methods

The technique developed for measuring mechanical properties of hydrogels involves a mechanical actuator that harmonically drives a stainless steel biopsy needle placed in the medium. Narrowband cylindrical shear waves are imaged (SonixRP, Ultrasonix Medical Corporation, 1D array) using pulsed Doppler techniques. Doppler pulses synchronized to the vibrating needle were acquired for 300 ms (PRF=10 kHz) in a plane near the needle. Velocity is estimated off line using poly-phase estimators to minimize errors.

Shear moduli were computed from velocity using two approaches. First, a phase gradient (PG) technique is applied to measure shear-wave speed. Spatially averaged speeds between 50 and 450 Hz were numerically fit to a mathematical model relating dispersion and complex modulus. The second approach is an algebraic inversion technique that directly estimates local shear moduli. The accuracy of both approaches was verified through comparisons with rheometry and radiation force techniques.

Results

The elastic shear modulus of a collagen hydrogel was measured, $\mu = 640 \pm 14$ Pa, using a commercial rheometer as a standard. An acoustic radiation-force step response method gave elastic ($\mu = 680 \pm 136$ Pa) and viscous ($\eta = 0.14 \pm 0.028$ Pa s) shear moduli. The phase gradient approach yielded frequency-independent moduli, $\mu = 571 \pm 67$ Pa and $\eta = 0.16 \pm 0.09$ Pa s, and the algebraic inversion approach produced the elastic modulus $\mu = 529 \pm 146$ Pa. In all cases, $N \geq 3$.

Discussion and Conclusions

Phase gradient (PG) estimates of shear moduli compare closely to those from rheometer and acoustic radiation-force step experiments. The algebraic inversion (AI) estimates are less accurate but more precise than PG. Thus AI is preferred for imaging nodules while PG is best for mechanobiology experiments. Preliminary results in 3D human fibroblast cultures show that stiffness doubles two days following growth factor stimulation. Immunofluorescence shows significant differentiation of fibroblasts to myofibroblasts, thus confirming a relationship with known tumor mechanisms.

3E-4

12:15 PM **Shear Modulus Imaging by Spatially Modulated Ultrasound Radiation Force**

Stephen McAleavey¹; ¹BME, University of Rochester, Rochester, NY, USA

Background, Motivation and Objective

Spatially Modulated Ultrasound Radiation Force (SMURF) imaging is a technique for quantitative shear modulus imaging. In order to track changes in tissue over time, and to assess diffuse stiffening, quantitative modulus data are required. SMURF uses impulsive acoustic radiation force to generate a shear wave of known spatial frequency in a medium of unknown shear modulus. The velocity of the induced shear wave, and hence the shear modulus of the medium, is determined from the period of the induced shear wave. Here we present the first experimentally obtained images of shear modulus using the SMURF method.

Statement of Contribution/Methods

All imaging was performed with a Siemens Antares scanner (Siemens Medical Solutions, USA, Ultrasound Group) and linear array transducer (Siemens VF7-3) at 4.2 MHz. In each SMURF ensemble, tissue motion was induced by two focused (F/4.5) 200 cycle pulses, with a shared focal depth of 1.5-4 cm, separated laterally by 2.5mm and temporally by 130 μ s. The resulting shear wave was tracked along a single A-line by normalized cross-correlation of RF echo data. The time T between peaks of the induced shear wave is estimated from the tracked tissue motion signal as the wave propagates past the observation point. The shear modulus is estimated as $G=p(\Delta x/T)^2$. Modulus data for the region between two scan lines is acquired in a single ensemble. Images are formed by sweeping the push and track beams across a region of interest. Targets scanned included 1 cm spherical inclusions in a commercial elastography phantom (CIRS Model 049), uniform samples of ZerdineTM, and tissue-mimicking

Tuesday
Oral

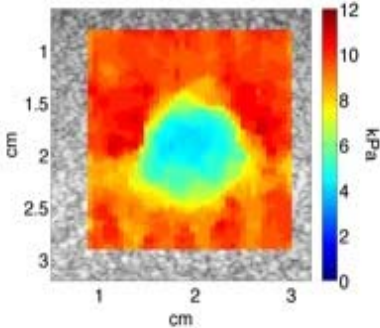
hydrogels containing a soft conical inclusion. Calibration was verified through unconfined compression testing of Zerdine and hydrogel samples.

Results

Images of spherical (shown below), conical, and step edge phantoms are presented. Agreement within 8% is found between SMURF and unconfined compression measurements of uniform phantoms. Image resolution on the order of the push beam spacing is observed.

Discussion and Conclusions

A key advantage of this method is that tracking is performed along a single a-line, avoiding correlated noise bias errors encountered in multiple-track location methods. We describe the source of this noise. Modulus estimates are obtained without extensive spatial averaging, allowing high resolution to be obtained.



3E-5

12:30 PM Measurements of swine renal cortex shear elasticity and viscosity with Shearwave Dispersion Ultrasound Vibrometry (SDUV)

Carolina Amador¹, Matthew W. Urban¹, Lizette V. Warner², James F. Greenleaf¹; ¹Ultrasound Research Laboratory, Department of Physiology and Biomedical Engineering, Mayo Clinic College of Medicine, Rochester, MN, USA, ²Reno-Vascular Research Laboratory, Mayo Clinic College of Medicine, Rochester, MN, USA

Background, Motivation and Objective

Evaluation of renal fibrosis by conventional imaging modalities is difficult. Changes in kidney elasticity measured by magnetic resonance elastography (MRE) have been shown to indicate renal scarring in animal models (*Magn Reson Med*, vol. 52:56-64). The purpose of this study is to evaluate the feasibility of SDUV for *in vitro* measurements of renal cortex elasticity and viscosity in swine kidney.

Statement of Contribution/Methods

Shearwave Dispersion Ultrasound Vibrometry (SDUV) applies a focused ultrasound beam to generate shear waves that propagate outward from the vibration center (*IEEE Trans. UFFC*, vol. 56:55-62). The shear wave propagation speed is estimated from its phase measured at multiple locations along its propagation path. Shear wave speed thus measured at several frequencies is used to inversely solve for tissue viscoelasticity through a Voigt dispersion model. A freshly excised swine kidney was used in this *in vitro* SDUV experiment. Shear waves were generated 5 mm deep into the kidney surface using a 3 MHz focused transducer with 44 mm diameter and 70 mm focal length. Shear waves were detected by a 5 MHz focused transducer with 12.7 mm diameter and 50 mm focal length. SDUV measurements were obtained at 5 different ROIs (Region of Interest), each measured about 5 mm by 5 mm. Shear wave propagation speeds at frequencies 50-500 Hz were measured and fit by the Voigt model to solve for shear elasticity and viscosity over each ROI.

Results

The shear elasticity and viscosity of the renal cortex estimated from 5 ROIs are 1.81 ± 0.40 kPa and 1.89 ± 0.29 Pa·s, respectively.

Discussion and Conclusions

There are limited studies regarding the *ex vivo* elastic properties of the kidney. An ongoing *in vivo* renal MRE [presented on ISMRM, 2009] study suggests that shear elasticity increases with perfusion pressure: the renal artery was occluded from 20% to 100% by 20% increments giving shear elasticity of 3.37, 3.23, 2.90, 2.85 and 2.93 kPa, respectively. The *in vitro* SDUV measurements are somewhat less than the *in vivo* MRE results, but still within a reasonable range. Indeed, we would expect that *in vitro* shear elasticity be less than that at total occlusion because the *in vitro* kidney is devoid of any residual perfusion. In summary, this study shows the feasibility of SDUV to estimate both shear elasticity and viscosity of renal cortex *in vitro* with good precision. Future work includes *in vivo* measurements of renal viscoelastic properties under different physiological conditions and further comparison with MRE.

Disclosure: Dr. Greenleaf and Mayo have a potential financial interest in SDUV. Patent applications have been filed for the technology, which has been licensed.

3E-6

12:45 PM Radiation dose imaging with ultrasound shear-wave elastography and radiation sensitive gels

Remo Crescenti¹, Jeffrey Bamber¹, Nigel Bush¹, Steve Webb^{1,†} Joint Physics Department, Institute of Cancer Research and Royal Marsden NHS Foundation Trust, Sutton, Surrey, United Kingdom

Background, Motivation and Objective

Radiation-sensitive polymer gels may be employed as 3D dosimeters in modern radiotherapy. Previously we have shown that Young's modulus is dependent on the radiation dose and have determined dose contrast in such gels using pseudo-static ultrasound elastography combined with inverse reconstruction. The success has been limited by the influence of friction at the boundaries, noise in the measurement and smoothing introduced by the inverse reconstruction.

Here we investigate the potential of shear-wave elastography for 3D gel dosimetry and compare it with pseudo-static elastography.

Statement of Contribution/Methods

A block (4 x 4 x 12 cm³) of radiation-sensitive polymer gel was irradiated to produce a relatively stiff rod-shaped volume (1 x 1 x 12 cm³). Ultrasound B-mode and Young's modulus images were acquired with the Aixplorer (Supersonic Imagine, Aix-en-Provence, France) with the gel in a water bath.

Results

Figure 1 shows the B-mode image with the Young's modulus map. The irradiated area is clearly visible as a hard and bright region (mean: 7.2 kPa) in a softer and dark background (mean: 2.4 kPa).

Discussion and Conclusions

The shape and size of the irradiated area was accurately preserved, which is an improvement when compared to pseudo-static elastography. Also, no influence of the boundaries was observed. Further advantages include the ease of rapidly obtaining 3D Young's modulus data. The background noise level was similar as in pseudo-static elastography. Higher accuracy may be gained by optimizing the shear-wave elastography sequence for gel dosimetry. For example, a smaller distance between radiation force pushes may help achieving better accuracy but would lead to longer measurement times. However, this is acceptable, because real-time elastography and avoidance of movement artefacts are important in clinical applications but are not an issue in gel dosimetry. A further optimization could be an increase in Young's modulus imaging depth by the use of a lower ultrasonic frequency for the applied radiation force.

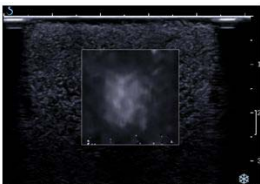


Figure 1: B-mode image (scan-depth in cm) with overlaid Young's modulus map.

Tuesday
Oral

4E. Array Imaging

Tarragona

Tuesday, September 22, 2009, 11:30 am - 1:00 pm

Chair: **Massimo Pappalardo**
University di Roma TRE

4E-1

11:30 AM Flexible Ultrasonic Transducers for Structural Health Monitoring of Pipes at High Temperatures

Jeanne-Louise Shih¹, Makiko Kobayashi², Cheng-Kuei Jen^{2,1} *McGill University, Canada, ²Industrial Materials Institute National Research Council Canada, Canada*

Background, Motivation and Objective

Structural health monitoring (SHM) and non destructive evaluation (NDE) of pipes in power, chemical and petroleum plants and other structures have become increasingly important in the improvement of safety and in the extension of these structures' lifespans. In these applications, ultrasonic transducers (UTs) may need to be conformed to structures that have surfaces with different curvatures and may need to be operated at elevated temperatures. Conventional piezoelectric UTs having rigid flat end surfaces may not be convenient for such type of inspections due to poor signal to noise ratio (SNR) in the pulse-echo mode. The main goal of this research is to develop a simple and an economical on-site sensor fabrication approach. One objective is to develop piezoelectric flexible ultrasonic transducers (FUTs) including those formed in array configurations that can be made in the lab. Another objective is to develop an on-site bonding technique such as brazing to bond FUTs onto pipes to achieve excellent bonding for permanent SHM and NDE purposes.

Statement of Contribution/Methods

The sol-gel fabricated thick piezoelectric films coated directly onto 75 μm thick steel or titanium membranes serving as FUTs have been developed with a rapid thermal treatment and a poling under ultraviolet light technique. Top electrodes, electrical wire, conductive bonding and connectors were also developed for operation at up to 500°C. Array configurations in 1D and 2D were made by varying the arrangements of the top electrode layouts. Special induction heating techniques were developed to braze such FUTs directly onto steel pipes, where the brazing material between the FUT and the external surface of the pipe served as a permanent high temperature couplant for SHM and NDE applications.

Results

At room temperature, the ultrasonic signal strengths of the developed FUTs made of PZT composite films were the same as those of the commercially broadband UTs centered at 5 – 10 MHz. Such FUTs centered at around 11 MHz and brazed onto steel pipes with a 26.6 mm outer diameter and a 2.5 mm pipe thickness showed ultrasonic echoes with a signal-to-noise ratio (SNR) of at least 26 dB at 150°C in pulse-echo mode. FUTs made of bismuth titanate composite films and centered around 12 MHz were also made and brazed onto steel pipes and their operation temperature reached up to 500°C. Individual ultrasonic performance of the 16-element 1D and 2D FUT arrays also showed to be similar.

Discussion and Conclusions

FUTs and arrays are small, lightweight and have a high level of sensitivity that is comparable to commercially available broadband UTs at room temperature. They can be conformed to pipes and this ensures high SNR during pulse-echo measurements. Since FUTs together with all necessary electrical connections can operate at up to 500°C and can be fabricated on-site, they are excellent candidates for the purposes of SHM and NDE of pipes.

Tuesday
Oral

4E-2

11:45 AM **Direction of Arrival Estimation of Multimodal Lamb Waves Using 2-D Arrays**

Tadeusz Stepinski¹, Marcus Engholm²; ¹*Signals and Systems, Uppsala University, Uppsala, Uppland, Sweden,*
²*Signals and Systems, Uppsala University, Sweden*

Background, Motivation and Objective

Monitoring of the structural integrity of thin planar structures that consist in detecting and localizing impact or damage at any point of the structure requires normally a relatively dense network of uniformly distributed ultrasonic sensors. A phased array with all-azimuth angle coverage would be extremely useful in the structural health monitoring (SHM) of such structures. One way of achieving 360° azimuth coverage is to use 2-D ultrasonic arrays, e.g. uniform circular arrays. Estimating direction of arriving (DOA) waves is one of the fundamental issues when using arrays in SHM applications. Although a number of DOA estimation techniques have been developed, none of them can efficiently cope with dispersive and multimodal Lamb waves (LWs).

Statement of Contribution/Methods

In the paper we propose two novel high-resolution spectral estimation techniques that are capable of handling broadband LWs sensed by 2-D arrays, the modified Capon method, and the modified multiple signal classification technique (MUSIC). Both techniques require no prior information about the characteristics of the material and can be applied to arbitrary array geometries.

Results

Performance of the proposed techniques is compared, first, using simulated multiple-mode LWs, and then verified using experimental data. The experimental data was obtained by means of a prototype circular array used for sensing dispersive waves propagating in thin plates. The prototype array consisted of 16 separate pinducers (diam. 1.5mm) with a relatively flat frequency response below 1 MHz, assembled in a plastic ring. The array design facilitated firm contact of the pinducers with monitored structure and acoustic coupling was obtained using a suitable coupling agent. The array was provided with an analog multiplexer that enabled recording signals received by the individual elements using a digital oscilloscope. The array was used for the reception of ultrasonic pulses sent by a broadband piezoelectric transmitter and propagating in an aluminum plate.

Discussion and Conclusions

The results presented in the paper demonstrate both DOA estimation and source separation ability of the proposed techniques. The Capon technique has been shown to be a very flexible and powerful approach for Lamb wave characterization, especially since it can be used for any array geometry. MUSIC performs even better than Capon on simulated data but it is only capable of detecting the presence of a signal arriving from a certain direction with certain wavenumber. Unlike Capon, MUSIC cannot be used as a beamformer since it is not able to calculate an array weighting vector based on the data. Its other drawback is the need to determine the size of the noise subspace, that is, the number of signal sources. A common weakness of both high-resolution techniques is their difficulty in handling correlated signals. In the paper we outline directions of our future work aimed at improving their performance for correlated signals.

4E-3

12:00 PM **Echographic Imaging of plates**

Francisco Montero de Espinosa¹; ¹*Acoustics, CSIC, Madrid, Madrid, Spain*

Background, Motivation and Objective

Lamb waves are commonly used in the field of Non Destructive Testing (NDT). Their capacity to propagate along plates over large distances with little attenuation makes them attractive. However, because they are dispersive, multiple modes can be excited for a given frequency making defect identification difficult.

Statement of Contribution/Methods

The echographic techniques based on ultrasonic array transducers can be used to detect and size defects on metallic and CRF plate structures if care is taken to excite only one mode. The use of linear array transducers bonded on the plates make very effective the excitation and detection of Lamb waves but the strong physical coupling with the plate also originate a large death zone on the images decreasing the capability of detecting flaws near the transducer placement.

Results

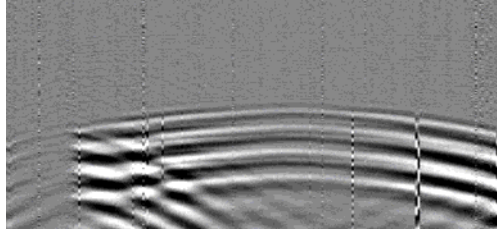
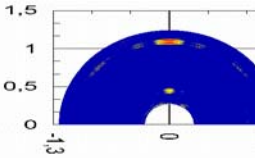
Optical interferometry is used to both the observation of the propagation of lamb waves in the specimens - figure 1- and to obtain the dispersion curves.

Tuesday
Oral

Array transducers with different apertures and configuration – linear, concave, segmented- based on piezoceramics and piezocomposites bonded to the plates are used to perform echography. The transducer designs look for the selection of a certain mode. Images of metallic and CRF plates using synthetic aperture and new multichannel electronics system specially designed for low frequencies are presented- figure 2-

Discussion and Conclusions

When Lamb mode selection is performed via a special array design and a previous study of the propagation of the waves in the finite structure is made, a correct interpretation of the images and defect sizing can be made.



4E-4

12:30 PM Monitoring of fatigue damage using subharmonic phased array for crack evaluation (SPACE)

Yoshihiko Ohara¹, Hiroaki Endo¹, Makoto Hashimoto¹, Yohei Shintaku¹, Kazushi Yamanaka^{1,1} *Department of Materials Processing, Tohoku University, Sendai, Miyagi, Japan*

Background, Motivation and Objective

Nonlinear ultrasound has been expected as a most promising approach to detect closed cracks. However, no method had monitored growth of closed fatigue cracks in three dimensions. We have developed a novel imaging method, subharmonic phased array for crack evaluation (SPACE)^{1,2)} (Fig. 1(a)). It has a better selectivity for open and closed parts of cracks than previous nonlinear methods, which has been demonstrated in closed fatigue^{1,2)} and stress corrosion cracks³⁾. Here we monitor growth of a closed fatigue crack for the first time.

Statement of Contribution/Methods

The fatigue crack was formed in a compact tension (CT) specimen (A7075) with a maximum stress intensity factor of $9.0 \text{ MPa}\cdot\text{m}^{1/2}$ and a minimum stress intensity factor of $0.6 \text{ MPa}\cdot\text{m}^{1/2}$. To examine the distribution of the crack depths and closure behavior in the length direction, the measurement was done at 5 positions. Then we examined the dependence of the fundamental and subharmonic images on a static tensile load which reduces the effect of the closure stress.

Results

We found that the crack depths in the subharmonic images were larger than those in the fundamental images at each position, as shown in Fig. 1(b). Specifically, the difference was larger at near the side surface than at the center. This suggests that the crack tip was closed with higher closure stress. The percentage of the closed part was 63 % at near the surface after 48000 fatigue cycles, whereas it decreased to 20 % after 87000 cycles.

Under the tensile load, the fundamental images changed in the stress intensity factor range of 0 to $1 \text{ MPa}\cdot\text{m}^{1/2}$, whereas the subharmonic images changed in the wider range of 0 to $2 \text{ MPa}\cdot\text{m}^{1/2}$. This suggests that the behavior at the closed parts, referred to as the area of contact acoustic nonlinearity (CAN), was more diverse than at the linear scatterers.

Discussion and Conclusions

We monitored crack depth and closure behavior by subharmonic phased array for crack evaluation (SPACE). We demonstrated that the comparison of the fundamental and subharmonic images provides detailed information about the open and closed parts in overall cracks.

Refs. 1)Y. Ohara, et al., Appl. Phys. Lett. 90 (2007) 011902, 2)Y. Ohara, et al., Jpn. J. Appl. Phys. 47 (2008) 3908.

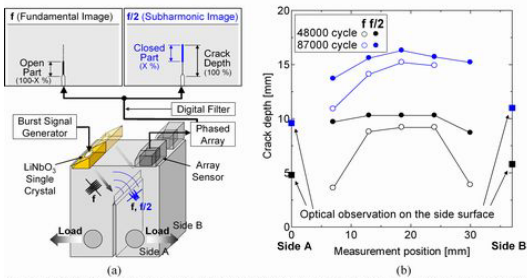


Fig. 1. Experimental setup and results: (a) SPACE. (b) distribution of crack depth measured by SPACE.

4E-5

12:45 PM High-Resolution Acoustic Imaging Using Multi-Carrier Waveforms Synthesized by Genetic Algorithm

Toshio Ito¹, Masanori Sugimoto¹, Hiromichi Hashizume^{2,1}, *Department of Electrical Engineering and Information Systems, University of Tokyo, Bunkyo-ku, Tokyo, Japan, ²National Institute of Informatics, Japan*

Background, Motivation and Objective

This paper presents a new method of acoustic imaging, which is based on techniques called synthetic transmit aperture (STA) and pulse compression (PC). The originality of our method is to transmit multi-carrier acoustic signals which are optimized by our genetic algorithm to improve resolution and dynamic range. The key to implement STA and PC is low cross-correlations and a sharp auto-correlation peak of transmitted waveforms. In conventional methods, signals modulated with M-sequences are often used because of their relatively low correlation coefficients. However their correlation coefficients are still far from ideal, having spurious peaks that introduce noise in resulting images. Therefore we tried to find more suitable waveforms for STA and PC than M-sequence signals.

Statement of Contribution/Methods

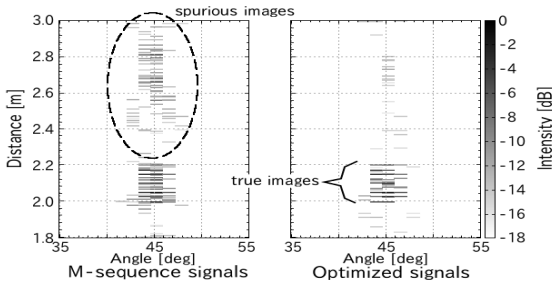
In our method, we express the signal as a summation of sub-carriers of different frequencies. By tuning amplitudes and phases of the sub-carriers, we can obtain any waveform which has predefined time duration and frequency bandwidth. The amplitudes and phases are then optimized by the genetic algorithm to synthesize signals which have improved correlation coefficients and resolution.

Results

We compared the optimized multi-carrier signals with M-sequence signals. The time duration and the bandwidth of both signal types were about 4.7 ms and 26.7 kHz, respectively, resulting in 125 sub-carriers in the multi-carrier signal. Spurious peaks in the correlation coefficients of the optimized signals were flatter and lower. The improvement in SNR was 7.5 dB. Using computer simulation, both signals were then used for imaging by STA and PC. As shown in the figure, the image obtained by the optimized signals (right) had almost no spurious images, and the dynamic range was improved by 4.9 dB. The optimized signals also improved resolution due to the effective use of the available bandwidth.

Discussion and Conclusions

Although physical experiments will be conducted in the future, the simulation result clearly showed that our proposed signals can improve dynamic range and resolution. This is because our method can generate better approximations of ideal white noise, which are often called pseudo-noises. Pseudo-noise is important in many fields of engineering, such as communication engineering, thus the possibility to apply our method and signals to other fields should also be investigated.



Tuesday
Oral

5E. BAW II

Pergamo

Tuesday, September 22, 2009, 11:30 am - 1:00 pm

Chair: **Gernot Fattinger**
Triquint Semiconductor

5E-1

11:30 AM Improved Coupled Resonator Filter Performance using Carbon-Doped Oxide Decoupling Layer

Stephen Gilbert¹, Phil Nikkel¹, Rich Ruby¹, Tiberiu Jamneala¹, John Larson III^{1,2} *Wireless Semiconductor Division, Avago Technologies, San Jose, CA, USA*

Background, Motivation and Objective

The coupled resonator filter (CRF) has been proposed as a means to reduce the size and extend the capability of film bulk acoustic resonator (FBAR) ladder filters. CRF provides filtering, single-ended to differential port conversion, and impedance transformation within an ultra-miniature die. This is achieved by stacking two resonators on top of one another, separated by a low impedance, quarter wave acoustic decoupling medium. In conventional CRF, this is a multilayer Bragg reflector, whereas we have demonstrated a simplified approach that uses a single layer of the dielectric SiLK [1] - [3]. Here we describe a newly developed decoupling material that has enabled significant improvements in filter performance over our previous reports.

Statement of Contribution/Methods

Carbon-doped silicon oxide (SiOCH) replaces SiLK, significantly improving the performance of the resulting CRF filters. The SiOCH films are integrated into the standard CRF device stack using an appropriate process flow. In contrast to the spin-on and curing process used for SiLK, the SiOCH films are deposited by plasma enhanced chemical vapor deposition (PECVD). Because little is known of the acoustic properties of SiOCH in the frequency range of interest, extensive characterization and optimization was required to develop a decoupling layer with the necessary characteristics. Material parameters were determined by physical analysis of the SiOCH and through fits of filter S-parameters using a 1-D Mason model [3].

Results

The CRF filters reported here possess several key advantages over earlier SiLK-based devices. For SiOCH films with impedance of 4.8 MRayls, acoustic attenuation is 600 dB/cm at 1GHz. This is much lower than the SiLK attenuation of 2100 dB/cm [3], and reduces filter insertion loss by more than 0.5 dB.

The conformal step-coverage provided by the PECVD process eliminates passband anomalies that were often observed with SiLK. These anomalies degraded insertion loss and bandwidth, and were caused by thickness non-uniformity in the SiLK near the perimeter of the resonator. This is difficult to avoid using a spin-on process.

Use of SiOCH also dramatically reduces the temperature coefficient of frequency (TCF). On the high frequency side of the passband, TCF decreases from -84 ppm/°C for a SiLK-based device [2] to -30 ppm/°C for SiOCH. On the low frequency side of the passband, TCF increases from -15 ppm/°C for SiLK to -23 ppm/°C for SiOCH. Overall TCF is improved, making bandwidth specifications easier to achieve.

Discussion and Conclusions

CRF filters with SiOCH as the decoupling layer show improved insertion loss, bandwidth, and TCF compared to SiLK-based filters reported earlier.

[1] J.D. Larson III, US Patent 6946928, Sept. 20, 2005. J.D. Larson III, S. Ellis, US Patent 7242270, July 2007.

[2] M. Small et al, Proc. IEEE Ultrason. Symp., pp. 604-607, Oct. 2007.

[3] T. Jamneala et al, IEEE Trans. Ultrason. Ferroelect. Freq. Control, v. 55, pp. 2320-2326, Oct. 2008.

5E-2

11:45 AM GPS and WiFi Single Ended to Differential CRF Filters using SiOCH as a De-Coupling Layer

Rich Ruby¹, Steve Gilbert¹, Allen Chien¹, Tiberiu Janneala¹; ¹Avago Technologies, USA

Background, Motivation and Objective

Coupled resonator filter (CRF) filters are a natural entry into single ended to differential (SE2DE, or un-balanced to balanced) filter applications for Bulk Acoustic Resonator Technologies. Unlike the “classic” FBAR [1], a CRF can be used in a traditional “transformer” configuration, allowing for excellent common mode rejection, balanced differential output, and impedance transformation. Furthermore, since the two FBARs are processed with one on top of the other (separated by the SiOCH de-coupling layer), the total area of these filters is significantly smaller than standard FBAR filters. CRF filters only have zeros at dc and infinity, thus the impulse response of these filters is very low, making them an excellent choice for OFDM applications. However, without the zeros near poles (as in “classic” FBAR filters), the roll-off is poor. This issue can be overcome by placing two CRF devices in series.

Statement of Contribution/Methods

In this work, we present a GPS filter that uses a DSBAR [2] in series with a FACT [3, 4] CRF transformer to obtain a high rejection filter with balanced output. The goal is a filter with large rejection below 1453 MHz and above 1710 MHz. We extracted the acoustic attenuation for a given acoustic impedance of the SiOCH for a range of devices having different SiOCH acoustic impedances. We then used fits of these parameters inside Agilent’s ADS optimizer to find the balance between losses and maximum impedance mismatch. Another filter goal was to have minimum insertion loss at 1575MHz (US GPS system) and 1601 MHz (Russian GPS – GLONASS), as well as VSWR less than 2 for the GPS and GLONASS frequencies. We will also present simulations and measurements of Wi-Fi SE2DE filters. Both filters can be made in a small form factor –approximately, 0.28 mm² in area.

Results

Discussion and Conclusions

Careful fits of a variety of DSBARs were made using different SiOCH films and a parametric fit of SiOCH film attenuation to acoustic impedance was generated. Based on this and other fits to measured devices, we simulated and optimized a series of GPS filters and Wi-Fi filters. Simulated impulse response of these filters are on the order of 10 to 20 nsec. Simulated impulse response of “classic” FBAR filters struggles to get below 90 nsec. Results of measured parts will be presented.

- [1] R. Ruby, P. Merchant, “Micromachined Thin Film Bulk Acoustic Resonators”, Freq. Control Symp., pp.135-138, 1994
- [2] M. Small et al, Proc. IEEE Ultrason. Symp., pp. 604-607, October 2007.
- [3] J.D. Larson III and R.C. Ruby, “Thin film acoustically-coupled transformer,” US Patent 6946928, September 20, 2005. J.D. Larson III, “Stacked bulk acoustic resonator band-pass filter with controllable pass bandwidth,” US Patent 7019605, March 28, 2006.
- [4] S.R. Gilbert et al, Micro. Symp. Digest, 2008 IEEE MTT-S, pp. 839-842, June 2008.

5E-3

12:00 PM Investigation for Nonlinear Distortion of Acoustic Devices for Radio-Frequency Application and Suppression of Nonlinearity.

Masanori Ueda¹, Masafumi Iwaki¹, Tokihiro Nishihara¹, Yoshio Satoh¹, Ken-ya Hashimoto²; ¹Satoh Fellow Group, FUJITSU LABORATORIES LTD., Japan, ²Graduate School of Engineering, Chiba University, Japan

Background, Motivation and Objective

Requirements given to RF acoustic devices are becoming stringent year by year. In addition to very low insertion loss and a steep cut-off characteristic, reduction of the inter-modulation distortion (IMD) is vital for the use in the wideband code division multiple access (WCDMA) or third generation systems. Therefore, simulation and reduction of acoustic device nonlinearities become very important.

We proposed a circuit model for the analysis of RF BAW resonators' non-linear behavior [1].

Statement of Contribution/Methods

This paper is composed of three parts. First, it clarifies nonlinearities on SAW and BAW resonators and indicates the importance to suppress the even-order nonlinearity of BAW resonators. Second, we demonstrate the further effectiveness of our proposed method using several types BAW duplexers and present how to reduce nonlinearities. Third, BAW duplexers with low IMD products are introduced.

Results

First, we measured experimentally 2nd and 3rd order harmonics in both a BAW and a SAW one-port resonator for an input power of 26 dBm. The 3rd order distortion of BAW was about 15 dB better than that of SAW while, the 2nd order distortion of FBAR was about 30 dB worse than that of SAW. We also investigated so-called triple-beat-products on SAW and BAW resonators, as a result, BAW resonators indicate better performance than SAW resonators.

Next, aiming at demonstrating the effectiveness of our IMD simulation technique [1] and suppressing even-order IMD products, we manufactured BAW band 1 duplexers having unique circuit and filter topologies for the 2 GHz WCDMA system. The simulation was in good accordance with the experimental results for both the IMD2 and IMD3 characteristics. It was confirmed in both simulations and experiments that IMD products could be enough suppressed. We could obtain the duplexer with an IMD power level lower than -110 dBm.

Discussion and Conclusions

We discussed the nonlinear performance difference between SAW and BAW resonators, and accuracy and efficiency of the proposed simulation technique on BAW devices could be validated by comparison to experimental data. This qualifies it as a high performance tool for the prediction of BAW device nonlinearities. Finally, we could realize the excellent BAW duplexer with low IMD products.

[1] M. Ueda, M. Iwaki, T. Nishihara, Y. Satoh and K. Hashimoto, "A Circuit Model for Nonlinear Simulation of Radio-Frequency Filters Employing Bulk Acoustic Wave Resonators", IEEE Trans. on Ultrasonics, Ferroelectrics, and Frequency control, vol.55, 2008, pp. 849-856.

5E-4

12:15 PM Unified model for nonlinear effects in BAW resonators

Eduard Rocas¹, Carlos Collado¹, Enrique Iborra², Robert Aigner³, ¹Signal Theory and Communications, Universitat Politècnica de Catalunya, Barcelona, Spain, ²Grupo de Microsistemas y Materiales Electrónicos, Universidad Politécnica de Madrid, Madrid, Spain, ³R&D Acoustic Technologies, Triquint Semiconductor, Apopka, Florida, USA

Background, Motivation and Objective

A complete physical model for intermodulation distortion and harmonics prediction is presented for thin film BAW resonators. The model consists on an extension of the Nonlinear Distributed KLM one that includes the significant role of thermal effects on material properties, which lead to IMD and harmonics generation

Statement of Contribution/Methods

Integrated physical circuit model.

The nonlinear effects are modeled with a stress and temperature dependent elasticity.

The material layers, thermally represented as a cascade of series thermal resistances and shunt heat capacitances, are coupled to the acoustic domain by dissipation and self-heating effects (Fig.1). The materials stack configuration and the packaging set the thermal dynamic response. The unified model allows to know the temperature distribution along the device, which depends on the slow time-varying instantaneous dissipated power.

Third order IMD (3IMD) results from the contribution of both the stress dependent elasticity and the thermal effects.

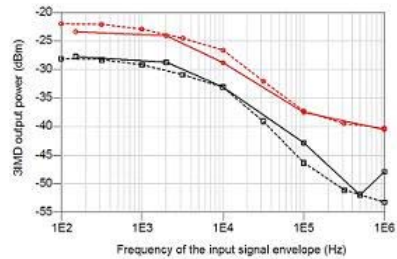
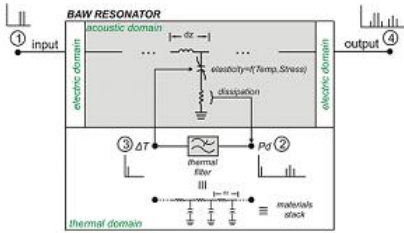
Results

Simulation results show good agreement with measurements of second harmonics and 3IMD performed on BAW resonators of different areas. Figure 2 shows the simulated results (dotted lines) and measured (continuous lines) 3IMD output power at 2f1-f2 for two resonators (circles and squares). The 3IMD power depends on the input signal envelope because the existence of thermal effects.

Tuesday
Oral

Discussion and Conclusions

The importance of having a unified model that accounts for the electric, mechanic and thermal domains is key to predict the nonlinear behavior of BAW resonators. The accurate modeling of the IMD generation mechanism is a significant step towards more linear designs of BAW filters for high power applications.



5E-5

12:30 PM Considerations on Measurement Setup for Second-Order Nonlinearity in Radio Frequency Bulk Acoustic Wave Duplexers

Yiliu Wang¹, Florian Thalmayr¹, Nan Wu¹, Ken-ya Hashimoto¹; ¹Graduate School of Engineering, Chiba University, Japan

Background, Motivation and Objective

Non-linearity is a vital matter for the use of radio frequency (RF) surface and bulk acoustic wave (SAW/BAW) duplexers in communication systems. It can generate unwanted signals in the receiver (Rx) band through the mixing of jammer signals with a relatively strong transmitter (Tx) signal.

Although the non-linearity measurement is a daily task for active devices, its methodology is not directly applicable to the RF SAW/BAW duplexers. Namely, since non-linearity in the duplexers is weak, non-linear signals generated in the peripheral circuit must be completely suppressed. In addition, since the duplexer characteristics are sensitive to the port impedances, all the ports must be terminated by 50 Ω not only for the Rx and Tx frequencies but also those of jammers and non-linear signals. This is particularly important for the second-order intermodulation distortion (IMD2) because jammer frequencies can be far from the operation bands.

Statement of Contribution/Methods

This paper discusses influence of the setup on the measurement reliability and reproducibility for the IMD2 generated in the RF BAW duplexers.

Results

A US PCS FBAR duplexer (KT084) supplied by Avago technologies was used as a specimen. Fig. 1 shows a typical measurement setup.

It is shown that the IMD2 level can be measured reliably and reproducibly provided that the port termination is properly applied. For example, a filter and a relatively large (>20 dB) attenuator are necessary between the oscillator 2 (OSC2) and the Ant port to suppress the non-linear mixing in OSC2 and the impedance mismatching of the filter at the out-of-band. If order of these two devices is reversed, the IMD2 level changes significantly. Although an isolator is commonly used to stabilize the power amplifier (PA) output level, a proper attenuator must be added for the impedance matching in a wide frequency range.

We also report the key know-how necessary for the reliable measurement. For example, (a) prior to the measurement, the PA output should be applied to the setup for the warm up, and (b) two OSCs and the spectrum analyzer (SA) should be synchronized to reduce frequency fluctuation.

Discussion and Conclusions

The IMD2 measurement setup is discussed for the FBAR duplexers.

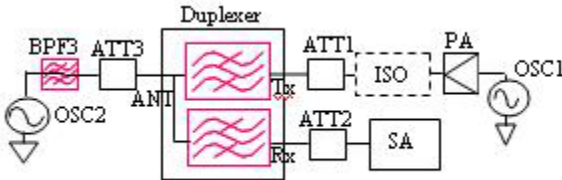


Fig. 1 Typical measurement setup

5E-6

12:45 PM **Stacked Crystal Resonator (SCR): A highly linear BAW Device**

Martin Handtmann¹, Kabula Mutamba², Bernhard Gebauer¹, Martin Franosch^{1,2} *Avago Technologies, Munich, Germany, ²Infinion Technologies AG, Regensburg, Germany*

Background, Motivation and Objective

Besides small size, exceptional insertion loss and outstanding isolation, BAW filters and duplexers are often the preferred choice in the transmit path of mobile frontend due to their excellent power handling capabilities. Thereby, they exhibit a non-linear behavior as been observed by Aigner et al., causing generation of higher harmonics and sensitivity of the resonance frequency towards a voltage bias. We will present a new BAW device, a stacked crystal resonator (SCR), which intrinsically cancels out the even order non-linearities and compare it to a normal BAW resonators and current solutions for improved linearity.

Statement of Contribution/Methods

A parallel circuit in anti-parallel configuration is a commonly used approach to reduce non-linearities in BAW filters. Figure 1 depicts a SCR, which is obtained by applying this approach to a stacked crystal filter (SCF). The thus formed electrical constraint reduces the resonance modes of the SCR to the ones of a normal resonator, and together with the acoustical coupling of the similar oriented piezoelectric layers a cancelation of the even order non-linearities is achieved. Additionally the SCR benefits from an active area reduction by a factor of 2.

Results

Measurements of first devices demonstrate the improved linear behavior. Figure 2 shows a 30dB improvement in worst case 2nd harmonic generation of a SCR over a normal solidly mounted BAW resonator. Further, the frequency sensitivity on a voltage bias was reduced by a factor of 20 and the coupling coefficient increased by 10%.

Discussion and Conclusions

The presented stacked crystal resonator is a intrinsically highly linear BAW resonator, which is well suited to be used as basic building block for filters in the transmit path of mobile frontends.

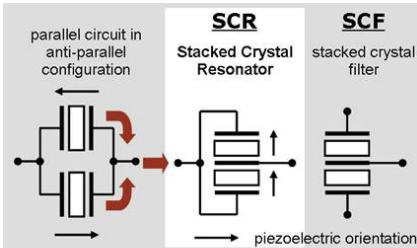


Figure 1: Application of the parallel circuit in anti-parallel configuration to a SCF results in a stacked crystal resonator.

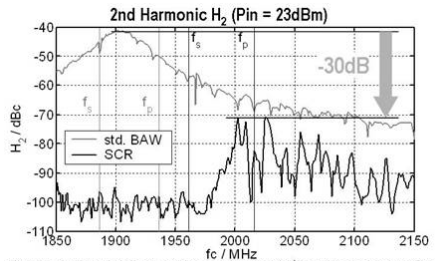


Figure 2: Comparison of the measured 2nd harmonic generation of a standard BAW versus a SCR.

Tuesday Oral

6E. Ultrasonic Linear Motors

Baalbek

Tuesday, September 22, 2009, 11:30 am - 1:00 pm

Chair: **Takefumi Kanda**
Okayama University, Japan

6E-1

11:30 AM Ultrasonic linear motor using traveling surface acoustic wave

Minoru Kurosawa^{1,2}: *Department of Information Processing, Tokyo Institute of Technology, Yokohama, Kanagawa, Japan*

Background, Motivation and Objective

Twenty five years ago, traveling wave type ultrasonic linear motors were studied but in vain. It was because a huge vibration system using beding vibration and low power density at low operation frequency around several tens kHz. For example, to obtain 1 m/s slider speed, 1.2 kW driving electric power was required. Ever since, study on traveling wave type linear motor has been stopped in the bulk transducer ultrasonic motor field.

Statement of Contribution/Methods

Since the early '90th, we have been developing a surface acoustic wave motor as shown in Fig. 1. The surface acoustic wave (SAW) motor is based on the MEMS technology; surface micro machining and thin films are used to fabricate devices. The fabrication process of the SAW motor is different from conventional ultrasonic motors. In addition, piezoelectric material of the SAW motor is different; the transducer material is not PZT but lithium niobate crystal material. An outstanding difference is a traveling wave motor in spite of linear motion.

Results

The SAW motor which operates at 9.6 MHz has superior performances such as 1 m/s slider speed or 10 N only with 35 W driving electric power. The SAW device was 60 mm by 14 mm by 1 mm, 128 degree y-rotated x-propagation lithium niobate. The transducer weight was only 4 g which produces 10 N output force. The maximum mechanical output power was about 2 W. Hence the mechanical output force and power per transducer weight are as high as conventional ultrasonic motors. From a physical modeling simulation, conversion efficiency from the mechanical vibration to mechanical thrust motion was investigated. The simulation result indicated that the conversion efficiency was around 50 %; the efficiency is as high as superior ultrasonic motors.

Discussion and Conclusions

A state-of-the-art SAW motor is explained detail and futur works will be discussed.

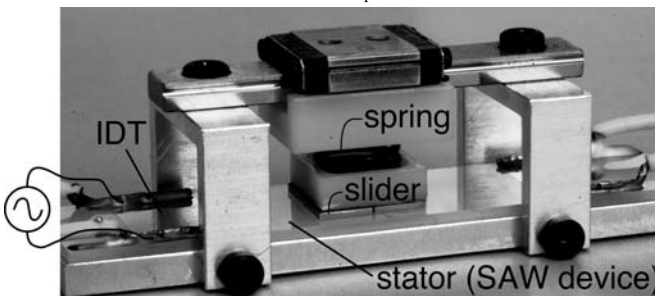


Fig. 1 An example of surface acoustic wave linear motor.

6E-2

12:00 PM Segment-Structured Diamond-Like Carbon Films Installed on Driving Surface of Surface Acoustic Wave Linear Motor

Mitsuru Nakamura¹, Yosuke Fujii², Hiroyuki Kotani², Masaya Takasaki², Takeshi Mizuno², Tsuyoshi Kuroda³, Naoto Ohtake³, ¹Mechanical engineering, Saitama university, Japan, ²Saitama university, Japan, ³Nagoya university, Japan

Background, Motivation and Objective

A surface acoustic wave (SAW) linear motor is a kind of ultrasonic motors, which has many merits such as high thrust force, thin structure, precise positioning and so on.

On the other hand, wear is one of problems in the motor due to friction drive principle. To solve this problem, segment-structured diamond-like carbon (S-DLC) films had been considered to be applied as a wear resistant material on the driving surface. Under trial driving by the LiNbO₃ transducer with S-DLC films, reduced driving performance was observed. The reason was seemed to be nonuniform shapes and heights of the S-DLC segments. Additionally, exfoliations of the S-DLC films were observed. The reason of this problem was that preparation method of the S-DLC films on LiNbO₃ substrate was not optimized. The purpose of this report is to solve these problems.

Statement of Contribution/Methods

The reason of nonuniform profile of the segment was seemed to be due to a meshed mask to prepare the S-DLC films. To solve this problem, preparation of S-DLC films without the mask is required. In this report, we propose a new S-DLC transducer. Figure 1 shows a schematic view of the new segment structure of the DLC film. At first, segment-structured chromium (S-Cr) films were prepared on substrate. Then DLC films was coated on whole area. We call this stator S-Cr/DLC stator.

Results

Using an optical measurement instrument of roughness, uniform heights and shapes of S-Cr/DLC films segment was confirmed. Figure 2 shows projections shape of the S-Cr/DLC. To compare S-Cr/DLC transducer and conventional S-DLC transducer, driving characteristics of the transducers were observed. S-Cr/DLC transducer performed better driving performance than that of S-DLC transducer.

Discussion and Conclusions

We confirmed improvement of driving performance using S-Cr/DLC transducer.

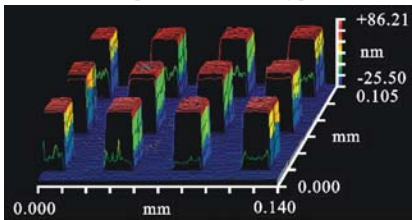


Fig. 2 3D measurement result of segments.

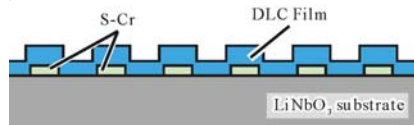


Fig. 1 Schematic view of the new S-DLC substrate.

6E-3

12:15 PM Butterfly-shaped piezoelectric linear ultrasonic motor using multilayer ceramics

Won Hee Lee^{1,2}, Byeong Kwon Ju², Chong Yun Kang¹, Yong Wook PARK³, Seok Jin YOON^{1,2} ¹Korea Institute Science and Technology, Korea, Republic of, ²Korea University, Korea, Republic of, ³Namseoul University, Korea, Republic of

Background, Motivation and Objective

Recently, imaging and consumer devices such as mobile phones, PDAs, and micro-positioners, which have a requirement to be very thin, as well as having very low energy consumption and manufacturing cost, call for linear motors with extremely low profile. In particular, various piezoelectric linear motors have been widely studied for many applications due to their advantages such as quick response, compact and possible linear motion, etc. In this study, a butterfly-shaped piezoelectric motor has been designed and fabricated using multilayer ceramics for being operated at low voltages.

Statement of Contribution/Methods

The butterfly-shaped piezoelectric motor is simply composed of an elastic plate, which includes a coupling tip for energy transfer and two protrusions to fix it, and two piezoelectric ceramics as shown in figure 1. To reduce driving voltage, thin multilayer ceramics fabricated by a tape casting method were adopted to the motor. The thickness of each ceramic layer and internal electrode were $\sim 35\mu\text{m}$ and $\sim 2\mu\text{m}$, respectively. The motor is driven by two sinusoidal electrical signals with 90 phase difference.^o

Results

Dynamic characteristics of the motors were measured. Both the velocity and the force linearly increase as the applied voltage increases. The driving force of 50 g and velocity of 13 mm/s were achieved when the preload between the coupling tip point and moving slider was 150 g and the applied voltage is 5 Vp-p.

Discussion and Conclusions

This paper presents dynamic properties of the piezoelectric linear motor for lower driving voltage and simple structure. The motor, with a very low profile of $\sim 1\text{mm}$ has been successfully driven having the following dynamic properties: a maximum velocity of 13 mm/s and a force of 50 g. These results confirm the suitability of the multilayer piezoelectric linear motor for applications to optical modules with compact size and high resolution.

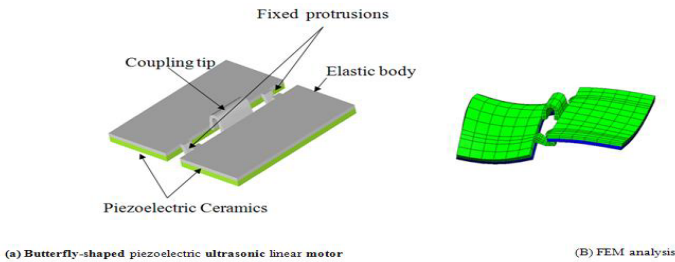


Figure. Configuration of the multilayer piezoelectric ultrasonic linear motor

6E-4

12:30 PM Linear ultrasonic motor using a quadrangular piezoelectric ceramics

Dong-Soo Paik¹, Sahn Nam², Piotr Vasiljev³, Chong-Yun Kang¹, Seok-Jin Yoon⁴, ¹Materials Science Eng., Korea University, Seoul, Korea, Republic of, ²Materials Science Eng., Korea University, Korea, Republic of, ³Ultrasound Lab., Vilnius Pedagogical University, Lithuania, ⁴Korea Institute of Science and Technology, Korea, Republic of

Background, Motivation and Objective

Piezoelectric linear ultrasonic motors are attractive for the application to camera modules of imaging devices such as personal/mobile computers, mobile telephones and PDAs. In particular, various types of ultrasonic motors with compact size have been suggested to have a wide range of optical device applications. The compact ultrasonic motor exhibits higher flexibility compared to that of the conventional electromagnetic motors whose efficiency significantly decreases with miniaturization. A tiny linear ultrasonic motor with a fixed piezo-ceramic as a motionless stator has been previously reported. In addition to the developed motor, another design with a mobile stator is suggested to enhance the simplicity of motor structure.

Statement of Contribution/Methods

The suggested inertia micromotor consisted of thin quadrangular piezoelectric ceramics and holder joined to a shaft as shown in Fig.1. The piezoelectric ceramics comprise of 6 layers of piezoelectric sheets 0.05mm in thickness and brass elastic body 0.2mm in thickness. The holder plays a role of connector between the stator and the shaft and the spring binds both of them tight to the shaft.

Results

As a result of frequency response analysis for the holder(stator) materials and dimensions, it was found that the stator material with low acoustic coefficient such as a carbon fiber exhibited excellent dynamic properties and the

length of stator should be no longer than 5mm. The piezoelectric linear ultrasonic inertia motor shows a speed of 20mm/s and a torque of 8g at a driving frequency of 140kHz and a driving voltage of 4.5Vrms.

Discussion and Conclusions

From the experimental results, the micromotor is a promising candidate for optical applications because of a simple structure and a low driving voltage.

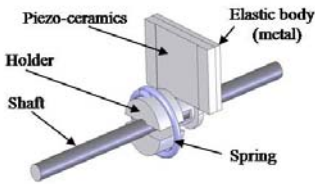


Fig. 1 Piezoelectric linear ultrasonic motor.

Tuesday
Oral

6E-5

12:45 PM **Design and Dynamic Properties of Omni-directional Piezoelectric Thin-typed Actuator**

Chong-Yun Kang¹, Woo-Suk Jung¹, Seok-Jin Yoon¹; ¹KIST, Korea, Republic of

Background, Motivation and Objective

Generally, Piezoelectric actuators have many advantages compared with conventional motor as follows; No magnetic disturbance, rapid response characteristic, no breaking mechanism, simple and light, and so on. Owing to these merits, these actuators have been widely applied and studied for various applications such as robots, optic device, camera, stage. But most of developed actuators had one DOF, to apply multi-DOF system is required more than two actuators. Also, according to the advance of machinery and handheld device industry, system is requiring the smaller and lighter to use in limited space. Therefore, this paper represents a piezoelectric thin-typed actuator capable of omni-directional movement for applying a tiny stage, robot eye and joint, which only made of a elastic body and ceramics.

Statement of Contribution/Methods

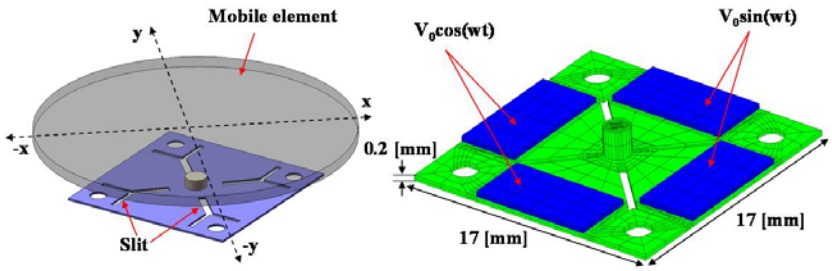
The actuator can be driven at frequencies being elliptical vibrations combined with the longitudinal and transverse vibrations. In other words, elliptical vibration on the tip enables to linear movement, when sine and cosine waves were applied to each ceramic. In order to maximize the elliptical vibration, the actuator was simulated by ATILA to confirm electro-mechanical coupling coefficients and displacements according to change slits on elastic body and size of ceramics. Finally, to verify movements of the alumina tip was verified by OFV-551 Laser vibrometer.

Results

Through results of simulation, when the actuator attached ceramic size of 8x4 [mm²] exists all slits on elastic body, it had the higher electro-mechanical coupling coefficients and displacements at resonance frequencies. Based on the simulation results, the actuator was manufactured and then confirmed elliptical vibrations for linear motion between the transverse and longitudinal vibrations. The actuator could be verified movement to desired directions by change of input signals applied each ceramics.

Discussion and Conclusions

This paper presents the piezoelectric thin-typed actuator capable of omni-directional movements, which has a volume of 17x17x1[mm³]. The actuator was successfully driven with the dynamic properties of maximum velocity about 150mm/s and thrust force about 100g. Therefore, the proposed actuator could be expected to apply the precise positioning stage, robot eye and joint as well as devices with the limited s



1F. Therapeutic Applications

Sala 1

Tuesday, September 22, 2009, 2:30 pm - 4:00 pm

Chair: **Charles Cain**
Univ. of Michigan

1F-1

2:30 PM **Kidney Stone Fragmentation Using Histotripsy**

Alexander Duryea¹, Adam Maxwell¹, William Roberts², Zhen Xu¹, Charles Cain^{1,1} *Biomedical Engineering, University of Michigan, Ann Arbor, Michigan, USA, ²Urology, University of Michigan, Ann Arbor, Michigan, USA*

Background, Motivation and Objective

Shock wave lithotripsy can result in residual stone fragments of significant size (>2mm) that may cause ureteral obstruction and facilitate the aggregation of new stones. Previous work has shown that cavitational-based pulsed ultrasound therapy (histotripsy) can mechanically fractionate soft tissue into fine debris. We explored the use of histotripsy for treatment of kidney stones, investigating its potential to minimize fragment size and collateral tissue damage while maintaining comparable stone disintegration rate.

Statement of Contribution/Methods

Ultrasound-calcium phosphate-based cement was used as a model stone in a comparative study between histotripsy and shock wave lithotripsy. Histotripsy treatments employed a spherically-focused 1-MHz transducer, generating 5-cycle pulses delivered at a 1 KHz rate and 14MPa/45MPa peak negative/positive pressures. Lithotripsy was performed with a Wolf Piezolith 3000, using a 2 Hz pulse rate and 14MPa/76MPa peak negative/positive pressures. In each case, stones were sonicated for 5 minutes, and stone fragments were collected and sieved using filter sizes of 100um, 1mm, and 2mm. Collateral tissue damage was assessed by sonicating stones embedded in a tissue-mimicking agarose phantom containing red blood cells. Damage showed clearly as a color change in areas of the phantom where cells were destroyed. Acoustic backscatter was recorded during histotripsy to correlate stone disintegration with cavitation activity.

Results

1) Histotripsy produced no fragments greater than 100um in diameter, while 24% of those produced by lithotripsy exceeded 2mm. 2) On average, 14% of a 0.8ml stone was eroded by histotripsy during the 5 minute treatment, while lithotripsy fractionated 76 % of the stone in the same time course. 3) Collateral damage patterns produced by histotripsy and lithotripsy in the gel phantom both consisted of sparsely distributed micro-lesions located within a zone extending less than 5mm from the stone edges. Micro-lesions produced by histotripsy and lithotripsy were 100-300um and 300-500um in diameter, respectively. 4) Acoustic backscatter suggested that loss of stone mass is strongly correlated to bubble cloud initiation by histotripsy.

Discussion and Conclusions

Preliminary results demonstrate that histotripsy can erode model kidney stones into fine fragments while maintaining a minimum level of collateral damage in a tissue-mimicking phantom. Stone fragments resulting from histotripsy were significantly smaller than those produced by conventional lithotripsy. Although the histotripsy disintegration rate is currently below that of lithotripsy, it should be noted that the histotripsy parameters have not yet been optimized. As such, histotripsy shows promise in avoiding problems associated with residual fragments in lithotripsy.

1F-2

2:45 PM **Moving stones inside a kidney using acoustic radiation force**

Oleg Sapozhnikov¹, Michael Bailey¹, Bryan Cunitz¹, Peter Kaczkowski¹, Ghanem Oweis²; ¹Applied Physics Laboratory, University of Washington, Seattle, WA, USA, ²Department of Mechanical Engineering, American University of Beirut, Beirut, Lebanon

Background, Motivation and Objective

Acoustic radiation force imparted remotely on a small scatterer can be used to move the scatterer in a desirable direction. Such a need exists during treatment of kidney stone disease, because residual kidney stone fragments often remain after extracorporeal shockwave lithotripsy, ureteroscopic laser lithotripsy, and percutaneous nephrolithotomy, and new stones may grow from those fragments. The goal of this work is to study the possibility of using radiation pressure and streaming created by transcutaneous focused ultrasound to manipulate the location of stone fragments within the collecting system in order to facilitate passage of residual stone fragments.

Statement of Contribution/Methods

In the theoretical part, we simulated the radiation force imparted on a kidney stone by a focused ultrasound beam. First, acoustic scattering was modeled using finite differences based on elasticity equations. Then the radiation stress tensor was calculated and the radiation force was obtained given stone position and size. In the experimental part, we studied both radiation force and acoustic streaming as possible ways to displace stones inside the kidney collective system. The stones were placed in a transparent kidney phantom consisting of gel surrounding a water-filled space and in cadaveric porcine kidneys. Stone motion was observed visually in the kidney phantom and using diagnostic ultrasound in the porcine kidneys. The focused ultrasound therapy system was an annular array of 2 MHz with focal lengths in the range 4.5-8.5 cm. Longer bursts of higher amplitude ultrasound were applied than are applied in diagnostic ultrasound (4-MPa bursts for 100 ms to 1 s). The ensuing fluid flow field was measured using cross-correlation particle imaging velocimetry (PIV) that is based on timed-CCD-imaging of minute tracer particles seeded into the flow and illuminated with a laser sheet. Acoustic streamlines were visualized and the velocity values were measured in the transparent kidney phantom.

Results

Numerical calculations showed that moderate intensity focused ultrasound could create radiation force that exceeds the stone weight. This was confirmed experimentally. Stones in kidney phantom were seen to move. Stone velocities were on the order of 1 cm/s and quickly moved out of the ultrasound focus. Acoustic streaming also contributed to the stone motion. No evidence of thermal necrosis of kidney tissue was observed on gross examination.

Discussion and Conclusions

Radiation force and streaming created by focused ultrasound can be used to move stones within the collecting system. Further studies are required to assess minimum ultrasound exposures necessary to move stones, bio-effects caused by the ultrasound, and whether passage of fragments is facilitated. Work supported by NIH DK43881 and NSBRI SMST001601.

1F-3

3:00 PM **Arrest of tumor growth and reduction of tumor size in vivo by combination of ultrasound and intravascular microbubbles**

Chien Ting Chin¹, Talent Shevchenko², Balasundar Raju¹, Alexander Klibanov²; ¹Ultrasound Imaging & Therapy, Philips Research North America, Briarcliff Manor, NY, USA, ²University of Virginia, Charlottesville, VA, USA

Background, Motivation and Objective

High-intensity ultrasound can be used to treat tumor by thermally-induced necrosis. We recently observed that moderate focal ultrasound exposure after intravenous injection of microbubbles leads to transient reduction of tumor blood flow. In this work we report suppression of tumor growth in a murine model following repeated insonation of microbubbles. Insonation were chosen to avoid temperature elevation or acute damage to the tissue and vasculature.

Statement of Contribution/Methods

Half a million MC38 tumor cells were injected subcutaneously in the left thigh of female C57BL/6 mice (day 0). Tumor-bearing mice were divided into four groups (n = 7 each): C0 (no intervention), CU (ultrasound exposure), CB (microbubble injection) and E (microbubble injection followed by ultrasound exposure). Perfluorobutane microbubbles stabilized with a phosphatidylcholine and PEG stearate monolayer shell (mean size ~2 μm) were injected intravenously (dose of 50 million particles in 0.1 ml saline) twice daily. Therapeutic ultrasound (TIPS, Philips) consisted of 3 series of 10 pulses with the following parameters: f = 1.2 MHz, P = 5.0 MPa, 10⁵ cycles, PRF = 1 Hz, applied to the tumor after each of the two microbubble injections. These interventions were applied to experimental animals daily when tumors reached observable size (typically day 5). Treatment was skipped if no

measurable tumor was observed that day. Ultrasound imaging (Philips HDI5000 & CL15-7) was used for spatial guidance and blood flow monitoring. Tumor size was measured with a caliper. Animals were euthanized when the tumor size exceeded 16 mm.

Results

Low MI ultrasound contrast imaging showed the tumors were well perfused. Both high MI imaging and TIPS exposure destroyed microbubbles in the tumor vasculature. Microbubble replenishment within a few seconds was seen after destruction by high MI diagnostic imaging as expected but not after TIPS exposure. Blood flow in the treated region is stunned for several minutes. From day 5 through 17, control tumors showed rapid growth (C0: 12 ± 4.5 , CB: 10.2 ± 1.8 , CU: 16 ± 2.5 mm²/day). The E group showed reduction of tumor size: a trend of -0.33 ± 2.6 mm²/day over the same period. From day 10 onwards, the tumor size of E group was significantly smaller, than in the other groups ($p < 0.001$). Some temporary skin ulceration in the E group over the treated area was observed.

Discussion and Conclusions

Moderate insonation of microbubble can temporarily disrupt, or "stun", tumor blood flow. Repeated treatments arrested and even reversed tumor growth. Temperature elevation during ultrasound exposure was $< 2.5^\circ\text{C}$, ruling out thermal effects. Both microbubbles and ultrasound are required to induce stunning of blood flow and control of tumor growth. Destruction of bubble contrast was necessary but not sufficient to induce either outcomes. Ongoing studies suggest that stunning occurs in the tumor but not in normal vasculature.

1F-4

3:15 PM The role of compressional pressure in formation of dense bubble clouds in histotripsy

Adam D. Maxwell¹, Tzu-Yin Wang¹, Charles A. Cain¹, J. Brian Fowlkes¹, Oleg A. Sapozhnikov², Michael R. Bailey², Zhen Xu¹¹Biomedical Engineering, University of Michigan, Ann Arbor, MI, USA. ²Applied Physics Laboratory, University of Washington, Seattle, WA, USA

Background, Motivation and Objective

The onset of tissue fractionation by histotripsy pulses has been shown to coincide with initiation of a dense cavitating bubble cloud. Histotripsy pulses are short (< 20 cycles) and highly non-linear, with high peak rarefactional pressures (> 10 MPa) and compressional pressures (> 30 MPa). How a histotripsy pulse forms a dense cloud in tissue is not clearly understood. Using high-speed imaging, we studied bubble cloud formation induced by a histotripsy pulse and the role of the positive pressure phase in cloud formation.

Statement of Contribution/Methods

Bubble clouds were generated in a gelatin tissue phantom using histotripsy pulses. A focused, 1-MHz transducer (aperture = 10 cm, $f\# = 0.9$) was used to apply single 15-cycle pulses with peak negative/positive pressures of 19/70 MPa. Shadowgraphic images of pulse propagation and bubble cloud formation were recorded with a high-speed camera at 0.1-10 million fps. To assess the importance of the compression phases of the pulse in forming bubble clouds, an 80-um thickness steel foil was placed between the transducer and focus to reflect the high frequency components found in the positive shock. As a result, the transmitted positive pressure was reduced by 48%, while peak negative pressure remained unchanged.

Results

High speed images show that in the first 3-5 cycles of the ultrasound pulse, a sparse field of single cavitation bubbles with maximum radii of 50 - 120 um was formed within 5 mm of the focal region. During subsequent cycles, a dense cavitation cloud erupted from one of the single bubbles at the focus, and grew in length opposite the direction of ultrasound propagation until all 15 cycles passed the focus. After the pulse ended, the cloud ceased growth and collapsed. Images suggest that the cavitation cloud started to form directly after incidence of the shock front on the single bubble. When the positive pressure at the focus was reduced, single bubbles still formed, but a bubble cloud was never observed.

Discussion and Conclusions

Bubble clouds nucleate from the location of a single cavitation bubble. After single bubbles are generated, a high compression component of the ultrasound cycle is necessary to induce cavitation clouds. Based on these results, we hypothesize that the backscattered shock from a single cavitation bubble is inverted, resulting in extremely high rarefactional pressure, which is responsible cloud formation.

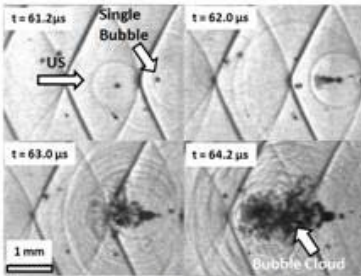


Fig. 1 – Bubble cloud forming from single bubble during 3 cycles of a histotripsy pulse

1F-5

3:30 PM Measurements of Blood Clot Displacements Induced by Pulsed Focused Ultrasound

Cameron Wright¹, Kullervo Hynynen¹, David Goertz¹; ¹Imaging Research, Sunnybrook Health Sciences Centre, Toronto, ON, Canada

Background, Motivation and Objective

Despite a significant body of work establishing the feasibility of ultrasound potentiated thrombolysis, there remains considerable uncertainty about the specific mechanisms involved in this process. Proposed mechanisms include acoustic streaming, thermal effects, cavitation, and radiation pressure, though the relative roles of each will likely depend upon the acoustic conditions that are employed. Thrombus displacements due to acoustic radiation forces have been hypothesized to improve the penetration and action of lytic agents and to induce strains that may promote clot degradation. Their role in thrombolysis is however poorly constrained due to an absence of direct experimental data. The objective of this study is to perform displacement measurements of clots in a focused ultrasound beam.

Statement of Contribution/Methods

A high frequency ultrasound imaging system was employed with an imaging transducer (20 MHz) situated with its plane at an angle of 30 degrees to a focused therapy beam (1.5 MHz, $f\#$ 0.8, -3 dB width 0.8mm). The focal regions of both transducers were colocalized in a blood clot that was situated in a 4 mm diameter channel within agar. The control of imaging and therapeutic pulses and data acquisition was conducted under the control of an arbitrary waveform generator. Therapy pulses (1ms duration) were interleaved (0.1ms spacing) with imaging pulses and successive imaging traces were acquired and processed using a 2D autocorrelator approach to extract displacement information along a given line of sight. Acoustic powers ranged from 0.1 to 20W.

Results

Thrombus displacements were found to vary linearly with acoustic power, as has been observed in other tissues. For example, after a 16 pulse sequence it was found that the peak displacements at 1 and 8 watts were 25 and 200 microns respectively. It was also observed that 'overshoot' occurred after pulse turn-off, consistent with inertial effects. The time for recovery to initial position varied with power; at 8 watts it was 55 ms. Displacements were found to be negligible by a distance of 1.5 mm laterally from the therapy beam axis.

Discussion and Conclusions

These results provide the first direct evidence of clot displacements induced by a focused ultrasound beam. Substantial displacements of blood clots can be achieved under exposure conditions that are viable in a clinical situation. This information will be relevant to understanding and exploiting this effect in the context of sonothrombolysis.

3:45 PM **Ultrasound-inducible fluorescent particles for internal tattooing**

Olivier Couture^{1,2}, Nicolas Pannacci³, Patrick Tabeling³, Vincent Servois⁴, Mathias Fink³, Mickael Tanter^{3,5}, ¹Institut Langevin - Ondes et Images, ESPCI ParisTech, Paris, France, ²Fondation Pierre-Gilles de Gennes, France, ³ESPCI ParisTech, France, ⁴Institut Curie, France, ⁵INSERM, France

Background, Motivation and Objective

Despite registration methods such as guiding wires, resecting diseased tissue previously detected with medical imaging remains challenging for surgeons. Our objective is to selectively and non-invasively deposit markers under image guidance for internal tattooing. This study describes the production and guided delivery of ultrasound-inducible particles carrying large payloads of fluorescent markers.

Statement of Contribution/Methods

Our particles are double emulsions. The primary emulsion consists of nanoparticles of fluorescein-saturated water encapsulated in perfluorohexane. This emulsion is then encapsulated in aqueous Pluronic (1%) using a flow-focusing microfluidic system. The vaporisation threshold of these particles is measured with a 2.25 MHz transducer (f: 38 mm, f#1) focused in an Opticell plate and observed under an inverted fluorescence microscope.

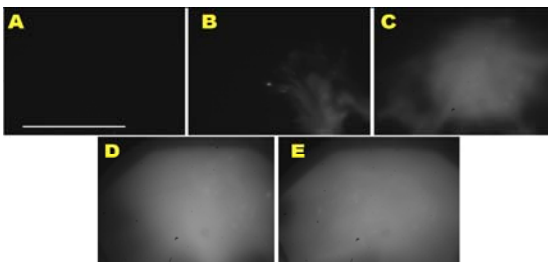
Results

The composite particles are monodisperse with a diameter of 5 microns. The fluorescein-containing water represents about 70% of the particles' content and they are stable for more than 2 weeks. When submitted to 2.25 MHz pulses, the particles vaporise at 4 MPa peak-negative pressure. In the microfluidic channel, a violent increase in volume is observed. In the Opticell plate, the microparticles are invisible prior to ultrasound-induced release. During disruption, jets of fluorescein are generated. After several seconds, a brightly-fluorescent dot (0.5 mm diameter) is observed at the focus of the transducer.

Discussion and Conclusions

Two third of the composite particles consists of payload that can be released at the focal spot of the transducer. Such a large amount of fluorescein could be observed under fluorescence endoscopy. This payload can also contain other hydrophilic markers and chemotherapy. The combined effect of the vaporisation of these particles and sonoporation is now being tested in the vascular-bed of fertilised chicken eggs.

Fig 1: Ultrasound-induced release of fluorescein in an Opticell plate observed under fluorescence-microscopy (15X) over 10 seconds.



2F. Contrast Agent Imaging

Sala 2

Tuesday, September 22, 2009, 2:30 pm - 4:00 pm

Chair: **Nico de Jong**
Erasmus Medical Centre

2F-1

2:30 PM **Ultrafast imaging of ultrasound contrast agents**

Olivier Couture^{1,2}, Souad Bannouf¹, Gabriel Montaldo¹, Jean-François Aubry¹, Mathias Fink¹, Mickael Tanter^{1,3}; ¹Institut Langevin - Ondes et Images, ESPCI ParisTech, Paris, France, ²Fondation Pierre-Gilles de Gennes, France, ³INSERM, France

Background, Motivation and Objective

The rate of dissolution of microbubbles post-disruption depends on their environment (hydrostatic pressure, dissolved gas, temperature, geometry). Unfortunately, conventional scanners do not have the time-resolution to exploit dissolution as a contrast mechanism over entire images. In this study, ultrafast plane wave imaging is used for dissolution imaging of flowing and bound microbubbles.

Statement of Contribution/Methods

An ultrafast 2D ultrasound scanner (Supersonic Imagine, France) was adapted to emit a disruption pulse between two series of imaging pulses at 500 Hz frame rate. Each image was composed of 11 compounded views obtained with plane waves at different angles. An 8 MHz linear array was used to emit the pulses. Imaging was performed on microbubbles (1/10000 v/v, Bracco Research SA) that were floating in a wall-less vessel phantom or bound to a gelatin surface.

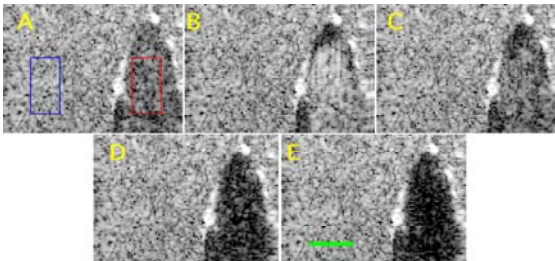
Results

Before disruption (fig 1 A), the microbubbles were hypoechoic in fundamental mode. After the disruption pulse (B), the microbubbles backscattering intensity increased by 10 dB in the centre of the vessel before decreasing in the next 100 ms (C,D,E) to -5dB. Ultrafast B-mode images also showed that disruption is heterogeneous as the microbubbles at the top of the vessel disappeared much faster than those in the centre. In the case of microbubbles bound to a surface, the drop in intensity after disruption occurred in less than 4 ms.

Discussion and Conclusions

Contrary to conventional perfusion imaging using contrast agents, Ultrafast imaging of microbubbles' disruption gives access to transient bubbles dynamics just after shell disruption. Such transient dynamics could help distinguish free-flowing microbubbles from confined ones in B-mode images. It also provides a mean to measure the effect of radiation pressure on microbubbles, along with the geometry of the vessels in which they are flowing.

Fig 1: Disruption of microbubbles in a wall-less vessel phantom (A) Prior to the disruption (B) 4 ms after disruption (C) 24 ms (D) 36 ms (E) 100 ms. The scale bar is 1 cm long.



2F-2

2:45 PM **High-resolution in-vivo ultraharmonic contrast imaging using a dual-frequency transducer**

Ryan Gessner¹, Mike Lee², Marc Lukacs², F. Stuart Foster², Paul Dayton¹; ¹Biomedical Engineering, University of North Carolina at Chapel Hill/North Carolina State University, USA, ²University of Toronto, Canada

Background, Motivation and Objective

With recent advances in animal models of disease, there has been great interest in capabilities for high-resolution ultrasound imaging. The ability to detect small numbers of contrast agents in a tissue background is particularly important for molecular imaging or perfusion imaging. Microbubble contrast agents are unique in that they scatter ultrasound energy at higher and lower harmonics than the fundamental imaging frequency. These broadband harmonics, due to the contrast agents' nonlinear response, have been shown to be most intense when insonified near the MCAs' resonant frequencies. To date, efficiently exciting harmonic response has not been possible with high-frequency imaging systems since most contrast agents are resonant in the 1-5 MHz frequency range. We hypothesized that a dual frequency transducer, which could excite microbubbles near resonance and detect harmonic content above 25 MHz, would provide high sensitivity to contrast agents with high resolution and superior tissue rejection. Our objective was to design a probe for high-sensitivity ultrasonic molecular and perfusion imaging.

Statement of Contribution/Methods

Our team has developed and tested a unique dual-frequency confocal transducer for a VisualSonics imaging system which enables low frequency excitation at 2-4 MHz and high frequency detection near 30 MHz. Preliminary in vivo tests with this probe have been performed on three rats. Images of the animals' left kidneys were obtained for multiple bolus injections in both dual-frequency imaging and standard B-mode imaging modes. The resulting contrast-to-tissue ratios within the imaging ROIs were determined offline and compared. Additionally, susceptibility to tissue motion was compared against standard power Doppler imaging.

Results

Using this ultraharmonic imaging approach, we demonstrate spatial resolution near that of the high-frequency element (30 MHz), and contrast-to-tissue ratios 15 dB greater using the ultraharmonic imaging approach compared to standard 30 MHz B-mode in all three animals. Ultraharmonic imaging is demonstrated to be not affected by tissue motion.

Discussion and Conclusions

Our studies have demonstrated that ultraharmonic imaging can be implemented on a high-resolution ultrasound system by utilizing a dual-frequency transducer, with a substantial improvement in contrast-to-tissue detection compared to B-mode imaging, and robustness in the presence of tissue motion compared to signal-subtraction or power-Doppler contrast detection techniques. This technology could provide a substantial improvement in sensitivity for ultrasonic molecular imaging and slow-flow perfusion imaging in animal models.

2F-3

3:00 PM **Nonlinear Contrast Agent Imaging with a Linear Array Based Micro-Ultrasound System**

Andrew Needles¹, James Mehi¹, Marcel Arditi², Emmanuel Gaud², Peter Frinking², Desmond Hirson¹, Stuart Foster^{1,3}; ¹VisualSonics, Canada, ²Bracco Research, Switzerland, ³Sunnybrook Research Institute, Canada

Background, Motivation and Objective

Recently, a linear array based micro-ultrasound system with a 64 channel beamformer has been developed (Foster et al. UMB 2009). This talk will focus on the implementation of a real-time nonlinear contrast mode on this array based system, and the challenges faced in high-frequency contrast imaging, namely nonlinear propagation in tissue. The array transducer, beamforming techniques, digital sampling and signal processing will be described, along with in vitro and in vivo results.

Statement of Contribution/Methods

A modified micro-ultrasound scanner (Vevo 2100, VisualSonics) was operated at 18-24 MHz with a 256 element linear array transducer (MS-250, $f_c = 21$ MHz). In vitro imaging was conducted with MicroMarker (VisualSonics) contrast agent flowing at 30 mm/s through a 1 mm wide vessel within a polyvinyl alcohol (PVA) cryogel phantom. Low amplitude (350 kPa) narrowband pulses (6 cycles) were used with the following multi-pulse sequences: pulse-inversion (PI), amplitude-modulation (AM) and their combination (PIAM). These sequences isolate nonlinear

Tuesday
Oral

bubble echo signals at the subharmonic (SH) and also fundamental (FUND - only for AM and PIAM) frequencies. The signals were digitally bandpass filtered (BPF) around the SH, FUND or SH+FUND frequency bands. Mean echo power values were calculated for bubbles and PVA, and contrast-to-tissue-ratios (CTR) were determined.

Results

Fig. 1a summarizes the in vitro results; compared to raw non-processed echo signals, the improvement in CTR at 18 MHz was maximized (13 dB) with either AM or PIAM, whereas at 24 MHz the highest improvement in CTR (15 dB) was obtained with PI + SH. Guided by these results, in vivo images were obtained with small animals (mice, rats) in a variety of applications (abdominal, cardiac, xenograft tumours). Figure 1b and 1c show the abdomen of a mouse pre- and post-bolus, respectively, highlighting perfusion in the kidney (K), pancreas (P), and spleen (S).

Discussion and Conclusions

Real-time nonlinear contrast imaging is now possible with an array based system in the 18-24 MHz range. Significant advantages of nonlinear fundamental detection have been demonstrated, but these advantages appear to diminish with increasing frequency. As frequency increases, pulse sequences extracting the SH are preferred. For many applications, nonlinear imaging will offer improved performance for contrast studies in small animals.

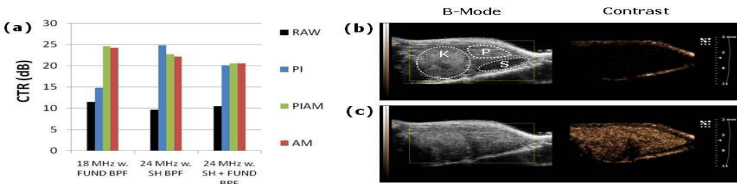


Figure 1

2F-4

3:15 PM High-frequency contrast ultrasound imaging of size-isolated microbubbles in mice

Shashank Sirsi¹, Jameel Feshitan¹, Shunichi Homma², Mark Borden^{1,2} *Chemical Engineering, Columbia University, USA, ²Cardiology, Columbia University, USA*

Background, Motivation and Objective

High-frequency ultrasound is enhanced through the use of lipid-coated microbubble contrast agents for anatomical, functional and molecular imaging. Previous in vivo studies have relied on highly polydisperse microbubble suspensions, which may provide a complex and varied acoustic response. We have developed a rapid and robust method for isolating large quantities of size-selected microbubbles from a polydisperse suspension [Feshitan et al., *J. Colloid Interface Sci.*, 2009]. The purpose of this paper is to examine the in vivo acoustic response and circulation persistence of size-selected microbubbles for a range of concentrations using high-resolution ultrasound.

Statement of Contribution/Methods

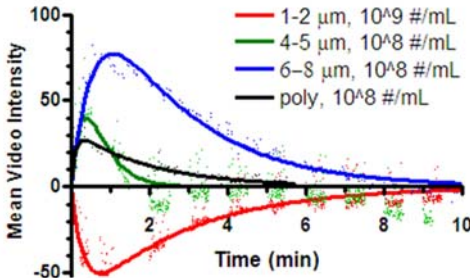
Microbubbles of 1-2, 4-5, and 6-8 μm diameter were isolated using differential centrifugation and characterized using multiple sizing/counting techniques. Ultrasound imaging of the mouse kidney was performed at 40 MHz using a Visualsonics Vevo 770 during bolus injections of size-sorted and unsorted microbubble suspensions (0.1 mL; 10^7 to 10^9 #/mL). Time-intensity ultrasound contrast curves were generated and fit to a single-compartment pharmacokinetic model. Area under the curve (AUC) and circulation persistence (t^*) were assessed in the studies.

Results

Our results demonstrate that contrast enhancement at 40 MHz is a strong function of microbubble size. The AUC increased over 4-fold for 4-5 μm vs. 6-8 μm diameter microbubbles ($10^8 \text{ \#}/\text{mL}$). Likewise, the AUC increased by 83% from 10^7 to $10^8 \text{ \#}/\text{mL}$ for 6-8 μm microbubbles. Shadowing occurred for all microbubble sizes at high enough concentrations; the threshold concentration for shadowing decreased for larger microbubbles. Surprisingly, 1-2 μm diameter microbubbles exhibited only shadowing for all of the concentrations tested. Contrast persistence was also found to increase with microbubble size and concentration. For example, t^* increased from $120 \pm 26 \text{ sec}$ to $442 \pm 102 \text{ sec}$ for 4-5 μm vs. 6-8 μm microbubbles ($10^8 \text{ \#}/\text{mL}$).

Discussion and Conclusions

For high-frequency imaging in mice, large microbubbles strongly increase contrast, while small microbubbles mainly attenuate. The results suggest that larger microbubbles require orders of magnitude lower concentrations without sacrificing persistence, which may be important for molecular imaging and drug delivery.



2F-5

3:30 PM Prostate cancer localization by contrast-ultrasound diffusion imaging

Massimo Misch¹, Maarten Kuenen¹, Hessel Wijkstra², Ad Hendriks³, Erik Korsten¹, ¹Eindhoven University of Technology, Netherlands, ²Academic Medical Center Amsterdam, Netherlands, ³Catharina Hospital Eindhoven, Netherlands

Background, Motivation and Objective

Prostate cancer is the form of cancer with the highest incidence in men in western countries, accounting for 25% and 10% of all cancer diagnoses and deaths, respectively. The low specificity of available diagnostics hampers the implementation of a general screening, which would lead to a significant reduction of mortality rates.

New techniques are therefore necessary for a noninvasive early detection of those forms of cancer that are clinically significant. Imaging techniques are particularly interesting as they would permit cancer localization and, therefore, efficient use biopsy targeting of focal therapies. As cancer aggressiveness relates to microvascular growth, several imaging techniques have been proposed for the detection of blood perfusion. However, up until now, reliable cancer detection has not been achieved.

We propose a different ultrasound imaging method for prostate cancer detection that is based on the quantification of the (intravascular) local diffusion of ultrasound contrast agents. Local diffusion is expected to correlate better than perfusion with the complexity of cancer microvasculature.

Statement of Contribution/Methods

Local diffusion is estimated by an intravenous injection of an ultrasound contrast agent bolus. In this study, a 2.4 mL bolus of SonoVue® (Bracco, Milan) was injected. The bolus passage through the prostate is measured by transrectal contrast-enhanced ultrasound imaging. A large set of indicator dilution curves (IDCs) is measured from the received acoustic intensity at the resolution of the ultrasound scanner. To this end, the ultrasound B-mode videos are compensated for the logarithmic compression of the signal dynamic range. The measured IDCs are fitted by the Local Density Random Walk model. This model is a solution of the convective diffusion equation and, therefore, provides a physical representation of the diffusion process. A fast model fitting is presented for the estimation of a diffusion parametric image of the prostate. The estimation robustness is improved by dedicated spatio-temporal filtering based on specific IDC-noise modeling. A preliminary validation was carried out by comparison with histology data obtained from a patient after radical prostatectomy at the Academic Medical Center in Amsterdam.

Results

The results showed a good agreement (sensitivity 86.0%, specificity 89.5%) between the parametric diffusion images and the histology assessment. This agreement was superior to that obtained by estimation of the other IDC parameters proposed in the literature, such as the IDC time to peak, mean transit time, appearance time, peak intensity, and area.

Discussion and Conclusions

Local UCA-diffusion quantification by contrast ultrasonography is a promising method for prostate cancer localization, with potential to permit accurate targeting of biopsy and focal therapy. Further validation is however necessary to optimize the method and compare it with other techniques.

2F-6

3:45 PM Contrast Improvement by Combining Pulse Inversion with EMD and EEMD

Ai-Ho Liao¹, Che-Chou Shen², Pai-Chi Li¹; ¹National Taiwan University, Taiwan, ²National Taiwan University of Science and Technology, Taiwan

Background, Motivation and Objective

Ultrasound nonlinear imaging using microbubble based contrast agent has been widely investigated. Nonetheless, its contrast is often limited because acoustic wave propagation in tissue is also nonlinear. In this study, an ultrasound contrast imaging method which combines pulse-inversion technique with empirical mode decomposition (EMD) and the ensemble empirical mode decomposition (EEMD) in Hilbert-Huang transform (HHT) is explored to enhance the contrast between bubbles and surrounding tissues.

Statement of Contribution/Methods

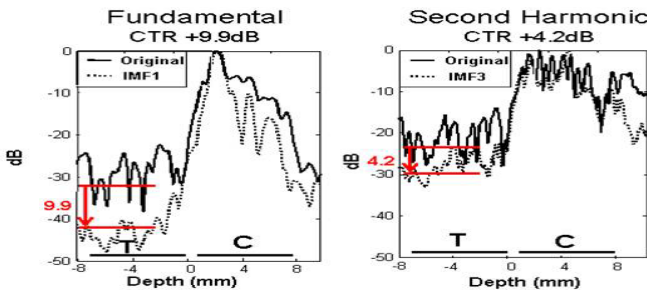
The EMD is a method associated with HHT that allows decomposition of the data into a finite number of intrinsic modes (IMF). To overcome the scale mixing problem in EMD, EEMD method further utilizes the ensemble of IMF with added white noise to better differentiate the nonlinear microbubble signal from the nonlinear tissue signal. This hypothesis was tested on pulse-inversion (PI) nonlinear imaging, which is generally regarded as one of the most effective nonlinear imaging methods, using both simulations and PI A-line measurements.

Results

Our results showed that, when imaging with certain IMF, the contrast-to-tissue ratio (CTR) in the fundamental band and the second harmonic band was improved by 9.9 and 4.2 dB after EEMD. The EMD method is shown to be less effective in CTR improvement especially in second harmonic imaging due to its weakness in decomposing signals in the presence of frequency mixing.

Discussion and Conclusions

By extracting microbubble component and suppressing background noise, it is demonstrated both numerically and experimentally that the EEMD could noticeably improve image contrast in both PI fundamental and second harmonic imaging. Further investigation is still required to warrant practical applications of EMD and EEMD in ultrasound nonlinear imaging.



3F. Cardiac Imaging

Sala 4

Tuesday, September 22, 2009, 2:30 pm - 4:00 pm

Chair: **James Miller**
Washington University

3F-1

2:30 PM **Tangential sound field oscillations for 2D motion estimation in echocardiography**

Hervé Liebgott¹, Abderraouf Ben Salem¹, Adrian Basarab¹, Hang Gao², Piet Claus², Jan D'Hooge², Philippe Delachartre¹, Denis Friboulet¹, ¹CREATIS-LRMN, France, ²Katholieke Universiteit Leuven, Belgium

Background, Motivation and Objective

Last year at this conference the application of transverse oscillations (TO) for 2D motion estimation in echocardiography was presented. The results showed the feasibility of obtaining a PSF with oscillations in the direction perpendicular to beam axis for typical cardiac phased array transducers. It has been shown by computer simulation that the lateral translation of a translating square numerical tissue phantom can more accurately be estimated using a phase-based estimator combined with TO compared to conventional block matching (BM).

Statement of Contribution/Methods

The aim of this study was to further investigate the proposed methods in a more realistic setting. Hereto, the squared numerical tissue phantoms were deformed as well as translated assuming conservation of volume and applying axial strains of 0% to 2%. The accuracy between the phase-based estimator combined with TO and BM was compared and the influence of depth was investigated. Secondly, images from a more complex kinematic model of the heart were generated as previously described [Gao et al. IEEE UFFC 56(2)] but using a look-up-table of a sound field with TO. The quality of the motion estimates was visually verified.

Results

Displacement estimation using TO was limited to values below 1/4 of the axial or lateral wavelength. As the beams diverge with depth, larger displacements at larger depths could be estimated. At 90mm it was possible to estimate axial and lateral displacement up to 0.03 and 0.5mm, respectively with a mean error below 0.003 and 0.038mm, respectively. Although the mean estimation was similar for the TO and BM methods, TO showed a smaller standard error (for 0.03mm axial and 0.5mm lateral displacement the standard error are 0.001mm and 0.025mm for TO and 0.003 mm and 0.043 for BM). This remained the case when deformation up to 2% is applied.

The 2D displacement map (Fig 1) between two frames from the numeric heart sequence shows the feasibility to estimate 2D motion using the TO method for myocardial wall kinetics.

Discussion and Conclusions

The proposed combined TO - phase-based estimator approach showed to estimate 2D myocardial motion more reproducibly than conventional block matching under realistic cardiac motion/deformation and imaging conditions. This method can thus be implemented on currently available hardware and might be a step forward in multi-dimensional motion and strain estimation of the heart.

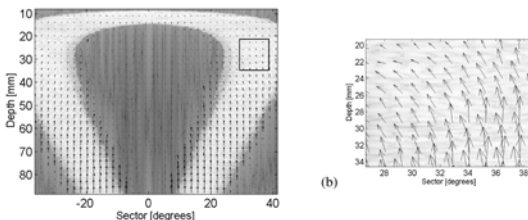


Fig 1: (a) 2D displacement map obtained between two images from the cardiac sequence simulated. (b) Zoom in the box marked in a by the black rectangle. The representation is done in a polar coordinate system.

Tuesday
Oral

3F-2

2:45 PM 3-D Motion Tracking Using Raw Data and a Matrix Array: Phantom and In Vivo Cardiac studies

Brett Byram¹, Greg Holley², Daniel Need², Doug Giannantonio¹, Gregg Trahey¹, ¹Biomedical Engineering, Duke University, Durham, NC, USA, ²Ultrasound Division, Siemens Medical Solutions, USA, Inc., Mountain View, CA, USA

Background, Motivation and Objective

Researchers have demonstrated three dimensional (3-D) speckle tracking using detected data at low volume rates. However, the effect of volume rate, kernel size and data type (raw and detected) has not been sufficiently explored. First comparisons are made within the stated variables for 3-D speckle tracking.

Statement of Contribution/Methods

Ultrasound volumetric, raw baseband data in an IQ format were acquired using a matrix array attached to a Siemens SC2000 scanner (Siemens Healthcare Sector, Ultrasound Business Unit, Mountain View, CA). Data were acquired from a phantom with controlled translation, and data were acquired of left ventricle short-axis views of a human volunteer. The data were used to demonstrate the feasibility of 3-D motion tracking using raw data in both phantom and in vivo scenarios using a matrix array. Data volumes were acquired at volume rates up to 1000 Hz for a 10°x12° lateral and elevational extent, respectively, and to an axial depth of 14cm. The acquired volumes consisted of 120 receive beams acquired in sections of 30 beams received in parallel. Kernels within acquired data were tracked using phase-sensitive normalized cross-correlation. Subsample estimation, in the lateral and elevational dimensions, was performed using the grid-slopes algorithm. Kernel sizes of 1.2x.85x.85mm, 2.2x1.7x1.7mm, and 4.3x3.5x3.5mm (axial x lateral x elevational) were used for the analysis.

Results

Acquired data were used to examine the effect of volume rate, kernel size and data type on 3-D speckle tracking. The effect of volume rate was analyzed by comparing velocity estimates from lower frame rates against velocity estimates derived from 1000 Hz volume rate data which were summed appropriately to simulate the lower volume rate estimates. This comparison was made for both raw and detected data. The resulting lateral and elevational tracking performance is similar for both IQ and detected data. The axial tracking performance is best when the IQ data is used, but this is primarily due to lower estimation jitter. The performance of tracking axial displacement using detected data is still better than the tracking performance in the lateral or elevational dimensions, which is consistent with the literature. Additionally, the results show little improvement when tracking above 200 Hz (although this is kernel dependent). For the largest kernel (4.3x3.5x3.5 mm) there is little perceived benefit for tracking at volume rates above 100 Hz. The employed tracking method and data shows, qualitatively, good temporal and spatial stability (for independent kernels) at high volume rates.

Discussion and Conclusions

3-D speckle tracking with IQ data has been validated on phantom data, and 3-D speckle tracking limits have been explored using *in vivo* cardiac left ventricle data.

3F-3

3:00 PM Assessment of regional myocardial function using 3D cardiac strain estimation: comparison against conventional echocardiographic assessment

Gabriel Kiss¹, Daniel Barbosa², Krasimira Hristova², Jonas Crosby³, Fredrik Orderud⁴, Piet Claus², Brage Amundsen¹, Dirk Loeckx⁵, Jan D'hooge^{1,2}, Hans Torp³, ¹Medical Imaging Laboratory, Norwegian University of Science and Technology, Norway, ²Lab on cardiovascular imaging and dynamics; department of cardiovascular diseases, Catholic University of Leuven, Belgium, ³Department of Circulation and Medical Imaging, Norwegian University of Science and Technology, Norway, ⁴Computer Science Department, Norwegian University of Science and Technology, Norway, ⁵Centre for the Processing of Speech & Images; department of electrical engineering, Catholic University of Leuven, Belgium

Background, Motivation and Objective

Recent work of our labs introduced methods to assess regional myocardial function by estimating all normal strain components in all left ventricular (LV) segments from volumetric ultrasound data. RCTL-BURDOCK is a method in which a subdivision surface is first deformed by edge detection (RCTL), and then the resulting mesh is refined by BURDOCK based on a 3D speckle-tracking approach, while splineMIRIT is a B-spline transformation-based elastic registration method.

Statement of Contribution/Methods

The aim of the present study was to test and contrast the diagnostic accuracy of both approaches in the clinical setting.

Volumetric ultrasound data was acquired in 7 healthy volunteers and 9 patients with proven coronary artery disease (GE Vivid7 Dimensions, Vingmed, Horten, Norway). Wall motion scoring (WMS) (0=normo-kinetic; 1=hypo-kinetic; 2=a-kinetic; 3=dys-kinetic) was carried out. An end-diastolic subendocardial mesh was automatically obtained through segmentation performed by RCTL. The mesh nodes were subsequently tracked during the cardiac cycle using both BURDOCK and splineMIRIT. Three standard apical views and 3 short axis slices at different levels in the LV where generated on which the mesh was visualized. The tracking quality was visually scored on a segmental basis (0=bad; 1=good) by a trained cardiologist blinded to the data and compared among methods using a paired t-test.

The dynamic meshes were then used to calculate segmental circumferential and longitudinal strain as length changes between nodes. Bull's-eye plots of the end-systolic strain were generated and used by a trained cardiologist to identify the presence of the ischemic regions. The methods ability to detect infarcted patients was tested by computing per patient sensitivity and specificity values (WMS as reference). Differences in longitudinal strain values in normal and unhealthy segments of high 3D quality have been also compared.

Results

Overall, tracking quality was better for splineMIRIT, 85% vs. 79% of segments, p-value < 0.01 paired t-test. Sensitivity values for detecting MI were 70% and 40% for BURDOCK and splineMIRIT, while specificity values were 81.82% and 90.91% respectively, p-value = 0.37 (McNemar test). Mean and standard deviation values for end-systolic longitudinal strain in normal segments were -14.47%±10.22 BURDOCK, -14.80%±11.22 splineMIRIT and -9.65%±9.22 BURDOCK, -10.67%±10.31 splineMIRIT in segments showing abnormal motion. The ANOVA test yielded significant differences among normal and abnormal segments for both methods (p-value < 0.01).

Discussion and Conclusions

The proposed methods are fully automatic and can distinguish between normal and unhealthy segments in clinical recordings. BURDOCK reported significantly higher sensitivity scores for detecting MI, while splineMIRIT achieved better tracking quality results. A quantitative comparison of both methods against a reference method is the subject of ongoing work.

3F-4

3:15 PM Forward-Looking Volumetric Intracardiac Imaging Using a Fully Integrated CMUT Ring Array

Amin Nikoozadeh¹, Omer Oralkan¹, Kai Thomenius², Aaron Dentinger², Douglas Wildes², Kalyanam Shivkumar³, Aman Mahajan³, Douglas N. Stephens⁴, Matthew O'Donnell⁵, David Sahn⁶, Pierre T. Khuri-Yakub¹:¹Stanford University, Stanford, CA, USA, ²General Electric Corporate Research & Development, Niskayuna, NY, USA, ³University of California, Los Angeles, Los Angeles, CA, USA, ⁴University of California, Davis, Davis, CA, USA, ⁵University of Washington, Seattle, WA, USA, ⁶Oregon Health and Science University, Portland, OR, USA

Background, Motivation and Objective

Atrial fibrillation is the most common type of cardiac arrhythmia that now affects over 2.2 million adults in the United States alone. Currently fluoroscopy is the most common method for guiding interventional electrophysiological procedures.

We are developing a 9-F forward-looking intracardiac ultrasound catheter for real-time volumetric imaging. This catheter not only improves visualization and ultimately procedural success but also reduces the undesirable use of fluoroscopy.

Statement of Contribution/Methods

We designed and fabricated a 64-element 10-MHz CMUT ring array with through-wafer via interconnects. The outside and inside diameters of the ring measure 2.6 mm and 1.6 mm, respectively. The central opening of the ring can potentially be utilized to deliver a variety of devices such as HIFU transducers, RF ablation electrodes, and optical fibers for photo-acoustic imaging.

We also designed custom front-end electronics to be closely integrated with the CMUT array at the tip of the catheter for improved SNR. This integrated circuit (IC) is composed of preamplifiers and protection circuitry, and can directly interface a standard imaging system. This multi-channel IC is designed in a high-voltage process and is capable of passing up to ±50 V bipolar pulses. Every channel in this IC is composed of two separate paths that

Tuesday
Oral

meet at both the input and output of the channel: the transmit path, which is only composed of diode expanders, and the receive path, which contains a transimpedance amplifier and a buffer. Both the amplifier input and buffer output are protected from high voltage pulses using diode limiters.

An 8-channel front-end IC was fabricated based on this circuit topology. Additionally, a flexible PCB (flex) was designed that is composed of 8 long and narrow legs that intersect at the center of the flex. The ring array is flip-chip bonded to the center of the flex and one IC is flip-chip bonded to each leg to address a total of 64 channels. The flex legs are then folded around the ring array for final integration with the catheter.

Results

The IC was wire-bonded to a ring array for bench-top testing. We successfully applied up to ± 50 V bipolar pulses to the IC and measured an amplifier recovery time of less than 300 ns. We performed a pulse-echo experiment with the ring array immersed in oil. The CMUT array was biased at negative 70 V and a 2-burst ± 45 V sine wave was applied to an element. We measured a SNR of about 30 dB for the echo from the oil-air interface that was about 5.2 mm away. In another experiment, with the array biased at negative 60 V and a ± 45 V 8-MHz tone burst input, we measured an acoustic pressure of 1.4 MPa_{r-p} at the face of the array element.

Discussion and Conclusions

The presented experimental results demonstrate the performance of the main components of our forward-looking volumetric intracardiac imaging approach. We are currently working on the final catheter integration and backend imaging system development.

Supported by the NIH under grant HL67647.

3F-5

3:30 PM Ultrafast imaging of the heart using Circular Wave Synthetic Imaging using Phased and curvilinear Arrays

Mathieu COUADE¹, Mathieu Pernot², Mickael Tanter², Emmanuel Messas³, Alain Bel³, Maguette Ba³, Albert-Alain Hagege³, Mathias Fink²: ¹SuperSonic Imagine, France, Metropolitan, ²Institut Langevin, ESPCI ParisTech, CNRS UMR 7587, INSERM, France, Metropolitan, ³Hôpital Européen Georges Pompidou, INSERM U633, France, Metropolitan

Background, Motivation and Objective

An important limitation of conventional Tissue Doppler Imaging is the necessary trade-off, between N, the number of acoustic transmit firings (field of view) and FR, the imaging frame rate, for a given pulse repetition frequency (PRF = N x FR). To overcome this limitation, we propose the use of synthetic imaging with a small number of broad beams (typically then than 5) insonifying a large field of view 100 mm depth, 80° wide sector with a phased array) with a very high frame rate (>1000 images/sec). The aim of this study is to demonstrate in-vivo the feasibility of ultrafast Tissue Doppler Imaging using conventional curvilinear and cardiac phased array probes.

Statement of Contribution/Methods

Synthetic imaging is performed using a coherent summation of receive only focusing images. Performances of synthetic imaging using circular wave transmit were optimized in vitro to obtain a high acquisition frame rate. Then, in vivo experiments were performed on 12 sheep. After a lateral thoracotomy, the transducer was placed directly on the lateral wall of the left ventricle to obtain different typical views of the heart. Continuous loops of 1200 frames with a frame rate above 1200 Hz were collected and an ECG were recorded simultaneously. A complete axial displacement movie of a single heart cycle was obtained using conventional 1D and 2D cross-correlation technique on IQ beamformed images.

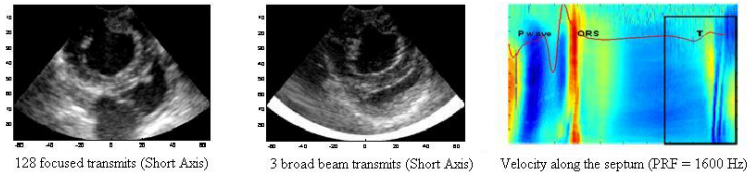
Results

Single transmit was found to be sufficient for imaging tissue displacement in the myocardium with a curved probe. For phased array probe, the coherent summation of a few number of transmits (between 3 and 5) dramatically reduces the clutter noise. With 3 angles, the contrast between blood in ventricular cavity and the myocardium was found to be 5 dB smaller than in conventional focused image. Using this technique in vivo, it was possible to observe at high frame rate both the global contraction motion and the propagation of mechanical waves in the myocardium during a complete cardiac cycle.

Discussion and Conclusions

This preliminary study shows the potential of applying synthetic broad beam imaging to image a wide sector of the heart at a very high frame rate. Without requiring any triggering with the ECG signals, such ultrafast sequences are

demonstrated here to image over a large field of view the propagation of natural mechanical waves along the septum at different stages during a single heart cycle.



3F-6

3:45 PM **Segmentation in 3D Echocardiography Based on Temporal Correlation of the Radio Frequency Signal.**

M.M. Nillesen¹, R.G.P. Lopata¹, H.J. Huisman², J.M. Thijssen¹, L. Kapusta³, C.L. de Korte¹; ¹Clinical Physics Laboratory, Department of Pediatrics, Radboud University Nijmegen Medical Centre, Nijmegen, Netherlands, ²Department of Radiology, Radboud University Nijmegen Medical Centre, Nijmegen, Netherlands, ³Pediatric Cardiology, Department of Pediatrics, Radboud University Nijmegen Medical Centre, Nijmegen, Netherlands

Background, Motivation and Objective

Semi-automatic segmentation of the endocardial surface in three-dimensional (3D) ultrasound images might substantially support clinical diagnosis of heart disease. In particular in children with congenital heart disease, segmentation should be based on echo features solely, since incorporation of *a priori* knowledge on the shape and anatomy of the heart might induce erroneous segmentation results.

The low echogenicity of the myocardium in some regions imposes strong demands on the segmentation algorithm. High resolution information derived from the radio frequency (rf) ultrasound signal might be crucial in these critical regions. We evaluated the possible contribution of the correlation between subsequently acquired echo signals for segmenting the cardiac wall.

Statement of Contribution/Methods

Transthoracic full volume rf-image sequences (ECG-gated) were acquired in long/short axis views in four healthy children. A Philips iE33 ultrasound system was used with a pediatric X7-2 matrix array transducer (2-7 MHz) and an rf-interface. A semi-3D technique using a 2D coarse-to-fine displacement estimation algorithm was used to locally determine temporal maximum cross-correlation (MCC) values from the rf-data as a feature for distinguishing between blood and myocardium. The MCC values in end-diastolic frames were used as an additional external force in a deformable model. The segmentation method was tested using a) adaptive filtered, demodulated rf-data, b) MCC-data and c) a combination of both. The methods were evaluated by calculating the mismatch ratio between automatically segmented contours and interactive segmentation results by an expert.

Results

In low echo contrast regions of the myocardium, MCC values could still differentiate between blood and myocardial tissue, whereas blood and myocardium could not be classified using adaptive filtered data only. Combining the MCC force with the adaptive filtering force in the deformable model led to improved segmentation of the ventricular cavity in datasets containing low contrast regions. The average mismatch ratio decreased from 0.18 (adaptive filtering) and 0.19 (MCC) to 0.12 (combination of adaptive filtering and MCC).

Discussion and Conclusions

Preliminary results revealed that MCC values have additional value for segmentation of cardiac tissue. Using MCC, temporal information is included in the deformable model as an extra feature that might facilitate segmentation in regions where contrast between blood pool and endocardial border is too low to perform gray-level based segmentation. Although the frame rate of full volume imaging is still limited in terms of accurate cross-correlation values throughout the entire cardiac cycle, the MCC based model could be used in the end-systolic and end-diastolic phase to assess cardiac output and as a more robust initialization for segmentation of the other frames in the cardiac cycle.

Tuesday
Oral

4F. NDE Signal Processing

Tarragona

Tuesday, September 22, 2009, 2:30 pm - 4:00 pm

Chair: **Eric Furgason**
Purdue University

4F-1

2:30 PM Three dimensional ultrasound gestural interface

Riccardo Carotenuto¹, Radu Ionescu¹, Pietro Tripodi¹, Fabio Urbani^{2,1}:¹DIMET, Università Mediterranea di Reggio Calabria, Italy, ²Department of Engineering, University of Texas at Brownsville, Brownsville, Texas, USA

Background, Motivation and Objective

Gestural interfaces are the most natural way to interact with machines and in the next future they will get more and more ubiquitous, due to their enormous impact on issues like office work, public health, social life, entertainment, etc. Touch screens and accelerometer-equipped game pads are only the first avant-garde of what can be expected in the next future. This work presents a localization system based on airborne ultrasounds capable to localize several position markers with sub-centimeter accuracy at a rate of about 25 Hz. Using the position markers, body movements can be measured fast and precisely enough to make possible the future implementation of a gestural interface using predefined 3D trajectories of body, limbs or fingers as code words or commands.

Statement of Contribution/Methods

The localization system is composed of a number of low-cost 3D remote position sensors and of a set of beacons that emit a sequence of ultra-acoustic pulses in the space region containing the position sensors. When impinged by the acoustic wavefronts, each sensor sends back a signal to a central unit through a suitable transmission channel. The central unit, knowing the positions of the acoustic beacons and the time of arrival of the sensor signals, computes the positions of the sensors, identifying and discarding possible false signals due to echoes and environmental noise.

In a first prototype implementation, four coplanar beacons, actually earphones, are placed at the corners of a PC screen, and are forced to emit pulses in the 20 – 40 kHz band. Each sensor is equipped with a wideband miniature microphone, which is wired to an acquisition board. All the computation, including signal filtering, time of arrival detection, and localization, is carried out by a notebook PC in real-time at 25 Hz.

Results

In Fig. 1 the experimental freehand trajectories of two sensors writing “hello” in front of the PC screen, are shown. The measured positioning standard deviation was about 3 mm in all the three spatial directions within a range of 70 cm.

Discussion and Conclusions

The proposed system showed a positioning and trajectory tracking accuracy good enough to make it possible a straightforward realization of a gestural interface, which is currently under investigation. At the best of the authors' knowledge, in literature there are no similar localization systems, concerning localization rate and position accuracy.

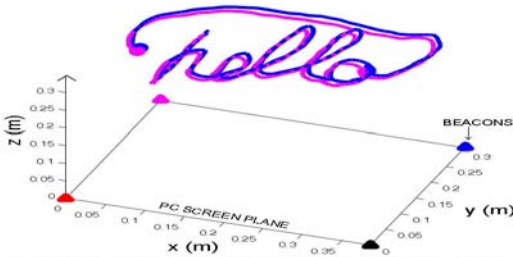


Fig. 1. Experimental 3D trajectory: freehand "air" writing in front of the PC screen using a pair of sensors (200 samples @ 25 Hz, the sensors separation is 7 mm).

4F-2

2:45 PM Adaptive 3D Ultrasonic Data Compression using Distributed Processing Engines

Christophe Desmouliers¹, Erdal Oruklu¹, Jafar Saniie¹, ¹Electrical and Computer Engineering, Illinois Institute of Technology, Chicago, IL, USA

Background, Motivation and Objective

Ultrasonic 3D imaging is an important tool in NDE applications for quality control, flaw detection, and material characterization. However, ultrasonic 3D images often encompass massive amounts of data, making it very challenging to perform real-time volumetric image analysis. In this work, a fast and scalable data compression architecture based on discrete wavelet transform (DWT) is proposed. This System-on-Chip (SoC) architecture can process B-scan and C-scan images in real-time and reduce the data and bandwidth requirements substantially without degrading the signal fidelity.

Statement of Contribution/Methods

We introduce an adaptive data compression algorithm that uses 3D wavelet transform and incorporates both local and global thresholding methods. The algorithm offers highest energy compaction due to optimal wavelet packet tree decomposition derived from ultrasonic signal models. This decomposition determines the subbands that can be discarded completely or thresholded aggressively without compromising the integrity of data. For hardware synthesis, a distributed wavelet processing engine (PE) hardware is proposed and implemented on a Xilinx Virtex-5 FPGA platform. An array of PEs computes multiple wavelet transform operations in parallel, reducing the computation time significantly. Since DWT is a separable transform, 3D wavelet transform can be implemented as three stages of successive 1D DWT. The architecture exploits the fact that after completion of each 1D DWT stage, transform coefficients can be significantly discarded. Furthermore, a hybrid 3D wavelet kernel is used. This approach uses high-order wavelet kernels for the axial resolution for improved data compaction and Haar transform for the remaining two spatial resolutions. Since Haar kernel can be realized with simple logic (no multiplications), the hardware requirements and computation time is reduced substantially.

Results

For a case study, experimental 3D ultrasonic data from a steel block are acquired by a pulse-echo system with a 5MHz transducer. The data dimensions are 128x128x2048 points which correspond to 5cmx5cmx5cm cubic region. Total size of data is more than 32 Megabytes. The compression algorithm is applied to ultrasonic RF signals and evaluated based on compression ratio vs. signal-to-noise ratio. The results indicate that compression ratios can reach and exceed 98% data reduction while still maintaining high signal fidelity. In addition, the proposed distributed processing engine hardware can process and compress this data in real time within data acquisition period.

Discussion and Conclusions

An adaptive 3D compression algorithm has been presented for ultrasonic signals. The performance of the compression algorithm has been quantified with experimental data and shown to offer significant resilience to different experimental data sets. An SoC architecture has been designed to deal with massive data bandwidth and real-time compression requirements.

4F-3

3:00 PM Anti-Collision Technique of SAW ID Tags at Unknown Temperature using Integer Programming

Maria Brandl¹, Stefan Schuster², Stefan Scheiblhofer², Andreas Stelzer^{1,1} *Institute for Communication and Information Engineering, Johannes Kepler University, Linz, Austria, ²Christian Doppler Laboratory for Integrated Radar Sensors, Johannes Kepler University, Linz, Austria*

Background, Motivation and Objective

Based on the synchronous separation method, a new identification algorithm for separating multiple asynchronous surface acoustic wave identification (SAW ID) tags at variable unknown temperature is presented. For identification of the codes, an estimation of the reflector delays (round trip delay times – RTDTs) is necessary. Reading out multiple tags simultaneously, these impulse response patterns superpose and the assignment between reflectors and tags is lost. Furthermore, the answer and thus, the delays of the tags are scaled, thus stretched or compressed due to external effects, e.g. temperature. The radial position results in a shift of the impulse response and is handled as an offset. In this paper, a novel technique is introduced, which estimates the offsets, scalings and codes.

Statement of Contribution/Methods

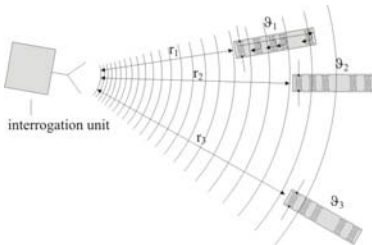
We use a least squares (LS) approach based on a linear combination of the RTDT data of the different tags. In a first step, the continuous parameters, namely the scalings and the offsets, are estimated separately. As a consequence, the resulting LS-cost function depends only on the RTDT data and the discrete sets of parameters. A fundamental prerequisite to achieve a precise model for the desired synthetically generated RTDT information is a good RTDT estimate. Here, the superresolving Relax algorithm has been chosen.

Results

In practice, only the sum of the scalings can be estimated precisely when using the sum of RTDTs as data. Thus a one-dimensional grid search is applied for the scaling. The offset is determined by means of a synchronization procedure. In an improvement step, the squared error between the time-domain data and a signal model based on synthetic RTDTs together with phase and amplitude information is minimized. This approach operates down to a signal-to-noise ratio (SNR) of as low as -8 dB, which is verified by means of substantial Monte Carlo simulations and measurements at different scalings and offsets.

Discussion and Conclusions

This novel separation method presents a flexible reliable anti-collision identification algorithm for a simultaneous interrogation of multiple SAW tags. The threshold level of the simulations and the measurements match well. The recently developed technique represents a high-quality and applicable extension for SAW ID tags at different temperature (ϑ) and radial distances (r) according to the figure shown below.



4F-4

3:15 PM Beamspace Transformation for Data Reduction using Genetic Algorithms

Minghui Li¹, Eddie Ho¹, Gordon Hayward^{1,1} *Centre for Ultrasonic Engineering, University of Strathclyde, Glasgow, Scotland, United Kingdom*

Background, Motivation and Objective

Estimation of the incident waveform directions, or direction of arrival (DOA) estimation, is an essential problem in sonar array processing. It may resolve closely spaced targets clustered when imaging. A sonar array usually consists of a large number of elements, as a consequence, the data processing complexity is extensive, typically requiring $O(M^3)$ operations for an M -element array. An approach to reduce the computation is to map the data from full-dimension element space (ES) into a lower dimension beam space (BS), through a linear transformation prior to signal processing.

Tuesday
Oral

A key issue in BS processing is transformation design. Among the proposed methods, maximum estimation accuracy (MEA) [1] and the adaptive approach [2] are the most promising. MEA is optimal in terms of DOA accuracy; but it is sensitive to out-of-sector interference. The adaptive approach yields robust estimates if the data covariance is estimated accurately. However, it is not the case since only a few samples can be taken into account to avoid mixing data from different distance cells. Furthermore, it encounters difficulties with correlated waveforms, which are usually inevitable.

In this paper, we present a flexible and robust approach for BS transformation design. The cost function evaluates DOA estimate accuracy and interference suppression capability simultaneously, and genetic algorithms (GA) are used for searching the global solution. This method is robust to interference, data sample scarcity, and incident waveform correlation.

Statement of Contribution/Methods

The cost function is defined by

$$f(T) = w_1 * n_1(T) + w_2 * n_2(T) + w_3 * n_3(T)$$

$n_1(T)$: BS DOA estimation accuracy by measuring the closeness between ES and BS Cramer-Rao bounds (CRB) [1], $n_2(T)$: interference suppression capability by comparing the gain pattern of T with the desired one, and $n_3(T)$: angle errors between sources representation subspaces.

Positive constants $w_1 - w_3$ are set on the basis of the expected variations of related terms and the desired balance among them. GA is applied to perform global minimization of $f(T)$.

Results

Simulations show that the BS DOA estimates obtained using this transformation are as accurate as those obtained using ES data samples in terms of mean squared errors (MSE), but the computing cost is significantly reduced, in the order of thousand times. Furthermore, the design yields superior DOA estimates under strong interference over MEA and the adaptive method.

Discussion and Conclusions

We present a novel scheme for BS transformation design under strong interference in sonar array processing, aiming for reduced computation. The approach is potentially useful for accurate target discrimination and localization in certain NDE applications.

[1] Anderson, S. On optimal dimension reduction for sensor array signal processing. *Signal Processing*, 30, 245-256.

[2] Eriksson, J. and Viberg, M. Adaptive data reduction for signal observed in spatially colored noise. *Signal Processing*, 80, 1823-1831.

4F-5

3:30 PM Underwater ultrasonic ranging by digital signal multiplexing with Hadamard matrix

Tadashi Ebihara^{1,2}, Keiichi Mizutani^{2,3}, Kojiro Nishimiya^{1,2}, Koichi Mizutani¹, Naoto Wakatsuki¹; ¹University of Tsukuba, Japan, ²Research Fellow of the Japan Society for the Promotion of Science, Japan, ³Tokyo Institute of Technology, Japan

Background, Motivation and Objective

Recently, there has been an increase in the amount of research on underwater acoustics. In this paper, we propose digital signal multiplexing with Hadamard matrix (DSM-H) which is a type of digital signal processing for underwater ultrasonic ranging system (URS), to improve signal-to-noise ratio (SNR) compared to existing underwater URS.

Statement of Contribution/Methods

DSM-H is a digital signal processing method which compiles multiple data vectors into one signal mathematically. By applying DSM-H to URS, multiple propagation properties are obtained in single measurement.

Fig. 1(a) shows the DSM-H process in modulator and demodulator. Transmitting signal is obtained by superimposing vectors which are Kronecker products between N -data vectors and rows of Hadamard matrix. N -propagation properties are obtained in a single measurement by applying matched filter to received signal.

We inspected this proposed system by a pass-band simulation. Each set of data vectors is different M-sequence. Transmission line matrix method is used for wave propagation and propagation environment is shown in Fig. 1(b). White Gaussian noise is added to signal. For comparison, we also inspected existing underwater URS which uses

Tuesday Oral

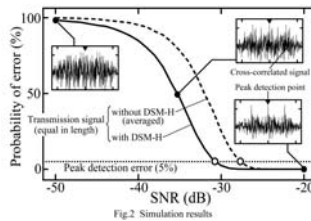
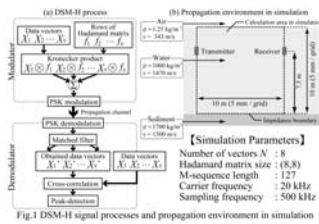
M-sequences without applying DSM-H and N -times averaged. Total signal lengths of applying DSM-H and without applying DSM-H are the same.

Results

Fig. 2 shows the simulation results. Applying DSM-H achieves 5% error at SNR -31 dB while without applying DSM-H at -28 dB. From these results, SNR can be improved about 3 dB by applying DSM-H to underwater URS.

Discussion and Conclusions

We evaluated the advantage of DSM-H to underwater URS. Compared to existing method, DSM-H can improve SNR effectively. Experimental evaluation of DSM-H in ocean is our future work.



4F-6

3:45 PM A new Split-Spectrum Algorithm for Dispersive Materials using Variable Bandwidth Filters

Alberto Rodríguez¹, Luis Vergara²; ¹Signal Processing and Communications, Universidad Miguel Hernández de Elche, Elche, Alicante, Spain, ²Depto. Comunicaciones, Universidad Politecnica de Valencia, Spain

Background, Motivation and Objective

Split-spectrum algorithms have been extensively applied to the suppression of grain noise in ultrasonic NDE. This algorithm is based on the frequency diversity phenomenon which appears when a wideband pulse is applied to a dispersive material. In terms of the filter bank, there are two main trends commonly followed. One is based on constant bandwidth Gaussian filters equally spaced in frequency and the other one uses wavelets as a multi-resolution time-scale method.

We have designed a series of modifications to this structures with the main objective of achieving high values of SNR with as less bands as possible, in order to improve the efficiency of the method

Statement of Contribution/Methods

We desing an alternative that combines both techniques. It is based in the use of variable bandwidth filters, but in this case equally spaced in frequency and energy gain equalized so all bands have the same contribution from the possible echo defect. With this new design we improve the insensitivity of the echo defect to the tuning frequency. We will also use the pruning technique to reduce the number of bands in the algorithm.

Regarding the recombination methods, the most used are those ones based on Amplitude Minimization and Polarity Thresholding. In this study we will also consider the Normalized Amplitude Minimization method and the Frequency Multiplication method, not very commonly used but revealed in this work as the best option when combined with the new filter bank proposed.

Results

We show the results obtained after simulations using non stationary models for the grain noise. Signal to noise ratio enhancement factor was selected as the figure of merit to make the comparisons among the different methods. These results are contrasted with real processed signal obtained in laboratory from pieces of cement 32.5.

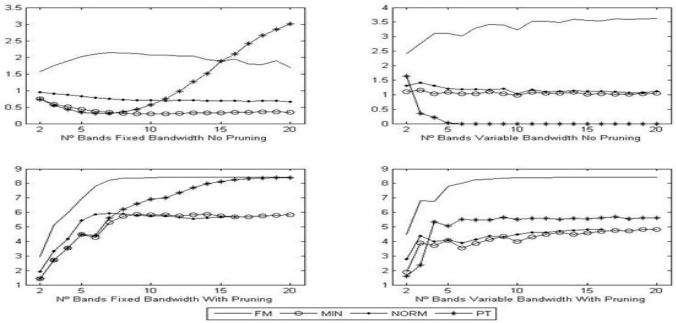
In figure are shown the results obtained after the recombination for all the algorithms and with the two filter bank structures and any band ruled out. In figure 2 are also shown the results obtained after the pruning for the best case.

Tuesday
Oral

Discussion and Conclusions

As we can see from the obtained results, the new filter bank design achieves an improvement in the SNR gain for a very low number of bands.

We have also shown that with pruning the SNR improves achieving the maximum value for very low number of bands, achieving a very efficient structure.



Tuesday
Oral

5F. SAW Device Design

Pergamo

Tuesday, September 22, 2009, 2:30 pm - 4:00 pm

Chair: **Leo Reindl**
University of Freiburg

5F-1

2:30 PM High Performance Microwave Acoustic Components for Mobile Radios

Maximilian Pitschi¹, Jürgen Kiwitt¹, Robert Koch¹, Karl Wagner¹, Robert Weigel^{2,1} *EPCOS AG, Munich, Germany,*
²*Institute for Electronics Engineering, University of Erlangen-Nuremberg, Germany*

Background, Motivation and Objective

Due to their outstanding characteristics acoustic components, such as SAW and – later on - also BAW filters, have been key components in wireless communication systems from their very beginning. Regarding mobile radio handsets the primary field of application of acoustic components has moved to the RF front-end sections. Here, with the increasing demand for WCDMA-FDD capable mobile phones, duplexers, which allow to separate the TX and RX paths while being simultaneously connected to the antenna, have become indispensable.

Regarding the specifications of the different operating bands the requirements on form factors, pass band characteristics, attenuations of the other signals (TX, RX, GPS, WLAN, ...), and isolations make them high performance components requiring a sophisticated acoustic as well as electromagnetic design. Regarding the requirements imposed on the duplexers in terms of, e.g., center frequencies, spacings of RX and TX bands, relative band widths, and shape factors, they also require application-specific acoustic structures.

As a consequence, in contrast to standard filters, duplexers are highly optimized components using leading-edge technologies. In order to achieve the best balance of the characteristic properties of the acoustic structures regarding, for instance, their quality factors, pole-zero distances, and temperature coefficients, the manufacturing processes of the acoustic chips are designed for the specific applications. Furthermore, optimizing the electrical characteristics a co-design of package and acoustic chip is applied.

Statement of Contribution/Methods

Results

In this paper we provide an overview of the different types of duplexers that have been the result of the focused specialization and optimization efforts. We classify them according to the type of acoustic structures, matching circuitry, and package being used. So far, purely SAW-based and BAW-based duplexers as well as hybrid duplexers using both SAW and BAW chips have been reported. Most of the matching circuitry is integrated in, for instance, an LTCC package using a distributed approach based on a $\lambda/4$ line or a lumped approach comprising coils and/or capacitors. Sometimes the matching circuitry is realized externally on the PCB.

Furthermore, we present recent integration successes, i.e., duplexer inserts, allowing the seamless integration of duplexers into modules without drawbacks on performance or module thickness.

Discussion and Conclusions

5F-2

3:00 PM Realization of Small and Low Profile Duplexer Using A CSSD Packaging Technique

Toshio Nishizawa¹, Satoru Ono¹, Motoyuki Tajima¹, Osamu Kawachi¹; ¹*Communication Devices Division, FUJITSU MEDIA DEVICES LIMITED, Yokohama, Kanagawa, Japan*

Background, Motivation and Objective

In the market, the RF architecture of cellular phones and the diversification of the system (NCDMA, GSM, WCDMA and LTE in the future) is rapidly evolving. This drives the need for multiband, multimode RF functions. As a result, further miniaturization and high reliability is required for Duplexers.

Tuesday
Oral

Statement of Contribution/Methods

In this paper, we discuss how small size, high reliability Duplexers can be achieved using the original CSSD (Chip Size SAW Devices) packaging structure. Good heat radiation, hermetic performance and small frequency drift against temperature shift are essential to achieve small size and highly reliable Duplexers. To make the reduction from 3025 package size to 2520 package size it is necessary to reduce the chip size by roughly 67%. It is then necessary to improve the effect of heat radiation by the corresponding amount giving the 2520 package size the same power handling capability as the larger 3520 package size Duplexer. Because of it is necessary to reduce the size of the chip for the miniaturization of Duplexer around 67% is needed to miniaturize package from 3025 size to 2520 size. Then, it is necessary to improve the effect of heat radiation done to correspond to about 67%. It means 2520 size duplexer can be realized same handling power capability of 3025 size duplexer. Our CSSD structure is effectively achieves this.

Results

Our CSSD structured duplexer has effectively achieved good heat radiation characteristics and realized hermetic performance. The 2520 package size Band 2 Duplexer (including matching circuit) realized better performance than 3025 package size Band 2 Duplexer.

Discussion and Conclusions

In this paper, we will report on the advantage of heat radiation and electrical performance characteristics of the CSSD structure. In addition, we will discuss the possibility of further miniaturization in the future.

5F-3

3:15 PM New SPUDT cells including fingers and gaps wider than a quarter wavelength

Guenter Martin¹, Hagen Schmidt¹, Sergey Biryukov¹, Bernd Steiner², Bert Wall²:¹IFW Dresden, Germany, ²Vectron International GmbH & Co. KG, Germany

Background, Motivation and Objective

The basic types of SPUDT cells like DART, EWC, Hanma-Hunsinger, FEUDT and TF include quite narrow fingers and gaps. For application in GHz SAW devices these fingers are too narrow to implement the electrode structures in the required quality by means of the available technologies. Lehtonen et al. [1] suggested SPUDT structures on 128°YXLiNbO₃ the fingers of which are a quarter or half a wavelength wide. The purpose of the proposed paper is to find SPUDT cells the fingers and gaps of which are wider than a quarter wavelength not only for 128°YXLiNbO₃.

[1] S. Lehtonen, V. P. Plessky, C. S. Hartmann and M. M. Salomaa, Proc. 2003 IEEE Ultrasonics Symposium, p. 817

Statement of Contribution/Methods

Apart from this condition there is not any limitation of the finger and gap widths leading to a variety of solutions with partly more favorable parameters than in [1]. Such solutions of SPUDT cells with wider fingers and gaps than a quarter wavelength on YZLiNbO₃ and 128°YXLiNbO₃ with 3, 4, 5 fingers and a length of 2, 3, 3 wavelengths (in the same order) are presented. The cells have been found by means of an optimization procedure comprising a MATLAB optimization function, a cell analysis software according to the theory in [2] and a MATLAB program creating the interface optimization function – cell analysis.

[2] S. V. Biryukov and M. Wehnacht, J. Appl. Phys. Vol. 96 (2004), p. 3117

Results

The structure data and the most important SAW parameters of some cells on YZLiNbO₃ and 128°YXLiNbO₃ as a result of the optimization are summarized. The sensitivity of the transduction-reflection phase difference to fluctuations of the finger widths and electrode layer thickness is considered, too. Due to bulk wave generation there is a relatively big loss. It can be a problem if the IDTs are too long. Therefore, short IDTs are required. In order to achieve a sufficient unidirectional effect in spite of the small number of fingers big reflection factors per wavelength are needed. The experimental study of a cell type with five fingers on YZLiNbO₃ which theoretically meets the requirement of a big reflection factor confirms the existence of a strong unidirectional effect pointing really to a big reflection factor per wavelength.

Discussion and Conclusions

Related to the compatibility with the available structuring technologies all the cells found are suitable for the GHz range. Because of the loss problem they are advantageous for wideband delay lines as well as for wideband remote

sensors and ID tags. It is shown that a larger sensitivity to fluctuations of the finger widths and electrode layer thickness can be accepted for wideband devices.

5F-4

3:30 PM SAW DUPLEXER DESIGN FOR WCDMA SYSTEM

Takashi Shiba¹, Osamu Hikino², Seima Kondo², Naoko Kamogawa²; ¹Hitachi Media Electronics, Yokohama-shi, Kanagawa-ken, Japan, ²Hitachi Media Electronics, Japan

Background, Motivation and Objective

SAW has been successfully employed in a number of signal-processing devices, such as RF filters, IF filters, duplexers and other SAW devices for recent digital mobile communications. It is expected to realize a high sensitivity and a high blocking performance against jamming signal for CDMA mobile terminals because of the concurrent communication of transmitter (Tx) and receiver (Rx) signals. The SAW duplexers are generally used for N-CDMA and WCDMA mobile terminals to achieve miniature sizes. Low loss, high outband rejection and high linear characteristics of SAW duplexer are desired for this purpose.

Statement of Contribution/Methods

Distortion coefficients of SAW duplexers are simulated by using a nonlinear equivalent circuit analysis and measured for 2.5mm and 2.0mm size SAW duplexers for Band1 WCDMA terminals.

Some relations between sensitivity performances and duplexer performances (losses, isolations between Tx and Rx terminals and distortion parameters) are obtained. We simulate system noise figure (NF) levels and blocker levels from duplexer performances with the above distortion parameters, low noise amplifier (LNA) parameters and mixer parameters by using a nonlinear NF model and a signal flow approximation.

Results

Good agreements between simulations and experimental results of intercept point values for B1 duplexer are observed.

Discussion and Conclusions

Consequently, desired duplexer performances to achieve sufficient system performances of WCDMA terminals are determined by these procedures.

5F-5

3:45 PM Wideband Multi-Mode SAW Filter Employing Pitch Modulated IDTs on Cu-Grating/15°YX-LiNbO₃-Substrate Structure

Ken-ya Hashimoto¹, Takashi Miyamoto¹, Tatsuya Omori¹, Masatsune Yamaguchi¹; ¹Graduate School of Engineering, Chiba University, Chiba, Chiba, Japan

Background, Motivation and Objective

Because of their balun- and transformer-functions in addition to their excellent out-of-band rejection, the longitudinally-coupled multi-mode SAW (MMS) filters are widely used in the RF section of modern mobile phones.

Their fractional passband width is inherently limited by the electromechanical coupling factor K^2 of a substrate. The authors have shown that a Cu-grating/15°YX-LiNbO₃ (15-LN)-substrate structure is most effective in developing extremely wideband and low-loss ladder-type filters.

Statement of Contribution/Methods

This paper attempts to apply the Cu-grating/15-LN-substrate structure to the development of extremely wideband MMS filters in GHz range.

Results

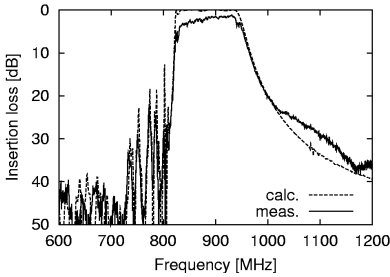
First, a design tool developed for the present purpose is detailed. A precise simulation is performed by the modified coupling-of-modes (COM) model, where the coupling of the propagating shear-horizontal-type SAWs with bulk acoustic waves is taken into consideration. Parameters necessary for the simulation are determined experimentally. Namely, a series of simple one-port resonators is fabricated on the Cu-grating/15-LN-substrate structure, and the parameters are determined by fitting the experimental admittance with the theoretically predicted characteristics.

Next, it is shown that the synthesis of extremely wideband MMS filters needs to use a certain number of resonances which are properly combined. In the design, we adopt the pitch-modulated IDTs proposed by the

authors, and demonstrate that a fractional bandwidth of more than 12% is achieved by a proper combination of seven resonances. Here, should the number of resonances be insufficient, the required IDT aperture length becomes extremely large resulting in a ohmic loss of the IDT fingers.

Discussion and Conclusions

An MMS filter composed of three IDTs was fabricated on a Cu-grating/15-LN-substrate structure. Fig. 1 compares the frequency response of the fabricated filter with the calculated result. The passband width of 12.8% and the minimum insertion loss of 1.2 dB were experimentally obtained around 900 MHz. Although the measured result totally agrees with the calculation, a small discrepancy is seen in the passband response. Its inclination is explained by the finger resistance. Other miscellaneous losses of 0.8 dB may be due to the SAW attenuation with propagation.



Tuesday
Oral

6F. Phononic Crystals-Propagation

Baalbek

Tuesday, September 22, 2009, 2:30 pm - 4:00 pm

Chair: **Vincent Laude**
CNRS

6F-1

2:30 PM **Defect-Mode Waveguide and Coupled-Mode Theory**

Toyokatsu Miyashita^{1,†} Dept. Electronics & Informatics, Ryukoku University, Otsu, Japan

Background, Motivation and Objective

Defect-mode waveguides (DMWSs) in artificial crystals are appreciated for practical usage due to high transmission and sharp band-pass characteristics. In the analysis of such prominent properties of DMWGs by the visualized FDTD simulations, that mechanism has been considered due to mode coupling between adjoining defects.

Statement of Contribution/Methods

We constructed a coupled mode theory which can analyze a chain of an arbitrary number of defects. Our coupled-mode model of a DMWG is shown in Fig. 1. Linear coupled-mode equations were derived subject to the conservation of energy. Their eigen-frequencies were solved analytically till 7 defects and numerically till 15 defects. Further, recursive formula was obtained for an arbitrary number of defects.

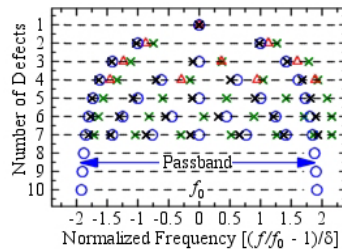
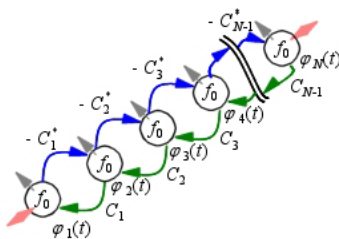
Results

The solved eigen-frequencies are partially shown in Fig. 2 by blue circles. The bandwidth defined by the spread width of the eigen-frequencies increases monotonically, and seems to converge into a constant of $4\delta f_0$, where f_0 denotes the resonance frequency of a single-defect, and δf_0 magnitude of the coupling coefficient.

The previously reported peak frequencies f which appear in the transmissions obtained by the FDTD simulation are plotted in Fig. 2 on a scale of normalized frequency $(f/f_0 - 1)/\delta$ for DMWGs in an acrylic-resin sonic crystal by green diagonal crosses, and those for DMWGs in a GaAs photonic crystal by black ones. Experimental ones are plotted by red triangles. Their bandwidths agree well with those by the coupled mode theory with differences of 1.3%, 2.3%, and 3.3% respectively in case of four defects.

Discussion and Conclusions

This coupled mode theory proved to be useful for DMWGs. It is expected to be developed further for complicated DMWGs in functional acoustic circuits including T-branches and crossroads.



Tuesday
Oral

6F-2

2:45 PM **Band gap of Lamb waves in one-dimensional phononic crystal plate**

Yong Li¹, Zhilin Hou¹, Badreddine ASSOUAR²; ¹South China University of Technology, China, People's Republic of, ²Institut Jean Lamour, Nancy University - CNRS, France

Background, Motivation and Objective

The propagation of elastic waves in periodic heterogeneous materials has received much attention in the last decade. The existences of absolutely band gap in such kind of materials suggest various potential applications. Recently, band gaps in one- and two-dimensional phononic crystal (PC) plate were also found. For a two-dimensional PC plate, to adjust the width and position of the band gap, various configurations, such as the square, triangle, and honeycomb lattices, are studied. But for the one-dimensional PC plate, only the structure that layer-stacked along the propagating direction are studied. In this structure, a band gap usually appears between the 0th symmetric and anti-symmetric Lamb mode. In this work, we study a 1D PC plate consisted of layers of circular inclusion in the thickness direction. We find that the width and the position of the band gap in such a system can be adjusted more easily by the size and the distance between the circular inclusions.

Statement of Contribution/Methods

It is shown in Ref. [1] that, in a PC plate with mirror plane, the Lamb modes can be separated into two uncoupled sets: the symmetric and anti-symmetric modes. So it will be convenient if we can discuss each of them separately. Based on the main idea of the Plane Wave Expansion method shown in Ref. [2], we found that such a separation can be done by taking the advantage of the symmetry of the wave fields. Because of the symmetric and anti-symmetric property of the displacement components, the trial wave solutions can be expanded respectively by the cosine and sine functions rather than Fourier series, and the eigenvalue equation associated with symmetric and antisymmetric modes can be obtained alternatively.

Results

By the method suggested above, we calculated the band structure of the Lamb wave in the PC plates containing one, two and three layer circulars in the thickness direction. Numerical results show that the width and position of the band gap in such kind of systems relies strongly on the size and position of the scatterers. For a PC plate with two and three layer scatterers, high frequency band gap can also be opened by adjusting the distance between the scatterers. Further investigation shows that partial band gap of the symmetric/anti-symmetric mode can usually be adjusted alternatively, so that the full band gap, which is the overlap of the partial ones, can be opened. A physical understanding of this phenomenon can be understood by checking the energy distribution of the modes in a uniform plate: a partial band gap can usually be opened if the scatterers are inserted in the area where the elastic energy of the corresponded mode is concentrated.

Discussion and Conclusions

The new PC structure we propose in this work deals with the control of the opening of complete band gap and the understanding of physical phenomenon occurring in 1D PC plate structured in thickness direction.

- [1]. Z. Hou, M. B. Assouar. J. Phys. D: Appl. Phys. 41, 215102 (2008)
- [2]. Z. Hou, M. B. Assouar. Phys. Lett. A, 372, 2091 (2008)

6F-3

3:00 PM **Properties of acoustic wave propagation in “double negative” metamaterial**

Ivan Lisenkov¹, Roman Popov¹, Sergey Nikitov¹; ¹Kotelnikov Institute for Radio Engineering and Electronics of RAS, Moscow, Russian Federation

Background, Motivation and Objective

Currently a lot of interest and research is attracted to “double negative” (DNG) media. In acoustics DNG media properties are represented by the material with simultaneously negative density and stiffness. Obviously, that such media could not be found on Earth, but such behavior could be observed in man-made composites, thus effective negative density and stiffness could be obtained in some frequency domain. Such media are called “metamaterials”.

Statement of Contribution/Methods

We consider the composite consisted of isotropic background material, called matrix, and embedded resonators in it. In the frequency band near the resonance the group response of resonators could be great enough to affect the

Tuesday
Oral

propagating wave in matrix in anti-phase, cause negative response. The frequency of a resonance is chosen in such manner that the wavelength in the matrix is much greater than the size of inclusions and the distance between them, so the composite is quite uniform.

Two methods for modeling elastic wave propagation in such composites are developed. The first one is build upon analytical effective media characteristics calculations based on scattering, namely, coherent potential approximation. In the work we obtained the analytical formulas for effective media. Close to the resonance frequency scattering changes dramatically (analog to Mie resonances), affecting totally the propagating wave.

The second method, based on FEM, is direct numerical calculations of the behavior of the one inclusion in matrix ("elementary cell") under alternating harmonic forces at the given frequency. If the acceleration of the cell is opposite to the force, the cell has negative mass, if the cell is expanding under the pressure, the cell has negative stiffness.

Results

In the model the inclusions in the form of solid multi-layered cylinders are taken, the waves are propagating perpendicular to inclusions generatrices. Cylinders are consisted of outer soft shells and rigid heavy cores causing structure resonances at low frequencies. The matrices were considered both liquid and solid. It is shown that such structures exhibit DNG regime in a narrow frequency domain. Zones of DNG regimes depending on geometry and inclusions mechanical properties are calculated, comparison between numerical and analytical methods is done. Also surface acoustic waves (SAW) propagation in the composite/free matrix interface is considered. It is found that the interface can support propagating SAW in a particular frequency domain, as an analogy to surface plasmon-polariton waves in electrodynamics.

Discussion and Conclusions

Possibility of developing acoustic metamaterial consisting of solid or liquid matrix with multi-layered cylindrical inclusions is considered. Frequency domains of DNG for different geometry and mechanical characteristics are found. The dispersion characteristics for the SAW propagating in such media are calculated.

The work is supported by RFBR grant #08-02-00785-a.

6F-4

3:15 PM **Simultaneous Photonic and Phononic Band Gaps in a two-dimensional Lithium Niobate Crystal**

Said Sadat-Saleh¹, Sarah Benchabane¹, Fadi Baida¹, Maria-Pilar Bernal¹, Vincent Laude^{1,2} *Institut FEMTO-ST, Besançon, France*

Background, Motivation and Objective

The possibility to obtain hypersonic phononic band gaps in artificial crystals presenting submicron lattice parameters has shown that phononic and photonic crystals can be made of comparable dimensions, hence opening the way to simultaneous elastic and electromagnetic band gaps. The existence of such «phoxonic» band gaps has been theoretically demonstrated in 2D crystals made of air holes in silicon [1]. Experimental evidence of the phenomenon has been reported in a 3D crystal [2]. However, these works have focused on simple lattice geometries and there is no guaranty that phoxonic band gaps can be obtained with materials exhibiting lower refractive index constrasts or crystal symmetry.

Statement of Contribution/Methods

We focused on the theoretical investigation of air/lithium niobate 2D phoxonic crystals. The conditions for the existence of a full photonic band gap in this material are demanding, due to its relatively low refractive index. This adds up with its anisotropy which slightly hinders the opening of large phononic band gaps. The most commonly used single-atom lattices, i.e. square and hexagonal, as well as multiple-atom hexagonal lattices were considered. In each case, photonic and phononic band structures were computed independently.

Results

It is observed that decreasing the lattice symmetry lattice by adding atoms of different sizes leads to larger phoxonic band gaps, though the largest photonic and phononic band gaps are not obtained for the same structure. The best compromise is reached with a hexagonal symmetry with three different atoms per unit cell. The low refractive index of the material prevents from opening complete phoxonic band gaps, as the gap maps for the optical transverse electric and transverse magnetic polarizations do not overlap in any of the considered structures. Yet, complete band gaps for either optical polarization can be found.

Discussion and Conclusions

The possibility to open simultaneous phononic and photonic band gaps in lithium niobate was theoretically demonstrated. Technologically feasible designs were proposed for operation at an optical wavelength of 1.55 μm and at acoustic frequencies in the GHz range. The simultaneous confinement of both elastic and electromagnetic energy in a same volume is then possible, provided that the incident light is polarized. Phoxonic crystals hold promises for the confinement and tailoring of sound and light waves in tiny volumes, with potential applications to acousto-optics and highly controllable photon-phonon interactions.

[1] M. Maldovan and E. Thomas, Appl. Phys. Lett. 88, 251907 (2006).
 [2] A. V. Akimov, et al., Phys. Rev. Lett. 101, 033902 (2008).

6F-5

3:30 PM **Influence of disorder on wave propagation and localization in 2D phononic crystals with a point defect**

Ali Chen¹, Yueheng Wang¹, Chuanzeng Zhang², ¹Institute of Engineering Mechanics, Beijing Jiaotong University, Beijing, China, People's Republic of, ²Department of Civil Engineering, University of Siegen, Siegen, Germany

Background, Motivation and Objective

In 1993, Kushwaha proposed the concept of phononic crystals (PNCs) for the first time. Since then significant effort has been devoted to the study of PNCs, which are periodic systems and exhibit acoustic band gaps. In recent years many results on defect states of the PNCs with point or line defects have been reported. However the study of the influence of random disorders on band structures and localization phenomenon of PNCs is yet very limited, although it is very important to the fabrication of wave filters which have an exact filtering frequency and hence an effective function to prohibit undesirable waves. In this paper, the influences of random disorders on band structures and localization phenomenon are studied for two-dimensional (2D) solid-solid PNCs with a point defect.

Statement of Contribution/Methods

The plane wave expansion method combined with the super-cell technique is used. As an example, we consider a PNC of a square lattice with a point defect and the PNC was made up of plumbum (scattering material) and epoxy (matrix material).

Results

The influences of the random disorders on the defect state and the first band gap of anti-plane wave mode of the PNC are investigated and the results are shown in Fig. 1 for the cases of the radius disorder (a) and the location disorder (b), respectively.

Discussion and Conclusions

From Fig. 1 it can be seen that the radius disorder has a more pronounced influence on the defect state and the width of the first band gap than the location disorder does.

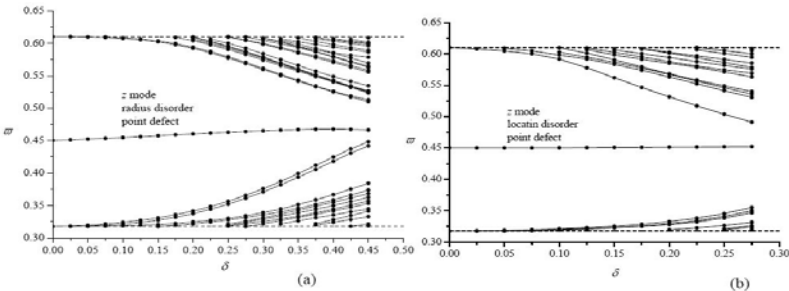


Fig. 1 The influences of the disorder degree on the defect state and the first band gap of the PNC with a point defect as well radius disorder (a) and location disorder (b), respectively.

Tuesday
Oral

6F-6

3:45 PM Negatively refracted transverse waves : study of the ultrasonic field at the exit of an elastic phononic crystal

bruno morvan¹, Anne-Christine Hladky-Hennion², jerôme vasseur², jean-philippe Groby², bertrand dubus², Alain Tinel¹, Bahram Djafari-Rouhani²; ¹LOMC-FRE CNRS 3102, France, ²IEMN-UMR 8520 CNRS, France

Background, Motivation and Objective

Research in the field of phononic crystals (PC) has undergone a rapid evolution in the last few years due to the interest for prospective applications like for example: superlensing effect, wave guiding, selective filtering and multiplexing devices. This work concerns the study of negative refraction of elastic waves that can occur in simple prism shape PC with an elastic matrix (periodic arrangement of holes in an elastic matrix).

Statement of Contribution/Methods

In a previous study [1] the authors have shown the negative refraction of an incident ultrasonic beam at an interface between the considered PC and a homogeneous medium. Despite the corrugation of the interface at the exit of the PC (periodic alignment of holes), the Snell's law gives a prediction of the angle of refraction of the transmitted ultrasonic beam. In order to better understand the negative refraction phenomenon that takes place at the interface between PC and the homogeneous surrounding medium, FEM calculations are performed. The displacements are studied along a direction parallel to the exit surface of the PC. An experimental study is also performed which allows to identify the refracted waves with negative refraction angles.

Results

At the exit interface of the prism shape PC, the incident wavefront is discontinuous because of the presence of the holes. The phenomenon of wavefront reconstruction after the PC is clearly shown. We define a "near-field distance" beyond which the wavenumber of the refracted wave is in good agreement with its theoretical value predicted from the band structure of the PC. Depending on the value of the angle of incidence and on the frequency, both a negatively refracted transverse wave and a positively refracted transverse wave are observed.

Discussion and Conclusions

The wave transmission through a Phononic crystal and more particularly the coupling between external plane waves and the Bloch waves inside the phononic crystals are detailed in this work. In the future, the role of the evanescent waves has to be considered in particular near the interface of the phononic crystal structure to progress towards the development of ultrasonic super lens.

[1] A.-C.Hladky-Hennion, J. O. Vasseur, B. Dubus, B. Djafari-Rouhani, D. Ekeom, B. Morvan, J. Applied Phys., 104, 064906 (2008).

Tuesday
Oral

1G. Therapy Microbubbles

Sala 1

Tuesday, September 22, 2009, 4:30 pm - 6:00 pm

Chair: **Kullervo Hynynen**
Univ. of Toronto

1G-1

4:30 PM **Change of cell membrane permeability by controlled microbubble cavitation**

Yun Zhou¹, Kun Yang¹, Jing Yong Ye¹, Cheri Deng¹; ¹*University of Michigan, USA*

Background, Motivation and Objective

Ultrasound induced microbubble cavitation has been exploited as a promising strategy to increase cell membrane permeability for intracellular drug and gene delivery. However, the detail process and mechanism have not been fully understood due to challenges in achieving controlled microbubble cavitation and real-time measurement of cell membrane permeability. This study developed techniques to study the change in cell membrane permeability affected by single bubble cavitation in a controlled fashion.

Statement of Contribution/Methods

To achieve controlled cavitation, a single bubble (15–20µm diameter) was generated and trapped stably a self-focused femtosecond (fs) laser beam, which was generated by a 250 KHz re-generatively amplified self-focused Ti:sapphire laser with an output duration of 100 fs and wavelength of 793 nm. A dual-frequency ultrasound transducer assembly (7 MHz and 1.5 MHz) was utilized to generate controlled cavitation by placing the bubble near the vicinity of cell membrane using the 7MHzpulses (10 KHz PRF, 1.5 MPa peak negative pressure) and to collapse the bubble at the desired position using the 1.5MHz exposure (one or multiple pulses at 9.68 MPa peak negative pressure). Microbubble dynamics were monitored by ultrasound imaging and high speed video microscopy with a fast frame camera. The transmembrane current (TMC) change obtained by whole cell voltage clamp techniques was used as a real-time membrane permeability assay using single *Xenopus* oocytes as a model system.

Results

Fast frame video microscopy revealed the dynamic bubble behavior such as microjetting and bubble collapsing near the cell membrane under different exposure conditions. Synchronized recordings from optical monitoring, acoustic backscatter signal and TMC obtained from our experiments relate the bubble cavitation with the change of cell membrane permeability. A total of 195 TMC measurements at two different pressures (9.68 & 11.14 MPa, peak negative pressure) showed how the acoustic pressure and microbubble-membrane distance affected cavitation and membrane permeability.

Discussion and Conclusions

By employing techniques for controlled bubble manipulation (such as trapping, displacement, and destruction) and real time assessment of cell membrane change, this study obtained quantitative results demonstrating the spatiotemporal process of a controlled single bubble cavitation and its effect on cell membrane sonoporation or ultrasound induced permeability change.

1G-2

4:45 PM **Acoustic Emissions Associated with Ultrasound Stimulated Microbubble Modulation of Tumor Blood Flow**

David Goertz¹, Raffi Karshafian², Kullervo Hynynen¹; ¹*Imaging Research, Sunnybrook Health Sciences Centre, Toronto, ON, Canada*, ²*Physics, Ryerson University, Toronto, ON, Canada*

Background, Motivation and Objective

We recently demonstrated the feasibility of using pulsed low intensity ultrasound (US) and microbubble (MB) to induce repetitive transient flow modulations in murine tumors over a period of 30 minutes, which were followed by

a sustained vascular shut-down. Notably, this was achieved at clinically viable agent doses. These effects may have implications for local drug delivery and potentiation. An understanding of MB behavior associated with these effects will be required to gain insight into mechanisms and to optimize insonation strategies. In this study we examine MB emissions associated with US exposures that induce flow-modifying effects in tumors.

Statement of Contribution/Methods

Subcutaneous murine tumors (PC3) were exposed to 1 MHz pulsed US (740 kPa) following a bolus injection of Definity MB (60 ul/kg). In previous experiments, the treatment exposure scheme consisted of a sequence of fifty 100 microsecond bursts sent at 1ms intervals, which was repeated at 20s intervals for 2 minutes following MB injection. These conditions produce a transient (<15 minute) flow shut-down, as indicated by 9 MHz contrast flow imaging. In this study, the primary insonation scheme was comprised of the above 2 minute treatment scheme followed by single sequence exposures transmitted at 15, 30, 45 and 60 minutes post-injection (n=4). The purpose of the latter insonations was to determine the longevity of cavitation sites available for treatment. In a second scheme, the 2 minute therapy sequences were omitted (n=2). Control experiments were conducted using a saline only injection (n=3). A broadband 580 kHz transducer was used as a passive cavitation detector, with inertial cavitation (IC) assumed to be associated with wideband signals, quantified between 0.7-0.8 MHz.

Results

IC and subharmonic (SH, 0.5 MHz) signals were detected during the treatment sequence following MB injection. For pulses within the 2 minute treatment period, similar levels of emissions were measured, with IC 38 dB above the noise floor. For the 15, 30, 45 and 60 minutes time points the IC values were, respectively, 35, 23, 12, and 0 db above the noise floor. In the case where the two-minute treatment sequence was omitted, comparable levels of IC were detected from 15-60 minutes. Contrast imaging performed during this time showed a peak in signal at 10-20s following MB injection, decaying by 12 dB at 2 minutes, with no agent detected by 15 minutes.

Discussion and Conclusions

This work has shown that both SH and IC signals are present under conditions that produce flow changes in tumors. An unexpected result was that significant IC signals could be induced for up to 45 minutes following an injection, indicating that populations of cavitation sites, the characteristics of which are unknown at present, remain either in general circulation or within the tumor. This suggests that insonation strategies might therefore be extended beyond the point at which agent is rendered undetectable with imaging.

1G-3

5:00 PM **Enhancement of ultrasonic heating with microbubbles and their localization in target tissue**

Shin-ichiro Umemura¹, Ken-ichi Kawabata², Rei Asami², Shin Yoshizawa¹, Yoichiro Matsumoto³, ¹Tohoku University, Aoba-ku, Japan, ²Hitachi Ltd., Aoba-ku, Japan, ³University of Tokyo, Aoba-ku, Japan

Background, Motivation and Objective

Ultrasound can form a well-localized focal spot, which provides great geometrical selectivity in therapeutic application. On the other hand, the smallness of the focal spot limits the throughput of the treatment. Sensitizing the target tissue to ultrasound may have potential to overcome this limitation.

Statement of Contribution/Methods

A microbubble, subjected to ultrasound at a frequency in the resonance range, converts the acoustic energy to heat through its volumetric oscillation [1]. If the microbubbles are distributed rather uniformly in the body, however, the significant portion of the ultrasonic power will be converted into heat in the intervening tissues before delivered to the ultrasonically focused target tissue. Recently two approaches have been proposed to selectively localize microbubbles in the target tissue: (i) an acoustic approach using pulse sequences to eliminate intervening microbubbles [3] and (ii) a biochemical approach using tissue selective nano-droplets whose phase changes with ultrasonic stimulation to produce microbubbles in situ [2].

[1] Umemura et al., IEEE Trans. UFFC, 52, 1690-1698 (2005).

[2] Kawabata et al., Jpn. J. Appl. Phys., 44(6B), 4448-4852 (2005).

[3] Utashiro et al., Proc. 14th Cavitation Symp. (in CD) (2009).

Results

The acoustic power converted to heat by a microbubble containing polyatomic gas through viscous heating was numerically calculated, and it was predicted that tissue ultrasonic absorption would be doubled if microbubbles are delivered to the tissue at a concentration in the order of 100 bubbles /mg. Exteriorized murine kidneys were

exposed to focused ultrasound at 3.2 MHz and the tissue temperature change was measured. Optison at a dose of 0.2 ml/kg multiplied the ultrasonically induced temperature elevation by several times [1]. In the approach (ii), nano-droplets containing mixture of two perfluoropentanes, with boiling temperatures around 30°C and 50°C were prepared. They were converted to microbubbles with a short ultrasound pulse with a few μ s duration at a few MPa and several MHz. They were also confirmed to selectively distribute in experimental tumors [2]. In the approach (i), it was demonstrated that the intervening microbubbles in a gel were eliminated with short ultrasound pulses with several μ s duration at a few MPa and 2 MHz [3].

Discussion and Conclusions

The localizing approach (i) can utilize both geometric and molecular selectivities of focused ultrasound and nano-droplets, respectively, for the treatment. This may be a great advantage over other non-invasive treatment methods. The approach (ii) does not have such synergistic selectivity, but no approval is needed before clinical application except for that of the instrument. Therefore, both approaches may be important for the future of focused ultrasound therapy.

1G-4

5:30 PM Ultrasonic delivery of a chemotherapeutic agent using Acoustic Droplet Vaporization (ADV)

Mario Fabilli¹, Ian Sebastian¹, Kevin Haworth¹, Oliver Kripfgans¹, Paul Carson¹, J. Brian Fowlkes¹; ¹University of Michigan, Ann Arbor, MI, USA

Background, Motivation and Objective

The phase-transitioning of micron-sized, superheated emulsions into gas bubbles using ultrasound (US), termed acoustic droplet vaporization (ADV), has been shown in vivo to selectively occlude blood flow to targeted organs. ADV also has the potential to be a localized drug delivery mechanism, while simultaneously reducing perfusion. This work focuses on the in vitro delivery of the chemotherapy drug chlorambucil (CHL) to Chinese hamster ovary (CHO) cells using ADV.

Statement of Contribution/Methods

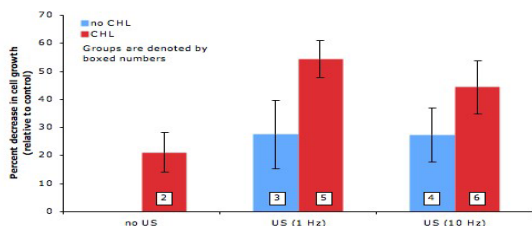
Emulsions were made using lipids, saline, perfluoropentane, and soybean oil – either with or without CHL. CHO cells were plated at $1.2 \cdot 10^4$ cells/cm² in OptiCell™ chambers (n = 24) 24 hours prior to treatment. The chambers were equally divided into six groups: (1) control of no droplets or US, (2) CHL droplets with no US, (3) sham droplets with US (1 Hz PRF), (4) sham droplets with US (10 Hz PRF), (5) CHL droplets with US (1 Hz PRF), and (6) CHL droplets with US (10 Hz PRF). A 10 MHz linear array (GE L9, contrast mode, MI = 0.9) was used to induce ADV across the chamber surface over one minute. The chambers were incubated for one-hour post treatment and then the medium was replaced following triplicate washings. The cells were allowed to grow for 48 hours post treatment. The cells in each chamber were trypsinized and counted using a Coulter counter.

Results

All groups were statistically distinct from control (1), with p-values <0.05, except (3) and (4). Relative to (1), the effect of CHL leaking from the emulsion (2) caused a mean decrease of 21% in cell growth, whereas the effect of US and CHL caused average decreases of 54% and 44% for (5) and (6), respectively. Comparing (2) versus (5) yields a p-value of < 0.01. The effect of ADV alone – (3) and (4) - caused an average decrease of 27% in both cases.

Discussion and Conclusions

The cytotoxicity enhancement using ADV to release CHL from the emulsions displays the potential of ADV-mediated drug release, especially for lipophilic agents like CHL. Relative to (2), a 33% and 23% decrease in cell growth was obtained for CHL with US at 1 Hz and 10 Hz, respectively. The cytotoxicity of ADV alone, (3) and (4), is statistically similar to the effect obtained from CHL leakage (2), thereby indicating that ADV can have an impact on cell growth. However, maximizing the drug load in the emulsion can increase the benefit of ADV-mediated drug delivery.



1G-5

5:45 PM **Controlled Cavitation for Controlled Release**Steve Wrenn¹; ¹Drexel University, Philadelphia, PA, USA**Background, Motivation and Objective**

Our objective is to develop a drug delivery technology that permits targeted and controlled drug release using ultrasound as a remote, mechanical trigger. Ultrasound-induced cavitation provides an On/Off switch for drug release, and the rate of drug release correlates with membrane phase behavior; the relative amounts of multiple phases determine the membrane permeability.

Statement of Contribution/Methods

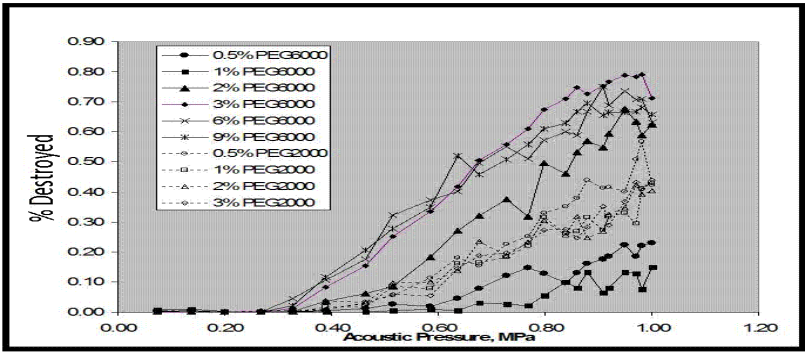
We have demonstrated that the experimentally measured cavitation threshold of a microbubble can be controlled in a systematic way by changes in the microbubble monolayer shell chemistry. This permits control over the extent of cavitation, which in turn facilitates control over the amount and rate of drug released. Moreover, we have shown that the rate of ultrasound-induced drug leakage also correlates with the number and size of small, insoluble domains present in multi-phase systems.

Results

Detailed results will be shared at the meeting concerning both measured cavitation thresholds (1) and measured leakage rates (2). Here are typical examples: 1) Increasing the mole fraction of PEGylated lipid in the microbubble shell from 1 mole% to 6 mole% decreases the inertial cavitation threshold from 0.62 MPa to 0.3 MPa and increases the fraction of microbubbles destroyed at 1 MPa from 15% to 70%. Similarly, decreasing the PEG molecular weight from 6000 to 2000 lowers the cavitation threshold to ~0.4 MPa and doubles the fraction of microbubbles destroyed. 2) In binary systems comprising the phospholipid DMPC and cholesterol, discontinuities in drug leakage are observed at cholesterol mole fractions of ~10% and ~30%, which coincide with phase boundaries for this system. Moreover, a minimum in leakage is observed at ~20% cholesterol, which corresponds to a maximal domain (and hence perimeter) size within the two-phase coexistence region. Similarly, a discontinuity exists at 26 mole% cholesterol in a ternary system comprising cholesterol plus equimolar amounts of the phospholipids DPPC and POPC; this coincides with a phase boundary marking entry into a single-phase region.

Discussion and Conclusions

Our results demonstrate that rational design of an ultrasound-based drug delivery vehicle, based on fundamental principles of colloid science, is feasible. The cavitation threshold can be set by simple changes in microbubble chemistry, and the rate of drug released can be further controlled by prescribing the number and size of domains present in a two-phase system.



Tuesday
Oral

2G. Tissue Characterization

Sala 2

Tuesday, September 22, 2009, 4:30 pm - 6:00 pm

Chair: **Michael Kolios**
Ryerson University

2G-1

4:30 PM **A Novel Technique for Measuring Ultrasound Backscatter from Single Micron-Sized Objects**

Omar Falou¹, Min Rui², Ahmed El Kaffas³, J. Carl Kumaradas², Michael Kolios^{1,2}; ¹*Dept. of Electrical and Computer Engineering, Ryerson University, Toronto, Ontario, Canada,* ²*Dept. of Physics, Ryerson University, Toronto, Ontario, Canada,* ³*Dept. of Medical Biophysics, University of Toronto, Toronto, Ontario, Canada*

Background, Motivation and Objective

The measurement of the ultrasound backscatter from individual micron-sized objects is required to gain an understanding of the behaviour of both weak (cells) and strong (contrast agents) scatterers for applications ranging from tissue characterization to molecular imaging. However, obtaining such a response remains a challenge. For instance, the presence of air bubbles in a suspension of cells during measurements of cell backscatter may lead to the incorrect interpretation of the backscattered signals. In addition, the size and shape of the single object that produces an ultrasound backscatter signal are critical input parameters to theoretical models, yet hard to be measured experimentally.

Statement of Contribution/Methods

In this work, a novel technique combining a Xenoworks microinjection system (Sutter, Inc., Los Angeles, CA) with co-registered Olympus IX71 inverted microscope (Olympus America, Inc., Center Valley, PA) and a VEVO770 Ultrasound imaging device (VisualSonics, Inc., Toronto, ON) was developed in which the ultrasound backscatter response from a single object was obtained under optical microscope guidance. This technique provides accurate information about the size and shape of the object. Two transducers of central frequencies of 25 and 55MHz were used (for a total spectrum of 12-58 MHz). The foci of the optical lens and the transducer were aligned to obtain optical and ultrasonic images of the same region. The object of interest was either maintained attached to the micropipette (using negative pressure) or initially attached and then released from the micropipette (using positive pressure) while imaging both optically and ultrasonically. In order to calibrate the system, a micropipette (inner and outer tip diameters of 1 μm and 3 μm , respectively) was used to grab a 20 μm polystyrene microsphere from a suspension of microspheres in de-ionized water by applying a pressure of -18.9 kPa. The microsphere was either held on the pipette tip or released by applying a pressure of +35.0 kPa. During the release, optical and ultrasonic raw RF lines (spaced 70 μm apart) were obtained. These lines were then used to obtain the power spectral plot of individual microspheres which were compared to analytical solutions.

Results

A very good agreement was found (error of 2%) between the measured backscatter response of microspheres and that of a Faran model of an elastic sphere. Extension of this method to prostate carcinoma (PC-3) cells showed a very good agreement (error of 5%) when compared to the Anderson fluid sphere model.

Discussion and Conclusions

This technique is capable of providing accurate measurements of the backscatter from individual objects and is currently being used to deduce the backscatter response from other cell lines of different sizes and from ultrasound contrast agents either in isolation or attached to a cell. The advantages of the technique along with its future applications are discussed.

Tuesday
Oral

2G-2

4:45 PM **Estimating Scatterer Properties in Rat Fibroadenomas Using Various Mathematical Form Factors**

Zachary T. Hafez¹, Lauren A. Wirtzfeld¹, Rita J. Miller¹, Sandhya Sarwate¹, Michael L. Oelze¹, Timothy J. Hall², William D. O'Brien Jr.^{1,2} *¹Electrical and Computer Engineering, University of Illinois, Urbana, Illinois, USA, ²Medical Physics, University of Wisconsin, Madison, Wisconsin, USA*

Background, Motivation and Objective

Quantitative ultrasound (QUS) imaging is a model-based approach aimed at lesion detection and classification. In this study, the RF backscattered signals from rat fibroadenomas were fit to various mathematical models to yield effective scatterer diameter (ESD) estimates which are tied to tissue microstructure. The goal of these experiments was to understand potential sources of scattering in live tissue across a wide frequency range and how results from different models compare to one another.

Statement of Contribution/Methods

The ESD was computed from the RF backscattered signals from Sprague Dawley rats with fibroadenoma tumors ranging in size from 1 to 6 cm in diameter. The tumors were scanned using three single-element transducers with center frequencies of 3.5, 7.5 and 13 MHz with a collective -10-dB frequency bandwidth of 1.4 to 18 MHz. A total of five parallel two-dimensional slices separated by 1 mm were acquired for each tumor. A reference scan for each transducer was acquired from a smooth Plexiglas plate. After scanning was complete, the rats were euthanized and the tumors were excised for histological classification and scatterer quantification. Theoretical models of scattering, i.e., form factors, were used to estimate the average ESD of all five slices of each tumor. Faran (considering solid spheres), fluid-filled sphere and spherical Gaussian form factors were used, allowing for a comparison between different models.

Results

Fourteen histologically confirmed fibroadenomas were included in the analysis. The ESD values calculated are for 3.5 MHz, 7.5 MHz, and 13 MHz respectively. The ESD values for the Faran form factor for all tumors were 159 $\mu\text{m} \pm 1 \mu\text{m}$ (mean \pm standard deviation), 98 $\mu\text{m} \pm 5 \mu\text{m}$, and 63 $\mu\text{m} \pm 4 \mu\text{m}$. The fluid filled sphere form factor ESD values were 206 $\mu\text{m} \pm 17 \mu\text{m}$, 115 $\mu\text{m} \pm 19 \mu\text{m}$ and 46 $\mu\text{m} \pm 14 \mu\text{m}$. The Gaussian form factor ESD values were 283 $\mu\text{m} \pm 27 \mu\text{m}$, 145 $\mu\text{m} \pm 19 \mu\text{m}$ and 50 $\mu\text{m} \pm 28 \mu\text{m}$.

Discussion and Conclusions

A trend of decreased ESD with increased frequency was observed for all three form factors, which fits with theory that the scattering at higher frequencies is due to smaller scatterers. The range of values obtained across the form factors and frequencies resulted in ESDs in the typical range of the acini of the rat fibroadenomas, which range in cross sections from 10s to 100s of micrometers. The high level of consistency in ESD estimates across the large number of tumors suggests that the analysis is able to lock in on a particular scale of structure within these tumors for each frequency. These specific size structures can then be correlated against the histological structures to aid in determining the ultrasound scattering sites for these tumors. This work was supported by NIH Grant R01CA111289.

2G-3

5:00 PM **Intrinsic Differences in Ultrasonic Backscatter Properties Between the Left and Right Ventricles of Fetal Hearts**

Mark Holland¹, Allyson Gibson¹, Joseph Hoffman¹, James Miller¹, Achiau Ludomirsky², Gautam Singh^{1,2} *¹Washington University in St. Louis, USA, ²New York University, USA*

Background, Motivation and Objective

It is thought that the cardiac chambers differ in their morphological and contractile properties from an early embryonic stage of development. We hypothesized that a non-invasive ultrasonic backscatter investigation might illustrate fundamental differences in myocardial properties of the two ventricles during heart development. The goals of this investigation were: 1) to measure the apparent level of backscatter from the left and right ventricular walls of excised, mid-gestational fetal pig hearts; 2) to measure the magnitude of the cyclic variation over the heart cycle of ultrasonic backscatter from the left and right ventricular free walls of mid-gestational fetal human hearts in utero; and 3) to determine if the observed cyclic variation of backscatter results are consistent with predictions relating overall backscatter levels and the magnitudes of cyclic variation.

Tuesday
Oral

Statement of Contribution/Methods

Broadband (30 to 60 MHz) integrated backscatter measurements were obtained from the left and right ventricular myocardium from 16 excised, formalin-fixed, mid-gestational fetal pig heart specimens using a 50-MHz single-element transducer measurement system. Separately, measurements of the magnitude of cyclic variation of backscatter from the left and right ventricular walls of the hearts of 16 structurally normal mid-gestational human fetuses were obtained from analyses of echocardiographic images obtained using a specially-configured commercial imaging system.

Results

For each of the 16 fetal pig hearts, the level of apparent integrated backscatter from the right ventricular myocardium was larger than that from the left ventricular myocardium exhibiting mean values of -35.9 ± 2.0 dB and -40.1 ± 1.9 dB (mean \pm SD; $p < 0.001$), respectively. For the human fetuses, the magnitude of cyclic variation of backscatter was found to be greater for the left ventricular free wall than for the right ventricular free wall (4.5 ± 1.1 dB vs. 2.3 ± 0.9 dB, respectively; mean \pm SD; $p < 0.0001$).

Discussion and Conclusions

Measurements of the level of apparent backscatter (fetal pigs) and cyclic variation of backscatter (human fetuses) demonstrate significant differences between the left and right ventricular myocardium. The measured results are consistent with previously described models relating overall backscatter levels and the magnitudes of cyclic variation that predict the magnitude of cyclic variation should decrease as the level of backscatter from the myocardium increases. Results of this study suggest cyclic variation measurements may offer a useful approach for characterizing intrinsic differences in myocardial properties of the two ventricles in assessing fetal heart development. [NIH R01 HL040302]

2G-4

5:15 PM *In vivo* ultrasound characterization of red blood cell aggregation using the Structure Factor Size and Attenuation Estimator

Emilie Franceschini¹, François T. H. Yu², François Destrempe², Guy Cloutier^{2,1} *Laboratory of Mechanics and Acoustics, LMA - CNRS UPR 7051, Marseille, France, ²Laboratory of Biorheology and Medical Ultrasonics, University of Montreal Hospital Research Center, Montreal, Quebec, Canada*

Background, Motivation and Objective

The ultrasound characterization of red blood cell (RBC) aggregation is an attractive tool to determine rheological blood flow disorders *in vivo* and *in situ*. The backscattered signals from blood can be spectrally analyzed to deduce the size and spatial distribution of RBC aggregates. One difficulty to apply this analysis *in vivo* is due to the frequency-dependent attenuation caused by intervening tissue layers that distorts the spectral content of backscattered echoes from blood microstructures. An optimization method was recently proposed to simultaneously estimate tissue attenuation and blood structure properties, and was termed the Structure Factor Size and Attenuation Estimator (SFSAE). With *in vitro* experiments, the method gave satisfactory estimates of attenuation and blood structure parameters with relative errors below 25%. The current work presents *in vivo* results to demonstrate the feasibility of the method.

Statement of Contribution/Methods

Measurements were performed on an arm's vein of a normal subject using an ultrasound scanner equipped with a 25 MHz center frequency probe. The probe was positioned in longitudinal view to examine three blood flow conditions: normal blood flow, stop flow with a proximal and distal constrictions of the region of interest, and finally complex flow in the vicinity of two closed venous valves. For each case, the aggregate diameter D , expressed in number of RBCs, the packing factor W and the total attenuation A were estimated by using the SFSAE, i.e. by comparing the spectrum of the backscattered radio-frequency echoes with newly developed models of RBC aggregate scattering.

Results

Quantitative ultrasound parametric images of D , W and A estimates were constructed. Table I summarizes mean parameters for the three blood flow conditions considered. For the two structural parameters D and W , statistically significant differences were observed between normal and stopped flow conditions, as well as between blood stagnation and circulation zones in the case of the two closed venous valves.

Discussion and Conclusions

To conclude, this work shows the SFSAE ability to estimate blood backscattering properties *in vivo* and *in situ*, and opens the way to parametric imaging for clinical studies in abnormal blood conditions.

Table I. Mean estimates of the aggregate diameter D expressed in number of RBCs, the packing factor W and the total attenuation A in dB cm/MHz for three blood flow conditions

	Normal blood flow	Stopped blood flow	Two closed venous valves	
			Circulation zone	Stagnation zone
D	1.61 ± 0.49	2.32 ± 1.03	1.09 ± 0.66	3.69 ± 0.81
W	0.91 ± 0.60	2.21 ± 1.11	0.86 ± 0.46	4.20 ± 1.34
A	0.209 ± 0.102	0.246 ± 0.105	0.342 ± 0.067	0.318 ± 0.036

2G-5

5:30 PM Implementation of scatterer size imaging on an ultrasonic breast tomography scanner

Roberto Lavarello¹, Michael Berggren², Steven Johnson², Michael Oelze^{1,†} *University of Illinois at Urbana-Champaign, USA, ²TechniScan Medical Systems, USA*

Background, Motivation and Objective

Quantitative ultrasound (QUS) techniques make use of frequency-dependent information from backscattered echoes normally discarded in conventional B-mode imaging. Using scattering models and spectral fit methods, properties of tissue microstructure can be estimated. The variance of QUS estimates is usually reduced by processing data obtained from a region of interest (ROI) whose dimensions are larger than the resolution cell of B-mode imaging, which limits the spatial resolution of the technique. The use of full angular (i.e., 360°) spatial compounding has been proposed as a means of improving the variance of scatterer property estimates and spatial resolution of QUS imaging. In this work, preliminary experimental results from a QUS implementation on an ultrasonic breast tomography scanner from TechniScan Medical Systems (TMS) are presented.

Statement of Contribution/Methods

The imaging target consisted of a cylindrical gelatin phantom of 7.8 cm diameter. The phantom contained uniformly distributed glass bead inclusions of 85 μm mean diameter. The TMS scanner provided reflection-mode data using arrays with 6 MHz nominal center frequency for 17 different angles of view distributed between 0 and 360°. Tomographic images of speed of sound were also generated by the TMS scanner and used for refraction-compensation and registration of the effective scatterer diameter (ESD) estimates corresponding to ROIs at different angles of view. The ESD estimates were obtained using the -9-dB bandwidth of the reflection-mode arrays. Only data from the surface of the array to the center of the tomography gantry were analyzed for each angle of view, which resulted in 8.5 effective angles of view per ROI.

Results

ESD estimates were obtained using ROIs of size 4 mm by 4 mm with a 50% overlap. The average mean and standard deviation of the single angle of view estimates considering the 17 data sets were 85.4 μm and 12.2 μm , respectively. The compounded QUS image was obtained by averaging the single angle of view ESD estimates from registered ROIs after discarding the two most significant outliers when compared to the median ESD estimate per pixel. The resulting ESD mean and standard deviation of the compounded image were 85.4 μm and 4.3 μm , respectively. The improvement in standard deviation by a factor of 2.8 agrees very well with the theoretical expected value of approximately 2.9.

Discussion and Conclusions

The preliminary experimental results presented here represent the first implementation of QUS on an ultrasonic breast tomography scanner and demonstrate some of the benefits of integrating these technologies, i.e., the availability of full angular spatial compounding and integration with tomographic speed of sound images. This method finds direct applicability for breast tissue characterization, for which full angular coverage is available. This work was supported by NIH grant R43CA12152.

2G-6

5:45 PM **Analysis of human fibroadenomas using three-dimensional impedance maps**

Michael King¹, Josephine Harter², Sandhya Sarwate³, Michael L. Oelze¹, James A. Zagzebski⁴, Timothy J. Hall⁴, **William D. O'Brien, Jr.**¹; ¹*Department of Electrical and Computer Engineering, University of Illinois at Urbana-Champaign, USA.* ²*Department of Pathology and Laboratory Medicine, University of Wisconsin-Madison, USA.* ³*Department of Pathology, University of Illinois at Urbana-Champaign, USA.* ⁴*Department of Medical Physics, University of Wisconsin-Madison, USA*

Background, Motivation and Objective

Three-dimensional acoustic tissue models are a unique means to study ultrasonic scattering by tissue microstructure. These models, called three-dimensional impedance maps (3DZMs), are created from serial sets of histological images which must be properly transformed to recreate the original tissue volume. A properly reconstructed 3DZM can then be used to estimate properties, such as the effective scatterer size, of the ultrasonic scattering sites in the underlying tissue. These estimates can, in turn, be empirically related to histological features of the tissue.

Statement of Contribution/Methods

In this work, previously developed 3DZM creation techniques were used to create 3DZMs from 10 sets of human fibroadenoma (a benign tumor of the breast) data. Each set of tissue data was used to create one or more 3DZMs with dimensions of 300x300x300 μm (650x650 pixels per slice, 100 slices). These volumes were then used to compute estimates of effective scatterer diameter using the fluid-filled sphere form factor. Estimates were made using the entire 300x300x300 μm volume as the analysis volume. Additionally, estimates were made from the volumes generated by dividing each volume into eight 150x150x150 μm volumes.

Results

For the set of 10 fibroadenoma 3DZMs, the effective scatterer diameter was estimated to be $84 \pm 40 \mu\text{m}$ when the entire volume was used for analysis and $70 \pm 30 \mu\text{m}$ when each volume was divided into 150x150x150 μm volumes for analysis. This result compared roughly to the size of the acini in the tissue, although a wide variation was observed in the histological layout of the tissue.

Discussion and Conclusions

This work demonstrates the application of 3DZM techniques to the analysis of scattering in a particular type of human tissue. This work was limited by the lack of other measurements (e.g., ultrasonic measurements) made on the tissue volumes from which the 3DZMs were ultimately produced; however, even with only the image data and the resulting 3DZMs, interesting results were obtained. This work was supported by NIH Grant CA111289.

Tuesday
Oral

3G. Cancer Imaging

Sala 4

Tuesday, September 22, 2009, 4:30 pm - 6:00 pm

Chair: **John Hossack**
Univ. of Virginia

3G-1

4:30 PM Performance of Three-Dimensional Sonoelastography in Prostate Cancer Detection: A Comparison between ex vivo and in vivo Experiments

Benjamin Castañeda¹, Karin Westesson², Liwei An³, Jorge Yao⁴, Laurie Baxter⁴, Jean Joseph⁵, Kenneth Hoyt⁶, John Strang², Deborah Rubens², Kevin Parker³; ¹Seccion Electricidad y Electronica, Departamento de Ingenieria, Pontificia Universidad Catolica del Peru, Lima, Lima, Peru, ²Department of Imaging Science, University of Rochester Medical Center, USA, ³Department of Electrical and Computer Engineering, University of Rochester, USA, ⁴Department of Pathology, University of Rochester Medical Center, USA, ⁵Department of Urology, University of Rochester Medical Center, USA, ⁶Department of Radiology, University of Alabama, USA

Background, Motivation and Objective

Previous work in ex vivo prostate glands showed that sonoelastography is a promising imaging technique for tumor detection. This work evaluates the performance of 3D sonoelastography for prostate cancer detection in vivo and ex vivo and compares their performance.

Statement of Contribution/Methods

11 patients underwent a TRUS examination prior to their scheduled radical prostatectomy. External vibration was induced by a specially designed plate using 2 mechanical actuators, each driven by a low frequency harmonic signal between 70 and 140Hz. Sonoelastographic and US volumes were acquired. The same gland was received after surgery and embedded in a gelatin mold. An external piston was used to vibrate the embedded gland at low frequencies (chords composed of 105, 140, 175 and 210 Hz). A GE Logiq 9 US scanner was used in conjunction with a positioning device to acquire B-mode and sonoelastographic volumes. In both, in vivo and ex vivo experiments, the surface of the gland was segmented from the B-mode images and the tumors from sonoelastographic images. After imaging, the gland was step-sectioned following a whole-mount histological procedure. Cancer and BPH in the histological images were outlined by an expert pathologist. From these, a volume was reconstructed and registered to the US volumes using the surface of the gland as a marker. To assess detection performance, findings from the in vivo and ex vivo sonoelastography were compared in size and position to 3D pathology.

Results

1 case was discarded due to poor contact between the gland and transducer. In vivo sonoelastography detected 12 tumors. Their average diameter measured 7.4 ± 4 mm vs. 7.5 ± 3.5 mm in the histological volume. The smallest detected tumor had an estimated diameter of 3 mm. 12 other deficits were depicted by sonoelastography. 6 of them corresponded to BPH and the rest remained unexplained. 7 tumors were undetected with an average diameter of 3.8 ± 1.7 mm. Ex vivo sonoelastography found 18 deficits. 9 of these corresponded to cancerous masses, 4 to BPH nodules, and 5 were unexplained false positives. 5 tumors were missed entirely. The average diameter of the detected tumors was 7.2 ± 3.1 mm measured in sonoelastography vs. 7.5 ± 3.5 mm measured on histology. The minimum estimated diameter of a detected tumor was 2.5 mm. The undetected tumors measured in average 5.3 ± 3.2 mm in diameter. When only tumors over 4 mm in diameter (as measured on histology) are considered for the analysis, in vivo sonoelastography showed 83% accuracy, 91% sensitivity and 81% specificity, whereas ex vivo sonoelastography showed 82% accuracy, 75% sensitivity and 84% specificity.

Discussion and Conclusions

In vivo and ex vivo sonoelastography showed similar performance in prostate cancer detection (over 80% accuracy for tumors > 4 mm in diameter). These results are an improvement over B-mode, but are not yet sufficient to replace biopsy. However, in vivo sonoelastographic scanning may be useful to improve yield over blind biopsy.

3G-2

4:45 PM **Correlation Between SWEI and ARFI Image Findings in Ex Vivo Human Prostates**

Liang Zhai¹, John Madden², Vladimir Mouraviev², Thomas Polascik², Kathryn Nightingale^{2,1} *Duke University, USA, ²Duke University, USA*

Background, Motivation and Objective

We have previously reported using Acoustic Radiation Force Impulse (ARFI) imaging methods to visualize normal prostate zonal anatomy and pathologic processes in prostate specimens. ARFI images portray the central zone stiffer than other anatomic zones, and BPH can appear heterogeneous and softer than the peripheral zone. Since displacements in ARFI images depend on both the underlying tissue stiffness and the amplitude of acoustic radiation force, one question that arises is: how are the relative displacements in ARFI images related to the underlying tissue stiffness? In this study, co-registered 2D ARFI datasets (relative displacement images: sequences monitor displacement within the radiation force region of excitation (ROE)) and shear wave elasticity imaging (SWEI) datasets (quantitative stiffness images: sequences monitor shear wave propagation outside of the ROE) were acquired from excised prostate specimens in order to evaluate the correlation between ARFI relative displacement images and local shear wave speed estimates, and to quantify the stiffness of prostate structures.

Statement of Contribution/Methods

4 prostate specimens were obtained immediately after radical prostatectomy, and imaged in an isotonic saline bath at room temperature with a modified AntaresTM scanner and VF10-5 array. In ARFI (F/#1.5) and SWEI (F/#2.0) sequences, push beams had a focal depth 15 mm, center frequency 5.7 MHz and duration 52 us, and were interspersed with tracking beams. Utilizing 4:1 parallel receive, displacements were tracked simultaneously at 4 lateral locations with a PRF of 9.5 kHz. In each axial/lateral ARFI imaging plane, 44 push and 176 track beams spanned a 26.4 mm FOV; SWEI sequences spanned this FOV with 4 push locations spaced 6.6 mm apart. 50 imaging planes were interrogated with 1 mm elevation spacing to interrogate the entire prostate. Tissue displacements were estimated using Loupas algorithm. Shear moduli were reconstructed using our previously reported Lateral-Time-To-Peak (LTTP) algorithm. Prostate zones and abnormalities were identified in ARFI images, and their shear moduli were determined from the corresponding SWEI data. ARFI findings were verified by comparison with histological sections analyzed by a pathologist blinded to the ARFI findings.

Results

ARFI images exhibit higher spatial resolution than the quantitative SWEI data. Depth-normalized ARFI displacements were inversely correlated with the reconstructed shear moduli ($\rho = 0.5$), consistent with the assumption that larger ARFI displacements are associated with more compliant tissues. The mean reconstructed shear moduli for the different structures identified in ARFI data (in n specimens) were: central zone (n=3): 11.7+/-3.9 kPa; peripheral zone (n=4): 5.4+/-1.5 kPa; BPH (n=3): 8.1+/-6.2 kPa; and prostate cancer (n=3): 19.1+/-4.4 kPa. These quantitative findings are consistent with other reports in the literatures.

Discussion and Conclusions

3G-3

5:00 PM **Prostate-cancer Imaging Using Machine-learning Classifiers: Potential Value for guiding Biopsies, Targeting Therapy, and Monitoring Treatment**

Ernest Feleppa¹, Mark Rondeau¹, Christopher Porter², Paul Lee¹; ¹Lizzi Center for Biomedical Engineering, *Riverside Research Institute, New York, NY, USA*, ²Urology, *Virginia Mason Medical Center, Seattle, WA, USA*

Background, Motivation and Objective

Prostate cancer (PCa) remains a major health concern in many countries. It is one of the few cancer types that cannot be imaged reliably by any commonly used imaging modality. As a consequence, ultrasound-guided needle biopsies are performed systematically with respect to overall gland anatomy, but blindly to PCa lesions, which causes a high false-negative rate. Advanced ultrasonic and magnetic-resonance methods are being investigated and show some promise for providing needed PCa-imaging reliability. Of the two modalities, inexpensive and rapid ultrasound would be the preferable modality if proven to be reliable. Our objective is to develop and test an ultrasonic method based on spectrum analysis of radio-frequency ultrasound echo signals and on classification using current machine-learning tools for reliably imaging PCa and thereby guiding biopsies, targeting therapy, and eventually, monitoring treatment of PCa.

Statement of Contribution/Methods

Radio-frequency (RF) data were acquired in the biopsy plane of 617 prostate biopsy cores obtained from 64 suspected prostate-cancer (PCa) patients. RF data were digitized and stored immediately before insertion of the biopsy needle, and spectral computations subsequently were performed in a region of interest that spatially matched the tissue-sampling location. Spectral-parameter estimates, level of serum prostate-specific antigen (PSA), histologically determined tissue-type of each biopsy, and level of suspicion (LOS) for PCa based on B-mode appearance at the biopsy site were recorded in a data base. Four non-linear classifiers were trained using these data: artificial neural networks (ANNs), logitboost algorithms (LBAs), support-vector machines (SVMs), and stacked-restrictive Boltzman machines (LBM). Cross-validation and leave-one-patient-out methods were employed to obtain tissue-category scores. Areas under ROC curves (AUCs) were used to assess classifier performance in comparison with LOS-based performance. Tissue-type images (TTIs) were generated using look up tables (LUTs) derived from these classifiers.

Results

AUCs for the ANN, LBA, SVM, and RBM respectively were 0.84 ± 0.02 , 0.87 ± 0.04 , 0.89 ± 0.04 , and 0.91 ± 0.04 . In comparison, the LOS-based AUC was 0.64 ± 0.03 . TTIs revealed subsequently histologically confirmed cancerous foci that were undetected prior to prostatectomy pathology.

Discussion and Conclusions

The ultrasonic imaging methods described here show significant potential for achieving needed reliability. The set of AUCs and generated TTIs imply that a clinically significant beneficial reduction in false-negative biopsy procedures would be possible if TTIs based on these methods were used to guide biopsies. Similar clinically significant benefits would result from using TTIs to target focal treatment and reduce toxic side effects. Potentially, such TTIs also could be used for assessing changes in tissue over time for surveillance or therapy monitoring.

3G-4

5:15 PM **Differentiation of solid benign and malignant breast masses by quantitative analysis of ultrasound images**

Chandra Sehgal¹, Phoebe Harvey², Peter Arger¹, Emily Conant¹:¹University of Pennsylvania, USA, ²University of Pennsylvania, USA

Background, Motivation and Objective

Although breast sonography is highly accurate at distinguishing solid from cystic lesions, it is less precise when differentiating benign and malignant masses. The goal of this study is to evaluate quantitative methods for differential diagnosis of solid breast masses.

Statement of Contribution/Methods

B-Mode imaging of the breast masses was performed in radial and antiradial planes of 207 patients with proven biopsy. Three margin features were extracted for each mass: margin brightness, margin sharpness, and angular variation. These features and age of the patient were used with logistic regression to classify the lesions as malignant or benign. Receiver-operating characteristic (ROC) analysis was performed to assess the diagnostic performance of each feature individually as well as collectively. In each case, classification performance was evaluated using a leave-one-out cross validation method. The robustness of the diagnostic algorithm was determined by studying effects of sample size and training level on the overall performance of the classifier.

Results

Of the 207 masses, 139 (67.1%) were benign and 68 (32.9%) were malignant. The average sizes of the benign and malignant masses were 12.5 ± 29 mm and 10.0 ± 6.0 mm, respectively. The difference was not significant ($p=0.33$). Margin brightness gave the highest ROC value ($Az = 0.77 \pm 0.04$), followed by age ($Az = 0.74 \pm 0.04$), sharpness ($Az = 0.68 \pm 0.04$), and angular variation ($Az = 0.61 \pm 0.04$). When all four features were used together, the ROC performance increased to $Az = 0.83 \pm 0.03$. With smaller samples (50 cases) chosen randomly from 207 cases such that malignant to benign ratio of 2:1 was maintained, the ROC area under the curve increased to 0.89. The area under the ROC curve increased progressively from 0.73 to 0.83 as the training:testing ratio was increased from 1:3 to 4:1.

Discussion and Conclusions

While there was no statistical difference in the size of benign and malignant lesions, their margin characteristics varied significantly, differentiating the two groups. The patients with malignant masses were older than those with

benign masses. This difference was significant and added to diagnostic performance. When all the features were used together, the probability of malignancy for the solid breast masses could be determined with ROC area ranging from 0.83 to 0.89. Diagnostic accuracy was notably influenced by the size of the database, relative distribution of malignant to benign ratio, and the training level of the algorithm.

Quantitative image analysis is a promising tool for clinical diagnosis of breast masses. Significant diagnostic performance can be attained using margin characteristics of the lesions and logistic regression classifiers. Further gains in diagnostic performance may be achieved by adding new features and classifiers to the analysis.

3G-5

5:30 PM Axial shear strain imaging for breast mass differentiation

Tommy Varghese¹, Min Rao², Haiyan Xu³, Sara Baker⁴, Amy Sommer⁵, Gale Sisney⁶, Timothy Hall⁷, Elizabeth Burnside⁸, ¹Medical Physics, University of Wisconsin-Madison, Madison, WI, USA, ²Swedish Cancer Institute, USA, ³Electrical Engineering, University of Wisconsin-Madison, USA, ⁴University of Wisconsin-Madison, USA, ⁵Medical Physics, University of Wisconsin-Madison, USA, ⁶Radiology, University of Wisconsin-Madison, USA

Background, Motivation and Objective

Breast cancer remains the second-leading cause of cancer deaths in women, and over 200,000 new cases of invasive breast cancer are expected in the USA this year. Promising data suggest that axial strain imaging has an important role in breast tissue classification. However, another important parameter, the shear strain has only recently been recognized as having great potential. We examine the feasibility of utilizing in-vivo axial shear strain imaging for differentiating benign from malignant breast masses.

Statement of Contribution/Methods

A VFX13-5 linear array transducer was utilized to acquire in-vivo radiofrequency echo data on 38 patients using a Siemens SONOLINE Antares real-time clinical scanner at the University of Wisconsin Breast Center. Free-hand palpation imaging with deformation up to 10% was utilized to acquire radiofrequency data loops to generate strain images. In this study, we report on 6 malignant tumors and 15 fibroadenomas to demonstrate the potential of shear strain imaging, compared to biopsy results that were considered the diagnostic standard. Axial strain and axial component of shear strain are estimated using an algorithm based on 2D cross-correlation. Areas of the axial-shear strain, normalized to the lesion size, applied strain and strain contrast was utilized for differentiating benign from malignant masses.

Results

Our results indicate that the normalized axial-shear strain area is significantly larger for malignant tumors when compared to benign fibroadenomas. Axial-shear strain pixel values greater than a specified threshold, including only those with correlation coefficient values greater than 0.75, were overlaid on the corresponding B-mode image to aid in diagnosis. Scatter plot of the normalized area feature demonstrate the feasibility of developing a linear classifier to differentiate benign from malignant masses.

Discussion and Conclusions

Our preliminary results demonstrate the potential to utilize axial-shear strain features to classify a tumor as benign or malignant for breast cancer imaging. Most of the malignant masses had normalized shear strain areas greater than 0.5, while for benign masses, the shear strain areas were lower than 0.4.

Acknowledgements: This work is supported by Komen Foundation Grant BCTR0601153.

3G-6

5:45 PM Derivation of a mean sound velocity in the female breast for artifact reduction in Full Angle Spatial Compounding

Christian Hansen¹, Nils Hüttebräuker¹, Markus Hollenhorst², Lothar Heuser², Gernot Schulte-Altendorfer², Helmut Erment¹, ¹Research Group High Frequency Engineering, Ruhr-University Bochum, Germany, ²Institute of Radiology, Neuroradiology and Nuclear Medicine, Ruhr-University Bochum, Germany

Background, Motivation and Objective

Full Angle Spatial Compounding (FASC: incoherent superposition of single ultrasound images (SUI) from aspect angles all around an object) yields an isotropic resolution and reduces speckle and artifacts. To apply FASC to

breast imaging, we developed an add-on system to a conventional ultrasound echo scanner. With this system the distribution of Speed of Sound (SoS) inside the breast can also be reconstructed using a reflector behind the breast. Next to diagnostics SoS-images are used to geometrically correct FASC-images and avoid artifacts. However, since attenuation in the breast and reflections on its boundary are high, the registration of the reflector and the SoS-reconstruction may fail. To still correct FASC-images, we developed an image based method to compute a mean SoS for the breast on the basis of a typical double-line artifact (Fig 1a).

Statement of Contribution/Methods

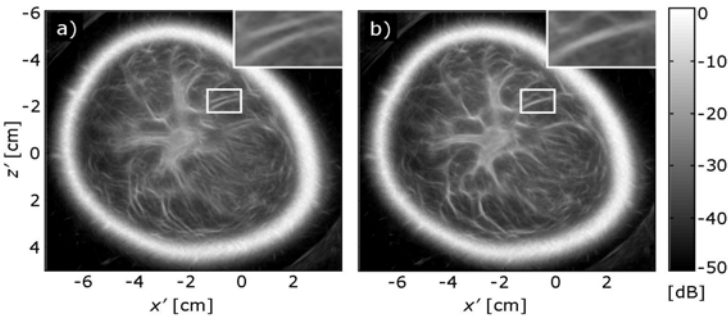
A low frequency curved array is automatically moved around a female breast in a water tank. From all aspect angles beamformed rf-data is acquired using a Siemens Acuson Antares. For a correction, A-lines of SUIs are aligned before superposition with respect to the transit time inside the breast and refraction at its boundary. A mean SoS of the breast is derived in two steps by inspecting an ROI with a double-line artifact: a) ROIs of all uncorrected SUIs are correlated with the ROI of an uncorrected FASC-image to find two SUIs that cause the artifact. b) For different SoS-values the corrected ROIs of these SUIs are superimposed and correlated with each other. The optimal SoS maximizes this correlation. Finally, all SUIs are corrected with the optimal SoS before FASC.

Results

We scanned female volunteers to evaluate our method. Fig 1 shows the uncorrected (a) and corrected (b) FASC-image of a healthy woman. Even in uncorrected FASC-images breasts are depicted in whole with a high isotropic resolution and structures inside are clearly visible. However, the correction by a mean SoS helped to reconstruct the correct geometry and to minimize the loss in resolution. The proposed method saved computation power and was time-efficient.

Discussion and Conclusions

In-vivo results show high potential of FASC for breast imaging. A geometric correction of FASC-images is necessary and can sufficiently be conducted using the mean SoS from the proposed method. Further clinical studies will evaluate FASC in comparison to mammography or MRI.



Tuesday
Oral

4G. Nanoscale Acoustic Sensing

Tarragona

Tuesday, September 22, 2009, 4:30 pm - 6:00 pm

Chair: **John Vetelino**
University of Maine

4G-1

4:30 PM **Carbon nanotubes applied to chemical and biological sensors**

F Xavier Rius^{1,2}: *Analytical and Organic Chemistry, University Rovira i Virgili, Tarragona, Catalonia, Spain*

Background, Motivation and Objective

Carbon nanotubes have been described as a revolutionary material. This adjective is based on the combination of different extraordinary properties displayed by this nanostructured allotropic form of carbon.

Among the distinct physical characteristics, carbon nanotubes (CNTs) exhibit outstanding mechanical tensile strength, very low density and electrical resistivity or very high thermal conductivity. Additionally, several features related to their chemical structure are also noticeable. The very high surface to volume ratio, together with the high adsorption ability of different species onto the sidewalls, makes nanotubes very appropriate sorbents useful in different methodologies. Their semiconducting or metallic character, the capacity to act as ion-to-electron transducers or as wavelength-specific markers, have been used to develop different mass, electrochemical or optical sensors.

Statement of Contribution/Methods

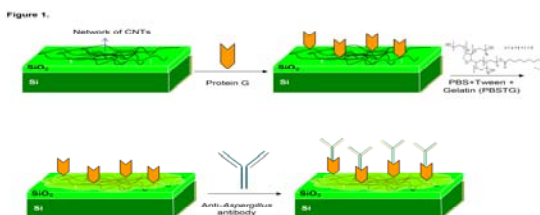
In this communication, I will review the main properties of carbon nanotubes and their relationship to the applications in different chemical sensors and biosensors. The sensing mechanism will be also revised and discussed.

Results

Field effect transistors based on networks of carbon nanotubes have been proven very useful to detect a whole range of species, from very low molecular mass gases to whole cells. Figure 1 shows an scheme of the deposition of carbon nanotubes onto a layer of SiO₂. Carbon nanotubes are further functionalized to incorporate the antibodies that will confer selectivity to the sensor.

Discussion and Conclusions

Ultrasonic sensors often utilize films deposited on the surface of the piezoelectric device to sense chemicals and biological analytes. Nanotubes have been used as coating in different devices and their treatment and deposition processes are well studied. This may give clues about the possibilities of using CNTs in the area of piezoelectric based sensing.



Tuesday
Oral

5:00 PM **Ultra-Thin AlN Contour-Mode Resonators for Sensing Applications**

Matteo Rinaldi¹, Chiara Zuniga¹, Gianluca Piazza¹; ¹Electrical and Systems Engineering, University of Pennsylvania, Philadelphia, PA, USA

Background, Motivation and Objective

Resonant sensors are required to operate in frequency ranges dictated by commercial standards. In available sensors, based on QCMs or FBARs, the operating frequency is related to the sensitivity of the device and the two parameters cannot be set independently. Differently, for AlN Contour-Mode resonators (CMR) the frequency of operation can be set lithographically, while the required value of sensitivity can be independently attained by scaling the thickness of the device. This paper reports on the design and experimental verification of a new class of ultra thin (250 nm) CMRs suitable for high sensitivity gravimetric sensors. In this first demonstration the frequency of the device is set to 180 MHz and sensitivity of 25 KHz*μm²/fg is achieved. This demonstrates the unique capability of CMRs to decouple resonance frequency from mass sensitivity. In addition, the advantage of measuring mass loading by monitoring device admittance at a fixed frequency is demonstrated and a 100X gain factor in sensitivity is achieved.

Statement of Contribution/Methods

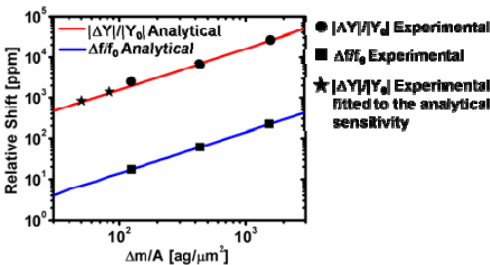
The sensitivity to mass per unit area for a CMR device is given by: $S=f_0/(2*\rho*T)$ (f_0 is the device frequency, ρ its density and T its thickness). This analytical expression is verified by exposing the fabricated device to different concentrations of methanol (4-50% vapor pressure) and extracting the variation of motional inductance ($\Delta L/L_0$) due to the mass (Δm) adsorbed on the gold surface. The fractional mass change is also measured by monitoring the admittance amplitude ($|\Delta Y|/|Y_0|$) at a fixed optimum frequency (inductive region between series and parallel resonances).

Results

The sensitivity to mass per unit area of the CMR is 25 KHz*μm²/fg in agreement with the theory. The relative frequency shift ($\Delta f/f_0$) is 0.14 ppm*μm²/ag, whereas the relative admittance amplitude shift ($|\Delta Y|/|Y_0|$) is instead 16.8 ppm*μm²/ag, showing a 100X gain in sensitivity. This gain translates experimentally into a better limit of detection down to 50 ag/μm².

Discussion and Conclusions

The capability of CMRs to increase the mass sensitivity by scaling the device thickness independently of the frequency is demonstrated and a 100X enhancement in sensitivity is attained by monitoring changes in the device admittance amplitude.



5:15 PM **170 MHz electrodeless quartz-crystal microbalance for high sensitive biosensors**

Hirotsugu Ogi¹, Hironao Nagai², Yuji Fukunishi², Masahiko Hira²; ¹Graduate School of Engineering Science, Osaka University, Toyonaka, Osaka, Jordan, ²Osaka University, Japan

Background, Motivation and Objective

Quartz crystal microbalance is a promising biosensor allowing the real-time monitoring of reaction between proteins through the change in the resonance frequency of the quartz-plate oscillator. Because it principally detects the mass adsorbed on the receptor immobilized on the oscillator surfaces, its sensitivity (the amount of the

frequency change) highly increases as the oscillator thickness decreases. Conventional QCM sensors, however, need heavy electrodes on both surfaces of the oscillator, deteriorating the sensitivity.

Statement of Contribution/Methods

We then develop a wireless-electrodeless method to excite and detect the shear vibrations of the naked quartz crystal using a flat antenna with the noncontacting manner, and achieve a high-frequency QCM system with the fundamental resonance frequency of 170 MHz. We demonstrate its high sensitivity and usefulness by applying it to the specific adsorption of human immunoglobulin G (hIgG) and *Staphylococcus aureus* protein A (SpA).

Results

Using the high nonspecific-adsorption ability of SpA on the naked quartz surfaces, we detected hIgG. (hIgG shows high specific adsorption ability with SpA.) The amount of the frequency decrease was beyond 60 kHz when 60 nM IgG solution was injected, showing much higher sensitivity than the conventional 5 or 10 MHz QCMs.

Discussion and Conclusions

The QCM sensitivity is proportional to the square of the fundamental resonance frequency, and the sensitivity of the 170 MHz QCM is estimated to be higher than the conventional 5 or 10 MHz QCM by ~ 1000 or ~ 300 , respectively. Furthermore, the electrodeless quartz crystal can use both surfaces as the active sensor regions, while the conventional QCM uses only one side for the sensing area. Thus, the high-frequency wireless-electrodeless QCM will contribute to the study of label-free interaction among bimolecular materials.

4G-4

5:30 PM The Electromagnetic Fields Radiated From a Monolithic Spiral Coil Acoustic Transduction Sensor

Donald McCann¹, John F Vetelino^{1,†}Laboratory for Surface Science and Technology, University of Maine, Orono, ME, USA

Background, Motivation and Objective

The monolithic spiral coil acoustic transduction (MSCAT) sensor platform is a novel bulk acoustic wave (BAW) device which is excited by a gold spiral coil antenna photolithographically deposited on one side of an AT-quartz wafer. The MSCAT platform can operate at very high frequencies by efficiently exciting high harmonic transverse shear modes (TSMs) with the application of a high frequency RF signal to the spiral coil. Since one surface of the MSCAT device is bare, this device can be used as a sensing platform upon which one deposits analyte selective chemical or biological films. The bare surface allows the detection of analyte induced mechanical (mass and viscoelasticity) and electrical (conductivity and dielectric constant) property changes in the film. Although previous work has shown that the MSCAT sensor is a highly sensitive sensor platform for chemical and biological analyte detection, the mechanism by which the spiral coil excites the TSM in the AT-quartz sensor substrate is not well understood. It is the purpose of the present work to develop the theory associated with the MSCAT sensor platform.

Statement of Contribution/Methods

Finite element analysis (FEA) was used to obtain the electromagnetic fields radiated by the spiral coil antenna deposited on AT-cut quartz. The theoretical results were compared to experimental measurements for specific spiral coil geometries.

Results

The spiral coil antenna was shown to produce electric fields that have components in both the lateral and thickness directions. These fields were responsible for exciting the TSM in the MSCAT sensor platform. Further, it was also shown that liquid properties on the sensor surface significantly alter the form of the radiated electric field. The relative magnitude of the electric field in the near field vary significantly dependent on operating frequency and the spiral coil geometry. The spiral coil geometry found to operate most efficiently at high frequencies consisted of 8 turns, 250 μm spacing, and 515 μm line widths and was shown to operate at 495 MHz (99th harmonic).

Discussion and Conclusions

A theoretical understanding of how the spiral coil antenna in an MSCAT sensor platform excites TSMs in AT-quartz has been developed. It was found that the spiral coil antenna produces electric fields in both the lateral direction and thickness direction which excite the TSM. It was also found that the spiral coil geometry has a

significant effect on the overall performance of the MSCAT sensor platform and that liquid properties on the sensor surface can significantly alter the form of the electric field radiated by the spiral coil.

4G-5

5:45 PM **Miniaturized Laser-Based Photoacoustic Sensor of Trace Gases**

Alexander Gorelik¹, Andrew Ulasevich¹, Vladimir Starovoitov^{1,1} *B.I.Stepanov Institute of Physics, NASB, Minsk, Belarus*

Background, Motivation and Objective

The miniaturized spectroscopic hardware is a promising field of application for the photoacoustic (PA) trace-gas detection technique powered by tunable infrared diode lasers. The principle of the technique is based on measuring the amplitude and phase for the acoustic pressure oscillation arising due to absorption of a modulated laser beam by molecules of gas inside a photoacoustic cell. The photoacoustic detection is realized with an enhanced sensitivity if the modulation frequency coincides with an acoustic resonance of the cell. Therefore, the modulation frequency should be correlated with the cell-resonator sizes: the frequency increases with reducing the sizes. Implementation of laser-beam modulation at ultrasonic frequencies ranged from tens kilohertz up to the submegahertz scale allows to reduce the cell sizes down to a few millimeters.

Statement of Contribution/Methods

In the report we discuss an approach to miniaturizing the resonant PA cell. The approach implies an optimization of design for the internal cell cavity in order to reduce the negative effect of parasite signals (the background due to absorption of the laser beam in the cell windows and the noise initiated by external acoustic disturbances), which can play a great role for the small-sized PA cells. The optimization is performed with the help of numerical simulation of the acoustic signals generated inside the cell.

Results

We analyze also our practical experience in the field and present optimized Brewster-windowed PA cells with the internal volume V from 30 to 500 mm³. A couple of our recent PA cells are shown in Figure. The left cell (ZnSe windows) has the internal volume $V \sim 500$ mm³ and clear aperture $d = 8$ mm. The right one (Ge windows) is a cell with $V \sim 80$ mm³ and $d = 4$ mm. Our tests testify to good performance for the cells. The threshold detectable absorption for the cells is $\sim 10^{-8}$ cm⁻¹ W Hz^{-0.5}. Such a millimeter-sized cell powered, for instance, by a minute DFB laser diode with a typical output power of ~ 20 mW will allow to detect trace gases at a sensitivity level, which can be attained by the absorption spectroscopy techniques along an optical path of 20 km.

Discussion and Conclusions



Tuesday
Oral

5G. Novel SAW Materials and Structures

Pergamo

Tuesday, September 22, 2009, 4:30 pm - 6:00 pm

Chair: **Mauricio Pereira da Cunha**
University of Maine

5G-1

4:30 PM Characterization of surface acoustic wave focusing by an annular interdigital transducer

Vincent Laude¹, Kimmo Kokkonen², Sarah Benchabane^{1,†} *Institut FEMTO-ST, Centre National de la Recherche Scientifique, Besancon, France,* ²*Optics and Molecular Materials Laboratory, Helsinki University of Technology, Helsinki, Finland*

Background, Motivation and Objective

The concept of annular interdigital transducer (AIDT) on a piezoelectric substrate has been introduced recently [1]. The fingers of the AIDT are curved to match the shape of the wave surface, in order to launch SAWs that form a focal spot at the center of the device. In the first demonstration of this principle [1], a clear focusing of SAW energy to a spot smaller than half a wavelength was observed. In this paper, we use a phase sensitive heterodyne interferometer [2] to further characterize the behavior and the formation of the focal spot as a function of frequency. These observations further allow us to identify possible shortcomings of our first design and to propose potential improvements.

Statement of Contribution/Methods

We study an AIDT on Y-cut lithium niobate, with an average acoustic wavelength of 50 μm . The device operation is characterized by measuring the vibration fields in the device at a number of frequencies. The whole aperture of the AIDT is scanned with a lateral step size of 5 μm , providing an overview of the device behavior. The center of the device is also scanned with a lateral step size of 2 μm in order to provide more detailed information of the wave behavior in the focal region. Animations computed from experimental data and showing the wave motion will be shown. 2D Fourier transforms are utilized to obtain the angular spectrum content of the acoustic displacement field, and hence, e.g., to characterize how uniformly the waves are excited.

Results

It is generally found that the AIDT generates a focal spot on a much wider bandwidth than the electrical response of the AIDT alone would indicate. The Fourier transforms of the acoustic displacement fields show that the angular spectrum content is given by the slowness curve for the SAW on the free surface times an emission factor that depends both on frequency and emission angle, and is governed by SAW transduction in the AIDT fingers. Once this emission factor is estimated, it is used to simulate numerically the AIDT by a superposition of all emitted plane waves. Simulations show that the frequency and angle dependence can be compensated for by the geometrical design of the AIDT in order to obtain the maximal displacement at the focus.

Discussion and Conclusions

The AIDT is a promising solution to obtain an acoustic point source on a surface, for instance for the probing or excitation of phononic crystal waveguides or for localized actuation in sensors and transducers. Due to anisotropy, proper design of an AIDT must accurately take into account both the transduction and the propagation of SAWs. These properties are represented by measurable angle- and frequency-dependent quantities, which provide feedback to refine simulation models and to further optimize device designs.

[1] V. Laude et al., Appl. Phys. Lett. 92, 094104 (2008).

[2] K. Kokkonen et al., Appl. Phys. Lett., 92, 063502 (2008).

5G-2

4:45 PM **An acoustic waveguide using doubly-bonded silicon/thinned PPT/silicon structures for RF applications**

Florent Bassignot¹, Roger Petit², Emilie Courjon¹, Gwenn Ulliac¹, Thierry Laroche¹, Julien Garcia¹, Samuel Queste¹, Jean-pierre Romand¹, Sylvain Ballandras^{1,1}*FEMTO-ST, France*, ²*CELAR, France*

Background, Motivation and Objective

Surface Acoustic Waves resonators may be used for the frequency stabilization of electrical oscillators until a few Gigahertz (GHz). In some cases, these resonators are limited by technical and compactness specifications imposed by radar applications. Consequently, passive components using guided acoustic waves are well-suited for such an application. Periodically poled transducers (PPTs) have been investigated recently as an alternative to classical inter-digital transducers for the excitation and detection of guided acoustic waves. We propose here a new compact structure allowing high frequency operation with a simplified package as the wave is trapped in a sandwich structure based on Si/LiNbO₃/Si material combination. We investigate the capability of such devices to answer the above specifications.

Statement of Contribution/Methods

We explain the PPTs fabrication principle and present experimental results on 3" and 4" LiNbO₃ and LiTaO₃ wafers. We then report theoretical analysis results of the PPT operation obtained, using our finite and boundary element simulation tool. Thanks to the analysis of the transducer dispersion properties providing the optimum operating points and the temperature coefficient of frequency (TCF) analysis, we have chosen the best combination Si/PPT/Si to fabricate test vehicles. Poled LiNbO₃ wafers are first bonded on silicon (Si) using Au/Au compression, then thinned down to a few dozen microns. The resulting stack is metalized to process a second wafer bonding on Si. These devices exhibit a 50 μm period, yielding operating frequencies near 80 MHz.

Results

We have pointed out the existence of elliptically polarized guided modes for various material combinations and technological parameters. We also have identified the possibility to excite partially guided longitudinally polarized waves. The control of the ferroelectric material thickness has been achieved (lapping and polishing). The comparison between theoretical and experimental TCF shows that we are able to accurately predict the thermo-elastic behavior of the material stack.

Discussion and Conclusions

Several devices have been successfully fabricated with different thicknesses and tested. As predicted, we have measured both contributions of elliptic and longitudinal modes near the expected contributions. Besides, we prove that the final device can be packaged easily in a low cost housing.

Acknowledgement : This work is supported by the Délégation Générale de l'Armement (DGA) under grant #0734020

5G-3

5:00 PM **fabrication of GHz range oscillators stabilized by nano-carbon-diamond-based surfcae acoustic resonators**

Roland Salu¹, Céline Gesset², Samuel Saada², Ventsislav Yantchev³, Badreddine Assouar¹, Fabien Bénédic¹, Philippe Bergonzo², Frank Omnes¹, Vincent Edon⁴, Denis Rémiens⁴, Omar ElMazria², Ilia Kartadjev³, Sylvain Ballandras¹; ¹*CNRS, France*, ²*CEA, France*, ³*Uppsala University, Sweden*, ⁴*Université de Valenciennes, France*, ⁵*Université de Nancy, France*

Background, Motivation and Objective

A significant amount of work has been performed to evaluate Diamond-like Carbon (DLC) films for the development of high frequency surface acoustic wave (SAW) devices for various Radio-Frequency (RF) applications. Major advantages of this material are its very high acoustic phase velocities. Its use for SAW applications, however, requires a piezoelectric overlay for wave excitation as well as detection. The quality of the final device using DLC films then is directly affected by the piezoelectric layer and the diamond as well. Until now, rather modest values of quality factors of SAW resonance on such layered substrates have been reported and only a few studies have been devoted to overcome the corresponding limitations.

Tuesday
Oral

Statement of Contribution/Methods

In this work, different research groups are collaborating to identify the capability of diamond-based substrates for the development of SAW resonators at 5 GHz and above, for use in high performance RF oscillators in that frequency range. Various combinations of materials are tested in this project in order to identify the best solution for the above-mentioned source application. Nano-crystal diamond (NCD) particularly is investigated in that matter, coupled with piezoelectric layers such as aluminum nitride (AlN), zinc oxide (ZnO) and lithium niobate (LiNbO₃). The different diamond films and piezo-layer deposition approaches are described and the main characteristics of each material are presented.

Results

Design of single and double port SAW resonators operating near 5GHz are reported. Experimental results are reported for SAW resonators built atop AlN/Diamond/Silicon, ZnO/Diamond and LiNbO₃/Diamond/Silicon substrates operating near 5 GHz and compared to theoretical predictions. We particularly emphasize the need for processing the so-called nucleation side as surface roughness appears a major issue for the fabrication of high quality SAW devices. The oscillator application is achieved using double port resonators built on ZnO/Diamond substrates. The oscillator principle is described and its phase noise measured and discussed.

Discussion and Conclusions

These results allow the identification the best material combination for the development of sources for direct frequency synthesis in the GHz range. Further, ways to improve device performance are identified. An objective comparison with the state-of-the-art is finally given.

This work is supported by the French Délégation Générale de l'Armement (DGA) under grant #636974 0680238016

5G-4

5:15 PM A New Photoimageable Epoxy as an Acoustic Absorber for IF Surface Wave Filter

Rodolfo Chang¹, Suzanne Combe¹, George Grama^{1,†} *TriQuint Semiconductor, Apopka, Florida, USA*

Background, Motivation and Objective

It is a well recognized practice to apply some sort of acoustic absorber material at the ends of the piezoelectric surface and also on certain portions of the metal transducers as well as the multi-strip coupler of an IF SAW filter. Most SAW companies use a family of rubber materials known as RTV or epoxy resins in either manual or automatic fashion for the suppression of unwanted acoustic energy, such as waves that reflect off the chip edges. One drawback of epoxy resins is that the method of application is very coarse, the material "bleeds out" expanding the required real estate. Another drawback is that the resin not only attenuates the wave but also causes strong reflections from the edge of the absorber itself degrading the pass band response therefore increasing the error vector magnitude (EVM) of the filter.

Statement of Contribution/Methods

In the past we have tried to use Photoimageable epoxy like Polyimide, as described in [1], but we found out the material is not very effective at frequency ranges of 70 to 350 MHz. TriQuint has developed and presented a new way of applying an epoxy based Photo-definable photo resist for the purpose of acoustic absorption of unwanted reflections present on the surface of a piezoelectric substrate. The Photo-Imageable-Epoxy (PIE), belongs to a family of epoxies which are commonly used in the semiconductor industry for IC and MEMS device.

[1] C.A Johnson et al., "Polyimide as an acoustic absorber for high frequency SAW applications", 1988 IEEE Ultrasonics symp. pp279-288

Results

With the help of a simple test mask, we measured the transmission capabilities of the new absorber (PIE) and compared with the standard SA absorber for 3 different frequencies ranges. We also compared the reflection capabilities of the new material with the standard SA absorber over 3 different operating temperatures for a real filter application

Discussion and Conclusions

The PIE was used for the first time as an absorber, and showed comparable Transmission capability as the current Screen Absorber (SA) method for frequencies higher than 150 MHz. The PIE exhibited lower reflectivity as compared to the SA, particularly over the cold temperature range. As a result, the Error Vector Magnitude (EVM) of an IF filter was improved from 3.3% to 2.1% at cold Temperature.

5G-5

5:30 PM Surface acoustic wave reflection characteristics of electrodes in ZnO/diamond structures

Ruyue Lee¹, Ruyen Ro¹, Yuan-Feng Chiang², Cha-Chi Sung², Sean Wu^{3,1}-I-Shou University, Taiwan, ²National Taiwan University, Taiwan, ³Tung-Fang Institute of Technology, Taiwan

Background, Motivation and Objective

Zinc oxide (ZnO) films were combined with diamond to be a composite surface acoustic wave (SAW) substrate showing high velocity and high coupling coefficient. In this study, Rayleigh SAW reflection characteristics of Cu or Al electrodes in (100) or (002) ZnO films on (111) diamond structures were analyzed using the finite element method (FEM). The extracted coupling-of-mode (COM) parameters were employed to design a dual mode SAW (DMS) filters for wideband code division multiple access (WCDMA) applications.

Statement of Contribution/Methods

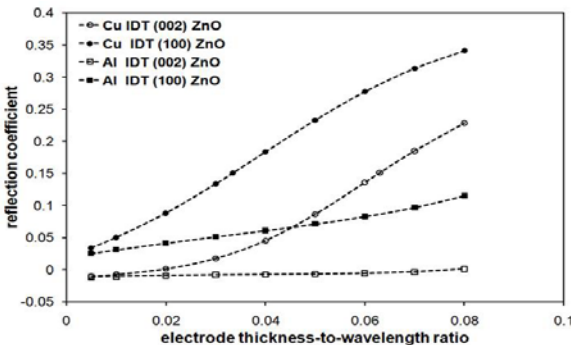
The resonance and anti-resonance frequencies obtained using the FEM are used to compute the effective phase velocity, coupling coefficient, and reflectivity of SAWs in IDT/ZnO/diamond structures with optimized films thickness-to-wavelength ratio and different electrode thickness-to-wavelength ratios. The extracted COM parameters are substituted into the transmission matrix method for the design of the DMS filter for WCDMA applications.

Results

SAW operating in the second mode, Sezawa mode, exhibits the highest coupling coefficient among the first five modes in the ZnO/diamond structures. The attached figure shows the SAW reflection characteristics of Cu or Al electrodes in (100) or (002) ZnO films on (111) diamond structures versus electrode thickness with optimized films thickness ratios for the Sezawa mode. With the optimized films thickness ratio ($h_f/\lambda = 0.44$) and Al electrode thickness ratio (h_e/λ) of 0.05, Sezawa mode in the IDT/(100) ZnO/(111) diamond structure possesses the phase velocity of 5438 m/s, coupling coefficient of 5.1%, and reflectivity of 0.071. The tailored DMS filter using these COM parameters yields a RF filter operating at 2140 MHz with 3 dB bandwidth of 80 MHz, insertion loss of 2.02 dB, shape factor of 1.17, and sideband suppression of 28.83 dB.

Discussion and Conclusions

SAW characteristics in (100) or (002) ZnO films on (111) diamond structures were analyzed using the FEM. The former structure exhibits better performances than the latter case. The use of Al IDT/(100) ZnO/(111) diamond structure to design the DMS filter applicable for WCDMA systems is also demonstrated.



Tuesday Oral

5G-6

5:45 PM **Quasi-Periodic Surface Green's Dyad of a Piezoelectric Half-Space**

Carlos Jerez-Hanckes¹, Vincent Laude²; ¹*Seminar for Applied Mathematics, ETH Zurich, Zurich, Switzerland,*
²*Département Micro Nano Sciences & Systèmes, Institut FEMTO-ST, Besançon, France*

Background, Motivation and Objective

Miniaturization of SAW IDTs has brought into attention many of the so-called transversal effects. However, typical FEM/BEM models neglect these phenomena by regarding wave propagation solely along the sagittal plane in order to reduce the number of unknowns. Recently, several achievements have been made towards a more comprehensive model: the computation of a 3-D surface piezoelectric Green's dyad for a single excitation; and, a hybrid boundary elements scheme that successfully copes with the electrodes's large length-to-width ratios. Unfortunately, these improvements are still insufficient to account for the large number of electrodes present in typical IDTs. Based on the agreement between periodic 2-D models and experiments, the present work seeks to compute a Green's dyad for a periodic excitation lying solely along the propagation direction.

Statement of Contribution/Methods

We present a complete treatment of the quasi-periodic 3-D surface Green's function. For this, we derive a Poisson's summation formula along one direction whose terms are based on the spectral single-excitation Green's function. For numerical stability, the latter is decomposed into: SAW single poles; asymptotic behaviors for large and small slownesses; and, a remaining regular part. Closed forms for the inverse Fourier transforms of the first two spectral terms require extensive use of complex and Fourier analysis as well as distribution theory techniques. Summation is carried out for each contribution, obtaining finite sums for all of them except for the asymptotic terms, whose divergent series has to be dealt with differently.

Results

Spectral SAW poles render plane waves as expected. Behavior at small speed -- large slowness -- is given by an infinite series of modified Bessel functions dependent on parity. Thus, logarithmic singularities show up for small longitudinal wave numbers as well as a fast oscillatory decay along transverse direction. Regular terms can be directly computed via FFT. First tests in the hybrid boundary element formulation for the isotropic case are consistent with theory.

Discussion and Conclusions

At the sagittal plane, new singularities -- periodically distributed -- arise from the quasi-periodic excitation, in accordance to previous 2-D models. The fast computation of near-field effects remains a challenge, though integral representations provide interesting approximations. Numerical results are quite promising for an attempt at a fast 3-D SAW IDT model.

Tuesday
Oral

6G. High Frequency Transducers & Arrays

Baalbek

Tuesday, September 22, 2009, 4:30 pm - 6:00 pm

Chair: **Geoff Lockwood**
Queen's University

6G-1

4:30 PM **Fabrication of 20 MHz Convex Array Transducers for High Frequency Ophthalmic Imaging**

Hyung Ham Kim¹, Jonathan Cannata¹, Jay Williams¹, Jin Ho Chang¹, K. Kirk Shung^{1,2} *Dept. of Biomedical Engineering, University of Southern California, Los Angeles, CA, USA*

Background, Motivation and Objective

Ophthalmic imaging is one of main applications of high frequency ultrasound. Especially, there has been an increasing demand for imaging the posterior segment of the eye to diagnose retinal disease. Most of currently available ophthalmic imaging systems employ single element transducers, which are mechanically translated to form sector-shaped images. The major drawback of this scanning technique is that it has a fairly low frame rate. B-scan is still the main mode of clinical diagnosis. We have proposed 20 MHz convex array transducers to make use of the benefit of arrays over single element transducers. This convex array is a linear array curved along the azimuth direction in a convex way to create a sector-shaped viewing area large enough to cover the entire eye in one image, and also curved in the elevation direction in a concave way for geometric focusing. This array allows for a higher frame rate with electronic translation, the creation of multiple focal zones with beamforming and dynamic aperture, the implementation of color flow mapping, and 3D imaging with add-on mechanical translation.

Statement of Contribution/Methods

20 MHz 192-element convex array transducers have been designed with 111 μm pitch, 24 mm radius of curvature, 52° maximum view angle, 7 mm elevation width and 30 mm geometric focus. A 32-element test array with 100 μm pitch has been fabricated and tested. A 1-3 composite with high dielectric piezoceramic and polymer was fabricated with a ceramic post width of 36 μm and a polymer kerf width of 14 μm . The ceramic volume fraction was approximately 60%. Two ceramic posts and a polymer kerf formed one element in the azimuth direction. A custom designed flexible circuit was aligned and attached to a scratch-diced composite and 75 Ω micro-coaxial cables were interconnected. A single matching layer and a backing medium were used for acoustic matching.

Results

All 32 elements of a fabricated test array were active without any short or open circuits. The pulse-echo response for a typical element acquired at the axial peak, 31.1 mm, matched with a designed geometrical focusing at 30 mm, had a center frequency of 20.0 MHz and approximately 60% of -6 dB fractional bandwidth. The estimated insertion loss at 20 MHz after compensating diffraction, attenuation and reflection was -20 dB and the maximum crosstalk was -17 dB and -22 dB for the nearest and for the next-nearest element respectively.

Discussion and Conclusions

The flexibility of the 1-3 composite with a matching layer allowed the acoustic stack to be conformed both in azimuth and elevation directions without misalignment or breakage. Since this test array has not yet been optimized in terms of piezoelectric material, thickness of flexible circuit, bonding tooling and matched coaxial cables, its sensitivity, crosstalk and temporal and spectral characteristics may be significantly improved. Full size, 192-element array prototypes following further modifications are underway now.

6G-2

4:45 PM **Functional Characterisation of High Frequency Arrays based on Micro-moulded 1-3 Piezocomposites**

Christine E.M. Demore¹, Anne L. Bernassau¹, Nigel Bush², Luis Garcia-Gancedo³, Florent Dauchy³, David Hutson¹, Tim W. Button³, Jeffrey C. Bamber², Sandy Cochran¹; ¹*Institute for Medical Science and Technology, University of Dundee, Dundee, United Kingdom*, ²*Joint Department of Physics, Institute of Cancer Research, Sutton, Surrey, United Kingdom*, ³*Functional Materials Group, University of Birmingham, Birmingham, United Kingdom*

Background, Motivation and Objective

High frequency (>30 MHz) ultrasonic transducer arrays are needed to improve high-resolution medical imaging in areas such as dermatology and ophthalmology by allowing electronic scanning, thus improving image quality compared to the single-element transducers now standard in such systems. Both fine-scale piezocomposite substrates and methods to define the array elements are required for sufficiently sensitive high-frequency arrays. Our approach is to use micro-moulded 1-3 piezocomposites as the substrate for photolithographically patterned array electrodes. These processes have the potential to extend the frequency range of imaging arrays towards 100 MHz. In this paper we report prototype fabrication and functional characterisation of linear arrays suitable for high frequency imaging.

Statement of Contribution/Methods

The fine-scale nature of the devices and the composite material requires new approaches to the problems of scaling down the size of ultrasonic arrays based on piezoelectric ceramics. A fully mask-based, scalable fabrication process beginning with ceramic powder, through to array interconnect, has been developed for high frequency transducer arrays. Micro-moulded piezocomposites were fabricated with 20 µm diameter pillars and 43% volume fraction ceramic, filled with an epoxy compatible with photolithography. 20-element linear arrays with 50 µm pitch (30 MHz) and 15 µm pitch (100 MHz) were patterned on the surface of piezocomposite coupons and lapped to 55 and 45 µm thickness respectively. Array electrodes were wired to electrical connectors, and the packaged devices were back filled with an unloaded epoxy. No matching layers were incorporated for initial functional testing. Electrical impedance and pulse-echo response of the arrays were measured.

Results

The electrodes show good definition and adhesion to the composite surface for both array patterns, and elements have a consistent electrical response. Typical electrical impedance of the 2 mm long elements of the lower frequency array, prior to adding an epoxy backing, is approximately 500 Ω at resonance and $k_{\text{eff}} = 0.4$. The reflected pulse for a typical element has a 200 ns pulse envelope and a 30% -6 dB fractional bandwidth about the 31 MHz centre frequency. Although the composite substrate was not optimised for the higher frequency array, the electrical impedance response indicates functionality, with a resonant frequency of 42 MHz, confirmed by pulse echo response measurements.

Discussion and Conclusions

The prototype devices reported here demonstrate the feasibility of high frequency arrays based on micro-moulded 1-3 piezocomposites for high resolution imaging. The fabrication processes developed for these arrays can be scaled for arrays operating at 100 MHz with the potential for small wafer-scale commercial fabrication. Functional testing indicates suitable performance for electronic scanning of tissue.

6G-3

5:00 PM **Piezoelectric Thin Films for a High Frequency Ultrasound Transducer with Integrated Electronics**

Flavio Griggio¹, Hyunsoo Kim², Insoo Kim³, Thomas Jackson², Kyusun Choi³, Richard Tutwiler⁴, Susan Trolier-McKinstry^{1,3}; ¹*Materials Science and Engineering, The Pennsylvania State University, USA*, ²*Center for Thin Film Devices and Department of Electrical Engineering, The Pennsylvania State University, USA*, ³*Computer Science and Engineering, The Pennsylvania State University, USA*, ⁴*Applied Research Laboratory, The Pennsylvania State University, University Park, USA*

Background, Motivation and Objective

High frequency ultrasound devices (50 MHz-1 GHz) can be used to image smaller organs or surfaces such as skin, the gastrointestinal tract, and intravascular imaging of blood vessels. Increased operation frequency and improved image resolution can be achieved adopting arrays of fine pitch piezoelectric elements as the resonating structures. However, as transducer size decreases, close-coupling of the electronics is necessary. We report here on the fabrication of linear arrays of PZT elements by thin film processing and micromachining techniques and testing of the device with a close coupled COMS chip.

Statement of Contribution/Methods

Chemical solution deposition was used to prepare PZT ($\text{PbZr}_{0.52}\text{Ti}_{0.48}\text{O}_3$) and PNN-PZT ($\text{PbNi}_{0.33}\text{Nb}_{0.66}\text{O}_3 - \text{PbZr}_{0.45}\text{Ti}_{0.55}\text{O}_3$) films. The PZT films were then integrated into prototype one dimensional array transducers. The geometry used for transducer arrays is a xylophone-bar type with a length width aspect ratio greater than 5:1 in order to isolate the desired length and width extensional modes. For this purpose, the PZT and remaining films in the stack were patterned using ion-beam etching and partially released from the underlying silicon substrate by XeF_2 etching. The fabricated device is packaged into a 16-pin ceramic package and tested.

A CMOS transceiver chip was fabricated in a standard 0.18 μm technology and prototyped for the ultrasound transducer. It contains 16 receive and transmit channels with preamplifiers, time-gain compensation amplifiers, a multiplexed 250 MHz 6 bit analog/digital converter with 4 Kbyte of FIFO buffers.

Results

It was found that dense, randomly oriented, pyrochlore – free PNN-PZT thin films show a dielectric constant as high as 1500, a remanent polarization of 20 $\mu\text{C}/\text{cm}^2$ and $\epsilon_{31,f}$ equal to -10.6 C/m^2 for thicknesses lower than 300 nm. The Curie temperature for the studied composition is 250 $^\circ\text{C}$.

Impedance measurements on the fabricated structures showed resonance frequencies between 3 and 70 MHz for fully and partially released structures depending on the transducer dimensions and vibration modes. In-water pulse-echo tests demonstrated transmit and receive functionalities. A bandwidth on receive of 66 % has been determined for partially released structures.

The receive channel bandwidth and gain of the CMOS chip are 100 MHz and 55 dB respectively.

Discussion and Conclusions

The tests performed on prototype transducers using the custom control chip show that the resulting PZT linear array is compatible with low-voltage CMOS (<3.3 V) and that the device could meet the sensitivity and bandwidth requirements for portable ultrasound imaging systems.

6G-4

5:15 PM **Electroacoustic performance of high frequency PZT based transducer fabricated by electrophoretic deposition: comparison with screen printing technique**

Guy Feuillard¹, Danjela Kuscer², Louis Pascal Tran-Huu-Hue¹, Emmanuel Le Clezio³, Marija Kosec², Marc Lethiecq³, ¹IC-CUP, ENIVL, Université François Rabelais, Blois, France, Metropolitan, ²Jožef Stefan Institute, Ljubljana, Slovenia, ³IC-CUP, Université François Rabelais, ENIVL, Blois, France, Metropolitan

Background, Motivation and Objective

The electrophoretic deposition process (EPD) is a fast and inexpensive method that requires simple equipment. It enables processing of thick films not only on flat but also on curved substrates in a wide range of thicknesses.

EPD is an alternative to the screen printing technique for the fabrication of PZT thick films. The objective of the work is to compare the functional properties of piezoelectric thick films fabricated by EPD and screen printing technique and to evaluate their impact on high frequency ultrasonic transducer performance.

Statement of Contribution/Methods

PZT PbO thick films were fabricated by EPD process. PZT and PbO particles, stabilized in ethanol using ammonium polyacrylate as a dispersant, have been deposited onto platinised Al_2O_3 substrate at constant current of 0.8 mA for 30 seconds. After sintering at 900 $^\circ$ and 950 $^\circ$ in PbO-rich atmosphere, 27 and 17 (for sintering at 950 $^\circ\text{C}$) micrometers thick PZT PbO films have been prepared. The structural properties of the films are reported. The electrical impedance of the integrated structure is measured and the functional properties are determined by adjusting the input parameters of the KLM electrical equivalent circuit to the experimental data. Electromechanical characterizations are compared to those of a PZT/PGO film fabricated by screen printing technique. The performance of a high frequency transducer based on these two types of thick films are then modeled and compared. The transducer consists in a thick film with electrodes deposited onto a porous PZT with an acoustical impedance of 20 MRayl.

Results

The films fabricated by EPD possess an effective density estimated at 7000 kg/m^3 while the films fabricated by screen printing technique have a density around 5800 kg/m^3 . The relative dielectric constant is 400 and the dielectric losses are around 2 %, the thickness coupling coefficient is 47 %. The effective acoustic impedance of the PZT PbO film is close to 30 MRayl.

Tuesday
Oral

Discussion and Conclusions

The potential of EPD for the fabrication of thick films for transducers is demonstrated. The measurements of the relative dielectric constant and loss tangent confirm the high densification of the films compared to those fabricated by screen printing technique. The effective properties of the PZT PbO films are closer to those of bulk PZT. When designing a transducer, benefit of this higher acoustical impedance compared to that of the backing results in a higher sensitivity of the transducer. The functional properties of PZT PbO films prepared by EPD process exhibit that they are interesting alternative for processing high frequency annular arrays transducers.

6G-5

5:30 PM 1-3 Piezocomposite Design Optimised for High Frequency Kerfless Transducer Arrays

Christine Demore¹, Luis Garcia-Gancedo², Florent Dauchy², Tim Button², Sandy Cochran¹, Jeff Bamber^{3,1} *Institute for Medical Science and Technology, University of Dundee, Dundee, United Kingdom, ²Functional Materials Group, University of Birmingham, Birmingham, United Kingdom, ³Joint Department of Physics, Institute of Cancer Research, Sutton, Surrey, United Kingdom*

Background, Motivation and Objective

Transducer arrays operating at frequencies above 30 MHz have been under investigation for some time because of their many potential biomedical imaging applications and improved image quality compared to the single element transducers presently in use. Very fine scale 1-3 piezocomposite material is required for such arrays, but its development has been limited by the geometrical limitations of dice-and-fill fabrication techniques. An alternative approach is to use micro-moulded piezocomposites. These offer particular advantages because of the small dimensions possible ($<10 \mu\text{m}$), and because the ceramic phase can be positioned within the polymer matrix wherever best suited for a particular device. In this paper we report composite design techniques and fabrication processes aimed at kerfless high frequency arrays with minimised interelement coupling for devices operating up to 100 MHz.

Statement of Contribution/Methods

Advances in micro-moulding techniques with improved ceramic slurries have been made, along with innovative approaches to composite design. Because kerfless array element electrodes are defined photolithographically on the surface of the composite, the design of the composite must take into account the array element geometry to minimize unwanted modes and maximize performance. Finite element analysis (FEA) has been crucial in the design of composite patterns that suppress spurious modes and are also suitable for micro-moulding. Composites with volume fractions up to 45% and with a variety of ceramic geometries have been fabricated using mask-based micro-moulding. Ceramic structures with height-to-width aspect ratios greater than 10 and dimensions suitable for high frequency operation have been made with sufficient green strength for de-moulding and sintering. Epoxy was used as the filler and after poling the composites were lapped and electroded for electrical impedance testing.

Results

A minimum separation of $4 \mu\text{m}$ between ceramic structures and a minimum ceramic width of $8 \mu\text{m}$ were achieved with micro-moulded composites. Electrical impedance measurements correspond to FEA of composite pattern vibration modes. Modeled composites with a specific distribution of ceramic dimensions within the range feasible for micro-moulding have been shown to have thickness mode mechanical resonance up to 95 MHz without significant lateral modes, and $k_T = 0.68$ for a composite with 40% volume fraction ceramic operating at 45 MHz.

Discussion and Conclusions

Micro-moulding has been shown to be suitable to fabricate unusual ceramic geometries for 1-3 piezocomposite material for high frequency kerfless transducer arrays. FEA has shown that spurious modes can be suppressed by using a distribution of ceramic geometries and dimensions. Thus the advantages of 1-3 piezocomposites can be gained, along with other beneficial properties, when device design is not limited by conventional fabrication techniques.

Tuesday
Oral

5:45 PM **Techniques for Wirebond Free Interconnection of Piezoelectric Ultrasound Arrays Operating Above 50 MHz**

Anne Bernassau¹, David Flynn², Farid Amalou², Marc Desmulliez², Sandy Cochran^{1,3} *¹Institute for Medical Science and Technology, University of Dundee, Dundee, United Kingdom, ²MicroSystems Engineering Centre, Heriot-Watt University, Edinburgh, United Kingdom*

Background, Motivation and Objective

Interconnects between high frequency ultrasound (HFUS) arrays and external circuitry are difficult and expensive because of the small element pitch, as low as 15 μm , and the large number of elements, up to 256. The wire bonding commonly used can be time consuming and also difficult to achieve on piezocomposite material because of the soft filler material. Also, the minimum pitch is limited by the need for the bonding head to be big enough to be visible. This requires creation of a fanout for frequencies above about 50 MHz, in turn increasing the size of the array package; this is disadvantageous for medical applications such as ophthalmology. This paper focuses on wirebond free interconnection for HFUS piezocomposite arrays operating at frequencies above 50 MHz. The suggested solution is integration of an ultrasound "chip" with a silicon (Si) wafer using state-of-the-art semiconductor industry fabrication techniques.

Statement of Contribution/Methods

The fabrication method involves flip-chip bonding a piezocomposite substrate to a Si wafer, on which tracks have been patterned and an aperture opened for a backing layer. Cr-Au tracks were prepared on the Si wafer with lift-off photolithography; the same process and materials were used for the array elements on the piezocomposite. Photoresist was patterned to define the growth of plated Au for the connection bumps for flip-chip bonding. The aperture through the Si for the backing layer was achieved by powder blasting with 9 - 30 μm alumina particles through a photosensitive mask. Bonding was achieved with a semiconductor industry flip-chip bonder operating at a low process temperature, compatible with the polymer matrix in the piezocomposite. Fabrication of through Si via (TSV) connections from the back of the Si have been investigated with both laser machining, using a high-repetition rate ns-pulse diode-pumped Nd:YVO₄ laser, and powder blasting.

Results

Electroplated gold bumps have been achieved with a height of about 6 μm , characterised with a surface profiler. Powder blasting has been shown to be efficient to create a 1 x 2 mm² aperture, the same size as the piezocomposite, in a 400 μm thick Si wafer, in less than 45 s. The piezocomposite was bonded to the Si die with anisotropic conductive film with a force parameter of 30 Kg, and arm and chuck temperature 180°C. For the TSV connections, powder blasting created holes tapered with the back opening 60% less than the front opening. By laser machining, the back dimensions were only 40% less than the front dimensions.

Discussion and Conclusions

External connections in conventional ultrasound arrays are achieved by dicing flex circuits. For high frequency arrays, wire bonding has been used, but this has major limitations. The work reported here has demonstrated techniques based on developments in the semiconductor industry that may reduce bonding cost, enhance reliability and allow small wafer-scale fabrication of arrays operating above 50 MHz.

Tuesday Poster Sessions

P2-A. Therapy: Monitoring, Control and Quality Assurance

Sala Orange

Tuesday, September 22, 2009, 10:00 am - 11:30 am

Chair: **Emad Ebbini**
Univ. of Minnesota

P2-A-01

Optimal monitoring of high intensity ultrasound therapy in the focal plane using backscattered pulse echo diagnostic ultrasound

Gavriel Speyer¹, Peter Kaczkowski¹, Andrew Brayman¹, Lawrence Crum¹, ¹*Applied Physics Laboratory, University of Washington, Seattle, WA, USA*

Background, Motivation and Objective

Pulse-echo diagnostic ultrasound (DU) is a recognized modality for identifying changes in temperature between captured frames. This technology is typified by using non-parametric estimates in which the relative displacements between regions in two ultrasound frames are associated with temperature differentials. The use of parametric modeling to relate the therapy delivered by high intensity focused ultrasound (HIFU) to the observed displacements between DU frames provides a means for bounding estimates, characterizing estimator performance, and identifying optimal estimators.

Statement of Contribution/Methods

We seek to both characterize the limitations of therapy monitoring and identify a means for attaining optimal performance for the special case of DU frames captured entirely in the focal plane of the HIFU transducer. To this end, the frames of ultrasound used for therapy monitoring are assumed to result from a known beam pattern modulated by an unknown source over a well defined interval. The motion in the focal plane is assumed known, as are the physical properties and manner of heat diffusion in the medium. By ascribing a statistical model to the measurement noise, the Cramer Rao bound is determined for coefficients in a functional expansion for the unknown time-varying heating. The functions in this expansion are identified from the analysis as the orthonormal basis providing independent coefficient estimates with minimum variance.

Results

Although heating is nonlinearly related to the distortion between DU frames, the performance of the optimal orthonormal basis functions for estimating heating can be shown to be fully characterized by a nominal operating point of applied heating. Not only have we identified tests for evaluating performance away from the nominal operating point, but both simulation and experiment confirm that the proposed set of basis functions attains the Cramer-Rao bound under nominal conditions, and either outperforms or remains characterized by this bound. We consider two primary cases of interest: lateral scans, in which the HIFU transducer moves parallel to the DU scanhead, and depth scans, in which the HIFU transducer moves perpendicular to the DU scanhead. The point scan is also considered, which is a special case of the other two when the position of the HIFU transducer is fixed. Analytic bounds are determined, and these are compared to simulation and experiment.

Discussion and Conclusions

A method for characterizing temperature and heating estimators using DU frames captured in the focal plane is presented. Estimators are proposed and analyzed, and these are shown to be fully characterized by the lower bound on the variance of coefficient estimates.

Tuesday
Poster

P2-A-02

Feasibility of a closed-loop controlled noninvasive ultrasonic glucose sensing and insulin delivery system

Nadine Smith¹, Eun-Joo Park², Jacob Werner³, Devina Jaiswal^{1,3} *Graduate Program in Acoustics, The Pennsylvania State University, University Park, PA, USA, ²Bioengineering, The Pennsylvania State University, University Park, PA, USA, ³Animal Resource Program and Department of Dairy and Animal Science, The Pennsylvania State University, University Park, PA, USA, ⁴Bioengineering, The Pennsylvania State University, University park, PA, USA*

Background, Motivation and Objective

To prevent complications in diabetes, the proper management of blood glucose levels is essential. Previously, ultrasonic transdermal methods using a light-weight cymbal transducer array has been studied for noninvasive methods of insulin delivery for Type-1 diabetes and glucose level monitoring. In this study, the ultrasound systems of insulin delivery and glucose sensing have been combined by a feedback controller. This study was designed to show the feasibility of the feedback controlled ultrasound system for the noninvasive glucose control. For perspective human application, in vivo experiments were performed on large animals that have a similar size to humans.

Statement of Contribution/Methods

Four in vivo experiments were performed using about 200 lbs pigs. The cymbal array of 3x3 pattern has been used for insulin delivery at 30 kHz with the special-peak temporal-peak intensity (Isptp) of 100 mW/cm². For glucose sensing, a 2x2 array was operated at 20 kHz with Isptp = 100 mW/cm². Based on the glucose level determined by biosensors after the ultrasound exposure, the ultrasound system for the insulin delivery was automatically operated. For comparison, the glucose levels of blood samples collected from the ear vein were measured by a commercial glucose meter.

Results

With a reference glucose level of 115 mg/dl, the ultrasound system for insulin delivery and glucose sensing was operated by the closed-loop, feedback controller. The glucose levels of four pigs were determined every 20 minutes and continuously controlled for 120 minutes. In comparison, the glucose levels determined by the biosensor were close to the levels measured by the commercial glucose meter.

Discussion and Conclusions

The results of in vivo experiments indicate the feasibility of the feedback controlled ultrasound system using the cymbal array for noninvasive glucose sensing and insulin delivery. Further studies on the extension of the glucose control will be continued for the effective method of glucose control.

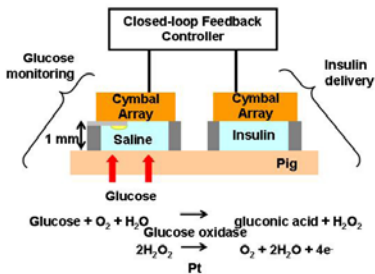


Figure1. The ultrasonic glucose sensing and insulin delivery system have been combined by a closed-loop feedback controller. The insulin delivery system was triggered by the results of glucose sensing.

P2-A-03

A Closed-loop System for Monitoring High Intensity Focused Ultrasound Treatment Based on Acoustic Backscattered Signal Processing

Xinliang Zheng¹, Shahram Vaezy¹; *¹Bioengineering, University of Washington, Seattle, WA, USA*

Background, Motivation and Objective

High Intensity Focused Ultrasound (HIFU) has been investigated for applications such as the treatment of tumor, internal bleeding and atrial fibrillation. However, a key problem is the lack of robust methods of treatment monitoring. One current technique is MRI that provides temperature mapping. However, this method is hindered

Tuesday
Poster

by its slow acquisition speed, MR-compatible HIFU device requirements, and high cost. These disadvantages can be overcome by ultrasound-based monitoring techniques. The objective of this study is to investigate the use of ultrasound radiofrequency (RF) signals in pre-treatment targeting, intra-treatment monitoring, and post-treatment evaluation of necrotic lesions formation in tissues.

Statement of Contribution/Methods

For targeting, sub-ablative HIFU intensity was first applied to ex-vivo chicken breast tissue, while collecting RF data. The region with the highest rate of increase in RF amplitude was found to indicate the focal region. The accuracy of the targeting was verified by comparing the estimated region with the location of hyperecho after HIFU treatment at ablative intensity, and also the location of the necrotic lesion in the tissue. During HIFU treatment, the correlation between RF data at the same location in two different frames with 5 seconds interval was calculated. The temporal change in the correlation coefficient during the exposure was quantified to study the time of lesion formation. The final step of lesion evaluation was performed by calculating the rate of decrease in RF amplitude after exposure. The region with the highest decreasing rate was found to localize the location of lesion, as verified by gross inspection.

Results

For targeting, the difference between predicted focus locations based on RF data and hyperecho was measured to be 1.92 ± 1.02 mm (mean \pm standard deviation), with no statistically significant difference. The anticipated time for lesion formation based on RF data was approximately 5 seconds earlier than the lesions visualized in sliced tissue. Comparing the locations of the necrotic lesions estimated from RF and those measured in tissue, the axial and lateral difference were 2.00 ± 2.31 mm and 0.85 ± 2.15 mm, respectively, with no statistically significant difference between lesion coordinates (axial: $p=0.37$ and lateral: $p=0.15$).

Discussion and Conclusions

We propose a novel technique based on RF data for monitoring of HIFU treatment. The feasibility of this method was demonstrated in ex vivo experiments. By integrating the three stages of targeting, intra- and post-treatment monitoring and evaluation, a closed-loop guidance and monitoring system could be developed. Although tested off line, the technique can be implemented in real-time. The proposed technique has a great potential to be used in HIFU treatment to improve the safety and efficacy of HIFU therapy.

P2-A-04

Unequal Heating Duration to Reduce The Treatment Time in High-Intensity Focused Ultrasound Therapy

Ji Xiang¹, Shen Guofeng¹, Bai Jingfeng¹, Chen Yazhu¹; ¹Shanghai Jiao Tong University, China, People's Republic of

Background, Motivation and Objective

Cooling periods are usually intervened between two consecutive sonications to avoid near-field heating during high-intensity focused ultrasound (HIFU) therapy, which leads to a long treatment time. A possible strategy to shorten the treatment time is to eliminate the cooling intervals. An unequal heating duration method without the cooling time is proposed to reduce the treatment time during HIFU.

Statement of Contribution/Methods

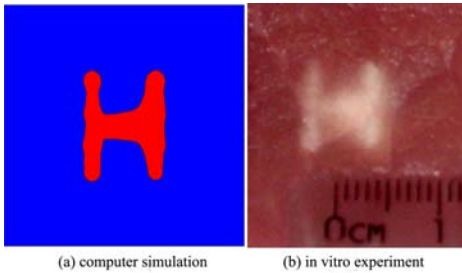
The starting focal point in the target region is set with the longest duration. Two unequal periods with a long-short pattern are prepared for two sequential focal points begun with that starting point; with the two points, the previous one is heated for a long duration while the latter is heated for a short duration. The durations for the rest focal points are set by analogy. If the distance between a point and its previous heated point is more than double focal spacings, it is set as a new starting point with a long heating period.

Results

Computer simulations and ex vivo experiments with the focus scanned by a 90-element spherical phased array had been carried out. An H-shaped lesion consisting of 17 single lesions about 2 mm in diameter was generated with a 2-mm focal spacing using the proposed method, and average time per point was reduced by 65% and 76% respectively in simulation and experiment. Moreover, in simulation 2 separate prefocal lesions (< 3 mm in diameter) were generated 2 mm proximal of the focal plane while no lesion was generated 5 mm proximal of the focal plane.

Discussion and Conclusions

The results demonstrated the proposed method was able to effectively shorten the treatment time by setting unequal heating durations for consecutive focal points and sparing the cooling interval through sonications. The results also indicated that it was promising to alleviate nontarget surrounding tissue damage in HIFU treatments by optimizing heating duration distributions of focal points.



P2-A-05

Characterisation of High Intensity Focused Ultrasound (HIFU) Lesions with Magnetic Resonance Imaging (MRI) at 7 T

Chaturika Jayadewa¹, Yann Jamin², James McLaughlan¹, Simon Walker-Samuel², Simon Robinson², Martin Leach², Gail ter Haar¹, Ian Rivens¹; ¹Joint Department of Physics, Institute of Cancer Research, Sutton, United Kingdom, ²CRUK and EPSRC Cancer Imaging Center, Institute of Cancer Research, Sutton, United Kingdom

Background, Motivation and Objective

HIFU treatment requires (i) target identification and treatment planning, (ii) acoustic energy delivery for conversion into heat and (iii) treatment monitoring. Clinically, ultrasound (US) imaging or MRI is used for (i) and (iii). Although not real time, T2 weighted (T2-w) and contrast enhanced T1-w MRI data (at 1.5 T) have shown better correlation with the size of HIFU damaged regions (lesions) than those from diagnostic US to date. Because of the current trend towards using higher clinical MR field strengths (3 & 7 T), this project uses high resolution MR (7 T) images of HIFU lesions in *ex vivo* bovine liver to assess whether quantitative MR parameters such as R2 (1/T2), R2* (1/T2*), and Apparent Diffusion Coefficient can be used to differentiate between lesions types.

Statement of Contribution/Methods

Three types of HIFU lesions (i) purely thermal ($\leq 320 \pm 32$ W/cm² for 180s), (ii) acoustic cavitation induced (790 ± 100 W/cm² for 6s) and (iii) those due to both acoustic cavitation and boiling (1000 ± 100 W/cm² for 4s) were created. Cavitation activity was monitored continuously during HIFU exposure (1.69 MHz, f number 1.79, focal length 15 cm, transducer) using, simultaneously, 1 and 10 MHz focused passive cavitation detectors, electrical drive power fluctuations and audible emissions. In brief, boiling lesions could be identified by the presence of both drive fluctuations and audio emissions, acoustic cavitation lesions were characterised by simultaneous broadband and half harmonic emissions, and purely thermal lesion formation resulted in the absence of all monitored indicators. MRI was performed at 7 T with a T2-w (SE, 12 echoes, TE 12-144ms, TR 3s), and T2*-w (MGE, 8 echoes, TE 6 – 28ms, TR 500ms) sequence.

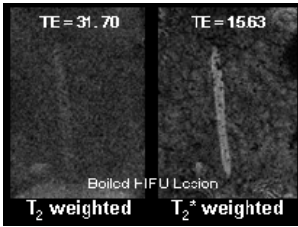
Results

Lesions were unexpectedly difficult to identify on T2-w images, but T2*-w images provided better lesion to normal tissue contrast, as shown in the figure. The parametric R2* map could not distinguish between the different lesion types.

Discussion and Conclusions

This study suggests that T2-w MRI is not as effective as T2*-w for the visualisation of HIFU lesions at higher field strength (7 T). The potential for diffusion weighted MRI to visualise these lesions is currently being investigated. The study will be repeated at a more clinically relevant field strength (1.5 T) for direct comparison with 7 T data.

Tuesday
Poster



P2-A-06

Photoacoustic thermometry for therapeutic hyperthermia

Parag Chitnis¹, James McLaughlan², Jonathan Mamou¹, Todd Murray², Ronald Roy^{2,1}, F. L. Lizzi Center for Biomedical Engineering, Riverside Research Institute, New York, NY, USA, ²Department of Mechanical Engineering, Boston University, Boston, MA, USA

Background, Motivation and Objective

Local hyperthermia is widely studied as a treatment option for small tumors. Hyperthermia results in tumor ablation when local temperature exceeds 56°C for 2 s. Our current work investigates the feasibility of exploiting the photoacoustic (PA) effect to monitor in situ temperature rise during high intensity focused ultrasound (HIFU) exposures.

Statement of Contribution/Methods

PolyAcrylamide phantoms with a cylindrical inclusion (3x20 mm) of graphite (0.01 g/ml) were heated using 30 s exposures from a 2 MHz HIFU transducer (focal distance 60 mm, aperture 70 mm). The transducer focus was aligned to the tip of a wire thermocouple (diameter 0.13 mm) embedded in the inclusion. A 532 nm laser (pulse duration 10 ns, PRF 10 Hz) was used to illuminate the inclusion. A 15 MHz broadband transducer (focal distance 19 mm, aperture 9 mm) was employed as a passive receiver (PR) to detect the PA response, which was an ultrasonic pulse emanating from the inclusion due to thermoelastic expansion induced by optical absorption. The native temperature and PR signals were recorded pre-, during-, and post-HIFU exposure. Singular-value-decomposition (SVD) was performed on the matrix consisting of the PR signals to extract temperature data. The eigenvector whose decomposition coefficients contained the most energy after low-pass filtering (i.e., discarding broadband cavitation and system noise) was selected. The temperature profile was obtained by linear fitting to the thermocouple data, and median filtering the decomposition coefficients on the selected eigenvector.

Results

HIFU intensities of 38 W/cm², 89 W/cm², and 169 W/cm² were employed with a 5 min between each run. The thermocouple measurements indicated a temperature increase from a baseline of 22°C to temperatures ranging from 45 to 55°C as shown by the black curve in Fig. 1. SVD-deduced temperatures shown by the blue, green, and red curves were obtained from the PA signals and correlated well with the thermocouple measurements (RMS error of 1 to 5°C). The net increase in temperature corresponded to a 20 to 30% increase in PA amplitude.

Discussion and Conclusions

The PA temperature-measurement technique was able to track heating and cooling phases over a range of temperatures characteristic of HIFU-induced hyperthermia. The dependence of PA amplitude on temperature can be described adequately using a linear fit.

Tuesday
Poster

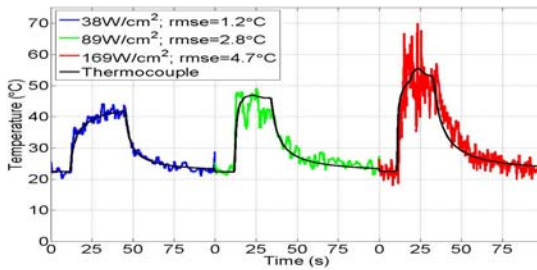


Figure 1. Temperature profiles obtained from the embedded thermocouple and the photoacoustic methods for three HIFU intensities.

P2-A-07

Temperature Estimation in HIFU with Lateral Speckle Tracking

Eunsul Baik¹, Jongbum Seo^{1,†} *Biomedical Engineering, Yonsei University, Wonju-si, Gangwon-do, Korea, Republic of*

Background, Motivation and Objective

High intensity focused ultrasound (HIFU) can induce thermal coagulation in cancerous tissue noninvasively. Thermal dose in tumor region should be elevated to a threshold so that tissue necrosis can be assured. The adequate increase of temperature and the duration is critical for the thermally induced damage. The aim of this study is to provide a model pertinent to temperature monitoring based on the ultrasound imaging for HIFU.

Statement of Contribution/Methods

The temperature estimation method based on the lateral speckle displacement tracking is proposed and tested in the presentation. A homogenous tissue with randomly distributed point scatterers and a linear thermal expansion model were used for this simulation study. The linear thermal expansion model indicated temperature rise of $2.78\text{Å}^{\circ}\text{C}$ induces $1\text{Å}/\text{m}$ lateral displacement of individual scatterer. To measure the lateral displacement in the focal zone of HIFU transducer precisely, we propose an algorithm using lateral speckle tracking technique with a specific spatial filter. A modified cross correlation algorithm with synthetic lateral phase is developed to reduce computation for real-time implementation. The size of the focal zone of HIFU transducer is used as prior information for the spatial averaging filter. In order to increase the accuracy in the lateral direction, both interpolation and interleaving are tested and analyzed.

Results

The average lateral tracking shows approximately 10% error with interleaving data compared to 30% error with/without interpolation data. These results imply that the increasing lateral spatial sampling rate is a critical parameter in the lateral speckle tracking. Standard deviations were reduced at least by a factor of 2 as a result of applying the spatial averaging filter. The simulated results indicated that the lateral tracking $1\text{-}5\text{Å}/\text{m}$ could be used for the temperature estimation. Since $1\text{-}5\text{Å}/\text{m}$ lateral displacement is equivalent to $2.78\text{-}13.9\text{Å}^{\circ}\text{C}$ changes in the temperature according to the linear thermal expansion model, the minimum resolution of temperature estimation is expected to be on the order of $3\text{Å}^{\circ}\text{C}$.

Discussion and Conclusions

The feasibility of a temperature estimation based on the lateral speckle tracking demonstrated. For the reduction of calculation time a modified algorithm is developed. The amount of computation is reduced by a factor of 8 with equivalent outcome. Considering the temperature monitoring targeting up to $65\text{-}70\text{Å}^{\circ}\text{C}$, the only three or four times of cross correlation will be required. Hence, the thermal dose calculation might be implemented almost real time during operation. The experimental verification is required in order to confirm this simulation research.

Tuesday
Poster

P2-A-08

Multi-Frequency Harmonics Technique for HIFU Tissue Treatment

Andrey Rybyanets¹, Andrey Nasedkin², Anastasia Rybyanets³, Maria Lugovaya³, Tomara Domashenkina^{1,1} *Institute of Physics, South Federal University, Russian Federation, ²South Federal University, Russian Federation, ³Physical Faculty, South Federal University, Russian Federation*

Background, Motivation and Objective

HIFU methods are extensively used to perform local therapeutic and/or surgical procedures on a patient's tissue. Various studies have indicated that efficacy of tissue lysis using HIFU can generally be enhanced by applying more than one frequency of ultrasound to the region. The objective of the present paper is development and experimental study of a new technique for enhancing of tissue lysis and enlarging treatment volume in during one HIFU sonification.

Statement of Contribution/Methods

New technique for enhancing of tissue lysis and enlarging treatment volume during one HIFU sonification is proposed. The technique consists in simultaneous or alternative (at optimal repetition frequency) excitation of single element HIFU transducer on a number of frequencies corresponding to odd natural harmonics of piezoceramic element. Calculation and FEM modeling of transducer vibrations and acoustic field patterns for different frequencies sets were performed. Acoustic pressure in focal plane was measured in water using calibrated hydrophone and 3D acoustic scanning system. In vitro experiments on different tissues and phantoms confirming the advantages of multi-frequency harmonic method were performed. In the experiments the HIFU transducer was excited simultaneously or sequentially on frequencies corresponding to 1st, 3rd and 5th harmonics at ultrasound energy levels sufficient for producing cavitation, thermal or mechanical damage of fat cells at each of aforementioned frequencies.

Results

Enhancement of the lysis was reached due to simultaneous or sequential influence of harmonic frequencies providing cavitation or mechanical lysis of tissue, formation of inhomogeneous ultrasound beam patterns with enhanced pressure gradients and shear deformations, and generation of difference and summary frequencies as a result of non linear parametric and radiation pressures interactions of main frequencies. Additional increase in lysis activity is provided by optimal repetition frequencies, bursts lengths and sonification times that correspond to specific resonance/relaxation times of cavitation "clouds" and/or tissues as well as natural body reaction times. The experimental results have also shown that at proper focusing and intensity levels the harmonics technique could further improve ultrasonically assisted transdermal drugs delivery mainly because of dynamical ultrasonic influence and inhomogeneous field pattern at the skin surface.

Discussion and Conclusions

Applications of multi-frequency harmonic technique for ultrasonic surgery, hyperthermia, therapy and body aesthetics were considered. The multi-frequency harmonic technique brings a new approach to accelerate treatment of big volumes of adipose tissue or tumors ablation with HIFU and also provides a miniaturization of the conventional HIFU transducers.

P2-A-09

Tissue Coagulation Imaging based on Bi-Plane RF Cross-Correlation during High Intensity Focused Ultrasound Therapy

Takashi Azuma¹, Ken-ichi Kawabata¹, Rei Asami¹, Shin-ichiro Umemura² *Hitachi CRL, Japan, ²Tohoku University, Japan*

Background, Motivation and Objective

Tissue expansion imaging based on echo time-shift detection is presented for monitoring high intensity focused ultrasound (HIFU) treatment. Echo-shift imaging can detect thermal reversible changes and irreversible changes caused by lesion formation. Since one of the most important purposes of monitoring is the visualization of the profile of the HIFU-treated region, we focused on detecting irreversible tissue change, especially tissue expansion after coagulation. A split HIFU method has good throughput, because coagulation size formed by one shot of the split HIFU beam is 1 cubic cm. In our previous study, tissue expansion during the split HIFU exposure was imaged by echo-shift between two consecutive frames. In this study, we used an orthogonal bi-plane imaging system with two linear arrays to discriminate volume change of tissue from other parameter changes.

Tuesday
Poster

Statement of Contribution/Methods

The experimental system as shown in fig.1 consisted of an 8-split-beam HIFU transducer, an EUB-8500 ultrasound scanner with two 9 MHz linear arrays, and a PC to store RF data. One imaging beam of the linear array A is parallel to the HIFU beam and the other imaging beam of the linear array B is perpendicular to the HIFU beam. An excised lobe of swine liver in a water tank was exposed to HIFU with frequency of 3.25 MHz. Echo-shift images were calculated on the basis of the cross-correlation between the RF data in two consecutive frames.

Results

The upstream part of the focal tissue moved toward to the array and the downstream part moved away from the array in both planes, which indicated that the observed echo time-shift was due to tissue expansion as shown in fig.2. The focal tissue gradually expanded upto about 12-15% in each direction. This expansion ratio is larger than that of thermal expansion by an order of magnitude. The HIFU-induced tissue expansion started suddenly at 6 s after the start of HIFU exposure and did not change when the exposure was stopped.

Discussion and Conclusions

This also suggests that the observed tissue expansion may have been caused by irreversible changes of the tissue. Since it is important to detect irreversible change at lesion to feedback to the next HIFU shot, bi-plane echo-shift imaging should be useful for detecting coagulation lesions.

Part of this work was supported by the New Energy and Industrial Technology Development Organization, Japan.

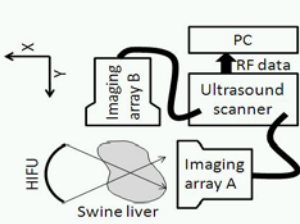


Fig.1 experimental setup

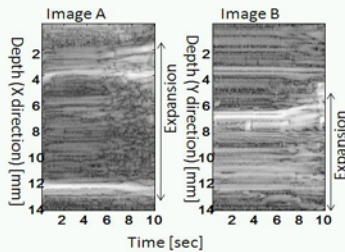


Fig.2 two M-mode image during HIFU

Tuesday
Poster

P2-A-10

Comparison of acoustic power calibration methods for therapeutic ultrasound transducers using PVDF membrane hydrophone, scanning laser vibrometry and radiation force measurements

Junho Song¹, Kullervo Hynynen^{1,2} *Sunnybrook Health Science Centre and Department of Medical Biophysics, University of Toronto, Toronto, ON, Canada*

Background, Motivation and Objective

Therapeutic high intensity focused ultrasound (HIFU) has been extensively investigated as a tumor treatment modality over the last several decades. Its potential has been shown in various applications for noninvasive cancer treatments. The understandings of the acoustic pressure field and power radiated from HIFU transducers are of great importance for the safety of the patients in clinical applications. A number of calibration methods are commonly used to investigate the characteristics of the HIFU transducers.

In this paper we compared the three common calibration methods for HIFU transducers: pvdf membrane hydrophone, “brush” target radiation force balance, and scanning laser vibrometer. The advantages and limitations of each calibration methods were studied at different frequency and acoustic power.

Statement of Contribution/Methods

Two spherically curved HIFU transducers (10-cm diameter, 8-cm focal length) were used in the experiments. The first transducer had the fundamental, 3rd, and 5th harmonic frequencies of 0.58, 1.74 and 2.85MHz, respectively. The second transducer had fundamental and 3rd harmonic frequencies of 0.56 and 1.69 MHz, respectively. The transducers were electrically matched to 50-Ohm load with a L-C matching network. A tone burst signal was used to drive the transducers.

An absolutely calibrated 25 um thick, bilaminar pvdf membrane hydrophone (GEC-Marconi, UK) was used to measure the acoustic pressure. It has the sensitivity of 0.046 uV/Pa and 7% uncertainty over the frequency range between 0 and 20 MHz. As the second calibration method, a constructed in-house 15-cm diameter “brush” target

radiation force balance was used to measure the time-averaged acoustic power. As the third method, scanning laser vibrometer (Polytec, USA) was used to measure the particle motion at the desired location. It measures vibration velocity from 0.02 um/s to 10 m/s in the frequency range between 0 Hz and 1.5 MHz, and the maximum displacement was ± 75 nm between 30 kHz and 24 MHz, respectively.

Results

Using the three calibration methods, the acoustic pressure/power amplitudes measurements had good agreement each other within a margin of 5% in the measurable acoustic power range. The hydrophone showed good signal-to-noise sensitivity and broadband dynamic range (e.g. 9.3 MPa at 2.85 MHz) while it was not able to measure very high acoustic pressure due to the safety of the system. The radiation force balance showed the highest measurable maximum acoustic power range in the experiment. The scanning laser vibrometer was the fastest calibration method than the other methods. It could measure the maximum acoustic pressure of approximately 20 MPa at 0.58 MHz.

Discussion and Conclusions

Three common calibration techniques for the HIFU transducers were investigated by the comparison of the acoustic pressure/power measurements. The difference showed lower than 5% in the measurable range.

P2-A-11

Function Approximations to Accelerate 3-D Beam Predictions for Thermal Dose Calculations

Dustin Kruse¹, Chun-Yen Lai¹, Katherine Ferrara¹; ¹*Biomedical Engineering, University of California at Davis, Davis, CA, USA*

Background, Motivation and Objective

Tissue heating with ultrasound has application to drug delivery for cancer therapy using thermally-sensitive drug carriers that release encapsulated contents between 39 and 42°C. Temperatures above 42°C maintained for long periods of time can cause protein unfolding, thermal tolerance and cell death. Robust and safe control of tissue heating requires predictions of beam location, temperature and thermal dose in order to optimize the spatial and temporal distribution of acoustic power. Our objective is to identify methods to speed up such computationally-intensive calculations. We will demonstrate the application of fast algorithms for the prediction of 3-D field and temperature distribution in pre-clinical studies.

Statement of Contribution/Methods

Here, we considered the monochromatic first Rayleigh-Sommerfeld solution, which relies heavily on complex exponentials. We have identified a fast approximation for the evaluation of a complex exponential using a reduced-complexity polynomial that minimizes absolute error to a maximum of 0.001, and we have quantified errors on beam intensity and total acoustic power (TAP) for a 64 physical element transducer array. The array was subdivided into 1024 mathematical elements, and the field was calculated in a 2-D plane consisting of 128x128 field points. The fast approximation was hand-coded in assembly using x86 vector instructions. We also compared the results obtained in Field II, MATLAB and compiled C code, in both single and double precision when possible.

Results

Table 1 shows calculation times and accuracies recorded for the codes tested. A 22x speed-up was obtained for the approximate calculation compared to the compiled C single precision algorithm, which is primarily a consequence of the fast approximation. The errors in the spatial intensity (0.43%) and TAP (0.094%) were larger for the fast approximation, yet remain relatively negligible for the purpose of calculating temperature rise.

Discussion and Conclusions

Since TAP is the more relevant quantity for thermal diffusion-limited heating, the small error of less than 0.1% indicates a better measure of the fast approximation compared to maximum intensity error. The fast approximation may be applied to other beam prediction methods. Here, we will apply these fast calculations to predict beam and heating profiles. (NIH: R01CA103828, 1R21EB009434)

Table 1. Computation times and accuracy*.

Computation	time (s)*	Intensity Error %	TAP Error %
Field II, #†, dp	21.7	n/a	n/a
R-S, Matlab, dp	4.99	ref	ref
R-S, Matlab, sp	4.98	1.3e-2	2.7e-5
R-S, compiled C, dp	3.49	1.3e-11	1.6e-14
R-S, compiled C, sp	3.43	1.6e-2	1.2e-5
R-S, x86 approx., sp	0.157	4.3e-1	9.4e-2
R-S: Rayleigh-Sommerfeld *Intel Duo P8400 @ 2.26 GHz †10% bandwidth ‡100 MHz sample rate			

P2-A-12

Use of quantitative ultrasound to detect temperature variations in biological phantoms due to heating

Goutam Ghoshal¹, Michael Oelze^{1, †}, ¹Department of Electrical and Computer Engineering, University of Illinois at Urbana-Champaign, USA

Background, Motivation and Objective

High intensity focused ultrasound (HIFU) is a noninvasive technique that has great potential for improving thermal therapies. To target specified regions accurately for treatment, a robust imaging technique is required to monitor HIFU application. Therefore, the development of an ultrasonic imaging technique for monitoring HIFU treatment is highly medically significant. Quantitative ultrasound (QUS) is a novel imaging technique that may improve monitoring of HIFU treatment by quantifying tissue changes.

Statement of Contribution/Methods

Two types of phantoms were constructed and examined using ultrasound versus increases in temperature from 37 to 50°C in 1°C increments. The phantoms were biological phantoms made of agar and containing either 4T1 mouse carcinoma cells or CHO cells as scatterers. All scatterers were uniformly distributed spatially throughout the phantoms. Sound speed and attenuation were measured in the phantoms versus temperature through insertion loss methods. Two parameters were estimated from the backscatter coefficient (effective scatterer diameter (ESD) and effective acoustic concentration (EAC)) and two parameters were estimated from the envelope statistics (k parameter and μ parameter) of the backscattered echoes versus temperature. Spectral estimates were based on a fluid-filled sphere model and envelope parameters were estimated using the homodyned K distribution.

Results

The estimates of sound speed increased monotonically in both phantoms from 1520 to 1570 m/s with increases in temperature. With increases in temperature the attenuation coefficient was observed to decrease by 0.03-0.04 dB/cm/MHz in both phantoms. No significant variations in the ESD were observed over the temperature range for the 4T1 and CHO phantoms. However, the EAC for 4T1 phantom was observed to decrease from -1.0 dB/mm³ to -2.1 dB/mm³, and for CHO the EAC decreased from -0.5 dB/mm³ to -4.8 dB/mm³. In the CHO phantom the k parameter was observed to increase from 0.35 at 37°C to 0.72 at 50°C. The k parameter for 4T1 did not show significant variations with increase in temperature. The μ parameter for the 4T1 phantom increased from 0.28 at 37°C to 0.43 at 50°C. No significant trends in the μ parameter were observed in the CHO phantom versus temperature.

Discussion and Conclusions

Ultrasonic backscatter experiments were performed on two types of phantoms to understand the variations in QUS parameters with increases in temperature. From the results it was observed that some parameters were more sensitive to temperature changes than the others for a particular type of sample. The results of this study suggest that QUS has the potential to be used for noninvasive monitoring of temperature changes in tissues. This work is supported by NIH R01-EB008992.

Tuesday
Poster

Improved Exosimetry on Diagnostic Ultrasound Equipment Using Broadband Pulse Deconvolution: Assessment for Five Different Hydrophones

Volker Wilkens¹, Hans-Peter Reimann^{1,†} *Physikalisch-Technische Bundesanstalt, Braunschweig, Germany*

Background, Motivation and Objective

Exposure measurements for medical ultrasound equipment are essential as regards aspects of safety and quality assurance. Recently, the new standard IEC 62127-1 Ultrasonics-Hydrophones Part 1: Measurement and characterization of medical ultrasonic fields up to 40 MHz, has been published. A significant difference to its predecessor is the introduction of the pulse deconvolution method to compensate for nonideal hydrophone frequency responses. Specific criteria are given in which cases this method shall be applied. However, little experience is available so far regarding the possible improvement of the results in practical exposure measurement situations.

Statement of Contribution/Methods

Exemplar acoustic output measurements were performed on a commercial diagnostic system using five different needle-type, membrane-type and capsule-type hydrophones. Two different transducer heads were investigated: a 3.5 MHz convex array and a 7.5 MHz linear array. The output beams for M and pD mode with different focal length and pulse repetition frequency settings were characterized by axial line scans and by beam profile scans at focus. Spatial peak temporal average intensity I_{spta} and maximum compressional p_c and rarefactional pressure amplitudes p_r were determined. All parameters were derived using both voltage-to-pressure conversion techniques, the hydrophone transfer factor $M(f_{\text{awr}})$ at the working frequency f_{awr} and the broadband transfer function $M(f)$ for pulse deconvolution. The various beam plots and output parameters obtained with both methods are compared.

Results

The results qualitatively show a similar behaviour for all hydrophones. The largest differences between both conversion methods occur for large pressure amplitudes, e.g. in the case of strong nonlinear distortion of the waveforms. The I_{spta} values obtained by deconvolution were systematically lower, with typical deviations ranging from 0 % up to 26 %. The results for p_c obtained by deconvolution were also systematically lower. Here, the deviations were between 0 % and 50 %. For p_r , the deconvolution method led to higher values with deviations up to 10 %. In cases with significant differences, the location of I_{spta} was always found at slightly lower distance from the transducer using the deconvolution method.

Discussion and Conclusions

The investigation shows that pulse deconvolution is an effective method to be applied in practise to compensate for nonideal hydrophone frequency responses. Systematic errors in measurements on common diagnostic ultrasound systems can be avoided. This is particularly important since the uncertainty of hydrophone measurements is already relatively large due to typical uncertainties in the range of ± 10 % of absolute hydrophone calibration data.

P2-B. Therapy Microbubbles

Sala Orange

Tuesday, September 22, 2009, 10:00 am - 11:30 am

Chair: **Greg Clement**
Harvard Medical School

P2-B-01

Molecule-cell membrane interaction: a key process for sonoporation?

Kadija Kaddur¹, Rustem Uzbekov², Julien Piron¹, Ayache Bouakaz¹; ¹UMR INSERM U930-CNRS ERL 3106, Université François Rabelais, Tours, France, ²Département des microscopies, Université François Rabelais, Tours, France

Background, Motivation and Objective

Sonoporation is explored as a physical mean to incorporate molecules into cells. However the mechanism of incorporation of these molecules is still misunderstood. The main hypothesis assumes that ultrasound (US) and microbubbles (MB) increase the membrane permeabilization through transient pore formation process. Nevertheless, recent results demonstrated the possible implication of endocytosis pathways in sonoporation. To understand and clarify the mechanism of permeabilization induced by sonoporation, we observed, using scanning electron microscopy (SEM), the effect of the interaction of US and MB on the cell membrane of a human glioblastoma cell line. In parallel, we quantified the incorporation and the localization of gold nanoparticles (NGPs, average diameter: 20 nm) after sonoporation into the cells using transmission electron microscopy (TEM).

Statement of Contribution/Methods

A solution containing NGPs (10% V/V) and BR14 MB (Bracco research, Geneva) were added to a suspension of cells. Cells were then insonified at 1MHz, 400 kPa, duty cycle of 40% during 30 seconds. Immediately after US exposure, the cells were fixed. For each group (NGPs alone, NGPs+US and NGPs+US+BR14 (5 MB per cell)), 20 cells were selected for further analysis. The number of NPGs was quantified and the localization of each NGP was determined (inside the cytosol, in the nucleus or in contact with the cell membrane).

Results

In comparison to control cells, SEM showed that US alone did not induce any modification of cell membrane. However, in the presence of MB, US affected significantly the cell membrane reducing its roughness and removing the microvilli from its surface. Using TEM, the results showed that the majority of NGPs (71%) interacts with the extracellular side of the cell membrane, 29% of NPGs were incorporated into the cytosol, but no localization into the nucleus was identified. NPGs presence at the cell membrane level was 7 times lower in control condition (NPGs alone), and no nanoparticles were detected into the cells (nucleus+cytosol). US alone produced an intermediate effect and the number of NPGs at the cell surface was 3 times lower in comparison with US+BR14 condition and only 5% of total NPGs were located into the cytosol.

Discussion and Conclusions

Our observations demonstrate that US and MB enhance the interaction of molecules with cell membrane as well as the incorporation of molecules into the cytosol. It is the first experiment that demonstrates an enhancement of interactions between molecules and cell membrane during sonoporation. The smoothing of the cell membrane as induced by sonoporation as shown with SEM plays likely a major role in facilitating the attachment of extracellular molecules with cell membrane and possibly enhancing thus endocytosis pathways. Such interactions could be an initial but essential step before the internalization of the molecules into the cell.

Ultrasound mediated gene silencing with short-hairpin RNA

Chien Ting Chin¹, Alexander Ghanem², Clemens Troatz², Christopher S. Hall¹, Klaus Tiemann^{3,1} Ultrasound Imaging & Therapy, Philips Research North America, Briarcliff Manor, NY, USA, ²Dept. of Cardiology, University of Bonn, Bonn, Germany, ³Dept. of Cardiology and Angiology, Hospital of the University of Münster, Münster, Germany

Background, Motivation and Objective

Ultrasound-mediated gene delivery especially with the enhancement of microbubble or nanoparticle agents has been demonstrated for some years. Translation to pre-clinical disease models faces many challenges. For guidance, existing scanners are well suited for imaging the anatomy as well as the microbubble agent but they lack power and flexibility needed to optimize delivery, activation of the payload and side effects.

Statement of Contribution/Methods

An integrated system for image-guided local delivery of drug and gene materials was developed. The system consists of a therapeutic ultrasound module, an imaging system and a PC-based architecture for overall control and coordination. The therapeutic ultrasound module is equipped with an 8-ring F/1 annular array transducer with a natural focus at 80mm. A motion system provides programmable steering of ultrasound focus in the lateral dimensions. The system is capable of firing arbitrary waveform ultrasound centered at 1.3 MHz (62% BW) at P. upto 6.5 MPa and a maximum CW acoustic output of 40 W. The imaging system can be one of many available scanners. The user interface is designed to offer power to technical investigators and simplicity to medical researchers. Acoustic characterization was performed using computer modeling, hydrophone and radiation force balance measurements.

Preliminary feasibility for gene silencing using short-hairpin RNA (shRNA) was performed. With image-guidance, the focal zone of the ultrasound device was placed in the anterior heart wall of ROSA26 transgene (LacZ) mice, which express β -galactosidase (β -Gal) in the entire animal. Subsequently, microbubbles and a plasmid which encodes a shRNA against the LacZ gene, were infused in a femoral vein. After the arrival of microbubbles was detected on the imaging system, the operator started a therapeutic ultrasound protocol. Satisfactory location of focal zone and reperfusion of fresh bubbles between firings were verified by imaging. Expression of β -Gal was detected with X-Gal staining two days after ultrasound treatment. Finally, β -Gal activity was quantified using the Galactostar assay.

Results

Tissue slides stained for β -Gal, troponin and nuclei showed silencing of LacZ gene with no signs of cell damage. Quantitative assay showed $70 \pm 10\%$ suppression of β -Gal activity in the focal target area whereas the off-target posterior wall showed only $26 \pm 10\%$ suppression. Control studies confirmed that ultrasound, microbubbles and plasmid are each an essential prerequisite for gene silencing. Animals receiving nonsense plasmid showed silencing is dependent on cognate sequence.

Discussion and Conclusions

This paper presents an integrated system dedicated for preclinical image-guided ultrasound-mediated gene delivery. Non-viral delivery of plasmid encoding shRNA was demonstrated. Silencing at 70% efficacy proved that a significant fraction of cardiac myocytes were reached.

Detection of blood-brain barrier disruption by contrast-enhanced high frequency ultrasound image: small animals study

Ching-Hsiang Fan¹, Po-Hong Hsu², Hao-Li Liu², Chih-Kuang Yeh¹, ¹Department of Biomedical Engineering and Environmental Sciences, National Tsing Hua University, Hsinchu, Taiwan, ²Department of Electrical Engineering, Chang Gung University, Taoyuan, Taiwan

Background, Motivation and Objective

Contrast-enhanced magnetic resonance imaging (MRI) were used to detect the increase of BBB permeability induced by high intensity focus ultrasound (HIFU) with ultrasound contrast agents (UCAs). However, the transient response after disrupting BBB is still unknown since it is very challenging to use MRI to dynamically observe the physiological change with the temporal resolution of $< 1s$. In this study, contrast-enhanced high-frequency ultrasound imaging (25 MHz) was used to detect the enhancement of BBB permeability in small animal experiments. The higher temporal resolution of high-frequency ultrasound imaging provides a potential to monitor the UCAs leakage into the surrounding brain parenchyma.

Statement of Contribution/Methods

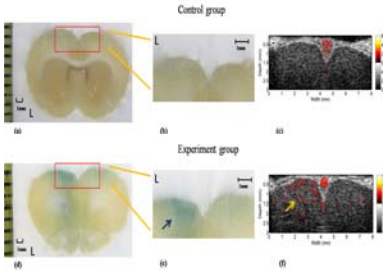
Six Sprague-Dawley rats were performed craniotomy before the HIFU sonication. One 1.5 MHz HIFU was delivered to the left hemisphere brain with 2.45 MPa pressure. Prior to sonication, UCAs were injected to enhance BBB permeability. Control group rats were sonicated without UCAs injection. Before and after sonications, the rats were individually injected UCAs and immediately a sequence of B-mode images (8 mm by 3 mm) were acquired at a frame rate of 7 fps. Note that the UCAs act as imaging indicators at this moment. We monitored the BBB disruption 6 hours in total and repeated the above mentioned process every hour. The BBB disruptions were verified by means of Evans blue extravasation (Figs. a,b,d,e). Image alignment by speckle tracking was applied across frames to reduce the motion artifacts. To map contrast replenishment after UCAs injection, the echo power in each voxel (following the wall-filter filter applied across pulses) was summed over the time direction (Figs. c, f).

Results

The results show the power intensity in experiment group is higher than the control group ones. In experiment group, the power intensity in left hemisphere brain is higher than the right side and the power intensity decreases over time (6h: 8% left). In addition, the spatial map of power consists with the Evans blue histology results.

Discussion and Conclusions

The results indicated that the contrast-enhanced high-frequency ultrasound imaging is feasible to detect the enhancement of BBB permeability. Potential applications include estimation the duration between BBB disruption and recovery in small animals.



P2-B-04

Ultrasound-activated Microbubbles as Novel Enhancers of Radiotherapy in Leukemia Cells *In Vitro*

Raffi Karshafian¹, Anoja Giles², Peter N. Burns^{2,3}, Gregory J. Czarnota^{2,3}, ¹Department of Physics, Ryerson University, Canada, ²Sunnybrook Health Sciences Centre, Canada, ³University of Toronto, Canada

Background, Motivation and Objective

Microbubbles are used as diagnostic contrast agents in ultrasound imaging, and as therapeutic agents with ultrasound to improve drug delivery. The aim is to develop a novel ultrasound-microbubble mediated vascular-based method to enhance the effects of ionizing radiation on tumours. The objectives of this study are to investigate the potential of ultrasound-activated microbubbles as a radiosensitizer, and the effect of ultrasound, microbubble and ionizing radiation exposure parameters on cell viability.

Statement of Contribution/Methods

Acute myeloid leukemia (AML-5) cells in suspension were exposed to ultrasound pulses of 500 kHz, 32 μs pulse duration, 3 kHz pulse repetition frequency and 30 s insonation time, and to ionizing radiation using 160 kVp X-rays at 200 cGy/min dose rate. Variations in insonating acoustic pressure (125-570 kPa), Definity microbubble concentration (0-3% v/v), ionizing radiation dose (0-8 Gy) and treatment order of ultrasound and radiation were investigated. The effect on cell viability (V_{PI}) was assessed using flow cytometry with propidium iodide immediately, and 24, 48 and 72 hours following treatment. Clonogenic cell viability (V_C) was assessed through the ability to form a cell colony. Electron microscopy images were acquired of untreated, treated with ultrasound and microbubbles, treated with ionizing radiation and treated with the combined modalities.

Tuesday
Poster

Results

Ultrasound-activated microbubbles can enhance the effect of ionizing radiation in AML-5 cells. Cell death increased by ~35% with the combined treatment of ultrasound and ionizing radiation ($V_{PI}=42\pm6\%$) compared to ultrasound ($V_{PI}=77\pm5\%$) and radiotherapy ($V_{PI}=71\pm7\%$) 48 hours following the treatments. The ability of ultrasound and microbubbles to enhance therapeutic effect of radiotherapy depended on ultrasound pressure and microbubble concentration. Higher acoustic pressures (570 kPa) and microbubble concentrations (greater than 1.5% v/v) were more effective at increasing cell death in the combined treatment. The induced enhancement was not sensitive to treatment order with one hour between treatments. Clonogenic survival assay showed a reduced viability in the combined treatment ($V_C\sim2\%$) compared to ultrasound and microbubble treatment ($V_C\sim30\%$) and ionizing radiation ($V_C\sim11\%$). Microscopy images of cells treated with both systems showed a more pronounced membrane deformations compared to images of cells with each treatment.

Discussion and Conclusions

Ultrasound-activated microbubbles can enhance the therapeutic effects of ionizing radiation. It was found that the enhancement of radiotherapy depends on both ultrasound and microbubble exposure parameters. Data from animal experiments indicated that this effect could be reproduced to yield enhanced tumour cell kill in xenograft models.

P2-B-05

Translational Studies of Pulsed HIFU Enhanced Tissue Permeability: Mechanisms in Mice and Rabbit Models

Brian O'Neill¹, Elisabetta Sassaroli¹, Christof Karmonik¹, King Li¹: ¹The Methodist Hospital Research Institute, Houston, TX, USA

Background, Motivation and Objective

Enhanced tissue permeability resulting from pulsed high intensity focused ultrasound (pHIFU) has been studied for over a decade now. Most of these studies have been in mouse models. To proceed to the clinic, two questions remain to be answered, first, what is the mechanism of action, and second, does it scale to humans. The goal of our ongoing research is to provide clear answers to these questions.

Statement of Contribution/Methods

An Insightec ExAblate 2000 3T MRI guided focused ultrasound device was used to sonicate the thigh muscle of rabbits. The sonication parameters were similar to those successfully used in the many earlier mouse studies. The temperature and cavitation were continually monitored during sonication. The effect of the treatment on tissue transport and physiology were assessed using T2 and contrast enhanced MR imaging at 0, 24, and 48 or 72 hours post treatment.

Experimental work was supplemented with theoretical modeling, using Comsol Multiphysics to test earlier assumptions regarding tissue heating and radiation force induced strains, using computer models of mouse and bulk muscle.

Results

Of the 13 treatments with parameters typical of earlier mouse experiments, not one showed significantly improved MRI contrast delivery. Temperatures for a single sonication in the bulk muscle were 1-2°C lower than those in measured in mouse models. Further tests looked at acoustic powers up to 80W, or at lower powers with longer duty cycles. Of the treatments at 5% duty cycle, only 70 and 80 W treatments showed enhanced contrast uptake, typically associated with elevated thermal doses (temperatures of $\geq 47^\circ\text{C}$). Some of these treatments resulted in thermal necrosis at the center of the enhanced region, but a few had observable contrast uptake without ablation. Cavitation signatures sometimes appeared due to occasional couplant problems, but were never correlated with enhanced delivery. With improved contrast uptake, there was also co-localized enhancement of the T2 weighted images. Histology later confirmed that this was edema. Contrast enhancement and edema could still be found near necrotic lesions at 72hrs, but was absent from sites without lesions by 24hrs.

Results of the theoretical modeling yielded greater heating and lower radiation force strains in mice models than predicted in previous studies where boundary effects were ignored. The strains achieved during sonication are found to be boundary dependent but were no more than 2%, despite tissue displacements of over 100µm. In bulk muscle displacements and strains were even lower. Predicted temperatures in hot spots, ie. near the bone, could briefly reach 47°C.

Discussion and Conclusions

Our results suggest that the thermal dose, rather than peak acoustic or half-harmonics power, appears as the best indicator of improved transport. These studies indicate that the parameters and assumptions from earlier studies in mouse models must be re-evaluated for larger animals and humans.

The effect of microbubble to skin-like soft material

Kazuya Obata¹, Kenji Yoshida¹, Akira Tsukamoto², Takashi Ushida², Yoshiaki Watanabe¹; ¹Doshisha University, Japan, ²Tokyo University, Japan

Background, Motivation and Objective

There are some reports about transdermal administration with the use of ultrasound in medicine. In this technique, it is thought that ultrasonic cavitation bubbles play important roles to introduce medicines into a skin. Therefore, We need to understand the bubble behaviors inside or at the surface of the skin, and should clarify the effect of bubbles on a skin. In this study, we examine the effect of microbubble to skin-like soft material with the aim of figuring out the mechanism and safety of transdermal administration.

Statement of Contribution/Methods

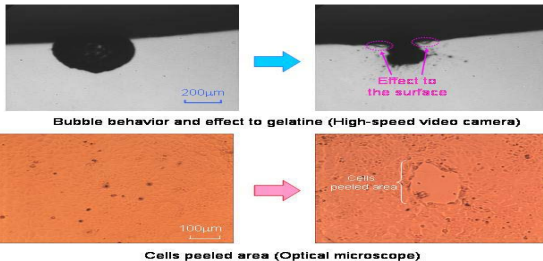
Using a high-speed video camera and an optical microscope, we examined the effect of microbubble driven by ultrasound to MDCK cells, kidney epithelial cells of dog, cultured on bovine gelatine. First, we observed the surface of gelatine covered with MDCK cells, using the microscope. Second, we observed the real-time bubble behaviors on the gelatine with the high-speed video camera. Third, we observed the gelatine surface again and investigated the effect of the bubble by comparing the gelatine surfaces before and after ultrasound irradiation.

Results

We observed bubble vibration, repetition of expansion and contraction, with high-speed video camera. Additionally, optical observations demonstrated that the surface of gelatine was pressed during bubble expansion, and pulled during bubble contraction. Using optical microscope, we observed the hole where cells were peeled from gelatine. This hole was not observed before ultrasound irradiation.

Discussion and Conclusions

The peeling of cells on gelatine seems to be related to bubble behaviors because 1) it was not observed before ultrasound irradiation, 2) the surface of gelatine was pressed and pulled by the bubble, 3) the peeling area was about the same size as the bubble. For these reasons, we suggest that the vibrating bubble peels the cells from gelatine. Assuming that the same phenomenon occurs in transdermal administration, it is possible that the administrations of medicines into a skin are enhanced through the peeled area. We expect that this study contributes to clarify mechanism of transdermal administration.



Enhancement of doxorubicin effect on cancer cell mortality with ultrasound and microbubbles

Julien Piron¹, Kadija Kaddur¹, Ayache Bouakaz¹; ¹UMRS INSERM U930, CNRS ERL 3106, Université Rabelais de Tours, France

Background, Motivation and Objective

Potential use of clinical ultrasound (US) in enhancing the anti-cancer drugs effects in the treatment of cancers has been recently reported. Moreover US in combination with microbubbles have proven its efficiency in improving molecule uptake into cells through sonoporation mechanism. In this work, we want to verify that low intensity US and microbubbles could enhance anticancer-drug effect.

Statement of Contribution/Methods

In this study, we evaluate the benefit of sonoporation in enhancing cell mortality using anti-cancer drug doxorubicin and U87MG cells (human glioma cells). Experiments were conducted in five groups: non treated, doxorubicin treated, US-microbubble treated, doxorubicin + US, and doxorubicin + US-microbubble. Cells were exposed to 5 μ M doxorubicin and sonicated at 1 MHz (with 40% duty cycle for 30s and acoustic pressures from 0.4 to 0.8 MPa). Six and 24h after treatment, cell mortality was evaluated by Trypan blue dye exclusion test. Three experimental microbubble types were investigated: BR14, Vevo MicroMarker and Poly lactide Shelled microbubbles.

Results

The results showed that for all microbubble types, a significant enhancement in doxorubicin effect was achieved when it was co-administered with microbubbles in comparison to the drug alone.

The highest effect was obtained at 800 kPa Vevo MicroMarker microbubbles which doubled the cell mortality. Cell mortality in doxorubicin + US group was comparable to doxorubicin alone (25.3 \pm 5.6 % versus 22.2 \pm 4.9 % at 6h and 20.5 \pm 4.1 % versus 29.8 \pm 4.7 % at 24h). When Vevo MicroMarker microbubbles were co-administered with doxorubicin, cell mortality percentage reached 45.8 \pm 4.6 % and 51.0 \pm 4.5 % at 6h and 24h respectively. Using Poly lactide Shelled microbubbles and BR14 microbubbles, cell mortality at 24h reached respectively 42.8 \pm 2.4 % and 57.6 \pm 8.8 %.

Thus, at 24h, ratios of doxorubicin + US-microbubble condition and doxorubicin alone are 2.2 and 1.5 for BR14 and Poly lactide Shelled microbubbles respectively. The highest ratio is obtained with Vevo MicroMarker micro bubbles: 2.4.

Discussion and Conclusions

Our results demonstrate that low intensity US and microbubbles could enhance anti-cancer drug effect, suggesting that this combination might be a useful tool for the cancers therapy.

P2-B-08

Mechanism of sonoporation: Ultrasound and Microbubble Mediated Generation of Transient Pores on Cell Membranes *In Vitro*

Raffi Karshafian¹, Peter N. Burns^{2,3,1} *Department of Physics, Ryerson University, Toronto, Ontario, Canada,*
²*Department of Medical Biophysics, University of Toronto, Canada,* ³*Sunnybrook Health Sciences Centre, Canada*

Background, Motivation and Objective

The therapeutic efficiency of biologically active molecules that exert their effect within the cell is ultimately constrained by the inability of complex molecules to cross the plasma membrane. The application of ultrasound increases cell membrane permeability and allows molecules to cross the otherwise-impermeable plasma membrane and enter the intracellular space, a phenomenon referred to as sonoporation. This work investigates the mechanism of sonoporation. The objectives of this study are to directly observe bioeffects on the surface of cell membranes induced by ultrasound and microbubbles with electron microscopy methods and to correlate them with flow cytometry data on cell permeability.

Statement of Contribution/Methods

KHT-C cells in suspension were exposed to ultrasound pulses of 500 kHz centre frequency, 570 kPa peak negative pressure, 32 μ s pulse duration, 3 kHz pulse repetition frequency and two minutes insonation time in the absence and presence of microbubble contrast agents (Definity at 3.3% v/v and Optison at 6.7% v/v). Cell permeabilisation was assessed with a permeability marker (FITC-dextran, 70 kDa) added 60 s before and 60 s after the termination of the ultrasound treatment. Following treatment, reversible permeability (P_R) and cell viability (V_{PI}) were measured with flow cytometry. P_R is defined as the number of cells stained with FITC-dextran and unstained with propidium iodide (PI). V_{PI} is defined as the number of cells unstained with PI. Cell membrane morphology was observed using electron microscopy.

Results

P_R 's of 71% and 44% were achieved with ultrasound in combination with Definity and Optison, respectively, with the FITC-dextran added before ultrasound exposure. P_R 's similar to control (~0.5%) were achieved with ultrasound alone, and with FITC-dextran added 60 s following termination of the treatment. Untreated cells exhibited continuous plasma membrane morphology as assessed with electron microscopy. Ultrasound and microbubble treated cells demonstrated generation of pores as large as 400 nm on the membrane, immediately

following treatment. The pores resealed within five minutes following the termination of the ultrasound and microbubble treatment. No pores were observed on cells exposed to ultrasound alone.

Discussion and Conclusions

Pore generation on cell membranes was congruent with intracellular uptake of FITC-dextran molecules indicating that the mechanism underpinning sonoporation is the generation of transient pores on cell membranes induced with ultrasound-activated microbubbles. This study may be applied to guide the development of sonoporation-mediated therapies.

Tuesday
Poster

P2-C. Contrast Agents: Characterization and Modeling

Sala Orange

Tuesday, September 22, 2009, 10:00 am - 11:30 am

Chair: **Christopher Hall**
Philips Research North America

P2-C-01

Acoustic size distribution analyzer for microbubbles

David Maresca¹, Marie Muller^{1,2}, Marcia Emmer¹, Hendrik J. Vos¹, Antonius F.W. van der Steen^{1,3}, Nico de Jong^{1,3}, ¹Biomedical Engineering, Erasmus Medical Center, Rotterdam, Netherlands, ²Laboratoire Ondes et Acoustique, Université Paris Diderot, Paris, France, ³Interuniversity Cardiology Institute of the Netherlands, Netherlands

Background, Motivation and Objective

Ultrasound contrast imaging depends largely on the harmonic behavior of bubbles. It is acknowledged that bubble size has a great impact on the amplitude of harmonic generation. However the size distribution of the contrast bubbles after human administration is unknown. High above resonance, bubble responses depend on their physical cross section only [1]. Our objective is to take advantage of this feature to measure single bubble sizes with ultrasound.

Statement of Contribution/Methods

A 25 MHz single element focused transducer (2.5 cm focus) was mounted in a water tank filled with a highly diluted Definity® population (1/500,000). Pressures scattered by the bubbles responding to 400 kPa pulses ($MI < 0.1$) were acquired. To determine a bubble position with respect to the acoustic axis, two consecutive pulses of 20 and 30 MHz were transmitted, taking advantage of the beam profile differences at the two frequencies. A bubble was considered on axis when the difference in backscattered amplitudes at the two frequencies was smaller than 20%. The transducer was calibrated with a hydrophone so that absolute pressure values could be derived from the measurements. High above resonance, the backscattered pressure p_b relates to the bubble radius r as $p_b = r \cdot \rho \cdot \dot{p}_i / d$, where d is the transducer-bubble distance and p_i the incident pressure hitting the bubble.

Results

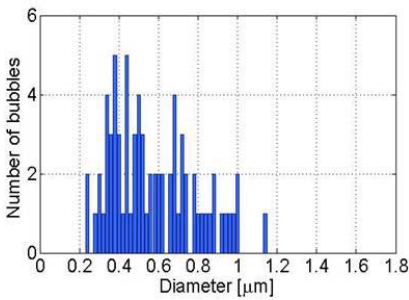
With our approach we sized 74 bubbles from a Definity vial showing a mean diameter of 0.6 μm and a standard deviation of 0.2 μm (See figure). As an indication, a Coulter counter characterization of the same vial resulted in a mean diameter of 0.9 μm and a standard deviation of 0.7 μm . Note that the amount of bubbles sized via each method is not comparable.

Discussion and Conclusions

The acoustically determined size distribution is comparable in shape with that of the Coulter counter but appears shifted to lower radii. The 20% uncertainty of the hydrophone used to calibrate the transducer could be a reason for the observed shift. The size distribution obtained acoustically is also narrower than expected. The reason for this is currently unknown. An application of our method could be to analyze bubbles administered in superficial arteries as it potentially estimates the standard deviation of a bubble population noninvasively.

[1] J Sijl, et al., "Acoustic characterization of single ultrasound contrast agent microbubbles", JASA, 2008

Tuesday
Poster



P2-C-02

Acoustic characterization of individual monodisperse contrast agents with an optical-acoustical system

Mehmet Kaya¹, Steven Feingold¹, Kanaka Hettiarachchi², Abraham P. Lee², Paul A. Dayton^{1,1} *Joint Department of Biomedical Engineering, University of North Carolina-North Carolina State University, Chapel Hill, North Carolina, USA, ²Department of Biomedical Engineering, University of California, Irvine, USA*

Background, Motivation and Objective

To date, all of the microbubble contrast agents manufactured commercially for diagnostic purposes have consisted of populations that have large size variances due to their manufacturing methods. We hypothesize that significant improvements in contrast imaging and microbubble-enhanced therapeutics may result from monodisperse microbubbles. Parameters such as the destruction threshold, the amount of radiation force experienced, and the resonant frequency, are all affected by microbubble diameter. For vehicles in the 1-7 micron range, which is the ideal range for intravascular microbubbles, all of these parameters change drastically with small differences in diameter

Statement of Contribution/Methods

We have developed a microfluidic flow-focusing system which has the capability to produce lipid-encapsulated microbubbles in the 2-10 micron diameter range with nearly identical diameter. By altering the gas pressure and liquid flow rate, the size distribution of manufactured bubbles can be adjusted. Monodisperse microbubbles are pumped from the microfluidic chamber through a 200 micron cellulose tube, across the confocal region of a microscope objective and two single-element broadband transducers. A high-speed camera is used to record the diameter of the microbubbles as they pass through the acoustic focus. Bubble production rate is slow enough so that individual bubbles can be resolved both optically and acoustically. In this study, we study the acoustic responses of monodisperse microbubbles formulated with this system as a function of bubble diameter and excitation frequency. Results are compared to simulations from a modified Rayleigh-Plesset model.

Results

Acoustic studies show scattered echo amplitude from single microbubbles as a function of frequency are in excellent agreement with simulations. Acoustic responses from monodisperse contrast agents are highly correlated (correlation of ~ 0.9), compared echoes from a polydisperse microbubbles (~ 0.7). Data indicate that maximum acoustic response for each bubble occurs when excited near its resonant frequency, and the magnitude of the acoustic response can be enhanced by several fold simply by near-resonance excitation within a frequency range as small as 2 MHz. Data also indicate that larger bubbles produce a larger scattered echo.

Discussion and Conclusions

Microfluidic flow focusing is a method to make lipid-encapsulated microbubbles with controlled size distribution. Although the production rate of a single chamber is too slow to produce enough contrast for large studies, the system works well for detailed studies of acoustic behavior of contrast agents as a function of diameter. Results are in agreement with simulations from a modified Rayleigh-Plesset model and confirm our hypothesis that for a given bubble size, optimal scattered echo is obtained when the bubbles are excited near the resonance frequency.

Ultrafast Framing Optical and Acoustical Recordings of Nonlinearly Oscillating Microbubbles

Hendrik J. Vos¹, Riccardo Mori², Jacopo Viti², Jeroen Sijl³, Francesco Guidi², Piero Tortoli², Nico de Jong¹; ¹Biomedical Engineering, Thorax Center, Erasmus MC, Rotterdam, The Netherlands, ²University of Florence, Italy, ³University of Twente, Enschede, Netherlands

Background, Motivation and Objective

Characterization of single ultrasound contrast agent (UCA) microbubbles (MBs) is necessary to improve detection strategies. In general terms, MB nonlinear behavior such as harmonic distortion, subharmonic oscillations and thresholding improves detection efficacy, but not all of the MB sizes present in a dispersed UCA population will contribute to the detection signal. In this paper, we experimentally study the relation between size and nonlinear responses of single MBs.

Statement of Contribution/Methods

Single Definity MBs, held in a transparent tube, are positioned in the focal region of both a microscope and two ultrasound transducers (2.5cm focus). One excites the MBs with 15-cycle tone burst pulses at ~ 60 kPa amplitude. The frequency cyclically changes from 2 - 4 MHz in steps of 0.5 MHz over consecutive pulses so that the behavior of a same bubble at different frequencies is observed. The second transducer, suitably calibrated, records the echo. Both are connected to a custom coherent TX/RX low-noise electronic system. The optical images from the microscope are instantaneously captured by the Brandaris-128 ultrafast-framing camera operating at ~ 12.5 million frames per second, allowing full capture of MB size, shape, and oscillation. The MBs show a slow acoustically-induced deflation during subsequently transmitted sequences, allowing for studying the size-dependency of the response to multiple frequencies. Furthermore, numerical transformation of the radial oscillation into a radiated pressure allows direct comparison of optically-predicted echoes with the acoustically-recorded ones.

Results

Sixteen MBs having radii between 1.2 and 3.6 μm were recorded. The echo amplitude was 0.4 – 10 Pa for the fundamental-frequency response and 0.2 – 2.5 Pa for the second and subharmonic-frequency responses. All such values depended strongly on the initial bubble radius. The coherent TX/RX allowed observing that the fundamental-echo phase shift was on the order of $\pi/2$ around resonance. Larger second-harmonic response was shown at two size ranges: around the resonant size, and at the smallest size reached by the end of the deflation process. The optical records clearly showed that in the latter case the microbubble oscillation was characterized by a strong compression-only behavior. Subharmonics were found when the transmit frequency was roughly twice the resonance frequency. Agreement within ~1 Pa over the range of 1 – 5 MHz (including nonlinear responses) was found between the echoes predicted from the optical recordings and the recorded echoes.

Discussion and Conclusions

The combined acoustical/optical setup allows for a detailed study of the dynamics of differently-sized microbubbles. Even at low excitation levels ($MI < 0.04$) highly nonlinear oscillations, such as compression-only for smallest and subharmonics for larger microbubbles, have been identified; the predicted echo levels of these effects agree well with the recorded ones.

An investigation of contrast agent shell rupture threshold in response to overpressure

Parag Chitnis¹, Paul Lee¹, Jonathan Mamou¹, Jeffrey Ketterling^{1,†}, F. L. Lizzi Center for Biomedical Engineering, Riverside Research Institute, New York, NY, USA

Background, Motivation and Objective

The stiffness of contrast agent (CA) shells is a critical parameter that determines responsiveness to acoustic excitation and half-life in circulation. This study investigates the static pressure threshold for CA rupture, which can be used to infer the material properties of the CA-shell and predict the response to acoustic excitation.

Statement of Contribution/Methods

Polymer-shelled CAs (POINT Biomedical) with nominal mean diameter of 3 μm and a constant shell-thickness-to-radius ratio (STRR) were subjected to overpressure in a cylindrical test chamber with a microscope reticule at the top and a glass window at the bottom. A CCD-based video-microscope (50X magnification, 128 μm FOV, 1 Mpixel) was used to image CAs. Water was introduced into the chamber at a flow rate of 5 mL/hr to increase the

static pressure from 0.5 to 22 psi, which was monitored using a pressure sensor. Each pressure measurement was accompanied by a corresponding image of CAs. The first frame was used to define sub-images containing each CA and these were extracted from all subsequent frames for automated post-processing involving: 1) a 0.5x0.5 μm median filter, 2) binarization and Sobel-based edge detection, and 3) Hough transform to obtain the diameter of CAs. CAs that migrated outside of the FOV or “clumped” together were discarded. Change in diameter as a function of static pressure was obtained for all remaining CAs.

Results

Four trials resulted in 68 valid CAs. The majority of CAs did not respond to static pressure change until the threshold for shell rupture was exceeded, resulting in an abrupt destruction. The density function of rupture pressures exhibited 4 main lobes. A k-means algorithm separated the data into 4 clusters (Tab. 1). Mean rupture pressures in each cluster were statistically different but the corresponding mean diameters were statistically the same. Further, a linear fit indicated that rupture pressure was marginally dependent on diameter for three clusters.

Discussion and Conclusions

Classical theory for a spherical shell predicts that the critical compression load is a function of STRR. Measurements agree with this theory and indicate that the CA sampled might consist of 4 different STRR, thus resulting in rupture pressures clustered around 4 different means that were relatively independent of diameter. This method can be used for inferring and comparing shell properties of different CAs.

Table 1: Results from the k-means algorithm and Anova test obtained from CA rupture data. * indicates statistical difference from other clusters. Slope and intercept were obtained by fitting the pressure-diameter data to a straight line.

#	N	Mean Diameter (μm)	Mean Rupture Pressure (psi)	Slope (psi/μm)	Intercept (psi)	RMS Error (psi)
1	6	3.6±1.1	1.7±1.5*	0.2	1.0	1.3
2	29	4.7±0.9	8.1±1.0*	0.3	6.5	0.9
3	22	3.9±1.0	10.5±1.0*	0.2	9.9	1.0
4	11	4.3±1.2	16.3±2.4*	-1.2	21.3	1.9
All	68	4.3±1.1	9.7±4.0	0.1	9.4	4.0

Tuesday
Poster

P2-C-05

A new theoretical model for cracked bubbles

Padraig Looney¹, David Thomas¹, Robin Steel¹, Tom Anderson¹, Nikos Pelekasis², Vassilis Sboros¹; ¹Medical Physics, School of Clinical Sciences and Community Health, Edinburgh University, Edinburgh, United Kingdom, ²Mechanical Engineering, University of Thessaly, Volos, Greece

Background, Motivation and Objective

The response of the rigid shelled contrast agent biSphere® has been previously studied optically and acoustically over a range of MI. Free bubble models have been used to model the behaviour of rigid shelled MBs. In this work a new theoretical model is proposed and is compared with existing models in terms of agreement with experimental acoustic responses from single MBs

Statement of Contribution/Methods

Approximately 400 single biSphere® echoes were captured using driving pulses with MIs ranging from 0.12 to 0.87. The absolutely calibrated harmonic and fundamental responses of each MB were found. These were compared with three models: a. A Keller-Miksis free bubble model, b. A Hoff-like model with elastic shell and c. A new “cracked” bubble model. The new model has been developed to account for the movement of gas in and out of a MB. The Keller-Miksis equation was modified to approximate the volume of gas moving in and out of the shell and forming a free MB. These models used the experimentally measured radius distribution of the contrast agent biSphere and the calibrated transmitted pulse to calculate the scattered pressure wave at the face of the transducer and achieve direct comparison with the single microbubble acoustic data.

Results

For the lowest MI (0.12) the cracked model showed that the majority of MB responses were below the noise level of the imaging system. For MI of below 0.5 the cracked model gave good agreement with the experimental data while the free model and the shelled model disagreed with the experimental distribution. As an example for MI of

0.4 ninety percent of MBs above noise had a fundamental RMS response a. for the Keller-Miksis free bubble model below 18Pa, b. for the Hoff-like model below 5Pa, c. for the new “cracked” bubble model below 3Pa and d. for the experimental data below 3Pa. Above a MI of 0.5 the Keller-Miksis free bubble model gave good agreement with the fundamental response but not with the harmonic response. Imposing the previously optically observed radius threshold (Bouakaz et al 2005) for inducing a bubble cracking the disagreement of the free bubble model with the experimental results increased while the cracked model was unaffected.

Discussion and Conclusions

The free bubble model and the shelled bubble model have been shown to be inadequate in modelling the acoustic response of biSphere as it produces much larger scatter responses than measured in all cases. The new ‘cracked microbubble’ model is in agreement with the experimental results for MIs lower than 0.5 as it accommodates for the volume deficit of the gas behaviour outside the shell. It therefore implies that at high MIs this model fails, as more violent processes make the model assumption inadequate and the free bubble model achieves then a reasonable agreement with the experimental data.

P2-C-06

Ultrasound phase velocities in SonoVue as a function of pressure and bubble concentration

Kathryn Hibbs¹, Robert Eckersley², Alison Noble¹, Meng-Xing Tang^{3,1} *Department of Engineering Science, University of Oxford, United Kingdom, ²Imaging Sciences Department, Imperial College London, United Kingdom, ³Department of Bioengineering, Imperial College London, United Kingdom*

Background, Motivation and Objective

It is widely known that the presence of bubbles causes a change in the speed of sound in a liquid, but this fact has never been exploited in contrast-enhanced ultrasound (US) using microbubbles. However changes in the speed of sound, measured using strain estimation techniques, are already used in other areas of US, for example the measurement of changes in local tissue stiffness and the measurement of temperature changes during HIFU treatment. The aim of this study is to establish the parameters affecting speed of sound in the US contrast agent SonoVue and to determine whether the speed of sound changes are significant enough to enable strain estimation techniques to be applied to contrast-enhanced US. This is the first step towards a novel imaging technique that is less susceptible to artifacts than current techniques [1] and furthermore may permit the quantitative estimation of local microbubble concentration.

Statement of Contribution/Methods

Measurements of US transmission through SonoVue diluted in saline (0.9%, w/v) were made using a 3.5 MHz transducer and a needle hydrophone. The SonoVue was placed in a beaker with acoustic windows between the transducer and hydrophone. 9 broadband pulses, consisting of a Gaussian enveloped sinusoidal signal of 2 cycles with peak negative pressure ranging from 13 to 128 kPa, were transmitted through the sample 100 times. This was repeated for 8 different SonoVue concentrations varying from 0 to 1200 ul/l. A broadband phase spectroscopy technique [2] was used to find the phase velocity at each insonating pressure and for each SonoVue concentration.

Results

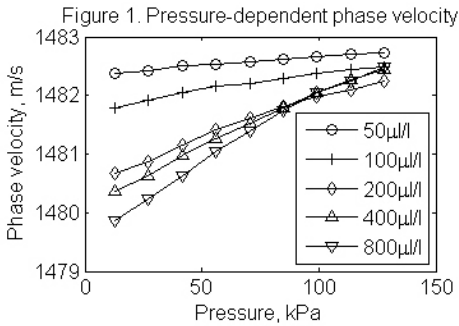
Phase velocity was found to vary with frequency, insonating pressure and SonoVue concentration. Figure 1 shows the pressure-dependent phase velocity for a range of concentrations calculated at 3.4 MHz. Phase velocity was found to increase approximately linearly with pressure and the rate of change increased with concentration.

Discussion and Conclusions

The phase velocity of US through SonoVue varies significantly with frequency, pressure and concentration. This magnitude of dispersion suggests that strain estimation techniques can be applied in contrast-enhanced imaging. The adaptation of a strain estimation algorithm for use with contrast-enhanced US images is currently underway.

[1] M Tang and RJ Eckersley. IEEE UFFC 2006;53:2406-2415

[2] J Mobley et al. J Acoust Soc Am 1998;103:2145-2153



P2-C-07

Theoretical model for the threshold onset of contrast microbubble oscillations

Alexander Doinikov¹, Ayache Bouakaz¹; ¹INSERM U930 CNRS ERL 3106, Université François Rabelais, Tours, France

Background, Motivation and Objective

Emmer et al. (UMB 2007;33:941) investigated experimentally the onset of radial oscillation of phospholipid-coated microbubbles and reported that for microbubbles with resting radii $R_0 < 2.5 \mu\text{m}$ there is a threshold for the acoustic pressure amplitude below which little or no oscillation is observed. The bubble oscillation was not detected until the acoustic pressure reached the threshold value, and as the resting radius of the microbubbles decreased, the threshold pressure increased.

Statement of Contribution/Methods

This paper suggests that the observed threshold behavior is a consequence of the plastic properties of the phospholipid encapsulation. A theoretical model is proposed for the description of this behavior.

Results

The proposed theory is based on the assumption that a phospholipid layer, as a viscoplastic material, has a yield threshold. As a result of this property, the oscillation of a microbubble with a phospholipid shell does not start until the acoustic pressure amplitude P_a exceeds a critical value. Our theoretical development has shown that the critical value of P_a is given by $P_a^{cr} = 3\epsilon\tau_0/R_0$, where ϵ is the shell thickness and τ_0 is the threshold bulk shear stress of the phospholipid coating. Using the measurements of Emmer et al., one can estimate the magnitude of the product $\epsilon\tau_0$ and thereby validate the proposed theoretical model. The validation of the model reveals that for a 1 nm thick phospholipid shell, τ_0 is on the order of 40 MPa. This is a reasonable figure in accordance with the experimental data of Marmottant et al. (JASA 2005;118:3499) from which it follows that the bulk elastic modulus of a 1 nm thick phospholipid layer is on the order of 333 MPa. For $\tau_0 = 40 \text{ MPa}$ and $\epsilon = 1 \text{ nm}$, the model predicts that P_a^{cr} increases from 34 MPa to 100 MPa as R_0 decreases from 3.5 μm to 1.2 μm , which is in agreement with Emmer et al.'s observations.

Discussion and Conclusions

The assumption that the threshold onset of radial oscillation of phospholipid-coated microbubbles is a consequence of the plastic properties of a phospholipid layer allows one to suggest a simple physical explanation for this experimental observation. The explanation is that a phospholipid layer, as a physical material, has a yield threshold which in turn results in the threshold onset of bubble oscillation. The derived expression for the critical acoustic pressure reveals that the observed dependence of the threshold pressure on the resting bubble radius is a geometrical factor that results from the spherical shape of the phospholipid coating. The presence of the threshold can be modeled by integrating the corresponding condition into the modified Rayleigh-Plesset equation.

Numerical study of the ultrasonic propagation in a solution of ultrasound contrast agent at high frequency

Belfor Galaz¹, Guillaume Haiat², Nicolas Taulier¹, Jean-Jacques Amman³, Wladimir Urbach¹; ¹Laboratoire d'Imagerie Paramétrique, CNRS, Paris, France, France, ²B2OA UMR 7052, CNRS, Paris, France, France, ³Department of Physics, de Santiago de Chile (USACH), Santiago, Chile

Background, Motivation and Objective

Specific ultrasound contrast agents (UCA) offer new avenues in therapeutic treatment by allowing *in situ* drug delivery in combination with ultrasound imaging. However, high frequency acoustic wave propagation in solutions of UCA remains unclear due to the complex interaction between ultrasound and the coated particles (mode conversion, scattering, multiple reflections). The aim of this study is to assess the potentiality of 2-D numerical simulation tools to model the propagation in such medium around 50 MHz. We aim at deriving the sensitivity of the ultrasonic parameters to the physical parameters of UCA suspensions.

Statement of Contribution/Methods

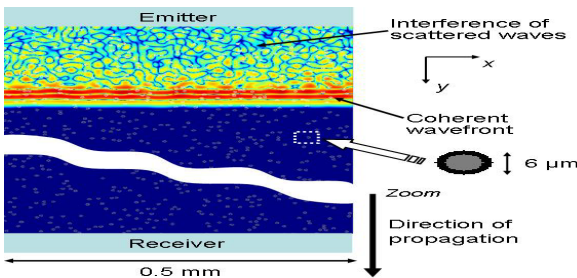
To address this problem, a 2-D Finite Difference Time Domain numerical simulation code was used to model the ultrasonic propagation in an aqueous solution with particles made of i) polystyrene and ii) fluid surrounded by a polymeric capsule. A dedicated iterative method was devised to construct 2-D binary numerical models of UCA solution (see Figure). For each set of parameters, the results were averaged for 15 UCA solutions with randomly located particles.

Results

The numerical simulation tool is validated by comparing the results with an analytical model derived from the Faran theory. A good agreement between the experimental and numerical results is obtained for the polystyrene particles. For the coated 6 μm diameter particles, the attenuation coefficient at 50 MHz (AC50) and the relative backscattered intensity (RBI) increases non-linearly with the concentration. When the size of the membrane thickness increases from 0.45 μm to 1.65 μm , AC50 decreases from 170 to 25 dB/cm whereas RBI decreases from -14 to -22 dB (respectively increases from -22 to -17 dB) for thin (< 1 μm) (respectively thick, > 1 μm) membranes. AC50 decreases (respectively increases) when the longitudinal (respectively transverse) wave velocity of the membrane increases. The variations of the ultrasonic velocity versus the solution parameter are in agreement with an effective medium model.

Discussion and Conclusions

Mode conversion effects are shown to play a role in the ultrasonic propagation through a UCA solution. Multiple scattering phenomena may explain the variation of AC50 and of RBI as a function of the membrane thickness and of the concentration. This study may have important implications in the conception of new particles used in UCA suspension.



P2-D. Ultrasound Systems and Devices

Sala Orange

Tuesday, September 22, 2009, 10:00 am - 11:30 am

Chair: **Pai-chi Li**
National Taiwan University

P2-D-01

GPU-Based Color Doppler Ultrasound Processing

Li-Wen Chang¹, Ke-Hsin Hsu¹, Pai-Chi Li¹; ¹National Taiwan University, Taiwan

Background, Motivation and Objective

Color Doppler ultrasound is a routinely used diagnostic tool for assessing blood flow information in real time. The required signal processing is computationally intensive, involving autocorrelation, linear filtering, median filtering, and thresholding. Due to the large amount of data and high computational requirement, color Doppler signal processing has been mainly implemented on custom-designed hardware, with software-based implementation; particularly on general-purpose central processing units; not being successful. In this paper, we will describe the use of a graphics processing unit for implementing signal-processing algorithms for color Doppler ultrasound.

Statement of Contribution/Methods

The signal-processing algorithms involved in color Doppler include clutter filtering, flow estimation, thresholding, persistence processing, median filtering and image mapping. They are implemented in GPU-based software using the CUDA platform. These algorithms are combined into three kernels for effective usage of the processing power and data communication bandwidth.

Results

The memory-copy command for data transfer between the mainboard memory and graphics memory is an additional time-consuming step that is not needed for a pure CPU-based implementation. Although these memory copy steps take extra time, the overall processing speed achieved by the GPU platform still outperforms that of the CPU platform. The performances of the CPU-based and GPU-based implementations are compared and shown in the attached table. The total execution is about 70-fold faster on the GPU than on the CPU, and the frame rate is dramatically improved from about 2 fps on the CPU to more than 160 fps on the GPU.

Discussion and Conclusions

With the GPU-based platform, efficient computations for color Doppler ultrasound are feasible. It would be possible to integrate other ultrasound signal-processing algorithms into this platform to further simplify the system hardware, provided that the data transfer between the imaging system and the PC is sufficiently fast.

Table: Execution time for each kernel

Execution Time (ms)		CPU	GPU	Speed-up
Copy Data to GPU			2.353	
Kernel 1		166.2	2.547	65
Kernel 2	1×1	3.7	0.033	112
	3×3	39.1	0.177	220
	5×5	82.8	0.438	189
Kernel 3		225.6	0.281	802
Copy Data to CPU			0.548	
Total	1×1	392.7	5.734	68
	3×3	431.6	5.876	73
	5×5	473.6	6.137	77

Design of a Multi-Channel Pre-Beamform Data Acquisition System for an Ultrasound Research Scanner

Ivan K. H. Tsang¹, Billy Y. S. Yu¹, Dave K. H. Cheung¹, Harry C. T. Chiu¹, Chris C. P. Cheung², Alfred C. H. Yu¹;
¹Medical Engineering Program, The University of Hong Kong, Pokfulam, Hong Kong, ²Ultrasonix Medical Corporation, Richmond, BC, Canada

Background, Motivation and Objective

Access to the pre-beamform data of each array channel on an ultrasound scanner is important to experimental investigations on imaging research topics like adaptive beamforming and synthetic aperture imaging. Through such data access, we can obtain in-vitro or in-vivo insights on various imaging methods without resorting to hardware implementation. Our aim in this work is therefore to develop a pre-beamform data acquisition (DAQ) system that can collect data from 128 array elements simultaneously.

Statement of Contribution/Methods

Our DAQ system is intended to interface with a Sonix-RP research scanner through a probe connector port. As shown in the figure, this design comprises three major blocks: 1) a connector board that interfaces with the array probe and the scanner; 2) a main board that triggers data acquisition and controls data transfer to a computer; 3) four receiver boards that are each responsible for acquiring 32 channels of digitized raw data and storing them to the on-board DDR2 memory. The probe-connecting end of this system is interfaced with TX810 chips (Texas Inst.) to facilitate switching between transmit and receive modes. When receiving data, the incoming analog signal is first passed into a low-noise amplifier (MD3880; Supertex). These signals are then sent into AFE5805 chips (Texas Inst.) on the four receiver boards to perform time gain compensation, anti-alias filtering, and 12-bit data sampling at a 40MHz rate. Subsequently, the digitized signal samples are de-serialized using a Virtex-5 FPGA (Xilinx) and are stored into DDR2 memory. To facilitate data retrieval, we implemented a Virtex-5 FPGA on the main board to initiate data transfer, and if preferred, to perform on-board beamforming (programmable by user) prior to sending data to a computer through a USB 2.0 link.

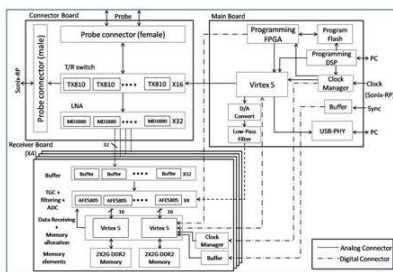
Results

For our prototype, we used 16GB of DDR2 memory for data storage. With a frame rate of 100Hz, a 10cm depth-of-view and 128 transmit firings per frame, this DAQ system is capable of collecting pre-beamform data from all array channels for 2.5 seconds. We are currently completing the prototype development in collaboration with Ultrasonix.

Discussion and Conclusions

The reported DAQ system can facilitate research at the pre-beamform stage of ultrasound imaging. In turn, it can contribute to the design of improved imaging paradigms with sharper contrast and/or faster frame rates.

Tuesday
Poster



Software-based Hand-held Ultrasound Color Doppler Imaging System

Hyuntaek Lee¹, Hak-yeol Sohn¹, Yang Mo Yoo¹, Tai-kyong Song¹:¹Electronic Engineering, Sogang University, Seoul, Korea, Republic of

Background, Motivation and Objective

Due to improved portability and patient acceptability, a recently-developed hand-held ultrasound machine (e.g., P10, Siemens Medical Systems, Mountain View, CA, USA) has been tested in various emerging clinical applications, e.g., ambulatory healthcare. For miniaturization, in a hand-held ultrasound machine, application-specific integrated circuits (ASICs) are widely used. However, since the clinical utility of a hand-held ultrasound machine is continuously evolving, it would be appropriate to have improved functional flexibility, especially in mid- and back-end processing. In this paper, we present a software-based hand-held ultrasound system architecture where a single digital signal processor (DSP) is utilized to support real-time color Doppler imaging.

Statement of Contribution/Methods

To demonstrate the feasibility of the proposed software-based ultrasound system architecture, we have developed a custom built hand-held ultrasound machine where front-end processing (e.g., beamforming) is carried out in a FPGA (Virtex 4, Xilinx, San Jose, CA, USA) while mid- and back-end processing for color Doppler imaging is performed with a DSP (TMS320C6416T, Texas Instruments, Dallas, TX, USA). For system control and user interface, an Intel PXA270 processor is embedded. To maximize the usage of a DSP, the memory stall caused by external memory access was minimized by utilizing EDMA. In addition, the register utilization rate was also increased by employing accumulation and shift register structure.

Results

Table 1 summarizes the real-time execution time of the DSP utilized for a single excitation event in color Doppler processing when an imaging depth is 16 cm. As indicated in Table 1, the total execution time to perform color Doppler mid- and back-end processing (i.e., 146.02 us) is faster than the acquisition time which is approximately 200 us. It means that the developed hand-held ultrasound machine is capable of supporting real-time color Doppler imaging.

Discussion and Conclusions

In this paper, the new software-based hand-held ultrasound machine which can support real-time color Doppler imaging using a single DSP was presented. The developed hand-held ultrasound machine has improved functional flexibility so that it could quickly adopt evolving clinical applications.

Table 1. Execution time for color Doppler mid-end processing and Color Doppler back-end processing for a single excitation event on a single DSP in the developed hand-held ultrasound machine when imaging depth is 16 cm

Mid- end processing	Time[μ s]	Color Doppler processing	Time[μ s]
DC canceling	37.39	Data reorganization	2.39
TGC	9.96	Clutter filtering	5.02
Down conversion	17.90	Autocorrelation	3.72
Decimation	61.86	Axial filtering	0.78
		Velocity estimation	6.40
		Color mapping	0.60
Total	127.11	Total	18.91

P2-D-04

Compact Modular Doppler System with Digital RF Processing

Marcin Lewandowski¹, Mateusz Walczak¹, Andrzej Nowicki¹; ¹Institute of Fundamental Technological Research, Polish Academy of Sciences, Warsaw, Poland

Background, Motivation and Objective

Doppler instruments are widely used for evaluation of the hemodynamics of vascular circulation. A broad range of instruments, from the simplest ones to advanced multi-channel systems, is commercially available. The objective of the work was to develop the modular acquisition and processing system to enable the construction of various class instruments on one platform. Unification of the electronic subsystems that are common for different instruments as well as separation of the transmission-receiving part and the acquisition part offer high potential for the adaptation of the instrument at minimum costs. Application of modern high-speed digital systems makes the implementation of advanced algorithms of Doppler processing directly on RF signals feasible.

Statement of Contribution/Methods

The developed system consists of two electronic boards with dimensions of 130x90 mm in sandwich configuration. The first of them contains digital interfaces (USB, Ethernet) and digital signal processing. The transmitter-receiver systems and the analog-to-digital converter have been placed on the second board. Digital signal processing was based on an efficient DSP (Blackfin BF537, Analog Devices, USA) with 128 MB RAM and an FPGA (Cyclone II EP3C25, Altera, USA). Fast digital interface LVDS of the acquisition board enables the operating of two separate Doppler channels. The transmitter-receiver and acquisition board contains the mixed signals systems and it can be easily adapted to specific solutions without modifying the digital processing board. The modular Doppler system can work as a standalone device (with the limited user interface) or as a PC peripheral under the control of application software.

Results

The dual channel transcranial PW Doppler flowmeter with multi-gate processing has been the first application of the developed system. The acquisition module provides the A/D sampling at 64 MSPS rate with 14-bits resolution and supports ultrasonic transducers within the range of 1-16 MHz. The applied arbitrary waveform transmitter enables coded transmission signals. The digitized RF echo signals are quadrature demodulated and filtered in the FPGA. Then after the decimation the signal enters the DSP where it undergoes further processing. More advanced signal processing can be implemented on the PC. The PC software performs visualization of color Doppler, spectrum (up to 8 gates simultaneously) as well as audio output from one selected gate. The recording of raw data enables long time monitoring and off-line elaboration of the data for all range gates.

Discussion and Conclusions

The developed system is a modern technical solution which enables to build portable Doppler instruments of different classes. Modular construction of electronics systems and digital signal processing facilitate the adaptation of the system to new applications. The developed prototype of transcranial Doppler will be introduced into production soon.

P2-D-05

A Transmission Method of 200MHz Range Ultrasonic Wave Using a Fused Quartz Fiber

Takasuke Irie^{1,2}, Norio Tagawa², Tadashi Moriya², Kouichi Itoh^{3,1}; ¹Microsonic co.,Ltd., Tokyo, Japan, ²Division of Information and Communications Systems Engineering, Tokyo Metropolitan University, Tokyo, Japan, ³Hitachi-Omiya Saiseikai Hospital, Ibaraki, Japan

Background, Motivation and Objective

In the current pathological examination, the high cost diagnosis using CT and MRI are required before the established diagnosis of the tissue whether it is malignant or benign. Furthermore, the tissue diagnosis in the current pathological examination takes time because it requires a tissue sample obtained by the biopsy and the observation using an optical microscope, and gives burden on the patient. The main objective of the study is to enable an operator to observe directly microscopic images of the tissue without taking out the tissue sample from patient. In order the objective, we are developing a needle type ultrasonic microscope that uses a thin fiber as an ultrasound probe. Since the diameter of the probe is so small that can it be inserted into body tissue without placing a severe burden on the patient and still retain non-invasiveness.

Tuesday
Poster

Statement of Contribution/Methods

We reported that the ultrasonic pulse waves generated by 50 and 220 MHz transducers were transmitted in the transmission line (included the fused quartz fiber) and reflected at the end face. In this paper, we describe experimental results for the propagation in a fused quartz fiber and the penetration into the acoustic coupling medium of the ultrasonic pulse wave in the 200MHz range. In the experiment, the system consists of a pulser/receiver (Panametrics model 5900PR), a 220MHz transducer (Panametrics model V2113) for transmitting, a tapered fused quartz fiber (length; 24.3mm, diameter of the large surface side; 3.07mm, diameter of the small surface side; 0.69mm) and a 170MHz transducer (Panametrics model V3878) for receiving. In order to transmit the ultrasonic waves efficiently from the transducer to the fiber, we attached the transducer at the large surface of the fused quartz fiber. The receiving transducer was attached at the other side of the fiber. As the contact media between the fiber and the transducer, the ultrasound gel was used. The ultrasonic pulse (approximately 50Vp-p amplitude) with the wide frequency-band width (95~278 MHz) was transmitted into the fiber.

Results

The reflected wave from the end of the fiber with the frequency of approximately 160MHz and the amplitude of approximately 970mV at the end of the fiber was obtained. And the penetrated waves with the frequency of approximately from 160MHz to 100MHz and the amplitude of approximately from 970mV to 160mV through the ultrasound gel (maximum depth 1.2mm) were detected respectively.

Discussion and Conclusions

The wavelengths of the 100MHz and 160MHz were approximately 15 μm and 10 μm respectively. If the ultrasonic image with the resolution higher than the half of the wavelengths could be obtained using the penetration method, it will be expected that the microscopic image of the tissue can be seen directly. We will continue to study to increase the sensitivity of the penetrated wave and improve the efficiency of the transmission.

P2-D-06

Electronic Fresnel Focusing for Low-Cost Portable Ultrasound Imaging

Jesse Yen¹, Jay Mung¹, Man Nguyen¹, Samer Awad^{1,†} *University of Southern California, USA*

Background, Motivation and Objective

As ultrasound systems become more portable, new system architectures with fewer channels than standard cart-based systems are desired. To reduce channel count, we propose a new method based on the Fresnel lens concept. We note that there have been few publications describing an electronic Fresnel lens for imaging in recent years. This is likely due to the prevalent use of analog delay lines and digital methods for traditional time delay-and-sum (DAS) beamforming (BF). Here, we investigate the use of a modified electronic Fresnel-based BF method for low-cost portable ultrasound systems.

Statement of Contribution/Methods

With Fresnel focusing, the traditional time delay associated with each element is replaced with an equivalent phase shift that always ranges from 0 to 360 deg. For a sampled system, discrete phase shifts would be used. In our case we investigate the use of 4- and 8-phase systems. A 4-phase system would have possible phase shifts of 0, 90, 180, and 270 deg only. The primary advantage of this technique is that a system with 4 transmit and 2 receive channels can be used to steer and focus an array with 64 to 128 elements. Each channel is assigned a different phase shift. Single-pole/single-throw switches such as the ADG1413 (Analog Devices) can be used to cluster elements with identical phase shifts. Furthermore, echo data requiring a 45 deg phase shift can be achieved by applying a 0 and 90 deg phase shift via a digital Hilbert transform followed by summation. We performed Field II computer simulations to characterize the performance of the system in terms of -6, -20, and -40 dB beamwidths. For our experimental setup, we imaged an ATS ultrasound phantom consisting of axial-lateral wire targets and 3 mm diameter cylindrical anechoic cysts. A full synthetic aperture RF data set was collected and sampled at 40 MHz using an Ultrasonix Sonix RP ultrasound system with a L14-5/38 linear array and a 2-cycle 5 MHz transmit pulse. First, offline DAS BF was performed using Matlab to serve as a gold standard. Next, the RF data were beamformed based on the Fresnel focusing technique. Contrast ratio and lateral wire target size were used as image quality metrics.

Results

In the Field II simulations, the lateral -6, -20, and -40 dB beamwidths for DAS BF were 0.53, 0.96, and 2.97 mm respectively. For 8-phase BF, the beamwidths were 0.66, 1.36, and 6.22 mm. For 4-phase BF, the values were 0.62, 1.93, and 15.59 mm with clutter present at the -40 dB level. For a 3 mm diameter cyst, the contrast ratios were

26.2 , 23.5, and 20.0 dB for traditional DAS BF, 8-phase, and 4-phase Fresnel focusing technique, respectively. The lateral wire target sizes were 0.60, 0.66, and 0.62 mm, respectively.

Discussion and Conclusions

The -6 and -20 dB beamwidths for an 8-phase system were similar to DAS. Fresnel focusing may be a suitable alternative for low-cost portable ultrasound systems due to the reduced channel count. Future work will involve improving the -40 dB beamwidth and developing a prototype Fresnel-based system.

P2-D-07

5DOF Trajectory Reconstruction for Handheld Ultrasound with Local Sensors

Philipp Stolka¹, Joyce Choi², Joseph Wang², Emad Boctor^{1,3}; ¹Computing Science, Johns Hopkins University, Baltimore, MD, USA, ²Biomedical Engineering, Johns Hopkins University, Baltimore, MD, USA, ³Department of Medical Imaging Physics, Johns Hopkins Medical Institutions, Baltimore, MD, USA

Background, Motivation and Objective

For intra-operative imaging, handheld ultrasound/US excels because of its simplicity, real-time nature, and no radiation. However, it is not easy to spatially interpret the 2D images. In addition to the difficulty to highlight relevant 3D features, handheld US imaging is an "immediate" modality since volume reconstruction usually only happens as a mental exercise. This makes registration of new US data with pre-operative data sets difficult.

Algorithms for 2D image slice positioning and 3D volume reconstruction can be classified by the sensors used to constrain positions of single 2D slices. Mostly, they are either tracking-based approaches (using absolute-position external sensors like electromagnetic/EM or optical trackers, encoder arms, or robot-based solutions) or sensorless 3D reconstructions (approaches that require specific trajectories or complex image-based reconstructions).

Statement of Contribution/Methods

We propose to replace absolute probe tracking with simple local sensors, which only provide a limited range of sensor values and limited positioning information. However, by combining them into a local sensor ensemble, iterative global trajectory reconstruction is feasible. This has a very small footprint in complexity and hardware, allowing very low-cost 3D US generation without sophisticated tracking mechanisms.

To provide independent information sources that do not suffer from drift or jitter, two sensor types are attached to the handheld US probe: high-precision optical mice for relative lateral and elevational motion as well as a 3-axis accelerometer, used as an absolute 2DOF orientation sensor, having no drift, but subject to acceleration artifacts. To increase the stability of the system against spurious mouse jumps, two mice will be used on both sides of the US array. This also recovers rotational motion around the gravity vector (the DOF missing from the orientation sensor) in many cases.

Motions m_i and orientations R_i are cumulated into positions P_i : $P_n = \sum_{i=1..n} R_i m_i$.

Results

Experiments regarding the (perpendicular) motion drift of optical mice have shown it to be below 6%, depending on the surface. With the driftless 2nd accelerometer precision, calculations led to expect a vectorial $\approx 7\%$ error on linear motions. Trajectories on curved surfaces exhibited errors of 10..17% (4DOF reconstructions using one mouse and one accelerometer, compared with ground truth from optical tracking).

Discussion and Conclusions

We have shown the usefulness of very limited local sensor sets for successful US probe trajectory reconstruction. The trajectories can then serve as either sole input for 3D US, or can initialize image-based algorithms.

Drift errors can be partly explained by uneven and rough surfaces making tracking difficult. Further experiments will focus on including a 2nd mouse for 5DOF reconstructions.

P2-E. Acoustic Radiation Force Imaging

Sala Orange

Tuesday, September 22, 2009, 10:00 am - 11:30 am

Chair: **Kathy Nightingale**
Duke University

P2-E-01

Optical Quantification of Acoustic Radiation Force Impulse-Induced Dynamics in a Translucent Phantom

Richard Bouchard¹, Jason Streeter², Mark Palmeri¹, Paul Dayton², ¹Duke University, USA, ²UNC Chapel Hill / NC State University, USA

Background, Motivation and Objective

Despite their practical utility, ultrasonically-based tissue displacement estimators are hindered by a few fundamental limitations: poor tracking resolution in the lateral dimension, sampling limitations due to interference from previous pulses, and a large effective tracking kernel. Optically-based (i.e. visible spectrum) tracking, which is impractical in most clinical applications due to near-field scattering, can overcome some of the aforementioned limitations in an experimental setting that utilizes a translucent phantom. Past research groups have successfully tracked the acoustic radiation force impulse (ARFI)-induced dynamic response in a phantom with optically-based techniques that relied on a laser source. These techniques, however, had either limited spatial/temporal resolution or were restricted to uniaxial tracking. We propose an optically-based technique that utilizes conventional microscopy to investigate, with good spatial/temporal displacement resolution, the ARFI-induced response in a translucent, tissue-mimicking phantom.

Statement of Contribution/Methods

Suspended 10- μ m microspheres were tracked axially and laterally at multiple locations throughout the field of view (FOV) with 0.5- μ m tracking resolution, in both dimensions, and at frame rates of up to 36 kHz. Induced dynamics were successfully captured before, during, and after the ARFI excitation at depths of up to 4.8 mm from a translucent phantom's proximal boundary. Results are presented for tracked axial and lateral displacements resulting from on- and off-axis (i.e. shear wave) acquisitions; these results are compared to matched finite element method (FEM) modeling and independent ultrasonically-based empirical results.

Results

In axial data sets, displacement peaks occur later in time and with decreasing amplitude as the FOV becomes more offset, which is characteristic of shear wave propagation. From these data, shear wave velocities resulting from all three acquisition techniques (i.e. optical, ultrasound, FEM) differ by < 3%. In lateral data sets, displacement occurs almost immediately after the excitation while times to displacement peaks do not share a direct relationship with FOV offset, which is characteristic of a Poisson effect. From these data, a "lateral-displacement" wave speed can be obtained; this speed differs by < 8% between optical and FEM estimates.

Discussion and Conclusions

Optical tracking of ARFI-induced dynamics in a translucent, tissue-mimicking phantom was successfully achieved at frame rates of up to 36 kHz and with sub-micron displacement resolution in the axial and lateral dimensions. These tracking data show good agreement with matched FEM modeling and independent ultrasonically-based results early in time (up to 4 ms). Despite the restricted clinical applicability of this tracking technique, it could assist in gaining a greater understanding of complex, radiation force dynamics in tissue-mimicking phantoms.

In Vivo ARFI Imaging of the Mechanical Properties of Muscle in a Dog Model of Duchenne Muscular Dystrophy

Mallory Scola¹, Joe Kornegay², Caterina Gallippi¹; ¹Biomedical Engineering, University of North Carolina at Chapel Hill, USA, ²Pathology and Laboratory Medicine, University of North Carolina at Chapel Hill, USA

Background, Motivation and Objective

Duchenne muscular dystrophy (DMD) is an X-linked recessive disorder caused by a mutation in the gene for dystrophin leading to a loss of the dystrophin protein from muscle cell (myofiber) membrane. There is resultant myofiber necrosis and subsequent progressive replacement of muscle by fibrous tissue and fat. The fibrosis and fatty deposition, along with myofiber regeneration, can lead to initial muscle enlargement (hypertrophy), generally followed by muscle loss (atrophy). We hypothesize that ARFI imaging is capable of differentiating changes in muscles affected by DMD.

Statement of Contribution/Methods

ARFI imaging was performed with a Siemens SONOLINE Antares™ imaging system equipped for research purposes and a VF7-3 transducer (Siemens Medical Solutions USA, Inc. Ultrasound Division). Imaging was performed in vivo on the rectus femoris (RF) and cranial sartorius (CS) muscles of two age-matched golden retriever cross littermates, one normal and the other with a dystrophin gene mutation analogous to that of DMD. Two ARFI excitation methods were employed: (1) a single 70 μ s ARFI excitation impulse, and (2) a double excitation impulse, with the two 70 μ s impulses administered in the same region of excitation 2ms apart. Both methods were followed by 4:1 parallel receive tracking for 1D axial displacement measurement using cross-correlation. ARFI imaging was implemented in planes transverse and parallel to muscle fibers. Depth was controlled for using a displacement profile obtained from a homogeneous agar tissue mimicking phantom imaged with the same ARFI methods. Physiological motion was rejected, and parametric images of peak displacement (single-excitation) and difference in peak displacements (double-excitation) were rendered.

Results

In the RF muscle region, as segmented from the B-Mode image, transverse plane peak displacements were 0.78 mm \pm 0.23 and 0.24 mm \pm 0.18 in DMD and control dogs, respectively. Differences in peaks were 1.44 mm \pm 0.48 and 0.60 mm \pm 0.26. Parallel plane peak displacements were 0.97 mm \pm 0.29 and 0.25 mm \pm 0.13, and differences in peaks were 1.77 mm \pm 0.77 and 0.59 mm \pm 0.26. Smaller ($p < 0.02$, paired t-test) ARFI-induced displacements achieved in the RF of the DMD dog suggest that the DMD RF is more stiff, and smaller ($p < 0.02$, paired t-test) difference in peaks suggest that the DMD RF is less elastic, which is consistent with expected fibrosis. In contrast, peak displacement and difference in peak results for the CS muscle were similar in the DMD and control dog in both transverse and parallel planes. However, the DMD CS was larger and more homogeneous in ARFI imaging, consistent with expected hypertrophy.

Discussion and Conclusions

Results showed significant differences in peak displacement in the RF for DMD vs control dog, but similar ARFI results in the CS. These results are consistent with the variable disease progression seen among muscles in DMD and suggest that ARFI could be relevant to monitoring therapy in affected individuals.

Axial Resolution Measurement of an ARFI Imaging System using Cone Phantoms

Manoj Menon^{1,2}, Stephen McAleavey^{1,2}; ¹Biomedical Engineering, University of Rochester, USA, ²Rochester Center for Biomedical Ultrasound, USA

Background, Motivation and Objective

Assessing the mechanical properties of small tissue structures is useful for the characterization, diagnosis, and treatment of a variety of conditions, such as atherosclerotic vessels and cancerous tumors. Acoustic Radiation Force Impulse (ARFI) imaging finely measures the mechanical properties of tissue by generating a local acoustic radiation force using a standard diagnostic ultrasound scanner. Short duration, high intensity ultrasound pulses induce impulsive acoustic radiation forces that result in micron-scale tissue displacements. Displacements are tracked using ultrasound tracking pulses and are quantified using conventional correlation-based methods. In this study, we measured the axial resolution of an ARFI imaging system by imaging tissue phantoms with compliant cones embedded in stiff background. It is crucial to understand the resolution limits in order to apply this to applications in which resolving small objects is important.

Statement of Contribution/Methods

The ARFI Imaging system was a Siemens Antares ultrasound scanner (Siemens Medical Systems) with a VF7-3 linear array transducer using a 2 cm lateral focal depth and 5.33 MHz excitation frequency. Beam sequences included a 30 microsecond pushing pulse followed by 30 – 0.15 microsecond tracking pulses (at a pulse repetition frequency (PRF) of 12.7 kHz), during a period of 1.2 ms. A gelatin phantom was fabricated with a 5 kPa Young's modulus cone and 17 kPa background, providing the necessary elastic contrast to visualize the cone tip. A MATLAB simulation was developed to model the system. Scatterer positions and amplitudes were defined, and convolved with a 2-cycle pulse to generate echoes. Part of the echo was shifted to simulate displacements which were estimated using windowed normalized cross-correlation. Windows ranged in length from 0.6 mm to 5.1 mm. The location on the cone axis where the displacement was half the maximum displacement at the base of the cone was identified and the cone width at that axial location was reported as the resolution.

Results

Axial resolution measurements were proportional to correlation window length. Resolution was approximately 0.6 mm given a 1 mm correlation window. We also computationally investigated the effects of the reflections at the cone-background boundary.

Discussion and Conclusions

We have successfully developed a way to experimentally, and computationally estimate the resolution of an ARFI imaging system by assessing its ability to image the tip of a compliant cone. This analysis may be used by others to quantify the resolution of elastographic imaging methods that employ correlation-based displacement estimation techniques.

P2-E-04

In Vivo Hemostasis Detection at Human Femoral Arteriotomy by ARFI Ultrasound

Russell Behler¹, Mallory Scola¹, Timothy Nichols², Melissa Caughey³, Melrose Fisher³, Hongtu Zhu⁴, **Caterina Gallippi¹**; ¹Biomedical Engineering, The University of North Carolina at Chapel Hill, Chapel Hill, NC, USA, ²Medicine, Pathology and Laboratory Medicine, The University of North Carolina at Chapel Hill, USA, ³Division of Medicine, The University of North Carolina at Chapel Hill, USA, ⁴Biostatistics, The University of North Carolina at Chapel Hill, USA

Background, Motivation and Objective

Patient care could be improved, and medical expenses reduced, by individualizing manual compression and time to ambulation following cardiac catheterization. Individualizing treatment requires near real-time monitoring of bleeding during compression at femoral artery puncture sites (arteriotomies). *We hypothesize that hemostasis onset at femoral arteriotomies can be monitored noninvasively by ARFI ultrasound.*

Statement of Contribution/Methods

We conducted a randomized, reader-blinded study of 20 patient volunteers who underwent diagnostic percutaneous coronary catheterization. After sheath removal, patients were randomized to treatment with either standard of care manual compression alone or, to expedite hemostasis, manual compression augmented with a pGlcNAc fiber-based hemostatic dressing (Marine Polymer Technologies, Danvers MA). Concurrent with manual compression, ARFI imaging was performed with a Siemens SONOLINE Antares™ imaging system (Siemens Medical Solutions USA, Inc. Ultrasound Division). ARFI imaging began at the time of sheath removal, with an acquisition every minute for 15 min. Serial data sets were processed with custom software that exploits variance in 1D axial cross-correlation measures to identify pools of extravasated blood. The time at which estimated extravasated blood area stopped increasing was considered time to hemostasis onset, and hybrid ARFI/B-Mode images were rendered to highlight extravasated blood.

Results

Average ARFI-derived times to hemostasis in patient volunteers treated with manual compression alone (n=10) and manual compression augmented by hemostatic dressing (n=9) were, respectively, 13.00 ± 1.56 and 9.44 ± 3.09 min ($p \leq 0.0065$, Wilcoxon). Arteriotomies were more displaceable than adjacent arterial wall tissue during suspected bleeding, and large displacements relative to surrounding soft tissue were observed in suspected extravasated blood pools. Notably, ARFI imaging delineated rebleeding in a patient volunteer treated with manual compression alone who later developed a hematoma.

Discussion and Conclusions

Our preliminary results, which show statistically significantly faster ARFI-derived times to hemostasis when a hemostatic dressing is used to augment manual compression, suggest that ARFI imaging is capable of noninvasively monitoring hemostasis onset at femoral arteriotomies. Future work will employ longer serial ARFI imaging duration.

P2-E-05

Analysis of Cross-Correlation Coefficients for Subcutaneous Blood Signal Detection by ARFI Imaging

Mallory Scola¹, Elizabeth Mauldin², Caterina Gallippi¹; ¹Biomedical Engineering, University of North Carolina at Chapel Hill, USA, ²College of Arts and Sciences, University of North Carolina at Chapel Hill, USA

Background, Motivation and Objective

ARFI subcutaneous blood detection is relevant for monitoring femoral puncture post cardiac catheterization as well as numerous other clinical applications. Blood signal isolation by conventional means is challenged by overlapping frequency spectra and low blood to surrounding tissue signal ratios. However, the correlation of signals arising from blood displaced by ARFI is expected to be lower than that of signals arising from soft tissue. We hypothesize that cross correlation coefficients can be exploited to enhance identification of subcutaneous blood pools in ARFI imaging.

Statement of Contribution/Methods

Imaging was performed ex vivo on a porcine muscle injected with a blood mimicking fluid using a Siemens SONOLINE Antares™ imaging system specially equipped for research purposes and VF7-3 transducer (Siemens Medical Solutions USA, Inc. Ultrasound Division). ARFI and spatially matched B-Mode data were serially acquired before, during, and after injection of the fluid. ARFI induced displacements were then measured using 1D axial cross-correlation. Fluid signal was isolated by performing filtering based on (1) variance of displacement, (2) mean cross-correlation, (3) variance of cross-correlation, (4) variance of first derivative of cross-correlation, and (5) variance of second derivative of cross-correlation.

Results

Filtering based on variance of ARFI induced displacement detected a pool of fluid with a cross-sectional area of 100.82 mm². The method based on mean cross-correlation detected a 104.98 mm² area of fluid. The variance of cross-correlation filter isolated an area of 104.46 mm². The variance of the first derivative of cross-correlation produced a 100.81 mm² area of fluid, and variance of the second derivative of the cross-correlation found a pool of fluid with an area of 105.44 mm². Since the detected fluid area is within 3% of the mean area for all of the filters, no significant difference was observed in the filtered images. Figure 1 shows the fluid signal isolated by filtering based on the second derivative of the cross correlation value.

Discussion and Conclusions

All five methods of filtering were successful at isolating pools of fluid. In theory, exploiting displacement variance will enhance discrimination at high correlation values, as described by the jitter equation. In addition, time derivations accentuate variance of periodic correlation values.

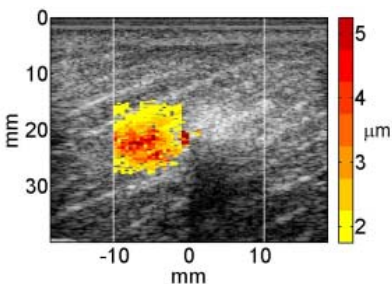


Image Reconstruction of Local Shear and Viscosity Moduli for a Finite Amplitude Modulated Acoustic Radiation Force

Alexia Giannoula¹, Richard Cobbold²; ¹*Institute of Biomaterials & Biomedical Engineering, University of Toronto, Toronto, Ontario, Canada*, ²*Institute of Biomaterials & Biomedical Engineering, University of Toronto, Toronto, Canada*

Background, Motivation and Objective

An efficient way to remotely generate narrowband low-frequency shear waves within tissue, is by the modulated acoustic radiation force, resulting from the interference of two finite-amplitude confocal quasi-CW ultrasound beams with slightly different frequencies. Furthermore, relatively large ultrasound source pressures may be needed, thereby, leading to the generation of narrowband shear components at both the fundamental and harmonics of the modulation frequency [1]. In this work, we present the method and results obtained using a FEM model, to simulate the induced shear displacement within a homogeneous viscoelastic medium, containing a circular inclusion (lesion). It is shown how images of the local shear modulus and viscosity can be reconstructed, using an implementation of the inverse-problem approach. Several components of the shear-wave spectrum are examined and the corresponding reconstructed images are assessed with several modified elastography-based quality metrics.

Statement of Contribution/Methods

Initially, the finite-amplitude acoustic radiation force, created by the interference of two confocal quasi-CW ultrasound beams, is calculated using a modified 2nd-order operator-splitting algorithm. Subsequently, the propagation of the generated narrowband low-frequency shear waves in a viscoelastic medium with a circular lesion are studied, using finite-element simulations, assuming the Voigt model. In the following, an inverse algorithm is applied on the calculated shear-displacement ‘movie’, thereby, enabling the reconstruction of 2-D maps of the local shear modulus and viscosity. Not only the fundamental, but also the higher-harmonic and low-frequency (LF) components of the shear-wave spectrum are employed. The performance of the reconstructed images of the local viscoelasticity are evaluated based on the lesion contrast, contrast-transfer-efficiency (CTE), and contrast-to-noise ratio (CNR).

Results

Efficient reconstruction of shear modulus and viscosity images is demonstrated, for both low and high viscosity conditions. In the first case, not only the fundamental, but also the higher harmonics of the shear spectrum are shown to provide reliable estimates of viscoelasticity. The calculated contrast and CTE are very good for hard or soft lesions with low contrast and for hard lesions with high contrast, for all harmonics. For increased viscosities, the low-frequency component, arising due to the effects of dispersion, exhibits superior reconstruction and contrast performance.

Discussion and Conclusions

Images of the local shear and viscosity moduli were successfully reconstructed, using a FEM model, followed by an inverse algorithm. A wide range of lesion shear moduli, viscosities and diameters was investigated. The potential of improving the viscoelastic estimates by combining information from different spectral components was also considered.

[1] A. Giannoula et al., IEEE Trans. UFFC, 56, 575-588, 2009.

Acoustic Radiation Force Impulse Imaging for Aneurysms

Aine Tierney¹, Douglas Dumont², Tim McGloughlin³; ¹*M&AE, University of Limerick, Limerick, Limerick, Ireland*, ²*Duke University, USA*, ³*University of Limerick, Ireland*

Background, Motivation and Objective

Current diagnosis of Abdominal Aortic Aneurysms (AAA) relies on the maximum diameter criterion – that is if the maximum diameter of the aneurysm is 5cm or greater, surgical intervention is deemed necessary. It is known that some aneurysms rupture at a relatively small diameter while others grow to a large diameter without rupture, indicating that there are limitations associated with the use of diameter alone as a diagnostic tool. In aortic aneurysm tissues, weakening of the mechanical properties of the degenerated tissues may progress the expansion of the aneurysm. Therefore, a method for the reliable, noninvasive estimation of AAA wall mechanics may be a useful clinical tool for the assessment of rupture potential. Acoustic radiation force impulse (ARFI) imaging characterizes the mechanical properties of tissue by measuring displacement resulting from applied ultrasonic

radiation force. ARFI imaging has been shown to be effective in monitoring liver ablations, differentiating cysts from potentially malignant masses in breast imaging and also the mechanical properties of vascular tissue in vivo in the carotid artery. This study explores the feasibility of using ARFI imaging to characterize AAA behaviour

Statement of Contribution/Methods

An ex vivo AAA model was developed from an excised porcine aorta, with an elastase treatment. The behavior of the AAA model was characterized through pressurization and analysed using ARFI imaging and shear wave techniques to demonstrate differences between aneurysmal and normal aortic tissue. Opening angle measurement showed a four fold decrease from healthy aorta to AAA model, this elastin degradation was verified by pathological analysis. At each pressure step through physiological pressure ranges, diametrical measurements of the AAA model were consistently between 20mm and 40mm greater than healthy aorta measurements. Shear wave velocities, between 80mmHg and 180mmHg, varied from 4.2mm/ms² to 7mm/ms² for healthy tissue and 4.6mm/ms² to 8.26mm/ms² for the aneurysmal tissue.

In vivo aorta was imaged to demonstrate the feasibility of ARFI imaging on aortic aneurysms. B-mode and ARFI images were acquired of one healthy and one diseased aorta in female volunteers. Cardiac motion was minimized using ECG-triggered beam sequences, and ARFI images were acquired during diastole. Residual motion was treated with a linear motion filter. The healthy aorta showed uniform displacement at the wall of excitation. Diseased aortic images revealed greater displacement in the intraluminal thrombus than the wall of the aorta.

Results

Discussion and Conclusions

ARFI induced displacement was demonstrated in ex vivo phantoms, in vivo healthy aorta and in vivo diseased aorta. ARFI imaging was shown to have potential as a useful diagnostic tool for AAA examination.

Acknowledgements: This work is supported by NIH Grants HL075485 and 5T32EB001040, and the FAS Science Challenge

P2-E-08

A comparison between 1D and 1.5D arrays for the formation of spatially modulated ultrasound radiation force beams.

Etana Elegbe^{1,2}, Stephen McAleavey^{1,2}, ¹Biomedical Engineering, University of Rochester, USA, ²Rochester Center for Biomedical Ultrasound, USA

Background, Motivation and Objective

The Spatially Modulated Ultrasound Radiation Force (SMURF) method is a technique for estimating the shear modulus of an elastic material [1]. SMURF determines shear modulus through measurement of the frequency of shear waves of known wavelength propagating in a medium of unknown modulus. Shear modulus is then computed using the relationship $G = (\lambda f)^2 \rho$. The spatial frequency k of the force variation is equal to the desired spatial frequency of the shear wave, that is, $k = 2\pi/\lambda$. Because acoustic radiation force is proportional to intensity, generation of this spatially varying force is a matter of determining how to generate an equivalently varying ultrasound intensity field.

Presented in this study is the Focal Fraunhofer method, which is one of the techniques we have developed to create the desired beam intensity pattern within a region of interest. To create a push that results in discernible displacements while minimizing tissue heating in the near field, we investigate the use of both a linear and a multi-row 1.5D array. A 1.5D array allows for more aggressive focusing in the elevation direction and thus a greater intensity in the region of interest. The efficacy of both configurations is analyzed based on the ability to generate beams of the desired well-defined spatial wavelength at various focal depths, as well as the ability to localize the pushing beam to the region of interest.

Statement of Contribution/Methods

Both configurations are simulated using Field II [2] for tissue attenuation values of 0 and 0.7dB/cm/MHz. The linear array transducer is simulated with 96 elements. The 1.5D array has 7 x 96 elements. Both transducers have a center frequency of 5.33 MHz, a mechanical focus at 3.75cm and a 100-cycle pushing beam. The ratio of the intensity in the near field region to that within the region of interest is an indication of the efficiency in energy deposition at the ROI.

Results

For a given F/#, the 1.5D array showed a significant improvement in the localization of the intensity field at the region of interest, more so in the case of an attenuation level of 0.7dB/cm/MHz (approximately 2.5 times more energy at the ROI than the 1D case). For an F/3 system, the 1.5D array had an effective focal range of 4.1cm, while the 1D array was limited to a range of 2cm. There is also a significant improvement in terms of the overall intensity for both the F/3 and F/5 configurations with the 1.5D array.

Discussion and Conclusions

The use of a 1.5D array transducer increases the intensity deposited in the ROI as well as the effective depth of focus due to the ability to control the elevation focus at various depths.

Reference:

- [1] McAleavey, S.A., M. Menon, et al. (2007). "Shear-modulus estimation by application of Spatially Modulated impulsive acoustic radiation force." *Ultrasonic Imaging* 29(2): 87-104.
- [2] Jensen, J. A. and N. B. Svendsen (1992). "Calculation of pressure fields from arbitrarily shaped, apodized, and excited ultrasound transducers."

Tuesday
Poster

P2-F. Hard Tissue and Bone

Sala Orange

Tuesday, September 22, 2009, 10:00 am - 11:30 am

Chair: **Georg Schmitz**
Ruhr-Universität Bochum

P2-F-01

Measurement of longitudinal wave velocity in trabeculae by micro-Brillouin scattering

Masahiko KAWABE¹, Mami MATSUKAWA¹, Norikazu OHTORI²; ¹Doshisha University, Japan, ²Niigata University, Japan

Background, Motivation and Objective

Bone has complicated properties which depend on the multi-scale structure. The quantitative ultrasound technique (QUS) is used to know "bone quality", such as structural properties and elastic properties. However, the conventional QUS technique gives us mixed information from multi-scale properties in the area where ultrasonic waves passed through. In order to extract pure material properties of bone without the effects of other characteristics like structures, we have tried to measure longitudinal wave velocity in one trabecula using a non-contact micro-Brillouin scattering technique.

Statement of Contribution/Methods

The micro-Brillouin scattering measurement was performed using a JRS type Fabry-Perot interferometer, with an argon ion laser ($\lambda=514.5\text{nm}$). Wave velocities in the minute area (diameter of $10\mu\text{m}$) can be obtained by the measurement of very weak scattered laser light from thermal phonons in the sample. Considering the transparency for light scattering measurements, we have fabricated thin layer samples (thickness $150\mu\text{m}$) from the trabecular bone in the distal part of a bovine femur. Two types of samples, where trabecular aligns along the bone axis direction or anterior-posterior direction, were prepared.

Results

We have succeeded in measuring longitudinal wave velocities in 20 trabeculae. Velocity measurement error was approximately 1%. The aspect ratio (diameter/length) of the measured trabeculae were from 0.14 to 0.36. We measured wave velocities in the trabecular alignment direction at 12 different positions in each trabecula. There was no recognizable pattern in the velocity distribution. The measured wave velocities were in the range of $4.58\text{-}5.16 \times 10^3 \text{m/s}$ in the trabeculae along bone axis direction, whereas those along the posterior-anterior direction were $4.60\text{-}5.09 \times 10^3 \text{m/s}$. The relations between the aspect ratio and wave velocities are shown in the figure. The effects of trabecular direction and aspect ratio on the velocity were not statistically significant.

Discussion and Conclusions

The observed velocities in each trabecula did not depend on the aspect ratio and trabecular direction. This tells us the possibility that the average elastic properties are similar in all trabeculae.

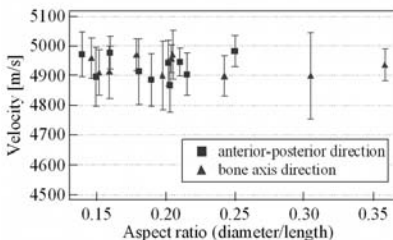


Fig. The relations between the aspect ratio and average velocity with SD of each trabecula.

Tendinopathy Discrimination Using Spatial Frequency Parameters and Artificial Neural Networks

Pengfei Song¹, Kristopher R. Linstrom², A. John Boye³, Kornelia Kulig³, Judith M. Burnfield⁴, Greg Bashford¹,²*Biological Systems Engineering, University of Nebraska-Lincoln, Lincoln, Nebraska, USA*, ²*Neurintel LLC, Lincoln, Nebraska, USA*, ³*Division of Biokinesiology and Physical Therapy, University of Southern California, Los Angeles, California, USA*, ⁴*Institute for Rehabilitation Science and Engineering, Madonna Rehabilitation Hospital, Lincoln, Nebraska, USA*

Background, Motivation and Objective

Healthy tendon's structural characteristics are related to the anisotropic speckle pattern observed in ultrasonic images. Tendon damage (e.g., with advanced tendinopathy) disrupts the speckle pattern. Quantification of the structural appearance of tendon shows promise in creating a tool for early diagnosis, prognosis and tracking of changes in tendon organization over time. Previously we showed the feasibility of using spatial frequency parameters and Linear Discriminant Analysis (LDA) to categorize tendon tissue as normal or tendinopathic with better than 80% accuracy. The current work aimed to improve accuracy by using a more sophisticated classifier, the Artificial Neural Network (ANN). Our objectives were to develop the ANN classifier and compare its results with those achieved in our previous LDA work.

Statement of Contribution/Methods

Ultrasound B-Mode images of the Achilles and Tibialis Posterior (TibPost) tendons from 40 subjects were scanned with a commercial system (Siemens Antares). Subjects were divided into four groups, N=10 each: Achilles tendinopathy, Achilles controls, TibPost tendinopathy, TibPost controls. Within the images, eight spatial frequency parameters from the spectra of 32x32 pixel (2 mm²) kernels were extracted. A sample kernel is shown (Fig. 1, top left). Peak spatial frequency (i.e., radius of paired peaks) was one parameter studied (Fig. 1, top right; ~2 mm⁻¹ here). Note the contrast with the lower images in Figure 1. The eight parameters served as inputs into two different ANNs: one trained with Achilles images and one with TibPost images. Independent test sets from each group were tested against each of the two ANNs.

Results

For the Achilles tendons tested with an Achilles-trained ANN, the correct classification rate (CCR) was 99.1%. The CCR was 94.6% for TibPost tendons tested with a TibPost-trained ANN. However, when testing a tendon with an ANN trained for the other tendon type, the results were 71.9% for the TibPost tested against Achilles-trained ANN, and 75.2% for the Achilles tested against TibPost-trained ANN.

Discussion and Conclusions

The high CCRs obtained using the tendon-specific ANNs suggest that this novel discrimination strategy may offer strong promise as a tool for diagnosing and monitoring a degenerated tendon's response to treatment. The ANN CCR was higher than the highest CCR of 82.6% obtained by the LDA used in our previous work.

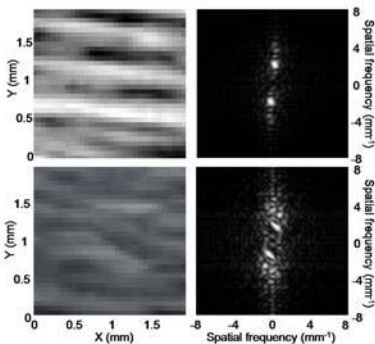


Fig. 1. Space domain – spatial frequency domain. Top left, normal tendon image kernel. Top right, corresponding spatial spectrum. Bottom left and right, tendinopathy image and spectrum respectively.

P2-F-03

Tooth Characterization using Ultrasound with Fractional Fourier Transform

Sevan Harput¹, Steven Freear¹,¹*Ultrasound Group, School of Electronic and Electrical Engineering, University of Leeds, Leeds, United Kingdom*

Background, Motivation and Objective

The diagnostic applications of ultrasound have been used in dentistry since the 1960s. The pulse-echo technique is exploited for producing an image of the tooth enamel and underlying dentino-enamel junction. Although long-duration excitation provides a better penetration, short-duration pulses are preferred to avoid the overlapping caused by the successive reflections inside the enamel and dentin layers, which makes time or frequency analysis nearly impossible. However, by using long-duration linear frequency modulated chirp excitation, it is possible to maintain separation in time and frequency by exploiting the fractional Fourier transform (FrFT). In this work, we present an application of the fractional Fourier technique to tooth imaging by analyzing and filtering chirp signals, overlapping in both time and frequency domains, where the common time or frequency based filtering is not applicable.

Statement of Contribution/Methods

For applications like tooth imaging, the ultrasonic attenuation makes signal detection more problematic for short-duration/high-frequencies pulses. Thus, a long-duration chirp is chosen to increase the excitation energy. However, in the experiments it is observed that the enamel-dentin boundary creates numerous internal reflections, which causes the chirp signals to interfere arbitrarily. The resulting waveform is not identifiable in the time domain. In the frequency domain, constructive and destructive interference of the phase of each individual chirp exists. When the frequency components in each ultrasonic pulse are not in phase with that of successive overlapping pulses an irregular waveform is created in the frequency domain. Therefore, the interfered chirp signals are filtered in the fractional domain, where the rotation angle is calculated according to chirp rate. The filtered signals are transformed back to the time domain and the time-of-flight between consecutive chirp signals are measured. Finally, the thickness of layers can be calculated through prior knowledge of the speed of sound in that material.

Results

The experiments are performed in water by using 2.25MHz Olympus V323 transducers (Olympus NTD Inc., Waltham, MA). A tooth phantom is constructed by bonding two 1 mm thick glass plates between a 2 mm gap, since glass and enamel have similar acoustic properties including speed of sound and acoustic impedance. Results indicate that the thickness of the glass and the intervening gap can be measured with an accuracy of less than 5% error.

Discussion and Conclusions

In this work, we have successfully demonstrated the application of the FrFT in the separation of overlapping chirps. The dentino-enamel junction for a tissue phantom has been accurately characterized. The tissue boundaries within the tooth phantom could not be differentiated with traditional techniques. However, chirp coded excitation together with FrFT was able to produce an accurate tissue boundary measurement.

P2-F-04

Assessment of Articular Cartilage Morphological, Acoustic and Mechanical Properties using High Frequency Ultrasound

Yong-Ping Zheng¹, Shu-Zhe Wang¹, Yan-Ping Huang¹,¹*The Hong Kong Polytechnic University, Hong Kong, China, People's Republic of*

Background, Motivation and Objective

Osteoarthritis (OA) is a common joint disorder which affects millions of individuals all over the world. The articular cartilage (artC) degeneration in OA is related to changes in material properties. In order to detect OA in the early degeneration stage and provide better treatment, researchers have tried different methods other than the most clinically used x-ray or arthroscopy to monitor the changes in the properties of the artC, since those traditional techniques are not suitable for the early detection of artC degeneration. Ultrasound has been treated as one of the most promising methods for the early diagnosis of artC degeneration. In this study, high frequency ultrasound systems were used to quantitatively measure the morphological, acoustic and mechanical properties of bovine artC in vitro.

Tuesday
Poster

Statement of Contribution/Methods

A total of 40 artC disks were prepared from twenty bovine patellae ($n=20 \times 2$) and divided in to two groups, for later collagenase and trypsin digestion, respectively. The surface condition of artC was measured by ultrasound using ultrasound roughness index (URI), which indicates the roughness of the artC surface. Acoustic parameters and thickness of the samples were also assessed before and after the enzyme degeneration treatment. And a newly developed ultrasound water jet indentation system was used to assess the mechanical properties of artC.

Results

The results showed URI increased significantly ($p < 0.05$) after collagenase digestion, while no significant difference of URI ($p > 0.05$) was found in trypsin digestion group. Acoustic parameter integrated reflection coefficient (IRC) decreased significantly ($p < 0.05$) in collagenase digestion group while no significant change ($p > 0.05$) was found in trypsin digestion group. Apparent integrated backscatter (AIB) suggested insignificant change in collagenase group ($p > 0.05$) but significant decrease in trypsin group ($p < 0.05$). Both enzymatic degeneration groups showed no significant difference ($p > 0.05$) in integrated attenuation (IA) results and significant increase ($p < 0.05$) in integrated backscatter (IBS) results. The stiffness measured by ultrasound water jet suggested that artC from both groups became significantly softer ($p < 0.05$) after the enzyme degeneration. A linear relationship was noted between the acoustic parameters IRC and URI. Stiffness measured by water jet indentation test showed linear relationships with the stiffness obtained by standard mechanical indentation test. Inverse and power relationships were also noted between stiffness and URI in the collagenase treatment group.

Discussion and Conclusions

This study showed that ultrasound can be a useful tool to quantitatively assess and systematically analysis the morphological, acoustic and mechanical properties of artC. Since a single arthroscopic ultrasound probe is able to provide all these parameters, a comprehensive assessment of artC early degeneration can be achieved only use ultrasound.

P2-F-05

Ultrasonic guided wave propagation in long bones with varying cortical thickness

Dean Ta¹, Kailiang Xu¹, Petro Moilanen², Sulin Cheng³, Weiqi Wang¹; ¹Department of Electronic Engineering, Fudan University, Shanghai, China, People's Republic of, ²Department of Physics, University of Jyväskylä, Jyväskylä, Finland, ³Department of Health Science, University of Jyväskylä, Jyväskylä, Finland

Background, Motivation and Objective

The propagation of ultrasonic guided wave (GW) in the long bone is very sensitive to bones' shape, properties and cortical thickness (CTh). Most of the previous studies on the GW propagation in long bones mainly focused on the bones with uniform CTh. However, it is necessary to understand the impacts of CTh variation, such as mode conversion. Therefore, an adequate analysis on GW propagating in long bones with varying CTh is essential for the precise calibration of the quantitative measurement of the long bone. The aim of this study is to use a modified boundary element method (BEM) to analyze the GW propagation characteristics in long bones with varying CTh.

Statement of Contribution/Methods

Numerical analysis implemented by the BEM and cylindrical mode expansion method were employed to calculate the transmission coefficients for various incident GW modes, frequency, and CTh. In the cases of incident longitudinal tube modes L(0,1), L(0,2) and L(0,3) at frequencies 0.05 - 2.0 MHz, gradual CTh variations from 6 mm to 10 mm were considered. Mode conversion phenomena due to varying CTh were investigated.

Results

Results for a series of numerical simulations showed that extremely different mode conversion and transmission phenomena took place for the same GWs incident depending on the propagation direction in the sample with varying CTh, especially when excited at the thick end of the sample. Both L(0,1) and L(0,2) modes had good penetrations through the CTh at low frequencies. The transmission coefficients of any mode for L(0,1) and L(0,2) incidents were strongly dependent on frequency, particularly at high frequencies. Transmission coefficients do not increase or decrease monotonically with the difference between thin and thick side in most situation, only it is clear that the transmission coefficients of L(0,2) at low frequencies have the monotonic trend.

Discussion and Conclusions

The direction of the GW propagation is very important due to significant differences in resulting mode conversion phenomena when using the GW to assess the actual long bones. The modified BEM method used enabled

optimization of GWs for the bone assessment. Results of this work can thus be used to improve inspection sensitivity for the assessment of long bones with varying CTh.

P2-F-06

Ultrasonic characterization of a cortical bone slab: model-based approach

Roberto Longo¹, Quentin Grimal², Josquin Foiret², Pascal Laugier², Steve Vanlandui¹, Patrick Guillaume¹
¹Department of Mechanical Engineering, Vrije Universiteit Brussel, Bruxelles, Belgium, ²Laboratoire d'Imagerie Paramétrique, Université Pierre et Marie Curie-Paris6, Paris, France

Background, Motivation and Objective

Millimeter-scale material properties of compact (cortical) bone are spatially heterogeneous due in particular to the variations mineralization and micro-porosity. The heterogeneity of bone properties, in particular elasticity, has been the focus of several research papers because it is essential for the understanding of the biomechanical response of the tissue to local strain and stresses. Mappings of acoustic velocities have been obtained based on the time delay of transmission of plane wave through a bone slab of given thickness. With such a technique, the mapping of elasticity is not possible because this would require in addition the knowledge of the density at each point. In this paper a system identification technique in the frequency domain is presented, for parametric modelling of transmission experiments performed in water for a bovine bone specimen at normal incidence. It is shown that this approach allows simultaneous determination of acoustic velocity, mass density, damping and sample thickness. The ultrasonic excitation is a multisine signal, compressed in amplitude. The proposed procedure is based on a maximum likelihood estimator.

Statement of Contribution/Methods

The bovine bone was attached to a support and immersed in a water tank, between two ultrasonic transducers. The excitation consisted in a "compressed multisine signal" with optimized phase resulting in a small crest factor and energy between 10 kHz and 4 MHz. The transfer function associated with the model of wave propagation corresponding to the experiment was derived under the assumption of plane wave propagation in absence of dispersion. The acoustic velocity in water was measured independently, so that the model can be expressed with four independent parameters.

Results

The accuracy of the method for the simultaneous determination of density, velocity and sample thickness was found to be below 2% on homogeneous samples of copper, aluminium and Perspex samples. Similar results were obtained for the bovine bone. The method was then used with transducers of diameter 6 mm in the frequency range 4-6 MHz to map the properties of a cross-sectional slab of bovine bone. Significant variations of the density, velocity and thickness (due to the preparation of the sample) could be measured. In particular, 80 % of the velocity values were found between 4111 and 4428 ms⁻¹. The precise assessment of density was possible only far enough from the specimen edges.

Discussion and Conclusions

In this paper a modelling approach in the frequency domain for ultrasonic characterization of bovine bone has been presented. The physical parameters for the bovine were derived at the same time in the same sample directly from the model parameters. Future works will involve the use of this technique for ultrasonic characterization of human bones using focused transducers.

P2-F-07

Effects of Structural Anisotropy on the Two-wave Phenomena in Cancellous Bone - Numerical and Experimental Study -

Yoshiki NAGATANI¹, Mami MATSUKAWA², Katsunori MIZUNO³:¹Kobe City College of Technology, Japan, ²Doshisha University, Japan, ³Panasonic Corporation, Japan

Background, Motivation and Objective

Ultrasonic technique is considered as a strong tool for more reliable and less onerous diagnosis system of osteoporosis, because wave properties directly reflect the elasticity. In order to improve the accuracy of ultrasonic diagnosis system, our group has proposed a new evaluation idea, focusing on the separation of longitudinal waves that pass through the cancellous bone. In vivo measurement systems often use focus transducers, however, the observed waveforms change easily due to the subtle difference of the incident wave conditions. This comes from the complicated structure of the bone.

In this study, therefore, making use of the cylindrical specimens of bovine cancellous bone, the effect of anisotropic trabecular structure was investigated by both experiments and numerical simulations.

Statement of Contribution/Methods

The cylindrical specimens, which were about 40-70 mm in length and 11.00 ± 0.05 mm in diameter, were fabricated from the distal part of a bovine femur. For the 3-dimensional elastic FDTD simulations, spatial structure of specimens were obtained by X-ray CT data with cube lattice of 23.7 μm .

In the experiments and simulations, focus transmitters were used. We placed the focal point of wave on the central axis of the cylindrical specimen. By rotating the specimen, we changed the incident angle of wave transmission. The direction of the incident wave was always perpendicular to the side surface of the cylindrical specimen. A single sinusoidal wave was used as the initial transmitted wave. The bone samples were fully immersed in water.

Results

The two-wave phenomena were observed when the incident angle of wave was parallel to the alignment direction of trabeculae. In both experiments and simulations, the arrival times and peak amplitudes of the waves showed clear periodicity due to the incident angle: the maximum wave speeds and minimum amplitudes in the parallel propagation. We always found this negative correlation between wave speeds and amplitudes.

Discussion and Conclusions

The wave speeds and amplitudes were related to the structural anisotropy of the trabeculae which was derived from CT data. The tendency was similar in both simulations and experiments. This tells us that numerical data from FDTD simulation can reflect the alignment direction of trabeculae within the propagation area.

The simulated waveforms, however, were not exactly identical with measured waves although the conditions and specimens were same. The disagreements seem to come from the several lacks of simulation: such as absorption in medium, friction loss between liquid and solid, poor estimation of the acoustical constant of trabecula, and low resolution of the CT images etc. We should consider these problems in the future work for the practical use of simulations to help the development of new diagnosis systems.

P2-F-08

Low-frequency axial ultrasound velocity measurements in children and adults: correlations with bone mineral density and cortical thickness in the radius and tibia

Vante Kilappa¹, Petro Moilanen¹, Leiting Xu², Jussi Timonen¹, Sulin Cheng^{2,1}, *Physics, University of Jyväskylä, Finland, ²Health Sciences, University of Jyväskylä, Finland*

Background, Motivation and Objective

Skeletal quantitative ultrasound (QUS) has in several studies been shown to discriminate fractured subjects from non-fractured ones, and to being thereby capable of predicting osteoporotic fracture risk. The axial transmission (AT) QUS method based on the first arriving signal is responsive to material properties of cortical bone. In particular, at low frequencies (LF; 0.2-0.4 MHz) AT provides good sensitivity to cortical thickness and properties of endosteal cortical bone in the radius and tibia in comparison with high-frequency (HF, c. 1 MHz) ultrasonometers. This improved sensitivity of LF AT has, however, not been reported yet for in vivo studies of adult and elderly subjects. The objectives of this study are thus to evaluate the extent to which an LF AT assessment of bone reflects its cortical thickness and bone mineral density, and to compare the results of such assessment with those of HF AT.

Statement of Contribution/Methods

A cross-sectional study was conducted on 131 girls (10-19 y), 144 adults (20-58 y) and 109 elderly female subjects who had undergone menopause (43-88 y). Speed of sound of the first arriving LF signal (VLF) was assessed in the tibial shaft and radius shaft by a custom-made ultrasonometer (CV_{rms} = 0.5%). The VHF of these subjects was determined at the same sites with an Omnisense ultrasonometer (Sunlight Medical, BeamMed Ltd). The site-matched volumetric total bone mineral density (BMD), cortical bone mineral density (CBMD), subcortical bone mineral density (ScBMD) and cortical thickness (CTh) of the subjects were measured with pQCT (XCT2000, Stratec Medizintechnik GmbH).

Results

In the elderly subjects, VLF correlated best with CBMD in the radius ($R = 0.862$, $p < 0.001$), but significantly also with ScBMD and CTh ($R = 0.755$, $p < 0.001$, and $R = 0.748$, $p < 0.001$, respectively). VHF provided moderate correlation with CBMD ($R = 0.505$, $p < 0.001$), but correlation with ScBMD and CTh was weak (ns., and $R = 0.358$,

$p < 0.05$, respectively). Results for the tibia, and for the children and adult subsets, were similar but weaker than those for the radius of the elderly subjects.

Discussion and Conclusions

It was thus demonstrated for the first time in an in vivo study of adult and elderly subjects that an LF AT assessment of bone provides a better prediction for its cortical thickness as well as subcortical properties than HF AT. This indicates that LF AT is more sensitive to osteoporotic changes which occur deep in the endosteal bone.

P2-F-09

Relationships between speed of sound (5MHz) of cortical bone and bone quality factors

Julien Grondin¹, Kazufumi Yamamoto², Yuichiro Yaoi², Quentin Grimal¹, Mami Matsukawa², Fabienne Rupin¹, Amena Saied¹, Pascal Laugier¹; ¹Laboratoire d'Imagerie Paramétrique, Université Pierre et Marie Curie-Paris 6; CNRS, LIP UMR 7623, Paris, France, ²Laboratory of Ultrasonic Electronics, Doshisha University, Kyotanabe, Japan

Background, Motivation and Objective

Quantitative ultrasound clinical devices measure the speed of sound (SOS) in the MHz-range. SOS has been shown to reveal useful information on bone quality. The detailed nature of what determines SOS, however, depends on complicated interdependencies among multiple bone properties. A rigorous insight into what factors are the main SOS determinants could provide a better clinical acceptance of the technique. The objective of the present study was to investigate the relationships between SOS in cortical bone and a set of independent bone characteristics, such as bone mineral density, mean crystals orientation, microstructure and microelasticity.

Statement of Contribution/Methods

Four human femurs from female donors were included in the study. Femurs were removed during multi-organ collection which complied with the requirements of the French Transplant Administration. One 10 mm-thick cross-section was cut perpendicularly to the bone long axis (BA) in the mid-shaft of each femur. Seven regions around the cross-section were marked with pencil. The posterior part was excluded from the study because of its high porosity. Longitudinal velocity (SOS) was measured in through-transmission at 5MHz with the sample immersed in saline. Dual X-Ray absorptiometry provided bone mineral density (BMD). Measurement of the proportion of crystals (PCBA) oriented along the BA was assessed using X-Ray diffraction profiles. PCBA was obtained by computing the area under (0002) peak normalized by BMD. Mean acoustic impedance (Z) and porosity (Por) were obtained from 50-MHz scanning acoustic microscopy (SAM). The spatial resolution of SAM measurements was 23 μm . The measurements were site-matched for each region.

Results

Significant relationships were found between SOS and BMD ($R^2 = 0.67$), Z ($R^2 = 0.52$) and Por ($R^2 = 0.32$). No correlation was found between SOS and PCBA. Up to 74% of SOS could be explained with a linear combination of BMD and Z.

Discussion and Conclusions

These results suggest BMD as the main determinant of SOS. The absence of correlation between SOS and PCBA contrasts with another study on plexiform bovine cortical bone showing a significant relationship between crystals orientation and SOS. The discrepancy between the two studies is unclear. We hypothesize that different structural organization of cortical bone from different species (plexiform in bovine and haversian in human) may have a different impact on SOS values. Future studies should clarify this issue.

P2-F-10

Effect of Porosity Distribution in a Propagation Direction on Ultrasound Waves through Cancellous Bone

Atsushi Hosokawa¹; ¹Department of Electrical and Computer Engineering, Akashi National College of Technology, Japan

Background, Motivation and Objective

To realize high reliability in ultrasound diagnostic apparatuses for osteoporosis, the detailed elucidation of the complex ultrasound propagation in cancellous bone is required. Cancellous bone is a porous material comprising numerous trabecular elements, and its porosity changes with position in the bone. As the position shifts inward, in

general, the porosity becomes higher. In this study, the effect of the porosity distribution in the propagation direction on ultrasound waves through cancellous bone has been numerically investigated using finite-difference time-domain (FDTD) simulations.

Statement of Contribution/Methods

Numerical models of bovine cancellous bone were reconstructed from 3-D microcomputed tomographic images. To generate the trabecular structures without and with porosity distribution, the trabecular elements in each cancellous bone model were eroded using 2 procedures. In one procedure, the erosions were uniformly distributed in the whole region. In the other procedure, the distribution of the erosions was changed in the direction of the trabecular orientation. For ultrasound propagation in the trabecular-oriented direction, pulse waveforms through the cancellous bone models without and with the porosity distribution in the propagation direction were simulated by the viscoelastic FDTD method.

Results

In the simulated waveforms, two waves, called as "the fast and slow waves", could be observed, as shown in Fig. 1. The amplitudes of both the fast and slow waves simulated using the cancellous bone models with the porosity distribution tended to be larger than those using the models without the porosity distribution. On the other hand, the propagation speed of the fast wave tended to slightly decrease owing to the porosity distribution, and a significant variation in the slow wave speed was not observed.

Discussion and Conclusions

It was previously shown that both the fast and slow wave amplitudes were mainly correlated with the mean lengths of the trabecular elements and pore spaces in the direction perpendicular to the propagation direction. The porosity distribution can cause the spatial variations in the trabecular and pore lengths. It can therefore be considered that the effect of the porosity distribution in the propagation direction on the fast and slow waves is associated with the trabecular and pore lengths in the perpendicular direction.

Tuesday
Poster

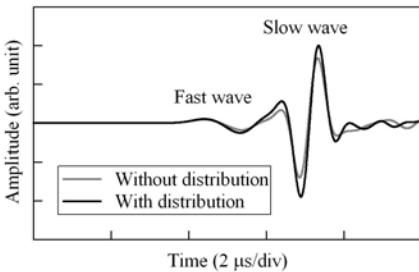


Fig. 1 Simulated waveforms.

P2-F-11

Correlations between signal spectrum of ultrasonic backscatter and cancellous bone microstructure

Dean Ta¹, Kai Huang¹, Weiqi Wang¹, Haiyan Zhang^{2,1} *Department of Electronic Engineering, Fudan University, Shanghai, China, People's Republic of, ²School of Communication and Information Engineering, Shanghai University, Shanghai, China, People's Republic of*

Background, Motivation and Objective

Osteoporosis is a bone disease characterized by bone mass loss, deterioration of bone microstructure. Ultrasonic backscatter can provide additional micro-structure information. The aims of this work are to investigate the correlations between signal spectrum maximum shift (SMS) of ultrasonic backscatter and cancellous bone micro-structure.

Statement of Contribution/Methods

Twenty-six bovine cancellous bones in vitro were scanned in a plane by moving transducer in 0.142mm steps. Correlations were studied between mean /standard deviation (SD) of SMS values within a ROI (14.2

mm×14.2mm) of bone samples and bone micro-structural parameters obtained from a μ -CT 3-D reconstruction, which are mean trabecular thickness (Tb.Th), mean trabecular spacing (Tb.Sp), bone volume/total volume ratio (BV/TV), bone surface/volume ratio (BS/BV), and bone material density (BD).

Results

Results demonstrated that SMS has mediate and significant correlations with all the parameters obtained from μ -CT (Tb.Th, $r=-0.699$, $p<0.01$; Tb.Sp, $r=0.477$, $p<0.05$; BV/TV, $r=-0.675$, $p<0.01$; BS/BV, $r=0.663$, $p<0.01$; BD, $r=0.663$, $p<0.01$). The SD of SMS values was also significantly ($p<0.01$) correlation with bone micro- structural parameters (Tb.Th, $r=-0.720$; Tb.Sp, $r=0.771$; BV/TV, $r=-0.754$; BS/BV, $r=0.802$).

Discussion and Conclusions

The SMS parametric image displays the distribution of ultrasonic energy lost when ultrasound penetrates into and propagates inside bone micro- structure. The mean/standard deviation (SD) of SMS may help characterize bone quality and osteoporosis diagnosis.

P2-F-12

Characterizing Biot constants from ultrasound through trabecular bone

Guillermo Rus¹, Michal Pakula², Quentin Grimal², Pascal Laugier²; ¹Structural Mechanics, University of Granada, Granada, Spain, ²UPMC-Paris6, CNRS, Laboratoire d'Imagerie Paramétrique, Paris, France

Background, Motivation and Objective

Reliable quantification of mechanical constants of bone tissue is an open issue with relevance for the diagnostic of bone quality disorders, such as osteoporosis. The reconstruction of such parameters from nondestructive testing based on ultrasonic transmission of pulses and model-based solution of the identification inverse problem is proposed as a novel technique with high potential not only due to the reduced cost and its non-ionizing nature, but for the direct relationship and sensitivity of the propagation of those mechanical waves to the mechanical strength of bone, which defines the ultimate criterion for diagnosis.

This work is aimed at (i) evaluating the feasibility of the model-based inverse problem to reconstruct the mechanical constants that govern Biot theory, and quantify its accuracy and error for trabecular bone specimens. A second goal is (ii) to validate to which extent the Biot theory assumed in the model of wave propagation is valid, and if any corrections can empirically be suggested to overcome inconsistencies. Finally, (iii) the obtained Biot constants are cross-correlated and a parametric study is carried out to extract practical parameters for final bone quality assessment.

Statement of Contribution/Methods

An ultrasonic transmission setup (pulsed at a central frequency of 500kHz), was applied to 27 prismatic samples of human femoral condyle to measure the transmitted signal.

A model-based Inverse Problem is applied to reconstruct the values of the Biot constants that best fit the experimental measurements. Two inputs need to be introduced: i) the parametrization, responsible for which parameters of the model control the characterization of the sought model and ii) the experimental measurements. A cost functional is defined to find which Biot mechanical parameters minimize the mismatch between the time, frequency, attenuation and phase velocity in the experimental and numerical response simulated by a semianalytical model of the propagation through a poroelastic medium.

A genetic algorithm is used to search the Biot parameters, due to its capability of doing a robust and global search where the cost functional has several local minima that may produce wrong answers, at the cost of larger computational resources.

Results

Some of Biot constants can be clearly reconstructed by inversion based on matching the time-frequency domain signals: the porosity, tortuosity, tissue elasticity and Characteristic length. Other constants appear to be coupled together, like tortuosity with porosity (this has also been observed by other types of measurements), while others cannot be identified.

Discussion and Conclusions

As a conclusion, the model-based inversion using genetic algorithms proves as a technique to quantify several mechanical and geometrical trabecular bone properties simultaneously from a single measurement. The precision is to be validated against independent laboratory measurements excluding mechanical wave propagation.

Is the Biot's theory adequate for modelling wave propagation in cancellous bone?

Michal Pakula^{1,2}, Frederic Padilla², Mariusz Kaczmarek¹, Pascal Laugier²; ¹*Institute of Environmental Mechanics and Applied Computer Science, Kazimierz Wielki University, Bydgoszcz, Poland*, ²*Laboratoire d'Imagerie Parametrique, University Pierre et Marie Curie, Paris, France*

Background, Motivation and Objective

The paper is focused on comparative theoretical and experimental studies of ultrasonic wave propagation in cancellous bones. The main objective is to verify if the commonly used for modeling of elastic wave propagation in cancellous bone (macroscopic Biot's model) is adequate for mathematical description of the phenomenon in the material.

Statement of Contribution/Methods

In the isotropic case, the model requires dozen macroscopic input mechanical and structural parameters. Most of them were measured individually for 31 pure human femoral trabecular bone specimens. Then, frequency dependent wave parameters (phase velocity and attenuation coefficient) predicted by the model were compared with the results of ultrasonic tests performed on the same specimens. In order to simulate real experimental conditions, modeling was complemented by the theoretical solution of the boundary problem of interaction of plane harmonic wave with the slice of cancellous bone treated as a porous material saturated with fluid.

Ultrasonic measurements were performed in immersion following the insertion method. The wave parameters (phase velocity and attenuation coefficient as a function of frequency) were computed from the ratio of the spectrum of the broadband pulse transmitted through the specimen to the spectrum of the reference pulse recorded when there is no specimen between the transducer and receiver.

Results

The sensitivity analysis of the model (studies of the influence of the variability of input parameters on the phase velocity and wave attenuation), shows that the accordance between experiment and the model can be achieved only in the case when porosity is very high and the tortuosity reach its lower limit (around 1).

It was established significant contribution of the fluid/bone and bone/fluid boundaries on the global attenuation loss. The corrected values of attenuation coefficient (including the effect of boundaries) are of the same order of magnitude compared to measured values, but the frequency dependence of the parameter was not well predicted by the model.

Moreover, the theoretical results exhibit, observed in experiments, higher attenuation of fast wave compared to that of the slow wave.

Discussion and Conclusions

The main conclusion is that Biot's theory can be used for modelling of wave propagation in cancellous bone for highly oriented (tortuosity close to 1) and highly porous (about 90%) specimens.

For lower porosities strong differences between the model predictions and experimental results are observed.

The most probable source of discrepancy in the frequency dependence of attenuation and phase velocity comes from the basic assumption of Biot's theory, which was introduced for wavelengths much higher than the typical dimension of heterogeneities and therefore does not account for important physical interactions such as scattering.

Warped Signal Dictionaries for the Analysis of Ultrasonic Guided Waves in Long Bones

Luca De Marchi¹, Kailiang Xu², Dean Ta², Alessandro Marzani³, Cristina Gentilini³, Salvatore Caporale¹, Nicolo Speciale¹; ¹*DEIS, University of Bologna, Italy*, ²*Department of Electronic Engineering, Fudan University, China, People's Republic of*, ³*DISTART, University of Bologna, Italy*

Background, Motivation and Objective

The analysis of ultrasonic guided wave (GW) propagation in long bones has interested several researchers in the last years. For a given excitation frequency, many GW modes can propagate in long bones each with defined wavelength, phase velocity, and attenuation. These quantities can be used in the assessment of osteoporosis and in the evaluation of fracture healing. The objective of this work is to analyze these wave propagation phenomena

through dedicated simulations and experimental acquisitions. To this aim, we developed a new signal processing method, capable to highlight the different mode characteristics.

Statement of Contribution/Methods

The proposed method is based on a warped-basis pursuit (W-BP) algorithm. The ultrasonic wave is represented as a linear superposition of elementary signals, called atoms. Atoms are designed to match the spectro-temporal structures of the acquired waveforms. This can be done by using a warped frequency transform (WFT) which generates signals with the same dispersive behaviour of GWs. The WFT acts by reshaping the time-frequency plane according to different warping maps, each one suitable for the analysis of a particular GW propagating mode. Atoms generated by a given warping map are grouped in subsets, which are finally summed to build the whole set of atoms, called the Dictionary. The Dictionary is overcomplete, i.e. the atoms number is greater than the dimensionality of the waveform space. This requires a criterion to select among the many possible representations; in particular, W-BP seeks the one that minimizes the L1 norm of the coefficients used in the superposition. The coefficients distribution produces a new time-frequency representation suitable to characterize GWs, as each coefficient can be associated to a subset, and then to a propagating mode.

Results

An application to propagating GWs in long bones is presented to show the potential of the proposed procedure. Time-transient events obtained both numerically, from dedicated FEM simulations, and experimentally, via a piezoelectric ultrasonic set-up applied to a bovine tibia, are considered. In FEM simulations, the bone is considered as a hollow cylinder with inner and outer diameter of 18.8 and 24.7 mm, respectively, and linear poroelastic material properties in agreement with the low level of stresses induced by the waves. The results show that WFT limits interference patterns between modes and produces a sparse representation suitable for dispersion characterization using ridge detection methods.

Discussion and Conclusions

This work proposes a decomposition method capable to analyze the dispersive behaviour of GWs that propagates in long bones. The new tool efficiently represents the different GWs with non-linearly frequency modulated atoms. In the proposed decomposition, energy extraction is a simpler task and can be performed to obtain reliable mode representation and characterization.

P2-G. Cardiac, Vascular and General Tissue Characterization

Sala Orange

Tuesday, September 22, 2009, 10:00 am - 11:30 am

Chair: **Guy Cloutier**
Univ. of Montreal

P2-G-01

Generation and tracking of mechanical waves with Radiation Force using a single transducer: Vascular Applications

Douglas Dumont¹, Aine Tierney², Jeremy Dahl¹, Stephen Hsu¹, Gregg Trahey¹; ¹Duke University, USA, ²University of Limerick, Ireland

Background, Motivation and Objective

In this abstract, we describe our technique for generating and tracking radiation-force induced mechanical waves in both the circumferential and longitudinal direction using a single transducer. Radiation-force induced wave velocimetry is demonstrated for axisymmetric and non-axisymmetric cryogel phantoms, *ex vivo* porcine aortas, and *in vivo* arterial tissue

Statement of Contribution/Methods

Axisymmetric and non-axisymmetric phantoms of varying moduli (20-120kPa) were constructed, mounted in a water-tank, and pressurized with a gravity head. Circumferentially non-axisymmetric phantoms consisted of an approximately 45 degree arc composed of one modulus, and a 315 degree arc composed of another modulus. Radiation-force induced mechanical waves were generated and tracked with the phantoms oriented both in the longitudinal and circumferential imaging plane of the transducer. Estimates of longitudinal wave group velocity (LWGV) were obtained using previously described lateral time-of-flight algorithms [3]. Estimates of right-traveling (RT) and left-traveling (LT) circumferential wave group velocities (CWGV) were obtained by converting the displacement data into polar coordinates, and fitting a regression line to the angular time-of-flight data. The non-axisymmetric phantom was rotated about the transverse axis such that a heterogeneous section was located at either the two-o'clock or the ten-o'clock position in order to determine the effect of asymmetry on the propagation velocity of the LT and RT waves. Estimates of arterial wave velocity were then obtained from *ex vivo* porcine aortas mounted in a water tank, and *in vivo* in the carotid artery of a healthy, normal volunteer.

Results

Results indicate that radiation-force induced waves can be tracked successfully in the longitudinal and circumferential directions using a single transducer that both excites and tracks the propagating wave. Over the physiological pressure range (80-120mmHg), LGWVs were found to vary from 3.2 ± 0.5 and 6.4 ± 0.9 mm/ms, with faster group wave velocities associated with stiffer phantom moduli. For *ex vivo* data (n= 3 excised porcine aortas), LWGVs were found to vary from 5.1 ± 0.9 and 6.8 ± 1.8 mm/ms over the physiological pressure range. In the axisymmetric phantom, CWGVs were found to be 61 ± 9 deg/ms and 68 ± 11 deg/ms for the LT and RT waves. In the non-axisymmetric phantom, CWGVs were determined to be 28 ± 5 deg/ms and 63 ± 9 deg/ms for the LT and RT waves with the heterogeneous section oriented at the ten-o'clock position and 72 ± 15 deg/ms and 23 ± 9 deg/ms with the heterogeneous section oriented at the two-o'clock position.

Discussion and Conclusions

Radiation-force induced elastic wave velocimetry was demonstrated in vascular phantoms and in arterial tissue using a single transducer. Circumferential material asymmetry can be determined by tracking the group wave velocity for the left-traveling and right-traveling wave.

Simple and noninvasive analysis of the pulse wave for blood vessel evaluation

Masashi Saito¹, Yuya Yamamoto¹, Mami Matsukawa¹, Yoshiaki Watanabe¹, Mio Furuya², Takaaki Asada²:¹Doshisha University, Japan, ²Murata Manufacturing Co., Ltd., Japan

Background, Motivation and Objective

The evaluation of the pulse wave has become important for screening arteriosclerosis. The pulse wave is composed of an incident wave and a reflected wave. Because the reflected wave propagates to the peripheral artery, the wave properties strongly depend on the viscoelastic properties of blood vessels. The evaluation of blood vessels, then, may be possible by the analysis of this reflected waveform [1]. We propose a simple, noninvasive, and in vivo technique to extract the reflected wave component from the observed pulse wave, using a commercial piezoelectric transducer. We actually applied this technique to young and elder subjects to check the applicability.

Statement of Contribution/Methods

Pulse waves and blood flow velocities at the carotid artery were measured simultaneously from subjects. A piezoelectric transducer (Murata MA40E7R) was used to measure the pulse wave as the displacement of surface skin. The obtained pulse waveform was in good agreement with that observed by the mechano-cardiogram (Fukuda Denshi MES-1000). An ultrasonic diagnostic system (Toshiba Medical Systems Aplio SSA-700A) was used to measure the blood flow velocity. To extract the reflected wave component from the observed pulse wave, we have first estimated an inner pressure waveform from the blood flow velocity waveform by the equation of continuity and an elastic pipe model. Next, an incident wave was presumed from the inner pressure applying an optimum Voigt model. The model brought the estimated incident waveform whose initial part is similar to that of the observed pulse waveform. We have then assumed the reflected wave by subtracting this incident wave from the observed pulse wave.

Results

We obtained data from four young (mean ages 23 years) and four senior (mean ages 66 years) subjects. There are remarkable differences in the observed waveforms due to age. The maximum amplitudes of the estimated reflected waves are shown in Fig.1. Values of senior subjects are always higher than those of junior subjects. There was a statistically significant difference between two groups.

Discussion and Conclusions

The elasticity of the vessel walls increases due to age [1]. Our current results are in agreement with the character, showing high attenuation of reflected waves due to the soft vessel walls of junior subjects.

Ref. [1]: W. W. Nichols et al., McDonald's Blood Flow in Arteries, Hodder Arnold, 2005

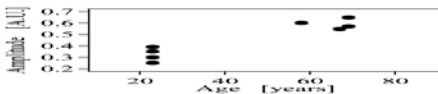


Fig.1 The relationships between age and maximum value of estimated reflected wave.

Nonlinear Tissue Characterization with Intravascular Ultrasound Harmonic Imaging

Sushma Srinivas^{1,2}, Chaitanya Chandrana^{1,3}, Vladimir Zagrodsky¹, Shuvo Roy¹, Aaron Fleischman^{1,1}:¹Biomedical Engineering, Cleveland Clinic Foundation, Cleveland, OH, USA, ²Chemical and Biomedical Engineering, Cleveland State University, Cleveland, OH, USA, ³University of Toronto, Toronto, Canada

Background, Motivation and Objective

Current Intravascular ultrasound (IVUS) techniques of tissue characterization are morphology based, a characterization based on surface echogenicity and spectral parameters from the fundamental imaging alone. Complex harmonic signals develop as a result of heterogeneous composition of nonlinear tissue such as calcified lipids, not easily characterized in the fundamental mode. Tissue harmonic imaging (THI) offers substantial advantages such as nonlinear information, better lateral resolution, higher contrast resolution, low near field spatial variation and decreased sidelobes. The objective is to enhance tissue characterization with the extent of tissue nonlinearity for a better diagnosis using broadband transducers.

Statement of Contribution/Methods

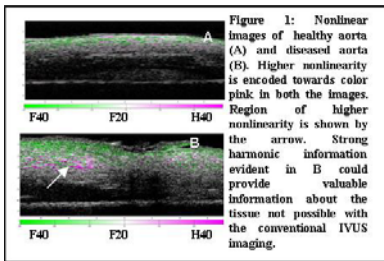
Broadband high resolution polymer transducers enabling harmonic imaging were fabricated. Cadaver human aorta and rabbit aortic grafts with neointimal growth were imaged. Fundamental (at 20MHz and 40MHz) and Harmonic signals (at 40MHz and 80MHz) from the tissue were obtained in one scan line using a previously established pulse inversion technique with 60% bandwidth Gaussian pulses. The frequency spectrum from fundamental imaging was extended with additional parameters around the second harmonic frequency representative of tissue nonlinearity. A combined tissue nonlinear parameter β/ρ was estimated from the harmonics. The image from fundamental mode was modulated with the tissue nonlinear parameter and color coded. Regions of higher value of nonlinear parameter were considered to be lipid laden. Histological correlation was done to estimate the significance of nonlinear tissue characterization.

Results

Transducers exhibited good axial resolution (~ 19 μ m) and broad bandwidth (~ 130%) facilitating harmonic imaging. Harmonic modulation of the fundamental image yields a continuous color perception of linear and nonlinear tissue properties as shown in Figure 1. Neointimal growth over the graft was better seen with nonlinear imaging due to higher harmonics from the endothelium compared to the graft. Nonlinear spectral parameters from THI better classify the tissue components as they extend the set of parameters from fundamental imaging used for tissue classification in 'Virtual Histology'.

Discussion and Conclusions

Nonlinear tissue characterization better classifies tissue components.



Tuesday
Poster

P2-G-04

On the characterization of left ventricular function with acoustic radiation force impulse imaging

Stephen Hsu¹, Richard Bouchard¹, Douglas Dumont¹, Patrick Wolf¹, Gregg Trahey¹; ¹Duke University, Durham, NC, USA

Background, Motivation and Objective

Extensive research has been devoted to the quantification of left ventricular (LV) function for the detection and diagnosis of a variety of cardiac diseases. The primary focus of these studies has been to track the changes in elastic properties of the myocardium at specific points of the cardiac cycle and correlating them with the performance of the heart. The clinically accepted method for the measurement of LV function utilizes pressure-volume (PV) analysis to measure an elasticity metric known as elastance. Previous investigations into PV analysis have demonstrated its potential in providing measurements of myocardial performance and function, however the underlying simplifications and assumptions in tissue geometry and distribution of loads within the heart lend them susceptible to artifacts. Another relatively new technique for the assessment of tissue elasticity is with acoustic radiation force impulse (ARFI) imaging. As ARFI imaging has been shown to be capable of measuring myocardial stiffness through the cardiac cycle, beat-to-beat variations within the ARFI-induced displacement curves may provide corollary insight into LV function.

Statement of Contribution/Methods

An ovine heart was imaged under an open chest preparation. The transducer, inserted into a vacuum apparatus, was placed directly on the LV epicardium, along the long axis of the heart. A pacing wire was sewn onto the left atrium of the exposed heart and used to pace the heart at rates above the normal sinus rhythm. Baseline M-mode ARFI images of the LV free wall were acquired on every other beat across seventeen heartbeats (nine total). Four

factors that determine myocardial performance (preload, afterload, heart rate, and contractility) were independently varied, and the subsequent ARFI images were inspected for changes from the baseline measurements that could be attributed to changes in LV function. An ARFI imaging-based rate of systolic stiffening is introduced for the characterization of LV function during systole.

Results

Changes within the ARFI-induced displacement curves reflected changes in LV function as observed when altering four factors of myocardial function in these experiments. More encouragingly, the results can generally be corroborated by previous investigations and theories of myocardial elastance and LV function. For example, the ARFI imaging-derived end-systolic stiffness was seen to be load independent and increased with an increase with contractility. The rate of systolic stiffening was also observed to vary in accordance to the Frank-Starling law of the heart.

Discussion and Conclusions

By continuously sampling through the cardiac cycle and across multiple heartbeats, the preliminary results indicate that ARFI imaging is capable of providing additional insight into LV function not previously available with traditional PV analysis.

P2-G-05

Algorithm for Estimating the Attenuation Slope from Backscattered Ultrasonic Signals

Alexander Haak¹, Zachary T. Hafes¹, Janelle J. Anderson², Maria-Teresa Herd², Kibo Nam², Ernest L. Madsen², Timothy A. Bigelow³, Timothy J. Hall², William D. O'Brien¹, ¹Electrical and Computer Engineering, University of Illinois at Urbana-Champaign, USA, ²Department of Medical Physics, University of Wisconsin-Madison, USA, ³Department of Electrical and Computer Engineering, Department of Mechanical Engineering, Iowa State University, USA

Background, Motivation and Objective

In vivo measurements of the acoustic attenuation slope (AS) have been used to characterize tissue. The correction for diffraction loss (DL) is a major problem for many AS measurements. An existing algorithm corrects for DL approximating the axial beam profile by a Gaussian function. This algorithm was enhanced by correcting for DL using a reference scan of a planar reflector.

Statement of Contribution/Methods

In the proposed algorithm the down-shift of center frequency is utilized to estimate AS. The depth of field of a focused single element transducer was range gated into sections (giving a 17 mm region of interest) and the average spectral amplitude (ASA) was estimated from several adjoined A-lines. The ASA at each depth was divided by the corresponding reference spectral amplitude in order to correct for diffraction. The center frequency and bandwidth of the corrected spectra were estimated assuming a Gaussian shape of the spectral amplitude and linear frequency dependency of the attenuation. The attenuation slope was then estimated by a linear fit of the center frequency vs. depth.

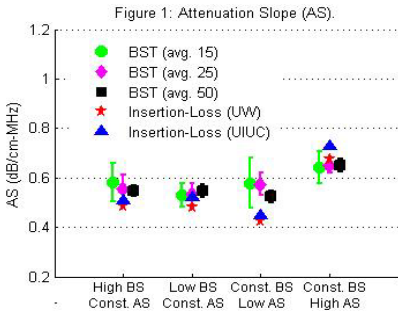
The method was tested on two pairs of tissue mimicking phantoms, with AS within a typical range of soft tissue (0.5 to 0.75 dB/cm-MHz), made of randomly distributed glass spheres embedded in a gel matrix. One pair of phantoms had the same attenuation but different backscatter (BS) intensity. The other pair had the same backscatter intensity but different attenuation.

Results

A focused single element transducer (7.8 MHz, $f/4$) was used to estimate AS using the backscatter technique (BST). The ASA was obtained from 15, 25 and 50 adjacent RF lines. In Fig. 1 the BST results, obtained from 5 measurements, are plotted together with the insertion-loss measurements. The error bars represent the standard deviation.

Discussion and Conclusions

The estimated ASs using the BST method agree well with the values estimated using the insertion loss technique. The standard deviation around the mean value was less than 5% when 50 average spectra were used to calculate AS and less than 10% and 18 % when 25 and 15 average spectra were used respectively. The estimated AS, using 50 average spectra, changed by less than 10% compared to the estimate using 15 average spectra indicating that the proposed algorithm is quite robust and high lateral resolution of AS can be achieved. [This work was supported by NIH Grant CA111289].



P2-G-06

Inter-laboratory comparison of backscatter coefficient estimates for tissue-mimicking phantoms

Janelle J. Anderson¹, Maria-Teresa Herd¹, Michael R. King², Alexander Haak², Zachary T. Hafez², Jun Song², Michael L. Oelze², William D. O'Brien, Jr.², Ernest L. Madsen¹, James A. Zagzebski¹, Timothy J. Hall^{1,3}^{Medical Physics, University of Wisconsin Madison, Madison, WI, USA, ²Electrical Engineering, University of Illinois Urbana Champaign, Urbana, IL, USA}

Background, Motivation and Objective

The backscattered intensity of ultrasound ("echogenicity") is a useful property for characterizing tissues. However, current clinical imaging systems display only relative backscatter instead of measurements on an absolute scale. Additionally, there are several potential backscatter-derived parameters that could also be helpful in tissue characterization if the backscatter is measured accurately and consistently. While previous inter-laboratory comparisons of backscatter coefficient (BSC) estimation have been reported, the BSC estimates have only included a relatively narrow frequency range and lacked reference to the values predicted by Faran's theory. With highly variable results and no claim of a right answer, these were simply comparisons among results. Our goal is to compare Faran scattering theory with cooperatively measured backscatter coefficients for low- and tissue-like attenuating phantoms containing different size distributions of spherical scatterers for frequencies extending up to 12MHz.

Statement of Contribution/Methods

Backscatter coefficients were measured with two different techniques in two laboratories for eight different phantoms. One set of phantoms had a broad distribution of glass bead diameters (5-30 μ m). A second set of phantoms had a narrower diameter distribution (45-53 μ m). The third phantom set had a well-characterized narrow diameter distribution (38-43 μ m) for which we could easily calculate the expected backscatter coefficients using Faran's theory. A fourth set of phantoms had relatively large diameter beads (150-180 μ m) for comparisons at relatively high ka. Both BSC estimation methods used a planar interface for system calibration. Measurements were made by the WI and IL groups for all phantoms and compared.

Results

Results showed good agreement between both labs' BSC measurements from 2.5 to 12MHz. The best overall agreement was found with the narrow diameter distribution where the average fractional error over the frequency range was 20% for IL and 16% for WI. Samples containing broader diameter distributions had slightly worse agreement. WI measurements were biased less than 6% high, and IL measurements were biased approximately 2% low. Importantly, the frequency dependence of both groups' BSC measurements agreed with that predicted by Faran's theory which would lead to accurate effective scatterer size estimates.

Discussion and Conclusions

These results have demonstrated backscatter measurement accuracy from 2.5 to 12MHz for different methods implemented by both groups. Excellent agreement with the predictions of Faran's theory demonstrates the ability to accurately estimate both effective scatterer size and acoustic concentrations. Future work will continue this BSC comparison extending to higher frequencies and use in ultrasound scanners for tissue characterization. [NIH CA111289]

P2-G-07

Estimation of Ultrasound Tissue Attenuation Along the Propagation Path by Applying Multiple Filters to the Backscattered Echoes

Timothy Bigelow¹; ¹Electrical and Computer Engineering, Iowa State University, Ames, IA, USA

Background, Motivation and Objective

Quantifying the correlation length of the tissue microstructure has shown potential for diagnosing between benign and malignant tumors. In order to implement these advances in the clinic, the total frequency dependent attenuation along the propagation path must be determined on a patient specific basis. Previously, an algorithm was developed to estimate this attenuation using echoes from multiple sources. In this study, the developed algorithm was extended to echoes from a single source by filtering the echoed signal into multiple frequency bands. This step was needed because it would be challenging to scan exactly the same tissue region using multiple sources in the clinic.

Statement of Contribution/Methods

Computer simulations were conducted to verify the attenuation could be determined by filtering the echoes from a single source. The simulations utilized a spherically focused single element source (5 cm focal length, f/4, 14 MHz center frequency, 50% bandwidth) exposing a homogeneous tissue region. The simulated tissue had Gaussian scattering structures with effective radii of 5 to 55 μm (one size per simulated case) placed at a density of 250/mm³ (~5 scatterers/resolution cell for 14 MHz transducer). The attenuation of the tissue was also varied from 0.1 to 0.9 dB/cm-MHz. The simulations explored the dependence on scatterer size, attenuation, and region of interest (ROI) size.

Results

The error in the total attenuation estimate varied from 0.036 \pm 0.045 dB/cm-MHz for an attenuation of 0.1 dB/cm-MHz to -0.0004 \pm 0.032 dB/cm-MHz for an attenuation of 0.9 dB/cm-MHz when the effective radius of the scatterers was 25 μm . Likewise, the error in the estimates varied from 0.036 \pm 0.048 dB/cm-MHz for an effective scatterer radius of 5 μm to 0.043 \pm 0.039 dB/cm-MHz for an effective scatterer radius of 55 μm when the tissue attenuation was 0.5 dB/cm-MHz. The accuracy and precision of the estimates could be further improved by increasing the size of the ROI.

Discussion and Conclusions

The computer simulations confirmed that the total attenuation along the propagation path can be determined by appropriately applying multiple filters to the backscattered echoes from a single source. The accuracy and precision of the estimates were slightly worse than when using multiple independent sources. This is likely due to the reduced bandwidth available when using a single source as compared to using multiple sources. (Supported by NIH Grant CA111289 and Iowa State University)

P2-G-08

Preparation and Characterization of Microstructured Poly(Vinyl Alcohol) Phantoms Mimicking Fibrous Tissue

Andrew Dawson¹, Paul Harris², Gideon Gouws^{1,1} *School of Chemical and Physical Sciences, Victoria University of Wellington, Wellington, New Zealand, ²Industrial Research Limited, Wellington, New Zealand*

Background, Motivation and Objective

Tissue is usually treated as homogeneous, however when viewed at the micron length scale it is found to be formed from microstructures. Microstructure is known to influence the wave velocity and modes depending on the frequency and microstructure dimension; an oriented microstructure causing anisotropic propagation. As an example the dermis at 200 MHz is expected to be locally anisotropic whilst at 5 MHz highly echogenic, both a consequence of collagen and its microstructure. Anisotropic microstructured PVA [poly(vinyl-alcohol)] phantoms mimicking tissue have been developed to investigate the influence microstructure has on 20 to 200 MHz waves, and the results compared with standard PVA phantoms.

Statement of Contribution/Methods

Highly structured PVA phantoms have been prepared using freeze casting techniques. Initially a PVA slurry (5-10 % by weight) is cryogenically frozen at a slow rate of 2-8 mm/min. The samples are then cut to 1-2 mm thickness and freeze dried; this removes the ice crystals by sublimation leaving behind the resultant microstructured PVA. The samples can then be stored for long periods. When immersed the hydrophilic samples preserve their structure for several days depending upon the PVA average molecular weight and degree of hydrolysis.

Tuesday
Poster

Focused Panametrics immersion transducers have been used for a transmission measurement over the frequency range 20 to 200 MHz. A measurement without the sample provides transducer alignment and a reference propagation time for the transmission velocity calculation. Sample thickness is measured accurately using a pulse echo measurement.

Results

Horizontal cross-sections of the samples viewed with an SEM reveal highly regular porous microstructures. The longitudinal sections show a structure similar to that observed in fibrous tissue - a microstructure with a preferred orientation with localised variations. Samples with a 5 mm/min immersion rate consist of pore wall thicknesses of 5-10 μm with a pore spacing of 20-40 μm .

Initial results reveal acoustic impedance and attenuation properties similar to those for tissue. Tensile strength is greater along the direction of microstructure alignment compared to other directions. Experimental velocity variations with frequency and acoustic impedance measurements will be presented.

Discussion and Conclusions

Fabricated porous PVA phantoms possess acoustic properties (velocity, attenuation, impedance) and structural properties (anisotropy, local variations, microstructure dimensions) similar to those found in fibrous tissue. These phantoms can be easily fabricated with similar properties suggesting the freeze casting technique developed may be a valuable method for constructing these new tissue phantoms.

P2-G-09

Development Of Silicon-Based Materials For Ultrasound Biological Phantoms

Luis Maggi¹, Elisabeth Monteiro², Marco Antonio Kruger³, Wagner Pereira⁴, ¹biomedica Engineering Program, Federal University Of Rio De Janeiro, Rio De Janeiro, Rio De Janeiro, Brazil, ²instituto De Macromoleculas, Federal University Of Rio De Janeiro, Rio De Janeiro, Rio De Janeiro, Brazil, ³biomedical Engineering Program, Federal University Of Rio De Janeiro, Rio De Janeiro, Rio De Janeiro, Brazil, ⁴biomedical Engineering Program - Coppe, Federal University Of Rio De Janeiro, Rio De Janeiro, Rio De Janeiro, Brazil

Background, Motivation and Objective

Ultrasound (US) phantoms are made of materials that mimic acoustic properties of human soft tissue. Ideally, such materials should mimic US velocity (1435 to 1631 m.s⁻¹), attenuation (0.22 to 1.47 dB.cm-1MHz-n with n ranging from 1.09 to 1.15), density (916 to 1100 kg.m-3) and scattering. Many of the tested materials have some of the desired properties like Agar, polyvinyl alcohol gel and polyacrylamide gel, however, they are susceptible to dehydration and biological attacks. This fact imposes a frequent material renewal, being other source for inaccuracies and uncertainties for measurements. Silicone rubbers are stable materials, but present higher attenuation and lower US velocity compared to tissues. This work investigates the mixing of silicone rubber with other substances to bring its properties close to biological tissues, and evaluates its stability along time.

Statement of Contribution/Methods

According to literature (Onda Corporation, 2003), the RTV 615® Silicone rubber has the lowest acoustic attenuation (1 dB.cm-1 at 0.8 MHz), and US velocity 1020 m.s⁻¹. Then we mixed it with materials of lower attenuation and higher US velocity. It was tested about 25 material types at various concentrations. Stability was studied by measuring US velocity and attenuation over time, by standard transmission methods.

Results

The three best mixtures were silicone rubber with silicone oil (40% in weight) or glycerin (33%) or Vaseline (23%). US velocity and attenuation were measured using three transducer pairs at 1, 2.25 and 5 MHz in a tank with distilled water at 25°C, and at five positions for each phantom (Table I). Attenuation was reduced for silicone rubber with silicone oil or with Vaseline. In the first case, US velocity remains unchanged, while, in the second case, it is slightly increased. For silicone rubber with glycerin, we achieved the highest increase in US velocity; however, attenuation has also increased. The phantoms acoustic properties were assessed for 16 months and no significant changes were detected.

Discussion and Conclusions

It was presented a study of materials intended to mimic basic acoustic properties of biological tissues with stability over time. Preliminary results show that acceptable values of attenuation were achieved and the phantoms can be used for certain applications. US velocity still needs to be improved by 25%.

FREQUENCY MATERIAL	Attenuation (dB.cm ⁻¹)			Velocity (m.s ⁻¹)		
	1 MHz	2.25 MHz	5 MHz	1 MHz	2.25 MHz	5 MHz
SILICONE RUBBER	1.59 ± 0.01	3.49 ± 0.01	10.11 ± 0.09	1063.79 ± 0.87	1044.94 ± 0.43	1053.84 ± 0.18
SILICONE + OIL SIL 40%	1.06 ± 0.00	1.96 ± 0.03	5.68 ± 0.02	1053.47 ± 0.48	1036.56 ± 1.13	1023.57 ± 0.15
SILICONE + GLYCERIN 33%	1.91 ± 0.09	3.97 ± 0.10	9.33 ± 0.03	1183.10 ± 3.59	1177.46 ± 2.78	1173.46 ± 0.13
SILICONE + VASELIN 23%	0.79 ± 0.05	2.02 ± 0.03	5.24 ± 0.02	1136.98 ± 3.11	1135.03 ± 3.78	1118.92 ± 0.21

Tuesday
Poster

P2-H. Wave Propagation and Energy Harvesting

Sala Orange

Tuesday, September 22, 2009, 10:00 am - 11:30 am

Chair: **Michal Bezdek**
Endress+Hauser Flowtec AG

P2-H-01

A synthetic Lamb wave tomography method combining wave-equation traveltimes and waveform data

Haiyan Zhang¹; ¹Shanghai University, China, People's Republic of

Background, Motivation and Objective

The use of ultrasonic Lamb waves for non-destructive evaluation (NDE) of platelike structures is effective due to their long propagating distance. However, the existence of multiple modes and the dispersive character of the modes make it difficult to understand and interpret. Tomography is a non-invasive imaging technique allowing for the visualization of the internal structures of an object. In recent years, Lamb wave tomography has been an attractive technique since it can produce quantitative maps that can be easily interpreted by technicians. Researchers attempted to adopt existing mature tomographic algorithms in seismic wave inversion to the specifics of Lamb waves in order to image plates. However, current traveltimes tomography that only uses the time-of-flight information may be discarding a wealth of information in the amplitude and phase of the Lamb wave. In seismic wave tomography, traveltimes inversion and wave-equation inversion are two extremes, and they have complementary strengths and weakness. Many researchers made use of the complementary nature of traveltimes tomography and waveform imaging to form high resolution images from crosshole seismic data. Motivated by these researches, a synthetic Lamb wave tomography method combining wave-equation traveltimes and waveform data is developed in this paper.

Statement of Contribution/Methods

In this method, an initial velocity model is solved firstly by wave-equation traveltimes tomography, and then a detailed velocity model is solved by the waveform tomography. In the wave-equation traveltimes tomography, Lamb waves are simulated numerically using finite element method. The velocity model is perturbed until the traveltimes from the computed waveforms are best fitted to the measured traveltimes in a least square sense. The traveltimes tomography will be taken as the starting model in waveform inversion. A gradient optimization method is used to minimize the squared error between the measured and computed Lamb waveforms.

Results

The synthetic wave-equation traveltimes and waveform tomography method is applied to the computed and measured crosshole data collected in an aluminium plate with one or multiple strong scattering through hole defects. Results show that the synthetic method is effective in eliminating reconstruction artifacts of traveltimes inversion, therefore improving the resolution and quality of reconstruction images.

Discussion and Conclusions

This paper describes the derivation of a new velocity inversion method, wave-equation traveltimes + waveform inversion. The method borrows the best characteristics of traveltimes inversion and waveform inversion. No traveltimes picking or ray tracing is necessary, and there are no high frequency assumptions about the data. Simulated and measured data tests show that this synthetic method provides a tomogram with the smooth and the detailed parts of the velocity model, and enhances the resolution of traveltimes Lamb wave tomography.

Semi-analytical finite element method for dispersion curves using higher order elements for Long Range Ultrasonic Testing.

Jose A. Otero¹, Nekane Galarza², Benjamin Rubio², Eduardo Moreno¹:¹Ultrasonic Group, ICIMAF, Vedado, Ciudad Habana, Cuba, ²Seguridad Industrial, Leia, Vitoria, Basque Country, Spain

Background, Motivation and Objective

Guided waves are suitable for detecting defects in pipes and others guided structures like rail, plates and bars. In these objects there are different modes of propagation, where the phase and group velocity depend on the frequency. These relations are known as dispersion curves and have been calculated by analytical and numerical methods. The use of analytical methods only is possible to use for the case of simple geometries like plates and bars. For others geometries it is necessary to use numerical methods. One of the more important is the Semi-analytical Finite Element Methods or SAFEM. Different authors have been used where the cross section for instance the plane xy , of the guided elements are discretized into small section. The longitudinal direction, the z axis it is described by an exponential orthogonal function which depends of the wave vector. The models used by different authors, assume a finite element associated with a displacement wave vector that are only linear depending of x , y and xy . In this paper it is proposed new elements which that include a quadratic dependence with a better performance in the precision of dispersion curves.

Statement of Contribution/Methods

It was developed a software of Semi-analytical finite element method in Matlab. In this case it was used higher order elements such as eight-node quadrilateral and six-node triangle elements.

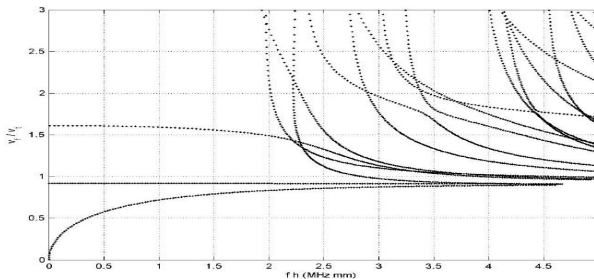
Results

It was obtained the dispersion curves of phase and group velocities from different elements such as, rail, pipes and rods. This is presented as a toolbox in Matlab using a GUI. Fig. 1 shows and example for the case of square bar.

Discussion and Conclusions

The dispersion curves obtained by this method are compared with other authors. Hayashi, Song and Rose (1) presented a model using four-node quadrilateral elements. Our approximation presents a better performance in the zone of low frequency of dispersion curves.

(1) Hayashi T., Song W.J., Rose J. Guided wave dispersion curves for a bar with an arbitrary cross-section, a rod and rail example. *Ultrasonics* (2003) 175-183.



Numerical Simulation of Sound Wave Propagation Using Hybrid Technique Combining FDTD Method and CIP Method

Masaki Ohmiya¹, Kan Okubo¹, Takao Tsuchiya², Norio Tagawa¹:¹Tokyo Metropolitan University, Japan, ²Doshisha University, Japan

Background, Motivation and Objective

Numerical simulation in time domain has been investigated widely for sound wave propagation with computer technologies. The finite difference time domain (FDTD) method is one of the most widely used schemes in computational acoustics. Although FDTD is simple to implement and model compared to other numerical techniques, using Yee's leapfrog algorithm, finite difference approximation certainly causes error because of

numerical dispersion. For that reason, large-scale simulations of sound wave propagation cannot be analyzed exactly. Therefore, those simulations require a low-dispersion method. The CIP method is known as a method that causes less numerical dispersion error. In this study, we examine a hybrid technique combining FDTD method and CIP method for large-scale simulations.

Statement of Contribution/Methods

To combine FDTD and CIP, the treatment of boundary is very important, because FDTD uses the staggered grids, while the collocated grids are used in CIP calculation. Moreover, CIP method utilizes not only the acoustic field values but also their spatial derivatives on grid points. Figure 1 shows the boundary of the domains of the two methods. p and v respectively represent the pressure and the particle velocity. We apply one-side finite difference approximations in order to obtain the values on CIP grids from the values of FDTD grids. On the other hand, the values on FDTD grids are given by applying the Hermite interpolation with those on CIP grids.

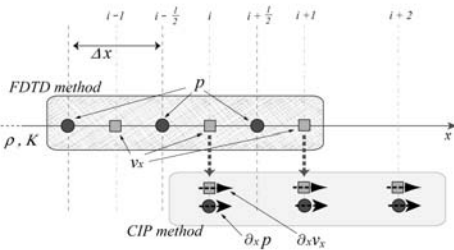
Results

To evaluate numerical error, a comparison study between the proposed method, conventional methods and exact solution was made for the calculation model of sound radiation from a point source. The reflection coefficient of the boundary is approximately less than -50 dB at over 10 CPW (cells per wavelength). However, numerical dispersion error of a hybrid FDTD-CIP scheme is less than conventional FDTD scheme.

Discussion and Conclusions

We investigate a hybrid FDTD-CIP scheme for solving the long wave propagation problem. The handling of boundary between the domains of the two methods is considered in this study. The numerical results demonstrate that the hybrid FDTD-CIP analysis provides higher accuracy concerning phase than conventional FDTD analysis.

Tuesday
Poster



P2-H-04

Sustainable Vibration Energy Harvesting based on doped PMN-PT Piezoelectric Single Crystal Cantilevers

Seung Eon Moon¹, Sung Q Lee¹, Sang Kyun Lee¹, Kang-Ho Park¹, Jongdae Kim¹; ¹ETRI, Korea, Republic of

Background, Motivation and Objective

In this study, to increase the generating power, we report the performances of the piezoelectric energy harvesting device with doped PMN-PT piezoelectric single crystal having higher piezoelectric strain constant d and higher piezoelectric voltage constant g over conventional piezoelectric materials. And to acquire the reliable piezoelectric energy harvesting device, the proper modeling was adapted to the measured results.

Statement of Contribution/Methods

Piezoelectric energy harvesting device was consisted of the PMN-PZT single crystal beam bonded to the FR4 substrate of 0.55 mm thickness with same size. For the PMN-PZT single crystal beam, gold electrode was coated on the both side and electrically poled sufficiently. The output power generated from the piezoelectric energy harvesting device is determined by the measured voltage across the load resistor connected to the device. The electrical properties of the fabricated devices were measured by using Agilent 4194A, Agilent 35670A, digital oscilloscope and probe station, etc. The frequency dependant impedance/phase angle, capacitance/quality factor values, FFT spectrum and mechanical damping ratio etc were measured.

The experimental set-up for measuring the performances of the piezoelectric energy harvesting device is shown in Fig. 1 (b). The vibration exciter (B&K, Type 4808) was used to supply reliable mechanical vibrations to the device. The shaker was controlled by HP 33120A function generator and power amplifier (B&K, Type 2719). The accelerometer sensor was located under the base of the PCB jig and measured the acceleration on the device. The measured acceleration on the sensor and the output voltage by the device were displayed on the oscilloscope (Tektronix, TDS3012B).

Results

The maximum output power of about 0.08 mW and 0.28 mW was obtained with a 2.3 k Ω resistive load resulting in a maximum power density of about 1 and 3.5 mW/cm³ for 0.5 g and 1 g acceleration, respectively. The power density was calculated using the generated power divided by the effective volume of the device, which is much higher than the reported value. The output power of the piezoelectric energy harvesting device was increased with the acceleration applied in the device.

Discussion and Conclusions

We fabricated piezoelectric energy harvesting device using doped PMN-PT piezoelectric single crystal beam. The devices generated 0.28 mW power and 3.5 mW/cm³ power density with an optimal resistive load of about 2.3 k Ω from 1 g acceleration at its resonant frequency of 630 Hz, which were well matched with the calculated values. The improved power was ascribed to the Zr doping effects and the large piezoelectric coupling factor of the [110] poled piezoelectric crystal

P2-H-05

Array configurations for higher power generation in piezoelectric energy harvesting

Daisuke Koyama¹, Kentaro Nakamura^{1,2}*Precision and Intelligence Laboratory, Tokyo Institute of Technology, Yokohama, Kanagawa, Japan*

Background, Motivation and Objective

Electric power generation efficiencies using a vibration of a piezoelectric element with array configurations were discussed. We have been investigating the piezoelectric energy harvesting using a polyurea thin film, which can be fabricated on the micro array structure. In our previous work, it was predicted that the higher power generation efficiency could be obtained with the shorter cantilever configuration. To realize the piezoelectric energy harvesting device with the larger volume energy density, the energy conversion efficiencies of the different array configurations were investigated.

Statement of Contribution/Methods

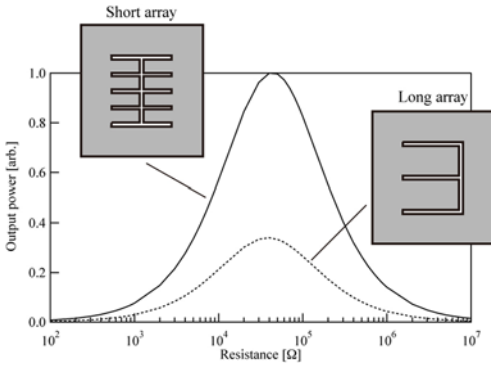
The energy conversion efficiencies and the volume energy densities of the energy harvesting element with several array configurations were calculated through the finite element analysis (FEA). Two energy harvesting devices with the different array configurations were designed. In the same volume of 22 \times 19 \times 1 mm³, the large array configuration has two long cantilevers (18 \times 9.5 \times 1 mm³) and the small one has eight short cantilevers (9 \times 4.25 \times 1 mm³) as illustrated in Fig. 1. The 1-mm-thick PZT elements were attached on the surface of each aluminum cantilever. The harmonic vibration in the vertical direction at the fundamental resonance frequencies of the cantilevers was applied by using a vibration generator, and the electric power generation was measured by connecting the load resistance.

Results

The larger volume energy density as an electric power generator could be obtained with the shorter array configuration. The larger output power was generated with the larger applying vibration. The relationship between the load resistance and the output power was investigated and the optimum values of load resistance on the short and long array configurations were both 40 k Ω (Fig. 1). The volume energy density ratio of the short array configuration to that of the long one was estimated to be 2.95.

Discussion and Conclusions

Much larger volume energy density is expected by using the micro array configuration with a polyurea thin film.



P2-H-06

Free-standing thick-film piezoelectric multimorph cantilevers for energy harvesting

Swee Leong Kok¹, Neil Maurice White¹, Nicholas Robert Harris^{1,†}, *School of Electronics and Computer Science, University of Southampton, United Kingdom*

Background, Motivation and Objective

Usually piezoelectric materials are fabricating on thin substrates, such as stainless steel, into a cantilever structure and operating at the resonant frequency of the system. As the substrate material is non-functional, it does not contribute directly to the electrical power output but merely serves as a base material. The aim of this paper is to describe a novel structure for a thick-film piezoelectric cantilever in a free-standing form, which minimises the movement constraints on piezoelectric materials and therefore maximises the electrical output power.

Statement of Contribution/Methods

Novel thick-film multilayer free-standing structures in the form of a multimorph cantilever were fabricated. The multimorph structure consists of three individual PZT layers with equal thickness of about 40 μm separated physically and electrically by Ag/Pd conductors. Each piezoelectric plate was polarised in its thickness direction with two different modes: series and parallel. In series mode, both the outer electrodes plates were polarised in the same direction with respect to the centre plates, while it was polarised in the opposite direction for parallel mode.

Results

In a low-level ambient vibration of 5 ms⁻², the series polarised multimorph structure was found to produce an electric power of 40 μw (two times more than parallel polarised multimorph), when driving a resistive load of 37.5 kΩ at resonant frequency of 400 Hz.

Discussion and Conclusions

A correct combination of electrode terminate within the multimorph determines the electrical output of the device. Series polarised multimorph was found to be more efficient in generating output power compared to parallel polarised multimorph. Free-standing multimorph cantilevers, can generate enough energy for powering microsystems.

P2-H-07

Measurement of Granule Strength in Particle Beds using Ultrasonic Velocity

Peter Coghill¹, *CSIRO Minerals, Australia*

Background, Motivation and Objective

Measurements of ultrasonic velocity have been used to determine cohesion and setting in many materials such as sinter and cement. These properties are also important for industrial granular materials such as pellets and powders. Current test methods of granular material are usually some form of attrition test or individual crushing of pellets.

Tuesday
Poster

These methods suffer disadvantages of being time consuming or difficult to relate to fundamental properties of the particle or both. In many of these cases a measurement of the average ultrasonic velocity of these particles could be related to the particle strength. This paper sets out to demonstrate a method that would allow this measurement to be made despite the effects on sound transmission due to the granular structure of the material.

Statement of Contribution/Methods

For certain conditions of pressure, particle size, and wavelength effective medium theories (EMTs) can be used to describe sound propagation through granular material. These usually take the constituent properties of the particles as a given and calculate sound velocity. We construct a test apparatus designed to operate in these conditions to perform the inverse and determine intrinsic particle properties from the sound measurement.

First the EMT and measurement regime is tested on standard particles. Then the efficacy of sound velocity measurement when related to individual crush tests is demonstrated for iron ore pellets. An attrition test comparison is then made with alumina hydrate powder.

Results

In 50 gram samples of 100 micron glass bead standards, measurements are carried out with a reproducibility of 1%.

Three batches of iron ore pellets with different crush test results are measured in a single layer to demonstrate the relationship between the sound speed measurements and crush test results. In this case there was a correlation coefficient of 0.96 between the measurements. The single layer sound measurement reduced the variability by a factor of 5.

For 40 gram alumina powder samples the bulk sound velocity measurement and the bulk density were correlated to attrition measurements with a correlation co-efficient of 0.96 for 11 industrial samples.

Discussion and Conclusions

This paper investigates a new area for the use of ultrasonics in material evaluation: particle strength in granular materials. The strength of two industrially important test materials has been successfully measured. In the first, iron ore pellets, individual crush strength is the traditional quality control measurement, and in the second, alumina powder, an attrition test is the traditional quality control measurement. The second case is of particular interest as a sample comprised of hundreds of thousands of particles. An instrument developed along these lines has the potential to conveniently measure particle strength for a range of granular materials where the individual particle strength is related to sound velocity, such as those formed by binding agents or agglomeration.

P2-H-08

Compacting of Various Metal Alloy and Ceramic Powder Using 20 kHz Ultrasonic Vibration Compacting Equipment with Upper and Lower Vibration Punches

Jiromaru Tsujino¹, Yasunori Saotome², Noboru Shimada³, Eiichi Sugimoto^{4,1} *Faculty of Engineering, Kanagawa University, Yokohama, Kanagawa, Japan,* ²*Osaka Center for Material Research, Tohoku University, Sakai, Osaka, Japan,* ³*Portie Co. Ltd, Kumagaya, Saitama, Japan,* ⁴*Asahi EMS Co. Ltd, Tokyo, Tokyo, Japan*

Background, Motivation and Objective

Compacting of metal, alloy and ceramics powder is important process for powder metallurgy which is used for producing small and precise mechanical parts and required for various industry fields including electronics. Some complex metal alloy, amorphous alloy and fine ceramic powder are impossible to compact using only static pressure. Metal alloy and amorphous alloy powder which contains Zr, Cu, Al, Ni or Cu, Zr, Al, Ag for producing high strength material are impossible to compact although under very high static pressure of over 5 GPa.

Statement of Contribution/Methods

20 kHz ultrasonic compacting equipment with 5-mm-diameter upper and lower vibrating punches is developed and compacting characteristics are studied (Fig. 1). The vibration systems consist of 50-mm-diameter BLT transducers, stepped catenoidal horns and 5.0-mm-diameter hard metal punches. These vibration systems are driven under various vibration phase differences 0° to 180°(in-phase to anti-phase mode) using two 2 kW power amplifier systems. This system could be driven the compact specimen in vibration node (vibration stress maximum position) using node punches.

Results

Compacting characteristics of copper, iron alloy, amorphous alloy and ceramic powder are studied using various phase differences under vibration amplitude of over 15 μm (peak-to-zero value). Maximum static force is 10 kN (0.5 GPa). Figure 2 shows copper and iron alloy specimens compacted using upper and lower ultrasonic vibration punches.

Discussion and Conclusions

Various powder including copper, iron alloy and ceramic powder used for IC ceramic packages were successfully compacted using ultrasonic vibration. Vibration conditions for compacting various powder including amorphous alloy and conditions of compacts are under studying.



Fig. 1 20 kHz ultrasonic compacting equipment with 5-mm-diameter upper and lower vibration punches.



Fig. 2 5-mm-diameter copper and iron alloy powder compacts using 20 kHz ultrasonic compacting equipment with upper and lower vibration punches.

Tuesday
Poster

P2-H-09

Ultrasonic characterization of unconsolidated granular media undergoing compaction

LEGLAND Jean-Baptiste¹, TOURNAT Vincent¹, GUSEV Vitaliy²; ¹LAUM UMR CNRS 6613, Le Mans, France, ²LPEC UMR CNRS 6087, Le Mans, France

Background, Motivation and Objective

Granular media are present in nature or in industry, and they consequently interest a wide community : geophysics, mechanics. Many methods exist to study their properties but elasticity of unconsolidated granular media remains poorly understood, especially at low static pressure. Ultrasonic methods are the only one able to probe accurately the elasticity of a 3-D granular packing. In order to reach a large number of different mechanical states of the granular structure, we use the well known compaction process. The objective is to understand the influence of parameters like static pressure and compacity on the linear and nonlinear elasticity.

Statement of Contribution/Methods

In order to measure the elastic parameters of the granular packings (made of glass beads) along compaction, we specially built a setup which is composed of a container with a movable bottom (vertical compaction). To excite and to measure the standing longitudinal acoustic waves between the vertical walls of the container two ultrasonic transducers are used. The first resonance of the granular layer is about 3 kHz which corresponds to a 120 m/s wave velocity. Each experiment consists, for a given number of solicitations, to measure the :

- average compacity (ϕ),
- static pressure (p_0),
- temperature (T_0),
- longitudinal velocity (C_l) from which is deduced the effective elastic modulus (E_{eff}).

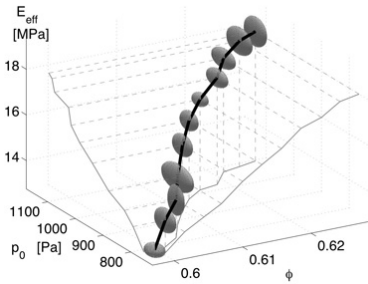
First, this elastic parameter is measured for weak excitation amplitudes. Other methods are implemented in order to measure nonlinear parameters such as the nonlinear resonance method. Harmonic generation and self-demodulation effects at high level of ultrasonic amplitude is currently studied.

Results

The evolution of the effective elastic modulus as a function of the average compacity and the pressure is shown in the figure where all points are averaged over five experiments (black one). The dependences of compacity and the elastic modulus on static pressure are shown by the projections (gray one).

Discussion and Conclusions

Many parameters change during compaction process and the results show that the increase in velocity is associated with the increase in static pressure and average compacity. We currently quantify the role of each of them on the elasticity. The evolution of nonlinear parameters due to hysteresis and nonlinear dissipative effects is currently studied.



P2-I. Ultrasonic Signal Processing

Sala Orange

Tuesday, September 22, 2009, 10:00 am - 11:30 am

Chair: **Ramazan Demirli**
Canfield Scientific

P2-I-01

Wavelet Cycle-Spinning Denoising of Ultrasonic Traces Acquired from Austenitic Steel

Jose Luis San Emeterio¹, Emilia pardo¹, Miguel Angel Rodriguez²: ¹*Señales, Sistemas y Tecnologías Ultrasonicas, Instituto de Acustica (CSIC), Madrid, Spain,* ²*ETSI Telecomunicación, Universidad politecnica de Valencia, Valencia, Spain*

Background, Motivation and Objective

Ultrasonic non-destructive evaluation of austenitic steel components or welded unions usually presents difficulty for small flaw detection, due to complex structure and wave scattering at grain boundaries. Ultrasonic signals from small flaws are masked by grain or structural noise that partially overlaps the frequency response of the ultrasonic transducer. The main objective of this work is the application and performance analysis of a cycle-spinning undecimated wavelet transform (UWT) processor for denoising ultrasonic traces acquired from a test block made of austenitic steel.

Statement of Contribution/Methods

A Panametrics 5052 Ultrasonic analyzer, an M103 transducer of 1 MHz centre frequency and a digital oscilloscope have been used in the experimental set-up. A cycle-spinning (CS) implementation of UWT has been developed and applied to denoise ultrasonic traces. Performance is evaluated in terms of SNR, defined as the peak value in the target zone of the trace divided by the standard deviation of the whole trace. CS denoising of ultrasonic traces has been compared with the classical discrete wavelet transform (DWT) denoising. Different mother wavelets (Daubechies db1, db6, and db12) and several threshold selection rules (Universal, Minimax and SURE) have been assessed. Soft thresholding, zero padding for border treatment and decomposition level dependent thresholds (appropriated for correlated noise) have been used in all cases.

Results

It has been found that the DWT denoised traces are frequently worse than the initial traces when Universal thresholds are used. This fact seldom happens with the corresponding CS processing. CS denoising is almost always better and more stable than DWT denoising, which presents some fluctuating performance. The best results are generally obtained by CS processing with Minimax thresholds while SURE thresholds usually attains an intermediate performance. The particular values of DWT thresholds and the corresponding mean values of CS thresholds have been computed and compared at the different scales, showing similar values. It has also been observed that SNR results for short filters (i.e. db1, L=2) are generally better than for long filters (db12, L=24). Nevertheless the visual quality of the denoised traces with very short filter length (db1) is worse than for intermediate length filters (db6, L=12).

Discussion and Conclusions

CS is an effective approach to denoise ultrasonic signals contaminated with grain noise. CS presents a general tendency to higher SNR, improved visual quality of the denoised traces and greater robustness of the processing in relation to the classical DWT denoising. In addition, CS denoising is a versatile approximation from which alternative processing schemes can be derived.

Evaluation of Chirp and Binary Codes as Excitation Pulses for 3D USCT Transducers

Michael Zapf¹, Badreddine Derouiche¹, Nicole Ruiter¹; ¹Forschungszentrum Karlsruhe, Germany

Background, Motivation and Objective

At Forschungszentrum Karlsruhe we are developing a new imaging method for early breast cancer detection: ultrasound computer tomography (USCT).

The USCT system consist of hundreds of ultrasound transducers, sparsely positioned in 3D in walls of the measurement container. This SAFT (synthetic aperture focusing technique) setup relies on transducers with a critical trade-off in active transducer area, to fulfill opening angle and as well signal SNR requirements.

This work tries to relax this crucial trade-off by extending the SNR through usage of advanced coded excitation and matched filter signal processing techniques known from radar and sonar.

Statement of Contribution/Methods

The evaluation was done with a special transducer measurement setup, which allows geometrical arbitrary positioning of an emitter-receiver combination in contrast to the fixed USCT 3D aperture.

The setup consisted of an USCT transducer prototype which acted as emitter and a calibrated hydrophone, arbitrarily positioned to the emitter, which acted as receiver.

On a measurement run the emitter was excited by an arbitrary digitized code generated by an AWT (arbitrary waveform generator). A PC digitization card was triggered and measured the emitted sound-wave pressure. Signal processing and analysis was done with MATLAB.

The test cases to analyze robustness and quality of the different codes and the signal processing chain were an empty measurement and a tissue mimicking object measurement.

Evaluated codes were a damped sine pulse, a Barker code with 13 elements, a Golay code sequence with 16 elements and a linear modulated Chirp. For all codes the same mean frequency (f_c) and the same bandwidth (f_b) was taken, therefore the time duration is diverging.

Results

The figure shows the SNR for evaluated codes with the parameters $f_c=2.75\text{MHz}$ and $f_b=1.4\text{MHz}$ for an empty measurement which was averaged 512 times.

The Golay code shows the highest SNR for empty measurement (56dB) and the object measurement (42dB), followed by the barker code then the chirp code. The sine code has by far the lowest SNR.

Discussion and Conclusions

The evaluated Golay code is a promising option as excitation code for USCT, with downside of a doubled DAQ time because of code sequence. Therefore, the Barker code without this disadvantage, is also an option for extending the signal SNR without reducing the opening angle of the transducers.

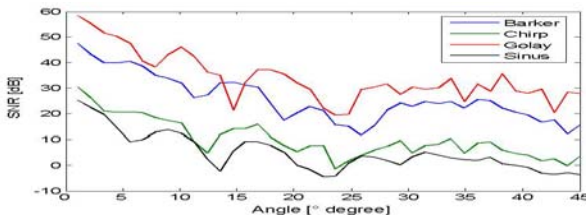


Figure: Y-axis gives the SNR of the excitation codes, x-axis is the difference angle to face-to-face position of emitter and receiver, therefore representing the emitter opening angle

Performance Evaluation of Time-Frequency Distributions for Ultrasonic Flaw Detection

Erdal Oruklu¹, Semih Aslan¹, Jafar Saniie¹; ¹Electrical and Computer Engineering, Illinois Institute of Technology, Chicago, IL, USA

Background, Motivation and Objective

In ultrasonic NDE applications such as detecting fatigue cracks, void and delamination in large grain materials, defect echoes are often concealed by clutter resulting from grain scattering. In the past, studies have been performed to improve flaw visibility based on frequency diversity. In Rayleigh region where the echo wavelength is larger than the grain size, the scattering is highly dependent on the frequency of interrogation. Consequently, when testing the materials using a broadband transducer, there is an upward shift in the expected frequency of scattered echoes. On the contrary, the echoes from defects represent a downward shift with respect to transducer frequency due to the effect of frequency-dependent attenuation. This paradox in frequency shift is advantageous for locating the defect. Therefore, methods that meet the criteria for improved flaw detection are time-frequency (T/F) distributions. T/F processing of signals extracts the features produced by the concentration of signal energy in two dimensions (time and frequency) instead of only one. Hence, the objective of this study is to analyze T/F distributions for optimal ultrasonic flaw detection.

Statement of Contribution/Methods

In this study, we have examined Gabor transform (GT), Wigner-Ville distribution (WVD), Wavelet transform (WT), and Chirplet transform (CT) for flaw detection. These distributions are not unique and they display signal information differently on T/F plane. A methodology is presented with respect to each T/F distribution method, describing the necessary steps to achieve maximum flaw echo visibility enhancement. These steps include choosing the optimal time and frequency window sizes (based on Heisenberg principle), and the appropriate post-processing detection method to minimize the effect of null-observations. To demonstrate the validity of the methods, we discuss and draw an analogy between T/F distributions and the conventional Split-Spectrum Processing (SSP) flaw detection method.

Results

For performance evaluation, experimental measurements from steel blocks (type 1018 with different grain sizes including single or multiple defects) are acquired using an ultrasonic pulse-echo system with 5 MHz and 10 MHz broadband transducers. The comparative results show the strengths and deficiencies of each method. T/F distributions are particularly effective, matching and exceeding SSP performance when the signal is analyzed with a priori information about the transducer bandwidth and the expected frequency-shift due to scattering and attenuation.

Discussion and Conclusions

In this work, we have developed and analyzed methods for improved ultrasonic flaw detection using T/F distributions. T/F representation exploits the frequency sensitivity of grain scattering and focuses on the T/F region where the flaw-to-clutter ratio is maximal. The analytical and experimental studies verify the feasibility of the T/F techniques for NDE applications.

Hilbert Transform for Ultrasonic NDE Applications: Pitfalls and Solutions

Erdal Oruklu¹, Yufeng Lu², Jafar Saniie¹; ¹Electrical and Computer Engineering, Illinois Institute of Technology, Chicago, IL, USA, ²Electrical and Computer Engineering, Bradley University, Peoria, Illinois, USA

Background, Motivation and Objective

Hilbert Transform (HT) is an effective tool for estimating the signal envelope and instantaneous frequency (IF). However, IF computation based on HT is highly sensitive to noise and also to interfering multi-component echoes such as ultrasonic scattering signals. Furthermore, HT works well with narrowband signals but broadband signals may not satisfy the well-behaved analytic signal model based on the Bedrosian theorem. In this study, we analyze and model complex ultrasonic signals using HT, leading to efficient characterization of materials with respect to frequency-dependant scattering, attenuation and dispersion effects. We present the challenges/pitfalls associated with HT and introduce remedies to overcome the limitations of HT when it is applied to ultrasonic signals.

Statement of Contribution/Methods

We aim to address two key issues related to HT based IF measurements with this investigation. First, in order to minimize the effect of the noise, a weighted smoothing function based on envelope estimates is introduced. The duration of this smoothing function is governed by the resolution of the required ultrasonic testing system. By reducing the noise components, the accuracy is significantly increased at locations where the signal envelope is small. Second, to qualify the ultrasonic signal for HT, we decompose it to multiple narrowbands using a filterbank structure and estimate IF within these narrowbands. Any erroneous frequency estimation beyond these bands can be discarded. Finally, the entire T/F representation with HT can be obtained by recomposing IF components obtained by each narrowband. An important advantage of this approach is separating echoes within different frequency bands and consequently minimizing the time-overlap among them. This decomposition operation also satisfies the Bedrosian identity by limiting the bandwidth of the signal.

Results

We apply the proposed HT methods to various experimental ultrasonic data sets and examine microstructure scattering, effects of attenuation in large grained materials, flaw/crack detection in the presence of high grain scattering noise, characterization of complex shapes defects, and study of reverberation in thin layers. Simulation studies and experimental results support the accuracy of the IF estimation. Enhanced IF technique provides tractable frequency estimates and makes it possible to quantify physical phenomena such as spectral shifts due to attenuation and scattering and dispersion effects.

Discussion and Conclusions

HT can be very effective for instantaneous frequency estimation in ultrasonic NDE applications. However, it may result in misinterpreting echo signals if not used correctly. Therefore, two methods have been introduced to increase the robustness of the HT method by reducing its sensitivity to noise and by ensuring true analytic signal representations with the narrowband decomposition.

P2-I-05

Real Time Adaptive Parametric Equalisation of Ultrasonic Transducers

Sean G. Mc Sweeney¹, W.M.D Wright¹; ¹Electrical and Electronic Engineering, University College Cork, Cork, Ireland

Background, Motivation and Objective

Parametric equalisation is often used to achieve a desired response from an audio transmitter, but is rarely applied to ultrasonic transducer systems. The ability of a broadband ultrasonic transmission and reception system to adapt its frequency and time domain response to changing acoustic conditions would be a distinct advantage in certain applications. Ultrasonic remote monitoring systems would benefit significantly from this ability, as signal levels could be minimised and consequently the transmitter power consumption decreased. This work presents a real-time adaptive ultrasonic parametric equaliser using optimisation driven Matlab code to control the coefficients of a switched capacitor filter network implemented in a Cypress PSOC (Programmable System On a Chip).

Statement of Contribution/Methods

In this work, adaptive parametric magnitude equalisation of a through-transmission ultrasonic system using CUTs (Capacitive Ultrasonic Transducers) has been achieved in real time by tracking a desired SNR (signal to noise ratio) across the operational frequency spectrum. A Matlab neural network was developed to control the equalisation filter coefficients based on the received frequency response data. The adaptive parametric equaliser adjusts the magnitude of the driving signal to maintain the desired SNR as closely as possible. The neural network was trained using PSO (Particle Swarm Optimisation) back-propagation, based on a state space model of the system developed from frequency response data. The developed equalisation circuitry, which is switched capacitor based and was fully implemented on the PSOC, is also described.

Results

Simulation and experimental results of the adaptive equalisation of a CUT through-transmission pair operating up to 100kHz in air using Cypress PSOC switched capacitor modules have shown a decrease in excess of 15% in the average energy consumption of a continuous operation system with changing acoustic characteristics, such as the path length. The frequency range was limited by the capabilities of the PSOC used. Transient and small signal response data of the equaliser has been charted highlighting performance parameters within the various modes of operation of the following realisable filter elements: Butterworth, Chebychev, Bessel and Gaussian. These filters were selected by the system based on the critical response criteria; flat passband response, stopband attenuation, damping maximisation or transient response, respectively.

Discussion and Conclusions

It has been shown that for CUT through-transmission systems, adaptive parametric equalisation may be used to compensate for changing frequency dependant attenuation in real time to maintain a desired SNR. The principles of this work are valid for any transducer arrangement, frequency range, or equalisation method. A potential application is the control of individual array elements, which could result in improved focusing in inhomogeneous media.

P2-J. Bulk Wave Effects

Sala Orange

Tuesday, September 22, 2009, 10:00 am - 11:30 am

Chair: **Jan Brown**
JB Consulting

P2-J-01

Characterization of bulk acoustic wave transducers and resonators based on low temperature sputtered AlN thin films

Cinzia Caliendo¹; ¹*Istituto dei Sistemi Complessi, Consiglio Nazionale delle Ricerche, Rome, Italy, Italy*

Background, Motivation and Objective

Hexagonal aluminum nitride (AlN) substrate is an excellent candidate for the realization of low cost, high frequency surface and bulk acoustic wave (SAW and BAW) devices thanks to its high SAW and BAW propagation velocities in the c plane, good electromechanical coupling constant (0.3%) and an almost negligible temperature coefficient of delay (TCD = -30 ppm/°C). The BAW resonators fabricated in the thin film technology offer high performance and small physical size. Thin film bulk acoustic resonators (TFBAR) have recently been adopted as alternatives to SAW resonators in high frequency devices, due to their inherent advantages, such as low insertion loss, low cost, high power handling capability and small size.

Statement of Contribution/Methods

AlN films were grown by RF reactive magnetron sputtering system at 80°C on the surface of Si(100) and Al₂O₃(100) covered with an Al or Pt film (0.12 μm thick). An Al top electrode, 0.12 μm thick, was sputtered and patterned on the free surface of the AlN layer. The contour lines (the form factor M for different electrode and piezoelectric film thickness) and the theoretical frequency response of the BAW transducers was simulated. The scattering parameter S₁₁ of the electroacoustic transducers was tested in the frequency and time domain by means of a vectorial network analyzer. The time delay and operation frequency of the BAW transducers were measured and found in good accordance with the theoretically calculated values. TFBARs were realized on a Si₃N₄ membrane, 200 nm thick, chemically etched on a Si substrate. The TFBAR input impedance was measured and the equivalent-circuit modified Butterworth Van Dyke (MBVD) model was derived to simulate the electrical behavior of the TFBAR in the vicinity of the film resonance.

Results

AlN-based BAW transducers were realized and their frequency response was tested for different piezoelectric film thicknesses. The experimental data were compared and found in good accordance with the theoretically calculated ones. The TFBAR performances were tested for different piezoelectric film thickness values. TFBARs showing high effective electroacoustic constant and quite good Q were obtained. A lumped element, equivalent circuit model was derived to extract the parameters of the tested devices.

Discussion and Conclusions

The frequency response of BAW transducers was tested for different piezoelectric film thicknesses and found in good accordance with the theoretically calculated one. The experimental BAW velocities were equal to 9425 and 10355 m/s for the Si- and Al₂O₃-based BAW transducers, confirming the higher piezoelectric quality of the AlN films grown on Al/Al₂O₃ respect to those grown on Al/Si. TFBARs showing K₂= 3.8 % and Q=156 were obtained. The parameters of the modified Butterworth Van Dyke model of the TFBAR were extracted. The obtained results confirm that AlN films are suitable for high frequency application even in the region of low temperature deposition values.

Tuesday
Poster

Determination of the Temperature Coefficient Piezoelectric Constant (TCe33) to Improve Thermal 1D Acoustic Tool for BAW Resonator design

David Petit^{1,2}, Brice Gautier², David Albertini², Emmanuel Defay³, Jacques Verdier², Daniel Barbier², Jean-François Carpentier¹, ¹STMicroelectronics, Crolles, France, ²INL, Villeurbanne, France, ³CEA-LETI-MINATEC, Grenoble, France

Background, Motivation and Objective

In the early 1960's piezoelectric thin films have been used in Surface Acoustic Wave (SAW) and Bulk Acoustic Wave (BAW) transducers, sensors and resonators. To predict the performances of acoustic resonator, the 1D acoustic model is currently used with the following parameters: density, elastic modulus, thickness, and piezoelectric coefficients. In this model the piezoelectric coefficient e_{33} represents the stress due to a given electric field when the crystal is clamped. Various piezoelectric coefficients (e_{ij} , d_{ij} , g_{ij} and h_{ij}) have been characterized with several specific techniques, among which, we find: RF measurement, interferometry, Piezoresponse Force Microscopy (PFM)... Based on the piezoelectric theory, we propose to evaluate the e_{33} coefficient as a function of the elasticity C_{33} , permittivity ϵ_{33} and the static piezoelectric coefficients ($d_{33\text{eff-s}}$). In working condition, the temperature environment modifies the behaviour of the material properties. The measurement technique for the Temperature Coefficient (TC) of elasticity C_{33} can be achieved using the picoseconds ultrasonic tool. The TC(e_{33}) coefficient is evaluated using RF measurement. The TC($d_{33\text{eff-s}}$) coefficient has been characterised using the PFM equipped with a heating system. The main issue of this work is the synthesis of specific rules to achieve good measurement of $d_{33\text{eff-s}}$ coefficient by means PFM technique. Then, the TC(e_{33}) coefficient has been deduced and introduced into the thermal 1D acoustic tool.

Statement of Contribution/Methods

First, the analytic piezoelectric formalism is presented in order to present the methodology in details. The PFM technique is based on the detection of local vibration induced by an AC signal applied between two Mo electrodes of the AlN piezoelectric layer. The local oscillations of the top electrode are transmitted to the tip and detected using a lock-in amplifier. The test samples used to characterize the $d_{33\text{eff-s}}$ coefficient are fabricated following specific rules. In order to validate the measurement technique, an effective piezoelectric coefficient based on a reference x-cut quartz is measured and compared with literature. Furthermore, the temperature can be changed during operation to characterize the TC($d_{33\text{eff-s}}$) coefficient of the AlN layer.

Results

Reproducible measurements of the $d_{33\text{eff-s}}$ coefficient are obtained using the PFM technique. Finite Element simulations confirm the specific rules applied of the measured $d_{33\text{eff-s}}$ coefficient. The evolution of this coefficient is shown on the +25 to +80°C temperature range. This result confirms the weak influence of the TC(e_{33}) coefficient comparatively the TC(C_{33}) coefficient.

Discussion and Conclusions

We propose a method to assess the TC(e_{33}) coefficient based on the piezoelectric theory. We also discuss the uncertainty temperature coefficients in the thermal 1D acoustic model in comparison to the thermal measurement of the BAW resonator.

BAW SMR Filter Reliability Investigation Using Lock-In Thermography

Nizar BEN HASSINE¹, Denis MERCIER², Christian SCHMIDT³, Philippe RENAUX², Christophe BILLARD², Guy PARAT², Pierre BAR¹, Cedrick CHAPPAZ¹, Patrice WALTZ¹, Skandar BASROUR⁴, ¹STMicroelectronics, Crolles, France, ²CEA-LETI/MINATEC, DRT, Grenoble, France, ³Fraunhofer Institute for Mechanics of Materials, Halle, Germany, ⁴TIMA CNRS-UJF-INPG Micro-Nano-Systems Group, Grenoble, France

Background, Motivation and Objective

Bulk Acoustic Wave (BAW) Solidly Mounted Resonator (SMR) technology offers key advantages for RF filtering applications in term of miniaturization, power handling and thermal stability. However, the tendency toward reducing the device size leads to enormous power density and causes reliability problems. Consequently, it is important to study the characteristics of SMR filters under high power level. This paper aims to provide a contribution for a better characterization and understanding of SMR filters behaviour under high AC signals by using an original technique: the Lock-In Thermography (LIT).

Statement of Contribution/Methods

LIT principle consists in stimulating the SMR filter by a modulated RF source that produces a thermal response imaged with a highly sensitive IR camera. LIT advantages are the detection sensitivity ($<100\mu\text{K}$), the spatial resolution (up to $1.2\mu\text{m}/\text{pixel}$) and the reduction of lateral heat spreading. A specific RF bench is developed to measure the power dissipated inside the filter (FIG.1).

Results

SMR filter characteristics under high power level are investigated using the proposed technique. Self-heating and heat repartition in different resonators are reported as a function of the applied signal frequency (FIG.2). The electric equivalent model is used to estimate the dissipated power in each resonator for correlation with thermal results. No electromigration effect is observed in Molybdenum electrodes for the studied filter up to 36dBm.

Discussion and Conclusions

LIT is demonstrated to be an interesting technique for BAW thermal characterization. Future characterizations in a stand-alone resonator should be interesting for an accurate thermal modeling.

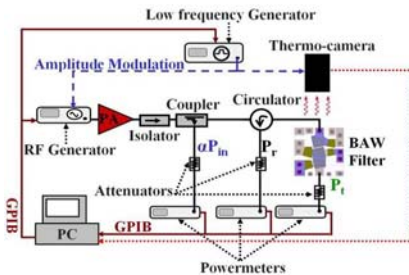


FIG.1: Setup used for SMR filter characterization

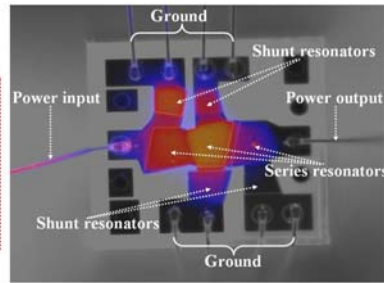


FIG.2: SMR filter lock-in thermogram for $f_{\text{Lock-in}}=25\text{Hz}$, $P_{\text{in}}=31\text{dBm}$ and $f=1.8\text{GHz}$

P2-J-04

Application of torsional resonance technique to temperature-range studies of shear viscoelastic properties of crude oil and crude-saturated sands

Oleg Zozulya¹, Igor Esipov², Andrew Fokin², ¹SMR, Schlumberger, Moscow, Russian Federation, ²Physical Acoustics Lab, Andreyev Acoustics Inst., Moscow, Russian Federation

Background, Motivation and Objective

Production forecasts for conventional oil stimulate interest in new methods of exploitation of unconventional resources such as heavy oil. Heavy oil has reserves that are estimated to be more than double the world reserves of conventional oil. One of the main challenges in heavy oil production comes from its high viscosity. Cold production has recovery efficiency of less than 10% whereas heating methods by reducing the oil viscosity by several orders increase the efficiency up to 80%. An important aspect of heating production is solid-liquid front monitoring which can be inferred from seismic data. This can not be implemented at length without acquiring the knowledge on the rheology of unconsolidated media saturated with viscous fluid.

Statement of Contribution/Methods

A torsional resonance technique is developed for the temperature-range studies of the shear viscoelastic properties of bulk fluids and fluid-saturated unconsolidated media at single frequency in the range 10-20KHz. The technique is based on the torsional resonance curve registration for the empty and the sample-filled finite-length tube and on the subsequent determination of the resonance frequency shift and the attenuation change caused by sample loading. To determine the resonance frequency and the attenuation the method of nonlinear simplex approximation is used.

Results

A simplified theoretical model is developed which describes the propagation of torsional mode waves in elastic tubes filled with viscoelastic material. The model relates the real and imaginary parts of the sample shear modulus with the frequency shift and the attenuation change of torsional oscillations.

To verify the results of the theoretical modeling and estimate the measurement errors the test experiments are carried out for glycerol, i.e. for the fluid that exhibits no viscoelastic behavior in the temperature and frequency ranges used. The accuracy of the measurements is about 6% for the range of viscosities 0.1-10 Pas.

The measurement carried out with bulk crude oil from Mordovo-Karmalskoe field (Russia) in temperature range -10-60C shows that the crude undergoes glass phase transition at temperatures below 30C which is characteristic of wax precipitation.

To investigate the temperature effect on the viscoelastic properties of crude-saturated unconsolidated media a number of commercially available proppants with different particle size distributions (PSD) are studied in temperature range 1-60C. The results show that the crude-saturated proppants exhibits viscoelastic behavior in the whole temperature range. The shear loss modulus is shown to be influenced by the proppant PSD, however the correlation with the proppant permeability holds only for temperatures up to 20C.

Discussion and Conclusions

The torsional resonance technique developed is a valuable tool for temperature-range characterization of shear viscoelastic properties of fluid-saturated unconsolidated media at logging-tool frequencies.

P2-J-05

The Experimental Study of Acoustic Waves of Frequency about 40GHz

Boris Zaitsev¹, Mikhail Grigoriev²:¹SF IRE RAS, Saratov, Russian Federation, ²Saratov State University, Saratov, Russian Federation

Background, Motivation and Objective

In 60-80 years of XX century acoustic waves of frequencies ~10 GHz were actively studied in the wide temperature ranges. It has been found that some crystals have relatively low attenuation and may be used for development of the signal processing devices operating at the room temperature. In these years the papers devoted to study of acoustic waves in quartz at higher frequencies (24, 40, 70, and 114 GHz) in temperature range 4.2 – 30K were also published. But the crystals, which are prospective for acoustic waves at frequencies ~10 GHz, have not been studied at the higher values of frequency. This paper is devoted to study of acoustic waves of frequency ~40 GHz.

Statement of Contribution/Methods

We have investigated such crystals as ruby, lithium niobate, and magnesium aluminate spinel (MAS) with various ratio of magnesium and aluminum oxides. The samples under study had the shape of stepped cylinder of diameters 1 and 3.5 mm and length 2-5 mm with the unparallelism of edges less than 15 seconds. As transducers for the samples of ruby and MAS the films of zinc oxide with thickness ~1000 Å were used. As for lithium niobate the excitation and reception of acoustic waves were performed directly from the sample surface. As electro-dynamic system for applying the electromagnetic wave to the transducer we used the quasi-static resonator having the inner diameter 3 mm. The adjustment of the resonator on the resonant frequency was performed by changing the distance between the sample edge and capacitive lug. The coefficient of the single transformation was equal 30-40dB. We investigated the temperature dependencies of attenuation of longitudinal and shear waves in crystals under study in temperature range starting from 78K. The measurement of the wave attenuation was performed by standard echo-pulse method. At first attenuation was estimated at 78K as the averaged value of the ratios of the neighboring echo-pulses. Then with increase of the temperature we registered only the change in pulse amplitude as a change in attenuation.

Results

We have measured the temperature dependencies of attenuation of: (i) longitudinal and shear waves in lithium niobate, (ii) longitudinal waves in ruby, and (iii) longitudinal and shear waves in MAS. For the most crystals and wave types the temperature range ended by the value ~150K, i.e. the strong attenuation did not allow to watch echo-pulses at the room temperature. The exemption was the shear wave in MAS with the ratio of oxides 1:2, for which we could confidently watch echo-pulse at 300K delayed on 0.8 μs. The comparison of attenuation of this wave at frequencies 36.5 GHz (54 dB/μs) and 9.4 GHz (3.5 dB/μs) at 300K showed the quadratic frequency dependency.

Discussion and Conclusions

The obtained results show the real possibility of developing the signal processing devices of 8 mm radio region operating at the room temperature with insertion loss ~ 110 dB and time delay ~ 1 μ s.

P2-J-06

The effect of viscosity on the Love waves in piezoelectric structures

Jianke Du¹, Xiaoyu Cheng¹, Yonk-Kong Yong², Ji Wang¹:¹Ningbo University, China, People's Republic of, ²Rutgers University, USA

Background, Motivation and Objective

Love waves propagating in piezoelectric materials are widely used in resonators, sensors and transducers. The layered structures with inhomogeneous boundary conditions, for example, a thin film on a substrate, are currently adopted to achieve high performance for these devices. Almost all the modeling and analysis of wave propagation are based on the linear theory of piezoelectricity with quasi-electrostatic approximation, where the medium is assumed to be perfectly elastic and perfectly insulating to electric current. As operating frequencies get higher and sizes of acoustic wave devices become smaller, the dissipation of energies becomes more significant and should be considered in more realistic theories or modeling. As presented in references, an approach to treat with viscous dissipation of piezoelectric material is to assume that elastic modulus, piezoelectric coefficient, and dielectric permittivity coefficient are all complex constants, so the attenuation and other effects of the viscosity on the structural vibrations or the propagation of waves can be considered and analyzed. However, there are very few studies using viscoelastic models for surface acoustic waves in piezoelectric solids.

Statement of Contribution/Methods

We investigate analytically the effect of the viscous dissipation of material on the dispersive and attenuated characteristics of Love wave propagation in a layered structure, which involves a thin viscoelastic layer bonded perfectly to an unbounded piezoelectric substrate. The effects of the viscous coefficient on the phase velocity of Love waves and attenuation are presented and discussed in detail. The analytical method and the results can be useful for the design of the resonators and sensors.

Results

The effect of the viscosity on the velocity of the second and the third modes is more significant than that of the first modes. The velocity decreases with the viscous coefficient for a certain nondimensional wavenumber. The relationship between the attenuation and the viscosity coefficients is approximately linear for the first mode, but it is nonlinear for the second and the third modes, either for electrical open or shorted case, and the attenuations of the second and the third modes are larger than that of the first mode. It is obvious that the attenuation increases with the increase of the viscosity coefficients.

Discussion and Conclusions

Love wave propagation in piezoelectric layered structures with consideration of dissipation is investigated analytically. The electrically open and shorted cases are taken to solve the problem, respectively. The phase velocity and attenuation are figured and discussed in detail. Effects of viscous coefficients on the characteristics of dispersion curves are examined. We can find that the viscous coefficient has significant effect on the phase velocity and the attenuation. The analytical method and the results can be useful for the design of the resonators or sensors.

P2-J-07

The Calculation of Electrical Parameters of Film Bulk Acoustic Wave Resonators from Vibrations of Layered Piezoelectric Structures

Ji Wang¹, Jiansong Liu¹, Jianke Du¹, Dejin Huang¹:¹Mechanics and Engineering Sciences, Ningbo University, Ningbo, Zhejiang, China, People's Republic of

Background, Motivation and Objective

Film bulk acoustic wave resonators (FBARs) are new generation piezoelectric resonators with higher frequencies and manufacturing process compatible with existing semiconductor technology. With the successful development of FBAR products for wireless communication applications, the FBAR technology has been extensively studied for new technology, products, and applications. The sophistication of the FBAR technology and demands for precision products, it is natural to make use of the full analysis of acoustic waves propagating in the FBAR structures for design and calculate electrical parameters before the fabrication.

Statement of Contribution/Methods

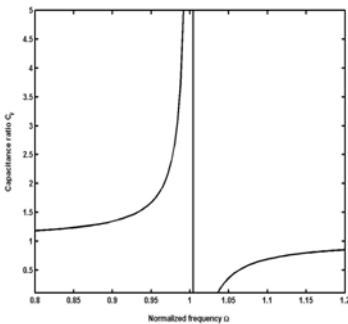
With solutions of deformation and electrical field, essential electrical parameters of a FBAR, like the capacitance ratio, can be evaluated straightforwardly. Additional parameters such as the resistance, and more importantly, the quality factor, have to be calculated with the consideration of material viscosity so the dissipation of energy can be accounted for. By assuming isotropic metal electrodes with a constant viscosity coefficient, complex material properties enter the equations of motion and solutions, including the frequency, will be complex and the electrical field can also be used for the calculation of energy dissipation.

Results

With the one-dimensional model of the layered structures of typical FBARs, a procedure for the analysis of vibrations with the consideration of piezoelectric effect and driving voltage is established. The electrical parameters, including the capacitance ratio, resistance, and quality factor, are obtained as a function of the resonator structure and vibration frequency. Such results are important for the device modeling and improvement.

Discussion and Conclusions

The analytical approach based on wave propagation in layered structures will be important in improving design and conceiving new products. The introduction of material viscosity will enable the formulation and calculation of FBAR properties with solutions of wave propagation. Current formulation based on one-dimensional approach can be easily extended to the finite structure of smaller FBARs for improved analysis and design. The formulation can also be extended to work with numerical methods which are widely adopted in the FBAR design and analysis.



Tuesday
Poster

P2-J-08

Two-dimensional FDTD Simulation for the Acoustic Propagation in a Piezoelectric Superlattice

Chao Zhang¹, Yiqiang Qin¹, Gang Zhao², **Yongyuan Zhu**^{2,1}:¹Department of Materials Science and Engineering, Nanjing University, China, People's Republic of, ²Department of Physics, Nanjing University, China, People's Republic of

Background, Motivation and Objective

The Piezoelectric Superlattice (PSL) is a kind of microstructure material with piezoelectric coefficient artificially modulated, which can be realized in domain engineered piezoelectric materials such as PPLN and PPLT. In recent years, the acoustic and optical properties of PSL have been studied intensively with various research groups, both theoretically and experimentally, and many interesting results have been found. In one-dimensional (1D) case, a commonly used theoretical method to analysis the acousto-optical properties of PSL is the so-called \bar{A} -function model, which can be solved efficiently with the Green's function method. However, this method is only available in the 1D case and is difficult to extend to the two-dimensional (2D) and three-dimensional (3D) cases.

Statement of Contribution/Methods

In this paper, we have developed a new method to solve this problem. The new method is based on the Finite-difference time-domain (FDTD) algorithm and is convenient to study the 2D and 3D wave propagation processes in PSL.

Results

A simulation result for the acoustic field distribution in a 1D PSL at the resonance frequency is shown in Figure 1 as an example. The simulation presented here is performed in the 2D case and it can be extended to the 3D case with little difficulty.

Discussion and Conclusions

To improve the simulation speed, the Compute unified device architecture (CUDA) technique has been applied in our FDTD simulation. The calculated results of our method was compared with the pervious Green's function method in the condition of which the PSL structure is degenerated to the 1D structures, and the results are found to be agreed well with each other.



Figure 1. FDTD simulation result for the acoustic field distribution in a 1D PSL at the resonance frequency

P2-K. Laser Interactions

Sala Orange

Tuesday, September 22, 2009, 10:00 am - 11:30 am

Chair: **David Feld**
Avago Technologies

P2-K-01

Acousto-electron and Acousto-optic Phenomena in Laser Heterostructures

Ljudmila Kulakova¹, Ilya Tarasov¹, Vitaly Voloshinov²; ¹Russian Academy of Sciences, Ioffe Physico-Technical Institute, St.Petersburg, Russian Federation, ²Department of Physics, M V Lomonosov Moscow State University, Moscow, Russian Federation

Background, Motivation and Objective

Tunable midinfrared sources are needed for high-resolution laser spectroscopy and optical communication systems. Applications such as fast process control or optical FM communication require fast tuning methods. Direct electrical tuning of the optical transition in multisectional lasers or by the Stark effect remains the problem unsolved because the fine spectroscopy application requires continuous frequency tuning and a high level of stability of intensity of laser emission, which are lacking with these methods. As was recently found, ultrasonic strain can influence the process of optical wavelength emission, thus providing fast time response and more precise wavelength adjustment. This adjustment becomes possible due to acousto-optic and acousto-electronic interactions taking place in laser heterostructures. This statement was proved for what we believe to be the first time in our investigations of the influence of alternating strain (produced by bulk ultrasonic waves) on InGaAsP/InP heterolaser emission.

Statement of Contribution/Methods

Therefore, one of the goals of this paper was to present earlier basic and new results of a study carried out on the subject. Another goal of the research was to develop the techniques of fine spectroscopy. We implemented fine experimental techniques for dynamic spectral analysis. First of them is based on the dependence of the resonant wavelength of a Fabry-Perot etalon on the angle of incidence, so that the etalon can be used as a high precision tunable narrow-band optical filter. The second one uses acousto-optic filter cell to analyze a direction propagation change of the laser emission. Application of the techniques made it possible to reveal the effects produced by the Rayleigh surface acoustic wave (SAW) on the frequency and space spectrum of a single and multimode InGaAsP/InP laser operated at wavelengths near 1.48 μm

Results

Both the wavelength and the propagation direction modulation of the laser modes (in the single mode generation) have been observed, induced by the time dependent periodic deformation field of the SAW. Some very important effects were discovered in the case of multifrequency generation mode. So-called "burning" of carriers, resulting in an instability of the emission spectrum, was removed by the sound introduction due to cancelation of the local depletion of carriers.

Discussion and Conclusions

The approaches to fine dynamic spectrum analysis have been developed. We have specified two major contributions to the modulation mechanism. The first is due to the acoustic modulation of the effective refractive index of the laser mode, the second to the bandgap modulation in the optically active layers. Both contributions are shown to have commensurable values and the same phase, which implies the opportunity for fast and continuous tuning of the emission frequency in the range of 40 GHz on the scale of the sound period.

The authors are grateful to the RFBR (pr. no.07-02-00557) for financial support.

New Acousto-optical Effect – Constant High Diffraction Efficiency in Wide Range of Acoustic Power

Valery Proklov¹, Alexander Vainer¹, Yuri Rezvov^{2,1} / Lab. 254, IRE RAS, Moscow, Russian Federation, ²NIRChTY, Novomoskovsk, Tula Region, Russian Federation

Background, Motivation and Objective

Classic Bragg acousto-optic (AO) interaction obeys the relationship: $I = \sin^2(v/2)$, where I is the diffraction efficiency and v denotes the phase modulation index. As the acoustic amplitude is increased, the periodical full power transfer between the initial and the diffracted optical beams is observed. It was theoretically shown [1] that this relationship is violated in case of considerable curvature of acoustic wave fronts in the diffraction plane. The appropriate curvature is observed at significant distance from the plane piezoelectric transducer. The necessary distance is lowered in case of low acoustic frequency, small transducer width, and strong acoustic anisotropy of the media.

The aim of this work was to investigate theoretically and experimentally the effect of that curvature upon Bragg AO diffraction.

Statement of Contribution/Methods

The experiment was carried out using the highly acoustically anisotropic single crystal TeO₂ in Bragg regime with acoustic frequency 6 MHz.

Results

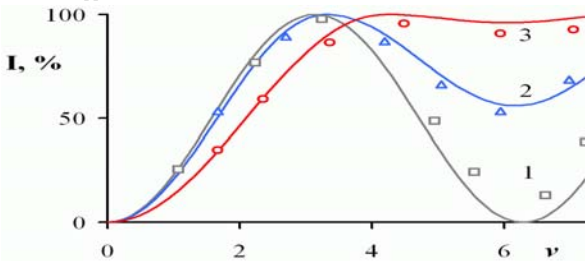
The figure shows the calculated (curves) and measured (dots) diffraction efficiency as a function of phase modulation index at different distances from the transducer: 1.4 mm (1), 4 mm (2), 12.5 mm (3). One can see that as the AO interaction region is moved from the transducer the efficiency loses its canonical sinusoidal relationship to v and becomes stabilized at high level in a wide range of acoustic amplitude.

Discussion and Conclusions

A new feature of Bragg AO diffraction is experimentally realized – the suppression of backward optical power transfer from the diffracted light beam to the initial one due to the curvature of acoustic wave fronts in the diffraction plane. The effect takes place at condition: $\Lambda B X \geq 2L^2$, where X stands for the distance from the transducer, L is the transducer width, Λ denotes the acoustic wavelength, and B is the anisotropy factor of the media. The effect might be used to improve stability of AO devices.

The research was supported by the RFBR, projects #07-02-00414-a and #08-02-13502-ofi-c.

[1] Acoustooptical interaction in the field of a decaying ultrasonic wave with a quadratic phase front in an anisotropic medium / A. S. Zadorin and S. N. Sharangovich // Radiophysics and Quantum Electronics – 1990. – V. 33, N. 3. – pp. 271-277.



SIGNAL PROCESSING METHODS FOR MATERIALS DEFECTS DETECTION

BOUDEN Toufik¹, Dib Samira², Aissous Kamel², Grimes morad^{2,3}, ¹Automatic, NDT lab, Jijel University, Jijel, Algeria, ²Electronic, NDT lab, Jijel University, Jijel, Algeria, ³Electronis, NDT lab, Jijel University, Jijel, Algeria

Background, Motivation and Objective

The NDT (Non Destructive Testing) play a very important role in the economy. They have become the essential tool for evaluating the mechanical properties of materials in order to detect defects.

Statement of Contribution/Methods

In this work, considered the pulse echo method to characterize materials using ultrasound, in which a piezoelectric transducer transmits ultrasonic energy. The signals reflected from the opposite side of the field, or discontinuity, empty or elements included in the material are received by the same transducer where energy converted into an electrical signal is processed by a computer and displayed on a screen.

The display can show the relative thickness (depth), or localized defects. Also, one can calculate the speed of propagation determines the nature of the material if the latter is unknown and the position of different interfaces, so the size of the sample. The ultrasonic detection principle involves the fundamental concept that a propagating wave will be reflected and/or partly transmitted when it encounters a defect or boundary. From the speed of the propagating wave at selected locations, the presence of a defect and its location can be deduced. Therefore, precise detection and identification of defects in materials requires an appropriate method for analyzing the signal.

Many methods proposed for analyzing ultrasonic signals mainly apply analyses of frequency or time domain, but the non-stationary nature of ultrasonic signals, as with many real-world signals, makes those analyses unsatisfactory since their frequency components change with time.

Results

In this work, we have presented a comparative study (advantages and limitations in NDT field) to the signal processing methods: Hilbert transform, cross-correlation function, split spectrum processing (SSP) and wavelet transform.

The performances are tested on synthetic signals in order to generalize the application of these methods for the detection of interfaces and therefore defects if they exist.

Discussion and Conclusions

The simulation results show that the application of signal processing methods, allows the detection of interfaces and hence the location of faults and if necessary materials characterization. Indeed, the Hilbert transform allows detection of the envelope signal locating and met interfaces. However, this approach ignores the sign gradients encountered because it considers only the absolute value. The cross-correlation function solves this problem of sign and gives a good location interfaces. The use of wavelet transform solves the problems encountered by the two other methods. Indeed, it allows a good location interfaces and therefore better detection of defects.

Resonant Acoustic Calorimetry of the Interaction of Laser Radiation with Nonlinear-Optical Crystals

Aleksei Konyashkin¹, Aleksei Doronkin², Valentin Tyrtshnyy², Daniil Myasnikov³, Oleg Ryabushkin^{1,4} *Kotelnikov Institute of Radio-engineering and Electronics of RAS, Fryazino, Russian Federation, ²Moscow Institute of Physics and Technology, Dolgoprudny, Russian Federation, ³NTO «IRE-Polus», Fryazino, Russian Federation*

Background, Motivation and Objective

During interaction of light with crystals some part of the radiation energy converts into heat leading to the modifications of the crystal acoustical properties.

Statement of Contribution/Methods

An original method has been recently proposed for the determination of the linear and nonlinear optical absorption coefficients in crystals. It is based on the registration of the crystal acoustical resonance frequency change caused by the interaction of the low-power [1] and high-power laser radiation [2].

Results

KTP piezoelectric resonance frequency shift Δf_c during homogeneous heating linearly depends on crystal temperature ($df_c/dT = -53$ Hz/K). Resonance line form changes due to the interaction with the laser radiation (unpolarized pulse fiber laser, $\lambda = 1.064$ mkm, pulse duration 100 ns, pulse repetition rate 20 kHz, average power is up to 19 W) and due to the uniform crystal heating without the laser radiation influence occur in the same way.

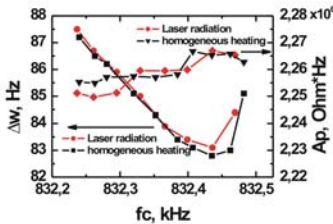
Figure shows Line width (Δw) and the Peak value (A_p) of the real part of the KTP crystal electrical impedance approximated by the Lorentz function: $\text{Re}(Z(f)) = Z_0 + (2A_p/\pi)(\Delta w/(4(f-f_c)^2 + \Delta w^2))$, during homogeneous heating, and for the different laser powers, f_c - Lorentz peak position frequency.

Discussion and Conclusions

For this power range it is valid to characterize inhomogeneous crystal heating by the equivalent crystal temperature T_{eq} . Equivalent crystal temperature change (ΔT_{eq}) is directly determined from the measured piezoelectric resonance frequency shift: $\Delta T_{eq} = \Delta f_c / (df_c/dT_a)$. For higher laser powers as well as during nonlinear-optical interaction piezoelectric resonance frequency shift will exhibit nonlinear dependence on the laser power [2]. In real high-power laser application processes thereby determined temperature $T_{eq}(P) = T_{eq}(0) + \Delta T_{eq}(P)$ is the fundamental factor for the quantitative determination of the true inhomogeneous crystal temperature distribution $T(x,y,z,P) = T_{eq}(P) + \Delta T(x,y,z,P)$. Experimental results presented here prove that $\Delta T(x,y,z,P) \ll T_{eq}(P)$.

References

- [1] J. Bezancon, J. Mangin et al, IEEE J. of Quant. Electron. 37, 1396 (2001).
 [2] O. Ryabushkin, D. Myasnikov, A. Konyashkin, Proc. EOS Annual Meeting 2008, TOM 6 808 (2008).



P2-K-05

Analysis of the leaky surface acoustic wave radiation in YX-LiTaO3 for symmetric and non-symmetric IDTs

Paulius Kazdailis¹, Romualdas Rimeika¹, Daumantas Ciplys^{1,1} *Radiophysics dept., Vilnius University, Vilnius, Lithuania*

Background, Motivation and Objective

Acousto-optic interaction is a powerful tool for control of light parameters for signal processing and sensing purposes. The acousto-optic probing of leaky surface acoustic wave (LSAW) radiation has been reported in our previous works [1,2]. Knowledge of the interdigital transducer (IDT) radiation characteristics is of great practical importance for design and implementation of LSAW based sensors. For certain purposes, the IDTs with nonequal electrode and gap widths (non-symmetric IDTs) are used. Our goal is to study the spatial distribution of LSAW radiation into the crystal bulk from the non-symmetric IDT and to compare it with that of the symmetric IDT.

Statement of Contribution/Methods

The experiment was performed using YX-LiTaO3 crystal with LSAW propagation along X axis. Two IDT configurations were used: a) with electrode and gap widths 16 μm and 8 μm , respectively, and b) both equal to 12.5 μm . The number of finger pairs was practically the same, 35 and 36. The anisotropic diffraction of 633 nm wavelength He-Ne laser light from the bulk wave radiated by LSAW was investigated. The spatial distribution of radiated wave intensity was determined by angular measurements with the high-precision optical goniometer.

Results

The dependencies of diffracted light intensity on light incidence angle are shown in Fig 1. The radiation patterns can be unambiguously determined from these curves. For non-symmetric IDT, the radiation pattern is wide and is well described by Gaussian distribution, in contrast to that of symmetric IDT exhibiting the sharp peak.

Discussion and Conclusions

The symmetric and non-symmetric IDT radiation patterns in YX-LiTaO3 exhibit different shapes. Variation of the IDT electrode/gap width ratio enables to adjust spatial distribution of the radiated acoustic beam intensity and can be applied to fit certain design requirements of LSAW based sensors.

- [1] R. Rimeika, D. Ciplys, P. Kazdailis, and M. S. Shur, Appl. Phys. Lett. 90, 181935 (2007).
 [2] P. Kazdailis, R. Rimeika, D. Ciplys, Acoustics'08 Paris Conference Proceedings (Paris, 2008), p. 2085 - 2089.

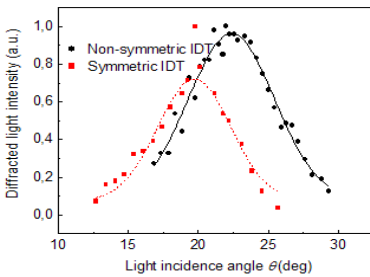


Fig. 1. Diffracted light intensities versus light incidence angle for symmetric and non-symmetric IDTs.

P2-K-06

Kinetics of the Nonlinear-Optical Crystal Equivalent Temperature during the Interaction with Single-Mode High-Power Laser Radiation

Aleksei Doronkin¹, Aleksei Konyashkin², Valentin Tyrtshnyy¹, Daniil Myasnikov¹, Oleg Ryabushkin³; ¹Moscow Institute of Physics and Technology, Dolgoprudny, Moscow region, Russian Federation, ²Kotelnikov Institute of Radio-engineering and Electronics of RAS, Fryazino, Russian Federation, ³NTO "IRE-Polus", Fryazino, Russian Federation

Background, Motivation and Objective

Acousto resonant spectroscopy technique gives the opportunity to measure true nonlinear-optical crystal temperature T_c during linear [1] as well as nonlinear interaction [2] of the laser radiation with crystals.

Still for the high-power laser application processes inhomogeneous heating of the crystals should be taken into account. Here it is fundamentally valid to characterize inhomogeneous crystal heating by the equivalent crystal temperature T_{eq} . Value of the T_{eq} is directly determined from the measured piezoelectric resonance frequency f_i (i – resonance mode) providing that dependence of the f_i on temperature T for the case of the homogeneous heating is known. Kinetics data of the $T_{eq}(t)$ for the different piezoelectric resonances enable to estimate stationary distribution of the inhomogeneous crystal temperature $T_c(x,y,z)$.

Statement of Contribution/Methods

External electric field of the radiofrequency fixed into the resonance band affects the KTP crystal. The dependence of the piezoelectric resonance frequency on time $f_i(t)$ is started to register. Hereon the KTP crystal was irradiated with the CW single-mode polarized fiber laser, $\lambda = 1064$ nm, power up to 14 W.

Results

Time dependencies of the piezoelectric resonance frequency $f_i(t)$ were measured using different laser powers for the characteristic piezoelectric resonances of the crystal. Dependencies of the slopes $k_i(P) = d(f_i(t))/dt$ on the laser power P are shown in the figure for several resonances. Optical absorption coefficients a_i are calculated through known KTP crystal mass (m), length (l), KTP specific heat (c), measured coefficient df_i/dT and assuming linear dependence of the $k_i(P)$ on the laser power.

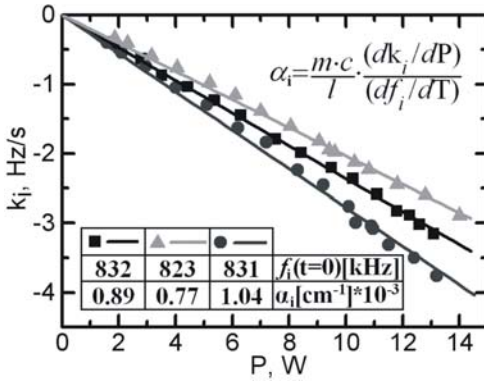
Discussion and Conclusions

Value discrepancy of the obtained absorption coefficient is due to the different sensitivity of the acoustical modes to the inhomogeneous crystal heating. Kinetics of the acoustic resonances enable determination of the inhomogeneous crystal temperature distribution $T_c(x,y,z,t,P)$.

References

- [1] J. Bezancon, J. Mangin, P. Stimer, M. Maglione, IEEE J. of Quant. Electron. 37, 1396, 2001.
 [2] O. Ryabushkin, D. Myasnikov, A. Konyashkin, Proc. EOS Annual Meeting 2008, TOM 6, 808, Paris 29 Sept. – 2 Oct. 2008.

Tuesday
Poster



Tuesday
Poster

P2-L. Bubbles and Beads

Sala Orange

Tuesday, September 22, 2009, 10:00 am - 11:30 am

Chair: **Jan Brown**
JB Consulting

P2-L-01

Ultrasonic trapping of beads in a straight channel

Rosie Boltryk¹, Shungo Hirawa², Tetsuo Okada², Peter Glynne-Jones¹, Martyn Hill^{1,2} ¹University of Southampton, Southampton, Hampshire, United Kingdom, ²Department of Chemistry, Tokyo Institute of Technology, Tokyo, Japan

Background, Motivation and Objective

This work studies the acoustic radiation trapping forces within a chamber (figure) designed to detect counterions based on the aggregation position of ion-exchange resin beads; certain counterions alter the water content of the beads, their acoustic properties and thus the acoustic force acting on them. However, the trapping of particles or cells in this way is relevant to a range of biological, chemical and medical analyses, for example, those involving cell washing, cell separation or testing of reagents.

Statement of Contribution/Methods

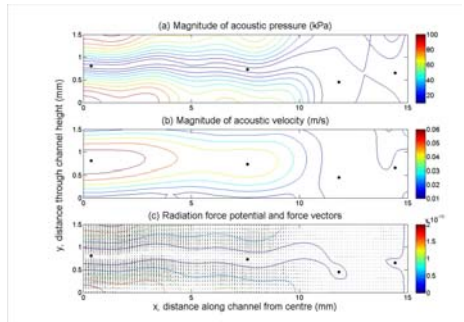
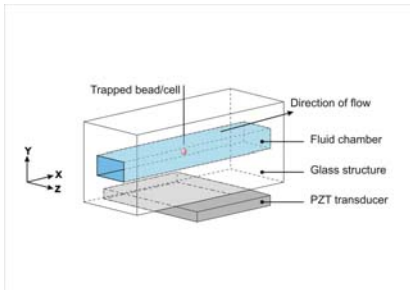
We investigate the trapping forces along the length of a small aspect ratio rectangular channel when an analyte is flushed past a bead. We study how these forces are influenced by the geometry of the transducer and channel structure using both measured and simulated results.

Results

In characterising the device, typical trapping forces have been measured and the trapping locations imaged over a range of resonant frequencies. Finite element (ANSYS and MATLAB) has also been used to predict trapping locations for a series of resonant frequencies, with results similar to that seen in practice. Simulations show that acoustic variations along the length of the chamber give rise to trapping forces and thus trapping locations can be predicted (figure). This reveals that variations in the acoustic velocity profile are an important factor.

Discussion and Conclusions

Finite element analysis is used to predict particle trajectories and agglomeration patterns and reveals the importance of transducer and structural geometry, and modes contained within these structures, to generate lateral forces in a "featureless" channel. An extension of this is to predict spatial and temporal concentration distributions using previously published techniques applied to 1-d acoustic fields.



Tuesday
Poster

Comparison of bubble behaviors on two different wall-materials in low frequency ultrasonic field

Kenji Yoshida¹, Taisuke Yoshikawa¹, Kazuya Obata¹, Yoshiaki Watanabe¹; ¹Doshisha University, Japan

Background, Motivation and Objective

Dynamics of a bubble near a wall is desired to be clarified in various fields. Vibrating bubbles near a rigid wall is known to induce cleaning effect in ultrasonic cleaning. In medical applications of ultrasonic techniques to gene delivery and transdermal drug delivery, it is necessary to understand bubble behaviors on a cell or tissue. An important factor affecting bubble behaviors is the wall-material near a bubble. We aim to investigate how the properties of the wall such as acoustic impedance and elasticity affect bubble behaviors.

Statement of Contribution/Methods

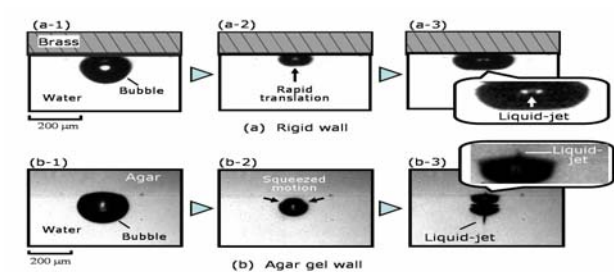
Two different materials, a brass and an agar gel, were used as a wall to which a bubble was adhered. Using a high-speed video camera, the bubble behaviors were observed in a transient acoustic standing wave with the center frequency of 27 kHz. Observations were conducted at various conditions of bubble size and sound pressure. Effects of the wall-material on the bubble behaviors were qualitatively investigated by comparing the bubble behaviors on these two different materials.

Results

Optical observations demonstrated that the difference of wall-material led to differences of the bubble behaviors, particularly generation processes of a liquid-jet at large sound pressure (see Figure). In case of the brass wall, a liquid-jet was generated toward the wall when the gravity point of contracting bubble rapidly moved toward the wall. In case of the agar wall, two liquid-jets were simultaneously generated when the contracting bubble was divided due to its squeeze motion. In this case, the remarkable bubble translation toward the wall did not occur.

Discussion and Conclusions

It seems that the bubble translation leading to liquid-jet generation on the brass wall is induced by secondary Bjerknes force associated with the sound reflection at the wall. This effect should depend on the difference in acoustic impedances between the wall and surrounding water. In case of the agar wall, we think that the remarkable bubble translation does not occur due to the small differences in acoustic impedances between the wall and water. The generations of the liquid-jets on the agar wall are associated with the agar wall deformation. This means that the elasticity of the wall can significantly affect the bubble behaviors. Our observed results characterize the effect of acoustic impedance and elasticity of the wall on bubble behaviors.



Sound propagation in thin-walled elastic pipe with viscous liquid-bubble mixture

Rudolf Bergman¹, Semyon Levitsky¹, Jehuda Haddad¹; ¹Sami Shamoon College of Engineering, Beer Sheva, Israel

Background, Motivation and Objective

Fine gas bubbles even in small amounts may change essentially sound speed and attenuation in liquid flows in tubes. Dynamic properties of waveguides with liquid-bubble mixture are important for different applications, e.g. hydraulic machinery, shock wave absorbers, etc. From theoretical point of view elastic tube with bubbly liquid is characterized by two ranges of acoustic dispersion, one being connected with inertia of the tube wall (attached

mass of the waveguide) and the second – with the liquid inertia, influencing radial pulsations of bubbles in the wave. While the first frequency range in the absence of bubbles is well covered at present both theoretically and experimentally, the second one needs more in depth analysis. In the present study sound propagation in coaxial waveguide with bubbly liquid is investigated. It is assumed that the central part of the pipe is occupied by a circular elastic rod, the tube wall can be treated as a thin elastic shell, and the liquid is pure viscous. Volume concentration of free gas is supposed to be small. The goal of the study is to estimate theoretically acoustic properties of such waveguide for different gas concentrations, bubble sizes, liquid viscosities and gap width.

Statement of Contribution/Methods

General scheme of the problem solution is based on conjugated description of three cylindrical layers interaction (elastic shell, liquid with bubbles and internal rod) in monochromatic wave. Tube wall dynamics is described within Kirchhoff-Love approximation; the flow of viscous liquid in the wave is treated within quasi-one-dimensional approach; the central circular rod is supposed to be pure elastic. Compressibility and dissipative properties of bubbly liquid in the wave can be almost entirely attributed to the gas phase; dynamics of the later is highly frequency dependent. All basic losses (thermal, viscous and acoustic) at bubble-liquid interaction are accounted for; the resulting dispersion equation for the waveguide is obtained and studied numerically.

Results

Results of simulations illustrate strong influence of liquid, gas, elastic shell and rod parameters on sound dispersion and attenuation. It is shown that free gas leads to essential decrease of the sound speed on the low frequency branch of dispersion curve. Sound speed in a high frequency range exhibits drastic non-monotonic changes with frequency. The scale of these changes, the same as sound attenuation in this range, is highly sensitive to bubble's size, gas concentration and the gap width.

Discussion and Conclusions

Theoretical model describes the basic features of sound propagation in the gap between thin circular elastic shell and coaxial elastic central rod, filled by viscous liquid with fine bubbles. The results cover wide frequency range and can find application in description of acoustic signals propagation in complex hydraulic waveguides.

P2-L-04

A prototype of small-size and self-oscillate thermoacoustic system

Kohei Hotta¹, Shin-ichi Sakamoto², Daichi Tsukamoto¹, Yoshiaki Watanabe³; ¹Faculty of Engineering, Doshisha University, Kyotanabe, Kyoto, Japan, ²Department of Electronic Systems Engineering, University of Shiga Prefecture, Hikone, Shiga, Japan, ³Faculty of Life and Medical Sciences, Doshisha University, Kyotanabe, Kyoto, Japan

Background, Motivation and Objective

Recently, the problem of heat dissipation has increased concomitantly with the increasing popularity of electronic devices. A thermoacoustic cooling system is one of the best solutions for cooling technology in the future. The power source of thermoacoustic cooling system is heat energy, which can be obtained from waste heat of an electronic device. The heat energy will be converted to sound energy at the prime mover. Thereby, electric generation is realized by inserting a piezoelectric substance in the sound field. However, the total system length is several meters. Further miniaturization is then necessary for practical applications. We produced a small prototype of a thermoacoustic system, where heat energy can be converted to the sound energy.

Statement of Contribution/Methods

We used a straight tube with 130 mm total length and 25 mm inner diameter. One end of the tube was opened and the other end was closed. A 6-mm-long honeycomb ceramic stack was set 100 mm distance from the open end. A probe microphone (B&K type 4182) was used to measure the inner sound pressure.

The channel radius of stack is related to its energy conversion efficiency. We used two type of stack with different channel radii (0.35 mm or 0.45 mm); then the sound pressure was measured at 50 mm distance from the open end. The input energy was also changed from 1.5 to 56 W and generated sound pressures were measured.

Results

The experimental result is depicted in Fig. 1. Sound was generated clearly in this small thermoacoustic system. The resonance frequency was about 640 Hz. Furthermore, the sound pressure was 1300 Pa for the 0.35 mm channel radius with 56 W input energy. The input-output characteristic was almost linear in the input energy range of 25–56 W.

Discussion and Conclusions

In this study, we produced a small thermoacoustic system where heat energy can be converted into sound energy. For the future, it is expected that the cooling will be realized by introducing the heat pump stack in this resonance tube. Moreover, electric generation can be realized by inserting a piezoelectric substance into the open end.

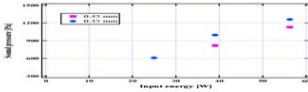


Fig. 1. Experimental result.

P2-L-05

Ultrasonic Measurements of Spherical Resonator Characteristics and Determination of their Errors

Ilona Ali Bláhová¹; ¹Department of Physics, Faculty of Electrical Engineering, Czech Technical University in Prague, Prague, Czech Republic

Background, Motivation and Objective

Spherical resonator is usually used for excitation of physical phenomena known as single-bubble cavitation and single-bubble sonoluminescence. It is evident that a creation of the cavitation bubble demands very specific conditions. A cell for these experiments has to have certain characteristics. Moreover characteristics of used liquid like speed of sound, density and kinematic viscosity should be known for precise description of the bubble dynamics. Described measurement method that follows is focused to determination of characteristics of used spherical resonator.

Statement of Contribution/Methods

The unique experimental set up was prepared. For measurements the spherical glass cell filled with liquid was used. Water was used as reference liquid. Piezoelectric circular transducers were used. They were stuck on the wall of a glass cell. One of them was used as a transmitter and the other one as a receiver. Agilent 4294A Precision Impedance Analyzer was used for transducer excitation by a sweep signal and for data recording. Signal processing has been made in system Matlab.

Results

At the beginning the influence of different experimental settings (different liquids, different cells, kind and area of used transducers, its position on the cell walls, different way of their sticking in the cells wall) on obtained frequency spectrum was studied. On the base of these experiments the proposal of an optimal experimental setting was prepared. Due to precise measurements of real and complex parts of received signals, the purity of obtained modes of measured resonator was assessed. The frequency intervals for future measurements were established. The fluid physical property characterisation was obtained on the base of Swept Frequency Acoustical Interferometry. The position of local frequency maxima and its widths were assessed and analysed. Sound speed, attenuation and liquid density were calculated. The accuracy of them was established.

Discussion and Conclusions

Physical characteristics of spherical resonator and their accuracies were determined. Results of these measurements will be used in measurements focused to dynamics of single-bubble cavitation and single-bubble sonoluminescence where spherical resonator will be used for creation of a cavitation bubble.

P2-L-06

Efficient ultrasonic atomization using a vibrating small gap

Kenta Tokumitsu¹, Daisuke Koyama¹, Kentaro Nakamura^{1,2} Precision and Intelligence Laboratory, Tokyo Institute of Technology, Yokohama, Nagatsuta, Kanagawa, Japan

Background, Motivation and Objective

Ultrasonic atomization has been utilized as an inhaler and a humidifier since it can generate the mist with particle size of several μm or around $10 \mu\text{m}$ without elevating temperature. Currently, ultrasonic atomization is expected for supplying fuel to burners to reduce the generation of unwanted materials. Supplying water mist to cooling tower is another promising application. However, it is difficult to produce a large amount of fine mist, because there is an inverse proportionality between the driving frequency and the particle size. High frequency transducer

of MHz region can produce fine mist, but its radiation surface is so small to process a large volume. In this study, we newly propose an ultrasonic atomization principle using a small gap between a vibrating surface and a wall. The particle size in the method is determined by the gap and free from the conventional dependence on the frequency. A large volume of small particles of around 10 μm in diameter can be produced by the vibrating gap even at lower frequencies in several 10 kHz, and the area for atomization can be extended. A relationship between the gap and particle size is experimentally studied in a circular configuration using a vibrating ring.

Statement of Contribution/Methods

The vibration system is composed of a duralumin ring of 70 mm in diameter and a Langevin transducer with a horn. The seventh twist-flexural mode is excited at 26 or 40 kHz along the circumference of the ring. The ring has a tapered cross-section to have higher vibration amplitude at the upper end. A duralumin cup is inserted in the ring and a gap of 10-100 μm is formed between them. The mist is generated from the top end of the gap, while water is automatically conveyed from the bottom to the top of the ring due to the vibration.

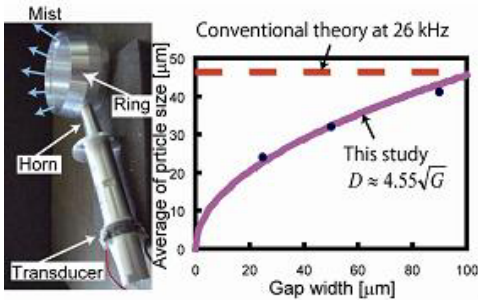
Results

The particle size is measured as a function of the gap. The particle of 24 μm is obtained even at low frequency of 26 kHz, and is dependent mainly on the gap. According to our experiments, the particle size D is expressed by the gap G as $D \approx 4.55\sqrt{G}$.

Discussion and Conclusions

It is important to introduce a mechanism to maintain the gap at every place along the circumference of the ring for the practical application. We suggest that the radiation force acting on the wall of the cup can be utilized for automatic control of the gap.

Tuesday
Poster



P2-M. High Intensity Ultrasound Application

Sala Orange

Tuesday, September 22, 2009, 10:00 am - 11:30 am

Chair: **Vitold Pozhar**

*Scientific and Technological Center of Unique Instrumentation of
Russian Academy of Science*

P2-M-01

Nonlinear and von Neumann reflection of elastic shock waves in soft solids.

Gianmarco Pinton¹, Jean-Luc Gennisson¹, Mickael Tanter¹, Mathias Fink¹, Francois Coulouvrat^{2,1} *Langevin Institute (CNRS UMR 7587), ESPCI ParisTech, INSERM, Paris, France, ²Universite Pierre et Marie Curie (CNRS UMR 7607), Paris, France*

Background, Motivation and Objective

In soft solids, such as biological tissue, the low value of shear elasticity allows the propagation of transverse waves with a high particle velocity when compared to the wave speed. With such a large Mach number shock waves can develop over a few wavelengths. We study the reflection of shocked shear waves traveling through a tissue-like medium, incident at a small angle on a rigid surface with numerical simulations and ultrasound based experiments.

Statement of Contribution/Methods

The nonlinear elastic wave equation is approximated by a paraxial wave equation and a third order nonlinear term. This equation is solved numerically with operator splitting and finite differences with a Crank-Nicolson scheme used for the diffractive term and a flux-conservative Rusanov scheme for the nonlinear term. Numerical results for shock propagation are verified analytically with a Burgers-Hayes solution and with self-similarity.

To mimic biological tissue a soft phantom with shear wave speed of 2.56 m/s was cast with 5% gelatin and 2% agar concentrations. A 100 Hz large amplitude shear wave pulse was generated by a vibrator attached to a plate embedded in the phantom. A transient elastography technique consisting of a medical transducer array connected to an ultrafast ultrasound scanner was used to measure the transverse displacement field at 3000 Hz with a displacement resolution of 1 μm .

Results

Numerical simulations demonstrate close agreement with the classical understanding of shock wave reflection and the different reflection regimes. For large angles a regular nonlinear solution is observed: the reflection angle of the incident shock is different from the angle of incidence. For small angles a three shock von Neumann-type solution is observed with an additional Mach shock at the interface. The transition between regular reflection and von Neumann reflection predicted by the simulations is given by the nondimensionalized angle

3.92 and theory predicts that angle to be 3.91. Experiments show that the different reflection regimes can be observed in tissue-like phantoms.

Discussion and Conclusions

The reflection of acoustic shock waves (with second order nonlinearity) has been previously studied, but we have examined for the first time the reflection of shear shock waves. We presented numerical methods to solve the paraxial wave equation with third order nonlinearity and demonstrated excellent agreement with theory. Simulations and experiments were used to describe different reflection regimes.

Tuesday
Poster

Laser Thermal Efficiency Increase by means of Fast Acousto-optic Beam Scanning

Sergey Antonov¹, Alexander Vainer², Yuri Rezvov^{3,1} Lab. 250, IRE RAS, Moscow, Russian Federation, ²Lab. 254, IRE RAS, Moscow, Russian Federation, ³NIRChTY, Novomoskovsk, Tula Region, Russian Federation

Background, Motivation and Objective

The laser thermal efficiency (LTE) has threshold nature, and thus the common Gaussian intensity distribution is not optimal for various laser material processing techniques like metal cutting or graving and etc. The most appropriate spatial diagram in this concern has to come closer to a rectangular one. This work considers the first time implementation of acousto-optic (AO) tools for laser beam control to increase its LTE parameter.

Statement of Contribution/Methods

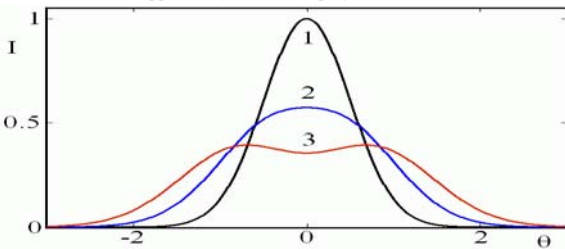
To increase LTE the fast angular AO scanning of the initial beam around its initial (central) position is proposed. The method is based on the laser beam refraction by standing ultrasonic wave. The increase of LTE might be obtained if the aperture of the beam is less than the half of ultrasonic wavelength and is provided by two effects: 1) laser beam scanning at ultrasonic frequency, 2) distortion of the directional diagram of the beam. If the period of the ultrasonic wave is sufficiently smaller than the characteristic time of the motion of the laser spot on the material, than it can be assumed that the refracted beam has a modified stationary intensity distribution. That distribution is wider than the initial one, thus an adjustment of the objective lens focus is necessary. The optimal parameters for LTE increase were found.

Results

An AO refractive scanner was designed and fabricated using LiNbO3 single crystal. The standing ultrasonic wave was generated using piezoelectric effect of the crystal. The scanner was illuminated with initial Gaussian single-mode non-polarized technological laser beam, having wavelength 1.06 μm. The figure shows experimentally measured angular distributions of the laser intensity I, where θ is the angle in the diffraction plane, normalized to the angular divergence of the initial beam. The curve 1 corresponds to zero power of the acoustic wave in the AO scanner, curve 2 – to unit power, curve 3 – to double power.

Discussion and Conclusions

The experiments showed satisfactory agreement with theoretical analysis. The portion of the optical power, enclosed in the central region of the Gaussian beam, limited by the intensity level 0.9 of the maximum, is equal to 34%. The proposed AO method increases that value to 55%, while the operating laser spot is widened in 3.8 times. The research was supported by the RFBR, projects #07-02-00414-a and #08-02-13502-ofi-c.



Ultrasonic rock drilling devices using longitudinal-torsional compound vibration

Andrea Cardoni¹, Patrick Harkness¹, Margaret Lucas^{1,1} Mechanical Engineering, University of Glasgow, United Kingdom

Background, Motivation and Objective

Space missions for planetary sampling are a hot topic. Nasa-funded studies have proven that ultrasonics is a viable technology for extraterrestrial drilling. Previous research by the authors has indicated that ultrasonic longitudinal-torsional coupled vibrations may improve rock excavation. In this study, the design of two drillers operating via longitudinal-torsional motion is pursued.

Statement of Contribution/Methods

Two design approaches are studied to obtain longitudinal-torsional oscillations. The first consists of a driller wherein modal coupling is achieved by matching longitudinal and torsional modal frequencies. Since the ultrasonic transducer consistently used in this work is of the Langevin-type with PZT poled in the thickness direction, torsional vibration is achieved via diagonal slits. In the second driller the excitation of combined torsional and longitudinal vibration is obtained via helical grooving (Fig.1).

Finite element analysis (FEA) is used to predict the devices' behaviour. FE predictions are validated via experimental modal analysis (EMA). Cutting tests are performed in sandstone.

Results

FE simulations of the electromechanical characteristics of the drillers are conducted using elastic and piezoelectric elements. Spectral plots of the current in the PZT and the mechanical displacement of the horn allow prediction of optimal driving frequencies. A sensitivity analysis is also carried out to study the effects of groove depth and position on the driller vibration. Predicted dynamics is validated by EMA, and electrical data are corroborated by impedance bridge measurements.

Discussion and Conclusions

The slitted driller provides higher versatility. Longitudinal or longitudinal-torsional vibrations can be excited via adjustments of the driving frequency, although optimal frequencies for suitable modal coupling may occur away from resonance thus implying difficult electrical driving. Design strategies to mitigate such difficulties are provided. The device with helical grooves is more easily driven. Rock cutting tests demonstrate the validity of both drilling solutions.

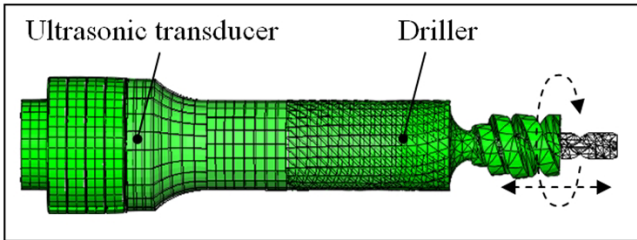


Fig. 1: Longitudinal-torsional vibration predicted by FEA

P2-M-04

Characterisation of nonlinear behaviour of power ultrasonic drilling horns

Andrew Mathieson¹, Andrea Cardoni¹, Patrick Harkness¹, Margaret Lucas¹; ¹Mechanical Engineering, University of Glasgow, United Kingdom

Background, Motivation and Objective

In ultrasonic applications such as drilling, cutting and welding it is necessary for devices to be driven at high power. This gives the device sufficient output motion to fulfil the application it is designed to perform. Unfortunately, it has been well documented that whilst power ultrasonic devices are driven at high power, it can be common for nonlinear behaviour to appear. If an attempt is not made to understand this behaviour and subsequently try to control it, it is likely that the ultrasonic device will suffer from poor performance and possible failure.

Statement of Contribution/Methods

The ultrasonic devices which are characterised in this study have been developed for drilling purposes. The drills consist of a tuned horn screwed into an ultrasonic exciter (transducer) and were designed to resonate in both the 1st longitudinal mode and the 2nd torsional mode through modal coupling. To improve the toughness of one of the titanium horns, a tungsten cap was fixed to the tip of the horn. This slight modification has changed how the device behaves, increasing its nonlinear response characteristic.

To assess the level of nonlinearity in the devices, measurements of the response characteristics near the tuned frequency are taken at varying power levels. The responses are detected with a 3D laser vibrometer, allowing both in and out of plane velocity measurements to be taken. Experimental modal analysis allows the mode shapes of the systems to be identified.

Results

Through these measurement techniques it is possible to show that both devices suffer from nonlinear phenomena, such as harmonics, frequency modulation and natural frequency shift. However it is revealed that the device with the tungsten tipped horn is characterized by an increased presence of such phenomena including a greater shift in natural frequency as well as the appearance of bifurcations.

Discussion and Conclusions

This study compares two similar devices and tries to understand the reason behind the increase of nonlinear behaviour in the one with the tungsten cap. To ensure that the transducer contribution to the level of nonlinearity is equal in both assemblies, the same transducer will be used for both devices. It is understood that the speed of sound through titanium and tungsten are considerably different and this is investigated in this study. Finally, knowledge obtained from this research will provide suggestions for future power ultrasonic tooling strategies.

P2-M-05

Ultrasonic Velocity In Magnetorheological Fluids Under Magnetic Fields Induced By Permanent Magnets

Jaime Rodríguez López¹, Yago Gómez-Ullate Ricón¹, Luis Elvira Segura¹, Francisco Montero de Espinosa Freijo¹; ¹Dept. Señales, Sistemas y Tecnologías Ultrasonicas., Instituto de Acustica CSIC, Madrid, Spain

Background, Motivation and Objective

Magnetorheological (MR) fluids are suspensions of micrometer-sized magnetic particles in a carrier fluid. Their main feature is that rheological properties change under the action of external magnetic fields. They are widely used in the automotive industry, nevertheless, only a few studies about their acoustical properties have been made. In contrast with previous works where electromagnet induced uniform fields were used, the change of sound velocity in a MR fluid under non uniform magnetic fields provided by small permanent magnets is analyzed. It is shown that the acoustical properties of the fluid can be changed tuning them at our discretion and in an easy way.

Statement of Contribution/Methods

The time-of-flight variations of 1MHz ultrasonic pulses were analyzed using a transmission-through technique, as they propagates through a MR fluid with a 20% volume fraction of particles. The magnetic field was applied by means of up to four 30x15x5mm NeFeB magnets. The magnetic field was changed both in geometry, intensity and uniformity using a different number of magnets placed in different configurations.

Results

The sound velocity in the MR fluid at 1MHz is 964 ± 2 m/s when no magnetic field was applied. When the magnetic field lines were normal to the ultrasonic propagation direction the velocity was found to decrease up to 10m/s. On the contrary, when the magnetic field lines were parallel to the ultrasonic propagation direction, a sound speed increment up to 18m/s could be measured. When the magnetic field was suppressed by taking off the magnets, the sound speed did not recover the initial value.

Discussion and Conclusions

When the magnetic field is applied, the particles in the fluid are ordered forming chain type structures aligned approximately with the magnetic field lines. These structures modify significantly the sound speed depending on their orientation. It was seen that some of these structures were maintained even when the magnetic field was suppressed, showing the hysteretic behavior of the fluid. These measurements are in qualitative agreement those reported by other authors working with fields induced by electromagnets. This work shows the possibility of changing the acoustic properties of a MR medium by simple modifications of the external magnetic field. These changes could be used for example as a method for the design of active matching layers for acoustical emission/reception purposes.

P2-M-06

The resonant amplification of shear phonon tunneling by the layer of magnetic 2d composite

Tetyana Lapyteva¹, Olga Sukhorukova¹, Sergei Tarasenko¹, Vladimir Shavrov²; ¹Donetsk A.A. Galkin Institute of Physics & Engineering of NASU, Donetsk, Ukraine, ²V.A. Kotelnikov Institute of Radioengineering & Electronics of RAS, Moscow, Russian Federation

Background, Motivation and Objective

At present, the analysis of electrodynamic properties of composite magnetic 1D and 2D materials and search for acoustics analogs of unique polariton effects in such media are actively investigating. However, in spite of such materials are acoustic continuous media the theoretical investigations of its acoustic properties haven't been done until now.

Statement of Contribution/Methods

In this work the conditions for resonance amplification by the layer of 2D magnetic composite both bulk and shear evanescent waves incident from without upon the materials' surface have been determined.

Results

As an example of composite medium the system of identical circular metal-coated ferro- and antiferromagnetic bars parallel to the Z-direction (it is also the easy axes) in the elastically isotropic nonmagnetic matrix are considered. The analyze of this dynamical problem was carried out in the frame of effective medium method.

Discussion and Conclusions

To this end the acoustic analog of Maxwell, Garnett and Sheng approximation that actively used in polariton dynamics of fine-dispersed media have been obtained. Received data was correlated with the results of shear bulk wave scattering by the isolated metal-coated ferro- and antiferromagnetic cylinders.

P2-M-07

Explosive Instability of Ultrasonic Triads under Frequency Modulated Electromagnetic Pumping

Vladimir Preobrazhensky¹, Philippe Pernod², Oleksandr Yevstafyev³; ¹LEMAR, Wave Research Center GPI RAS, Moscow, Russian Federation, ²LEMAR, IEMN-DOAE- U.M.R.CNRS 8520, EC Lille, Villeneuve d'Ascq, Nord, France, ³Physics, V.I.Vernadsky Taurida National University, Simferopol, Crimea, Ukraine

Background, Motivation and Objective

Explosive instability and localization of ultrasound under homogeneous electromagnetic pumping was recently predicted and observed in magneto-acoustic medium [1,2]. This kind of instability is developed as a result of three-phonon bound excitation in supercritical conditions easily achievable in magneto-elastic materials with soft magnetic subsystem. However in real crystals supercritical dynamics of wave triads is distorted by high order nonlinear acoustic effects, first of all by nonlinear phase- or frequency shifts of waves. The goal of this work is to remove this obstacle for observation of explosive amplification of ultrasound.

Statement of Contribution/Methods

The experimental observation of explosive dynamics of ultrasonic triads was achieved in a magneto-acoustic resonator using quasi-singular frequency modulation of supercritical electromagnetic pumping.

Results

The proper choice of modulation function allowed to compensate nonlinear frequency shift of acoustic vibrations and to reveal quasi- singular amplification typical for explosive instability. The figure shows typical time dependence of amplitude of ultrasonic vibrations in α -Fe₂O₃ magneto-acoustic resonator of eigen frequency $f_0=340$ kHz under electromagnetic pumping pulse $f=3f_0$, $\tau=370$ μ s with (a) and without (b) quasi- singular frequency modulation.

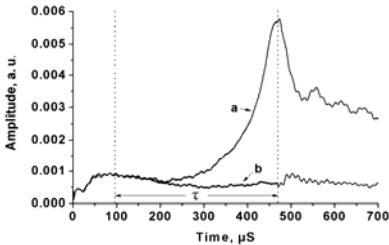
Discussion and Conclusions

Explosive behavior of ultrasonic triad in real media is confirmed experimentally. The results are in agreement with theoretical description of explosive dynamics elaborated taking into account high order magneto-acoustic nonlinearities and modulation of the pumping field.

Tuesday
Poster

The work was supported by RFBR (grant 09-02-00602-a), Program of RAS "Acoustics of natural media" and French Embassy in Ukraine.

[1] V. Preobrazhensky, O. Bou Matar and P. Pernod, Phys.Rev.E 78, 04 6603 (2008).
[2] V.L. Preobrazhenskii, V.V. Rudenko, P. Pernod, and V.I. Ozhogin, JETP Lett. 86, 348 (2007).



P2-M-08

The Effect of Electrical Current in Biological Tissues on Ultrasound Echoes

YUAN XU¹, OZKAN DOGANAY¹; ¹PHYSICS, RYERSON UNIVERSITY, TORONTO, ONTARIO, Canada

Background, Motivation and Objective

The imaging of the electrical properties has been used in various clinical applications because the electrical properties of biological tissues are closely related with the physiological and pathological status of the tissues. In this study, we investigate the effect of electrical current in biological tissues on the ultrasound echoes. This technique may provide a new perspective for understanding the dielectric properties of biological tissue.

Statement of Contribution/Methods

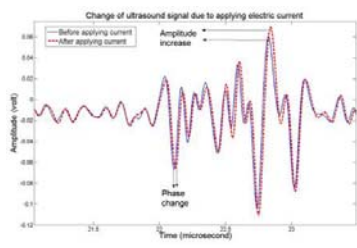
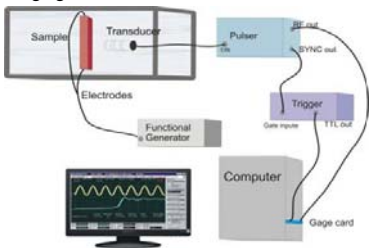
We compared the ultrasound echoes from various types of tissues before and after applying electric current to the tissues. The experimental setup is shown in Figure 1. Electric current is applied to the sample through the electrodes. Ultrasound pulses are transmitted and received by the transducer.

Results

Figure 2 shows a typical change of the ultrasound echoes induced by the electrical current in tissues. In some segments of the ultrasound signal, we can observe amplitude change and time shifting. These changes are repeatable, reversible, and correlated with the voltage we apply to the tissues. We also investigate how these changes are affected by the amplitude, frequency, and other parameters of the applied electrical source.

Discussion and Conclusions

We conclude that applying an electrical current to tissues can change the amplitude and phase of the ultrasound pulses reflected from the tissues. We think this change is related with both the electrical and mechanical properties of tissues. More studies are needed to investigate the mechanism behind this new effect and to develop new imaging methods based on this effect.



Tuesday Poster

P2-M-09

Development and Experimental Investigation of a Hand-operated Ultrasonic Knife

Jens Twiefel¹, David Oliva Uribe¹, Minzhe Shi¹, Jörg Wallaschek^{1,2} *Institute of Dynamics and Vibration Research, Leibniz University of Hannover, Hannover, Niedersachsen, Germany*

Background, Motivation and Objective

Ultrasonic cutting uses the superposition of small ultrasonic vibrations on the large macroscopic cutting motion of a knife. Most often resonating systems are used, with eigenfrequencies in the ultrasonic range. Typically the superimposed ultrasonic vibrations of the cutting blade are in longitudinal direction with respect to the tool. The main advantage of this technique is the often significant reduction in the mechanical friction between knife blade and cutting material. Typical industrial applications can be found in food industry to make thin slices of bread or cakes without critical deformations. Moreover, additional effects caused by the use of ultrasonic cutting like heat generation has been used in the textile industry to cut and seal some fabrics in order to prevent fraying. The present papers reports on the development and testing of an ultrasonic knife. Effects like coaptation and coagulation in biological tissues are utilized in medical field when using ultrasonic cutting (i.e. ultrasonic scalpels) for resection of tumours or coagulation of blood vessels, becoming especially common in laparoscopy. The advantages of the use of an ultrasonic scalpel in medical procedures are the reduction of tissue damage (below 3mm) and operation times, less blood loss, and more rapid healing in comparison with other surgical instruments.

Statement of Contribution/Methods

This paper reports the development of an ultrasonic scalpel prototype. The mechanical design of the knife has been performed utilizing transfer matrix and finite element methods. A self-oscillating circuit was developed to drive the system. The whole system has been manufactured and assembled. For verification of the system vibration shape measurements utilizing a 3-d laser interferometer have been performed. Further, the cutting performance has been demonstrated and force measurements show a clear reduction of the frictional forces.

Results

The results of measurements are in good agreement with model-based theoretical results. The cutting performance has been increased significantly compared to the knife without ultrasonic vibrations. An improved resulting cutting performance has been shown for different materials.

Discussion and Conclusions

In this work, the design of a new ultrasonic knife system including the mechanical dimensioning, the driving circuitry, and validation measurements has been presented. The prototype could be realized in a tiny dimension and showed a good performance. The knife will be topic for further investigations and improvements.

P2-M-10

Surface fine processing by ultrasonic radiation pressure

Nobuo OGAWA^{1,2} *Mechanical Engineering, Tokyo University of Science, Noda, Chiba, Japan*

Background, Motivation and Objective

Sandblast techniques that gas-solid jet impinges on surface of the work and process it are well known as surface processing techniques. In many cases gas is air in general and solid particles are metal, plastics and ceramics etc. The solid particles are accelerated by gas flow and impacts on the work and process the surface of the work. However fine solid particles stream away with gas flow without an impact on the work because of large viscosity. For fine processing by means of fine solid particles the viscosity resistance becomes serious obstacle to process the surface of the work. Then ultrasonic radiation pressure is introduced as power accelerating fine particles. When ultrasonic is radiated on the solid particles ultrasonic radiation pressure acts on the solid particles and accelerates it.

Statement of Contribution/Methods

Gas-solid jets through the nozzle with ultrasonic horn impinge on the work. In this case the solid particles are accelerated by gas flow and ultrasonic radiation pressure. So the fine solid particles can process the surface of the work without being streamed due to viscosity of air flow. Where output of the ultrasonic generator is 150 W and 28KHz. Horn is set up on the transducer and grinding performance of the work is measured by laser roughness indicator.

Tuesday
Poster

Results

Where size of the solid particle is #2000 (6.7 μ m mean diameter) of alumina powder. Grinding performance is improved largely for very fine powder by ultrasonic radiation pressure. Length between the blasting nozzle that is 1 mm in diameter and the surface of the work is 0.5, 1, 2, 3 and 15 mm. For 0.5 mm<ts<3 mm depth of grinding is measured in proportion to ts because that accelerating zone of the particles by ultrasonic radiation pressure becomes long with ts. So impact velocity of the solid particles on the work is large for large ts. On the other hand grinding performance for various sizes of the solid particles, #1000, #1500 and #2000 and ts=1 mm is investigated. Deep depth of grinding is measured for large particle size, because of large initial velocity and ultrasonic radiation pressure near the nozzle exit.

Discussion and Conclusions

Grinding performance depends on distance between the blasting nozzle and the work. Momentum of the particles supplied by gas flow decreases as increases ts. And velocity of the jets is strongly decreasing near the surface of the work so momentum of the particles due to jet flow decreases rapidly. On the other hand solid particles are accelerated by radiation pressure until impact on the work for ultrasonic radiation so grinding performance is improved. For ts=15 mm, the gas-solid jet diffuses and r-direction force acts on the particles and wide grinding area is seen in r-direction. The solid particles are given large initial velocity by jet flow and intense ultrasonic radiation pressure near the nozzle exit. And the particles continue accelerating by ultrasonic radiation pressure until impact on the work.

Tuesday
Poster

P2-N. Device Modeling

Sala Orange

Tuesday, September 22, 2009, 10:00 am - 11:30 am

Chair: **Jyrki Kaitila**
Infineon

P2-N-01

Experimental Optimization of Electrodes for High Q, High Frequency HBAR

Lukas Baumgartel¹, Eun Sok Kim²; ¹Physics, University of Southern California, Los Angeles, California, USA, ²EE-Electrophysics, University of Southern California, Los Angeles, California, USA

Background, Motivation and Objective

High-overtone bulk acoustic resonators (HBAR) have high quality factor (Q), making them good candidates for frequency reference resonators and frequency filters. We attempt to maximize the Q of an HBAR device that operates at frequency greater than 7 GHz.

Statement of Contribution/Methods

HBAR – consisting of piezoelectric film (ZnO) sandwiched between two electrodes, atop a low acoustic-loss substrate (sapphire) – can be modeled with a modified BVD equivalent circuit. In this model, the effective Q has a term that goes as the inverse of the series resistance, which is dictated by the electrode resistance. This is therefore an important parameter for HBAR electrodes. However, other considerations, such as acoustic properties, in addition to quality of piezoelectric crystal growth on the electrode, are important. Therefore, we experimentally investigated four parameters: electrode metal, deposition conditions for the metal with best performance, electrode thickness, and active area size. We fabricated three runs of HBAR that were identical except for electrode metal: molybdenum, aluminum, or gold. We then optimized deposition conditions with respect to resistivity. Finally, HBAR was fabricated with five different electrode thicknesses, and 11 different active area sizes, ranging from 0.06 μm to 0.14 μm , and 5,300 μm^2 to 23,600 μm^2 , respectively.

Results

The devices fabricated with Mo electrodes exhibited the highest Q. Mo was sputter deposited, and four-point probe method was used to determine that the lowest resistivity Mo film is achieved at a gas (Ar) pressure of 5 mT and an RF power of 300 W. Out of five Mo electrode thicknesses, the HBAR with 0.14 μm had the highest Q. An active area of 6,500 μm^2 was found to perform best. Out of all those fabricated, the optimum device had Q = 6501 at a frequency of 7.520 GHz, yielding $fQ = 4.49 \times 10^{13}$.

Discussion and Conclusions

Molybdenum – despite its moderate resistivity – is the best electrode metal, owing to its low acoustic loss and superior characteristics as a ZnO growth base-layer. Optimizing Mo sputter deposition conditions led to further improvements due to decreased resistance. Since most of the acoustic energy is contained in the sapphire substrate, mass loading of a heavier electrode does not lower Q. Thus, the thickest electrode with the lowest resistance is best. The small active-area HBARS had Q about three times that of the large ones. This could be due to acoustic loss in the lateral dimensions of the active area. The smaller devices also had higher ratio between impedance at series and parallel resonant frequencies.

Though the maximum resonance is expected to occur when an acoustic half-wavelength is equal to the thickness of the ZnO layer, our results show that the frequency range of maximum Q increases with decreasing electrode thickness. This is because the thickness of the electrode is not negligible compared to that of the ZnO, which is 0.35 μm thick for operation above 7 GHz.

Tuesday
Poster

A design procedure for an acoustic mirror providing dual reflection of longitudinal and shear waves in Solidly Mounted BAW Resonators (SMRs)

Sumy Jose¹, André Jansman², Ray Huetting¹, ¹Semiconductor Components, University of Twente, Enschede, Netherlands, ²Research, NXP Semiconductors, Eindhoven, Netherlands

Background, Motivation and Objective

The quality factor of the SMR is limited by substrate losses [1]. An acoustic mirror is traditionally employed for the reflection of longitudinal waves and not for shear waves. We propose a procedure, derived from optics, to design stacks that efficiently reflect both longitudinal and shear waves. This method can be applied for the acoustic mirror design for any material combination.

Statement of Contribution/Methods

The necessity for reflection of both types of waves was recognized earlier and some optimized stacks have been reported for specific material combinations [1, 2]. But to our knowledge no systematic design procedure with a solid theoretical background has been reported. Starting with the stop-band theory [3] and the principle of spacer layers [4] in Optics, we present a design procedure which gives the modified thicknesses for the reflector stack to efficiently reflect both the waves. FEM simulations [5] were performed for verifying the results based on the analytical model described in [6] showing good agreement.

Results

The performance improvement is seen from the mirror transmission curves as a function of frequency [1]. Fig.1 shows the transmission curves of a nine layer Ta₂O₅/SiO₂ optimized reflector stack with and without the spacer and fig.2 shows the curves demonstrated for different material combinations.

Discussion and Conclusions

With the optimized design, we can obtain a minimum transmission for longitudinal and shear waves of -25 dB and -20 dB at resonant frequencies for longitudinal and shear waves, respectively, for various reflector material combinations. With such optimized designs, devices can be designed that are no more limited by acoustic loss into the substrate.

- [1]S. Marksteiner et al., Proc. IEEE Ultrasonics Symposium, pp.329-332, 2005.
- [2]S. Marksteiner et al., US patent: 006933807B2
- [3]Optics of thin films, Z.Knittel, John Wiley & Sons, 1976.
- [4]GU Pei-fu,Zheng Zhen-rong., Journal of Zhejiang University Science A,2006 7(6),pp.1037-1040.
- [5]www.comsol.com
- [6]K. M. Lakin et al., IEEE Trans. Microwave Theory and Techniques, 41(12), pp. 2139-2146, 1993.

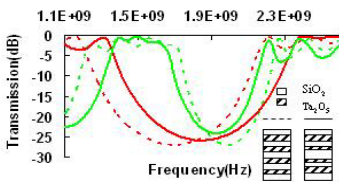


Figure1. Transmission of a nine layer Ta₂O₅/SiO₂ optimized reflector stack based on the new design procedure with and without the spacer layer. Red lines indicate longitudinal and green indicate shear waves. Solid lines represent the configuration with the spacer layer and dashed lines represent the one without the spacer layer.

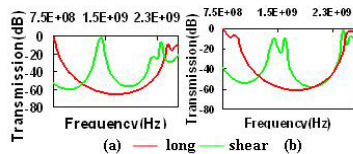


Figure2. Transmission curves of a nine layer optimized reflector stack of (a) W/SiO₂ and (b) SiOC/Ta₂O₅. In both the cases, the transmission of longitudinal and shear waves is well below -55dB. The new design procedure is also applied for other material combinations like SiOC/W, SiOC/P, SiOC/TiN and the optimized layer stacks show the efficient reflection of both longitudinal and shearwaves.

Tuesday
Poster

Influence of Mobile Charges in the Substrate of BAW Filters on High Resistivity Silicon

Amelie Hagelauer¹, Bernhard Bader², Gudrun Henn², Ansgar Schaeufele², Stephan Marksteiner², Karl Wagner², Robert Weigel^{1,†} *Institute for Electronics Engineering, University of Erlangen-Nuremberg, Germany, ²EPCOS AG, Germany*

Background, Motivation and Objective

BAW filters have emerged as an important technology for GHz filtering components. Especially the high quality factor and the good temperature coefficient make the BAW filters well suited for W-CDMA band II and band III devices. To meet the high requirements of these devices, it is essential to analyze and minimize possible loss mechanisms. One loss mechanism is the existence of mobile charges at the surface of high-resistivity silicon. These charges increase the insertion loss and influence the performance of SMR-BAW-filters.

Statement of Contribution/Methods

In this paper we investigate the influence of mobile surface-charge induced parasitic losses on the performance of our BAW filters at 1.9 GHz. Several approaches have been proposed in the field of RF-MEMS devices in the past few years to minimize this effect. The two methods that are most promising for BAW applications are ion implantation into the bulk silicon to reduce the surface charge mobility and the use of low charge silicon-dioxide to avoid the creation of mobile mirror charges in the silicon. At high temperatures the implanted silicon recrystallizes, eliminating the effect of the implantation. Since a BAW process involves several manufacturing steps at elevated temperatures (>400°C), it is questionable if the implantation survives the processing. Therefore, we designed test structures in order to verify the stability of the implantation with respect to the thermal budget of our BAW process. All test structures and filters were manufactured on the same wafer-type using different passivation methods. Additionally we used EM-simulations to evaluate the measurements of our test structures. An extended simulation model reflects the measured insertion attenuation of the filter performance pretty well.

Results

On statistical average, filters of sample nr. 3 show an improvement of 0.05 dB insertion attenuation compared to filters of sample nr. 1. Losses are reduced, resulting in steeper slopes and a larger passband width. An influence on other filter characteristics, e.g. stop band suppression is not observed. The usage of low-charge silicon-dioxide shows no influence on filter performance.

Discussion and Conclusions

Our filters, CPW as well as MS lines are suitable to investigate the influence of mobile charges in the silicon of BAW filters. The ion implantation reduces losses and yields an improvement of the filter performance.

Table 1: Overview of test samples with different test structures: BAW-filters, coplanar waveguide and micro strip lines

Sample Nr.	Wafer-Type	Surface mobility reduction	Oxide
1 (standard)	p-Si > 4k Ω cm	non	PECVD oxide
2 (reduced charges)	p-Si > 4k Ω cm	non	PECVD oxide with reduced charges
3 (implantation)	p-Si > 4k Ω cm	Ion-implantation	thermal and PECVD oxide

Wide bandwidth Bragg mirrors for multiband BAW filter chips

Jimena Olivares¹, Enrique Wegmann¹, Marta Clement¹, Jose Capilla¹, Enrique Iborra¹, Jesús Sangrador¹; *Grupo de Microsistemas y Materiales Electrónicos, Universidad Politécnica de Madrid, Madrid, Spain*

Background, Motivation and Objective

Bulk acoustic wave (BAW) filters are of great interest for wireless communications, such as mobile phones. The integration of different bandpass filters in the same substrate for duplexers or multiband systems is a challenging objective. The Bragg mirror, which is a key part of BAW Solidly Mounted Resonators, is a limiting element in the

multifrequency integration. The aim of this work is to investigate the possibility of achieving Bragg mirrors providing a good acoustic reflection in a wide frequency band.

Statement of Contribution/Methods

The width of the reflectance band in Bragg mirrors strongly depends on the acoustic impedance mismatch of the adjacent reflector layers. To maximize this mismatch we propose the use of iridium (Ir) as high acoustic impedance material and porous silicon dioxide (SiO₂) as low impedance layer. In this work, Bragg mirrors with Ir/SiO₂ are designed and fabricated. Ir and SiO₂ are deposited by pulsed-DC sputtering. The acoustic properties of the two materials were previously assessed by measuring their density and sound velocity.

Bragg mirrors design is based on the Mason model, taking into account both longitudinal and shear modes for the optimization. Special attention is paid to minimize the number of layers of the mirrors to improve the integration of the devices.

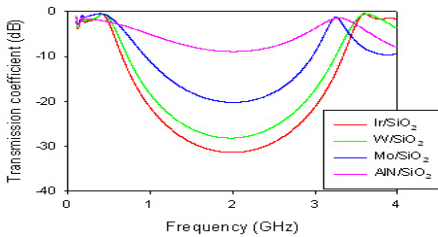
Results

The figure shows the simulated transmittance of a $\lambda/4$ Bragg mirror composed of only three layers of SiO₂/Ir/SiO₂. The transmittance of similar reflectors made with more conventional pairs of materials (SiO₂/AlN, SiO₂/Mo and SiO₂/W) is also depicted for comparison.

The bandwidth of the Bragg mirrors made of Ir and SiO₂ is experimentally evaluated using BAW structures with AlN stacks of different thicknesses to obtain resonators with substantially different frequencies.

Discussion and Conclusions

Results indicate that very low transmittance mirrors in a wide band are achieved with only three layers, thanks to the very large acoustic impedance mismatch between Ir and SiO₂ films. Additionally, the acoustic isolation achieved is similar to that obtained for Bragg mirrors with a greater number of layers of more conventional materials such as SiO₂/AlN. The Irse acoustic reflectors provide a suitable acoustic isolation in a wide frequency range.



Tuesday
Poster

P2-N-05

Reduced Order Finite Element Models of Bulk Acoustic Wave Resonators

Philip Katus¹; ¹IMTEK Laboratory for Electrical Instrumentation, Institute, Freiburg, Baden-Württemberg, Germany

Background, Motivation and Objective

Finite element (FE) simulation has become an important method in the modeling of bulk acoustic wave (BAW) devices. Unfortunately the FE method is very demanding on computational resources. Moreover most techniques to reduce the complexity of FE models are not applicable to piezoelectric materials. Although model order reduction using moment matching can be applied to piezoelectric materials this method is not commonly used by developers and scientists. In this work model order reduction using moment matching (MOR) is utilized to simulate BAW resonators. In particular, accuracy and cost of MOR is compared to harmonic and modal analysis. Because the quality of reduced models strongly depends on the underlying physics, the basic results may be relevant for different layouts of BAW resonators as well. In addition the basic principle of MOR is explained and recommendations are given

Statement of Contribution/Methods

Simulations are performed using Ansys-Software and an add-on for MOR developed at IMTEK [1]. In the procedure Ansys is utilized to obtain the second order system of equations ($\text{rank}=1e4..2e5$). Then MOR is used to reduce this system ($\text{rank}<300$) which then can be easily solved. MOR is based on the approximation of the first m moments of the corresponding transfer function at a specific expansion point. Moment matching is inherently achieved by calculating the Krylov subspace up to rank m . Because this leads to numerical instabilities, the Arnoldi algorithm is used to calculate the Krylov subspace. By projecting the system matrices onto a basis of the Krylov subspace, the reduced system is obtained.

[1] E. B. Rudnyi and J. G. Korvink, Model Order Reduction for Large Scale Engineering Models Developed in ANSYS, Lecture Notes in Computer Science, v. 3732, pp. 349-356, 2006.

Results

Typical BAW resonator models require a reduced system size of about 200 equations. In this case the relative error of admittance averages to 0.39 % and that of dominant displacement to 0.12 % for the chosen frequency interval. The interval is centered at main resonance (680 Mhz) and extends to ± 80 Mhz.

Increasing the size of the reduced system lowers the averaged error of all degrees of freedom (DOF). However, the accuracy of several DOF's can temporary decrease when increasing the system size.

Discussion and Conclusions

MOR is an efficient and precise method for the modeling of BAW resonators. But up to date no proof for an upper error bound exists. Therefore it is required to understand the characteristics of reduced models.

P2-O. MEMS and Sensors

Sala Orange

Tuesday, September 22, 2009, 10:00 am - 11:30 am

Chair: **Tuomas Pensala**
VTT

P2-O-01

A new thin-reflector mode for ultrasonic particle manipulation in layered resonators

Peter Glynne-Jones¹, Rosie Boltryk¹, Nick Harris², Pierre Baclet³, Martyn Hill¹; ¹School of Engineering Sciences, University of Southampton, Southampton, Hampshire, United Kingdom, ²Electronics and Computer Science, University of Southampton, Southampton, Hampshire, United Kingdom, ³ENSIAME, Université de Valenciennes et du Hainaut Cambrésis, Valenciennes, France

Background, Motivation and Objective

Previous literature has described two major classes of planar acoustic particle manipulation devices: (a) those where the dominant resonance is in the fluid layer, leading to agglomeration at one or more pressure nodes within the fluid layer; and (b) those where a resonant reflector layer provides a pressure release boundary condition, causing the agglomeration position to occur at a pressure node close to the fluid/reflector interface (Quarter-wave devices).

Statement of Contribution/Methods

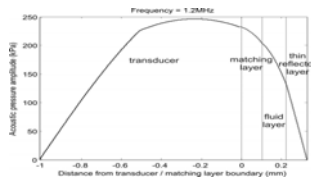
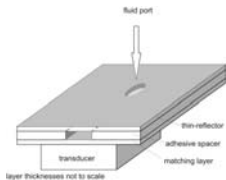
We describe here a new arrangement which operates at the first thickness resonance of a composite structure, with energy distributed across all layers of the device as shown in fig2. This leads to pressure nodes at the air boundaries of a device. By designing with only a thin reflector layer (a thickness of $\sim\lambda/15$ in this case) particles at all positions within the channel are forced to the reflector/fluid layer boundary.

Results

We model and experimentally characterise a device, and show that it can produce forces of order 50pN on a 10µm diameter polystyrene bead with transducer excitation of 25Vpp. We demonstrate that this configuration will work efficiently with lossy polymer reflector layers, and further show that by incorporating an additional thin plastic layer between the transducer and fluid layers it is possible to create a disposable sample cuvette that is easily mounted within a device.

Discussion and Conclusions

The advantages of this arrangement are energetic acoustic modes, thin device walls compatible with high N/A microscope objectives, and the possibility of creating cheap, disposable sample cuvettes. The design is also more stable than quarter-wave devices to small variations in chamber dimensions. We foresee this having applications in biosensing, cell handling and fractionation devices.



Tuesday
Poster

P2-O-02

Multi-band RF Filter Integrating Different Modes of AIN Resonator by CMOS-compatible Process

Takeshi Matsumura^{1,2}, Masayoshi Esashi², Hiroshi Harada¹, Shuji Tanaka²; ¹National Institute of Information and Communications Technology (NICT), Japan, ²Tohoku University, Japan

Background, Motivation and Objective

For future mobile phones based on the cognitive radio technology, a multi-band RF front-end module is required and a multi-band RF filter is one of the key components. In this study, we demonstrated a multi-band AIN/Si composite bulk acoustic wave (BAW) filter integrating different modes of AIN resonator to cover the frequency range from hundreds MHz to higher GHz.

Statement of Contribution/Methods

We developed a novel CMOS-compatible process technology to co-fabricate different modes of AIN resonator, FBAR and disk-type resonator, above LSI. First, an SOI wafer is bonded to a Si wafer, which is treated as a dummy LSI in this study, using a polyimide film. The handle layer and the BOX layer of the SOI wafer are etched away, and an AIN piezoelectric layer sandwiched by metal electrodes is fabricated on the device layer to form BAW structures. Finally, the underlying polyimide is ashed away by O₂ plasma to release BAW devices. All process techniques are compatible with the advanced LSI with a very small design rule.

Results

Figure 1 shows a top view of a fabricated mechanically-coupled 3 disk-array filter. The disk radius is 27μm, corresponding to a resonant frequency of ca. 292MHz in higher order wine-glass mode. From the filter response, a center frequency of 292.8MHz and 3dB band width of 3.4MHz (1.2%) were obtained. Figure 2 shows a filter response of a fabricated ladder-type FBAR filter. From the filter response, we obtained a center frequency of 7.71GHz and 3dB band width of 140MHz (1.8%).

Discussion and Conclusions

We successfully co-fabricated different modes of AIN resonator on the same wafer. We obtained center frequencies of 292.8MHz and 7.71GHz from the disk-type resonator filter and the FBAR filter, respectively, and indicated the possibility of multi-band RF filter for future mobile phones.

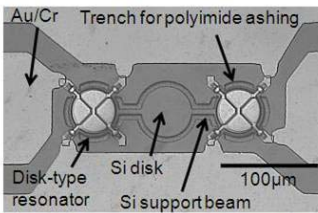


Fig. 1 Mechanically-coupled 3 disk-array filter

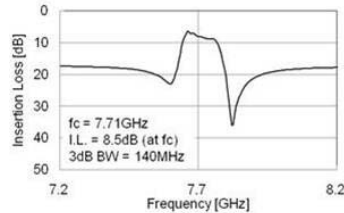


Fig. 2 S21 of the ladder-type FBAR filter

P2-O-03

PZT transduced high-overtone width-extensional resonators above 1 GHz

Hengky Chandralim¹, Sunil Bhave¹, Ronald Polcawich², Jeff Pulskamp², Roger Kaul²; ¹Electrical and Computer Engineering, Cornell University, Ithaca, New York, USA, ²US Army Research Laboratory, USA

Background, Motivation and Objective

PZT is an attractive transducer because it exhibits a large electromechanical coupling coefficient and DC bias dependent elastic modulus [1]. Several groups have demonstrated piezoelectric materials for transduction, while utilizing single-crystal silicon (SCS) as the resonating “carrier” material to enhance resonator quality factors (Q) [2,3]. A systematic study is essential to investigate the effect of silicon on Q, resonant frequency (fc) and develop and accurate BVD model of piezoelectrically transduced resonators at RF.

Tuesday
Poster

Statement of Contribution/Methods

This paper demonstrates the use of SCS as a carrier material to enhance Q and boost the frequency of high-overtone width-extensional mode (WEM) resonators to operate above 1 GHz. We developed a mature and reliable process with 70% yield to fabricate PZT-Only and PZT-on 3, 5 and 10 μm SCS resonators. In order to acquire a large transduction area to minimize the motional impedance (Rx) and excite high-overtone modes of vibrations to attain high fc, WEM resonators are excited by patterning IDTs like electrodes on top of the resonators (Fig. 1a and b).

Results

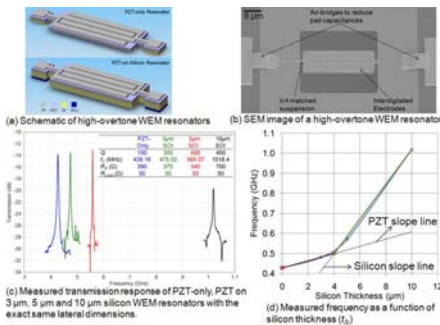
Resonators with identical lateral dimensions and thicker silicon exhibit higher Q, higher fc and lower Rx for frequency up to 1 GHz (Fig. 1c). These measurement results confirm that integrating PZT transduction with single-crystal silicon retains the mechanical energy within the high quality silicon device layer, resulting in a net decrease in Rx. The loss-tangent of PZT starts to dominate the loss and degrade the Q for frequency of operation above 1 GHz (Fig. 1c). This can be improved by engineering the PZT texture [4]. By varying the % mass of SCS in the resonator, we can define the desired Q and fc of the resonators (Fig. 1d).

Discussion and Conclusions

The excitation of high-overtone WEM resonators using IDT electrodes configuration exhibits high fc with low Rx. The air-bridge routing (Fig. 1b) cancels parasitic capacitances and enables frequency characterization to above 1 GHz. PZT-on-SCS technology will enable PZT transduced resonators that covers up to low-band GSM frequencies.

[1] Chandralahim et al, Appl. Phys. Lett., pp. 233504 (2008).
 [2] Abdolvand et al, IEEE Trans. UFFC, pp. 2596-2606 (2008).
 [3] Jaakkola et al, IEEE Ultrasonics Symposium, pp. 717 – 720 (2008).
 [4] Wasa et al, IEEE Ultrasonics Symposium, pp. 1920 - 1923 (2008).

Tuesday
Poster



P2-O-04

Suppression of Parasitic Resonance in Piezoresistively Transduced Longitudinal Mode Silicon MEMS Resonators

Jize Yan¹, Angel Lin¹, Ashwin Seshia¹, ¹University of Cambridge, United Kingdom

Background, Motivation and Objective

Silicon-based MEMS resonators have emerged as a potential candidate for applications relating to timing references, frequency selective signal processing and sensors due to their small size and potential for integrability with electronics. However, the efficiency of integrable transducer technologies and the presence of capacitive and motional parasitic elements has limited much of their applicability while there remain significant application drivers to scale operation to VHF and beyond. Capacitively actuated and piezoresistively sensed silicon MEMS resonators have been presented as a means for scaling to high frequencies with a 1.1. GHz fundamental mode silicon MEMS resonator demonstrated [1]. However, in this case the resonator topology was modified to accommodate device-layer piezoresistive transduction resulting in possible parasitic mechanical modes.

Statement of Contribution/Methods

This paper demonstrates an extension of the concepts presented in [1], wherein beams are electrostatically excited in a combined longitudinal mode. The response of the beam is sensed using both capacitive and piezoresistive transduction principles. The resonator consists of six parallel beams linked to a central anchor and a pair of symmetrical parallel beams that force the parallel beams to vibrate in-phase. Other mechanical modes are suppressed as compared to [1]. The paper also compares this topology to a square bulk mode resonator with similar electrical interfaces previously reported in [2].

Results

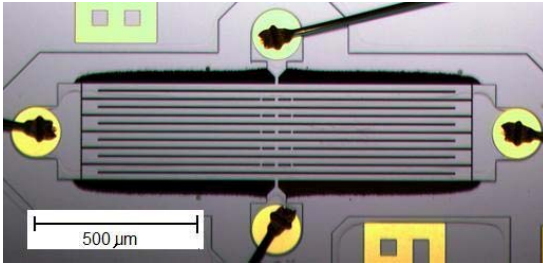
The open-loop transmission measurements for the silicon microfabricated resonator shown below demonstrate a quality factor (Q) of 0.936 million at 3.5 MHz using piezoresistive readout. By utilizing a second harmonic piezoresistive sensing approach [2], a Q of 8043 is observed in the air. Parasitic mechanical modes are suppressed as compared to previously reported resonator configurations.

Discussion and Conclusions

A novel piezoresistively-transduced and spurious mechanical mode suppressed longitudinal mode resonator is demonstrated with an associated f-Q product of 3.28×10^{12} . This topology allows for the scaling of the resonator transconductance at high Q by combining an arrayed beam approach while simultaneously rejecting spurious mechanical modes.

[1] J.T.M.van Beek et al, Proc. IEDM 2007.

[2] A.T-H.Lin et al, Proc. Transducers 2009.



P2-O-05

Microresonant Impedance Transformers

Roy Olsson¹, Kenneth Wojciechowski^{1,†} Sandia National Laboratories, USA

Background, Motivation and Objective

Contour mode AIN resonators are of interest for advanced radios due to their small size, high-Q, low impedance and ability to obtain 0.01-10GHz frequencies on a single substrate. The ability of AIN MEMS resonators to realize impedance transformers with a wide range of turns ratios without added fabrication complexity has not been extensively explored. Impedance transformation through microresonator filters allows ideal noise matching of amplifiers to antennas, reduced power and size in IF stages and improved phase noise in MEMS oscillators with displacement limited power handling.

Statement of Contribution/Methods

Equivalent models of 2 (Fig. 1), 3 and 4 port microresonant impedance transformers have been developed and demonstrate excellent agreement with measured results. The real admittance seen looking into a microresonator port (Y11) is proportional to the electrode area (EA) of that port squared, while the through admittance (Y21 and Y12) is proportional to the product of all electrode areas, providing the opportunity to realize low loss impedance transformers. Since, for a resonator of fixed dimensions, the real impedance looking into a port is proportional to $1/EA^2$ while the shunt capacitance loading the port is proportional to EA, the effective k_t^2 at one port can be increased with a corresponding k_t^2 decrease at another. This is useful when high capacitive loading is seen on one port such as in channelizing filter banks.

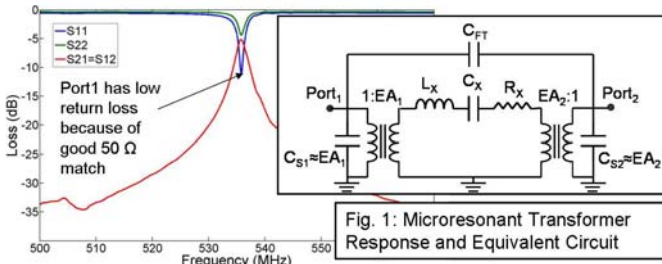
Tuesday
Poster

Results

The measured results (50 Ω termination) for a 2-port, 536 MHz microresonant impedance transformer with, $EA_1=1.35EA_2$, for a transformation ratio of $(EA_1/EA_2)^2=1.82$ are shown in Fig. 1. As predicted by the model, the impedance seen looking into ports 1 and 2 is 52 and 95 Ω while the through impedance is 70 Ω. A 3-port microresonant transformer at 110 MHz has also been realized with $EA_1=EA_2=6EA_3$ that transforms a single-ended 4320 Ω impedance into a differential 120 Ω system.

Discussion and Conclusions

Low loss microresonant transformers have been realized with turns ratios as high as 6:1. This new class of filters enable, for example, matching of low impedance antennas to CMOS LNAs that exhibit lower noise when driven from higher impedance sources.



Tuesday
Poster

P2-O-06

PMBAR as an alternative to QCM

Evgeny Milyutin¹, Paul Mural¹; ¹Swiss Federal Institute of Technology, Switzerland

Background, Motivation and Objective

BAW and SAW resonators are potential alternatives to QCMs for sensor applications. BAW resonators based on thin films of AlN or ZnO show a superior sensitivity in comparison to SAW resonators and QCM. However, BAW shear mode resonators based on standard AlN sputter techniques were not realized, so far. In a previous work we published modeling and experimental results for homogeneous AlN films combined with interdigitated electrodes. The longitudinal component present below the electrode fingers limited the quality factor. In this work, the piezo-modulated bulk acoustic resonator (PMBAR) is studied as a solution for avoiding this.

Statement of Contribution/Methods

A novel shear mode bulk acoustic wave (BAW) resonator based on an AlN(001) thin film was studied for sensor applications as an alternative to quartz microbalances (QCM) and surface acoustic wave (SAW) devices. The patented design of this device enables operation in liquid, using standard c-axis oriented AlN in combination with interdigitated electrodes. The main novelty behind this concept is the use of AlN films with modulated piezoelectric properties (fig. 1a), ideally between full (piezo) and zero (nonpiezo) piezoelectric effect.

Results

The device in immersed operations was simulated for various ratios between piezoelectric properties of “good” and “bad” AlN. The coupling coefficient of the device decreases with lowering the piezoelectric portion in the film. For this reason, the possibilities of fabricating a “bad” AlN was studied, which resulted in production of the film with a piezoelectric coefficient $d_{33}=2.4\text{pm/V}$. This is half of the normally observed coefficient in good AlN. The sensitivity was simulated for a device with this experimentally realized materials that results in high sensitivity - 500m2/kg after some design optimization.

Discussion and Conclusions

Modeled resulting sensitivity values for the device are approximately 10 times larger than for SAW resonators (e.g. one used by Samsung for HBAG immunosensor, sensitivity is 54m2/kg) and about 180 times that typically obtained with QCM (value 3.3m2/kg is taken). This is a promising outlook for PMBAR sensors.

The Effect of Ultraviolet (UV) Radiation on the Temperature Coefficient of Resonant Frequency (TCF) of ZnO Based Film Bulk Acoustic-wave Resonator (FBAR)

Xiaotun Qiu¹, Ziyu Wang², Jie Zhu¹, Jonathon Oiler², Cunjiang Yu³, Hongyu Yu^{1,2,4}:¹Electrical Engineering, Arizona State University, USA, ²school of earth and space exploration, Arizona State University, USA, ³Mechanical and Aerospace Engineering, Arizona State University, USA

Background, Motivation and Objective

Film Bulk Acoustic-wave Resonators (FBARs) have been drawing considerable attention both as filters and as high sensitivity mass sensors in recent years. However, it has been found that the resonant frequency of FBAR is highly temperature dependent. Previous studies attributed this phenomenon to the changes of piezoelectric layers' stiffness and densities with temperature. In this study, we demonstrated that for ZnO based FBAR, ultraviolet (UV) light also affected its temperature coefficient of resonant frequency (TCF), which decreased under UV illumination due to attenuation of oxygen absorption.

Statement of Contribution/Methods

The FBAR was fabricated on top of a SiN diaphragm, consisting of an Al/ZnO/Au sandwich structure. A versatile ultraviolet lamp (365 nm) was used as UV source. The temperature of the FBAR was modulated by a heater. The resonant frequency was monitored with an Agilent E5071C network analyzer.

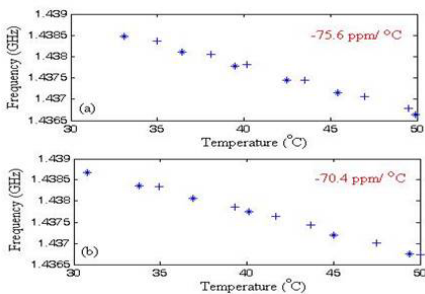
Results

The resonant frequency of the FBAR was around 1.44 GHz with a quality factor (Q) of 550. Figure 1 shows the FBAR resonant frequency changes vs. temperature measured (a) in the dark and (b) under UV (720 $\mu\text{W}/\text{cm}^2$) illumination (two measurements were conducted in each condition). The average TCF was around -75.6 ppm/°C in the dark, while under UV light, TCF changed to -70.4 ppm/°C.

Discussion and Conclusions

It is known that oxygen is absorbed on the ZnO film through capturing electrons from the film. When temperature increases, ZnO attempts to absorb more oxygen onto its surface. This process may increase the density of the film, which will decrease the acoustic velocity inside the film, resulting in the decrease of resonant frequency. So for the ZnO FBAR in the dark, both softening of the material (e.g. decrease of the stiffness) and oxygen absorption with increasing temperature contribute to the measured TCF.

When there is UV illumination on the FBAR, electron-hole pairs are generated inside the ZnO film. The holes produced by light absorption migrate to the surface and discharge the negatively charged adsorbed oxygen ions. When an oxygen ion is discharged by the capture of a hole, it will be thermally desorbed. So UV can cause oxygen desorption from the ZnO surface. In this way, the oxygen absorption during the rise of temperature will be attenuated, resulting in smaller TCF under UV compared to the value obtained in the dark.



Multilayer shear wave resonator consisting of c-axis tilted ZnO films

Naoki Morisato¹, Shinji Takayanagi¹, Takahiko Yanagitani², Mami Matsukawa¹, Yoshiaki Watanabe¹:¹Laboratory of Ultrasonic electronics, Doshisha University, Kyotanabe, Kyoto, Japan, ²Graduate School of Engineering, Nagoya Institute of Technology, Nagoya, Aichi, Japan

Background, Motivation and Objective

A shear wave resonator is suitable for the sensors to measure mass loading in the liquid. In previous presentation, we have reported c-axis 23° tilted ZnO films for shear wave excitation. These films have large electromechanical coupling, however, they excites spurious longitudinal wave.

Statement of Contribution/Methods

We propose new multilayered resonator consisting of c-axis tilted ZnO films (Fig. 1). Each layer has same thickness. The c-axis tilt directions in odd and even layers are symmetric with respect to the surface normal. In this resonator structure, layer thickness can be increased without change of shear mode resonant frequency. This enables the expansion of sensing area (in 50 Ω matching) and high power operation. Moreover, longitudinal wave excitation is expected to be suppressed because resonant frequency of thickness extensional mode should become lower.

Results

In the first attempt at multilayer sputter deposition, preferential orientation could not be obtained in the second and third layers. We then next tried to introduce buffer amorphous SiO₂ layers between the ZnO layers. As a result, strong preferentially oriented layers could be formed only on the SiO₂ layer fabricated at low temperature. Degree of the 3-dimensional orientation and electromechanical coupling coefficient of the each layer has been estimated by XRD pole figure analysis and Mason's equivalent circuit analysis, respectively.

Discussion and Conclusions

The longitudinal and the shear wave conversion loss curves of the four layered resonator are shown in Fig. 2. We can see highly efficient shear wave excitation with relatively suppressed longitudinal wave excitation. More suppression is expected by increasing the number of layers.

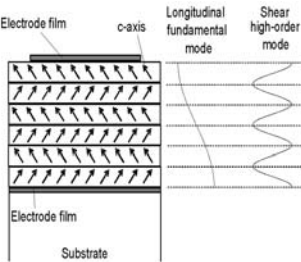


Fig.1 Multilayer structure of c-axis tilted ZnO films

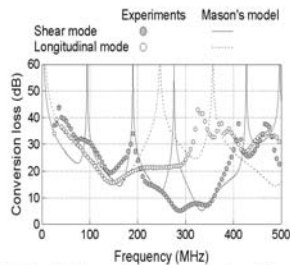


Fig.2 Longitudinal wave and shear wave conversion losses of the resonator consisting of four layer of c-axis tilted ZnO

Tuesday
Poster

P2-O-09

Integrated Finite Element Analysis of an Electrostatically-Driven Vibrating Beam used as a Gyro Sensor

Maisonnet jerome¹, Dulmet Bernard¹; ¹time and frequency, FEMTO-ST, besancon, France

Background, Motivation and Objective

Flexural vibrating beam have been widely proposed for gyro sensor applications. Designing multi-beam structures is an efficient way to drastically reduce energy losses at the clamping zone of the beams. Nevertheless, the numerical modeling of multi-beams gyros is complicated by the order of multiplicity of eigenvalues, and a prescribed gyration is barely seen as a possible input in the dynamic modules of structural analysis software. Furthermore, high-Q monolithic structures are better analyzed in the framework of modal analysis, where the primary step simply computes eigenvalues, while the driving terms are taken into account only during the further steps of the model. As a consequence, accurately modeling such a gyros cannot be performed in an integrated manner, so that optimizing them remains a long and difficult task.

Statement of Contribution/Methods

In this paper, we rely on a simple finite element description which takes the gyration along the axis of a beam as a prescribed initial parameter of the analysis. Thus, we can describe the behavior of the vibrating beam in a suitable way, inasmuch as the eigen-frequencies can still be computed through closed-form formulas. Thereafter, we explicitly introduce the electrostatic excitation through the work of external forces in Hamilton's principle, and the

complete behavior is obtained after the dynamic incremental terms are extracted by means of a Taylor's expansion of the actual gap in real time. Following this procedure, we obtain all components of the mechanical displacement of the

beam in terms of the applied voltage and a prescribed gyration at constant rate. Thus, the non-linear mechanical softening arising from the electrostatic actuation is taken into account at the same level as the linear effect of Coriolis force.

Results

In this manner, we set up a convenient modeling tools in the purpose to compute the gyroscopic sensitivity of electro statically-actuated vibrating beams which are the kernel elements of many MEMS gyro sensors.

Discussion and Conclusions

The approach can be extended to electrostatically-driven multi-beam sensing structures provided that the primary model be completed to also support the effects of a gyration around an axis perpendicular to the beam axis.

P2-O-10

Gyroscopic Effect for SAW in Common Piezoelectric Crystals

Sergey Biryukov¹, Hagen Schmidt¹, Manfred Weihnacht¹; ¹*IFW Dresden, Dresden, Germany*

Background, Motivation and Objective

To the best of our knowledge the first paper, in which a dispersion of the classical Rayleigh wave in rotating media is investigated, has been published in 1973 [1]. There are now several dozens of papers about the gyroscopic effect for SAW, some of them are reviewed shortly in [2]. The papers are oriented mostly on the complex procedure of a dispersion equation derivation in an explicit form to find then its numerical solution. However, SAWs in rotating common piezoelectric crystal cuts have never been considered. It is interesting to estimate the gyroscopic effect for such cuts with an eye to rotation rate sensors.

Statement of Contribution/Methods

In the present work the gyroscopic effect is taken into account by a simple way using the well-known numerical procedure for SAW calculation in arbitrary crystals. To take into account the medium rotation it is enough to introduce Coriolis and centrifugal forces into the piezoelectric medium equations of motion. Such modification changes only slightly some coefficients of these equations, which are related with the medium density. The boundary conditions on the free surface therewith are not changed. Further, as a result of standard procedure, the SAW velocity is calculated as a function of the medium rotation rate.

Results

The rotation of medium about each coordinate axis is considered: about direction of SAW propagation, about transversal direction in plane, and about an external normal to surface. A relative shift of the SAW phase velocity dV/V is calculated as a function of the ratio g of the rotation rate to the angular SAW frequency. Because the parameter g is normally very small the first term in the expansion of dV/V in power of g is most important. The following results for these terms are obtained. For STX-quartz $dV/V=(-1.7g^2, 0.14g, -0.011g)$ respectively to the axis order above; for 128YX-LiNbO₃ $dV/V=(-29.4g^2, 0.094g, 0.021g)$; for YZ-LiNbO₃ $dV/V=(-28.6g^2, 0.026g, -0.203g^2)$; for X112Y-LiTaO₃ $dV/V=(-0.39g, 0.056g, -0.57g^2)$; for Z cut of AlN $dV/V=(-7.5g^2, 0.018g, -0.12g^2)$.

Discussion and Conclusions

The calculations show that in spite of the quite large numerical coefficients between dV/V and power of g , the gyroscopic effect itself is very small due to the smallness of g . For example, for a rotation rate of 300 revolutions per second and a SAW frequency of 30MHz the parameter $g=10^{-5}$. In the case of quartz rotating about the transversal axis the relative velocity shift and hence the corresponding relative frequency shift in a rotating SAW resonator is 1.4×10^{-6} . If the quality factor of a resonator is about 10^4 then modern signal processing can resolve such frequency changing. So, in principle, a use of the gyroscopic effect for SAW by sensors is possible.

[1] M. Schoenberg and D. Censor, "Elastic waves in rotating media," Q. Appl. Math., 31, 115-125, 1973.

[2] M. Destrade, "Surface acoustic waves in rotating orthorhombic crystals," Proc. R. Soc. Lond. A 460, 653-665, 2004.

P2-P. BAW Materials

Sala Orange

Tuesday, September 22, 2009, 10:00 am - 11:30 am

Chair: **Dave Feld**
Avago Technologies

P2-P-01

Nanomagnet Fabrication on FBAR for Magnetic Sensor Applications

Humberto Campanella¹, Rafael Pérez del Real², Marina Diaz-Michelena², Marta Duch³, Héctor Guerrero², Jaime Esteve³, José A. Plaza^{3,1}, *Instituto de Microelectrónica de Barcelona IMB-CNM (CSIC), Bellaterra, Barcelona, Spain,*
²Instituto Nacional de Técnica Aeroespacial Manuel Terradas INTA, Spain, *³Instituto de Microelectrónica de Barcelona IMB-CNM (CSIC), Spain*

Background, Motivation and Objective

Thin-film bulk acoustic wave resonators (FBAR) made of aluminum nitride (AlN) have demonstrated high frequency sensitivity to external force loading due to its high resonance frequency and the acoustic and mechanical properties of AlN. However, few magnetic sensors have been explored using AlN-based MEMS, and most implement a soft magnetic material like nickel iron (NiFe) alloys.

Previously, we succeeded on extracting a nanomagnet from a rare-earth quarry and attaching it to a MEMS device. Also, we have explored and demonstrated the high sensitivity of FBARs in mass detector and accelerometer applications. Technological applications and fundamental research on micro- and nanomagnetism have motivated the study of reduced-size magnetic structures as well. Thus, our objective is to exploring the possibilities of magnetic sensors based on both FBARs and reduce-sized hard magnets.

Statement of Contribution/Methods

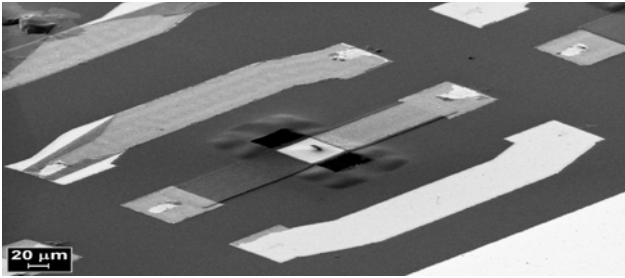
The main contribution of this work is a method for fabricating and attaching a rare-earth nanomagnet on top of an FBAR. An FBAR-based magnetic sensor is proposed, the magnetic-sensitive element being the nanomagnet, and the resonant detection being performed by the FBAR. Whenever a magnetic force arises between the nanomagnet and an external magnetic source, the added stress on the FBAR changes its mechanical configuration, thus shifting its resonance frequency.

Results

The figure shows an NdFeB nanomagnet placed on the top electrode of an FBAR embedded on a coplanar test structure. The nanomagnet was extracted from a macroscopic NdFeB quarry, milled, attached to a tungsten tip, placed on the FBAR, bonded to it, and de-attached of the tip by means of ion-assisted deposition and milling using a focused ion beam (FIB) machine. The FBAR is made of AlN and Pt electrodes, and it was released through front-side reactive-ion-etching (RIE) of the silicon substrate. Experimental measurements and FEM simulations confirm the mass-loading on the FBAR due to the nanomagnet attachment.

Discussion and Conclusions

We have demonstrated the method by extracting and placing a reduced-size magnet on top of an FBAR. Preliminary force analysis shows that the resonance frequency of the FBAR shifts up directly proportional to the magnitude of the magnetic force. On-going work is currently being done to test the sensitivity of the FBAR magnetic sensor.



P2-P-02

Discussion of Millimeter Wave FBAR with Very Thin AlN Film Fabricated Using MOCVD Method

Shoichi Tanifuji¹, Yuji Aota¹, Suguru Kameda¹, Tadashi Takagi¹, Kazuo Tsubouchi^{1,1} Research Institute of Electrical Communication, Tohoku University, Sendai, Miyagi Prefecture, Japan

Background, Motivation and Objective

The band pass filters based on the film bulk acoustic resonators (FBAR) have a great advantage of the good cut off characteristics at over 2GHz. We have fabricated 5GHz FBAR using aluminium nitride (AlN) film because AlN has higher acoustic velocity than other piezoelectric materials. We have successfully grown the c-axis oriented AlN film using metal organic chemical vapor deposition (MOCVD) method on SiO₂/Si substrate. In previous work, we reported that high oriented AlN(0002) film was achieved at the FBAR structure and realized the good FBAR resonance characteristics at 5 GHz using the Ru/AlN/Ru/Ta/SiO₂/Si(100) structure. Moreover, full width at half maximum (FWHM) of AlN(0002) was excellent value under 1.2° at less than 500nm thickness. In this paper, we discuss millimeter wave FBAR with very thin AlN film fabricated using MOCVD Method.

Statement of Contribution/Methods

We fabricated FBAR with Ru/AlN/Ru/Ta/SiO₂/Si(100) structure. Top and bottom Ru electrodes and Ta film was deposited by RF magnetron sputtering method. The Ta layer of 5nm was formed as the adhesive layer between bottom Ru electrode and SiO₂/Si(100) substrate. AlN was deposited using MOCVD method with source gasses of NH₃ and Tri-methyl Aluminum (TMA). Before AlN deposition, H₂-annealing was carried out in order to improve electrode crystallization and remove surface oxidation layer at 1050°C. After H₂-annealing, NH₃-annealing was carried out to stabilize the NH₃ gas flow. Then AlN deposition was carried out after the TMA gas was introduced at same temperature. In this way, we fabricated Ru/AlN/Ru/Ta/SiO₂/Si(100) structure. Then, we formed cavity under membrane structure used by Deep-Reactive Ion Etching (D-RIE) method. Finally, we measured FBAR resonant characteristics.

Results

After H₂-annealing, mean surface roughness (Ra) of Ru bottom electrode was less than 5Å and FWHM of Ru(0002) was 1.1° in actual measurement. On the other hand, FWHM of AlN(0002) on bottom Ru electrode was excellent value of 1.2°. Even if AlN film thickness less than 100nm, FWHM of AlN(0002) was under 1.5°. For example, if AlN film thickness was 37nm, FWHM was 1.3°. In the case of top and bottom Ru electrode thickness of 20nm and AlN thickness of 30nm, we obtain resonant frequency over 30GHz FBAR in simulation.

Discussion and Conclusions

We successfully achieved to obtain the high oriented very thin AlN film using MOCVD process. FWHM of AlN(0002) was excellent value under 1.5° at less than 100nm thickness. Since we obtain excellent crystalline thin AlN film by MOCVD method, FBAR is expected to be applied to millimeter wave band resonant devices.

Influence of AlN quality on the transversal and longitudinal coupling coefficients of acoustic devices

José Capilla¹, Marta Clement¹, Jimena Olivares¹, Jesús Sangrador¹, Enrique Iborra¹, ¹Grupo de Microsistemas y Materiales Electrónicos, Universidad Politécnica de Madrid, Madrid, Spain

Background, Motivation and Objective

Aluminum nitride (AlN) polycrystalline films are frequently used as piezoelectric material in BAW, SAW, and MEMS devices. The performance of all these devices depends on the piezoelectric quality of the AlN films. The relationship between the main piezoelectric coefficients, d_{33} and d_{31} , is well known for AlN bulk single crystals. However, this relationship is not well-established for polycrystalline AlN used in layered devices. In such devices the existence of microscopic defects, like misaligned grains or grain boundaries, could affect in a different way the distribution of stress in the longitudinal or transversal direction generated by the applied electric field. Therefore, the effective electromechanical coupling factors, longitudinal and transversal, are more adequate than d_{33} and d_{31} to describe their behavior.

Statement of Contribution/Methods

We present the study of the electromechanical coupling factor of BAW and SAW devices fabricated simultaneously on the same AlN layer. We use AlN films with variable crystalline properties in order to investigate the origin of the lack of proportionality between both coupling factors.

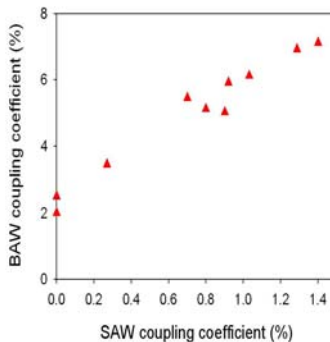
AlN thin films were grown by reactive sputtering under different conditions on Bragg mirrors covered with metal layers. The crystallographic properties were determined by XRD. BAW and SAW devices were fabricated on these samples to determine the coupling factors: longitudinal coupling was derived from the fitting of the electrical response of BAW devices using the Mason's model, while transversal one was obtained from the electrical response of SAW delay lines.

Results

The figure shows the relationship between both coupling coefficients for several samples with different crystal qualities. It can be observed that the transversal coupling drops faster than the longitudinal one. Additionally, the AlN films with the lowest BAW response present a null SAW response.

Discussion and Conclusions

The AlN films with the largest lack of proportionality between the two coupling coefficients are those with non-pure c-axis orientation, even for films with a narrow rocking curve around the c-axis. This indicates that the presence grains with orientation other than c-axis has a great importance for the propagation of surface waves. Therefore, the requirements of the crystal quality for transversal mode devices are stronger than those for longitudinal mode ones.



P2-P-04

Piezoelectric coefficients measured by picosecond ultrasonicsPatrick Emery¹, Nizar Ben Hassine², Arnaud Devos¹, Emmanuel Defay²; ¹CNRS, France, ²CEA-LETI, France**Background, Motivation and Objective**

The needs for materials in thin films characterization are increasing with the raising interest for Micro-Electro-Mechanical-Systems. Picosecond Ultrasonics (PU), a non-contact and non-destructive technique, has been largely developed to answer the mechanical metrology requirements of thin films technology, particularly in the field of Bulk Acoustic Wave (BAW) resonators [1]. The PU technique uses a pulsed laser source to excite and detect longitudinal acoustic waves at very high frequencies (100 GHz to 1 THz) [2]. Basically, the technique enables longitudinal sound velocity measurements and thickness control [3].

Statement of Contribution/Methods

It has been shown that the insertion of a wavelength tunable laser source improves the accuracy of the measurements [4]. Moreover, this particular configuration enriches the measurable parameters of thin films (acoustic attenuation [5], temperature coefficients [6], transverse sound velocity [7]). To go further, we explored the capability of the technique concerning piezoelectric characterization.

Results

In this poster, we demonstrate that the PU technique is able to measure sound velocity variations induced by a DC voltage. The experimental setup is associated with electrical probes that enable the application of a DC voltage on a BAW-type sample (here a Mo/AlN/Mo stack). The impact of a DC voltage on the sound velocity can be related to the stiffness variation of the piezoelectric layer. These results suggest that PU can also perform piezoelectric measurements in thin films.

Discussion and Conclusions

- [1] P. Emery, A. Devos and P. Ancey, "Picosecond Ultrasonics : the preferred tool for Bulk Acoustic Wave characterization", IEEE Ultrasonics Symposium, 2008.
- [2] H. T. Grahn, H. J. Maris, and J. Tauc, "Picosecond ultrasonics", IEEE J. Quantum Electron., vol. 25, p. 2562, 1989.
- [3] H.-N. Lin, R. J. Stoner and H. J. Maris, "Ultrasonics Experiments at Ultra-High Frequency with Picosecond Time-Resolution", IEEE Ultrasonics Symposium, 1990.
- [4] A. Devos, P. Emery, G. Caruyer and P. Ancey, "An Improvement of the Picosecond Ultrasonics Technique Based on a Tunable Laser : Application to Bulk Acoustic Wave Resonator Characterization", IEEE Ultrasonics Symposium, 2006.
- [5] P. Emery and A. Devos, A. Volatier and P. Ancey, "Attenuation measurements in thin films using picosecond ultrasonics", IEEE Ultrasonics Symposium, 2006.
- [6] P. Emery, D. Petit, A. Devos and P. Ancey, "Temperature Coefficients Measured by Picosecond Ultrasonics on Material in Thin Films for Bulk Acoustic Wave Technology", IEEE Ultrasonics Symposium, 2007.
- [7] P.-A. Mante, J.-F. Robillard and A. Devos, "Complete thin film mechanical characterization using picosecond ultrasonics and nanostructured transducers : experimental demonstration on SiO₂", IEEE Ultrasonics Symposium, 2008.

P2-P-05

Zero Mass Loading Sensitivity of the S₀ Lamb Wave resonance in Thin Film Plate Acoustic Resonators (FPAR)Ventsislav Yantchev¹; ¹Solid State Electronics, Uppsala University, Uppsala, Sweden**Background, Motivation and Objective**

During the last five years, a new class of thin film microacoustic devices, based on the utilization of lateral plate guided waves, is being developed. Plate guided waves in thin films have been traditionally observed as a spurious and degrading content in the response of thin film bulk acoustic resonators (FBARs). Among the variety of plate modes observed, the lowest order symmetric Lamb wave (S₀) in thin AlN membranes has attracted special attention due to its weak dispersion, acoustic velocity in excess of 10 000 m/s and moderate electromechanical coupling (up to 3.5%). Number of prove of principle studies has recently reveal to a certain extent the potential and the physical limitations of the FPAR technology, but its full capabilities are yet to be realized. In this work, studies toward minimization of technologically induced tolerances in FPARs are initiated.

Statement of Contribution/Methods

Synchronously designed FPARs are typically operating at the upper edge of the frequency stopband due to the negative reflection coefficient of the S0 Lamb wave in periodical strip gratings. Most generally, the upper stopband edge is relatively insensitive to electrode thickness variations due to the partial compensation between slowing down and reflection, both induced by the presence of grating strips [1]. In here, the possibility to achieve 0-sensitivity of the upper stopband edge is discussed for AlN based FPARs. Both Floquet-Bloch Harmonic analysis and COMSOL FEM experiments are used towards the identification of the 0-sensitivity FPAR topologies.

Results

Topologies with 0-sensitivity of the upper stopband edge with respect to technological tolerances in electrode thickness are identified in the 400MHz - 3GHz frequency band. For a given resonance frequency, variety of 0-sensitive topologies with different AlN thickness and grating pitch are identified, providing thus the opportunity to select the topology with the optimum reflectivity and/or electromechanical coupling. 0-sensitive topologies of intrinsic temperature compensated FPARs are further discussed in here.

Discussion and Conclusions

0-sensitivity of the FPAR resonances with respect to technological tolerances in the grating strip thickness are demonstrated. The described effect is a result of the complete compensation between the mass loading and the reflection at the upper stopband edge, both induced by the presence of a periodic grating. The latter, presumes significant role of the metallisation ratio as well. It is further noted the generality of the above described phenomena with respect to other acoustic devices operating at the upper stopband edge (SAWs in ZnO, 128 Y-LiNbO3 etc.).

[1] V. Yantchev and I. Katardjiev, "Propagation characteristics of the fundamental symmetric Lamb wave in thin aluminum nitride membranes with infinite gratings," J. Appl. Phys., vol. 98, pp. 849101, 1-7, Oct. 2005

Supported by the Goran Gustafsson Foundation and the WISENET Vinnova

P2-Q. Sensors, High Frequency, CMUTs & Micromachining

Sala Orange

Tuesday, September 22, 2009, 10:00 am - 11:30 am

Chair: **Mark Schafer**
Sonic Tech

P2-Q-01

Patterning of 30MHz Ultrasonic Fresnel Zone Plate by Optical Poling of PVDF-TrFE Film

Hirota **Yanagida**¹, Yasutaka Tamura², Tatsuhsa Takahashi^{3,1}, *Informatics, Yamagata University, Yonezawa, Yamagata, Japan, ²Yamagata University, Japan, ³Mathematical Information Science, Asahikawa Medical College, Asahikawa, Japan*

Background, Motivation and Objective

Poly vinyliden fluoride-co-trifluoro-ethylene is a widely investigated piezoelectric material used in ultrasound transducer applications. Thin film of the copolymer is suitable for high frequency applications. However, directivity control of high frequency transducer is a difficult problem because ultrafine processing is required.

The optical poling method was proposed by M. Date for the microscopic size patterning of ferroelectricity. We have adopted the technique in the directivity control of flat thin film transducers. In this paper, we attempt to fabricate a 30MHz ultrasound Fresnel zone plate by using optical poling method.

Statement of Contribution/Methods

PVDF-TrFE films with copolymer content of 78/22mol% were used for the laser poling. The thickness was 20 micro meters. The 12mW of He-Ne laser was used. To confirm the minimum width of the patterning line in our system, pyroelectric current was measured for various laser scan rate. After the confirmation, the Fresnel zone plate was designed. We measured the distribution of sound pressure.

Results

The effect of laser scan rate for ferroelectricity was shown in Fig.1. The 0.1mm of ferroelectricity line was obtained when 0.7mm/s of laser scanning rate was used. Using this method, we succeeded that the 30MHz ultrasound Fresnel lens was fabricated. The measured sound pressure was shown in figure 2. The solid line was the Fresnel lens and dotted line was the results of flat type transducer. When the Fresnel zone plate transducer, the focusing area was 70% of the flat type transducer.

Discussion and Conclusions

The 30MHz ultrasound Fresnel zone plate was made by optical poling. In our system, we concluded that the smallest patterning line was 0.1mm. Our 30MHz ultrasound Fresnel lens made the 70% smaller focusing area than the flat type transducer.

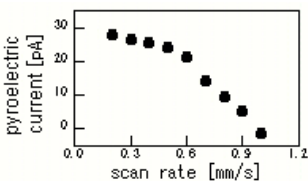


Fig.1 Effect of scan rate for the pyroelectric current

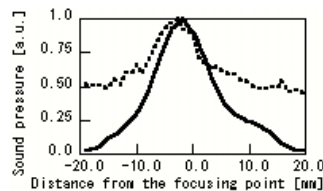


Fig.2 Distribution of the sound pressure

Tuesday
Poster

Carotid Peak Blood Velocity Detection using a 5-Plane CMUT Array with Asymmetric Acoustic Lenses: Initial Results

Der-Song Lin¹, Xuefeng Zhuang¹, Jessica Faruque², Ömer Oralkan¹, Sandy Napel², R Brooke Jeffrey², Butrus T. Khuri-Yakub¹; ¹E. L. Ginzton Laboratory, Stanford University, Stanford, CA, USA, ²Radiology, Stanford University, USA

Background, Motivation and Objective

Ultrasound measurement of peak blood velocity (PBV, correlated to carotid stenosis) requires accurate determination of Doppler angle and is subject to intra- and inter-operator variability. We report the initial results for a 5-plane CMUT array built on a single silicon substrate for operator-independent carotid artery screening.

Statement of Contribution/Methods

We propose to use 5 parallel 1D CMUT arrays on a single substrate with asymmetric lenses to obtain 5 parallel short-axis B-mode and color flow images of the carotid artery. Custom-built board-level electronics interface the 5-plane array with a commercial imaging system. We designed the circuitry to switch between the arrays and multiplex the CMUT arrays output into the system to minimize modification to the ultrasound system. In the elevation direction, asymmetric acoustic lenses mold-casted by PDMS steer the acoustic beam at fixed angles for color Doppler measurements. A finite element model was developed to study the effect of the PDMS coating on the CMUT arrays. Then a hemi-cylindrical PDMS lens centered on a single-array CMUT was made to verify the focus design parameters. The off-axis steering capability was also verified by testing on an off-centered cylindrical lens on the CMUT. For testing, we use a software package that we developed to automatically compute the vessel trajectory, Doppler angles, and angle-corrected peak velocities.

Results

We designed and fabricated a CMUT containing 5 parallel arrays, where each 1D array consists of 132 elements, each 200 μm by 4 mm in size. The fabricated CMUT arrays showed a center frequency of 8.1 MHz and a fractional bandwidth of 103% in immersion. In resonant frequency measurement in air, the uniformity across the array is excellent, with a standard deviation of 0.18% of the mean. Studies of PDMS coating on CMUT surfaces showed no change in the pull-in voltage and minimum impact on the frequency response. The experimental on-axis output pressure profile matches the design, exhibiting a focal depth of 11 mm. Initial experiments on the off-centered cylindrical lens CMUT verified the off-axis steering capability. The in-house software package calculated the PBV with an error of less than 5% for Doppler angles less than 40° in a flow phantom.

Discussion and Conclusions

A new screening method for carotid stenosis is proposed. We have completed the first generation 5-plane CMUT arrays. The arrays showed excellent element-to-element uniformity, and are suitable for the proposed application. Preliminary experimental results validate the viability of the asymmetric acoustic lenses. An in-house software package has been developed for PBV calculation once the five color flow Doppler images are obtained.

CMUT Design Equations for Optimizing Noise Figure and Source Pressure

Ira Wygant^{1,2}, Mario Kupnik², Butrus Khuri-Yakub²; ¹National Semiconductor, USA, ²Stanford University, USA

Background, Motivation and Objective

We previously demonstrated that a 1D spring-mass-damper model accurately describes a circular CMUT cell's electromechanical behavior. This model enables efficient transient simulations and a straightforward derivation of the small-signal equivalent circuit. The work presented here extends this analysis to develop simplified high-level design equations that estimate source pressure and noise figure at the CMUT's center frequency.

Statement of Contribution/Methods

Several assumptions simplify the analysis. We assume a clamped thin plate, negligible deflection due to atmospheric pressure, a dc bias voltage close to the pull-in voltage, and a plane-wave radiation impedance. Medical imaging CMUTs, for example, typically satisfy these criteria with the exception that the bias voltage may vary between 50% and 90% of the pull-in voltage and the real part of the radiation impedance is less than the plane-wave impedance. Despite these approximations, the resulting equations provide a useful design starting point and show how performance varies with the design variables.

Results

Expressions (1-3) give the CMUT cell thickness (t), radius (a), and gap (g0) in terms of the mechanical resonance frequency (f0), quality factor (Q), pull-in voltage (Vpi), and material properties (E, ρ, and ν). We evaluate each expression using values (a-g), which are typical parameters for a 2D array element and a low-power amplifier. Assuming the bias voltage equals the pull-in voltage we calculate an equivalent parallel resistance and capacitance at resonance (4-5). The term γ describes the parasitic capacitance. Classic two-port noise analysis gives the noise figure, (6), in terms of the amplifier’s input-referred noise. To estimate the transmit pressure, (7), we assume the pulse voltage is a fixed percentage, 20%, of the pull-in voltage. We also derive (6) and (7) for an ideal parallel-plate transducer, which for values (a-g) shows a 0.5-dB improvement in noise figure and a 70% increase in source pressure compared with a circular CMUT cell.

Discussion and Conclusions

These results show that increasing Q and Vpi increase source pressure at the expense of bandwidth and a higher transmit voltage; for minimum noise figure, the design optimum depends on the amplifier’s noise parameters. Using (1-7), we can quickly estimate a CMUT design and its performance for a variety of ultrasound applications.

$$\begin{aligned}
 f_0 &= 10 \text{ MHz} \quad (\text{a}) \\
 Q &= 0.3 \quad (\text{b}) \\
 V_{pi} &= 100 \text{ V} \quad (\text{c}) \\
 A &= 250 \mu\text{m} \times 250 \mu\text{m} \quad (\text{d}) \\
 \epsilon_0 &= 5.8 \text{ nF}/\sqrt{\text{Hz}} \quad (\text{e}) \\
 I_0 &= 10 \text{ fA}/\sqrt{\text{Hz}} \quad (\text{f}) \\
 R_{int} &= 1.5 \text{ MRays} \quad (\text{g}) \\
 t &= 0.543 \frac{R_{int} Q}{\rho \omega_0} = 17.7 \mu\text{m} \quad [1] \\
 a &= \frac{1.27}{\omega_0} \sqrt{\frac{QR_{int}}{\rho}} \sqrt{\frac{E}{1-\nu^2}} = 26.4 \mu\text{m} \quad [2] \\
 g_0 &= 1.87 \left(\frac{\epsilon_0^2 I_0^2}{R_{int} Q \omega_0} \right)^{1/3} = 274 \text{ nm} \quad [3] \\
 R_p &= 1.54 \frac{R_{int}}{\epsilon_0 A Q \omega_0} = \frac{2.88}{A} \left(\frac{V_{pi}}{\epsilon_0 \sqrt{R_{int} Q^2 \omega_0^2}} \right)^{2/3} \\
 &= 40 \text{ k}\Omega \quad [4] \\
 C_p &= 1.22 \frac{\epsilon_0 A}{g_0} = 0.65 A \left(\frac{\epsilon_0^2 QR_{int} \omega_0}{V_{pi}^2} \right)^{1/3} = 2.5 \text{ pF} \quad [5] \\
 F &= 1 + 0.72 \frac{1}{AKT} \left(\frac{V_{pi}}{\epsilon_0 \sqrt{R_{int} Q^2 \omega_0^2}} \right)^{2/3} I_0^2 + \\
 &\quad 0.087 \frac{A}{kT} \left(\frac{\epsilon_0 Q^2 \omega_0^2 \sqrt{R_{int}}}{V_{pi}} \right)^{2/3} (1 + \frac{3.5(\gamma+1)^2}{Q^2}) \epsilon_0^{-2} \\
 &= 6.1 \text{ dB} \quad [6] \\
 T_{sr} &= 0.59 \left(\frac{\epsilon_0 (R_{int} Q \omega_0)^2}{V_{pi}} \right)^{1/3} \frac{V_{pi}^2}{5} = 490 \text{ kPa} \quad [7]
 \end{aligned}$$

P2-Q-04

Modeling the Pulse-echo Response of a 2D CMUT Array Element

F. Yalcin Yamaner¹, Ayhan Bozkurt¹; ¹Faculty of Engineering and Natural Sciences, Sabanci University, Istanbul, Turkey

Background, Motivation and Objective

Front-end integrated circuit design for 2D ultrasonic array elements is challenging due to reduced element sensitivity. The pulse driver and return echo amplifier circuits can be optimized by the use of a precise circuit model of the transducer array at the design stage. An equivalent circuit that models transmit and receive operations of the array enables the matching of the IC to the transducer. This helps the designer to optimize the front-end IC before fabrication.

Statement of Contribution/Methods

In this paper, we present an equivalent circuit model for a 2D CMUT array element to assess the overall pulse-echo behavior. The circuit is a modified version of the conventional model in which the radiation term in the Mason equivalent circuit has been replaced by the RLC network to model the finite size of the transducer. The new circuit includes (i) an RC network to model the frequency dependent diffraction losses and attenuation in the transmitted and reflected acoustic waves, (ii) transmission lines for propagation delays, (iii) a VCVS to model the reflection from the imaging surface (which is the oil-air interface in our experiments). Component values of this model circuit were calculated using analytic expressions for the electro mechanic transformer ratio of CMUTs, based on the work in [1] and [2]. Pulse-echo measurements were carried out using a front-end IC designed in AustriaMicroSystems H35 high-voltage CMOS technology. An array element of 14x14 CMUT elements of 20 fEm radius and 1 fEm membrane thickness was wire-bonded to the IC. The resulting pulse and pulse echo response responses were then compared to the simulation results based on the developed model.

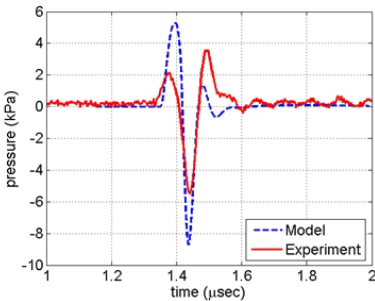
Results

The equivalent circuit model was verified by running simulations on Cadence Spectre. The post-layout extracted netlist of the IC is combined with the proposed equivalent circuit that models the wire bonded array elements. The elements were fired with a unipolar pulse of 20 Volts and the signal at the amplifier output was than compared to the experimental data. Figure 1 shows a comparison of the experimental data and simulation result.

Tuesday
Poster

Discussion and Conclusions

We demonstrated that the information obtained from the pulse-echo model is consistent with experimental results and can be used for further IC designs to enhance overall system performance.



P2-Q-05

Modeling of Capacitive Micromachined Ultrasonic Transducer (cMUT) for Harmonic Balance Analysis

Huseyin Oguz¹, Selim Olcum¹, Niyazi Senlik¹, Abdullah Atalar¹, Hayrettin Koymen¹; ¹Electrical and Electronics Engineering, Bilkent University, Ankara, Turkey

Background, Motivation and Objective

Finite element method (FEM) simulation packages are powerful tools and used for analysis of cMUTs extensively. FEM transient dynamic analysis is particularly useful to observe nonlinear behavior of the membrane. Although, FEM analysis predicts the performance of a particular design very well, excessive time required for the simulation makes it unsuitable for the design stage. Conversely, *harmonic balance* analysis provides an accurate estimate of the response of nonlinear circuits very quickly.

Statement of Contribution/Methods

It is inadequate to terminate Mason's mechanical LC section by a rigid piston's radiation impedance for an immersed cMUT. Transient FEM analysis reveals that the radial distribution of both the fundamental component and the harmonics in the membrane displacement can be modeled as clamped radiators given in [1]. We used the *normalized radiated power of a clamped radiator* definition in [1] to model the radiation impedance of a cMUT membrane.

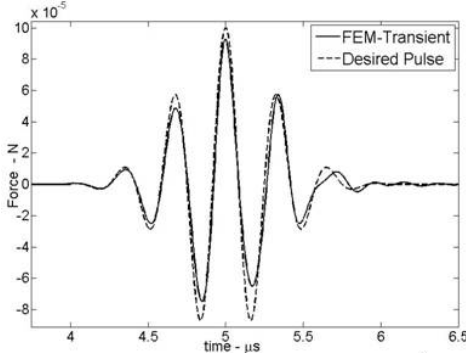
Results

Also we employed the root mean square (rms) of the velocity distribution on the membrane surface as the equivalent circuit variable rather than the average velocity. With this definition of the through variable, the kinetic energy of the membrane mass is preserved in the model. The inductance in the new equivalent circuit is equal to the mass of the membrane as opposed to 1.8 times the mass, which is the case in Mason's model. In order to preserve the resonance frequency in vacuum, the stiffness of the membrane becomes 1.8 times of the Mason's expression. We employed the linear parametric model for membrane mechanics and modified them to match the rms velocity definition.

Discussion and Conclusions

We derived the force and current equations for a clamped radiator and implemented them using a harmonic balance simulator. We observed much better agreement between FEM and the proposed equivalent model, compared to the conventional model. Using the equivalent model equations and parameters, we demonstrated the use of the proposed method by designing a desired radiating acoustic signal at the output and calculated the required excitation voltage, which is then tested in FEM transient analysis and resembled the desired pulse shape.

[1] Greenspan, M. "Piston radiator: Some extensions of the theory," J. Acoust. Soc. Am. Vol. 65, pp. 608-621



(1979).

P2-Q-06

Basic Studies of Application of Piezoelectric Chiral Polymeric Film Improved by Supercritical Carbon Dioxide Treatment to Sound Shielding Technology

Yoshiro Tajitsu¹, Yoshiro Tajitsu^{2,1} *Electrical Engineering Department, Kansai University, Suita, Osaka, Japan, ²Kansai University, Japan*

Background, Motivation and Objective

We have reported a novel technique for controlling the elastic coefficient of piezoelectric lead zirconate titanate (PZT) by connecting an electric circuit that behaves as a "negative capacitor" (negative-capacitance circuit(NCC)) [1]. In other words, NCC softens the piezoelectric material. Also, NCC shows the effect when the material has the large piezoelectric constant. Our goal is to apply our novel technique to sound shielding in the surrounding of the daily life. However, it is difficult to get PZT ceramics with a large area and flexibility. Thus, we plan to use the chiral piezoelectric polymer film, such as poly-L-lactic acid (PLLA).

Statement of Contribution/Methods

PLLA was subjected to supercritical carbon dioxide (s-CO₂) treatment to change its high-order structure, realizing an improvement in its piezoelectricity. The NCC experimental procedure is as follows: First, the PZT (left side in Fig. 1) was vibrated using a pulse oscillator. The elastic waves propagated in the order of the left brass bar, the center sCO₂-PLLA film connected to the NCC, and the right brass bar, as shown in Fig. 1. Finally, the elastic waves were measured using the detection PZT attached to the right end brass bar.

Results

The piezoelectric constant of sCO₂-PLLA film was five times that of PLLA film fabricated by the conventional method. From observation by atomic force microscopy, it was found that, upon treatment with s-CO₂, the grain structure in sCO₂-PLLA film becomes homogeneous, compared with that in PLLA film without s-CO₂ treatment. Next we found in the NCC experiment that the maximum attenuation factor in transmission loss of sCO₂-PLLA film connected to the NCC was about 20 dB.

Discussion and Conclusions

The attenuation factor of sCO₂-PLLA film was markedly improved compared to the results (3dB) of PLLA film without s-CO₂.

[1] Y. Tajitsu, K. Tahara, H. Ueda, K. Imoto, M. Date and E. Fukada: *Ferroelectrics*, 351, 43, 2007.

Tuesday
Poster

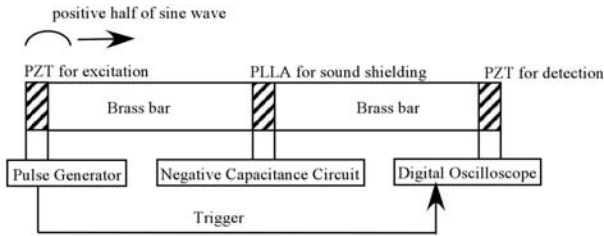


Figure 1 Schematic diagram of experimental system.

P2-Q-07

PMN-PT Piezoelectric Thick Film For High Frequency Ultrasonic Transducer Applications

Benpeng Zhu¹, Qifa Zhou¹, K.Krik Shung¹, Y.H Huang^{2,1} *University of Southern California, USA, ²Chemat Technology Inc., USA*

Background, Motivation and Objective

Many applications of very high frequency (>100MHz) ultrasound are envisioned including eye, skin and intravascular imaging. It is very difficult and time-consuming to lap down and mechanically machine very thin piezoelectric ceramics or crystal in the fabrication of high frequency single element transducers and arrays. Therefore, piezoelectric thick-film technology is an attractive low-cost alternative. The permittivity of the thick film, a crucial parameter, plays an important role in the electrical impedance matching of transducers to the electronic system because the electrical impedance of the element is inversely proportional to the permittivity of the piezoelectric material. With the miniaturization of the transducer and array, there has been more demand for high dielectric constant piezoelectric thick films, especially for high frequency applications.

Statement of Contribution/Methods

This paper reports the fabrication and testing of 12 μm piezoelectric 0.65Pb(Mg1/3Nb2/3)O3-0.35PbTiO3 (PMNPT) thick film on the (111) Pt/Ti/SiO2/Si substrate using a ceramic power/sol-gel solution modified composite method. The PMNPT composite solution was prepared from PMNPT powder (Chemat Technology Inc.) and PMNPT solution (0.4M) in mass ratio 1: 4. A 1-min rapid thermal anneal (RTA) at the desired temperature was performed to crystallize each layer.

Results

X-ray diffraction analysis and scanning electron microscope revealed that the film was in the well-crystallized perovskite phase and cracked free. The film exhibited good dielectric and ferroelectric properties. At 1 KHz, The dielectric constant and the loss were 2100 and 0.037, respectively. The remnant polarization was 17.2μC/cm2 at room temperature. A high frequency single element acoustic transducer was designed and fabricated with the PMNPT thick film. It showed a bandwidth at -6 dB of 30% at 120 MHz without matching layer.

Discussion and Conclusions

The dielectric constant of the film was much larger than those of the PZT films reported in the literature and previous work. Due to piezoelectric properties and large dielectric constant, PMNPT thick film is one of promising candidates for high frequency ultrasound linear array. The fabrication of this kind of array is ongoing.

P2-Q-08

High-frequency Micromachined Ultrasonic Annular Arrays

Dawei Wu¹, Changgeng Liu², Qifa Zhou¹, Frank Djuth², Kirk Shung¹; *¹Biomedical Engineering, University of Southern California, Los Angeles, CA, USA, ²Geospace Research, Inc., El Segundo, CA, USA*

Background, Motivation and Objective

Annular arrays have many advantages – they are conceptually simple offering dynamic focussing for a large depth of field (DOF) with compact electronics. Often PVDF or copolymers are used in a kerfless form. For intravascular

Tuesday
Poster

ultrasound (IVUS) imaging, a small overall diameter (~ 1 mm), a large DOF and good signal levels are essential. Piezoceramics offers a good outcome if fabrication is possible. Dicing provides near ideal element independence for phase steering, however conventional dicing of circular elements is not possible and laser dicing can be expensive. In this work we explore MEMS technologies to fabricate miniature annular arrays.

Statement of Contribution/Methods

The 1.3-mm aperture array comprises six equal area (0.25 mm^2) rings separated by $16\text{-}\mu\text{m}$ kerfs. 1500 \AA of Cr/Au was sputtered onto a polished CTS-3023HD PZT disc, and patterned to form a seed layer for electroplating nickel as a hard mask. Inductively Coupled Plasma Reactive Ion Etching (ICP-RIE) SF6 dry etching was then used to etch the kerfs to a depth of $\sim 25 \mu\text{m}$. The kerfs were filled with Epotek-301 and the surface lapped leaving the diced ceramic. The Cr/Au layer was re-patterned to form the electrodes, Epotek-301 loaded 25% by weight with tungsten powder used as a backing. The un-etched (front) side was lapped to attain a $20 \mu\text{m}$ sample thickness, and Cr/Au sputtered onto it and a brass mount to provide the ground connection; a $6\text{-}\mu\text{m}$ parylene layer was added for matching. Ultrasonic wire bonding was used to connect the array electrodes to the micro-coaxial cable connectors.

Results

Piezo-CAD modeling indicates a 100 MHz centre frequency and 45% bandwidth (6 dB), an insertion loss of 20 dB (two-way) and $\sim 10 \Omega$ impedance. The nearest-element crosstalk was found to be between -20 dB and -35 dB (80-120 MHz) with PZFlex. The SEM indicates the sharp etched edges, the profile angle is 86 degrees. Measurements show a water loaded 107 MHz centre frequency with 9Ω impedance, and a thickness coupling coefficient of 0.52. Further characterization of the array including pulse-echo, radiation patterns, etc will be presented.

Discussion and Conclusions

A miniature 100 MHz annular array made using microfabrication techniques has been realized. MEMS dry etching shows great promise in the fabrication of miniature devices e.g. IVUS arrays. Modeling results and preliminary measured data of the array are very promising.

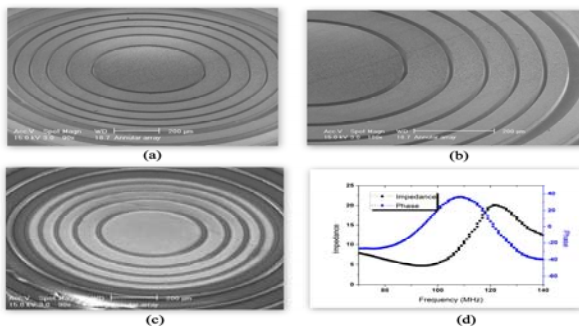


Fig.1: (a) and (b) are side view of the etched array; (c) is the array after patterning electrodes and filling the kerfs; (d) is the measured electrical impedance.

P2-Q-09

Characterization of cMUT by Digital Holography Microscopy

Nicolas S en egond¹, Dominique Certon¹, Jean-Edouard Bernard¹, Franck Teston¹, ¹UMR Universit e Fran ois Rabelais de Tours INSERM U930 CNRS ERL3106, France

Background, Motivation and Objective

The comparison of numerical simulations to real cMUT behavior is essential to adapt and perform the process. In order to characterize all the physical parameters of cMUT, several devices were employed (FIB, SEM, impedance meter, laser interferometer, etc). In this context, we propose to use a full-field measurement device, a Digital Holography Microscopy (DHM), which acquires static and dynamic in-plane and out-of-plane measurements of many membranes with single acquisition and then provides most of required parameters. This paper presents the principle of this device, its performances comparing to other ones and its limits.

Statement of Contribution/Methods

DHM (LynceTec®) generates cMUT 3D images using the principle of holography. Holograms are induced by combining a coherent reference wave with the wave received from the cMUT by reflection and recorded by a CCD camera. Their reconstructions are dealt numerically in real-time and provide an intensity image and a phase image where out-of-plane quantitative data are extracted. The dynamic acquisition is provided with a stroboscopic module up to 100 kHz (under this value, the acquisition real-time is sufficient) and synchronized with the cMUT applied excitation.

Results

Complete characterization array element based on $20 \times 20 \mu\text{m}^2$ and $25 \times 25 \mu\text{m}^2$ square shape cMUT was conducted. At first, a static analysis is managed: roughness and widths of different layers as well as gap height are calculated. The initial deflections of membrane and variations of their displacements with the DC bias voltage value are measured on large cell populations. With the help of Finite Element Model, these measurements allow computing initial stress and Young modulus of layers. Lastly, a temporal study is performed: cMUT element is excited by a several MHz frequency sinusoid signal on which a continuous voltage is superimposed and membranes motions are acquired.

Discussion and Conclusions

Collapse voltage and deflection depending on bias voltage are compared and present good agreements with data extracted from impedance analyzer. We show that relative deviation is due to the disparity of cMUT cell population. The evolution of membrane shape during sinusoid excitation is compared to measurement with laser heterodyne interferometer. DHM presents advantage of a full-field acquisition but is limited by its stroboscopic working frequency. Limits of this device are then discussed. Indeed, while out-of-plane width is around the half of laser wavelength (around 340nm), measurement is very difficult to extract from phase information. Finally, DHM adds to cMUT characterization by its ability to obtain both statistical and local cMUT behavior: it is midway between local characterizations obtained by interferometry and full-element characterizations by impedancemetry.

P2-Q-10

Transurethral ultrasound catheter-based transducer with flexible polyimide joints

Martin Culjat¹, Aaron Dann², David Bennett², Hua Lee³, Warren Grundfest², Rahul Singh^{3,1} *Center for Advanced Surgical and Interventional Technology (CASIT), UCLA, Los Angeles, CA, USA, ²UCLA, USA, ³UCSB, USA*

Background, Motivation and Objective

Prostate cancer is the most common non-skin cancer found in men in the U.S. and is the second leading cause of cancer death in men. Improved imaging techniques may not only further reduce deaths by increasing the ability to detect prostate cancer, but may also improve surgical outcomes and monitoring. Ultrasound imaging techniques, such as transrectal ultrasound (TRUS), are ideal for pre-, intra-, and post-operative imaging of the prostate. However, TRUS is limited in resolution and by shadowing. Transurethral ultrasound (TUUS) imaging may enable higher resolution imaging due to shorter required penetration depth, and at the same time eliminate shadowing effects that are prevalent in TRUS by imaging from within rather than through the prostate.

Statement of Contribution/Methods

A TUUS transducer has been developed that features a 2D array of piezoelectric elements embedded within a catheter body. Fabrication of the arrays has been made possible with a highly durable MEMS-based microfabrication process that allows the array to be rolled to the desired curvature with flexible polyimide joints, greatly simplifying fabrication of the cylindrical transducer.

Results

A transducer prototype was fabricated and features bulk lead zirconate titanate (PZT) elements mounted on an array of silicon islands formed by partitioning a silicon wafer via deep reactive ion etching (DRIE). Polyimide was patterned to form bendable joints, which allow substrate flexibility and encapsulate metal film interconnects. The silicon islands fulfill the dual roles of mechanical substrate and acoustic matching layer to soft tissue in conjunction with a deposited parylene film. Polyimide was selected because it is mechanically strong, readily patternable by photo-lithographic techniques, and resistant to chemicals used in microfabrication processes. The prototype 2×28 element TUUS transducer prototype has 400 μm element width, 500 μm pitch, and a pulse width of 300 ns in water. The transducer joints have withstood more than 10,000 bending cycles without visible damage or measurable deterioration of the interconnects.

Discussion and Conclusions

Flexible TUUS transducers were successfully fabricated and tested, with the transducer fabrication technology allowing for scaling to smaller element dimensions, larger array sizes, and to small diameter catheters. TUUS has the potential to provide considerable improvement to prostate imaging, image guidance, and monitoring as a new high resolution, real-time imaging tool.

P2-R. Various Transducer Topics

Sala Orange

Tuesday, September 22, 2009, 10:00 am - 11:30 am

Chair: **Mark Schafer**
Sonic Tech

P2-R-01

Extension of CHOTs technology to the optical generation and detection of very high frequency elastic waves: Evanescent Cheap Optical Transducers (eCHOTs)

Ahmet Arca¹, Theodosia Stratoudaki¹, Richard J. Smith¹, Matt Clark¹, Mike Somekh¹; ¹*Division of Electrical Systems and Optics, Faculty of Engineering, Nottingham University, Nottingham, United Kingdom*

Background, Motivation and Objective

Cheap Optical Transducers (CHOTs) have been demonstrated for the generation and detection of elastic waves at typical NDE frequencies between 0.5 and 100MHz. In this paper, we discuss how the CHOT operates and how this breaks down at high frequencies. We also show that it is possible to extend the frequency range upwards towards the multi GHz region using a new evanescent wave CHOT.

The “evanescent” CHOT has a different mode of operation from the normal CHOT, since the latter depends on diffracted orders, whereas such orders are evanescent for the excitation wavelength in the former. In this study we show how the operation principles and specifications of CHOTs [1] are affected by the move to very high frequencies to eCHOTs [1].

Statement of Contribution/Methods

We have designed and optimized these transducers using Finite Element modelling to link the physical displacements caused by the elastic waves with the optical behaviour. In addition to operating in the very high frequency regime the new eCHOT exhibits higher sensitivity and a wider window of operation making it an ideal candidate for GHz / nano scale ultrasonics.

Results

We have found that even though the superficial geometry of the eCHOT is similar to that of CHOTs [1], their operation is fundamentally different. While the CHOTs depend on an energy gain-loss system dominated by the diffracted orders, the eCHOTs depend on a system dominated by resistive heating losses as there are no diffraction orders. By optimizing this mechanism we can show enhanced sensitivity over a wider range of parameters than possible with a device designed for conventional CHOT specifications

Discussion and Conclusions

We have extended the range of operation for CHOTs transducers up to and beyond the optical resolution limit by introducing a sub-wavelength mechanism which can be remotely operated in order to generate and detect surface acoustic waves in the range of GHz. We have verified that the operation of this small ultra-high frequency device is dependent on the increase and decrease of resistive heating as the device interacts with

the surface acoustic wave. This suggests that more exotic structures could be built to enhance the sensitivity of these devices.

[1] T. Stratoudaki, J. A. Hernandez, M. Clark, and M. G. Somekh, Cheap optical transducers (chots) for narrowband ultrasonic applications," Measurement Science and Technology, vol. 18, 2007.

P2-R-02

Lowering the centre-frequency of thick film PZT devices using acoustically matched backing layers

Stephen Ellwood¹, Steven Freear¹; ¹*Ultrasound Group, School of Electronic and Electrical Engineering, The University of Leeds, Leeds, West Yorkshire, United Kingdom*

Background, Motivation and Objective

Our current research effort is directed towards fabricating PZT thick-films for use in industrial process monitoring transducers.

The use of thick films in this application confers a number of benefits. The tape casting method permits rapid and straightforward fabrication of ultrasound devices onto both flat and curved metal surfaces in arbitrary shapes. Additionally, the non-invasive device placement on the process vessel exterior improves reliability and eliminates the requirement for problematic coupling media.

Despite the promise shown by this technique, a major obstacle remains: the low-thickness of the deposited film devices. This leads to generation of ultrasound at relatively high frequencies (eg 40MHz for 50 μ m film). These high frequencies are problematic for two main reasons.

Firstly high-frequency sound is attenuated more readily than lower frequencies, limiting the maximum attainable penetration depth. Secondly, to achieve good quality synthetic aperture imaging reconstruction transducers are required to act as point sources. Point sources at such high frequencies are difficult to achieve because the lateral transducer dimensions required are comparable to the device wavelength. These wavelengths are small at such high frequencies.

In this paper we suggest a technique that can be used to lower the centre-frequency of the sound generated by a film device of a given thickness. We provide theoretical arguments and modelling results to prove the efficacy of this technique.

Statement of Contribution/Methods

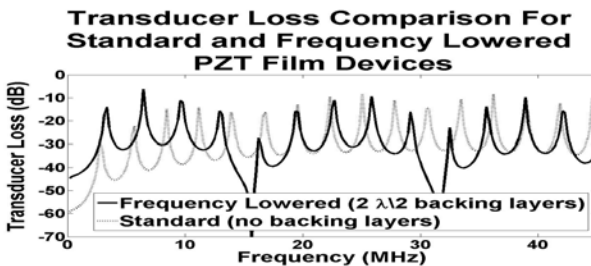
The centre frequency of the film devices is lowered by attaching a number of impedance-matched half-wavelength acoustic backing layers to the active PZT film layer. This lowers the centre frequency of the device with a minimal change in device transducer loss at other frequencies.

Results

The new design demonstrates improved low-frequency performance. An improvement in transducer loss of up to 8dB is achieved over the frequency range 0-10MHz.

Discussion and Conclusions

Here we present the design of a PZT thick-film derived process measurement transducer with improved low-frequency performance. The transducer loss of this new design is improved by up to 8dB in the frequency range 0-10MHz. This is in comparison with equivalent existing devices that lack the additional backing layers and other improvements described in this paper.



Edge-Connected, Crossed-electrode Array using Non-linear Transducer

Ichiro Fujishima¹, Yasutaka Tamura¹, Hiroataka Yanagida¹, Jyubei Tada¹, Tatuhisa Takahashi²; ¹Informatics, Yamagata University, Yonezawa, Yamagata, Japan, ²Mathematical Informaton Science, Asahikawa Medical Colege, Asahikawa, Hokkaido, Japan

Background, Motivation and Objective

Two-dimensional transducer arrays are key devices for various ultrasound applications such as 3-dimensional imaging and biomedical treatment. However, two dimensional arrays require a huge number of elements which should be connected to electronic signal channels. This rises cost of the electronic circuits. Connection between the elements and the circuits has technical difficulties such as cross-talk and cable assemblies.

H. C. Schau proposed 2-dimensional array structure of edge-connected, crossed-electrode array. The proposed 2-dimensional array permits the control of $M \times N$ elements with $N + M$ signal channels. Schau's crossed-electrode array, however, dose not have ability of 2-dimensional beam-steering.

The objective of our research is to realize a two dimensional array which enables us to form arbitrary transmitting wavefront using the edge-connected, crossed-electrode geometry.

Statement of Contribution/Methods

To solve the problems of Schau's array, we have proposed to adopt nonlinear electromechanical coupling devices to the edge-connected, crossed-electrode structure. This new structure permits arbitrary beam steering with decreased cost and complexity of the electronic drive circuit.

We have proposed several conversion methods of generating two sets of drive waveforms for row and column electrodes from given 2-dimensional wavefront. In this paper, we describe a conversion method for continuous sinusoidal wave which utilizes difference frequency between the low and column electrodes.

A high efficient nonlinear electromechanical coupling devices is needed for our purpose. We have proposed an edge-connected, crossed-electrode capacitive transducer array, and constructed the array operates in air for the preliminary experiment.

Results

In the preliminary experiment, the ability of generating focused acoustical sound wavefronts using the difference frequency method was demonstrated. Accuracy of focus position was evaluated for two calculating methods using computer simulations.

Discussion and Conclusions

We proposed an edge-connected, crossed-electrode 2-dimensional array using nonlinear electromechanical coupling transducers. We also proposed signal processing method to generate the sets of driving signals. This geometry requires only $N + M$ electrode leads to drive $N \times M$ elements for arbitrary waveform generation.

We described an edge-connected, crossed-electrode capacitive transducer array operates in air. The preliminary constructed array demonstrated the ability of focusing wavefront of continuous sinusoidal wave using the difference frequency method.

Feasibility Study of a Membrane-type Magnetostrictive Acoustic Transducer for Ultrasonic Thrombolysis

Seung Hyun Cho¹, Hong Jin Kim², Yoon Young Kim²; ¹Center for Safety Metrology, Korea Research Institute of Standards and Science, Daejeon, Korea, Republic of; ²School of Mechanical & Aerospace Engineering, Seoul National University, Seoul, Korea, Republic of

Background, Motivation and Objective

It is well known that ultrasound helps increase the efficiency of thrombolysis when used together with tissue plasminogen activator. Recently, a catheter device mounting a piezoelectric ultrasonic transducer on its tip has been proposed. However, this device has some limitations because the supply of high-voltage electric power to piezoelectric elements in the transducer can be dangerous to a human. To overcome this limitation, the use of a magnetostrictive acoustic transducer instead of piezoelectric one was considered. A magnetostrictive transducer can generate ultrasound by the magnetic field not by electric field. So, flowing electric current inside of a human body is not necessary since magnetic field can be applied to the magnetostrictive transducer wirelessly outside of a human body. The objective of this work is to investigate the feasibility of a magnetostrictive transducer as a device for thrombolysis.

Statement of Contribution/Methods

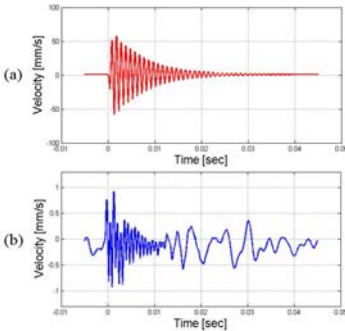
In this feasibility study, the research was focused on the shape or configuration of a magnetostrictive transducer so a scaled-up transducer was considered and experiments were conducted to examine the transducer performance in water. Specifically, a membrane-type magnetostrictive transducer was considered since a membrane shape was thought to be more appropriate to generate ultrasound than a cylinder block shape. The transducer comprises a thin magnetostrictive membrane, two permanent magnets for bias magnetic field. The membrane was made of nickel or iron-cobalt alloy. For experiments, the transducer was submerged under water and actuated. Then the velocity of water surface was measured by a laser vibrometer to evaluate the efficiency of the ultrasound generation by the transducer. A conventional hydrophone was not used to exclude the effect of electrical crosstalk from the excitation coil.

Results

Figure 1 shows the measured velocities of the magnetostrictive membrane of the transducer and the water surface when pulsed magnetic field was supplied.

Discussion and Conclusions

The results show that the membrane vibration was effectively transferred to acoustic wave in water. This means that the proposed transducer using a thin magnetostrictive membrane can be a potential device for ultrasonic thrombolysis. The effects of excitation current and bias magnetic field intensity on the membrane vibration were also investigated.



P2-R-05

Linear hydrophone arrays for measurement of shock wave lithotripter acoustic fields

Jeffrey A. Ketterling¹, Paul Lee¹, Wayne Kreider², Michael R. Bailey², Robin Cleveland³; ¹Lizzi Center for Biomedical Engineering, Riverside Research Institute, New York, NY, USA, ²Applied Physics Laboratory, University of Washington, Seattle, WA, USA, ³Department of Mechanical Engineering, Boston University, Boston, MA, USA

Background, Motivation and Objective

Lithotripter acoustic field characterization is based on single-element hydrophone measurements even though many clinical lithotripters do not have highly repeatable sound fields. The ability to instantaneously capture the acoustic field at many points would permit more accurate characterization of lithotripters and would have broad implications for advancing the understanding of how lithotripters fragment stones and damage kidney tissue. Here, linear hydrophone arrays composed of 20 elements measuring 0.5 by 0.5 mm and spaced 1.25 mm center to center are described and characterized.

Statement of Contribution/Methods

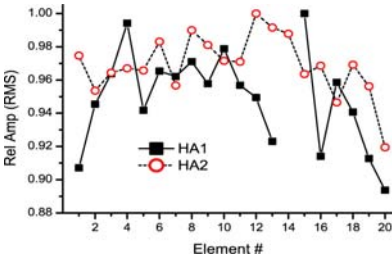
Two arrays were fabricated by bonding a 9 μm piezopolymer film to a flex circuit containing an array pattern formed using standard printed-circuit-board etching techniques. After bonding, the devices were backed with an epoxy plug in order to provide structural support and the plug was secured in an acrylic mount. A 30 cm ribbon cable connected the array to an interface box that then fanned out to standard coaxial cables of 2.1 m length. The sensitivity of each hydrophone element was measured using a 5.25 MHz focused transducer with an annular element (35 mm focal length, 7.1 mm ID, and 9.45 mm OD) as the source. Excitation consisted of a 14-cycle tone burst and measurements were made at a distance of 41 mm in order to broaden the pressure field relative to the hydrophone element size. A preamp was used prior to digitizing the signals.

Results

RMS voltages were measured for each hydrophone element for a peak-incident pressure of 4.5 kPa and the values were normalized across each array. The normalized RMS voltages were quite uniform across each array and between arrays (Fig. 1, HA1: mean = 0.95 and $\sigma = 0.029$; HA2: mean = 0.97 and $\sigma = 0.018$) with one non-functioning element (# 14 on HA1). Prior to amplification, the element voltages were ≈ 1 mV peak.

Discussion and Conclusions

The linear hydrophone arrays had very consistent performance element to element. For lithotripter pressure levels on the order of 40 MPa, the arrays are expected to generate ≈ 9 V peak and no pre-amplification will be necessary. Digitizing the array channels simultaneously will permit an instantaneous measurement of the acoustic field in one dimension. The next phase of testing will determine element lifetime when exposed to repeated lithotripter shockwaves. [Work supported by NIH DK081119]



Tuesday
Poster

Wednesday Oral Sessions

1H. Optical and Photoacoustic Imaging

Sala Orange

Wednesday, September 23, 2009, 8:00 am - 9:30 am

Chair: **Stanislav Emelianov**
Univ. of Texas at Austin

1H-1

8:00 AM **Orthogonal Unipolar Golay Codes for Multispectral Photoacoustic Coded Excitation Imaging**

Martin P. Mienkina¹, Annika Eder¹, Claus-Stefan Friedrich², Nils C. Gerhardt², Martin R. Hofmann², Georg Schmitz^{1,2} *¹Institute of Medical Engineering, Ruhr-University Bochum, Bochum, Germany, ²Institute of Photonics and Terahertz-Technology, Ruhr-University Bochum, Bochum, Germany*

Background, Motivation and Objective

In photoacoustics (PA) ultrasound is generated by laser irradiation of tissue. By employing multiple light wavelengths for PA imaging, it is potentially possible to derive clinically relevant tissue parameters like total hemoglobin concentration and blood oxygen saturation. Commonly, Nd:YAG lasers in combination with optical parametric oscillators are used as sources for spectroscopic PA but it would be desirable to use less expensive laser diodes instead, which emit light at several wavelengths in the near infrared spectrum. Since laser diodes combine low pulse energy with high pulse repetition frequency (PRF) compared to Nd:YAG lasers, averaging procedures can be employed to increase the SNR. In order to prevent range ambiguities the PRF of the laser diodes must be limited to the inverse of the echo time.

Statement of Contribution/Methods

We propose to use coded excitation for pulsed PA to increase the PRF beyond this limit for higher SNR. Furthermore, by using orthogonal unipolar Golay codes (OUGC) it would be possible to acquire PA data generated by two laser diodes at two different wavelengths simultaneously and separate them afterwards. Emitting two wavelengths simultaneously increases the SNR gain per time unit and reduces motion artifacts. Thus, we derive a theoretical estimation of the SNR gain due to OUGC and demonstrate the feasibility of using multispectral PA coded excitation (MS-PACE) by experiments. Orthogonal Golay codes consist of 2 orthogonal pairs of complementary sequences. For MS-PACE the codes must be split into 8 unipolar sequences since no negative light emission is possible. Due to orthogonality, 2 specific sequences can be emitted simultaneously. For sending one code, 4 light emissions are necessary and 2 of the received ultrasound responses are subtracted before being correlated with the bipolar codes. For the experiments, a pulse pattern generator provides an 8 bit OUGC and synchronizes two pulsed laser diodes emitting light at 850 nm and 905 nm (both pulse duration 31 ns, PRF 5 kHz, pulse energy approx. 4 μ J) with a clinical ultrasound system (Ultrasonix Sonix RP), which is reconfigured for single channel data acquisition. The laser diodes irradiate a metal slab and the resulting PA signals are acquired using a 128 element linear array (L 14-5/38). The data sets are decoded and PA images are reconstructed using the synthetic aperture focusing technique.

Results

Based on the theoretical calculations the SNR gain ranges from 9.0 dB to 30.1 dB for code lengths between 8 bit and 1024 bit, respectively. The decoded multispectral PA images allow a clear discrimination between the signals generated by the two wavelengths, showing two adjacent illumination spots. The SNR gain due to coding is calculated as 8.1 dB for 905 nm (code 1) and 8.5 dB for 850 nm (code 2), respectively.

Discussion and Conclusions

This work showed that MS-PACE using OUGC is a feasible technique for acquisition of PA signals simultaneously generated by two different light sources.

8:15 AM Contrast enhancement in photoacoustic imaging

Sheng-Wen Huang¹, Janet Eary², Congxian Jia³, Lingyun Huang¹, Shai Ashkenazi⁴, Matthew O'Donnell¹;
¹Bioengineering, University of Washington, Seattle, WA, USA, ²Radiology and Orthopedic Surgery, University of Washington, Seattle, WA, USA, ³Biomedical Engineering, University of Michigan, Ann Arbor, MI, USA, ⁴Biomedical Engineering, University of Minnesota, Minneapolis, MN, USA

Background, Motivation and Objective

To increase specific contrast over background absorption in photoacoustic (PA; also called optoacoustic) imaging, absorbing contrast agents such as gold nanoparticles can be functionalized to target specific cells. However, contrast may be severely limited because of PA signals from finite intrinsic background absorption. If background signals can be suppressed, the molecular dynamic range of contrast agents can be greatly expanded, enhancing contrast and therefore the sensitivity and specificity of PA imaging.

Statement of Contribution/Methods

We propose differential-absorption photoacoustic (DAPA) imaging for contrast enhancement. A pump beam illuminates the imaged object, changing absorption from unexcited ground-state absorption to transient absorption. Conventional PA imaging measures ground-state absorption, while DAPA imaging detects the difference between transient and ground-state absorption by subtracting the conventional PA image from a transient PA image taken after pump beam illumination. When parameters are properly chosen so that a region of interest has finite change in absorption whereas the background has negligible change, the DAPA image will provide high contrast between the region of interest and the background, resulting in background suppression. Finite changes in absorption can be obtained using photoluminescent molecules or contrast agents.

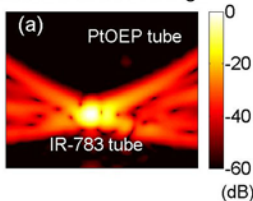
Results

Two tubes were imaged. One contains a Pt(II) octaethylporphyrine (PtOEP) dye solution and serves as an object of interest while the other contains an IR-783 (from Sigma-Aldrich) dye solution and serves as an object to suppress. The pumping and probing wavelengths were 532 and 760 nm, respectively. Although the IR-783 tube dominates the conventional PA image [Figure (a)], it is suppressed by over 40 dB and consequently significantly overwhelmed by the PtOEP tube in the DAPA image [Figure (b)].

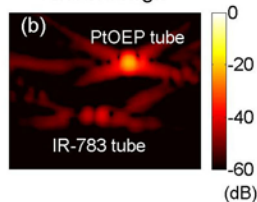
Discussion and Conclusions

The potential of DAPA imaging in suppressing undesired objects and spotting regions of interest has been demonstrated using PtOEP. To achieve enough penetration in biomedical applications of DAPA imaging, photoluminescent contrast agents that can be pumped between 600–800 nm, e.g. oxyphor G2 (Oxygen Enterprises, Philadelphia, PA), are preferred. Imaging depth in this mode has also been analyzed and will be presented.

conventional PA image



DAPA image



8:30 AM Free-hand 3D optoacoustic imaging of vasculature

Marc Fournelle¹, Holger Hewener¹, Hans-Joachim Welsch¹, Heinrich Fonfara¹, Robert Lemor¹; ¹Fraunhofer IBMT, Germany

Background, Motivation and Objective

Optoacoustic techniques allow imaging of tissue structures with optical contrast and acoustical resolution. This modality is ideal for visualization of blood vessels since haemoglobin is one of the best-absorbing tissue chromophores. It therefore can provide vasculature images with much higher contrast than pure ultrasound. If compared with standard techniques for blood imaging such as Doppler ultrasound, the advantage of optoacoustics

is scalability allowing a resolution down to several μm . The availability of biologically conjugated nanoparticles further allows using this technique for molecular imaging where a localization of the abundance of biomolecules is desired in 2D and 3D. The strong spectral dependence of blood absorption properties will potentially allow multispectral optoacoustics for investigation of oxygenation level. While the location and size of vessels can be obtained with optoacoustic b-scans, the understanding of the network requires 3D data. We propose the use of a stereo-camera in order to track the transducer position for fast and convenient acquisition of 3D optoacoustic data.

Statement of Contribution/Methods

Optoacoustic signals are generated using a q-switched Nd:YAG laser at 1064nm. The resulting signals are acquired by different linear 1d-array transducers in the range of 5 to 20 MHz and transferred to our multichannel hardware platform DiPhAS (Digital Phased Array System, Fraunhofer IBMT) for amplification and digitization. The position and orientation of the transducer are recorded using an optical position tracking system (Spectra, Northern Digital Inc) and handled with each measured data. Within seconds, a complex volume reconstruction is computed on an integrated PC based on an adapted optoacoustic software beamforming algorithm and position based 3d reconstruction. The resulting optoacoustic volume data can be viewed using common visualization techniques.

Results

The potentials of our system were evaluated on optoacoustic phantoms. Experiments were conducted using point absorber mimicking structures in order to characterize the 3d optoacoustic PSF for determination of volume resolution. For reconstruction, 2D and 3D sum-and-delay algorithms were implemented and evaluated. Further, we acquired first 3D optoacoustic in-vivo data of blood vessels in a human forearm. Vessel branches could be visualized with high contrast against background tissue.

Discussion and Conclusions

We combined optoacoustic imaging with freehand-3d-ultrasound reconstruction and were able to measure and visualize the 3d vascularisation of the forearm. The recording speed is limited by the Nd:YAG-laser-PRF of 20 Hz and results in 10 seconds needed to acquire 150 to 200 optoacoustic slices as input for 3d reconstruction. The system setup and operation can be improved by integrating a commercial electromagnetic tracking system into the transducer housing for easier probe handling in the future and a faster laser with higher PRF.

1H-4

8:45 AM High resolution optoacoustic detection of nanoparticles on living cells

Wolfgang Bost¹, Yvonne Kohl¹, Frank Stracke¹, Marc Fournelle¹, Robert Lemor¹, ¹Fraunhofer IBMT, Sankt Ingbert, Saarland, Germany

Background, Motivation and Objective

In optoacoustic imaging acoustical signals are generated when short light pulses are absorbed according to the absorption coefficient of the examined biological sample. This imaging modality combines advantageous features of optics and acoustics (high contrast and high resolution). To increase the intrinsic contrast in tissue, absorbing particles are of great interest because of their considerable capacity to absorb light at visible and near-infrared wavelengths. We developed a technology platform for optoacoustic imaging down to diffraction limited microscopy for in vitro detection of nanoparticle exposed cells. Different nanoparticles types were investigated regarding their suitability as optoacoustic contrast agent.

Statement of Contribution/Methods

Our high-resolution photoacoustic microscopy platform based on the SASAM[©] acoustic microscope (kibero GmbH, Germany) is designed for the investigation of optoacoustic contrast agents in cell cultures and allows a resolution down to 5 μm . It consists of an inverted optical microscope (Olympus IX 81, Japan), a kHz repetition rate Nd:YAG laser (Teem photonics, France) arranged in a confocal setup, the SASAM 1000 electronics system with different transducers attached allowing generation and detection of laser-induced ultrasound signals in a frequency range up to 400 MHz.

A critically underdeveloped area in optoacoustics is the development of contrast agents. Here we present a broad evaluation of different nanoparticles as photoacoustic contrast agents. Different particulate contrast agents like plasmon resonant gold particles, biodegradable polymeric nanoparticles and magnetite particles were synthesized and characterized. Cytotoxicity experiments were performed using two different cell culture systems and the cell viability was determined. Following three different times of exposure to the nanostructures and different concentrations, the cell viability was determined using cytotoxicity assays and Live/Dead staining.

Results

The -6 dB lateral resolution of the system was experimentally determined to 5 μm independently of the used transducer by measuring the point spread function. The high resolution allows high contrast imaging of cell systems charged with functionalized contrast agents. The in vitro cytotoxicity experiments did not show any cytotoxic effect till the concentration of 1×10^8 NP/ml. In addition, the cells were incubated with particles at a concentration of 50 $\mu\text{g/ml}$ and a high-resolution optoacoustic image could be obtained with high SNR.

Discussion and Conclusions

We demonstrate the suitability of our optoacoustic microscope for attending the development of new contrast agent types by characterizing them in terms of generated signal amplitudes. The synthesized particles are biocompatible and can be used as a contrast agent in biomedical imaging technologies. Current work focuses on modifying the particles for targeted delivery.

1H-5

9:00 AM **Optical coherence tomography: recent technical developments and the impact on clinical utility**

Melissa Suter¹, Brett Bouma¹, Guillermo Tearney¹; ¹Harvard Medical School, Boston, Massachusetts, USA

Background, Motivation and Objective

Optical coherence tomography (OCT) is a high-resolution ($<10 \mu\text{m}$), non-contact, optical imaging modality that provides cross-sectional images of tissue microstructure. The diagnostic potential of OCT has been successfully demonstrated in both gastrointestinal and coronary applications, however OCT to date has not been widely adopted as a clinically viable tool due in part to limitations in the imaging speeds achievable resulting in the acquisition of only very small fields of view.

Statement of Contribution/Methods

Optical frequency domain imaging (OFDI) is a high speed second generation OCT imaging technology that utilizes a rapidly tuned wavelength swept laser source to provide spectrally resolved interference between a sample arm and a stationary reference arm. The inherent signal-to-noise gains of OFDI as well as the high rates of the tuning laser result in significantly improved image acquisition speeds compared to conventional OCT, without sacrificing image quality. Coupled with appropriate catheter designs, optical rotary devices, and linear translation, OFDI images can be rapidly acquired in helical scanning patterns facilitating large area comprehensive volumetric microscopy of luminal organs.

Results

Volumetric OFDI images of the entire distal esophagus in patients undergoing routine screening and surveillance of Barrett's esophagus, a precursor to esophageal adenocarcinoma will be presented. The OFDI images show a variety of microscopic features that are consistent with histopathologic findings, including squamous mucosa, cardia, and specialized intestinal metaplasia both with and without dysplasia. In addition, in vivo comprehensive intracoronary OFDI of arterial segments approaching 5 cm in length will be presented. Thin-capped fibroatheromas, calcific nodules, macrophages, cholesterol crystals, thrombus, and stent struts both with and without neointimal hyperplasia will be highlighted.

Discussion and Conclusions

The ability to rapidly perform comprehensive microscopy of luminal organs using second generation OCT imaging technology may have a significant impact on current clinical practices. In the management of Barrett's esophagus where current screening and surveillance protocols suffer from biopsy sampling errors, comprehensive OFDI may aid in reducing this diagnostic uncertainty. Likewise, rapid in vivo comprehensive microscopy of long arterial segments may provide insights to the natural history and the management of coronary artery disease.

2H. Medical Imaging

Sala 2

Wednesday, September 23, 2009, 8:00 am - 9:30 am

Chair: **Anne Hall**
GE Healthcare

2H-1

8:00 AM **A comparison between methods for automatic quantification of global left ventricular function**

Daniel Barbosa¹, Gabriel Kiss², Piet Claus¹, Krasimira Hristova¹, Brage Amundsen², Dirk Loeckx³, Fredrik Orderud², Hans Torp², Jan D'hooge^{1,2}, ¹Cardiovascular Diseases, Catholic University of Leuven, Leuven, Belgium, ²Circulation and Medical Imaging, NTNU, Trondheim, Norway, ³Electrical Engineering, Catholic University of Leuven, Leuven, Belgium

Background, Motivation and Objective

Quantitative analysis of 3D cardiac ultrasound data requires a significant amount of user interaction. Recently, we introduced methods that could help in automating this process. On the one hand, an edge detection algorithm in combination with a deformable subdivision surface was presented for automatic segmentation of the LV cavity. A real-time, dynamic implementation (RCTL) of this approach allows tracking the subendocardial boundary throughout the cardiac cycle. On the other hand, an automatic 3D motion estimation algorithm was presented in which subsequent image volumes are elastically registered using a B-spline transformation field (splineMIRIT).

Global functional parameters such as stroke volume (SV) and ejection fraction (EF) can thus be estimated using either RCTL or splineMIRIT. The aim of this study was to contrast both methods for their accuracy in a clinical setting.

Statement of Contribution/Methods

3D data sets were acquired in 5 healthy volunteers and 8 patients with coronary artery disease at a frame rate of 28.1 ± 3.9 Hz (GE Vivid7, GE Vingmed, Norway). The end-diastolic (ED) volume was automatically segmented using RCTL and the resulting subendocardial mesh was then tracked using both RCTL and splineMIRIT. As a reference, both ED and end-systolic volumes were manually contoured using commercially available tools (EchoPac, GE Vingmed, Norway). From both automatically and manually defined volumes, SV and EF were derived. Correlations of the automatic methods against the reference method were made as well as a Bland-Altman analysis to determine agreement.

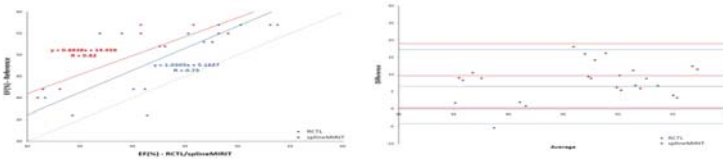
Results

The correlations and Bland-Altman plots for the EF are shown in Figure 1. The regression coefficients were not significantly different ($p=0.66$) with similar results for SV ($R=0.81$ and $R=0.86$). Bias and limits of agreement were -6.5 [-17.2 - $+4.2$]% and -9.6 [-19.0 - $+0.3$]% respectively. While there was no systematic difference between splineMIRIT and RCTL for the normal volunteers, splineMIRIT gave lower values ($38 \pm 7\%$) than RCTL ($42 \pm 7\%$) for the infarct patients ($p < 0.05$).

Discussion and Conclusions

Both methods show a good correlation with the reference method and might thus be used for fully automated estimation of SV or EF. Given that RCTL is a fully integrated method, it seems to be the better option. However, splineMIRIT might improve the measurement of regional functional parameters (i.e. strain).

Wednesday
Oral



2H-2

8:15 AM **A novel fast algorithm for tracking of the longitudinal movement of the arterial wall using ultrasound B-mode data**

Tobias Nilsson¹, Åsa Rydén Ahlgren², Tomas Jansson¹, Hans W Persson¹, Kjell Lindström¹, Magnus Cinthio¹;
¹Department of Measurement Technology and Industrial Electrical Engineering, Lund Institute of Technology, Lund University, Lund, Sweden, ²Department of Clinical Sciences, Clinical Physiology and Nuclear Medicine Unit, Lund University, Malmö, Sweden

Background, Motivation and Objective

We have recently demonstrated a distinct longitudinal movement of the arterial wall and a resulting shear strain within the wall. This new information of great importance for cardiovascular research has been determined using a recently developed 2D echo-tracking algorithm on ultrasonic B-mode image. The algorithm is based on cross correlation and is limited to track points with a local maximum intensity. Further, cross correlation rely on multiplication operations and is computationally relatively slow. Also the algorithm requires the arterial walls to be oriented horizontally in the image. Here, a new improved method based on sum of absolute difference (SAD) is presented.

Statement of Contribution/Methods

The 2D movement was estimated in three steps. Initially the positions of the walls were estimated, giving the radial movement and the orientation of the arterial walls in the image. This enabled identification of the intima-media segment where a rough pre-estimation of the longitudinal movement was performed. Finally, a user specified point in the arterial wall was tracked using SAD and the given data above. By interpolating the region of interest (ROI) sub-pixel accuracy was achieved. The information acquired from the first two steps significantly decreased the region of interest - minimizing the calculation time.

The new algorithm was evaluated by comparing it with the existing one using *in vivo* ultrasound measurements during 2 to 5 cardiac cycles in ten normotensive volunteers (aged 25-49). Three distinct movements denoted LMov1, LMov2 and LMov3, respectively, were paired for each cardiac cycle.

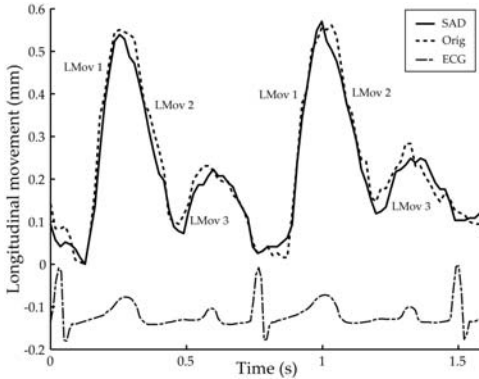
Results

The figure shows the longitudinal movement during two cardiac cycles of a 28-year-old female calculated by the two algorithms. The longitudinal movements were $345 \pm 230 \mu\text{m}$ (mean \pm SD), $-750 \pm 307 \mu\text{m}$ and $580 \pm 268 \mu\text{m}$, respectively. The mean difference between methods was $3 \pm 74 \mu\text{m}$.

Discussion and Conclusions

The comparison showed that the algorithms gave consistent results. The variance, less than the distance between the ultrasonic beams, might be explained by the fact that the algorithms are optimized for tracking different features of the same echo. The new algorithm offers less calculation time, which make it suitable for real time measurements, more flexibility in which echo to track as well as insensibility to the orientation of the arterial wall.

Wednesday
Oral



2H-3

8:30 AM MR-guided ultrasonic brain therapy : high frequency approach

Jean-Francois Aubry¹, Laurent Marsac², Mathieu Pernot¹, **Mickaël Tanter**¹, Benjamin Robert², Yves Martin², Claude Cohen-Bacrie², Jacques Souquet², Mathias Fink^{1,2} *ESPCI, Institut Langevin, Paris, France, ²Supersonic Imagine, Aix-en-Provence, France*

Background, Motivation and Objective

Brain therapy with transcranial focused ultrasound is a scientific and technological challenge. The choice of the working frequency has important outcomes on the treatment precision and safety. A novel prototype is presented here, working at the highest frequency envisioned for transcranial brain treatment (1MHz). Increasing the frequency optimizes the focusing precision and the antenna gain. However the aberrations induced by the skull are increasing with frequency, so that a precise adaptive focusing correction is mandatory. A non invasive time-reversal focusing technique based on CT scans is performed for that purpose.

Statement of Contribution/Methods

An MR-compatible high power prototype has been designed and constructed. It is made of 512 transducers able to deliver up to 20 W/cm² at 1MHz. Pressure distribution around focus has been mapped in a water tank with calibrated hydrophones and the total acoustical power has been measured with a radiation force balance. The system has been installed and tested in a 1.5T Philips Achieva. Temperature rise has been mapped every 1s with a proton resonance frequency shift MR sequence in two orthogonal planes. Three dimensional finite difference time domain simulations were used to compute the propagation of the wave field through three human skulls. The simulated phase distortions were used as inputs for transcranial correction and the corresponding pressure fields were scanned in the focal plane.

Results

For a total electrical power ranging from 200W to 5kW, the efficiency of the transducers was equal to 57% with a 2.6% standard deviation. At maximum power, the peak negative and peak positive pressure at focus were measured respectively to 5.0 MPa and 9.2 MPa. At half of the maximum power (10W/cm² on the surface of the transducers), necroses were induced 2cm deep in turkey breasts placed behind a human skull. In vitro experiments on human skulls show that simulations restore more than 85% of the pressure level through the skull bone when compared to a control correction performed with an implanted hydrophone.

Discussion and Conclusions

A MR-guided brain therapy device operating at 1MHz has been successfully developed and tested. It should be particularly suited for precise targeting in the brain and the first clinical applications will be brain metastases and essential tremors.

2H-4

8:45 AM **Functional Imaging of the Rat Brain with Micro-Ultrasound**

John Sun¹, Liis Lindvere¹, Adrienne Dorr¹, Bojana Stefanovic¹, Stuart Foster^{1,2}:*Sunnybrook Health Sciences Center, Canada*

Background, Motivation and Objective

Linear array based Micro-Ultrasound provides 40-150um resolution over a significant depth of field at frames rates as high as 1000fps. Current imaging modalities for investigating in vivo brain function are challenged to provide this combination of imaging parameters. Therefore, the present experiment was carried out to investigate the potential of micro ultrasound in neuroimaging of rodents.

Statement of Contribution/Methods

Adult male Sprague-Dawley rats was anesthetized with isoflurane. To enable high frequency ultrasound imaging of the brain, stereotaxic surgery was done to prepare a small cranial window. Ultrasound contrast agent was infused through the tail vein and an electrical stimulus was applied to the forelimb to assess changes in brain perfusion. Ultrasound imaging was performed using high frequency linear array (Vevo2100, VisualSonics), equipped with a probe with a 20-MHz center frequency. The probe was positioned appropriately to reveal 2 regions of interest, the forelimb representation in the primary somatosensory cortex (S1FL) and primary motor cortex (M1). Ultrasound contrast agent (Micromarker, VisualSonics) was continuously infused at a rate of 40uL/min at 2x10⁹ microbubbles/mL concentration. The imaging was done using non-linear (pulse inversion and amplitude modulation) contrast mode. When signal intensity reached a steady state, a contrast disruption pulse was delivered. Average signal intensity from S1FL and M1 regions were fit to a monoexponential model so as to estimate the slope and plateau values for the reperfusion curves.

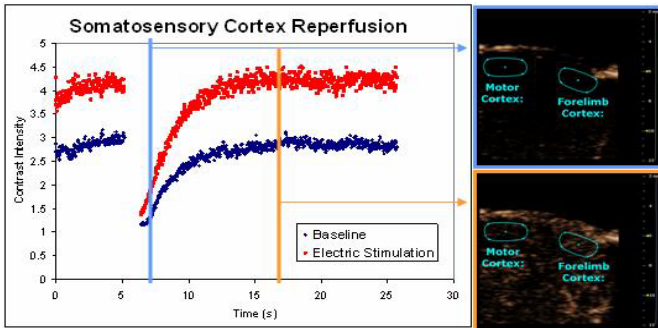
Results

Forepaw stimulation produced a significant increase in both the initial slope of the reperfusion curve and the plateau signal intensity in S1FL (p<0.01). In contrast, these changes in M1 were not significant. As expected, the forelimb stimulation was thus found to result in a transient increase in cerebral blood flow and volume.

Discussion and Conclusions

These data demonstrate the great potential of the use for micro ultrasound for functional brain imaging in animal models. The imaging parameters tradeoff afforded by nonlinear contrast micro ultrasound with depth penetration sufficient to enclose the entire cerebrum - provides a unique window into the study of cerebral hemodynamics, both in the cortex and in the deep grey matter.

Wednesday Oral



2H-5

9:00 AM **Natural brain tissue pulsatility measurement : A pilot study in older depressed patients**

Mélouka Elkateb Hachemi¹, Thomas Desmidt², Frédéric Pataf², Vincent Camus², Jean-pierre Remenieras^{1,2}:*INSERM U930 CNRS ERL 3106, France, ²INSERM U930 CNRS ERL 3106, Hospital of Tours, France*

Background, Motivation and Objective

It was shown that natural brain displacement is composed of a cardiac component of low amplitude and short duration and a slower respiratory component with high-amplitude. During the systolic phase, the cardiac

component consists of a rapid displacement followed by a slow return to the initial configuration during diastole. Tissue Pulsatility Imaging (TPI) is a new ultrasound technique used to assess natural brain tissue displacement. The aim of this study was to use TPI technique to find a potential correlation between Brain Tissue Pulsatility (BTP) and elderly depression in patients with cardiovascular risk factors. In fact, there are growing evidences that depression in the elderly is associated with cerebrovascular abnormalities

Statement of Contribution/Methods

BTP of depressed and non depressed diabetic patients was compared. 25 diabetic patients were then recruited and underwent a clinical examination by a psychiatric. They were classified into two groups. A group of 11 diabetic depressed patients diagnosed (mean age 62 ± 7 years) and a group of 14 diabetic patients without depressive symptoms (mean age 66 ± 7 years). Ultrasound (US) recordings were realized using a medical US Siemens Scanner (Antares). Transcranial acquisitions were performed with a 2 MHz phased array probe through the right temporal bone window. A direct access to the beamformed radiofrequency (RF) signals is allowed by a User's Interface Research mode installed on the Scanner. The acquisition of six cardiac cycles was realized on each patient with 25 frames/s. Off-line estimation of displacements was performed by 1D correlation methods on the RF lines of the collected 2D data. With this configuration, the measured displacements correspond to the medial component (on the ultrasound beam axis) of the total displacement. Displacement was then filtered around the cardiac frequency to remove the respiratory component.

Results

The displacement was found to be greater around wall arteries and diminish away from them. Its results probably from arteries pulsations and its magnitude is linked to their properties (distensibility and compliance). A significant decrease in BTP magnitude was observed in the group of depressed patients ($45 \pm 7 \mu\text{m}$) compared to the group of non depressed patients ($70 \pm 15 \mu\text{m}$).

Discussion and Conclusions

This pilot study is the first to test TPI in clinical conditions including depressive patients older than fifty. Decreased BTP in depressive patients supports the involvement of specific cerebrovascular disorders in the pathophysiology of depression. We argue specific brain endothelial dysfunction caused by high blood level of cortisol is a key biological mechanism to explain reduced brain pulsatility in depression. We have recruited at this stage of the study 21 other patients, clinical examination and US acquisitions were performed and calculation of the BTP is in progress. Further and larger clinical and biological studies are needed to complete our hypothesis.

2H-6

9:15 AM **Ultrasound Current Source Density Imaging of a time-varying current field in a multielectrode nerve chamber**

Ragnar Olafsson¹, Pier Ingram¹, Zhaohui Wang¹, Qian Li¹, Russell Witte¹ ¹Radiology, University of Arizona, Tucson, Arizona, USA

Background, Motivation and Objective

Interventional neurosurgery requires precise mapping of cortical activity prior to resection to minimize the loss of function. This laborious and time consuming mapping procedure is performed with surface and penetrating electrodes. We have developed Ultrasound Current Source Density Imaging (UCSDI), a new technique that can potentially improve this procedure. UCSDI maps electrical current distributions based on the acoustoelectric (AE) effect, an interaction between ultrasound and electricity. The potential advantages of UCSDI are high spatial resolution defined by the ultrasonic point spread function, automatic registration to B-mode ultrasound, and fast mapping with electronically steered beams.

Statement of Contribution/Methods

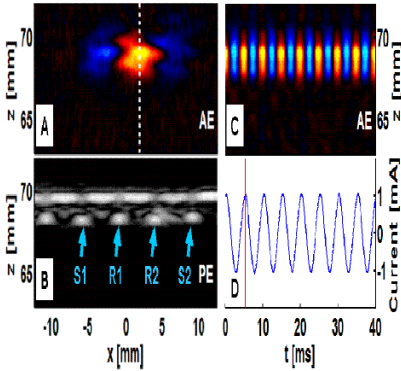
We describe the mapping of dynamic electric current in a nerve analog (excised porcine specimen). The nerve analog was placed on top of a grid of stainless steel electrodes and immersed in mineral oil. A burst of electric current (Plot D, 1 mA, 200 Hz sine wave, 20 cycles) was injected through one pair of electrodes (Plot B, S1, S2) while voltage was measured with another pair (Plot B, R1, R2). A 2D data set was acquired by scanning an ultrasound transducer (2.25 MHz, $f/1.8$, focal length = 69 mm) along the nerve analog. At each step the transducer was triggered (250 triggers, trigger interval=306 us) in synchrony with the current burst. These are the first UCSDI images of dynamic electric current in a well controlled multielectrode nerve chamber.

Results

The figure depicts pulse echo (PE) images of a nerve lying on top of a grid of electrodes (Plot B, white hyperechoic circles) and the AE current source density map of the nerve (Plot A). Plot C is an M-mode AE image corresponding to the white dashed line in plot A. Plot D shows the current waveform, captured simultaneously. Maximum SNR was 34 dB and maximum signal was 345 μ V. Based on nerve analog diameter of 1.5mm, the sensitivity was 6 μ V/(mA/cm²) and the noise equivalent current density was 1.1 mA/cm²--the same order of magnitude as biological current density.

Discussion and Conclusions

We have imaged dynamic electric current in a multielectrode nerve chamber with UCSDI. These experiments are consistent with what we have shown previously in the live rabbit heart, further suggesting that the sensitivity of UCSDI is sufficient to map current in excited neural tissue.



3H. Bone I

Sala 4

Wednesday, September 23, 2009, 8:00 am - 9:30 am

Chair: **James Miller**
Washington University

3H-1

8:00 AM **Ultrasonic Characterization of Backscatter from Human Cancellous Bone with a Renyi Entropy Metric: Correlation with X-Ray Bone Mineral Density**

Kirk D. Wallace¹, Brent K. Hoffmeister², Lewis J. Thomas, III³, Sue C. Kaste^{4,5}, Gregory M. Lanza¹, Samuel A. Wickline^{1,2} *Dept. of Cardiology, Washington University School of Medicine, Saint Louis, MO, USA,* ²*Dept. of Physics, Rhodes College, Memphis, TN, USA,* ³*University of Missouri School of Medicine, Columbia, MO, USA,* ⁴*College of Medicine, University of Tennessee, Memphis, TN, USA,* ⁵*Dept. of Radiological Sciences, St. Jude Children's Research Hospital, Memphis, TN, USA*

Background, Motivation and Objective

Ultrasound backscatter has the potential to provide information useful for the diagnosis and monitoring of bone disorders (e.g., osteopenia, osteoporosis, and hard tissue sarcomas). We hypothesize that the Renyi entropy, previously shown to be sensitive to subtle changes in scattering from soft tissues, may also have some utility in characterizing properties of bone. The goals of the present work were to investigate and compare the ability of energy- and entropy-based analyses of radio-frequency ultrasonic backscatter, to assess material properties of cancellous bone with respect to conventional quantitative computed x-ray tomography (QCT).

Statement of Contribution/Methods

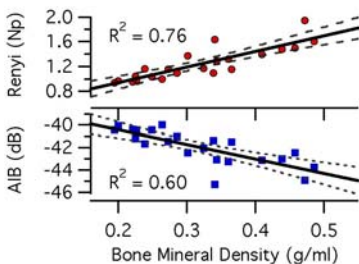
Twenty-two (22) specimens of cancellous bone were prepared from 14 fresh frozen human femoral heads. A bandsaw was used to segment the specimens and shape them into cubes with a mean lateral dimension of 14.7 ± 0.7 mm. Bone marrow was removed from the specimens using a water jet. Specimens were placed in physiologic saline, degassed under vacuum, and maintained at 4°C until imaging. Ultrasonic C-scan measurements were performed, interrogating all 6 faces of each cube, rastering a 7.5 MHz (12.7 mm diam., F/4) transducer in a 49×49 grid. Backscatter data (500 MS/s, 8-bits) were analyzed using the Renyi entropy as well as a frequency-domain integrated backscatter approach.

Results

Bone mineral density (BMD) values, assessed by QCT (GE LightSpeed Ultra, 80 kV, 360 mA·s), spanned a range from 0.19 to 0.49 g/ml. Consistent with published results [Hoffmeister *et al.*, TUFFC 2008;55:1442-1452], the apparent integrated backscatter was inversely proportional to the BMD ($R^2 = 0.60$). Renyi entropy analysis of these same data showed an increasing relationship with BMD and an improved correlation ($R^2 = 0.76$).

Discussion and Conclusions

To our knowledge, this study represents the first reported application of ultrasound entropy analysis to investigate the hard tissue of bone. The enhanced correlation between the Renyi entropy metric and the x-ray measurements suggests the potential for this approach in detecting and quantifying loss of bone mineral density.



3H-2

8:15 AM **Extracting fast and slow wave velocities and attenuations from experimental measurements of cancellous bone using Bayesian probability theory**

Christian Anderson¹, Michal Pakula², Adam Bauer¹, Karen Marutyan¹, Mark Holland¹, Larry Bretthorst¹, Pascal Laugier², James Miller^{1,2} *Washington University in St. Louis, St. Louis, MO, USA, ²Universite Paris 6, Paris, France*

Background, Motivation and Objective

The consensus among many laboratories is that the attenuation coefficient of cancellous bone exhibits an approximately linear-with-frequency dependence. In the majority of cases, the phase velocity decreases with frequency. This negative dispersion appears to be inconsistent with the causality-imposed Kramers-Kronig (KK) relations for media with a linear-with-frequency attenuation coefficient.

The porous structure of cancellous bone can generate two compressional waves, known as a fast wave and a slow wave, that can overlap in time. Our laboratory has sought to explain the observed negative dispersion as an artifact of analyzing rf data containing two interfering waves as if only one wave were present. In this study, the inverse problem of how to recover the individual fast and slow waves from interference data was addressed. Waves transmitted through bone samples were analyzed using Bayesian probability theory to recover the individual properties of the fast and slow waves.

Statement of Contribution/Methods

Data at nine independent sites were acquired on a bovine femur condyle sample using broadband 500 kHz center frequency transducers. Each rf line served as input to a Bayesian analysis program. In the Bayesian calculation, ultrasonic wave propagation through cancellous bone was modeled as the superposition of two plane waves characterized by a linear-with-frequency attenuation coefficient and a logarithmic-with-frequency increasing phase velocity. The calculation employed Markov chain Monte Carlo (MCMC) to obtain estimates of the joint posterior probability for all parameters in the model.

Results

In all cases where the data processed by conventional means exhibited negative dispersion, two waves with positive dispersions were recovered with Bayesian analysis. The mean \pm SD fast and slow wave velocities for the nine sites analyzed were (2072 \pm 42) m/s and (1519 \pm 22) m/s, respectively. The mean \pm SD slopes of the attenuation coefficients were (17.2 \pm 9.7) dB/cm/MHz and (10.8 \pm 5.3) dB/cm/MHz for the fast and slow waves, respectively.

Discussion and Conclusions

Many complicating factors, including phase cancellation at the face of a piezoelectric receiver and diffraction effects, are not explicitly accounted for in the present model. Nevertheless, the Bayesian models proved to be a reliable method for recovering fast and slow waves from data that yielded negative dispersions when processed as if a single wave were present.

NIH R01 AR057433-01

3H-3

8:30 AM **Monitoring of trabecular bone induced microdamage using a nonlinear wave-coupling technique**

Hélène Moreschi¹, Rony Harb², Anne-Sophie Eveno², Marielle Defontaine¹, Sandra Guerard², David Mitten³, Samuel Callé¹, Guillaume Renaud⁴; ¹*Imagerie et Cerveau équipe 5, INSERM U930 CNRS ERL 3106 F.Rabelais University, France, Metropolitan*, ²*Arts et Métiers ParisTech, CNRS, LBM, 151 Bd de l'Hôpital, Paris, France, Metropolitan*, ³*Université de Lyon, F-69622, Lyon, France; INRETS, UMR-T9406, LBMC; Université Lyon 1, Lyon, France, Metropolitan*, ⁴*LIP-UMR CNRS 7623, Paris, France, Metropolitan*

Background, Motivation and Objective

Bone tissue contains microcracks which may affect its mechanical properties as well as the whole trabecular structure. Efficient nonlinear (NL) ultrasound methods have been widely developed for nondestructive testing and geophysical applications to detect microdamage. A Dynamic Acoustoelastic Method, was developed to monitor microdamage induced by fatigue testing in trabecular bone samples.

Statement of Contribution/Methods

The method consists in using a low frequency (LF) wave (2.8 KHz) acting as a tension/compression quasi-hydrostatic pressure and ultrasound (US) pulses (10 pulses/LF period) used to measure NL viscoelastic properties

(Time Of Flight Modulation, TOFM) and dissipative nonlinearities (Relative Amplitude Modulation, RAM) in bone samples. Twenty calcanei samples, extracted from 10 human donors, were machined into parallelepipeds and divided in 2 groups: A, endcaps samples (resin epoxy) and B, free ends samples. Our purpose is to check for end artifacts on mechanical testing. Uniaxial compressive fatigue tests were carried out on 7 specimens in each group. Both groups included 3 controls (not mechanically tested). The loading frequency was fixed at 2 Hz (close to gait frequency) with a strain range from 0.2 to 0.5 %. Moduli were calculated throughout the fatigue loading and a decrease of 50% was used to stop the tests.

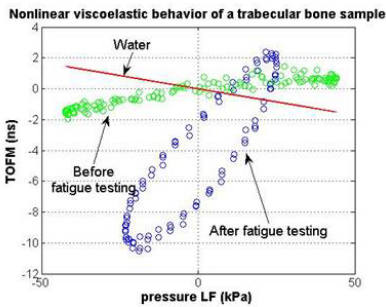
Nonlinear US measurements were performed just before and after the fatigue tests on both groups. TOFM and RAM curves are plotted as a function of LF pressure amplitude.

Results

The figure shows an example of TOFM curves obtained before and after fatigue. A NL classical behavior is observed in pure water. As expected, the corresponding nonlinear parameter β , obtained from the slope of TOFM curve, was found to be 5. In bone samples, a negative slope, an asymmetry in tension/compression phases and a hysteresis are observed most of the time, and is characteristic of a NL non classical behavior.

Discussion and Conclusions

Maximum TOFM and RAM amplitudes in both tension and compression phases and hysteresis levels are compared to Young's moduli and residual strains before and after fatigue. We expect the endcaps process to improve the distribution of stresses into the specimens and to find increased NL TOFM and RAM amplitudes after fatigue. Besides, for mechanical parameters a decreased Young's moduli and increased residual strains are expected.



3H-4

8:45 AM Fluid properties influence the phase velocity but not the attenuation coefficient of fluid-filled cancellous bone between 0.35 and 2.5 MHz

Michal Pakula¹, Frederic Padilla¹, Pascal Laugier¹; ¹Laboatoire Imagerie paramétrique UMR CNRS 7623, Université Pierre et marie Curie-Paris6, Paris, France

Background, Motivation and Objective

It remains unclear to what extent the inherent material properties of the saturating fluid significantly affect ultrasonic properties measured in cancellous bone, particularly if the absorption and/or scattering conditions are different with different filling fluids.

Statement of Contribution/Methods

The paper is focused on comparative in vitro ultrasonic experiments of cancellous bones filled with different fluids with the goal of evaluating the contribution of different fluid physical properties to velocity dispersion, absorption and scattering mechanisms. Twenty six trabecular plates were prepared from fresh human condyles obtained from 13 individuals. Ultrasonic measurements were performed in through-transmission at room temperature using three pairs of transducers with centre frequencies of 0.5, 1 and 2 MHz. The specimens were measured first with the intact marrow inside and subsequently with water and alcohol filling the pores after marrow removal.

Results

Overall, no significant influence of the fluids was evidenced on the attenuation coefficient of cancellous bone between 0.35 and 2.5 MHz. Given the absence of impact of viscosity (marrow vs. water) of the saturating fluid, we

hypothesize that the source of wave attenuation can be associated with viscoelastic absorption in the solid phase and with scattering by the solid trabeculae. Significant alteration of scattering conditions (alcohol vs. water) obtained by changing the acoustic impedance mismatch between the saturating fluid and the trabeculae was reflected neither in the attenuation nor in its slope. The attenuation remains nearly linearly frequency dependent in a broad frequency range. This led us to suggest that attenuation is associated with the trabecular network and that LS scattering together with absorption in the solid phase are candidates as main sources for the attenuation. In contrast, the elastic properties of the fluid are main determinants of the phase velocity.

Discussion and Conclusions

These findings are particularly significant in the context of in vivo measurements, because they demonstrate that the subject-dependent properties of marrow may partly explain the inter-subject variability of SOS values. For in vitro investigations of the influence of bone material or microstructural properties, our suggestion is that marrow can be advantageously replaced by water, because attenuation will not be affected by the change and the variability of SOS measurements will be reduced to the impact of the bone properties only.

3H-5

9:00 AM **Model-based Parameter Estimation in the Frequency Domain for Quantitative Ultrasound Measurements of Bone**

Stefanie Dencks^{1,2}, Reinhard Barkmann³, Claus Glüer³, Georg Schmitz⁴:¹Physikalisch-Technische Bundesanstalt, Germany, ²Ruhr-Universität Bochum, Universitätsklinikum Schleswig-Holstein, Germany, ³Universitätsklinikum Schleswig-Holstein, Germany, ⁴Ruhr-Universität Bochum, Germany

Background, Motivation and Objective

For the prediction of osteoporotic fracture risk Quantitative Ultrasound (QUS) can be used to assess skeletal status: short pulses with center frequencies of 0.5 to 1 MHz are transmitted through the bone and characteristic transfer parameters associated with bone strength are determined from the received signals. Recently, we showed that systematic but hardly predictable uncertainties arise if conventional techniques for the calculation of standard QUS parameters are applied to signals resulting from multipath transmission [1], a phenomenon frequently occurring during bone inspection. Therefore, we proposed the implementation of a model-based signal separation in the time domain [2]. However, the success of this algorithm strictly depends on the possibility of analytically modeling the transmitted signals in the time domain.

Statement of Contribution/Methods

To overcome this restriction a new signal analysis was developed, which is based on a parametric model of the transfer function in the frequency domain. The parameters are estimated by applying nonlinear optimization procedures which are integrated in an iterative Space Alternating Generalized Expectation-Maximization algorithm (SAGE). Moreover, an approach relying on the signal analysis method of matching pursuits provides a good initial guess of parameters which is essential for correct optimization. This method is independent of transducer characteristics and excitation modus. Thus, this signal analysis is applicable to arbitrary signals.

Results

The accuracy and robustness of the algorithm were analyzed. By comparing the Cramér-Rao lower bounds derived in the frequency domain with results of Monte Carlo Simulations it is shown, that the algorithm approximates the true parameter values and has variances close to the lower bounds. Additionally, simulations were performed to evaluate limitations and uncertainties to be expected in case of superimposed signal components. Improved parameter estimation by signal separation is clearly demonstrated comparing the conventional with the model-based signal analysis. E.g. the uncertainty in the estimation of the broadband ultrasound attenuation is expected to be reduced by more than 50% for typical measurement conditions.

Discussion and Conclusions

The model-based parameter estimation in the frequency domain allows for characterizing single signal components of multipath transmission signals without restrictions on the shape of the transmit signal. Thus, uncertainties in the calculation of the standard QUS parameters are substantially reduced. Additionally, it may become feasible to characterize the mechanical competence of different bone compartments.

[1] Dencks et al. "Improvement of Measurement of Broadband Ultrasound Attenuation in Cancellous Bone by Signal Component Separation." International Congress on Ultrasonics, Vienna Austria, 2007.

[2] Dencks et al. IEEE Trans Ultrason Ferroelec Freq Cont 55:1304-1315, 2008.

3H-6

9:15 AM **Time-domain model of the ultrasonic wave propagation in an inhomogeneous anisotropic viscoelastic fluid/solid multilayer medium: application to cortical bone**

Guillaume Haiat¹, Salah Naili², Mai Ba Vu², Quentin Grimal³, Marilyne Talmant³, Christophe Desceliers⁴, Christian Soize⁴, ¹B2OA UMR 7052, CNRS, Paris, France, ²Laboratoire de Mécanique Physique, Université Paris 12 – Val de Marne, Creteil, France, ³Laboratoire d'Imagerie Paramétrique, Université Paris 6, Paris, France, ⁴Laboratoire de Modélisation et Simulation Multi-Echelle, MSME FRE3160, Université Paris Est, Marne la vallée, France

Background, Motivation and Objective

Cortical bone quality is assessed in clinical practice using axial transmission (AT) devices, which allow the measurement of quantitative ultrasonic parameters such as the first arriving signal (FAS) velocity. However, the physical interaction between an ultrasonic wave and cortical bone remains poorly understood due to the complex nature of the bone structure. Cortical bone and the surrounding soft tissues are attenuating media, which might affect the results obtained with AT devices. Moreover, cortical bone is highly heterogeneous and a gradient of material properties from the outer to inner part of the cortical shell has been reported. The aim of this work is to evaluate the effect of anisotropic heterogeneous dissipative phenomena occurring in bone and in soft tissues on the ultrasonic response of the bone structure.

Statement of Contribution/Methods

A two-dimensional finite element time-domain method is derived to model transient wave propagation in a three-layer medium composed of an inhomogeneous transverse isotropic viscoelastic solid layer sandwiched between two dissipative acoustic fluid layers. The model couples acoustic propagation in both dissipative acoustic fluid media with the response of the solid whose constitutive equation is based on the linear theory of viscoelasticity without memory. Bone viscoelasticity is assumed to be heterogeneous and a constant spatial gradient of viscoelastic properties is considered for two values of bone thicknesses corresponding to a relatively thick and thin bone.

Results

Realistic variations of the viscosity of the soft tissues within the physiological range do not affect the FAS velocity in any configuration. However, when the viscoelastic bone parameters vary within their physiological range, changes of the value of the FAS velocity (up to 341 m/s) are comparable to what has been obtained for variation of the elastic parameters [1]. The components of the viscoelastic tensor affecting the results are the same as those of the stiffness tensor found in [1]. For a thin bone, the FAS velocity can be predicted by considering the spatially averaged bone properties. For a thick bone, the FAS velocity may be qualitatively predicted using a signal processing technique.

Discussion and Conclusions

The results allow the derivation of a contributing depth (CD) for a thick bone width. In the case of a gradient of viscoelasticity, $CD \sim 1.6$ mm, in the case of a gradient of C_{11} , $CD \sim 0.6$ mm and in the case of a gradient of mass density, $CD \sim 1$ mm. However, in the case of a gradient of porosity, the determination of the contributing depth is not possible due to the simultaneous variation of all bone parameters. Our results highlight the importance of accounting for absorption phenomena occurring in cortical bone for the analysis of ultrasonic measurements with AT device.

This study was supported by the Agence Nationale de la Recherche (Contract BoneChar n° BLAN06-2_144779).

[1]: Haiat et al. J Acoust Soc Am (in press)

4H. Acoustic Imaging and Characterization

Tarragona

Wednesday, September 23, 2009, 8:00 am - 9:30 am

Chair: **Bob Addison**
Rockwell Science Center

4H-1

8:00 AM **Two-dimensional Array Design Considerations for NDE Applications**

Paul Wilcox¹, Alexander Velichko¹:*Mechanical Engineering, University of Bristol, Bristol, Bristol, United Kingdom*

Background, Motivation and Objective

One-dimensional (1D) ultrasonic arrays are in routine use in many NDE applications and enable a 2D plane to be inspected. 2D arrays can be manufactured and have the potential to image a 3D volume of a component, but their full potential has yet to be realized in NDE. The number of channels available on commercial array controllers is typically limited to 128. Significant increases in channel count beyond this raise the practical problem of providing robust connectivity between each array element and the controller. Therefore, determining the optimum configuration of a limited number of elements in a 2D aperture and the associated data processing is of great importance and provides the motivation for the work in this paper.

Statement of Contribution/Methods

For 2D arrays in NDE applications the limited channel count precludes large apertures if it is assumed that the element pitch must satisfy the half-wavelength criterion in both dimensions. In the case of 1D arrays NDE operation is almost always in the near-field, but the smaller aperture of 2D arrays means that the distinction between far and near-field operation becomes important. For far-field operation, a fully populated 2D array contains redundant data. By using the effective aperture concept it is possible to significantly reduce the number of elements required without compromising performance. The optimum element layout for this scenario is investigated via simulation. In the near-field, there is no data redundancy but it is shown that a reduction in element count of 70% can be achieved by optimizing the element layout without significantly compromising performance. However, this still does not enable 2D arrays with apertures anywhere near as large as those of 1D arrays to be designed. Such an array would necessarily have to sacrifice some information. The question of which information to sacrifice is then investigated in the context of defect characterization.

Results

The optimum element layout for far-field operation is a single circular ring of elements at approximately half-wavelength pitch. A slightly less efficient layout is to space the elements around the perimeter of a regular polygon. Experimental results demonstrate the use of reduced element count in the far-field are presented using only the perimeter elements of a commercial square matrix array. The optimum design of a fully-populated 2D array is presented, along with simulated results. A candidate sparsely populated 2D array with elements distributed along the boundaries of a honeycomb pattern is shown. Simulated results from a number of canonical scatterers are presented and show the potential of using such an array for 3D defect characterization.

Discussion and Conclusions

The optimum configurations for far-field operation and near-field operation without information loss have been presented. A possible layout for a sparsely populated 2D array has also been shown, but whether this is the optimum remains an open question.

4H-2

8:15 AM **Evolutionary algorithms for optimal ferroelectret arrays design**

Javier Rodrigo Villazón Terrazas¹, Alberto Ibáñez Rodríguez¹, Joao Ealo Cuello^{1,2}, Jorge Camacho Sosa¹, Carlos Fritsch Yusta³; ¹END, Instituto de Automática Industrial, La Poveda - Arganda del Rey, Madrid, Spain, ²School of Mechanical Engineering, Universidad del Valle - Cali, Colombia., Colombia

Background, Motivation and Objective

The array technology is commonly used in ultrasonic applications due to its capability for electronically steering and focusing the ultrasonic beam at different angles and depths. The number of elements and the inter-element spacing are among the parameters that affect the cost of the array and the performance of the desired steering response.

Our research lab built a ferroelectret-based array transducer. This array presents an acceptable response of the main lobe at different frequencies; however, when steering is applied, the grating lobes level greatly increases because the inter-element spacing is greater than half wavelength ($\lambda/2$).

To improve the response of the array, we propose a new approach design for full arrays, which allows us to control the grating lobes level without changing the basic characteristics of the array, i.e. the size of the radiant aperture and number of elements.

Statement of Contribution/Methods

Recently, the array transducers based on ferroelectret technologies have been introduced for airborne ultrasonic applications. Their simple manufacturing procedure allows us to build prototypes rapidly and inexpensively. Besides, this technology is easy to use and exhibit a high mechanical flexibility, which makes it possible to design customizable directivity devices fabricated on substrates of complex-developable surface.

Considering these advantages, we propose an evolutionary algorithm based method for designing the array layout that consists of the following steps:

- 1) To divide the elements of the full array in two or more cells, depending on the radiant space surface.
- 2) To redistribute the cells of the elements, maintaining the distance between the elements.
- 3) To use the evolutionary algorithms in order to find the different positions of the cells around the full array. Cell overlapping condition is not allowed.

Results

An optimized array was obtained having the same characteristics of the fabricated array prototype, i.e. number of elements, inter-element spacing greater than 1 wavelength (λ) and the radiant aperture. However, the grating lobes level was reduced more than 5 dB. Simulation results were validated experimentally using the fabricated ferroelectrets-based array.

Discussion and Conclusions

The evolutionary algorithm opens up new possibilities in the optimal design of arrays. The proposed method proved efficient for the array optimized operation and can be extended to 2-D arrays, regardless the transducer technology.

4H-3

8:30 AM **Optimization of complex shape part inspections with phased arrays**

Marco Aurélio Brizzotti Andrade¹, Alberto Ibáñez², Montserrat Parrilla³, Julio Cezar Adamowski⁴, Carlos Fritsch⁵; ¹Escola Politécnica - Universidade de Sao Paulo, Brazil, ²Instituto de Automática Industrial-CSIC, Spain, ³Instituto de Automática Industrial - CSIC, Spain, ⁴Escola Politécnica - Universidade de Sao Paulo, Brazil, ⁵Instituto de Automática Industrial- CSIC, Spain

Background, Motivation and Objective

The NDE inspection of complex shape parts is usually performed by immersion. In state-of-art phased array equipments, a focus is defined for every scan line in emission and dynamic focusing is used in reception. The scan lines are commonly defined based on Fermat's Principle or Snell's law. To achieve the highest resolution and

sensitivity, the reception foci should be located on the path defined by the maximum field intensity of the emitted beam. In complex part inspections, it is common that the path defined by the maximum field intensity does not coincide with the path determined by the Fermat's principle. In such cases, resolution and sensitivity are degraded. In order to increase the image resolution and sensitivity, it is proposed a fast algorithm to determine the scan lines that coincide with the maximum field intensity of the emitted beam.

Statement of Contribution/Methods

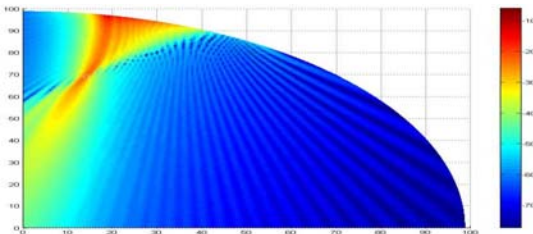
From the geometry involving the array, the couplant, the part and the region of interest, a set of emission foci are defined. Then, a fast field simulation procedure based on a solution of the wave equation for harmonic waves is performed for each focus. The proposed algorithm determines a set of scan lines that coincide with the path of the maximum field intensity. Finally, a Fast Focal Law computing algorithm provides the set of time-delay laws to generate the image.

Results

The proposed method was verified by comparing the images obtained by the classical approach with that obtained by using the proposed algorithm. A 96 element subaperture of a 128-element, 5 MHz array (Imasonic, France) was used in the inspection of a 100-mm radius cylindrical aluminum piece with several side drilled holes. The array signals were acquired by a SITAU 128-128 ultrasound system (Dasel S. L., Spain). The image comparison shows that the proposed method can increase the image resolution and sensitivity, especially when the emission focus is defined close to the part interface.

Discussion and Conclusions

A technique to optimize the inspection of parts by immersion is proposed. Differently from other techniques, it provides the highest resolution and sensitivity obtained with an array for a given inspection arrangement for arbitrary shape parts. The resulting tool is fast enough to be used in an interactive mode.



4H-4

8:45 AM Ultrasonic holography of 3D objects

Sergey Tsysar¹, Oleg Sapozhnikov²; ¹Department of Acoustics, Physics Faculty, Moscow State University, Moscow, Russian Federation, ²Center for Industrial and Medical Ultrasound, Applied Physics Laboratory, University of Washington, Seattle, WA, USA

Background, Motivation and Objective

Holography is a method of recording wave scattering from an object such that the object's shape and position can be reconstructed later. An experimental realization of acoustic holography that uses scanned measurements in place of a transducer array has been reported for studying the vibrations of piezoelectric sources [Sapozhnikov et al. IEEE UFFC Symp. 2004, 2006]. In addition to such measurements of surface vibration, it is of practical interest to record acoustic holograms of 3D objects. The goal of the current paper is to demonstrate such a technique in the ultrasonic frequency range.

Statement of Contribution/Methods

The holographic approach used here relies on the principle of a time-reversal mirror and the Rayleigh integral. An ultrasonic beam consisting of long tone bursts is directed at a target object and the resulting acoustic field is measured at a large number of points surrounding the object. In one implementation, a computer-controlled positioning system is used to scan a small broadband hydrophone across a grid of measurement points in a single

plane near the target. Object reconstruction is then accomplished numerically by back-propagating the acoustic field from measurement locations to a 3D region representing the object. Theoretically, the accuracy and the optimal parameters of the method were studied by modeling forward and backward propagation from a point scatterer. Experimentally, two targets were investigated: (1) a set of 3-mm diameter plastic beads and (2) a piece of styrofoam with a rough surface and a diameter of several cm. Ultrasound frequencies from 1 to 1.5 MHz were considered, while hologram measurements were collected with grid spacings between 0.3 and 0.4 mm.

Results

Both theory and measurements show that the spatial resolution of 3D ultrasonic holography is limited by diffraction effects. Theoretically, the image of a point scatterer is an ellipsoid with a lateral size on the order of a wavelength and a somewhat larger axial size (relative to the scanning plane). However, discrete scatterers larger than a wavelength are well-resolved. When recording a hologram of 3D objects, the surface roughness is also an important factor: smooth objects provide a specular reflection so that only part of the surface is visible in the reconstructed image. This feature of ultrasonic holography is identical to that of optical holography.

Discussion and Conclusions

Using this 3D ultrasonic holography method, it is possible to reconstruct the position and shape of objects or collections of objects that do not involve a significant amount of multiple scattering. Because the spatial resolution of the method has a typical diffraction limit on the order of a wavelength, improved spatial resolution can be achieved with higher frequencies. Work supported by RFBR 08-02-00368, ISTC 3691 and NIH R01EB007643.

4H-5

9:00 AM Perpendicular fluid flow measurement with a spatial array of ultrasonic transducers

James S. Hall¹; ¹*Electrical and Computer Engineering, Georgia Institute of Technology, Atlanta, GA, USA*

Background, Motivation and Objective

Ultrasonic methods are in commercial use for measuring the average flow rate of a gas or liquid. These techniques estimate the flow rate by measuring a change in propagation velocity, which requires that the propagation path have some non-negligible directional component in the flow direction. The proposed method overcomes this limitation by using a spatial array of transducers to estimate the angle-of-arrival of a reflected ultrasonic wave and thus measure flow perpendicular to the path of propagation.

Statement of Contribution/Methods

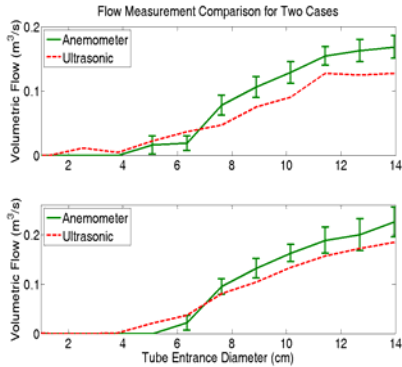
Numerical simulations were conducted to characterize the viability of perpendicular flow measurement using two-dimensional array configurations. Experimental data was then obtained to physically validate the algorithm using a three-transducer linear array. A 5.5" diameter 80" long hard plastic tube was used to condition the flow, mount the transducers, and reflect the waves. Flow rate was adjusted by restricting the tube opening closest to the flow source. At the other end of the tube, a vane-anemometer was used to independently measure the flow. A data-driven calibration method was developed to characterize the relative positions of the transducers. System phase stability issues were addressed via minor phase adjustments based on intermediate calibration data.

Results

Numerical simulations indicate that, as expected, relative transducer locations and phase stability are critical to flow measurement accuracy. Experimental ultrasonic flow measurements are shown in the figure to be in close agreement with anemometer readings. Discrepancies between the experimental and reference measurements can be attributed to the chaotic nature of the undeveloped turbulent flow within the tube.

Discussion and Conclusions

Both numerical and experimental results demonstrate the feasibility of a spatial array for perpendicular flow measurement. Measurement accuracy is limited only by system phase stability and relative location resolution. Although high resolution beamforming techniques worked well with numerical simulations, conventional beamforming was found to be more robust to discrepancies in phase and model mismatch. Experimental results confirm the viability of this method while highlighting important subtleties about implementation.



4H-6

9:15 AM Integrating A Spatial Ultra-directional Steerable Acoustic Source and Electronic Speckle Pattern Interferometry for Vibration Analysis

Yu-Chi Chen¹, Chih-Chiang Cheng¹, Kuang-Chong Wu^{1,2}, Chih-Kung Lee^{1,3}, ¹Institute of Applied Mechanics, National Taiwan University, Taipei, Taiwan, ²National Applied Research Laboratories (NARL), Taipei, Taiwan, ³Industrial Technology Research Institute (ITRI), Hsinchu, Taiwan

Background, Motivation and Objective

Large-size flexible panel is leading the developing trend in display fields. It should be noted that mechanical vibration should be taken into account in designing large-size display. More specifically, large-size optical thin film based flexible displays face unique structural response challenges as their low modulus and extreme thinness make structure warp and wrinkle at the presence of thermal stresses.

Statement of Contribution/Methods

To study and to understand the vibration characteristics of large-area thin film structures, a full-field non-destructive optical detection method and a suitable excitation source must be integrated to establish the testing platform. Electronic speckle pattern interferometry (ESPI) was chosen as the optical metrology technique due to its maturity in pursuing large-area metrology needs. A newly developed directivity-controlled ultra-directional ultrasonic array was chosen as the excitation source as it will not exert unnecessary constraint onto the flexible specimen. More specifically, steerable acoustic exciter was chosen to achieve acoustic impedance matching and to determine the forcing positions precisely [1]. The ultrasonic array developed was driven by an amplitude-modulated ultrasonic signal with a sinusoidal carrier of 40 kHz so as to radiate a steerable and ultra-directional demodulated audible beam coupled to the large-area thin film. The layout of this testing platform is detailed herein (Figure 1). Through controlling the direction and position of the steering beam to alter the forcing positions on the thin film, the corresponding vibration modes of interests would be detected through the ESPI setup.

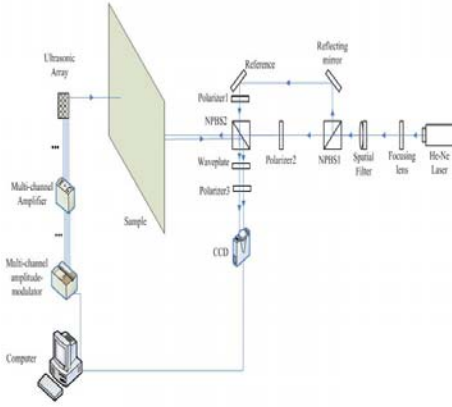
Results

Both the design and the experimental results obtained on this newly developed testing platform.

Discussion and Conclusions

This newly developed testing platform is a full-field non-destructive optical detection method for large-area thin film structures.

[1] C. H. M. Jenkins and U. A. Korde, "Membrane vibration experiments: An historical review and recent results," *J. Sound Vib.*, vol. 295, pp 602-613, 2006



Wednesday
Oral

5H. Novel Devices & Systems

Pergamo

Wednesday, September 23, 2009, 8:00 am - 9:30 am

Chair: **Paul Reynolds**
Weidinger Associates, Inc.

5H-1

8:00 AM **Biologically Inspired Ultrasound-its Applications in NDE**

Gordon Hayward¹; ¹*Centre for Ultrasonic Eng University of Strathclyde, Scotland, United Kingdom*

Background, Motivation and Objective

Mammalian creatures such as bats and cetaceans are known to possess powerful ultrasonic systems that are capable of environmental discrimination, communication and echolocation of food items. For example, many species of bat can discriminate sub-millimetre target structures while emitting centimetre ultrasonic wavelengths, a capability currently beyond most engineered ultrasonic systems. This work describes some aspects of bat behaviour and their potential applications for ultrasonic non-destructive evaluation (NDE).

Statement of Contribution/Methods

Firstly, a technique for accurate measurement and synthesis of bat emissions is described, using an ultrasonic sensor that is mounted directly on the bat and communicates to a data analysis system via a wireless link. A methodology for practical synthesis of such signals is presented, using a combination of inverse filtering and wideband electrostatic transducer technology. Potential applications for range finding and navigation are discussed, in the context of autonomous, remote sensing agents, which have considerable potential for NDE scanning of structures. Secondly, the concept of using optical monitoring techniques to create 'intelligent' transducers which are directly aware of their signal output, is presented. Optical fibre systems, comprising polarimetric and multi-sensor Bragg gratings are introduced and experimental data is presented, along with potential NDE applications. Thirdly, the use of naturally occurring, self similar patterns in sparse 2-D ultrasonic arrays is described, using both simulation and experimental data.

Results

Accurate synthesis of bat ultrasonic signals is demonstrated, in conjunction with their potential for high resolution range finding using miniature, autonomous robotic sensors. The feasibility of using optical monitoring for calibration, control and processing of ultrasonic transducer data is demonstrated successfully, along with applications in target discrimination for improved NDE. Experimental sparse array images are presented, using a commercial NDE imaging system and these show good agreement with theoretical prediction.

Discussion and Conclusions

This work demonstrates the significant potential for using biologically inspired ultrasound in the field of NDE, using three very different examples of natural phenomena. Many others exist and some of these will be reported at a later date.

5H-2

8:30 AM **Moving towards an ideal frequency response with Fibre-Optic hydrophones**

Paul Morris¹, Andrew Hurrell¹, Paul Beard²; ¹*Precision Acoustics Ltd, Dorchester, Dorset, United Kingdom*,
²*Department of Medical Physics and Bioengineering, University College London, London, United Kingdom*

Background, Motivation and Objective

The accurate characterisation of high frequency ultrasound fields (such as those found in diagnostic medical ultrasound) requires hydrophones with small active elements to avoid spatial averaging. However, with piezoelectric hydrophones, it can be difficult to achieve a sufficiently small element size with adequate sensitivity since the latter scales with active area. The polymer film Fabry-Perot fibre-optic hydrophone does not suffer from this limitation and can provide an optically defined element diameter of around 10 μm with high broadband

sensitivity. However, a drawback is that its frequency response is non-uniform due to acoustic diffraction at the tip of the fibre. The aim of this study was to address this by (i) modifying the geometry of the fibre tip in order to improve the uniformity of the response and (ii) correcting for any residual non-uniformity through the use of a deconvolution routine.

Statement of Contribution/Methods

A finite difference model of acoustic propagation in fluid and elastic media was used to investigate the factors which affect the response of fibre-optic hydrophones. As a direct result of this modelling, a hydrophone with a rounded tip was designed and fabricated. The frequency response was measured experimentally and compared to that calculated numerically and that of a fibre-optic hydrophone with a plane tip. In addition, measured waveforms were de-convolved using the methods proposed in the recently released standard IEC62127-1 and compared to those obtained using a PVdF membrane hydrophone.

Results

The finite difference model reveals a strong correlation between experimental and numerical results. In addition, the performance characteristics of the hydrophone are seen to arise from the relatively complex layered structure of the sensor. When an acoustic wave interacts with the sensor tip, up to 9 separate edge wave components are generated. These waves combine and interfere, leading to the non-uniform frequency response.

Results from the modelling reveal that rounding the fibre tip reduces edge wave generation, significantly improving the uniformity of the frequency response, a finding that was confirmed by experimental measurements.

Discussion and Conclusions

The frequency response of the Fabry-Perot fibre-optic hydrophone has been significantly improved by using a rounded tip geometry. Combined with deconvolution, this allows the fibre-optic hydrophone to be used to make accurate measurements of the output of medical ultrasound devices operating at high frequencies without sacrificing sensitivity. Previous work, outlining the ability of this hydrophone to make simultaneous measurements of temperature and acoustic pressure, combined with the results presented here, indicate that this type of fibre-optic hydrophone may be a useful tool for characterising the output of both diagnostic and therapeutic medical ultrasound devices.

5H-3

8:45 AM Development of Texture in Lead Zirconate Titanate (PZT) by Applying Electric Field during Gelcasting

Sedat Alkoy¹, M.Yunus Kaya^{1,1}Gebze Institute of Technology, Kocaeli, Turkey

Background, Motivation and Objective

Grain oriented (textured) polycrystalline piezoelectric ceramics can provide single-crystal like properties without experiencing any difficulties of single crystal growth process. There are various processes to obtain texture such as; hot pressing (HP), templated grain growth (TGG), orientation under a high magnetic field during a gelation process. However, high pressures at high temperatures are required for HP, anisometric template particles are required for TGG and anisotropic particles are required for magnetic alignment. These methods have not been used for piezoelectric lead zirconate titanate (PZT) ceramics. This study reports a method to obtain texture in PZT ceramics by application of an electric field during gelation of a gelcast slurry.

Statement of Contribution/Methods

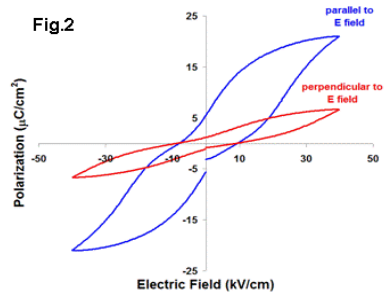
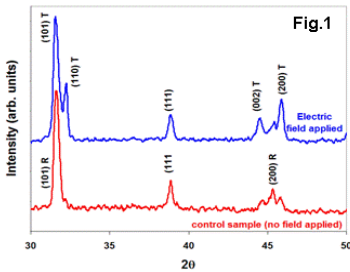
MAM (monomer), PEGDMA (crosslinker) and dispersant were dissolved in DI water to form a premix. Hard PZT (PZT-4) powder was dispersed in this premix. Before casting into the mold, APS (initiator) and TEMED (catalyzer) were added to the slurry. An electric field of 3 kV/cm was applied to the slurry for 30 min at room temperature during gelation. Sintering was done at 1260°C for 4 h.

Results

XRD pattern of sintered samples in Fig.1 indicates that PZT has rhombohedral symmetry but develops a tetragonal symmetry as a result of electric field applied during gelation. Dielectric constants and piezoelectric d_{31} coefficients along and perpendicular to E-field are 1070 & 450 and 390 & 280 pC/N, respectively. Hysteresis loops are compared in Fig.2.

Discussion and Conclusions

Gelcasting provides a means to lock the particles aligned under the application of a high electric field via gelation and this alignment in green body was retained after sintering. Electrical properties are greatly enhanced along the E-field direction.



5H-4

9:00 AM Fiber optic Sagnac interferometer for characterizing ultrasound biomicroscopy transducers

Matthew Churgin¹, Mengyang Liu¹, Takashi Buma¹; ¹University of Delaware, USA

Background, Motivation and Objective

There is a lack of hydrophones with sufficient spatial resolution and bandwidth for accurate measurements of ultrasound biomicroscopy transducers. Optical techniques achieve extremely fine spatial resolution and broad detection bandwidth. Furthermore, fiber optic technology can significantly improve portability and ease of use.

Statement of Contribution/Methods

We demonstrate a fiber optic Sagnac interferometer with an immersible probe head for characterizing high frequency ultrasound transducers. The fiber-coupled probe head contains optical components as well as the acoustic sensing surface, which is made from polydimethylsiloxane (PDMS). The entire probe head is encapsulated with PDMS for immersion applications. The fiber optic hydrophone is used to characterize a 100 MHz $f/1$ zinc oxide transducer (2 mm focal length). The detection bandwidth of the hydrophone is 250 MHz, limited by the internal fiber delay-line within the interferometer. The transducer is laterally scanned over a 50 x 50 grid in 2 m increments. The signal from each location is averaged 32 times by a 500 MHz 8-bit digital oscilloscope.

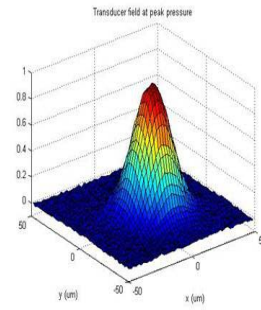
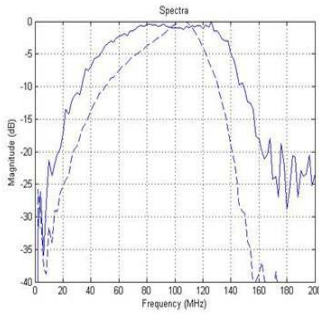
Results

Figure 1 shows the spectra of the fiber optic hydrophone signal (solid line) and the transducer pulse echo signal (dashed line). The slight difference is expected since the pulse echo spectrum is shaped by both the transmit and receive response of the transducer. Figure 2 shows a surface plot of the peak transducer field spanning 100 x 100 μm . The -3 dB transmit beam width is 20 μm along both x and y axes.

Discussion and Conclusions

These results demonstrate that a fiber optic Sagnac interferometer with an immersible probe head is well suited for characterizing ultrasound biomicroscopy transducers.

Wednesday
Oral



5H-5

9:15 AM High Temperature Guided Acoustic Wave Transducers Using Mechanical Gratings

K.-T. Wu¹, W.-L. Liu¹, M. Kobayashi², C.-K. Jen², Y. Ono³, M. Takeuchi⁴, ¹Electrical and Computer Engineering, McGill University, Canada, ²Industrial Materials Institute, National Research Council Canada, Canada, ³Carleton University, Canada, ⁴Tamagawa University, Japan

Background, Motivation and Objective

Guided acoustic waves are of attraction for structural health monitoring (SHM) and NDT applications because they may inspect parts or structures of a large area within a short time period using a few ultrasonic transducers (UTs). For aerospace industry such SHM and NDT may require that the UTs operate from -80°C to 100°C . The main motivation of this research is to develop miniature and light weight integrated and flexible guided acoustic wave transducers involving the use of line-shape mechanical gratings for the application within such temperature range.

Statement of Contribution/Methods

Mechanical line-shape gratings have been machined with different dimensions and number of gratings to convert longitudinal (L) waves into plate (PAWs) or surface acoustic waves (SAWs) depending on the substrate thicknesses. Piezoelectric lead-zirconate-titanium (PZT) composite films served as L wave integrated UTs (IUTs) were made by a sol-gel sprayed technique onto the opposite surface of the metallic substrate having the mechanically gratings. If the substrate is thick, then such a layout is an integrated guided acoustic wave transducer configuration. The merit of this approach is that IUT can be at the internal surface of a structure and mechanical gratings at the external surface. If the substrates are $75\mu\text{m}$ thick membranes, then it is a flexible guided acoustic wave transducer design. Theoretically simulations of the mode conversion from L wave to guided acoustic waves are also carried out.

Results

Line-shape mechanical gratings with a line interval of 0.6 mm, a width of 0.3 mm, a depth of 0.04, 0.06 mm or 0.12 mm, an aperture of 10 mm and different numbers of gratings have been made onto stainless steel (SS) or aluminum substrates of 10 mm, 0.15 mm and 0.075 mm thick. Thick PZT composite films have been made as IUTs at the direct opposite side of these gratings and their center frequencies of the IUTs are between 5 and 12 MHz. The ultrasonic signals were obtained in transmission and pulse-echo modes up to 150°C . The signal-to-noise ratio of the received signals is better if the substrate is thinner. The line interval of gratings determines the center frequency of the L wave converted guided PAWs or SAWs as confirmed by the theoretical simulation using a finite difference computer program. The higher is the number of the gratings, the narrower is the bandwidth of the guided acoustic waves. The line gratings and IUT made onto the $75\mu\text{m}$ thick SS membranes as flexible guided acoustic wave transducers attached to another 2 mm thick aluminum plate were used for NDT of the defects artificially made onto the aluminum plate.

Discussion and Conclusions

Integrated and flexible guided acoustic wave transducers have been made using line shape mechanical gratings together with sol-gel fabricated IUT at the opposite side. They can operate up to 150°C . If the substrate is thin, then such flexible guided acoustic wave transducers may be attached or bonded to parts even with curved surfaces and used for NDT or SHM purposes.

6H. Phononic Crystals-Devices, Filters, Couplers

Baalbek

Wednesday, September 23, 2009, 8:00 am - 9:30 am

Chair: **Toyokatsu Miyashita**
Ryukoku University

6H-1

8:00 AM Acoustic Filter based on Coupled Resonator Acoustic Waveguides in phononic crystal slabs

Abdelkrim Khelif¹, Saeed Mohammadi², Ali Adibi^{2,1}UMI, CNRS/ GeorgiaTech Joint Laboratory, Atlanta, Georgia, USA, ²ECE, Georgia Institute of Technology, Atlanta, Georgia, USA

Background, Motivation and Objective

Recently, phononic band gap materials, the so-called phononic crystals, have been made possible by using periodic structure by analogy to photonic and semiconductor crystals. These materials allow the propagation of elastic waves to be regulated. In other words, they play the role of perfect mirrors for elastic waves in the frequency window of the band gap, i.e., forbidding elastic waves for all polarizations and directions. This area of research has received much attention because of the fundamental interest in localization of elastic energy and the vast potential applications. Among the promising prospects are acoustic devices that have been extensively used for high-frequency applications, such as radio-frequency filters for mobile phones and wireless networks in the form of surface acoustic wave devices or thin film bulk acoustic resonators. In this paper, we focus on employing the phononic band gap concept in the conventional acoustic systems to enhance the performance or even widen their range of applications. The coupled resonator acoustic waveguide (CRAW) structure is an illustration of the capabilities of these new materials to confine the elastic energy and enable novel functionalities through control and engineering of the dispersion of acoustic waves by only using the geometry of the phononic crystal structure.

Statement of Contribution/Methods

In this paper we demonstrate experimentally the possibility of forming a new acoustic filter structure based on the CRAWs with superior performance over the conventional filters. The structures are made by etching an array of microsize holes in a silicon membrane. This phononic slab structure exhibit a complete phononic band gap. The filter is composed of several single resonators that are coupled periodically through evanescent waves due to the complete acoustic band gap of the slab. Under certain conditions, selective filter modes occur within the omnidirectional band gap. In this case, the elastic energy is localized in the extended defect formed by the collective coupled resonators. The frequencies of the filters are sensitive to the geometrical parameter of the defect line and to the separation distance between the single resonators.

Results

The phononic crystal slab structures are made by etching a honeycomb array of microsize holes with 15 μm period in a silicon membrane. The thickness of the membrane is equal to 15 μm . This phononic slab structure exhibits a complete phononic band gap in the frequency range of (115-150 MHz). An acoustic filter based on CRAW within the band gap frequency range with excellent flat frequency response over a relative bandwidth of 10% is demonstrated.

Discussion and Conclusions

Using the evanescent waves coupling between several single resonators that occur within complete acoustic band gap of the phononic slab, we have demonstrated a new acoustic filter. Such research should be invaluable for the evaluation of future acoustic devices and for revealing the physics of the interaction of acoustic waves with phononic crystals.

6H-2

8:15 AM **Ultra High Frequency (UHF) Phononic Crystal Devices Operating in Mobile Communication Bands**

Roy Olsson¹, Yasser Soliman², Drew Goettler², Mehmet Su², Ihab El-Kady¹, Zayd Leseman²; ¹Sandia National Laboratories, USA, ²University of New Mexico, USA

Background, Motivation and Objective

Microfabricated phononic crystals (PhonC) with integrated acoustic transducers and PhonC devices (resonators and waveguides) have recently been reported at VHF (30-300MHz). PhonCs are of great interest for miniaturizing and improving performance of next generation acoustic signal processing devices for mobile communications. To have broad impact on wireless communications, PhonCs must be scaled to relevant RF frequency bands.

Statement of Contribution/Methods

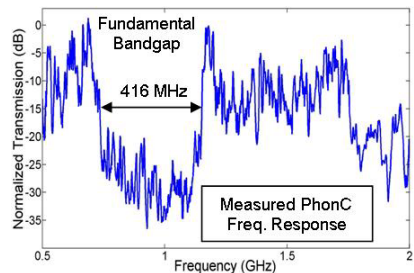
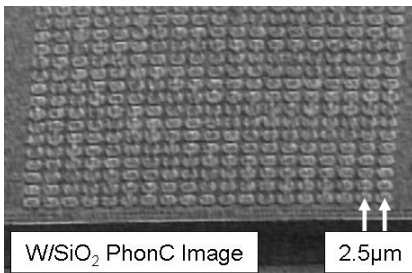
The frequency range of PhonC slabs is expanded by nearly an order of magnitude into the commonly used GSM-850 and GSM-900 cellular phone bands. Utilizing a cermet topology of high acoustic impedance W inclusions in a silica low acoustic impedance membrane, PhonC devices in wireless bands have been realized. Ensuring that the inclusions and host medium have low acoustic velocity mismatch allows scaling to GHz frequencies with minimum feature sizes greater than 1 μ m.

Results

The fabricated PhonC devices are composed of 1.4 μ m diameter W rods arranged in a 2.5 μ m pitch square lattice inside a 1.85 μ m thick suspended silica membrane. AlN acoustic transducers are used to characterize the response. The measured phononic bandgap is centered at 943MHz and is 416MHz wide, a frequency span that covers both the GSM-850 and GSM-900 cellular bands. The maximum bandgap depth is 35dB for an 18 period PhonC. PhonC based waveguides exhibit less than 3dB of normalized loss. W/Si PhonCs currently in fabrication are expected to achieve higher frequencies and lower losses.

Discussion and Conclusions

Scaling of PhonCs to cellular frequency bands allows this emerging technology to be applied to signal processing for wireless communications. Potentially interesting devices include high-Q resonators, filters, waveguides, combiners and dividers.



Wednesday
Oral

6H-3

8:30 AM **Transmission Properties of 1D and 2D Phononic Crystal Sensors**

Ralf Lucklum¹, Jing Li²; ¹Institute for Micro and Sensor Systems, Otto-von-Guericke-University, Magdeburg, Saxonia-Anhalt, Germany, ²Otto-von-Guericke-University, Germany

Background, Motivation and Objective

Phononic crystals (PnC), which are periodic composite materials, will be introduced as a new platform for sensing liquid properties in small cavities. A 1-dimensional realization consists of a periodic repetition of 2 layers with different acoustic properties. A 2-dimensional device consists of scattering centers with acoustic properties different to a homogeneous matrix surrounding the scatterers. The most strikingly feature of PnC are frequency bands (stop bands) within which sound cannot propagate through the structure. Since the spatial modulation of the material parameters of the PnC is in the same order as the acoustic wavelength in the stop band, they can be realized in a wide geometric dimension range. With frequencies in the MHz-range phononic crystal sensors should

especially give access to dimensions common in microfluidic devices where the number of sensors applicable for material property determination in microchannels or microreactors is rather limited.

Statement of Contribution/Methods

The sensor concept is based on monitoring changes of characteristic features of the transmission properties of the phononic crystal with changes of properties of one component that builds the PnC. Here we use the dependence of frequencies of transmission peaks within the band gap which are correlated to material properties of a liquid confined between a solid. As proof of concept a 1-dimensional realization with a single liquid gap as well as a 7-layer arrangement have been modeled and experimentally verified with two external piezoelectric transducers coupled to the device. A 2-dimensional phononic crystal sensor has been developed and optimized which consists of a solid matrix and a certain number of periodically arranged holes which are filled with the liquid of interest.

Results

A transmission peak sensitive to speed of sound, c , of the liquid has been predicted between 600 and 800 kHz from 1-dimensional transmission line model calculations and experimentally found both in the impedance plot of the piezoelectric transducer and the transmitted signal. It has been examined for a mixture of water and propanol. The measurements recover the literature values of c vs. x , the molar ratio of the mixture incl. the maximum in c for $x_{\text{propanol}} = 0.2$. Calculations with the layer multiple scattering theory predict similar features for the 2-dimensional phononic crystal sensor.

Discussion and Conclusions

The frequency shift of the resonant peak with speed of sound of the liquid is a function of frequency, its bandwidth a function of the number of layers. The resolution in concentration of our single fluidic gap arrangement is about 0.1 % for a molar ratio of 0 ... 0.1 and therefore already experimentally of great relevance. With the 7-layer arrangement we have found an optimal design with a resolution of more than 2 kHz frequency shift for a 1% change in speed of sound. With a 2-D phononic crystal sensor one can reduce the shape of the liquid cavity from a sheet to a channel.

6H-4

8:45 AM High-quality Factor Piezoelectric-on-substrate Phononic Crystal Micromechanical Resonators

Saeed Mohammadi¹, Ali Asghar Eftekhari¹, Abdelkrim Khelif², Ali Adibi^{1,3} *Electrical and Computer Engineering, Georgia Institute of Technology, Atlanta, Georgia, USA, ²CNRS-Georgia Tech Joint Laboratory, USA*

Background, Motivation and Objective

Phononic crystal (PnC) structures are gaining a growing attention due to their ability to engineer the properties of acoustic modes in mechanical structures. The possibility of achieving complete phononic band gaps (CPnBGs) for a wide range of frequencies in PnC structures has enabled the confinement and guidance of mechanical energy at small footprints. High-frequency, high-quality factor (Q) MM resonators are perhaps the main building blocks for realizing functional devices such as filters, multiplexers, and de-multiplexers for wireless communications and sensing applications. Therefore, realization of high-Q, high-frequency PnC resonators can lead to functional PnC-based devices with potentially better performance compared to their conventional counterparts.

Statement of Contribution/Methods

In this paper, we report, a high-Q, PnC piezoelectric-on-substrate MM resonators operating at VHF frequencies. The PnC structure in this work is based on a hexagonal lattice PnC formed by etching a hexagonal array of holes in a free-standing silicon slab. The PnC resonator is created by embedding a defect, [e.g., by removing (i.e., not etching) a number of PnC holes], in the periodic PnC structure. Metal electrodes and a thin ZnO piezoelectric layer are placed directly on the resonant structure for input/output coupling of the electric signal to the mechanical mode in the resonator. In such a structure, the number of the PnC layers around the resonator defect area can be increased to reduce the loss due to leakage of the mechanical energy through the PnC structure; consequently the loss of the mechanical energy will be limited to material and friction losses only. Furthermore, by tailoring of the geometry of the metal electrode on top of the resonant structure, it is possible to maximize the coupling of the applied input electrical power to the mechanical mode inside the PnC resonator and therefore, obtain lower electrical impedance in a smaller footprint.

Results

High-Q PnC resonators are demonstrated by embedding defects in hexagonal-lattice PnC fabricated in free-standing Si slab. Q's more than 10,000 have been obtained at frequencies as high as 130 MHz. The acoustic mode in the PnC resonator is directly excited by fabricating the transducer directly on the PnC resonator for piezoelectric

excitation. A relatively low input impedance is obtained by tailoring the shape of the metal electrode to match the field profile of the acoustic mode in the PnC resonator.

Discussion and Conclusions

PnC structures enable high-Q resonators as they can completely suppress losses due to in-plane leakage of the mechanical energy from the resonators mechanical supports. The Q of the PnC resonator in such structures will be solely limited to the intrinsic acoustic loss of the materials. Direct excitation of the PnC and tailoring the metal electrodes to minimize the input/output impedance of the PnC resonators enable low impedance PnC resonators. In summary, PnC structures provide a flexible platform for the design of high quality, low-impedance, and low-insertion loss MM devices for use in wireless communications and sensing.

6H-5

9:00 AM Design of Acoustic Couplers Using Gradient-Index Phononic Crystals

Sz-Chin Lin¹, Bernhard Tittmann¹, Tony Huang¹; ¹*Engineering Science and Mechanics, The Pennsylvania State University, University Park, PA, USA*

Background, Motivation and Objective

Phononic crystal waveguides (PCWGs) can efficiently guide acoustic waves along predefined defects in a compact space on the wavelength-scale, a feature useful for micro/nanoscale acoustic circuits. However, the dimension mismatch between an input acoustic beam and a PCWG could cause a great deal of energy loss, which is undesirable for practical applications. To fully realize the functionality of a PCWG, we designed an acoustic beamwidth compressor based on a concept called gradient-index phononic crystals (GRIN PCs) to efficiently couple acoustic energy into the waveguide over its working bandwidth.

Statement of Contribution/Methods

An acoustic coupler that consists of a GRIN PC butt-coupled with a straight PCWG was studied. The PCWG is obtained by simply removing the center row of cylinders from a square-lattice gold/epoxy PC. The GRIN PC contains a square array of solid cylinders embedded in epoxy. By gradually modulating the material properties of cylinders that comprise the GRIN PC, we induce a parabolic acoustic velocity gradient along the modulating direction that converges wide beam plane waves at a focal zone with a full-width at half maximum (FWHM) of one wavelength and a gain of 8 dB. The GRIN PC is not frequency-dispersive and can stably focus acoustic waves over the operating frequencies of the PCWG.

Results

The FDTD-calculated steady-state transmitted acoustic energy at the outlet of the PCWG shows a transmission enhancement of 7.2 times compared to a stand-alone PCWG. An average transmission rate of 80% and a beam-size conversion ratio of 6.5:1 were obtained over the operating frequencies of the PCWG. Up to a 90% transmission rate was observed at a range close to the design frequency of the GRIN PC.

Discussion and Conclusions

We computationally prove that a GRIN PC-based beamwidth compressor can exhibit a beam-size conversion ratio of 6.5:1 and average/maximum transmission efficiency of 80%/90% over the working frequency range of a straight PCWG. The methodology described in this work can be useful in applications relating to signal processors and acoustic sensors.

6H-6

9:15 AM Peculiar refraction phenomena in a solid/air phononic crystal

Jerome vasseur¹, Jim Bucay², Pierre Deymier², Eleonore Rousselet³, Anne-Christine Hladky-Hennion³, Yan Pennec³, Khrishna Muralidharan¹, Bahram Djafari-Rouhani³, Bertrand Dubus³; ¹*EPHONI, IEMN, Villeneuve d'Ascq, France*, ²*DMSE, University of Arizona, Tucson, Arizona, USA*, ³*IEMN, France*, ⁴*University of Arizona, USA*

Background, Motivation and Objective

Phononic crystals (PCs) consist of periodic arrangements of inclusions in a physically dissimilar matrix. The periodicity as well as the differences in the impedance of the constituent materials can cause Bragg scattering, leading to a selectivity in which, at certain frequencies, wave propagation is forbidden. The band structure of these artificial composite materials may also present dispersion curves with a negative slope. This opens the way for devices exhibiting peculiar refraction properties.

Statement of Contribution/Methods

We present a theoretical and experimental study, in the audible frequency range, of the refraction properties of a PC consisting of a square array of cylindrical Polyvinylchloride (PVC) inclusions in air. Theoretical results based on the Plane Wave Expansion (PWE) method, the Finite Difference Time Domain (FDTD) method and the Finite Element (FE) method show, in full agreement with the measurements, that the PC exhibits positive, negative, or zero angle refraction depending on the angle of the incident sound beam. Zero angle refraction means that in a specific range of angle of incidence, the acoustic beam is self-collimated inside the PC as can be observed through a usual waveguide.

Results

Due to a lattice parameter in the cm range (2.7 cm), the refraction phenomena occur in the audible frequency range and can be observed using a very usual experimental setup. We observed three different refraction phenomena occurring at the two sides of the PC. Moreover upon exiting the crystal, all allowed angles of incidence underwent beam splitting. We explained these features in terms of the system's equifrequency surfaces (EFS's). It was found that a number of characteristics must be present in the EFS's in order to produce the observed behaviors. These included EFS's which were nearly square and whose size and position allowed more than one EFS to overlap with half the EFS of the incident media. This allows all types of wave refraction on the input side of the PC, as well as creates beam splitting upon exit of the PC. We showed also that focusing of acoustic waves at the exit of the PC may occur under certain specific conditions.

Discussion and Conclusions

Positive, negative, and zero angle refraction can be obtained in the PVC/Air PC by varying the angle of the incident beam at a single frequency. These properties result from the unique geometry of the PC's equi-frequency surfaces as compared to that of the incident media. This allows for all types of wave refraction on the input side of the PC, as well as creates beam splitting upon exit of the PC. These properties, observed in the audible frequency range, remain valid for ultrasonic waves by reducing the lattice parameter of the PC.

1I. Elasticity and Thermal Effects

Sala 1

Wednesday, September 23, 2009, 11:30 am - 1:00 pm

Chair: **Michael Insana**
Univ. of Illinois at Urbana-Champaign

1I-1

11:30 AM Temperature dependence of shear modulus in ex vivo muscle assessed by ultrasound

Emilie SAPIN¹, Jean-Luc GENNISSON¹, Mathieu PERNOT¹, Mickael TANTER¹, Mathias FINK¹; ¹Langevin Institute, Laboratoire Ondes et Acoustique, ESPCI ParisTech, CNRS UMR 7587, INSERM, PARIS, France

Background, Motivation and Objective

Ultrasound-based techniques to monitor HIFU treatments, combining temperature and elasticity mapping, requires better understanding of the thermal effects on soft tissues elasticity. Hence, the study aims at evaluating the temperature dependence of the shear modulus of ex vivo bovine muscles.

Statement of Contribution/Methods

20 samples of roast beef were slowly heated into a thermally-controlled saline bath. Thermocouples were used to assess temperatures both into water and muscles. Local elasticity was assessed using Supersonic Shear Imaging. 4 successive shear plane waves were created along different echographic lines (probe L7-4, 5MHz), thanks to the radiation force generated by 4 “pushing” beams for 200 μ s at 4 depths along the same line. The shear wave propagation was acquired with 30 images at 5000 frames/s, from which the elasticity map was recovered. Shear modulus was computed as the median of the local values into a manually-chosen region of interest. Samples were heated from 20°C to 70°C by steps of 10°C and 20 minutes long and cooled back at room temperature. Elasticity assessment was achieved every minute, either along or perpendicular to the muscular fibres. To identify reversibility-irreversibility thresholds, samples were heated from 20°C to successively 30°C, 40°C, 50°C, 60°C and 70°C for 20 minutes and cooled back at 20°C for 20 minutes.

Results

Shear moduli decreased linearly with increasing temperature up to about 60°C, with a change in slope around 45°C-50°C, and then exponentially increased (irreversible changes) for higher temperatures. Cool-down behaviour depended on the ratio: shear modulus at the end of the heating / initial shear modulus. Ratio < 1 led to a constant modulus during cool-down whereas ratio > 1 led to increasing modulus. Perpendicularly to the fibres, the initial modulus was 1.5 lower than along the fibres.

Discussion and Conclusions

The present study experimentally assessed the thermal-induced changes in the shear modulus of ex vivo bovine muscles using ultrasound. The thermo-mechanical behaviour is consistent with changes in collagen at the micro-scale. Indeed, the shear modulus decreases with increasing temperatures up to 60°C, because of the collagen unfolding process. Above 60°C, collagen is irreversibly transformed into a random structure, which leads to an exponential irreversible increase in the muscular elasticity. A change in slope is observed around 45°C-50°C for all the samples and an original pattern was shown: the cool-down behaviour depends on the shear modulus at the end of the heating relative to the initial value. Time effects and water absorption in the medium have to be explored to complete this work. This study gives promising prospects for the use of a full-ultrasound-based technique to monitor thermal effects on tissues.

11-2

11:45 AM **Complex Shear Modulus of Thermally-Damaged Liver**

Marko Orescanin¹, Muqem Qayyum², Kathleen Toohey², Michael Insana²; ¹Electrical and Computer Engineering, University of Illinois at Urbana-Champaign, Urbana, IL, USA, ²Bioengineering, University of Illinois at Urbana-Champaign, Urbana, IL, USA

Background, Motivation and Objective

Ablative procedures for initiating coagulative necrosis surrounding unresectable liver tumors receive attention as potential cancer treatments. Experience shows that thermal lesions are significantly stiffer than surrounding untreated liver. Therefore elasticity imaging has promise for monitoring lesion growth during ablation. We measured time-varying shear properties of normal and thermally damaged liver as a function of strain amplitude and strain rate to develop a constitutive model of shear wave propagation in liver.

Statement of Contribution/Methods

Shear wave imaging techniques were applied to measure complex shear moduli of liver samples, ex vivo. Porcine livers were obtained minutes after harvesting and samples were measured in saline within 8 hours. Samples from the same organ were heated for 1.5 hours at 47C to stimulate the protein degradation in ablative therapies and measured using the same techniques. A vibrating needle placed in samples generated cylindrical shear waves (50 - 300 Hz) at various strain amplitudes that were imaged using pulsed Doppler methods (SonixRP, linear array) to measure viscoelastic properties. Through shear speed dispersion fitting, complex shear moduli $\mu - i\omega\eta$ were estimated. Standard indentation tests provided estimates of the relaxed elastic shear modulus (<1 Hz).

Results

The elastic shear modulus of fresh and thermally-damaged porcine liver samples were found using indention techniques to be $\mu = 107 \pm 35$ Pa and $\mu = 200 \pm 95$ Pa, respectively. Conversely, shear wave imaging between 50-300 Hz yielded frequency-independent moduli: $\mu = 1757 \pm 733$ Pa and $\eta = 1.72 \pm 0.48$ Pa s for fresh liver and $\mu = 3851 \pm 3233$ Pa and $\eta = 8.9 \pm 2.9$ Pa s for thermally-damaged liver. While the measurement techniques yielded very different results, in each case the elastic modulus doubled for damaged liver. These values were found to vary significantly with strain amplitude, suggesting that liver is a highly nonlinear medium.

Discussion and Conclusions

Similar discrepancies between indenter and shear wave imaging results were found in the literature for fresh bovine liver and may be explained in terms of the strain amplitude and strain rate dependencies of nonlinear media. Our measurements show that the elastic modulus doubles and is independent of frequency while the viscous modulus η increases five-fold with unknown frequency dependence. The frequency independence of μ suggests that the lesion contrast in strain imaging will be similar for all measurement techniques. The larger change in η values suggests time-varying strain images may offer larger contrast for tracking thermal lesion growth.

We are developing a theoretical framework that nondimensionalizes the governing equations to propose parameters, similar to Reynolds number, to determine dynamic similitude between different experimental cases when comparing mechanical properties.

11-6

12:00 PM **Elastic Modulus Imaging (EMI) for Visualizing Thermal Ablation Zone: Initial Experience in A Porcine Model**

Jingfeng Jiang¹, Chris Brace², Anita Andreano², Ryan DeWall¹, Nick Rubert¹, Fred Lee², Tomy Varghese¹, Timothy Hall¹; ¹Medical Physics, University of Wisconsin, USA, ²Radiology, University of Wisconsin, USA

Background, Motivation and Objective

Effective tumor localization and intra-procedural monitoring are critical to treatment success during thermal ablation. Although conventional B-mode ultrasound is ineffective at depicting the margin of tissue coagulation, more advanced ultrasound-based parametric imaging methods such as the proposed elastic modulus imaging (EMI) method showed great potential in determination of the size and shape of the ablated area where protein denaturation and water vaporization cause an increase of the tissue modulus. Our aim in this study is to investigate the feasibility of using the EMI method for evaluation of thermal ablation zones.

Statement of Contribution/Methods

A regularized block-matching algorithm was used to obtain displacement data between a pair of pre- and post-deformation (induced by the ablation applicator) ultrasound echo fields. 2D strain (i.e. axial gradients of displacements) and elastic modulus images were then reconstructed from their corresponding displacement data.

Wednesday
Oral

More specifically, the EMI method iteratively adjusts local modulus values to enforce a biomechanical model to produce displacements close to those obtained from ultrasonic speckle tracking. A total of 14 radiofrequency (RF) and microwave ablation zones (1-3 cm in diameter) were created in vivo in 5 porcine animals with normal livers. After open-abdominal ablation, RF ultrasound echo data were acquired under the guidance of a real-time strain imaging system. Ablation areas at gross pathology in the corresponding imaging planes were then compared to imaging results obtained by the EMI and strain imaging methods.

Results

Comparing ablation area measurements, EMI had higher correlation with gross pathology measurements than strain imaging (EMI Pearson coefficient = 0.965, $p < 0.0001$; strain Pearson coefficient = 0.857, $p < 0.0001$). We also found that EMI more accurately depicts thermal ablation zone size than strain imaging (area underestimation of 8.2% versus 13.7%, respectively). Furthermore, the EMI method improved contrast-to-noise ratios by approximately a factor of 2 compared to strain images.

Discussion and Conclusions

These preliminary results support the hypothesis that EMI may potentially enhance the ability to visualize thermal ablation zones, thereby improving assessment of ablative therapies. Our future work will be directed to test the EMI method in tumor-bearing animal models and to rigorously validate our results with histology in these models.

11-4

12:15 PM Comparison of different compression methods for ultrasound elastography in order to detect HIFU ablations in the liver: preliminary in vivo results.

Jeremy Chenot¹, David Melodelima¹, Hubert Parmentier¹, Michel Rivoire², Jean-Yves Chapelon¹; ¹unit 556, inserm, Lyon, France, ²Institut de Chirurgie Expérimentale, Centre Léon Bérard, Lyon, France

Background, Motivation and Objective

Guiding HIFU treatments using elastic properties of ablated tissues is gaining attention since it is non-invasive and can provide new information. Good-quality elasticity imaging requires highly controlled compressions, which are often challenging to obtain with hand-held devices. Here we report the comparison of 4 compression methods for the detection of HIFU ablations created in the liver during surgery.

Statement of Contribution/Methods

This work was performed in vivo in 12 pigs. HIFU lesions of 20 cm³ were produced in the liver during surgery using a previously validated toroidal HIFU device working at 3 MHz. Ablations were imaged with conventional ultrasound imaging and elastography. Two probes were used: a 7.5 MHz sectorial array placed in the centre of the HIFU device and a conventional 12 MHz linear array. During elastography, the probe was placed directly on the liver and compression was performed using four different methods: (i) the probe was used to manually exert a periodic pressure on the liver, (ii) the liver was compress manually between the hand of the operator and the probe, (iii) the liver was compress manually between a PVC cylindrical plate (diameter 75mm, height 5mm) and the probe, and (iv) the compression was performed by the probe fixed on a motorized arm. Seven days after the treatment, ablations were imaged again using the same methodology. The resulting images were analyzed and compared by calculating CNRe, SNRe and contrast. Dimension of ablation measured with sonography and elastography were compared to those measured on gross pathology.

Results

The mean elastography contrast was similar for each compression method (17.6 dB for hand-held compression, 19.8 dB if the liver was compressed between the probe and the hand, 18.2 dB using the PVC plate and 20.1dB using the motorized compression). The quality of elastograms was also similar for all compression methods, CNRe ranged between 1.23 and 1.96, SNRe ranged between 0.90 and 1.04. The correlation between dimensions measured on elastograms and on gross pathology were higher in the case of elastography obtained by compression with the plate ($R^2=0.79$). In the other cases the correlations were: $R^2=0.63$ for manual compression, $R^2=0.69$ for compression of the liver between the probe and the hand of the operator and $R^2=0.46$ for motorized compression. Compared with sonograms, all elastography methods shown higher contrast and better estimation of ablation dimensions.

Discussion and Conclusions

The best compromise between image quality, flexibility of the compression method, motion artifacts and the accessibility of all parts of the liver was judge to occur when using the plate. Nevertheless this approach is feasible only because the treatment is performed during surgery. Hand-held compression is also a good approach with broader possible applications.

11-5

12:30 PM **Real-Time Ultrasound Elasticity Imaging For Liver RF Ablation Assessment: Preliminary ex vivo and in vivo Animal Studies**

Hua Xie¹, Anna Fernandez², Unmin Bae³, Sheng Xu¹, William Pritchard⁴, John Karanian⁴, Alberto Chiesa⁴, Bradford Wood⁵, Jochen Kruecker^{1,2}, *Philips Research North America, Briarcliff Manor, New York, USA*, ²*Booz Allen Hamilton, Rockville, Maryland, USA*, ³*Philips Medical Systems, Bothell, Washington, USA*, ⁴*Lab. of Cardiovascular and Interventional Therapeutics, FDA, Laurel, Maryland, USA*, ⁵*Clinical Center, NIH, Bethesda, Maryland, USA*

Background, Motivation and Objective

We had previously demonstrated the feasibility of using RF electrodes to induce tissue deformation for ultrasound elasticity imaging in ex vivo and clinical liver radio frequency ablation (RFA) assessment, with the strain images formed by off-line processing. In clinical applications, however, only real-time elasticity imaging will have the ability to identify ablated regions and provide immediate feedback to determine the need for additional ablations during the same treatment session.

Statement of Contribution/Methods

In this study, a real-time compression based elasticity imaging prototype was developed and evaluated for liver RFA assessment under ex vivo and in vivo conditions. The prototype was implemented on a commercial ultrasound system (iU22, Philips Healthcare) for an L12-5 linear transducer and a C5-1 curvilinear transducer. Under the ex vivo condition, bovine liver samples were degassed and embedded in a gelatin phantom. Under the in vivo condition, pigs were anesthetized and mechanically ventilated. Ultrasound elasticity imaging experiments were performed during breath-hold in order to reduce respiratory motion artifacts. Post-RFA strain images were compared against several imaging modalities including MRI, contrast-enhanced CT and gross pathology.

Results

For the ex vivo case, a Rita Starburst probe (AngioDynamics, Queensbury, NY) was used to perform RFA and induce tissue deformation for strain imaging. Real-time strain images were generated pre- and post-RFA. After the ablation, the liver phantom was imaged by a Panorama 1-T MRI system, then it was dissected along the approximate ultrasound imaging plane for lesion dimension measurement using a caliper. The post-RFA strain images depicted an ablation zone with increased stiffness that was well correlated with the physiological changes observed in the T1-weighted MR image and gross pathology. The strain image revealed an ablation zone of 4.9 cm x 2.9 cm, and the MR image and gross pathology showed a zone of 4.6 cm x 3.2 cm and of 4.9 cm x 3.6 cm, respectively. For the in vivo study, three different commercial RFA needles were employed: the Covidien (Mansfield, MA) CoolTip single prong and triple-cluster probes, and the Rita Starburst probe. The animals underwent contrast-enhanced CT imaging immediately after RFA. They were then sacrificed and the ablated liver lobes were dissected for ex vivo MRI. All three imaging modalities showed comparable measurement of lesion dimensions. The triple-cluster Covidien probe and the Rita probe with expanding tines seemed to perform better with elasticity assessment than the Covidien single probe.

Discussion and Conclusions

Preliminary results from this study demonstrate that real-time ultrasound strain imaging is potentially a valuable tool for assessing liver RFA. Further technical development of this prototype will advance toward real-time clinical use.

11-3

12:45 PM **In vivo Ultrasound Electrode Displacement Strain Imaging**

Nicholas Rubert¹, Shyam Bharat¹, Ryan DeWall², Anita Andreano³, **Tomy Varghese⁴**, Christopher Brace³, Jingfeng Jiang¹, Lisa Sampson³, James Zagzebski¹, Fred Lee^{1,2}, *Medical Physics, University of Wisconsin-Madison, USA*, ²*Biomedical Engineering, University of Wisconsin-Madison, USA*, ³*Radiology, University of Wisconsin-Madison, USA*, ⁴*Medical Physics, University of Wisconsin-Madison, Madison, WI, USA*

Background, Motivation and Objective

The incidence of primary and secondary liver tumors has increased significantly worldwide over the last two decades. Due to co-morbidity, poor liver function and/or number and distribution of lesions, only a minority of these patients can be treated with surgery. As an alternative to surgical resection, percutaneous RF ablation is used to thermally destroy the tumor in situ, having the advantage over surgery of being minimally invasive. Effective treatment monitoring in real-time is an important factor in the success of RF ablation, and ultrasound elastography could become a convenient, cost-effective means to delineate boundaries of the ablated zone for clinical personnel during the procedure.

Wednesday
Oral

Statement of Contribution/Methods

This study assessed electrode displacement-based strain imaging for monitoring abdominal RF ablation procedures that are difficult to access with conventional elastography on 5 porcine animal models. We present results utilizing a novel approach of displacing the ablation electrode itself to introduce the mechanical stimuli required for strain imaging. A Siemens Antares clinical ultrasound scanner equipped with a research interface, using a linear array transducer to acquire data. Ultrasound RF data were acquired immediately following ablation of the porcine liver using a Radionics Cooltip electrode. The porcine liver was excised following the procedure, sliced along the imaging plane and the dimensions of the ablation zone measured. Strain images of the ablation zones were produced offline using block-matching and multi-level motion tracking algorithms. The area of the lesion on the strain image was compared to the area of the lesion in pathology images obtained from nine separate lesions.

Results

The estimated linear correlation coefficient between pathology and the strain images over 9 lesions was 0.903 ($p < 0.004$). The area of the ablation zone in the strain image slightly underestimated the area measured using gross pathology, consistent with earlier ex-vivo experiments.

Discussion and Conclusions

The high contrast between ablated and normal liver tissue makes strain imaging far superior to B-mode imaging for clinical use. The results of this in-vivo experiment show good agreement between ablation zone area identified on the strain image and actual ablation size. This is an important step towards demonstrating the reliability of this method for routine clinical use.

This work was supported by NIH-NCI grant R01CA112192-02.

2I. Beamforming

Sala 2

Wednesday, September 23, 2009, 11:30 am - 1:00 pm

Chair: **Kai Thomenius**
GE Global Research

2I-1

11:30 AM **Adaptive Receive and Transmit Apodization for Synthetic Aperture Ultrasound Imaging**

Iben Kraglund Holfort¹, Andreas Austeng², Johan-Fredrik Synneväg³, Sverre Holm², Fredrik Gran⁴, Jørgen Arendt Jensen¹:¹Dept. Electrical Engineering, Technical University of Denmark, Kgs. Lyngby, Denmark, ²Dept. Informatics, University of Oslo, Oslo, Norway, ³Bergen Oilfield Services AS, Bergen, Norway, ⁴GN ReSound A/S, Ballerup, Denmark

Background, Motivation and Objective

The application of adaptive, data-dependent beamformers to the field of ultrasound imaging has provided significant results in terms of increased resolution and contrast compared to the conventional delay and sum (DAS) beamformer. Previously, the adaptive minimum variance (MV) beamformer has been applied to the receiving aperture of synthetic aperture ultrasound (SA) data. This has provided single emission images with increased resolution. The set of single emission images are combined by a weighted sum to form the full SA image; these weights represent the transmit apodization. So-far only data-independent transmit apodization weights have been used.

Statement of Contribution/Methods

This paper suggests a framework for utilizing adaptive, data-dependent apodization weights both on the receiving and transmitting aperture for SA. The suggested approach is based on the MV beamformer and consists of two steps. A set of uniquely designed receive apodization weights are applied to pre-summed element data forming a set of adaptively weighted images; these are in SA literature conventionally referred to as low-resolution images. The adaptive transmit apodization is obtained by applying MV across the full set of single emission images before summation.

Results

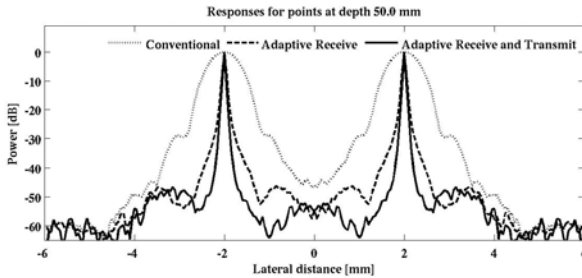
The proposed method has been applied to simulated SA data of 13 point targets at depth from 40 mm to 70 mm, obtained using Field II. A 5.5 MHz, 64-element linear array transducer is used. The SA sequence consisting of 64 emissions is obtained using virtual sources with 11 active elements. For the MV beamforming, diagonal loading and a sub-array size of $L = 32$ are used both in receive and transmit.

The proposed method is compared to two data-independent transmit weighted methods; DAS using Hanning weights with $f/2.5$ in receive and boxcar in transmit, and MV in receive and boxcar in transmit.

For two point targets placed laterally at a depth of 50 mm, the three methods provide main lobe widths (at -30 dB) of {2.20, 0.47, 0.26} mm. The included figure shows the lateral variation over two points at a depth of 50 mm for the responses.

Discussion and Conclusions

The investigations show that the suggested receive and transmit data-dependent approach increases the resolution significantly. Compared to the two data-independent transmit apodization approaches, the resolution (at a depth of 50 mm) is increased by a factor of 8.5 and 1.8, respectively.



21-2

11:45 AM **Grating-lobes reduction by application of Phase Coherence Factors**

Jorge Camacho¹, Montserrat Parrilla¹, Carlos Fritsch¹, ¹Departamento de Sistemas, Instituto de Automática Industrial, Arganda del Rey, Madrid, Spain

Background, Motivation and Objective

To avoid grating lobes, the array elements pitch must be $d \leq \lambda/2$. Therefore more elements must be used to increase resolution without grating-lobes. The cost is a more complex electronics and a higher data volume. This is relevant for 3-D imaging with 2-D arrays, where the number of active elements can be large, also for small apertures. For high frequency ultrasound, manufacturing constraints may prevent the inter-element pitch from satisfying the Nyquist spatial sampling criteria, giving rise to grating lobes.

Phase Coherence Imaging (PCI) has been recently proposed by the authors as a robust method to improve the image quality [1]. It is an adaptive beamforming algorithm based on a statistical analysis of the instantaneous phase of the aperture data. PCI simultaneously reduces the side and grating-lobes level and the main lobe width. The main objective of this work is the application of this technique to reduce the grating lobe level in sparse apertures.

[1] J. Camacho, M. Parrilla and C. Fritsch, "Phase Coherence Imaging", IEEE Trans. on UFFC, 56, 5, pp. 958-974, 2009.

Statement of Contribution/Methods

A theoretical analysis of the expected performance as a function of transducer bandwidth and the number of array elements is presented. Then, some simulations are conducted to evaluate grating-lobes reduction and the ability to detect low-amplitude scatters. Experimental data is also presented, with a 2-D matrix array ($d=\lambda$) and a perspex phantom. A second experiment with a standard tissue-mimic phantom and a $d=2\lambda$ array allowed evaluating the grating lobe reduction performance for medical images.

Results

The application of the PCI technique simultaneously reduces grating-lobe artifacts and side-lobe levels. Grating lobes reduction performance is close to the theoretically expected for both, simulations and experimental data. Improvements in lateral resolution were also observed. For the tissue mimic phantom a slight improvement in the image contrast was also achieved (Figure 1).

Discussion and Conclusions

It has been proven that the PCI technique provides an effective method to suppress grating-lobes artifacts in sparse apertures, while simultaneously reducing side-lobes level and increasing the lateral resolution. Furthermore, it is well suited for real-time implementation, operating with a single bit per element in some cases.

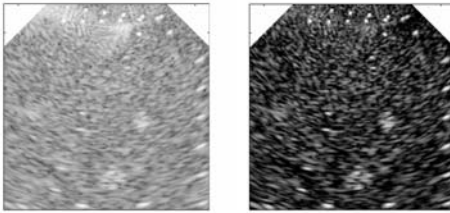


Figure 1. Tissue mimic phantom images with a 2.5 MHz array, 16 elements and $d = 2\lambda$. (Left) Original Image (Right) Weighted by PCF. Dynamic range is 50 dB for both images

2I-3

12:00 PM Time Reversal in Speckle Noise

Gabriel Montaldo¹, Mickael Tanter¹, Mathias Fink^{1,2} / Institut Langevin (CNRS UMR 7587), ESPCI, France

Background, Motivation and Objective

Adaptive focusing is a major research topic in wave physics embracing a wide variety of applications in radar optics and ultrasound. In the last decade, the concept of time reversal has been proven to be a way to find such optimal wave to focus inside an heterogeneous medium. Iterative time reversal methods are very efficient to focus on some targets such as point-like reflectors embedded in a heterogeneous medium. However, a limitation of time reversal processing was its incapacity to focus in media containing a lot of very small scatterers ("speckle" medium) randomly distributed in space. This limitation was limiting the applicability of time reversal in Ultrasound medical imaging. The proposed method solves this problem by demonstrating that a virtual bright reflector can be generated inside a speckle medium and then be used for adaptive focusing using time reversal.

Statement of Contribution/Methods

The proposed concept is illustrated using a strongly aberrating layer that distorts the propagating wavefield both in amplitude and phase. The aberrating medium is placed on the surface of a medium containing a lot of randomly distributed scatterers (speckle medium) (agar gelatine phantom). Waves are transmitted and recorded using a linear ultrasonic array of 128 elements (5MHz central frequency) driven by an electronic system of 128 independent transmit/receive channels.

The proposed method starts by prefocusing a set of waves in a set of points inside an isoplanatic patch surrounding the desired focus, each backscattered signal corresponding to an independent realization of the speckle. By rephasing adequately each speckle realization it is possible to add constructively the contribution of the different realizations and to create a virtual point-like reflector. The application of a time reversal procedure with this virtual reflector enables to refocus optimally through the strongly aberrating layer.

Results

The performance of the method is shown by comparing the Green's function obtained with the modified time reversal process in speckle noise and the true Green's function measured by placing a real point-like reflector in the focal point. A very good agreement between both measurements is observed. As an application, a complete corrected image of an ultrasonic test phantom is made through an aberrating layer.

Discussion and Conclusions

As the proposed technique only requires the assumption of the presence of Rayleigh scatterers randomly distributed in space in the imaging zone, it could have potential applications in many application fields of wave physics. In medical ultrasound, it could open the way to transcranial imaging with performant aberration corrections. Finally, as the implementation of the technique is based on the use of very simple signal processing and time reversal operations, it can be implemented in real time for medical applications.

21-4

12:15 PM **A Tunable Analog Delay Element for High-Frequency Dynamic Beamforming**

Gökce Gurun¹, Alper Sisman², Mustafa Karaman², Paul Hasler¹, Levent Degertekin^{1,1}: *Georgia Institute of Tech., USA, ²Isik University, Turkey*

Background, Motivation and Objective

Implementing beamforming for high frequency arrays is challenging because of the accurate delay requirements at high frequencies. High frequency digital beamforming is not suitable for catheter based applications as large number of cables is required between the array and the external beamformer. A possible solution is to perform analog beamforming on an integrated circuit adjacent or monolithically integrated to the imaging array.

Statement of Contribution/Methods

In this study, we introduce an improved voltage in voltage out low pass filter as an analog delay cell for high frequency dynamic beamformers. This circuit can generate three times more delay with a given bandwidth when compared to conventional low pass filters. Delay of circuit is tunable and the gain of the cell is inherently very close to unity with its current mirror based design. The proposed delay cell operates single ended and therefore is more suitable for CMUT operation which generates single ended output.

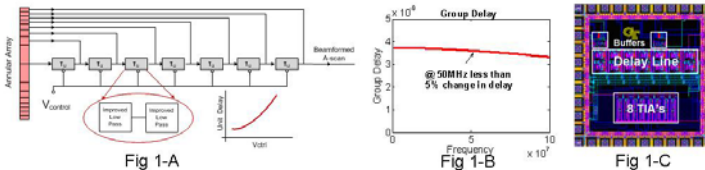
Results

We designed a test beamformer for a 30MHz equal area annular array with 100% bandwidth using the proposed delay cell and the unit-delay focusing architecture (Fig. 1-A) [1]. To focus an 8-element annular array with 400- μm radius, between $f/2$ and $f/4$, maximum required delay values are calculated to be between 15 ns and 30 ns. Improved delay cell is shown to generate 3.75ns delay that is 5% linear up to 50MHz (Fig 1-B). Hence required delays are implemented using a delay line made up of 14 improved delay elements with delays tunable between 1.1ns and 2.2ns. To demonstrate functionality we designed and fabricated a custom front-end IC in a 0.5 μm standard CMOS process. The IC chip consists of 8 transimpedance amplifiers, the analog dynamic beamformer and two buffers (Fig. 1-C). We will present testing results and investigate the effect of delay quantization.

Discussion and Conclusions

An improved analog delay cell, based on a low pass filter that is suitable for dynamic receive beamforming of high frequency arrays for intravascular ultrasound is designed and implemented. Proposed delay cell is also suitable to perform analog elevation beamforming for 1.5D arrays.

[1] J. R Talman, S. L. Garverick, C. E. Morton, G. R. Lockwood, "Unit-delay focusing architecture and integrated-circuit implementation for high-frequency ultrasound," IEEE Trans. Ultrason., Ferroel. Freq. Cont., vol.50, pp.1455-1463, Nov. 2003



21-5

12:30 PM **SURF imaging - Acoustics from a dual-frequency band annular array**

Svein-Erik Masoy¹, Thor Andreas Tangen², Oyvind Standal², Jochen M. Deibele², Sven Peter Nasholm², Rune Hansen^{2,3}, Bjorn Angelsen², Tonni F. Johansen^{2,1}: *Department of Circulation and Medical Imaging, Norwegian University of Science and Technology, Trondheim, Norway, ²Department of Circulation and Medical Imaging, Norwegian University of Science and Technology, Norway, ³Department of Medical Technology, SINTEF Health Research, Trondheim, Norway*

Background, Motivation and Objective

Measured acoustic propagation effects of dual-frequency wide-band pulses in a focused ultrasound system are demonstrated. A designed and manufactured dual-frequency band annular array capable of transmitting 0.9/7.5 MHz center frequency wide-band pulses using a single acoustic surface is presented and used for this purpose.

Statement of Contribution/Methods

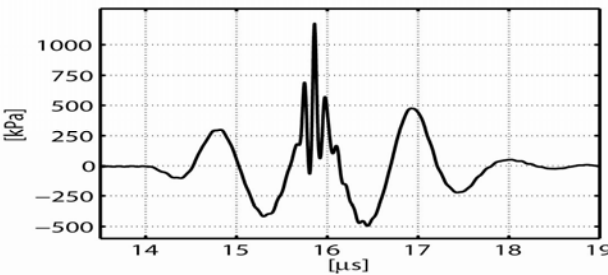
This group has developed a method named Second-order Ultrasound Field imaging, abbreviated SURF imaging. The SURF imaging technique is based on transmission of dual-frequency band pulses from the same acoustic source using a low-frequency (LF) manipulation pulse and a high-frequency (HF) imaging pulse, typically having a frequency separation of greater than 1:7. The two pulses are wide band, usually with a length less than 4 periods. The purpose of the LF pulse is to manipulate the scattering and propagation of the HF imaging pulse, and is only transmitted and not received. The HF imaging pulse is then used to image tissue or nonlinear scatterers under the influence of the manipulation pulse.

Results

Water tank measurements using a hydrophone demonstrate the function of the array by activating the low- and high-frequency layers individually and simultaneously. Activating the low- and high-frequency layers individually, results in less than -50 dB signal level from the high- and low-frequency layers respectively. Activating both layers simultaneously, produce a well defined dual-frequency pulse at the array focus (see Fig. 1). The presence of the low-frequency pulse leads to compression, expansion, and a time delay of the high-frequency pulse. There is a phase shift between the low- and high-frequency pulse as it propagates from the array to the focus. This makes the latter described effects also dependant on the array configuration. By varying the low-frequency pressure, a shift of up to 0.5 MHz in center frequency and a time delay of up to 5.7 ns of a 8.0 MHz transmitted high-frequency pulse is observed at the array focus relative to no low-frequency pulse present.

Discussion and Conclusions

The results show that the array works as intended and demonstrate the high propagation complexity of dual-frequency pulses.



Wednesday Oral

21-6

12:45 PM Contrast Enhancement of Adaptive Ultrasound Imaging Using Eigenspace-Based Minimum Variance Beamforming

Babak Mohammadzadeh Asl¹, Ali Mahloojifar¹, *Biomedical Engineering, Tarbiat Modares University, Tehran, Iran*

Background, Motivation and Objective

Recently, adaptive beamforming methods have been successfully applied to medical ultrasound imaging, resulting in significant improvement in image quality compared to non-adaptive delay-and-sum (DAS) beamformer. Most of the adaptive beamformers presented in the ultrasound imaging literature are based on the minimum variance (MV) beamformer which can improve the imaging resolution while retaining the contrast. The main objective of this research is to present a beamformer which could improve the imaging resolution and contrast, at the same time.

Statement of Contribution/Methods

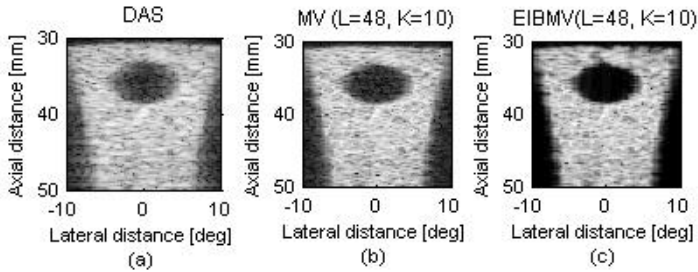
In this paper, we have applied the eigenspace-based MV (EIBMV) beamformer to medical ultrasound imaging and shown the simultaneous improvement in imaging resolution and contrast. EIBMV beamformer utilizes the eigenstructure of the covariance matrix to enhance the performance of the MV beamformer. The weight vector of the EIBMV is found by projecting the obtained MV weight vector onto a vector subspace constructed from the eigenstructure of the covariance matrix. Using EIBMV weights instead of the MV ones leads to reduced sidelobes as well as improved contrast, without compromising the high resolution of the MV beamformer.

Results

The excellent performance of the proposed beamforming approach is demonstrated by a number of simulated phantoms including point targets and a circular cyst. EIBMV beamformer shows a significant reduction in the sidelobe levels while representing the same mainlobe width as the MV. Specifically, in the point targets phantom, the proposed method decreases the sidelobes about 9 dB and 22 dB compared to MV and DAS, respectively. Furthermore, as shown in the figure, the proposed method increases the contrast of simulated cyst phantom about 8.55 dB and 13.9 dB and also improves the contrast-to-noise ratio about 32% and 61%, compared to MV and DAS, respectively.

Discussion and Conclusions

It is demonstrated that the proposed EIBMV beamformer, by reducing the undesired contribution of the sidelobes, provides a significant enhancement in contrast, outperforming both the DAS and MV beamformers. These improvements are achieved while the high resolution of the MV beamformer is retained. The characteristics of the proposed method including selection of the number of the eigen vectors needed for constructing the signal subspace, and robustness against phase aberrations are also discussed.



3I. New Developments in Blood Flow Imaging

Sala 4

Wednesday, September 23, 2009, 11:30 am - 1:00 pm

Chair: **Jorgen Jensen**
Technical Univ. of Denmark

3I-1

11:30 AM **A fully automated multidimensional DCT-based penalized least-squares method for vector flow mapping from conventional color-Doppler imaging.**

Jonathan Hamel-Nunes¹, Sarah Dort¹, Gilles Soulez², Sophie Lerouge^{2,3}, **Damien Garcia**¹; ¹Laboratory of Biorheology and Medical Ultrasonics, Research Center, University of Montreal Hospital (CRCHUM), Montreal, Quebec, Canada, ²Department of Radiology, University of Montreal Hospital (CRCHUM), Montreal, Quebec, Canada, ³Department of Mechanics, École de Technologie Supérieure, Montreal, Canada

Background, Motivation and Objective

Conventional color-Doppler imaging is incomplete since it only captures the velocity components parallel to the ultrasound beam. Vectorial mapping of the blood flow can be reconstructed by combining coplanar measurements from different angles. Several dilemmas, however, hamper this process: 1) Doppler velocities are noisy, 2) gappy data appear due to signal loss, 3) turbulence generates outlying values and 4) accuracy is lost due to the small angular increment.

Statement of Contribution/Methods

To produce a vectorial blood flow mapping, we developed a fully automated algorithm based on the discrete cosine transform and allowing fast processing of multidimensional tensors. An iteratively reweighted method was also proposed to deal with occurrence of missing and/or outlying Doppler velocities. The performance of this new technique was evaluated on an analytical vortical flow which was made corrupted by the addition of white noise, gappiness and spurious velocity vectors. We then tested the method *in vivo*: two series of color-Doppler measurements were performed on a carotid sinus, at $\pm 17^\circ$, using an Ultrasonix scanner (Sonix RP).

Results

The analytical study demonstrated that complex flows can be rebuilt with high accuracy despite the presence of strong data corruption (Fig. 1). The reconstruction algorithm also allowed us to decipher the blood flow and the vortex formation in the carotid sinus of a healthy subject (Fig. 2).

Discussion and Conclusions

The novel algorithm allows the display of vectorial flow fields using conventional color-Doppler imaging. The proposed method is extremely fast, accurate and clinically compliant. This will offer the possibility of studying a number of unexplored aspects of blood flow dynamics in vascular diseases such as stenoses and aneurysms.

Corrupted vs. Reconstructed vortical flow

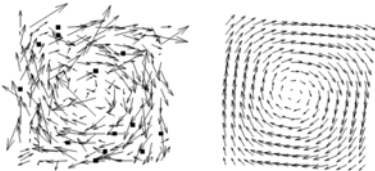


Fig. 1

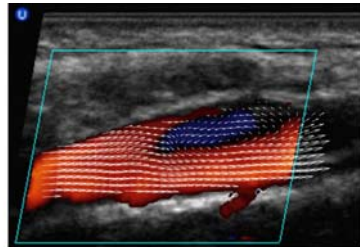


Fig. 2

3I-2

11:45 AM **Noninvasive Wall Shear Stress Measurements in Human Carotid Artery Using Echo Particle Image Velocimetry: Initial Clinical Studies**

Fuxing Zhang¹, Alex Barker¹, Phillip Gates², David Strain², Jonathan Fulford², Luciano Mazzaro¹, Angela Shore², Nick Bellenger², Craig Lanning^{3,4}, Robin Shandas^{3,4}; ¹University of Colorado at Boulder, USA, ²Peninsula Medical School, Royal Devon and Exeter Hospital, United Kingdom, ³University of Colorado at Denver, USA, ⁴Division of Cardiology, The Children's Hospital, Aurora, CO, USA

Background, Motivation and Objective

The accurate quantification of wall shear stress (WSS) in the human carotid artery, a region prone to plaque formation, would be of great help to investigate the mechanisms by which hemodynamic distortions cause atherogenesis. Currently, phase-contrast MRI (PC-MRI), ultrasound Doppler sonography and computational fluid dynamics (CFD) are used to quantify WSS, although all have limitations. We have developed a non-invasive and easy-to-use technique, called Echo Particle Image Velocimetry (EPIV), which overcomes the limitations of the aforementioned techniques. Echo PIV can generate accurate multi-dimensional, multi-component velocity information, with temporal resolution up to 0.7ms, for the direct calculation of in-vivo time-resolved WSS.

Statement of Contribution/Methods

Ten healthy volunteers were studied on the right common carotid artery (rCCA) by using both Echo PIV technique and PC-MRI. *Echo PIV*: Raw RF data of B mode microbubble images with high frame-rate (Illumasonix LLC, Boulder, CO) were recorded and processed to obtain two-dimensional velocity vector maps of rCCA, from which WSS information was calculated using a three-point, second-order polynomial curve fitting, assuming a blood viscosity of 3.2 cP. Typically 7 to 10 cardiac cycles of data were acquired and ensemble-averaged for each subject. *PC-MRI*: A 1.5T MRI scanner (Philips Medical Systems) was used. Five slices, orthogonal to the longitudinal axis of right carotid artery were obtained at the level of the bifurcation (voxel size, 0.5x0.5x6 mm). WSS information was calculated based on the 3D velocity vector fields with 3D paraboloid (3DP) fitting.

Results

Echo PIV and PC-MRI-derived WSS profiles over the cardiac cycle showed good agreement for all subjects. WSS values for peak systolic, end diastolic, and mean value of all heart phases were selected as representative measurements for quantitative comparison between the two techniques. The mean \pm SD (in dyne/cm², N=10 subjects) of WSS were for EPIV: 21.1 \pm 6.5, 4.0 \pm 1.7, 8.7 \pm 2.5; and for MRI with 3DP fitting: 17.0 \pm 3.4, 4.3 \pm 1.1, 7.7 \pm 1.5, for peak-systolic, end-diastolic and mean values, respectively. The overall error of EPIV against MRI was calculated as 10 \pm 28%. EPIV-obtained WSS values agree with results reported by others.

Discussion and Conclusions

The Echo PIV-derived WSS in human rCCA showed good correlation with those values obtained by PC-MRI with 3DP fitting. The factors most likely responsible for the difference between the two techniques are the difference of slice orientations, discrepancy of vessel wall localizations in two modalities, and inherent physiological variability in hemodynamics caused by the time between EPIV and MRI studies. Nevertheless, EPIV appears highly promising as a simple, easy-to-use, non-invasive means of directly measuring temporally and spatially resolved WSS in human carotid vessels.

3I-3

12:00 PM **In vivo investigation of real-time high frame rate flow imaging using plane-waves and parallel receive beamforming**

Lasse Lovstakken¹, Tore Bjastad¹, Torbjorn Hergum¹, Johan Kirkhorn², Siri Ann Nyrnes¹, Hans Torp¹; ¹Norwegian University of Science and Technology, Norway, ²GE Vingmed Ultrasound, Horten, Norway

Background, Motivation and Objective

The inherent trade-off between frame rate and image quality in color flow imaging (CFI) often leads to suboptimal images for medical diagnosis. Parallel receive beamforming (PRB) has been used to overcome this problem. However, using conventionally focused transmit beams, PRB is associated with image artifacts due to misalignments of transmit and receive beams. These artifacts are visible as discontinuities between PRB groups, and a high degree of PRB is therefore not utilized without substantial spatial smoothing.

Statement of Contribution/Methods

We investigated the use of plane (unfocused) transmit beams with a high degree of PRB to increase the frame rate in CFI. This approach has several advantages, 1) in principle no PRB misalignment artifacts are present, and 2)

lateral sampling requirements are reduced, increasing frame rate and lowering overall thermal effects. Simulations (Field II) were used to design transmit beams with a plane wave front region covering 16 receive beams. Using a GE Vingmed Vivid E9 ultrasound system, this setup was implemented for 16x PRB in 2D imaging for both B-mode and CFI, and also for Blood Flow Imaging (BFI), an angle-independent flow visualization technique based on the additional display of blood speckle movement.

Results

A tenfold increase in frame rate was achieved, which implied B-mode imaging at 1200 fps and duplex flow imaging at 150 fps for a 3x4 cm image size with twice the lateral sampling for CFI. In addition, a speckle image frame rate of 800 fps was achieved in BFI, amounting to a significant increase in flow information rate. Artifacts due to PRB were not visible in the images; however, the quality in B-mode was reduced due to the use of unfocused transmit beams. Simulated beam profiles showed that plane transmit beams with negligible ripple could be generated down to 4 cm for 16x PRB. A significant reduction in transmitted pressure was observed; however, as the setup was thermal limited, higher pulse amplitudes could be used since fewer beams were transmitted, reducing the overall degradation.

In vivo and experimental flow imaging was done using a GE 9L and 11L linear transducer for vascular imaging of the carotid bifurcation, congenital heart disease in neonates, and cardiac imaging of rats. Sufficient penetration of 4-5 cm in depth was achieved for CFI in all cases. Examples showed that significantly more detailed information of flow could be obtained. In the carotid bifurcation brief swirling flow events were depicted. In neonates, shunt flow in septal defects was more clearly visualized. Further, when imaging rats with a heart rate above 300 bpm, more than 20 duplex images per cycle with the whole heart in view was obtained.

Discussion and Conclusions

By utilizing parallel receive beamforming with plane-wave transmission, very high frame rates can be achieved with sufficient sensitivity for flow imaging in vascular and pediatric cardiac applications. The proposed setup also has a high potential for small animal imaging.

31-4

12:15 PM Two-dimensional flow velocity estimation in the carotid bifurcation: a study of crossed-beam vector Doppler and speckle tracking using computational fluid dynamics

Abigail Swillens¹, Patrick Segers¹, Hans Torp², Lasse Lovstakken²; ¹IBiTech, Ghent University, Belgium, ²Department of Circulation and Medical Imaging, NTNU, Norway

Background, Motivation and Objective

Multi-dimensional flow imaging may be beneficial for improving diagnosis and understanding of cardiovascular pathologies. Speckle tracking (ST) and crossed-beam vector Doppler (VD) methods have been investigated, but have yet to be validated against a ground truth for clinically relevant and potentially complex flow patterns. In this work we compare in detail ST and VD performance for simulated flow fields in a mildly stenosed 3D carotid bifurcation model based on computational fluid dynamics (CFD).

Statement of Contribution/Methods

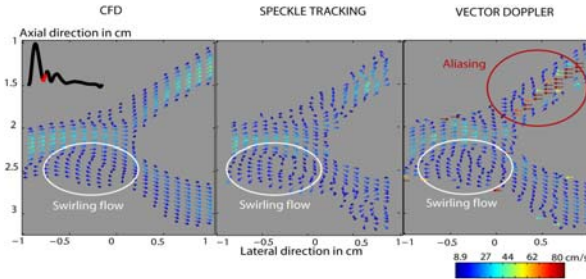
CFD simulations (Fluent v6.2) were done with pulsatile flow conditions in a 3D carotid model based on MRI scans. Blood was modeled as point scatterers moving according to the CFD flow field, and ultrasound RF-signals were obtained using Field II. Full 2x4 cm (WxH) linear scans were simulated for a full cardiac cycle ($f_0=5\text{MHz}$, $N_s=10$, $\text{PRF}=2/4\text{ kHz}$). Thermal noise and a FIR clutter filter were applied during post-processing. For ST, sum-of-absolute-differences (SAD) matching and parabolic SAD interpolation was employed within a scan interleave region. VD was implemented using common transmit ($F_n=2.5$) and electronically separated receive apertures ($F_n=4.5$). Receive beams were angled 12 deg. towards transmit, and expanding apertures were used in depth.

Results

CFD results included both high and low velocity flow, as well as complex swirling flow patterns. Performance summarized as the mean deviation of all velocity estimates over the cardiac cycle indicated that ST was the better lateral estimator and VD the better axial estimator. The mean deviation for ST was 4.2 / 3.2 cm/s for v_x / v_y respectively, while 13 / 2.9 cm/s for VD, compared to a reference mean velocity of 11 cm/s. Both methods were limited by the clutter filter in the ability to estimate low velocity swirling flow, with more severe errors observed for VD estimates. As shown in the attached figure, VD was further limited by aliasing for high velocities, depending then on the flow angle and each transmit-receive beam angles respectively. To achieve sufficient steering angles, scanning with VD was restricted by transducer geometry, and receive apertures were substantially reduced for a 2x4cm scan.

Discussion and Conclusions

Overall, ST provided more consistent results and a more practical approach to 2D velocity estimation in a stenosed carotid bifurcation model compared to crossed-beam VD.



31-5

12:30 PM Toward Non-Invasive, Real-Time Measurement of Volume Blood Flow Using 3D Color Doppler Ultrasound

Michael S. Richards¹, Oliver D. Kripfgans¹, Jonathan M. Rubin¹, Anne L. Hall², J. Brian Fowlkes¹; ¹Radiology, University of Michigan, Ann Arbor, Michigan, USA, ²GE Medical Systems, Milwaukee, Wisconsin, USA

Background, Motivation and Objective

Accurate measurement of blood volume flow (BVF) is important for many clinical applications, including monitoring of cardiac output, vascular diseases, and organ perfusion. A previously tested method, using surface integration of the color flow (CF) Doppler velocities, quantifies the flux of blood across a 3D CF coronal image plane cross-sectioning the vessel [1]. This method measures BVF with high accuracy (~10% error), comparing well with other invasive techniques [1]. Using standard CF data requires correction for biases induced by clutter rejection filters. For this method, many volumes are needed to estimate this correction. To obtain accurate measurements for single acquisitions a singular value decomposition (SVD) based filtering method was developed that uses both clutter and blood signals to calculate the integrated velocities.

Statement of Contribution/Methods

A flow phantom was created using latex tubing (4.8 and 3.2 mm inner diameter (i.d.), w/ 0.4 mm thick walls, Kent Elastomer Pro Inc) imbedded in a solution of 6% gelatin and 2% silica by mass. A CompuFlow 1000 System (Shelley Med Img Tech) was used to pump blood-mimicking fluid through the tubing at varying rates and flow profiles intended to mimic flow in humans. 3D CF IQ images were taken on a Logiq 9 (GE Med Sys) and a 3D swept, linear array probe at 5 MHz.

IQ data, ranged gated for Doppler packets across the tube, was isolated as a matrix. A fixed rank (2nd order) SVD filter was performed on each matrix to separate the blood from the clutter signals. The clutter signal was then scaled, based on the blood power values, and added back to the blood signal. Autocorrelation was then used to calculate the CF velocities and integrated to obtain BVF.

Results

BVF measurements are shown and compared to mean pumped values. The measurement means and standard deviations are calculated from ~30 volumes for each size and flow type. Volume sweep time was >3-beat cycles for the pulsatile flows.

Discussion and Conclusions

Measured values of BVF correspond very well to actual values with good accuracy and high precision in most cases. However, the large error in some measurements requires further investigation into the methods and possible sources of noise, prior to validation in the clinic.

Wednesday
Oral

[1] MS Richards, OD Kripfgans, JM Rubin, AL Hall, JB Fowlkes, "Mean Volume Flow Estimation in Pulsatile Flow Conditions", *Ultrasound in Medicine and Biology*, In Press.

Tube Size	Large Tube (4.8 mm i.d.)			Small Tube (3.2 mm i.d.)		
	Measured (mL/min)	Actual (mL/min)	% Error	Measured (mL/min)	Actual (mL/min)	% Error
Constant	11.6 ± 0.5	12.0	3.3%	3.2 ± 0.1	3.0	6.7%
"	99.6 ± 8.4	120.0	17.0%	26.5 ± 3.4	24.0	10.4%
"	264.1 ± 21.6	300.0	12.0%	63.1 ± 5.2	60.0	5.2%
Carotid	96.5 ± 8.8	90.0	7.2%	21.4 ± 1.5	18.0	18.9%
Femoral	32.7 ± 2.7	30.0	9.0%	9.9 ± 0.6	7.2	37.5%

3I-6

12:45 PM **Volumetric Blood Flow Assessment through Multigate Spectral Doppler**

Stefano Ricci¹, Magnus Cinthio², Lorenzo Francalanci¹, Piero Tortoli¹; ¹*Electronics and Telecommunications Department, Università degli Studi di Firenze, Italy,* ²*Department of Measurement Technology and Industrial Electrical Engineering, Lund University, Sweden*

Background, Motivation and Objective

Several difficulties are faced in volumetric blood flow measurements, which require the assessment of both the velocity distribution and the cross-sectional area of the vessel. For example, Doppler angle ambiguity hinders quantitative velocity measurements, the velocity estimation is typically made only for a single sample volume (SV) placed on the vessel axis, and the Doppler beam orientation is usually not suitable for accurate diameter measurements. A dual-beam approach is here presented and shown capable of producing accurate and reproducible volumetric flow measurements.

Statement of Contribution/Methods

A novel vector Doppler method has been recently proposed and validated (doi: 10.1109/ULTSYM.2007.610.) for measuring the velocity magnitude of blood crossing a SV. This method is based on the use of a reference beam (RB) and a measuring beam (MB): when the RB is transversely oriented to the flow, the MB performs a Doppler velocity measurement with known angle.

In this work, the method has been applied to 128 SVs aligned along the MB, while the transverse RB orientation has been exploited to obtain the diameter measurement through a combined threshold and linear interpolation algorithm applied on both the near and far wall. The approach has been implemented on a US system specifically designed for research, which, every 20 ms, calculates the vessel diameter, the velocity profile and, assuming cylindrical vessel geometry, the instantaneous volumetric flow.

Results

The new method has been tested with 20 in vitro experiments and preliminary in vivo measurements on 3 volunteers. The in vitro tests have been carried out on a flow phantom under several different experimental conditions (flow trends, Doppler angles, sample volume lengths, etc). We compared the measurements with the reference values obtained with independent volumetric methods, obtaining an average error of about 6%.

The volumetric flow in the common carotid artery of each volunteer has been measured 4 times, waiting 10 minutes between consecutive measurements. Each measurement was obtained by integrating the flow detected in 4 consecutive systolic peaks. For each volunteer, the variation coefficient, i.e. the ratio between the standard deviation and the mean of the 4 measurements resulted 5.7%, 4.8%, 9.2%, respectively.

Discussion and Conclusions

The proposed technique allows to obtain non invasive, quantitative assessment of the blood volumetric flow in large arteries. The in-vitro experiments have shown the method robustness under different conditions, and the in vivo tests produced encouraging results in terms of reproducibility.

Wednesday
Oral

4I. Energy Harvesting

Tarragona

Wednesday, September 23, 2009, 11:30 am - 1:00 pm

Chair: **Pierre Khuri-Yakub**
Stanford University

4I-1

11:30 AM Energy conversion improvement in ferroelectrics: application to energy harvesting and self-powered systems

daniel guyomar¹, mickael lallart^{1,2,†} LGEF, INSA Lyon, villeurbanne, france, France, ²LGEF, INSA, villeurbanne, France, France

Background, Motivation and Objective

The proliferation of consumer electronics, combined with the constant progress in ultra-low power devices and increasing demand in terms of autonomous sensors and sensor networks, has enabled the conception of systems powered up using ambient sources such as vibrations, hence allowing the replacement of batteries that present maintenance issues and environmental problems. However, the power output of microgenerators is still limited from a few tens of microwatts to a few milliwatts. The objective is to improve the energy conversion in order to increase the power output performances.

Statement of Contribution/Methods

The topic addressed here exposes the conversion enhancement principles for piezoelectric generators, using a simple, low-cost, embeddable and truly self-powerable concept based on an intermittent switching of the piezoelement, allowing a great increase of the piezoelectric conversion abilities and thus of the performance of energy harvesters. Due to the non-linear voltage processing, the voltage builds up and increases the mechanical to electrical energy conversion. Several schemes derived from this basic switching concept will be discussed, with a particular attention placed not only on the energy harvesting abilities of the microgenerators, but also on their realistic implementation and their use for powering up electronics devices (e.g., by considering the power output as a function of the connected load). The application of the conversion enhancement principles to semi-passive, self-powered or semi-active vibration control will be also presented, as well as its application to other conversion effects (e.g., pyroelectric). Finally, a truly self-powered wireless Structural Health Monitoring scheme using an efficient energy harvesting scheme will be described.

Results

The proposed approach permits to harvest up to 10 times more energy than the standard approach (rectifier and a storage capacitance).

Discussion and Conclusions

The harvester is efficient, self-powered and fully adaptative. No frequency tuning is required. The output power is compatible with some realistic applications

4I-2

12:00 PM Spiral Type Piezoelectric MEMS Power Generator with Shear Mode

Hyun-Cheol Song¹, Hyung-Chan KIM¹, Chong-Yun Kang¹, Seok-Jin Yoon¹; ¹Thin Film Materials Research Center, Korea Institute of Science and Technology, Korea, Republic of

Background, Motivation and Objective

Energy harvesting from the environment has been of great interest as a standalone power source of wireless sensor nodes for Ubiquitous Sensor Networks (USN). In particular, the piezoelectric energy harvesting from ambient vibration sources has intensively researched because it has a relatively high power density comparing with other energy scavenging methods.

Through recent advances in low power consumption RF transmitters and sensors, it is possible to adopt a micro-power energy harvesting system realized by MEMS technology for the system-on-chip. However, the MEMS energy harvesting system has some drawbacks such as a high natural frequency over 300 Hz and a small power generation due to a small dimension.

Statement of Contribution/Methods

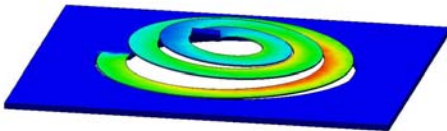
To overcome these limitations, we devised a novel power generator with a spiral spring structure as shown in the figure. The natural frequency of a cantilever could be decreased to the usable frequency region (under 300 Hz) because the natural frequency depends on the length of a cantilever. The MEMS cantilever with the spiral spring structure was fabricated by a silicon MEMS process. The piezoelectric thick film was formed by a screen printing method and then it was also treated by Cold Iso-static Press(CIP) to improve the properties of the thick film.

Results

In this study, the natural frequency of the energy harvester was a lower than a normal cantilever structure and sufficiently controllable in 50 - 200 Hz frequency region as adjusting weight of a proof mass. Moreover, the MEMS energy harvester had a higher energy conversion efficient because a shear mode (d15) is much larger than a 33 mode (d33) and the energy conversion efficiency is proportional to the piezoelectric constant (d).

Discussion and Conclusions

We expect the spiral type MEMS power generator would be a good candidate as a standalone power generator for USN.



Wednesday
Oral

4I-3

12:15 PM **Multi-cantilever piezoelectric MEMS generator in energy harvesting**

B S Lee¹, S C Lin¹, W J Wu¹, C K Lee^{1,2}, *¹Engineering Science & Ocean Engineering, National Taiwan University, Taipei, Taiwan, ²Institute of Applied Mechanics, National Taiwan University, Taipei, Taiwan*

Background, Motivation and Objective

With increasing interests in wireless sensor network applications, the ways to power these sensor devices have become an important issue over the past several years. Comparing all possible energy sources, mechanical vibration stands out to have the most potential as a power source. A piezoelectric transducer can be considered a good choice when compared with electromagnetic and electrostatic types due to its high energy density. A piezoelectric transducer which adopts MEMS technology is considered the best solution for miniaturization.

Statement of Contribution/Methods

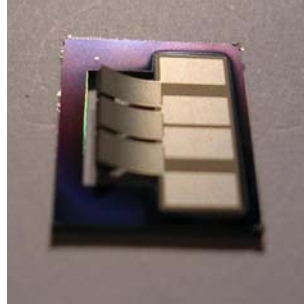
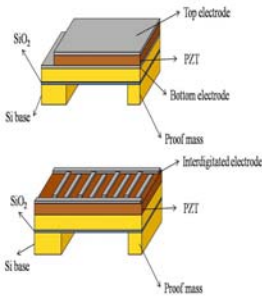
In this paper, we are going to present the development of a multi-cantilever piezoelectric MEMS generator. The configuration of d31 mode and d33 mode piezoelectric MEMS generator is shown in Figure 1. The output characteristics of these two devices are identical. Based on previously developed d31 mode and d33 mode devices, the performance of a combination of the d31 mode and d33 mode devices are studied.

Results

The multi-cantilever piezoelectric MEMS generator is based on the silicon process with laminated PZT material to transform mechanical strain energy into electrical charge by using the d31 and d33 mode of PZT. The proof mass made of silicon is build at the free end of the cantilever beam for adjusting the resonant frequency. Figure 2 shows the photo of a finished multi-cantilever piezoelectric MEMS generator that has single beam size of 3000X1500X10µm comprising 5µm PZT layer.

Discussion and Conclusions

A multi-cantilever type piezoelectric MEMS generator comprising d31 and d33 mode is developed and the output performance of the device is evaluated. The characteristics of serial and parallel connections of identical generator, including the relations between resistive load and output power/voltage, are also studied.



41-4

12:30 PM Genetic Algorithm Optimization of a Piezoelectric System for Energy Harvesting from Traffic Vibrations

Guoliang Ye¹, Jize Yan¹, Zi Jing Wong¹, Kenichi Soga¹:¹*Department of Engineering, University of Cambridge, United Kingdom*

Background, Motivation and Objective

Piezoelectric resonant systems have been seen as a promising approach to harvest energy from environmental vibrations. The systems are conventionally modeled and designed under the assumption of a purely sinusoidal excitation. However, real vibration sources usually have a broad bandwidth with multiple resonant peaks, which feeds difficulties in system design and parameter optimization. This paper investigates into using a genetic algorithm with numerical simulations to optimize the system, and also demonstrates the maximum power harvested from real traffic vibrations of manhole covers, bridges and tunnels.

Statement of Contribution/Methods

The piezoelectric resonant system is modeled as a cantilever structure. Its output power relates to the parameters of the mass, the stiffness of the cantilever, the effective piezoelectric coefficient, the capacitance, the mechanical damper and the resistive load r . A genetic algorithm runs initially with a random guess (or a guess from prior knowledge) to the parameters which are represented by a number of individuals. The output power of each individual is then evaluated through numerical simulations. The algorithm runs iteratively following the procedures of surviving good individuals which produce high output power, and eliminating poor individuals, until the parameters converge to produce maximum power. The advantage of using such a genetic simulation algorithm is that it allows the evaluation of the system output to be numerical, instead of restricting in an analytical solution which is difficult to be derived from real traffic vibrations.

Results

Experiments were carried out using offline acceleration data and the results were compared to a conventional system designed by assuming a purely sinusoidal excitation. The data were logged by an accelerometer in a sampling frequency of 1 KHz from the vibrations of manhole covers, bridges and tunnels excited by vehicles and trains. An example of the spectrum of the manhole cover data shows that multiple frequency components widely locate at 30-60 Hz, 120-150 Hz and 280-330 Hz, depending on different kinds of vehicles. Within 200 simulations, the optimized system harvests over 10 times more energy than the conventional system of the same mass and piezoelectric material. This is because the genetic simulation algorithm globally considers the effects of each parameter to produce an optimal frequency response to scavenge more energy from the real vibrations while the conventional system only captures the energy narrowly around the frequency of the assumed sinusoidal excitation.

Discussion and Conclusions

This paper has demonstrated the ability of a piezoelectric resonant system to harvest energy from real acceleration signals in manhole covers, bridges and tunnels. A novel genetic simulation algorithm has been introduced to

optimize the system, which shows a great potential to improve the conventional method of assuming a purely sinusoidal excitation.

4I-5

12:45 PM Sensing Physical Fluid Properties with CMUT Arrays

Marcel Thraenhardt¹, Peter-Christian Eccardt², Hubert Mooshofer², F. Levent Degertekin³, Peter Hauptmann¹;
¹Institute of Micro and Sensor Systems, University of Magdeburg, Magdeburg, Germany, ²Corporate Technology, Power and Sensor Systems, Siemens AG, Munich, Germany, ³G.W. Woodruff School of Mechanical Engineering, Georgia Institute of Technology, Atlanta, Georgia, USA

Background, Motivation and Objective

Fluid waves at the fluid/silicon interface of CMUT arrays have always been an issue in medical imaging applications.

We present the usage of dispersive guide mode waves ($c_{\text{wave}} < c_{\text{fluid}}$) at these interface for sensing fluid properties with no special modification of the membrane geometry.

The only modification is a mask on top of the CMUT array to confine the energy of this interface wave in the fluid on the area of active CMUT membranes.

With this slight modification the CMUT can still be used for ultrasonic imaging applications, which enables a variety of ultrasonic sensor applications such as sensing physical

fluid properties like viscosity, density, speed of sound and acoustic impedance with only one sensor device.

Statement of Contribution/Methods

Based on an analytic approach to CMUT surface waves we set up a FEM model to investigate the behavior of a CMUT array when driven as a resonant sensor. For this we applied forces with alternate directions to neighboring membranes by AC voltages with a 180° phase shift.

A resonance condition of the surface wave is expected when the half wavelength of the fluid wave matches the membrane pitch.

This mechanical resonance could be observed in the FEM simulations and in experiment as expected.

The electrical behavior of the CMUT was investigated by harmonic multiphysics FEM analysis resulting in an electrical impedance spectrum. A simple electrical equivalent circuit

was fitted to the impedance spectra to investigate the influence of physical fluid properties as speed of sound, density and viscosity to the electrical equivalent circuit components L_s , C_s , R_s .

The sensors are being implemented using CMUT arrays with dual-electrode structure which are fabricated using a low temperature silicon nitride deposition process. These CMUTs are especially suitable for sensing applications since they are shown to have high coupling coefficient ($k^2 > 0.7$) for a large DC bias range - above 90% of the collapse voltage.

Results

In FEM simulations the electrical equivalent circuit component L_s of the proposed sensor shows linear dependency on the fluid density. The dependency of ω to viscous damping by the viscosity of the fluid to R_s can be approximated by a root-law. It shows a linear dependency in double-log scale.

In addition experimental verification of the FEM results will be presented, differences will be discussed.

Discussion and Conclusions

We presented a new sensor principle based on the slight modification of CMUT Arrays. By simple electrical reconfiguration a CMUT Array can be used as an ultrasound transducer and also as a surface wave sensor. We used FEM simulations to characterize the electrical behaviour of the sensor and to estimate the operating range and the sensitivity to the fluid's density and viscosity. The proposed sensor principle was verified in experiment.

Wednesday
Oral

5I. Piezoelectric Transducer Materials

Pergamo

Wednesday, September 23, 2009, 11:30 am - 1:00 pm

Chair: **Scott Smith**
GE Research

5I-1

11:30 AM Electrical Properties of CuO doped-KNN Ceramics and 1-3 Piezocomposites

Ebru Mensur Alkoy¹, Melih Papila¹; ¹Faculty of Engineering and Natural Sciences, Sabanci University, Istanbul, Turkey

Background, Motivation and Objective

Lead free piezoelectric materials have been attracting increasing attention in recent years as new materials to prevent serious problems caused by the high toxicity of lead. Among lead-free materials, potassium sodium niobate [(K_{0.5}Na_{0.5})NbO₃ -(KNN)] is considered to be a promising candidate due to its comparable piezoelectric, ferroelectric properties to PZT and its high Curie temperature. The densification of KNN is problematic but it can be enhanced and one of them is addition of a sintering aid. There are no studies on lead-free piezoelectric materials in the fiber form which can find possible use in piezocomposite transducer applications. In this study, KNN was produced in two different forms; as bulk ceramics and as fibers. 1-3 composite ceramics were also prepared from fibers.

Statement of Contribution/Methods

KNN powders were prepared by the conventional solid state reaction method from oxide and carbonate powders. After the calcination of KNN, copper oxide (CuO) was added to the KNN powder as a sintering aid in three different ratios. The green KNN and KNN-CuO pellets were sintered at various temperatures ranging from 1070°C to 1110°C. The samples were poled by applying a DC electric field of 5 kV/mm for 30 minutes at 80°C. The KNN fibers with different CuO molar ratios were drawn using a novel alginate gelation technique. Fibers were dried 24 h at the room temperature and sintered at 1090°C-4 hour.

Results

Increasing CuO ratio was found to cause drastic changes on the microstructure. Addition of 0.5mol% CuO caused a densification of KNN whereas addition of 1.5mol% CuO led to further densification, formation of a liquid phase between the grains and grain growth. A similar trend was also observed in the microstructures of the KNN fibers. Well formed pure and CuO-added KNN fibers were produced with diameters from 150µm to 300µm. Dielectric constant and loss of 0.5mol% CuO added KNN were found to be 320 and %1.4, respectively at 100 KHz. 2Pr was determined to be ~32 µC/cm² and the coercive field (Ec) was measured as 10 kV/cm. The planar mode coupling coefficient (kp) and mechanical quality factor (Qm) of the KNN sample containing 0.5mol% CuO were calculated from admittance-frequency measurements taken from disc shaped thin pellets using the resonance method. The kp and Qm were 0.29 and 398, respectively. Piezoelectric coefficient d33 of this sample was measured as 120 pC/N. These measurements were also repeated for various CuO additions. The CuO added KNN fibers were embedded in to an epoxy matrix and 1-3 piezocomposites were prepared with various fiber volume ratios. The dielectric and piezoelectric properties of these piezocomposites with respect to fiber content were also investigated.

Discussion and Conclusions

The CuO addition was found to be a viable sintering aid to obtain dense KNN ceramics. This is a first report in the literature on fabrication of lead-free piezoelectric ceramic fibers and 1-3 piezocomposites.

5I-2

11:45 AM **Characterization Of CuInP2S6 Family Two Dimensional Crystals For Ultrasonic Transducers**

Vytautas Samulionis¹, Juras Banys¹, Yulian Vysochanski²; ¹Physics Faculty, Vilnius University, Vilnius, Lithuania, ²Institute of Solid State Physics and Chemistry, Uzhgorod University, Ukraine

Background, Motivation and Objective

The development of modern ultrasonic transducers for medical diagnostic applications requires continuously new lead free materials to cope with increasing demands. A promising family for this type of development is that of layered CuInP2S6 crystals. These crystals possess figures of merit for piezoelectricity comparable to that of widely used piezoelectric materials. In recent years such two dimensional crystals are obtained as thin plates and could be used as ultrasonic transducers in the frequency range of 5-15 MHz, almost without polishing, because they have ideal parallel surfaces. These crystals crystallize in a layered two-dimensional structure. In pure CuInP2S6 crystals piezoelectric sensitivity exists below the first order ferroelectric phase transition at $T_c = 312$ K.

Statement of Contribution/Methods

Recently the new crystals and solid solutions were obtained after substitution Cu to Ag, In to Cr or S to Se. In this contribution we present the experimental investigation results of ultrasonic and piezoelectric properties of these materials. The pulse-echo method was used for measurements of ultrasonic velocity and attenuation.

Results

The critical ultrasonic attenuation and velocity anomalies were observed at phase transition temperatures. After substitution In to Cr and S to Se phase transition temperature decreases and intermediate phases, possibly incommensurate, appear above ferroelectric phase transition point. After substitution Cu to Ag the ferroelectric phase transition also shifts to lower temperatures. The piezoelectric sensitivity was investigated by measuring of amplitude of ultrasonically detected piezoelectric signal. It was shown that piezoelectric sensitivity in the ferroelectric phase increases with bias DC field, then saturates, and after reversion of voltage the signal decreases, at field near coercive, changes sign, and saturates again at high voltage of opposite polarity. At the vicinity of coercive field the peaks of ultrasonic attenuation were observed. Therefore using our ultrasonic methods we could study the polar state of the crystal. When DC bias electric field was applied along the polar direction perpendicular to layers, the piezoelectric sensitivity due to electrostriction appeared in the paraelectric phase. In this case the large electromechanical coupling ($K_{33} = 20 - 30$ %) was observed in DC fields of order 30 kV/cm.

Discussion and Conclusions

The phase transition temperature can be increased to > 330 K in nonstoichiometric CuInP2S6, grown with excess of In. In such CuIn $_{1+\delta}$ P2S6

S6 crystals, at room temperature electromechanical coupling for thickness vibrations as high as 50 % could be obtained, after appropriate poling, what is important for medical diagnostics ultrasonic transducers applications.

5I-3

12:00 PM **Growth, Properties and Applications of PMN-PT based Giant-piezoelectric Crystals**

Pengdi Han¹; ¹H. C. Materials Corp., Bolingbrook, Illinois, USA

Background, Motivation and Objective

Significant progresses have been made in the development of PMN-PT based giant-piezoelectric crystal and products since its discovery in 1996. $\langle 001 \rangle$ -seeded single crystals of 3"-4" diameter are successfully commercialized, especially in medical ultrasound imaging industrials. The giant-piezoelectric crystal will be broadly utilized for the next generation of acoustic transduction devices. In this paper, the concepts and knowledge of the crystals will be presented and discussed in terms of applications.

Statement of Contribution/Methods

Following a review on crystal growth and commercialization of the "giant-piezoelectric crystals" PMN-PT based ferroelectric relaxor in the past decade; the detailed physical properties of the PMN-PT based crystals are presented and discussed in terms of applications in ultrasound transducers. At present time 4" diameter PMN-PT single crystal and 3" diameter PIN-PMN-PT crystals are commercially available. The achievement has led to a new era there are new opportunities readily to be explored for the next generation of acoustic transduction devices.

Wednesday
Oral

Results

In order to sufficiently utilize the advantages of the crystals, discussions focus at the followings:

- (1) The differences between single crystal and PZT ceramics
- (2) The concept so called “domain-engineering” (artificially domaining) in context of Elasto-Piezo-Dielectric matrices for three kinds of domain-symmetry, i.e., 3m, 4mm and mm2.
- (3) The relationships between the property and ferroelectric domain structure.
- (4) Suggestions how to choose the poling configurations for different vibration modes based on our topological survey for all cut directions for optimization of piezoelectric coefficient of the crystals.

Aimed to enhance the source level of sonar system, we have commercially developed a new ternary composition, PIN-PMN-PT single crystals of 3” in diameter using Bridgman growth method. The new crystals give strong $E_c(001)$ (electrical coercive field in $\langle 001 \rangle$) up to 3 x $E_c(001)$ of PMN-PT and higher depoling temperature (>120 °C). The detailed piezoelectric properties will be reported for the purpose of applications.

Discussion and Conclusions

In summary, the achievement of the development and fabrication of the giant-piezoelectric crystals has led to a new era there are new opportunities readily to be explored for the next generation of acoustic transduction devices.

This work is supported by Office of Naval Research through contract N00014-08-C-0857, N00014-07-C-0865 and N00014-09-C-0190.

51-4

12:30 PM Progress Update on Relaxor Piezoelectric Single Crystals

Jun Luo¹, Wesley Hackenberger¹, Shujun Zhang², Thomas Shroud², ¹TRIS Technologies, Inc., State College, PA, USA, ²Material Research Lab, Penn State, USA

Background, Motivation and Objective

Single crystal relaxor ferroelectrics exhibit excellent properties for piezoelectric transducer and actuator applications. Lead magnesium niobate-lead titanate (PMN-PT) crystal provides several key advantages based on their unique properties, including high elastic compliance, large piezoelectric coefficient, and extremely high electromechanical coupling. However, the performance of PMN-PT crystals is limited by low rhombohedral-to-tetragonal phase transition temperature ($T_{\pi} < 100^{\circ}\text{C}$), low coercive field ($E_c < 2.5\text{kV/cm}$) and low mechanical quality factor ($Q < 160$). Developing PMN-PT based crystals by composition modification can provide a variety of materials with optimum properties for transducer and actuator applications.

Statement of Contribution/Methods

A series of piezoelectric single crystals including PMN-PT and its isomorphs, pure and Mn-doped lead indium niobate-lead magnesium niobate-lead titanate (PIN-PMN-PT and Mn: PIN-PMN-PT), have been produced at TRS using modified Bridgman crystal growth. These single crystals have been successfully grown along different crystallographic orientations including $\langle 001 \rangle$, $\langle 110 \rangle$ and $\langle 111 \rangle$, with diameters up to 75mm. A multi-crucible Bridgman growth process has also been established for industrial production of these crystals.

Results

To expand the usage temperature range and electric drive field (limited by T_{π} and E_c , respectively), TRS produced large-size PIN-PMN-PT crystals with PIN concentration higher than 26% and diameter up to 75mm. PIN-PMN-PT with optimized composition possesses similar electromechanical properties to PMN-PT, while T_{π} and E_c are increased to 130-140°C and 4-6kV/cm respectively. Both quasi-static and dynamic measurements were used to fully characterize piezoelectric, dielectric and elastic properties of as-grown PIN-PMN-PT crystals.

The low mechanical Q of PMN-PT crystals implies mechanical losses that can result in heat generation for high drive and high duty cycle applications. Recently, TRS has successfully grown Mn doped PIN-PMN-PT crystals. It was demonstrated that by doping with Mn, mechanical Q can increase to above 700 in $\langle 001 \rangle$ -poled longitudinal mode vibrators without compromising k_{33} , T_{π} and E_c . The piezoelectric coefficient, d_{33} , and dielectric constant, K_p^T , were found to be in the range of 1080-1700pC/N and 2900-4500, respectively. This modified composition is being evaluated for high drive and high duty cycle sonar transducer applications.

Discussion and Conclusions

It is demonstrated that by composition modification, the electromechanical properties of PMN-PT based crystals can be optimized to expand operating temperature range, increase AC electric field, and reduce mechanical losses for the high power and duty cycle applications.

5I-5

12:45 PM **Crystal Growth and Improved Properties for Lead Indium Niobate-Lead Magnesium Niobate-Lead Titanate Ternary Piezoelectric Crystals**

Jian Tian¹, Pengdi Han¹, James Carroll², David Payne³; ¹H. C. Materials Corp., Bolingbrook, IL, USA, ²Sandia National Laboratories, Albuquerque, NM, USA, ³Department of Materials Science and Engineering, University of Illinois, Urbana, IL, USA

Background, Motivation and Objective

The excellent properties of the binary piezoelectric crystal, lead magnesium niobate-lead titanate (PMN-PT), have led to a broad range of research and application for medical ultrasound. Recently, the ternary piezoelectric crystal, lead indium niobate-lead magnesium niobate-lead titanate (PIN-PMN-PT), has demonstrated improvements in design characteristics for electrical and thermal stability, while maintaining excellent dielectric and piezoelectric properties. Now, we report crystal growth behavior and further understanding of composition-property relationships in the ternary system, PIN-PMN-PT crystals, for compositions between the two end-members, PMN-PT and PIN-PT.

Statement of Contribution/Methods

PIN-PMN-PT crystals were grown directly from the melt by a modified Bridgman method. The starting compositions were selected to cover the full range of the ternary system. In addition, compositions were chosen near the morphotropic phase boundary (MPB), in the rhombohedral region, for optimum dielectric and piezoelectric properties. From each crystal boule, plate and bar specimens were obtained from the base to the top of the crystal. Selected dielectric and piezoelectric properties were measured in the [001] crystallographic direction.

Results

Crystal growth experiments revealed that PIN-PMN-PT crystals, with compositions over a broad range, could be grown from a stoichiometric melt. We have grown PIN-PMN-PT crystals in the desired perovskite structure for compositions in the range 0-33 mol% PIN. High-quality crystals were obtained since a flux was not used in crystal growth. (However, for compositions with greater PIN content (>33 mol%) flux additions had to be used to obtain the perovskite structure). Measurements determined excellent properties for ternary crystals, with strain coefficient $d_{33} \sim 1000-2000$ pV/m, voltage coefficient $g_{33} \sim 30-45 \times 10^{-3}$ Vm/N, coupling factors $k_{33} \sim 0.87-0.92$ and $k_t \sim 0.56$. Desired increases in coercive field E_c , depoling temperature $T_{R/T}$, and Curie temperature T_c were obtained with increasing PIN content. By comparison with binary crystals, the measured values of dielectric constant K decreased with increasing PIN content.

Discussion and Conclusions

PIN-PMN-PT crystals could be grown from stoichiometric melts for compositions within 0-33 mol% PIN. Ternary crystals offer improvements in properties over PMN-PT, namely increases in coercivity (3 \times) and thermal stability (by 45 °C) as well as excellent piezoelectric and dielectric properties. Thus, new ternary crystals enable improvements to be realized for transducer characteristics by using higher drive fields with less temperature sensitivity. This leads to increased robustness and less problems in depoling.

Wednesday
Oral

6I. Acoustic Propagation

Baalbek

Wednesday, September 23, 2009, 11:30 am - 1:00 pm

Chair: **Georg Mansfeld**
Institute of Radio Engineering & Electronics/RAS

6I-1

11:30 AM Waveguide Localization in Graded Crystals with Antiguinding Acoustic Velocity Profile

Anton Kozlov¹, Vladimir Mozhaev¹, Anna Zyryanova¹; ¹*Faculty of Physics, Moscow State University, Moscow, Russian Federation*

Background, Motivation and Objective

Graded materials are promising candidates for various practical applications in diversified fields and they belong to the class of smoothly inhomogeneous media, where the waveguide effect can occur. For isotropic media with 1-dimensional inhomogeneity of wave properties, it is firmly established at present that the waveguide confinement appears along the lines of minimum wave velocity, while the inverse velocity profile with a local maximum does not produce any waveguide effect and so it is considered as antiguiding. The purpose of the present study is to show that the anisotropy of graded crystals can result in an inversion of common guiding and antiguiding velocity profiles if a local concavity appears on the acoustic slowness surface.

Statement of Contribution/Methods

For some multi-element compound crystals such as

$Al_xGa_{1-x}As$, the relative variations of mass density can be much more than those of elastic stiffnesses. This allows us to consider graded crystals with constant stiffnesses and spatially varying mass density. On the basis of this simplification, we study the wave localization for elliptic and hyperbolic models of acoustic anisotropy using both wave equation and ray approaches. Besides, the exact analytic solutions are found for (a) localized quasishear bulk waves in cubic graded crystals and (b) flexural waves in thin plates of cubic and tetragonal graded crystals.

Results

- (1) The study of pure shear wave propagation in graded crystals (elliptic model) predicts the waveguide effect under common guiding velocity profile (when the phase velocity decreases with distance from the waveguide axis).
- (2) The hyperbolic model predicts the existence of localized waveguide modes under antiguiding conditions, i.e. when the phase velocity falls down rather than grows with distance from the waveguide axis.
- (3) Both qualitative and quantitative ray considerations are consistent with predictions of the elliptic and hyperbolic models.
- (4) The exact particular solution for localized quasishear bulk waves does not confirm the predictions of the first two models and it seems to contradict them. However, the more detailed analysis explains the reasons for this disagreement.
- (5) The exact particular solution for flexural waves in thin crystal plates confirms the predictions of the simplified elliptic and hyperbolic models. It describes the existence of laterally localized waves under antiguiding conditions.

Discussion and Conclusions

We have theoretically demonstrated in this study the existence of new wave phenomenon. It consists in the acoustic waveguide localization under antiguiding conditions in graded anisotropic media with a local concavity of the acoustic slowness surface. On the basis of performed analysis, one can conclude that the predicted phenomenon should be general for waves of various nature under condition that the medium anisotropy produces the slowness surface concavities.

11:45 AM **The Velocity of Anti-Plane Surface Waves on a Body with Depth-Dependent Properties**

Jan Achenbach^{1,1} *Mechanical Engineering, Northwestern University, Evanston, IL, USA*

Background, Motivation and Objective

In this paper we discuss anti-plane surface waves on the flat free surface of a body with properties that depend on a normal coordinate z . The relevant material properties are the shear modulus $\mu(z)$ and the mass density $\rho(z)$, where z is the distance from the free surface. We have

$$\mu(z)=\mu_0g(z) \text{ and } \rho(z)=\rho_0h(z), \tag{1}$$

where

$$g(0)=g_0=1 \text{ and } h(0)=h_0=1 \tag{2}$$

Statement of Contribution/Methods

The main question to be addressed is: do anti-plane surface waves exist at all, and if they exist, are there limitations on the analytical forms of $g(z)$ and $h(z)$. An additional question is: what is the potential utility for QNDE purposes.

The analytical form of the surface wave is taken as

$$v(x,z,t)=V(z)e^{i(kx-\omega t)}, \tag{3}$$

where $V(z)$ must satisfy the equation

$$\mu(z)(d^2V/dz^2)+(d\mu/dz)(dV/dz)-k\mu(z)V(z)+\rho(z)\omega^2V(z)=0, \tag{4}$$

with boundary condition at $z=0$

$$\mu(0)(dV/dz)=0 \tag{5}$$

Wave motion of the kind discussed here is of primary interest in seismology and in the study of functionally graded materials.

Results

It is well-known that anti-plane surface waves do not exist on a homogeneous body with a free surface. A boundary condition that represents some constraint on the surface is required to support anti-plane surface waves.

To the author's knowledge no analytical solution of Eq. (4) exist for arbitrary depth dependence of μ and ρ . For applications in seismology the dependence of μ and ρ has been dealt with numerically by replacing the continuous inhomogeneity by a representative layering, or by a formulation which is amenable to a numerical approach by the Runge-Kutta technique.

In this paper we show significant advances toward a general analytical solution. We do in fact, derive an elegant expression for $V(z)$, see Eq. (3), for the case of high frequency, which is certainly acceptable for QNDE applications in the Mega-Hertz range. The principal result is an equation which relates the surface wave speed, the wave number, and derivatives of $g(z)$ and $h(z)$ at $z=0$. Curves will be displayed that show the relation between the surface wave speed and the wave number. Specific observation will be made with regard to the limitations on the derivatives of $g(z)$ and $h(z)$, in order that surface waves will exist.

Discussion and Conclusions

We will also discuss the possibility of the inverse problem of determining certain properties of $g(z)$ and $h(z)$ from measured values of the surface wave speed.

Wednesday
Oral

Finally we will discuss progress that will have been achieved in extending the method of this paper to determine the velocity of in-plane (Rayleigh) surface waves on a body with depth dependent properties.

6I-3

12:00 PM **Microstructured materials - propagation and use for impedance matching**

Paul Harris¹, Roger Young¹, Andrew Dawson², Russell Petherick¹, Frederic Lecarpentier¹; ¹Industrial Research Ltd, Lower Hutt, Wellington, New Zealand, ²Victoria University of Wellington, Lower Hutt, Wellington, New Zealand

Background, Motivation and Objective

To maximise signal levels designers incorporate matching layers. Often loaded epoxy is used to attain a 3-10 MRayl layer impedance since there is no useful solid in this range. However the attenuation is high - similar materials are often used for absorbing backings. Designers also use 1-3 composites to lower the active element impedance, but low ceramic fractions result in small signals.

The use of a highly collinear microstructured material as a matching layer could provide both low impedance and low attenuation. The microstructure dimension has to be small compared to the wavelength, which is an issue for high frequencies (>50 MHz). Highly collinear porous (pore diameter <100nm) aluminium looks suitable for this application.

Statement of Contribution/Methods

A range of highly regular porous aluminium samples have been prepared, the samples have pore diameter/spacing 30nm/60nm to 200nm/500nm. The 6mm diameter, 0.3mm thick samples have pores that extend from face to face. At low frequencies (<5MHz) dicing can also be used, 60um width pillars have been realised. Using quartz (~12 MRayl) the dicing base is then useful as an intermediate layer.

3D FEM has been undertaken to study the propagation within and at the interfaces of the samples. A range of lattice organizations (square and face-centred square) and dimensions (pore, pillar, kerf) have been modelled at varying wavelengths.

Broadband Panametrics transducers from 10 to 200 MHz have been used in a water bath, one as a emitter/reflection receiver and a second as a transmission receiver. A measurement without the sample provides alignment, and attenuation and time references. The custom receiver circuits and experimental setup will be described.

Results

The modelling and experimental work shows that propagation within the microstructure varies between the bulk P (0% porosity), and the Lamb (approaching 100% porosity) velocity for a square lattice. The reflectivity is dependent on the solid area fraction i.e. porosity and seems independent of lattice organization.

From the FEM analysis the modes and distribution of energy can be identified. Energy propagates as two waves, predominantly as a fast wave in the solid which has compact form and a characteristic pseudo-Lamb group velocity.

Discussion and Conclusions

How does energy cross an interface? The wave incident on the pore opening encounters no material impedance mismatch, however little energy propagates within the pore fluid. In fact the energy distribution is a consequence of modal propagation, and here the pore dimensions largely inhibits propagation in the water phase.

Based on current work an impedance of 4 MRayl for the microstructured material seems realizable.

6I-4

12:15 PM **Measurements of Acoustical Properties of ZnO Single Crystals by the LFB /PW Ultrasonic Material Characterization System**

Yuusuke Kourai¹, Sho Yoshida¹, Yuji Ohashi¹, Mototaka Arakawa¹, Jun-ichi Kushibiki¹, Noboru Sakagami¹; ¹Electrical Engineering, Tohoku University, Sendai, Miyagi, Japan

Background, Motivation and Objective

ZnO has been widely used for BAW devices, SAW devices, and so on. However, basic acoustic properties, viz., phase velocity and attenuation coefficient, have hardly been measured in the operating frequency ranges of these devices. We have been studying development and application of the line-focus-beam/plane-wave ultrasonic material characterization (LFB/PW-UMC) system. In this paper, we measured phase velocities and attenuation coefficients of ZnO single crystal in the VHF/UHF ranges using the LFB/PW-UMC system.

Statement of Contribution/Methods

A Z-cut ZnO single crystal specimen grown by the hydrothermal synthesis method was prepared. Three longitudinal-wave ultrasonic devices with different operating center frequency of 200, 420, and 600 MHz were used for measurements. Bulk acoustic properties were measured in 50-1000 MHz by the PW-UMC system. Two-dimensional velocity distributions of leaky SAWs (LSAWs) were measured on the both surfaces of the Z-cut specimen by the LFB-UMC system at 225 MHz.

Results

In the measured result of LSAW velocity distributions, 1.0-m/s decrease from the average value was observed for a part of region on -Z surface. Resistivity of this region was estimated to be relatively low from [1]. After that, the -Z surface was polished to remove the region by 500 μm. No velocity decrease was observed for the new -Z surface in LSAW velocity distributions. Fig. 1 shows the result of acoustic properties of Z-axis propagating longitudinal waves. The velocity dispersions were observed obviously before the removal and slightly after the removal. Attenuation coefficients after the removal decreased as compared with those before the removal.

Discussion and Conclusions

We compared the measurement results with the calculated values considering the resistivity [2-3]. From the frequency characteristics of velocities and attenuation coefficients, the resistivity of the specimen before and after the removal was estimated to be 10^2 - 10^3 Ωm and 10^3 - 10^4 Ωm, respectively. The LFB/PW-UMC system can successfully detect the variations of acoustic properties caused by slight changes of the resistivity of the specimen.

[1] J. Kushibiki et al, Appl. Phys. Express vol.2, 026501, 2009.
 [2] A. R. Hutson and D. L. White, J. Appl. Phys. Vol.33, p.40, 1962.
 [3] R. T. Smith, J. Acoust. Soc. Am., Vol. 46, p.105, 1969.

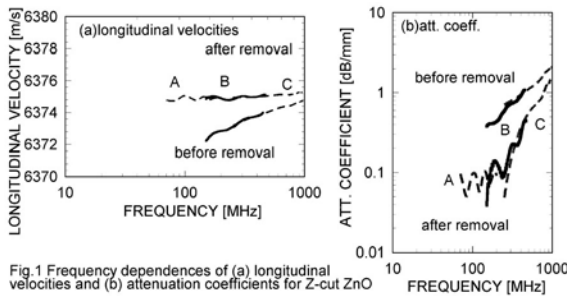


Fig.1 Frequency dependences of (a) longitudinal velocities and (b) attenuation coefficients for Z-cut ZnO

61-5

12:30 PM Fundamentals of Acoustics - Conditions of Existence of Acoustic Waves in Crystals with Surfaces and Interfaces

Vladimir Alshits¹; ¹Institute of Crystallography RAS, Moscow, Russian Federation

Background, Motivation and Objective

Acoustic waves in crystals are used in multiple devices which are based on different physical principles and intended for various aims. Accordingly, the numerous number of different wave types are in use: bulk waves, surface waves, leaky waves, interface waves, guided waves etc. Certainly it is necessary to know specific properties of these waves and conditions for their existence. However theoretical studies in this field are complicated because of an anisotropy of crystals. On the other hand, some of the wave types exist exclusively due to an anisotropy, being forbidden in isotropic bodies.

Statement of Contribution/Methods

Fortunately during last decades new theoretical methods were developed which allowed analytical studying of wave phenomena even in crystals of unrestricted anisotropy. Many types of acoustic waves were systematically investigated. Now we can sum up the results of these studies.

Results

In this paper we present a short review of some basic theoretical results in the acoustics of anisotropic media. The consideration will be concentrated on general criteria for the existence of different classes of acoustic waves in

Wednesday
Oral

anisotropic media with surfaces and interfaces. We shall discuss exceptional bulk acoustic waves, surface waves in purely elastic, piezoelectric and piezoelectric-piezomagnetic crystals, leaky waves of different types, interfacial waves of Stoneley type, Lamb waves (both fundamental and guided modes), Love waves etc. In addition, we shall shortly dwell on the relations between phase, group and ray velocities of bulk and surface acoustic waves and on the resonant reflection of acoustic waves due to a coupling with a leaky wave branch.

Discussion and Conclusions

Now it is clear that anisotropy is not at all reduced simply to more complex theoretical descriptions of properties and phenomena, which are very well known and compactly described for isotropic media. Anisotropy brings into existence new properties and phenomena that are principally absent in isotropic media. In addition, for theoreticians, anisotropy is a beautiful world of elegant mathematics, non-trivial theorems, unexpected peculiarities, singularities and topological catastrophes.

Some Relevant References

1. Alshits, V.I. and Lothe, J. (1979) Elastic waves in triclinic crystals, *Sov. Phys. Crystallogr.*, 24, 387-398, 644-648.
2. Barnett, D.M. and Lothe, J. (1985) Free surface (Rayleigh) waves in anisotropic elastic half-spaces. *Proc. R. Soc. Lond.*, A 402, 135-152.
3. Darinskii, A.N. (2000) On the theory of the elastic wave propagation in a crystal coated with a solid layer, *Proc. R. Soc. Lond. A* 456, 1897-1929.
4. Shuvalov, A.L. (2000) On the theory of wave propagation in anisotropic plates, *Proc. R. Soc. Lond. A* 456, 2197-2222.
5. Alshits, V.I. (2004) On the role of anisotropy in crystalloacoustics. In: *Surface Waves in Anisotropic and Laminated Bodies and Defects Detection*, Eds. R.V. Goldshtein & G.A. Maugin, Kluwer Acad. Publ., Dordrecht, pp. 3-68.

1J. Cardiovascular Elastography

Sala 1

Wednesday, September 23, 2009, 2:30 pm - 4:00 pm

Chair: **Chris de Korte**
Catholic Univ. of Nijmegen

1J-1

2:30 PM **Clinical Value of Two Compounding Techniques for IVUS Palpography**

Mikhail Danilouchkine¹, Frits Mastik¹, Antonius van der Steen^{1,2}; ¹*Biomedical Engineering, Erasmus Medical Center, Netherlands*, ²*Interuniversity Cardiology Institute of the Netherlands, Netherlands*

Background, Motivation and Objective

Recent validation studies proved the diagnostic value of IVUS palpography in semi-invasive characterization of atherosclerotic plaques in coronary arteries. The neighboring high and low strain regions are frequently associated with rupture-prone locations. However, IVUS probe motion hampers accurate determination of the mechanical properties at each location of the luminal surface and results in regions of void strain estimates.

This study aims at the in-vivo assessment of two compounding techniques for IVUS Palpography.

Statement of Contribution/Methods

To increase the elastographic contrast-to-noise ratio, Doyley et. al. proposed a compounding scheme for IVUS Palpography [1]. The neighboring IVUS frames acquired at diastole are paired to compute the luminal strain profiles or partial palpograms. Subsequently, the obtained strain maps are averaged to form a final compounded strain profile for a given cross-section of a coronary artery. This first scheme is further referred to as the classical compounding. The second scheme explicitly takes into account that the measured strains are only partially available. It attempts at reconstructing a missing elasticity value by using available strain information in its direct vicinity via the multilevel Normalized Convolution method. The improved partial strain profiles are subsequently averaged in the same manner as in classical compounding. This scheme was coined as reconstructive compounding.

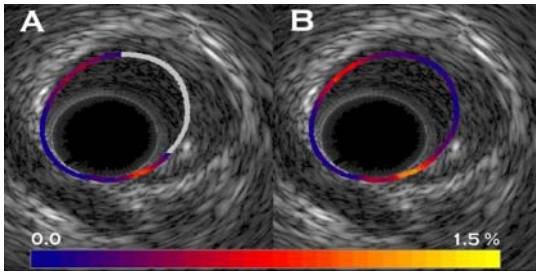
Results

The comparative analysis was performed on 8 in-vivo IVUS pullbacks. The percentage of valid strains was $28.6 \pm 13.7\%$ for the scheme without compounding, $94.3 \pm 4.4\%$ and $99.7 \pm 0.2\%$ for the classical and reconstructive methods, respectively. Figure shows the luminal strain distribution for a cross-section of a coronary artery with an atherosclerotic burden, computed with the classical (A) and reconstructive (B) compounding scheme. Due to the missing information about the cap stiffness, plaque vulnerability cannot be assessed with classical compounding. Reconstructive compounding restores the missing strain values and allows to judge about the plaque's rupture-proneness.

Discussion and Conclusions

Implementation of the compounding schemes significantly boosts the diagnostic information coming out of IVUS Palpography with the reconstructive scheme being the best.

[1] Doyley M.M. et.al. UMB 27(11), 1471-1480, 2001.



1J-2

2:45 PM Quantitative Imaging of Myocardium elasticity using Supersonic Shear Imaging

Mathieu COUADE^{1,2}, Mathieu Pernot², Mickael Tanter², Emmanuel Messas³, Alain Bel³, Maguette Ba³, Albert-Alain Hagege³, Mathias Fink², ¹Supersonic Imagine, France, Metropolitan, ²Institut Langevin, ESPCI ParisTech, CNRS UMR 7587, INSERM, France, Metropolitan, ³Hôpital Européen Georges Pompidou, INSERM U633, France, Metropolitan

Background, Motivation and Objective

Several techniques have been proposed for assessing mechanical properties of the heart, but none of these techniques can provide a quantitative and local measurement of elasticity in the myocardium. This is mainly due to the rapid variation of myocardial elasticity during the cardiac cycle. We propose to apply the concept of Supersonic Shear Imaging (SSI) for measuring instantaneously the myocardium elastic modulus at the different stages of the cardiac cycle.

Statement of Contribution/Methods

Experiments were performed in vivo on 12 sheep. After a lateral thoracotomy, the transducer was placed directly on the postero-lateral wall of the left ventricle. Then, a shear wave was generated on the myocardium using the acoustic radiation force induced by a conventional linear ultrasonic probe (8MHz). The shear wave propagation along the muscle was imaged in real-time using an ultrafast scanner (12 000 frames/s). The tissue velocities were obtained from conventional speckle tracking techniques and the shear wave phase velocity was derived at each frequency in the range of 100-1500Hz from a single broadband radiation force excitation. Each elasticity measurement was achieved in less than 20 ms and was repeated 20 times every 50 ms during 1 second allowing to measure variation of elasticity within one cardiac cycle. The electrocardiogram (ECG) was recorded and synchronized with the acquisitions. A transient (<30 minutes) and local myocardial infarction was induced by ligation of diagonal or obtuse marginal coronary arteries. Shear wave elasticity was performed before, during infarction and after reperfusion at the same myocardium location.

Results

The feasibility of inducing and imaging shear wave in the myocardium was demonstrated in-vivo up to 20 times per second allowing the observation of myocardium elasticity natural variation during the cardiac cycle. The mean shear wave velocity was found to be 4.8 +/- 1.1 m/s in the systolic phase and 2 +/- 0.3 m/s in the diastolic phase. Immediately after ligation and local myocardial infarction, a 20% diminution of shear wave velocity was measured in systole. After reperfusion, the initial elasticity was completely restored.

Discussion and Conclusions

The reproducibility and the accuracy of the measurement are discussed. The effect of the myocardial anisotropy is also discussed. This novel approach offers a promising technique for imaging quantitatively the elasticity of the myocardium. To our knowledge, this is the first time that the myocardial elasticity variation is measured locally and quantitatively.

Wednesday
Oral

3:00 PM 3D elasticity imaging on an open-chest dog heart

Congxian Jia¹, Ping Yan², Albert Sinusas², Donald Dione², Qifeng Wei³, Karl Thiele³, Theodore Kolias¹, Jonathan Rubin¹, Lingyun Huang⁴, Sheng-Wen Huang¹, James Duncan², Matthew O'Donnell^{1,2} *University of Michigan, USA, ²Yale University, USA, ³Philips Medical Systems, USA, ⁴University of Washington, USA*

Background, Motivation and Objective

Myocardial ischemia and infarction alter myocardial viability and contractility. We have hypothesized that contractility changes can be detected by ultrasound strain imaging. Current ultrasound strain imaging methods are mainly 1D and 2D. However, heart motion is complex and 3D. To address this, 3D RF data were acquired using a commercial 3D scanner on an open-chest dog heart before and after occlusion of the left anterior descending (LAD) artery. 3D speckle tracking was used to detect acute ischemia induced by occlusion of the LAD artery.

Statement of Contribution/Methods

According to a local animal protocol, 3D RF volume data were acquired on an open-chest dog heart using a commercial 2D phased array (iE33, Philips, Andover, MA) placed in front of the anterior wall of the left-ventricle with a small water stand-off. The LAD artery was occluded to produce acute ischemia. Data acquisition before and after occlusion of the LAD artery includes 52 volumes/cycle and 46 volumes/cycles (FR is 77), respectively. Each data volume covered 77.5 degrees in the azimuthal direction and 70 degrees in the zenithal direction and 6.5cm in depth (anterior wall) at a transmit frequency of 3.8 MHz. 3D speckle tracking was applied to estimate strain with tracking resolution of 1.2 mm in the axial direction and 4.5 mm in azimuthal and zenithal directions. Frame-to-frame tracking results were accumulated referenced to the heart geometry at the end of diastole.

Results

3D speckle tracking successfully estimated the displacement in three directions. Radial strains at the end of systole derived from accumulated 3D displacements referenced to the end of diastole in the zoomed region (shown in Fig. 1 (c)) detected abnormal wall thinning (Fig. 1 (b)) due to LAD occlusion contrasted to normal heart wall thickening (Fig. 1(a)).

Discussion and Conclusions

Unlike 1D or 2D methods, 3D speckle tracking can estimate myocardium's three dimensional motion. By accounting for out-of-plane motion, strain imaging using 3D tracking may allow more accurate detection of abnormal myocardial deformation associated with myocardial ischemia or infarction.

This work was supported in part by HL-082640, HL-67647, HL-68658 and CA-109440.

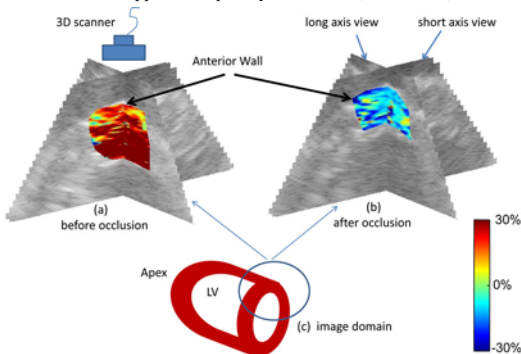


Fig. 1. Radial strain using 3D speckle tracking before and after occlusion at the end of systole.

1J-4

3:15 PM High quality non-invasive full 2D strain tensor imaging using a beam steered linear array ultrasound transducer

Hendrik Hansen¹, Richard Lopata¹, Chris de Korte¹, ¹*Clinical Physics Laboratory, Department of Pediatrics, Radboud University Nijmegen Medical Center, Netherlands*

Background, Motivation and Objective

Strain imaging has been performed using 1D, 2D and 3D ultrasound data. Usually, strain is only estimated in the beam direction, because of the availability of phase information. However, strain estimates in other directions are also desired, since most tissues are anisotropic. Beam steering enables measurement of different projections of the 2D displacement field while using phase information. The full 2D displacement vector and strain tensor can be derived using multiple projections. This study aims at deriving the full 2D strain tensor by measuring only displacement along the beam while steering the beam at three angles.

Statement of Contribution/Methods

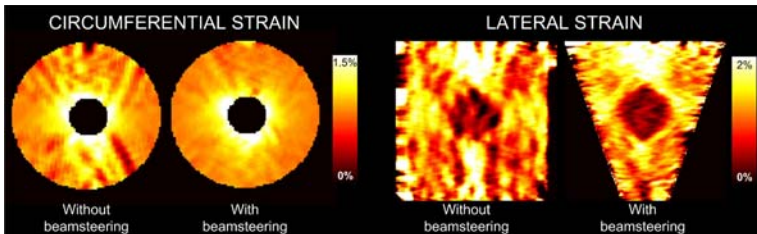
A Philips SONOS 7500, equipped with a linear transducer (11-3L, $f_c = 8.7\text{MHz}$) and an rf-interface, was used to acquire radiofrequency (rf) data at -30° , 0° , and 30° . The technique was applied on pre and post-compression data of a homogeneous gelatin vessel phantom placed in a water tank. A water column was attached and used to generate intraluminal overpressures of 10 and 14 mmHg. Displacements along the beams were iteratively estimated using 2D cross-correlations. The 0° acquisition yielded the vertical displacements. Projection of the -30° and 30° displacements yielded the horizontal displacements. The full 2D strain tensor was derived using 1D least squares strain estimators and rotated to obtain radial and circumferential strains. To test the technique's suitability for non vascular applications a block phantom of polyvinyl alcohol with a three times stiffer cylindrical inclusion was constructed. Rf data of the phantom were acquired before and after 2% vertical compression at beam steering angles of -20° , 0° and 20° . To quantify image quality, elastographic signal-to-noise (SNRe) and contrast-to-noise ratio's (CNRe) were calculated for radial and circumferential strain images of the vessel phantom, and for lateral strain images of the inclusion phantom.

Results

Strain images constructed with beam steering technique showed much more detail and contrast than images constructed without this technique: Radially, SNRe and CNRe increased with 6 dB and 19 and circumferentially with 3 dB and 9 dB for the vessel phantom. SNRe and CNRe increased with 5 dB and 11 dB lateral for the inclusion phantom.

Discussion and Conclusions

The full 2D strain tensor can be accurately measured by using three beam steering angles.



1J-5

3:30 PM Acoustic radiation force impulse imaging of cardiovascular tissue

Gregg Trahey¹, Jeremy Dahl¹, Stephen Hsu¹, Douglas Dumont¹, Richard Bouchard¹, Jason Allen¹, Patrick Wolf¹, ¹*Duke University, Durham, NC, USA*

Background, Motivation and Objective

Cardiovascular disease remains the most likely cause of death in developed countries, accounting for approximately 870,000 deaths in the United States alone in 2004. Virtually every form of cardiovascular disease involves modifications in tissue stiffness. Acoustic radiation force impulse (ARFI) imaging shows great promise in the regional characterization of tissue stiffness in a variety of clinical applications. Cardiovascular tissues

present unique challenges to ARFI imaging because of their dynamic changes in stiffness, high-amplitude physiological motion, and elevated stiffness levels compared to other tissues.

Statement of Contribution/Methods

We have implemented ARFI and shear wave elasticity imaging (SWEI) on a commercially available scanner. These imaging methods were employed on: dynamic vascular and cardiac phantoms; canine, porcine, and ovine models; and normal patients and those diagnosed with peripheral and carotid arterial disease. Interpolation and extrapolation filters, designed to eliminate artifacts from physiological motion, were implemented and evaluated. Stiffness measurements were obtained throughout the cardiac cycle and with various manipulations of tissue status (ie: radiofrequency ablation, blood pressure, and heart rate) under transcutaneous, intravascular, intracardiac, and epicardial imaging conditions.

Results

In both vascular and cardiac applications, ARFI imaging resolution was similar to corresponding B-mode images. The ARFI-induced displacement and recovery curves exhibited cyclic variations that reflected the expected changes in stiffness through the cardiac cycle. Calcified vascular plaques and ablated cardiac tissue demonstrated consistently high and stable stiffness throughout the cardiac cycle. High frame rate ARFI imaging was capable of visualizing the direction and speed of propagation of mechanical stiffness waves corresponding to myocardial contraction. Shear wave velocimetry was successfully implemented in cardiac and vascular tissues. Measured shear wave velocities, as expected, increased during systole and at elevated pressures. Shear wave velocities were also seen to vary with tissue orientation, resulting from underlying tissue anisotropy.

Discussion and Conclusions

Radiation force-based imaging offers myriad opportunities for contributing to the diagnosis of various cardiovascular diseases. It offers heretofore unavailable information on the local dynamic stiffness characteristics of tissue.

2J. Bioeffects

Sala 2

Wednesday, September 23, 2009, 2:30 pm - 4:00 pm

Chair: **William O'Brien**
Univ. of Illinois at Urbana-Champaign

2J-1

2:30 PM **Potential Mechanism for Vessel Invagination Caused by Bubble Oscillations**

Wayne Kreider¹, Hong Chen¹, Michael Bailey¹, Andrew Brayman¹, Thomas Matula^{1,2}:*Center for Industrial and Medical Ultrasound, Applied Physics Laboratory, University of Washington, Seattle, WA, USA*

Background, Motivation and Objective

In medical ultrasound, acoustically excited bubbles are relevant to both imaging and therapeutic applications and have been implicated in causing vascular damage. A current paradigm for understanding interactions between bubbles and vessels considers the dilation of small vessels to be the most likely damage mechanism. However, recent high-speed photographs suggest that bubbles oscillating in larger vessels can cause an invagination of the vessel wall that is associated with higher strains than any accompanying vessel dilation. The objective of this effort is to elucidate mechanisms whereby acoustically excited bubbles can cause such invaginations.

Statement of Contribution/Methods

By comparing the geometry of a bubble in a relatively large vessel with a bubble near a flat and rigid boundary, a Bernoulli-type equation is derived for pressure radiated by the bubble at the boundary. Considering an axis defined by the center of the bubble and the nearest point on the boundary, this equation assumes a locally cylindrical flow geometry between the bubble and boundary as well as incompressible, inviscid flow. Also, flow is assumed to diverge spherically with increasing radial distance from the bubble. Used in conjunction with radial bubble dynamics from experimental observations and/or numerical simulations, this approach estimates the impact of an oscillating bubble in terms of radiated pressure along the boundary. From the hypothesis that both instantaneous and averaged pressures at the boundary may provide insight into bubble-vessel interactions, a series of experiments were conducted in *ex vivo* tissue and simulations were compared to photographic observations.

Results

For two photographic sequences, simulations predict that instantaneous pressures at the vessel wall take on both positive and negative values in synchrony with nearby bubble oscillations. However, observed vessel deflections were not synchronous with bubble oscillations. Over the 3.9-microsecond time span represented by each sequence, average radiated pressures of -0.07 and -0.09 MPa were calculated at the vessel wall, thereby implying net tensile forces consistent with invagination. These predicted averages correspond with observed vessel deflections toward the lumen of 9 and 10 microns, respectively.

Discussion and Conclusions

A bubble oscillating near a boundary can lead to attractive forces, whereby the bubble may act like a straw that generates suction on a nearby vessel wall. Moreover, simulations suggest that the net tensile force would increase quickly if the vessel wall began to move toward the bubble. Because instantaneous pressures are not synchronous with vessel deflections, viscous characteristics of the vessel and surrounding tissue likely play a role in such bubble-vessel interactions. Work supported by NIH grants EB00350, DK43881, and DK070618.

Wednesday
Oral

2J-2

2:45 PM **Applications of Low Intensity Pulsed Ultrasound for Functional Bone Tissue Engineering using Adult Stem Cells**

Skylar Marvel¹, Elizabeth Loba¹, Paul A. Dayton¹, ¹Joint Dept of Biomedical Engineering, University of North Carolina-North Carolina State University, USA

Background, Motivation and Objective

Low intensity pulsed ultrasound (LIPUS) has been used to accelerate fracture healing for over a decade. In 1994 the FDA approved a LIPUS device for fracture healing and in 2000 for nonunions. Despite this, there is still a lack of understanding the effects of ultrasound (US) parameters on cell growth. There are very few published studies that examine US pulse repetition frequency (PRF), a crucial parameter in US dose. Also, most studies are limited to the parameter ranges available within the capabilities of commercially made systems, such as a 1 MHz sine wave, 30 mW/cm² intensity applied for 20 min. per day, pulsed for 200 μ s with a PRF of 1 kHz, giving a 20% duty cycle.

Statement of Contribution/Methods

We combine expertise in tissue engineering and US physics to study the effects of LIPUS parameters on stem cell differentiation for both human bone marrow derived (hMSC) and adipose derived (hASC) adult stem cells. We have built a custom LIPUS system, which has extreme flexibility over parameter selection, in order to determine separate optimal parameter settings that will increase calcium production while also decreasing adipose production for each cell type.

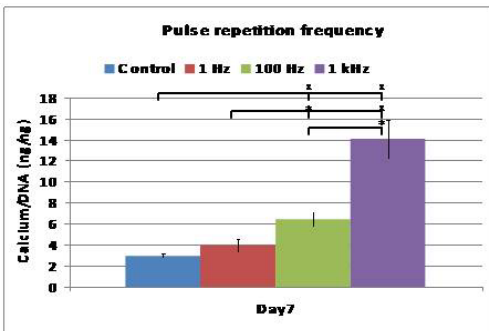
Results

In recent preliminary studies, our group has discovered significant effects of LIPUS on the differentiation of stem cells. Specifically, we have found that application of LIPUS to hMSCs is capable of increasing the calcium production per cell ($p < 0.05$ control/1 kHz, 100 Hz/1 kHz) while significantly decreasing adipogenic differentiation ($p < 0.05$ control/100 Hz, control/1 kHz, 1 Hz/1 kHz). The application of LIPUS to hASCs also significantly increases calcium accretion per cell (Figure 1, $p < 0.01$ control/100 Hz, control/1 kHz, 1 Hz/1 kHz; $p < 0.05$ 1 Hz/100 Hz, 100 Hz/1 kHz).

Discussion and Conclusions

Clearly more research needs to be done exploring the effects of LIPUS on stem cells. These two cell types can be used for creating bone constructs to fill critical bone defects. Our results are particularly exciting because hASCs are understudied and have only recently begun to gain interest to researchers since they are readily available, easily obtained and new lineage potentials are continually being discovered. One of the significant factors for LIPUS has been determined to be the PRF. Once proper parameters have been found, LIPUS can be incorporated into modern bioreactors as an additional stimulus to produce a desired differentiation.

Wednesday
Oral



2J-3

3:00 PM **Microbubble and Ultrasound Induction Gene Expression Associated with Novel Radiation Enhancing Therapy**

Gregory Czarnota^{1,2}, Raffi Karshafian³, Anoja Giles¹, Azza Al Mahrouki¹, Sara Irajji¹, *Radiation Oncology, and Imaging Research, Sunnybrook Health Sciences Centre, Toronto, Ontario, Canada,* ²*Radiation Oncology, and Medical Biophysics, University of Toronto, Toronto, Ontario, Canada,* ³*Physics, Ryerson University, Toronto, Ontario, Canada*

Background, Motivation and Objective

It is now appreciated that radiation not only damages the DNA inside tumour cells in vivo but may act by damaging the endothelial cells of the vasculature. Recent research indicates significant enhancements of radiation effects by exposing the endothelial cells in the vasculature to microbubble disruption. In this study we tested the hypothesis that exposure to microbubble agents in the presence of ultrasound can lead to significant changes in gene expression using cell culture in vitro.

Statement of Contribution/Methods

Adherent human umbilical endothelial cells (HUVEC) exposed to ultrasound for microbubble perturbation at a concentration of 1.0×10^{10} in 1 ml of phosphate buffered saline. Cells were exposed 500kHz ultrasound, 16 cycles tone burst, 3kHz pulse repetition frequency for 30 seconds, and 570 kPa peak negative pressure. Definity bubbles (Bristol Myers-Squibb) were (no bubbles, and 3.6×10^{10} microbubbles in 90 μ l added to 1 ml of cells). Cells were then exposed to 0, 2, and 8 Gy using 160 kVp X-rays at 200 cGy/minutes. Histology was carried using light microscopy using haematoxylin and eosin staining and with TUNEL staining for apoptotic cell death. Immunohistochemistry for ceramide expression was also carried out. Gene expression profiling and RT-PCR were used for assays of gene expression induction at 1, 4 and 12 hours after treatment.

Results

Immunohistochemistry indicated endothelial cell apoptosis and activation of the ceramide cell-death pathway to be caused by microbubbles. Gene analysis identified 19,264 genes total with, depending on treatment conditions 239 – 517 genes demonstrated more than a two fold up-regulation. This included a number of genes that are known to be involved in apoptosis and ceramide-induced apoptotic pathways. These included mitogen-activated protein kinase kinase 1 (MAP2K1), Sphingomyelin phosphodiesterase 2, neutral sphingomyelinase (SMPD2), acid sphingomyelin phosphodiesterase 1, (ASM; SMPD1), UDP glycosyltransferase 8 (UDP-galactose ceramide galactosyltransferase, UGT8), Cytochrome c oxidase (COX6B1), and Caspase-9. To verify these results, we performed real time RT-PCR, which indicated an upregulations that ranged from 2 to 199 fold, specifically in the combined treatment of ultrasound and radiation. This was observed when comparing the expression levels of the above mentioned genes in cells exposed to combined treatment to those of the control or to the levels observed in treatments with radiation only.

Discussion and Conclusions

Radiation effects have been recently demonstrated in vivo to synergistically enhance the effects of radiotherapy. Analyses carried out here in vitro indicate significant changes in gene expression in response to microbubbles and ultrasound alone, or when combined with radiation. Data indicate the activation of similar membrane-damage related biological pathways. This work forms the basis for ultrasound-induced radiotherapy enhancement.

2J-4

3:15 PM **Ultrasound-Enhanced Osteogenesis of Human Mesenchymal Stem Cells Encapsulated in Collagen Meshwork**

Hades C. T. Wong¹, Mei Yi Wong¹, Barbara P. Chan¹, Alfred C. H. Yu¹, *Medical Engineering Program, The University of Hong Kong, Pokfulam, Hong Kong*

Background, Motivation and Objective

Bone marrow derived mesenchymal stem cells (MSCs) are well-regarded as potential bone graft materials for regenerative medicine. An osteoinductive way of implanting these MSCs is to first encapsulate them into larger particles through collagen fiber meshes and then injecting these particles to the treatment site. Nevertheless, its ensuing osteogenic differentiation is known to be slow for human MSCs (hMSCs). As such, our objective has been to examine whether ultrasound stimulation can improve the osteogenesis of collagen-hMSC particles.

Statement of Contribution/Methods

We studied the in-vitro calcium deposition level over a three-week period for collagen-hMSC particles that were routinely exposed to ultrasound. In this study, the hMSCs were first cultured to the 6th passage in a growth medium and a 37°C humidified incubator environment (with 5% CO₂). Three days prior to the start of experiment, the hMSCs were entrapped using a Type I collagen solution to form disc-shaped particles with 2mm radius and 1mm thickness (concentration: 500,000 cells/ml; density: 2 mg/ml), and these particles were cultured in an osteogenic differentiation induction medium. During the experimental period which lasted 18 days, the collagen-hMSC particles were exposed to 1MHz pulsed ultrasound with 30mW/cm² intensity (SATA) and 20% duty cycle for 30min. daily outside the incubator environment. The ultrasound excitations were sent through an unfocused probe with 2.56cm diameter, and the particles were placed at the last maxima of the field profile (13.5 cm from probe). At the end of the experimental period, the collagen-hMSC particles were photographed using phase contrast microscopy, after which they were air-dried for 1 week. Their calcium deposits were extracted using 1%

trichloroacetic acid and the amount was quantified with a calcium assay kit. To facilitate comparison, we repeated the entire experimental protocol without ultrasound exposure. Also, we conducted a set of experiments that only applied the ultrasound exposure in the first 6 days to determine whether early-stage stimulation is important to the osteogenesis of collagen-hMSC particles.

Results

Our phase contrast images show that the ultrasound-exposed collagen-hMSC particles had a darker appearance than the unexposed ones because of the increased presence of calcium deposits. Also, in our calcium deposit assay, the ultrasound-exposed group had a 51% increase in their normalized calcium weight (N=6, $p < 0.05$). A statistically similar impact (K-S test: $p < 0.05$) was observed for the collagen-hMSC particles that were only exposed to ultrasound in the first 6 days, thereby confirming that ultrasound stimulation makes early impact on the osteogenic differentiation of these particles.

Discussion and Conclusions

Our initial evidence indicates that ultrasound stimulation has potential in improving the efficacy of injectable bone tissue engineering by enhancing the osteogenic process of collagen-hMSC particles.

2J-5

3:30 PM Use of vital staining to refine the thermal necrotic threshold for tissue exposed to high intensity focused ultrasound

Peter Kaczkowski¹, Andrew Brayman¹, Gavriel Speyer¹, Yak-Nam Wang¹, Steven Kargl¹, Lawrence Crum^{1,†} *Applied Physics Lab, University of Washington, Seattle, WA, USA*

Background, Motivation and Objective

Ablative thermal therapy using High Intensity Focused Ultrasound (HIFU) requires knowledge of the minimum necrotic dose, and we examine the hypothesis that simply raising tissue temperature to a minimum of approximately 60 degrees C is a sufficient condition for immediate necrosis. In support of this goal, we seek to test the hypotheses that (1) a non-subjective quantitative metric of HIFU-induced liver tissue discoloration (discoloration index, DI) is a valid and reliable indicator of tissue ablation, (2) the DI will correlate with numerical models of thermal dose (TD), (3) the discoloration metric and simulated TD will correlate with histological observations of HIFU-treated tissues using vital staining, and thus provide an acute necrotic threshold for the HIFU heating regime.

Statement of Contribution/Methods

Freshly excised bovine liver was transported from a slaughterhouse and sectioned into 5 cm³ blocks, placed in cassettes and carefully degassed in preparation for exposure with 3.5 MHz HIFU. Linear transverse scans at constant energy exposure (between 4 and 10 J/mm at focus) created linear lesion tracks which were surgically exposed at the focal depth within minutes after treatment, photographed, and sampled for vital staining (NADH). Total time from slaughter to fixation was less than 12 hours. A custom image processing tool was used to extract lesion characteristics from macroscopic and histological images. Lesion metrics were then compared to numerical simulations of temperature evolution using nonlinear acoustic (KZK) and Heat Transfer Equation (HTE) algorithms.

Results

Vital staining indicates a narrow transition zone between viable and ablated tissue, saturating in the ablated zone. The DI is highly correlated with the logarithm of the computed TD. Comparison of transverse lesion profiles obtained with the three methods indicates that the discoloration metric is sensitive below TD = 10 minutes @ 43° C, substantially less than the accepted necrotic threshold of 120 minutes. More importantly, the transition to saturation of the necrotic signal corresponds to about TD = 110±10 min (60 °C for 0.05 sec), and deviation from background viable tissue occurs at about TD = 7 min (46 °C for 60 sec). Thus, given the rate of temperature diffusion in the focal region, necrosis is highly probable if the tissue reaches a temperature of 60 degrees.

Discussion and Conclusions

The necrotic threshold for thermal ablative therapy using HIFU can practically and simply be defined by a minimum temperature rather than by thermal dose, but the time history of tissue temperature may be required to ensure viability. The newly defined tissue discoloration index is useful as a proxy for histological analysis in rapid assessment of HIFU treatment protocols. Survival studies of HIFU-induced bioeffects, allowing time for apoptotic processes to extend the necrotic region, are planned to refine the dose-response relationship. Work supported by NIH R01CA109557.

2J-6

3:45 PM The growth of Osteoblasts stimulated by low intensity pulsed ultrasounds of different exposure durationsShow-Huic Chen¹, Chun-Yi Chiu¹, Shyh-Hau Wang¹, Siao-Song Lee¹; ¹Chung Yuan Christian University, Taiwan**Background, Motivation and Objective**

The bone remodeling is a life long process with the regulation between bone formation and resorption to maintain a healthy bone. Osteoblasts (OBs) are cells responsible for bone formation. Although the proliferation of OBs was found to increase upon the simulation with low intensity pulsed ultrasounds (LIPUS), it remains unclear to what ultrasonic parameters accommodate bone cells with a beneficial effect for the growth. In this study, OBs were insonated with LIPUS of different exposure durations to extensively investigate ultrasound exposure on the growth of cells.

Statement of Contribution/Methods

Method and materials for this study were adopted from our previous studies in which the OBs were seeded and then were incubated for 24 hours to allow cells to be adhered on the culture plate. Subsequently, LIPUS of a fixed 100 mW/cm² intensity from a 1 MHz and 20% duty cycle within 1 kHz pulse repetition frequency was arranged to respectively stimulate various groups of passage OBs for 3, 5, 10 and 20 minutes daily. Another experiment was also arranged using the same protocol to insonify groups of differentiation OBs for 14 days. The insonification responses for those OBs were evaluated by cell morphology, viability, alkaline phosphatase (ALP) activity, Alizarin red-S staining, and mRNA expression by reverse transcriptase-polymerase chain reaction (RT-PCR).

Results

Results showed that the proliferation of those insonified OBs for 10 minutes tended to increase to around 1.1 fold compared to cells of the control group after the fourth day of experiments. Similar tendency for the ALP activity was observed, in which the largest activity and proliferation rate of OBs were measured to be at the sixth day after insonation. The largest mineralization of OBs enhanced by LIPUS insonification also corresponded to cells insonified for 10 minutes daily. Moreover, the RT-PCR analysis revealed that those cells insonified for 10 minutes daily tended to increase more mRNA levels of osteocalcin than those of control groups.

Discussion and Conclusions

The variations of temperature in the culture medium throughout each insonification procedure were measured to be less than 1 °C indicated that the insonification effect on OBs is associated to non-thermal effect of LIPUS stimulation. This study also demonstrated that both proliferation and activation of ALP synthesis of OBs may be enhanced by LIPUS stimulation and is exposure duration dependence in which a sufficient longer insonification duration brings more effective in promoting the OBs growth.

3J. Bone II

Sala 4

Wednesday, September 23, 2009, 2:30 pm - 4:00 pm

Chair: **Pascal Laugier**
Univ. Pierre et Marie Curie-Paris 6

3J-1

2:30 PM **Tissue acoustic impedance of cortical bone is determined by nanostructural characteristics hydroxyapatite**

Fabienne Rupin¹, Aurelien Gourrier^{2,3}, **Mathilde Mouchet**¹, Kay Raum⁴, Françoise Peyrin³, Amena Saied¹, Pascal Laugier¹; ¹Laboratoire d'imagerie Paramétrique, Université Pierre et Marie Curie, Paris, France, ²Laboratoire de Physique des Solides, Université Paris-Sud, Orsay, France, ³ESRF, Grenoble, France, ⁴Q-BAM Group, Dept. of Orthopedics, Martin Luther University of Halle-Wittenberg, Halle, Germany

Background, Motivation and Objective

The osteon is the fundamental functional unit of cortical bone at the tissue level. Each osteon consists of concentric lamellae, made of a composite material of mineral platelets (hydroxyapatite), with given size and orientation distributions, embedded in an organic matrix of collagen fibers. The elastic properties of lamellae of human cortical bone have been investigated using scanning nanoindentation and acoustic microscopy. Both the nanoindentation modulus and the acoustic impedance show a characteristic bimodal lamellar pattern of alternating high and low values. Previous reports suggest that the lamellar modulation of microelastic properties is related to the lamellar level modulation of the mineral content or to variations of the lamellar orientation. Both assumptions are plausible, however, the orientation of mineral platelets and collagen fibers were not directly assessed for a face-to-face confrontation with microelastic measurements. Furthermore, the influence of mineral platelets thickness on tissue level elasticity has not been investigated so far.

Statement of Contribution/Methods

The goal of this study was to look at the osteon level variation of acoustic impedance and to assess its relationship to mineral platelet orientation and size with a micrometre resolution. Data were acquired on a cross-section of a human femoral mid-shaft using 900-MHz scanning acoustic microscopy, synchrotron radiation micro-computed tomography (SR- μ CT) and small angle X-ray scattering (SAXS). The local variations of mineral content were determined from SR- μ CT and the relative variations of orientation of mineral platelets were obtained from the integrated SAXS intensity. Moreover, the mean thickness of mineral platelets in bone was deduced from the analysis of the SAXS patterns.

Results

The well-known lamellar level modulation was observed on both the SAM and SAXS images but not in the SR- μ CT images. While the absence of modulation on SR- μ CT images indicates a constant level of mineral in the explored region, the SAM and SAXS data indicate a modulation of microelasticity, orientation and thickness of the platelets. The local acoustic impedance showed also a strong positive correlation with the SAXS intensity ($R^2=0.91$, $p<0.0001$) and a much lower correlation with the platelets thickness ($R^2=0.35$, $p<0.0001$).

Discussion and Conclusions

This is the first study that combines SAXS, SR- μ CT and SAM in order to elucidate the impact of mineral platelets orientation and mean thickness on microelasticity. The alternating pattern of high and low impedance values across a human osteon was found in spite of a homogeneous distribution of mineral quantity. Our results suggest that the main factor contributing to these variations is the platelet orientation reflected in modulations of the integrated SAXS intensity and that the mean platelet thickness contributes only to a small extent to the variations in acoustic impedance.

3J-2

2:45 PM **Impact of a multi-frequency sequence of measurements on first arriving signal velocity on a bone plate model**

Thien-Ly Pham¹, Jean-Gabriel Minonzio¹, Maryline Talmant¹, Pascal Laugier^{1,2} *Laboratoire d'Imagerie Paramétrique, Université Pierre et Marie Curie-Paris 6; CNRS, LIP UMR 7623, France*

Background, Motivation and Objective

QUS axial transmission provides velocity of waves propagating along the cortex of long bones. Studies have shown that the first arriving signal (FAS) measured at the centre frequency of the probe is an indicator of bone status. Recently, it has been suggested to measure the frequency dependence of the FAS velocity to recover the cortical thickness. A difficulty arises due to the frequency dependence of the near field effect (governed by the emitter-receiver distance-to-wavelength ratio d/λ). Our goal is to characterize the near field effect on FAS velocity of plates of various thicknesses.

Statement of Contribution/Methods

Propagation was simulated using a finite difference method on homogeneous transverse isotropic 1 to 8 mm-thick plates immersed in water and on a semi-infinite interface. The probe contained an emitter and 31 regularly spaced receivers aligned parallel to the plate surface. Broadband pulses with centre frequencies increasing from 0.3 to 2MHz were used to excite the probe, resulting in variations of thickness-to-wavelength ratio Th/λ from 0.075 to 4 and of d/λ from 1.2 to 19.4. Local velocity was calculated by measuring the difference of time-of-flight between two adjacent receivers.

Results

Fig.1 illustrates the near field effect by plotting local velocity values against d/λ . A unique value of local FAS velocity is expected for fixed values of Th/λ under conditions of far field. In contrast, huge variations of local velocities were obtained as a function of d/λ . The pattern of variation exhibited by the local velocities as a function of d/λ depended on Th/λ . At a fixed value of Th/λ , under the same conditions of field i.e. for the same range of d/λ , local velocities on plates of different thicknesses presented the same evolution.

Discussion and Conclusions

Our results illustrate the additional complexities arising from the near field effect. FAS measurements at multiple frequencies imply taking into account both the ratio governing the thickness dependence and the ratio governing the near field effect. An accurate characterization of near field effect could aid in developing a correction procedure. Choosing regions in the space parameter where local velocity does not vary much minimizes near field effect.

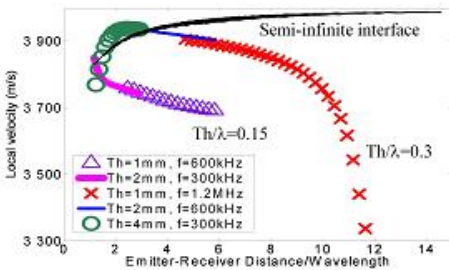


Fig. 1: Near field effect for a semi-infinite interface and for plates of different thicknesses for two values of Th/λ (0.15 and 0.3)

3J-3

3:00 PM **Measurement of guided mode phase velocities using multi-emitters and multi-receivers arrays in contact using transfer matrix analysis**

Jean-Gabriel Minozio¹, Maryline Talmant¹, Pascal Laugier^{1,2} *Laboratoire d'Imagerie Paramétrique, CNRS LIP UMR7623, Université Pierre et Marie Curie - Paris 6, Paris, France*

Background, Motivation and Objective

Structural and material properties of elastic waveguides can be characterized by fitting measured to theoretical guided waves phase velocities. Here emitters and receivers are placed in contact on the same side of the waveguide (i.e. axial transmission geometry). Multi-receivers arrays allow the determination of phase velocities using two dimensional spatio-temporal Fourier Transform, which requires a large distance probed by the receivers. Practical constraints, as in clinical inspection of cortical bones, may reduce the inspected spatial length and therefore the efficiency of this technique.

Statement of Contribution/Methods

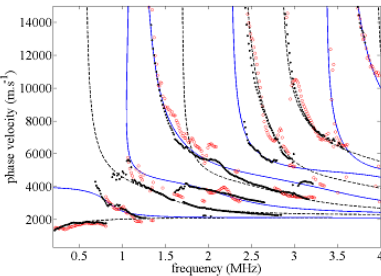
A technique, taking benefit of using both multiple emitters and multiple receivers, is proposed. The guided mode phase velocities are obtained using a projection in the singular vectors basis, obtained by the singular values decomposition of the transmission matrix between the two arrays at different frequencies.

Results

First experiments, carried out on different metallic plates are shown. Experimental velocities are in good agreement with Lamb waves theoretical values. Figure 1 shows the experimental guided modes phase velocities for a 2 mm thick copper plate measured with a 8-emitter and 14-receiver array. The theoretical Lamb wave velocities (lines) are compared with the experimental velocities obtained by the spatial-temporal Fourier Transform, (circle) and by the transfer matrix analysis (dot).

Discussion and Conclusions

The transfer matrix analysis method shows a real improvement compared the spatio-temporal Fourier Transform. These results allow a good evaluation of the thickness and the transverse and longitudinal bulk waves velocities. Further applications concerning evaluation of elastic properties of cortical bone are finally mentioned.



3J-4

3:15 PM **Dispersion of longitudinal wave velocity in swine cortical bone**

Takaaki Koizumi¹, Kazufumi Yamamoto², Tomohiro Nakatsuji¹, Mami Matsukawa¹; ¹Doshisha University, Kyotanabe, Kyoto, Japan, ²Hamamatsu University School of Medicine, Hamamatsu, Shizuoka, Japan

Background, Motivation and Objective

It is known that the apparent phase velocity of longitudinal wave in bone often shows negative frequency dispersion, owing to the degree of superposition of two waves. In case of bovine cortical bones, we reported the negative velocity dispersion of longitudinal wave which propagated the two layered structure [1]. In this study, we have investigated the frequency dispersion of wave velocity in the swine cortical bone, which has interesting two layered structure in the mid-shaft of femur.

Statement of Contribution/Methods

Three ring-shape cortical bone specimens were obtained from the swine femur with diaphysis length of 100 mm. We measured longitudinal wave propagating along the bone axis at 8 different positions of each specimen. Measurements were performed using a polyvinylidene fluoride (PVDF) transmitter and receiver. A single sinusoidal signal at 10 MHz was applied to the transmitter. The transmitted longitudinal wave propagated through NSS (Normal Saline Solution), sample, and NSS at temperature of 25.0 degrees C. Frequency dispersion of velocity was estimated from the phase spectra of obtained waves. The optical microscope observation showed that the ring bone specimens have two concentric layered structure, Haversian (inside) and plexiform (outside).

Results

The frequency dispersions of longitudinal wave velocities were almost positive. At frequencies from 5.5 to 6.5 MHz, the velocity increases were in the range from 3 to 17 m/s. However, the negative dispersions were found at a few measurement points. The figure shows an example of the negative velocity dispersion obtained at the posterior - medial area of a cortical ring specimen. The specimen was 15 mm distal part from the middle of the shaft. In this area, observed waveform showed the superposition of two longitudinal waves.

Discussion and Conclusions

The frequency dispersion of velocity in the swine cortical bone was investigated. In a few cases, we found longitudinal wave separation and the negative frequency dispersion of velocity. The mechanism of this apparent dispersion seems to result from the two layered structure, as pointed in the bovine cortical bone studies.

[1]G. Haiat et al., "Ultrasonic velocity dispersion in bovine cortical bone: An experimental study" J. Acoust. Soc. Am. 124 (3), 2008.9.

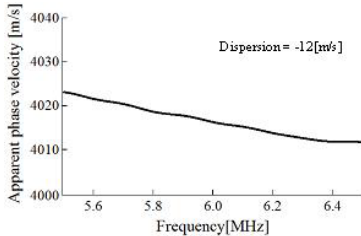


Fig. Negative dispersion of wave velocity.

3J-5

3:30 PM Diagnostically significant parameters of acoustic wave propagation along the tibia for osteoporosis assessment

Vladimir Egorov¹, Alexey Tatatrinov¹, Armen Sarvazyan¹; ¹Artann Laboratories, USA

Background, Motivation and Objective

A clinical validation study of Bone UltraSonic Scanner (BUSS), an axial transmission ultrasonometer developed by Artann Laboratories, demonstrated its sensitivity to early stages of osteoporosis development [Sarvazyan et al. Ultrasonics 49(3), 331-337, 2009]. Assessment of long bone conditions by BUSS is based on evaluating relative changes of the axial profiles of propagation parameters of bulk and guided acoustic waves generated in a wide frequency range. In this paper, we present results of further analysis of clinical data to rank diagnostically relevant parameters of acoustic wave propagation along tibia for osteoporosis assessment.

Statement of Contribution/Methods

A total of 134 patients enrolled in the clinical study were divided into six groups from normal to advanced osteoporosis according to their dual-energy X-ray absorptiometry (DXA) hip t-score. The 2-D waveform profiles at 0.1 MHz and 1 MHz were obtained by scanning 15 cm along the proximal tibia. An assessment of the statistical significance of each parameter for osteoporosis detection was completed with the aid of the statistical toolbox in MATLAB.

Results

Based on wavelet analysis, we derived 14 parameters characterizing propagation of bulk and guided acoustic waves along the tibia. For each parameter we analyzed its diagnostic significance with the use of one-way Analysis of Variance (ANOVA) testing a null hypothesis that there is no difference between normal and osteoporosis

conditions. If calculated p-value was below 0.05, it was considered as an indication that this parameter has a potential to be used for osteoporosis detection. We found 7 parameters satisfying this condition ($p < 0.05$). Applying principal component analysis to the group of parameters and taking into account the results of ANOVA tests we ranked the parameters according their statistical significance for osteoporosis detection. The first three most significant parameters are 1) guided wave "power" calculated as an integral of the modulus of complex Gaussian wavelet transform at 100 kHz; 2) shift of the frequency spectrum maximum for the guided wave pulse; 3) longitudinal wave "power" calculated as an integral of the modulus of complex Gaussian wavelet transform at 1 MHz.

Discussion and Conclusions

As a result of clinical data analysis, most informative acoustic parameters characterizing bone health are defined and the algorithms for evaluating these parameters are developed. The proposed set of acoustic parameters can be used for implementation of statistical classifier for osteoporosis detection to further improve BUSS diagnostic accuracy in osteoporosis detection at an early stage of development.

This work is supported by the National Institute of Health (USA), grant G017400.

3J-6

3:45 PM Influence of geometry on circumferential waves transmitted at the femoral neck

Julien Grondin¹, Quentin Grimal¹, Klaus Engelke², Pascal Laugier¹; ¹Laboratoire d'Imagerie Paramétrique, Université Pierre et Marie Curie-Paris 6; CNRS, LIP UMR 7623, Paris, France, ²Institute of Medical Physics, University of Erlangen-Nürnberg, Erlangen, Germany

Background, Motivation and Objective

Quantitative ultrasound (QUS) techniques are now widely accepted to assess bone quality and to evaluate fracture risk. QUS is currently limited to measurements of peripheral sites. Better risk assessment could be obtained if sites at highest risk of fracture such as hip could be directly measured. Recent studies have shown that transmission of ultrasound through femoral neck results in the transmission of multiple modes of propagation and in complex rf traces. We have shown previously that early signal arrivals correspond to circumferential waves guided by the cortical shell propagating at a much higher speed than waves transmitted directly through cancellous bone. We hypothesized that these guided waves convey relevant information on bone geometrical and material characteristics and thus have the potential to improve fracture risk prediction. Our objective is to investigate the relationships between the speed of guided circumferential waves and geometrical features of the neck that are known to be strong determinants of femoral strength.

Statement of Contribution/Methods

Eleven human femurs from elderly females (> 65 years) were included in the study. Proximal femur volumes reconstructed from X-Ray computed tomography (CT) acquisitions were segmented and the automatic calculation of an anatomical Neck Coordinate System (NCS) was performed using MIAF – Femur (Medical Image Analysis Framework – Femur option). Five equally spaced cross-sections were extracted from the 3-D cortical shell of femoral neck using the NCS. Two-dimensional (2-D) finite-difference time-domain simulations of the transmission (antero-posterior direction) of an ultrasonic plane wave through each femoral neck cross-section were performed and Time-of-Flight (TOF) of the guided wave was ascertained. Geometrical parameters including cross-sectional area (CSA), minimum moment of inertia (I_{min}) and section modulus (SM) were computed from the cortical compartment of femoral neck cross-section images.

Results

Significant statistical relationships were found between geometrical parameters and TOF. The position of the cross-section along the neck affected significantly the relationships. The highest correlation was obtained for I_{min} in the region between proximal and mid-femoral neck ($R^2 = 0.82$; $p = 10^{-4}$) whereas section modulus ($R^2 = 0.55$; $p < 0.01$) and cross-sectional area ($R^2 = 0.62$; $p < 0.005$) were best correlated with TOF in the mid-femoral neck.

Discussion and Conclusions

The significant correlations observed in this study suggest that circumferential waves at femoral neck convey relevant information on bone strength. Although cylindrical focalisation with appropriate parameters can be used experimentally to approach the two-dimensional configuration of this simulation study, the complex 3-D geometry of the femoral neck may affect these results. Future 3-D simulation studies are required to take into account the realistic three-dimensional shape of the neck.

4J. Ultrasound in Air

Tarragona

Wednesday, September 23, 2009, 2:30 pm - 4:00 pm

Chair: **Paul Wilcox**
University of Bristol

4J-1

2:30 PM **Simultaneous determination of physical and acoustical properties of a homogeneous plate in air**

Abdelhak EL MOUHTADI¹, Jean DUCLOS¹, Hugues DUFLO¹; ¹Groupe Ondes Acoustiques, Laboratoire Ondes et Milieux Complexes, FRE 3102 CNRS, Le Havre, France

Background, Motivation and Objective

Transmission of ultrasonic plane waves through an elastic plate is widely employed for studying acoustic properties of materials. The purpose of this work is to present an experimental technique for investigating the transmission coefficient through a solid plate using air-coupled transducers. This technique enables to determine simultaneously the velocity and the attenuation of ultrasonic waves, the density and the thickness of the sample.

This study is concerned with plane longitudinal waves that are normally incident upon a parallel face plate placed in air. A variety of materials has been studied such as Polyethylene, Plexiglas and carbon/epoxy composite. The comparison between theory and experiment of the transmission coefficient of each plate over the frequency bandwidth covered by the measurements has been exploited to estimate the four acoustic properties of the sample.

Statement of Contribution/Methods

The experimental system consists of two air-coupled transducers having 1 MHz central frequency and 25 mm diameters. Two independent signals are being exploited: the signal transmitted only through air, in the absence of the plate, called the reference signal and the first signal transmitted through the sample which has been placed between the transducers. The distance between transducers was $d = 6$ cm. The plate was carefully aligned parallel to the surface of the transducers by maximizing the amplitude of the reflected pulse and echoes. For each measurement, the transmitter is excited by a chirp signal; the signal from the receiving transducer is acquired by a digital oscilloscope, averaged to improve the signal-to-noise ratio and transferred to a computer for further processing. The FFT transforms of these signals allow the calculation of the complex transmission coefficient as a function of frequency.

Results

The measured transmission coefficient is compared with the theoretically predicted one which takes into account the substitution of the plate thickness by an equal layer of air. The theoretical relation contains six independent parameters and seven physical properties characterizing both the sample and air. The identification of the six parameters is carried out using the complex transmission coefficient. Then, assuming the wave velocity in air is known, we deduce the four parameters of the plate (thickness, longitudinal velocity, attenuation coefficient and density) as well as the density and the attenuation coefficient of air.

Discussion and Conclusions

The temperature and pressure instabilities were found to have a crucial effect on the transmission measurements. Therefore, all measurements were made in a constant temperature and pressure environment and an additional measurement of wave velocity in air was performed. The accuracy (10^{-3} for thickness and velocity) and reliability of these results justify the further study of inhomogeneous materials.

Wednesday
Oral

4J-2

2:45 PM **Determination of Plant Water Status using Air-Coupled Ultrasounds**

Tomás E Gomez¹, Domingo Sancho², Eustaquio Gil-Pelegrin²; ¹CSIC, Spain, ²Unidad de Recursos Forestales, Spain

Background, Motivation and Objective

Plant water status is a necessary indicator of a plant in order to know how to manage a forest or an agricultural field. It is especially important in arid and semi-arid climates where plant production depends mainly in an optimum water supply. Knowing the plant water status is easier to avoid stress due to drought and, therefore, to have a better quality of plant products; it is also useful in a lot of physiology, ecology and biology studies which involves water relations between the vegetation and the environment.

In plant physiology and agriculture, the pressure bomb technique pioneered by Sholander et al. (1965) to measure plant water potential ($\bar{\psi}$) or the calculation of the relative water content (RWC) by Barrs (1968) are widely accepted references to determine the plant water status. As a result of the combination of these two measurements appeared the curves pressure against volume (Tyree and Hammel, 1972) which among other parameters, are able to estimate the cell turgor pressure, critical water point in plant life. $\bar{\psi}$ and RWC are, therefore, good parameters to estimate plant water status but, however, as these methods are destructive, these measurements imply destruction of part of the plant and don't permit to monitor a plant using the same part more than one time. This is the main reason why recently (since 2006) many studies have been focused in non-destructive or non-invasive techniques.

The objective of this work is to investigate the possibility of using a non-destructive, non-contact and air-coupled ultrasonic technique to assess water content, water potential and turgor pressure of mature leaves from different branches of a single grown-up stand of poplar (*Populus x euroamericana*).

Statement of Contribution/Methods

Wide-band ultrasonic pulses in the frequency range 0.3-1.0 MHz were transmitted through the leaves and the phase and the magnitude of the transmission coefficient versus frequency were obtained. These spectra reveal a clear resonance which corresponds to the first thickness resonance of the leaves. From the analysis of this resonance we obtained: ultrasonic velocity and attenuation coefficient and thickness and density of the leaves. Water potential (using conventional methods) and relative water content (weighing the leaves) were measured simultaneously.

Results

A close relationship between ultrasonic parameters and water content and water potential measurements is obtained: as the leaves become drier, the attenuation coefficient increases and the frequency location of the thickness resonance goes down; this is related to a decrease of the velocity, produced by a decrease of the leaves elastic modulus.

Discussion and Conclusions

This suggests a sound relationship between the ultrasonic parameters and the loss of turgor pressure in the leaves which is a very important parameter. In conclusion, the use of a wide band air-coupled ultrasonic technique is powerful non-destructive and rapid technique to study plant water content.

4J-3

3:00 PM **Highly Anisotropic Beam Patterns for a Pot-like Ultrasonic Sensor with Penetrating Slots Configuration**

Chih-Chiang Cheng¹, Chia-Yu Lin¹, Jen-Huan Ho², Yu-Chi Chen¹, Wen-Jong Wu², Kuang-Chong Wu^{1,3}, Chih-Kung Lee^{1,4}; ¹Institute of Applied Mechanics, National Taiwan University, Taipei, Taiwan, Taiwan, ²Engineering Science & Ocean Engineering, National Taiwan University, Taipei, Taiwan, Taiwan, ³National Applied Research Laboratories (NARL), Taipei, Taiwan, Taiwan, ⁴Industrial Technology Research Institute (ITRI), Hsinchu, Taiwan, Taiwan

Background, Motivation and Objective

Obstacle detection by using ultrasonic proximity sensors has been adopted in automotive industry so as to improve safeties. A pot-like aluminum structure with a piezoelectric ceramic stuck on the inner bottom vibrating plate is usually used to generate and to receive ultrasound in this type of proximity sensor. In practice, the proximity sensor needs an anisotropic beam, whose beam-width is wide in the horizontal direction and narrow in the vertical direction, since ground is not perceived as a real obstacle in vehicle applications [1]. In this application, the design degree of freedom was typically constrained by a car designer. For the visual effect of a car body, a flat radiating surface was required and the size of the ultrasonic sensor was limited down to 15 mm in diameter.

Wednesday
Oral

Statement of Contribution/Methods

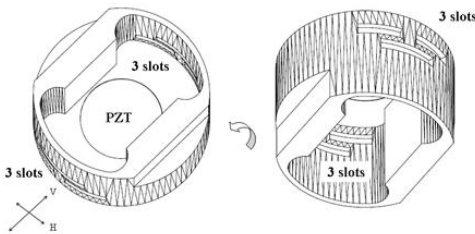
To obtain the narrower beam width in the vertical direction, raising its operating frequency has been an effective method adopted even though it also narrows the beam width in the horizontal direction and it results in higher sound absorption in air [2]-[3]. To circumvent the need to raise the frequency, a new configuration of a pot-like ultrasonic sensor with highly anisotropic beam pattern under previously defined constraints was developed in this research. This configuration (Fig. 1) was characterized by a pair of 3 penetrating slots on the opposite side of its cylindrical shell in the vertical direction. In this study, the frequency of the ultrasonic sensor was fixed at 48 kHz, which is identical to the frequency of today's parking ultrasonic sensor, and a finite element simulation was introduced in this configuration design. In addition, the far-field pressure beam patterns were measured using a standard microphone in an anechoic room.

Results

Finally, we identified that the isotropy of this type ultrasonic sensor, which is defined as an H/V ratio, exceeds 3.

Discussion and Conclusions

We concluded that the position of these penetrating slots referred to the bottom radiating surface would affect the source level and sensitivity of the ultrasonic sensor. Both the design methodologies and the experimental verifications will be detailed in this paper.



4J-4

3:15 PM Adaptable Emission Airborne Spiking Sonar

Fernando J. Alvarez¹, Roman Kuc², Teodoro Aguilera¹; ¹Electrical Engineering, Electronics and Automatics, University of Extremadura, Badajoz, Badajoz, Spain, ²Electrical Engineering, Yale University, New Haven, Connecticut, USA

Background, Motivation and Objective

The current trend in the field of airborne sonar is the development of biologically inspired systems capable to extract more information than just the Time-Of-Flight of the first detected echo. These systems are called biomimetic not only because they mimic the sensory structure of the animal with typically one emitter (mouth) and two receivers (ears), but also because the signal processing they perform is inspired by processes observed in nature.

A clear example of this type of system is the PAP-sonar developed by the intelligent sensors laboratory at Yale University, that uses a conventional ranging module and controls it in a nonstandard way to generate a sequence of spikes (Pseudo-Action Potentials) whose temporal density is proportional to the strength of the detected echo. This work proposes an improved version of this system that is capable to adapt the length of the emission to changing features of the environment, thus obtaining richest information from the objects surrounding the sensor.

Statement of Contribution/Methods

The new PAP-sonar incorporates a microcontroller unit (MCU) that not only controls the reception stage of the driving board to generate spikes, but also adapts the duration of the emission to the strength of the last received echo. This is made by generating a 50 kHz TTL signal to drive the base of the transistor included in the emission stage of the 6500 ranging module, base that has been previously isolated from the signal generator included in this module. Once the echo has been received and transformed into a sequence of spikes, the MCU counts them and selects the number of 50 kHz cycles to be emitted in the next firing.

Results

In the original PAP sonar, the emission stage included in the 6500 ranging module was used to generate an unchangeable ultrasonic pulse of 16 cycles at 49.4 kHz. Nevertheless, there are occasions where it would be desirable to shorten this pulse and increase the system resolution or conversely, to prolong it and increase the system sensitivity. This can be easily done by the new system thanks to the modifications carried out in the ranging module and the operation of the microcontroller.

New and more informative scans of complex reflectors such as foliage are obtained by the new sensor, increasing the capability of this system to perform identification tasks.

Discussion and Conclusions

Continuing with the philosophy of the previous PAP sonars, the main contribution of the system presented in this work is its capability to extract rich information from the environment while still using commercial electronic modules.

This capability has been notably enhanced through the adaptable emission feature, and still the new sensor can be easily assembled and at a very low cost, making it accessible to a wide community of researchers.

Moreover, the real-time adaptability provided by the MCU makes the system attractive for navigation applications, since the duration of every new emission can be selected depending on the spikes count of the last echoes.

4J-5

3:30 PM **Experimental Investigations of Ultrasonic Levitation in A Machine Tool Spindle System**

Su Zhao¹, Joerg Wallaschek^{1,1}*Institute for Dynamics and Vibration Research, Hannover, Germany*

Background, Motivation and Objective

Squeeze film ultrasonic levitation (also called near field acoustic levitation) can be observed when a planar object is brought close to an oscillating surface which vibrates at a high frequency (often in the ultrasonic range). The non-zero mean pressure in the air gap levitates the object above the oscillating surface at a distance of a few to a few tens microns. This technique has already been applied in several non-contact linear and rotational bearings. However all the previous prototypes had very limited load capacity and thus could not be applied in precision machine tools. The present study is devoted to develop an improved design of a squeeze film bearing which provides sufficient load capacity at reasonable power consumption.

Statement of Contribution/Methods

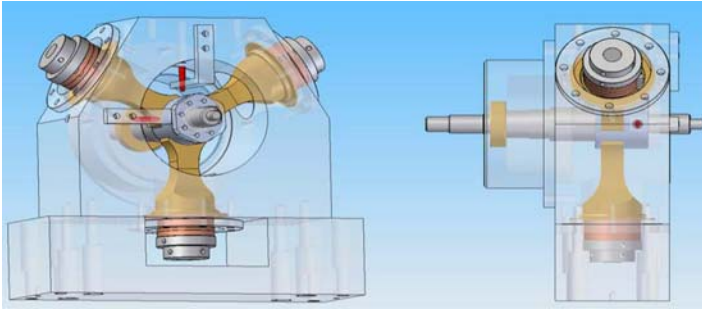
The proposed bearing uses in-air squeeze film ultrasonic levitation and consists of three high power piezoelectric transducers mounted on a housing (as shown in the figure). The concave radiation surfaces of the three transducers form the journal bearing. When the transducers are driven at their first longitudinal resonance, the ultrasonic levitation effect between the radiation surfaces and the spindle generates a repelling force in the air gap which suspends the spindle and automatically keeps the spindle at a stable equilibrium position.

Results

A mathematical model of the system was developed to predict the load capacity. The computational results show good agreement with experiment results. The proposed bearing system provides steady, non-contact suspension to the spindle. The actual position of the spindle center is monitored precisely during operation by the two inductive sensors, which allows a detailed investigation of the system's behavior. A load capacity of 70000 N/m² (i.e. 7 N/cm²) was achieved at a frequency of 20 kHz with an input power of 80 W.

Discussion and Conclusions

The load capacity of the presented bearing system is more than five times higher than that of previous prototypes reported in the literature. Its performance is already comparable to common air bearings with similar size. The stiffness and damping of the bearing will be further improved by implementing a PD controller which controls the position of the spindle by actively adjusting the individual input power of each transducer. The bearing will then also be able to compensate static loads and disturbances.



4J-6

3:45 PM Investigation of SAW Atomization

Aisha Qi¹, James Friend¹, Leslie Yeo¹; ¹*Department of Mechanical and Aerospace Engineering, Monash University, Melbourne, VIC, Australia*

Background, Motivation and Objective

Atomization is a technology that converts a bulk parent drop to a spray or mist, which is a collection of droplets with micron or submicron diameters. Unlike conventional atomization techniques, surface acoustic wave (SAW) atomization is driven at much higher frequencies (5-500 MHz). The SAW traverses the piezoelectric substrate surface as a transverse-axial elliptical (Rayleigh wave). It induces violent vibration of the drop, and consequently promotes the destabilization and breakup on the capillary waves.

It is a commonly used assumption that the capillary frequency is half of the SAW excitation frequency. However, it has been found that the capillary frequency is either resulted from the balance between the capillary force and the viscous stress, or the competition between the capillary force and the inertial force, depending on the characteristic length scale of a liquid drop or film. Therefore, the capillary frequency can never exceed 1 MHz, even though the SAW excitation is above 10 MHz. The motivation of this project is to investigate and analyze the capillary destabilization and breakup process.

Statement of Contribution/Methods

In order to determine the resonant frequency at which the capillary wave breaks up, we measured the frequencies on the liquid free surface by using the Laser Doppler Vibrometry (LDV). In addition, the breakup process on the liquid free surface is captured by the high speed camera and microscope. The time scale of the capillary breaking up matches the capillary frequency obtained by the LDV. Moreover, we used the laser diffraction based Spraytec technology to obtain the size distributions of atomized octanol aerosol and water aerosol.

Results

The LDV result that records the frequencies obtains a notable peak appearing at 10 kHz. It clearly shows that the capillary waves are excited at 10 kHz order frequency, when the liquid is stimulated by a 20 MHz SAW excitation. From the images captured by high speed camera, the time it takes for the liquid thread to drain and pinch-off, typically 10 ms, also indicates the capillary breaks up at 10 kHz frequency.

Regarding the aerosol size distribution, we obtained the mean diameter of octanol aerosol and water aerosol is in the range of 1-3 μm and 8-10 μm , respectively.

Discussion and Conclusions

The experimental results suggest that the capillary waves that are excited at the free surface of the drop always vibrate at the capillary-viscous resonant frequency, even if the frequency at which the drop is excited, in this case the SAW frequency, is several decades larger. The diameter of the droplet is close to the capillary wavelength which is in the order of 1-10 μm according to the viscous-capillary damping. This is contrary to a common assumption that has been made which has typically led to erroneous predictions in the droplet size in prior SAW atomization studies.

5J. Micromachined Ultrasonic Transducers

Pergamo

Wednesday, September 23, 2009, 2:30 pm - 4:00 pm

Chair: **Omer Oralkan**
Stanford University

5J-1

2:30 PM **A Wafer Bonded Capacitive Micromachined Underwater Transducer**

Selim Olcum¹, Muhammed Senlik¹, Kagan Oguz¹, Ayhan Bozkurt², Abdullah Atalar¹, Hayrettin Koymen^{1,1}^{Electrical and Electronics Engineering Dept., Bilkent University, Ankara, Turkey, ²Faculty of Engineering and Natural Sciences, Sabanci University, Istanbul, Turkey}

Background, Motivation and Objective

Large bandwidth and ease of electronic integration make capacitive micromachined transducers (CMUT) excellent candidates for underwater transducers. In this work we have fabricated and tested CMUTs in 10–50 KHz range.

Statement of Contribution/Methods

CMUT membranes with 1 cm diameter and 380 μm of thickness are fabricated. Unlike conventional methods, we have utilized the whole silicon wafer as the membrane and used anodic wafer bonding technology to bond it to a thick insulating glass substrate. A double side polished, 380 μm thick, highly doped silicon wafer is used as the membrane. First the vacuum cavity, which is 5 μm in height, is etched using an RIE reactor. A thermal wet oxidation reactor is used in order to create a 0.5 μm thick silicon oxide on the surface of the wafer for passivation. The silicon oxide at the back side of the wafer is etched using the RIE reactor and a 0.25 μm thick aluminum is deposited by RF sputtering in order to make an ohmic contact to the silicon wafer.

Having completed the membrane side, the substrate side is fabricated on a 3.2 mm thick 4 inches Borofloat Glass wafer. The substrate electrode, which is 100 nm of gold, is buried on the glass wafer. As a passivation layer and also for smoothing the surface for possible steps due to the electrode layer, 0.2 μm of silicon oxide is deposited using a PECVD reactor. The completed membrane and substrate wafers are anodically bonded and sealed under 500V of potential in 450°C and 1 mTorr of vacuum.

Results

The transducers are tested in air and underwater in our open water testing facility in Bilkent University Lake. The collapse voltage of the devices is measured to be 500V under atmospheric pressure. The resonance frequency of the transducers is measured 45 KHz and 25 KHz in air and underwater, respectively. The beam patterns of the immersed membranes are measured both as single CMUT and as single element array. The size of the array is limited with the silicon wafer size, which is in this work 3 inches.

Discussion and Conclusions

The design and fabrication process contain several trade-offs. Because of the ambient pressure under water, the membranes can accommodate a certain depth range. In this work this range has chosen to be 0–10 meters. The collapse voltage of the transducers is critical in that sense. It should be high enough to maintain the deeper end of the operational depth. On the other hand, high voltages require a thicker insulating silicon oxide layer and above 1 μm the bonding becomes impossible. Therefore, the operational depth range is limited by the anodic bonding process. Anodic bonding requires high voltages to be applied during bonding. The membranes should not collapse because of the applied bonding voltage. This requirement sets a lower limit on the collapse voltage of the transducers. Another critical parameter, the isolation layer thickness, should be high enough to withstand the collapse voltage and thin enough for the anodic bond to be successful. In this work, the silicon oxide isolation thickness is 0.7 μm .

5J-2**2:45 PM Challenges with acoustic backing of CMUT arrays on silicon with integrated electronics**

Sigrid Berg¹, Arne Rønnekleiv^{1,†} *Department of electronics and telecommunications, Norwegian University of Science and Technology (NTNU), Trondheim, Norway*

Background, Motivation and Objective

In capacitive micromachined ultrasonic transducers (CMUT) an acoustic backing is needed to damp the acoustic waves that penetrate into the silicon wafer. If not damped, these waves may reflect at the bottom of the silicon wafer and disturb the transducer wave front. Several aspects of acoustic backing of CMUT arrays will be discussed using a model for the wave propagation in the backing as introduced in [1].

Statement of Contribution/Methods

The discussion in [1] focuses on a structure where one or possibly several silicon layers are bonded together to form a stack of silicon layers which is then backed with a damping material such as tungsten filled epoxy. Here we will discuss the acoustic properties of some realistic bonding methods for such structures. Candidate methods are anisotropic conducting glue and solid liquid interdiffusion, SLID.

We will further look at the possibility of using two damping layers in the stack, one close to the top surface and the other at the bottom of the stack. Through the upper damping layer we will need vias for electrical signals to and from all elements in the array. We will look at the effects of making the upper damping layer of a tungsten filled epoxy with a sufficiently low tungsten content that it will not be conducting. This probably means a volume fraction of tungsten well below 40 %. Acoustic properties of the vias will be discussed.

Results

Analysis shows that to give good acoustic contact between layers in the stack the bond should cover a large fraction of the total area, and the bond layer should be thin or have high acoustic impedance.

Analysis also shows that to use an upper damping layer from non-conducting tungsten epoxy should provide sufficient damping of the surface wave at the water silicon interface.

Introducing a rough bottom surface in the backing may help scatter incoming waves into waves with high transverse k-vectors. Since silicon has rather high acoustic velocities, these waves do not easily propagate back to the top surface. This is due to effects similar to total reflection between backing and silicon. This will be quantified in the paper.

Discussion and Conclusions

The available bonding techniques for stacks of silicon wafers with interconnects and damping layers are not well established, and hence the exact effects of thicknesses, material parameters and area coverage can not be determined. The results here however indicate that it should be possible to integrate a substantial amount of electronics directly under the CMUT array, and still obtain reasonable acoustic properties for the array. The tasks to be done by the electronics are not discussed here, and also omitted are the problems that might arise due to the power consumption of the electronics.

[1] S. Berg and A. Rønnekleiv, "Backing requirements for CMUT arrays on silicon", 2005 IEEE Ultrasonics Symposium Proceedings, pp 1952 – 1955.

5J-3**3:00 PM 2-D CMUT Wafer Bonded Imaging Arrays with a Row-Column Addressing Scheme**

Andrew Logan¹, John Yeow¹; *Systems Design Engineering, University of Waterloo, Waterloo, Ontario, Canada*

Background, Motivation and Objective

Capacitive micromachined ultrasonic transducers (CMUTs) are a promising alternative to conventional piezoelectric transducers for medical imaging and diagnostics. They have demonstrated image quality on par with commercial piezoelectric transducers. The use of semiconductor fabrication technologies to manufacture ultrasonic imaging arrays permits the creation of high-frequency fully populated 2-D arrays capable of 3-D imaging without grating lobes.

Statement of Contribution/Methods

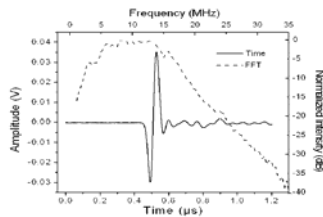
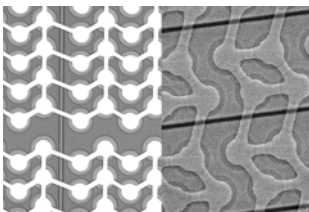
We report the fabrication and testing of 2-D CMUT arrays fabricated using a wafer bonding process whereby the membrane and the insulation layer are both silicon nitride. A row-column (RC) scheme is used to address individual elements. The use of an RC addressing scheme in conjunction with wafer bonding fabrication has the potential to greatly simplify the fabrication of 3-D imaging capable arrays by both minimizing the number of electrical connections required and keeping processing simple.

Results

A 32x32 element array with a center frequency of 15 MHz in air and 10 MHz in immersion and a 32x32 element array with a center frequency of 28 MHz in air are discussed. Figure 1 is an optical image of the 15 MHz device (left) and an SEM image of the 28 MHz device (right). Figure 2 shows the transmission pulse from one column of the 15 MHz device and its Fourier transform. The device is biased at 75 V and a voltage spike is applied using a commercial ultrasonic pulser/receiver. Signal is detected using a hydrophone 10 mm away. The device has an uncorrected -3 dB bandwidth of 98%.

Discussion and Conclusions

The devices discussed here are suitable for phased array imaging. The element dimensions are 150 μm x 150 μm and 45 μm x 45 μm for the 15 MHz and 28 MHz (in air) devices respectively. The devices will be used for biological imaging purposes.



5J-4

3:15 PM Evaluation of CMUT Annular Arrays for Side-looking IVUS

Alper SISMAN¹, Jaime Zahorian², Gokce Gurun², Mustafa KARAMAN¹, Mujdat Balantekin², F. Levent Degertekin², Paul Hasler², ¹Isik University, Electronics Eng. Dep., Turkey; ²Georgia Institute of Technology, USA

Background, Motivation and Objective

Side-looking (SL) IVUS probes are extensively used for management of cardiovascular diseases. Probes with single rotating piezoelectric transducer have simple front-end, but have fixed focused operation, and suffers from motion artifacts. Solid state SL-IVUS imaging probes use piezoelectric transducer arrays and electronic beamforming, and hence do not suffer from motion artifacts. Synthetic phased array processing of signals detected with small-sized array elements limits the SNR achievable with these probes. In this study, we explore, through experiments and simulations, a SL-IVUS probe architecture employing rotating phased annular CMUT array with integrated front-end microelectronic circuits for both low-cost, low-profile, and advanced IVUS probes.

Statement of Contribution/Methods

We designed and fabricated 840-μm diameter, 8 element CMUT annular arrays operating around 50-MHz using a low temperature process. The elements are discretized with 18-μm wide rings and arranged to have roughly equal area. We characterized the imaging performance of these arrays using wire target phantoms in water tank and verified our simulation methods for fixed and dynamic receive focusing arrays. We also produced simulated PSFs of rotating probe employing a fixed-focus transducer (at # 2) and a solid-state array probe with a 64-element ring array. We compared the simulated PSFs of the CMUT annular array with these two existing probe architectures.

Results

We performed imaging experiments with the CMUT annular arrays in water. The measured axial/ lateral resolution provided by 50-MHz arrays is 35μm/120μm, respectively for a target at f# of 3.8 using dynamic receive focusing. The array with parylene coating shows approximately 40% fractional bandwidth measured in water limited by the cross talk as predicted by FEA. The simulation results show that the proposed annular array produces better beam

quality in different depths than the fixed-focus single transducer and solid-state linear array. For example the beam widths at $f/3$ of the simulated PSFs of these three schemes are 4.4, 4.9 and 8.7 degrees respectively.

Discussion and Conclusions

CMUT based high frequency annular arrays with dynamic receive focusing provide significant improvement over single element fixed focus transducers as well as existing solid state SL-IVUS arrays. The crosstalk in CMUT arrays needs to be explored further to improve the axial resolution.

5J-5

3:30 PM An Area Hydrophone Based on CMUT Arrays

Paul Cristman^{1,2}, Omer Oralkan^{1,2}, Xuefeng Zhuang^{1,2}, Te-Jen Ma^{2,3}, Srikant Vaithilingam^{1,2}, Tom Carver², B. (Pierre) T. Khuri-Yakub^{1,2}, ¹Electrical Engineering, Stanford University, USA, ²E. L. Ginzton Lab, USA, ³Mechanical Engineering, Stanford University, USA

Background, Motivation and Objective

As the uses of ultrasonic transducers have increased so has the need to measure and characterize their pressure fields. Currently available hydrophones are limited by long scan times, and multiple source pulses to measure large area fields. Using a capacitive micro-machined ultrasonic transducer (CMUT) array and associated electronics we are able to improve on these limitations. The CMUT inherently allows for a tunable sensitivity by changing DC bias. Motivated by the need to improve the characterization of megasonic cleaners used in semiconductor processing we were able to implement such an area hydrophone.

Statement of Contribution/Methods

In the first implementation an existing 2D CMUT array originally developed for medical imaging was used. The array was flip chip bonded to electronics. The measurements were preformed in DI water after encapsulation of the CMUT array and electronics.

Results

With this array we successfully measured an ultrasonic pressure field distribution over a 4 mm x 4 mm area with a 250 x 250 micron pitch and no mechanical scanning. The array has sensitivities ranging from 1.04 to 76 micro-V/Pa depending on DC bias (1 to 30 V). This array had a minimum detectable pressure of 1.8 mPa/root(Hz). The maximum detectable pressure for the CMUT array used was 347 kPa peak. The maximum detectable pressure is limited by the gain and the maximum output voltage swing of the existing electronics currently designed for imaging. The minimum and maximum pressures are both functions of DC bias and both quantities span 2 orders of magnitude. The pulse echo bandwidth for this array was only 3.5 MHz. However, pulse echo is not the best measure of the array bandwidth as a hydrophone. The bandwidth can be easily improved in future designs.

Discussion and Conclusions

Operating the CMUT array in receive only mode allows for greater flexibility in front end electronics. The packaging flexibility of the CMUT array will allow the hydrophone to correctly match the boundary conditions in the desired application. This is critical in the characterization of megasonic cleaners where the presence of the wafer can significantly impact the pressure field. Several such arrays could be positioned on a silicon wafer to measure the pressure field across the entire wafer with nearly identical boundary conditions as the real wafers. By adjusting the DC bias of the CMUT the sensitivity of the hydrophone array can be optimized for the pressure range of interest. The CMUT array has excellent sensitivity across a wide range of pressure and frequency. The CMUT makes a perfect candidate for measuring area pressure distributions. The number of elements, element size, element frequency, and element sensitivity can all be optimized for high sensitivity applications. Also, the array can be optimized for large bandwidths and large pressure applications as well. While only a proof of concept the initial results for CMUT array hydrophones are promising.

Work supported by Intel Corporation Santa Clara, CA USA 95054

3:45 PM **A Flexible Capacitive Micromachined Ultrasonic Transducer (CMUT) Array with Increased Effective Capacitance from Concave Bottom Electrodes for Ultrasonic Imaging Applications**

Ching-Hsiang Cheng¹, Chen Chao¹, Xiaomei Shi², Wallace W. F. Leung^{1,1} *Research Institute of Innovative Products and Technologies, The Hong Kong Polytechnic University, Hung Hom, Kowloon, Hong Kong,* ²*Department of Electronic and Information Engineering, The Hong Kong Polytechnic University, Hung Hom, Kowloon, Hong Kong*

Background, Motivation and Objective

A CMUT can transmit and receive ultrasound by vibrating its membrane like a drum. DC bias is applied to bring the membrane closer to the bottom electrode for increasing its sensitivity. However, most of the developed CMUTs have flat bottom electrode, which can not comply with the deflected membrane as a concave surface. Since the capacitance is inverse-proportional to the gap distance between the electrodes, this makes only the 25% central area more sensitive to the capacitance change and the other 75% of the area is considered as parasitic capacitance without coverage of the top electrode.

Statement of Contribution/Methods

Based on the theoretical analysis, when using concave bottom electrodes, the effective capacitance can increase 10 times comparing with using the flat bottom electrode. For CMUTs using flat bottom electrodes, the capacitance change reaches its maximum of 22% when the diameter of the top electrode is 84 μm. The maximum capacitance at collapsed mode can only reach 0.06 pF. For CMUTs using concave bottom electrodes, the capacitance change can increase up to 79% when enlarging the diameter of the top electrode up to 99.8 μm. The maximum capacitance at collapsed mode can reach up to 0.69 pF.

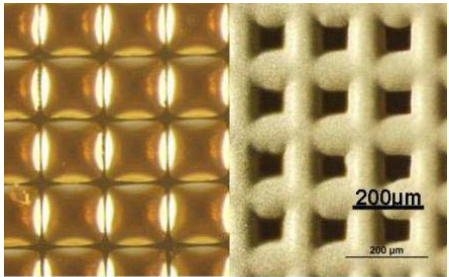
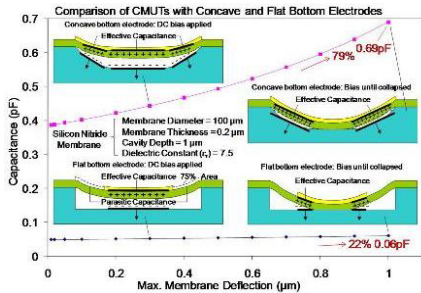
Results

The fabrication steps are reversed to have the membrane on the substrate bottom and then build the cavity and bottom electrode on the top. This allows us to form the concave bottom electrode on top of the reflowed photoresist in convex spherical shape using over-plating technique, which can not be achieved by the conventional bottom-up surface-micromachining technique.

Discussion and Conclusions

By using the concave bottom electrode to increase the effective area of the membrane, it can increase the effective capacitance to improve the fill factor, output pressure, bandwidth, and sensitivity of the transducer.

Wednesday
Oral



Photoresist Reflow Over-Plating

6J. RF MEMS

Baalbek

Wednesday, September 23, 2009, 2:30 pm - 4:00 pm

Chair: **Sunil Bhave**
Cornell University

6J-1

2:30 PM **RF MEMS : Focusing on the Next Step**

Takeo Oita¹; ¹Nihon Dempa Kogyo Co., Ltd., Tokyo, Tokyo, Japan

Background, Motivation and Objective

Radio frequency and mixed signal semiconductor technologies have been improving and play a big role in the rapidly growing market of wireless communication. Higher integration of CMOS technologies due to "More Moore"s Law is helping this success. In parallel, some of the RF micro device technologies have been very popular, especially for frequency selection such as Piezo-material devices by using MEMS technology.

On the other hand, there are many wireless services already in existence such as various kind of cellular standards, many private systems representing IEEE 802.11/15 WLAN, Bluetooth, and public mobile services, and also there are coming up new systems such as "Ultra Wide Band", and "Wireless Sensor Network". Since all these services have different carrier frequencies, channel bandwidth, and various kinds of modulation systems a single solution is not tenable. This led the industry toward the concept of the "Software Defined Radio". This has been discussed for many years, leading to a vision of a "Cognitive Radio". Expectation of a "Cognitive Radio" is that it can change its radio functions by swapping software instead of replacing hardware. It is clear that conventional A/D converters with high data rates and large dynamic range will not suffice. Thus, it has been said that RF MEMS is a strong contender as a complimentary technology, allowing "More Than Moore" to enable the ubiquitous connectivity.

Statement of Contribution/Methods

Discuss current status of the RF MEMS technology briefly including switches, LC, oscillators/filters using Piezo-materials, Silicon, and Metal, besides focusing on the next step of RF MEMS with the keyword of "Tunable", "Selectable" and "Combination".

Results

The focus for RF MEMS for the next step will be demonstration of "Antenna Switches", "Matching modules", "Front Ends", "Filter Banks", "Improving the resonator performances for the wireless application" and "Creating new functions for RF MEMS".

Discussion and Conclusions

The next step for RF MEMS is not only technology discussions, but also the international standardization for the RF MEMS industry and wireless communication products.

6J-2

3:00 PM **Super High Frequency Width Extensional Aluminum Nitride MEMS Resonators**

Kenneth Wojciechowski¹, Roy Olsson III¹, Melanie Tuck¹; ¹Sandia National Laboratories, USA

Background, Motivation and Objective

There has been recent progress in extending aluminum nitride (AlN) resonator frequencies to super high frequency (SHF) bands using electron beam lithography. We present SHF (up to 6.8 GHz) width extensional (WE) resonators that are patterned optically. In the past contour mode resonators have been anchored using quarter wave beams to minimize anchor loss. In this work we compare the performance of solidly anchored resonators to resonators anchored with quarter wave beams. Finally, it is assumed that as resonator area is scaled its insertion loss (IL) will decrease. However the shunt capacitance from the resonators input/output to ground causes their IL to decrease less than expected. We investigate this effect.

Statement of Contribution/Methods

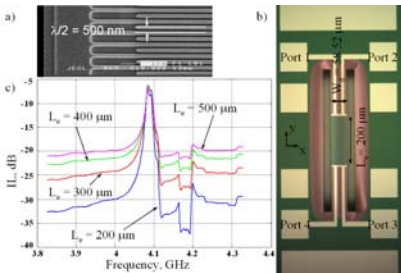
SHF resonators were fabricated with a simplified, 2 mask AIN process without a bottom electrode or dielectric. The simplified process yields better AIN performance and higher resonator sound velocity enabling the use of optical lithography. Figure 1a shows a SEM of optically patterned electrodes for a 10 GHz device. It was hypothesized that the acoustic wave (launched in the x-direction, Fig. 1b) is well confined and has minimal propagation in y-direction. Hence, anchoring loss should not change significantly between solidly anchored resonators and resonators anchored with beams. To test this hypothesis, resonators with beam anchors of the same size were fabricated. Also, a comparison was done varying resonator length (L_c) for a 4.1 GHz device to investigate area scaling.

Results

The beam and solidly anchored resonators had similar Q (400) but the beam anchored insertion losses were 4 dB higher. In fact, the solidly anchored resonators demonstrated 4 dB lower IL, two dB of which is due to wider metal routing. Increasing electrode area via L_c did very little to improve IL (Fig. 1c).

Discussion and Conclusions

SHF AIN resonators have been fabricated using optical lithography for the first time. Solidly anchored WE resonators were shown to be superior to beam anchored resonators of the same size and it was verified that simply scaling resonator area does not improve IL due to shunt capacitance. Resonators with an IL of 7.2 dB into 50 ohms at 4.1 and 6.8 GHz have been demonstrated. This type of performance at 6.8 GHz is unprecedented for contour mode resonators and represents a 12.6 dB improvement over recently reported SHF AIN resonators.



6J-3

3:15 PM CMOS Integrated Micro and Nanomechanical Resonators

Maxim Zalalutdinov^{1,2}, Jeffrey Baldwin², Jeremy Robinson², Joshua Cross³, Bojan Ilic³, Jeevak Parpia³, Eric Snow², Brian Houston².¹Global Strategies Group Inc., USA, ²Naval Research Laboratory, USA, ³Cornell University, USA

Background, Motivation and Objective

Micro and nanomechanical resonators are envisioned as core devices for sensing applications, as well as frequency-determining elements of various systems for RF signal processing including frequency generators, filters, modulators, etc. Integration of these mechanical devices with on-chip electronics, that would maintain high figures of merit (i.e. high quality factor, high frequency, small footprint, low motional resistance, etc.), is a key factor that determines the range of potential applications.

Statement of Contribution/Methods

We present methods of CMOS integration for micro- and nano-mechanical (MEMS, NEMS) resonators implemented in polysilicon, single crystal silicon, and graphene-based materials approaching a single atomic layer.

Results

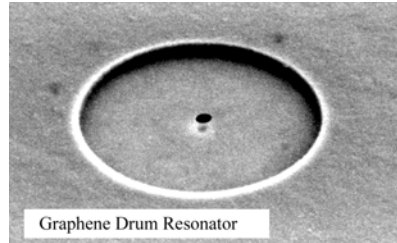
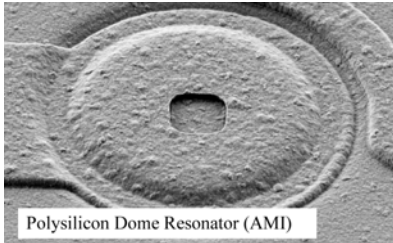
We demonstrate high frequency ($f \sim 50$ MHz), high quality factor ($Q \sim 5000$) resonators from each of the materials listed above, as well as routes to achieve device integration for each. Polysilicon resonators (figure 1: $f = 47$ MHz, $Q = 7980$) fabricated within the flow of the generic CMOS process will be presented, as well as single-crystal devices implemented in the thin "active" layers (40 nm) of the 3D FDSOI process (MIT Lincoln Lab). Physical mechanisms limiting the performance of these silicon devices will be compared to that of graphene resonators

Wednesday
Oral

(figure 2: $f = 20$ MHz, $Q = 7400$). Finally, we present progress toward post-CMOS, wafer-level integration of nanomechanical graphene resonators.

Discussion and Conclusions

In conclusion, we will discuss the prospects for novel devices and signal-processing methods implemented in mechanical domains. We will consider systems that exploit nonlinear dynamics (including emerging behavior featured by systems of coupled oscillators) and benefit from mutiplicability inherent to an integrated design.



6J-4

3:30 PM Effects of mechanical and electrical coupling on parametric sensitivity of mode localized sensors

Pradyumna Thiruvakanathan¹, Jize Yan¹, Ashwin Seshia^{1,†} *Department of Engineering, University of Cambridge, Cambridge, Cambridgeshire, United Kingdom*

Background, Motivation and Objective

Vibration localization has been employed as a means of attaining sensitivities that are orders of magnitude greater than corresponding resonant frequency variations. Further enhancements in sensitivity depend on the ability to control and predict the strength of the internal coupling between the resonators (with weaker coupling springs resulting in higher sensitivity). In this paper, we compare and contrast the effects of two distinctly different mechanisms of coupling (mechanical and electrical) on the parametric sensitivity of these sensors. Furthermore, we experimentally investigate the effects of electrical spring tuning on the sensitivity of the sensors and realize a sensor with sensitivity tunable by over 60%. Such high tunability in parametric sensitivities allow for a new class of sensors whose sensitivity can be tailored to the application.

Statement of Contribution/Methods

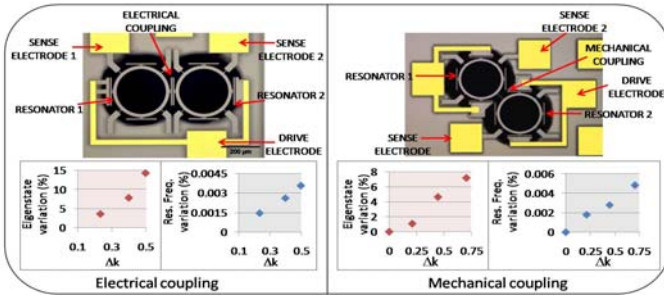
Two flexural wine glass mode ring resonators coupled using mechanical and electrical coupling springs (refer fig. 1) were used to experimentally investigate the coupling spring effects on the parametric sensitivity of mode localized sensors. One of the resonators in each configuration was subjected to electrostatically induced stiffness perturbations and the resulting relative shifts in the eigenstates and resonant frequencies were studied.

Results

Relative shift in eigenstates of over two orders of magnitude greater than corresponding resonant frequency shifts was observed in case of the mechanically coupled system while sensitivity enhancements of over three orders of magnitude were observed in the electrically coupled case.

Discussion and Conclusions

Such enhancements in sensitivity suggest that either coupling configuration could potentially be employed based on the constraints of the application. Furthermore, tunability in coupling spring constant of over 60% is demonstrated in the electrically coupled system consequently enabling the realization of a sensor with tunable sensitivity.



6J-5

3:45 PM **Power Handling and Related Frequency Scaling Advantages in Piezoelectric AlN Contour-Mode MEMS Resonators**

Chengjie Zuo¹, Matteo Rinaldi¹, Gianluca Piazza¹; ¹Department of Electrical and Systems Engineering, University of Pennsylvania, USA

Background, Motivation and Objective

Defining power handling limits of micro/nanomechanical resonators is of paramount importance since it sets the type of application in which a filter can be used and directly affects the phase noise of oscillators. By directly scaling the lateral dimensions for different frequency of operation, piezoelectric Aluminum Nitride (AlN) contour-mode MEMS/NEMS resonators have been demonstrated from 10 MHz up to 10 GHz. Nonlinearities in AlN MEMS/NEMS contour-mode resonators have never been studied to date. In this paper, we present theoretical and experimental verification of mechanical nonlinear limits for AlN contour-mode resonators and show how they are advantageously impacted by the geometrical scaling into micrometer (nanometer) range and microwave frequency of operation.

Statement of Contribution/Methods

Mechanical nonlinearity in piezoelectric resonators can be modeled via nonlinear 1st and 2nd order correction terms (Y1 and Y2, respectively) of the material Young’s modulus (Y0). A one dimensional and isotropic analysis was applied to model the nonlinear behavior of AlN contour-mode MEMS/NEMS resonators. By assuming the bifurcation point as a measure of maximum usable vibration amplitude, the critical current (ic), power (pc) and power per unit area (pc/A) that a thickness-field-excited (TFE, to distinguish from LFE: lateral-field-excitation) AlN contour-mode resonator can handle can be derived as:

Equation (1), Equation (2), Equation (3)

where ε is the dielectric permittivity of the piezoelectric material; Q is the quality factor of the resonator; ρ is the mass density; L, W and T refer to the length, width and thickness of a sub-resonator (finger) respectively; n is the number of sub-resonators that form the final single-body resonator; and kt2 is the effective electromechanical coupling coefficient.

Results

Please refer to Table I.

Discussion and Conclusions

The main conclusions of this study are that: i) the critical current does not decrease with increasing frequency (independent of W) and can be properly controlled by adjusting the value of the device effective length, nL; ii) the power handling per unit area is inversely proportional to finger width, W, which indicates advantages of scaling (i.e. miniaturization) of the piezoelectric AlN contour-mode resonators to higher frequencies.

Wednesday
Oral

$$i_c \approx \frac{4\sqrt{2}\pi\sqrt{\epsilon}Y_0}{\sqrt{\sqrt{3\rho}|9Y_0^2 - 10Y_1^2|}} \frac{nLk_1}{\sqrt{Q}}$$

Equation (1)

$$P_c \approx \frac{4\pi^3 Y_0^{3/2}}{\sqrt{3\rho|9Y_0^2 - 10Y_1^2|}} \frac{nLT}{Q^2}$$

Equation (2)

$$\frac{P_c}{A} \approx \frac{4\pi^3 Y_0^{3/2}}{\sqrt{3\rho|9Y_0^2 - 10Y_1^2|}} \frac{T}{Q^2} \frac{1}{W}$$

Equation (3)

Table I. Experimental results on power handling of resonators operating at different frequencies and with different geometries

	<i>f</i> [MHz]	<i>Q</i>	<i>k</i> ²	<i>W</i> [μm]	<i>n</i>	<i>L</i> [μm]	<i>T</i> [μm]	<i>I</i> _c [mA]	<i>p</i> _c [dBm]	<i>p</i> _c /A [μW/μm ²]
TFE	177	2500	2.0%	25	3	200	2	9.1	4.9	0.20
TFE	223	1400	2.0%	20	3	200	2	9.4	7.9	0.52
TFE	223	1800	2.0%	20	3	200	2	9.3	7.0	0.42
TFE	3047	500	1.5%	1.2	37	17	0.25	2.2	0.5	1.49
LFE	1170	2200	1.0%	4	15	80	3	3.0	1.0	0.26
LFE	1643	1450	0.4%	2	19	60	3	2.4	2.7	0.82

1K. Dynamic Elastography

Sala 1

Wednesday, September 23, 2009, 4:30 pm - 6:00 pm

Chair: **James Greenleaf**
Mayo Clinic

1K-1

4:30 PM **High resolution quantitative imaging of cornea elasticity using the Supersonic Shear Imaging technique.**

mickael tanter¹, jean-luc gennisson¹, david touboul², thu-mai nguyen¹, jeremy bercoff¹, mathias fink¹; ¹Institut Langevin - Laboratoire Ondes et Acoustique, France, ²Hopital Pellegrin, France

Background, Motivation and Objective

High-resolution measurements of cornea elasticity could turn out to have many applications in ophthalmology. It could help to understand corneal pathologies such as Keratoconus, to evaluate the biomechanical response of the cornea after refractive surgeries (LASIK) and to estimate the efficiency of new cornea treatments such as cornea transplant using femtosecond laser or Riboflavin/UV-A induced corneal collagen cross-linking (UVA CXL). It could also provide the first tool enabling a precise and non-invasive measure of the intraocular pressure. Furthermore, enlarging the technique to the lens could lead to the conception of a new process to treat presbyopia using the femtosecond laser. In this work, the Supersonic Shear Imaging technique (SSI) is proposed to map the biomechanical properties of the cornea.

Statement of Contribution/Methods

The SSI technique is based on the radiation force induced by a conventional ultrasonic probe to generate a planar shear wave into tissues. Then shear wave propagation throughout the corneal layer is caught in real time thanks to an ultrafast ultrasound scanner (up to 10000 frames/s) driving a high-frequency ultrasonic probe (15 MHz). A study has been conducted ex vivo on 10 porcine eyes in order to correlate corneal elasticity measurements with the intraocular pressure and to estimate corneal elasticity changing after UVA CXL. In vivo data have also been acquired on sheep's eyes.

Results

The results obtained ex vivo show a variation of corneal elasticity while changing the intraocular pressure. Besides, a significant corneal elasticity increase of 50% has been measured after UVA CXL treatment. Quantitative elasticity maps have been obtained on in vivo sheep's eyes. The phase velocity of the shear wave has also been extracted to investigate the shear wave dispersion. The results were compared to 3D finite differences simulations. The mechanical wave propagation corresponds to a leaky Lamb wave. Analytical and numerical dispersion curves are compared to experimental results and exhibit a very good agreement in the 400 – 3000 Hz range.

Discussion and Conclusions

This initial investigation demonstrates the ability of ultrafast and high resolution echographic systems to provide a real-time and quantitative mapping of corneal elasticity. Quantitative elasticity maps were acquired ex vivo on porcine cornea using the SSI technique. This technique can perform real-time, high resolution and quantitative maps of corneal elasticity. It could be straightforwardly adapted for in vivo investigations.

1K-2**4:45 PM Robust Hepatic Shear Modulus Reconstruction using Acoustic Radiation Force and RANSAC**

Michael Wang¹, Mark Palmer¹, Ned Rouze¹, Kathryn Nightingale¹; ¹*Biomedical Engineering, Duke University, Durham, NC, USA*

Background, Motivation and Objective

Liver stiffness may be useful for the staging and management of hepatic fibrosis. Liver shear modulus can be quantified by measuring the shear wave speed (SWS) in the liver using time of flight (TOF) methods. In this approach, the shear wave arrival time is measured at different locations along the direction of propagation. Least squares linear regression is then used to reconstruct the SWS. This method has previously been validated on simulated and phantom data. However, its application on patients is more challenging due to the effects of physiological motion, which cause gross measurement errors. Linear regression and averaging are not suitable for dealing with this type of error, which can lead to skewed SWS reconstructions. Therefore, the use of RANSAC, an iterative fitting approach robust to outliers, was investigated for estimating SWS from patient livers.

Statement of Contribution/Methods

Shear waves were generated in patient livers using acoustic radiation force in an IRB approved study. SWS measurements were repeated 3-6 times with the probe at an intercostal superior location in each liver. Shear wave arrival times were measured using its time-to-peak (TTP) in a 22 x 24 mm (depth x lateral) region of interest laterally offset from the excitation focus. The SWS is given by the slope of this plane in the lateral dimension (the assumed direction of shear wave propagation). TTP measurement noise distribution for shear wave data not corrupted by physiological motion was measured from a homogeneous elastic phantom, and used to set a noise threshold to identify subsets of consistent data (inliers). The best fit plane from all RANSAC iterations was chosen to minimize the number of outliers and sum of the square errors of the inliers. A valid reconstruction is returned only if a minimum for this cost function occurs within physically realistic limits for the SWS (0-5.8m/s).

Results

Out of 299 SWS measurements on 71 patients, RANSAC was able to successfully perform reconstructions in 225 cases. In total, 46 patients (65%) had consistent repeated shear modulus reconstructions using RANSAC. In comparison, using the same data, our previous TOF algorithm with no outlier removal scheme was able to achieve consistent modulus reconstructions in 42 patients (59%). Inconsistent repeated measurements yielding a standard deviation greater than half the mean shear modulus were discarded for both methods. The mean precision for all patients with consistent reconstructions was 1.2 kPa and 0.7 kPa for the TOF and RANSAC methods, respectively. The range of hepatic shear moduli obtained with RANSAC was 1.4-29 kPa and occurred in patients with fibrosis stages F0-F4, with increasing stiffness being correlated with increasing fibrosis stage.

Discussion and Conclusions

RANSAC is able to improve the precision of in vivo radiation force based hepatic shear modulus reconstructions, leading to a greater yield in the number of patients with consistent repeated shear modulus measurements.

1K-3**5:00 PM Adaptive Radiation Force Ultrasound for Monitoring Hemostasis in Whole Blood**

F William Mauldin, Jr.¹, Francesco Viola¹, Xiefan Lin-Schmidt¹, Michael Lawrence¹, William Walker¹; ¹*Biomedical Engineering, University of Virginia, Charlottesville, VA, USA*

Background, Motivation and Objective

Over-activation or under-regulation of hemostasis plays a central role in the onset of diseases that represent leading causes of morbidity and mortality in the developed world. Current diagnostic technologies have had limited success in characterizing hemostasis due to several limitations including reagent variability, complicated sample preparation, and a disregard for contributions of cellular components of the blood.

Statement of Contribution/Methods

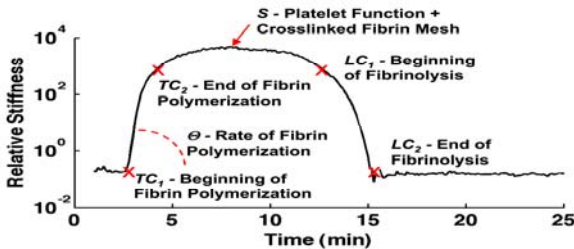
We describe a novel technique, termed sonorheometry, which uses acoustic radiation force to monitor the dynamic changes in mechanical properties of whole blood during clot formation and dissolution in vitro. An adaptive force technique was used to adjust the pulse repetition frequency during each experiment, which improved the dynamic range of sonorheometry and allowed for full characterization of hemostasis (Figure below).

Results

Inhibition of the plasma coagulation factor, fibrinogen, with 4 mM of GPRP peptide resulted in an average increase of approximately 500% in times to clot TC_1 and TC_2 along with a 95% decrease in baseline stiffness S . A dosage of 12 μg of monoclonal antibody abciximab, which inhibited platelet aggregation, resulted in an average decrease in baseline stiffness of roughly 90%. When 200 IU of a plasminogen activator, urokinase, was added to blood samples, clot dissolution was accelerated, which was indicated by an average decrease in time to lysis TL_1 and TL_2 of approximately 200%. Sonorheometry exhibited low coefficients of variation for coagulation parameters ($< 6\%$) and good correlation was observed between time to clot and partial thromboplastin time ($r=0.74$ for TC_2 ; $n=20$). We also present results showing a linear response to heparin dosages between 0-5 IU (average $r > 0.98$ for TC_2 ; $n=5$) and the ability of sonorheometry to characterize heparin reversal via protamine at a ratio of 1.2:1, in agreement with previously published results.

Discussion and Conclusions

The data presented in this paper indicate that sonorheometry quantifies all phases of hemostasis, and is thus a viable tool for rapid assessment of increased thrombotic or bleeding risks in basic research and clinical settings. This work was supported by NIH grant EB005433 and the Wallace H. Coulter Translational Partnership Award at the University of Virginia.



1K-4

5:15 PM Estimation of Mechanical Properties of Arteries and Soft Tubes Using Shear Wave Speeds

Miguel Bernal¹, Matthew W. Urban¹, James F. Greenleaf^{1,2} *Physiology and Biomedical Engineering, Mayo Clinic College of Medicine, Rochester, MN, USA*

Background, Motivation and Objective

Arterial elasticity has gained importance in the past few decades as a predictor of cardiovascular diseases and mortality [1]. We propose a noninvasive technique using ultrasound radiation force and measurement of shear wave speed to calculate the mechanical properties of arteries and soft tubes noninvasively.

Statement of Contribution/Methods

We used ultrasound radiation force to generate shear waves in the walls of excised pig carotid arteries or soft urethane tubes. Using pulse-echo ultrasound we measured the shear wave speeds by analyzing the arterial wall motion along a length of the artery. The carotid arteries used in these experiments were harvested from pigs, frozen the same day and thawed the day of the experiment. Two soft tubes were made using an injection technique from urethane with different amounts of softener to change the mechanical properties. Samples of the mixtures were also poured for testing in a DMA machine. The arteries or tubes were embedded in gelatin to simulate the surrounding tissues of vessels. A column of water was used to change the transmural pressure of the system from 10 to 100 mmHg in increments of 10 mmHg.

Results

For the pressure range used, the average speed of the tube with no softener added was 9.07 m/s while the speed for the tube with softener added was 7.33 m/s. Using these speeds, the modified Moens-Korteweg equation and the variation of the radius and the thickness measured from the ultrasound echoes, we calculated the Young's modulus of each tube for the different pressures. The Young's modulus was almost constant for all pressures with average values of 0.403 and 0.314 MPa respectively which agrees with mechanical testing values of 0.416 MPa for the stiffer tube and 0.345 for the softer one. In contrast to the results on the tubes, the artery wave speeds significantly increased with transmural pressure. The speed at 10 mmHg was 4.24 m/s and increased to 5.99 m/s at 100 mmHg.

Using the radius from pulse echo signal and assuming similar changes in thickness as the ones in the tubes, the Young's modulus for the carotid was 0.16 MPa at 10 mmHg and increased to 0.64 MPa at 100mmHg.

Discussion and Conclusions

This feasibility study shows that mechanical properties of vessels and soft tubes can be measured using shear wave propagation induced by ultrasound radiation force. The Moens-Korteweg equation seems to be good approximation to estimate the Young's modulus, as the results in the soft tubes agreed very well with the mechanical testing results. Implementation of this technique in conventional ultrasound machines would provide a clinical tool for assessing local arterial wall stiffness.

[1] E. Dolan, L. Thijs, Y. Li, N. Atkins, P. McCormack, S. McClory, E. O'Brien, J. A. Staessen, and A. V. Stanton, "Ambulatory arterial stiffness index as a predictor of cardiovascular mortality in the Dublin Outcome Study," *Hypertension*, vol. 47, pp. 365-70, 2006.

1K-5

5:30 PM Coherent Plane Wave Compounding for Very High Frame Rate Ultrasound Imaging and Transient Elastography

Gabriel Montaldo¹, Mickael Tanter¹, Jeremy Bercoff², christophe Fraschini², Mathias Fink^{1,2}*Institut Langevin (CNRS UMR 7587), ESPCI, France, ²Supersonic Imagine, France*

Background, Motivation and Objective

The emergence of ultrafast frame rates in ultrasound imaging was impelled by new imaging modalities such as Transient Elastography. Data acquisition rates reaching more than thousands of images per second enable to track shear mechanical waves propagating in biological tissues which convey information about local tissue elasticity. A first proposed approach for reaching such ultrafast frame rates consists in transmitting plane waves into the medium. However, as the beamforming process is restricted to the receive mode, resulting images suffer from a low quality and it has consequences on the robustness of the Transient Elastography mode. It is here proposed to improve the beamforming process by using a coherent recombination of compounded plane waves transmissions in order to recover high quality echographic images without degrading the high frame rate capabilities.

Statement of Contribution/Methods

Conventional B-mode imaging using line by line transmit focusing is compared with a synthetic imaging approach based on the successive transmission of plane waves with different steering angles. The coherent recombination of backscattered echoes for successive plane wave transmits permits to reconstruct set of signals virtually backscattered from each point in the imaged area. Contrast to noise ratio and resolution are compared for conventional B-mode and coherent plane wave compounding (CPWC) respectively for different numbers of transmit focal depths and numbers of compounded plane waves. Then, focused pulses dedicated to acoustic radiation force generation are added to the coherent plane wave compounding sequence. Shear waves generated by acoustic radiation force are tracked using 1D speckle correlation. Resulting tissue displacement movies are compared for single plane wave insonifications and for CPWC.

Results

Theoretical predictions are confirmed by in vitro and in vivo experiments. In typical configurations (128 elements, 8 Mhz, 6 cm depth imaging, Supersonic Imagine prototypes V1 and V2), CPWC reaches better quality (CNR and resolution) than conventional Bmode imaging (four transmit focal depths) while increasing the frame rate by a factor higher than 10. In Transient Elastography experiments using the Supersonic Shear Imaging, ultrafast frame rate higher than 1000 Hz were reached with a strongly improved quality (10 dB contrast and 40% resolution improvement) of the ultrafast image. In vivo experiments in breast show that CPWC enables to increase the elasticity reconstructed area by 50%.

Discussion and Conclusions

It is shown that the coherent summation of flat compounded insonifications is promising for ultrasound imaging as it provides high-end image quality while strongly increased temporal resolution. The classic compromise between temporal resolution and image quality is broken, and new perspectives can be envisioned: Fast B and color modes could be of significant interest for cardiac and 3-D applications.

1K-6

5:45 PM **Image Reconstruction from Shear Wave Modulated Ultrasound Echo Data**

Stephen McLeavey¹; ¹BME, University of Rochester, Rochester, NY, USA

Background, Motivation and Objective

Conventional ultrasound imaging uses delay-and-sum beamforming for focusing. Lateral resolution is determined by aperture size and wavelength. A sound speed of 1540m/s is typically assumed; sound speed variations may degrade the focus. We present a novel method in which lateral resolution of the target is obtained by using traveling shear waves to encode the lateral position of the scatters in the phase of the received echo. This method separates the lateral resolution of the imaging system from the properties of the ultrasound aperture. We demonstrate image formation with an unfocused transducer in phantoms of uniform shear modulus.

Statement of Contribution/Methods

Consider a weakly focused or unfocused ultrasound beam propagating in the +z direction in a weakly scattering medium of known shear modulus. A z-polarized plane shear wave propagating normally to this ultrasound beam (+x direction) induces a phase modulation in the echo signal from scatterers within the medium. The phase of the echo signal from a scatterer at lateral position x is modulated by $(4\pi A/\lambda)\cos(\omega t - kx)$, where k is the shear wave number, ω the shear wave frequency, A the shear wave amplitude, and λ the ultrasound wavelength. We demonstrate that the phase modulation of the total RF echo signal as a function of wavenumber can be expressed in terms of a Fourier transform of the lateral scatterer distribution. The inverse transform, obtained by measurements of the phase modulation over a range of shear wave spatial frequencies, yields the lateral scatterer distribution. Range data is recovered from time of flight as in conventional US, yielding a B-mode-like image.

Results

The analytical solution is verified through combined finite-element/Field II simulations modeling a single, unfocused 5MHz transducer in media of uniform shear modulus and with a 10% stiffer inclusion. We present images of a hyperechoic, 12mm diameter cylinder in a gelatin phantom. RF echo data were collected using a single element of a 5MHz linear array, vibrated over a 200-1.2kHz range using an electromagnetic shaker. Comparisons with standard B-mode imaging in the presence of near-field phase-screen aberrators demonstrate the relative insensitivity of the new technique to ultrasound phase aberration. Image SNR is shown to improve with vibration amplitude. Lateral resolution for low amplitude vibration is equivalent to shear wavelength, but enhanced at higher amplitudes.

Discussion and Conclusions

We demonstrate a new method for imaging using a combination of shear and ultrasound waves. This method shows promise for image reconstruction in the presence of aberrators.

Wednesday
Oral

2K. Signal Processing

Sala 2

Wednesday, September 23, 2009, 4:30 pm - 6:00 pm

Chair: **Svetoslav Nikolov**
BK Medical

2K-1

4:30 PM Real-time Calculation of a Limiting form of the Renyi Entropy For Detection of Subtle Changes in Scattering Architecture

Michael Hughes¹, John McCarthy², Victor Wickerhauser², Jon Marsh³, Jeffrey Arbeit⁴, Ralph Fuhrhop³, Kirk Wallace¹, Kwesi Agyem³, Gregory Lanza¹, Samuel Wickline^{1,2} *School of Medicine, Washington University, USA, ²Mathematics, Washington University, USA, ³Washington University, USA, ⁴Internal Medicine, Washington University, USA*

Background, Motivation and Objective

In earlier studies we reported on the application of Renyi entropy, $I_f(r)$, $r < 2$, for detection of precancerous lesions, by quantification of subtle changes in backscattered waveforms, $f(t)$, that occurred as neovascular targeted perfluorocarbon nanoparticles accumulated near the lesion. Signal energy and conventional B-mode imaging were unable to detect this change. Although computational requirements precluded its clinical application with currently available equipment, that study raised the possibility of further sensitivity improvements using values of r closer to the limiting value of 2, where $I_f(r)$ approaches infinity. In this study, we investigate sensitivity improvements obtained at this limit.

Statement of Contribution/Methods

We do this by extracting the asymptotic form of $I_f(r)$ as $r \rightarrow 2$. While our algorithm involves use of the second derivatives of $f(t)$ at its critical points, the resulting signal processing scheme, surprisingly, doesn't sacrifice sensitivity and the operation count in this approach is lower than that used to produce the signal envelope, currently the standard for real-time ultrasonic imaging display.

Results

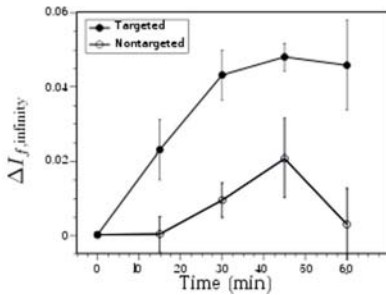
The results obtained after injection of targeted nanoparticles or nontargeted nanoparticles (which serve as a control) by $I_{f,\infty}$ receiver, are shown in the Figure. Both curves show the time evolution of the change (relative to 0 minutes) in mean value of receiver output in the enhanced regions of images obtained from the four animals in the targeted and the four animals in the nontargeted groups. Standard error bars are shown with each point. At fifteen minutes the change in mean value of $I_{f,\infty}$ is more than two standard errors from zero, implying statistical significance at the 95% level. There is no significant change in image brightness for the nontargeted nanoparticles group.

Discussion and Conclusions

As the results show, the algorithm for computation of $I_{f,\infty}$ is stable in the presence of experimental noise. Moreover, reduction of the accumulation time required to reach detectability from 30 to 15 minutes is clearly of significance, potentially reducing both patient discomfort and increasing clinical throughput. Moreover, the operation count in this approach is suitable for implementation in a real-time imaging system.

Funded by NIH EB002168

Wednesday
Oral



2K-2

4:45 PM Shannon Entropy: A Specular Echo-Insensitive Imaging Metric Showing Myocardium Anisotropy

Ya-Jian Cheng¹, Michael Hughes²; ¹Biomedical Engineering Dept, Washington University in St Louis, St. Louis, MO, USA, ²Washington University in St Louis, St Louis, MO, USA

Background, Motivation and Objective

Ultrasonic images are often corrupted by specular echoes which obscure features near interfacial boundaries. This problem can be especially severe for in vitro examination of excised tissues that must often be sliced into thin sections to permit examination by other techniques beside ultrasound. For instance, in our laboratory, excised cardiac specimens are sliced and subjected to optical, MRI, and histological examination in addition to ultrasonic scanning to characterize infarct region size and myofiber orientation. In many of these studies myocardial anisotropy was impossible to detect without removal, by gating, of specular echoes (SE), which is often a subjective process. In this study, we show that entropy imaging visualizes myocardial anisotropy without gating.

Statement of Contribution/Methods

Short axis slices of mouse heart (n=3) were C-scanned on a 150x150 grid (0.025 mm stepsize). At each point in the scan, one 8-bit, 2048 point RF A-line was acquired. These were analyzed using three signal receivers, log variance, log energy (sum of squared voltages) and Shannon entropy, to produce one pixel value at each location in the C-Scan. The Shannon entropy was computed, via the standard formula, using the probability density function (PDF) of the backscattered RF (obtained by normalizing the histogram of 8-bit digital values in each RF A-Line). For one of the specimens, a diffusion tensor MRI at 12T was also made as an additional check of the ultrasonic result.

Results

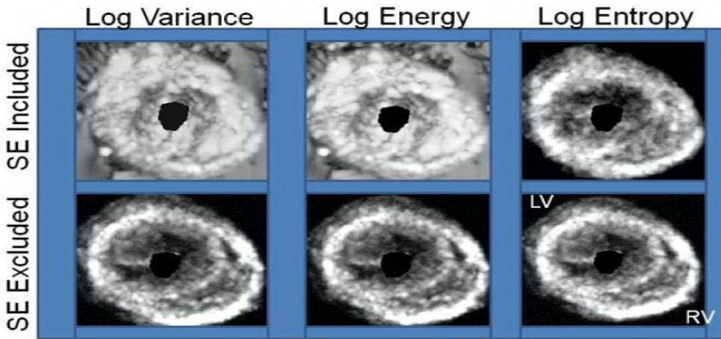
Figure 1 is typical of our results. It shows that Shannon Entropy is sensitive to myocardial anisotropy. These results agree with a quantitative analysis of all 6 images from all mice performed by conservatively defining regions of interest for epi-, mid-, and endo-myocardium, and computing the mean signal receiver value within each ROI. Entropy imaging had highest contrast between mid and epi/endo myocardium in both gated and ungated cases.

Discussion and Conclusions

Our results show that it is possible to easily visualize myocardial anisotropy using ungated ultrasonic data if Shannon entropy analysis is used. This is primarily due to the fact that the specular echo, which has a big impact on variance and energy, has only a small impact on backscattered PDF. Thus, this signal receiver can serve as the basis for objective analysis of backscattered ultrasonic data.

Study supported by NIH CA119342, NSC-095-SAF-I-564-051-TMS

Fig.1 Anisotropy visualized by entropy, even when specular echo(SE) is included.

**2K-3****5:00 PM A Model-Based Synthetic Aperture Image Reconstruction Technique for High-Frequency Ultrasound**

Joern Opretzka¹, Michael Vogt¹, Helmut Ermert^{1,†} *High Frequency Engineering Research Group, Ruhr-University Bochum, 44801 Bochum, Germany*

Background, Motivation and Objective

In high-frequency ultrasound (HFUS) systems, fixed-focus single element transducers are still widely-used, since HFUS array transducers are not yet technically mature. However, the small depth-of-field of fixed-focus transducers limits the imaging range, and the signal-to-noise-ratio (SNR) rapidly decreases out of the focus area. This can be overcome by using synthetic aperture focusing techniques, which yield a depth independent lateral resolution. Delay-and-sum-algorithms have successfully been applied in the far-field of the transducer, assuming, that the focal point is a virtual point source for spherical waves. However, the assumption of spherical waves is only valid for strongly focused transducers.

Statement of Contribution/Methods

In this contribution a mono-static synthetic aperture image reconstruction technique is suggested, which is based on correlation of the recorded echo signals with a simulated point spread function of the system. The simulation is based on the real transducer geometry. In this way, the echo signal's phase and direction-dependent magnitude are taken into account for reconstruction.

For each imaging depth the rf point spread function (PSF) is simulated using the Field II simulation program and saved in a look-up table. For image reconstruction the correlation between a 2D (axial / lateral axis) rf echo signal dataset and the PSF is calculated, whereat the depth-dependence of the PSF is taken into account. The reconstructed image is then obtained by calculation of the echo signal's envelope.

Results

The proposed method was evaluated using a 20 MHz ultrasound system with a spherically-focused transducer (focal length 15 mm, f-number 2.36, lateral resolution (-6 dB) in focus approx. 180 μm), which is mechanically scanned along the lateral direction. The lateral distance between adjacent image lines was less than half a wavelength to fulfill sampling requirements. Field II simulations of the system show a lateral resolution (-6 dB) of 750 μm and 950 μm at 12 mm and 20 mm depth in conventional B-mode images, while after applying the reconstruction algorithm the lateral resolution was below 250 μm in the whole depth range.

These results were confirmed by measurements on a wire phantom: A tungsten wire (7 μm diameter) was imaged in depths from 12 mm to 22 mm. After reconstruction with the proposed algorithm, the lateral resolution was below 300 μm (mean 220 μm , standard deviation 52 μm). Further results obtained from ex-vivo measurements on small animals are presented.

Discussion and Conclusions

The suggested synthetic aperture image reconstruction technique is based on simulated PSFs of the used transducer. It improves the lateral resolution outside of the transducer's focus area. The method can be applied in both the near- and the far-field and also works for transducers with relatively high f-numbers.

This work is supported by the German Research Foundation (Deutsche Forschungsgemeinschaft, DFG), grant ER 94/31-1.

2K-4

5:15 PM **Dual pulse frequency compounded super harmonic imaging for array transducers**

Paul van Neer¹, Mike Danilouchkine¹, Guillaume Matte¹, Martin Verweij², Nico de Jong¹; ¹Biomedical Engineering, ErasmusMC, Rotterdam, Zuid-Holland, Netherlands, ²Electrical Engineering, Mathematics and Computer Science, Delft University of Technology, Delft, Zuid-Holland, Netherlands

Background, Motivation and Objective

Second harmonic imaging is currently the standard in commercial echographic systems. A new modality, super harmonic imaging (SHI), is based on combining the 3rd to 5th harmonic generated during sound propagation in tissue. This emerging modality could further enhance resolution and quality of echographic images. To meet the bandwidth requirement for SHI an interleaved phased array was developed. Array elements used in transmission generally have bandwidths of ~80% leading to gaps between harmonics in the spectral domain. This causes ripple artifacts in the echo image. Last year we introduced a new dual pulse frequency compounding method to reduce these artifacts and showed initial single element results [1]. In this work we implement and optimize the dual pulse method for an interleaved array on an ultrasound system and research its imaging characteristics, ie point spread functions (PSF).

Statement of Contribution/Methods

In the dual pulse SHI method each trace is constructed by the summing of two firings, the second slightly frequency shifted compared to the first. To study the dual pulse method's performance an interleaved array (44 1 MHz and 44 3.7 MHz elements, optimized for echocardiography) was used in combination with a fully programmable ultrasound system. Initial estimates for the frequencies of the first and second pulses were derived using an algorithm based on the Fubini solution and then optimized experimentally.

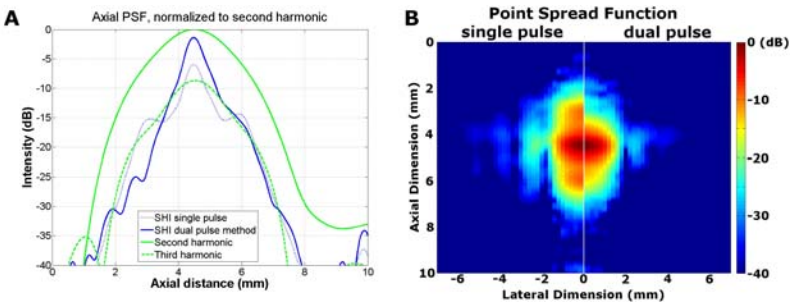
Results

The optimized center frequency of the first pulse was 0.85 MHz and of the second 1.19 MHz. Fig 1A shows that dual pulse SHI has axial widths of 0.95, 1.5 and 3.3 mm at -6, -10 and -20 dB levels respectively. These values are lower than for both single pulse SHI – axial widths of 1, 3.3 and 4.5 mm at -6, -10 and -20 dB – and the third harmonic – axial widths of 2.3, 3.6 and 5.1 mm –. The dual pulse SHI peak intensity is only 2 dB below the second harmonic. The dual pulse SHI PSF is significantly improved compared to the single pulse SHI PSF (fig 1B).

Discussion and Conclusions

The optimized dual pulse SHI method practically eliminates the ripple artifacts due to the gaps between harmonics. The dual pulse SHI PSFs show an on-axis intensity almost equal to the second harmonic, but with an off-axis energy distribution similar to the third harmonic.

[1] Matte G.M., et al. "A new frequency compounding technique for super harmonic imaging." In proc IEEE Ultrasonics symp 2008.



Wednesday
Oral

2K-5**5:30 PM Evaluation of an Analytical Solution to the Burgers Equation Based On Volterra Series**

Martin Schiffrer¹, Michal Mleczko¹, Georg Schmitz¹; ¹*Institute of Medical Engineering, Ruhr-University Bochum, Bochum, NRW, Germany*

Background, Motivation and Objective

The effects caused by nonlinear propagation of ultrasonic waves, e. g. generation of harmonics, are increasingly exploited in the development of state-of-the-art diagnostic ultrasound imaging systems and their imaging modes. They constitute the basis of tissue harmonic imaging (THI) and are used for tissue characterization. Recent concepts for the detection of ultrasound contrast agents take them into account.

Sophisticated physical models for nonlinear wave propagation exist in terms of nonlinear differential equations. Among those, the Burgers equation is widely-used to predict the combined influences of nonlinearity and dissipation on the propagation of plane waves in homogeneous fluids. It is usually solved numerically. However, simple, well-interpretable, and explicit analytical solutions are a desirable complement. They could enable the derivation of models for the complete signal chain of ultrasound imaging systems which serve as starting points for optimizations, e. g. optimal pulse sequences.

This contribution demonstrates that nonlinear system theory utilizing Volterra series provides an explicit analytical solution to the Burgers equation with these properties. The corresponding Volterra polynomials can be evaluated with scalable and small relative errors compared to numerical solutions.

Statement of Contribution/Methods

The Burgers equation is solved analytically in Laplace domain employing a Volterra series. Investigating the resulting Volterra kernels, it is demonstrated that their associated multilinear systems can be decomposed into nonlinear interconnections of two types of linear time-invariant systems: Gaussian low-pass filters and ideal integrators. The interconnections enable the efficient computation of the acoustic pressure for arbitrary boundary conditions.

For an initially Gaussian pressure waveform (center frequency 3.5 MHz, fractional bandwidth 1) in distilled water, the output signals of the Volterra polynomials up to degree 10 are compared to a widely-used reference solution to the Burgers equation employing Strang-Marchuk splitting combined with a Crank-Nicolson finite difference method. The quality of approximation is assessed in terms of the l_2 -norm of the error.

Results

A simple, well-interpretable explicit analytical solution to the Burgers equation is obtained. Numerical calculations show that the relative errors achieved by the Volterra polynomials of degree 2 and 3 with respect to the reference solution are 4.22 % and 1.35 %, respectively, after a propagation distance of 10 cm in steps of 5 mm for an initial acoustic pressure of 500 kPa. These decrease for Volterra polynomials of higher degrees.

Discussion and Conclusions

Volterra polynomials of low degrees approximate the widely-used numerical solution to the Burgers equation with small relative errors. They enable the derivation of models for the signal chain of diagnostic ultrasound imaging systems with scalable accuracy.

2K-6**5:45 PM Effects of Nonlinearity on Propagation Through the Skull**

Gianmarco Pinton¹, Jean-Francois Aubry¹, Mickael Tanter¹, Mathias Fink¹; ¹*Langevin Institute (CNRS UMR 7587), ESPCI ParisTech, INSERM, Paris, France*

Background, Motivation and Objective

As an ultrasound wave propagates nonlinearly energy is transferred to higher frequencies where it is more strongly attenuated. Compared to soft tissue the skull has a strongly heterogeneous material parameters. We characterize with experiments and establish a numerical method that can describe the effects of the skull on the nonlinear components of ultrasonic wave propagation for application to high intensity focused ultrasound (HIFU) therapy in the brain.

Statement of Contribution/Methods

A degassed desiccated human skull was placed in a water tank and insonified with a single 0.7 mm 1 MHz circular transducer from a custom array designed for HIFU treatment. Two dimensional scans were performed preceding

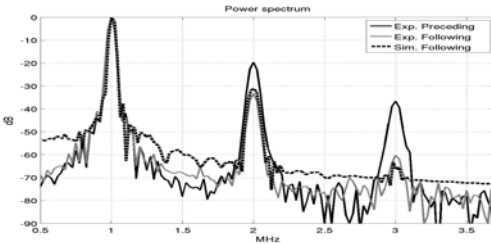
and following propagation through the skull with a calibrated hydrophone. Data from the scan preceding the skull were used as an input to a three dimensional finite difference time domain (FDTD) simulation that calculates the effects of diffraction, density, attenuation with linear dependence on frequency via relaxation mechanisms, and second order nonlinearity. A previously established equation was then used to transform a computed tomography scan to a set of registered maps of these four material properties and the skull morphology.

Results

Prior to propagation through the skull the second harmonic component was 19 dB lower than the fundamental, and the third harmonic component was 37 dB lower. Following the skull the second harmonic component was 35 dB lower and the third harmonic was 55 dB lower. As shown in the figure, the simulation is in agreement with the measurements to within 0.5 dB across the considered frequency range and shows good agreement across the 2d scan.

Discussion and Conclusions

We have established a three dimensional FDTD simulation that accurately models the effects of nonlinearity and attenuation for propagation through the skull. Experimental validation shows good agreement across a broad frequency range and spatial extent. These results will be used to improve treatment planning.



3K. Surgical Automation

Sala 4

Wednesday, September 23, 2009, 4:30 pm - 6:00 pm

Chair: **Gregg Trahey**
Duke University

3K-1

4:30 PM Development of an ultrasound imaging system for needle guidance

Rahul Singh¹, Michael Lee², David Bennett², Aaron Dann², Warren Grundefest², Hua Lee³, Martin Culjat²; ¹Electrical and Computer Engineering, University of California, Santa Barbara, Santa Barbara, CA, USA, ²UCLA, USA, ³UCSB, USA

Background, Motivation and Objective

Ultrasound transducers are commonly used for guidance during needle biopsies and central line placement. However, these procedures require the user to simultaneously insert a needle while holding a transducer. This technique is highly user dependent and is associated with a steep learning curve. A thin flexible ultrasound transducer that can be placed conformally on curved body surface, allowing a needle to be inserted directly through the substrate, may potentially simplify ultrasound guidance procedures while also providing high quality 3D imagery.

Statement of Contribution/Methods

A conformal ultrasound imaging system has been developed that features a flexible ultrasound transducer array. The array has been paired with a custom built transceiver and a backward propagation-based image reconstruction technique to produce a system that is able to image while a needle pierces the array substrate, greatly simplifying needle biopsy procedures (Fig 1). The transducer array features bulk ceramic PZT elements operating in thickness-mode, mounted on etched silicon islands connected by patterned flexible polyimide joints.

Results

The concept was first demonstrated through simulations in Matlab using the backwards propagation algorithm. The ultrasound imaging system was then implemented and used to generate preliminary imagery of a needle in a cylindrical soft tissue phantom.

Discussion and Conclusions

The ultrasound imaging system and generated images demonstrate that a needle can be imaged while it pierces the transducer array. The advances show preliminary success and initial feasibility of the conformal ultrasound approach to needle biopsy and central line placement. If successfully applied clinically, the proposed conformal ultrasound approach may considerably simplify these medical procedures.



3K-2

4:45 PM **Needle path detection for brachytherapy dosimetry based on lateral power imaging and template matching**

Mehdi Moradi¹, Xu Wen¹, Ehsan Dehghan¹, W. J. Morris², S. E. Salcudean¹; ¹Electrical and Computer Engineering, University of British Columbia, Vancouver, BC, Canada, ²British Columbia Cancer Agency, Canada

Background, Motivation and Objective

Brachytherapy is a treatment for prostate cancer with highly successful outcomes. Radioactive 125I seeds are implanted in and around the prostate based on a designed plan. However, due to prostate deformations during the procedure, the implanted seeds do not always match the plan. Hence image-based methods for seed localization and dosimetry are important. We propose a method to reliably identify the needle paths in ultrasound images. The needle paths can be used to limit the search area for individual seeds in TRUS images, or for line-based image registration to fluoroscopy images.

Statement of Contribution/Methods

A motorized brachytherapy stepper was designed which enabled us to acquire images of prostate in sagittal planes in the range of -45 to 50 degrees, with 0.3 degree intervals. The needle paths appear as curvilinear patterns of high brightness in the lateral direction of the sagittal images. In order to identify the paths, the power along the lateral direction of the RF frames was computed and averaged over overlapping segments of the rows in the RF frames. While ultrasound artifacts usually appear randomly, the seeds appear in up to 30 images in the sequence of the sagittal images with a Gaussian pattern of change in power. The seed-specific temporal templates of lateral power were extracted by imaging a seed implanted in a gelpad at three different orientations relative to the ultrasound probe. Template matching was performed based on the normalized cross correlation. The row segments in RF frames which satisfied a threshold of similarity to the templates and also an intensity threshold were identified as seeds. Fuzzy C-Means Clustering (FCM) was applied to the extracted seed locations. The points within each cluster were subjected to a linear regression algorithm. The resulting paths were ranked based on the number of segments belonging to the corresponding cluster and the level of their similarity to the templates.

Results

The method was applied to a brachytherapy prostate phantom (CIRS, Norfolk, VA) with seeds implanted along 26 needles. We set the number of clusters in the FCM step to 30. 29 of the acquired lines matched the needle paths with some needle paths characterized by more than a line. These repeated lines were removed by spatial filtering. Ten extracted lines were used to register the 3D US data to a 3D fluoroscopy reconstruction of the seeds. A line to line registration algorithm based on exhaustive search was employed. The registration error was 2.1 mm. A limited clinical study based on ultrasound data acquired from two different patients showed that in both cases, at least the five high scoring lines extracted from ultrasound images accurately matched needle paths.

Discussion and Conclusions

The method accurately identifies the needle paths in phantoms and has promising results in a limited clinical study. Data for an extensive clinical study is acquired. The set of templates will be expanded to include several seed orientations.

3K-3

5:00 PM **Time of Flight Trilateration for Localization of Minimally Invasive Surgical Instruments**

Jay Mung¹, Sukgu Han², Samantha Cunningham¹, Fred Weaver², Jesse Yen¹; ¹Biomedical Engineering, Viterbi School of Engineering, University of Southern California, Los Angeles, CA, USA, ²CardioVascular Thoracic Institute, Keck School of Medicine, University of Southern California, Los Angeles, CA, USA

Background, Motivation and Objective

This work explores the use of ultrasound signals to provide real time, 3D coordinate data for minimally invasive surgical instruments. This system provides 3D coordinate data and not images. The coordinates can be registered with preoperative, 3D CT image data to provide a "GPS" like navigation system for minimally invasive surgery.

Statement of Contribution/Methods

Three ultrasound piston transducers were used as transmitters and held at fixed locations. A custom catheter based transducer was moved within the transmitted ultrasound field. For each catheter position, the time of flight for the ultrasound signal to arrive from each transmitting transducer was obtained by either pulsed signal thresholding or

Wednesday
Oral

frequency modulated continuous wave (FMCW) range-finding. 3D coordinates for the catheter were then obtained with trilateration, given the sound speed of the medium and the spatial coordinates of the transmitters.

The localization procedure was performed in a DI water tank and a porcine tissue phantom. In the tank experiment, the catheter was moved in 1 mm increments for two 10 cm runs, once towards the plane of the transmitters (axially) and once parallel to the plane of the transmitters (laterally). Performance was evaluated with linear regression. The porcine phantom was prepared by implanting a model silicone aorta beneath the skin surface and was imaged with a CT scan. The catheter was mounted on a semi-rigid wire and advanced in 1 mm increments laterally into the phantom. Performance was evaluated by plotting coordinates on the CT images.

Results

The slope and linear regression fits for the axial and lateral translation coordinates obtained by thresholding were $m = 0.976$ with $r^2 = 0.987$ and $m = 0.709$ with $r^2 = 0.991$, respectively. For FMCW, the values were $m = 1.015$ with $r^2 = 0.999$ and $m = 0.949$ with $r^2 = 0.986$. The porcine phantom results obtained by thresholding are shown in the figure below.

Discussion and Conclusions

The linear regression values show better performance with FMCW range-finding. The registration methods used with the porcine phantom did not account for out-of-plane misalignment of the CT images. Still, the path and the anatomical environment show good agreement.

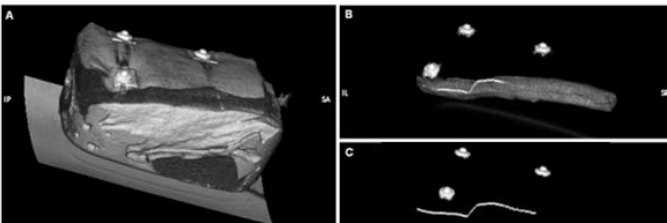


Figure: 3D reconstruction of CT image data. A: full reconstruction. B: "aorta" and path only and C: path only. Note: "nipples" are EKG electrodes affixed as fiducial markers.

3K-4

5:15 PM Line filtering for detection of microtools in 3D ultrasound data

Marian Uhreik¹, Jan Kybic¹, Christian Cachard², Herve Liebgott²: ¹Center for Machine Perception, Department of Cybernetics, Faculty of Electrical Engineering, Czech Technical University, Prague, Czech Republic, ²CREATIS LRMN, Universite de Lyon, INSA-Lyon, Universite Lyon 1, CNRS UMR 5220, Inserm U630, Villeurbanne, France

Background, Motivation and Objective

Minimally invasive surgical procedures involve an insertion of a thin tubular microtool such as a needle or an electrode of diameter 1 mm and less. The goal is to increase the contrast of such microtool and improve the robustness of its automatic detection in 3D ultrasound data of biological tissue.

Statement of Contribution/Methods

Tubular structures can be detected using a second order derivative analysis. Eigenvalues of the Hessian matrix describe the local structure. For the tubular structure, one eigenvalue (along the line) is much smaller than other two. A single function quantifying the tubularity has been proposed.

In this work, line filtering is used for visual enhancement of microtool (with a fixed diameter) in 3D ultrasound data. Secondly, a classifier based on thresholding detects voxels belonging to the tool which is then automatically localized using model fitting using RANSAC procedure. The tool axis model is a low order polynomial curve. Voxels close to the axis are required to have high intensity in the original image and to be classified as a tubular structure in the filtered image.

Results

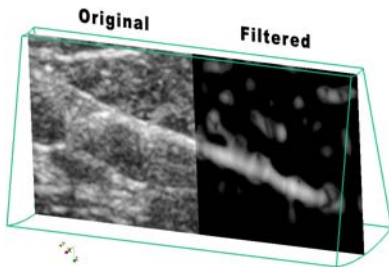
Simulation study was done on a set of simulated ultrasound images (using FIELD II) with varying location of the tool in the inhomogeneous background. Experiments on real 3D data were done for a PVA Cryogel phantom with a microelectrode of diameter 0.3 mm and on data from breast biopsy with a thin needle of diameter 1 mm (Figure).

The Weber contrast is increased 5 times when filtering is applied. The number of true positive voxels in classifier is 2 times higher for the same false alarm rate. The localization algorithm robustness against incorrect detecting of 2D structures such as fat tissue is improved, while the accuracy remains better than 1 mm. Line filtering is done in pre-processing phase and takes at most few seconds. The model fitting algorithm runs in near real-time.

The figure contains 3D volume of breast biopsy with needle. The left part of the slice contains the original data and the right part contains the filtered data.

Discussion and Conclusions

We have proposed an improved technique for microtool visual enhancement and localization in 3D ultrasound data which exploits the 1-dimensionality of the tool for more robust localization.



3K-5

5:30 PM **Evaluation of 3D Reconstructed Lower Limb Vessel Geometries with an Ultrasound Robotic Imaging System**

Marie-Ange Janvier¹, Gilles Soulez², Guy Cloutier¹, ¹Laboratory of Biorheology and Medical Ultrasonics, University of Montreal Hospital Research Center (CRCHUM), Montreal, Quebec, Canada, ²Department of Radiology, University of Montreal Hospital, Montreal, Quebec, Canada

Background, Motivation and Objective

Atherosclerosis is the principal cause of peripheral arterial disease (PAD) that leads to progressive narrowing of lower limb arteries. The localization of lesions, the length and the degree of stenosis are the most common criteria used to assess the severity of PAD. Moreover, to plan the appropriate therapy, a 3D representation of the vessel is desirable. To investigate arterial lesions in lower limbs, ultrasound (US) imaging is the first line imaging method. Because current US imaging techniques cannot visualize the entire lower limb vascular tree within an acceptable time frame at a high precision, other imaging modalities such as CT, MR and catheter-based angiography are routinely used to provide complete mapping of lower limb arteries. 3D-US imaging has the potential to form a complete lower limb vessel representation non-invasively with no ionization, but presently, most 3D-US developments are not optimally adapted for this particular clinical application. The goal of this study was to develop a prototype 3D-US imaging robotic system that can control and standardize the image acquisition process for any scanning distance from the iliac down to popliteal arteries.

Statement of Contribution/Methods

Because calibration has a major impact on the quality of reconstructed geometries enabling precise 3D visualization, planning and accurate image-guided interventions, a customized calibration procedure was first implemented. A phantom embedding Z-fiducial markers was conceptualized to determine the optimum spatial transform that relates the US probe image plane to the robotic system coordinates. The calibration transform was evaluated with a reconstruction precision < 1.20 mm for chosen US image settings. Additionally, the accuracy of the calibration transform was evaluated on 3D known vessel geometries (i.e., ground true prototype vessels) fabricated in vascular phantoms. The first gold standard geometry was an axisymmetric cylinder with a stenosis and the second, a realistic reproduction of a diseased lower limb artery (iliac artery with multiple stenoses).

Wednesday
Oral

Results

Geometrical errors of 3D reconstructions were assessed on a pixel base and in terms of lumen diameter reductions and cross-sectional areas across the vessel length. At optimum US settings, the mean reconstruction error was 0.39 ± 0.35 mm for the first phantom, whereas it was 1.38 ± 1.29 mm for the second. The mean lumen diameter and cross-sectional area errors were 1.49 ± 1.52 mm and 3.19 ± 2.30 mm², respectively, for the cylindrical shape with a stenosis and similarly, they were 0.80 ± 0.54 mm and 7.65 ± 6.61 mm² for the iliac geometry.

Discussion and Conclusions

Altogether, these results demonstrate the potential of the robot to represent adequately lower limb vessels for the clinical evaluation of stenoses. Further validation will require in vivo comparison of 3D-US robotic reconstructions with CT-scans.

3K-6

5:45 PM 3-D Ultrasound Guidance of Autonomous Surgical Robotics: Feasibility Studies

Edward Light¹, Kaicheng Liang¹, Albert Rogers¹, Daniel von Allmen², Stephen Smith¹, ¹*Biomedical Engineering, Duke University, Durham, North Carolina, USA,* ²*University of North Carolina School of Medicine, Chapel Hill, North Carolina, USA*

Background, Motivation and Objective

Our long-term goal is 3D ultrasound guidance of autonomous surgical robots for routine medical tasks such as breast needle biopsies and foreign body extraction for reduced cost. In previous studies, our lab showed that a matrix array 3D endoscope and matrix array catheters, could be used to guide a surgical robot. The robotic tasks, in water tank studies, included touching pin tips and cyst punctures using target coordinates from the 3D measurement package of the scanner with user selection of the target. These tasks were accomplished with an rms error of less than 2mm.

Statement of Contribution/Methods

In this paper we describe feasibility studies of autonomous robot biopsies in excised turkey breasts using real time 3D ultrasound combined with simple thresholding algorithms. We used a Volumetrics Medical Imaging, Inc. 3D scanner with a 2.5 MHz matrix array. The biopsy needle was attached to the arm of a Cartesian Robot with 3 degrees of freedom. The robot autonomously processed 3D image volumes received from the ultrasound scanner. The coordinates for both the biopsy needle tip (x, y, z) and the target ($x\hat{a}\epsilon^{TM}$, $y\hat{a}\epsilon^{TM}$, $z\hat{a}\epsilon^{TM}$) were acquired. The differences ($Dx = x - x\hat{a}\epsilon^{TM}$, $Dy = y - y\hat{a}\epsilon^{TM}$, $Dz = z - z\hat{a}\epsilon^{TM}$) were calculated followed by a transform from the 3D scanner coordinate system to the robot coordinate system using a fiducial mark on the transducer. The needle probe was then moved by the robot, Dx, Dy, Dz relative to its original location toward the target.

In the first experiment of five trials, using a thresholding algorithm to reject all image voxels below the brightest echo, the robot guided the biopsy needle to the tip of a 3 mm metal rod target embedded in a turkey breast simulating a calcification. In the second experiment of five trials, using an algorithm to reject all image voxels above a threshold, the robot guided the biopsy needle to the interior of a water-filled void in the breast tissue simulating a cyst. Finally in the third experiment of five trials, we used a 60 Hz alternating magnetic field to vibrate 2 mm long needle fragments in a water tank simulating ferrous shrapnel. Using real-time 3D color Doppler and a thresholding algorithm to reject all image voxels below the brightest Doppler echo, the robot guided the biopsy needle to the needle fragment.

Results

In all experiments no user input was required. The total time for each biopsy procedure ranged from 1- 3 minutes. The real time 3D scanner was used to monitor the results in the breast tissue showing the impact of the biopsy needle on the rod tip and the penetration of the cyst in each trial. In the 3D Doppler/shrapnel experiment, the robot jog operation was used to measure an RMS error of 1.06 mm.

Discussion and Conclusions

Our long-term goal is 3D ultrasound guidance of autonomous surgical robots for routine medical tasks such as breast needle biopsies and foreign body extraction for reduced cost. In each trial, the robot guided the biopsy needle to the target with a typical time of 1-3 minutes.

4K. Material and Defect Characterization

Tarragona

Wednesday, September 23, 2009, 4:30 pm - 6:00 pm

Chair: **Roman Maev**
University of Windsor

4K-1

4:30 PM Efficient Finite Element Modelling of Elastodynamic Scattering

Paul Wilcox¹, Alexander Velichko^{1,†} Mechanical Engineering, University of Bristol, Bristol, Bristol, United Kingdom

Background, Motivation and Objective

The scattering of elastic waves by defects is the physical basis of most ultrasonic and guided wave NDE/SHM. Accurate models of elastodynamic scattering behaviour are therefore central to the interpretation of experimental results and the development of new techniques. In the case of ultrasonic arrays, defects are probed from a range of incident angles and the scattered field is recorded over a range of incident angles. For this reason efficient modeling techniques that can predict the scattered field for any combination of incident and scattering angle are required. This leads to the concept of a scattering or S-matrix that describes the amplitude and phase of the scattered field as a function of incident and scattering angle. The purpose of this paper is to describe a general technique for efficiently predicting the S-matrices of an arbitrary-shaped scatterer using a commercial finite element (FE) package.

Statement of Contribution/Methods

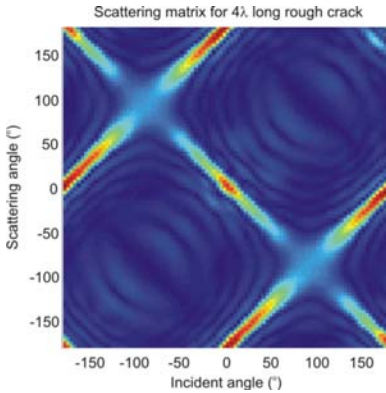
A robust and efficient technique for producing the S-matrices for an arbitrarily-shaped defect and that can be implemented in a commercial FE package is described. The spatial size of the modeling domain around the defect is made as small as possible to minimize computational expense. The underlying principle is to contain the defect wholly within a closed surface on which the Kirchhoff-Helmholtz integral is evaluated for both incident and scattered fields. Conceptually, this allows a incident plane wave to be injected onto the defect from a specified direction and the scattered field to be decomposed into plane waves in different directions.

Results

Example S-matrices from various 2D scatterers in isotropic media are presented. These include those from a circular void, which are compared to analytical solutions leading to estimates of modeling accuracy. It is shown that the amount of information contained in the S-matrices for a particular scatterer can be completely represented by a finite number of Fourier coefficients and how this relates to the number of FE model executions required. It is further shown how the information in the far-field S-matrices can be used to predict near-field scattering phenomena.

Discussion and Conclusions

The technique described is general and can theoretically be extended to 3D scattering, anisotropic media and guided waves. The technical challenges associated with these applications are discussed.



4K-2

4:45 PM Frequency spectrum spatially resolved acoustic spectroscopy for microstructure imaging

Wenqi Li¹, Steve Sharples¹, Matt Clark¹, Mike Somekh¹; ¹Electrical Systems and Optics Research Division, University of Nottingham, Nottingham, United Kingdom

Background, Motivation and Objective

The microstructure of a material influences the characteristics of a component such as its strength and stiffness. A previously described laser ultrasonic technique known as spatially resolved acoustic spectroscopy (SRAS) can image surface microstructure, using the local surface acoustic wave (SAW) velocity as a contrast mechanism. The technique is robust and tolerant of acoustic aberrations. Compared to other existing methods such as electron backscattered diffraction, SRAS is completely non-contact, non-destructive (as samples do not need to be polished and sectioned), fast, and is capable of inspecting very large components. The SAW velocity, propagating in multiple directions, can be used to determine the crystallographic orientation of grains.

Statement of Contribution/Methods

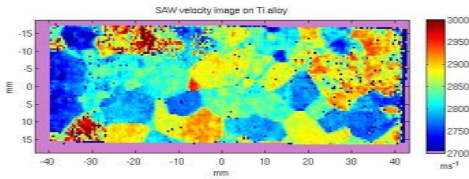
Previously, the method used a fixed frequency laser and variable grating period (k-vector) to determine the most efficiently generated surface waves, and hence the velocity. However, SRAS can also be implemented by using a fixed grating period with a broadband laser excitation source; the velocity is determined by analyzing the measured frequency spectrum.

Results

In this paper, experimental results acquired using this "frequency spectrum SRAS" (f-SRAS) method are presented for the first time. The results are illustrated as velocity maps of material microstructure in two orthogonal directions. The two different ways of performing SRAS measurements - f-SRAS and k-SRAS - are compared, and excellent agreement is observed.

Discussion and Conclusions

Furthermore, f-SRAS is much simpler, and is potentially much more rapid than k-SRAS because it can determine the velocity at each sample point in one single shot from the laser rather than scanning the grating period.



4K-3

5:00 PM **Precise Evaluation of Zero-CTE Temperature of TiO₂-SiO₂ Ultra-Low-Expansion Glass Using the Line-Focus-Beam Ultrasonic Material Characterization System**

Jun-ichi Kushibiki¹, Mototaka Arakawa¹, ¹Electrical Engineering, Tohoku University, Sendai, Japan

Background, Motivation and Objective

Ultra-low-expansion (ULE) glasses, of which coefficient of thermal expansion (CTE) becomes zero at a desired temperature, are required as the basic substrate materials suitable for photomask blanks and optical mirrors in extreme ultraviolet lithography (EUVL) systems.

We proposed and developed a super-precision CTE evaluation method of ULE glasses using the line-focus-beam ultrasonic material characterization (LFB-UMC) system. Evaluation is made by accurately measuring the phase velocity of leaky surface acoustic waves (LSAWs) excited and propagated on the water-loaded specimen surface. In this paper, an accurate relationship between LSAW velocities and CTE characteristics is discussed for TiO₂-doped SiO₂ (TiO₂-SiO₂) glass, to evaluate absolute CTE by our method.

Statement of Contribution/Methods

Specimens were prepared from two TiO₂-SiO₂ ultra-low-expansion glass (C-7972, Corning Inc.) ingots (A and B) and a synthetic silica glass (C-7980, Corning Inc.). LSAW velocities {V_{LSAW} (m/s)} were measured by the LFB-UMC system at 225 MHz. Absolute CTE was measured by an optical heterodyne interferometric dilatometer in a temperature range of 5-35°C at the National Metrology Institute of Japan.

Results

Relationships among V_{LSAW}, CTE at 22°C {CTE(22°C) (ppb/K)}, and zero-CTE temperature {T(zero-CTE) (°C)} are shown in Fig. 1. From these results, we can obtain the following equations: CTE(22°C) = 4.33 × (V_{LSAW} - 3303.29); T(zero-CTE) = -2.67 × (V_{LSAW} - 3303.29) + 22.5. LSAW velocity, at which CTE(22°C) becomes zero, was estimated as 3303.29 m/s, and the TiO₂ concentration was also estimated as 7.38 wt% from the relationship between V_{LSAW} and TiO₂ concentration we determined previously. Resolutions of CTE(22°C) and T(zero-CTE) by the LSAW velocity measurement were estimated as ±0.72 (ppb/K) and ±0.45°C (±2σ, σ: standard deviation) at 225 MHz.

Discussion and Conclusions

Both manufacturers and users can precisely inspect T(zero-CTE) for all EUVL-grade ultra-low-expansion glass substrates by this indirect evaluation method using the calibration line.

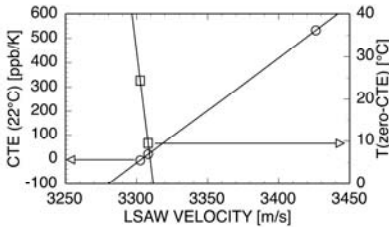


Fig. 1. Relationships among LSAW velocities, CTE at 22°C (open circles), and zero-CTE temperatures (open square) for $\text{TiO}_2\text{-SiO}_2$ ultra-low-expansion glasses.

4K-4

5:15 PM Investigation of transient processes in eutectic solidification with an ultrasound pulse-echo technique during unidirectional solidification

Anne Drevermann¹, Ulrike Hecht¹, Stephan Rex¹; ¹ACCESS e.V., Aachen, Germany

Background, Motivation and Objective

Ultrasonic (US) pulse echo technique was used for the investigation of complex eutectic transitional processes during unidirectional solidification. Previous publications describe the technique as an undisturbing tool to investigate the solidification velocity during unidirectional solidification. This time two different eutectic solidification processes were investigated, i.e. a) morphological transitions in coupled growth of an Al-Cu-Ag alloy and b) symbiotic eutectic growth of an Al-Si-Mn alloy.

Statement of Contribution/Methods

The unidirectional solidification takes place in a Bridgman Stockbarger furnace. Due to an effective liquid metal cooling a piezoelectric transducer can be attached to the cold solid end of the cylindrical sample. This US transducer generates and receives a guided wave that is reflected by the solid-liquid interface. During directional solidification the length of the solid part of the sample increases and accordingly the time-of-flight of the echo. This is evaluated by means of a phase-selective correlation.

Results

a) During unidirectional solidification of an Al – 32.1 wt.% Cu – 3.2 wt.% Ag alloy univariant eutectic growth takes place. The two phases $\alpha(\text{Al})$ and Al_2Cu grow coupled. Both phases segregate Ag into the melt. This gives the opportunity to trigger morphological transitions by carrying out well-defined velocity steps, e.g. the transition from lamellar planar to eutectic cellular growth. The US pulse echo measurement of the velocity was compared to image analysis of the evolution in eutectic patterns and to concentration profiles measured by EDX.

b) The second process is the symbiotic eutectic growth of an Al – 3 wt.% Si – 1 wt.% Mn alloy. During directional solidification of this alloy the secondary phase nucleates ahead of the planar primary phase solidification front and grows in interaction with it. During this process unexpected remelting events were observed with the US pulse echo technique. Thus an online correlation was implemented to quench the sample exactly in the remolten status and investigate its characteristics regarding particle distribution and solutal field.

Discussion and Conclusions

US pulse echo technique proved an excellent tool to contribute to the understanding of the complex dynamics of eutectic solidification processes.

4K-5

5:30 PM **Effects of Ultrasonic Capillary Dynamics and Pad Material on the Mechanics of Thermosonic Ball Bonding**

Yan Huang¹, Michael Mayer^{1,†} *University of Waterloo, Canada*

Background, Motivation and Objective

Thermosonic ball bonding is the most popular wire bonding process and an essential step in microchip production. The process uses a capillary tool for ultrasonic welding the beaded end of micro-wires to metal pads on integrated circuits using a frequency typically between 120 kHz and 140 kHz at elevated temperatures. Au wires 25 micron in diameter and 2 micron thick Al pads (Au-Al) are often used. To replace Au, Cu wire has emerged due to its potentially high performance/price ratio. However, Cu wire bonding frequently results in under-pad damage and subsequent failure of the microchip as Cu is harder than Au. Therefore, the under-pad stress fields (UPSFs) during the bonding process are studied. Ni is used as an alternative pad metallization due to its stiffness which is higher than that of Al. Can a Ni pad compensate for the UPSF increase caused by Cu wire? A finite element (FE) model is reported to find the answer. The innovative objectives of this contribution are to include the effect of ultrasonic dynamics and to analyze ways to reduce peak stresses by changing the pad material.

Statement of Contribution/Methods

A frequency response model for the first time combines the ultrasonic dynamics and material effects of the ball/pad system. The model includes chip, wire, and capillary tool. Results are compared with experiments from literature. A sub-model covering the capillary vibration only is adjusted to match the experimental data. No subsequent adjustment is necessary for the main model which then is used to produce results and conclusions. The UPSFs are calculated for various wire/pad material combinations.

Results

To achieve agreement between model and experiment, implementing an ultrasonic tool “nodding” effect is found necessary. UPSF increase caused by replacing Au wire with Cu wire and UPSF reduction due to the use of Ni are quantified. For the standard Au-Al process, the maximum principal stress magnitude (MPS) under the pad is 490 MPa and compressive. With the harder Cu wire instead of the Au wire, 3.7% less ultrasound amplitude is required while MPS increases by 6.2% with the same bond quality (interfacial shear) maintained. When Ni is used to replace the softer Al pad material, MPS is reduced by 4.9%. A Cu wire combined with a Ni pad results in 1.3% higher MPS than with Au-Al.

Discussion and Conclusions

The reported model is in excellent agreement to experimental results. It was found that calculated stresses are substantially off target unless ultrasonic dynamics are included. When changing the pad material from Al to Ni, the higher hardness effect of Cu compared to Au can be compensated almost completely. This confirms preliminary observations from industry. The reported model can be adapted to compare processes with varying material parameters and geometrical dimensions of the capillary, ball, pad and under-pad structure, chip, and die attach adhesive. Processes using different ultrasonic frequencies can also readily be compared with each other.

4K-6

5:45 PM **Evaluation of Elastic Inhomogeneity in ZnO Crystal by Means of the Micro-LFB Ultrasonic Material Characterization System**

Jun-ichi Kushibiki¹, Yuji Ohashi¹, Mototaka Arakawa¹, Sho Yoshida¹, Noboru Sakagami¹, [†]*Graduate School of Engineering, Tohoku University, Sendai, Japan*

Background, Motivation and Objective

We have been developing a method of evaluating resistivity of ZnO crystals using the line-focus-beam ultrasonic material-characterization (LFB-UMC) system. Characterization is made by accurately measuring the velocity of leaky surface acoustic waves (LSAWs) propagating on a water-loaded specimen surface. We have also developed a micro-LFB ultrasonic device achieving higher spatial resolution to detect steep velocity variations within the crystals. In this paper, we demonstrate applicability of the micro-LFB-UMC system for evaluating resistivity distributions in ZnO crystals related to the crystal growth processes and conditions.

Statement of Contribution/Methods

A small crystal ingot of ZnO (3x7x11 mm³) grown by the hydrothermal synthesis method was prepared. LSAW velocity distributions were first measured for +c plane [(001)], -c plane [(00-1)] and two m planes [(11-0) and (-1-10)] at 225 MHz. Next, to examine elastic homogeneities inside the specimen, we conducted same measurements

for two new specimen surfaces of +c and -c planes cut and optically polished at the positions of 2.5 mm and 0.3 mm from the original end surfaces, respectively.

Results

For the specimen before reforming, the averaged LSAW velocities were 2672 m/s for +c plane, 2618 m/s for -c plane, and 2650 m/s for the two m planes. These velocities correspond to low resistivity only for the as-grown -c plane and high resistivity for the other as-grown surfaces. We observed significant LSAW velocity distributions for the new +c and -c surfaces inside the as-grown crystal (Fig. 1). In this result, we can observe lower and higher velocity regions surrounding the higher one for the seed crystal. The same tendency was observed for the new +c specimen surface.

Discussion and Conclusions

From the above results, we can understand that relatively lower resistivity region grew first around the seed crystal with higher resistivity, then higher one further did around them except for the -c plane. According to our previous report [1], the regions with LSAW velocities from 2624 to 2673 m/s in Fig. 1(b) have the resistivities from 2.1 to 153 Ωm . Using the micro-LFB-UMC system, a detailed information associated with crystal growth processes and conditions can be obtained, and the results could be fed back to improvement of the growth conditions.

[1] J. Kushibiki et al., Appl. Phys. Express, Vol. 2, 026501 (2009).

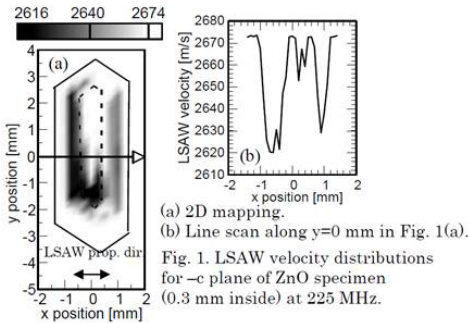


Fig. 1. LSAW velocity distributions for -c plane of ZnO specimen (0.3 mm inside) at 225 MHz.

5K. Medical Imaging and Therapeutic Transducers

Pergamo

Wednesday, September 23, 2009, 4:30 pm - 6:00 pm

Chair: **S. Cochran**
Dundee University

5K-1

4:30 PM Hybrid Dual Frequency Transducer and Scanhead for Micro-Ultrasound Imaging

Marc Lukacs¹, Mike Lee¹, Emmanuel Cherin¹, Jianhua Yin¹, Paul Dayton², Desmond Hirson³, Stuart Foster¹;
¹Sunnybrook Health Sciences Centre, Canada, ²Joint Department of Biomedical Engineering, UNC-NCSSU, USA,
³Visualsonics Inc., Canada

Background, Motivation and Objective

It is a common objective, for imaging transducers, to design a device with as broad a bandwidth, and as narrow a pulse response as possible. A bandwidth of > 80% is considered to be quite broad for piezo transducers used in soft tissue imaging applications. However, new and emerging ultrasound imaging techniques, such as coded excitation, radial modulation imaging and enhanced bubble contrast imaging, are placing new requirements on the frequency response of transducer design. For each of these applications, it is desirable to excite and/or destroy contrast bubbles while retaining the ability to generate high resolution images with a higher frequency B-mode pulse and thus exceed the bandwidth of a single piezo stack.

Statement of Contribution/Methods

The authors present a hybrid dual frequency annular transducer whereby the central element and the concentric annular ring operate with center frequencies of 30 MHz and 2 MHz respectively. The radius of curvature of each transducer, 12.7mm, was matched to achieve an overlap of focal depths along a shared axial axis.

A commercially available 30MHz polymer transducer from Visualsonics was used for the central element and the 2MHz transducer ring was fabricated using a 1-3 piezo-ceramic composite with triangular PZT pillars. The ring was calibrated to generate peak to peak pressure waves of up to 5 MPa to oscillate US contrast bubbles. The device was mounted onto an RMV Scanhead motor to allow for real time imaging.

Results

The ultrasound propagation and the effects of edge waves, from the ring transducer were found to match quite well to nonlinear propagation simulations. The 3dB focal depth/depth of field of each transducer was 10.9mm/6.6mm and 12.7mm/2.5 for the 2 and 30 MHz transducers respectively. The 3dB spot size was 360um and 115um respectively and the misalignment of the axial axes was 1 degree.

Discussion and Conclusions

The design, assembly and acoustic field characterization of the hybrid dual ultrasound transducer will be discussed. Real time images using a Visualsonics VEVO 770 will also be presented.

5K-2

4:45 PM New Ring Array Transducers for Real-Time 3D Intravascular Ultrasound

Edward Light¹, Victor Lieu¹, Stephen Smith¹;¹Biomedical Engineering, Duke University, Durham, North Carolina, USA

Background, Motivation and Objective

While the last decade has seen tremendous advances in the development and application of interventional medical devices, new imaging modalities to monitor these procedures in real-time have not kept pace. X-ray fluoroscopy with its inherent disadvantages is still the main imaging modality. Real time 3D ultrasound enables continuous monitoring of these same structures before, during and after deployment. We have previously demonstrated ring arrays of 2D transducer elements for real-time 3D ultrasound imaging for guidance of minimally invasive

procedures using W.L. Gore & Associates, Inc. micro-miniature ribbon cables. We have recently completed devices using cabling from Tyco Electronics and have early results from a transducer built on a single 46 cm long flexible circuit from MicroConnex.

Statement of Contribution/Methods

We have developed new miniature 2D array transducers integrated into a Cook Medical, Inc. vena cava filter deployment device. One transducer consists of 55 elements operating near 5 MHz. The interelement spacing is 0.20mm. It was constructed on a flat piece of copper clad polyimide and then wrapped around an 11 French catheter of a Cook, Inc. inferior vena cava (IVC) filter deployment device. We used a braided wiring technology from Tyco Electronics Corp. (Wilsonville, OR) to connect the elements to our real-time 3D ultrasound scanner. This technology included 64 signal wires along with individual ground wires for each signal wire, and an overall metal shield braid to reduce electronic pickup.

We have also built transducers on a 46 cm long single layer flex circuit from MicroConnex (Snoqualmie, WA) which terminates in an interconnect that plugs directly into our system cable. This transducer consists of 70 elements at 0.157 mm interelement spacing operating at 5 MHz. No extra cabling or soldering is required.

Results

Using the cabling from Tyco, typical measured transducer element bandwidth was 20% centered at 4.7 MHz and the 50 Ohm round trip insertion loss was -84 dB. The mean of the nearest neighbor cross talk was -37.0 dB. These measurements were made including the cabling. We made real-time 3D images of a Cook IVC filter with this device.

Using the 46 cm flex from MicroConnex, typical measured transducer element bandwidth was 29% centered at 4.8 MHz and the 50 Ohm round trip insertion loss was -94 dB. The mean of the nearest neighbor cross talk was -33.0 dB. These are preliminary data, and we have not yet imaged with this transducer.

Discussion and Conclusions

We were able to fabricate 2D array ring transducers using new interconnect technologies. Both show comparable numbers to our past transducers. The long flex circuit offers the chance to reduce costs by removing the need to solder wires to a smaller flex circuit and an interconnect to the system cable.

5K-3

5:00 PM **Ultrasound Catheter for Microbubble Based Drug Delivery**

Joseph Kilroy¹, Linsey C. Phillips¹, Abhay V. Patil¹, John Hossack¹, ¹*Biomedical Engineering, University of Virginia, Charlottesville, Virginia, USA*

Background, Motivation and Objective

Atherosclerosis is the leading cause of death in the developed world. Current methods of treating atherosclerotic occluded blood vessels include angioplasty followed by stent placement. Unfortunately, the potential for re-occlusion often requires the use of anti-proliferative agents. An intravascular ultrasound (IVUS) catheter that delivers drug coated microbubbles through radiation force and bursts the bubbles has been simulated and fabricated. The novel component of this device is the use of IVUS for combined radiation force for translation of bubbles into position followed by bubble breaking for drug delivery.

Statement of Contribution/Methods

Finite Element Analysis (FEA - PZFlex, WAI) was used to model the acoustic performance of an IVUS transducer for radiation force and destruction modes of operation. Microbubble translation was simulated with bubble diameters of 2, 2.5, and 4 microns based on minimum, maximum, and mean sizes for bubbles used in a flow phantom experiment. A custom IVUS transducer was designed to operate at 1.5MHz with 80 kPa and 170 kPa PNP for translation and destruction, respectively. Transducer acoustic performance was tested using a hydrophone in water when excited by a 1.5 MHz Gaussian ramped pulse.

Capacity to deliver drugs or genes was tested by breaking microbubbles carrying a red fluorescent reporter gene in proximity to rat smooth muscle cells in vitro with a -170 kPa PNP, 1.5 MHz Gaussian Pulse at a PRF of 1 kHz.

IVUS radiation was tested in a flow phantom with 4.5 mm diameter vessels coated with streptavidin to anchor bubbles once they contact the vessel surface. A solution of 2.5 micron mean diameter biotin bubbles concentrated at 4.1×10^6 bubbles/ml was flowed at 30 ml/min for 26 seconds. During flow the bubbles were exposed to a 1.5 MHz 80 kPa PNP Gaussian ramped pulse at 8 kHz PRF. The accumulation of bubbles along the vessel wall was

measured in terms of image intensity by transcutaneously scanning with an Ultrasonix Research Platform Scanner and bubble specific real time imaging software developed in our laboratory.

Results

The FEA of the transducer design compared with measured acoustic output of the transducer has a correlation coefficient of 0.98. Translation model results show 2, 2.5, and 4 micron bubbles move at mean velocities of 0.4, 1, and 3 cm/s respectively. The change in image intensity on the targeted wall of the vessel was 12.5 dB. In vitro gene transfection, as a surrogate for drug delivery, of rat smooth muscle cells was achieved with the new transducer.

Discussion and Conclusions

In this paper an IVUS catheter for microbubble based drug delivery was simulated, assembled, and tested. The IVUS catheter translated microbubbles across a flow phantom vessel using radiation force in accordance with the simulation results. Gene transfection was achieved using burst sequences. To the authors' knowledge this is the first demonstration of IVUS-mediated radiation force delivery of microbubbles to a simulated vessel wall.

5K-4

5:15 PM Real-Time Simultaneous Therapy and Imaging for Noninvasive HIFU Surgery of Prostate Tissue

Jong Seob Jeong¹, Jin Ho Chang¹, Jonathan M. Cannata¹, K. Kirk Shung^{1,2} *Biomedical Engineering, University of Southern California, Los Angeles, CA, USA*

Background, Motivation and Objective

In ultrasound image guided HIFU (high intensity focused ultrasound), real-time simultaneous therapy and imaging is more desirable because it allows for tracking tissue movement and monitoring feedback induced by a treated target. Unfortunately, reflected HIFU signals corrupt the quality of signals received by an imaging transducer during simultaneous therapy and imaging. The intention of this paper is to demonstrate that these interference signals can be significantly reduced in the formed B-mode image by implementing coded excitation and notch-filtering on reception. We also propose a design of an integrated image/HIFU phased array transducer for treatment of malignant prostate tissue to demonstrate our signal processing technique.

Statement of Contribution/Methods

The proposed integrated image/HIFU transducer is composed of three rows of phased array elements confocally aligned in elevational direction. The center row forms the 64-element 6 MHz imaging array and the two identical 64-element 4 MHz outer rows work together to produce the HIFU signal. Different stack configurations and piezoelectric materials were used to achieve the desired performance as a combination HIFU and imaging transducer. The total dimension of the HIFU array was 14.4 mm x 20 mm, which in our preliminary experiments was sufficient to generate spatial peak intensity more than 1000 W/cm² at a focal spot. A 13 bit Barker code with a conventional sidelobe suppression filter was used for implementing coded excitation. The second order infinite impulse response notch filters were used to remove the HIFU array generated 4 MHz fundamental and 8 MHz harmonic signals from the 6 MHz imaging array echo response. The -6 dB bandwidth of 6 MHz array should be large enough to include the critical frequency components of imaging signals but narrow enough to minimally overlap with the notch frequencies.

Results

A 14.4 mm x 28 mm prototype integrated imaging/HIFU transducer which consists of three single elements was fabricated as a preliminary experiment. When the HIFU and imaging transducers were activated simultaneously, high amplitude 4 MHz and 8 MHz signals were detected by the 6 MHz imaging transducer. After notch filtering, one scanline produced by the 13 bit Barker code with 2 cycles or 3 cycles per bit displayed a sidelobe level less than -40 dB while conventional 2-cycle pulse had a maximum sidelobe level of -20 dB. These results agree with those obtained with a Field II simulation.

Discussion and Conclusions

Our experimental results prove that the combination of coded excitation and use of notch filters on reception can minimize reflected HIFU signals efficaciously and thus the proposed design of an integrated imaging/HIFU transducer can be used for real-time simultaneous imaging and treatment of prostate tissue. In the future, the fabrication of an integrated imaging/HIFU phased array and the development of an electronics system for real time operation will be pursued.

5K-5

5:30 PM Reducing electrical impedance of therapeutic intracavitary phased arrays with lateral coupled paired elements

ALEKSANDRA KUKIC¹, KULLERVO HYNYNEN^{1,2}, ¹SUNNYBROOK RESEARCH INSTITUTE, TORONTO, Canada, ²MEDICAL BIOPHYSICS, UNIVERSITY OF TORONTO, TORONTO, Canada

Background, Motivation and Objective

Therapeutic phased arrays utilize elements of small width to thickness ratio and thus have high electrical impedance. High mismatch between the driving circuitry and the transducer results, requiring difficult L-C matching circuits. Lateral mode coupling has been used to reduce the electrical impedance of small cylindrical elements for high power phased arrays for use in therapeutic purposes such as tumor coagulation [1]. We propose lateral mode coupling use in therapeutic intracavitary linear phased arrays.

[1] Hynynen et al "Lateral Mode Coupling to Reduce the Electrical Impedance of Small Elements Required for High Power Ultrasound Therapy Phased Arrays", IEEE Trans. on UFFC, vol. 56, no. 3, Mar 2009

Statement of Contribution/Methods

A linear composite array was built using thickness poled PZT4-EC69 (EDO Salt Lake City UT). Pairs of elements (.155x1.4x14.5 mm) were stacked in a linear array; each element had its electrodes on its sides. In order for the surface of the array to emit sound, the elements were driven at the frequency corresponding to their height. Pairs of consecutive elements were driven via a common electrode.

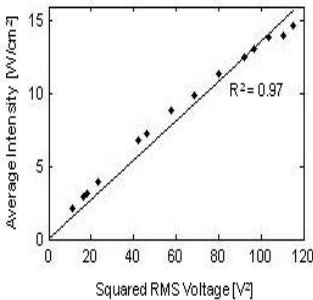
Electrical impedance of the elements was measured using a network analyzer (4195A Hewlett-Packard Palo Alto CA). A matched element pair was driven at lateral mode resonant frequency. The acoustic surface displacements were measured using a scanning laser vibrometer (PSV-400-M2-20 20 MHz Polytec Tustin CA).

Results

The electrical impedance at lateral mode coupling resonant frequency of 1.3 MHz (corresponding to the height of 1.4 mm) was 149 ohms at minimum phase peak of -33 deg. By comparison, an element of similar dimensions (.3x1.1x15 mm) and resonant frequency of 1.5 MHz exhibited an electrical impedance of 1.4 kohms at -22 deg. A matched pair of elements was able to achieve therapeutically significant spatially averaged acoustic intensity of 15 ± 5 W/cm² (Fig 1). The maximum displacement at each input power level varied spatially by $20 \pm 9\%$.

Discussion and Conclusions

Lateral mode coupling utilization combined with element pairing allows for smaller distance between the electrodes, and an increase in electrode area. This results in significant electrical impedance decrease. The paired elements provide at least 50% larger acoustic power output than has been reported with current arrays for the purposes of thermal therapy in intracavitary applications.



5:45 PM **Dual-mode Intracranial Catheters for Minimally-invasive Neuro-oncology: Feasibility Study**

Carl Herickhoff¹, Gerald Grant², Gavin Britz², Srinivasan Mukundan³, Edward Light¹, Patrick Wolf¹, Stephen Smith¹;
¹Biomedical Engineering, Duke University, Durham, NC, USA, ²Neurosurgery, Duke University Medical Center, Durham, NC, USA, ³Radiology, Brigham and Women's Hospital, Boston, MA, USA

Background, Motivation and Objective

We investigated the feasibility of dual-mode intracranial catheter transducers for visualization and treatment of tumors in the brain. A minimally-invasive, endovascular approach to administering localized ultrasound hyperthermia in the brain could provide targeted control of drug release from thermosensitive liposomes, enhancing chemotherapeutic efficacy.

Statement of Contribution/Methods

To demonstrate feasibility, we developed a 12 Fr, integrated matrix and linear array catheter transducer prototype for combined real-time 3D imaging and heating. This 3.6 MHz dual-mode catheter incorporated 153 matrix array elements and 11 linear array elements on a 0.2 mm pitch (8.4 mm × 2.3 mm total aperture). The prototype's imaging and therapy performance was compared in vitro with a Siemens 10 Fr AcuNav catheter as a gold standard. Each probe was used in a canine brain model to image anatomical structures and color Doppler blood flow and to attempt in vivo heating.

Considering the eventual need for a smaller diameter and more flexible catheter, we also modified a Boston Scientific 3 Fr IVUS catheter. The 40 MHz element was replaced by a 220 μm thick, 350 μm × 350 μm piece of PZT-4, and electrical impedance and pulse-echo measurements were taken. A test transducer with an identical element was constructed and driven with a 25 W power amplifier and custom impedance matching circuit to measure acoustic output and determine therapy potential.

Results

The dual-mode 3D catheter acquired B-scan and C-scan images of phantoms which were comparable to AcuNav B-scans, and achieved a 3.5°C temperature rise in tissue-mimicking material at a 2 cm focus. In vivo real-time 3D imaging of the canine brain from the venous sinus delineated the lateral ventricles and Circle of Willis using B-mode and color Doppler.

Electrical impedance and pulse-echo measurements for the modified 3 Fr IVUS catheter verified that the transducer was functional, with peak transmission at 5 MHz and 9 MHz. Intensity measurements at 3.85 MHz with the test transducer 4 mm from the hydrophone yielded an ISPTA of 0.58 mW/cm² at a 0.01% duty cycle.

Discussion and Conclusions

Compared to the AcuNav, the dual-mode 3D catheter exhibited satisfactory image quality. The prototype also created a 3.5°C temperature rise without using electrical impedance matching circuits, which could boost power output by as much as 30%. Our in vivo experiment showed that intracranial RT3D imaging improves on 2D imaging by enabling the operator to more quickly and definitively orient the catheter's field of view and identify structures in the cranial cavity.

We also demonstrated a retrofit of a 3 Fr IVUS catheter with a low-frequency, high-power transducer element. Extrapolation of our intensity measurement indicates that such an element could output an ISPTA of 5.8 W/cm², which may be sufficient to create local hyperthermia.

6K. Industrial Ultrasonics

Baalbek

Wednesday, September 23, 2009, 4:30 pm - 6:00 pm

Chair: **Jiromasu Tsujino**
Kanagawa University

6K-1

4:30 PM **Joint Estimation of Fibers and Fines Concentration in Paper Pulp Suspensions Using a Combined Optical and Acoustic Technique**

Jan Niemi¹, Johan E. Carlson², Torbjörn Löfqvist¹; ¹*EISLAB, Dept. of Computer Science and Electrical Engineering, Lulea University of Technology, Lulea, Sweden,* ²*Div. of Systems and Interaction, Dept. of Computer Science and Electrical Engineering, Lulea University of Technology, Lulea, Sweden*

Background, Motivation and Objective

The pulp and paper industry develops numerous different types of paper products today. The demands on efficient use of both raw materials and energy, in combination with the increased use of recycled paper, make it important to develop the production system in terms of control and pulp consistency.

The fibers in the pulp can be divided into two size classes, fibers and fines (i.e. fibers shorter than 200 μm). The ratio of fibers to fines is important since it significantly affects the properties of the final paper, but today there is no technique available for online measurement of both. This paper presents a technique based on combined optical and ultrasonic measurements for joint online estimation of fiber and fines mass fraction in paper pulp suspensions.

Statement of Contribution/Methods

The method proposed in this paper measures four quantities: Time of flight and intensity of light transmitted through the pulp, and speed of sound and attenuation of pulse-echo ultrasound. The optical technique is much more sensitive to the smaller fines than to the fibers, although not unaffected by the larger fibers, while the ultrasound technique is less sensitive to the fines. The two techniques do not, however, contribute with completely independent information, which motivates the use of a multivariate technique for the analysis. Consequently, the measurements were then used to build a statistical model (based on Partial Least Squares, PLS) relating the four quantities above to the mass fractions of fibers and fines.

Results

The method is evaluated with experiments on softwood pulp suspensions for total mass fractions in the range of 0-0.5%, with varying fiber-to-fines ratios. One experimental run was used as calibration data, and a second for validation and evaluation of the PLS prediction model. Results of using the combined optical/acoustic technique or the two techniques by themselves were then compared. The prediction yielded a Q^2 value of around 0.98, for both the fines and fiber mass fractions. This indicates that the variance of the prediction errors is only around 2 % of the total variance of the measured responses. Using only the optical technique the prediction capability of fiber mass fraction was reduced significantly. For the ultrasound techniques, the same was true for the fines mass fraction.

Discussion and Conclusions

The results show that by using a combined optical and ultrasonic technique, in combination with PLS regression, it is possible to estimate the mass fractions of both fibers and fines in paper pulp suspensions. The predictive capabilities are significantly increased by using the combined data than the optical or ultrasonic methods by themselves. Furthermore, the method is computationally efficient, making it suitable for online implementation.

6K-2

4:45 PM **Cleaning Membranes with Focused Ultrasound Beams for Drinking Water Treatment**

Jian-yu Lu¹, Xi Du², Glenn Lipscomb^{2,1} *Bioengineering, The University of Toledo, Toledo, OH, USA, ²Chemical Engineering, The University of Toledo, Toledo, OH, USA*

Background, Motivation and Objective

Membranes such as nanofiltration (of pore sizes in the order of nanometers) and reverse osmosis (of pore sizes that allow water molecules to pass but stop sodium chloride) membranes are the state-of-the-art technologies for the treatment of drinking water and desalination of sea water, respectively. However, due to the small pore sizes of these membranes, fouling is a major problem. Conventional methods for membrane cleaning use chemicals that produce secondary pollutions and stop the water treatment process during the cleaning. Ultrasound has been studied to clean the membranes to avoid the problems of chemical cleaning. However, so far there are no methods that can integrate ultrasound transducers into commercial membrane systems for water treatment.

Statement of Contribution/Methods

In this paper, we study the efficacy of a focused ultrasound beam on membrane cleaning. This study is significant since ultrasound intensity is increased greatly at the focus, potentially allowing polymer-based (such as polymer, copolymer, or homopolymer) transducers to be used. Compare to PZT (lead zirconate titanate) ceramic types of transducers, polymer-based transducers have low transmission efficiency but they are flexible, non-brittle, and have a low cost. The flexibility of the polymer-based materials is necessary for integrating transducers into the spacer structures of existing commercial membrane units such as spiral wound membrane systems with minimal modifications. The focused ultrasound that produces a high intensity at focus can be steered by phased array transducers that are formed by printing electrode patterns on polymer surfaces to sweep the beam over the surfaces of membranes for cleaning.

Results

To show the efficacy of focused ultrasound beam in membrane cleaning, an experiment was performed. In the experiment, an Ultrafiltration (pore sizes of tens of nanometers) instead of Nanofiltration membrane was used because the pump in our lab does not produce more than 40 psi pressure. To reduce the time for ultrasound cleaning, the membrane was covered with tapes except for an area of 1 square inch. Before fouling, a flow rate of 3.47 milliliters/minute (mL/min) was measured with a GE Sepa CF II Foulant system. After fouling with a 10% of yeast solution that was cooked in microwave until boiling, the flow rate was reduced to 0.128 mL/min in 15 minutes. The fouled membrane was then cleaned with an ultrasound beam of about 2.7 MPa (peak) at focus and 671 KHz. The beam has 300 cycles per burst with about 50 Hz pulse repetition rate for the bursts to avoid damaging to the transducer. The beam was scanned over the uncovered membrane surface at 1 mm/s speed with a table-top scanning system to clean the membrane. After the cleaning, the flow rate was restored partially to about 1.67 mL/min.

Discussion and Conclusions

This study shows the efficacy of focused ultrasound beams for membrane cleaning, potentially allowing transducers of relatively low power rating to be used.

6K-3

5:00 PM **Ultrasound Thermometry for Monitoring Internal Temperature Gradient in Heated Material**

Ikuo Ihara¹, Manabu Takahashi², ¹Mechanical engineering, Nagaoka University of Technology, Nagaoka, Niigata, Japan, ²Nagaoka University of Technology, Japan

Background, Motivation and Objective

In the fields of science and engineering, there are high demands for monitoring internal temperature and its distribution in a heated material. This is because such temperature is an important factor that is closely related to the material properties. Although some conventional techniques using thermocouples or infrared radiation are widely used for temperature measurements, they are not acceptable for the internal temperature monitoring. Ultrasound, because of its high sensitivity to temperature, is expected to be an alternative means for temperature measurements. The objective of this work is to develop a new ultrasound thermometry for monitoring internal temperature gradient in a material.

Wednesday
Oral

Statement of Contribution/Methods

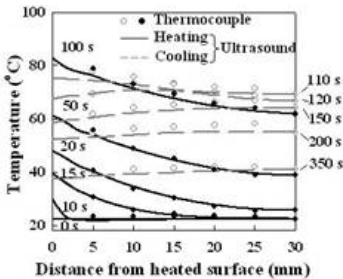
In this work, an effective ultrasonic technique for measuring internal temperature gradient is proposed and its practical feasibility is demonstrated through experiments with a steel plate under heating and cooling. The technique consists of an ultrasonic pulse-echo measurement and an inverse analysis coupled with a one-dimensional finite difference calculation. The advantages of the technique are that no boundary condition at the heating surface of a material is needed and the computation time is relatively fast for the temperature estimation.

Results

Ultrasonic pulse-echo measurements are performed for the steel plate of 30 mm thickness whose single side is heated by a heater of 200 °C and subsequently cooled down by water. The measured transit time of ultrasound across the steel is then used for the inverse analysis to determine temperature gradient in the steel. The variation in the estimated temperature gradient with elapsed time is shown in figure, where the estimated results by the ultrasonic technique are compared with those measured using thermocouples. The time shown in the figure denotes the elapsed time after the heating starts. It can be seen that the temperature gradient estimated ultrasonically and its variation almost agree with those measured using thermocouples.

Discussion and Conclusions

It is verified that the present ultrasonic technique provides an effective measurement of the internal temperature gradient in a heated material. This technique is expected to be an effective means for on-line monitoring of materials being processed at high temperatures.



6K-4

5:15 PM A quantitative assessment for the orientation and distribution of carbon fibers in the bipolar plate of fuel cell using high frequency ultrasound

Yi-Hsun Lin¹, Chih-Chung Huang², Shyh-Hau Wang^{1,1} Chung Yuan Christian University, Taiwan, ²Fu-Jen Catholic University, Taiwan

Background, Motivation and Objective

Conductive polymer composites fabricated by adding a certain amount of conductive fillers into a polymer substrate are commonly used as the material of the bipolar plate in fuel cells. The electrical conductivity of polymer composites is affected by the distribution and orientation of fillers and is therefore crucial to be assessed. This study is to develop methods and techniques for nondestructively measuring properties of carbon fibers in the conductive polymer composite using a 50 MHz high frequency ultrasound system.

Statement of Contribution/Methods

The experiments were carried out from samples, fabricated by an injection molding machine, composed of a 5x5 cm polycarbonate added with carbon fibers of 6µm diameter and 3mm length and those of weight percentage at 0, 0.1, 0.2, and 0.3%. The C-scan images corresponding to depths at 0.15 and 0.3 mm under the surface of conductive polymer composites were reconstructed. The orientation of filler carbon fibers parallel or perpendicular to the surface of conductive polymer composites were calculated according to their respective percentages of pixel content in the image.

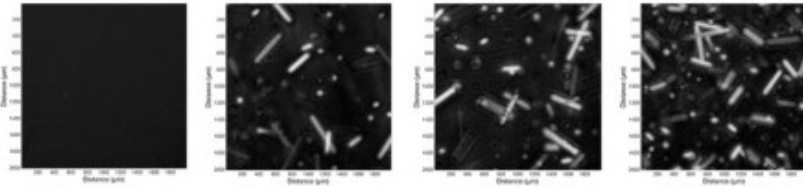
Results

Results showed that percentages of pixel contents for fillers of parallel orientation at the depth of 0.15 mm under the surface of sample for those 0.1, 0.2, and 0.3 wt% filler carbon fibers were calculated to be 2.50±1.13, 5.19±1.70, and 5.93±1.29, respectively, and those of 0.3mm were to be 2.91±1.46, 6.18±1.60, and 6.42±1.77,

respectively. Moreover, those percentages of pixel contents for fillers of perpendicular orientation with respect to depth of 0.15mm were 1.49 ± 0.89 , 2.49 ± 0.96 , and 3.62 ± 0.95 , respectively; those of 0.3mm were 1.39 ± 0.72 , 2.70 ± 0.62 , and 3.97 ± 0.94 , respectively. A highly linear relationship can be found between the calculated percentage of pixel content and the added carbon fiber concentration.

Discussion and Conclusions

This study demonstrated that current high frequency ultrasound image incorporated with the analysis method is feasible to be applied to quantitatively and rapidly assess the distributions of fillers in conductive polymer composites.



C-scan images of materials filled with 0, 0.1, 0.2 and 0.3wt% of carbon fibers (left to right)

6K-5

5:30 PM Characterization of Material Properties in Solid Oxide Fuel Cells using a Laser Ultrasound Technique

Sheng-Wei Tang¹, Che-Hua Yang²; ¹Institute of Mechatronic Engineering, National Taipei University of Technology, Taipei, Taiwan, ²Department of Mechanical Engineering, National Taipei University of Technology, Taipei, Taiwan

Background, Motivation and Objective

Solid oxide fuel cell (SOFC) has attracted much attention as a promising source of electrical power generation because of its high efficiency in converting chemical energy to electrical power. The main structure of SOFC is a three-layered structure with the electrolyte sandwiched by anode and cathode (Fig. 1). The ceramic materials make the SOFC capable of operating at elevated temperatures in the range of 500-1000 degree, however, also suffers from the difficulties in the control of geometrical and mechanical properties.

Statement of Contribution/Methods

This research is aimed at the characterization of anode and electrolyte properties in a nondestructive way. Plate-shape anode and electrolyte samples are tested. A procedure employing a laser ultrasound technique (LUT) together with an inversion algorithm is used to characterize the ceramic SOFC layer properties.

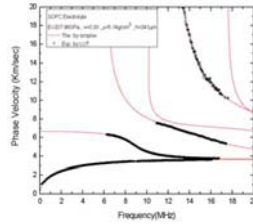
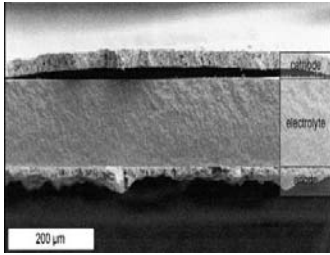
Results

Fig.2 shows the measured dispersion spectra for the electrolyte. Followed by the inversion algorithm, thicknesses and properties such as elastic moduli for the anode and electrolyte are obtained. Also shown in Fig. 2 are theoretical dispersion spectra calculated using the inversion-determined properties.

Discussion and Conclusions

While independent measurement using an optical microscope is used as a reference, the inversion-determined thickness has an accuracy of better than 1%. The obtained material properties are compared with those in the literature where destructive methods are employed. The determined Young's modulus shows errors of 3.9% for the anode and 1.9% for the electrolyte. The current research is leading towards to determining all the properties from a complete 3-layered SOFC structure after finishing the study in the current stage where each layer is treated separately.

Wednesday
Oral



6K-6

5:45 PM **Welding Characteristics of Aluminum, Copper, Nickel and Aluminum Alloy with Alumina Coating Using Ultrasonic Complex Vibration Welding Equipments**

Jiromaru Tsujino¹, Terumichi Murakoshi², Eiichi Sugimoto³:¹Kanagawa University, Yokohama, Kanagawa, Japan, ²YKK AP Co. Ltd, Kurobe, Toyama, Japan, ³Asahi EMS Co. Ltd, Tokyo, Tokyo, Japan

Background, Motivation and Objective

Ultrasonic complex vibration welding could be used for joining same and different metal and ceramics, and has superior quality compared with conventional welding with linear vibration locus. Welding of aluminum-copper, aluminum nickel plate specimens and aluminum alloy is essential for fuel cell, battery or EDLC electrodes for electric or hybrid automobile and other various industry fields.

Statement of Contribution/Methods

15 to 40 kHz complex vibration welding systems were developed using (1) multiple transducers integrated with a transverse vibration disk, (2) complex vibration converter with diagonal slits and (3) longitudinal-transverse vibration rod driven eccentrically by longitudinal vibration source shown in Figure 1. Elliptical to circular vibration loci are obtained at the welding tip and they are driven using 2 kW to 5 kW amplifiers. Required vibration velocity and damage by vibration fatigue are small compared with conventional welding.

Results

Welding characteristics of aluminum, copper, nickel and aluminum alloy plate specimens are studied. Structure of these welded areas are observed using SEM and TEM (transmission electron microscope). Figure 2 shows TEM images (100 nm) of cross sections of (1) aluminum-copper and (2) aluminum-nickel plate welded specimens. These specimens were joined directly without any inter-metallic compound, mutual diffusion and any different structures.

Discussion and Conclusions

Different metal specimens were welded directly without any special structure using the complex vibration welding equipments. Required vibration velocity was one-third to quarter compared with conventional welding and weld strength near to material strength was obtained independent of specimen position and direction, and multiple or continuous welding is possible.

Wednesday
Oral

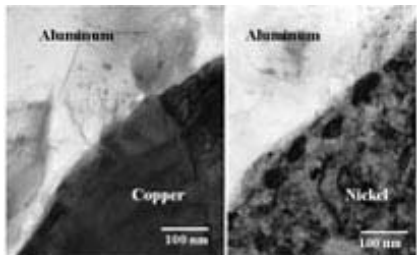


Fig. 2 TEM images of cross sections of welded aluminum-copper and aluminum-nickel plate specimens, welded using ultrasonic complex vibration welding.

Wednesday Poster Sessions

P3-A. Tissue Characterization

Sala Orange

Wednesday, September 23, 2009, 10:00 am - 11:30 am

Chair: **Michael Oelze**
University of Illinois

P3-A-01

Investigating Pseudoarthrosis With Ultrasound Backscattered Signals

Daniel Matusin¹, Wagner Pereira¹, Manoel Ferreira², Alberto Schanaider²; ¹Biomedical Engineering Program - COPPE, UFRJ, Rio de Janeiro, Rio de Janeiro, Brazil, ²Experimental Surgery, UFRJ, Rio de Janeiro, Rio de Janeiro, Brazil

Background, Motivation and Objective

Quantitative ultrasound (QU) has been well explored in the characterization of biological tissues. In the last decade QU has been applied bone quality studies (e.g., osteoporosis). Pseudoarthrosis, a disease related to bone quality, comes from a failure in the regeneration/consolidation process of bone fracture, resulting in non-union of fragments. Its diagnosis and follow-up is usually done by X-rays.

Backscatter parameters have demonstrated to be sensible to small variations of tissue microstructure (bone included). Nevertheless, their capacity in the characterization of the fibrocartilaginous tissue of the pseudoarthrosis lesion has not been explored.

This study aims to investigate the ability of two backscatter parameters (Apparent Integrated Backscatter – AIB, and Frequency Slope of Apparent Backscatter - FSAB) in differentiating normal and pseudoarthrotic bone from in vitro US signals.

Statement of Contribution/Methods

Three samples (one of each Wistar rat) of femurs with surgically produced pseudoarthrosis were used. The bone fracture was made by a saw and the tensor fasciae latae muscle was sewn between both fragments to prevent consolidation, leaving some level of movement between fragments.

The samples were immersed in physiologic serum at 25°C, in the focal region of a 5-MHz circular transducer (Panametrics V326) focalized at 40 mm. They were scanned in a plane parallel to their surfaces and the transducer was displaced in steps of half size of beam diameter in focal region. An average of five US signals was collected for each sample. A reference signal was also collected from a steel plate placed at the same distance of the sample. Signals were transferred to a PC where AIB and FSAB parameters were estimated.

Results

The average values of AIB and FSAB for normal bone was -45.6 ± 5.04 dB and 0.04 ± 0.24 dB/MHz, respectively while for pseudoarthrosis it was -37.6 ± 0.8 dB and -5.41 ± 4.37 dB/MHz. Both parameters are statistically significant using Kruskal-Wallis ANOVA.

Discussion and Conclusions

In our data, parameters AIB and FSAB were able to differentiate pseudoarthrosis from normal bone. AIB values for pseudoarthrosis were smaller compared with normal bone of the same sample. FSAB for normal bone was close to zero, different from previous studies where the scattering values diminish when frequency increases (trabecular bone). The number of signals per sample is limited compared with other studies because of the small acquisition sites and by the convex format of the bone diaphysis.

It was studied the behavior of AIB and FSAB obtained from US signals of normal and pseudoarthrotic bone samples; They were able to detect statistically significant differences between both conditions. This is a preliminary study and more data is now being collected. It is previewed the use of combined parameters to enhance the detection and characterization of pseudoarthrosis stages. This study envisages a future application in living subjects as a means to follow-up bone healing evolution.

P3-A-02

Multi-parametric Study to Identify the Hepatic Fibrosis Stages

Mahmoud Meziri¹, Pereira wagner Coelho de Albuquerque², Christiano Bittencourt Machado³, Naceur tiah⁴, Razika Bouzitoune¹, Frédéric Padilla², Pascal Laugier²; ¹Laboratoire LM2S, Université Badji Mokhtar, BP 12, Annaba, Algeria, ²Biomedical Eng. Program - COPPE, Federal University of Rio de Janeiro, Brazil, ³UPMC-Paris6, CNRS, Laboratoire d'Imagerie Paramétrique, 15 rue de l'École de Médecine, 75006, Paris, France, ⁴Département de Mathématiques, Université Badji Mokhtar, BP 12, Annaba, Algeria, ⁵University of Michigan, Department of Radiology, 1301 Catherine Street, Ann Arbor, MI 48109, USA

Background, Motivation and Objective

Ultrasonic parameters such as sound velocity (SOS), backscatter coefficient (Bc), attenuation coefficient (Ac), mean scatterer spacing (MSS) and spectral slope (SS), ... have shown their potential to differentiate between healthy and pathologic samples in different organs (eye, breast, prostate, liver...). Recently, our group has looked into the characterization of hepatic fibrosis stages using the parameters cited above. The results have shown that none of them was able to individually differentiate between the different stages. Therefore, our aim is to explore a multi-parametric approach by combining these parameters to test their potential to discriminate between the liver fibrosis stages F0, F1, F3 and F4 according to Metavir Score.

Statement of Contribution/Methods

The radiofrequency (RF) signals backscattered from 20 specimens were acquired with an acoustic backscatter microscopy system with a 20-MHz frequency transducer. Ultrasonic parameters were then evaluated. First, a classification of functions was evaluated for the most pertinent parameter. Second, we have built all combinations of pairs. A discriminant analysis, standard method, was applied to test the best combination to discriminate the fibrosis stages

Results

The classification of the functions has shown that the most relevant individual parameter was Bc followed by SOS, SS, MSS and Ac, respectively. The discriminant analysis has shown that the combinations of (Bc, SOS) or (Bc, Ac) were the best to differentiate between the fibrosis stages and have correctly classified 85% of the liver samples with a high significant level ($p < 0.0000$).

Discussion and Conclusions

Our multi-parametric study has shown the capacity of (Bc, SOS) or (Bc, Ac) ultrasonic parameter combinations to discriminate between all fibrosis stages. It is interesting to note that Ac alone has the worst performance among the parameters; however, when combined with Bc, it forms the best pair. Combination of more than 2 parameters, though possible, is not supposed to be used in this case, due to the small number of samples. These results are a good indication that association of tissue parameters can play an important role to aid in the liver fibrosis diagnosis.

P3-A-03

Artificial skin classification with high frequency ultrasound radio-frequency signal analysis using self-organizing map

Takahiro Iwamoto^{1,2}, Yoshifumi Saijo³, Naohiro Hozumi⁴, Kazuto Kobayashi⁵, Nagaya Okada⁶, Akira Tanaka⁶, Makoto Yoshizawa^{7,1}; ¹Tohoku University, Japan, ²Research Fellow of the Japan Society for the Promotion of Science, Japan, ³graduate school of Biomedical Engineering, Tohoku University, Japan, ⁴Aichi Institute of Technology, Japan, ⁵the Research and Development Headquarters, Honda Electronics Co. Ltd., Japan, ⁶Faculty of Symbiotic Systems Science, Fukushima University, Japan, ⁷Cyber Science Center, Tohoku University, Japan

Background, Motivation and Objective

In the past decades, noninvasive and high-resolution visualization of skin structures within the dermis and hypodermis has become possible due to the development of high-frequency ultrasound (HFUS) imaging systems. HFUS system allows high-resolution cross-sectional imaging and is a less expensive, noninvasive, non-ionizing imaging tool compared to radiology and magnetic resonance imaging tool.

Besides conventional gray-scale B-mode echo-image analysis, tissue characterization of skin by analysis on the radio-frequency (RF) ultrasound signal was also investigated by several groups.

In the present study, ultrasonic tissue characterization for cultured skin, Vitrolife-Skin®, is proposed by analyzing spectra of RF ultrasound signal from HFUS imaging system. And by applying self organizing map (SOM) for tissue classification.

Statement of Contribution/Methods

The HFUS imaging system, which realizes high resolution B-mode imaging of tissue, was developed by our group. A spherically focused, single-element broadband ultrasound PVDF transducer, which enables high resolution B-mode imaging of the tissue, is used for imaging. The transducer has a nominal center frequency of 100 MHz, a focal length of $z_0=3.2\text{mm}$, and aperture diameter of $D=2.4\text{mm}$.

RF signals of HFUS imaging system from artificial skin were digitized and stored into a workstation. Saline is used as sound propagation medium between the transducer and skin surface. Frequency spectrum of each 128-points was calculated using a fast Fourier transformation. Further, the calculated spectra were used to compute 8 spectral parameters. We used SOM, a neural network approach to the data clustering, for data classification.

Results

We prepared 400 spectra from each of three regions, which were dermis, epidermis, and background regions, of the artificial skin. 80 percents of the total of 1200 spectra were used for training data and rests were used for test data for the SOM classifier. Finally, the average sensitivity and specificity of classified area by the SOM classifier were 90.4% and 97.9% respectively for the training data, and 86.3 % and 93.9% respectively for the test data.

By using the SOM classifier, cross-sectional skin image was segmented by four colors, which are learned three areas and other area (unlearned area).

Discussion and Conclusions

In conclusion, spectral parameters are useful for classification of epidermis and dermis in the artificial skin model. These results suggest that the proposed technique is useful for automatic classification of structures of the artificial skin model. This system could be useful for the noninvasive and nondestructive evaluation tool of skin.

P3-A-04

Periodicity estimation under variations of scatterers spacings, thickness and pulse frequency: a 2D simulation study

Christiano Bittencourt Machado¹, Mahmoud Meziri², Wagner Coelho de Albuquerque Pereira³, Frédéric Padilla⁴, Pascal Laugier⁵, ¹Laboratoire d'Imagerie Paramétrique, Université Pierre et Marie Curie, Paris, France, ²Laboratoire LM2S, Université Badji Mokhtar, Algeria, ³Biomedical Engineering Program - COPPE, Federal University of Rio de Janeiro, Brazil, ⁴Department of Radiology, University of Michigan Medical Center, USA, ⁵Laboratoire d'Imagerie Paramétrique, Université Pierre et Marie Curie, France

Background, Motivation and Objective

Bone quantitative ultrasound characterization has been extensively explored in the last decades, mainly with the purpose of osteoporosis diagnosis. Several techniques and acoustic parameters were applied with reasonable efficiency, but the use of the mean scatterer spacing (MSS) to assess the trabecular bone status is not yet well explored. MSS can be estimated by spectral analysis methods, and it has been applied to many types of tissues. The aim of this study was to evaluate MSS responses to scatterer spacings (SS) variations (V%), transducer central frequency (f_0) and scatterers thickness (ScTh) by 2D simulations, as a first approach to study the cancellous bone microarchitecture.

Statement of Contribution/Methods

Propagation medium was modeled as seven 1.0-mm thick solid cylindrical scatterers (six SS) with MSS's of 0.8 and 1.2 mm, with bone elastic constants, immersed in water. Several situations were simulated (150 signals each), using the custom-made software SimSonic2D (using a finite-difference time-domain method). It was used transmission f_0 of 1 and 3.5 MHz (pulse lengths of 4.28 and 1.26 mm in water, respectively). V% of 0, 10, 20 and 30% were applied, as well as a gaussian variation on ScTh (mean = 0.08 mm). To estimate MSS, it was applied the Spectral Autocorrelation (SAC), the Singular Spectrum Analysis (SSA), the quadratic transformation (SIMON) and the Multiple Signal Classification (MUSIC). For statistical analysis, Student t-tests ($\alpha = 0.05$) were used.

Results

For a simulated MSS = 0.8 mm, methods estimated values from 0.9 to 1.9 mm at 1 MHz. However, at 3.5 MHz, they obtained approximate values, for all jitter values. For a simulated MSS = 1.2 mm, in both frequencies the methods can provide good estimations. The estimations often did not follow a Gaussian distribution ($p > 0.05$), and multimodal histograms were observed. The variation of ScTh did not alter significantly MSS estimates in almost all cases ($p > 0.05$).

Discussion and Conclusions

As indicated in literature, tissue periodicity characterization seems to be difficult with only the parameter MSS, since there can be multimodal histograms from the estimates. With a pulse length of 4.28 mm (1 MHz), it was possible to separate SS in the order of 1.2 mm, but not of 0.8 mm. According to other works, trabecular spacings range from 0.2 to 1.5 mm, so, the best analysis frequency may be between the two tested in this work. The variation in trabecular thickness may not play a role in the variation in MSS estimates.

P3-A-05

Integrated reflection coefficient correction with respect to surface inclination and axial distance

Nils Maennicke^{1,2}, Martin Schoene^{1,2}, Kay Raum^{1,2}; ¹*Q-BAM group, Dept. of Orthopaedics, University Halle-Wittenberg, Halle (Saale), Germany*, ²*Berlin-Brandenburg School for Regenerative Therapies, Charité Campus Virchow-Klinikum, Berlin, Germany*

Background, Motivation and Objective

The Integrated Reflection Coefficient (IRC) has been shown to be an important US parameter for tissue characterization. However, the IRC suffers from large variations within samples that vary in inclination and axial distance to the transducer. In this work the dependence of the IRC on these surface parameters is investigated and applied as a correction to native samples. Assuming that the reflection coefficient is homogenous within a test sample, a valid correction should reduce the variance of the IRC. The ultimate goal of this work is to reduce the variation introduced by the IRC in order to more confidently reach statistical conclusions regarding the tissue morphology.

Statement of Contribution/Methods

A planar reflector was measured and simulated with varying inclinations and axial distances at 40 MHz. For the simulation, Field II was used to model a pulse echo from a plane with a width of 1.5 mm at angles of 0 to 10 degrees and axial distances of 7 to 12 mm. The experiment was performed as Bz-scans of an agar phantom with axial distances of 7 to 12 mm and angles of 0 to 9 degrees. For both setups the focal length was 9.2 mm with a lateral -6dB width of 125 μ m. Resulting IRCs of both datasets were fitted by a polynomial of degree 3 and used as a correction function, normalized to the IRC of the focus and without inclination. The validity of the IRC correction when applied to real data is exemplified by applying the fits to 6 C-scan measurements of healthy cartilage tissue on tibia plateaus obtained from sheep. Regions of interest in the sample were arranged as a grid with a lateral width of 150 μ m. Their corresponding inclination and axial distance were deduced from the time of flight of the first echo above a threshold.

Results

The mean IRC of the samples was -46.48 ± 7.68 dB. Applying the polynomial fits from experimental and simulated reflectors changed the average IRC to -37.02 ± 5.92 dB and 36.83 ± 6.47 dB, respectively. The average decrease of the standard deviation of the IRC after the fit was 1.76 ± 1.05 dB and 1.21 ± 0.86 dB. The models showed an average agreement of $R^2 = 0.39$ and $R^2 = 0.28$ with the native samples.

Discussion and Conclusions

A correction model for surface inclination and distance to the transducer appears to decrease the variance of the IRC. The results indicate that the experimental model shows a more effective adjustment to the data than the simulated model, however both corrections seem to improve the accuracy of the IRC. Optimizing the models by measuring a larger variation of surface inclinations will lead to further improvement of the correction.

P3-A-06

Supersonic Shear Waves Generation in Soft Tissue

Andrey Rybyanets¹, Maria Lugovaya², Anastasia Rybyanets^{2,3}; ¹*South Federal University, Russian Federation*, ²*Physical Faculty, South Federal University, Russian Federation*

Background, Motivation and Objective

The use of supersonic shear waves for real time visualization of soft tissue viscoelastic properties has recently been reported. Ultrasound focused beams were employed for remote ultrasonic generation of a shear source moving at a supersonic speed inside the body. The purpose of the present paper is a modelling and experimental study of a supersonic shear waves generation in soft tissue.

Statement of Contribution/Methods

In present paper a new technique for supersonic shear wave generation in soft tissue is described. The technique is based on cyclic generation of discrete off-axis focal zones with a predetermined space location and rotation of these focal zones around acoustic axis of HIFU transducer at optimal angular frequency. Shear waves remotely induced by the radiation force of a focused ultrasonic beam in each focal zone are constructively interfere creating intense Mach "spiral" structure. Modeling of acoustic field patterns for different HIFU transducer array configurations as well as supersonic shear wave propagation were performed.

Results

An experimental setup comprising HIFU transducer array, controller and multi-channel driving circuitry was designed and successfully applied in vitro for different tissues and phantoms. HIFU transducer array for generating off-axis focal zones was designed as a spherical piezoelectric cap divided circumferentially into plurality of "N" regular sectors. The controller was coupled to the multi-channel drive circuitry and configured to simultaneously drive all "N" transducer sectors with respective drive signals that have phase shift values being based upon a predetermined temporal function. For continuous rotation of off-axis focal zones around acoustic axis of HIFU transducer the controller simultaneously excites all sectors while leaves at least one sector dormant and successively changes which element is dormant with appropriate rate corresponding to shear wave propagation velocity.

Discussion and Conclusions

Intensive low frequency supersonic shear wave in adipose tissue in vitro and in vivo were detected experimentally using specially designed measurement cell equipped by shear deformation piezoelectric sensors. Possible applications of a new technique for diagnostic and therapeutic applications were considered.

P3-A-07

Signal Analysis for estimating mechanical properties of viable cells using Acoustic GHz-Microscopy

Sebastian Brand^{1,2}, Eric Strohm³, Michael Kolios³, Kay Raum²; ¹Fraunhofer Institute of Material Mechanics, Halle, Germany, ²Department of Orthopaedics, University of Halle, Halle, Germany, ³Department of Physics, Ryerson University, Toronto, Canada

Background, Motivation and Objective

The current study aimed on the method development for the estimation of mechanical properties of individual biological cells. Cells investigated ultrasonically were kept under culture conditions and no chemical markers have been applied in order to not alter the cells chemical conditions. For the estimation of mechanical properties namely thickness and sound velocity ultrasonic waves in the GHz range have been used. The major benefit of employing acoustic GHz-microscopy is the contact-free and therefore non-destructive mode of operation in combination with a lateral resolution in the 1 μ m range.

Statement of Contribution/Methods

The acoustic GHz-microscope employed tone-burst pulses of 20 ns duration at a frequency of 1 GHz. Unprocessed radio frequency (rf) -echo signals of HeLa cells have been acquired. Signals were processed using a numerical deconvolution technique which has proven to be reliable and robust in low-frequency ultrasonic applications. Applying this technique echo positions of the cell membrane and the substrate were computed. Using the echo position of the cell membrane versus the position of the substrate outside the cell the local cell thickness was derived. Cell thickness estimates in combination with the substrate echo recorded behind a cell lead to the estimation of the local sound velocity inside an individual cell. For verification of acoustically estimated thickness values cell thicknesses have also been estimated using laser scanning microscopy and scanning electron microscopy.

Results

Individual cells showed varying thicknesses with values ranging from 5 μ m to 15 μ m depending on the cell topography. Sound velocities however varied in a range between 1600 m/s and 1800 m/s. Thickness estimates of scanning laser microscopy and ultrasonic GHz-microscopy are in acceptable agreement. Results of the scanning electron microscopy are currently under evaluation but preliminary results support the ultrasonically obtained estimates.

Discussion and Conclusions

It was noticed that the cell-thickness estimation shows a higher accuracy in regions of the cells nucleus vs. the surrounding cytoplasm. That fact may be caused by the much smaller thickness of the cell in extra-nuclear regions of adhering cells. Thickness values obtained by laser scanning microscopy showed an artefact at the cells nuclear region, however the values obtained at both edges of the nucleus agree well with the ultrasonically obtained data. The current study contributes towards the estimation of cellular changes of individual cells during chemo-therapy and the development of a low-frequency technique for an in-vivo monitoring of treatment responses in cancer therapy.

P3-A-08

Quantitative Ultrasound for Evaluating Human Cervical Microstructure

Lisa Reusch¹, Kibo Nam¹, Helen Feltovich^{1,2}, Mark Kliewer³, Josephine Harter⁴, **Timothy Hall**¹:¹Medical Physics, University of Wisconsin - Madison, USA, ²Maternal Fetal Medicine, Allina Hospitals & Clinics, USA, ³Radiology, University of Wisconsin - Madison, USA, ⁴Pathology, University of Wisconsin - Madison, USA

Background, Motivation and Objective

Preterm birth rates are increasing alarmingly in the face of ineffective therapies. Collagen alignment in the cervix contributes to cervical strength and undergoes rearrangement long before gross changes (shortening, softening) can be seen, thus understanding cervical microstructure seems paramount to understanding cervical dysfunction. A quantitative assessment of these changes in women has been challenging due to a lack of noninvasive technology sophisticated enough to interrogate the microstructure of the cervix. We explored quantitative ultrasound techniques for detection of cervical collagen using prototype catheter transducers with diameters about the size of the cervical opening.

Statement of Contribution/Methods

Hysterectomy specimens were scanned with two prototype catheter transducers (Siemens). Radiofrequency (RF) data were acquired with the endocervical canal parallel to the transducer face. The angle between the acoustic beam and tissue was used to assess anisotropic acoustic propagation by electronic control of transmit and receive angles from -40° to $+40^\circ$. A region of interest (ROI) was selected (locations varied to assure result consistency) and the RF signals computed for each angle. Similar data from a phantom with spherical scatterers was used for system calibration.

Results

Power spectra of the backscattered RF signals from the cervix were higher at normal incidence (beams perpendicular to tissue) than beams steered to large angles regardless of ROI position. The spectral shapes for normal and steered beams were nearly identical, suggesting absence of a frequency-dependent absorption or scattering effect. While both the backscattered power from the control phantom and the cervix decreased with increasing steering angle, the difference in power was larger from the cervix compared to the control phantom. The difference in the backscattered power loss, comparing the cervix to the phantom data, was statistically significant for all steering angles beyond 5° . This excess power loss is consistent with scattering from an aligned cylindrical structure (i.e. collagen).

Discussion and Conclusions

This approach reliably and noninvasively detects a cylindrical, aligned component of cervical microstructure. Collagen is overwhelmingly the most likely candidate. Further studies will aim to definitively identify and quantify this component throughout pregnancy. Early detecting of changes in microstructure may open pathways to earlier, more specific interventions for preterm delivery.

P3-A-09

Development of an Ultrasonic Steatosis Index for the Evaluation of Fatty Liver Disease

Magali Sasso¹, Véronique Miette¹, Laurent Sandrin¹:¹R&D department, Echosens, Paris, France

Background, Motivation and Objective

Steatosis designates the intracellular accumulation of fat in liver. The worldwide prevalence of steatosis is very high (from 20 up to 80%) and is associated with several risk factors such as obesity, diabetes, alcohol, viral hepatitis. In many cases, steatosis can be accompanied with liver hepatitis which might induce cirrhosis. Biopsy is the gold standard for steatosis assessment. However, biopsy has a potential sampling error, is invasive and might

induce severe complications. Furthermore, steatosis is a silent condition and the decision for the hepatologist to refer to biopsy is often difficult.

Fibroscan® is an ultrasound-based transient elastography system that can be used for the diagnosis of liver fibrosis and cirrhosis by measuring the liver stiffness.

The objective of this work is to demonstrate the feasibility of a novel Ultrasonic Steatosis Index using our vibration-controlled transient elastography device.

Statement of Contribution/Methods

An Ultrasonic Steatosis Index (USI) has been developed based on the ultrasonic properties of the radio-frequency back-propagated signal. This index is evaluated between 25 and 65 mm, in the same zone as the liver stiffness measurement using the M-probe of the Fibroscan®.

The ability of this index has been evaluated in a retrospective study including 345 patients in four etiologic groups: 171 with Viral Hepatitis C, 64 with Viral Hepatitis B, 56 with alcoholic and 55 with non-alcoholic liver disease. All patients' livers were assessed using both Fibroscan® and histology. Steatosis was quantified on the biopsy as the percentage of hepatocytes with macrovesicular accumulation of fat (S0: 0% of hepatocytes, S1: 1~10%, S2: 11~33%, S3 > 34%).

Performance of the USI is appraised using the AUROC (Area Under the Receiver Operating Curve), taking the histological quantification of liver steatosis as gold standard.

Results

Using the USI, AUROC is equal to 0.84 and 0.93, in alcoholic and non-alcoholic liver disease, respectively, for the detection of more than 34% of steatosis (S3).

In VHC (VHB, resp.) AUROC is equal to 0.73 (0.82, resp.) for the detection of more than 1% of steatosis, 0.92 (0.93, resp.) for the detection of more than 11% of steatosis and 0.90 (0.93, resp.) for the detection of more than 34% of steatosis.

Results indicate that the USI might detect steatotic liver from 10% of cells infiltrated with fat.

Discussion and Conclusions

This preliminary study shows the potential of the USI to diagnose hepatic steatosis. A larger retrospective clinical study is currently conducted in 830 patients (700 VHC, 90 with alcoholic liver disease and 40 with non-alcoholic liver disease) where some threshold would be determined for the quantification of steatosis. In addition, the influence of steatosis on the liver stiffness measurement will be analysed.

The combination of both USI and liver stiffness measurement evaluated using the Fibroscan® might discriminate patients from simple steatosis to patient with steatohepatitis lesions.

P3-A-10

High Resolution Ultrasonic Method for 3D Fingerprint Recognizable Characteristics In Biometrics Identification

Anna Maeva¹, Fedar Seviaryn², Eugene Bakulin²; ¹University of Windsor, Windsor, Ontario, Canada, ²University of Windsor, Canada

Background, Motivation and Objective

Biometrics is an important and rapidly evolving method for personal identification based on ones unique biological characteristics. Its primary application is restriction of access to areas, information and personal data. Several techniques have been utilized; fingerprint, hand shape, retinal scanning and facial recognition, thermographic imaging, etc. Fingerprint recognition stands out due to low cost, accuracy and a well-developed operation of a historically accumulated large database.

Statement of Contribution/Methods

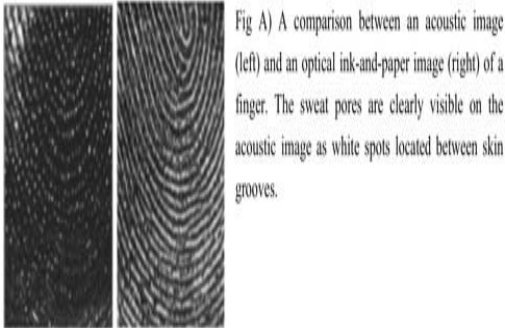
This paper describes further developments of fingerprint imaging by proposing a new method for characterizing not only the imprint but also key features of the tissue. The method is based on an acoustic microscopy approach where a two-dimensional image is formed from acquiring reflected signals by scanning using a focused ultrasonic transducer. Varying the C-scan gate position and width gives the ability to visualize acoustic reflections from any appropriate depth inside the skin. In particular, distribution of sweat pores can be easily visualized by setting the C-scan gate right under the skin surface. This provides additional means of personal identification unaffected by the fingers' surface conditions.

Results

The device output is a high resolution 3D set of data containing information not only about the imprint surface but also defining characteristics of the finger itself such as sweat pores, marks and scars. Also, the system is able to differentiate between an artificial finger from a carcass and a living being. The method allows adhering similar characterization techniques for the fingernail and its underlying surface, which provide even more valuable information for identification.

Discussion and Conclusions

This new method of acoustic characterization allows for the imprint of a fingerprint to be obtained with high-resolution, minimal mess and time. An acoustic image can be compared to a paper imprint and processed in existing databases. Further development of this method and corresponding apparatus will provide reliable and convenient identification technique for wide variety of applications.



P3-A-11

Intravascular Ultrasound (IVUS) as a Potential Tool for the Arthroscopic Assessment of Articular Cartilage

Yong-Ping Zheng¹, Yan-Ping Huang¹; ¹The Hong Kong Polytechnic University, Hong Kong, China, People's Republic of

Background, Motivation and Objective

Ultrasound has been recently demonstrated to be a potential tool for assessment of earlier degeneration of cartilage using acoustic, morphological, and mechanical properties. Intensive studies have showed that these properties are correlated to the status of cartilage degeneration. However, up to now no miniaturized ultrasound transducer has been specifically designed and commercialized for the arthroscopic use, particularly with imaging functions. In this study, intravascular ultrasound (IVUS), which is originally designed for imaging blood vessels, was introduced as a potential tool for quantitative evaluation of cartilage.

Statement of Contribution/Methods

An IVUS system (Volcano) with a catheter-based probe was used to measure the thickness and surface acoustical reflection amplitude from normal bovine patellar articular cartilage disks ($n = 16$), and the results were compared before and after degeneration induced by enzyme treatments (trypsin, $n=8$ and collagenase, $n = 8$). Similar measurement was also performed using an ultrasound biomicroscopy system (Vevo 770) and the results obtained by the two systems were compared.

Results

The thickness measured using IVUS was highly correlated ($r = 0.985$, $p < 0.001$) with that obtained by Vevo (Fig. 1). IVUS measurement showed that after enzyme digestions the cartilage thickness did not have a significant change ($p > 0.05$) but there were a significant reduction of the surface reflection amplitude ($p < 0.05$) for both enzyme digestions, with a larger effect from the collagenase treatment. Measurement performed by Vevo confirmed these results.

Discussion and Conclusions

The current results obtained by IVUS were consistent with previous studies using high frequency ultrasound. IVUS has a small transducer with the size of 1 mm in diameter and with the function of high resolution ultrasound imaging. Therefore, it is proper for use where the space is limited and tissue imaging is necessary. Therefore, IVUS can be recommended for the quantitative assessment of articular cartilage, with its ready-to-use arthroscopic feature. Its in vivo operation inside a joint should be further investigated in future studies.

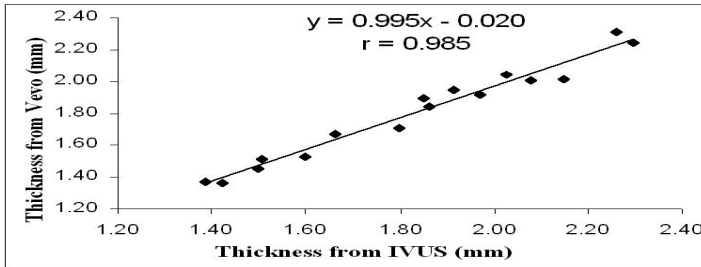


Fig. 1 Correlation of thickness measurement from two ultrasound systems before enzyme treatments

P3-A-12

Improved estimation of parameters of the homodyned K distribution

David Hruska¹, William D. O'Brien, Jr.¹, Michael Oelze¹; ¹University of Illinois at Urbana-Champaign, USA

Background, Motivation and Objective

The amplitude distribution of the envelope of backscattered ultrasound is dependent on tissue microstructure. By fitting measured envelope data to a model, parameters can be estimated to describe properties of underlying tissue. The homodyned K (HDK) distribution is a general model that encompasses scattering situations modeled by the Rice, Rayleigh, and K distributions. However, parameter estimation for the HDK distribution is not straightforward because the model is analytically complex. Furthermore, effects of frequency-dependent attenuation on parameter estimates need to be assessed.

Statement of Contribution/Methods

An improved parameter estimation algorithm was developed to efficiently estimate parameters of the HDK distribution, i.e., the μ (effective number of scatterers per resolution cell) and k (ratio of coherent to diffuse energy) parameters. Parameter estimates were found by fitting estimates of SNR, skewness, and kurtosis of fractional-order moments of the envelope with theoretical values.

To assess effects of attenuation, the resolution cell was modeled as a cylinder with a radius and height each proportional to the acoustic wavelength. The effects of frequency dependent attenuation were approximated by assuming a Gaussian pulse to determine the shift in center frequency of the pulse and hence change in volume of the resolution cell. Computational phantoms were created with varying attenuation coefficients and scanned using a simulated $f/4$ transducer with a center frequency of 10 MHz. An average of two scatterers per resolution cell (based on the phantoms with no attenuation) was used.

Results

The new estimation algorithm was tested and compared with an existing algorithm (based on the even moments of the HDK distribution). The new estimation algorithm was found to produce estimates with lower bias and variance. For $\mu=2$ and k ranging from 0 to 2, the average variance in the estimated μ and k values were 0.067 and 0.0069 for the new algorithm and 0.42 and 0.048 for the old algorithm, respectively. Estimate bias was also reduced with the new algorithm.

In the simulations with no attenuation, the μ parameter estimate was 2.53 ± 0.18 . In the phantoms with a linear attenuation coefficient of $0.5 \text{ dB} \cdot \text{MHz}^{-1} \cdot \text{cm}^{-1}$, the estimate was 4.64 ± 0.54 . This compared well with the predicted μ value of 4.98.

Discussion and Conclusions

The improved parameter estimation algorithm allowed the analytically complex HDK distribution to be used effectively to model the envelope of backscattered ultrasound.

The results of the simulations suggest that attenuation can substantially alter estimates of the number of scatterers per resolution cell. By better understanding these effects, it is hoped that effects of attenuation can be compensated. This work was supported by NIH Grant R01CA111289.

P3-B. Imaging Methods

Sala Orange

Wednesday, September 23, 2009, 10:00 am - 11:30 am

Chair: **Tom Thomas**
Boston Scientific

P3-B-01

3D Regularized Speed-Map Reconstruction in Ultrasound Transmission Tomography

Radovan Jirik¹, Igor Peterlik¹, Jiri Jan¹, Michael Zapf², Nicole Ruiter²; ¹Dept. of Biomedical Eng., Brno University of Technology, Czech Republic, ²IPE, Forschungszentrum Karlsruhe, Germany

Background, Motivation and Objective

Ultrasound transmission tomography is a potentially promising alternative to standard X-ray imaging in medical diagnosis, especially in mammography, mainly due to the non-ionizing character of ultrasound and high information content of the measured signals that could potentially result in high-resolution imaging. Sound speed is one of diagnostically significant parameters related to tissue pathology. Sound speed images could be directly used for diagnosis or for correction of reflectivity imaging using UCT.

Statement of Contribution/Methods

Reconstruction of sound-of-speed (SOS) maps from data recorded with a 3D ultrasound transmission tomograph is investigated. Algebraic reconstruction technique is used. Large overdetermined system of linear equations is formed from line integrals corresponding to each sender-receiver combination. The equation system is regularized and solved as non-linear least-squares problem. The main contribution is the solution of the problem of fairly sparsely distributed transducers and high noise level by extending a published method of 2D regularization in transmission tomography (based on edge-preserving potential related to total variance regularization in image deconvolution) to 3D and applying it to ultrasound transmission tomography.

Results

The 3D reconstruction has been implemented using Matlab Distributed Computing Toolbox. It has been tested on synthetic data and on real data measured with a 3D ultrasound transmission tomography prototype using a human breast phantom. During the reconstruction, 632832 equations were assembled to reconstruct a volume divided into 28800 voxels. The resulting spatial SOS map followed the object shape and the estimated velocity values were in accordance with the expected range.

Discussion and Conclusions

To reconstruct a reasonable image, the use of regularization was essential due to sparse transducer distribution and noise. In the classical approach of filtered backprojection with heavily interpolated projections, the neighboring projection samples would be assumed to be related. Here, the transducer sparsity is approached by assuming neighboring voxels of the reconstructed image to be related. This is a more realistic assumption. Furthermore, the character of the used regularization leads to preserved edges, to some extent. Finally, the time needed for the reconstruction could be reduced considerably when employing distributed computing resources.

P3-B-02

Adaptive Spatial Compounding for Ocular Imaging

Leo Pan¹, Robert Rohling¹; ¹University of British Columbia, Canada

Background, Motivation and Objective

Ultrasound (US) imaging of the eye is useful for several clinical applications ranging from assessing risk of glaucoma to monitoring corneal diseases such as keratoconus and Fuchs dystrophy. There is a need for portable, hand-held systems using low-cost conventional transducers so that US eye examinations can be performed more easily and widely, but such systems have difficulty depicting specularly-reflecting surfaces, such as the cornea.

Spatial compounding (SC) by beam steering may solve this problem with the tradeoff of blurring. Adaptive spatial compounding with warping (ASCW) was developed to solve these problems while retaining the benefits. The main objective of this work is to determine whether ASCW produces depictions of the cornea and lens that are un-blurred and independent of angle.

Statement of Contribution/Methods

Ten bovine eyes were obtained within 5 hours of slaughter and placed in a water bath. A linear array transducer (L12-5W, Ultrasonix Medical Corporation, Canada) was used to acquire pre-scan converted data along 10 slices spaced 2.3mm apart. For each plane, 9 data sets were obtained through electronic steering over a range of $\pm 12^\circ$. Two parameters of the ASCW (search region and search block size for the warping registration) were optimized for eye imaging and kept constant for all tests. SC images and ASCW images were compared to the conventional uncompounded image. In order to assess image quality automatically, a metric was devised. The cornea in each image was fitted with a circle to determine the center point, from which 11 lines, at 5° increments, were drawn outward to intersect the cornea and the pixel intensity values along each line are recorded. The intensity curves at the cornea and the lens were then separately fitted by Gaussian function to determine the FWHM. A thin sharp response with small deviation along the surface is considered ideal.

Results

The FWHM of the cornea, expressed as mean (standard deviation) in mm are: conventional=0.4841 (0.0821), SC=0.8859 (0.1743), and ASCW=0.4719 (0.07251). The standard deviation (SD) of the corneal FWHM are: conventional=0.2280 (0.07950), SC=0.4454 (0.1179), and ASCW=0.1305 (0.02382). The FWHM of the lens are: conventional=0.7272 (0.09752), SC=1.085 (0.1038), and ASCW=0.8553 (0.09473). The SD of the lens FWHM are: conventional=0.2353 (0.07486), SC=0.3658 (0.2936), ASCW=0.2652 (0.09548). Paired t-tests were performed and the results showed that ASCW's outperformed the conventional method in corneal FWHM SD, tied in corneal FWHM and lens FWHM SD, and showed higher value in lens FWHM. ASCW outperformed SC in all four categories.

Discussion and Conclusions

Based on the performed analysis, ASCW is a promising method for improving imaging of the eye with a conventional transducer.

P3-B-03

2D Noninvasive Acoustical Image Reconstruction of a Static Object through a Simulated Human Skull Bone

Kiyanoosh Shapoori¹, Jeff Sadler², Eugene Malyarenko³, Fedar Seviaryn², **Roman Gr. Maev**⁴, ¹Tessonics Inc., Windsor, Ontario, Canada, ²Department of Physics, University of Windsor, Windsor, Ontario, Canada, ³Tessonics Corp., Birmingham, MI, USA, ⁴Institute for Diagnostic Imaging Research, Windsor, Ontario, Canada

Background, Motivation and Objective

Timely, on-site diagnostics of life-critical brain injuries facilitates administration of medical treatment and greatly increases survivability. This work aims at the development of a portable, non-invasive ultrasonic transcranial examination tool for use by battlefield first responders and emergency crews. Despite its potential usefulness, practical realization of this imaging modality faces significant challenges due to high attenuation and scattering of ultrasonic waves by the human skull.

Statement of Contribution/Methods

A new ultrasonic imaging method for 2D image reconstruction of foreign substances in the brain, i.e. any reflectors existing in the brain tissue, such as hematomas, bone fragments, pieces of shrapnel, etc. is under investigation. The method is based on noninvasive transcranial ultrasound propagation through skull bone and brain tissue. In what follows, the mathematical theory of the method and the preliminary results of computer modeling and laboratory testing are presented. A simulation has been developed to predict the scattering behavior of acoustical fields transmitted through a human skull bone and also to process the data from experiment and reconstruct an image showing the position of the foreign object. The new algorithm has been designed to work with a linear array of 128 receivers, a simulated skull bone (scattering medium) and a reflector as a secondary source of ultrasound (all at the optimized frequency of 1.7MHz). To experimentally check the validity of the algorithm, a skull phantom was prepared for use in the laboratory tests. After passing through the phantom layer, the secondary ultrasound field originated from the reflector is recorded by the array of receivers. Then, the detected field distribution is signal processed to compensate for the distortion by the scattering layer and to reconstruct an image containing data about the reflector's position.

Results

Due to high attenuation of ultrasonic waves in the skull bone and brain tissue, it has been determined that the method works as an efficient reconstruction system for the reflector's position at a maximum distance of 15cm from the array of receivers, at 1.7MHz, which is far enough to cover all inside of a typical human skull.

Discussion and Conclusions

The algorithm combining the time reversal and matched filtering approaches has been successfully applied to the reconstruction of point-like and extended reflectors. The reconstructed images demonstrated adequate lateral resolution at distances ranging from one half to double the array length.

P3-B-04

Displacement Vector Measurement based on Two-dimensional Modulation Method with Hyperbolic Scanning

Tsuyoshi Shiina¹, Kengo Kondo², Makoto Yamakawa³; ¹Graduate School of Medicine, Kyoto University, Kyoto, Kyoto, Japan, ²Graduate School of Systems and Information Engineering, University of Tsukuba, Japan, ³Advanced Biomedical Engineering Research Unit, Kyoto University, Japan

Background, Motivation and Objective

Measurement of multidimensional displacement is required for quantitative imaging of blood-flow and tissue movement. The lateral modulation method proposed by Jensen et al. is a unique approach to obtain lateral displacement by generating a laterally oscillating RF signal. However, the method is basically designed for linear scan mode and requires large-sized aperture for measuring the wide area, consequently it is not suited to small-sized probe. We propose a method for 2-D displacement measurement which is applicable for small-sized aperture for cardiovascular diagnosis by designing a suitable beam scan path and lateral modulation.

Statement of Contribution/Methods

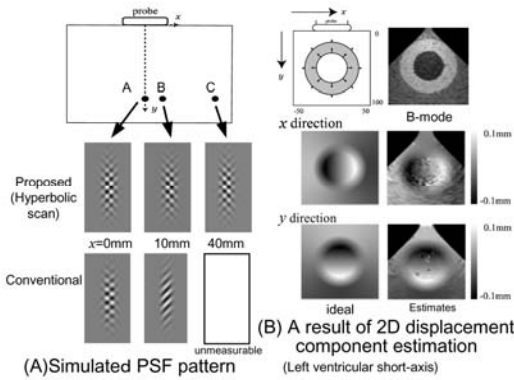
In the lateral modulation approaches, laterally oscillating signals is generated by a specific apodization function with two peaks, and the proper size of aperture increases in proportion to the depth to keep a constant precision. Although separable point spread function (PSF) is desired, the PSF is distorted far from the center of the aperture. We propose a method of continuously focusing on a hyperbola using a synthetic aperture beam-forming approach. The phase difference between the spherical waves generated at two foci of the hyperbola is constant at any point on the hyperbola. As a result, the proposed method yields the same PSF pattern at any point with fixed aperture size regardless of the lateral position or the depth. To measure 2D displacement from 2D-RF signals, we extended 1D Combined Autocorrelation (CA) Method proposed for tissue elasticity imaging to the 2D-CA method.

Results

Results of simulation verified that the PSF even far from the center of the aperture was not distorted in our proposed method. The left ventricular motion was also simulated, and the displacement vector distribution was estimated by proposed method. The result proved that the estimate of displacement vector components coincided highly with the ideal image as shown in figure.

Discussion and Conclusions

We proposed a new approach for measuring 2D displacement vector by producing separable and uniform 2D oscillating PSF over the entire image with small-sized aperture. The validity of the hyperbolic scan method and the effectiveness of the 2D-CA method with hyperbolic scanning were demonstrated by simulation of displacement vector estimation. In the next stage, we will verify the applicability of the proposed method by phantom experiments.



P3-B-05

Tissue Characterization Using Optically Assisted Ultrasonic Velocity-Change Imaging Method

Hironichi Horinaka¹, Satoshi Ishibashi¹, Daisuke Sakurai¹, Hajime Sano¹, Tetsuya Matsuyama¹, Kenji Wada¹, Toshiyuki Matsunaka^{1,2} *Physics and Electronics, Osaka Prefecture University, Sakai, Osaka, Japan*

Background, Motivation and Objective

We have already proposed the optically assisted ultrasonic velocity-change imaging for medical diagnosis. This method was applied to construct the ultrasonic velocity change images of the chicken meat phantom including the gold nano-rods or the ICG (indocyanine green) which individually had specific optical absorption spectra of the near-infrared region. Temperature change converted from the measured ultrasonic velocity change corresponded to the optical absorption properties of light-absorbing materials. This means that the optical absorption property can be obtained from the ultrasonic velocity-change due to light illumination.

In this study, we considered experimentally the possibilities of application of the optical assisted ultrasonic velocity-change imaging method to tissue characterization.

Statement of Contribution/Methods

Diode lasers with 660, 780, 813 and 910nm were used as light sources because the optical absorption of biological tissue was low in the wavelength region from 700nm to 950nm. The light was guided by the optical fiber around the array transducer to illuminate the phantom. In addition, the halogen lamp attached by the optical filter was used as a light source emitting the near infrared light which was absorbed into water and fat. The phantom was made of the chicken meat including beef fat.

Results

The ordinary B-mode image of the phantom is shown in Fig.1 (a). The fat distribution is not clear in Fig.1 (a). The ultrasonic velocity-change image obtained after illumination of 40 seconds is shown by gray scale in Fig.1 (b). The ultrasonic velocity-change profile along the line A-B is also shown in upper part of Fig.1 (b).

Discussion and Conclusions

The temperature change rate of the ultrasonic velocity in water is +2m/s degree and that in fat is -4m/s degree in bodily temperature. The ultrasonic velocity increases in muscle and internal organs with high percentage of water content and decreases in fat.

In the ultrasonic velocity change profile in Fig.1 (b), the negative velocity change area corresponds to the distribution of fat in the chicken meat.

Experimental results showed the possibility that the biological tissue could be characterized using the optically assisted ultrasonic velocity-change imaging method.

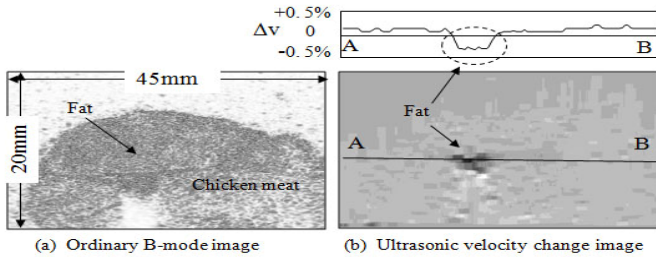


Fig. 1 Ultrasonic images of chicken meat including fat

P3-B-06

Speckle removal from heterogeneous-tissue signals using independent component analysis

Tadashi Yamaguchi¹, Tomoyuki Iwashina², Jonathan Mamou³, Naohisa Kamiyama⁴, Hiroyuki Hachiya^{5,1} *Research Center for Frontier Medical Engineering, Chiba University, Chiba, Japan, ²Graduate School of Advanced Integration Science, Chiba University, Chiba, Japan, ³F. L. Lizzi Center for Biomedical Engineering, Riverside Research Institute, New York, USA, ⁴Ultrasound Systems Division, Toshiba Medical Systems Corp., Tochigi, Japan, ⁵Graduate School of Engineering, Tokyo Institute of Technology, Tokyo, Japan*

Background, Motivation and Objective

In several diseases, tissue features that would enable distinguishing diseased tissue intermingled with healthy tissue is difficult or impossible because of the masking effects of speckle. Independent component analysis (ICA) is being investigated as a means of reducing the detail-masking effects of speckle. This study evaluates the effects of the ultrasound-beam and system properties on the ability of ICA to improve visualization of fine tissue structures by reducing speckle.

Statement of Contribution/Methods

The ICA algorithm requires two input signals. The first input signal is the tissue signal; it has two independent components: the signal reflected from diseased tissue structures and the speckle signal. The second input signal is a reference speckle signal; it is obtained from a tissue-mimicking reference phantom that generates speckle similar to that of normal tissue, and fabricated to match the attenuation, speed of sound, and speckle of normal tissue. The ultrasound beam and system properties were varied, and the two input echo signals were acquired for a wide range of settings on clinical US diagnostic equipment. The center frequency was varied between 2 and 6 MHz; the focal distance was varied between 20 and 80 mm; and the receiver gain was varied between 72 and 88 dB. The ICA-algorithm was tested on patients (mammary gland calcification and liver fibrosis) and phantoms. Performance in terms of fine-structure visualization was evaluated as a function of ultrasonic parameters by the S/N ratio calculated by comparing two output results from different second inputs.

Results

In most cases, ICA processing enabled separation of the speckle signal from the other large signal components. Therefore, diseased tissues and vessel walls that were masked by speckle and were difficult to visualize in the original image were more-clearly visualized on the image generated using the ICA method to remove the speckle contribution. The sizes of the extracted structures depended on the ratio of the speckle sizes between the two inputs. Similar results were obtained when focal depths were varied. Changing the receiver gain had no effect on performance. However, when the ICA method was applied in a highly attenuating medium, more than two independent components were returned and fine-scale speckle-masked structures were poorly visualized in the ICA-derived images.

Discussion and Conclusions

Results were consistent with theory predicting ICA to be independent of linear gain change. Furthermore, ICA performed successfully when the acoustical parameters of the phantom input were equivalent to those observed on normal tissues, and satisfactory results were obtained when the speckle size of both inputs were similar. However, when attenuation was higher in the test material than in the speckle-reference phantom, then ICA incorrectly corrected for speckle in the superficial and deep parts of each input signal. The automatic gain compensation will heighten the precision of ICA.

Wednesday
Poster

Enhancement of Muscle Visualization in Ultrasonography Using Gabor Filter Bank

Yong-Jin Zhou¹, Yong-Ping Zheng¹; ¹The Hong Kong Polytechnic University, Hong Kong, China, People's Republic of

Background, Motivation and Objective

In the study of musculoskeletal tissues, sonography yields anatomic information during both active and passive muscle contractions. It has been widely used to measure the changes in fascicular geometry, such as muscle thickness, muscle fiber pennation angle and fascicle length. The traditional way of manual sonogram reading for these parameters suffers from several drawbacks, such as operator fatigue and operator bias. In previous study, we have reported an automatic pennation angle estimation method using Hough transform, of which the performance is closely related to the image quality. In this study, we focus on the enhancement of longitudinal oriented patterns of muscles in sonograms, to enhance the performance of automatic measurements of muscle morphological changes.

Statement of Contribution/Methods

Since the muscular bundles are hypoechoic and the perimysiums surrounding fascicles are hyperechoic, in longitudinal view, sonograms of major muscle bundles, such as those of biceps and gastrocnemius muscle, often exhibit an alternating pattern of bright and dark with rather coherent orientation tendencies. Inspired by these apriori visual clues, we used Gabor filter bank to enhance the sonograms. Gabor filters have both frequency-selective and orientation-selective properties and have optimal combined resolution in both spatial and frequency domains. The proposed method comprised three steps, including orientation field estimation using Rao's method, frequency map computation and Gabor filtering. We applied this technique to biceps and gastrocnemius sonograms.

Results

The method was first evaluated using a simulated image distorted with multiplicative speckle noises, where the "muscles" were arranged in a bipennate fashion with a central "aponeurosis". After the enhancement using the proposed method, 92.3% of the original hyperechoic bands in the simulated image could be recovered and the noises in other locations were eliminated. The results of biceps gastrocnemius sonograms also demonstrated that proposed method is effective for the enhancement of the visualization of muscle structures. Fig 1 shows a typical image of biceps before and after the enhancement.

Discussion and Conclusions

This study demonstrated that using Gabor filter bank to enhance muscle visualization in sonogram is feasible. Further development for real-time processing is being continued.

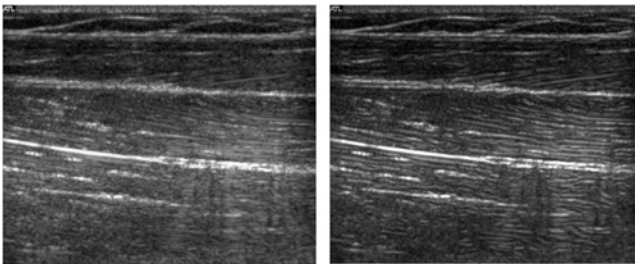


Figure 1. (a), original image, (b) enhanced

P3-B-08

Mechanisms of Image Quality Improvement Utilizing Harmonic Imaging

Gianmarco Pinton¹, Jeremy Dahl², Gregg Trahey², ¹Langevin Institute (CNRS UMR 7587), ESPCI ParisTech, INSERM, Paris, France, ²Biomedical Engineering, Duke University, Durham, NC, USA

Background, Motivation and Objective

Although harmonic imaging is used extensively, the mechanisms for image quality improvement are still poorly understood. In the simplified case of a homogeneous medium the improvements in harmonic imaging can be linked to reductions in the main lobe width and the height of side lobes. It has been suggested, however, that the primary benefit of harmonic imaging is reduction of clutter noise and less sensitivity to phase aberration. This requires complex simulations or experiments that incorporate the effects of tissue heterogeneities and multiple scattering, which has imposed significant challenges in describing and quantifying the mechanisms of image quality improvement with harmonic imaging.

Statement of Contribution/Methods

We investigate and quantify the losses in image quality for fundamental and harmonic imaging due to three sources of image quality degradation using a novel numerical algorithm that simulates ultrasonic propagation in a medium with heterogeneities in nonlinearity, attenuation, density, and speed of sound. The numerical simulations generate the full pressure waveforms at every point in the simulated field and therefore allow great flexibility in calculating the ultrasound images and PSFs. This numerical implementation models the fine structure of human tissue and the arrangement of the tissue in the human body. The simulation of a 2.1 MHz diagnostic transducer through a measured representation of the human abdominal layer generated the transmit-receive PSFs.

Results

A comparison of the theoretical and simulated power spectrum of the backscatter from a field of randomly distributed scatterers in the Rayleigh regime is presented. Transmit-receive PSFs were calculated for a typical 0.6 fractional bandwidth ultrasonic pulse. These PSFs distinguish between clutter occurring in the isochronous volume, in the region preceding the pulse, and in the region trailing the pulse.

Discussion and Conclusions

There are three distinct conclusions that can be drawn from the presented data. First the primary source of image degradation in the fundamental PSF comes from reverberation in the near-field abdominal structures. Measurements of the reverberation clutter alone indicate that it is 26 dB higher for the fundamental PSF compared to the harmonic PSF and that it is the single largest source of clutter. Second phase aberration is the largest source of clutter in the harmonic PSF. When phase aberration is removed using a uniform velocity and unchanged impedance medium the harmonic PSF exhibits an 11 dB improvement in the isochronous volume, which is significantly larger than the 0.9 dB improvement from reverberation clutter subtraction. Finally clutter in the PSFs occurs primarily from low level contributions distributed over a large area, especially in the fundamental PSF where plots of the radial distribution show no appreciable decrease with increasing distance.

P3-B-09

Automatic Real-time View Detection

Sten Roar Snare¹, Svein Arne Aase¹, Ole Christian Mjølstad¹, Håvard Dalen¹, Fredrik Orderud², Hans Torp¹
¹Circulation and Medical Imaging, NTNU, Trondheim, Norway, ²GE Vingmed Ultrasound, Oslo, Norway

Background, Motivation and Objective

With the introduction of smaller, portable and handheld devices, it is expected that ultrasound scanners will be used in the general practitioners office. Thus, a new and less experienced user group is expected. Algorithms to aid the user during the examination and analysis should be developed.

This work presents an algorithm capable of classifying an echocardiographic view as either an apical two chamber view, four chamber view or long axis view. It also provides a score on the overall image quality.

Statement of Contribution/Methods

The algorithm is based on a deformable non uniform rational B-spline (NURB) model updated in an extended Kalman filter framework. Models are constructed for each of the three standard views. The model pose and position of the control points become states in the Kalman filter. The model is updated using a combination of edge and speckle-tracking measurements, where weak edges and edges strongly deviating from their neighbor edges are discarded. The most probable standard view is found using feature detection and general successfulness in detecting edges. The apical four chamber is mainly recognized by the presence of a right ventricle. The apical long

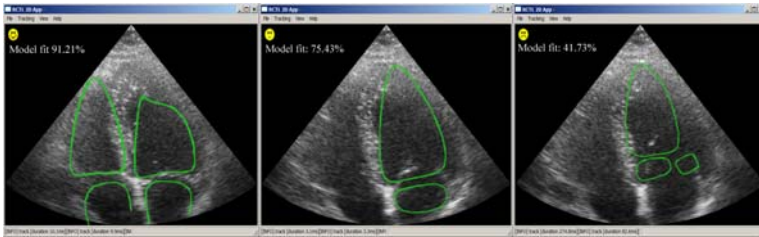
axis is identifiable by the aortic outlet tract. The percentage successfully detected edges is used as a measure of overall view quality.

Results

The algorithm has been trained and validated using 68 recordings from the Norwegian HUNT database. An echocardiographer classified each recording as one of three standard views. 33 randomly chosen recordings, with approximately 10 of each view, were used for training. The other 35 recordings were used for validation. The algorithm successfully classified the view in 30 of 35 cases (85.7%). Each classification is accompanied by a score, which can be used to assess image quality. The figure below illustrates how the models are fitted to a standard four chamber view, where the four chamber model receives a score of 91%, the two chamber 75% and the long axis model 42%. The model is thus classified as a four chamber view, and the score of 91% indicates a good image quality.

Discussion and Conclusions

An algorithm for separating between the three standard echocardiographic apical standard views has been developed and tested successfully. The method is general and can be extended to other standard views. It can hopefully become a helpful tool for the untrained user of ultrasound equipment.



P3-B-10

CREASIMUS: a fast simulator of ultrasound image sequences using 3D tissue motion

Adrien Marion¹, Didier Vray^{1,†} University of Lyon, CREATIS-LRMN; CNRS UMR5220; INSERM U630; University Lyon 1; INSA-Lyon, France

Background, Motivation and Objective

Data simulation is an important research tool to evaluate algorithms. Two types of methods are currently used to simulate medical ultrasound (US) data: those based on an acoustic model such as Field II, Ultrasim or Dream and those based on the Meunier & Bertrand's convolution model. The Field II simulation is more realistic than the convolution-based simulation because it uses a PSF that depends directly on the physical parameters. However, its main drawback is the high computation time, which is a strong limitation to simulate image sequences of tissue or blood motion. The purpose of the paper is to propose a fast simulator of sequences of US data with 3D moving scatterers.

Statement of Contribution/Methods

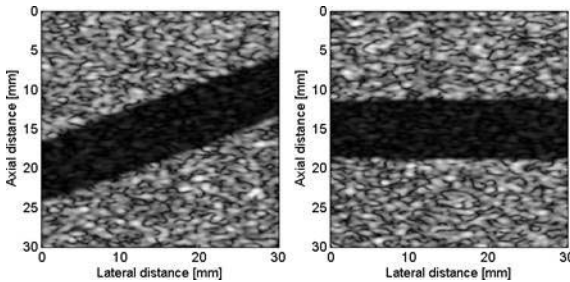
Assuming several hypotheses, Meunier & Bertrand suggested using a 2D convolution instead of a 3D convolution to reduce computation time. This proposition is severely limited since all scatterers remain within the imaging plane during a moving sequence. In this paper, we propose projecting scatterers onto the imaging plane before using a 2D convolution. The projection preserves the distance between the scatterers and the transmitter to avoid the loss of phase information. Furthermore, amplitudes are weighted to account for the azimuthal shape of the PSF. The scatterers are then approximated to a sampled grid before to be convolved with the 2D PSF.

Results

We show that our simulator provides realistic data in terms of first- and second-order statistics. We also study the influence of the size of the grid mesh on the simulated image. With a standard mesh, the computation time required to create an image of 1040*400 pixels with 130,000 scatterers is approximately equal to 0.27 s. Our simulator is available on demand. The user has only to provide to the simulator the PSF, the parameters of the sequence (image size, number of images, frame rate) and the scatterers' positions for each time, which can be calculated from a finite element model for example. The modification of the simulation parameters directly affects simulated images. We simulated in Fig. 1 some blood flow sequences at 5 MHz to illustrate results obtained with our simulator.

Discussion and Conclusions

We presented in this paper a fast simulator based on a 3D convolution methodology to simulate large sequences of US data. In our research work, these US image sequences are used to evaluate motion estimation and segmentation algorithms.



P3-B-11

Compensation of the Transducer Response

Jinhyoung Park¹, Changhong Hu¹, Dawei Wu¹, Qifa Zhou¹, K.Kirk Shung^{1,2} Biomedical Engineering, University of Southern California, Los Angeles, California, USA

Background, Motivation and Objective

Many approaches have been studied for the enhancement of penetration depth and spatial resolution in ultrasonic imaging. It has been shown that depth of penetration may be enhanced with coded excitation and a windowed chirp has been applied as a transmission method. A drawback of windowed chirp imaging is that it needs wideband transmission in high frequency.

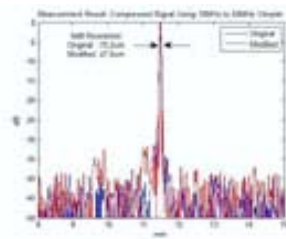
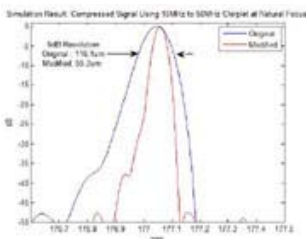
Statement of Contribution/Methods

A novel approach in which the windowed chirp transmission is inverse filtered with the impulse response of transducer was investigated. A focused LiNbO3 single element transducer at 30MHz center frequency with a 16 MHz of bandwidth is used. The impulse response of the transducer is acquired by pulse-echo measurements. The frequency of the Hanning windowed chirp is from 10MHz to 50MHz. Both the windowed chirp and the impulse response of transducer are Fourier transformed and the frequency response of the windowed chirp is divided by the frequency response of the response of transducer. This divided signal is inverse Fourier transformed to convert to the time domain. The resulted signal is used as new windowed chirp. The proposed method is evaluated with a high frequency ultrasonic imaging (UBM) system. The new windowed chirp is used as transmit using function generator. The echo signal is compressed by windowed chirp. The approach is also tested using Field II

Results

The experimental data shows that the received signal without compensation for the transmitted signal has frequency component only from 15 MHz to 50 MHz. Upon the the proposed approach, the received signal almost all frequency components from 10MHz to 50MHz are preserved. The resolution of the compressed signal without compensation is 70.2 μm which is improved to 47.0 μm following compensation. This agrees with simulation result

Discussion and Conclusions



P3-B-12

Asynchronous Telemedicine with Ultrasound: Improving Maternal Health in Developing Countries

Michele Solano¹, Eung-Hun Kim², Mark Christiansen², Cornie Scheffer³, Thomas Easterling⁴, Lut Geertz⁵, Kirk Beach⁶, **Yongmin Kim**^{2,1}*School of Nursing, University of Washington, Seattle, WA, USA.* ²*Bioengineering, University of Washington, Seattle, WA, USA.* ³*Mechanical Engineering, Stellenbosch University, Stellenbosch, South Africa.* ⁴*Obstetrics & Gynecology, University of Washington, Seattle, WA, USA.* ⁵*Obstetrics & Gynecology, Stellenbosch University, Stellenbosch, South Africa.* ⁶*Surgery, University of Washington, Seattle, WA, USA*

Background, Motivation and Objective

The UN selected improving maternal health as Millennium Development Goal #5. To achieve this goal, Maternal Mortality Ratio (MMR), the number of maternal deaths per 100,000 live births, has to be reduced substantially. In Sub-Saharan Africa, MMR is about 100 times higher than that in developed countries. Delays in seeking help, transporting to or receiving appropriate care upon arrival to a facility can be ameliorated by expanding access to routine prenatal ultrasound (US) in these regions. The objective of this study is to assess the feasibility of an electronic medicine system facilitating collaboration between specialists in maternal-fetal health and midwives new to obstetric ultrasound.

Statement of Contribution/Methods

Using a web-based asynchronous telemedicine system for consultation enabled by information and communication technology, our system consists of a portable US machine (SonoSite MicroMaxx®) and an Internet-capable laptop (Dell 530) both deployed in South Africa, and the main server (IBM x345) located at the University of Washington. We deployed the system in late 2008 and evaluated it with a midwife in South Africa and three OB/GYN specialists in the U.S. The midwife acquired US images from pregnant women and uploaded them via the laptop to a secure website hosted by the server. Asynchronous communication between the midwife and OB/GYN specialist consisted of direct annotation on US images using colored lines, shapes and free text associated with each case. A specialist's review consisted of 1) inspection of each US image, 2) annotation of key features (e.g., fetal lie and dating measurements) and 3) responding to queries from the midwife.

Results

During the 2-month study period, the system received 114 review requests for 91 women. A total of 704 US images were uploaded for 114 consultation cases. A total of 1,166 annotations were added to those 704 images. Specialists noted 25 "high-risk" conditions associated with 15 patients, which included breech presentation (9), fetal malformation and growth restriction (9), gestational diabetes (3), placenta previa (2), multiple gestation (1), and intra-uterine infection (1). Feedback from all the users indicated satisfaction with system reliability and operation. A midwife made good progress in learning essential US techniques and communicated effectively with specialists.

Discussion and Conclusions

Findings suggest that 1) it is technically feasible to expand routine availability of prenatal ultrasound to populations with restricted access to this service and 2) a midwife can be successfully coached in obstetric ultrasound acquisition and interpretation skills via a web-based asynchronous educative system. We believe that ultrasound imaging could play a major role in reducing the maternal mortality in developing countries. However, non-technical issues, e.g., how to scale up and business model, remain to be tackled.

P3-B-13

Efficient Arbitrary Volume Reslicing for Pre-Scan-Converted Volume in an Ultrasound Backend

Junqing Shang¹, Ravi Managul^{2,3}, Yongmin Kim^{1,2,1}*Electrical Engineering, University of Washington, Seattle, Washington, USA.* ²*Bioengineering, University of Washington, Seattle, Washington, USA.* ³*Hitachi Medical Systems of America, Twinsburg, Ohio, USA*

Background, Motivation and Objective

Several 3D ultrasound modes, e.g., multiplanar reconstruction (MPR) and tomographic ultrasound imaging (TUI), utilize arbitrary volume reslicing to generate 2D planes that are not usually available with traditional 2D ultrasound. There are two approaches for arbitrary volume reslicing (AVR), i.e., pre-scan-converted (pre-SC) or post-scan-converted (post-SC). For post-SC AVR, 3D SC is firstly performed to generate a post-SC volume, and then 2D AVR planes are generated from this volume. On the other hand, pre-SC AVR avoids the 3D SC step and directly uses the pre-SC volume to generate 2D AVR planes. AVR is typically performed on a PC system external

to the ultrasound frontend and backend, but the need to transfer the pre-SC volume from the ultrasound backend to the PC increases the response time. In this paper, we present an efficient pre-SC AVR algorithm in an ultrasound backend system. The backend supports AVR natively with other backend functions, so the PC system does not need to compute 2D AVR planes from 3D volumes.

Statement of Contribution/Methods

We used *in vivo* and synthetic datasets to evaluate the pre-SC and post-SC approaches. Computation and input/output requirements were estimated based on different viewing parameters. We also optimized the computation by a lookup table approach that pre-computes inversely-mapped addresses and coefficients as well as utilizing data-level parallelism and intelligent data loading and storing. We mapped the pre-SC AVR on a multi-core processor, Cell, which is used as the embedded computation unit for backend and 3D ultrasound processing inside an ultrasound machine.

Results

The post-SC AVR involves two steps, 3D SC and 2D AVR plane generation, where each step involves interpolation for resampling. On the other hand, the pre-SC AVR generates 2D AVR planes in one step, thus retaining more details due to less blurring introduced. The differences between two approaches depend on the spatial frequency content in pre-SC volume. RMSE was calculated to evaluate the differences. We evaluated the differences as a function of the spatial frequency in synthetic data. A larger difference can be observed when the frequency is high. *In vivo data* generally contain low frequency information, so the difference was smaller. Using one of eight computation cores in Cell, our algorithm generated a 1024×768 16-bit 2D image in 30.2 ms with a 512×136×64 16-bit input volume. Seven other cores are utilized for other backend and 3D functions, so all the modules of backend and 3D ultrasound processing including pre-SC AVR can run in the same backend system. If we use all eight cores in Cell, the AVR execution time is less than 5 ms.

Discussion and Conclusions

We developed an AVR algorithm that efficiently generates output images from pre-SC volumes. We compared it with post-SC AVR and mapped it on an ultrasound backend system rather than supporting it in a separate PC.

P3-B-14

Volume Rendering Algorithms for Three-Dimensional Ultrasound Imaging: Image Quality and Real-Time Performance Analysis

Ravi Managuli^{1,2}, Kerem Karadayi³, Canxing Xu¹, Yongmin Kim⁴, ¹Department of Bioengineering, University of Washington, Seattle, WA, USA, ²Hitachi Medical Systems of America, Twinsburg, Ohio, USA, ³Department of Electrical Engineering, University of Washington, Seattle, WA, USA, ⁴Department of Bioengineering and Electrical Engineering, University of Washington, Seattle, WA, USA

Background, Motivation and Objective

The real-time 3D ultrasound (US) volume rendering is challenging due to the large amount of computation required. Many rendering techniques have been developed, e.g., shear-warp, shear-image-order, pre-integration and direct-ray-casting. Each of these techniques has the pros and cons in terms of image quality, artifacts and computational efficiency. In this paper, we will compare the major rendering algorithms in terms of algorithm complexity and image quality. Also, we will present our new rendering algorithm, called pre-integrated-shear-image-order (PISIO), which overcomes the image-quality limitations of current algorithms while achieving real-time performance.

Statement of Contribution/Methods

The image quality achieved via each of these algorithms is compared in terms of the ability to preserve fine details and potential artifacts. We used a conventional rendering pipeline, consisting of a $3 \times 3 \times 3$ boxcar filter to preprocess the data, followed by shading, classification and rendering stages. For each algorithm, we used several 3D *in vivo* dataset as well as synthetic data to evaluate the artifacts and access the fine details in the rendered images. We also mapped our new algorithm on IBM's Cell multi-core processor to demonstrate its real-time performance.

Results

Direct-ray-casting is computationally very expensive due to its complex data handling and incoherent memory access pattern. Shear warp is the fastest, but suffers from aliasing and venetian-blind artifacts and fine details are lost. Pre-integration with shear-warp overcomes the aliasing artifact with a slight increase in computation but cannot preserve details and venetian-blind artifacts remain. The shear-image-order preserves details and removes venetian-blind artifacts while maintaining storage-order data access, but suffers from aliasing artifacts. Our new

algorithm tries to combine the advantages of both pre-integration and shear-image-order algorithms. This new algorithm enjoys computing advantages while preserving details and overcoming aliasing and venetian-blind artifacts. In addition, we found that by upsampling the input US volume by 2x in the depth direction, we can achieve image quality similar to that of direct-ray-casting. We incorporated this algorithm on a Cell processor, and found that more than 40 vols/s can be achieved for a 1923 volume using all the 8 SPEs on a single Cell processor.

Discussion and Conclusions

Since ultrasound systems are increasingly developed using programmable processors, such as Intel's core 2 and TI's C64x, our analyses can help system developers decide upon an algorithm that best meets the system requirements. In addition, the pre-integrated shear-image order algorithm is shown to overcome image artifacts while achieving real-time performance. In the next step, we plan to evaluate this algorithm for multi-volume rendering, such as, BW with power, BW with velocity, as well.

P3-B-15

A Real-Time Ultrasound Imaging System for Assessing Airway Wall Mechanics In-Vitro

Adam LaPrad¹, Arnab Majumdar¹, Bela Suki¹, Kenneth Lutchen¹, Thomas Szabo¹; ¹Biomedical Engineering, Boston University, Boston, MA, USA

Background, Motivation and Objective

Excessive airway constriction is a defining characteristic of asthma, but little is known about what mechanical conditions can transition the airway into this highly contractile state. Measurements of airway responses to induced constriction and pressure fluctuations simulating breathing have been limited to indirect or invasive optical methods at one cross-section along the airway length. The goal of this work was to design a real-time, non-invasive system for measuring airway wall mechanics in-vitro.

Statement of Contribution/Methods

We developed a complete ultrasound imaging measurement system for characterizing luminal diameter, wall thickness, wall stiffness, and active stress in intact airways. Using a portable ultrasound imaging system, a 7 MHz broadband ultrasound transducer was partially submerged in a fluid-filled tissue bath and mounted over the center axis of the fluid-filled intact airway in the longitudinal orientation. Transmural pressure oscillations to simulate breathing were delivered to the airway via a hydrostatic pressure column and computer-controlled syringe pump. Airway constriction was induced with acetylcholine added to the tissue bath (ACh, 10^{-5} M) while ultrasound videos were acquired (20 s, 8 fps). Each frame was processed with an edge detection algorithm to determine the airway wall inner and outer boundaries, from which luminal diameter and wall thickness were calculated for the full airway length. Using thick-walled cylinder stress equations, we also estimated the Young's modulus of the airway wall and the active stress developed by the airway smooth muscle.

Results

During induced airway constriction, the ultrasound system was able to fully characterize the dynamically changing airway wall mechanics along the full airway length. Luminal diameter decreased in parallel with increases in wall thickness, Young's modulus, and active stress. The validity of these measurements was confirmed via independent experiments in a force-length stretching apparatus using a strip of airway wall tissue. Also, we determined that our boundary detection algorithm resulted in underestimation of luminal diameter and overestimation of wall thickness (errors less than 5%). The errors were due to the pulse width thickness, which varied with depth due to focusing, absorption through the airways walls, and the nonlinear grayscale mapping in the image. A correction scheme was devised, based on radio frequency data, which accounts for these variables when calculating luminal diameter and wall thickness from the wall boundaries.

Discussion and Conclusions

This work demonstrates the feasibility of characterizing airway mechanics in response to pressure fluctuations simulating different breathing sequences and bronchoconstrictors. Our developed system is a novel research approach to determine the causes of excessive airway narrowing in asthma, and can also be applied to measuring arterial mechanics in health and disease.

Filtering and Scan Conversion of 3D Displacement Vectors from a 4D Curvilinear Transducer

Eric Pospisil¹, Robert Rohling¹; ¹Electrical and Computer Engineering, University of British Columbia, Vancouver, British Columbia, Canada

Background, Motivation and Objective

Recent advances in elastography and cardiac strain imaging on motorized curvilinear array transducers now provide axial, lateral and elevational displacement measurements in 4D (real-time 3D). When calculating displacements from such dual-radius transducers, scan conversion must convert both the measured 3D displacements and their locations into Cartesian coordinates (CC) at the rate of data acquisition. Although quasi-3D scan conversion methods exist, such as two sequential 2D conversion steps, there is a need for a computationally-efficient 3D vector scan conversion method for curvilinear transducers. Curvilinear 4D transducers pose unique problems for geometrically-correct non-aliased scan conversion.

Statement of Contribution/Methods

Displacement vectors obtained using time domain cross-correlation of radiofrequency data were created in the transducer coordinate (TC) system of R, θ, ϕ , where R and θ were measured about the transducer array center, and ϕ about the motor's axis of rotation – hence a dual-radius system. The 3D vector scan conversion performed component-wise trilinear interpolation of data in TC, using a backwards-mapping approach. The mapping from CC to TC was similar to a mapping from CC to spherical coordinates, but also utilized the orthogonal distance from the array center to the motor's axis to transform a given point P from CC to TC. CC displacements were found by displacing P in TC by the interpolated TC vector components, and then mapping the displaced point Q from TC to CC. The displacement was then obtained by subtracting P from Q in CC. The anti-aliasing filter was sized by comparing the sample spacing in TC to the output resolution. Linearly separable Gaussian filters were applied in R, θ , and ϕ individually. The variance of the filter was determined as a function of R in the θ and ϕ directions to maintain a constant spatial filter size in CC.

Pre-computed look up tables were used for trigonometry, the Gaussian filters, and coordinate mapping to realize significant speedup.

Results

Geometric accuracy was confirmed in AutoCAD Inventor by revolving a sector scan about a line to form a known geometrically correct volume, and using the measurement tools to validate both the mapping and vector conversion of the results from scan conversion. The implementation was found to be geometrically correct to floating point accuracy. The filters prevented aliasing for any choice of output data spacing in CC. Calculations on standard PC hardware took less than 26 ms for 10 frames of 100 scan lines of 80 displacement measurements.

Discussion and Conclusions

This research shows that it is feasible to implement full 3D scan conversion of 3D vector data with geometric accuracy on standard hardware at the rate of ultrasound data acquisition. This work is a key step for 3D elastography inversion methods using a 3D finite element models.

P3-C. Beamforming

Sala Orange

Wednesday, September 23, 2009, 10:00 am - 11:30 am

Chair: **Peter Hoskins**
Univ. of Edinburgh

P3-C-01

Preserving Speckle Statistics in Minimum-Variance Beamformed Images: the Effectiveness of Spatial Compounding.

Francois Vignon¹, Michael Burcher^{1,1} *Philips Research North America, Briarcliff Manor, NY, USA*

Background, Motivation and Objective

Data-dependent apodization techniques such as the minimum-variance beamformer (MVB) can beat the diffraction limit of the conventional Delay-and-Sum (DAS) beamformer, yielding enhanced resolution and contrast. However, the MVB algorithm strongly increases the speckle variance. This needs to be compensated in order for the MVB algorithm to be clinically successful. This paper evaluates the effectiveness of Spatial Compounding, an established technique for reducing speckle variance, in addressing this issue.

Statement of Contribution/Methods

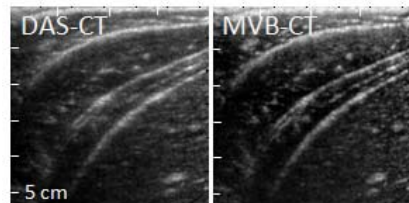
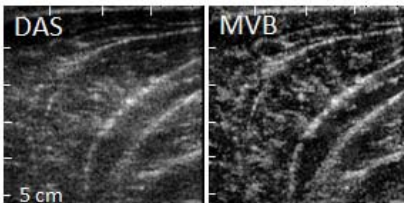
The Philips L12-5 38mm array and HDI 5000 scanner are used to image a tissue-mimicking phantom and the liver of a healthy volunteer, with and without spatial compounding (SonoCT TM). In a custom SonoCT mode (CT), the medium is imaged from 4 different view angles and the 4 resulting images are incoherently combined. DAS, DAS-CT, MVB, and MVB-CT images are generated by off-line beamforming. For the MVB-CT images, the MVB algorithm is first applied to each of the 4 component images before combining them.

Results

Quality metrics of the phantom images demonstrate the superiority of the MVB-CT mode over all others. Sidelobes are down by 20 dB compared to DAS methods, while the lateral resolution (0.4 mm) and speckle standard deviation (DAS: 4.4 dB, DAS-CT: 3.3 dB, MVB: 6.9 dB, MVB-CT: 5.5 dB) are preserved. MVB-CT also provides 9 dB of SNR enhancement at high depths compared to DAS. The in vivo images are shown in the Figures for qualitative evaluation. MVB-CT exhibits decreased clutter compared to DAS and DAS-CT, without the grainy appearance of MVB or even DAS.

Discussion and Conclusions

Combining the minimum variance beamformer with spatial compounding yields unprecedented image quality. Computational complexity remains a major obstacle for real-time implementation.



Wednesday
Poster

Mapping Skull Attenuation for Optimal Probe Placement in Transcranial Ultrasound Applications

Francis Vignon¹, William Shi¹, Ramon Erkamp¹, Emil Radulescu¹, Vijay Shandasani², Jeffrey Powers²,¹Philips Research North America, Briarcliff Manor, NY, USA, ²Philips Healthcare, Bothell, WA, USA

Background, Motivation and Objective

It takes skill and time to place an ultrasound probe on the optimal acoustic window for transcranial insonification. This hinders efficient ultrasound imaging and therapy of the brain. This paper investigates two approaches for automatically identifying the best transtemporal window, using an imaging probe and a point source on the contralateral temple.

Statement of Contribution/Methods

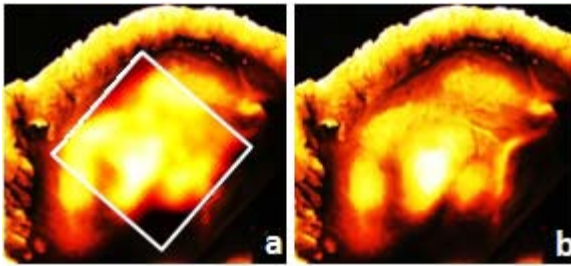
In a water tank, an X7-2 matrix probe driven by an iE33 scanner (Philips Healthcare) is placed at 5 mm in front of a temporal bone sample, in a typical transcranial imaging configuration. The focus of a single-element transducer ($\sigma=2.5$ cm, $F\#=2$, $f_0=3.5$ MHz) acts as a “contralateral” point source at a distance of 14 cm from the imaging probe. The signals coming from the point source through the skull are recorded by each individual probe channel, and their amplitudes are extracted to produce a 2D attenuation map of the skull under the probe footprint. The process is repeated for 9 non-overlapping probe positions to map an area of 3 cm x 3 cm. Smoothing, interpolation, and log-compression are then applied to the attenuation map. For comparison, the bone thickness is indicated by an optical attenuation map (a photograph with backlight illumination). In another approach, the amplitude of the beam-summed signals from the contralateral source is recorded for 81 overlapping probe positions, mapping an area of 2.5 cm x 2.5 cm. The optimal position is where the contralateral source appears brightest.

Results

Attenuation maps of 2 temporal bones were acquired with both per-channel and beam-sum approaches. An example per-channel-based attenuation map (30 dB dynamic range), as shown within the white box in Fig. a, is overlaid to the optical attenuation map (also in Fig. b), showing good correspondence. The beam-sum-based maps (not shown) indicate that the transcranial attenuation can increase by up to 20 dB when the probe is moved away from the optimal position by 1 cm.

Discussion and Conclusions

The skull attenuation can be mapped using a commercial imaging probe with the aid of a contralateral point source. While the per-channel map directly indicates the bone thickness and requires a shorter mechanical scanning time, the beam-sum-based mapping is more readily implementable on a commercial scanner. The tools developed in this study should help accelerate clinical workflow and improve image quality in transcranial ultrasound.



Simulation of Acoustic Fields from Arbitrary Transducer Stacks using a FEM Transducer Model and Nonlinear Wave Propagation

Martijn Frijlink¹, Hans Torp^{1,†} *Department of Circulation and Medical Imaging, Norwegian University of Science and Technology (NTNU), Trondheim, Norway*

Background, Motivation and Objective

Acoustic field simulations support ultrasound transducer development. The layered structure of a piezo-electric based acoustic stack defines the electro-mechanical behavior, which determines the way the electrical excitation pulse is converted into an acoustic one. Field simulations benefit from an accurate estimation of this acoustic pulse. However, the electro-mechanical transfer function used for field simulations is often approximated by 1D models or Gaussian curves.

In this study, we combined a 2D/3D Finite Element Method (FEM) model of the transducer stack, with a two-port model of the transmit circuit, and a simulation program for nonlinear wave propagation. These simulation tools were then used to calculate second harmonic (SH) fields for different acoustic stacks in order to study the effect of elevation size and type of piezo-electric material.

Statement of Contribution/Methods

A 2D/3D FEM model is used to calculate the average surface velocity and complex electrical impedance of a transducer element as a function of frequency. A two-port model connects the transducer impedance to an electrical transmit circuit (e.g. resistors, cable, tuning), and calculates the acoustic pressure pulse for arbitrary excitation pulses. The pressure pulse is then the input to Abersim, a simulation program for 3D nonlinear wave propagation for arbitrary transducer geometries.

To illustrate the use of these simulations, we first studied the effect of the elevation size of a cardiac array (PZT based, $f_c = 2.5$ MHz, 64 elements, elevation & lateral focus at 60 mm) on the generated SH field in an attenuating medium (0.3 dB/cm/MHz). Secondly, the effect of using single-crystal versus PZT composite was investigated.

Results

For a transmit circuit with a cable and tuning (dependent on the elevation width), and a square wave excitation pulse (1.9 MHz, 3 half cycles, $80 V_{pp}$), the maximum simulated SH amplitude was 1.02, 0.88, and 0.71 MPa for the cardiac array with elevation widths of 13, 11, and 9 mm respectively. If the excitation amplitude was adjusted to a normalized MI of 1.5, excitation voltages of 56, 66, and $80 V_{pp}$ were required for elevation widths of 13, 11, and 9 mm, respectively. The simulated SH 6-dB lateral beam width at focus was 2.3, 2.7 and 3.6 mm respectively.

A single crystal based stack ($f_c = 2.5$ MHz) resulted in a 6.5 dB higher maximum SH level than a similar PZT-based stack, for the same transmit circuit and excitation pulse (1.9 MHz, $70 V_{pp}$). Inductive tuning increased the SH level as generated by the PZT-based model by 5.5 dB.

Discussion and Conclusions

A comprehensive simulation tool, including a 2D/3D FEM transducer model and 3D nonlinear wave propagation, resulted in harmonic field simulations for arbitrary transducer stacks, transducer geometries, transmit circuits and excitation pulses. Examples showed that these simulations could be used to optimize the elevation width of an array, and guide the choice of piezo-electric material.

Spatial Refinement of Ultrasound Pressure Fields using Polycarbonate Lenses: Model and Experimental Validation in the context of Sonoporation

Hans O. Rølfesnes¹, Donald A. McLean¹, Paul A. Campbell^{1,†} *Carnegie Physics Laboratory, University of Dundee, Scotland, United Kingdom*

Background, Motivation and Objective

Sonoporation holds promise as a modality for the targeted delivery of molecules into a range of diseased or dysfunctional tissues. Often, the approach is executed using a standard single element focused transducer, however, as target regions will obviously vary in size, any individual transducer is unlikely to produce a focal region that covers a reasonable range of anticipated target volumes. In addressing this challenge, a number of approaches have been considered, such as simply employing different transducers with a range of focal properties, or else elected to exploit the versatility of phased array transducers, which facilitate 3D control of the pressure field but at increased cost and engineering complexity. Probably the least expensive route to achieving enhanced transducer versatility is by the application of ultrasonic lenses in order to modify the focal region. In the work presented here, we have investigated this latter approach at length via optimisation modelling, and also experimental validation.

Statement of Contribution/Methods

We designed and manufactured two different sector-vortex type lenses (mode 1 and mode 2) for modifying the focal area of a 1 MHz focused ultrasound transducer (Figure 1). Lens design was performed using a numerical model (in Matlab) for calculating deposition of ultrasound energy within layered media. The lenses were manufactured in-house, using low-cost polycarbonate. Prototypes were tested in a water bath using an automated ultrasound scanning system and with needle hydrophone mapping to characterise the resultant pressure fields. Heating effects were quantified with a tissue mimicking polyacrylamide gel containing fresh egg white to compare lesion sizes over the available parameter space. Finally, we sonoporated cells using the same configurations and compared the size of the region of cells that were affected by the ultrasound using a fluorescent probe of membrane disruption.

Results

Mathematical models of the two lens designs increased the transverse diameter of the focal region from 1.8 mm to 3.5 mm and 5.2 mm respectively, and ultrasound field measurements showed very good compliance with these numerical calculations. Lesion sizes achieved in gel phantoms were also of comparable dimensions. Corroboration with bioeffect on planar monolayers of sonoporated cells was also estimated over the full range of ultrasound parameters at our disposal.

Discussion and Conclusions

The application of ultrasonic lenses appears to be an extremely cost-effective route to achieving flexibility in effective ultrasound pressure fields for controlled sonoporation. Moreover, our straightforward approach to the model appears to capture the essential characteristics in an accurate, and therefore useful, fashion. We anticipate that acoustic lenses could now find a range of renewed interests in applied ultrasonics, given their intrinsic effectiveness, and low cost.

P3-C-06

APES Beamforming Applied to Medical Ultrasound Imaging

Ann E. A. Blomberg¹, Iben Kraglund Holfort², Andreas Austeng¹, Johan-Fredrik Synnevåg³, Sverre Holm¹, Jørgen Arendt Jensen², ¹Department of Informatics, University of Oslo, Norway, ²Department of Electrical Engineering, Technical University of Denmark, Denmark, ³Bergen Oilfield Services AS, Norway

Background, Motivation and Objective

Recently, adaptive beamformers have been introduced to ultrasound imaging. The primary focus has been on the minimum variance (MV) (or Capon) beamformer. Previous investigations have shown that the MV may provide a significant increase in resolution compared to the conventional delay-and-sum (DAS) beamformer, when used with the right parameters. However, the MV suffers from two potential drawbacks; sensitivity to the assumed wavefield parameters and difficulty in handling coherent echoes. Robustification methods such as diagonal loading and subarray averaging are used in order to obtain reliable amplitude estimates. Still, the MV underestimates the amplitude of scatterers in some cases. Temporal averaging is also necessary in order to obtain reasonable speckle statistics.

Statement of Contribution/Methods

This paper investigates an alternative but closely related adaptive beamformer; the Amplitude and Phase Estimation (APES) beamformer. APES was developed to give improved amplitude control at the expense of resolution. The purpose of this study was to see how APES performs on medical imaging data, since correct amplitude estimation often is just as important as spatial resolution.

Results

APES was applied to Field II simulated ultrasound data using a 96-element linear array transducer. Data was obtained for point targets and for a cyst in speckle. The performance of the beamformer is quantified using the full width at half maximum (FWHM), the resolvability index (RI), and the amplitude control in terms of peak amplitude. RI is defined as the relative difference between the peak amplitude of two laterally spaced point targets and the saddle point between them. Speckle statistics are quantified using the pixel signal-to-noise ratio (SNR_p) (1.91 for fully developed speckle).

The performance of the APES beamformer was investigated using subarray lengths of L from 24 to 48 in steps of 4. For a relatively robust set of parameters; $L = 44$ and a diagonal loading factor corresponding to 10 % of the

signal energy, the three methods {DAS, MV, APES} provide FWHM = {1.30, 0.16, 0.37} degrees, RI = {7, 21, 12.5} dB and amplitude estimates of {0, -3, 0} dB.

As a result of the increased amplitude control, APES provides speckle patterns similar to that of DAS without the need for temporal averaging. For {DAS, MV, APES}, the SNR_p was found to be {1.88, 1.19, 1.77}.

Discussion and Conclusions

Our results show that APES provides peak amplitude estimates equivalent to that of DAS, whereas MV with the given parameters underestimates the signal strength by up to 3 dB. The robustness of the APES beamformer comes at the expense of a slightly increased mainlobe width compared to the MV, which also affects the resolvability. However, APES performs significantly better than DAS in terms of resolution. Furthermore, APES provides a speckle pattern similar to that of DAS, without the need for temporal averaging.

P3-C-07

Adaptive parametric beamformation in ultrasound imaging

Sayed Mahmoud Sakhaei¹; ¹Mazandaran University of medical sciences, Sari, Mazandaran, Iran

Background, Motivation and Objective

Medical ultrasound beamforming is conventionally done using classical delay and sum (DAS) beamformer. This simple method uses preset weightings to combine the signals received by channels. These weightings control the sidelobe level at the expense of resolution. Moreover, its performance degrades by the presence of a strong off-axis scattering. Therefore, using adaptive beamforming such as Minimum Variance (MV), which controls the energy received from off-axis directions, instead of controlling the sidelobe level, can be more useful. In MV method, the energy at the output of beamformer is minimized subject to a constraint ensuring that the on-axis signal passes completely.

Several studies have been done about applying MV beamformer in medical ultrasound imaging. It is well known that a few problems should be solved before using MV in ultrasound imaging. First one arises from the fact that off-axis signal and on-axis signal are highly correlated, which leads to the performance degradation of beamformer. The second problem concerns to uncertainty of speed of sound, which causes constraining condition (steering vector) not be known precisely. This error can lead some interest signals to be missed. In addition, new weights should be calculated dynamically for each receive focus. Therefore, computational burden is another problem and simple algorithms are preferred for implementation.

Statement of Contribution/Methods

In this paper, to overcome the first problem, we use weighted spatial smoothing technique, which is superior to the conventional spatial smoothing in decorrelating signals and so the resolution. To have a robust beamformer, we utilize a parametric apodization similar to Taylor window. This parametric apodization guarantees that the signals coming from main axis and some around it pass from the beamformer. Moreover, the unknown parameters in the apodization which should adaptively be calculated are very smaller than the elements number in the array and so it has low computational burden.

Results

Our proposed method is applied on simulation data obtained by FIELDII. For a 96 elements phased array operating at 4 MHz, and for 2 types of targets, point and cyst target, the image obtained by our method are compared to those by DAS. The subarray elements used for spatial smoothing were 24 elements. They show significant improvement in resolution and contrast, while good robustness on 10% error in speed of sound, e.g. our simulations have demonstrated that for a point target laying at distance 40mm and by transmit focus at 60 and dynamic receive focusing, response of the adaptive beamformer is 60% narrower in FWHM than obtained by DAS.

Discussion and Conclusions

Using weighted spatial smoothing can improve the resolution which is diminished in conventional spatial smoothing as a result of decreased length of subarray aperture. In addition, parametric window enhances the robustness of the adaptive beamformer while decreasing the computational burden.

Super-Resolution Image Reconstruction With Reduced Computational Complexity

Michael Ellis¹, William Walker¹; ¹University of Virginia, Charlottesville, VA, USA

Background, Motivation and Objective

Though widely used, medical ultrasound is limited in its efficacy by image resolution. Recently, we have developed an adaptive image reconstruction (IR) algorithm, called dTONE, that significantly increases both image contrast and resolution by performing a global optimization assuming a discrete set of hypothetical source locations. A complete system model that is massive in scale is required, making this algorithm computationally burdensome. Here we have developed an alternative image reconstruction algorithm – called quick-TONE, or qTONE – that achieves comparably enhanced contrast and resolution with a reduced computational burden.

Statement of Contribution/Methods

The computational complexity of both algorithms can be decreased using a reduced rank form of the system model. However, the reconstructed images increasingly degrade as the system model rank is reduced. qTONE suffers far less image degradation than dTONE, allowing it to achieve comparable image quality to non-reduced dTONE at a fraction of the computational cost.

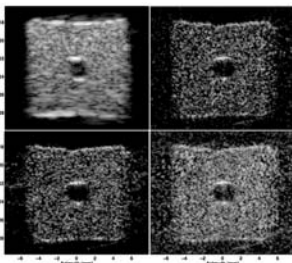
We performed a series of experiments using an Ultrasonix Sonix RP (6MHz with 80% bandwidth) to test the performance of qTONE. Conventional IR was applied using the default parameters of the Ultrasonix scanner, whereas dTONE and qTONE were applied on single-channel, unfocused data with plane wave transmit. Hypothetical sources were placed every 120 um laterally and 95.6 um axially. A 3 mm diameter anechoic region of 7% acrylamide gel was embedded in a 1 x 1 x 7 cm region of acrylamide containing Sephadex scatterers. This was then embedded in a 5 x 5 x 8 cm anechoic region of acrylamide and imaged using the parameters described above.

Results

The figure below shows, clockwise from the top-left, conventional IR, dTONE with a full model, dTONE with a reduced rank model, and qTONE with a reduced rank model. The full dTONE image required 1725 seconds to reconstruct on a desktop PC whereas the reduced rank dTONE and qTONE images required 163 seconds and 145 seconds, respectively.

Discussion and Conclusions

Both dTONE and qTONE provide superior contrast and resolution to conventional IR. Reducing the system model rank causes degradation of the dTONE image but very little degradation of the qTONE image. The results of these experiments show that qTONE significantly reduces computation time while maintaining the contrast and resolution enhancements of non-reduced dTONE.



Wednesday
Poster

P3-C-09

Image amplitude estimation with the minimum variance beamformer

Andreas Austeng¹, Are Fritz Charles Jensen¹, Johan-Fredrik Synnevåg², Carl-Inge Colombo Nilsen¹, Sverre Holm¹: ¹Department of Informatics, University of Oslo, Oslo, Norway, ²Bergen Oilfield Services AS, Bergen, Norway

Background, Motivation and Objective

The adaptive minimum variance (MV) beamformer has recently been adapted to active wideband imaging systems. It is vital that proper averaging in both the spatial and temporal domains as well as regularization must be used to produce images of acceptable image quality. It has also been shown that MV may provide a significant increase in resolution when tuned correctly. Studies showing this have focused on imaging points and cysts. Less focus has been put on how well the MV beamformer estimates the true image amplitude. As correct estimation of amplitude often is just as important as spatial resolution in medical imaging, this is the focus here.

Statement of Contribution/Methods

We have investigated how well the MV beamformer estimates the amplitude levels in speckle of different intensity. The performance of the MV beamformer is quantified with respect to reproduction of speckle intensity together with point and edge resolution. The results are compared to a conventional delay-and-sum (DAS) beamformer where we have applied either a uniform or a hamming weighting.

Results

We have applied the MV and DAS beamformers to Field II simulated ultrasound data. A 2.5MHz 64-element linear array transducer is used. For the MV beamformer, subarray lengths of L from 24 to 32, temporal averaging over three wavelengths and a diagonal loading factor corresponding to 1% or 10% of the signal energy were used. The temporal averaging gives MV images with speckle statistics comparable to DAS images. Speckle images containing areas with 10 different intensities with a relative intensity difference ranging from -3 dB to -40dB were then simulated. The images also included bright point targets on speckle background. All images were normalized to have the same speckle intensity in one of the areas.

For a relatively robust set of parameters ($L=24$, 1% diagonal loading) the MV beamformer gives point responses with the same amplitude level, but approximately 1/3 of the -6dB beamwidth and up to 5dB better sidelobe suppression compared to the DAS beamformer. The edges between the different intensity areas were also more well defined. The amplitude estimate of the various speckle intensities showed larger deviation. For speckle levels having RF signals of large amplitude, the DAS and MV beamformer produced comparable intensity levels, but for areas with low-value RF amplitudes the MV beamformer was able to produce much more accurate results. The deviation here was up to 10dB. The reason for this is that the MV beamformer has lower sidelobe leakage compared to the DAS beamformer.

Discussion and Conclusions

Our investigations show that the MV beamformer, when tuned correctly, is able to estimate the amplitude level of different speckle areas equally well or better than the DAS beamformer. The chosen parameters thus both give more accurate amplitude estimates as well as reproduce previously known results for a significant increase in resolution.

P3-C-10

A Time Domain Spectral Element Method for Propagation of Pulses in Nonlinear Materials

Halvard Kaupang¹, Bjørn Angelsen¹: ¹Department of Circulation and Medical Imaging, Norwegian University of Science and Technology, Trondheim, Norway

Background, Motivation and Objective

Simulations has throughout the years been more and more common in ultrasound beamforming and probe research. Several computer programs are able to simulate phenomena encountered in ultrasound research such as diffraction, attenuation, nonlinear effects and forward and back scattering, but few programs are capable of handling all of these effects. Programs suited for back scattering are often limited to linear propagation, and most nonlinear tools are based on propagation in only one direction. Several nonlinear tools are based on the KZK equation, but some solve the full wave equation. Simulation tools based on directional models handles forward scattering, or phase aberrations, well, but does not easily handle back scattering. Attenuation is handled by most available programs.

Statement of Contribution/Methods

A solution to the full wave equation in a nonlinear material is sought. The problem is modeled as a coupled system of two first order equations as presented by Tabei et al. in Ref. [1], but the spatial discretization is based on a Spectral Element (SE) approach using high order orthogonal polynomials rather than a k-space formulation. The method is implemented for nonlinear and homogeneous materials, and is bench marked to an existing simulation tool for directional nonlinear wave propagation: Abersim [2]. Abersim solves the directional full wave equation and not the approximative KZK equation. Two different transducer setups are tested and compared with both linear and nonlinear propagation. The transducer has transmit center frequency of 1.75 MHz, an aperture of 18 mm and is either focused at 54 mm or unfocused.

Results

Comparison of on-axis pulses and frequency spectra show a good overlap between the SE and Abersim solutions for both transducers, and both linear and nonlinear propagation. Focal point beam profiles for the main lobe and first side-lobe show that the SE solution are 0.5-1.0 dB lower relative to the Abersim solution for the maximum pressure, and <0.1 dB lower for the RMS value of the pressure. For nonlinear propagation the SE solution is <1.0 dB lower than the Abersim solution for the maximum pressure profiles, <0.2 dB higher for the RMS profiles. The second harmonic of the SE solution is 0.5 dB higher than the Abersim solution for both the maximum and RMS profiles. For the unfocused transducer, the same behavior is seen for both linear and nonlinear propagation.

Discussion and Conclusions

A time domain SE method has been developed to study propagation of ultrasonic pulses in nonlinear materials. Compared to one other simulation tool, the SE method shows good performance, and the deviations are <1 dB for the presented setups. Although attenuation, forward and back scattering are not implemented at the moment, these are vital aspects to address in order to investigate more complex simulation setups.

[1] Tabei, M., T. D. Mast and R. Waag, JASA 111 (1), pp. 53-63, 2002.

[2] Frijlink, M., H. Kaupang, S.-E. Måsøy, In Proc. IEEE IUS 2008, pp. 1282-1285, 2008.

P3-C-11

Model-Based Reconstruction for Photoacoustic Tomography with Finite Aperture Detectors

Meng-Lin Li¹; ¹Dept. of Electrical Engineering, Natinal Tsing Hua University, Hsinchu, Taiwan

Background, Motivation and Objective

So far most rigorous reconstruction algorithms for photoacoustic tomography (PAT), for example, the modified back-projection algorithm, have been developed based on ideal point detectors. Nonetheless, because of the issue of poor signal-to-noise ratio from point-like detectors, finite-size flat transducers are commonly used in PAT, thus introducing the finite aperture effect - the tangential resolution in PAT deteriorates as the imaging point moves away from the circular scanning center.

Statement of Contribution/Methods

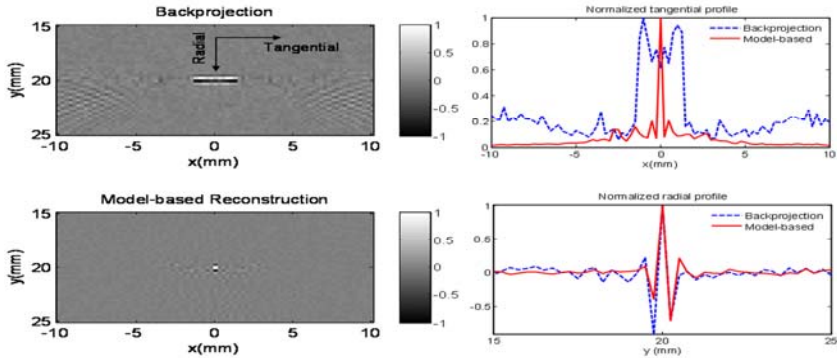
Such finite aperture effect and degradation in tangential resolution result from the spatial impulse response of the finite-size flat transducer. In this study, we adopt a model-based reconstruction method to improve the degraded tangential resolution for a photoacoustic tomography system with finite-size flat transducers. This method is based on a linear, discrete model of the photoacoustic detection system developed using matrix formalism. Using this model, a spatiotemporal optimal filter designed in minimum mean square error sense is used to deconvolve the spatial impulse responses associated with a finite-size flat transducer at every imaging point; thus retrospective restoration of the tangential resolution can be achieved.

Results

The performance of the model-based reconstruction method is verified using simulation data. In the simulation, a point absorber, which is 20 mm away from the circular scanning center, is scanned with a 6-mm flat transducer, and the scanning radius is 40 mm. Left panels of the figure are the reconstructed images using backprojection of the simulated signals (top) and the model-based reconstruction method (bottom); right panels show the normalized tangential and radial profiles of the images in the left panels. For a finite aperture detector, it is clearly shown that compared with that reconstructed by the backprojection algorithm, the tangential resolution obtained using the proposed method is significantly improved while the radial resolution is retained.

Discussion and Conclusions

It is demonstrated by simulation that the proposed method effectively improves the degraded tangential resolution for PAT with finite-size flat transducers. In addition, by taking electrical impulse response of the transducer into account, the proposed method can potentially improve the radial resolution, too.



P3-C-12

Nonlinear Field Computation using Operator Splitting with Nondiffracting Beams

Paul Fox¹; ¹Institute of Sound and Vibration Research (ISVR), University of Southampton, Southampton, Hampshire, United Kingdom

Background, Motivation and Objective

The work continues previous research into nonlinear field computation using operator splitting [1-3]. There currently exist various approaches to nonlinear field simulation, but each with its advantages and disadvantages. The motivation and objective here have been both to improve on previous related work and to offer a new design methodology.

Statement of Contribution/Methods

The work introduces a new methodology for computing nonlinear fields. In [2,3] these were computed by combining linear impulse response (Field II) field computation with operator splitting [1]. A set of virtual planes were propagated in a two stage process : a linear propagation from one plane to the next, and a nonlinear distortion of the linear propagation. The second phase required definition of an appropriate propagation distance through which to apply the nonlinear distortion, which is ambiguous using the spatial impulse approach due to the field at each location on one plane being a sum of contributions from all locations on the previous plane. In this work nondiffracting beams are used for the linear propagation since by definition they all propagate perpendicularly to the transducer surface and thereby share a common propagation distance.

Results

The resulting nonlinear simulations appear more accurate and robust than using the impulse response approach. The attached figure shows the surface pressure for a simple 10mm diameter piston array pulsed at 2MHz, 2MPa, 5 cycles (upper) and the subsequent centreline nonlinear field calculated at 45mm (lower). The characteristic sawtooth shape of the nonlinear field is clearly evident, along with the asymmetric +/- peak values (+4.5MPa, -2.6MPa).

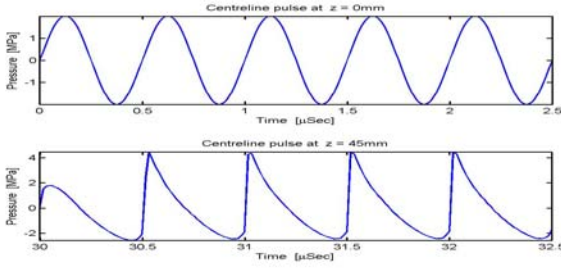
Discussion and Conclusions

A new technique is introduced which improves on previous related work. The numerical example given is for an annular array, but in principle the technique may also be applied to fully 2D arrays without any geometry or beamsteering constraints. (Note : This work was originally accepted for Beijing 2008 but had to be withdrawn due to unexpected financial problems. However, presentation at Rome 2009 is guaranteed).

[1] Tavakkoli, Cathingol, Souchon. JASA 104, pp. 2061-2072, 1998.

[2] Jensen, Fox, Taylor, Schlaikjer. Proc. IEEE Ultr. Symp., pp. 1690-1693, 2002.

[3] Fox, Proc. IEEE Ultr. Symp., pp. 1732-1735, 2007.



P3-D. Signal Processing

Sala Orange

Wednesday, September 23, 2009, 10:00 am - 11:30 am

Chair: **Piero Tortoli**
Univ. of Firenze

P3-D-01

Multiresolution Analysis of Intravascular Ultrasound Harmonic Signals to Image pre-rupture Plaques

Sushma Srinivas^{1,2}, Chaitanya Chandrana^{1,3}, Shuvo Roy¹, Aaron Fleischman¹; ¹Biomedical Engineering, Cleveland Clinic Foundation, Cleveland, OH, USA, ²Chemical and Biomedical Engineering, Cleveland State University, Cleveland, OH, USA, ³University of Toronto, Toronto, Canada

Background, Motivation and Objective

The pursuit of a definitive method of plaque diagnosis continues as there is an unmet need for clinical identification of vulnerable plaque before they rupture. Despite the efforts of current leading technologies like 3D volumetric analysis, wavelet analysis and virtual histology in imaging vulnerable plaque, these are not considered definitive due to their lack of identification of plaques likely to rupture, inability to differentiate vulnerable from stable plaque characteristics and primarily, the inability to image at high resolution. There is a need for a higher resolution IVUS device and a method to characterize the thin cap fibroatheromas (TCFA) before they rupture causing an acute coronary event. The objective is the early detection of vulnerable plaque by multiresolution analysis (MRA) of IVUS radiofrequency (RF) signals from harmonic imaging.

Statement of Contribution/Methods

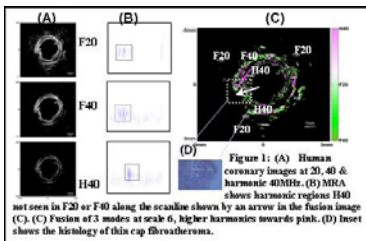
Broadband high resolution (~19 μ m) focused polymer transducers were fabricated. Fundamental (at 20MHz and 40MHz) and Harmonic signals (at 40MHz and 80MHz) from the tissue were obtained in one scan line using a previously established pulse inversion technique with 60% bandwidth Gaussian pulses. Multiresolution analysis was carried out by obtaining the wavelet coefficients with forward wavelet transform for fundamental and harmonic signals. Daubechies 4 wavelet filter was used to resolve components as close as 24 μ m. Fundamental and harmonic signals were analyzed at different resolutions to find an appropriate scale. Circumferential images of the coronary artery generated by inverse wavelet transform of wavelet coefficients from scales 4 to 8 were compared.

Results

Multiresolution analysis of the RF signals reveal that the fundamental and harmonic cross sectional images can be viewed at various scales, each scale offering unique diagnostic information. Harmonic signals identify tissue components not seen in fundamental at 20MHz and 40MHz. Figure 1 illustrates the MRA of fundamental and harmonic signals and the corresponding images of the excised human left anterior descending (LAD) coronary artery.

Discussion and Conclusions

MRA of harmonic signals leads to identification of plaque components at multiple frequencies providing additional diagnostic information. This technique may lead to an early detection of plaque, thereby reducing the incidents of acute myocardial infarctions (AMI).



Wednesday
Poster

Reverberation Artifact Rejection in Arterial ARFI Imaging

Russell Behler¹, Timothy Nichols², Elizabeth Merricks², Caterina Gallippi¹; ¹Biomedical Engineering, University of North Carolina at Chapel Hill, Chapel Hill, NC, USA, ²Pathology and Laboratory Medicine, University of North Carolina at Chapel Hill, USA

Background, Motivation and Objective

In arterial ultrasound imaging, interpretation of plaque geometry may be distorted by reverberation artifacts in the lumen. Reverberation and arterial wall signals are highly correlated, which precludes frequency domain or conventional regression filtering methods; however, decorrelation rates vary. *We hypothesize that exploiting variability in 1D axial cross-correlation (CC) measures reduces reverberation artifact while preserving wall signal in arterial ARFI imaging.*

Statement of Contribution/Methods

Matched B-Mode and ARFI imaging were performed *in vivo* in the iliac arteries of six hypercholesterolemic pigs using a Siemens SONOLINE Antares™ imaging system (Siemens Medical Solutions USA, Inc. Ultrasound Division). ARFI-induced displacements were measured by 1D axial CC. Reverberation and blood signals were rejected by applying thresholds to (1) B- Mode image amplitude ('amplitude'), (2) median CC values after recovery from ARFI excitation (~3 to 6 ms post excitation) ('correlation'), and (3) variances of the second time derivative of CC values after recovery ('variance'). The thresholds were used directly to reject reverberation and blood signal (in 'direct' application). The thresholds were also used to identify the upper and lower spatial bounds of the arterial lumen, and signal in the axial range between the bounds was rejected (in 'wall detect' application). Filter performance was compared as percent luminal rejection given at least 98% arterial wall preservation relative to manual segmentation by paired t-test.

Results

Results are shown in Table 1. In 5 of the 6 arteries, the variance filter in wall detect (n=4) or direct (n=1) application was the most effective method. However, the overall difference in the variance filter performance was only statistically significant (p<=0.025) in comparison to the amplitude filter in direct and wall detect applications (bold). The amplitude filter in wall detect application generally performed poorly because low amplitude regions in soft tissue were mistaken for lumen.

Discussion and Conclusions

The variance filter was found to be the most effective for reverberation signal rejection, but statistical significance was not consistently achieved in this pilot investigation. Similar methods may be relevant to reverberation artifact rejection in B-Mode imaging without a substantial reduction in frame rate.

% Lumen Remaining		Amplitude		Correlation		Variance	
Iliac Artery	Direct	Wall Detect	Direct	Wall Detect	Direct	Wall Detect	
1	85.8	100.0	2.6	8.9	1.4	0.0	
2	79.5	100.0	1.5	8.4	0.1	0.4	
3	91.9	100.0	41.4	73.5	5.2	4.3	
4	0.8	98.7	16.7	5.6	8.0	0.2	
5	96.4	100.0	81.4	100.0	32.3	100.0	
6	93.2	100.0	96.8	53.3	80.3	100.0	
T-test Results							
Filter Method	Amp - Direct	Amp - WD	Corr - Direct	Corr - WD	Var - Dir	Var - WD	
Amp - Direct	1	0.123	0.155	0.168	0.022	0.025	
Amp - WD		1	0.005	0.005	0.000	0.010	
Corr - Direct			1	0.949	0.390	0.829	
Corr - WD				1	0.348	0.784	
Var - Dir					1	0.607	
Var - WD						1	

Wednesday
Poster

Automatic Detection of micro-emboli by means of a synchronous linear prediction technique

Latifa Dreibine¹, Sébastien Ménigot¹, Nawal Meziati¹, Jean-Marc Girault¹; ¹UMR Université François Rabelais de Tours, Inserm U930, CNRS ERL 3106, Tours, France, Metropolitan

Background, Motivation and Objective

Detection of Micro-emboli is of great clinical importance to prevent cerebro-vascular events and to identify the causes of such events. Standard detection techniques implemented in the most commonly used systems are generally based on the passing of an energy threshold. The value of this threshold can be set just above the statistically highest detected energy of a Doppler signal related to circulating blood, i.e. during the systolic phase. This choice of threshold consequently prevents all detection of micro-emboli events whose energy might be lower than the systolic energy.

Statement of Contribution/Methods

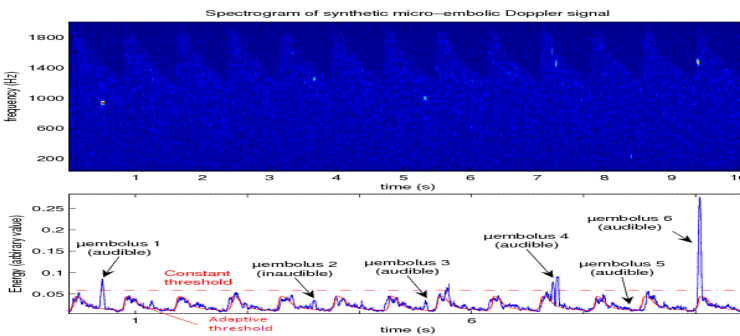
By assuming that the Doppler signal is cyclostationary, we hypothesize that energy is statistically periodic. Furthermore, by assuming that micro-emboli are unforecasted, we hypothesize that embolic signal are unpredictable. Joint used of synchronous and linear prediction techniques are candidate techniques to detect very small micro-emboli. If we periodically take and compare the values of the energy of the prediction error (or AR parameters) at different time points in the cardiac cycle, we can therefore detect the presence of non-periodic events such as micro-emboli.

Results

We have tested and compared our new technique to the standard technique (Fourier) using simulated and in vivo signals from patients with stenosis of high degrees of severity. From simulations, the standard automatic technique detects 60% of micro-emboli detected by our gold standard technique (auditory detection + sonogram visualization) whereas the synchronous linear prediction technique detects 97% (the false alarm rate being set at 0%). From clinic examinations, the standard automatic technique only detects 67% of micro-emboli detected by our gold standard technique (auditory detection + sonogram visualization) whereas the synchronous linear prediction technique detects 100% (the false alarm rate being set at 0%).

Discussion and Conclusions

This study demonstrates that our new technique detects micro-emboli hitherto not identified by classical methods. Large micro-emboli are all detected, but small micro-emboli are only detected with our new technique. This latter technique opens up new prospects to detect small emboli, despite the need for further studies to incorporate technique "on line".



P3-D-04

Performance Evaluation on High Frame-Rate Speckle Tracking

Shih-Ying Wu¹, Shun-Li Wang¹, Pai-Chi Li¹; ¹National Taiwan University, Taiwan

Background, Motivation and Objective

Doppler ultrasound for quantifying blood and tissue motion is angle-dependent and has maximum detectable velocity limitation. Speckle tracking can be utilized to estimate velocity vectors. The combination of high frame-rate imaging and speckle tracking has the potential to achieve accurate motion estimation but the computation requirement may be a concern. In this study, we evaluate performance of high frame-rate speckle tracking under different speckle decorrelation conditions, and compare it to speckle tracking in normal imaging conditions.

Statement of Contribution/Methods

A modified commercial scanner from Zonare was used for high frame rate imaging experiments. The main factors affecting performance of speckle tracking are target translation, SNR, flow gradients, and computation power. Experiments and simulations using plane-wave excitation with parallel beamforming are performed using the sum-absolute-difference (SAD) algorithm. First, phantom experiments (transducer: center frequency=4.1MHz, aperture width=19.2mm) were performed to study the estimation accuracy assuming no flow gradients occur. Effects of SNR were also studied. Second, laminar flow simulations with 0.5 m/s maximum velocity and 6 mm wide lumen (transducer: center frequency=6.6MHz, aperture width=19.2mm) using FIELD II were performed to study effects of velocity gradient. The constant flow experiment with a 4 ml/s flow rate is conducted. Finally, the computational complexity of speckle tracking at different frame rates was analyzed.

Results

The estimation errors from phantom experiments (SNR=28 dB) were within 5% when displacement was smaller than 5 mm and 8 mm for lateral and axial directions, respectively. In simulations, errors of 10±2% can be achieved when imaging frame rate is from 800 to 2000 Hz. The errors were 14±2% at 1000 Hz frame rate in flow experiments using a modified commercial scanner (Zonare). The computational complexity is generally proportional to the imaging frame rate.

Discussion and Conclusions

The use of high frame-rate imaging can reduce the range of search region as well as speckle decorrelation in speckle tracking. However, performance of speckle tracking is unreliable when the SNR is lower than 10 dB. The low SNR is a disadvantage of high frame-rate imaging due to the lack of transmit focusing.

P3-D-05

Angular Spectrum Simulation of Pulsed Ultrasound Fields

Yigang Du¹, Henrik Jensen², Jørgen Arendt Jensen¹; ¹Center for Fast Ultrasound Imaging, Department of Electrical Engineering, Technical University of Denmark, Lyngby, Denmark, ²BK Medical Aps, Herlev, Denmark

Background, Motivation and Objective

The optimization of non-linear ultrasound imaging should in a first step be based on simulation, as this makes parameter studies considerably easier than making transducer prototypes. Such a simulation program should be capable of simulating non-linear pulsed fields for arbitrary transducer geometries, for any kind of focusing and apodization. The Angular Spectrum Approach (ASA) is capable of simulating monochromatic non-linear acoustic wave propagation. However, to simulate ultrasound imaging, the simulation of the time response of each specific point in space requires a pulsed ASA simulation with multi temporal frequencies. Combining it with Field II, the generation of non-linear simulation for any geometry with any excitation array transducer becomes feasible. The purpose of this paper is to make a general pulsed simulation software using the modified ASA.

Statement of Contribution/Methods

Linear and phased array transducers are used to create the source plane, which is 2 mm from the transducer surface. Field II is applied to generate pulses for all the points in the source plane. Therefore, the 3D matrix data (1D time, 2D space) are obtained. The pulses in the simulated plane are calculated by the modified ASA, that is the 3D inverse Fourier transform of a series of planes corresponding to each temporal frequency. The planes are the multiplications between the 2D spatial Fourier transform of the pressure in the source plane and the ASA propagator for every temporal frequency components. The beam focusing is processed by Field II in the source plane.

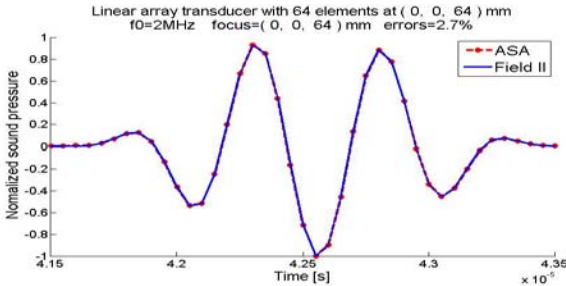
Wednesday
Poster

Results

A rectangular plane match to the shape of the transducer surface is chosen as the source. The plane has 33×407 points with the spatial interval of $\frac{1}{2}$ wavelength. The comparison of the pulse with the reference to Field II at the focus point (0, 0, 64) mm for a 64-element, 2 MHz linear array transducer is shown in the figure, and the error is 2.7%. For the further validation, 3 randomly selected points in the simulated plane make the errors be {12.5%, 13.3%, 23.4%} respectively corresponding to the positions of (3.9, -1.5, 64), (-1.9, 1.9, 64), (6.2, -4.2, 64) mm. The mean error for the pulses of all of points in the simulated plane is 10.9%.

Discussion and Conclusions

The good agreement between modified ASA and Field II simulation for the pulsed ultrasound fields obtained in this paper, makes it possible to expand Field II to non-linear pulsed fields.



P3-D-06

Correcting for focusing when estimating tissue attenuation from mean frequency shift

Jerzy Litniewski¹, Ziemowit Klimonda¹, Elzbieta Szymanska², Marcin Lewandowski¹, Andrzej Nowicki¹;
¹Department of Ultrasound, Institute of Fundamental Technological Research, Warsaw, Poland, ²Dermatology Clinic, CSK MSWIA Hospital, Warsaw, Poland

Background, Motivation and Objective

The attenuating properties of biological tissue are of great importance in ultrasonic examination even though its anatomical variability limits diagnostics effectiveness. Also, the accurate estimation of the frequency-dependent attenuation is important due to the need to its compensation when evaluating scattering properties of tissue or statistical characteristics of the backscatter.

We intend to use a self-developed high frequency ultrasonic scanner for the skin and cutaneous lesions characterization by evaluating its attenuating and scattering properties. To estimate in vivo the attenuation we use the downshift in mean frequency (DMF) of echo signals calculated using the mean frequency correlation estimator (I/Q algorithm) adopted from the Doppler technique. It is important to compensate the effects of focusing when calculating DMF to estimate the attenuation coefficient. Otherwise, in regions in front of the focus the attenuation is underestimated and in regions beyond the focus is overestimated.

Statement of Contribution/Methods

We propose the diffraction/focusing effects correcting (FC) technique that compensates mean frequency shift (MFS) induced by focusing. The method corrects mean frequency estimates derived from echo pulses propagating in attenuating tissue with locally varying attenuation coefficient. The FC procedure applies the diffraction correcting coefficients obtained experimentally from the probing pulses focused in water for assessing the expected values of MFS of pulses focused in attenuating tissue. The calculations involves the pulse 'history' that due to overall attenuation along the traveled path down-shifts the pulse spectrum what results in variation of the focusing-induced MFS.

Operation and accuracy of the FC procedure were verified by calculating the attenuation coefficient distributions in the tissue mimicking phantom (5MHz). Also, the B-scan images of the skin (30MHz) were processed to obtain attenuation parametric images.

Results

The results obtained from phantom measurements (DFS phantom, Denmark) show the uniform distribution of attenuation within the phantom. High agreement between the measured attenuation coefficient ($0.53 \pm 0.05 \text{ dB/MHzcm}$) and the one given by the manufacturer ($0.51 \pm 0.02 \text{ dB/MHzcm}$) was found. The parametric images of the skin are more complicated to interpret but the high attenuating area of dermis clearly differs from the less attenuating hypodermis.

Discussion and Conclusions

The proposed FC technique correctly estimates the MFS related to focusing. It can be applied even when only echoes instantaneous mean frequency is measured directly from the backscattered ultrasounds. The last corresponds to the I/Q frequency estimation algorithm used by us. Application of this procedure increases the accuracy of attenuation determination in tissue and is required in reliable parametric imaging.

P3-D-07

Huffman Sequence Design for Coded Excitation in Medical Ultrasound

Alessandro Polpetta¹, Paolo Banelli¹; ¹*Electronic and Information Engineering Department, University of Perugia, Italy*

Background, Motivation and Objective

This paper deals with coded-excitation (CE) for ultrasound medical echography. In the CE framework, binary and chirp sequences are largely used although they optimize performance either in frequency independent (FI) or frequency dependent (FD) attenuating mediums. In order to design a code that provides good contrast resolution (CR) and signal-to-noise ratio (SNR) both in FI and FD mediums, we propose Huffman linear codes (LCs) to combine amplitude with phase coding

Statement of Contribution/Methods

We identify the family of Huffman LC that, thanks to their impulse-like autocorrelation function, guarantees high CR. Then, among these codes, we explain how to select that one that maximizes the SNR. Interestingly, this procedure, which is inspired by chirp sequence properties, selects a LC with ridge ambiguity function (AF) and, consequently, it provides very good performance both in FI and FD mediums

Results

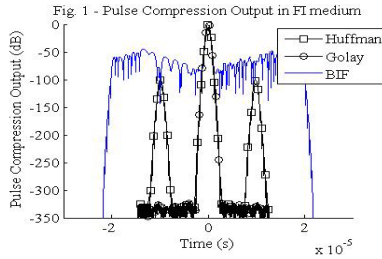
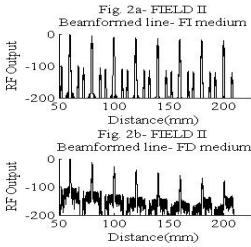
We compare the performance of this specific Huffman design with two known LCs: "near optimal sequence" with inverse filtering (BIF), and double-transmission Golay codes. As shown in Fig. 1, in FI medium, the BIF provides quite good

performance and Golay method, which is penalized by frame-rate reduction and motion artifacts, is optimum as concern the CR. However, both of

them highly suffer FD attenuation. Fig. 2 is obtained by FIELD II simulation of a phased array probe with 8 equally spaced reflecting scatterers, and it shows a beamformed line for the proposed Huffman LC, which confirms its very good performance both in FI and FD mediums, where it outperforms both BIF and Golay LC.

Discussion and Conclusions

We present an approach for CE that, to the best of our knowledge, is new in medical ultrasounds. It is based on Huffman coding theory and provides very good performance both in FI and more practical FD mediums



P3-D-08

A Novel Technique for High Resolution Ultrasound Imaging Using Super Resolution FM-Chirp Correlation Method (SCM)

Masaki Fujiwara¹, Kan Okubo¹, Norio Tagawa¹; ¹Department of Information and Communications, Tokyo Metropolitan University, Hino, Tokyo, Japan

Background, Motivation and Objective

This study addresses the issue of the super-resolution pulse compression technique (PCT) used for ultrasound imaging. The time resolution of the ultrasonic echoes using the FM-Chirp PCT is limited by the bandwidth of the sweep-frequency, therefore, the PCT resolution is insufficient when multiple scatterers are in close formation. To solve this limitation in this paper, we propose the Super resolution FM-Chirp Correlation Method (SCM) and evaluate its performance.

Statement of Contribution/Methods

SCM is based on the multiple signal classification (MUSIC) algorithm. The outline of SCM is as follows. The FM-chirp signal with a certain center frequency is transmitted several times. The echo signals are received and the same process is repeated with slight variation of the center frequency. Analytic signals are obtained from the compressed echo signals by applying an orthogonal detector. Subsequently, the covariance matrix of the above analytic signals, which is averaged with respect to the center frequency, is calculated. By solving the general eigenvalue problem defined by the covariance matrix calculated above and the matrix calculated using the envelope of the auto-correlation function of the transmitted signal, we can obtain the resultant signals with higher resolution than that of the original compressed echo signals.

Results

For the twelve-scatterer model, the computer simulations on resolution improvement by the super-resolution technique proposed in this paper were conducted. The broken line and the dotted line in Fig. 1 represent the PCT results of the transmitted chirp signals with 2 MHz (9–11 MHz) and 4 MHz (8–12 MHz) bandwidth, respectively. The solid line presents the results of the high-resolution estimation obtained using SCM. Figure 1 shows that we can estimate the position using the proposed method, where the PCT results estimate spurious peaks.

Discussion and Conclusions

In this paper, we propose the super resolution FM-chirp correlation method (SCM), which is based on PCT and the MUSIC algorithm. We analyzed the performance of the proposed method for the estimation of the time delays of the multiple echo signals. The results clarified that the super-resolution profile achieves higher resolution estimation than the conventional PCT.

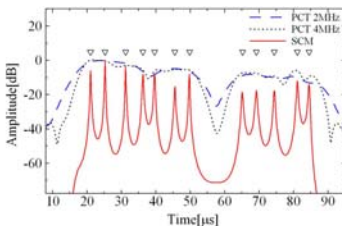


Fig. 1: Comparison of PCT and SCM in the case of twelve scatterers

Wednesday
Poster

P3-D-09

Fast Simulation of Second Harmonic Ultrasound Fields

Nicola Testoni¹, Karin Hensel², Monica Siepmann², Nicolò Speciale¹, Georg Schmitz², ¹ARCES/DEIS, Università di Bologna, Bologna, Italy, ²Lehrstuhl für Medizintechnik, Ruhr-Universität Bochum, Bochum, Germany

Background, Motivation and Objective

Numerical modeling of nonlinear (NL) ultrasound (US) beam propagation has a key role in designing state-of-art medical US systems due to the improvements in image quality coming from the use of second harmonic overtones. Describing the combined effects of diffraction, absorption and nonlinearity, the Khokhlov-Zabolotskaya-Kuznetsov (KZK) equation is the most commonly used model to address this simulation problem. Except when the source is an infinite plane, an exact solution of this equation is yet unknown, so computational models are used to simulate NL US fields. However, numerical schemes usually exploit stepping techniques to deal with propagation along the depth direction, causing prediction accuracy and computational cost to be strongly related to depth itself. This work introduces an algorithm capable to ease both these problems by providing good estimations of pressure profiles at arbitrary depth without requiring stepping techniques.

Statement of Contribution/Methods

Our proposal consists in a perturbative approach to the solution of the KZK equation cast in a discrete Fourier-Bessel (F/B) domain applicable for axisymmetric propagation from circular transducers. Basing on the assumption that pressure field at arbitrary distance from the US source admits a proper series representation, an approximate solution is obtained in a constructive way. The simulation consists of two steps: first, virtual sources with depth independent F/B coefficients are estimated from the real source ones; then, corrections to the predicted US field at arbitrary depth are applied. By properly addressing internal approximations, fine tune between accuracy and computational cost is possible.

Results

Simulated pressure profiles from two versions of the proposed algorithm and the output of a publicly available NL KZK solver (KZKTexas) were compared to experimental measurements conducted in a water tank. A Precision Acoustic HPM1/1 1mm needle hydrophone mounted on a tri-axial positioning system was used to measure the US pressure field generated by a Panametrics A392S flat immersion NDT transducer emitting a 5 cycle 1MHz sinusoidal train at different source amplitudes. Computational times and normalized root mean square error between simulated fundamental (RMSE1) and second harmonic (RMSE2) terms were recorded for each simulation. At 330kPa, simulation with KZKTexas lasted 1011.6s and provided -16.4dB RMSE1 and -17.3dB RMSE2; at the same pressure level, full precision algorithm resulted in 863.2s, -16.8dB RMSE1 and -19.0dB RMSE2; finally fast implementation yielded 88.6s, -16.8dB RMSE1, -12.6dB RMSE2. Very similar results were obtained for 108kPa.

Discussion and Conclusions

The proposed algorithm is capable of simulating NL US fields with accuracy at least comparable to other standard approaches to the same problem and significant computational savings. Performance improvements in the range of 2dB were recorded as well as cost reductions in excess of 90%.

P3-D-10

Small Calculus Detection for Medical Acoustic Imaging Using Cross-Correlation between Echo Signals

Hirofumi Taki¹, Takuya Sakamoto¹, Makoto Yamakawa², Tsuyoshi Shiina³, Toru Sato¹, ¹Graduate School of Informatics, Kyoto University, Kyoto, Japan, ²Advanced Biomedical Engineering Research Unit, Kyoto University, Kyoto, Japan, ³Graduate School of Medicine, Kyoto University, Kyoto, Japan

Background, Motivation and Objective

Small calculus detection in breast screening is important to differentiate malignant from benign masses. Despite several advances of acoustic imaging, medical acoustic imagers have insufficient ability to detect small calculus in comparison to X-ray imagers. Therefore the improvement of the calculus detection ability in acoustic imaging is strongly desired to serve an effective and low-cost screening technique without ionizing radiation. In this study, we proposed a novel method to detect small calculus using cross-correlation between echo signals behind a measurement point.

Statement of Contribution/Methods

Wednesday
Poster

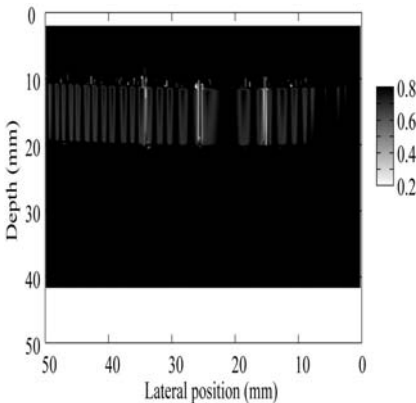
The proposed method employs a cross-correlation coefficient between echo signals of adjacent scan lines. The cross-correlation window is set behind a measurement point. When a small calculus exists in an acoustic beam, the waveform of a transmit wave changes severely. Therefore the echo waveform of a scan line with a calculus is quite different from that without a calculus, where the echoes return from a range behind the calculus. We can presume the existence of a calculus from a dip in the cross-correlation.

Results

We evaluated the effect of the proposed calculus detection method experimentally. We utilized RF signals of a medical acoustic imager (EUB-8500; Hitachi Co., LTD.). The center frequency of a transmit pulse is 7.5MHz. We employed three different copper wires 0.2, 0.29 and 0.40mm in diameter. The wires are set in a 4% agarose gel block for a 2cm depth, and the wire interval is 1cm. A polyethylene sheet 0.1mm thick is put close behind the wire. Agar gel contained 0.5% spherical polymer particles 7 μ m in diameter (Tech Polymer; Sekisui Plastics Co., LTD.). We set the correlation window as 8.3mm behind a measurement point. Figure shows the cross-correlation coefficient profile with a Wiener filter. In the profile dips exist at the points of three copper wires. The dips extended along the range direction to the length of correlation window. We also confirmed the effectivity of the proposed calculus detection method by computer simulations.

Discussion and Conclusions

We proposed a novel calculus detection method using cross-correlation between echo signals. The experimental study indicates the possibility that the proposed method has the ability to detect a small calculus 0.2mm in diameter.



P3-D-11

Multi-Dimensional Sub-Sample Motion Estimation: Initial Results

Reza Zahiri Azar¹, Orcun Goksel¹, Tim Salcudean¹; ¹Electrical and Computer Engineering, University of British Columbia, Vancouver, BC, Canada

Background, Motivation and Objective

Motion estimation in ultrasound images is important for many modern applications. We have recently presented pattern matching function interpolation techniques to determine motion in multi-dimensions with sub-sample accuracy. In these techniques, a multi-dimensional polynomial is fitted to the maximum of the discrete pattern matching coefficients and its neighboring lags. An estimation of the sub-sample motion in all directions is then achieved by finding the maximum of this fitted polynomial. In this work, the performance of these techniques is studied in 3D to determine the axial, lateral, and elevational components of motion with sub-sample accuracy using both simulated and experimental data.

Statement of Contribution/Methods

Following the coarse estimation of the motion within the sampling accuracy by locating the maximum of the discrete pattern matching function in 3D, a quartic polynomial with three variables $f(x,y,z)$ is fitted to the maximum of the discrete pattern matching function and its neighboring lags in the axial (x), lateral (y), and elevational (z) directions using a least squares fit. The sub-sample displacement is the estimated by locating the maximum of this fitted 3D polynomial using Newton's method.

Results

A virtual phantom was simulated and displaced over a 5x5x5 3D grid with a spacing of 1/4 of a sample in each direction. This grid spans ± 0.5 of a sample in all three axes. RF echoes corresponding to each of these configurations were generated using the FieldII simulation software. The proposed estimator was then applied to these simulated RF volumes in order to evaluate its performance in terms of bias and standard deviation. The mean absolute axial, lateral, and elevational bias of the proposed 3D quartic polynomial fitting was found to be 0.0060, 0.0075, and 0.0047 of a sample (corresponding to 120nm, 2.24 μ m, and 710nm), respectively. The performance of the method was also evaluated experimentally. A 3D motor-driven curved-linear transducer (4DC6-3/40) of a Sonix RP ultrasound machine (Ultrasonix, Richmond, Canada) was mounted on a 3-axis AIMS ultrasound scanning system (Onda Corp., Sunnyvale, CA) with 10 μ m resolution in each axis and submerged into a water tank equipped with a water conditioner. The motion of the probe was tracked by imaging a tissue mimicking phantom. The maximum tracking error of the proposed method was measured to be 12 μ m in all three axes which is very close to the accuracy of our experimental setup.

Discussion and Conclusions

The performance evaluation of a novel pattern matching function interpolation scheme, in simulations and experiments, demonstrates that it is suitable for accurate estimation of 3D motion. The proposed method outperforms other pattern matching interpolation methods presented in the literature in 3D motion estimation. Specific applications in medical ultrasound include fine 3D tissue motion tracking, motion vector estimation, strain tensor estimation, and tissue elasticity estimation.

P3-D-12

A BEM Study on Ultrasound Guided Wave Propagation in Bone-mimicking plates with microstructural effects

Maria Vavva¹, Alexios Papacharalambopoulos², Vasilios Protopoulos¹, Dimitrios Fotiadis¹:¹Dept of Material Science and Engineering, University of Ioannina, Greece, ²Dept of Mechanical Engineering and Aeronautics, University of Patras, Greece

Background, Motivation and Objective

Ultrasound guided wave propagation in bones has been largely based on the classical theory of elasticity. However, the mechanical behavior of materials with microstructure such as bone can be successfully modeled macroscopically using enhanced theories of elasticity. In a recent work, we used the simple Mindlin Form II gradient elastic theory to analytically derive the dispersion curves of the modes propagating in isotropic two-dimensional (2D) bone-mimicking plates with microstructure. We showed that microstructure results in significantly modified dispersion curves than those predicted by the Lamb theory, even at medium frequencies, i.e. 0.7-1 MHz, commonly used in ultrasonic bone studies.

In this work, we proceed to the numerical investigation of guided wave propagation in 2D bone models with microstructure, by using a Boundary Element Method (BEM). The results are compared to the theoretically obtained wave dispersion curves.

Statement of Contribution/Methods

The bone was modeled as an isotropic elastic material plate (4mm thick, density 1.5 g/cm³, longitudinal and shear velocity 4107 m/s and 1842 m/s, respectively). Two additional terms were introduced to account for bone's microstructure i.e., the gradient coefficient g and the micro-inertia term h , whose values were at the order of the osteons size. Computational simulations were performed for four different combinations between g and h in which $g \neq h$.

The analysis was performed numerically using the advanced Boundary Element Method/Fast Fourier Transform code which is able to solve dynamic gradient elastic problems. We used a transmitter-receiver configuration in which the emitted wave was simulated by a vertical transient loading, whereas the received signal waveform was the time history of the vertical displacements recorded at a 35 mm distance. The bone was considered free of stresses and double stresses. The modes were analysed in the time-frequency (t-f) domain. In order to validate the computational results we superimposed the theoretical dispersion curves on the t-f representation of the waveforms.

Results

The time-of-flight velocity was close to the bulk velocity value as predicted by the gradient elastic theory which is higher than the bulk wave in the classical case. In most cases, several modes could be well characterized in the t-f domain by the theoretical curves. The effect of microstructure was dependent on the absolute values of the coefficients and was less pronounced for the smallest value of h .

Discussion and Conclusions

Bone's microstructure was found to significantly affect mode dispersion in the 2D bone plates by inducing geometrical and material dispersion. Thus, microstructure is an important factor and should be considered in theoretical and computational bone studies. However, 3D bone models with microstructure accounting for bone's irregular geometry and anisotropy are needed so as to improve our understanding of wave guidance phenomena in real bones.

P3-E. Elasticity Methods: Clinical Applications

Sala Orange

Wednesday, September 23, 2009, 10:00 am - 11:30 am

Chair: **Jean-Yves Chapelon**
INSERM, Lyon

P3-E-01

Use of Ultrasound Elastography as a Tool for the Selection of Needle Gauges for Biopsy

Kishore Kumar¹, Suresh S², Jayashankar V¹; ¹Electrical Engineering, IIT Madras, Chennai, Tamilnadu, India, ²Ultrasound, Mediscan Systems, Chennai, Tamilnadu, India

Background, Motivation and Objective

In conventional ultrasound cysts appear dark due to its anechoic nature. Many instances sonologist found that fluid aspirated from the cysts is not just simple fluid like water but made up of complex fluids like puss, blood etc.

Three types of biopsy procedures are performed depending upon the abnormalities present – fine needle aspiration cytology (FNAC), core biopsy (CB) and cyst cytology. All biopsies are carried out using needle ranging from 21 gauge for FNA, 14 gauge for CB. Studies have shown that there are highly significant differences in pain scores with procedure type and needle size. The level of pain decreased significantly from a needle size of 21 gauge to needle size of 14 gauge. Due to the improper selection of needle gauge, biopsy may fail to collect sufficient sample and may lead to incomplete assessment. In order to collect sufficient samples either procedure may be repeated with same needle or with different gauge needle. This will lead to unnecessary pain and discomfort to the patient. The objective of this work is to explore the use of cyst elastogram in differentiating constituents of cyst fluids so that simple and complex cysts can be distinguished. This may avoid many unnecessary cyst cytology or fine needle aspiration (FNA) or help in the selection of proper needle gauges for biopsy.

Statement of Contribution/Methods

Polyacrylamide based tissue mimicking phantoms embedded with lesions of varying stiffness and cysts filled with fluids of varying viscosity are designed for the study. These phantoms are also used to teach or practice ultrasound guided core biopsy or FNAC. For solid lesion gauge selection is based on a five point elasticity score derived from elastogram of the lesion with score one corresponding to benign lesion. Characterization of cyst fluid is based on the parameters measured from color elastogram – mean and variance of R,G and B color components, relative chromaticity of lesions with surroundings etc. Using these parameters a grading is assigned to the complexity (viscosity) of fluids in the cysts. This grading is used to select the needle gauge for aspiration.

Results

Preliminary results using the phantoms have shown the promising results in differentiating simple and complex cysts. Grading system developed for the complexity of cyst fluid based on parameter measured from the color elastogram is useful in the selection of gauges. If the fluid is found to be viscous from the grading then sonologist must select an appropriate gauge needle so that sufficient sample can be collected for histopathological studies.

Discussion and Conclusions

Cyst elastogram can be used in differentiating simple and complex cyst so that unnecessary biopsy can be avoided. Elastography can aid in the selection of needle gauge for core biopsy and FNA so that unnecessary pain, patient discomfort and incomplete assessment can be avoided. Methods should be extended to biological lesions so that it can be used in clinical practice.

Monitoring Local Temperature Changes in Soft Tissues by Time-Reversal Elastography

Nicolás Benech¹, Stefan Catheline², Carlos Negreira¹; ¹Facultad de Ciencias, Laboratorio de Acústica Ultrasonora, Montevideo, Montevideo, Uruguay, ²Maison des Geosciences, Laboratoire Géophysique Interne et Tectonophysique, Grenoble, Saint Martin d'Heres, France

Background, Motivation and Objective

Elastography is a potential tool to evaluate local elasticity changes produced by thermal therapy ultrasound. The protein denaturation of tissue cells produces an irreversible increase in local stiffness. Thus elastographic methods are able to evaluate where and if this critical point has been reached. In previous works we have employed 1D transient elastography to monitor local changes in the shear elastic modulus in bovine skeletal muscle. In this work we include time-reversal elastography (TRE) experiments to evaluate temperature-induced changes on the local elasticity. TRE is currently a developing method in our laboratory. It is based on the time inversion of the low-frequency field recorded by speckle tracking methods. The method has the advantages of time-reversal experiments: it is independent of boundary conditions, is applicable in non-homogeneous media and is robust as regard to the low-frequency source shape and position. Thus it overcomes some limitations of 1D transient elastography.

Statement of Contribution/Methods

The low-frequency particle velocity field on the direction of the ultrasound beam (z direction) is measured at the volume of the soft solid by the transient elastography technique. The observation time is several hundreds of milliseconds (typically 500 ms) composed of speckle signals acquired at 1000 Hz pulse repetition frequency. The observation depth is 38 mm. The speckle correlation method allows to divide it in 38 measuring points separated 1 mm between them. The recorded field at a given position is time reversed and reemitted by the source. The resulted field converges at that position. The shear wave speed is deduced from the spatial and temporal focalization. In particular, the spatial width of the focal spot is directly related to the shear wavelength.

An electrical resistance was added inside the tissue sample to create a spatial dependent temperature profile. The TRE experiments are performed while the medium is heated and cooled. The spatio-temporal focalization process varies with time because the shear wave speed is temperature dependent. These variations are monitored by subtracting the reference field (recorded at time 0) from the actual field. The subtraction enhances small changes on the elastic field allowing to better monitor the heat induced changes.

Results

The preliminary results indicate changes on the spatio-temporal focalization of the TR field. The focal width is narrower around the heated zone. For low deposition rates ($\Delta T_{\max} \sim 12^\circ\text{C}$) these changes are reversible

Discussion and Conclusions

Limitations to TRE could arise in high attenuating media where the system is not time-invariant and thus the refocalization process is degraded producing a broadening in the spatial focusing with respect to theoretical limits. However, since subtraction of the reference field was performed, the method allows to estimate relative changes in the shear elasticity.

Exploration of abnormal skin tissue (Marfan Syndrome) with 2D high resolution elastography.

Gahagnon Solène¹, Gwendal Josse², Thomas Edouard³, Frederic Ossant^{1,4}; ¹INSERM U930, Tours, France, ²Research institute Pierre Fabre, Toulouse, France, ³CHRU Purpan, Toulouse, France, ⁴Bretoneau University Hospital, Tours, France

Background, Motivation and Objective

Many diseases directly affect the mechanical properties of biological tissues. Skin mechanical behavior can be explored using 2D high frequency elastography. We described and validated in previous work [1][2] an elastographic imaging system based on combination of two devices: an extensometer that submitted skin to an uniaxial stress cycle (stretching-holding-releasing) of ten seconds and a high resolution echographic system with an axial resolution of 150 μm (20 MHz) which acquired 10 images per second. This method allowed a mapping of internal displacement submit to mechanical stress stretching. We have also highlighted a complex behavior of the skin, behavior conditioned by the residual stress of the skin.

The purpose of the present study was to compare mechanical properties of healthy and diseased human skin with 2D high resolution elastography. The diseased subjects were stuck down by Marfan Syndrom, a disorder of connective tissue which notably affects the skin. A clinical study was conducted on 68 subjects: 23 subjects with Marfan's disease and 45 healthy subjects.)

Statement of Contribution/Methods

The high-frequency elastography system was used to perform axial strain kinetics during all the stress-cycle for a maximum uniaxial stretching of 20 % applied on the volar forearm for folded and tensed arm. The thickness of the dermis, the maximum effort applied with the extensiometer, the axial strain as well as the integral and the slope of axial strain kinetics were compared between the two groups of subject.

Results

Children with Marfan syndrome presented maximum effort, effort related to the thickness of the dermis, maximum and integral axial strain respectively greater than 32%, 49%, 78% and 76% compared to the control group. In addition, the levels of significance p are between 0,004 and 0,056. For the adults, there was no significant difference between the two groups.

Discussion and Conclusions

Finally, elastography allowed to differentiate the group of healthy subjects of the affected group with Marfan's syndrome.

[1] S.Gahagnon et al., "In-vivo exploration of the mechanical properties of healthy and pathological human dermis with 2D high resolution elastography", IEEE Ultr.Symp. Vancouver, 2006.

[2] Mofid Y et al., "High frequency elastography for in-vivo study of the mechanical behavior of skin", IEEE Trans. On Ultr., Fer. and Freq. Contr., Vol.53, N°5, 925-936, 2006.

P3-E-04

Imaging Tissue Mechanics in the Vicinity of Flow Channels: Phantom and *in vivo* results

Yayun Wan¹, Dalong Liu², Emad Ebbini¹, ¹Electrical and Computer Engineering, University of Minnesota, Minneapolis, MN, USA, ²Biomedical Engineering, University of Minnesota, Minneapolis, MN, USA

Background, Motivation and Objective

Accurate imaging of tissue motion and fluid flow at the boundary of major arteries may yield important information about the normal and disease states of these arteries. Traditionally, M-mode ultrasound was used to capture both flow and tissue motion profiles along a user-defined line of sight through the vessel walls. The recent introduction of ultrasound scanners with programmable imaging sequences and access to the beamformed RF data is allowing for new 2D imaging modes for simultaneous imaging of flow and tissue motion using 2D speckle tracking methods. Towards this end, we have designed an experimental evaluation of a robust 2D speckle tracking method for imaging tissue motion fields in the presence of flow channels, e.g. the carotid artery.

Statement of Contribution/Methods

We have recently introduced a robust 2D speckle tracking method, which employs the true 2D complex cross correlation to find sub-pixel displacements in both axial and lateral directions. The method was shown to achieve fine lateral tissue displacements with minimal lateral interpolation compared to previously published methods, even algorithms that utilize the analytic nature of the complex cross correlation in the axial direction. We have also modified the imaging sequence on a Sonix RP scanner to allow high frame rate 2D data collection in a limited field of view covering the cross section of the flow channel (M2D-mode imaging). In this mode, it is possible to track the 2D tissue motion at the boundaries of the channel with sufficient reliability to characterize the operation of the channel.

Results

Cross sectional M2D images of a 4-mm flow channel in an ATS Model 524 phantom were collected under controlled flow conditions (using a roller pump). Axial and lateral displacement fields in the tissue-mimicking regions surrounding the channel were evaluated using our 2D phase-coupled displacement tracking algorithm and were shown to reliably reflect the changes in flow conditions. In addition, we collected M2D-mode cross sectional images of the carotid artery of a healthy volunteer to characterize the tissue motion field in the vicinity of the artery. The axial displacements showed remarkable continuity at frame rates as low as 90 fps and allowed for smooth and contiguous evaluation of the axial strain and axial shear strains. These, in turn, provided fine definition of the boundaries of the vessel and their motion in both axial and lateral directions.

Discussion and Conclusions

The results from the flow phantom and *in vivo* experiments suggest strongly that the tissue mechanics in the vicinity of arteries can be captured reliably with high spatial and temporal resolution using ultrasound. Extending the results to 3D scanning of the vessel of interest (e.g. for screening purposes) will allow for an easy and rapid characterization of abnormalities in the boundaries of the flow region (e.g. due to abnormalities in the wall stiffness).

P3-F. Motion Tracking and Elasticity Imaging

Sala Orange

Wednesday, September 23, 2009, 10:00 am - 11:30 am

Chair: **Mark Palmeri**
Duke University

P3-F-01

B-mode Image Contrast Improvement and 2-D Strain Estimation Using Satellite-View Imaging Method

Makoto Yamakawa¹, Kengo Kondo², Tsuyoshi Shiina³, ¹Advanced Biomedical Engineering Research Unit, Kyoto University, Kyoto, Japan, ²Graduate School of Systems and Information Engineering, University of Tsukuba, Japan, ³Graduate School of Medicine, Kyoto University, Japan

Background, Motivation and Objective

The contrast of B-mode images is poorer than that of CT/MRI images, and only axial direction blood flow or strain is measurable with sufficient accuracy. Therefore, we improved the contrast of B-mode images by measuring an object from many viewpoints using two or more probes (satellite-view imaging) and by transmit dynamic focusing with a virtual point sound source. We also measured 2-D strain with sufficient accuracy using this satellite-view imaging method and quantitatively evaluated tissue elasticity.

Statement of Contribution/Methods

For the satellite-view imaging, we made a system that can control two probes freely within the same measurement plane. We also made a 128-channel ultrasonic transmitting and receiving system that can perform transmit dynamic focusing with a virtual point sound source. First, we estimated the relative position of two probes using multi-view targets. Next, in each probe, we performed transmit dynamic focusing using virtual point sound source transmission employing 32 elements. Finally, we compounded the signals measured in each probe based on the relative probe position and created a satellite-view image. We were able to estimate the axial displacement in each probe by the extended combined autocorrelation method we developed previously and calculated the 2-D strain by vector composition of these displacements based on a relative probe position. We also defined the 2-D strain ratio (the ratio of volume strain) based on the elastic equations for a more quantitative tissue elasticity evaluation.

Results

The relative probe position estimation accuracy was 0.076mm. In a phantom experiment, the contrast (defined as the difference between signal level of the object and the circumference divided by the signal level of the circumference) of a conventional B-mode image was 13.6%. However, the contrast of the satellite-view image was improved to 34.3%. Moreover, in an experiment using a phantom containing a hard inclusion with lateral compression, the lateral strain estimation accuracy of the conventional method was inadequate, and a 4mm inclusion could not be imaged. However, the satellite-view imaging method was able to image the inclusion. Moreover, it was quantitatively determined by the 2-D strain ratio that the inclusion is about seven times harder than the circumference.

Discussion and Conclusions

The contrast of a satellite-view image became about 2.5 times that of a conventional B-mode image. However, the resolution did not improve this time in spite of employing transmit dynamic focusing. Therefore, we will try to further improve the precision of the relative probe position. The satellite-view imaging method can estimate lateral strain with sufficient accuracy, and we can perform a quantitative tissue elasticity evaluation using 2-D strain ratio. In contrast, the conventional method is inaccurate and cannot image a 4mm inclusion.

P3-F-02

On the Imaging of Slip Boundaries Using 3D Elastography

Leo Garcia¹, Christopher Uff¹, Jeremie Fromageau¹, Jeffrey Bamber¹; ¹Joint Department of Physics, Institute of Cancer Research, Sutton, Surrey, United Kingdom

Background, Motivation and Objective

Elastography has been found to provide indication of the degree of bonding (or mobility) at tumour-tissue boundaries, a clinically useful property due to its dependence upon tumor pathology. It is hypothesised that three-dimensional (3D) elastography, now possible through 2D ultrasound transducers which are swept elevationally, may aid this assessment.

Statement of Contribution/Methods

This study aims to examine the appearance of a mobile tumour in elastography through 3D finite element (FE) analysis in comparison with experimental 3D ultrasound data acquisition conducted upon an approximately equivalent phantom, such that we may compare the results and gain experience in utilizing and analyzing 3D strain data from mobile tumours.

A 3D model of a sphere inside a cube, intended to approximate a tumor surrounded by healthy tissue, was generated using commercial FEM software COMSOL Multiphysics v3.5a (COMSOL, USA). The inclusion was four times as stiff as the background and the coefficient of friction at the tumor interface was approximately zero. A quasi-static axial compression of 1 % the model height was applied at the upper model surface and the resulting displacements and strain predicted. Gelatin phantoms (of equal dimensions to the model) were manufactured such that the inclusion could slip freely against its surroundings through the injection of water onto the inclusion surface, and compressed (as above) whilst its displacement was monitored with a 3D ultrasound probe utilising 3D ultrasound elastography acquisition software Stradwin 3.6 (University of Cambridge, UK).

Results

There is good agreement between FEM results and experimental results. Both show the occurrence of a discontinuity in displacement data at the tumor boundary, caused by the surrounding tissue slipping past the tumour. Both results show a region of high axial strain surrounding the tumor surface due to high mobility of the tissue compared to the tumour and not, as may be assumed in traditional elastographic interpretation, low Young's modulus. It has also been found that elevational (orthogonal to traditional 2D scan plane) displacement is higher in mobile tumours than in tumours adhered to their surroundings. 3D visualisation of axial strain data allows for detection of regions of mobility on the entire tumour surface.

Discussion and Conclusions

There is good evidence that we may trust our simulations for future studies into how we may exploit elastography to detect tumour boundaries and also our method of introducing tumour mobility in phantoms. It has been shown that 3D elastography allows visualisation of the entire boundary of a mobile tumour; information which we hope holds clinical potential for intra-operative tumour resection surgery in the brain, where tumour boundary definition is vital yet often difficult. It may also provide an approximate method of tumour volume estimation. A clinical *in vivo* study using the 3D elastography system reported is already underway.

P3-F-03

Robust Motion Estimation Using Complex Principal Components

F William Mauldin, Jr.¹, Francesco Viola¹, William F Walker^{1,1}; ¹Biomedical Engineering, University of Virginia, Charlottesville, VA, USA

Background, Motivation and Objective

Motion estimation is central to a variety of clinical ultrasound applications. In each of these applications, bias and variance errors are introduced by a variety of sources including electronic noise, decorrelation, aliasing, and inherent algorithm limitations. Unlike electronic noise, decorrelation is a noise source with coherence over time and with the same power spectrum as the signal. Thus, reducing decorrelation is impossible through frequency domain filtering or simple averaging and must be achieved through other methods.

Statement of Contribution/Methods

In this paper we introduce a novel motion estimator, termed the principal component displacement estimator (PCDE). This technique is capable of removing noise sources even if they overlap with the signal of interest in the frequency domain and maintain coherence over time. PCDE was compared to normalized cross-correlation with

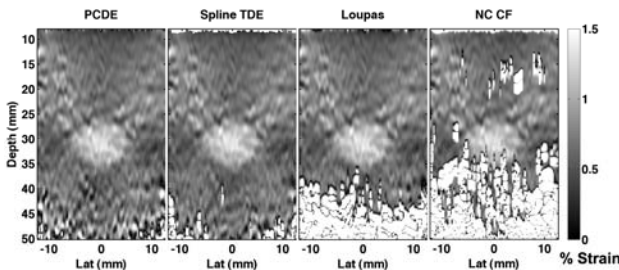
cosine fitting, Loupas' 2D autocorrelator, and spline-based time delay estimation (sTDE) in simulation and experimental elastography data. Compressions of approximately 1% were applied to a CIRS elastography phantom with 10.4 mm diameter lesions that had a contrast modulus ranging between -10 and 12 dB. PCDE was also applied to echo data from an acoustic radiation force imaging technique, termed sonorheometry, which is used to monitor blood hemostasis.

Results

PCDE outperformed other algorithms in terms of bias and standard deviation across a wide range imaging parameters. Under typical acoustic radiation force imaging conditions, PCDE reduced bias and standard deviation in simulation by over 33% compared to other algorithms. When operating on experimental elastography data, PCDE exhibited robust performance to decorrelation noise. Displacement variance at imaging depths between 40 and 45 mm was reduced by more over an order of magnitude and average improvements in CNR were as much as 8.64 dB over Loupas. Computational speed in MATLAB for PCDE is on the same order of magnitude or faster than for Loupas, depending on ensemble length.

Discussion and Conclusions

The data presented in this paper illustrate that PCDE is a robust motion estimator with a relatively minimal computational cost, making it superior for real-time imaging applications that are currently limited by decorrelation errors. This work was supported by NIH grant EB005433.



P3-F-04

Novel 2D displacement Estimation using Free-shape Kernels of RF-Data in Rotating and Shearing Structures

R.G.P. Lopata¹, H.H.G. Hansen¹, M.M. Nillesen², J.M. Thijssen², C.L. de Korte^{1,2} *Clinical Physics Lab, Department of Pediatrics, Radboud University Nijmegen Medical Center, Nijmegen, Netherlands, ²Clinical Physics Lab, Children's Hospital, University Medical Center St Radboud, Nijmegen, Netherlands*

Background, Motivation and Objective

2D and 3D RF-based strain imaging techniques are being used in a variety of applications. However, in cardiac and vascular applications, rotational movement of tissue often occurs. This fundamental study examines the feasibility of measuring rotation and the performance of strain estimation in shearing and rotating structures using four different RF-based methods.

Statement of Contribution/Methods

A block (5 cm x 5 cm) containing 3.5 million scatterers was used as input for Field II©. The block was subjected to a shear strain of 2.0, 4.0 and 6.0% in combination with an applied load of 0.0, 1.0 and 2.0% vertical strain. Secondly, experiments with the block rotated over a range of 0.5° to 5.0° and 10° (with again 0.0 – 2.0% vertical strain) were performed. RF-data were simulated for a linear array transducer (fc = 8.7 MHz, pitch = 135 µm), resulting in images of 5.0 cm x 3.0 cm. Displacements were estimated using a coarse-to-fine strain algorithm with sub-sample aligning and stretching of data using 1D and 2D pre-compression kernels (method I and II, respectively). A different approach was developed in which the search area was not limited to a box-shaped 2D region: Axial displacements were used to deform the kernel in the axial direction freely, resulting in shapes such as parallelograms (method Ia and IIa). All four methods were applied to the simulated data and the displacements, strains and rotations were estimated.

Wednesday
Poster

Results

The study revealed that method IIa outperformed the other methods. The root-mean-squared error (RMSE) between applied and measured, unfiltered displacements was calculated. The shearing experiment showed a significant improvement for higher shear strains for each applied load (up to 33% and 40% lowered axial and lateral RMSE, respectively). The RMSE of the axial strain reduced with 70% and the elastographic SNR (SNRe) increased by 10 dB. Rotations could be measured up to 5.0° by all methods. The maximum axial and lateral displacements at 5.0° were ± 1.4 mm. Method IIa outperformed the other methods and the axial and lateral RMSE decreased with 47 – 94% and 18 – 36%, respectively. For increasing angles, the measured cross-correlation decreased from 0.92 to 0.50 for method II and from 0.91 to 0.65 for method IIa. After reconstruction, the mean angles were 0.5° , 0.9° , 1.9° , 2.8° , 3.8° , 4.8° , with a standard deviation of 15% on average. The SNRe of the strain estimates reduced significantly for increasing angles. Method IIa showed a drop in axial SNRe from 37 to 22 dB thereby outperforming method II (drop of -65dB). The lateral SNRe revealed a negative correlation (-5dB/degree) for all methods. Again, method IIa outperformed the other methods by +24 dB.

Discussion and Conclusions

In conclusion, the proposed 2D free-shape method (IIa) enhances the measurement of rotation and of shear strains. Rotations can be measured up to 5.0° . Additional experimental validation of the method has to be performed.

P3-F-05

The spatio-temporal strain distribution in inhomogeneous poro-elastic phantoms.

Jeremie Fromageau¹, Gearoid Berry¹, Jeff Bamber^{1,1} Joint Department of Physics, Institute of Cancer Research and Royal Marsden NHS Foundation Trust, Sutton, Surrey, United Kingdom

Background, Motivation and Objective

Several studies described the technique to estimate the poroelasticity in homogeneous tissues using ultrasound elastography. Indeed, the time dependent strain to a sustained force gave information on the capacity of the fluid to diffuse in the porous structure. The case of two poroelastic media together, where the liquid can flow both in a porous vasculature network or be transferred in the surrounding matrix, is less documented. In this case two different behaviours can be observed. When the pressure in the vasculature is high the fluid transfer occurs from the vessels to the surrounding matrix, or, in the opposite, if an external load is applied to the surrounding medium the fluid is expelled thru the porous vessels. In this study we propose to study the latter case.

Statement of Contribution/Methods

Finite element analysis software (Mentat, Msc Software) was used to model a cylinder embedded in a cube. The cylinder was chosen with a high permeability whereas the background was quasi-elastic. A load in two phases was applied. First a linearly increasing load was applied on the top surface of the cube for 1 s, and then the load was sustained for 60 s.

An experiment with similar geometry and boundary conditions was also performed. The poroelastic cylinder consisted in a network of fibers used in a dialysis filter (BIO-1000WET, Asahi medical corp), and the surrounding matrix consisted in a mix of gelatine and agar. The phantom was observed with a ultrasound scanner (DIASUS, Dynamic Imaging), using a 7 MHz probe. The probe was connected to a test instrument (Instron 3342), permitting to control its displacement with a stepper motor and also to record the pressure applied during the whole experiment. The strain in the phantom was estimated from the RF signals using a 2D cross-correlation elastography method.

Results

The elastograms obtained experimentally clearly showed 3 regions with very different strain. A homogenous strain was observed in the surrounding matrix, a high strain in a circular region around the cylinder was also observed, whereas in the middle of the cylinder the strain appeared lower and more constant along the time. In the three regions, the time release, in order of the s, was smaller that what was expected from previous studies. In comparison the finite element analysis also showed the three different regions at the beginning of the load, but the strain at the interface and in the cylinder became more homogeneous along the time.

Discussion and Conclusions

The circular high strain region showed that the fluid transfer is more important at the interface between the cylinder and the background, but not in the core of the cylinder. This difference of behaviour between simulation and experiment can be explained by the fact that the network of fibers in the cylinder is not a perfect homogenous medium. The quantitative poroelastic parameters will also be presented.

An ultrasonic technique for imaging of tissue motion due to muscle contraction

Jason Silver¹, Yuu Ono¹, Andy Adler¹; ¹Carleton University, Canada

Background, Motivation and Objective

There are currently various techniques used to study muscles and their motion, such as mechanomyography, electromyography and acceleromyography. However, these methods give only global information about the musculature and its movement. Ultrasonic techniques provide promising methods that allow detailed study of muscles internally and locally. An objective of this research is to develop an ultrasonic technique by means of a tissue motion simulator, which could measure a tissue displacement accurately for real-time imaging of muscle contraction.

Statement of Contribution/Methods

A tissue-mimicking 3-layer phantom was constructed with 1 w% and 3 w% agar layers and a Plexiglas plate, having a thickness of 9 mm, 20 mm and 12 mm, respectively. Graphite powder was dispersed into the agar layers as ultrasound scatterers. This phantom simulates a structure of fat, muscle and bone. An ultrasonic probe having a center frequency of 6 MHz was attached to the top surface of the phantom. In order to simulate muscle contraction, one side of the agar layer was horizontally compressed by a piston using an electric motor while the opposite side was fixed. This resulted in a vertical motion of the agar layers beneath the probe. A method was also developed that allowed for accurate displacement measurements including an algorithm to remove motion artifacts. This algorithm is essential because a commonly employed clutter filter may not be applicable due to the frequency proximity between the desired muscular motion and unwanted probe or body motion.

Results

Radio frequency (RF) ultrasonic signals reflected from the interfaces between the layers and from the scatterers in the phantom were acquired using an M-mode. The sampling frequency was 33.3 MHz and the pulse repetition rate was 980 Hz. The phantom specimen was compressed at a rate of 4 Hz using the developed simulator. The vertical displacement at each depth was obtained by analyzing the phase variations of the RF signals using a quadrature demodulation and autocorrelation technique. The displacement velocity was also obtained by taking the derivative of the displacement with respect to the time. The periodic 4 Hz displacement was clearly observed for all depths except those in which the signal-to-noise ratio of the RF signal was very poor.

Discussion and Conclusions

Body motion may cause vertical movement of the ultrasonic probe held manually during RF signal acquisition. This will result in a measurement error of the tissue displacement. Since it can be assumed that bone is not compressed due to muscle contraction, a variation of the time delay of an echo reflected from a bone may be used to estimate probe movement. An algorithm and procedure to calibrate the effect of such movement has been developed and applied in a phantom experiment. The motion artifact from probe movement was effectively corrected by the proposed technique. The results of in vivo experiments of an arm stimulated with an electric muscle stimulator have also been discussed.

P3-G. Vascular Elastography

Sala Orange

Wednesday, September 23, 2009, 10:00 am - 11:30 am

Chair: **Hiroshi Kanai**
Tohoku University

P3-G-01

Reflected Shear Wave Imaging (RSWI) of Atherosclerosis

Russell Behler¹, Timothy Nichols², Elizabeth Merricks², Caterina Gallippi¹, ¹Biomedical Engineering, University of North Carolina at Chapel Hill, Chapel Hill, NC, USA, ²Pathology and Laboratory Medicine, University of North Carolina at Chapel Hill, USA

Background, Motivation and Objective

Atherosclerotic risk stratification may be improved by identifying soft lipid-rich or necrotic plaque regions, fibrous caps, calcium deposits, and other plaque components with disparate mechanical impedances. Mechanical impedance interfaces reflect acoustic radiation force (ARF)-induced shear waves. *We hypothesize that these shear wave reflections can be detected by tracking in the region of ARF excitation and that the reflections are indicative of nearby plaque components with different mechanical impedances in RSWI.*

Statement of Contribution/Methods

RSWI was performed using ARF excitation with a Siemens SONOLINE Antares™ imaging system specially modified for research purposes and VF7-3 transducer (Siemens Medical Solutions USA, Inc. Ultrasound Division). Shear wave reflections in the region of excitation were detected as inflections in (zero-crossings in the 2nd time derivative of) median-filtered (0.4 ms time window) 1D axial displacement profiles. Parametric images of the number of shear wave reflections and time of shear wave reflections were rendered. Shear wave velocity (SWV) was calculated in SWRI using a least squares fit of $SWV=2*\Delta d/\Delta T$, where Δd is the lateral distance traveled and ΔT is arrival time difference of the reflected shear wave. RSWI was performed in an agar tissue mimicking phantom (Young's modulus ~ 97 kPa) with a 1 mm glass bead inclusion, in two familial hypercholesterolemic (FH) pig iliac arteries ex vivo, and in one FH pig iliac artery in vivo. Phantom RSWI measures of SWV were compared to those of SWEI imaging, and RSWI results in pig arteries were validated by spatially matched immunohistochemistry.

Results

In phantom experiments, negative shear wave reflections were detected in the region of ARF excitation beside the glass bead across the lateral FOV (7.5 mm), which supported a RSWI SWV measurement of 3.92 +/- 0.08 m/s (versus 3.97 +/- 0.07 m/s by SWEI). In ex vivo RSWI of a large focal plaque, multiple negative shear wave reflections were detected in a necrotic region positioned between a fibrous cap and a large calcium deposit with collagen deposition. The RSWI SWV measurement in this region was 16 +/- 2 m/s. In ex vivo RSWI of a second large focal plaque, negative shear wave reflections were detected across a 6 mm lateral span that corresponded to a highly heterogeneous region containing both lipid and collagen deposits. Notably, this region did not appear to be highly displaceable or heterogeneous by conventional ARFI imaging. In in vivo RSWI of a plaque, negative shear wave reflections were detected inside an atheromatous core containing a small calcium deposit, and RSWI SWV was 4.98 +/- 0.83 m/s.

Discussion and Conclusions

These pilot results suggest that RSWI improves identification of soft, lipid-rich or necrotic plaque regions near fibrous cap, calcium, and collagen deposits. RSWI supports SWV estimation, which may be useful for quantitative ARF-based imaging.

Wednesday
Poster

Application of a transient elastography technique to the characterization of the arterial wall elasticity

Javier Brum¹, Nicolas Benech¹, Daniel Bia², Ricardo Armentano², Carlos Negreira^{1,1} *Instituto de Física, Facultad de Ciencias, Universidad de la República, Montevideo, Uruguay.* ²*Departamento de Fisiología, Facultad de Medicina, Universidad de la República, Montevideo, Uruguay*

Background, Motivation and Objective

Modifications of the biomechanical properties of the arterial wall can be associated with various diseases, for example arteriosclerosis and atherosclerosis. The early detection of these modifications allows an early diagnosis of these pathologies. With this objective several ultrasonic methods have been developed (i.e. Pulse Wave Velocity, M-mode Imaging, Intra Vascular Ultra Sound) to evaluate the different mechanical parameters which characterize the arterial wall. However, more accurate methods remain to be developed. The objective of this work is to adapt a transient elastography technique to evaluate the shear elasticity of the arterial wall and its in vivo application.

Statement of Contribution/Methods

Experiences in an arterial phantom made of Alcohol Polyvinil Cryogel (PVA), 1% PVA diluted in water with 1% of Sigmacell Cellulose as ultrasound scatter, were performed. The PVA material, from where the arterial phantom was made, was previously characterized by transient elastography. The phantom has a 3 mm inner radius and a 2 mm wall thickness. The arterial phantom was surrounded by an agar-gelatin based phantom (3% gelatine diluted in water with 1% agar as scatter), which mimics the surrounding tissue. A low frequency source (~ 100 Hz) acts on the sample's free surface generating shear waves inside the volume of the sample. A 10 MHz ultrasonic transducer is placed on the sample surface. The low frequency excitation is synchronized with the ultrasonic reception via the PC. Each A-Scan is sampled at 40 MHz with 1 kHz repetition rate. The shear wave propagation as a function of time and depth is obtained through a speckle cross correlation technique.

Since the goal of this work is the in vivo application of this technique, a second in vitro experience is conducted. The sample is connected to a circulating loop capable of mimicking the physiological pressure and flow conditions inside an artery. The circulating loop consists of an artificial heart (Jarvik model 5, Kolff Medical) coupled to a perfusion line. The artificial heart is driven by a pneumatic pump which provides the desired heart rate and pressure values.

Results

Studying the phase variation of the shear wave as a function of depth, a local estimation of the shear elasticity is obtained. At a depth of 15 mm a change in the local shear elasticity is observed due to the presence of the arterial phantom. The obtained elasticity for the arterial phantom and its surroundings are 16.08 kPa and 1.7 kPa respectively. A general agreement within 10% was found with the measurements using transient elastography. Three arterial phantoms of different shear elasticity were evaluated.

Discussion and Conclusions

In all three cases the obtained results are in good agreement with the previous characterization through transient elastography. Future works concern the application of this technique in in vitro and in vivo measurements on real arteries

Theoretical and experimental studies on group velocity for estimating the elasticity of arteries

Xiaoming Zhang¹, James Greenleaf^{1,1} *Physiology and Biomedical Engineering, Mayo Clinic, Rochester, Minnesota, USA*

Background, Motivation and Objective

Increased stiffness of arteries has recently gained acceptance as an independent risk factor for cardiovascular diseases. Pulse wave velocity (PWV) is widely used for estimating the stiffness of an artery. However, PWV is an average indicator of artery stiffness between two measuring points, and therefore does not identify local stiffness. We have developed a noninvasive method for generating and detecting the wave propagation in the arterial wall [X. Zhang et al., IEEE Trans. Ultrason. Ferroelect. Freq. Contr., vol. 52, pp. 642-652, 2005]. The phase velocity can be measured accurately over a few millimeters. The elasticity of the artery can be estimated from the phase velocity.

Statement of Contribution/Methods

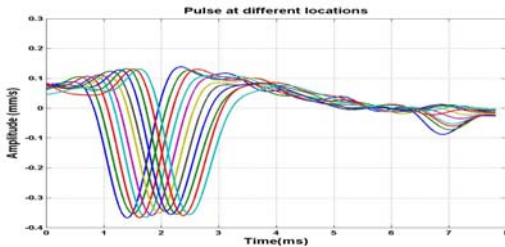
For in vivo artery studies, a short tone burst of ultrasound radiation force is preferred for generating an impulse wave in artery which reduces heat effects to the artery. In this paper, a mathematical model for group velocity analysis is developed from a three-dimensional cylindrical shell theory.

Results

Experimental studies on group velocity are carried out on natural latex tubes in air. A short pulse is generated with one cycle of 1000 Hz sinusoidal wave on the tube by an electromechanical shaker. The impulse response of the tube is measured by a laser vibrometer. Fig. 1 shows eleven impulse waves measured every 2 millimeters for 20 millimeters along the tube. The group velocity is measured by cross correlation analysis of the pulses at different locations. The measured group velocity is 17.83 ± 0.23 m/s for a tube with 4.8 mm outer diameter and 0.8 mm thickness. The group velocity calculated by our theory, given the properties and geometry, is 17.22 m/s at the 1000 Hz.

Discussion and Conclusions

A mathematical model is developed to calculate the group velocity of impulse propagation in viscoelastic tubes. The theoretical analysis agrees with the experiments well. The theory can be used for estimating the elasticity of arteries from the group velocity measurements.



P3-G-04

Non-invasive assessment of shear strain in the carotid arterial wall based on ultrasound radiofrequency data

Tim Idzenga¹, Hendrik Hansen¹, Richard Lopata¹, Chris de Korte¹; ¹Clinical Physics Laboratory, Dept. of Paediatrics, UMC St. Radboud, Nijmegen, Netherlands

Background, Motivation and Objective

Stroke is a major cause of death and is often caused by rupture of plaques in the carotid artery. Some of these plaques are vulnerable and prone to rupture, while other plaques are stable. It is hypothesized that the pulsating blood flow induces shear strain in the adventitial layer surrounding the artery, which might be related to the vulnerability of plaques. In this study we examined the feasibility of accurately assessing shear strain in the adventitia using non-invasive ultrasound.

Statement of Contribution/Methods

Ultrasound data of a carotid artery, consisting of three layers, were simulated using Field II. Longitudinal displacements (1 – 200 μm) were applied to the inner layer (arterial wall) with respect to the outer layer (surrounding tissue). This resulted in shear strain (0.1 – 20%) in the middle layer (adventitia). Furthermore, we constructed a three layered phantom from PolyVinyl Alcohol and applied displacements (50 – 500 μm) to the inner layer in longitudinal direction. Radiofrequency (rf) data were acquired using a (simulated) linear array transducer (11-3L, $f_c = 7.5$ MHz, pitch = 135 μm). Longitudinal displacement (and subsequently shear strain) were estimated using a coarse-to-fine strain algorithm. We also acquired a series of sequential images of the carotid artery in a human volunteer during five cardiac cycles and estimated the shear strain in the adventitial layer.

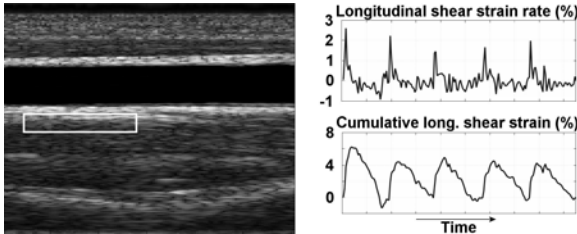
Results

In both simulations and phantom data the estimated shear strain increased linearly (Linear Regression, $p < .05$) with the applied displacement. The simulation estimates were similar to the applied values (root-mean-square-error

(RMSE) between 2 and 5 %). In the phantom, the calculated values underestimated the applied values (RMSE between 7 and 30 %). This is probably due to simultaneous displacement of the outer layer and/or compressibility of the material. In vivo the estimated shear strain was cyclic and reproducible over five cardiac cycles (see Figure 1). The estimated cumulative shear strain in the adventitia is a factor 10 smaller than earlier reported values in the intimal layer.

Discussion and Conclusions

In simulations and in a phantom we have shown that accurate assessment of shear strain is feasible using radiofrequency data. It was shown in vivo that this technique allows reproducible shear strain estimation in the adventitia during the cardiac cycle.



P3-G-05

Ultrasound wall-tracking diameter distension for assessment of arterial distensibility: an urgent need for direct stiffness measurement

Patrick Segers¹, Abigail Swillens¹, Thomas De Schryver¹, Sebastian Vermeersch¹, Ernst Rietzschel², Marc De Buyzere²:¹Ghent University, Belgium, ²Ghent University Hospital, Belgium

Background, Motivation and Objective

Arterial stiffness is increasingly used as an early marker of atherosclerosis and for the individual's assessment of cardiovascular risk. Ultrasound wall tracking allows assessing circumferential strain in arteries as $\Delta D/D$ (with D diastolic diameter and ΔD cyclic diameter change) or the distensibility coefficient $DC = (\Delta D/D)/\Delta P$ with ΔP the local pulse pressure (applanation tonometry). DC is systematically used as a measure of arterial stiffness in clinical research. Although DC depends on intrinsic stiffness, it also depends on geometry. As arteries remodel with age and in response to hemodynamic stimuli, it is anticipated that arterial structure and stiffness interfere, complicating the interpretation of DC. In this study, we reconcile arterial stiffness measured within the framework of the Asklepios population study.

Statement of Contribution/Methods

Diameter, intima-media thickness (IMT) and DC of the left common carotid artery were assessed in 2315 (1191W) apparently healthy subjects (age 35-56), using vascular ultrasound (Vivid 7, 12L probe) and wall tracking (media-adventitia transition) techniques. Subjects were stratified according to gender and age (4 categories). Evolution of DC and IMT/D with age was evaluated within the context of a theoretical framework linking DC, IMT/D and the Young elasticity modulus E [$DC = 1/(2.E.IMT/D)$].

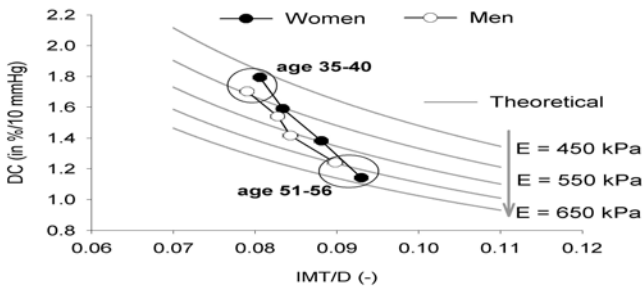
Results

The figure displays the theoretical relation (grey lines) between DC and IMT/D for E = 450 to 650 kPa. Symbols display measured data for men and women, averaged over 4 age categories. DC was higher in women than in men for age (35-40), while the inverse was true at age (51-56), suggesting a more rapid increase in stiffness in women. This evolution in DC is partly explained by arterial remodelling (increase in IMT/D) accompanied by an increase in intrinsic stiffness. While DC decreases by >30%, our data suggest an increase in intrinsic stiffness of about 25% over the studied age range. The relation between IMT/D and DC is virtually parallel for men and women.

Discussion and Conclusions

Clinically used measures of arterial stiffness, derived from ultrasonic measurement of circumferential strain, are intrinsically dependent on arterial geometry. Direct measurements of stiffness are highly needed to avoid the ambiguity between an artery's cinematic behaviour and its intrinsic mechanical properties.

Wednesday
Poster



P3-G-06

Lateral Motion Estimator for Measurement of Artery-Wall Displacement

Hideyuki Hasegawa¹, Hiroshi Kanai²; ¹Graduate School of Biomedical Engineering, Tohoku University, Japan, ²Graduate School of Engineering, Tohoku University, Japan

Background, Motivation and Objective

Artery-wall motion due to the heart beat is thought to occur only in the arterial radial direction because the main source of the motion is blood pressure. However, it has recently been reported that the artery also moves in the longitudinal direction. Therefore, both the radial (axial) and longitudinal (lateral) displacements should be estimated. Methods based on 2D correlation of RF echoes are often used to estimate the lateral displacement. However, these methods require much interpolation to achieve a sufficient spatial resolution. To overcome this problem, Jensen et al. modulated the ultrasonic field in the lateral direction to utilize the lateral phase. This method is useful but special beamformers are required. The present paper describes a phase-based method which can be used with a conventional beamformer.

Statement of Contribution/Methods

When an object moves in the lateral direction, the lateral profile of the echo amplitude is shifted depending on the magnitude of object's displacement. This lateral displacement can be estimated if the fluctuation frequency and phase (denoted as lateral phase ϕ) of the lateral echo amplitude profile can be determined. However, it is usually difficult to use the lateral fluctuation frequency because it is not determined by the ultrasonic frequency but is determined by the spatial distribution of reflection coefficient of the object. We propose a method to estimate the lateral displacement by determining the relationship between the change in the lateral phase and the lateral displacement. This relationship can be estimated by calculating the complex correlation functions between complex echo signals in two consecutive frames at multiple lags in the lateral direction because it can be considered that the lateral displacement is increased by a known quantity (= spacing of scan lines) when the lateral lag increased by one. This procedure yields the relationship (assumed to be linear) between the change in the lateral phase (= phase of the correlation function) and the lateral displacement. Complex echo signals were generated by the Hilbert transform applied to the echo amplitudes with respect to the lateral direction.

Results

The proposed method was validated using a cylindrical phantom made from silicone rubber. The error in the lateral displacement estimated by the proposed method was 13.5% (to the true displacement of 0.5 mm) with a correlation kernel size of 0.6 mm in the lateral direction, which was slightly smaller than the width at -20 dB of the maximum of lateral ultrasonic field (about 0.8 mm). This error was smaller than that (64.0%) obtained by the lateral modulation method with a larger kernel size of 3.6 mm.

Discussion and Conclusions

In this study, we developed a phase-based method for the estimation of lateral displacements with a good accuracy, that can be used with a conventional beamformer.

P3-H. Ultrasound Segmentation

Sala Orange

Wednesday, September 23, 2009, 10:00 am - 11:30 am

Chair: **Olivier Basset**
CREATIS, Lyon

P3-H-01

Level-set segmentation of myocardium and epicardium in ultrasound images using localized Bhattacharyya distance

Martino Alessandrini¹, Denis Friboulet¹, Olivier Basset², Jan D'Hooge³, Olivier Bernard²; ¹CREATIS-LRMN, villeurbanne, France, ²CREATIS-LRMN, France, ³Department of Cardiovascular Diseases, Belgium

Background, Motivation and Objective

Level sets have successfully been used for segmentation of the endocardial border in cardiac US images. Robust methods have been proposed within a Bayesian framework [1]. However, segmentation of the whole myocardial wall is still challenging given that the epicardial boundary is highly heterogeneous and discontinuous. The presence of papillary muscles may also complicate endocardial boundary detection. We propose a novel level set technique for combined endo- and epicardial boundary segmentation. Hereto a localizing approach is used to overcome limitations associated with global techniques. A comparison with the approach presented in [1] is made.

Statement of Contribution/Methods

The Bhattacharyya distance, which is a statistical measure of the similarity between two histograms, has recently been used for level set based segmentation. Here we adapt this framework to US data by incorporating a Rayleigh model for the envelope signal. Moreover a localizing strategy is used: for each point on the zero level only pixels within a neighborhood are used to compute the velocity field that steers the evolution of the level set, i.e. only local values of the Bhattacharyya distance affects the evolution of the curve. This ensures a good behavior when inhomogeneous contours and missing boundaries occur.

We compared the behavior of the proposed method and [1] for a set of five envelope images in a parasternal short axis view (2.5MHz, Toshiba Aplio). Initial contours were set by the user by positioning six points only. Manual segmentations drawn by an expert were used as a reference.

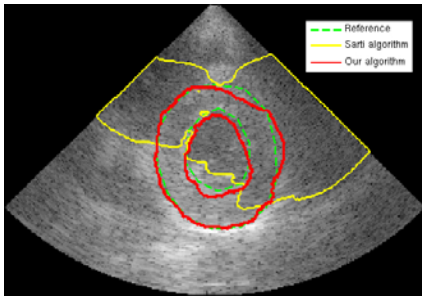
Results

While [1] failed due to its global evolution strategy, the proposed method managed to retrieve both endo- and epicardial boundaries with a good precision (cf. figure). Qualitative measures using the Dice coefficient were calculated: the mean matching value corresponding to the degree of similarity between our results and the ones of the expert was 0.8 (a value of 1 meaning a perfect fit).

Discussion and Conclusions

We introduced a new level set tool dedicated for the segmentation of the whole myocardial wall in ultrasound recordings. Thanks to the localization and the Bhattacharyya distance, this algorithm overcomes most of the difficulties typically encountered with such images.

[1] A. Sarti et al, "Maximum Likelihood Segmentation of Ultrasound Images with Rayleigh Distribution". IEEE UFCC, vol. 52, no.6, June 2005.



P3-H-02

Preliminary results of an ultrasound segmentation method based on statistical unit-root test of B-scan radial intensity profiles

Mehdi Moradi¹, Julian Guerrero¹, Robert Rohling¹, S. E. Salcudean¹; ¹Electrical and Computer Engineering, University of British Columbia, Vancouver, BC, Canada

Background, Motivation and Objective

Delineation of the perimeter of hollow structures, such as veins and arteries, from ultrasound images is an important step in US-based medical interventions. A simple and efficient approach is proposed for US segmentation and applied to clinical images of superficial femoral vein (SFV).

Statement of Contribution/Methods

Intensity edge profiles were created by extending radii in polar coordinates, in 5 degree intervals, from a user-determined seed point within the cross section of the vein in the B-scan images. Our statistical analysis on the partial autocorrelation function of the intensity values along the radii in the veins showed that the profiles can be modeled by stationary autoregressive AR(1) processes. An edge, or transition to fully developed speckle at the border of the vein, breaks this pattern of stationarity.

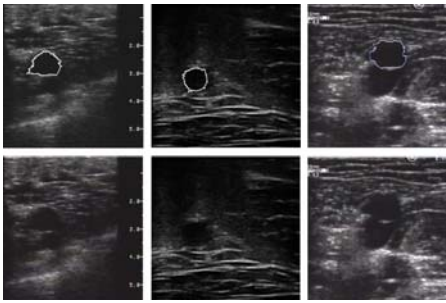
The augmented Dickie-Fuller (ADF) test, a very popular tool in econometric time series studies, examines the null hypothesis of non-stationarity which is equivalent to the existence of a unit root, against the hypothesis of stationarity for AR(1) processes. We used this test along the intensity edge profiles, starting from a minimum user-determined distance from the seed point, and looked for points along the radii where the null hypothesis of unit root could not be rejected. The contours of the veins were determined by these points. While no specific shape model was applied, the maximum distance of the contour points from the seed point was pre-determined.

Results

The Figure below illustrates some of the SFV segmentation results acquired on three different subjects. The maximum distance threshold was needed in around 6% of the radii. For validation, five images were selected and each segmented by five different radiologist experts. We used the mean of the expert-segmented veins as gold standard. The error area in the automatically segmented veins was 4.9%, 4.2%, 6.9%, 3.7% and 4.1% of the gold standard area for the five studied images. The length deviation along the radius was less than 5 pixels on average. We compared the performance of the proposed approach with that of the Canny edge detector which resulted in an average area error of 10.5%.

Discussion and Conclusions

The proposed method is fast (under 0.2 S for one image in a Matlab implementation) and requires minimal user interaction. The method can be easily modified to be used within a model-based segmentation approach.



P3-H-03

Evaluation of Segmentation Algorithms for Vessel Wall Detection in Echo Particle Image Velocimetry (EPIV)

Fuxing Zhang¹, Luiz Murta², Jiusheng Chen¹, Alex Barker¹, Luciano Mazzaro¹, Craig Lanning^{3,4}, Robin Shandas^{3,4},
¹University of Colorado at Boulder, USA, ²University of Sao Paulo, Brazil, ³University of Colorado at Denver, USA,
⁴Division of Cardiology, The Children's Hospital, Aurora, CO, USA

Background, Motivation and Objective

Recent in-vitro and in-vivo validation studies confirmed the accuracy of Echo Particle Image Velocimetry (EPIV), a simple non-invasive means of measuring multi-component blood velocity vectors. EPIV should also be useful for direct measurement of wall shear stress (WSS) in clinical studies. However, calculation of WSS requires accurate delineation of the vessel walls on the ultrasound images, which may be problematic when conventional segmentation techniques are used. We propose two new methods for overcoming these limitations.

Statement of Contribution/Methods

Two automatic algorithms were proposed for segmentation of contrast enhanced B-mode images. The first is based on the intensity profile of ultrasound images, termed intensity-based edge detection (IBED) and the second is based on the movement of microbubbles, termed movement-based quadratic difference (MBQD). In IBED, a temporal ensemble-averaging filter is applied before the edge detection to reduce the invariance of intensity inside the lumen and to enhance the edge. The wall boundaries are detected beamline by beamline by optimally modifying the threshold obtained by Otsu's method. The MBQD method detects the quadratic difference of two consecutive images with the assumption that the artery wall moves significantly slower than the microbubbles. The window size and overlap ratio are optimized to increase signal to noise ratio and improve resolution of the difference map.

Results

The parameters for the two methods were optimized over large sets of microbubble images obtained in human carotid vessels using an EPIV system (Illumasonix LLC, Boulder, CO). A comparison study between the two proposed algorithms plus the established active contour algorithm was carried out against manual delineations on both common carotid artery (CCA) and carotid bifurcation images, with 20 frames for each group. The inter-observer variability of three manual delineations, in pixels, was 0.9+/-0.4, 1.3+/-0.6, 1.3+/-0.6 on CCA images, and 2.5+/-1.0, 3.9+/-1.1, 2.3+/-1.1 on bifurcation images. The mean+/-SD of absolute difference between each computer-generated contour and ground truths, which were taken as the average of manual delineations, were 1.3+/-0.8, 3.8+/-0.8, 5.3+/-0.5 on CCA images, and 2.3+/-0.9, 4.6+/-1.3, 6.3+/-0.6 on bifurcation images, for MBQD, IBED and active contour methods, respectively.

Discussion and Conclusions

The proposed MBQD method shows comparable accuracy with manual delineations in segmenting the carotid artery walls on contrast enhanced ultrasound images with better performance than IBED and active contour algorithms. The performance of MBQD, however, depends on the concentration of microbubbles; this issue is currently being evaluated. An optimized MBQD algorithm should provide similar segmentation of the vessel lumen with manual delineation, and should thus lend itself to real time WSS imaging for vascular hemodynamics using EPIV.

Wednesday
Poster

Segmentation of Plaques in Sequences of Ultrasonic B-Mode Images of Carotid Arteries Based on Motion Estimation and Nakagami Distributions

François Destrempes¹, Gilles Soulez², Marie-France Giroux², Jean Meunier³, Guy Cloutier^{1,4} *Laboratory of Biorheology and Medical Ultrasonics, University of Montreal Hospital Research Center (CRCHUM), Montreal, Quebec, Canada, ²Department of Radiology, University of Montreal Hospital, Montreal, Quebec, Canada, ³Department of Computer Science, University of Montreal, Montreal, Quebec, Canada*

Background, Motivation and Objective

The goal of this work is to perform a segmentation of atherosclerotic plaques in view of evaluating its burden and to provide boundaries for computing properties such as the plaque elasticity distribution (elastogram).

Statement of Contribution/Methods

The echogenicity of a region of interest comprising the plaque, the lumen, and the adventitia in an ultrasonic B-mode image is modeled by a mixture of three Nakagami distributions. To each of these three tissues corresponds a specific weighted sum of these three distributions, which yields the pseudo-likelihood of a Bayesian model. The pseudo-prior of that model includes a geometrical smoothness constraint, as well as an original spatio-temporal cohesion constraint, based on the estimation of the motion field of the plaque in the video sequence. The Maximum A Posteriori (MAP) of the proposed model is computed with a variant of the Exploration/Selection (ES) algorithm. The overall proposed procedure follows a Learning-Prediction-Correction (LPC) strategy: learning the shape, position, and appearance of the plaque from solutions at previous frames; prediction of the shape, position, and appearance of the plaque at the current frame using the learning step; correction of the prediction using the observable data at the current frame. The starting point is a manual segmentation of the first frame.

Results

The proposed method is quantitatively and qualitatively compared with manual segmentations of all frames by an expert technician. Various measures have been used for this evaluation, including the sensitivity and specificity of the receiver operating characteristic (ROC) analysis, the kappa test, and the error of area of the plaque. We report a sensitivity of $83.7 \pm 8.3\%$, a specificity of $94.0 \pm 4.3\%$, a kappa index of $84.7 \pm 7.5\%$ and a percentage of error of the plaque area of $-2.5 \pm 8.0\%$.

Discussion and Conclusions

The results obtained on 94 sequences of 33 patients (for a total of 8988 images) compare favorably with previous studies.

Breast Ultrasound Phantom for Image Segmentation Assessment

Isabela Carvalho¹, Rodrigo Basto¹, Antonio Infantosi¹, Marco Antonio von Kruger¹, Wagner Pereira¹; *¹Biomedical Engineering Program, COPPE/UFRJ, Rio de Janeiro, Rio de Janeiro, Brazil*

Background, Motivation and Objective

Ultrasound (US) phantoms are testing objects built to simulate basic human soft tissue ultrasonic properties. In diagnostic imaging, breast phantoms are an important tool for performance assessment of medical ultrasound systems as well as for medical training purposes. Due to breast anatomical variations, such as size, shape and composition, phantoms are usually developed with only the most common characteristics like glandular and adipose tissues, cysts and lesions in different shapes, sizes. The aim of this work is to develop a US phantom that simulates breast lesions with regular and irregular contours, and known geometric dimensions, intended to be used to create an image database for application as a gold standard for methods of image processing (segmentation in special) and to support Computed – Aided Diagnosis System (CAD) developments.

Statement of Contribution/Methods

The experimental strategy follows four steps: (i) preparation of tissue-mimicking matrix with similar values to the properties of glandular tissue; (ii) lesions design and fabrication; (iii) final assembly of the phantom (matrix with lesions included); (iv) image acquisition in different scanning plans. An ideal material for constructing ultrasound phantoms should have the same ranges of speed of sound, attenuation coefficients and density as soft tissues. The phantom matrix is a mixture of agar, glycerin and graphite and PVC powders. The lesions were made of polyacrylamide using a series of molds with known dimensions. Two commercial breast scanning equipments were used for generating the images of phantom inclusions.

Results

The values for density, attenuation, US speed and impedance for the matrix are compatible with literature. Concerning the lesions, the US speed value obtained is inside the range accepted for biological tissue US speed variation (less than 2% of difference). The value of attenuation at 1 MHz for the polyacrylamide lesions is still around 20% smaller than literature values. The images were segmented with the method described by Gómez et al. (2008) and analyzed by a specialist that concluded that the visual appearance is compatible to the real ones. He also concluded that the lesions contours obtained by the segmentation method are in agreement with the shape of the phantom.

Discussion and Conclusions

A first version of a breast ultrasound phantom able to mimic the appearance of lesions in routine exams has been developed, and qualitatively approved by a specialist. We are presently implementing methods to assess quantitatively the lesion images, with the help of a segmentation method already mentioned. We are also working to improve the phantom so as to mimic the texture of nodules, ducts and lymphnodes. We believe such a phantom can give a substantial support in the development diagnose methods based on image processing (as CAD, e.g.).

P3-H-06

Classification of benign and malignant breast tumors by the contour analysis and scatterers characterization

Yin-Yin Liao¹, Po-Hsiang Tsui², Chien-Cheng Chang², Chih-Kuang Yeh¹; ¹Department of Biomedical Engineering and Environmental Sciences, National Tsing Hua University, Hsinchu, Taiwan, ²Division of Mechanics, Research Center for Applied Sciences, Academia Sinica, Taipei, Taiwan

Background, Motivation and Objective

Ultrasound B-mode image is an important clinical tool in noninvasive diagnoses of breast cancer. The Nakagami image estimated from ultrasonic backscattered envelope has been demonstrated to be useful in complementing conventional B-mode scans when classifying breast masses. It is interesting to compare these two ultrasonic imaging methodologies. The B-scan reflects the intensity of the reflected echoes, and is clever at a clear description of tumor contour to provide knowledge of morphology. Although the resolution of the Nakagami image is not as good as that of the B-scan, the Nakagami image reflects the statistical distribution of local backscattered signals, which is associated with the arrangements and concentrations of scatterers in tumors. In this circumstance, the B-mode image and the Nakagami image may be imagined as two linear independent vectors mathematically. This implies that additional clues for better classifying benign and malignant breast tumors may be obtained if we combine the B-mode image with the Nakagami parametric image for simultaneously analyzing the tumor contour and characterizing scatterers in the tumor.

Statement of Contribution/Methods

This study explored the clinical performance of combining the B-scan-based tumor contour analysis and the Nakagami-image-based tumor characterization in classifying benign and malignant breast tumors. Clinical rawdata obtained from 60 cases was acquired to construct the B-mode and Nakagami images. The B-mode images were used to calculate the standard deviation of the shortest path for contour feature analysis, and the Nakagami images were applied to estimate the average Nakagami parameters in the region of interests (ROI) in tumors. The receiver operating characteristic (ROC) curve was plotted to evaluate the ability of each parameter in classifying breast tumors. Subsequently, fuzzy c-means clustering (FCM) algorithm was applied to evaluate the performances of the Nakagami parameter combined with the standard deviation of the shortest path.

Results

The ROC analysis showed that the Nakagami parameter had a diagnostic accuracy of 80%, sensitivity of 73.3%, and specificity of 86.7%. The standard deviation of the shortest path had a diagnostic accuracy of 81.7%, sensitivity of 86.7%, and specificity of 76.7%. When we combine the Nakagami parameter with the standard deviation of the shortest path, it was found that the diagnostic accuracy was 81.7%, sensitivity was 80%, and specificity was 83.3%.

Discussion and Conclusions

The results indicated that the two-dimensional analysis based on the B-scan and the Nakagami image for simultaneously characterizing the tumor contour and the scatterer properties can enhance both the sensitivity and specificity to have a better performance to discriminate benign and malignant tumors.

P3-I. Acoustic Sensors

Sala Orange

Wednesday, September 23, 2009, 10:00 am - 11:30 am

Chair: **Kentaro Nakamura**
Tokyo Institute of Technology

P3-I-01

Nonlinear viscoelastic measurements in fluids using “Acoustical Rheology”

Samuel Collé¹, Helene Moreschi¹, Guillaume Renaud², Marielle Defontaine¹:¹Université François Rabelais, UMR Imagerie et Cerveau, INSERM U930, CNRS ERL 3106, Tours, France, ²LIP - UMR CNRS 7623, Paris, France

Background, Motivation and Objective

Remote Dynamic Acoustoelastic Testing (RDAT) was first developed to assess microcracks in trabecular bone tissue. However, the method appears to offer larger applications, especially in fluids, to investigate nonlinear rheological behaviors. The purpose of this work is to validate the technique’s sensitivity and to characterize the viscoelasticity in fluids, and particularly in non-Newtonian fluids which exhibit complex viscoelastic properties such as shear-thinning, shear-thickening or thixotropy.

Statement of Contribution/Methods

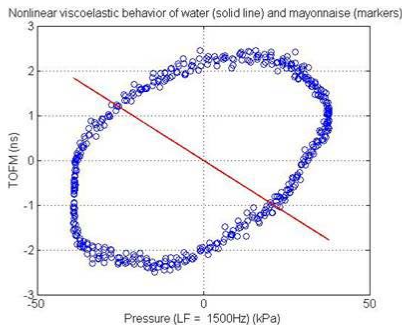
RDAT provides non-contact and localized measurements of viscoelastic and dissipative nonlinearities. It consists in the interaction of two acoustic waves: a low-frequency (LF) wave generated by a piston induces a dynamic tensile/compression quasi-hydrostatic loading on the material, while ultrasound (US) pulses are emitted perpendicularly. Celerity and amplitude variations of US pulses are analyzed to extract viscoelastic (Time Of Flight Modulation, TOFM) and dissipative (Relative Energy Modulation, REM) nonlinearities, respectively. We particularly studied several food products (Ketchup, mayonnaise) and cosmetics (lipid-based and water-based creams) well-known for their “counterintuitive” behaviors.

Results

TOFM and REM curves are plotted as a function of instantaneous LF pressure amplitude (figure 1). Because TOFM is linked to viscoelastic modulus, this kind of graph is closed to rheological diagrams used to describe fluids mechanical behavior under stress. Nonlinear viscoelastic and dissipative measurements have shown strong asymmetry in tension/compression, hysteric behavior and high level of nonlinearities.

Discussion and Conclusions

RDAT applies a bulk deformation into the medium. Hence, US viscoelastic measurements can’t be directly compared to shear stress measurements (rheometers), but provide an additional and complementary viscoelastic information. In perspective, we plan to correlate an instrumental rheological approach to a sensorial characterization (texture, uncton, spreadability, fluidity, consistence, firmness, ...).



Self-Temperature-Compensation Characteristics at 1st- and 3rd- Harmonic Frequencies for SAW Gas Sensor Used in Sensor Network

Mitsutaka Hikita¹, Y Hirazumi¹, H Aoki¹, J Matsuda¹, T Watanabe^{1,2} *Kogakuin University, Japan*

Background, Motivation and Objective

A novel SAW gas sensor with self-temperature-compensation has been proposed for use in sensor network (ref.1). The sensing dynamic range can be extended by utilizing both the 1st- and 3rd-harmonic frequencies. Experimental results showed the validity.

Statement of Contribution/Methods

D-1, D-2, and D-3 which have propagation lengths of L , $L+\lambda/2$, and $L+\lambda/4$ are used in the gas sensor (Fig. 1). Phase differences between the outputs (2) and (3) are $\pi/2$ and $3\pi/2$ at the 1st- and 3rd-harmonic frequencies respectively. The D-1 is used as a sensor. The D-2 and D-3 are isolated from sensing gas, which give standard phases. Phase shifts due to temperature have same values for all outputs. The projected values of (1) onto the axes for directions of (2) and (3) respectively provide phase shifts caused only by the sensing-gas irrelevant to temperature.

Results

A modified-finger-width IDT provides almost same excitation for both frequencies. A 128° Y-X LiNbO₃ was used. Experimental temperature characteristics for phases of (1), (2), and (3) at 75 MHz and 225 MHz, i.e. 1st- and 3rd-harmonic frequencies, are shown in Fig. 2. Phase differences between (2) and (3) are exactly $\pi/2$ and $3\pi/2$ at 1st- and 3rd-harmonic frequencies respectively. Phase shifts due to temperature are also same for all phases.

Discussion and Conclusions

From Fig. 2, projecting (1) onto the axes for directions of (2) and (3) can provide correct phase shift due only to the sensing-gas over wide temperature. Utilizing both frequency SAWs indicates a wide-dynamic range by switching frequencies. Projection procedure can be operated by mixing (1) with (2) and (3). The 1st- and 3rd-harmonic signals can be generated from RF circuits in 2.4-GHz ZigBee-based sensor network (ref.1).

1. M. Hikita, et al., PIERS, March, 2008, pp. 301-

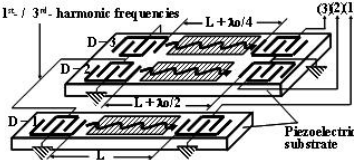


Fig. 1 New gas sensor consisted of three SAW delay lines. D-1: sensing delay line, D-2 / D-3: delay lines providing standard phases.

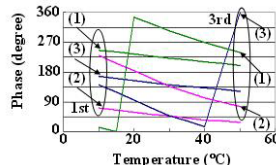


Fig. 5 Experimental temperature characteristics for output phases.

305.

Wednesday
Poster

Polymer Characterisation on Langasite Delay Lines

V. Carolina Ayala¹, Katrin Moosmann¹, Ismail Shrena¹, David Eisele¹, Oswald Prucker¹, Jürgen Rühle¹, Leonhard Reindl^{1,2} *Department of Microsystems Engineering, University of Freiburg - IMTEK, Freiburg, Germany*

Background, Motivation and Objective

The detection of ever diminishing masses is currently becoming of increasing importance by chips working with small volumes in chemical applications. For the detection of small masses (10^{-10} g) micro acoustic wave devices are used. To detect specific molecules, a sensitive layer is attached to the piezoelectric material, where a selective binding is produced.

Different substrates such as quartz (SiO₂), langasite (La₃Ga₅SiO₁₄, LGS), and lithium tantalate (LiTaO₃, LT) are used for the fabrication of surface acoustic wave (SAW) devices. LGS presents a higher electromechanical coupling coefficient than quartz and a better Q factor than LT. Cuts of LGS are also available with zero temperature coefficient delay (TCD), which allows high precision measurements using sensitive layers even without temperature compensation.

Statement of Contribution/Methods

In this paper a sensitive layer for the detection of diols, such as sugars or neurotransmitters, has been realized by attaching a polymer layer to a LGS (0°, 138.5°, 26.6° cut, zero TCD cut) delay line with double split finger configuration. The polymer consists of *N,N*-dimethylacrylamide, 4-vinylphenylboronic acid and a photo-crosslinkable unit P(DMAA-*co*-VPBA-*co*-MABP).

The transfer function (S_{21}) of the delay line was analyzed by a sophisticated signal processing algorithm. By this method the SAW velocities in the delay line and the center frequencies of the interdigital transducers (IDT) are obtained.

The influence of the polymer in the delay line device is studied and the sensitivity analyzed with different delay line configurations.

Results

Analyzing the SAW velocity of the center frequencies in the delay line, a change in the velocity due to the presence of the polymer can be detected. The third and fundamental harmonics are used for this purpose, because of their good signal strength. The higher harmonics (fifth and seventh) show a high attenuation due to bulk wave conversion. The polymer was characterized using ellipsometry and atomic force microscopy (AFM). The surface roughness of the polymer was also measured by AFM achieving 5 nm in a 50 μm scan size.

Discussion and Conclusions

Different methods of depositing the polymer are discussed. Furthermore, different polymer concentrations, which determine respective layer thickness, are analyzed. In addition, the temperature dependence of the new velocity is determined in a climate chamber.

A polymer layer has been successfully attached to LGS surfaces and has shown a long term chemical stability, making it adequate for future applications. Its properties have been studied with different delay line configurations.

P3-I-04

Monitoring of several complex materials with ultrasonic sensors array

Emmanuel Caplain¹, Stéphane Serfaty¹, Pascal Griesmar¹, **Loïc Martinez¹**, Jean-Yves LE HUEROU¹, ¹SATIE, Université Cergy-Pontoise, Cergy-Pontoise, France

Background, Motivation and Objective

Bulk acoustic wave sensors such as Thickness Shear Mode Resonator (TSMR) can be used to investigate the viscoelasticity of liquids or polymers in formation. However the material to investigate can present heterogeneous phases (for instance biphasic middle such as water/oil). Furthermore, for one considered phase, it can happen that the physical and chemical properties evolve versus time (for example in case of polymer formation). For a given phase, TSMR gives access to mechanical parameters such as the complex shear modulus $G^* = G' + iG''$ where G' and G'' represent respectively the elastic and viscous moduli. Using a network analyser, we measure the variation of the impedance of the TSMR around its resonance frequency. From this impedance measurement, we have shown in previous works that G^* can be extracted using an appropriate electrical model. For inhomogeneous materials it is not conceivable to use separated devices to determinate simultaneously the different G^* of the different phases.

Statement of Contribution/Methods

To perform a spatial monitoring, we use a new sensor made of a TSMR array. Our device consists of interconnected resonators made on separate substrates. The thickness of the different substrates has been chosen to get different resonant frequencies. This device gives local impedance at different points of the inhomogeneous material with a high sensitivity. Our array is designed to avoid acoustic interference between TSM resonators.

A new electrical model is used to extract simultaneously the local elastic and viscous moduli at different frequencies from the impedance evolution of the TSMR array. In this work, this TSMR array is made of two resonators: TSMR1 and TSMR2 resonant at respectively 6 MHz and 9 MHz.

Results

In the first step, we present here a validation of this model using two separated media representative of biphasic material. Water, taken as a reference, is the load of the TSMR1. TSMR2 is used to measure different water-glycerol mixture. We have obtained a good agreement with the tabulated values: the error is less than 5%. In the second step, we have performed our TSMR array with the same reference model (TSMR1 in water). In this case, TSMR2 measures a wide dynamical range of G' and G'' of an inorganic polymer (elaborated by sol-gel process) in formation.

Discussion and Conclusions

This device is particularly suitable to investigate inhomogeneous fluids and no miscible fluids. Using the different harmonics mode, we have a wide range of frequency investigation and gives access to a multi-scale study of inhomogeneous material.

P3-I-05

Development of Ball SAW Gas Chromatograph for Natural Gas Components

Yutaro Yamamoto¹, Shingo Akao², Hiroki Nagai¹, Noritaka Nakaso³, Toshihiro Tsuji¹, Kazushi Yamanaka¹; ¹Department of Materials Processing, Tohoku university, JST-CREST, Japan, Sendai, Miyagi, Japan, ²Tohoku University, Toppan Printing Co. Ltd, JST-CREST, Japan, Japan, ³Toppan Printing Co. Ltd, JST-CREST, Japan

Background, Motivation and Objective

For energy exploitation with natural gas and oilfield, handy multiple-gas sensors are essential. The gas chromatograph (GC) is frequently used as a multiple-gas sensor but it is not handy. We have developed the ball surface acoustic wave (SAW) sensor, where SAW makes multiple roundtrips without diffusing by the diffraction, realizing ultra-high sensitivity. Based on this excellent property, we propose a highly sensitive handy multiple-gas sensor.

Statement of Contribution/Methods

We developed a prototype of ball SAW GC system (Figure. 1(a)). To separate and detect lower hydrocarbons, we fabricated a micro-electro-mechanical-system (MEMS) column packed with styrene divinylbenzene beads for the first time by introducing a compression jacket. Then we fabricated a ball SAW GC system combining the packed MEMS column, a ball SAW sensor, a small pump and an injector. We detected three mixed lower hydrocarbons (methane, ethane and propane) using this system.

Results

Figure. 1(b) shows a chromatogram of the amplitude response of the ball SAW sensor. We successfully separated and detected sample gases. The signal was obtained with leaky loss whose measurement is a typical advantage of a ball SAW sensor over planer SAW sensors [1]. Though thermal conductivity detector and flame ionization detector which can detect these gases, they need heating up to 200 degrees or more. In contrast, we achieved the detection at room temperature (23 degrees) using the ball SAW sensor.

Discussion and Conclusions

Combining a packed MEMS column and a ball SAW sensor, we developed a ball SAW GC system. Using this, we succeeded at separation and detection of lower hydrocarbons at room temperature. Since a ball SAW sensor needs no heating mechanism, it is very useful in handy GC with an excellent explosion proof. It is therefore concluded that a handy GC is feasible.

[1] N. Iwata et al, JJAP 46 (2007) 4532.

Wednesday Poster

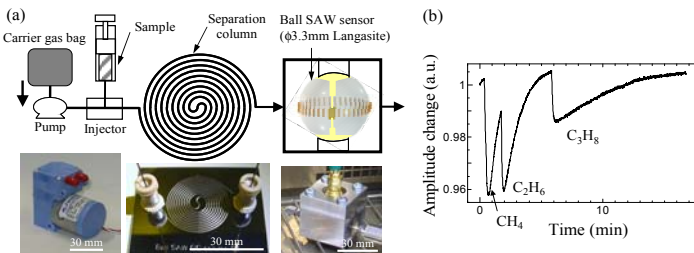


Fig. 1 Prototype of ball SAW GC system (a) schematic diagram (b) Gas chromatogram of methane (CH₄), ethane (C₂H₆) and propane (C₃H₈)

P3-I-06

A Novel Approach in Liquid-Level Sensing by Trapped-Energy-Mode Thickness Vibrator

KEN YAMADA¹, SHUHEI HORIUCHI¹, HISATO HONDA¹, TETSUYA KINAI¹; ¹TOHOKU GAKUIN UNIVERSITY, TAGAJI, MIYAGI, Japan

Background, Motivation and Objective

The detection and sensing of liquid level by ultrasonic techniques have widely been used thus far. Most of these techniques employ a pulse-echo method. This conventional method is a powerful means of detecting such variation on the centimeter scale or more. However, it is inadequate for measurement in a very small distance range because echo pulses are often screened off by transmit pulses. In recent years, the measurement of liquid level on the millimeter scale or less has become an important subject in, for example, biological and chemical fields.

Statement of Contribution/Methods

In this paper, a new method that employs a piezoelectric thickness vibrator operating in a trapped-energy mode for detecting a small-scale variation in liquid level is presented. In a piezoelectric plate operating in a trapped-energy mode, an evanescent field is created in the surrounding region of the plate. When this region is dipped in a liquid, a small leakage of vibration energy occurs. The amount of leakage varies depending on how deep the surrounding region, i.e., the evanescent field is in the liquid. Therefore, small variations in liquid level are detected by observing the changes in the resonance characteristics of the vibrators, such as quality factor Q_m and the electric conductance G .

Results

A thickness-poled Pb(Zr,Ti)O₃ (PZT) plate (NEPEC-6) of 30 mm diameter and 1 mm thickness having a 4-mm-diameter electrode was employed as the vibrator material. The resonance frequency was around 2.09 MHz and Q_m was about 400. The plate was supported vertically by clamping its fringe without affecting the main mode of vibration. Then, the plate was dipped in a liquid to be tested. The test liquids employed were water, glycerin, castor oil, and honey. The depth h was varied step by step using a pulse-motor stage moved in the vertical direction. The variation in G against h at the resonance point was measured using an impedance/material analyzer. Preliminary experiments have shown that almost linear variations in G against dipping depth can be obtained within a few millimeter range.

Discussion and Conclusions

Several advantages are expected in using the trapped-energy modes. First, it is free from spurious responses resulting from contour vibration modes. Therefore, the single-resonance characteristic of the principal mode is easily obtained. Furthermore, supporting the surrounding region does not deteriorate resonance characteristics, such as Q_m . This brings about easiness in holding the device when it is used as the sensor. Moreover, the gradual variation in the distribution of vibration over the electroded and unelectroded regions is convenient for obtaining moderate sensitivity to the liquid-level variation. The technique presented here will be an effective means for sensitively detecting variations in liquid level on a small scale.

P3-I-07

Separation and measurement of mixed hazardous gases by ball SAW gas chromatograph with sensitive film fabricated using off-axis spin-coating

Toshihiro Tsuji¹, Yuki Kawai², Kentaro Kobari¹, Yutaro Yamamoto¹, Shingo Akao³, Noritaka Nakaso³; ¹Tohoku University, JST-CREST, Japan, ²Tohoku University, Japan, ³Toppan Printing Co. Ltd., Tohoku University, JST-CREST, Japan

Background, Motivation and Objective

For social and environmental security, hazardous mixed hydrocarbon (HC) gases must be identified and measured. Although gas chromatograph (GC) can do this task, compact and high-performance system has not been established. Thus, we're developing ball surface acoustic wave (SAW) GC [1,2]. However, we had difficulty in multiple roundtrips of SAW in organic sensitive film. In this study, off-axis spin-coating (OAS) method to fabricate low-attenuation sensitive film on spherical surface was applied to sick-house gasses.

Statement of Contribution/Methods

In conventional spin-coating chucking the ball on the rotation axis, the flow of the coating solution is unstable and abrupt emission might occur from the propagation route of SAW since the direction of centrifugal force is normal to the surface; thus the film becomes thick and irregular. However, in the OAS shown in Fig. 1, the flow is smooth

on the propagation route and excess solution is effectively removed since the direction of the centrifugal force is tangential; thus the film becomes thin and uniform.

Results

Langasite ball SAW sensor ($\phi 3.3\text{mm}$, 150MHz) was coated with poly(dimethylsiloxane) by OAS. Figs. 2 show chromatograms for benzene, toluene, and xylene mixed by equivalent mole fraction, measured using (a) delay time and (b) amplitude changes of the 66th turn's waveform at 35°C and (c) signal of thermal conductivity detector of GC at 200°C, respectively. Each component was successfully separated and identified using the column [2] and sensitively detected by the ball SAW sensor.

Discussion and Conclusions

The measurement at high turn was useful for the reduction of the relative noise, leading to the decrease of limit of detection. The OAS will play an essential role in the ball SAW GC as a handy and intelligent hazardous gas sensor. [1]Iwata et. Al., JJAP 46 (2007) 4532. [2]Akao et. al., JJAP 47 (2008) 4086.

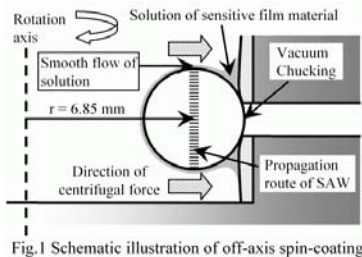


Fig.1 Schematic illustration of off-axis spin-coating

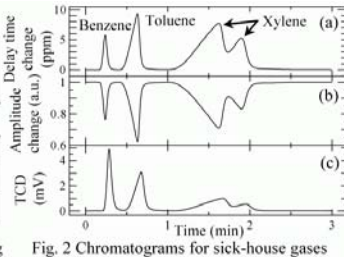


Fig. 2 Chromatograms for sick-house gases

P3-I-08

(yx1)21.82° LiNbO3 pseudo-LFE acoustic wave sensor

Tingfeng Ma¹, Chao Zhang², Zhitian Zhang¹, Wenyan Wang¹, Guanping Feng², ¹Department of Precision Instruments and Mechanology, Tsinghua University, Beijing, China, People's Republic of, ²Research Institute of Tsinghua University in Shenzhen, Shenzhen, Guangdong, China, People's Republic of

Background, Motivation and Objective

Bulk acoustic wave devices based on lateral field excitation (LFE) have been found sensitive to liquid electrical property (conductivity or permittivity) changes. Previous studies mainly concentrate on AT-cut quartz LFE sensors, which have been proved to be working on pseudo-LFE mode (the observed thickness shear mode (TSM) is not excited by the lateral field but the thickness field with the liquid acting as an analog electrode). However, due to the low piezoelectric coupling factor, the sensitivity of the AT-cut quartz LFE device to liquid electrical property changes is limited. In order to obtain LFE sensors with higher electrical sensitivities, pseudo-LFE on (yx1)21.82° lithium niobate was studied both theoretically and experimentally.

Statement of Contribution/Methods

Theoretical calculations show that the (yx1)21.82° LiNbO3 LFE device works on pseudo-LFE mode with a very high piezoelectric coupling factor of 24.41% for slow shear c mode, which is almost 3 times higher than that of AT-cut quartz. Several 5 MHz LFE devices on (yx1)21.82° lithium niobate were then designed and fabricated. NaCl water solutions and 2-propanol water solutions were used to test the devices' sensitivities to liquid conductivity and permittivity changes respectively. The devices' responses were measured using the PLO-10 phase-locked oscillator and FC-1300 frequency counter. The results were also compared with those of 5 MHz AT-cut quartz LFE devices.

Results

It has been shown that the 5 MHz (yx1)21.82° LiNbO3 LFE device is almost 20 times more sensitive to liquid conductivity changes than the 5 MHz AT-cut quartz LFE device, which is shown in Fig.1. As for the permittivity, about 3 times higher sensitivity was obtained for the 5 MHz (yx1)21.82° LiNbO3 LFE device.

Wednesday
Poster

Discussion and Conclusions

It is found that the $(yx)1.82^\circ$ LiNbO₃ LFE device works on pseudo-LFE mode, which is similar to AT-cut quartz LFE device. The electrical sensitivities of the $(yx)1.82^\circ$ LiNbO₃ pseudo-LFE sensor were measured and compared to AT-cut quartz LFE sensor. Two orders of magnitude higher sensitivity to the liquid conductivity change was obtained for the $(yx)1.82^\circ$ LiNbO₃ pseudo-LFE sensor. Theoretical analysis for the high electrical sensitivity was presented.

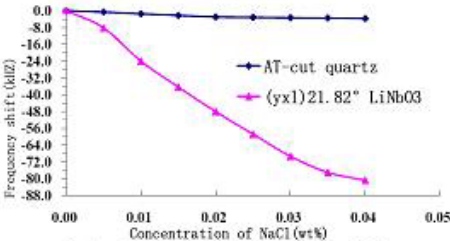


Fig. 1: Frequency shift of two kinds of LFE devices as a function of NaCl concentration in water

P3-I-09

Passive SAW OFC Pressure Sensor

Michael Roller¹, Donald Malocha²; ¹University of Central Florida, Winter Springs, Florida, USA, ²University of Central Florida, USA

Background, Motivation and Objective

NASA has expressed an interest in small, wireless, passive RFID pressure sensor systems. A surface acoustic wave (SAW) pressure sensor employing orthogonal frequency coding (OFC) can address this need. The use of wireless SAW sensors have been well-researched, but these devices have been limited in their use in multi-sensor environments due to their passive nature. Resonator type SAW devices have been widely used as pressure sensors; however, their inability to be coded handicaps their use in a multi-sensor system. In this work, an itemized approach exploring differing fabrication methods, proof of concept using a cantilever device, and initial experimental results from a diaphragm device are discussed. These devices utilize OFC to ensure minimal signal collisions when interrogating numerous sensors.

Statement of Contribution/Methods

The goal of this research is to demonstrate a systematic approach to creating a practical SAW pressure sensor drawing on OFC technology. A 250MHz device fabricated on lithium niobate with a transducer, OFC reflectors, and a diaphragm between the transducer and one of the reflectors is the embodiment of the final diaphragm device. The change in time delay of the differential correlation peak corresponds to the change in displacement of the diaphragm under pressure. Compared are various fabrication approaches attempted in creating the diaphragm from chemical etching to micro-ablation. Using micro-ablation, which may be a new way of fabricating the diaphragm, proves to be a very simple and quick process. Having established a method for creating these devices, a simple experiment on a cantilever device to confirm a time change in differential correlation peaks will be discussed. Finally, the initial results from experiments on the diaphragm devices will be shown.

Results

Results from both the cantilever device and the diaphragm device indicate these fabrication techniques can produce an operational sensor. A linear change in the differential correlation peak time delay is found to correspond to the change in strain on the cantilever device. A theoretical model has also been compared to these findings and exhibits a strong correlation with the experimental results.

The diaphragm device has indicated a clear "on/off" response under strained to unstrained conditions.

Discussion and Conclusions

This work will show that an OFC SAW pressure sensor device can be successfully fabricated and tested within a laboratory environment. The 250MHz device on lithium niobate shows a strong linear response to strain on the

device from initial cantilever device testing. The more complex diaphragm device which draws upon the same principles of operation as the cantilever device has shown strong on/off response to strained and unstrained states. Current work will hopefully demonstrate similar linear responses to changes in the diaphragm as those in the cantilever.

P3-I-10

Capacitive Method to Measure Flying Height of Slider in HDD using Surface Acoustic Wave Device

Jaegun Kim¹, Kyoung-Su Park², No-Cheol Park³, Young-Pil Park⁴, Taek-Joo Lee⁵, Soo-Cheol Lim⁶; ¹Mechanical Engineering, Yonsei university, Seoul, Korea, Republic of, ²Mechanical engineering, Yonsei university, Seoul, Korea, Republic of, ³Yonsei university, Korea, Republic of, ⁴Mechanical engineering, Yonsei university, Korea, Republic of, ⁵ITF. Co., Ltd, Korea, Republic of, ⁶Samsung electro mechanics. Co., Ltd, Korea, Republic of

Background, Motivation and Objective

Surface acoustic wave (SAW) device as physical/chemical sensors or their signal processing unit was widely studied in various industries. But the application to measure the several nanometer level's gap like flying height(FH) which is the gap between slider and recording media in HDD was not studied. The basic function of SAW device is band pass filter. So, the gap sensor with high precision and large SNR can be expected when the gap sensor with high precision using SAW device was realized. In this study, the high precision gap sensor using SAW device was proposed and applied to measure the FH in HDD.

Statement of Contribution/Methods

In this study, the SAW device whose center frequency is 13.56MHz, inter digital transducer's pairs are 30 and apodization is 9mm was used. First, the analytical approach by electro acoustic equivalent circuit modeling was used. Using commercialized capacitor, theoretical model was ensured. After the works, parallel plate capacitor(0.3X0.3 millimeter square) comprised using silicon wafer whose surface was layered by aluminum and recording media. Finally, SAW response by the plate's gap change when HDD was driving was measured.

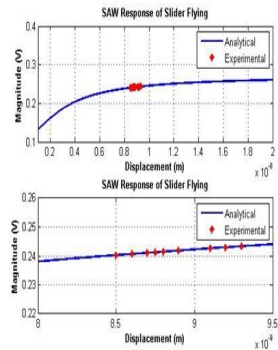
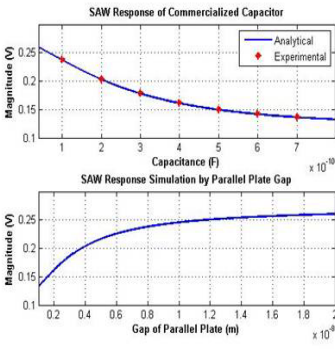
Results

In figure 1, the results which are the analytical solution and SAW response were compared. The maximum relative error rate was 3 percent.

In figure 2, the dynamic response by the media rotation is showed. The measured flying height is distributed from 8.5 to 9.5 nanometer and corresponding capacitance was distributed from 855 to 940 pico farad.

Discussion and Conclusions

In this study, gap measurement system with high precision using SAW device was modeled and its validity was confirmed through experiment. And it was applied to measure the flying height in HDD. So the result are valid and SAW device is proper as a high precision gap measurement system.



Wednesday
Poster

P3-I-11

Mitigating Spurious Compressional Waves in Multi-Measurand TSM Sensors

Jeffrey Andle¹, Reichl Haskell¹, Maly Chap¹, Daniel Stevens¹, Richard Gomes¹, Long Nguyen¹:*SenGenuity, Vectron, Hudson, NH, USA*

Background, Motivation and Objective

In situ monitoring of lubricant quality is of increasing interest in mobile and fixed asset applications.

To give an accurate picture of the quality of the lubricant, multiple measurands need to be monitored. Interpretation of these multiple measurands lead to key parameters of interest including fuel dilution, water or coolant contamination, soot load, and additives depletion (as total base number or total acid number).

It is the objective of the current work to combine acoustic wave viscosity and density measurement with temperature, conductivity and dielectric measurements to achieve a multimeasurand sensor capable of giving a complete picture of lubricant condition.

Statement of Contribution/Methods

A multi-measurand sensor platform has been created by combining a viscosity/temperature sensor with a parallel plate conductivity/dielectric sensing element. A langasite monolithic crystal filter (MCF) element and a RTD temperature sensor is housed in a T0-X style package providing viscosity and temperature measurement, while a parallel plate electrode structure provides a means for measuring conductivity and dielectric. Due to the nature of compressional mode radiation with thickness shear mode (TSM) based sensors, integration of parallel plate C/D electrodes immediately in front of the viscosity sensing surface poses an enormous design challenge. The present work compares various parallel plate structures for their ability to absorb or redirect the unwanted compressional modes enabling conductivity and dielectric measurement without compromising the quality of the viscosity measurement. Even with the electrode modifications, the energy lost as compressional modes will be interpreted by the sensor electronics as erroneous increase in viscosity-density product. Additionally, it is determined that the increase is due to elasticity-density product of the compressional wave in the fluid. Extraction of density and/or elasticity is explored to compensate for the compressional mode effects of the multi-measurand sensor platform in addition to providing additional measurands.

Results

Data is presented for multiple measurands including viscosity, temperature, conductivity and dielectric. Also, results clearly show the effect of the parallel plate electrode design on the performance of the MCF viscosity element. The geometrical design modifications of the C/D electrodes to enable better viscosity measurement are characterized to show impact of conductivity and dielectric parameters and measurement capability. Furthermore, results are shown on the use of dual mode resonance of the MCF to estimate and compensate the compressional wave radiation effect.

Discussion and Conclusions

It is shown that the integration of multiple measurands into a compact and manufacturable sensor is possible. Future work to improve the performance of the prototypes reported herein is outlined.

P3-I-12

Novel Air-Borne Ultrasonic sensor Using Nanofoam and a Laser Doppler Vibrometer

Takuya Iwamoto¹, Hidetomo Nagahara¹, Yuriko Kaneko¹, Ushio Sangaawa¹, Masahiko Hashimoto^{1,2}:*Panasonic Co., Ltd., Kyoto, Japan*

Background, Motivation and Objective

Ultrasonic echolocation systems are required for autonomous robots and security systems so that they can recognize their environments and adapt to them. However, ultrasonic wave interference is a serious problem when two or more echolocation systems are operated simultaneously in the same area. To avoid this problem, frequency or code multiplexing of ultrasonic waves should be performed using wideband sensors. In this report, we propose a novel ultrasonic sensor that can operate over a wide frequency range and provide high sensitivity for echolocation systems.

Statement of Contribution/Methods

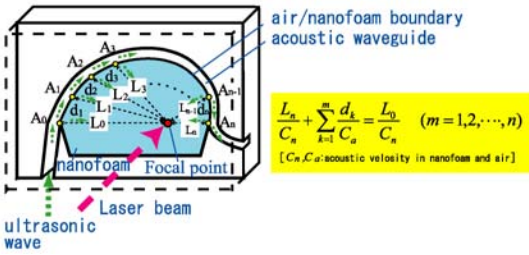
The novel features of our ultrasonic sensor are that it uses a particular material called nanofoam and detects ultrasonic waves using a laser Doppler vibrometer (LDV). Nanofoam is a nanoporous material composed of silica, which has extremely low acoustic impedance as a solid. Ultrasonic waves traveling in air are absorbed efficiently by nanofoam because of the small impedance mismatch. Moreover, the acoustic velocity in nanofoam is very slow (50 to 150 m/s, which is slower than in air). This enables the design of a focusing structure, as shown in the figure. Using this structure, ultrasonic waves entering the nanofoam from any point on the air/nanofoam boundary reach the focal point simultaneously. When an ultrasonic wave propagates in the nanofoam, its refractive index changes. Our sensor uses an LDV to detect this refractive index change at the focal point.

Results

A prototype device was produced for testing. The density of the nanofoam was 110 kg/m³, its acoustic velocity was 50 m/s, its refractive index was 1.02, and the refractive index change was $1.2 \times 10^{-7} \text{ Pa}^{-1}$. The focal length was $L_0 = 22 \text{ mm}$ (see the fig.) and the thickness was 10 mm. The LDV wavelength was 633 nm. We evaluated the device by measuring a wideband ultrasonic pulse wave from a tweeter (CF: 40 kHz, BW: (-6 dB) 20 kHz). We obtained waveforms that corresponded closely to the input pulse wave.

Discussion and Conclusions

We verified the operation of the proposed ultrasonic sensor. Current ultrasonic sensors apply resonance of a vibration to a diaphragm to obtain high sensitivity, which limits their frequency range. Our sensor can achieve high sensitivity and a wide frequency range simultaneously, because it does not use a diaphragm.



P3-I-13

A new type of MEMS Ultrasonic separator based on 2-D normal mode

Yuxiang Wang¹, Jiexiong Ding¹, Chenhui Hua^{1,2} *School of Mechatronics Engineering, University of Electronic Science and Technology of China, Chengdu, Sichuan, China, People's Republic of*

Background, Motivation and Objective

There are great advantages in separating suspended particles from small dosage by ultrasonic radiation force. There is more extensive application foreground by associating this method with MEMS. The research on MEMS ultrasonic separator is proceeding with some progresses, but almost all separators operated on one-dimensional normal mode. And there are some inherent defects, such as the difficulty of disposing outlets, the turbulence of clean and turbid stream. The objective of this paper is supplying a feasible approach to overcome these inherent defects.

Statement of Contribution/Methods

The method is employing two anti-phase PZT transducers to generalize two-dimensional normal mode (Fig.1), which drives particles to congregate in the lateral direction. Then the outlets would be easily located along this direction (Fig.2). The wedge shape training wall near the outlets is designed to divide the streams more smoothly. This separator is fabricated with MEMS process, and SOI is selected to form separating cavity, which ensures the precision of depth and the smoothness of bottom.

Wednesday
Poster

Results

In the separating experiment, this new type of separator shows advantages on driving the suspended particles (yeast) to the flanks of lateral direction. The turbid stream with particles is expelled from the side outlets, and the clean stream is expelled from the middle outlet.

Discussion and Conclusions

Based on the theory and experiment, it is proved that this new type of ultrasonic separator can drive suspended particles to form special patterns along lateral direction. Then the outlets are easily and reasonably positioned on the bottom of MEMS device, while turbulence near the outlets will decrease.

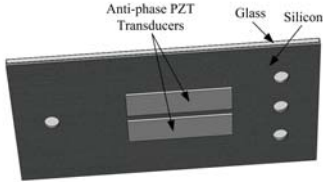


Fig.1 The reverse of this new type of separator

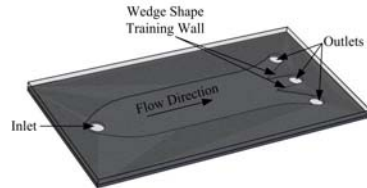


Fig.2 The obverse of this new type of separator

P3-I-14

Performing microdroplets mixing using an acoustic transducer with low vibration frequencies

Faten KARDOUS¹, Réda Yahiaoui¹, Jean-François Manceau¹; ¹MN2S, Femto-ST, Besancon, France

Background, Motivation and Objective

In the micro- and nano-fluidics field, the mixing of liquids is a difficult challenge. This function is usually achieved by mixing two or more continuous flows via their injection in the same micro-channel. An alternative approach to continuous microfluidic systems is the manipulation of discrete droplets.

Statement of Contribution/Methods

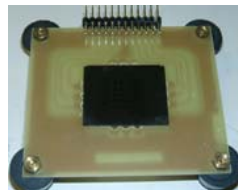
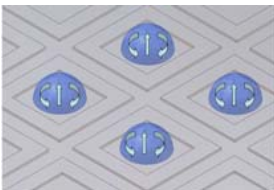
We have developed a liquid droplet mixer based on local acoustic field generation using low frequency vibrations. The ability of a rapid mixing using a minimum area and small volumes of liquids is an important criterion for chemical and biological applications. Our transducer permits the creation in parallel of an active mixture in a matrix of 25 microdroplets that are localized on a surface.

Results

The acoustic transducer was designed to avoid contamination between droplets while they are excited. Experiments showing the independent and active mixture of droplets were realized. In this work, we performed samples mixing. Indeed, the mixing behaviour depends on a number of parameters namely volume, viscosity, surface tension, exciting membrane mode, and vibration velocity. In order to study the reaction kinetic, mixing is visualized using CCD camera coupled to a microscope.

Discussion and Conclusions

First experiments related to droplet mixing validate the transducer structure proposed in this work. This result opens the door to experimenting the transducer in chemical and biological applications.



Acoustic particle manipulation in a microchannel narrower than half a wavelength: stability of the node of pressure

Iciar Gonzalez¹, Luis Fernandez², Tomas Gomez¹, Javier Berganzo²; ¹CSIC, Spain, ²IKERLAN, Spain

Background, Motivation and Objective

Ultrasonic micromanipulation is emerging as a new noninvasive competitive technology for diverse biotech and medical applications. This technique is highly efficient because it is based on the action of hydrodynamic forces acoustically induced on each single particle. These microdevices are usually made of silicon, making relatively expensive their market.

A new design of ultrasonic micromanipulator made of a cheaper material can provide added interest, representing the objective of the authors.

Statement of Contribution/Methods

A plastic microdevice is presented in this work to carry out ultrasonic particle micromanipulation within a channel along which suspensions flow. It was built in a soft material, SU-8 (apparently not suitable from the acoustic point of view), what is new in this type of devices, with a microfluidic channel and a piezoelectric ceramic attached to one of its outer edges. A second novelty of the device concerns to the way it works, behaving as a resonant multilayer system where all the layers are involved in the establishment of a standing wave across its width (including the channel). The part of the wave established within the channel includes a node of pressure, strategically located, toward where the flowing particles are driven by a radiation force acoustically induced, perpendicular to the flow direction and not on the isolated resonance of the channel of treatment.

The width of the channel is somewhat larger than a quarter of a wavelength, which does not fit any of the conventional models but it represents an intermediate situation.

Results

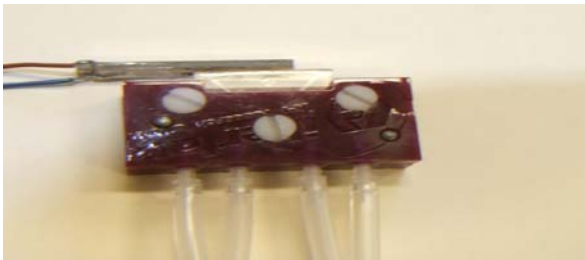
Experiments were made to analyse the stability of the device on the particle motion within the channel considering the influence of acoustic and spatial parameters involved. The influence of the acoustic frequency was clear; slight variations of this parameter (of approx. 10%) produced apparent displacements of the node of pressure in the channel.

To analyse the influence of spatial parameters within the channel diverse designs of the device were required, generating complex results.

Discussion and Conclusions

The feasibility of a new design of ultrasonic micromanipulator made of a plastic material is evidenced in this work, based on a multilayer resonance behaviour.

A complex correlation between the different parameters involved in the design of the device and the stability of its efficiency was found in the experiments.



P3-J. Defects and Characterization

Sala Orange

Wednesday, September 23, 2009, 10:00 am - 11:30 am

Chair: **Bernhard Tittman**
Pennsylvania State University

P3-J-01

Non-contact ultrasonic assessment of the properties of vacuum-packaged dry-cured ham

Tomas Gomez¹, E Corona², J Benedito²; ¹CSIC, Spain, ²UPV, Spain

Background, Motivation and Objective

Ultrasonic parameters such as velocity and attenuation have been used to assess physicochemical properties of many foods (fish analogues, meat mixtures, chicken meat and pork meat).

Industries that manufacture dry-cured ham, suffer from a high heterogeneity in the raw materials resulting in very heterogeneous final products which lowers the quality of the production. The final quality of dry-cured hams is highly dependent on the fat content, its distribution and its fatty acid composition. The texture of the dry-cured ham is also an important quality factor very appreciated by the consumer.

Hence, the seek for non-destructive techniques, like ultrasounds, that can be used to assess the fat content and distribution as well as the texture in sliced dry-cured ham is of great interest. The use of ultrasonic techniques in this field is promising, however, one of the main problems for its industrial development is the need of couplants. The objective of this work was to assess the feasibility of using a non-contact ultrasonic system to assess the properties and the quality of dry-cured ham

Statement of Contribution/Methods

Sliced dry-cured ham was purchased from a local market and vacuum packaged in the laboratory in three different thicknesses (5.6, 7.7 and 19.5 mm) which are usual in the retail distribution of this product. The experiments were performed on samples at 2 °C. Results obtained from a conventional contact measurement are compared with those obtained using air-coupled ultrasounds. In the first case, a couple of narrow-band ultrasonic transducers (1 MHz, 0.75'' crystal diameter) were used. A digital height gage was designed and built, to measure the sample thickness (± 0.01 mm). The ultrasonic velocity in the sample was computed from the time of flight, and the thickness read from the height gage. In the second case, a couple of wide-band air-coupled transducers (0.75 MHz) made from random 1-3 composites and a several matching layers were used

Results

Measured magnitude and phase spectra of the transmitted signal reveal the classical resonance pattern for sound transmission through a wall. As an important novelty, a special procedure is applied to determine the thickness of the packages from the frequency location of the thickness resonances and the phase value at these points. Velocity and attenuation are derived from the comparison between measured spectra and theoretically calculated ones. Typical data are about 1700 m/s for the velocity and 100 Np/m for the attenuation. Non-normal incidence and shear wave propagation is also investigated for this propagation mode contains significant information about the fat in the ham.

Discussion and Conclusions

We demonstrate that the non-contact technique is capable to assess the ultrasonic properties of vacuum-packaged dry-cured ham, and that it is a powerful technique as it can also provide information about the attenuation coefficient, the dispersion relations and it does not require measuring the thickness of the package

Nonlinear Resonance Ultrasound Spectroscopy (NRUS) to monitor the tightening of bolts

Jacques Rivière¹, Guillaume Renaud¹, Sylvain Hauptert¹, Paul A. Johnson², Maryline Talmant¹, Pascal Laugier¹;
¹Laboratoire d'Imagerie Paramétrique, UPMC Univ Paris 06, PARIS, France, ²Los Alamos National Laboratory, Los Alamos, NM, USA

Background, Motivation and Objective

The context of this work is the development of ultrasonic non-destructive methods for monitoring medical implant sealing. The aim of this study is to evaluate the sensitivity of Nonlinear Resonance Ultrasound Spectroscopy (NRUS) to torque changes, in a system composed of a bolt tightened in a block of different materials. The system investigated in this work offers the advantage of simplicity while it is assumed to model the more complex real-world configuration of an implant.

Statement of Contribution/Methods

A bolt is first tightened at different torques (range 15-75 N.cm) in an aluminum plate, then in a Plexiglas® block. For both experiments, two piezoelectric sensors are bonded on the material, one is used as an emitter, the other as a receiver. Different modes, identified using Finite Element Modelling, are studied in the range 1-20 kHz. For each mode, nonlinear parameters expressing the importance of resonance and damping variations are extracted.

Results

For the aluminum plate, when torque increases, these parameters decrease by one or two orders of magnitude, while linear resonance frequencies increase by about 1%. After identification of modes, the influence of the mode type on the sensitivity of nonlinear parameters is discussed. First modes from 1 to 10 kHz, corresponding to the first bending modes of the plate, show weak nonlinearity and little sensitivity to torque variations. Modes in the range 10-20 kHz, also corresponding to bending modes of the plate, are larger and more sensitive to torque changes, especially in the range 15-35 N.cm. Furthermore, screw bending modes only appear for torque exceeding 35 N.cm, and show a good sensitivity to torque increase.

In the case of Plexiglas® block, the identification of modes is more arduous, due to higher damping in this material. Indeed, high damping causes an overlapping of modes. Nevertheless, a decrease of nonlinear parameters is observed during tightening.

Discussion and Conclusions

These results suggest that NRUS can be an appropriate and sensitive method for monitoring of bolt tightening. The application of this method for monitoring implant sealing will be investigated in the near future.

Inclusion and Pore Classification in Rolled and Unrolled Steel Samples

Ville Kananen¹, Joonas Eskelinen¹, Edward Hægström^{1,2} *Department of Physics, University of Helsinki, Helsinki, Helsinki, Finland*

Background, Motivation and Objective

Inclusions and pores are formed into steel during the production process. Ultrasound is used in the steel industry for quality control to count and to locate inclusions and pores in steel. When large inclusions/pores (FBs) are found, the sample is cut and the FBs are analyzed using a scanning electron microscope (SEM) to determine the FB material content. This kind of FB characterization is laborious (the sample is measured, cut, ground to find FB, and SEM imaged to clarify the inclusion material). Signal processing techniques have provided new methods to characterize steel sample FBs. Our aim is to develop an instrument for quantitative inclusion and pore characterization in rolled and unrolled steel samples.

Statement of Contribution/Methods

This study has developed a stand-alone software relying on digital signal processing to classify FBs in steel samples. This produces new information of inclusion content shape and material distribution in rolled and unrolled steel samples.

The instrument features a 11.4 MHz focused transducer (14 cm focal length, 100% -6dB relative bandwidth). The water immersed sample was scanned across the top surface at 50 µm steps keeping the transducer focal point at the FB depth. FBs were cut out to verify the FB material and shape by means of optical microscopy. Data was digitally processed off-line (MathWorks MATLAB 7.4). The recorded echoes were corrected for attenuation. FBs were

separated into three classes by material (oxides, sulphides, pores) and three classes by shape (point-shaped, line-shaped, FB group). Continuous wavelet transform (CWT), short-time Fourier transform (STFT), and cross-correlation techniques were used to determine the differences between these classes' echo amplitude and frequency content. These differences were then used to classify FBs in steel samples.

Results

We report FB classification results for rolled ball-bearing steel 100Cr6 samples by FB material and for CH23MnB rolled steel samples by calcium-aluminate (CaAl) inclusion shape. For 100Cr6, CWT allowed highest FB classification accuracy 87% for 45 point-shaped FBs whereas STFT allowed highest FB classification accuracy 80% for 56 line-shaped FBs. For CH23MnB, CWT allowed highest FB classification accuracy 65% by FB shape for 23 CaAls. Scattering theory in Rayleigh regime was used to describe the sound-matter interaction in steel to aid FB classification by characterizing FB shape, size, and material effect on FB echo. Results for unrolled CH23MnB steel samples where pores are discriminated from CaAl inclusions are also shown.

Discussion and Conclusions

The FB classification software improves steel sample quality control by saving laboratory resources and time. The method allows class estimation for all FBs in sample and therefore gives more accurate information of steel quality compared to SEM method. However, FB characterization at transducer off-focal depths requires quantitative corrections into FB echo for correct FB classification.

P3-J-04

Material Evaluation with New Modulation Method in Photoacoustic Technique

Akiyuki Minamide¹, Kazuya Takemata², Yoshiaki Tokunaga²; ¹Kanazawa Technical College, Kanazawa, Ishikawa, Japan, ²Kanazawa Institute of Technology, Ishikawa, Japan

Background, Motivation and Objective

It is well-known that a photoacoustic microscope (PAM) is powerful equipment for 3D imaging research containing depth profiles. However, the time for data treatment takes very long time, and the operation process also becomes complicated.

In order to reform this disadvantage, we have proposed a new method the simultaneous measurement of multiple frequencies (SMMF). This method, however, has a weak point that a signal-to-noise-ratio (SNR) in high frequency components of the PA signals deteriorates than that in low frequency components.

Statement of Contribution/Methods

In this study we propose a new method reformed simultaneous measurement of multiple frequencies (RSMMF). Figure 1 shows comparison with principles of the RSMMF and the SMMF methods. In both methods, a complicated wave formed from a pulse train in the frequency range using inverse fast Fourier transform (IFFT) is applied to an acoustooptic modulator (AOM) as an output voltage of a computer and the modulated laser light passing through the AOM is irradiated to the sample. After the analog PA signal obtained from the microphone is treated by a FFT analyzer.

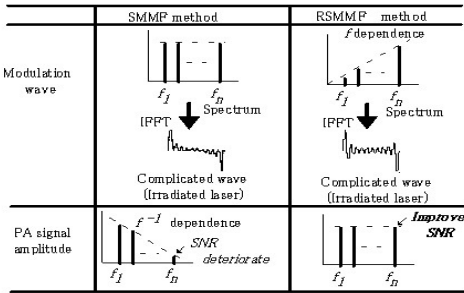
Because continuation laser is resolved into a pulse train of each frequency component in the SMMF, the energy strength of the single pulse component deteriorates. The SNR deteriorates greatly because the PA signal amplitude in a high frequency component decrements according to f^{-1} dependence. In the RSMMF, the amplitude of the pulse train of the laser beam is made to increase in proportion to f . As a results, it is possible that the measuring PA signal amplitudes in the high frequency component are sufficiently large, and the SNR can be also improved.

Results

A graphite without a defect was measured, SNR of the RSMMF has been improved from the SMMF 13dB at 100 Hz. Next, the graphite with an internal defect was measured. For the lower frequency components, in the both methods, the increase of the amplitude at the defect was clearly observed. On the other hand, the change of amplitude should be observed because the thermal diffusion length of the graphite at 60 Hz (0.7 mm) was same as depth of the defect. For the 60 Hz component, though the change of the amplitude was not almost observed in the SMMF, it was observed in the RSMMF.

Discussion and Conclusions

It was found that the RSMMF method could display better image of the internal defect than the SMMF method in the higher frequency components.



P3-J-05

Pattern Recognition and Quantitative Evaluation of Defects Using Ultrasonic Chirplet Signal Decomposition

Yufeng Lu¹, Erdal Oruklu², Jafar Saniie²; ¹Electrical and Computer Engineering, Bradley University, Peoria, Illinois, USA, ²Electrical and Computer Engineering, Illinois Institute of Technology, Chicago, IL, USA

Background, Motivation and Objective

In ultrasonic nondestructive testing, the pattern of scattering echoes is highly dependent on the impulse response of the ultrasonic transducer, physical properties of the propagation path, and the shape, size, orientation and location of defects. The inhomogeneity and/or structural disposition of materials results in nonstationary and dispersive ultrasonic scattering echoes. Therefore, for material characterization and flaw detection applications, it becomes a challenging problem to unravel such complex signals using only direct measurement and conventional signal processing techniques.

Statement of Contribution/Methods

Chirplet is a type of wavelet model often used in ultrasound, radar, sonar, and seismic signals. The chirplet signal decomposition (CSD) algorithm is utilized to decompose the ultrasonic scattering signal into a linear combination of chirplets and efficiently estimate the echo parameters, which can be correlated to the structure of defects. In this investigation, we present a quantitative method for pattern recognition and defect characterization using CSD. The geometry of defects contributes significantly to the echo shape when the defect size is about the same or bigger than the wavelength of ultrasound. The time-of-arrival, amplitude and the number of estimated echoes (i.e. chirplets) are critical in the quantitative evaluation of defects. For experimental studies, planar and focused transducers with different center frequencies (i.e., 5 MHz and 10 MHz) have been used for testing the embedded defects in a specimen at normal or oblique refracted angles. A variety of defects including disc-shaped cracks in a diffusion-bonded titanium alloy and a set of flat-bottom and side-drilled holes of different sizes positioned at various depths have been used to examine the echo scattering patterns and to predict the defect shapes and to validate the accuracy of the CSD algorithm.

Results

In this study, we demonstrate the application of the CSD algorithm for quantitative nondestructive evaluations using ultrasound. Through extensive experimental studies, it has been shown that the CSD algorithm offers an efficient approach for defect pattern recognition. Furthermore, CSD successfully associates the estimated chirplets and their parameters as a quantitative method to characterize defects.

Discussion and Conclusions

Numerical and experimental results signify that the CSD algorithm is successful for ultrasonic signal analysis accounting for a broad type of echoes including narrowband, broadband, symmetric, skewed, dispersive or nondispersive echoes. This algorithm also can be utilized in the analysis of ultrasonic signals often encountered in nondestructive testing for flaw detection and pattern recognition.

Wednesday
Poster

P3-J-06

An annular array with fiber composite microstructure for far field NDT imaging applications

Sivaram Nishal Ramadas¹, Jerzy Dziejewicz¹, Richard L O'Leary¹, Anthony Gachagan¹, Alexander Velichko², Paul D Wilcox²; ¹Centre for Ultrasonic Engineering, University of Strathclyde, United Kingdom, ²Mechanical Engineering, University of Bristol, United Kingdom

Background, Motivation and Objective

Two-dimensional (2D) array ultrasound transducers have received much attention in recent years. A typical 2D array configuration consists of a rectangular grid of miniature piezoelectric elements, each being addressed individually. The wavefronts generated from each of these elements can be time-delayed and synchronized to create an ultrasonic beam for which the beam parameters, such as the steering angle, focal distance and focal spot size, can be modified electronically. This is extremely advantageous for NDT applications as it allows dynamic focusing, electronic scanning and volumetric imaging of a test piece, all with direct influence on inspection time and accuracy. While 2D arrays offer numerous advantages, their use in NDT applications is often subject to many technological limitations.

Statement of Contribution/Methods

This paper describes the design and fabrication of a reduced element count annular array for far field NDT imaging application, built with a random fiber piezoelectric composite microstructure. An annular array design is considered, as it offers axi-symmetry layout while reducing number of array elements, which results in a significant reduction in the cost and complexity of building an ultrasonic volumetric imaging system.

Specifically, the fabrication process involved, manufacturing a range of ring shaped array moulds (approximately 30mm high and 20mm outer radius) using advanced 3D printing technique. PZT-5A piezoelectric fibers (105µm and 250µm diameter) are packed into the mould with hard setting polymer to form the fiber composite structure. Thin layers are then sliced and poled from this mould, to be used as active layers for the annular array. For the prototype study, device frequency between 1.5MHz to 3MHz, for operation into a steel load, is considered. The connections to the individual array elements are achieved by a flexible printed circuit board based interconnect system. The device is backed and matched with a particle loaded epoxy material to reduce pulse ring-down time, and increase efficiency.

Results

Performance evaluation of the fiber composite array including operational impedance, directivity, and cross-talk measurements are reported. Also, pulse experiments were performed to characterize the array for generating volumetric imaging of solid test pieces, and compare against conventional fully populated rectangular matrix array.

Discussion and Conclusions

The design and fabrication of a reduced element count, annular array with fiber composite microstructure has been presented. Work to date has indicated that such an approach provides an efficient and cost effective way of building NDT imaging systems. Future work will extend the philosophy to build an optimized array design, with particular emphasis on spatial distribution of elements and electrical interfacing. This will be reported at a later date.

P3-J-07

Characterization of the rheological properties of wheat dough using ultrasound

Fred Gates¹, Ari Salmi¹, Timo Karppinen¹, Edward Hæggestöm¹; ¹Department of Physics, University of Helsinki, Helsinki, Finland

Background, Motivation and Objective

In Europe bread, fresh pastry goods and cakes generated 28 billion EUR in value added in 2004 [1]. Quality control, in particular the measurement of flour water absorption, is essential to ensuring that there are no interruptions to processing. Water addition changes the rheological properties of the dough, influencing its behavior during processing and bubble growth in the dough. Nondestructive methods are required to allow online measurement of dough rheology. The velocity and attenuation of ultrasound in dough range from 80 m/s [2] to 3500 m/s [3] and attenuation values up to 500 dB/cm [4]. The aim of the study is to determine the reason for the wide range of values reported in the literature. In addition we aim to provide data for future online measurement purposes.

Statement of Contribution/Methods

We demonstrate how water content, frequency and measuring time cause variation in ultrasound velocity in wheat dough. We measured the ultrasound velocity in unfermented dough with different water additions using a pitch-catch method at various frequencies.

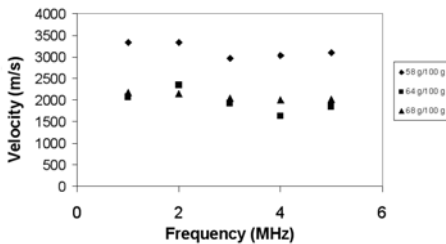
Results

Ultrasound velocity in dough is shown at 3 levels of water addition at frequencies between 1 – 5 MHz (Fig. 1). The time of arrival of the first arriving peak decayed exponentially over the first 30 minutes, from $8.90 \pm 0.04 \mu\text{s}$ to $8.84 \pm 0.02 \mu\text{s}$ through 3 mm of dough with optimal water content for baking (63.5 g water / 100 g flour). There was no noticeable difference between samples stored for similar periods before measurement and this effect was not due to drying.

Discussion and Conclusions

Water addition had the greatest effect on ultrasound velocity. Some frequency dependence was observed between 1 and 5 MHz. The ultrasound velocity depended on how long the dough was stressed between the transducers. The high attenuation limited the separation to around 3 mm, which made accurate velocity determination challenging.

[1] EUROSTAT (2007). European Business Facts and Figures.
[2] Kidmose et al (2001) J. Texture Studies 32:321-334
[3] Lee et al. (1992) J. Food Eng. 16:127-150
[4] Letang et al. (2001) Ultrasonics 39:133-141



P3-J-08

Ultrasonic Stiffness Measurements of Single Plant Fibers during Humidity Cycling

Risto Montonen¹, Kimmo Mustonen¹, Timo Karppinen¹, Ari Salmi¹, Edward Hægström¹; ¹Department of Physics, University of Helsinki, Finland

Background, Motivation and Objective

Mm-size fibers are structural elements in reinforced composites, woven- and non-woven fabrics and paper. The mechanical properties of wood fibers are important when paper behavior is studied under stress. Mechanical properties of individual fibers are commonly evaluated by pull- and torsion measurements, where the strain induced by a known amount of stress is quantified. Conventional measurements on mm- or sub-mm long fibers are slow and laborious. These tests tend to be destructive because clamping and straining alters the fibers structurally and mechanically. Consequently, studying e.g. the effect of temperature/humidity(RH) cycling on fiber properties is difficult.

Statement of Contribution/Methods

We developed an ultrasound time-of-flight measurement for single 4 to 5 mm long and $30 \pm 10 \mu\text{m}$ thick wood fibres. The measurements were done with a fixed transmitter (TX)-receiver (RX) distance. The transducers were custom built comprising a tungsten-carbide needle glued onto a 1MHz PZT disc. The TX and RX were glued to the fiber with a tiny droplet of cyanoacrylate to ensure good acoustic coupling. The waveforms of the through transmitted acoustic signals (450±270 kHz, -6dB BW, spike) were recorded. The stiffness was determined by

Wednesday
Poster

measuring the time-of-flight of the signal and calculating the stiffness from sound velocity and density (from tables). Our results correspond to earlier results of plant fiber pull measurements [1]. Cycled RH (30 to 90 % RH, 21 x 30 min cycles) was probed at constant 23 °C.

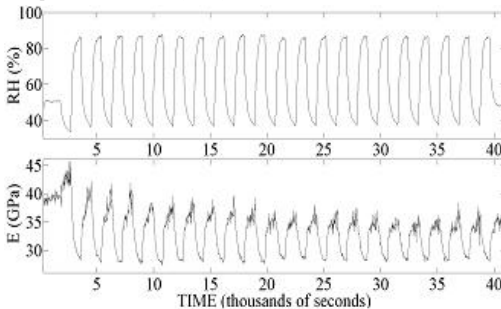
Results

Figure 1: first the larch fiber stiffness returned to nearly its native (dry) value, but after four cycles the maximum value decreased (0,7%/cycle)

Discussion and Conclusions

We characterized stiffness of single mm-scale fibers and observed the degradation of wood fiber stiffness in the longitudinal direction as a function of humidity cycling. The irreversible stiffness alteration is partially induced by the breaking of the H-bonds between the cellulose chains in the fiber wall by the water molecules. This stiffness drop may be caused by increasing residual moisture in the fiber but we find it unlikely because the cycling duration is long enough to allow the fiber equilibrate to surrounding humidity.

[1] C. Baley, Analysis of the flax fibres tensile behaviour and analysis of the tensile stiffness increase, Composites: Part A 33 (2002) 939-948



P3-J-09

Contact Measurement of Stiffness Depth Profile by Surface Acoustic Waves

Ari Salmi¹, Fred Gates¹, Tom Fabritius¹, Edward Haeggström^{1,1} Department of Physics, Division of Materials Physics, University of Helsinki, Helsinki, Finland

Background, Motivation and Objective

Depth profiling of stiffness in laminate structures is widely studied by high-frequency methods including photoacoustics, Brillouin scattering and acoustic microscopy [1]. Advances in the laseracoustic field have shown potential for thin layer characterization in hard solids, e.g. glass or ceramics [2]. However, the attenuation of high frequency waves in soft materials such as polymers is high which limits the effective probing depth of these techniques. In addition, none of the above methods offer portability; they require skilled operators and expensive equipment. We therefore try to create an affordable, portable and simple method to characterize the stiffness profile of laminated polymer structures into the depth direction.

Statement of Contribution/Methods

We used a needle ultrasonic transducer to excite surface waves. Laminates with two layers of polyethylene were prepared, the stiffness of the unbonded layers differed (2.1 vs 1.6 GPa). The upper layer was 2 mm thick and was heat sealed to an 11 mm thick base layer. We launched surface waves at varying frequencies (100-500 kHz) and measured the time-of-flight of the first discernible wave mode whose phase velocity was comparable to the longitudinal surface wave.

Results

Our data show phase velocities comparable to those calculated from the known material properties and layer thicknesses. Acoustic microscopy results confirmed the predicted thickness and adhesion, e.g. bonding between the layers. Data from different frequencies is shown and compared to theoretical dispersion curves. Surface waves

probe material to a depth of one wavelength, which allows determining a stiffness depth profile if different frequencies are excited.

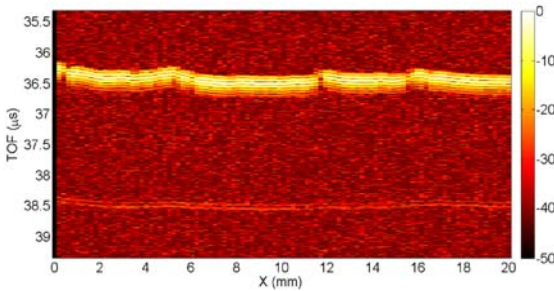
Figure 1: Acoustic microscopy image of the laminate structure, top surface and the boundary of the two layers of the laminate are shown.

Discussion and Conclusions

The results showed statistically significant difference between the mechanical properties of the laminate structures and the native polymers, which proves the feasibility to use the method to characterize such samples. The detected layer depth matched that obtained with the acoustic microscopy. The results show potential for rapid, affordable and portable characterization of stiffness depth profiles in polymeric samples.

[1] Every, A.G. Meas. Sci. Technol. 13 (2002) R21–R39

[2]Goossens, J. et al. J. Appl. Phys. 102 (2007) 053508



P3-J-10

The Glassy Rail – Advanced Ultrasonic Rail Inspection

Thomas Heckel¹, Hans-Joachim Montag², Sven Rube³, Steffen Fenger⁴; ¹VIII.43, Federal Institute for Materials Research and Testing, Berlin, Berlin, Germany, ²Federal Institute for Materials Research and Testing, Germany, ³PLR Pruftechnik Linke und Ruhe, Germany, ⁴PLR Pruftechnik Linke und Ruhe, Germany

Background, Motivation and Objective

One of the main challenges of automated rail testing is the high inspection speed. Because of a very dense overall traffic it became necessary to operate rail inspection trains up to more than 60 km/h. This speed is very close to the physical limits for ultrasonic testing methods, especially. To overcome these limits it is necessary to use digital signal processing algorithms which maintain resolution and detection quality independent of operation speed.

Statement of Contribution/Methods

A continued development of testing methods for the rail inspection trains was carried out over the years, for example the use of additional ultrasonic probes for the detection of SQUATs.

For data acquisition a recently developed inspection system is applied. It uses state of the art ultrasonic testing techniques which allow a speed independent resolution of 3 mm for volume scans. Up to fourteen ultrasonic probes per rail can be handled. 14-Bit A-Scan data and up to four interactive controlled gates are recorded continuously for each probe channel.

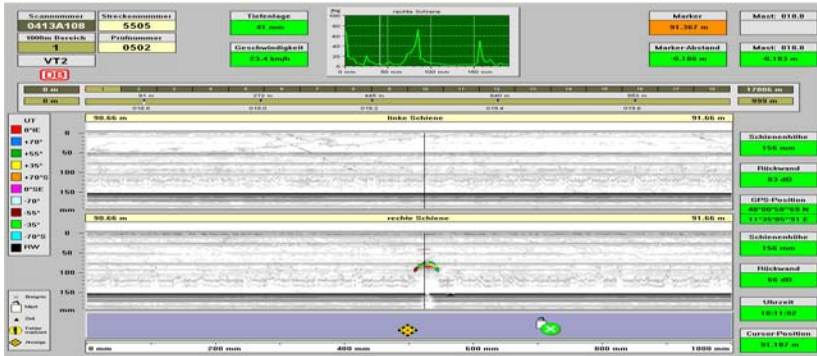
Results

The large amount of incoming measurement data poses additional challenges for the evaluation and the reviewing of the collected data. To keep evaluation of data simple to the operator automated classification algorithms had to be developed and adapted. The testing results are shown in a newly developed high resolution “Glassy Rail” diagram, which allows a very fast evaluation of data and sizing of defects. The detected findings are registered and fixed in position by GPS markers.

Wednesday
Poster

Discussion and Conclusions

Due to the large amount of different rail types and profiles, the adaptation and optimization of algorithms is still in progress. Additional data acquisition for non destructive eddy current methods for the detection of damages caused by rolling contact fatigue can also be applied and evaluated.



Wednesday
Poster

P3-K. Thin Films-Characterization

Sala Orange

Wednesday, September 23, 2009, 10:00 am - 11:30 am

Chair: **Cinzia Caliendo**
Instituto dei Sistemi Complessi

P3-K-01

Unusual increase in Poisson's ratio of nanocrystalline diamond thin films: Acoustic measurements and ab initio calculation

Kenichi Tanigaki¹, Hiroshi Tanei¹, Hirotugu Ogi¹, Nobutomo Nakamura¹, Koichi Kusakabe¹, Masahiko Hirao¹;
¹Graduated School of Engineering Science, Osaka University, Toyonaka, Osaka, Japan

Background, Motivation and Objective

Nanocrystalline diamond (NCD) thin films are deposited by CVD method by adding a small amount of nitrogen gas. They are candidates for high-efficiency acoustic and electronic devices, because they show highly smooth surfaces. The increase of the nitrogen gas concentration decreases the average grain size, and generates non-sp³ bonded region in the structure of NCD. In this study, we evaluate the effect of non-sp³ bonded region on the elastic constants using acoustic measurements and ab initio calculations.

Statement of Contribution/Methods

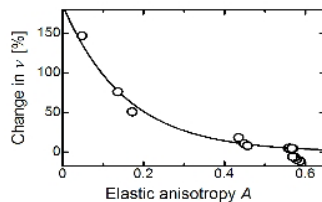
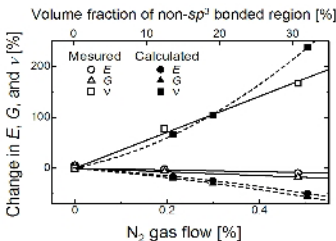
We measure the in-plane elastic constants of the NCD thin films using resonant ultrasound spectroscopy coupled with laser-Doppler interferometry and the out-of-plane modulus by Brillouin oscillations stimulated by picosecond ultrasound.

Results

The increase in the nitrogen gas concentration decreases Young's modulus and shear modulus slightly, while it drastically increases Poisson's ratio by 200% (Open dots in Fig. 1).

Discussion and Conclusions

In order to explain such an unusual elastic behavior, we consider an atomic-scale model for NCD, consisting of grains of sp³-bonded diamond structure and grain boundaries of non-sp³ bonded regions. The macroscopic elastic constants are determined using ab initio calculations, which consistently explain the behavior of the measured elastic property (Filled dots in Fig. 1). Figure 2 shows a significant correlation between Poisson's ratio and Zener's elastic anisotropy at the local non-sp³ bonded region, indicating that high elastic anisotropy caused by the non-sp³ bonded region have dominant influence on the macroscopic elastic constants of NCD. Thus, a combination of ultrasound measurement and theoretical calculation is found effective to analyze the relationship between microscopic structures and macroscopic property of solids.



Wednesday
Poster

P3-K-02

Annealing effect on elasticity of Cu thin films studied by resonant-ultrasound spectroscopy

Nobutomo Nakamura¹, Takeo Nakashima¹, Soichiro Oura¹, Hirotsugu Ogi¹, Masahiko Hirao^{1,2} *Graduate School of Engineering Science, Osaka University, Toyonaka, Osaka, Japan*

Background, Motivation and Objective

Polycrystalline thin films often contain incohesive bonding regions and nano-scale defects at grain boundaries, and the elastic constants are comparable to or smaller than those of the bulk materials; their decrement ratio depends on the shape and the volume fraction of the defects. Annealing treatment is an important technique to recovery and recrystallize thin films and to improve their physical properties. In this study, we measure the elastic constants of annealed Cu thin films deposited on Si substrates using resonant-ultrasound spectroscopy (RUS) and evaluate the correlation between the elastic constants and the annealing temperature. Furthermore, the effect of recrystallization and recovery is discussed.

Statement of Contribution/Methods

Cu thin films were deposited on monocrystal Si substrates by the RF-magnetron sputtering, and the substrates were heated after the deposition. The annealing temperature was 80 or 200 °C. In-plane elastic constant of Cu thin films was determined by RUS, and the crystallographic orientation was evaluated by x-ray diffraction method.

Results

X-ray diffractions spectra revealed that the crystallographic orientation changes depending on the annealing temperature: the as-deposited film showed <111> texture in the thickness direction and it became the random orientation as the annealing temperature increased. Elastic constant also increased, as the annealing temperature increased.

Discussion and Conclusions

There are two possible factors causing the increment in the elastic constant: recrystallization and recovery. We calculated the changing ratio of the elastic constant caused by the change in the crystallographic orientation using Hill's approximation. In this calculation, the orientation of grains in the thickness direction was determined from the x-ray diffraction spectra, and we assumed that the grains are randomly oriented around the thickness direction. Thus calculated elastic constant decreased as the annealing temperature increased, which is opposite to the observation. Therefore, we consider that the recrystallization hardly contributes to the increment of the elastic constant, and recovery is the dominant factor. The measured elastic constants were then compared with the bulk material's values that were calculated considering the crystallographic orientation of each film. By the comparison, we found that the elastic constant of the as-deposited film was smaller than the bulk value by 10% and it was recovered to the bulk value by the annealing at 200 °C. This result is explained by considering that incohesive bonding regions at the grain boundaries are cured and binding condition between the grains is improved by the annealing.

P3-K-03

Comparison between picosecond ultrasonics and nanoindentation characterization in thin film

Pierre-Adrien Mante¹, Arnaud Devos¹, Gaetan Raymond², Pierre Morin², Pascal Ancyey², ¹IEMN-CNRS, France, ²ST-Microelectronics, France

Background, Motivation and Objective

Mechanical characterization of thin films is a main issue in the microelectronic industry. The knowledge of these properties is necessary in many fields such as copper line interconnection and bulk acoustic wave resonators. A few techniques are reliable at this scale. Nanoindentation can't be directly effective in films thinner than 500nm due to substrate effects. Picosecond ultrasonics is an efficient method to excite and detect vibrations within a thin film. A strong optical pulse warms a transducer, which leads to the creation of an acoustic wave propagating at the sound velocity. It is a really competitive technique to characterize thin films but require a nanostructure of the transducer.

Statement of Contribution/Methods

In picosecond ultrasonic we use a metallic very thin film as a transducer and only longitudinal waves can be generated. Due to that the full mechanical properties of thin layer cannot be measured. Recently we showed[1,2] that thanks to a nanostructuring of the transducer, in-plane propagating waves are added using the same

experimental setup. In the case of an isotropic medium, we have now access to Poisson's ratio and Young's modulus.

Results

Our samples consist of a film of silica on a silicon substrate. The thickness of the silica film is varying from 200 nm to 600 nm. We performed nanoindentation measurements on those samples. Then we realized picosecond ultrasonics experiments.

Discussion and Conclusions

We will discuss the results for both techniques: limitations, size reduction effect and substrate effect. Further results obtained on other materials will be also presented.

[1]P.A. Mante, J.F. Robillard, A. Devos, Appl. Phys. Lett. 93, 71909 (2008)

[2]P.A. Mante, J.F. Robillard, A. Devos, IEEE Ultrasonics Symposium 2008

P3-K-04

Quality Factor of MEMS and NEMS AIN Contour-Mode Resonators in Liquid Media

Chiara Zuniga¹, Matteo Rinaldi¹, Gianluca Piazza¹; ¹Department of Electrical and Systems Engineering, University of Pennsylvania, Philadelphia, PA, USA

Background, Motivation and Objective

Miniaturized resonant sensors for bio applications are required to operate in liquids and their quality factor (Q) is important in setting the limit of detection. This work presents the first theoretical analysis and experimental verification of the behavior in liquids of AIN Contour Mode M/NEMS Resonator (CMR). CMRs are based on in-plane lateral vibrations and therefore deemed to perform well in liquids, similarly to shear-based devices. This study shows that the Q in water of 4 CMRs with different frequencies of operations on the same die (182 MHz to 3.45 GHz) increases with frequency of operation in agreement with the theory and is independent of its surface area. Therefore miniaturization and frequency scaling can be advantageously exploited to operate in liquids.

Statement of Contribution/Methods

A 1D model based on the theory of an oscillating plate in a viscous media was used to describe the behavior of AIN CMRs in liquids. Viscous damping and loading were modeled into an equivalent electrical circuit (Fig. 1) and the resonator Q in fluid (Qf) was found to be:

$$Q_f = \text{Est}/E_{\text{diss}} = [T \cdot (\pi \cdot f_s)^2 / (1/2)] / [2 \cdot (\mu f \cdot \rho f) / (1/2)]$$

where T and fs are the device thickness and frequency, and μf and ρf the density and viscosity of the fluid. Experimental verification of Eq.1 was performed by immersing in 2 μL drops of water 4 devices fabricated on the same die, formed by 250 nm thick AIN and operating between 182 MHz and 3.45 GHz. Their responses were fit to the proposed equivalent electrical model and the value of Qf extracted.

Results

The devices experienced a drop in Q (with respect to air) because of the additional damping introduced by the liquid media. Unlike QCMs, whose Q drops with increasing frequency, these devices demonstrated a reverse trend in agreement with theory, which shows a direct relationship between Q and (fs)², leading to higher Q at higher frequency (Fig.1).

Discussion and Conclusions

The behavior of CMRs in fluids has been studied showing the net advantages of scaling the technology to higher frequencies of operation in terms of quality factor enhancement, sensitivity (proportional to fs) and ultimate limit of detection. The theory also highlights how the device Qf is immune to surface to volume ratio effects and proves that miniaturization is effective in developing resonant bio-sensors.

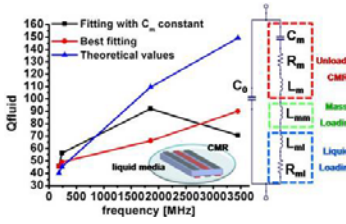


Figure 1. Experimental and theoretical Q_y of CMR in liquid media. The Q_y was extracted from the equivalent electrical model of the device. Two different kinds of fittings are reported, either best fitting curve or assuming constant stiffness of the device (C_m).

P3-L. Lamb Waves

Sala Orange

Wednesday, September 23, 2009, 10:00 am - 11:30 am

Chair: **Yook-Kong Yong**
Rutgers University

P3-L-01

Anisotropy propagation of Lamb waves in thin piezoelectric plates under the influence of bias electric field

Boris Sorokin¹, Sergei Burkov¹, Olga Zolotova¹; ¹Condensed Matter Physics, Siberian Federal University, Krasnoyarsk, Russian Federation

Background, Motivation and Objective

Producing of perspective devices for acoustoelectronics and non-destructive control would be found on basis of Lamb waves in piezoelectric crystals. Essential interest associates with such effect as phase velocity (or frequency) changing by the action of static electric field E and further optimal choice of propagation direction and E-application for crystal element of devices. So we have carried out the detailed analysis of Lamb waves anisotropic propagation in piezoelectric crystals under the above mentioned conditions.

Statement of Contribution/Methods

Analysis of influence of homogeneous static electric field E on Lamb wave anisotropy propagation conditions in piezoelectric crystalline plate has been considered on the basis of the theory published earlier [1].

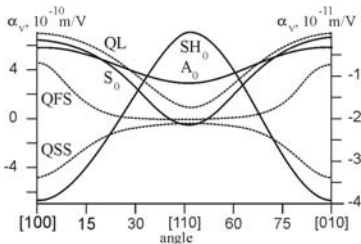
Results

By the basic dispersive equations obtained the analysis of changing by E-application for such propagation characteristics as phase velocity, electromechanical coupling coefficients and wave energy flow of Lamb wave in a lot of crystal directions has executed. We are taken into account such physical effects as a crystal symmetry decrease and effective material constants modification. Figure gives us an example of controlling coefficients anisotropy for Lamb waves propagating along directions in (001) plane (left ordinate axes) in comparison with ones for bulk acoustic waves (right ordinate axes). Electric field acts along wave propagation direction.

Discussion and Conclusions

Detailed computational calculations of Lamb wave propagation peculiarities on examples of Bi12GeO20 and La3Ga5SiO14 crystals under the E various variants application have obtained. The attention was mainly paid to dispersive behavior of first three modes and its anisotropy dependences. Hybridization effects and the repulsion of dispersive curves arising as a result of E-application have been considered for a various order modes. The data obtained can be useful for the design of controlling acoustic devices and for non-destructive control in which Lamb waves were found manifold applications.

1. Burkov S.I., Zolotova O.P., Sorokin B.P. Influence of the external electric field on propagation of Lamb waves in thin piezoelectric sheets // Proc. 2008 IEEE Intl. Ultrasonics Symp. (Beijing, China, November 2-5, 2008), pp. 1812-1814



P3-L-02

Guided Waves Propagating in a Bi-layer System Composed of a Piezoelectric Plate and a Dielectric Fluid Layer

Chia-Han Wu¹, Che-Hua Yang¹:¹Institute of Manufacture Technology, National Taipei University of Technology, Taipei, Taiwan

Background, Motivation and Objective

While Lamb waves are applied for the purpose of liquid sensor, very often there exists a condition that the plate substrate is loaded by a fluid layer. Studies in this category of problem are more involved with the condition with the fluid layer thickness large compared with the piezoelectric solid. However, some applications need to deal with a fluid layer thickness comparable with the plate. This study is focused on the theoretical modeling and experimental measurements for the dispersion relations of guided waves propagating in a piezoelectric plate loaded by a fluid layer of similar thickness.

Statement of Contribution/Methods

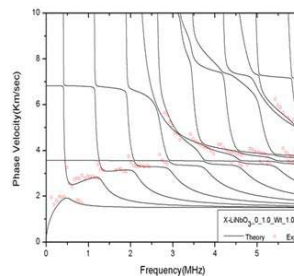
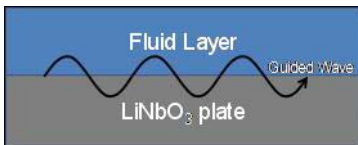
Our studied bi-layer system, as shown in Fig. 1, include a LiNbO₃ plate with a thickness of 1.0 mm and a fluid layer with its thickness varying from 1 to 3 mm. A theoretical model based on a recursive asymptotic stiffness matrix method (RASM) is used to model the dispersion spectra of guided waves propagating in the bi-layer system. The RASM model is used to study the effects of parameters including crystal-cut direction, azimuthal angle, plate/fluid thickness and density ratios, dielectric permittivity constant and conductivity. A laser ultrasound technique (LUT) is used to measure the dispersion relations.

Results

Fig. 2 shows the modeled and measured dispersion spectra for a bi-layer system with good agreement, which is also observed for other investigated cases.

Discussion and Conclusions

Mode couplings originating from individual modes pertaining to the single solid or liquid layer are identified and characterized in the theoretical modeling and measurements. While complete dispersion spectra can be constructed with the theory, dispersion data in the experiment is available only in the condition that the solid plate dominates the particle motion in the bi-layer system.



P3-L-03

Ultrasonic wave propagation in piezoelectric semiconductor plates under biasing fields

Bernard COLLET¹:¹Université Pierre et Marie Curie, (Paris 6), Institut Jean Le Rond d'Alembert, CNRS-UMR-7190,case162, Tour 65, Paris, Paris Cedex 05, France

Background, Motivation and Objective

The piezoelectric materials are either dielectrics or semiconductors. An ultrasonic wave propagating in a piezoelectric crystals or piezoelectric ceramics is usually accompanied by an electric field. When the crystal is also semiconducting, the electric field produces currents and space charges resulting in dispersion and acoustic loss. Several interesting phenomena involving the interaction of ultrasonic waves and electrons have been observed in piezoelectric semiconductors. These include in particular the process of ultrasonic amplification and nonlinear harmonic generation. It was shown experimentally and proved theoretically that an ultrasonic wave travelling in a

Wednesday
Poster

piezoelectric semiconductor can be amplified by the application of an initial dc electric field. The acoustoelectric amplification of ultrasonic waves have led to the development of acoustic devices.

Statement of Contribution/Methods

Piezoelectric semiconductor devices often have structural design of plates or beams. Here we study the thin piezoelectric semiconductor plates. Two-dimensional equations for coupled extensional, flexural and thickness-shear motions of plates are obtained systematically from the three-dimensional equations by retaining lower order terms in power series expansions in the plate thickness coordinate. Two-dimensional equations are specialized to obliquely cut of crystals of hexagonal (6mm) symmetry. In the presence of a depletion layer, the two-dimensional equations are generalized to the case of bilayered piezoelectric-semiconductor plates.

Results

The propagation of thickness-shear and flexural waves and their amplification by a dc electric field are analyzed.

Discussion and Conclusions

It is shown that the semi-conduction induces dispersion and acoustic loss in the propagation of thickness-shear and flexural waves. The equations are useful in analyzing plate structures for acoustoelectric devices.

P3-L-04

Complexity of elastic modes of a chaotic Silicon wafer

Olivier XERIDAT¹, Patrick SEBBAH², ¹Laboratoire de Physique de la Matière Condensée, CNRS UMR 6622, Nice cedex 2, France, ²Laboratoire de Physique de la Matière Condensée, CNRS UMR 6622, Nice Cedex 2, France

Background, Motivation and Objective

A closed quantum system is fully defined by a set of orthogonal discrete states. When channels are progressively opened and the system is being coupled to the environment, mode lifetime becomes finite as a result of leakage. Consequently, the spectral line of the modes broadens and their eigenfunctions become complex-valued with their standing wave component being progressively replaced by a component traveling toward the system boundaries.

We report non invasive measurements of the complex field of elastic modes of a 2" silicon wafer with chaotic shape. The amplitude and phase spatial distribution of the modes are directly obtained by Fourier transform of time measurements. We investigate the crossover of the wavefunction from real to complex, when absorption is progressively increased. The complexity factor q , which characterizes the degree to which a wavefunction is complex-valued, is measured for non-overlapping modes. Here we are interested in relating q to the mode spectral width Γ , which comes down to comparing the change in the spatial nature of the mode with its spectral characteristics.

Statement of Contribution/Methods

The ultrasounds are optically generated using a Nd:YAG Q-switched laser and detected by an interferometric heterodyne probe which measures a time response proportional to the plate normal displacement at one point. We measure the effect of increasing losses on spectral and spatial characteristics of the modes. Leakage channels are progressively opened by sticking absorbent elastomer strips with different dimensions on one edge of the chaotic sample. For each configuration, the acoustic field spatial distribution, the phase probability distribution, q and Γ are measured for individual non-overlapping modes.

Assuming spectral overlap to be negligible for the considered mode, Γ is obtained by fitting the complex spectrum around the resonance with a complex Lorentzian; q is obtained from the ratio of the variances of the imaginary and real parts of the wavefunction at resonance.

Results

We observe a linear dependence between q and Γ . The deviation from the linear fit is below 3%. From this fit, q extrapolates to 0 for $\Gamma=70.5\text{Hz}$. This value corresponds to the homogeneous contribution to the losses resulting from uniform surface-coupling with air.

Discussion and Conclusions

We measured the complex-valued wavefunction and spectral width of modes of a Silicon Chaotic plate. The complexity factor q is found to increase linearly with the spectral width Γ of the mode. This is in agreement with recent theoretical predictions. This is to our knowledge the first report of a direct comparison of q and Γ measured for a given mode. Although limited by the small number of non-overlapping modes, a systematic study over a larger number of modes should allow a statistical exploration of the spatial and spectral characteristics of the wavefunctions.

P3-L-05

On the nonlinear dynamics of plate-transducers

Andrea Cardoni¹, Enrique Riera², Alfonso Blanco³, Juan Antonio Gallego-Juarez^{2,1}. *Mechanical Engineering, University of Glasgow, United Kingdom, ²Instituto de Acustica (CSIC), Spain, ³Instituto de Fisica Aplicada, Spain*

Background, Motivation and Objective

Power ultrasonics finds an increasing range of industrial and medical uses. Among the applications involving liquids and gases, power ultrasonic plate-transducers play a key role. In these devices, the excitation of opportunely tailored flexural motions of plate elements allows high-directional propagation of sound waves through a variety of media. Plate-transducers are high-Q multi-component systems that at high power are vulnerable to nonlinearities which hamper their scale-up to large industrial plants. This work aims to study the vibration characteristics of plate-transducers by looking at the dynamic effect brought by their constitutive components (i.e. piezoelectric sandwich, mechanical amplifier, and plate radiator).

Statement of Contribution/Methods

The authors have previously characterized the vibration behaviour of ultrasonic devices identifying several nonlinear phenomena. This work progresses those findings by seeking novel solutions for the mitigation of nonlinear effects, and identifying drive regions within which tuned systems can operate stably. Sine sweep excitations near the operation frequency at increasing power levels are experimentally carried out to study the level of nonlinearity within the tested components. Since it has been shown that the vibration response of ultrasonic tools is highly influenced by temperature, a burst driving method has been adopted to eliminate thermal effects.

Results

The piezoelectric core of plate transducers appears to be the main source of nonlinearity. Fig. 1 shows the response characteristics near the tuned frequency of the piezoelectric component detected at increasing power levels (Fig. 1(a)), alongside two spectral velocity measurements (Fig. 1(b-c)). The effect of the other tuned units on the global system dynamics is also investigated.

Discussion and Conclusions

At low power the velocity response detected on the piezoelectric sandwich component is weakly nonlinear (Figs. 1(a-b)). At higher excitation a moderate softening characteristic appears (Fig. 1(a)). At further increased power the response becomes highly distorted and a wide-band response spectrum occurs (Fig. 1 (c)) at the excitation frequencies between A and B (Fig. 1(a)). This nonlinear behaviour can be advantageously modified by the addition of the other transducer components.

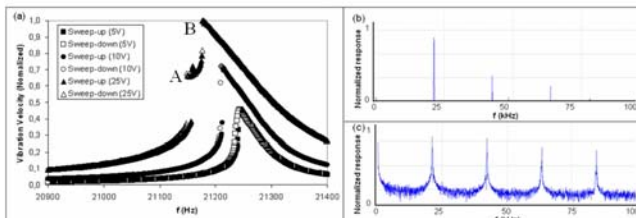


Figure 1. Vibration behaviour of the piezoelectric sandwich component using laser vibrometry: velocity response characteristics at three excitation levels (a), spectral measurements at low power (b), and high power (c).

P3-L-06

General Properties of the Anisimkin Jr. Plate Modes

Vladimir Anisimkin¹, *¹IRE RAS, Russian Federation*

Background, Motivation and Objective

Recently, new plate modes characterized by dominant depth-independent longitudinal displacement u_1 and propagation velocity v_p close to the velocity of the longitudinal BAW v_L has been found in 3 trigonal crystals. Though the crystals belong to the same symmetry, existence conditions and mode properties are rather different. The goal of the paper is finding general properties of the modes.

Wednesday
Poster

Statement of Contribution/Methods

By varying plate thickness, dispersion curves $v_n(h/\lambda)$ for all existing modes are numerically calculated (n – mode order, h - thickness, λ - wavelength). For modes with $v_n = v_L$ depth profiles and dispersion slopes $dv_n/d(h/\lambda)$ at relevant $(h/\lambda)_n$ are determined. Basing on the results, classification of the modes with $v_n = v_L$ is accomplished. To examine a link between these modes and bulk waves the thickness $(h/\lambda)_n$ are compared with the thickness h/λ_{TR} , supporting transverse BAW resonance between plate faces. The strategy is applied to the plates with free and shorted faces, with and without piezoelectric effect. Test materials include orthorhombic 2mm $Ba_2NaNb_2O_{15}$, tetragonal 4/m $PbMoO_4$, tetragonal 42m KDP, tetragonal 4mm $Li_2B_4O_7$, tetragonal 4/mmm TiO_2 , tetragonal 422 TeO_2 , trigonal 32 quartz and Te, hexagonal 6mm ZnO, cubic m3m Si, and isotropic fused quartz. Plate orientations are “traditional” (0, 130, 0) and “chaotic” (89, 37, 104).

Results

Three types of the plate modes with $v_n = v_L$ are found for various materials and orientations – Lamb, Anisimkin Jr. (u_1 is dominant and depth-independent), and quasi-longitudinal (QL) (u_1 is dominant, but depth-dependent). Shorting plate faces and avoiding piezoelectric effect do not affect the mode type. For any crystal symmetries all Lamb modes approach $v_n = v_L$ at irregular $(h/\lambda)_n$ and at large $dv_n/d(h/\lambda) \approx 10^3$ m/s. For the same symmetries all other modes are characterized by periodic $(h/\lambda)_n$ and low dispersion ($dv_n/d(h/\lambda) \leq 10^2$ m/s). The set of $(h/\lambda)_n$ is close to the set of periodic $(h/\lambda)_{TR}$ for transverse BAW resonance.

Discussion and Conclusions

3 general properties ($v_n \approx v_L$, $(h/\lambda)_n \approx (h/\lambda)_{TR}$, $dv_n/d(h/\lambda) \leq 10^2$ m/s) are inherent for Anisimkin Jr.’ and QL-modes. It is these properties rather than anisotropy and piezoelectricity of the plates play an important role in existence of the modes.

P3-L-07

Effects of Electrode Inertia and Stiffness on Vibration of Piezoelectric Plate with Dissipation

Jianke Du¹, Xin Yin¹, Yook-Kong Yong², Ji Wang¹; ¹Ningbo University, China, People's Republic of; ²Rutgers University, USA

Background, Motivation and Objective

It was well known that piezoelectric materials are widely used in resonators, sensors and transducers. Almost all the modeling and analysis of vibration and wave propagation are based on the linear theory of piezoelectricity with quasi-electrostatic approximation, where the medium is assumed to be perfectly elastic and perfectly insulating to electric current. As operating frequencies get higher and sizes of acoustic wave devices become smaller, the dissipation of energies becomes more significant and should be considered in more realistic theories or modeling. In resonator manufacturing, one electrode is deposited first with a pre-determined thickness. Then the electrode on the other side of the piezoelectric plate has a thickness that is determined by the desired frequency of the electroded plate. If the electrodes on the crystal plate are very thin, their mechanical effects can be neglected. When the electrodes are not very thin, their mechanical effects, e.g. inertia and stiffness, need to be considered.

Statement of Contribution/Methods

An approach to treat with viscous dissipation of piezoelectric material is to assume that elastic modulus, piezoelectric coefficient, and dielectric permittivity coefficient are all complex constants, so the attenuation and other effects of the viscosity on the structural vibrations or the propagation of waves can be considered and analyzed. Numerous investigations of damping in solid represented by viscoelastic model have been undertaken for the isotropic materials by researchers in various disciplines because of its important applications. However, there are few studies using viscoelastic models for vibration with consideration of electrode inertia and stiffness in piezoelectric solids.

Results

We calculated the frequency for different piezoelectric materials and gold or silver electrodes with consideration of dissipation of piezoelectric plate. We can find that the gold electrode has more remarkable effect than the silver electrode on the frequency for same viscous dissipation because gold is heavier than silver.

Discussion and Conclusions

From the results we can find, for piezoelectric crystal, such as quartz or langasite, the viscosity is always so small that the effect on the frequency can be neglected, but the frequency with consideration of dissipation provides a method to calculate the electric parameters. For piezoelectric ceramics, such as BaTiO₃, the viscosity has a

remarkable on the frequency. On the base of the frequency with dissipation, we can calculate the electric circuit parameters of resonators.

P3-M. Optical Interactions

Sala Orange

Wednesday, September 23, 2009, 10:00 am - 11:30 am

Chair: **Valeriy Proklov**
Institute of Radio Engineering & Electricity

P3-M-01

Cascaded Acousto-Optic Filtering of Unpolarized Light

Konstantin Yushkov¹; ¹*Physics Dept., Oscillation Physics Chair, M.V. Lomonosov Moscow State University, Moscow, Russian Federation*

Background, Motivation and Objective

Bragg diffraction of electromagnetic radiation by ultrasonic waves in birefringent crystals is widely used for spectral filtering of light. Selection of transmitted light spectrum is performed by means of adjusting frequency and power of the acoustic wave. Typically, an acousto-optic tunable filter (AOTF) operates with linearly polarized incident light. In the report, a novel method of processing arbitrarily polarized light that is based on consequent application of two ultrasonic waves is observed.

Statement of Contribution/Methods

A cascaded set of two acousto-optic cells for processing optical beams with arbitrary polarization was developed. Two similar paratellurite-based AOTFs with wide angular aperture were used. Diffraction of orthogonally polarized components of the optical beam was provided by different cells. Due to a special orientation of the cells, diffracted beams of ordinary and extraordinary polarization propagated collinearly at the output of the system and beam splitting caused by birefringence of the crystals was compensated. Similarity of the cells provided equal ultrasonic frequency and diffraction efficiency in both AOTFs.

Results

Each of the AOTFs provides diffraction of correspondent linearly polarized component of the incident optical beam. In the experiment, efficiency of the diffraction exceeded 96%. At the same time, orthogonally polarized components of the optical beam were diffracted by side lobes of radiation pattern of a piezoelectric transducer. Analysis revealed that six beams may be observed at the system output if a plain monochromatic optical wave is incident. Diffraction pattern consists of the zero-order beam, a pair of combined first-order diffracted beams with wide acceptance angle, and three additional diffraction maxima. In traditional acousto-optic systems, the additional maxima are not observed because linear polarization of light is properly adjusted at the input of the AOTFs. Intensity of these maxima depends on the parameters of ultrasonic field in the crystal. Efficiency of diffraction for additional maxima was lower than 4%.

Discussion and Conclusions

The developed system may be applied either for notch filters or bandpass filters for white light with arbitrary polarization. Optical image processing is possible due to a wide angular aperture. If a monochromatic light is used, modulation of the optical beam can be performed. Practical absence of optical losses in the system makes it suitable for operation with radiation of powerful lasers. Appearance of additional beams at the output of the system is caused by a combination of tandem AOTF application and operation with unpolarized light.

P3-M-02

Peculiarities of collinear acousto-optic diffraction in non-homogenous acoustic field

Sergey Mantsevich¹, Vladimir Balakshy^{1,2} *M.V. Lomonosov Moscow State University, Moscow, Russian Federation*

Background, Motivation and Objective

Collinear diffraction of light on a diffraction grating is a very interesting physical phenomenon. This type of diffraction is widely used in acousto-optic tunable filters and other optoelectronic devices where the phase diffraction grating is created by travelling acoustic wave.

It is clear from general considerations that the divergence of a filtered optical beam and the complicated structure of the acoustic field has to affect characteristics of the AO diffraction spectrum. In papers devoted to AO collinear diffraction, this problem was usually solved in the plane-wave approximation, and the influence of the light divergence was taken into account only through the parameters of the utmost lateral plane-wave components of the incident light beam. The acoustic field structure is usually considered to be homogenous. Besides, the anisotropy of an AO medium either was not taken into account at all or was taken but not quite correctly.

Statement of Contribution/Methods

In this work, the theoretical research of collinear AO interaction characteristics is carried out with taking into account all optical beam components, structure of acoustic field and AO interaction medium anisotropy. The calculations are fulfilled for two well-known AO crystals: calcium molybdate (CaMoO₄) and tellurium dioxide (TeO₂).

These crystals demonstrate essentially different diffraction characteristics because of peculiar features of optical and AO anisotropy.

CaMoO₄ is used precisely for collinear AO filter fabrication. In contrast, TeO₂ is not employed in collinear filters due to the absence of the AO effect in the plane XY perpendicular to the optical axis Z.

Results

Discussion and Conclusions

We have investigated the influence of the optical beam divergence on characteristics of collinear AO diffraction theoretically, taking into account all the peculiarities that appear when a strongly divergent beam is scattered by an acoustic field excited in an anisotropic medium. The diffraction pattern has been calculated for different directions of propagation of interacting waves relating to the crystallographic axes and for different ultrasound frequencies. The variations of the two-dimensional transfer function with the acoustic power, the optical wavelength, and the acoustic frequency have been analyzed. The dependence of the integral diffraction efficiency and the transmission band of the collinear AO filters on the optical beam divergence have been studied.

P3-M-03

Recognition of Optical Layered BPSK Labels Using Collinear Double-Stage Acoustooptic Processor for Hierarchical Photonic Routing

Nobuo Goto¹, Yasumitsu Miyazaki^{2,1} *The University of Tokushima, Japan, ²Aichi University of Technology, Japan*

Background, Motivation and Objective

Optical processing for packet routing can overcome bottleneck in large-capacity photonic networks. We have studied on collinear acoustooptic (AO) switches and applications to optical label recognition in label routing networks. We proposed recognition of each layer label encoded in on-off-keying (OOK) format with an AO processor consisting of optical delay waveguides, parallel AO switches, and electric multipliers. In this paper, we propose an AO processor for recognition of layer-structure binary-phase-shift-keying (BPSK) labels for hierarchical routing control.

Statement of Contribution/Methods

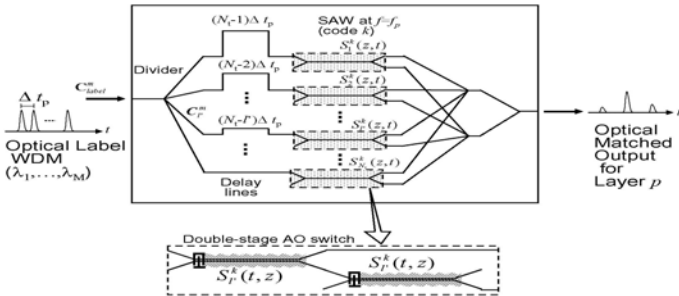
We consider M-layer labels, where each layer label consists of Nt-bit BPSK coded pulses. Each layer label has a different wavelength. The proposed integrated-optic processor consists of parallel AO switches and delay lines as shown in Fig.1. Each AO switch consists of double-stage collinear AO switches to compensate optical frequency shift due to AO interaction. The incident label is divided into Nt pulse trains at first. A layer label to be recognized is represented by SAWs in the AO switches. The AO switched and unswitched outputs are optically combined and the interference output corresponds to the correlated output between the stored label and the optical incident label.

Results

The recognition characteristics are analytically discussed and are confirmed numerically with computer simulation. It is shown that each layer label encoded in orthogonal BPSK codes can be recognized with the proposed circuit. A contrast ratio between auto-correlation and cross-correlation is theoretically found to be 14.0dB for the case of $Nt=7$ and $M=2$. The scalability of the recognizable label is also discussed.

Discussion and Conclusions

Since the optical label for a different layer has a different wavelength, the different label can be recognized by using SAWs at a different frequency. Although the response time of AO devices is slow, the proposed AO processor can handle higher-bit-rate pulses since SAWs are supposed not to change during the recognition process. The label to be recognized can be changed in a few micro seconds. Since the output from the processor is an optical pulse signal, a kind of transparent processing can be realized.



P3-M-04

AOTF characteristics in amplitude and frequency modulation mode

Vitold Pozhar¹, Vladislav Pustovoi¹, Sergey Beryoz¹:¹Scientific Technological Center of Unique Instrumentation of RAS, Moscow, Moscow region, Russian Federation

Background, Motivation and Objective

Control of characteristics of acousto-optical tunable filters (AOTF) via ultrasound wave modulation is one of the most promising tasks aimed at development new functional spectral elements. However, absence of analytical description of the effect of modulation prevents their development. Previously, we calculated in details AOTF characteristics for the case of alternating phase manipulation [1] and reported challenging properties of such AOTFs and demonstrated them experimentally [2], in particular differential capabilities. In this report, we have calculated AOTF characteristics for amplitude and frequency modulation modes.

Statement of Contribution/Methods

We have considered collinear-type diffraction of light on ultrasonic modulated waves and low-efficiency (single-scattering) approximation. In such approach we have deduced expressions described dependence of periodical output signal of photodetector on parameters of ultrasonic modulation signal. In particular, there are presented transmission functions corresponding to all harmonics of modulation frequency.

Results

Analysis demonstrates that just as for phase manipulation case, transmission function at zero frequency (time-averaged signal) is variable and can be significantly broaden in comparison to classical (non-modulated) AOTF. And for broadening purposes frequency modulation is preferable than amplitude one. Besides, in contrast to phase manipulation mode, amplitude modulation does not exhibit differential properties.

Discussion and Conclusions

This first analytical solution of diffraction problem in ultrasound modulation mode ensures calculation of diffraction characteristics at any harmonic of arbitrary modulation function and makes possible analytical

Wednesday
Poster

investigation of effect. There are significant differences in amplitude, frequency, and phase modulation modes. These results provide basis for development AOTFs with real-time controllable characteristics.

1. V.I.Pustovoit, V.E.Pozhar. Controlling Characteristics of the Collinear Acousto-optical Filter by Ultrasound Modulation. *Journal of Communications Technology and Electronics*, 1998, v.43, No.1, p.115-120.

2. V.E.Pozhar, V.I.Pustovoit, S.Bereza. Ultrasound fast modulation mode AOTFs for differential photoluminescence spectroscopy. 2007 IEEE Ultrasonics Symposium (New York, Oct. 28-31, 2007).

P3-M-05

Acoustic modes transformation in crystal of tellurium dioxide and applications for the design of acousto-optic devices

Nataliya Polikarpova¹, Vitaly Voloshinov¹; ¹*Faculty of Physics, M.V. Lomonosov Moscow State University, Moscow, Russian Federation*

Background, Motivation and Objective

Propagation and reflection of plane elastic waves in the tellurium dioxide is examined. The reflection of the waves from a free and flat boundary separating the crystal and the vacuum is studied in case of arbitrary oriented planes.

Statement of Contribution/Methods

The analysis shows that as much as two elastic waves may be reflected from the crystal surface. Energy flow of one of the reflected waves in paratellurite propagates in a quasi-back direction with respect to the incident energy flow so that both energy flows are separated by an angle as narrow as a few degrees. It is found that a relative intensity of the unusually reflected wave in the acousto-optic crystals may be close to a unit in a wide variety of crystal cuts. Possible applications of the examined phenomena in acousto-optic devices are discussed.

Results

It is found that propagation of acoustic waves in the crystalline materials possessing strong anisotropy of their elastic properties may be accompanied by a peculiar quasi-back reflection of acoustic energy from a free surface separating the crystals and the vacuum. The peculiarity of the reflection is in the fact that the unusual reflection follows the inclined incidence of the elastic energy on a crystal facet. Relative intensity of the extraordinary reflected waves in such acousto-optic crystals as paratellurite may be as high as 100%.

Discussion and Conclusions

Unique cases of the acoustic reflection are interesting not only from the point of view of fundamental knowledge but also of applied sciences. For example, new types of acousto-electronic and acousto-optic instruments may be designed on base of the examined effects. Tunable acousto-optic filters with collinear and non-collinear propagation of beams as well as acousto-electronic delay lines with low consumption of expensive crystalline materials are the most evident examples of possible applications.

P3-M-06

Modern problems of AOTF development and implementation

Vladislav Pustovoit¹, Vitold Pozhar¹; ¹*Scientific Technological Center of Unique Instrumentation of RAS, Moscow, Moscow region, Russian Federation*

Background, Motivation and Objective

Forty years have passed since development of the first acousto-optical tunable filter (AOTF). For this period ultrasound-controlled optical filters have evolved from promising optical element to key component of complex spectral systems. And variety of AOTFs amounts to many tens of different modifications and many of them are produced commercially. If so, following question is appropriate and rather interesting: are there any unresolved scientific problems in this field?

Statement of Contribution/Methods

To answer this question we have analyzed world-wide AOTF applications as well as our particular experience of development of AOTFs (since 1972) and AOTF-based systems (starting from 1983 airborne prototype apparatus for Earth remote sensing). And also we have compared modern state of technology to our fifteen-year prognosis [1].

Results

One of the most complex and multi-aspect problem is light diffraction on acoustic waves of complex form and composition (modulated waves, multi-frequency ultrasound, etc.). There was created and demonstrated AOTF with phase manipulation providing a set of specific sign-reversing instrument functions. However, theoretical substantiation of amplitude and frequency modulation of ultrasound for AOTF transmission function shaping is still required. The only method of ultra-short light pulse compression using linear-chirped ultrasonic waves, which we have suggested and grounded [1], was successfully put into practice.

Another actual problem is optimization of acousto-optical cell design for miniaturization, spectral range spreading, increasing spectral resolution, decreasing tuning time and so on. It should be recognized that there is no exact algorithm for developing AOTF having defined characteristics.

Two fundamental problems of AOTFs applications in spectroscopy is waiting their solution. First, correction of instrument function distortions was analyzed and a numerical approach was suggested. Second, determination of optimum measurement procedure is under investigation now [2].

Discussion and Conclusions

This analysis provides a clear representation of current state of AOTF technologies with focusing on physical and technical problems, which have not still solved adequately, while should be.

1. V.I.Pustovoi, V.E.Pozhar. Collinear diffraction of light by sound waves in crystals: devices, application, new ideas". Ultrasonics World Congress (Berlin, 1995, Sept. 3-7). Proc., v.1, p.217-224.
2. V.E.Pozhar, V.I.Pustovoi. "Adaptive Acousto-Optical Spectrometric Systems", Proc. IEEE Ultrasonics Symposium, Vancouver, Oct. 3-6, 2006, p.162-163.

P3-M-07

Refracto-Vibrometry for Visualizing Ultrasound in Small-Sized Channels, Cavities and Solid Objects

Lothar Zipser¹, Hans-Dieter Seelig¹, Heinz Franke^{1,†}*Electrical Engineering, HTW University of Applied Sciences, Dresden, Germany*

Background, Motivation and Objective

The generation and propagation of ultrasound in small-sized channels, cavities and solid objects is complicated. Therefore, it is desirable to visualize these actually invisible phenomena. Visualization can improve both understanding and optimisation of diverse ultrasonic effects and techniques in real miniaturized configurations.

Statement of Contribution/Methods

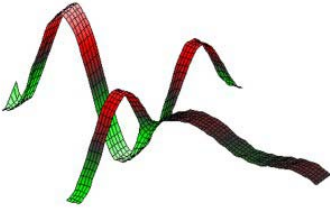
A novel non-contact method for measuring and visualizing the generation and propagation of ultrasound in transparent media was developed and tested by the authors. This method uses as measuring effect the variation of the optical refractive index n of a medium, caused by the passage of ultrasonic waves. This justifies the denomination "refracto-vibrometry". The measuring system required is based on a scanning Laser-Doppler vibrometer. Therewith, ultrasonic fields in gases, fluids and even in pellucid solid objects can be measured and subsequently visualized as animated videos. The paper describes preliminarily the theoretical fundamentals and the technical equipment for the new method.

Results

Instructive examples are presented for generation, propagation, reflexion, absorption and interference of ultrasonic waves in small volumes of air and water as well as in cm-sized perspex objects. Moreover, the fine structures of ultrasonic fields in small cavities and channels at different operating conditions are shown. The animated presentation of the measuring results as videos is very impressive and instructive. For instance, the figure shows a measured and 3D-visualized ultrasonic wave in a narrow channel with perpendicularly arranged branch lines. By means of destructive interference between the incoming wave and a standing wave in the branch lines the outgoing wave is nearly eliminated.

Discussion and Conclusions

Capabilities and limits of the refracto-vibrometry are discussed in detail. The novel method has a large potential in the fields of education and acoustics design. It turned out to be a useful completion of simulation and calculation. Refracto-vibrometry makes ultrasonics clearer and more feasible for application.



P3-N. Novel Ultrasonic Motors II

Sala Orange

Wednesday, September 23, 2009, 10:00 am - 11:30 am

Chair: **Eun Sok Kim**
University of Southern California

P3-N-01

A Study on the Crab Type Ultrasonic Motor

Jwo Ming Jou¹ *Mechanical Engineering, Cheng Shiu University, Kaohsiung County, Taiwan, Taiwan*

Background, Motivation and Objective

The main motivation and objective of this study is to hope to offer a kind of crab type ultrasonic motor (shown as Fig. 1~2) that it can apply to the precise movement platform or optic-electro-mechanical system. It has advantages of driving easy, simple structure, assembling conveniently and high movement velocity.

Statement of Contribution/Methods

The crab type ultrasonic motor in this study, it is made up by a crab type base and two piezoelectric actuating components; Its characteristic lies in: This piezoelectric actuating component is installed at the edge of oblique side of left and right sides of crab type base separately; While operating, so long as exert driving voltage and resonance frequency on the piezoelectric actuating component can let the crab type ultrasonic motor movement fast.

Results

According to the experimental results, the maximum movement velocity of the crab type ultrasonic motor is 385mm/sec and 274mm/sec under conditions of 160Vp-p driving voltage, 33kHz resonance frequency and 26.5gw net weight. And the maximum climbing velocity of the crab type ultrasonic motor is 71mm/sec under conditions of 200Vp-p driving voltage, 33kHz resonance frequency, 26.5gw net weight and the slope of 7.5 degrees.

Discussion and Conclusions

- (1) The movement velocity of the crab type USM is in direct proportion to driving voltage basically, but too big driving voltage causes displacement to interfere and reduce movement velocity instead.
- (2) The climbing velocity of the crab type USM is in inverse proportion to slope.
- (3) The main factor of influencing movement velocity of the crab type USM is the resonance frequency, but not the installing the slope angles of the position or the inclined plane of the piezoelectric actuating component. So long as find the best resonance frequency, then can get the maximum movement velocity.

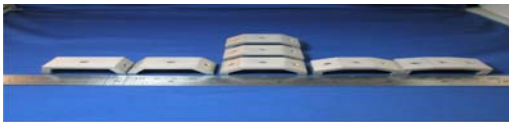


Fig.1 The bases of different size of the crab type USM.

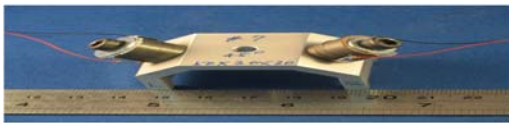


Fig.2 The prototype of the crab type USM.

A Study on the New Type Ultrasonic Motor

Jwo Ming Jou¹; ¹Mechanical Engineering, Cheng Shiu University, Kaohsiung County, Taiwan, Taiwan

Background, Motivation and Objective

The main motivation and objective of this study is to hope to offer a kind of new type ultrasonic motor. It has advantages of driving easy, simple structure, high loading ability and assembling conveniently. And it can apply to the precise fixed position platform or electromechanical system.

Statement of Contribution/Methods

The new type ultrasonic motor in this study, it includes piezoelectric actuating component, base, screw, spacer and nut. Its method or characteristic lies in: The piezoelectric actuating components put the inside within the base separately, and then lock in fixing holes of the base through screw, spacer and nut. While operating, only offer proper driving voltage, resonance frequency and loading on the piezoelectric actuating components that can let the ultrasonic motor movement fast on the platform. And so long as adjust the fixed position of piezoelectric actuating components and driving phase angle again that can reach the efficiency of change movement velocity and loading ability.

Results

According to the experimental results, the maximum movement velocity of the new type ultrasonic motor is 240mm/sec under conditions of 100Vp-p driving voltage, 548mA driving current, 108kHz resonance frequency, 90 degree of driving phase angle and 161gw net weight. And the maximum loading of the new type ultrasonic motor is 3.0kgw under conditions of 100Vp-p driving voltage, 548mA driving current, 108kHz resonance frequency, 90 degree of driving phase angle and 12.9mm/sec movement velocity.

Discussion and Conclusions

1. The piezoelectric actuating component install position to be lower, the movement velocity of the USM is faster.
2. Influenced by vibration modal, movement velocity right of USM is faster than movement velocity left.
3. The piezoelectric actuating component movement velocity by way of the installing of the same direction as fast as different way of installing of direction.
4. The loading ability of the new type USM is 18.6 times of the net weight.

Design and performances of shaftless ultrasonic motor for high torque generation

Jin-Heon Oh¹, Eui-Hwan Jeong¹, Kee-Joe Lim¹, Seong-Hwa Kang², Dae-Hee Park³; ¹Chungbuk National University, Cheongju, Chungbuk, Korea, Republic of, ²Chungcheong University, Cheongwon, Chungbuk, Korea, Republic of, ³Wonkwang University, Iksan, Jeonbuk, Korea, Republic of

Background, Motivation and Objective

Ultrasonic motors have been researched as one of the important actuators which used for robotic and planetary applications. In this application field of actuator, accurate and sensitive operation, small volume, certain level of mechanical output characteristics are required. Therefore, the ultrasonic motors are considered as appropriate actuators on the above mentioned sphere. However, these applications are limited at present because the currently available ultrasonic motors do not provide adequate high torque and power. And, ultrasonic motors need pressure mechanism between stator and rotor because of using the turning force created by the friction between them. To pressurize in these type motors, additional components and particular structure is required. So, these features act as limited elements in the realization of volume reduction, lightweight, simplification etc.

Statement of Contribution/Methods

In this paper, we propose a novel type shaft-less ring type ultrasonic motor. A traveling wave rotary type ultrasonic motor is selected as a base model. The newly designed stator has two piezoelectric ceramic rings which are bonded in sandwich shape as traveling wave generator. So we can expect to produce higher torque. The rotor structure is designed to produce the pressure by the stator vibration. Therefore, the proposed model has the rotor structure that coupled with the stator provokes the pressure, so this model do not install the separate plate any spring device.

Results

We used the finite element method to verify the operation principle and to compute the vibration mode. And, to demonstrate the simulation results, the prototype motor was fabricated and evaluated.

Discussion and Conclusions

This paper deals with the design, fabrication and evaluation of high torque traveling wave rotary type ultrasonic motor which has hollow structure. In conventional type of shaft-less motor, disk spring, similar accessories, or other structures are needed to keep the pressure mechanism between stator and rotor. Therefore, we propose a novel type ultrasonic motor with a new configuration which can realize simple structure and high torque simultaneously. The unique feature of this proposed motor will be suitable for the application of operating robot articulations.

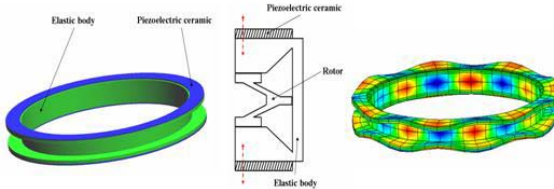


Fig. Shape of the proposed new type ultrasonic motor

P3-N-04

Design of Functionally Graded Piezoelectric Ultrasonic Motors using Topology Optimization

Wilfredo Montealegre Rubio¹, Emi-Io C. N. Silva¹, Glauco H. Paulino^{2,1} *Department of Mechatronics and Mechanical Systems Engineering, University of Sao Paulo, Sao Paulo, SP, Brazil, ²Newmark Laboratory, Department of Civil and Environment Engineering, University of Illinois at Urbana-Champaign, Urbana, IL, USA*

Background, Motivation and Objective

In this work, piezoelectric ultrasonic motors are designed based on the Functionally Graded Material (FGM) concept by using topology optimization. Essentially, ultrasonic piezomotors convert electrical energy into mechanical energy to obtain oscillation at specified resonance frequencies in the ultrasonic range, through the inverse piezo-effect. On the other hand, FGMs are composite advanced materials, which are made by changing gradually the properties with position inside material domain. The FGM concept applied to piezoelectric structures allows designing broadband piezoelectric transducers, reducing reflection waves inside them, and modifying their dynamic characteristics.

Statement of Contribution/Methods

In this work, Functionally Graded Piezoelectric Ultrasonic Motors (FGPUMs) are designed, aiming to find the optimal topology and gradation of the material properties along a specific direction to target desired eigenmode shapes. The design of FGPUMs is not an easy task to be accomplished by using trial and error methods. Thus, it suggests the use of optimization techniques to find the optimal topology and gradation of material properties. Hence, the Topology Optimization Method (TOM) is applied to reach this goal, which combines optimization algorithms with Finite Element Method (FEM) for determining solutions of complex multi-physics problems. FGPUMs are designed as traveling-wave motors, where the superposition of multiple standing waves creates a traveling wave. The traveling waves are generated by the combination of different vibration modes (different eigenmodes). The eigenmode control is achieved by maximizing and minimizing the structural displacement at certain user-defined points, while remaining portion of the domain is left without any kind of specification. The Modal Assurance Criterion is applied as mode shape-tracking method. To treat the material gradation, the Graded Finite Element is implemented, which incorporates the material property gradient at the size scale of the finite element. The optimization algorithm is implemented based on Sequential Linear Programming, and the Continuum Approximation of Material Distribution (CAMD), in which design variables inside each finite element are interpolated by using finite element shape functions.

Wednesday
Poster

Results

To show the improvement and the advantage of using FGM and TOM for designing FGPUMs, graded ultrasonic piezomotors, with material gradation along thickness direction, are considered. Results demonstrate that FGM and TOM concepts can be successfully applied as systematic tool to design piezoelectric ultrasonic motors.

Discussion and Conclusions

The work show the viability of using the TOM to design FGPUMs; specifically, the TOM can be applied to find both optimal topology and gradation function of FGPUMs, aiming to tailor user-defined eigenmodes and user-defined traveling wave patterns.

P3-N-05

Design and evaluation of low-profile micro ultrasonic motors driven by sector shaped piezoelectric vibrators

Takefumi Kanda¹, Takashi ICHIHARA¹, Koichi SUZUMORI^{1,†} *Okayama University, Japan*

Background, Motivation and Objective

In this paper, a design and evaluation of low-profile type micro ultrasonic motors which were driven by sector shaped piezoelectric vibrators has been presented. The aim of this research is to realize a thin and light micro actuator for micro mechatronics applications. For example, this type motor will be used for the driving of micro robotics and active devices on handheld digital terminals. Such type motor will be also available for the driving of micro devices, for example, micro pumps, valves and mixers embedded in micro fluidic systems which have card type shapes. We reported some types of micro ultrasonic motors for micro devices. The purpose of this paper is to improve the pre-load mechanism of low-profile micro ultrasonic motors.

Statement of Contribution/Methods

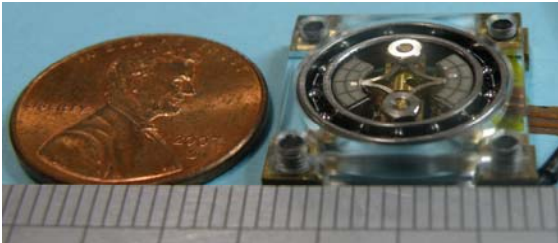
This motor has two sector-shaped vibrators and the pre-load mechanism. The driving principle of our actuator is based on an ultrasonic motor driven by a bar-type or rectangular plate type vibrator. The pre-load mechanism has horizontal structure and both vibrators and the pre-load mechanism were set in a wheel type rotor. The outer diameter and thickness of the unit were 10 mm and 0.6 mm. The weight of the vibrator unit was only 150 mg. By the FEM simulation, two different modes have been oscillated in vibrators. The structure of the horizontal pre-load mechanism was also optimized by using a finite element method simulation.

Results

Some basic performances are evaluated about the fabricated motors. The relationship between the output torque, rotation speed, preload and applied voltage were measured by using a laser surface velocimeter. When the driving voltage and the frequency were 20 Vp-p and 340 kHz, the maximum rotating speed and the maximum starting torque were 2350 rpm and 0.1 mNm, respectively. Additionally, wear resistant vibrators have been also fabricated. The contact points consisted of alumina ceramics at instead of stainless steel. Based on the analytical result by a finite element method, the motor which had realized high durability has been developed.

Discussion and Conclusions

In this research, the pre-load mechanism of the low-profile type motor was redesigned. The pre-load systems that used a new pre-load mechanism design were fabricated and evaluated. As a result, we have succeeded in fabricating the new low-profile micro ultrasonic motor and realizing improved driving performance.



Visualization of Flexural Wave Propagation in Helical Coiled Ultrasonic Waveguide

Ryo Tanaka¹, Masayuki Tanabe¹, Kan Okubo¹, Norio Tagawa^{1,2} *Department of Information and Communications, Tokyo Metropolitan University, Hino, Tokyo, Japan*

Background, Motivation and Objective

We have developed a miniature ultrasonic motor using a helical coiled waveguide as a stator [1]. In this motor, the elliptical motion of the surface particle due to the flexural ultrasonic waves rotates the rotor, which can be placed adjacently inside or outside the stator, via the frictional force. For high frequencies, rotational directions of both rotors are consistent with those of usual traveling wave-type ultrasonic motors. However, for low frequencies, the outer rotor rotates inversely. In [2] and [3], we examined the rotation direction and phase of the surface particle motion of a coiled waveguide for low frequencies, and we clarified that both rotation characteristics at both surfaces are the same. In this study, we examine a mechanism by which such a phenomenon is caused.

Statement of Contribution/Methods

We acquire the particle motions at both of inner and outer surface as a time-series signal densely at intervals of 2 degrees through FEM simulations using the PZFlex. Using the acquired time-series signals, we visualize vibration forms of the helical coiled waveguide due to propagation of flexural waves as an animation of a cross section image of a coil.

Results

The examples of the generated animations are shown in the figures. From the figures in the upper row representing a vibration form for high frequencies, we surely confirm that flexural wave patterns exist spatially in each one turn of the coiled waveguide. On the other hand, in the lower figures for low frequencies, we cannot see the flexural wave patterns, and a global eccentric motion can be seen in a cross section of the coil.

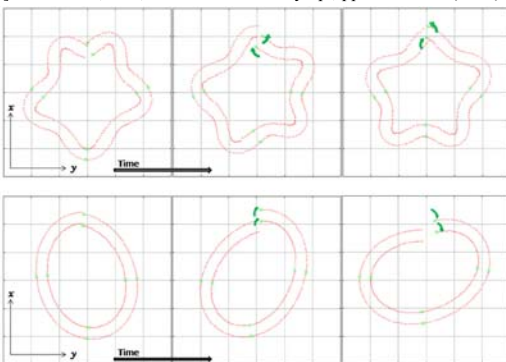
Discussion and Conclusions

For high frequencies, the wavelength of the flexural wave is shorter than the circumference of one turn of the coil, and hence there are some waves spatially in a one turn. This means that a convex shape of the coil's one turn is transformed into a concave shape during wave propagation. For low frequencies, the deformed shape of the coil keeps convex unlike that for high frequencies. Because of this, both rotations should be the same. This assertion is introduced intuitively, and in future, we are going to derive the quantitative condition with respect to the rotation direction theoretically.

[1] T.Moriya, et al., IEEE Ultrasonics Symp., pp.1546-1549 (2005)

[2] S.Xie, et al., IEEE Ultrasonics Symp., pp.2284-2286 (2007)

[3] K. Tomoda, et al, IEEE Ultrasonics Symp., pp.1461-1464 (2008)



P3-N-07

Theoretical And Experimental Investigations Of The Contact Mechanics in Standing Wave Type Piezoelectric Ultrasonic Motors

Jens Twiefel¹, Wiebold Wurpts¹, Jörg Wallaschek¹; ¹*Institute for Dynamic and Vibration Research, Leibniz Universität Hannover, Hannover, Germany*

Background, Motivation and Objective

Ultrasonic motors are a subject of intense research since many decades, as they offer several advantages compared to electromagnetic motors. Especially motors of the traveling wave type have been investigated in detail and their contact mechanics is well understood. The contact mechanics in ultrasonic motors of the standing wave type motor, however, is still an open research topic. The lack of a model based description of the contact behavior limits the quality of overall motor modeling and optimization.

Statement of Contribution/Methods

The present paper aims at filling the research gap on contact mechanics of standing wave type piezoelectric ultrasonic motors. We have experimentally investigated the trajectories of the contact tips by means of laservibrometer measurements for a wide parameter range. In particular preload, driving phase and driving frequency have been varied during the investigations. A shaking beam type standing wave motor was used on a rotational test bench. The experimental data is discussed and used for the validation of modeling assumptions.

Results

It became evident from the measured data that the trajectories of contact points are not purely elliptic. It was shown that in particular the velocity of the contact point has non-negligible higher harmonic components.

Since the experimental investigations mainly aim at validating modeling assumptions, the underlying model structure for the contact mechanics of standing wave type piezoelectric ultrasonic motors was studied in detail. A point contact model, which is capable to model the higher order harmonics of the trajectories was developed. It already allows to study the influence of the most important parameters. In combination with a model of the structural dynamics of the motor and a harmonic balance algorithm it allows a detailed description of the contact mechanics and overall motor performance.

Discussion and Conclusions

The presented measurements show clearly the presence of significant higher harmonic components in the trajectory of the investigated standing wave type ultrasonic motor. The presented numerical model includes those higher harmonics and allows the calculations of the motors characteristic for the steady state. The experimental and modeling results show that the common treatment of the tip's trajectory as pure elliptic movement not always leads to satisfying results.

P3-N-08

Miniature flat type inertial piezoelectric motor

Piotr Vasiljev¹, Dalius Mazeika²; ¹*Vilnius Pedagogical University, Vilnius, Lithuania*, ²*Vilnius Gediminas Technical University, Vilnius, Lithuania*

Background, Motivation and Objective

Piezoelectric motors are widely used for different devices such as micromanipulation and positioning systems, scanning microscopes, robotic systems and etc. Usually requirement to dimensions of the motor are defined by technical specification.

Statement of Contribution/Methods

A novel design of miniature linear piezoelectric motor is proposed and analyzed. Size of the motor not exceeds 150 mm³. Piezoelectric actuator consists of butterfly type oscillator and two piezoceramic elements that are glued to the oscillator (Fig. 1). Elliptical trajectory of the actuator is achieved on the connecting link of the two plates when the flexural oscillations of the plates with the phase difference by $\Pi/2$ are used. Harmonic or saw tooth type electric signal can be used for excitation. In this paper we present the study of inertial piezoelectric motor where saw tooth type electric signal is applied for actuator excitation. Advantages of this type of excitation are simpler electric circuit scheme, lesser dependence between the rotor torque and excitation frequency. These advantages allow to increase torque of the rotor without increasing dimensions of the actuator.

Wednesday
Poster

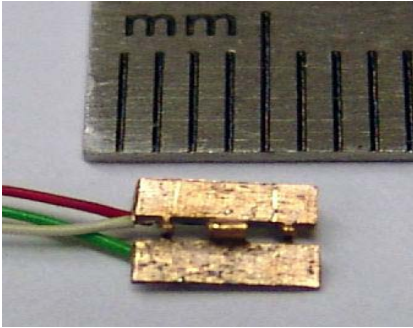
Results

Numerical investigation of the piezoelectric actuator using finite elements method was done to analyze natural frequencies, modal shapes and actuator response to the different excitation regimes.

The transient dynamic analysis of the motor was performed to simulate motion of the rotor and to calculate torque and speed of the rotor. Experimental prototype of the piezoelectric actuator was built and measurements of the output charecteristics were done.

Discussion and Conclusions

Results of numerical and experimental studies are in good cooperation. Investigated piezoelectric motor can be successfully used for different applications.



P3-O. Air-Coupled Ultrasonics

Sala Orange

Wednesday, September 23, 2009, 10:00 am - 11:30 am

Chair: **Vincent Laude**
CNRS

P3-O-01

Ultrasonic Air-coupled Wave Phase Conjugator for the Low Megahertz Frequency Range

Yuri Pylnov¹, Pavel Shirkovsky¹, Philippe Pernod², Vladimir Preobrazhensky³; ¹Moscow State Institute of Radio Engineering, Electronics and Automation, Russian Federation, ²Institute of Electronics, Microelectronics and Nanotechnology, France, ³Wave Research Center, General Physics Institute, RAS, Russian Federation

Background, Motivation and Objective

Parametric phase conjugation of ultrasound has in the present time many applications in NDT, medicine and velocimetry of liquid flows [1]. The properties of phase conjugate ultrasonic waves such as compensation of phase distortion of medium of propagation, autofocusing on ultrasound scatters and phase sensitivity to moving media permit to design new techniques with better characteristics. Great gain (~80dB) of ultrasonic wave in wave phase conjugator (WPC) made from magnitistrictive ferrite was conducive to study nonlinear effects in liquid at frequency 10MHz. On the other hand at last decade the ultrasonic diagnostics through air without contact liquid are developing [2]. Study of the possibility of WPC-technology to testing object in gas medium is the objective of the present work.

Statement of Contribution/Methods

The main problem to create aerial ultrasonic wave phase conjugator are enormous losses of intensity of ultrasonic wave when it crossing interface of solid-state active element and air (-86dB), and also huge attenuation of ultrasound in air ($\alpha = 16\text{dB/mm}$ for frequency 10MHz). To decrease these losses operating frequency of WPC was reduced to 7.5 MHz, in addition interface layers were used to matching acoustic impedances of WPC to air. Phase modulation of ultrasonic phase conjugate wave by pseudo noise M-sequence was also used to register super weak signals.

Results

The results of carried out research have shown that the best materials to prepare matching layers are porous membrane generally used for medical application. Quarter wave plate made of these materials glued on interface of WPC to increase the amplitude of phase conjugated wave. The gain of utilization of matching layer was about 20dB that permits to measure attenuation in air at frequency 7.5MHz ($\alpha = 9.4\text{dB/mm}$). The velocity distribution in the air jet was obtained by using WPC-technique with very high sensitivity of phase conjugated wave to velocity of air micro flow (~1rad/m/s).

Discussion and Conclusions

For the first time the propagation in the air of ultrasound parametrically phase conjugated by magnetostrictive ferrite in low megahertz frequency range was observed. Aerial velocity as well as ultrasound attenuation in air was measured at frequency 7.5MHz by air-coupled WPC. Application of wave phase conjugation in NDT and velocimetry of air micro flows is discussed.

The work was supported by the program of RAS "Acoustics of natural media".

[1] Pylnov Yu.V., Preobrazhensky V.L., Pernod Ph. and Smagin N.V. Flow Velocity Measurements by Means of Nonlinear Interaction of Phase Conjugate Ultrasonic Waves // Proc. IEEE Int. UFFC Conf., Rotterdam. – 2005. – p. 1612-1615.

[2] T.E. Gomes, "Acoustic Impedance Matching of Piezoelectric Transducers to Air", IEEE Trans. on UFFC, vol.51, no.5, pp. 624-633, 2004

Hartmann Ultrasound Generator Combined with Electrical Discharge

Rudolf Bálek¹, Stanislav Pekárek¹; ¹Department of Physics, Czech Technical University in Prague, Faculty of Electrical Engineering, Prague 6, Czech Republic

Background, Motivation and Objective

Environmental applications such as volatile organic compounds decomposition, destruction of nitrogen oxides or ozone generation utilize different chemical reactions. The efficiency of these reactions depends among others on the temperature, on the residence time (mixing of reactant medium) and also on the pressure in reaction volume. The increase of pressure in this volume can be achieved by application of ultrasound. At the same time many reactions can be enhanced by ionization of the reactant medium, which is most frequently performed by electrical discharges. The synergy of ultrasound with electrical discharges therefore opens new unique perspectives for many applications. The simple and reliable way which reflects these requirements is offered by the combination of Hartmann or Galton type power ultrasound generators with non-thermal electrical discharges.

Statement of Contribution/Methods

Hartmann gas-jet ultrasound generator in combination with the electrical discharge was investigated with the aim to clarify the effect of oscillating pressure gradients accompanied by ultrasound generation on performance of the electrical discharge between two electrodes (nozzle-resonator) in case of reduced gas flow rate through the nozzle.

Results

Efficient generation of ultrasound requires high gas pressure in the generator nozzle which results in high gas flow rate through the nozzle resonator gap. This high flow rate on the other hand causes low residence time, which decreases efficiency of chemical reactions. We therefore decided to modify the classical Hartmann generator in such a way that it efficiently generates ultrasound even when the gas flow rate is reduced.

We designed several modifications of the Hartmann - Galton generator combined with the electrical discharge with reduced gas flow rate. Our original idea involves a rod situated along the nozzle-resonator axis. New nozzle construction also enables to control electric field in nozzle-resonator gap.

Using the schlieren visualization of gas-jet and ultrasonic field we are able to detect the shape and structure of the discharge and to determine relation between the acoustic field and electrical discharge behavior.

Discussion and Conclusions

We describe a new setup of the Hartmann gas-jet ultrasonic generator combined with electrical discharge in the nozzle-resonator gap. It is proved that even for the reduced gas flow rate through the nozzle; the generator emits ultrasound, which effectively influences properties of the discharge. Apart of the fact that the discharge is stabilized and becomes more uniform, it increases its volume and decreases its impedance when the generator works in the regime of ultrasonic emission. At the same time the discharge light emission from the gap is more over uniform. In the regime without the ultrasonic emission the discharge light emission is fragmented.

Nonlinear acoustical waves in the air-filled resonator

Petr Konicek¹; ¹Department of Physics, CTU-FEE Prague, Prague, Czech Republic, Czech Republic

Background, Motivation and Objective

The main objective of this paper is the description of the properties of the nonlinear standing waves generated by a vibrating boundary in the acoustical resonator. The nonlinear oscillations of gas in the hard-walled resonator having one closed end and the other periodically oscillating are analysed in this work.

Statement of Contribution/Methods

The resonator is driven by a piston whose motions are characterized by superposed sinusoidal motions. All phenomena leading to a progressive distortion of the wave are supposed to be weak. The analytic approach to finite-amplitude standing waves in a resonator of a constant diameter is used, based on the inhomogeneous Burgers equation with a discrepancy.

Results

The nonlinear sound field in the cavity of the resonator can be approximately described as the sum of two Riemann or Burgers travelling waves. Each of these waves can be distorted significantly by nonlinear self-action, resulting

into the formation of a sawtooth-shaped profile from the initial harmonic one with no contribution from the cross-interaction of the two counterpropagating waves. Each wave is distorted by itself during the propagation, but there is no energy exchange between them. Each of two cross-secting waves generates its higher harmonics, but the cross-interaction process can be neglected if the waves are periodic in time.

When we want to describe a finite-amplitude sound field inside a circular resonator, we can use the inhomogeneous Burgers equation. In this paper we present the novel method of approximate solution of this equation in the stationary state.

Discussion and Conclusions

Described method is based on the matching principle technique. The procedure of calculation of inner and outer solution is presented. The outer solution V^0 represents the exact solution for the ideal fluid. This solution is valid in the whole interval of periodicity except the shock region. Over against, the inner solution V^1 describes correctly the sound field in the shock region only. The inner solution describes the behaviour of the real fluid, in which the thermoviscous attenuation take place.

P3-O-04

Parametric excitation of nonlinear standing waves in acoustic resonators

Michal Bednarik¹, Milan Cervenka², Petr Konicek²; ¹Physics, Czech Technical University in Prague - Faculty of Electrical Engineering, Prague, Czech Republic, Czech Republic, ²Czech Technical University in Prague - Faculty of Electrical Engineering, Czech Republic

Background, Motivation and Objective

The paper deals with parametric excitation of nonlinear standing waves. There are a number of methods which enable to generate intensive acoustic fields confined to resonators. The acoustic system, which is composed of an acoustic resonator and source, is often bulky and expensive. For this reason we designed a method which is inexpensive and at the same time enables miniaturization of the discussed acoustic system. This method is based on the use of a parametric acoustic piston source which radiates an amplitude modulated ultrasonic waves. The carrier ultrasonic wave is the finite amplitude one, and hence the nonlinearity of the fluid enables to self-demodulate the amplitude modulated ultrasonic waves. When a frequency of the demodulated wave is equal to some lower eigenfrequency of the resonator it is possible to excite nonlinear standing waves with its help.

Statement of Contribution/Methods

To study possibilities of the parametric excitations of nonlinear standing waves it is necessary to model an acoustic field inside the resonator. The inhomogeneous modified Burgers equation represents a suitable mathematical model. By means of this model equation it is possible to investigate how the depth of modulation and phase shift between the carrier and modulation wave influence the resulting acoustic field inside the resonator. This model equation also takes into account detuning of the parametric source. The detuning enables to suppress evolution of high-frequency components of the acoustic field.

Results

It follows from the spectrum analysis of the acoustic field inside the resonator that namely the phase shift between the carrier and modulation wave can affect the spectrum of nonlinear standing waves significantly. An approximate solution of the mentioned model equation was found for steady-state regime. The approximate solutions were gained on the basis of the multiple scales method. The validation of the approximate solutions was proved by comparison with numerical results. Because the numerical solutions are relatively time-consuming the approximate solutions appears as a suitable way how to investigate various modifications of the parametric excitation. The influence of the source detuning was also analyzed. It appears the suitable detuning can suppress the energy flow towards higher frequency components.

Discussion and Conclusions

On the basis of theoretical investigation it was found that the presented method is applicable for generation of intensive acoustic fields inside the resonators. The approximate solutions were found for the used model equation. From the realized analysis it follows that parametric excitation of nonlinear standing waves inside the acoustic resonators represents a perspective method. The theoretically studied the parametric excitation can be realized by means of an inexpensive piezoelectric transducer. This method appears as the very promising one in the case of its use for resonators with a variable cross-section.

UltraSonic Thruster (UST)

Alfred Tan¹, Franz Hover¹, ¹Mechanical Engineering, Massachusetts Institute of Technology, Cambridge, MA, USA

Background, Motivation and Objective

The UltraSonic Thruster (UST) uses the concept of highly directive, finite-amplitude ultrasonic wave to produce bulk fluid movement. Acoustic absorption reduces the momentum flux across an arbitrary control volume resulting in a net force along the axis and hence an overall streaming. We can exploit this novelty in the underwater as a source of thrust force to maneuver underwater vehicles. In this paper, the mechanism of UST is investigated based on the correlation between the net force and thrust exerted on the transducer when ultrasound is emitted into water.

Statement of Contribution/Methods

In this study, two separate water tanks are used to measure thrust and streaming visualization. For thrust, a torque meter is fitted with an L-shaft where a UST is located 50cm perpendicularly away from the torque meter axis. For the 2-D Particle Image Velocimetry (PIV) tank, a 532 nm Nd:YAG laser spreads out a sheet of laser illuminating the seeding particles. A CCD camera samples timed paired images for a 10cmx10cm plan view. DaVis software is used to post-process the streaming data. The UST consists of a Ø7.5mm PZT transducer attached to a waterproof housing and the other surface facing an air-gap backing. A function generator and power amplifier (ENI3100L) drive the UST, connected up by 50Ω coaxial cables.

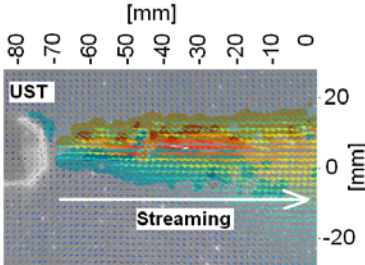
Results

Torque measurements are converted into thrust (force). Thrust generally varies quadratically with voltage (E.M. Allison et al, 2008). A maximum of 10mN thrust is obtained from driving the UST at 40Vpp at 7.1MHz with high repeatability. Particularly, it is observed that dominant thrust peaks at around 3 and 7MHz. The reason for this is still under investigation but could likely be due to the electrical resonance of the capacitive transducer load.

For the PIV results we used a lower voltage function generator(HP8114A). Flow velocity increases linearly in the nearfield. For 3.6MHz at 20Vpp, it reaches 2.1cm/s at around 60cm away from the transducer face. Increasing the voltage expectedly increases the nearfield velocity. The highest velocity is recorded at various frequencies and very similar peak patterns are observed as in thrust-frequency plot.

Discussion and Conclusions

Preliminary results show that, for a fixed transducer diameter and electrical power supply, certain frequencies give peak thrusts. It merits the idea that tuning the frequency could improve thrust efficiency.



P3-P. Acoustic Materials and Structures

Sala Orange

Wednesday, September 23, 2009, 10:00 am - 11:30 am

Chair: **Robert Weigel**
Friedrich-Alexander University

P3-P-01

Hybrid substrate for temperature compensated SAW filter

Yuji HORI¹, Hiroki KOBAYASHI¹, Kazutoshi TOHYAMA¹, Yasunori IWASAKI¹, Kenji SUZUKI¹; ¹NGK Insulators, LTD., Japan

Background, Motivation and Objective

The demand for temperature compensated SAW (TC-SAW) filter is becoming strong recently to compete with FBAR filter. Realization of good temperature property is the clue to achieve SAW duplexer in PCS application in particular. In the past years, several methods to improve SAW temperature characteristics have been proposed. The deposition of silicon dioxide film on piezoelectric substrate is a promising technology for that purpose. Another possible approach is to bond a piezoelectric substrate to a relatively low thermal expansion substrate.

Statement of Contribution/Methods

In this paper, we demonstrate a hybrid substrate which consists of a thin LiTaO₃ layer and a supporting substrate whose temperature expansion coefficient (TEC) is below about 5 ppm/°C. Polymer adhesive is used to bond two different substrates at room temperature. This bonding method has no restriction in regard of substrate materials. The thickness of LiTaO₃ layer is controlled by mechanochemical polishing.

Results

A 42Y-X LiTaO₃ wafer of 100 mm diameter was combined with Si(100) substrate by way of adhesive bonding. The thicknesses of LiTaO₃ and Si(100) wafers were 0.25 and 0.35 mm, respectively. The LiTaO₃ wafer of the hybrid substrate was roughly thinned by mechanical grinding at first, and then mechanochemically polished up to 30 μm within ±2 μm precision. The substrate was kept at 250°C in nitrogen ambient for half an hour for curing polymer adhesive. Even though the substrate was considerably warped due to the difference of TECs at such a high temperature, neither deformation nor delamination was observed at all. We fabricated a simple 1-port SAW resonator to verify the improvement of thermal coefficient of frequency (TCF). The resonant frequency was measured by vector network analyzer at temperature ranging from -30 to 85°C. The measured TCF was around -16 ppm/°C in this case, which indicates a large improvement compared with -40 ppm/°C of the bulk LiTaO₃ wafer.

Discussion and Conclusions

We proposed the hybrid substrate which is appropriate for TC-SAW filter. A large improvement of TCF was observed as expected. Further refinement, probably up to -10 ppm/°C, could be possible by combination of materials and thicknesses of bonding wafers. The high heat-proof of the hybrid substrate was demonstrated as well.

P3-P-02

Transformation of Surface Acoustic Waves into Boundary Waves in Piezoelectric/Metal/Dielectric structures

Natalya Naumenko¹; ¹Moscow Steel and Alloys Institute, Russian Federation

Background, Motivation and Objective

Application of boundary waves (BW) propagating along the boundary between piezoelectric substrate and dielectric overlay helps to avoid problems of packaging and to decrease sensitivity of device characteristics to the quality of crystal surface. In SAW devices utilizing boundary waves, the thickness of dielectric overlay usually does not exceed one-two wavelengths. Analysis of the boundary wave structure and, in particular, clarifying the

mechanism of transformation of SAW into BW, with increasing thickness of dielectric overlay, can help to estimate proper thickness of dielectric film and accurately simulate boundary wave devices.

Statement of Contribution/Methods

A universal technique based on matrix formalism was developed for analysis of SAW and BW in the Piezoelectric/Metal/Dielectric structures, with uniform metal film sandwiched between piezoelectric substrate and multi-layered dielectric half-space. This technique can be used for analysis of common SAW or LSAW in a piezoelectric substrate, in the substrate with metal film and in the same structure with dielectric film deposited over metal. The thickness of dielectric film can vary between zero (SAW) and infinite value (BW). Finite dielectric film is simulated as multi-layered dielectric, in which dielectric film of fixed thickness is covered by air half-space. This method was used for analysis of displacements as functions of depth, for different types of waves propagating in some Piezoelectric/Metal/Dielectric structures having application in SAW devices.

Results

As an example, 128°YX LN was investigated, with copper and isotropic glass films, and metal thickness sufficient to provide existence of two types of boundary waves. For each mode propagating in this structure, gradual transformation of the wave polarization and distribution of its energy along the vertical axis were analyzed, as functions of dielectric film thickness. It was found that two surface modes propagating in 128° YX LN with Cu film have mixed type of polarization for SC electrical boundary condition and SH-type or sagittal polarization for OC condition. For each surface wave, the energy is trapped near the surface. With increasing dielectric film thickness, the waves show different behavior. Part of the wave energy shifts from the surface into the metal film or stays close to the top surface of dielectric film. As a result, SAW transforms into BW or not. The same analysis was made for higher-order modes, which appear at certain nonzero film thickness and can be also transformed into BW.

Discussion and Conclusions

The found dependences of wave polarizations and distribution of the wave energy along vertical axis on the thickness of dielectric overlay, in Piezoelectric/Metal/Dielectric structures, reveal mechanisms of wave transformation from SAW to BW. The same mechanisms work when uniform metal film is replaced by periodic metal grating.

P3-P-03

Analysis of Acoustic Mode Propagation in Layered Structures Using Compound Matrix Method

V.I. Fedosov¹, Yu.V. Gulyaev¹, I.I. Chusov¹, M. Benetti², D. Cannata², F. Di Pietrantonio², E. Verona²; ¹*Institute of Radioengineering and Electronics "V.A. Kotel'nikov" RAS, Moscow, Russian Federation*, ²*Istituto di Acustica "O.M. Corbino" CNR, Rome, Italy*

Background, Motivation and Objective

One way out of many others to improve features of electro-acoustic devices is to study the characteristics of acoustic modes in layered structures. Calculations of the acoustic mode properties for different materials, cuts and orientations are essential in investigations of surface acoustic wave (SAW) and Pseudo-SAW (leaky) modes. It is of large interest to calculate these properties for layered structures with thick films not only from practical point of view, but from theoretical one as well.

Statement of Contribution/Methods

As shown in [1], the use of compound matrices in the matrix formalism make possible to calculate acoustic mode velocities (SAW and PSAW) in layered structures in case of thick film layers (5 wavelengths and more). We describe a procedure of using compound matrices in calculations of acoustic mode parameters for SAW and PSAW. Moreover, we use compound matrix method to calculate dispersion curves of SAW and PSAW mode velocities on the thickness of AIN thick film in the layered structure: AIN/single-crystal diamond substrate for which experimental and theoretical results were reported in recent work [2].

Results

On examples of calculations of acoustic mode parameters, we point out that one of reasons of the more stable algorithm obtained using the compound matrix method in comparison with initial matrix method, is a violating of associativity property of matrix multiplication during the computer analysis performed by these methods. The calculations of dispersion curves of SAW and PSAW mode velocities are presented for a thickness of AIN film up to 10 wavelengths (ten times more than theoretical results in [2]) and for diamond substrate orientation: [001] - cut and [100] - propagation direction.

Discussion and Conclusions

It is reported about the procedure of using compound matrix method to calculate acoustic mode propagation in layered structures with thick films. Using several SAW and PSAW modes in AlN/diamond structure, as an example, it is discussed a "relation" between SAW and PSAW modes, previously discussed in a number of works, and which may be seen from theoretical dispersion curves of SAW and PSAW velocities on fig.1 [2].

[1]. V.I. Fedosov, Yu.V. Gulyaev, I.I. Chusov, M. Benetti, D. Cannatà, F. Di Pietrantonio, E. Verona, Application of Compound Matrices to the Study of SAW and PSAW Propagation in Layered Structures, 2008 IEEE Ultrasonics Symp. Proc., pp.2233-2236.

[2]. M. Benetti, D. Cannatà, F. Di Pietrantonio, E. Verona, S. Almaviva, G. Prestopino, C. Verona, G. Verona-Rinati, Surface Acoustic Wave Devices on AlN/Single-Crystal Diamond for High Frequency and High Performances Operation, 2008 IEEE Ultrasonics Symp. Proc., pp.1924-1927.

P3-P-04

High Electromechanical Coupling Coefficient SAW Resonator on a Ta₂O₅/Al/LiNbO₃ Structure for Wide Duplex Gap Application

Hidekazu Nakanishi¹, Hiroyuki Nakamura¹, Rei Goto¹; ¹Panasonic Electronic Devices Co., Ltd., Japan

Background, Motivation and Objective

We have successfully developed the high electromechanical coupling coefficient (K^2) SAW resonator on a Ta₂O₅/Al/LiNbO₃ structure. The K^2 is one of the important parameter to determine the duplex gap of the SAW duplexer. Regarding UMTS bands, Band IV system has duplex gap of 355 MHz. To realize the duplexer with small size and high performance for Band IV system, the SAW resonator having very high K^2 is required. Therefore, the substrate and material structure appropriate for the Band IV duplexer need to be developed.

Statement of Contribution/Methods

We have developed the shape control SiO₂/Al/5°YX-LiNbO₃ structure and realized the high performance SAW resonator without spurious responses for Band I and Band IV duplexer. However, this structure has the K^2 of about 15%. It needs to study new structure with higher K^2 for further improvement performances for the Band IV duplexer. We employed the Ta₂O₅/Al/5°YX-LiNbO₃ structure to realize the resonator with higher K^2 than that of SiO₂/Al/5°YX-LiNbO₃ structure. The density of Ta₂O₅ is higher than that of SiO₂. So there is a possibility that the Ta₂O₅ thickness decreases more than the SiO₂ thickness for non leaky type SAW. We studied the phase velocity, the K^2 , the insertion loss, and the attenuation of the SAW resonator dependence of the Ta₂O₅ thickness. Moreover, we optimized the Ta₂O₅ thickness to suppress the Rayleigh mode spurious response.

Results

We have successfully cleared the optimum Ta₂O₅ thickness to realize the high performance SAW resonator without Rayleigh mode spurious response. The Ta₂O₅ thickness normalized by the wavelength of the acoustic wave (λ) is 0.025 λ and decrease appreciably compared to SiO₂ thickness. And the K^2 is very high of 23%, the insertion loss is good of 0.17dB. Furthermore, in the resonator characteristic, Rayleigh mode spurious response was suppressed.

Discussion and Conclusions

We have established the Ta₂O₅/Al/5°YX-LiNbO₃ structure for wide duplex gap application as the alternatives to the SiO₂/Al/5°YX-LiNbO₃ structure. The developed SAW resonator shows the excellent performances which are the high K^2 , the low insertion loss, and the high attenuation. The SAW resonator could be applied sufficiently for the Band IV duplexer.

Highly Oriented Ta₂O₅ Piezoelectric Thin Films Prepared by RF-Magnetron Sputtering

Shoji Kakio¹, Takeshi Mitsui¹, Akinori Tsuchiya¹, Yasuhiko Nakagawa¹; ¹Interdisciplinary Graduate School of Medicine and Engineering, University of Yamanashi, Kofu, Yamanashi, Japan

Background, Motivation and Objective

For the development of high-performance piezoelectric devices, piezoelectric thin films with high coupling, high stability, low loss, and high frequency are required. An X-axis-oriented Ta₂O₅ piezoelectric thin film is a relatively new material developed by Nakagawa, one of the authors, and has a strong piezoelectric property similar to that of ZnO thin films and a high dielectric constant. The authors also reported that, in the deposition of KNbO₃ thin films using an RF-magnetron sputtering system with a long-throw sputter cathode and an O₂-radical source, strong (110) orientation and a smooth surface were obtained. In this study, the X-axis-oriented Ta₂O₅ thin films were deposited on SiO₂ or MgO using the RF-magnetron sputtering system.

Statement of Contribution/Methods

A metal tantalum target with 50 mm diameter was used and the distance between the target and the substrate was 100 mm. The substrate temperature T_s was varied from 650°C to 750°C. The RF power applied to the cathode and the radical source was 150 W. The flow rate of the O₂-radical source was varied from 4 to 10 ccm, while the Ar gas flow rate and the gas pressure were fixed to 33 ccm and 0.75 Pa, respectively. The degree of orientation was evaluated from X-ray diffraction patterns. To measure the coupling factor (K^2) for the Rayleigh-type surface acoustic wave (SAW), interdigital transducers with a period λ of 20 μ m were fabricated using an Al film. The surface morphology was observed by atomic force microscopy.

Results

The deposition rate ranged from 0.54 to 1.73 μ m/h for the deposition time of 5 h. It was found that supplying the RF power to the O₂-radical source markedly enhanced the preferential (200)-axis orientation, increased K^2 , and reduced the surface roughness. The degree of orientation and the piezoelectric property were sensitive to changes in T_s and the O₂ flow rate. When T_s was 700°C and the O₂ flow rate was 10 ccm, the strongest piezoelectric property was obtained and K^2 of the Ta₂O₅/SiO₂ structure was 0.88% for the normalized thickness h/λ of 0.21 at the center frequency of 120.2 MHz. For a higher mode of the Rayleigh-type SAW in the Ta₂O₅/MgO structure, K^2 of 1.42% was obtained for h/λ of 0.23 at 256.3 MHz.

Discussion and Conclusions

The above-mentioned K^2 of the Ta₂O₅/SiO₂ structure is about 3/4 of that for the previously obtained thin film using a DC-diode sputtering system. Further optimization of sputtering conditions will be investigated with the aim of obtaining a stronger piezoelectric property.

In-Situ Monitored Deposition of SiO₂ on Longitudinal Wave Based Resonator

Sergei Zhgoon¹, Alexander Shvetsov¹, Mihir Patel², Kushal Bhattacharjee²; ¹Moscow Power Engineering Institute, Moscow, Moscow, Russian Federation, ²RF MD, USA

Background, Motivation and Objective

Longitudinal waves are interesting in high frequency wideband applications. It has been shown that with coating by SiO₂ overlay the temperature stability of a wave on YZ LiNbO₃ may be improved and useful characteristics can be obtained.

Statement of Contribution/Methods

In our previous publication [1], both theoretical and experimental results were presented on temperature compensation of longitudinal wave by SiO₂ overlay. However, one intriguing feature was the gradual transformation of the longitudinal wave (LLSAW) into a "modified" LLSAW as the SiO₂ thickness was increased. In this work an attempt has been undertaken to verify the validity of modeling results by in-situ monitoring of the frequency response of a resonator on YZ LiNbO₃ during SiO₂ sputtering. The in situ monitoring provides a picture of gradual waning of the LLSAW mode and the birth of the "modified LLSAW" mode. The synchronous resonator with 20 electrodes in the IDT and in each grating was formed with a period of 1.9 micron (wavelength 3.8 microns). The electrode material was 100 nm gold on 5 nm Ti. The deposition process was magnetron sputtering from a SiO₂ target at room temperature, while monitoring was performed with Agilent E5070a VNA by observation and registration of the resonator admittance.

Results

The obtained dispersion data was compared to the modeled dispersion curves. The vanishing of the first mode and the birth of the subsequent mode were clearly observed in the monitored response. The validity of the modeling results has been confirmed. The modeled resonator response with coating has been compared to the experimental response.

Discussion and Conclusions

The initial LLSAW and the subsequent “modified” LLSAW modes predicted in modeling exist, and their change occurs by means of vanishing of the initial mode and the birth of the subsequent mode. The modeling in Comsol Multiphysics correctly predicts the main features of this wave in an almost quantitative way.

[1] “Temperature Compensation of Longitudinal Leaky SAW with Silicon Dioxide Overlay”, M.S. Patel, K. Bhattacharjee, J. Reed, and S. Zhgoon, IEEE Ultrasonics Symp. Proceedings, 2008

P3-Q. Device Design

Sala Orange

Wednesday, September 23, 2009, 10:00 am - 11:30 am

Chair: **Maximilian Pitschi**
EPCOS AG

P3-Q-01

Phase Linear-Flat Wide Band-Low Loss Filters using Dispersive Unidirectional Up-Chirp and Down-Chirp Inter-Digital Transducers

Yusuke Sato¹, Kazuhiko Yamanouchi¹; ¹Tohoku Institute of Tech., Japan

Background, Motivation and Objective

In order to obtain the high performance Surface Acoustic Wave (SAW) devices, it is very important for the interdigital transducer (IDT) to be made the unidirectional ones (UIDT) together with SAW materials. Especially mobile communication and UWB communication systems require the phase linear-wide band-low-loss filters at GHz-ranges. We proposed new UDT of the SiO₂ and TeO₂ very thin grating films with 1.0dB insertion loss at 2GHz-range and unidirectional dispersive IDT (UDIDT) for the elastic convolvers. The dispersive IDTs (DIDT)s with up-chirp or down-chirp phase linear characteristics have the flat wide band and sharp cut-off characteristics without amplitude weighting of $\sin X/X$. Also transversal types of SAW filters have better power duration of IDT electrode than those of resonator types of filters with no phase linear. The phase linear and flat wide band are obtained by combining of up-chirp and down chirp dispersive interdigital transducers. Also, low loss filters with about 0dB insertion loss will be obtained by using the unidirectional up-chirp DIDT (UUDIDT) and unidirectional down-chirp DIDT(DUDIDT). Fan-shape IDT (FIDT) filters have flat wide band with sharp cut-off characteristics. But the FIDT can not use for low-loss filters, because the theoretical minimum insertion loss of unidirectional ones is about 3.5dB.

Statement of Contribution/Methods

We proposed the wide band filters combining DUDIDT and UUDIDT using the conventional UDT with the thin grating films. In this case, we could not obtain the low loss results.

Results

In this paper, experimental and theoretical results of phase linear, flat wide band and low loss filters using new configuration of DUDIDT and UUDIDT are described. The large directivities DUDIDT and UUDIDT are obtained by using the change of the electrode thickness, electrode width, and floating and short electrode as the reflectors.

Discussion and Conclusions

Calculation results for 128°Y-X LiNbO₃ showed below 0.5dB insertion loss with the bandwidth from 5% to 30% with the directivities of about 20dB and light amplitude weightings. The experimental results showed about 1.0dB insertion loss at 500MHz with bandwidth of 8% and sharp cut-off characteristics.

Also we describe about the dispersive double electrode IDTs with the TeO₂ thin film reflectors with wide bandwidth characteristics.

P3-Q-02

Design and analysis approach for SAW devices with string weighted tapered transducers

Svetlana Malocha¹, Rodolfo Chang¹; ¹Triquint Semiconductor, Apopka, Florida, USA

Background, Motivation and Objective

The string weighting technique for tapered transducers was first described in 2001 [1]. Similar to block weighting, string weighting is based on voltage division: the desired potentials on the transducer electrodes are achieved by dividing the transducer into groups of sub-transducers connected in series, and varying the number of sub-transducers in a group and the sub-transducer lengths.

The distinctive feature of string weighting is that the lengths of the sub-transducers are small (one wavelength) and maintained the same throughout the transducer. A specified weighting function is achieved by varying the number of sub-transducers connected in series (i.e. the number of transducers in the "string"). This technique combines flexibility of achieving the desired weighting function and the impedance value. It allows one to improve the rejection level in the devices with tapered transducers compared to what can be achieved using block or withdrawal weighting [1].

The great flexibility of string weighting results in complexity of the device structure. Therefore an analysis approach is required that takes into account specific electrical connections inside transducers and the resulting charge distribution on their electrodes.

Statement of Contribution/Methods

In this paper an analysis approach for devices with string weighted tapered transducers is presented. Special care is taken to ensure the accuracy of impedance calculation for the individual sub-transducers since the accuracy of the overall simulation depends on it.

The device containing two tapered transducers is subdivided into channels with constant electrode periodicity across the channel aperture. In each channel the transducers are subdivided into one-electrode cells, each cell starting and ending at the centers of the gaps adjacent to the electrode. P-matrices for cells are calculated based on the COM model and then cascaded.

The critical part of the analysis is the calculation of the COM parameters for each electrode cell, which are calculated with the specific electrical connections and charge distribution taken into account.

The implementation details of the analysis are presented.

An algorithm for implementing a given analog weighting function using string weighting is discussed.

Results

The analysis approach for SAW devices with string weighted tapered transducers is developed. The accuracy of the analysis is verified using commercial IF filters with string-weighted unidirectional tapered transducers built on LiNbO_3 .

Discussion and Conclusions

The advantages of string weighting are discussed. The analysis for the devices utilizing string weighting is developed.

Several examples of the devices with string weighted tapered transducers are presented which demonstrate good agreement between predicted and measured results.

[1] L. P. Solie and J. M. Bracewell. "A SAW basestation filter on langasite", IEEE 2001 Ultrasonics Symposium, pp. 305 – 308, 2001.

P3-Q-03

Acoustic Filter and Resonator on Periodical Poled LiTaO_3

Michio Kadota¹, Takashi Ogami², Kansho Yamamoto³, Yasuo Cho⁴, ¹Kadota Lab., Murata Mfg. Co. Ltd., Yasu, Shiga, Japan, ²Kadota Laboratory, Murata Mfg. Co.,Ltd., Yasu, Shiga, Japan, ³Tech. & Business Development Unit, Murata Mfg. Co.,Ltd., Yasu, Shiga, Japan, ⁴R.I.E.C., Tohoku University, Sendai, Miyagi, Japan

Background, Motivation and Objective

An in-line-filied model and a cross-field model by Smith are simple equivalent circuits of an interdigital transducer (IDT) of surface acoustic wave (SAW). Figs. 1(a) and (b) show an actual IDT model and a cross-field model by Smith, respectively. Fig. 1(c) shows a structure consisting of a top-electrode/periodical poled (PP) substrate/bottom-electrode. The cross-field model in Fig. 1(b) looks like the structure in Fig. 1(c). It is considered that a device composed of the structure in Fig. 1(c) can generate an acoustic wave. However, acoustic devices composed of a periodical poled PZT plate on Si substrate, a periodical poled $\text{Pb}(\text{Zr}_{0.2}\text{Ti}_{0.8})\text{O}_3$ thin film on (001) SrTiO_3 substrate, and a periodical poled Z-LiNbO₃ have previously reported only weak responses such as impedance ratio of 0.1 to 3dB.

Statement of Contribution/Methods

This reason is considered that their periodical poled devices have neither electrode fingers nor grating electrode reflectors, while conventional SAW devices have them. So they do not have any effective reflection to realize a good frequency response.

This time, authors have proposed effective reflectors for the periodical poled substrate device and attempted to fabricate the resonator and the resonator filter by applying the proposed reflectors to a periodical poled Z-LiTaO₃ (PPLT) plate, which is different from above-mentioned substrates.

Results

As the result, authors realized a resonator having an impedance ratio of 34 dB and a filter having an insertion loss of 2.6 dB and a relative bandwidth of 2.2 % as shown in Fig. 2 for the first time by applying the effective reflectors to the PPLT substrate.

Discussion and Conclusions

Authors could realize the PPLT resonator and the PPLT filter having good frequency characteristics by applying proposed effective reflectors to the PPLT structure for the first time. It is considered that PPLT resonators and/or PPLT resonator filters having more excellent characteristics could be realized by optimizing the design parameters such as an aperture and a number of PP period.

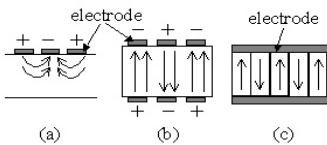


Fig. 1 Models of (a) actual IDT, (b) cross field equivalent model by Smith, (c) periodical poled structure.

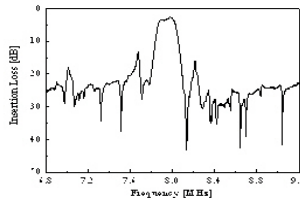


Fig. 2 Frequency characteristic of the filter consisting of periodical poled LiTaO₃ plate.

P3-Q-04

Revisiting of RAC devices

Li Xianyi¹, Victor Plesky², Thomas Weimann³, Paul Hartogh⁴, V.I. Grigorievsky⁵; ¹Max Planck Institut for Solar System Research, Katlenburg-Lindau, Germany, ²GVR Trade, Neuchatel, Switzerland, ³PTB, Braunschweig, Germany, ⁴Max Planck Institut for Solar System Research, Germany, ⁵Russian Academy of Science, Moscow, Russian Federation

Background, Motivation and Objective

Reflective Array Compressors (RAC) were intensively developed in 1970s and 1980s, and they are considered as one of the most sophisticated SAW devices. Until now they are still used in Radar systems and Chirp Transform Spectrometers, for processing wide band signals of 500MHz and more in real time. The basic parameter of such device is the BT product, which may reach 10000 and more. Meanwhile for many years the development effort of such devices was reduced. On the one side their earlier used fabrication methods such as variable profile grooves etching, is commercially not available now; and on the other side SAW device technology also has made significant progress during the last decades. The RAC devices were produced on piece by piece basis and were extremely expensive due to many fabrication steps such as phase correction which demands a unique approach for each device. The objective of this work is to develop RAC devices with BT values of 8000 using widely available technology nowadays.

Statement of Contribution/Methods

The development of RAC devices usually is focused on 2 goals, to minimize the insertion loss and phase deviation of S₂₁(f) from ideal quadratic dependence. To avoid the profile depth etching, we concentrated on methods of weighting on reflecting structures. Comparing different type of reflectors and different methods of weighting their reflectivity, we found that the best results can be obtained using grooves of uniform depth along the structure and weighting by variation of the duty cycle of grooves. For typical down chirp device with B=400MHz, T=20us this approach results in the variation of the groove width duty cycle from 10% to 50%. Then the narrowest width is about 220nm, i.e. out of range of resolution of photo lithography. Therefore we have used the standard e-beam lithography equipment for direct exposure of the weighted groove array. Another possibility which we studied is to combine this duty cycle weighting with aperture weighting which allows to keep critical dimension on the level of 0.4um where even optical lithography is sufficient.

Wednesday
Poster

Results

The fabricated RAC filter with time bandwidth product 8000($B=400\text{MHz}$, $T=20\mu\text{s}$) has a flat -53dB insertion loss and 23 degrees rms phase deviations in bandwidth.

Discussion and Conclusions

The modern lithography allows us to create structures which were impossible to fabricate 20 years ago, therefore we are able to produce ultra wideband devices with good specifications and reduced costs. We demonstrated here that RAC devices can be produced with new techniques, which are also applicable for SAW devices for UWB communication systems. The Chirp Transform Spectrometers using these RAC devices have advantages compared to real time Fast Fourier Transform spectrometers, in that they can perform broad band spectrum analysis with lower power consumption, this feature is especially important for space applications. In general small and passive SAW device as RACs remain highly competitive for a number of applications.

P3-Q-05

Ultra Wide Band Resonator composed of Grooved Electrode on LiNbO₃

Michio Kadota¹, Tetsuya Kimura², Yasuyuki Ida¹; ¹Kadota Laboratory, Murata Mfg. Co., Ltd., Yasu, Shiga, Japan, ²Kadota Laboratory, Murata Mfg. Co., Ltd., Yash, Shiga, Japan

Background, Motivation and Objective

A surface acoustic wave (SAW) device with a wide band is realized by using a substrate having a large electromechanical coupling factor such as 0°-15°YX-LiNbO₃. Hashimoto reported that a resonator composed of a Cu-electrode/15°YX-LiNbO₃ had a wide bandwidth of about 12 %. Authors attempted to fabricate a resonator with a wider bandwidth.

Statement of Contribution/Methods

Resonators composed of grooved Al electrode/LiTaO₃ and LiNbO₃ with same electrode thickness as the groove and with thinner electrode than that were reported by Kadota and Yamanouchi, respectively, but their bandwidths were narrower than above-mentioned resonator. Authors have realized a resonator with an ultra wide bandwidth of 17 % by composing thick grooves and same thick electrodes as the grooves as 0.1λ . Where λ is a wavelength of the SAW.

Results

Figs. 1(a) and (b) show side views of the structures composed of a conventional electrode/4°YX-LiNbO₃ and a grooved electrode/one. The thickness of the electrodes and the grooves is same as 0.1λ . Figs. 2(a) and (b) show their frequency characteristics. In spite of same electrode thickness, same λ , and same interdigital transducer, their characteristics are different. The latter has a wider bandwidth of 17 %, higher resonant and anti-resonant frequencies compared with those of the former. Furthermore, the latter has a small spurious due to Rayleigh wave in a lower frequency than the resonant one, though the former has a large spurious in a higher frequency than the anti-resonant one at a thick electrode and in a pass band at a thin electrode.

Discussion and Conclusions

The grooved electrode/LiNbO₃ has advantages that it has a large coupling factor, a wide band, a high frequency, and no spurious due to the Rayleigh in the pass band in spite of the electrode thickness compared with the conventional electrode/LiNbO₃. So, this structure is suitable for a high frequency device with a wide band.



Fig.1 Two structures: (a) Electrode/substrate, (b)grooved electrodes/substrate

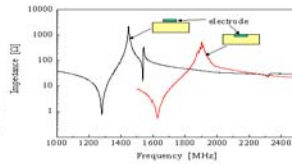


Fig.2 Frequency characteristics of resonators composed of (a) and (b) structures in Fig.1.

P3-Q-06

Design of New Lateral Field Excitation Langasite Resonant Sensors

Therese LEBLOIS¹, Colette TELLIER², ¹MN2S, Institute FEMTO-ST, Besançon, France, ²TF, Institute FEMTO-ST, France

Background, Motivation and Objective

Langasite (LGS) presents some interesting perspective for acoustic wave devices due to its strong piezoelectric coefficients, its moderate dielectric permittivity and its high working temperature. Moreover recent studies show that batch process such as wet micromachining can be adopted to fabricate LGS resonant structures. For bulk acoustic wave devices, lateral field excitation (LFE) presents some advantages such as reduced aging and increased frequency stability. Moreover up to now they are no investigation on LFE of LGS. The objective is thus to design new langasite resonant structures by combining modelling of piezoelectric excitation and simulation of micromachined structures.

Statement of Contribution/Methods

The study is composed of two parts. Part I is devoted to the selection of orientations that are suitable to excite a beam clamped at the two ends. For this purpose an analytical model based on Christoffel-Beckmann method is used to determine resonance frequency, electromechanical coupling coefficient and Q factor. The second part focuses on the simulation of the wet etching (HCl solution) of resonant structures with a special attention on commercial cuts (X, Y and Z cuts). The self elaborated simulator TENSOSIM allows us to select final orientations for which adequate etching shapes are obtained.

Results

Results are concerned with commercial cuts. The piezoelectric modelling predicts high coupling coefficients for these cuts. For specific orientations of the electric field we obtained higher electromechanical coefficients than for thickness excitation showing the interest of LFE. For each selected orientation the absence of coupling between the three modes of vibration which can be excited by LFE is verified. For this first selection of orientations the simulator furnishes 3D etching shapes of beams and corresponding longitudinal and transverse 2D sectional shapes. Owing to anisotropy of 3D and 2D etching shapes some selected orientations are rejected because of beam asymmetry or re-entrant cross sectional profiles. As a result among commercial cuts, only X cut with a Y alignment of the beam gives satisfactory metrological performances.

Discussion and Conclusions

The simulation of etching shapes and the computation of metrological performances of piezoelectric resonators show that the X commercial cut is very interesting to design new LFE langasite micromachined sensors that possess higher performances than quartz sensors. Clearly the present study can be extended to other singly or doubly rotated LGS plates. Two future objectives are:

- (i) the microfabrication of the X resonant structure,
- (ii) the establishment of a database (orientations, piezoelectric performances, 3D or 2D etching shapes, FEM analysis) for complete applications of LFE langasite sensors.

Wednesday
Poster

P3-R. Device Modelling (SAW)

Sala Orange

Wednesday, September 23, 2009, 10:00 am - 11:30 am

Chair: **Clemens Ruppel**
EPCOS AG

P3-R-01

Analysis of Additional Surface Mechanical Features in Micro-acoustic Devices – A Combined FEM-JTFA Approach

Glenn Matthews¹, Alireza Baghai-Wadji¹; ¹*School of Electrical and Computer Engineering, RMIT University, Melbourne, Victoria, Australia*

Background, Motivation and Objective

In this paper, we propose a hybrid method for the analysis of mechanical features added to the surface of micro-acoustic structures to enhance device performance. The technique has been successfully applied to evaluate the influence of additional mechanical features placed on a XY-LiNbO₃ Surface Acoustic Wave (SAW) device substrate surface as well as finite dimensioned electrode interactions on a Flexural Plate Wave (FPW) structure. Application of the Finite Element Method (FEM) followed by utilisation of a problem adapted Joint-Time Frequency Analysis (JTFA) allows a detailed study of additional surface features to be undertaken.

Statement of Contribution/Methods

It is well known that acoustic reflectors can be employed to enhance device performance, whilst absorbing materials can be applied to suppress unwanted modes. Using an adaptation of the FEM package ANSYS, a three-dimensional model of a XY-LiNbO₃ SAW structure has been developed. A SiO₂ isotropic wall, with dimensions of a 60µm wide and 10µm thick, was placed on the perimeter of the interdigital transducers (IDTs). A 1ns pseudo-impulse was applied to the input IDT and the device response calculated for a total of 350ns. The simulated device insertion loss characteristic was obtained and successfully compared with the authors' spectral domain Green's function.

Results

One known impediment in using the FEM to model micro-acoustic structures is the effect of triple transit interference. At the simulated device boundaries, acoustic energy reflects towards the IDTs, manifesting as unwanted ripple upon the insertion loss characteristic. In a fabricated device, the effect is lessened due to scattering. Since the insertion loss only considers the device frequency characteristic the time domain information is effectively discarded. Thus by employing JTFA, a more complete description of device behaviour can be obtained. An adaptive Wigner-Ville distribution has been utilised to distinguish between actual and triple transit signals. A differential time-frequency distribution has also been developed where the influence of the additional mechanical features can be clearly observed.

Discussion and Conclusions

Finally, we present guidelines to optimise the micro-acoustic device response by modifying the position, composition and dimensions of the additional mechanical features facilitating device fabrication with reduced substrate dimensions.

Erroneous Assumption of Superluminal Speeds in Green's Function Theory as the Origin of Singularities in BEM-based Modelling of SAW and BAW Devices

Alireza Baghai-Wadji¹; ¹*School of Electrical and Computer Engineering, RMIT University, Melbourne, Victoria, Australia*

Background, Motivation and Objective

The combined FEM-BEM analysis technique, introduced nearly two decades ago, has been widely accepted as a power technique in SAW and BAW community for modelling the massloading effect. It is also a widely acknowledged fact that simulations based on exclusive usage of BEM, whenever possible, produce the most accurate and reliable numerical predictions, which hardly can be surpassed by competing techniques. On the other hand, it is also common knowledge that the singularities occurring in Green's functions, and in their spatial derivatives, severely limit the applicability, implementation, accuracy, and the versatility of the BEM: At best it can be said that engineers and designers have learned to skilfully tame the beast to some reasonable degree and work with it. We sum up: FEM-BEM is currently an utmost useful tool in SAW and BAW modelling; BEM delivers most accurate numerical results; BEM is plagued with computational difficulties which require mastery in mathematical physics, which is not the primary domain of most engineers. Therefore, it can be concluded that the development and implementation of a BEM formulation, free of singularities, would be most desirable.

Statement of Contribution/Methods

This presentation introduces a method of analysis exclusively based on a modified version of BEM (BEM-BEM). The method allows us to achieve high accuracy to a degree that we can safely gauge the approximations obtained by alternative techniques, without being concerned with the aforementioned deficiencies associated with conventional Green's functions theory. We achieve this objective by basically showing that the Green's functions singularities originate in a physically inadequate assumption of superluminal speed of electrostatic- and elastostatic interaction propagation in piezoelectric media, which is implicitly embedded in conventionally constructed Green's functions.

Results

The practical implications of our method are manifold. A glimpse of the results obtained by our modified BEM includes: (i) the calculations of electric, magnetic, and elastic radiation resistance functions into the substrate; (ii) automatic and precise determination of the location of cut-off frequencies of Green's functions; (iii) construction of Green's functions without singularities; (iv) a dictionary of the modified Green's functions and their derivatives; (v) elastic scattering and transmission coefficients of surface waves on one or more massive and conductive electrodes, (vi) electromagnetic cross talk of a few metallic electrodes.

Discussion and Conclusions

Based on a fundamental insight it is shown that the analytical and numerical difficulties arising in the application of BEM can be avoided systematically by applying an easy-to-use (iterative matrix) method which will be presented for the first time. The proposed method promises to change the way how we view Green's functions and demystify the generally perceived difficulties in Green's functions.

Ab-initio Mesh-less Modelling of Three Dimensional Massloading Effect in SAW and BAW Devices

Hardik Vagh¹, Ali Reza Baghai-Wadji¹, Stephane Chamaly²; ¹*School of Electrical and Computer Engineering, RMIT University, Melbourne, Victoria, Australia*, ²*Research & Development, EPCOS PTE. LTD., Singapore, Singapore*

Background, Motivation and Objective

Brute force three dimensional simulation of the Surface Acoustic Wave(SAW) and Bulk Acoustic Wave (BAW) devices having massive finite-aperture metallic electrodes, massive busbars and massive protective closure structures is a prohibitively difficult task. This paper presents fundamentally new ideas and implementation tools based on a mesh-less analysis of the problem, to tackle the daunting challenge of modelling 3D massloading effect with high accuracy.

Statement of Contribution/Methods

The proposed method comprises the following steps: (i) Subdivide the device geometry of the massive structure into an adequate number of hexahedron elements, respectively, pentahedron elements in the case of complex

geometry of the devices. Thereby, it should be emphasized that, one electrode or the entire busbar is represented by one mesh-less hexahedron. (ii) Affine transform the hexahedron (pentahedron) elements to their corresponding master element, positioned at the origin of the coordinate system. (iii) Given our proposed recipe in this paper, construct a complete set of novel 3D orthogonal expansion functions. These functions possess richly detailed and refined features and are equipped with distinctive properties to describe the displacement- and traction variations in electrodes' interior, surface areas, their edges and corners with prescribed precision. (iv) Use a novel weak formulation, recently developed by these authors, to account for the effect of the massive structures, projected onto their support regions, on the surface.

Results

The above recipe enables the modelling of any arbitrary arrangement of electrodes with varying height, width and aperture length in terms of only one cubic master element characterized by our constructed basis functions, enabling 3D massloading analysis for the first time in SAW and BAW industry.

Discussion and Conclusions

The developed technique allows the computation of surface-to-bulk, bulk-to-surface wave conversion in 3D models of acoustic devices. Comparison with experimental data and with alternative simulations will be presented and discussed.

P3-R-04

Fabrication of SAW Devices with Small Package Size Using Through Substrate Via Technology

Hiroyuki Okitsu¹, Keishin Koh¹, Koji Hohkawa¹; ¹Kanagawa Institute of Technology, Japan

Background, Motivation and Objective

Recently mobile radio communication systems such as mobile phones have been remarkably improved becoming more compact and lighter. In these equipments, multiple SAW devices are used. Comparing the package size of active devices such as semiconductor IC, the package size of SAW devices is relatively larger because a capping structure to cover the surface of the SAW propagating substrate must be required. In order to realize SAW devices with smallest package size and investigate possibility of three dimension package of SAW devices, we propose the novel package method of SAW devices, in which two same SAW devices with half size of overlap length of the original device are bonded in face to face bonding and two same SAW devices are electrically connected in parallel by through substrate via technology. In this paper, we carry out basic study on fabrication process and will report basic experimental results.

Statement of Contribution/Methods

The process steps are 1) first, we formed via hole on piezoelectric substrate (wafer A) using sand blast milling from two side and formed through electrode by sputtering and plating process; 2) next, we fabricated SAW devices on two same piezoelectric substrate (wafer A and wafer B) and form solder metal bump on pad electrode; 3) we coated adhesive material using polyimide photo resist and patterned it on wafer A and Wafer B; 4) we bonded wafer A and wafer B by face to face using bonding equipment and carried out sealing process in vacuum equipment; 5) Finally, we dice the wafer to chip.

Results

We investigated processes conditions of through substrate via electrode for piezoelectric substrate with different thickness. We also investigated effect of some parameters such as several kinds of solder material, bonding conditions and size of metal bump. We fabricated test devices using LiTaO₃ and Quartz substrate and estimated frequency characteristics of devices.

Discussion and Conclusions

Experimental results indicated that there is no remarkable change in the frequency characteristics between half size devices bonded and original devices. The experimental results indicated that this package is possible to reduce package size of SAW devices. We also discussed possibility of three dimension package of SAW devices using this technology.

A Study of wafer Level Packaging of SAW Filter for Module Solution

Kaoru Sakinada¹, Akira Moriya¹, Msayuki Kitajima¹, Osamu Kawachi¹; ¹Communication Devices Division, FUJITSU MEDIA DEVICES LIMITED, Yokohama, Kanagawa, Japan

Background, Motivation and Objective

In the cellular market, the requirement for miniaturization becomes more severe each year. Multiband and multimode requirements have accelerated the need for further miniaturization of RF components. SAW devices, for the RF module function, require low insertion loss and high attenuation performance, while from the structural point, miniaturization and the ability to withstand high molding resisting pressure are demanded.

Statement of Contribution/Methods

Ceramic packaging with hermetic-seal has efficient reliability, from a structural point of view, for molding pressure in the module fabricating process. In contrast, the current WLP method is difficult to use in the practical mold process. A WLP method using resist with air-gap over the IDT is introduced as a solution for module fabricating. The issues of the resist structure with air-gap are humidity reliability and strength of the deformation. In this paper, we present the improvement method of humidity reliability and strength of the deformation.

Results

A WLP-SAW device for use in modules is realized by improvements in the reliability of IDT and the strength of molding pressure of the resist with air-gap. In the reliability test, the WLP-SAW device passed 500 hours in THB (85degC/85%, 2V), and passed 12MPa in Molding pressure. Device size is 0.93x0.92 mm and the height is 0.4mm typ.. In addition, electrical performance is improved compared to the current ceramic packaged devices due to decreased parasitic impedance from the package. An insertion loss improvement of 0.2dB was realized.

Discussion and Conclusions

In this paper, we would like to discuss the possibility of the WLP-SAW device for the resist structure with air-gap. Moreover, we would like to discuss the improvements in characteristics and molding resisting pressure with our WLP-SAW device.

P3-S. Medial Imaging Transducers

Sala Orange

Wednesday, September 23, 2009, 10:00 am - 11:30 am

Chair: **Kirk Shung**
USC

P3-S-01

Multi-row linear array using cMUTs and multiplexing electronics

Robert Wodnicki¹, Kai Thomenius¹, Rayette Fisher¹, Charles Woychik¹; ¹GE Global Research, Niskayuna, New York, USA

Background, Motivation and Objective

We are developing a large area reconfigurable imaging array which will have co-integrated cMUTs and control electronics. Our goal is a reconfigurable array with transducer subelements spaced at a pitch of 185um in X and Y dimensions.

Statement of Contribution/Methods

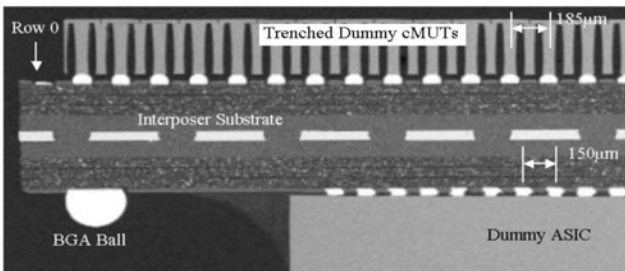
As a prototype demonstration of some of the goals of this effort, we have designed a multi-row linear array using cMUTs and existing multiplexing electronics.

Results

The attached figure shows a cross-section of our preliminary transducer assembly including mechanical test parts for the intended ASIC, interposer substrate, and trenched cMUTs. The interposer maps 150um pitch ASIC cell pads to 185um pitch cMUT transducer pads.

Discussion and Conclusions

In this paper we intend to show imaging and experimental acoustic results with the new cMUT-based probe, and compare these results to acoustic simulations. We also intend to describe results of the advanced packaging development which has allowed us to build this demonstration prototype.



Development of Transducer System for Tissue Harmonic Imaging of Long Coded Signal

Masayuki Tanabe¹, Kan Okubo¹, Norio Tagawa¹; ¹Department of Information and Communications Systems Engineering, Tokyo Metropolitan University, Hino, Tokyo, Japan

Background, Motivation and Objective

The objective of this study is to develop a transducer system which can obtain high spatial resolution and high signal-to-noise ratio signals using a pulse compression technique and tissue harmonic imaging. In the previous study, we proposed a multilayer transducer system which consists of a Pb(Zn_{1/3}Nb_{2/3})O₃-PbTiO₃ single crystal (PZN-PT) and two Poly(vinylidene fluoride) (PVDF) films, and clarified that the thickness of the PVDF film has an effect to the performance as a matching layer and as a receiver [1]. However, in consideration of actual use, we should suppress undesirable echo signals. In this study, we newly propose a system that solves the problem, and examine the feasibility of this system using the finite element method simulator *PZFlex* and the pseudospectral method simulator *SpectralFlex*.

Statement of Contribution/Methods

The figure shows the fundamental structure of the proposed system. The system consists mainly of a PZN-PT, two PVDF films, and a reflector. The PZN-PT transmits long coded signals with high transmission efficiency. Both PVDF films directly receive the transmitted signal, while just one of them receives the echo signals. By connecting lead wires shown in the figure, the echo signals can be extracted without a differential amplifier. In this system, the PVDF film does not only receive echo signals which contain harmonic components, but is also used as a matching layer of the PZN-PT. The reflector is placed for the purpose that a PVDF film receive only the transmitted signal.

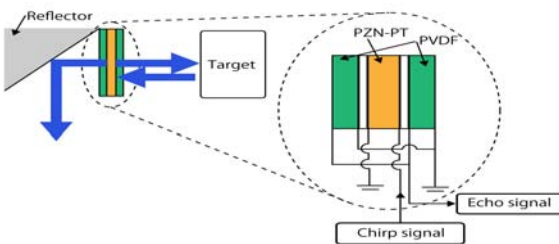
Results

We use a chirp pulse (5 μs, 18-22MHz, 30Vp-p, Hamming window) as a transmitted signal, and obtain an echo signal by the PVDF film (23μm thickness). The amplitude ratio between the 2nd harmonic component and the fundamental component of the obtained echo signal is -22 dB. Each width at half maximum of compressed signal using fundamental and 2nd harmonic component is 0.8 μm and 0.4 μm, respectively. Using a tungsten-loaded epoxy as a reflector, the echo signal directly received from the reflector is more suppressed than a stainless steel.

Discussion and Conclusions

It is clarified that we can extract harmonic components from the echo signals with high S/N when the PZN-PT receives the echo signals before finishing transmitting.

[1]M. Tanabe, et al., IEEE Ultrasonics Symp., pp.1765-1768 (2008)



P3-S-03

On sensitivity and surface temperature of multilayered linear ultrasound phased arrays for medical imaging: modeling, prototyping and experiments

Mihai State¹, Andrea Grandoni², Lorenzo Spicci², Peter Kerkhof³, Peter J. Brands³, Frans N. van de Vosse^{1,2} *Eindhoven University of Technology, Netherlands, ²ESAOTE Spa, Florence, Italy, ³ESAOTE Europe, Maastricht, Netherlands*

Background, Motivation and Objective

The advantages of the multilayer ultrasound transducers (MLT) compared to classic single layer transducers (SLT) are lower electrical impedance and better signal-to-noise ratio (SNR). These properties were emphasised in the last two decades. However, to our knowledge, unbiased receiving relative sensitivity results as well as surface temperature experiments for SLT and MLT based on similar piezoceramics were not reported to date. The present paper comparatively investigates designing and measuring of CTS 3203HD based SLT and MLT transducers for high sensitivity, fine pitch 2.5 – 3.3 MHz 128 elements ultrasound phased array. The effect of a parallel resistor heat sink on decreasing surface temperature is also being addressed.

Statement of Contribution/Methods

For manufacturing feasibility, multilayer prototypes had three similar piezoceramic layers. Based on frequency and time domain 2D finite element (FE) analyses (ANSYS 10.0 Multiphysics), reference single layer and new multilayer transducers were designed with heavy backing, kerf filler, adhesive bonds and two matching layers. The following methods were used for characterizing the prototypes: impedance analyses, scanning electron microscopy (SEM), pulser-receiver one-way transmit and receiving measurements, scanner one-way and pulse-echo measurements (ESAOTE MyLab30) and IR thermal mapping. In order to avoid overestimation of the MLT relative receiving sensitivity, the pulse-echo experiments were performed using an input voltage that determined far-field pk-pk pressure amplitudes similar to SLT. The influence of using a parallel resistor soldered on the PCB was monitored.

Results

The modelled impedance-frequency curves were validated through experimentally measured ones using f_c , k_{eff} and maximum impedance as evaluation parameters. Average thickness of the adhesive bonds calculated based on SEM images was approximately 5 micrometers. Transient transmit on-axis simulated pressure waveforms were validated by one-way water tank hydrophone measurements (PW @-6dB, f_c , BW @-6dB). When a parallel resistor was soldered on the multilayer transmit circuitry, IR measurements registered a 2 degrees Celsius decrease of the surface temperature. The resistor determined a ~ 5% increase of the transmit relative sensitivity and a ~ 4% decrease in BW @-6dB.

Discussion and Conclusions

Good correspondence between FE simulations and measurements was found for all the parameters investigated with differences less than 10 %. The manufactured adhesive bonds were thin enough to be acoustically invisible within the BW of interest. The MLT prototype had a 67 % higher transmit relative efficiency, similar relative receiving sensitivity but for 32% less applied voltage, 4.5 dB better SNR compared to SLT one. Due to a much lower equivalent resistance, MLT elements have a higher current draw than SLT ones. Parallel resistors are decreasing the self-heating and improve the electro-mechanical performance.

P3-S-04

Development of High Frequency Annular Array Ultrasound Transducers using Interdigital Bonded Composites

Hamid R. Chabok¹, Jonathan M. Cannata¹, Hyung Ham Kim¹, K. Kirk Shung^{1,2} *Dept. of Biomedical engineering, University of Southern California, Los angeles, CA, USA*

Background, Motivation and Objective

Conventional ultrasound imaging transducers operating in the 5-20 MHz range have a large footprint and inadequate spatial resolution to resolve fine structures in humans and small animals. Therefore, this research is intended to enhance the design and fabrication of high frequency (HF) composite annular arrays to allow for non-invasive, high-resolution imaging of small biological structures. The annular array transducer is a great alternative to linear and phased arrays because of its symmetric beam-profile, low electronic channel count, and more affordable fabrication cost. In this paper, the design, fabrication, and testing of HF 1-3 composite annular array transducers is presented.

Statement of Contribution/Methods

The composite annular array was developed using a piezoelectric ceramic with high dielectric permittivity and electro-mechanical coupling coefficient. The design parameters using computer simulations have been optimized. Then the annular array was fabricated using the 1-3 composite with ultra fine ceramic posts of $18 \mu\text{m}$ wide separated by a $8 \mu\text{m}$ polymer kerf, and an unloaded epoxy backing layer. Eight annuli electrodes were printed on a custom-designed double-sided flexible circuit to connect the composite annuli with 75 Ohm coaxial cables. Finally, an electroplated epoxy matching layer was used as the ground side to enhance the pulse-echo response of the array.

Results

One flat-aperture composite 8-element annular array has been fabricated. The annuli have been tested and were found to be in good agreement with KLM modeled results. The average pulse-echo response for the annuli was 30 MHz with 55 % -6 dB bandwidth. Element crosstalk was also measured. The maximum crosstalk for the nearest and next-nearest neighbor element was -31 dB and -40 dB, respectively.

Discussion and Conclusions

We believe that we have developed a reasonable fabrication procedure for high frequency composite annular arrays. During the array fabrication process we developed a simple and novel method to remove the chrome-gold electrode from polymer portions of the 1-3 composite without removing the electroplating over the ceramic posts. Therefore the fabrication process was greatly simplified because photolithography or laser ablation was not needed for electrode patterning. Also because all posts have independent electrodes, the alignment between the composite and flex circuit was not critical to the success of the fabrication process. As the next step, we plan to fabricate a miniature lightweight version of this array to be used in a very high frame rate sector imaging system.

P3-S-05

Multiple Frequencies Ultrasonic Imaging Using Multiple-Resonance Transducer

Iwaki Akiyama¹, Natsuki Yoshizumi¹, Kentaro Nakamura²; ¹Department of Electrical and Electronic Engineering, Shonan Institute of Technology, Fujisawa, Kanagawa, Japan, ²Tokyo Institute of Technology, Yokohama, Kanagawa, Japan

Background, Motivation and Objective

The aim of this study was realization of a broadband measurement system that is capable of effectively carrying out a frequency compound method. In this study we developed a bi-layer structure transducer with different thickness. This transducer has multiple resonance frequencies. The objective is to confirm the feasibility of the multiple-frequency imaging method for speckle reduction by using the multiple-resonance transducer.

Statement of Contribution/Methods

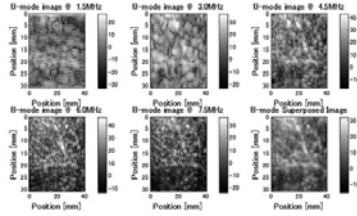
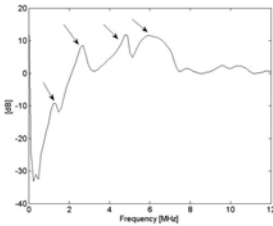
The multiple-resonance transducer which we developed was 6MHz transducer bonded with 2MHz transducer. When the 6MHz transducer was driven by an impulse voltage signal, the resonance frequencies of the whole are 1.5MHz and higher harmonic modes. Thus a pulse-echo imaging method by using this transducer was capable of simultaneous multiple frequencies imaging. Also the frequency compound method was capable of speckle reduction by superposing those images.

Results

The developed transducer insonified the waveform with multiple frequency bands, which was measured by a hydrophone at focal distance from the transducer. The spectrum was shown in the left figure. The peaks of the spectrum were observed at 1.5, 3.0, 4.5, and 6.0MHz as shown by arrows. The pork meat imaging experiments were carried out by using this transducer. The echo signals were divided into the frequency bands at each peak, thus we obtained the images at 1.5, 3.0, 4.5, 6.0 and 7.5MHz which were shown in the right figure. By superposing these five images we obtained the speckle reducing image as shown in the lower right of the right figure.

Discussion and Conclusions

We developed a bi-layer structure transducer of the multiple resonance frequencies. By using this transducer, we obtained the speckle reducing image by superposing the multiple-frequency images.



P3-S-06

Improving ultrasound imaging with integrated preamplifiers

Pascal Chatain¹, David Voisin¹, Mathieu Legros¹, Guillaume Ferin¹, Rémi Dufait¹, ¹Vernon S.A., France

Background, Motivation and Objective

We present a “transparent” receiving electronic architecture demonstrating high performance improvements for medical ultrasound imaging. The preamplifier was designed to be inserted with each coaxial cable and closer to active elements in order to keep compatibility with existing platform.

The foremost motivation of this work is to compensate cable losses and thus increase SNR for the global receive chain to finally expand depth penetration. Furthermore, the novel circuit strategy provides an interesting way for low power consumption, multi-channel and space saving and thus should be integrated close to 1D arrays.

The objective of this work is to identify the outstanding advantages of such a receiving electronic, hence its performances are demonstrated with experimental evaluations of multi-channel electronic boards integrated with 1D transducer arrays, and its imaging performances are highlighted.

Statement of Contribution/Methods

To meet all these specifications a particular attention was focused on HV pulses transmission, amplifier protection, Noise Figure, crosstalk, fast overload recovery and impedance matching on both sides : source(transducer) and load(cables from conventional ultrasound imaging).

Sets of measurement are performed to evaluate the different preamplifier stages in different modes (Transmit or/and Receive).

The multi-channel board design allows a plug and play feature with different standard piezocomposite head-probes. Consequently, comparisons with different configurations in term of bandwidth and impedance features are made with and without electronic.

Finally probes are plugged on conventional ultrasound systems and comparative image quality assessments are performed through quantitative methods.

Results

Integrated electronic exhibits an improvement of the SNR upon +15dB from B-mode images and showing a better “tissue to electronic noise” differentiation.

Furthermore, the electronic transfer function does not impact neither axial resolutions nor contrast performances. General imaging performances are specifically enhanced with higher depth where the SNR improvement is much better. The power consumption is about 10mW per channel and thermal imaging was performed on the entire probes and fits the regulations until 256 channels.

Discussion and Conclusions

Finding a solution to the given specifications was an actual challenge, and the electronic fits with different issues encountered in electrical transducer design(HV pulses, amplifier protection, space, consumption, compatibility with the T/R chain of conventional systems). The preamplifiers demonstrated high performances on a large panel of ultrasound probes(up to 20MHz)and meets the requirements of noise measurements, operational bandwidth, and consequently imaging performances enhancement. Moreover, boards are designed to drive other transduction technologies such as capacitive transducers, with specific add-on for bias voltage.

High frequency single-crystal ultrasound probe

Claire Bantignies¹, Pascal Mauchamp¹, Guillaume Ferin¹, Stéphane Michau¹, Rémi Dufait^{1,2} *Vermon, France*

Background, Motivation and Objective

Lead-based piezoelectric single crystals such as PZN-PT and PMN-PT have been first developed for under water applications by the U.S. Navy. Their outstanding piezoelectric properties (d_{33} as high as 2000pC/N and $k_{33} > 90\%$) make them valuable for high-end ultrasound transducers. Thus, they have been successfully used and commercialized in medical field mainly for cardiac imaging (2-5MHz) but manufacturing such a probe is critical since single crystal structures are more sensitive to thermal and mechanical stresses induced by standard micromachining process.

We propose in this paper to manufacture a high frequency ultrasound probe (15-20MHz) based on very thin single crystal materials ($<70\mu\text{m}$ thick) using low-stressing machining process and exhibiting improved electroacoustical performances.

Statement of Contribution/Methods

This paper presents the acoustical design, fabrication and evaluation of a 128 elements ultrasound array based on single crystal materials. The array specifications were a 3mm elevation, $100\mu\text{m}$ pitch, 20MHz center frequency.

A particular attention have been paid on manufacturing process in order to improve the used of single crystal structures in high frequency transducers.

Results

We demonstrated the feasibility to produce a PMN-PT single crystal probe with suitable performances for high resolution imaging. A complete electro-acoustical characterization has been done: bandwidth, pulse duration and directivity performances are then discussed and compared to classical PZT probes with the same specifications. Performances are close to those obtained with state-of-the-art piezocomposite transducers: bandwidth is competitive and a +3dB in sensitivity is reached.

Discussion and Conclusions

Polycrystalline ceramics like PZT have been widely used in high frequency transducers. Their granular structure limits the frequency range to typically 40MHz. Single crystal materials give access to higher frequency range (up to 60MHz) but require more sophisticated and softer manufacturing process. In this paper we have successfully manufacture a single crystal based transducer by controlling each critical process step such as lapping and dicing.

Non-scanning measurement of local curvature with an ultrasound annular array

Michael Lenz¹, Elfgard Kuehnicke¹, Joerg Sorber¹, Hans Georg Trier², Klaus-Peter Richter³, Gerald Gerlach¹; ¹Technical University of Dresden, Germany, ²TIMUG e. V., Germany, ³Richter Sensor and Transducer Technology, Germany

Background, Motivation and Objective

The use of annular arrays is a novel approach for curvature measurements with ultrasound. The objective is to measure the local curvature radii of buried structures with ultrasound, as for example the curvature radii of the eye lens, of cancerous tissue and inclusions in solid materials.

Statement of Contribution/Methods

To determine the curvature radius of an object, a 3MHz annular array with six elements was optimized. During the measurements, it was used in pulse echo mode and was directed toward the centre of different steel balls. The focus location was varied from a few millimetres in front of the ball to several millimetres behind the ball surface by synthetic focusing. Each time, the echo signal amplitudes on the single transducer elements were measured and plotted against the focus depth. To determine the ball diameters, we use the focus depths, at which these curves take their maxima.

Results

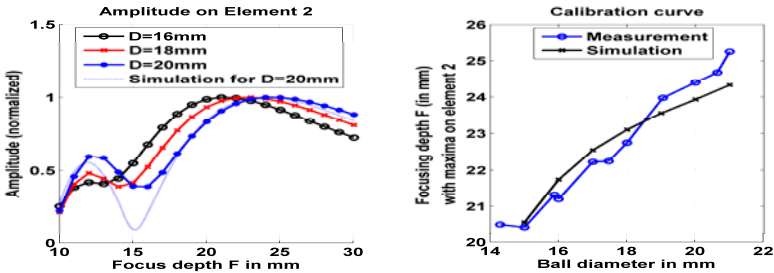
Fig. 1 shows the sound pressure on element 2 (the ring closest to the centre element) as a function of focus depth F for ball diameters of 16mm, 18mm and 20mm. The higher the ball diameter, the higher the focus depth at which element 2 receives the strongest echo signal. In fig. 2, the maximum positions of fig. 1 are plotted against the ball

diameter. Both simulation and measurement curves are monotonically increasing and can therefore be used as calibration curves for curvature measurements of unknown objects.

The simulations are based on sound field simulations with Green's functions. The good agreement with the measurements could be achieved by measuring the active transducer area of each single transducer element.

Discussion and Conclusions

The measurements show the high potential of the new method. To bring the measurement method into practice, further research will focus on ovoid objects, buried structures and robustness.



P3-S-09

Fine pitch non-uniform multilayered linear ultrasound phased arrays for medical imaging: design and testing

Mihai State¹, Andrea Grandoni², Lorenzo Spicci², Peter Kerkhof³, Peter J. Brands³, Frans N. van de Vosse¹;

¹Eindhoven University of Technology, Netherlands, ²ESAOTE Spa, Florence, Italy, ³ESAOTE Europe, Maastricht, Netherlands

Background, Motivation and Objective

Due to their higher transmit efficiency and better received SNR compared to single layer technology, multilayer transducers with uniform layers (MLU) are currently in research and use. Altering the intrinsic geometrical or material homogeneity (i.e. different thicknesses of the constitutive layers, piezoceramic/piezocomposite or piezoceramic/piezopolymer stacks) will increase the available degrees of freedom in transducer design. The paper presents parametric modeling and experimental results related to the development of a CTS 3203HD based fine pitch 2.5 MHz multilayered phased array with non-uniform thickness of the constitutive layers (MLNU). As reference transducer, a uniform multilayered phased array was developed in parallel.

Statement of Contribution/Methods

Considering the difficulty of handling, stacking and soldering very thin piezoceramic layers, the minimum viable thickness for the MLNU was 120 microns. A three-layers piezoceramic transducer was considered for industrial implementation. Preliminary frequency domain finite element (FE) parametric study (ANSYS 10.0 Multiphysics) determined the optimum individual thickness of the bottom and middle piezoceramic layers while the thickness of the top layer was constant. Consequently, by transient modeling, the optimum thickness of the matching layers was determined for both MLU and MLNU. Prototypes characterization considered: impedance analyses, pulse-receiver one-way transmit and receiving measurements, scanner one-way and pulse-echo measurements (ESAOTE MyLab30) and IR thermal mapping. By adjusting the applied voltage similar far-field pressure pk-pk amplitudes were obtained prior to pulse-echo measurements in order to have an unbiased receiving sensitivity evaluation.

Results

Compared to MLU, the predicted behaviour of MLNU (lower coupling constant at fundamental (keff), absolute position and relative amplitudes of the 2nd and 3rd harmonics) was confirmed by impedance and one-way pressure measurements with less than 10% relative differences. MLU and MLNU performance was comparatively assessed in terms of PW @-6dB, BW @-6dB, relative transmit and receiving sensitivities. To alleviate surface self-heating in order to comply with the standardized temperature limits, a parallel resistor was used as a heat sink.

Wednesday
Poster

Discussion and Conclusions

Based on pulser-receiver pulsed excitation measurements, MLNU prototypes exhibited a 12% and 15 % higher transmit and receive respectively BW @-6dB at centre frequency (f_c). In receiving, the 2nd harmonic level was ~ 13 dB down with respect to the f_c . However, considerable surface heating was measured in the case of MLNU. Using resistors placed in parallel with the active elements decreased MLNU equilibrium temperature by 47% while transmit and receive relative sensitivities improved by 38% and 22% respectively. In receiving, the parallel resistor determined a ~ 4dB drop of the 2nd harmonic amplitude.

P3-T. Transducer Modeling

Sala Orange

Wednesday, September 23, 2009, 10:00 am - 11:30 am

Chair: **Jian Yuan**
Boston Scientific

P3-T-01

Wideband multimode Tonpilz transducer with a cavity inside a head mass

Yongrae Roh¹, Saosometh Chhith¹; ¹*School of Mechanical Engineering, Kyungpook National University, Daegu, Korea, Republic of*

Background, Motivation and Objective

A typical Tonpilz transducer is suitable for generating high power ultrasonic waves. However, when a wide frequency bandwidth is also required, the conventional structure frequently fails to meet the requirement. To resolve the problem, polymeric impedance matching layers and series resonators have been added to the conventional. However, the polymeric impedance matching layers have caused lots of problems in high power applications, i.e. delamination of the layers due to acoustic cavitations is a representative problem. In this paper, a new Tonpilz structure has been designed to achieve the wideband bandwidth without the use of the polymeric matching layers while preserving the high power capability.

Statement of Contribution/Methods

The first step of widening the bandwidth was taken by achieving the dual-mode operation of the head mass. The first flapping mode of the head mass was coupled to the typical longitudinal mode to attain the wide bandwidth. The flapping mode frequency (f_r) was proportional to the head mass thickness. A wider bandwidth required a higher f_r , which in turn led to a larger head mass thickness. However, the larger thickness resulted in a heavier head mass, which decreased the bandwidth since the mechanical quality factor was proportional to the weight of the head mass. Hence, by inserting a cavity inside the head mass, the thickness was allowed to extend over a wider range without much increasing the head mass weight. The structure of the cavity was optimized to achieve the widest flat bandwidth of the transducer. The optimization process consisted of finite element analyses (FEA), statistical multiple regression analysis of the FEA results, and utilization of the genetic algorithm to determine the optimal head mass structure for the widest -3dB bandwidth. Once the head mass geometry was determined, the tail mass structure was also optimized, repeating the method used for designing the head mass.

Results

Superiority of the designed transducer was validated by comparing its performance with those of conventional transducers. The fractional bandwidth of a typical single mode transducer with matching layers was 13%, and that of a dual mode transducer with matching layers but without the cavity was 77% while that of the new Tonpilz transducer designed in this paper turned out to be 88%. When the matching layers were eliminated from the designed transducer, the bandwidth decreased to 84%, which was still far wider than the typical Tonpilz transducer with matching layers.

Discussion and Conclusions

The multimode Tonpilz transducer with a cavity inside a head mass invented in this work was shown to provide a much wider bandwidth than conventional Tonpilz transducers. Further, the matching layers that used to cause plenty of problems could be eliminated without much affecting the performance of the transducer. Hence, the new Tonpilz transducer is expected to overcome all the problems related with the polymeric matching layers in high power applications.

Wednesday
Poster

P3-T-02

Optimal design of a piezoelectric 2D array transducer to minimize the cross talk between active elements

Yongrae Roh¹, Wonsuok Lee¹, Susung Lee¹, ¹*School of Mechanical Engineering, Kyungpook National University, Daegu, Korea, Republic of*

Background, Motivation and Objective

Ultrasonic 2D array transducers have a much larger number of piezoelectric elements to do volumetric imaging than a traditional 1D array transducer. Since a larger number of elements mean a higher chance of cross-coupling between the elements, the cross talk between array elements is one of the most important factors affecting the performance of the 2D array transducer. There has been a strong need to find the means to reduce the cross talk level. In this paper, the structure of the piezoelectric 2D array transducer was optimized by means of the finite element method to minimize the cross talk level.

Statement of Contribution/Methods

The transducer under consideration is a planar 2D array transducer working at 3.5 MHz. The transducer is composed of 32 by 32 piezoelectric elements separated by major and minor kerfs, a thick backing layer, two impedance matching front layers, and an acoustic lens. Three-dimensional finite element models of the transducer were constructed using the commercial finite element analysis (FEA) code PZFlex.

The performance of an acoustic transducer is determined by the effects of many structural variables, and in most cases the influences of these variables are not linearly independent of each other. In this paper, through the FEA, the performance variation of the 2D array transducer was investigated by considering all the cross-coupled effects of its structural variables such as the thicknesses of the matching layers, and the width and depth of the major and minor kerfs. The backing layer was assumed to be thick enough to attenuate any backward waves. Through statistical multiple regression analysis of the FEA results, the functional forms of the cross talk level, pulse-echo sensitivity, center frequency, and acceptance angle of the 2D array were derived in terms of the structural variables. Then, by applying the constrained optimization technique, genetic algorithm, to the derived functions, the optimal combination of the structural variables, i.e. optimal structure of the transducer, was determined to provide the lowest cross talk level and the highest pulse-echo sensitivity while preserving a desired acceptance angle at the desired center frequency of 3.5 MHz.

Results

According to the results, of all the structural variables, the width of the minor kerf was most influential on the cross talk level and the sensitivity. Too much variation of the major kerf width and depth impaired the acceptance angle. The optimized structure turned out to have the cross talk level -8.2 dB lower than that of a typical 2D array structure reported in the literature.

Discussion and Conclusions

In comparison with conventional methods, the design method in this paper can determine the optimal geometry of the transducer with great efficiency and rapidity. Results of time domain transient analysis, frequency domain harmonic analysis, and spatial radiation pattern analysis are presented to describe the efficacy of the optimal design method to reduce the cross talk level.

P3-T-03

A wideband annular piezoelectric composite transducer configuration with a graded active layer profile

Sivaram Nishal Ramadas¹, Richard L O'Leary¹, Anthony Gachagan¹, Gordon Hayward¹, Robert Banks², ¹*Centre for Ultrasonic Engineering, University of Strathclyde, United Kingdom, ²Weidlinger Associates Inc, USA*

Background, Motivation and Objective

Ultrasound technology is routinely used in many application areas including underwater sonar, biomedicine, non destructive evaluation (NDE), materials characterisation and process control - all with direct routes into the vital economic sectors of energy, transportation, healthcare and food and drink. As technology demands have increased, device manufacturers are faced with a constant need to extend bandwidth and/or frequency response, while at the same time improve sensitivity, all combined with minimisation of size, complexity and cost. It is becoming increasingly apparent that the current transducer technology, with its emphasis on multi-element array systems, is nearing saturation and new approaches to ultrasonic system design and operation are needed to satisfy many future demands.

Wednesday
Poster

Statement of Contribution/Methods

This paper describes a new range of ultrasonic transducers that are applicable to a wide variety of engineering applications. Specifically, the design consists of a collection of concentric piezoelectric ring arrays, with different diameter rings having different resonant behaviour. This provides direct mechanical separation of different frequency bands in reception mode and the potential to generate complex waveforms in transmission. This design is further extended by employing a tapered active layer profile to form a multimode piezoelectric composite structure, with additional capability to focus without the need for matching layers.

Results

Extensive finite element (FE) modeling, using PZFlex, has been carried out, to study the variation of system performance with respect to the geometry variations. The results of a pilot study are presented. Initially a four ring stepped annular design is described, the device exhibit multiple thickness mode resonances, the range 0.5-2 MHz. The annular design is complemented by a comparable conical composite design. The experimental results to demonstrate the resonant behaviour of the devices, and are presented to validate the FE modelling. The surface dilation characteristics of a wide range of stepped annular and conical designs are then investigated using the FE model. This data is then used to predict the beam characteristics of each design for a range of excitation conditions.

Discussion and Conclusions

A wide bandwidth annular piezoelectric composite transducer design with a graded active layer profile is presented. The designs considered in this paper have extended impedance minimum characteristics, providing a much wider operational bandwidth than that currently associated with piezoelectric composites (typically around 30kHz for unbacked devices).

P3-T-04

Operation of a High Frequency Piezoelectric Ultrasound Array with an Application Specific Integrated Circuit

Anne Bernassau¹, Tim Button², Kyusun Choi³, **Sandy Cochran**¹, Christine Demore¹, Luis Garcia-Gancedo², David Hutson⁴, Tom Jackson⁵, Hyunsoo Kim⁴, Insoo Kim⁵, Carl Meggs², Susan Trolrier-McKinstry⁶, Rick Tutwiler⁷; ¹*Institute for Medical Science and Technology, University of Dundee, Dundee, United Kingdom*, ²*Functional Materials Group, University of Birmingham, Birmingham, United Kingdom*, ³*Department of Computer Science and Engineering, The Pennsylvania State University, State College, PA, USA*, ⁴*Center for Thin Film Devices and Materials Research Institute, The Pennsylvania State University, State College, PA, USA*, ⁵*Department of Electrical Engineering, The Pennsylvania State University, State College, PA, USA*, ⁶*Materials Research Laboratory, The Pennsylvania State University, State College, PA, USA*, ⁷*Applied Research Laboratory, The Pennsylvania State University, State College, PA, USA*

Background, Motivation and Objective

Integration of a piezoelectric high frequency ultrasound (HFUS) array with a microfabricated application specific integrated circuit (ASIC) has several advantages. It can reduce overall system dimensions for applications such as endoscopic ultrasound. The number of signal cables between the array/electronics and the data acquisition/imaging system can be reduced, cutting costs and increasing functionality. Electrical impedance matching is also simplified. The work reported here aimed to demonstrate ASIC operation with a piezocomposite HFUS array operating in the 30 – 40 MHz frequency range.

Statement of Contribution/Methods

The 20-element HFUS array was fabricated with micro-molded piezocomposite material and thin film Cr-Au electrodes using a mask-based process, then packaged in epoxy with external connectors. The mixed-signal transceiver ASIC has 16 channels, each with a programmable transmit beam former and receive amplifiers. An 8-bit 250 MS/s A/D converter digitizes signals from the receive channels, with data stored in a 3 Kbyte SRAM buffer. Fabricated with a 0.35 μm CMOS process, the ASIC area was 10 mm² and power consumption was 300 mW at 3.3 V supply voltage. The HFUS array was mounted on an interface board for connection to the ASIC and the combination was tested in several immersion configurations. Pitch-mode utilized an Olympus M316 external transducer with a Panametrics 5900PR pulser-receiver as an amplifier on reception. Catch-mode used the same external transducer with the 5900PR configured for transmission. Finally, the array was used for both transmission and reception in pitch-catch mode.

Results

Clear signals were seen in pitch-mode with excellent time resolution at separations around 5 mm. Mixed-signal noise from the ASIC was visible in some tests. Time resolution in catch-mode was also excellent and signal to noise ratio was much higher. This is because the combination of the external transducer/pulser and array reception/ASIC amplifier is better than the array/ASIC transmitter and external transducer/amplifier, principally

because the ASIC presently provides an uncoded transmit signal of only 3.3 V peak-to-peak. Pitch-catch mode with a 3.5 V external pulser generated signals with very low noise. Using the 3.3 V ASIC pulser and extra 20 dB gain from the 5900PR generated visible signals but with significant noise from mixed-signal sources in the ASIC.

Discussion and Conclusions

Integration of electronics and piezoelectric ultrasound devices has already been reported for 2D arrays at conventional frequencies. Integration will also be important for HFUS arrays. This paper reports the first results from the combination of a piezocomposite array operating at above 30 MHz with a custom-designed ASIC. Further optimization is needed, but the work demonstrates that all the basic components for an integrated piezocomposite-silicon electronics device now exist and that further development is viable and worthwhile.

P3-T-05

High Frequency Piezo-Composite Transducer With Hexagonal Pillars

Jianhua Yin¹, Mike Lee¹, Emmanuel Cherin¹, Marc Lukacs¹, Stuart Foster¹; *Imaging Research, Sunnybrook Health Science Centre, Toronto, ON, Canada*

Background, Motivation and Objective

Developing a high-frequency piezo-composite material is a challenge due to the extremely small pillar dimensions. The high frequency composites made by conventional dicing saw techniques will most likely have a low ceramic volume fraction and a large pillar width to height aspect ratio, because of the limitation of making narrow kerfs and small pitches. Previous studies on composite materials by Hossack et al have shown that electromechanical coupling and effective velocity are both dramatically decreased. when use of large aspect ratio pillars in a low ceramic volume ratio composite.

Statement of Contribution/Methods

Our previous work demonstrated that 45° triangular pillar composite has a wide band and best suppression of lateral resonance interference. However, the electromechanical coupling coefficient is only 0.37 when its volume ratio is 36% and aspect ratio is 0.6. In this work, we investigated a composite structure with hexagonal pillars. The performances of the composites have been simulated by using a finite element analysis tool (PZFlex). The composites with different volume ratios and aspect ratios were studied. The simulation results show that the composites with hexagonal pillars provide a significant improvement of performance over the composites with other shape pillars. A hexagonal pillar composite, with a volume ratio of 0.3 and an aspect ratio of 0.9, can maintain an effective electromechanical coupling coefficient of 0.6 with a drop in effective velocity of 20 percent. Secondary pulses, due to lateral resonances, are more than 20dB below the main pulse.

To verify the simulation findings, hexagonal pillar composites with low ceramic volume ratio have been fabricated by dice-and-fill technique.

Three sets of parallel kerfs, each with a 110µm index, and each offset by 120°, diced into PZT 5H with a 30µm thick blade, resulted in hexagonal pillars of equal side and a ceramic volume fraction of 0.32. The kerfs were filled with powder loaded epoxy. The composites were finished at four different thicknesses. Each of them has a backing of 30% PZT loaded epoxy and mounted on an SMA connector.

Results

The electromechanical coupling coefficients and effective velocities were calculated from the electrical impedance measurement of the transducers. For the composites with aspect ratio of 0.36, 0.48, 0.72 and 0.9, the electromechanical coupling coefficients are 0.61, 0.56, 0.76 and 0.62 and the velocities are 3315m/s, 3120m/s, 2530m/s and 2560m/s, respectively. The results agree well with the simulations.

Discussion and Conclusions

FEA simulations and experimental measurement have shown that the composite with hexagonal ceramic pillars has a significant performance improvement at low ceramic volume ratio and large pillar aspect ratio. The electromechanical coupling has been improved by more than 50% over previous geometry composites. This is a promising structure for fabrication of high frequency composite transducers and arrays.

P3-T-06

The second-order mode excitation mechanism of capacitive micromachined Lamb wave transducers

Li-Feng Ge¹; ¹*School of Electronic Science and Technology, Anhui University, Hefei, Anhui, China, People's Republic of*

Background, Motivation and Objective

Capacitive micromachined Lamb wave (or plate wave) transducers (mCLWT or mCPWT) possess potential as gravimetric sensors for chemical and biological detections. The kernel of CLWTs is a micro diaphragm-grating structure coupled with a thin plate working as an acoustic waveguide. Using the second-order bending mode of diaphragms to excite Lamb waves has been presented in order to minimize the acoustic radiation to surrounding medium since it is useless for CLWTs [Li-Feng Ge, SPIE, Vol. 6358, 635811-1, 2006]. This paper focuses on the other side, i.e., how to maximize the Lamb wave radiation desired, and further studies the effect of the second-order excitation mechanism on Lamb waves propagating in the silicon plate.

Statement of Contribution/Methods

The lowest order antisymmetric Lamb wave mode (A0 mode) of a thin plate has phase velocities much lower than the acoustic velocity in adjacent liquids if the plate is thin enough. This makes the acoustic energy be guided along the thin plate, avoiding the radiation energy loss of the plate. Therefore, to maximize the input energy exciting A0 wave propagating in the plate waveguide is mainly concerned. Note that a cell of CLWTs is the same with that of CMUTs with long rectangular diaphragms, so the TDK model for such CMUTs [Li-Feng Ge, Science in China (A), 42(12):1308-1315, 1999] is applied here. The input energy comes from the motion of long edges of diaphragms and is increased with the force and moment applied to these edges. It is revealed that second-order mode mechanism can excite effectively A0 wave by producing higher input energy and optimize the behavior of CLWTs.

Results

The computer simulation based on the analytical model further developed is given. The simulated device has long rectangular diaphragms with width of 100 μm and a thin silicon plate with thickness of 3 μm . Each diaphragm consists of a 1 μm thick LPCVD nitride film with residual stress of 280 MPa and a 150 nm thick aluminum electrode; the air-gap is 0.5 μm thick and filled by air for increasing further the restoring force of diaphragm; bias voltage is 30 V. The second-order bending resonance frequency calculated by the TDK model is 4.4 MHz, at which A0 wave is excited. The simulated results show that the second-order mode mechanism not only raises the electro-acoustical coupling efficiency, but also the mass sensitivity of the device due to using thinner plate. Also, a comparison between CLWTs and piezoelectric Lamb wave transducers (PLWTs) shows that CLWTs possess more pronounced advantages.

Discussion and Conclusions

The analytical model for CLWTs has been further developed. The second-order mode excited CLWTs are an attractive choice for chemical and biological measurements.

P3-T-07

Dynamic Response Estimation of Multilayer Ferroelectret-based Transducers using Lumped-Element Electromechanical Models

Joao Ealo^{1,2}, Fernando Seco¹, Carlos Prieto¹, Antonio Jiménez¹, Jorge Guevara¹; ¹*Instituto de Automática Industrial, Consejo Superior de Investigaciones Científicas-CSIC, Arganda del Rey, Madrid, Spain,* ²*School of Mechanical Engineering, University of Valle, Cali, Valle del Cauca, Colombia*

Background, Motivation and Objective

Cellular ferroelectrets exhibit remarkable characteristics which make them suitable for ultrasonic air applications such as non destructive evaluation, acoustic imaging, echo-localization, local positioning systems, etc. Because the increasing interest in its use, models are required to efficiently estimate the expected dynamic response of ferroelectret-based transducers of diverse configuration, e.g. multilayer devices, non-homogeneous surface transducers, prototypes combining layers of different characteristics, etc.

Quasi-static coupled models for predicting piezoelectric coefficient d_{33} and compliance of ferroelectret films have been reported by several researchers. Complex models using finite elements and micromechanical approaches have also been proposed to estimate the properties of these materials.

However, because damping cannot be measured statically, as can the mass or stiffness of a system, most of the models available are not satisfactory to estimate the dynamic response of the ferroelectret films in the ultrasonic frequency range.

In this work, we demonstrate that the dynamic response of a multilayer ferroelectret transducer can be predicted using a multi-degree of freedom electromechanical model of lumped-mass parameters. Layers are represented using the Kelvin-Voigt model of damping for viscoelastic behavior. The number of layers of the transducer equals that of the degree of freedom of the respective model.

Statement of Contribution/Methods

Flat transducers made of up to three layers were built and characterized using interferometric measurements on 256 points of the upper surface element, at frequencies ranging from 20 kHz to 400 kHz. Their corresponding farfield acoustic output was also measured. Using a least-square optimization scheme in the frequency domain, the parameters of the dynamic coupled models were found. First, the parameters of a single layer model were identified. Subsequently, these results were utilized as initial guess for the identification of the two and three-layers transducers.

Results

In spite of the anisotropy of the ferroelectret films and the measured inhomogeneity of the upper layer vibratory pattern, the average frequency response of the transducers in air is fairly well predicted with the electromechanical models developed. Estimation errors of less than 3 dB were obtained.

Discussion and Conclusions

The inner two layers of PP enclosing the air voids, along with the adhesive tapes used to built the prototypes, contribute to homogenize the vibratory pattern. The parameters obtained from the models identification can be directly related to the physical characteristics of the transducers: air void fraction, dynamic mass and stiffness, loss factor and thickness-extension resonances. Furthermore, preliminary results seem to indicate that by properly modifying the upper layer of a multilayer transducer it is possible to increase the acoustic bandwidth in the far field.

P3-T-08

Control of Ultrasound Direction with a Miniaturized Double-Transducer for Microwelding Applications

Michael Mayer¹, Peter Hess²; ¹University of Waterloo, Canada, ²Hess Innovation GmbH, Switzerland

Background, Motivation and Objective

Ultrasonic transducers have been used for many industrial tasks including welding and joining of various materials and products. In some of these joining applications, the direction in which the ultrasound vibrates determines the quality of the joint. The vibration should follow the direction of the work piece resulting in higher quality. To control the horizontal direction of a vibrating tool would be beneficial for e.g. the welding of fine wires in the thermosonic wire bonding process which is predominantly used to interconnect microsystems and microcircuits. As bonding wire diameters become smaller and smaller, directional variations become larger and larger with conventional unidirectional ultrasound, leading to suboptimal quality and delays in product miniaturization. It is the objective of this contribution to report on the optimization of a miniaturized ultrasonic double-transducer design to achieve complete control of vibration direction.

Statement of Contribution/Methods

A system with two piezo vibrators is designed using Ti as main material. The current amplitudes delivered to the piezos determine the desired vibration direction. A finite element (FE) model of the system calculates the harmonic frequency responses from 1 kHz up to 300 kHz. All resonances are determined and sorted according to their suitability for application. Geometrical parameters of the model are altered and the numerical analysis is repeated. The most suitable solution is determined and described. The interactions of the two vibrators are discussed, and a suitable control strategy to achieve any desired vibration direction is given. The results depend strongly on the damping ratio which was experimentally determined at one frequency and then assumed constant for all other frequencies. For this, the full-width at half-maximum of a Ti beam in resonance was measured and reproduced by a FE model of the same beam with adjusted damping ratio.

Results

The derived damping ratio is 0.0018 at 8 kHz. Several double-transducer designs were studied and compared with each other. There are 65 to 92 resonances per design. The optimized design fulfills a set of predefined conditions, measures $0.5 \times 2.0 \times 2.0$ mm, and has nine suitable resonances between 24.4 kHz and 232.3 kHz. For 232.3 kHz, the horizontal amplitude (HA) achievable with standard piezo-ceramic vibrators is 78 μm . The HA is 350 times higher than the vertical amplitude. The maximum von Mises stress in the system is below 51 MPa per micron HA.

Discussion and Conclusions

For the first time, the ultrasonic dynamics of a double-transducer design was studied and its parameters optimized with a FE model. The results suggest miniaturized high frequency transducers with directional control of the vibration are feasible. The directional control will lead to miniaturized products, while the miniaturized transducer design will lead to faster throughput in production by savings in dynamic mass.

P3-T-09

Toward more efficient matching layers for piezoelectric transducers

Franck levassort¹, Pierre Maréchal², Olivier Acher³; ¹Université François Rabelais, UMR Imagerie & Cerveau, INSERM U930, CNRS ERL 3106, Tours, France, ²Université Le Havre, LOMC, CNRS FRE 3102, FANO FR 3110, Le Havre, France, ³CEA DAM, Le Ripault, Monts, France

Background, Motivation and Objective

In ultrasonic medical imaging applications, piezoelectric transducers require inert layers or multilayers with specific characteristics to optimize the transmission coefficient toward the propagation medium in a large frequency range. This requirement of so-called "matching structure" is related to the physics of waves in layered media. In a former work, theoretical predictions concerning the ultimate properties of acoustical matching structures have been derived [1], following seminal work on the ultimate performance of multilayered electromagnetic absorbers. The purpose of this study is to evaluate the efficiency of matching layers that are commonly used in association with piezoelectric transducers and compare it to the ultimate performance of such structures.

Statement of Contribution/Methods

The so-called "harmonic" and "impulse" adaptation approaches were used to design different matching structures. They are made of several quarter-wavelength matching layers (from 1 to 4) between the piezoelectric (PZT) material and the propagation medium (water). Their reflection and transmission coefficients were computed with a one-dimensional model at normal incidence. The wideband performance of an antireflection matching structure was defined as an integral over a wide frequency band of a quantity related to the unwanted reflection between the PZT and water. Theoretical results have predicted that this quantity is bounded by a limit which has a simple expression. This limit is proportional to the surface mass of the structure divided by the acoustical impedance of the propagation medium.

Results

It is observed that as expected, the larger the mass of the matching structure, the larger the wideband performance. Two figures of merit were defined as the ratio of the wideband performance over the ultimate limit. Their values were reported for the different matching structures under investigation. Evolution of these parameters were studied as a function of the number of quarter-wavelength matching layers used.

Discussion and Conclusions

Results showed that relatively low values of these figures of merit were obtained with standard matching layers properties. As a consequence significant improvements can be expected through further design efforts. The present results can also be used to predict the mass of a matching structure as a function of the required bandwidth and residual reflection level.

[1] O. Acher, J.M.L Bernard, P. Maréchal, A. Bardaine, F. Levassort, "Fundamental constraints on the performance of broadband ultrasonic matching structures and absorbers", Journal of the Acoustical Society of America, Vol. 125(4), pp. 1995-2005, 2009.

A model for radial modes in a piezoelectric disc exhibiting non-uniform polarization: application to a bi-frequency transducer, method design, simulation and experiments.

Héctor Calás¹, Leslie Pérez-Fernández², Eduardo Moreno², Antonio Ramos¹, Jose. A Eiras³, ¹Instituto de Acústica, Spain, ²ICIMAF, Cuba, ³UFScar, Brazil

Background, Motivation and Objective

Piezoelectric ceramics are widely used in a variety of applications such as ultrasonic transducers, piezoelectric transformers, piezoelectric step motors and frequency control devices. Uniformly poled piezoelectric discs (UPDs) are the simplest configurations used for transducers, so their vibration characteristics are well known. On the other hand, some authors have applied non-uniformly poled discs (NUPDs) in applications like ultrasonic beam control. However, theoretical NUPDs behaviour is still poorly studied. In this contribution we present a model for radial modes in NUPDs.

Statement of Contribution/Methods

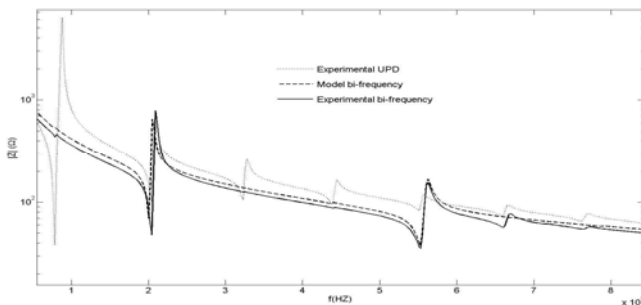
The proposed model is based in consider a linear relation between piezoelectric constants properties and the applied polarization function. An inhomogeneous first-order Bessel motion differential equation was obtained, and which is solved making an expansion of the polarization function in Fourier-Bessel series. Analytical expressions for radial displacements and for electrical impedance have been obtained. A method for applying this model to the control of radial modes is presented.

Results

In order to test the suitability of the model, this is applied for tow cases: a uniform poled piezoelectric disc and a Bessel transducer. The proposed model is particularly useful to study systems with piecewise constant polarizations functions. In addition, the model provides the possibility of designing the polarization function needed to obtain a particular electrical response. The model potentiality is shown by designing and constructing a bi-frequency radial transducer, using ceramic (PZT 53/47+1w% Nb). Major surfaces were parcelled into ring-like zones, which were covered by silver electrodes and then independently poled varying the percent of the applied field. The saturation poling field applied to electrodes was 3 kV/cm .

Discussion and Conclusions

In figure, the comparison between impedance frequency responses, for the bi-frequency and UPD transducers is shown. The theoretically predicted radial modes in our design are in good agreement with the experimental results. To conclude, we have proposed a model to describe the electromechanical behaviour of radial modes in NUPDs and a method for its application to control the frequency occurrence of radial modes.



Session Chairs

Addison, Bob.....	4H	Lerch, Reinhad.....	3A
Basset, Olivier.....	P3-H	Li, Pai-chi.....	P2-D
Bezdek, Michal.....	P2-H	Lockwood, Geoff.....	6G
Bhave, Sunil.....	6J	Lu, Jian-yu.....	P1-D
Bouakaz, Ayache.....	2E	Maev, Roman.....	4K
Brown, Jan.....	P2-J, P2-L	Mansfeld, Georg.....	6I
Cain, Charles.....	1F	Matula, Tom.....	1A
Caliendo, Cinzia.....	P3-K	McAleavey, Stephen.....	P1-H
Chapelon, Jean-Yves.....	P3-E	McCann, Donald.....	4C
Clement, Greg.....	P2-B	Miller, James.....	3F, 3H
Cloutier, Guy.....	P2-7	Miyashita, Toyokatsu.....	6H
Cochran, S.....	5K	Nakamura, Kentaro.....	P3-I
Dayton, Paul.....	1B	Nakamura, Nobutomo.....	P1-O
de Jong, Nico.....	2F	Nightingale, Kathy.....	P2-E
de Korte, Chris.....	1J	Nikolov, Svetoslav.....	2K
Demirli, Ramazan.....	P2-I	O'Brien, William.....	2J
Deng, Cheri.....	P1-C	Oelze, Michael.....	P3-A
D'Hooge, Jan.....	P1-G	Olsson, Roy.....	P1-L
Ebbini, Emad.....	2B, P2-A	Oralkan, Omer.....	5J
Emelianov, Stanislav.....	1H	Oruklu, Erdal.....	P1-K
Evans, David.....	P1-F	Palmeri, Mark.....	P3-F
Fattinger, Gernot.....	5E	Pappalardo, Massimo.....	4E
Feld, Dave.....	P2-P	Pensala, Tuomas.....	P2-O
Feld, David.....	P2-K	Pereira da Cunha, Mauricio.....	5G
Fink, Mathias.....	1E	Pitschi, Maximilian.....	P3-Q
Foster, Stuart.....	2D	Plesski, Viktor.....	P1-T
Furgason, Eric.....	4F	Pozhar, Vitold.....	P2-M
Greenleaf, James.....	1K	Proklov, Valeriy.....	P3-M
Greve, David.....	4B	Reindl, Leo.....	5F, P1-R
Haeggstrom, Edward.....	4A	Reynolds, Paul.....	5H
Hall, Anne.....	2H	Roh, Yongrae.....	3B
Hall, Timothy.....	3D	Ruppel, Clemens.....	5A, P3-R
Hall, Christopher.....	P2-C	Safafi, Ahmad.....	P1-U
Hoskins, Peter.....	P3-C	Saniie, Jafar.....	P1-I
Hossack, John.....	3G	Sboros, Vasilis.....	P1-B
Hynynen, Kullervo.....	1G	Schafer, Mark.....	P2-Q
Insana, Michael.....	1I	Schmitz, Georg.....	1C, P2-F
Jensen, Jorgen.....	3I	Shafer, Mark.....	P2-R
Kaitila, Jyrki.....	P2-N	Shung, Kirk.....	P3-S
Kanai, Hiroshi.....	P3-G	Sinha, Bikash.....	6D
Kanda, Takefumi.....	6E	Smith, Scott.....	5I
Kessler, Larry.....	P1-J	Suzuki, Atsuyuki.....	P1-P
Ketterling, Jeff.....	P1-A	Tanter, Mickael.....	3E
Khelif, Abdelkrim.....	6A	Thomas, Tom.....	P3-B
Khuri-Yakub, Pierre.....	4I	Thomenius, Kai.....	2I
Kim, Eun Sok.....	6C, P3-N	Tittman, Bernhard.....	P3-J
Kolios, Michael.....	2G	Torp, Hans.....	P1-E
Konofagou, Elisa.....	2C	Tortoli, Piero.....	2A, P3-D
Kupnik, Mario.....	4D	Trahey, Gregg.....	3K
Kuypers, Jan.....	5D, P1-Q	Tsujino, Jiromasu.....	6K
Lakin, Ken.....	5C	van der Steen, Ton.....	1D
Larson, John D.....	6B, P1-M	Vetelino, John.....	4G
Laude, Vincent.....	6F, P3-O	Wagner, Karl.....	5B
Laugier, Pascal.....	3J	Wang, Ji.....	P1-N

Weigel, Robert.....	P1-S, P3-P	Yuhas, Donald E.	PS
Wilcox , Paul	4J		
Yong , Yook-Kong.....	P3-L		
Yuan , Jian	3C, P3-T		

Author Index

- A**
- Aase, Svein Arne P1-G-01, P3-B-09
 Abbott, Ben 5B-4
 Abd Allah, Mohamed 5D-3
 Abdallah, Walid P1-C-03
 Achenbach, Jan 6I-2
 Acher, Olivier P3-T-09
 Adam, Dan P1-G-09
 Adamowski, Julio Cezar 4H-3
 Adamson, Rob 2D-1, P1-D-01
 Adibi, Ali 6H-1, 6H-4
 Adler, Andy P3-F-06
 Ageba, Ryo P1-U-09
 Agrawal, Dinesh 3A-2
 Aguilera, Teodoro 4J-4
 Agyem, Kwesi 2K-1
 Ahn, Dong-Ki P1-D-02
 Aigner, Robert 5E-4, P-S-6
 Akao, Shingo P3-I-05, P3-I-07
 Akil, Mariam P1-M-05
 Akiyama, Iwaki P3-S-05
 Al Mahrouki, Azza 2C-5, 2J-3
 Albertini, David P2-J-02
 Aleksandrov, Kirill P1-N-01, P1-N-02
 Alekseev, Sergey 6D-6
 Alessandrini, Martino P3-H-01
 Ali Bláhová, Ilona P2-L-05
 Alkoy, Sedat 5H-3, P1-U-20
 Allah, Mohamed Abd P-S-5
 Allemann, Pierre P1-H-02
 Allen, Jason 1J-5
 Allen, John S. 1B-2
 Alles, E.J. P1-N-11
 Alnot, Patrick P1-S-02
 Alqadah, Amel F. 1E-4
 Alsebai, Abubakr 2A-2
 Alshits, Vladimir 6I-5
 Alvarez, Fernando J. 4J-4
 Amador, Carolina 3E-5
 Amalou, Farid 6G-6
 Ambroziak, Andrzej P1-N-09
 Amman, Jean-Jacques P2-C-08
 Amundsen, Brage 2H-1, 3F-3,
 An, Liwei 3G-1
 Anastasiadis, Pavlos 1B-2
 Anaye, Anass P1-B-08
 Ancey, Pascal P3-K-03
 Anderson, Christian 3H-2
 Anderson, Christopher 1A-1
 Anderson, Janelle J. P2-G-05, P2-G-06
 Anderson, Tom P1-B-01, P1-G-03, P2-C-05
 Andle, Jeffrey 4C-5, P3-I-11
 Andreano, Anita 1I-3, 1I-6
 Angelini, Elsa P1-H-09
 Angelsen, Bjorn 2A-4, 2I-5
 Angelsen, Bjørn P3-C-10
 Anisimkin, Vladimir P3-L-06
 Antonov, Sergey P2-M-02
 Aoki, H P3-I-02
 Aota, Yuji P2-P-02
 Arakawa, Mototaka 4K-3, 4K-6, 6I-4,
 P1-M-01, P1-M-06
 Arapan, Lilia 5D-2
 Arbeit, Jeffrey 2K-1
 Arca, Ahmet P2-R-01
 Ardanuc, Serhan 6C-2
 Arditi, Marcel 1A-5, 2E-5, 2F-3, P1-B-08
 Arendt Jensen, Jørgen 3B-5, P3-D-05
 Arger, Peter 3G-4, P1-B-10
 Arif, Muhammad P1-A-04
 Aristizabal, Orlando 2D-2
 Armentano, Ricardo P3-G-02
 Arnaud, Caroline 5D-4
 Arnold, W. P1-J-11
 Asada, Takaaki P2-G-02
 Asami, Rei 1G-3, 2B-4, P1-B-12, P2-A-09
 Ashkenazi, Shai 1H-2
 Aslan, Semih P2-I-03
 Assouar, Badreddine 5G-3, 6F-2, P1-R-04,
 P1-S-02
 Astafiev, Konstantin P1-U-08
 Atalar, Abdullah 3C-4, 5J-1, P2-Q-05
 Aubert, Thierry P1-S-02
 Aubry, Jean-François 1E-3, 2B-1, 2F-1,
 2H-3, 2K-6
 Audière, Stéphane P1-H-09
 Austeng, Andreas 2I-1, P3-C-06, P3-C-09
 Averkiou, Michalakis 2E-3
 Avramov, Ivan 5D-2
 Awad, Samer P2-D-06
 Ayala, V. Carolina P3-I-03
 Azuma, Takashi 2B-4, P1-B-12, P2-A-09
- B**
- Ba, Maguette 1J-2, 3F-5
 Bachner, Noa P1-G-09
 Baclet, Pierre P2-O-01
 Bader, Bernhard P2-N-03
 Bae, Moo-Ho P1-D-02, P1-D-08
 Bae, Unmin 1I-5
 Bæk, David 3B-5
 Baek, Eunsol P2-A-07
 Baghai-Wadji, Alireza 5B-6, P3-R-01,
 P3-R-02, P3-R-03
 Baida, Fadi 6F-4
 Bailey, Michael 1B-4, 1F-2, 1F-4, 2B-6,
 2J-1, P2-R-05, P-S-1

Baker, Sara	3G-5	Bercoff, Jeremy	1K-1, 1K-5, P1-H-04
Bakulin, Eugene	P3-A-10	Berg, Sigrid	5J-2
Balakshy, Vladimir	P3-M-02	Berganzo, Javier	P3-I-15
Balantekin, Mujdat	5J-4, P-S-8	Berggren, Michael	2G-5
Baldwin, Jeffrey	6J-3	Bergman, Rudolf	P2-L-03
Bäle, Rudolf	P3-O-02	Bergonzo, Philippe	5G-3
Ballandras, Sylvain	5C-2, 5G-2, 5G-3	Bernal, Maria-Pilar	6F-4
Ballard, John	1E-2	Bernal, Miguel	1K-4
Bamber, Jeffray	3D-5, 6G-5, P1-C-06, P3-F-05	Bernard, Dulmet	P2-O-09
Bamber, Jeffrey	3E-6, 6G-2, P3-F-02	Bernard, Jean-Edouard	P2-Q-09
Bance, Manohar	2D-1, P1-D-01	Bernard, Olivier	P3-H-01
Banelli, Paolo	P3-D-07	Bernassau, Anne	6G-2, 6G-6
Banks, Robert	P3-T-03	Bernassau, Tanne	P3-T-04
Bannouf, Souad	2F-1	Berry, Gearoid	P3-F-05
Bantignies, Claire	P3-S-07	Beryzoa, Sergey	P3-M-04
Banys, Juras	5I-2	Bessonova, Olga V.	2B-6
Bar, Pierre	5D-4, P1-Q-02, P2-J-03	Bettinger, Thierry	P1-B-03
Barbier, Daniel	P2-J-02	Bharat, Shyam	1I-3
Barbosa, Daniel	2H-1, 3F-3, P1-G-04	Bhargava, Samarth	6C-3
Bardong, Jochen	5D-5, P1-S-05	Bhattacharjee, Kushal	P3-P-06
Barker, Alex	3I-2, P3-H-03	Bhav, Sunil	P-S-9
Barkmann, Reinhard	3H-5	Bhave, Sunil	6B-4, P2-O-03
Barthe, Peter G.	1E-4	Bia, Daniel	P3-G-02
Basarab, Adrian	3F-1, P1-D-07	Biagi, Elena	2A-6
Baseri, Babak	2C-2	Bigelow, Timothy	P2-G-05, P2-G-07
Bashford, Greg	P1-F-03, P2-F-02	Bigler, Emmanuel	P1-J-07
Basrou, Skandar	P2-J-03	Billard, Christophe	5D-4, P1-Q-02, P2-J-03
Basset, Olivier	1C-2, P1-D-07, P3-H-01, P-S-16	Biolluz, Nathalie	P1-B-03
Bassignot, Florent	5G-2	Biryukov, Sergey	5B-3, 5F-3, P2-O-10
Bastard, Cécile	P1-H-03, P1-H-06	Bittencourt Machado, Christiano	P3-A-04
Basto, Rodrigo	P3-H-05	Bjåstad, Tore Grüner	3I-3, P1-E-07
Battais, Amélie	2C-3	Blaak, S.	P1-D-06
Bauer, Adam	3H-2	Blalock, Travis	2A-5
Baumgartel, Lukas	P2-N-01	Blanc, Laurianne	4C-1
Bavencoffe, Maxime	6A-3	Blanco, Alfonso	P3-L-05
Bavu, Eric	P1-H-04	Blomberg, Ann E. A.	P3-C-06
Baxter, Laurie	3G-1	Blum, Daniel	P1-S-04
Beach, Kirk	P3-B-12	Boch, Anne-Laure	2B-1
Beard, Paul	5H-2	Boctor, Emad	P2-D-07
Bednarik, Michal	P1-N-04, P3-O-04	Boedecker, Sebastian	6B-4, P-S-9
Bedorf, D.	P1-J-11	Boissiere, Cedric	4C-1
Behler, Russell	P2-E-04, P3-D-02, P3-G-01	Boltryk, Rosie	4A-5, P2-L-01, P2-O-01
Bel, Alain	1J-2, 3F-5	Borden, Mark	2C-2, 2F-4
Bellenger, Nick	3I-2	Bornmann, Peter	P1-U-09
Belsito, Luca	2A-6	Bosch, J.G.	P1-D-06, P1-G-11
Belt, Lin	2E-4	Boser, Bernhard	3A-5
Ben Hassine, Nizar	P2-J-03, P2-P-04	Bosisio, Matteo	P1-H-03
Ben Salem, Abderraouf	3F-1	Bost, Wolfgang	1H-4
Benhabane, Sarah	5G-1, 6B-1, 6F-4	Bouakaz, Ayache	2E-1, P1-A-01, P1-A-03, P1-A-09, P2-B-01, P2-B-07, P2-C-07
Bender, Michael	P1-U-03, P1-U-03	Bouchard, Richard	1J-5, P2-E-01, P2-G-04
Benech, Nicolás	P3-E-02, P3-G-02	Bougrioua, Zahia	5A-2
Bénédic, Fabien	5G-3	Bouma, Brett	1H-5
Benedito, J.	P3-J-01	Bournebe, Zoumnone	P1-S-02
Benetti, M.	P3-P-03	Bouvot, Laurent	P1-S-02
Bennett, David	3K-1, P2-Q-10	Bouzitoune, Razika	P3-A-02
Bennett, Michael	P1-G-03	Boye, A. John	P2-F-02
		Bozkurt, Ayhan	5J-1, P2-Q-04

Cheng, Xiaoyu P2-J-06
 Cheng, Ya-Jian 2K-2
 Chenot, Jeremy 1I-4
 Cherin, Emmanuel 5K-1, P3-T-05
 Chertov, Andriy P1-K-04, P1-N-09
 Cheung, Chris C. P. P2-D-02
 Cheung, Dave K. H. P2-D-02
 Chhith, Saosometh P3-T-01
 Chiang, Yuan-Feng 4C-2, 5G-5
 Chien, Allen 5E-2
 Chiesa, Alberto 1I-5
 Chih-Chung, Huang 2D-4
 Chin, Chien Ting 1A-1, 1F-3, P2-B-02
 Chitnis, Parag P2-A-06, P2-C-04
 Chiu, Chun-Yi 2J-6
 Chiu, Harry C. T. P2-D-02
 Chiu, Yi-Yuan P1-A-06
 Chivukula, Venkata P-S-13
 Cho, Jeong P1-E-08
 Cho, Seung Hyun P2-R-04
 Cho, Yasuo P3-Q-03
 Choi, Hon Fai P1-F-02, P1-G-04
 Choi, James 2C-2
 Choi, Joyce P2-D-07
 Choi, Kyusun 6G-3, P3-T-04
 Choi, Yoon Young P1-U-10
 Christiansen, Mark P3-B-12
 Chuang, Shih 6D-2
 Chung, Cheng-Hsien 4B-2
 Churgin, Matthew 5H-4
 Chusov, I.I. P3-P-03
 Cinthio, Magnus 2H-2, 3I-6
 Ciplys, Daumantas P2-K-05, P-S-13
 Clark, Matt 4K-2, P2-R-01
 Claus, Piet 2H-1, 3D-3, 3F-1, 3F-3, P1-F-02, P1-G-04
 Clement, Marta P2-N-04, P2-P-03
 Cleveland, Robin P2-R-05
 Cloutier, Guy 2G-4, 3K-5, P3-H-04
 Cobbold, Richard P2-E-06
 Cochard, Etienne 1E-3
 Cochran, Sandy 2D-6, 6G-2, 6G-5, 6G-6, P3-T-04
 Coelho De Albuquerque Pereira, Wagner P3-A-04
 Coghill, Peter P2-H-07
 Cohen, Ivan 3D-6
 Cohen-Bacrie, Claude 2H-3
 Collado, Carlos 5E-4, P-S-6
 Collet, Bernard P3-L-03
 Combe, Suzanne 5G-4
 Conant, Emily 3G-4
 Coron, Alain 1C-3
 Corona, E. P3-J-01
 Cosgrove, David 1D-1
 Couade, Mathieu 1J-2, 3F-5
 Coulouvrat, Francois P2-M-01
 Courjon, Emile 5G-2

Couture, Olivier 1F-6, 2F-1, P1-B-06
 Crescenti, Remo 3E-6
 Cristman, Paul 5J-5
 Crosby, Jonas 3F-3
 Cross, Joshua 6J-3
 Crum, Lawrence 2B-6, 2J-5, P2-A-01
 Culjat, Martin 3K-1, P2-Q-10
 Cunitz, Bryan 1F-2
 Cunningham, John 4A-4
 Cunningham, Samantha 3K-3
 Czarnota, Gregory 2C-5, 2J-3, P2-B-04

D

D'Hooge, Jan 3D-3
 Dahl, Jeremy 1J-5, P2-G-01, P3-B-08
 Daigle, Ron P1-E-06
 Dalen, Håvard P1-G-01, P3-B-09
 Daniel, Tim 5B-4
 Danilouchkine, Mike 2K-4, P-S-16
 Danilouchkine, Mikhail 1J-1, P1-G-11
 Dann, Aaron 3K-1, P2-Q-10
 Danworaphong, Sorasak 6B-1
 Daridon, Jean Luc P1-M-03
 Darinskii, Alexandre P1-R-01
 Date, Munehiro P1-U-06
 Dauchy, Florent 6G-2, 6G-5
 Davies, Alexander 4A-4
 Dawson, Andrew 6I-3, P2-G-08
 Dayton, Paul A-4, 2F-2, 2J-2, 5K-1, P1-B-11, P1-C-02, P2-C-02, P2-E-01, P-S-3
 De Buyzere, Marc P3-G-05
 de Jong, N. P1-D-06, P1-N-06
 de Jong, Nico 1B-1, 2E-2, 2K-4, P1-B-02, P1-G-11, P2-C-01, P2-C-03, P-S-11, P-S-16
 de Korte, C.L. 3D-2, 3F-6, P3-F-04
 de Korte, Chris 1J-4, P3-G-04
 De Marchi, Luca P1-J-06, P2-F-14
 De Santis, Michele P1-I-05
 De Schryver, Thomas P3-G-05
 Defay, Emmanuel P2-J-02, P2-P-04
 Defontaine, Marielle 2E-1, 3H-3, P3-I-01
 Degertekin, F. Levent 2I-4, 4I-5, 5J-4, P1-D-03, P-S-8
 Dehghan, Ehsan 3K-2
 Deibebe, Jochen M. 2A-4, 2I-5
 Dejous, Corinne 4C-1
 Delachartre, Philippe 3F-1, P1-D-07
 Demi, L. P1-N-06
 Demirli, Ramazan P1-K-01
 Demore, Christine 6G-2, 6G-5, P3-T-04
 Dencks, Stefanie 3H-5
 Deng, Cheri 1G-1
 Deng, Cheri X. 2D-5
 Dentinger, Aaron 3F-4, P-S-2
 Dermitzakis, Aris P1-A-12
 Derouiche, Badreddine P2-I-02

Feng, Guanping4C-6, P3-I-08
 Fenger, Steffen P3-J-10
 Ferin, Guillaume P3-S-06
 Ferin, Guillaume P3-S-07
 Fernandez, Anna 1I-5
 Fernandez, LuisP3-I-15
 Ferrara, Katherine 1E-6, P2-A-11
 Ferreira, Manoel P3-A-01
 Feshitan, Jameel 2C-2, 2F-4
 Feuillard, Guy6G-4
 Finfer, Daniel 2E-06
 Fink, Mathias1E-1, 1F-6, 1I-1, 1J-2,
 1K-1, 1K-5, 2B-1, 2F-1, 2H-3, 2I-3, 2K-6,
 3D-6, 3F-5, P1-B-06, P1-H-04, P2-M-01
 Fisher, Melrose P2-E-04
 Fisher, Rayette P3-S-01
 Fleischman, Aaron P2-G-03, P3-D-01
 Flynn, David6G-6
 Flynn, John P1-E-06
 Foiret, Josquin P1-B-09, P2-F-06
 Fokin, Andrew P2-J-04
 Folks, Karri 2E-4, P1-H-05
 Fonfara, Heinrich 1H-3
 Fong, Hoi Yan 5A-6
 Foppen-Harteveld, Miranda 1B-1
 Foster, F. Stuart 1A-4, 2F-2
 Foster, Stuart 1A-3, 2F-3, 2H-4, 5K-1,
 P3-T-05
 Fotiadis, Dimitrios P3-D-12
 Fournelle, Marc 1H-3, 1H-4
 Fournier, Celine P1-H-01
 Fowlkes, J. B. 1C-5
 Fowlkes, J. Brian 1F-4, 1G-4, 2B-5, 3I-5,
 P-S-1
 Fox, Paul P3-C-12
 Francalanci, Lorenzo 3I-6
 Franceschini, Emilie 2G-4
 Francischelli, David P1-C-01
 Frank, Gary 2D-3, 3D-4
 Franke, Heinz P3-M-07
 Franosch, Martin 5E-6
 Franz, Georg 5B-1
 Fraschini, Christophe 1K-5
 Freear, Stephen 4A-4
 Freear, Steven P1-A-04, P2-F-03, P2-R-02
 Frey, Tim 3A-5
 Friboulet, Denis 3F-1, P3-H-01
 Friedrich, Claus-Stefan 1H-1
 Friend, James 4A-2, 4A-3, 4J-6, 5A-4
 Frijlink, Martijn P3-C-03
 Frinking, Peter 1A-5, 2E-5, 2F-3, P1-B-08
 Frinkley Bing, Kristin 1E-5
 Fritsch Yusta, Carlos 4H-2
 Fritsch, Carlos 2I-2, 4B-5, 4H-3
 Fritze, Holger P1-S-03
 Fromageau, Jeremie 3D-5, P3-F-02, P3-F-05
 Fuhrhop, Ralph 2K-1
 Fujihara, Yoko P1-H-08

Fujii, Yosuke 6E-2
 Fujikura, Kana 3E-1
 Fujikura, Takashi 5C-2
 Fujishima, Ichiro P2-R-03
 Fujiwara, Masaki P3-D-08
 Fukada, Eiichi P1-U-06
 Fukunishi, Yuji 4G-3
 Fulford, Jonathan 3I-2
 Fuller, Michael 2A-5
 Furuya, Mio P2-G-02

G

Gachagan, Anthony3B-6, P1-U-15, P3-J-06,
 P3-T-03
 Galarza, Nekane P2-H-02
 Galaz, Belfor P2-C-08
 Gallego-Juarez, Juan Antonio P3-L-05
 Gallimore, Dana P-S-15
 Gallippi, Caterina P2-E-02, P2-E-04,
 P2-E-05, P3-D-02, P3-G-01
 Gamble, Kevin 5B-4
 Gao, Hang 3F-1, P1-F-02
 Garcia, Damien 3I-1
 Garcia, Julien 5G-2
 Garcia, Leo 3D-5, P3-F-02
 Garcia-Gancedo, Luis 6G-2, 6G-5, P3-T-04
 Gaska, Remis P-S-13
 Gates, Fred P3-J-07, P3-J-09
 Gates, Phillip 3I-2
 Gaud, Emmanuel 2E-4, 2F-3
 Gautier, Brice P2-J-02
 Ge, Li-Feng P3-T-06
 Gebauer, Bernhard 5E-6
 Gedge, Michael 4A-5
 Geertz, Lut P3-B-12
 Gelat, Pierre 3B-1
 Gelehrter, Sarah 2C-4
 Gennisson, Jean-Luc 1I-1, 1K-1, 3D-6,
 P1-H-04, P2-M-01
 Gentilini, Cristina P2-F-14
 Geon, Sa-Gong P1-O-03, P1-O-04
 Gerhardt, Nils C. 1H-1
 Gerlach, Gerald P3-S-08
 Gesset, Céline 5G-3
 Gessner, Ryan 1A-4, 2F-2, P1-B-11
 Ghanem, Alexander P2-B-02
 Ghosh, Sourav 4C-3
 Ghoshal, Goutam P2-A-12
 Giannantonio, Doug 3F-2
 Giannoula, Alexia P2-E-06
 Gibson, Allyson 2G-3
 Gilbert, Stephen 5E-1
 Gilbert, Steve 5E-2
 Giles, Anoja 2C-5, 2J-3, P2-B-04
 Gilgenkrantz, Hélène P1-H-03
 Gil-Pelegrin, Eustaquio 4J-2
 Girault, Jean-Marc P1-A-09, P3-D-03

Girkin, John	2D-6
Giroux, Marie-France	P3-H-04
Gløersen, Per	P1-U-07
Glorieux, Christ	P1-N-08
Glüer, Claus	3H-5
Glushkov, Dmitry	P1-R-06
Glynne-Jones, Peter	4A-5, P2-L-01, P2-O-01
Goertz, David	1F-5, 1G-2
Goettler, Drew	6H-2
Goksel, Orcun	P3-D-11
Gol, Cem	P1-U-20
Gomes, Richard	P3-I-11
Gomez Fifer, Carlen	2C-4
Gomez, Tomas	4J-2, P3-I-15, P3-J-01
Gómez-Ullate Ricón, Yago	P2-M-05
Gonzalez, Iciar	P3-I-15
Gorelik, Alexander	4G-5
Gorelikov, Ivan	1A-3
Gorzkowski, E. P.	P1-U-19
Goto, Nobuo	P3-M-03
Goto, Rei	5A-1, P3-P-04
Gourrier, Aurelien	3J-1
Gouws, Gideon	P2-G-08
Grajal, Jesús	5A-2
Gramma, George	5G-4
Gran, Fredrik	2I-1, P1-E-04
Grandoni, Andrea	P3-S-03, P3-S-09
Grant, Gerald	5K-6
Gratier, Julien	5B-4
Greenleaf, J.F.	P1-H-07
Greenleaf, James	1K-4, 2A-1, 3E-2, 3E-5, P3-G-03, P-S-12
Greve, David	6C-3, 6C-5
Griesmar, Pascal	P3-I-04
Griggio, Flavio	6G-3
Grigoriev, Mikhail	P2-J-05
Grigorievsky, V.I.	P3-Q-04
Grimal, Quentin	3H-6, 3J-6, P2-F-06, P2-F-09, P2-F-12
Grizzle, William	2E-4
Groby, Jean-Philippe	6F-6
Grondin, Julien	3J-6, P2-F-09
Grundfest, Warren	3K-1
Grundfest, Warren	P2-Q-10
Guðbjörnsson, Sigmar	P1-U-07
Guerard, Sandra	3H-3
Guerrero, Héctor	P2-P-01
Guerrero, Julian	P3-H-02
Guevara, Jorge	P3-T-07
Guhr, Glen	4D-6
Guidi, Francesco	P2-C-03
Guillaume, Patrick	P2-F-06
Gulyaev, Yu.V.	P3-P-03
Guofeng, Shen	P2-A-04
Gurm, Hitinder S.	2C-1
Gurun, Gokce	2I-4, 5J-4, P-S-8
Gusev, Vitalyi	6A-1
Guyomar, Daniel	4I-1

H

Haak, Alexander	P2-G-05, P2-G-06
Hachiya, Hiroyuki	P3-B-06
Hackenberger, Wesley	5I-4
Haddad, Jehuda	P2-L-03
Haeggström, Edward	P1-I-06
Haeggström, Edward	P1-J-08, P1-K-02, P3-J-03
Haeggström, Edward	P3-J-07
Haeggström, Edward	P3-J-08
Haeggström, Edward	P3-J-09
Hafes, Zachary T.	P2-G-05
Hafez, Zachary T.	2G-2, P2-G-06
Hagege, Albert-Alain	1J-2, 3F-5
Hagelauer, Amelie	P2-N-03
Hägglund, Fredrik	P1-K-05
Hahn, Stephan A.	1B-3
Haiat, Guillaume	3H-6, P2-C-08
Hall, Anne L.	3I-5
Hall, Christopher S.	P2-B-02
Hall, James S.	4H-5
Hall, Timothy	1I-6, 2G-2, 2G-6, 3D-1, 3D-4, 3G-5, P2-G-05, P2-G-06, P3-A-08
Halvorsen, Einar	P1-U-18
Ham, Jeong-Ho	P1-D-08
Hamel-Nunes, Jonathan	3I-1
Han, Pengdi	5I-3, 5I-5
Han, Sukgu	3K-3
Han, Tao	P1-T-03, P1-T-05
Hanai, Kunihiko	P1-J-10
Handtmann, Martin	5E-6
Hansen, Christian	3G-6
Hansen, H.H.G.	P3-F-04
Hansen, Hendrik	1J-4, P3-G-04
Hansen, Karsten	P1-U-08
Hansen, Kristoffer L.	P1-E-04
Hansen, Rune	2A-4, 2I-5
Hara, Motoaki	5C-5
Harada, Hiroshi	P2-O-02
Harb, Rony	3H-3
Harkness, Patrick	P2-M-03, P2-M-04
Harput, Sevan	4A-4, P2-F-03
Harris, George	5A-3
Harris, Nicholas Robert	P2-H-06
Harris, Nick	P2-O-01
Harris, Paul	6I-3, P2-G-08
Hartenbach, Ellen	P1-H-10
Harter, Josephine	2G-6, P1-H-10, P3-A-08
Hartogh, Paul	P3-Q-04
Harvey, Phoebe	3G-4
Hasegawa, Hideyuki	P3-G-06
Hashiba, Kunio	3C-3
Hashimoto, Ken-Ya	4E-4, 5A-1, 5E-3, 5F-5, P1-Q-01, P1-Q-03, P-S-17
Hashimoto, Makoto	4E-4, P1-U-01
Hashimoto, Masahiko	P3-I-12
Hashizume, Hiromichi	4E-5

Haskell, Reichl	4C-5, P3-I-11	Holland, Mark	2G-3, 3H-2
Hasler, Paul	2I-4, 5J-4, P-S-8	Hollenhorst, Markus	3G-6
Hassan, Mawia	P1-D-04	Holley, Greg	3F-2
Hata, Masaki	1C-3	Hollister, S. J.	1C-5
Hattel, Author	P1-C-01	Hollman, Kyle	1C-5
Haugaard, Per	P1-F-01	Holm, Sverre	2I-1, P3-C-06, P3-C-09
Hauptert, Sylvain	P1-B-09, P3-J-02	Holmes, Jeffrey W.	P1-G-10
Hauptmann, Peter	4I-5	Holmgren, Olli	P1-Q-04
Hauser, Robert	5B-1	Homma, Shunichi	2F-4
Haworth, Kevin	1G-4	Honda, Hisato	P3-I-06
Hayward, Gordon	3B-2, 3B-6, 4F-4, 5H-1, P1-U-15, P3-T-03	Hong, Jongin	P1-U-10
He, Shitang	P1-T-01	Hori, Yuji	P3-P-01
He, Zhaojian	P1-L-03	Horinaka, Hiromichi	P3-B-05
Hecht, Ulrike	4K-4	Horiuchi, Shulei	P3-I-06
Heckel, Thomas	P3-J-10	Horsley, David	3A-5
Hehn, Michel	P1-S-02	Hosokawa, Atsushi	P2-F-10
Helge Gilja, Odd	P1-A-10	Hossack, John	1A-1, 1A-2, 2A-5, 5K-3, P-S-19, P-S-7
Hemmsen, Martin Christian	P1-F-01	Hotta, Kohei	P2-L-04
Hendriks, Ad	2F-5	Hou, Zhilin	6F-2, P1-R-04
Hendy, Amr	P1-D-04	Houston, Brian	6J-3
Henn, Gudrun	P2-N-03	Hover, Franz	P3-O-05
Hensel, Karin	1B-3, P3-D-09	Hoyt, Kenneth	2E-4, 3G-1, P1-H-05
Herd, Maria-Teresa	P2-G-05, P2-G-06	Hozumi, Naohiro	P1-J-10, P3-A-03
Hergum, Torbjørn	3I-3, P1-E-07	Hristova, Krasimira	2H-1, 3F-3, P1-G-04
Herickhoff, Carl	5K-6	Hruska, David	P3-A-12
Hess, Peter	6D-4, P3-T-08	Hsu, Ke-Hsin	P2-D-01
Hettiarachchi, Kanaka	P1-C-02, P2-C-02	Hsu, Po-Hong	P2-B-03
Heuser, Lothar	3G-6	Hsu, Stephen	1J-5, P2-G-01, P2-G-04
Hewener, Holger	1H-3	Hu, Changhong	P3-B-11
Hibbs, Kathryn	P2-C-06	Hua, Chenhui	P3-I-13
Higuti, Ricardo T.	P1-D-05, P1-J-02	Huang, Chih-Chung	6K-4
Hikino, Osamu	5F-4	Huang, Chih-Yung	4C-2
Hikita, Mitsutaka	P3-I-02	Huang, Dejin	P2-J-07
Hill, Jamie	4A-5	Huang, Kai	P2-F-11
Hill, Martyn	4A-5, P2-L-01, P2-O-01	Huang, Kang-Che	5A-5
Hillenbrand, Joachim	3A-3	Huang, Lingyun	1H-2, 1J-3, P1-G-08
Hiraizumi, Y	P3-I-02	Huang, Sheng-Wen	1H-2, 1J-3, P1-G-08
Hirao, Masahiko	4G-3, P3-K-01, P3-K-02	Huang, Tony	6H-5
Hirawa, Shungo	P2-L-01	Huang, Y.H	P2-Q-07
Hirooka, Daisuke	P1-P-02	Huang, Yan	4K-5
Hirson, Desmond	2F-3, 5K-1	Huang, Yan-Ping	P2-F-04, P3-A-11
Hiruma, Yuji	3A-1	Hubmayr, Rolf	3E-2
Hladky-Hennion, Anne-Christine	6A-3, 6F-6, 6H-6, P1-U-12	Huetting, Ray	P2-N-02
Ho, Eddie	4F-4	Hughes, Adam	4A-5
Ho, Jen-Huan	4J-3	Hughes, David Allan	2D-6
Ho, Shine-Tzong	6C-4	Hughes, Michael	2K-1, 2K-2
Hobson, Maritza	P1-H-10	Huijssen, J.	P1-N-06
Hoffman, Joseph	2G-3	Huisman, H.J.	3F-6
Hoffmeister, Brent K.	3H-1	Humayun, Mark	P1-C-03
Hofmann, Martin R.	1H-1	Hummels, Donald	5A-3
Hohkawa, Kohji	P1-O-05	Hurrell, Andrew	5H-2
Hohkawa, Koji	P3-R-04	Hutson, David	6G-2, P3-T-04
Hök, Bertil	P1-U-07	Hüttebräuker, Nils	3G-6
Holdsworth, David	P1-F-05	Hynnen Kullervo	5K-5
Holfört, Iben K.	P1-E-04	Hynnen, Kullervo	1A-3, 1F-5, 1G-2, 2A-3, P2-A-10
Holfört, Iben Kraglund	2I-1		

I

Ibáñez Rodríguez, Alberto	4H-2
Ibáñez, Alberto	4B-5, 4H-3
Iborra, Enrique	5E-4, P2-N-04, P2-P-03, P-S-6
Ichihara, Takashi	P3-N-05
Ida, Yasuyuki	P3-Q-05
Idzenga, Tim	P3-G-04
Igarashi, Juei	4D-1
Ihara, Ikuo	6K-3
Ilic, Bojan	6J-3
Imperatori, Patrizia	P1-O-01
Infantosi, Antonio	P3-H-05
Ingram, Pier	2H-6
Inoguchi, Hiroaki	P1-B-04
Insana, Michael	1I-2, 3E-3
Ionescu, Radu	4F-1
Iradji, Sara	2J-3
Irie, Takasuke	P2-D-05
Ishibashi, Satoshi	P3-B-05
Ishino, Yuji	P1-P-05
Ito, Toshio	4E-5
Ito, Yu	P1-P-06
Itoh, Kouichi	P2-D-05
Iula, Antonio	P1-I-05
Ivancevich, Nikolas	P1-F-06
Iwaki, Masafumi	5E-3
Iwamoto, Takahiro	P3-A-03
Iwamoto, Takuya	P3-I-12
Iwasaki, Yasunori	P3-P-01
Iwashina, Tomoyuki	P3-B-06
Izbicki, Jean-Louis	6A-3
Izumi, K.	1C-5
Izumi, Kentaro	6C-1
Izyumin, Igor	3A-5

J

J. Vos, Hendrik	P1-B-02
Jackson, Thomas	6G-3
Jackson, Tom	P3-T-04
Jafari, Sara	P1-B-09
Jaiswal, Devina	P1-C-01, P2-A-02
Jakob, Anette	P1-U-02, P1-U-03
Jamin, Yann	P2-A-05
Jamneala, Tiberiu	5E-1, 5E-2
Jan, Jiri	P3-B-01
Jansman, André	5C-4, P2-N-02
Jansson, Tomas	2H-2
Jantunen, Heli	P1-U-07
Janvier, Marie-Ange	3K-5
Jayadewa, Chaturika	P2-A-05
Jean-Baptiste, Legland	P2-H-09
Jeffrey, R Brooke	P2-Q-02
Jen, C.-K.	4B-3, 5H-5
Jen, Cheng-Kuei	4E-1, P-S-4
Jensen, Are Fritz Charles	P3-C-09
Jensen, Henrik	P3-D-05

Jensen, Jørgen A.	2I-1, P1-E-04, P1-F-01, P3-C-06
Jeong, Eui-Hwan	P3-N-03
Jeong, Jong Seob	5K-4
Jeong, Mok-Kun	P1-D-02, P1-D-08
Jerez-Hanckes, Carlos	5G-6
Jerome, Maisonnet	P2-O-09
Ji, Xiaojun	P1-T-03
Jia, Congxian	1H-2, 1J-3, P1-G-08
Jiang, Jingfeng	1I-3, 1I-6, 3D-1
Jiménez, Antonio	P3-T-07
Jingfeng, Bai	P2-A-04
Jin-Gyou, Kim	P1-O-03
Jirik, Radovan	P1-A-10, P3-B-01
Joblot, Sylvain	5D-4, P1-Q-02
Johannes, Ludger	P1-B-06
Johansen, Tonni F.	2A-4, 2I-5
Johansson, Linda	4A-6
Johansson, Stefan	4A-6
Johnson, Paul A.	P3-J-02
Johnson, Steven	2G-5
Jonathan, Mamou	2D-2
Jones, Robert	4A-5
Jose, Sumy	P2-N-02
Joseph, Jean	3G-1
Joshi, Shrinivas	P1-J-03
Josse, Gwendal	P3-E-03
Jou, Jwo Ming	P3-N-01, P3-N-02
Joung-Young, Sug	P1-O-03, P1-O-04
Ju, Byeong Kwon	6E-3
Judy, Michael	3A-5
Jung, Woo-Suk	6E-5
Jun-Tak, Lee	P1-O-03, P1-O-04
Jun-Yong, Choi	P1-O-03, P1-O-04
Juuti, Jari	P1-U-07

K

K. Kirk, Shung	2D-4
Kaczkowski, Peter	1F-2, 2J-5, P1-E-06, P2-A-01
Kaczmarek, Mariusz	P2-F-13
Kadah, Yasser	2A-2, P1-D-04
Kaddur, Kadija	P1-A-01, P2-B-01, P2-B-07
Kadota, Michio	P3-Q-03, P3-Q-05
Kadota, Yoichi	P1-U-09
Kahl, A.	P1-J-11
Kaitila, Jyrki	5D-3, P-S-5
Kaivola, Matti	P1-Q-04
Kakio, Shoji	P3-P-05
Kameda, Suguru	P2-P-02
Kamel, Aissous	P2-K-03
Kamiyama, Naohisa	P3-B-06
Kamogawa, Naoko	5F-4
Kanai, Hiroshi	P1-G-07, P3-G-06
Kananen, Ville	P3-J-03
Kanda, Takefumi	6C-6, P1-P-02, P3-N-05

Kaneko, Yuriko	P3-I-12	Kim, Jeesu	5C-1
Kang, Along	P1-T-05	Kim, Jongdae	P2-H-04
Kang, Chong Yun	6E-3	Kim, Jung-Hoon	5C-1
Kang, Chong-Yun	4I-2, 6E-4, 6E-5	Kim, Jungsoon	P1-P-07
Kang, Seong-Hwa	P3-N-03	Kim, Moojoon	P1-P-07
Kang, Shih-Tsung	P1-N-05	Kim, Sangwon	P1-E-05
Kapusta, L.	3F-6	Kim, Shin-Sung	P1-U-16
Karabutov (Jr.), Alexandr	P1-I-04	Kim, Yohan	2C-4
Karabutov, Alexandr	P1-I-04	Kim, Yongmin	P3-B-12, P3-B-13, P3-B-14
Karadayi, Kerem	P3-B-14	Kim, Yoon Young	P2-R-04
Karaman, Mustafa	2I-4, 5J-4, P1-D-03, P-S-8	Kimura, Tetsuya	P3-Q-05
Karanian, John	1I-5	Kinai, Tetsuya	P3-I-06
Kardous, Faten	P3-I-14	King, Daniel	P1-B-09
Kargl, Steven	2J-5	King, Michael	2G-6, P2-G-06
Karloff, Anthony	P1-K-04	Kinnick, Randall	3E-2
Karmonik, Christof	P2-B-05	Kirk, Katherine	P1-U-16
Karppinen, Timo	P3-J-07, P3-J-08	Kirkhorn, Johan	3I-3
Karshafian, Raffi	1G-2, 2C-5, 2J-3, P2-B-04, P2-B-08	Kiss, Gabriel	2H-1, 3F-3, P1-G-02
Kartadjev, Ilia	5G-3	Kitajima, Msayuki	P3-R-05
Karunakaran, Chandra Priya	1E-4	Kiwitt, Jürgen	5F-1
Kashiwa, Keisuke	P1-Q-01	Klibanov, Alexander	1A-1, 1A-2, 1F-3
Kaste, Sue C.	3H-1	Kliwer, Mark	P1-H-10, P3-A-08
Katarjev, Ilia	4A-6, 5D-2	Klimonda, Ziemowit	P3-D-06
Kato, Yasuhiro	P1-P-05	Ko, Herb	5C-1
Katus, Philip	P2-N-05	Kobari, Kentaro	P3-I-07
Kaul, Roger	P2-O-03	Kobayashi, Akihito	6C-6
Kaupang, Halvard	P3-C-10	Kobayashi, Kazuto	P1-J-10, P3-A-03
Kawabata, Kenichi	P1-B-12	Kobayashi, M.	4B-3, 5H-5
Kawabata, Ken-Ichi	1G-3, 2B-4, P2-A-09	Kobayashi, Makiko	4E-1, P-S-4
Kawabe, Masahiko	P2-F-01	Kobayashi, Takashi	3C-3
Kawachi, Osamu	5F-2, P3-R-05	Kobayashi, Hiroki	P3-P-01
Kawai, Yuki	P3-I-07	Koch, Christian	6B-5
Kawasaki, Hiraku	P1-I-02	Koch, Robert	5F-1
Kay, Matthew	P1-B-07	Kocimski, Janusz	P1-N-09
Kaya, M.Yunus	5H-3	Kodama, Hidekazu	P1-U-06
Kaya, Mehmet	P2-C-02	Koh, Keishin	P1-O-05, P3-R-04
Kazdailis, Paulius	P2-K-05	Kohl, Yvonne	1H-4
Kerkhof, Peter	P3-S-03, P3-S-09	Koizumi, Takaaki	3J-4
Ketterling, Jeffrey	2D-2, P2-C-04, P2-R-05	Kok, Swee Leong	P2-H-06
Khelif, Abdelkrim	6B-1, 6H-1, 6H-4	Kokkonen, Kimmo	5C-4, 5G-1, 6B-3, P1-Q-04
Khelladi, Hassina	P1-M-03	Kolar, Radim	P1-A-10
Khokhlova, Vera A.	2B-6	Kolias, Theodore	1J-3
Khuri-Yakub, Pierre T.	3F-4, 5J-5, P2-Q-02, P2-Q-03, P-S-2	Kolios, Michael	1C-4, 2G-1, P3-A-07
Kielczynski, Piotr	P1-M-02	Kondo, Kengo	P3-B-04, P3-F-01
Kilappa, Vantte	P2-F-08	Kondo, Seima	5F-4
Kilroy, Joseph	5K-3, P-S-7	Kondo, Takanori	P1-M-06
Kim, Eun Sok	P2-N-01	Kondoh, Jun	4A-1, P1-P-08
Kim, Eung-Hun	P3-B-12	Konicek, Petr	P1-N-04, P3-O-03, P3-O-04
Kim, Hong Jin	P2-R-04	Konofagou, Elisa	2C-2, 2C-6, 3E-1, P1-G-10
Kim, Hyung Ham	6G-1, P3-S-04	Konyashkin, Aleksei	P2-K-04, P2-K-06
Kim, Hyung-Chan	4I-2	Kooiman, Klazina	1B-1, P1-B-02
Kim, Hyun-Hoo	P1-P-01	Kook, Taeho	5B-4
Kim, Hyunsoo	6G-3, P3-T-04	Kornegay, Joe	P2-E-02
Kim, Insoo	6G-3, P3-T-04	Korsten, Erik	2F-5
Kim, Jaegeun	P3-I-10	Kosec, Marija	6G-4
		Kotani, Hiroyuki	6E-2, P1-P-03

Kourai, Yuusuke	61-4
Koyama, Daisuke	P1-P-06, P2-H-05, P2-L-06
Koymen, Hayrettin	3C-4, 5J-1, P2-Q-05
Kozlov, Anton	61-1
Kozlovski, Nikolai	P1-K-06
Kozyrev, Andrei	P1-O-02
Kraft, Martin	P1-S-05
Kraglund Holfort, Iben	P3-C-06
Kreider, Wayne	2J-1, P2-R-05
Kremer, Florence	3D-3, P1-F-02
Krempel, Sandro	P1-P-09
Kreutzbruck, Marc	P1-J-04
Kripfgans, Oliver	1G-4, 3I-5
Kristoffersen, Kjell	P1-E-07
Kruecker, Jochen	1I-5
Kruger, Marco Antonio	P2-G-09
Kruse, Dustin	1E-6, P2-A-11
Kuc, Roman	4J-4
Kudo, Nobuki	P1-A-11
Kuehnicke, Elfgard	P3-S-08
Kuennen, Maarten	2F-5
Kukic, Aleksandra	5K-5
Kulakova, Liudmila	P2-K-01
Kulig, Kornelia	P2-F-02
Kumar, Kishore	P3-E-01
Kumaradas, J. Carl	2G-1
Kumon, Ronald E.	2D-5
Kuo, S.	1C-5
Kupnik, Mario	P2-Q-03
Kuroda, Tsuyoshi	6E-2
Kurosawa, Minoru	6E-1
Kusakabe, Koichi	P3-K-01
Kuscer, Danjela	6G-4
Kushibiki, Jun-Ichi	4K-3, 4K-6, 6I-4, P1-M-01, P1-M-06
Kustron, Pawel	P1-N-09
Kuznetsova, Iren	P1-J-03
Kwon, Sung-Jae	P1-D-02
Kybic, Jan	3K-4

L

Lading, Lars	P1-L-05
Lai, Chun-Yen	1E-6, P2-A-11
Lal, Amit	6C-2
Lallart, Mickael	4I-1
Lamberti, Nicola	P1-P-04
Lampaskis, Marios	2E-3
Lancée, C.T.	P1-D-06
Lanning, Craig	3I-2, P3-H-03
Lanza, Gregory	2K-1, 3H-1
Laprad, Adam	P3-B-15
Laptyeva, Tetyana	P2-M-06
Laroche, Thierry	5G-2
Larrat, Benoit	1E-1, 2B-1
Larson Iii, John	5E-1
Larsson, Matilda	3D-3
Laude, Vincent	5G-1, 5G-6, 6A-5, 6B-1, 6F-4, P1-R-04
Laugier, Pascal	1C-3, 3H-2, 3H-4, 3J-1, 3J-2, 3J-3, 3J-6, P2-F-06, P2-F-09, P2-F-12, P2-F-13, P3-A-02, P3-A-04, P3-J-02
Lavarello, Roberto	2G-5, P1-I-03
Lawrence, Michael	1A-1, 1K-3
Le Clezio, Emmanuel	6G-4
Le Huerou, Jean-Yves	P3-I-04
Le Khanh, Hung	P1-U-12
Leach, Martin	P2-A-05
Leblois, Therese	P1-J-07, P1-M-05, P3-Q-06
Lecarpentier, Frederic	6I-3
Lediju, Muiyinat	P1-G-06
Lee Jr, Fred	1I-3
Lee, Abraham P.	P1-C-02, P2-C-02
Lee, B.S.	4I-3
Lee, C.K.	4I-3
Lee, Chih-Kung	4H-6, 4J-3
Lee, Fred	1I-6
Lee, Han-Woo	P1-D-08
Lee, Hua	3K-1, P2-Q-10
Lee, Hyuntaek	P2-D-03
Lee, Jaejin	P1-E-08
Lee, Jungwoo	3B-3
Lee, Michael	3K-1
Lee, Mike	1A-4, 2F-2, 5K-1, P3-T-05
Lee, Paul	3G-3, P2-C-04, P2-R-05
Lee, Ruyue	4C-2, 5G-5
Lee, Sang Kyun	P2-H-04
Lee, Siao-Song	2J-6
Lee, Sung Q.	P2-H-04
Lee, Susung	P3-T-02
Lee, Taek-Joo	P3-I-10
Lee, Wei-Ning	3E-1, P1-G-10
Lee, Won Hee	6E-3
Lee, Wonseok	P3-T-02
Lee, Yung-Chun	4B-2
Legros, Mathieu	P3-S-06
Lehnert, Tobias	P1-U-03
Lemor, Robert	1H-3, 1H-4, P1-U-03
Lenoir, Olivier	6A-4
Lenz, Michael	P3-S-08
Lerch, Reinhard	3A-4, 3B-4
Lerouge, Sophie	3I-1
Leseman, Zayd	6H-2
Lethiecq, Marc	6G-4, P1-U-12
Leung, K Y Esther	P1-G-11
Leung, Wallace W. F.	5J-6
Levassort, Franck	P1-U-12, P3-T-09
Levitsky, Semyon	P2-L-03
Lewandowski, Marcin	P2-D-04, P3-D-06
Ley, Klaus	1A-1
Li, Faqi	P1-C-07
Li, Hongyun	P1-T-03
Li, Jianbao	P1-L-02
Li, Jing	6H-3
Li, King	P2-B-05

Li, Meng-Lin P3-C-11
 Li, Minghui 4F-4
 Li, Pai-Chi 2F-6, P1-B-05, P2-D-01,
 P3-D-04
 Li, Qian 2H-6
 Li, Wenqi 4K-2
 Li, Yong 6F-2
 Liang, Kaicheng 3K-6
 Liao, Ai-Ho 2F-6, P1-B-05
 Liao, Yin-Yin P3-H-06
 Liebgott, Herve 3K-4
 Liebgott, Hervé 3F-1, P1-D-07
 Lieu, Victor 5K-2
 Light, Edward 3K-6, 5K-2, 5K-6, P1-F-06
 Lim, Jong-Nam P1-P-01
 Lim, Kee-Joe P1-P-01, P3-N-03
 Lim, Soo-Cheol P3-I-10
 Lin, Angel P2-O-04
 Lin, Angel T-H 4D-3
 Lin, Chia-Yu 4J-3
 Lin, Der-Song P2-Q-02
 Lin, Jiming P1-R-03
 Lin, S.C. 4I-3
 Lin, Sz-Chin 6H-5
 Lin, Yi-Hsun 6K-4
 Lin, Yu-Ting 6C-4
 Lindner, Gerhard P1-P-09
 Lindsey, Brooks P1-F-06
 Lindström, Kjell 2H-2
 Lindvere, Liis 2H-4
 Linfield, Edmund 4A-4
 Linkhart, Ken P1-E-06
 Lin-Schmidt, Xiefan 1K-3
 Linstrom, Kristopher R. P2-F-02
 Lipiäinen, Lauri P1-Q-04
 Lipscomb, Glenn 6K-2
 Lisenkov, Ivan 6F-3
 Litniewski, Jerzy P3-D-06
 Liu, Changgeng P2-Q-08
 Liu, Dalong 2B-2, P3-E-04
 Liu, Hao-Li P2-B-03
 Liu, He P1-U-18
 Liu, Jiansong P2-J-07
 Liu, Mengyang 5H-4
 Liu, W.-L. 5H-5
 Liu, Zhengyou P1-L-03
 Lloyd, Joseph 4D-5
 Lobo, Elizabeth 2J-2, P-S-3
 Lockhart, Mark 2E-4
 Loeckx, Dirk 2H-1, 3F-3, P1-G-04
 Löfqvist, Torbjörn 6K-1
 Logan, Andrew 5J-3
 Lohse, Detlef 2E-2
 Lomonosov, Alexey 6D-4
 Longbottom, Chris 2D-6
 Longo, Roberto P2-F-06
 Looney, Pdraig P2-C-05
 Lopata, R.G.P. 3D-2, 3F-6, P3-F-04

Lopata, Richard 1J-4, P3-G-04
 Lovstakken, Lasse 3I-3, 3I-4
 Løvstakken, Lasse P1-E-07
 Lu, Jian-Yu 6K-2
 Lu, Jimmy 2C-4
 Lu, Yufeng P2-I-04, P3-J-05
 Lucas, Margaret P2-M-03, P2-M-04
 Lucklum, Ralf 6H-3
 Ludomirsky, Achiau 2G-3
 Lugovaya, Maria P1-U-17, P2-A-08,
 P3-A-06
 Lukacs, Marc 1A-4, 2F-2, 5K-1, P3-T-05
 Luo, Jianwen P1-G-10
 Luo, Jun 5I-4
 Lutchen, Kenneth P3-B-15
 Lynnworth, Lawrence 4D-2

M

Ma, Te-Jen 5J-5
 Ma, Tingfeng 4C-6, P3-I-08
 Macé, Emilie 3D-6
 Machado, Christiano Bittencourt P3-A-02
 Machi, Junji 1C-3
 Machida, Shuntaro 3C-3
 Madden, John 3G-2
 Madsen, Ernest 2D-3, 3D-4, P2-G-05,
 P2-G-06
 Maeda, Hiraku 6C-6
 Maennicke, Nils P3-A-05
 Maev, Roman Gr. P1-K-04, P1-N-09,
 P3-B-03
 Maeva, Anna P3-A-10
 Maggi, Luis P2-G-09
 Maghnouj, Abdelouahid 1B-3
 Mahajan, Aman 3F-4, P-S-2
 Mahloojifar, Ali 2I-6
 Mahue, Veronique P1-A-02
 Majumdar, Arnab P3-B-15
 Makin, Inder Raj S. 1E-4
 Maleke, Caroline 2C-6
 Mallet, Vincent P1-H-04
 Malocha, Donald P1-K-06, P3-I-09
 Malocha, Svetlana P3-Q-02
 Malyarenko, Eugene P3-B-03
 Mamou, Jonathan 1C-3, P2-A-06, P2-C-04,
 P3-B-06
 Managuli, Ravi P3-B-13, P3-B-14
 Manceau, Jean-François P3-I-14
 Mansfeld, Georgy 6D-6
 Mante, Pierre-Adrien P3-K-03
 Mantsevich, Sergey P3-M-02
 Maréchal, Pierre 6A-4, P3-T-09
 Maresca, David P2-C-01
 Mari, Jean Martial P1-A-02
 Marie, Yannick 2B-1
 Marion, Adrien P3-B-10

Author
Index

Mark S., Humayun	2D-4	Medicken, Norman.....	P1-B-01, P1-G-03
Marksteiner, Stephan.....	P2-N-03	Mcgann, Jason.....	4C-4
Marsac, Laurent.....	2H-3	Mcgloughlin, Tim.....	P2-E-07
Marsh, Jon.....	2K-1	Mclaughlan, James.....	P2-A-05, P2-A-06
Martin, Carlos J.....	P1-D-05	Mclean, Donald A.....	P3-C-04
Martin, Guenter.....	5F-3	Meneilly, Alan.....	2E-3
Martin, Yves.....	2H-3	Medina, Lucia.....	P1-N-07
Martinez, Loïc.....	P1-N-08, P3-I-04	Meggs, Carl.....	P3-T-04
Martinez, Oscar.....	P1-D-05	Mehi, James.....	2F-3
Marushyak, Alexander.....	P1-N-01, P1-N-02	Meijer, G.C.M.....	P1-D-06
Marutyan, Karen.....	3H-2	Melodelima, David.....	11-4, 2C-3, P1-C-06
Maruyama, Kazuo.....	P1-A-11	Meltaus, Johanna.....	5C-4
Marvel, Skylar.....	2J-2, P-S-3	Ménigot, Sébastien.....	P1-A-09, P3-D-03
Marzani, Alessandro.....	P1-J-05, P1-J-06, P2-F-14	Menon, Manoj.....	P2-E-03
Masetti, Guido.....	2A-6	Mensur Alkoy, Ebru.....	5I-1, P1-U-11
Masotti, Leonardo.....	2A-6	Mercier, Denis.....	P2-J-03
Masoy, Svein-Erik.....	2A-4, 2I-5	Mercier, Laurent.....	P1-B-08
Masson, Jeremy.....	5C-2	Merkel, Aurélien.....	6A-1
Mast, T. Douglas.....	1E-4	Merrick, Elizabeth.....	P3-D-02, P3-G-01
Mastik, Frits.....	1J-1	Messas, Emmanuel.....	1J-2, 3F-5
Masuda, Hiroshi.....	P1-E-01	Meulendyk, Bennett.....	P-S-18
Masuyama, Hiroyuki.....	P1-I-01	Meunier, Jean.....	P3-H-04
Mathias, Fink.....	1E-3	Meuwly, Jean-Yves.....	P1-B-08
Mathieson, Andrew.....	P2-M-04	Meyer Jr., Richard J.....	P1-C-04
Mathieu, Jérôme.....	P1-K-03	Meynier, Cyril.....	3C-1
Matsuda, J.....	P3-I-02	Meziati, Nawal.....	P3-D-03
Matsuda, Osamu.....	5C-2, 6B-1, 6B-2	Meziri, Mahmoud.....	P3-A-02, P3-A-04
Matsukawa, Mami.....	3J-4, 6D-1, P2-F-01, P2-F-07, P2-F-09, P2-G-02, P2-O-08, P-S-14	Michau, Stéphane.....	P3-S-07
Matsumoto, Yoichiro.....	1G-3	Mienkina, Martin P.....	1H-1
Matsumura, Takeshi.....	P1-H-08, P2-O-02	Miette, Veronique.....	P1-H-01
Matsunaka, Toshiyuki.....	P3-B-05	Miette, Véronique.....	P1-H-09, P3-A-09
Matsuoka, Naoki.....	P1-C-03	Mikhailov, Anatoly.....	P1-O-02
Matsuura, Naomi.....	1A-3	Miles, Richard.....	3D-6
Matsuyama, Tetsuya.....	P3-B-05	Miller, James.....	2G-3, 3H-2
Matte, Guillaume.....	2K-4	Miller, Naomi.....	P1-C-06
Matthews, Glenn.....	P3-R-01	Miller, Rita J.....	2G-2
Mathies, Klaus.....	P1-J-04	Milner, Jaques.....	P1-F-05
Matula, Thomas.....	1B-4, 2J-1	Milyutin, Evgeny.....	P2-O-06
Matusin, Daniel.....	P3-A-01	Minamide, Akiyuki.....	P3-J-04
Mauchamp, Pascal.....	P3-S-07	Minonzio, Jean-Gabriel.....	3J-2, 3J-3
Mauldin, Elizabeth.....	P2-E-05	Mischi, Massimo.....	2F-5
Mauldin, Jr., F William.....	1K-3, P3-F-03	Mitake, Tsuyoshi.....	P1-H-08
Maxwell, Adam.....	1F-1	Mitri, Farid G.....	P1-H-07
Maxwell, Adam D.....	1F-4, 2C-1, P-S-1	Mitsui, Takeshi.....	P3-P-05
Mayer, Andreas.....	6D-4	Mitton, David.....	3H-3
Mayer, Elena.....	P1-R-02	Miwa, Takashi.....	P1-B-04
Mayer, Markus.....	5A-6, 5B-6, P1-R-05	Miyamoto, Atsushi.....	P-S-14
Mayer, Michael.....	4K-5, P3-T-08	Miyamoto, Takashi.....	5F-5
Mazeika, Dalius.....	P3-N-08	Miyashita, Toyokatsu.....	6F-1
Mazzaro, Luciano.....	3I-2, P3-H-03	Miyazaki, Yasumitsu.....	P3-M-03
Mc Sweeney, Sean G.....	P2-I-05	Mizuno, Katsunori.....	P2-F-07
Mcaleavey, Stephen.....	1K-6, 3E-4, P2-E-03, P2-E-08	Mizuno, Takashi.....	6C-6, 6E-2, P1-P-03
Mccann, Donald.....	4G-4	Mizuno, Takeshi.....	P1-P-05
Mccarthy, John.....	2K-1	Mizutani, Keiichi.....	4F-5
Mccormick, Matthew.....	2D-3	Mizutani, Koichi.....	4D-1, 4F-5, P1-I-01, P1-L-01
		Mjølstad, Ole Christian.....	P1-G-01, P3-B-09
		Mleczko, Michal.....	2K-5

Mofid, Yassine P1-H-09
 Mohamed, Elhassan 2A-2
 Mohammadi, Saeed 6H-1, 6H-4
 Mohammadzadeh Asl, Babak 2I-6
 Moilanen, Petro P2-F-05, P2-F-08
 Moleró, Miguel P1-N-07
 Montag, Hans-Joachim P3-J-10
 Montaldo, Gabriel 1E-1, 1K-5, 2F-1, 2I-3
 Montealegre Rubio, Wilfredo P1-U-21,
 P3-N-04
 Monteiro, Elisabeth P2-G-09
 Montero De Espinosa, Francisco 4E-3,
 P2-M-05
 Montonen, Leone P1-I-06
 Montonen, Risto P3-J-08
 Moon, Seung Eon P2-H-04
 Moonlight, Thomas P-S-15
 Mooshofer, Hubert 4I-5
 Moosmann, Katrin P3-I-03
 Morad, Grimes P2-K-03
 Moradi, Mehdi 3K-2, P3-H-02
 Moran, Carmel P1-B-01, P1-G-03
 Moreno, Eduardo P2-H-02, P3-T-10
 Moreschi, Hélène 2E-1, 3H-3, P3-I-01
 Morgan, David 5B-2
 Mori, Riccardo P2-C-03
 Morin, Pierre P3-K-03
 Morisato, Naoki P2-O-08
 Morita, Takeshi P1-U-09
 Moriya, Akira P3-R-05
 Moriya, Tadashi P2-D-05
 Morris, Paul 5H-2
 Morris, W. J. 3K-2
 Morvan, Bruno 6F-6
 Mosse, Ryan P1-C-04
 Mouchet, Mathilde 3J-1
 Mouraviev, Vladimir 3G-2
 Mozhaev, Vladimir 6I-1
 Mrasek, Heinz P1-J-04
 Mueller, Sebastian P1-H-01
 Mukundan, Srinivasan 5K-6
 Mulholland, Anthony J. P1-U-15
 Muller, Marie P2-C-01
 Mullin, Lee P1-B-11
 Mulvana, Helen P1-A-07
 Mung, Jay 3K-3, P2-D-06
 Muradoglu, Murat 5B-6
 Murakoshi, Terumichi 6K-6
 Muralidharan, Khrishna 6H-6
 Muralt, Paul P2-O-06
 Murray, Todd P2-A-06
 Murray, Victor 3B-2
 Murta, Luiz P3-H-03
 Mustonen, Kimmo P3-J-08
 Mutamba, Kabula 5E-6
 Mutton, Mark 4D-5
 Myasnikov, Daniil P2-K-04, P2-K-06

N

Nadimi Astaneh, Hasan P1-C-05
 Nagahara, Hidetomo P3-I-12
 Nagai, Hiroki P3-I-05
 Nagai, Hironao 4G-3
 Nagata, Hajime 3A-1
 Nagatani, Yoshiki P2-F-07
 Naili, Salah 3H-6
 Nakagawa, Yasuhiko P3-P-05
 Nakamura, Hiroyuki 5A-1, P3-P-04
 Nakamura, Kentaro P1-P-06, P2-H-05,
 P2-L-06, P3-S-05
 Nakamura, Mitsuru 6E-2
 Nakamura, Nobutomo P3-K-01, P3-K-02
 Nakanishi, Hidekazu 5A-1, P3-P-04
 Nakashima, Takeo P3-K-02
 Nakaso, Noritaka P1-T-02, P3-I-05,
 P3-I-07
 Nakatsuji, Tomohiro 3J-4
 Nalpas, Bertrand P1-H-04
 Nam, Kibo P2-G-05, P3-A-08
 Nam, Sahn 6E-4
 Napel, Sandy P2-Q-02
 Nasedkin, Andrey P1-U-17, P2-A-08
 Nasholm, Sven Peter 2A-4, 2I-5
 Naumenko, Natalya 5B-4, P3-P-02
 N'Djin, William 2C-3, P1-C-06
 Need, Daniel 3F-2
 Needles, Andrew 2F-3
 Negreira, Carlos P3-E-02, P3-G-02
 Nenadic, Ivan P-S-12
 Neubig, Bernd 5D-1, 5D-1
 Nguyen, Long P3-I-11
 Nguyen, Man P2-D-06
 Nguyen, Thu-Mai 1K-1
 Nichols, Timothy P2-E-04, P3-D-02,
 P3-G-01
 Nielsen, Espen P1-G-02
 Nielsen, Michael B. P1-E-04
 Niemi, Jan 6K-1
 Nightingale, Kathryn 1E-5, 1K-2, 3G-2
 Nikitov, Sergey 6F-3
 Nikkel, Phil 5E-1
 Nikolov, Svetoslav Ivanov P1-F-01
 Nikoozadeh, Amin 3F-4, P-S-2
 Nillesen, M.M. 3F-6, P3-F-04
 Nilsen, Carl-Inge Colombo P3-C-09
 Nilson, Daniel P1-L-05
 Nilsson, Tobias 2H-2
 Nishihara, Tokihiro 5E-3
 Nishimiya, Kojiro 4F-5, P1-L-01
 Nishizawa, Toshio 5F-2
 Nitta, Naotaka P1-E-01
 No, Kwangsoo P1-U-10
 Noble, Alison P2-C-06
 Nokrashy, Ahmed 2A-2
 Novell, Anthony 2E-1, P1-A-03, P1-A-09

Nowicki, Andrzej P2-D-04, 3-D-06
 Nunan, Kieran 3A-5
 Nylund, Kim P1-A-10
 Nymes, Siri Ann 3I-3

O

O'Donnell, Matthew 1H-2, 1J-3, 3F-4, P-S-2
 O'Leary, Richard L. 3B-6
 Obata, Kazuya P2-B-06, P2-L-02
 O'Brien, Jr., William D. 2G-2, 2G-6,
 P2-G-06, P3-A-12
 O'Brien, William P1-B-09, P2-G-05
 Octavio, Alberto P1-D-05
 O'Donnell, Matthew P1-G-08
 Oelze, Michael P2-A-12
 Oelze, Michael 2G-2, 2G-5, 2G-6, P1-I-03,
 P2-G-06, P3-A-12
 Ogami, Takashi P3-Q-03
 Ogawa, Nobuo P2-M-10
 Ogi, Hirotsugu 4G-3, P3-K-01, P3-K-02
 Ogi, Tsuneo P1-T-02
 Oguz, Huseyin P2-Q-05
 Oguz, Kagan 5J-1
 Oh, Jin-Heon P1-P-01, P3-N-03
 Ohara, Yoshikazu 4E-4, P1-U-01
 Ohashi, Yuji 4K-6, 6I-4
 Ohbuchi, Takeshi P1-I-01, P1-L-01
 Ohmiya, Masaki P2-H-03
 Ohtake, Naoto 6E-2
 Ohtori, Norikazu P2-F-01
 Oiler, Jonathon P2-O-07
 Oita, Takeo 6J-1
 Okada, Nagaya P3-A-03
 Okada, Tetsuo P2-L-01
 Okitsu, Hiroyuki P3-R-04
 Okubo, Kan P1-N-03, P2-H-03, P3-D-08,
 P3-N-06, P3-S-02
 Olafsson, Ragnar 2H-6
 Olcum, Selim 3C-4, 5J-1, P2-Q-05
 O'Leary, Richard L P1-U-15, P3-J-06,
 P3-T-03
 Oliva Uribe, David P2-M-09
 Olivares, Jimena P2-N-04, P2-P-03
 Olofsson, Tomas 4D-4
 Olsson Iii, Roy 6J-2
 Olsson, Roy 6H-2, P2-O-05
 Omnes, Frank 5G-3
 Omori, Tatsuya 5F-5, P1-Q-01, P1-Q-03,
 P-S-17
 O'Neill, Brian P2-B-05
 Ono, Satoru 5F-2
 Ono, Y 5H-5
 Ono, Yuu P3-F-06
 Oppenheim, Irving 6C-3, 6C-5
 Opretzka, Joern 2K-3
 Opretzka, Jörn P1-J-09
 Oralkan, Omer 3F-4, 5J-5, P-S-2

Oralkan, Ömer P2-Q-02
 Orderud, Fredrik 2H-1, 3F-3, P1-G-01,
 P1-G-02, P3-B-09
 Orescanin, Marko 1I-2, 3E-3
 O'Rorke, Richard 4A-4
 Oruklu, Erdal 4F-2, P2-I-03, P2-I-04,
 P3-J-05
 Oshiyama, Satoshi P1-O-05
 Osmanski, Bruno-Félix P1-H-04
 Ossant, Frederic P3-E-03
 Ostanin, Victor 4C-3
 Østbø, Niels P P1-U-07
 Otero, Jose A. P2-H-02
 Otis, Brian 5C-3
 Otsuka, Paul 6B-1
 Oudich, Mourad P1-S-02
 Oudry, Jennifer P1-H-02
 Oura, Soichiro P3-K-02
 Ouyang, Guangmin P1-U-18
 Overvelde, Marlies 2E2
 Oweis, Ghanem 1F-2
 Owen, Kevin 2A-5
 Owens, Gabe 2C-1

P

Padilla, Frédéric 3H-4, P2-F-13, P3-A-02,
 P3-A-04
 Paeng, Dong-Guk P1-C-03
 Pagnod-Rossiaux, Sylvie P1-B-03
 Paik, Dong-Soo 6E-4
 Pakula, Michal 3H-2, 3H-4, P2-F-12,
 P2-F-13
 Palanchon, Peggy P1-A-01
 Palmeri, Mark 1E-5, 1K-2, P2-E-01
 Palosaari, Jaakko P1-U-07
 Pan, Leo P3-B-02
 Pan, M. J. P1-U-19
 Pandey, Chandra Shekhar P1-M-04
 Pannacci, Nicolas 1F-6
 Papacharalambopoulos, Alexios P3-D-12
 Papila, Melih 5I-1
 Pappalardo, Massimo P1-I-05
 Parat, Guy 5D-4, P1-Q-02, P2-J-03
 Pardo, Emilia P2-I-01
 Park, Dae-Hee P3-N-03
 Park, Eun-Joo P1-C-01, P1-C-04, P2-A-02
 Park, Hyunkyu 3A-5
 Park, Jinhyoung P3-B-11
 Park, Kang-Ho P2-H-04
 Park, Kyoung-Su P3-I-10
 Park, No-Cheol P3-I-10
 Park, Yong Wook 6E-3
 Park, Young-Pil P3-I-10
 Parker, Katherine M. P1-G-10
 Parker, Kevin 3G-1
 Parmentier, Hubert 1I-4
 Parpia, Jeevak 6J-3

Parrilla, Montserrat.....2I-2, 4H-3
 Pasovic, Mirza1C-2, P-S-16
 Patat, Frédéric.....2H-5, 3C-1
 Patel, Mihir.....P3-P-06
 Patil, Abhay V.....5K-3, P-S-7
 Paulino, Glaucio H.....P3-N-04
 Pavan, Theo Z.....3D-4
 Payne, David.....5I-5
 Pedersen, Mads M.....P1-E-04
 Pedrós, Jorge.....5A-2
 Pekárek, Stanislav.....P3-O-02
 Pelekasis, Nikos.....P2-C-05
 Pennec, Yan.....6H-6
 Pennings, Ronald.....2D-1
 Pensala, Tuomas.....5C-4
 Pereira Da Cunha, Mauricio.....5A-3, 5B-5,
 P-S-15, P-S-18
 Pereira, Wagner.....P2-G-09, P3-A-01,
 P3-H-05
 Pérez Del Real, Rafael.....P2-P-01
 Pérez-Arjona, Isabel.....P1-L-06
 Pérez-Fernández, Leslie.....P3-T-10
 Périchon, Nicolas.....P1-H-02
 Pernod, Philippe.....P2-M-07, P3-O-01
 Pernot, Mathieu.....1E-1, 1I-1, 1J-2, 2B-1,
 2H-3, 3F-5
 Perois, Xavier.....5A-6
 Perrenoud, Geneviève.....P1-B-08
 Persson, Hans W.....2H-2
 Peter, Andreas.....P1-N-10
 Peterlik, Igor.....P3-B-01
 Peters, Christian.....4C-4
 Petherick, Russell.....6I-3
 Pethrick, Richard A.....P1-U-15
 Petit, David.....5D-4, P2-J-02
 Petit, Roger.....5G-2
 Peura, Marko.....P1-I-06
 Peyrin, Françoise.....3J-1
 Pflugrath, Lauren.....P1-E-06
 Pham Thi, Mai.....P1-U-12
 Pham, Thien-Ly.....3J-2
 Phillips, Linsey C.....1A-2, 5K-3, P-S-7
 Piazza, Gianluca.....4G-2, 6J-5, P3-K-04
 Picó, Rubén.....P1-L-06
 Pihl, Michael Johannes.....P1-F-01
 Pillai, Radhakrishna.....P1-B-03
 Pillen, S.....3D-2
 Pinton, Gianmarco.....2K-6, P2-M-01, P3-B-08
 Piron, Julien.....P2-B-01, P2-B-07
 Pitschi, Maximilian.....5F-1
 Plantier, Frédéric.....P1-M-03
 Plaza, José A.....P2-P-01
 Plessky, Victor.....P1-R-02, P3-Q-04
 Pochon, Sibylle.....1A-5, P1-B-03
 Poepping, Tamie.....P1-F-05
 Po-Hsiang, Tsui.....2D-4
 Pol, Stanislas.....P1-H-04
 Polascik, Thomas.....3G-2

Polcawich, Ronald.....6B-4, P2-O-03, P-S-9
 Polikarpova, Nataliya.....P3-M-05
 Pollard, Thomas.....5B-5
 Polpetta, Alessandro.....P3-D-07
 Polzikova, Natalia.....6D-6
 Popov, Roman.....6F-3
 Poppe, Erik.....P1-U-07
 Porter, Christopher.....3G-3
 Pospisil, Eric.....P3-B-16
 Powers, Jeffrey.....1A-5, P3-C-02
 Pozhar, Vitold.....P3-M-04, P3-M-06
 Prada, Claire.....1E-3
 Preobrazhensky, Vladimir.....P2-M-07, P3-O-01
 Prieto, Carlos.....P3-T-07
 Pritchard, William.....1I-5
 Profunser, Dieter.....5C-2, 6B-1, 6B-2
 Proklov, Valery.....P2-K-02
 Protopappas, Vasilios.....P3-D-12
 Provost, Jean.....3E-1
 Prucker, Oswald.....P3-I-03
 Prudan, Aleksandr.....P1-O-02
 Przybyla, Richard.....3A-5
 Ptashnik, Sergei.....P1-O-02
 Pulskamp, Jeff.....6B-4, P2-O-03, P-S-9
 Purchase, Thomas.....4A-5
 Pustovoit, Vladislav.....P3-M-04, P3-M-06
 Pye, Stephen.....P1-A-12
 Pylvov, Yuri.....P3-O-01

Q

Qayyum, Muqem.....1I-2
 Qi, Aisha.....4J-6
 Qiang, Bo.....2A-1, 3E-2
 Qifa, Zhou.....2D-4
 Qin, Yiqiang.....P2-J-08
 Qiu, Xiaotun.....P2-O-07
 Queste, Samuel.....5G-2

R

Radulescu, Emil.....P3-C-02
 Ræder, Henrik.....P1-U-07
 Raju, Balasundar.....1A-1, 1F-3
 Ramadas, Nishal S.....3B-6
 Ramadas, Sivaram Nishal.....P1-U-15, P3-J-06,
 P3-T-03
 Ramic, Zekija.....P1-U-18
 Ramos, Antonio.....P3-T-10
 Rao, Min.....3G-5
 Raum, Kay.....3J-1, P3-A-05, P3-A-07
 Raymond, Gaetan.....P3-K-03
 Rebiere, Dominique.....4C-1
 Redondo, Javier.....P1-L-06
 Reimann, Hans-Peter.....P2-A-13
 Reindl, Leonhard.....5D-5, P1-R-02, P1-S-01,
 P3-I-03
 Reinhardt, Alexandre.....5D-4, P1-Q-02

Sandrin, Laurent	P1-H-01, P1-H-02, P1-H-03, P1-H-06, P1-H-09, P3-A-09	Senlik, Niyazi	P2-Q-05
Sangawa, Ushio	P3-I-12	Seo, Chi Hyung	P1-G-08
Sangrador, Jesús	P2-N-04, P2-P-03	Seo, Jongbum	P2-A-07
Saniie, Jafar	4F-2, P1-K-01, P2-I-03, P2-I-04, P3-J-05	Seo, Koji	5A-1
Sano, Hajime	P3-B-05	Serfaty, Stéphane	P3-I-04
Sano, Hiroyuki	6D-1	Servois, Vincent	1F-6
Santin, Mathieu	P1-B-09	Seshia, Ashwin	4C-3, 4D-3, 6J-4, P2-O-04
Saotome, Yasunori	P2-H-08	Sessler, Gerhard M.	3A-3
Sapin, Emilie	1I-1	Seta, Ryo	P1-N-03
Sapozhnikov, Oleg	1F-2, 1F-4, 4H-4, P1-I-04, P-S-1	Seviaryn, Fedar	P3-A-10, P3-B-03
Sarens, Bart	P1-N-08	Sgambato, Kristopher	4C-4
Sarvazyan, Armen	3J-5	Shadmehr, Azadeh	P1-C-05
Sarwate, Sandhya	2G-2, 2G-6	Shamdasani, Vijay	P3-C-02
Sassaroli, Elisabetta	P2-B-05	Shandas, Robin	3I-2, P3-H-03
Sasso, Magali	P3-A-09	Shang, Junqing	P3-B-13
Sato, Toru	P3-D-10	Shapoori, Kiyanoosh	P3-B-03
Sato, Yusuke	P3-Q-01	Sharples, Steve	4K-2
Satoh, Yoshio	5C-5, 5E-3	Shavrov, Vladimir	P2-M-06
Sboros, Vassilis	2E-3, P1-A-12, P2-C-05, P-S-11	Shelton, Stefan	3A-5
Scavia, Guido	P1-O-01	Shen, Che-Chou	2F-6, P1-A-05, P1-A-06
Schaeufele, Ansgar	P2-N-03	Shevchenko, Talent	1A-1, 1F-3
Schanaider, Alberto	P3-A-01	Shi, Minzhe	P2-M-09
Scheffer, Cornie	P3-B-12	Shi, William	P3-C-02
Scheibhofer, Stefan	4F-3	Shi, Xianglong	P1-R-03
Schiffner, Martin	2K-5	Shi, Xiaomei	5J-6
Schmidt, Christian	P2-J-03	Shiba, Takashi	5F-4
Schmidt, Hagen	4D-6, 5B-3, 5F-3, P1-R-01, P2-O-10	Shih, Jeanne-Louise	4E-1, P-S-4
Schmitt, Martin	P1-P-09	Shiina, Tsuyoshi	P1-G-05, P1-H-08, P3-B-04, P3-D-10, P3-F-01
Schmitt-Landsiedel, Doris	5D-3, P-S-5	Shimada, Noboru	P2-H-08
Schmitz, Georg	1B-3, 1H-1, 2K-5, 3H-5, P1-A-08, P3-D-09	Shimamura, Hideki	P1-M-01
Schneider, Michel	P1-B-03	Shintaku, Yohei	4E-4, P1-U-01
Schoene, Martin	P3-A-05	Shirkovsky, Pavel	P3-O-01
Schönecker, Andreas	P1-U-04	Shivkumar, Kalyanam	3F-4, P-S-2
Schreuer, Jürgen	P1-M-04	Shore, Angela	3I-2
Schulte-Altendorneburg, Gernot	3G-6	Shrena, Ismail	5D-5, P1-S-01, P3-I-03
Schultz, Susan	P1-B-10	Shrout, Thomas	5I-4
Schulz, Michal	P1-S-03	Shui, Yongan	P1-R-03, P1-T-05
Schuster, Stefan	4F-3	Shung, K. Kirk	3B-3, 5K-4, 6G-1, P1-C-03, P1-U-03, P3-B-11, P3-S-04
Schweitzer, Patrick	P1-K-03	Shung, K. Krik	P1-U-19, P2-Q-07
Scipioni, Angel	P1-K-03	Shung, Kirk	P2-Q-08
Scola, Mallory	P2-E-02, P2-E-04, P2-E-05	Shur, Michael	P-S-13
Searfass, Cliff	3A-2	Shvetsov, Alexander	P3-P-06
Sebastian, Ian	1G-4	Siepmann, Monica	P1-A-08, P3-D-09
Sebbah, Patrick	P3-L-04	Sijl, Jeroen	2E-2, P2-C-03
Seco, Fernando	P1-U-05, P3-T-07	Silva, Emi-Lio C. N.	P1-U-21, P3-N-04
Seelig, Hans-Dieter	P3-M-07	Silver, Jason	P3-F-06
Segers, Patrick	3I-4, P3-G-05	Simsek, Ergun	P1-J-01
Sehgal, Chandra	3G-4, P1-B-10	Singer, Ferdinand	P1-P-09
Seilhean, Danielle	2B-1	Singh, Gautam	2G-3
Senégon, Nicolas	3C-1, P2-Q-09	Singh, Rahul	3K-1, P2-Q-10
Senlik, Muhammed	3C-4, 5J-1	Sinha, Bikash K.	P1-J-01
		Sinusas, Albert	1J-3
		Sirsi, Shashank	2F-4
		Sisman, Alper	2I-4, 5J-4, P-S-8
		Sisney, Gale	3G-5
		Slayton, Michael H.	1E-4

Tamon, Ryo	P1-P-03	Tokumitsu, Kenta	P2-L-06
Tamura, Yasutaka	P2-Q-01, P2-R-03	Tokunaga, Yoshiaki	P3-J-04
Tan, Alfred	P3-O-05	Tokutsu, Toji	3A-1
Tan, Ming	4A-3, 5A-4	Tomoda, Motonobu	6B-1
Tanabe, Masayuki	P3-N-06, P3-S-02	Toohy, Kathleen	1I-2
Tanaka, Akira	P3-A-03	Torbati, Zahra	2D-1, P1-D-01
Tanaka, Hiroki	3C-3	Torp, Hans	2H-1, 3F-3, 3I-3, 3I-4, P1-E-07,
Tanaka, Ryo	P3-N-06	P1-G-01, P1-G-02, P3-B-09, P3-C-03
Tanaka, Shuji	P2-O-02	Tortissier, Gregory	4C-1
Tanaka, Yukihiko	6B-1	Tortoli, Piero	1C-2, 3I-6, P2-C-03
Tanei, Hiroshi	P3-K-01	Touboul, David	1K-1
Tang, Mengxing	2E-6	Toufik, Bouden	P2-K-03
Tang, Meng-Xing	P1-A-02, P2-C-06	Tournat, Vincent	6A-1
Tang, Sheng-Wei	6K-5	Trahey, Gregg ...	1J-5, 3F-2, P1-G-06, P2-G-01,
Tangen, Thor Andreas	2A-4, 2I-5	P2-G-04, P3-B-08
Tanifuji, Shoichi	P2-P-02	Tran-Huu-Hu, Pascal	P1-U-12
Tanigaki, Kenichi	P3-K-01	Tran-Huu-Hue, Louis Pascal	6G-4
Tanner, Shawn	P1-U-13	Trier, Hans Georg	P3-S-08
Tanter, Mickael	1E-1, 1F-6, 1I-1, 1J-2,	Tripodi, Pietro	4F-1
.....	1K-1, 1K-5, 2B-1, 2F-1, 2H-3, 2I-3, 2K-6,	Troatz, Clemens	P2-B-02
.....	3D-6, 3F-5, P1-B-06, P1-H-04, P2-M-01	Troge, Alexandre	P1-U-15
Tarasenko, Sergei	P2-M-06	Trolier-Mckinstry, Susan	6G-3, P3-T-04
Tarasov, Ilya	P2-K-01	Tsadok, Yossi	P1-G-09
Tardy, Isabelle	1A-5, P1-B-03	Tsang, Ivan K. H.	P1-F-04, P2-D-02
Tas, Vahdettin	3C-4	Tsubouchi, Kazuo	P2-P-02
Tatatrinov, Alexey	3J-5	Tsuchiya, Akinori	P3-P-05
Taulier, Nicolas	P2-C-08	Tsuchiya, Takao	P1-N-03, P2-H-03
Tearney, Guillermo	1H-5	Tsui, Po-Hsiang	P3-H-06
Tekdas, Serkan	P1-U-11	Tsuji, Toshihiro	P3-I-05, P3-I-07
Tekel, Emre	P1-U-20	Tsujino, Jiroamaru	6C-1, 6K-6, P2-H-08
Tekes, Coskun	P1-D-03	Tsukamoto, Akira	P2-B-06
Tellier, Colette	P1-M-05, P3-Q-06	Tsukamoto, Daichi	P2-L-04
Ter Haar, Gail	3B-1, P2-A-05	Tsysar, Sergey	4H-4
Terada, Daisuke	P1-P-05	Tu, Cheng-Chiao	4C-2
Teston, Franck	3C-1, P2-Q-09	Tuck, Melanie	6J-2
Testoni, Nicola	P3-D-09	Tung, Yao-Sheng	2C-2
Tetelin, Angélique	4C-1	Turnbull, Daniel H.	2D-2
Thalhammer, Robert	5D-3, P-S-5	Tutwiler, Richard	6G-3
Thalmayr, Florian	5E-5, P-S-17	Tutwiler, Rick	P3-T-04
Theraulaz, Martine	1A-5	Tweedie, Andrew	3B-2
Thiele, Karl	1J-3	Twiefel, Jens	P2-M-09, P3-N-07
Thijssen, J.M.	3D-2, 3F-6, P3-F-04	Tyholdt, Frode	P1-U-07
Thirvenkatanathan, Pradyumna	6J-4	Tyrtshnyy, Valentin	P2-K-04, P2-K-06
Thomas, David	P1-A-12, P2-C-05, P-S-11		
Thomas, III, Lewis J.	3H-1		
Thomenius, Kai	3F-4, P3-S-01, P-S-2		
Thraenhardt, Marcel	4I-5		
Tiago, Marcelo Moreira	P1-J-02		
Tiah, Naceur	P3-A-02		
Tian, Jian	5I-5		
Tiefensee, Frank	P1-U-02, P1-U-03		
Tiemann, Klaus	P2-B-02		
Tierney, Aine	P2-E-07, P2-G-01		
Timonen, Jussi	P2-F-08		
Tin, Steven	6C-2		
Tinel, Alain	6F-6		
Tittmann, Bernhard	3A-2, 6H-5		
Tohyama, Kazutoshi	P3-P-01		

U

Ueda, Masanori	5C-5, 5E-3
Uemura, Tsutomu	P1-J-10
Ueno, Ei	P1-H-08
Uff, Chris	3D-5
Uff, Christopher	P3-F-02
Uhrcik, Marian	3K-4
Ulasevich, Andrew	4G-5
Ulliac, Gwenn	5G-2
Umamoto, Takeshi	P1-H-08
Umemura, Shin-Ichiro	1G-3, 2B-4, P2-A-09
Umphrey, Heidi	2E-4
Unnikrishnan, Sunil	1A-1

Urbach, Wladimir P2-C-08
 Urban, M.W. P1-H-07
 Urban, Matthew 1K-4, 3E-2, 3E-5, P-S-12
 Urbani, Fabio 4F-1
 Ushida, Takashi P2-B-06
 Uzbekov, Rustem P2-B-01
 Uzgur, Erman P1-U-16

V

V, Jayashankar P3-E-01
 Vaezy, Shahram 2B-3, P2-A-03
 Vagh, Hardik P3-R-03
 Vainer, Alexander P2-K-02, P2-M-02
 Vairac, Pascal P1-J-07
 Vaithilingam, Srikant 5J-5
 Vallet-Pichard, Anais P1-H-04
 van de Vosse, Frans N. P3-S-03, P3-S-09
 van der Steen, Antonius 1J-1, P1-G-11,
 P2-C-01, P-S-16
 van Dijk, J.P. 3D-2
 van Dongen, K.W.A. P1-N-11
 van Neer, Paul 2K-4, P-S-16
 van Stralen, Marijn P1-G-11
 van Wamel, Annemieke 1A-1, P1-B-02
 van Wijhe, Rene 2D-1
 Vanlanduit, Steve P2-F-06
 Varghese, Tomy 1I-3, 1I-6, 3G-5, P1-H-10
 Varray, François 1C-2
 Vasiljev, Piotr 6E-4, P3-N-08
 Vasseur, Jérôme 6F-6, 6H-6
 Vavva, Maria P3-D-12
 Veith, Michael P1-U-03
 Velichko, Alexander 4H-1, 4K-1, P3-J-06
 Venkatesh, T P1-U-14
 Verdier, Jacques P2-J-02
 Veres, Istvan A. 6B-2
 Vergara, Luis 4F-6
 Vermeersch, Sebastian P3-G-05
 Verona, E. P3-P-03
 Versluis, Michel 2E-2
 Verweij, M.D. P1-N-06
 Verweij, Martin 2K-4
 Vetelino, John 4C-4, 4D-2, 4G-4
 Vignon, Francois P3-C-01, P3-C-02
 Villareal, Alejandro P1-N-07
 Villazón Terrazas, Javier Rodrigo 4H-2
 Vincent, Tournat P2-H-09
 Viola, Francesco 1K-3, P3-F-03
 Virolainen, Teemu P1-K-02
 Vitalyi, Gusev P2-H-09
 Viti, Jacopo P2-C-03
 Vogl, Andreas P1-U-07
 Vogt, Michael 2K-3, P1-J-09
 Voigt, Jens-Uwe P1-F-02
 Voisin, David P3-S-06
 Voloshinov, Vitaly P2-K-01, P3-M-05
 Völz, Uwe P1-J-04

von Allmen, Daniel 3K-6
 von Kruger, Marco Antonio P3-H-05
 Vos, Hendrik P2-C-01, P2-C-03, P-S-11
 Vray, Didier P3-B-10
 Vree, C. P1-J-11
 Vu, Mai Ba 3H-6
 Vysochanskii, Yulian 5I-2

W

Wada, Kenji P3-B-05
 Wagner Coelho De Albuquerque, Pereira
 P3-A-02
 Wagner, H. P1-J-11
 Wagner, Karl 5F-1, P1-R-05, P2-N-03
 Wakatsuki, Naoto 4D-1, 4F-5, P1-I-01,
 P1-L-01
 Walczak, Mateusz P2-D-04
 Walker, William 1K-3, 2A-5, P3-C-08,
 P3-F-03
 Walker-Samuel, Simon P2-A-05
 Wall, Bert 5F-3
 Wallace, Kirk 2K-1, 3H-1
 Wallaschek, Joerg 4J-5
 Wallaschek, Jörg P2-M-09, P3-N-07
 Walti, Christoph 4A-4
 Waltz, Patrice P2-J-03
 Wamhoff, Brian R. 1A-2
 Wan, Yayun P3-E-04
 Wang, Hao P1-R-03
 Wang, Hsin-Ell P1-B-05
 Wang, Ji 6D-5, P2-J-06, P2-J-07, P3-L-07
 Wang, Joseph P2-D-07
 Wang, Kun 5C-1
 Wang, Lihong 6D-5
 Wang, Mengli P1-E-03
 Wang, Michael 1K-2
 Wang, Shougang 2C-2
 Wang, Shun-Li P3-D-04
 Wang, Shu-Zhe P2-F-04
 Wang, Shyh-Hau 2J-6, 6K-4
 Wang, Tzu-Yin 1F-4, 2B-5, P-S-1
 Wang, Weibiao P1-R-03, P1-T-03
 Wang, Weiqi P2-F-05, P2-F-11
 Wang, Wen P1-T-01
 Wang, Wenyan 4C-6, P3-I-08
 Wang, Yak-Nam 2J-5
 Wang, Yiliu 5E-5
 Wang, Yuesheng 6F-5
 Wang, Yue-Sheng 6A-2, P1-L-02, P1-L-04
 Wang, Yuxiang P3-I-13
 Wang, Zhaohui 2H-6
 Wang, Ziyu P2-O-07
 Warner, Lizette V. 3E-5
 Warram, Jason 2E-4, P1-H-05
 Watanabe, T P3-I-02
 Watanabe, Yoshiaki P2-B-06, P2-G-02,
 P2-L-02, P2-L-04, P2-O-08

Weaver, Fred 3K-3
 Webb, Steve 3E-6
 Weber, Sylvain P1-S-02
 Weber, Werner 5D-3, P-S-5
 Wegmann, Enrique P2-N-04
 Wei, Qifeng 1J-3
 Weigel, Robert 5F-1, P2-N-03
 Weihnacht, Manfred 4D-6, 5B-3, P1-R-01,
 P2-O-10
 Weimann, Thomas P3-Q-04
 Welsch, Hans-Joachim 1H-3
 Wen, Xu 3K-2
 Werner, Jacob P1-C-01, P2-A-02
 Westesson, Karin 3G-1
 White, Audrey P1-G-03
 White, Neil Maurice P2-H-06
 Wickerhauser, Victor 2K-1
 Wickline, Samuel 2K-1, 3H-1
 Wijkstra, Hessel 2F-5
 Wilcox, Paul 4H-1, 4K-1, P3-J-06
 Wildes, Douglas 3F-4, P-S-2
 Wilkens, Volker P2-A-13
 Willkie-Chancellor, Nicolas P1-N-08
 Willatzen, Morten 3B-5
 Williams, Jay 6G-1
 Williams, Jennifer 2C-4
 Williams, Ross 1A-3, P-S-10
 Willinger, Rémy P1-H-02
 Winterroth, F. 1C-5
 Wirtzfeld, Lauren A. 2G-2
 Witte, Russell 2H-6
 Wladimiroff, Juriy 1D-3
 Wodnicki, Robert P3-S-01
 Wojciechowski, Kenneth 6J-2, P2-O-05
 Wolf, Felix 3B-4
 Wolf, Patrick 1J-5, 5K-6, P2-G-04
 Wong, Emily P1-F-05
 Wong, Hades C. T. 2J-4
 Wong, Mei Yi 2J-4
 Wong, Zi Jing 4I-4
 Wood, Bradford 1I-5
 Wood, Christopher 4A-4
 Wood, Andrew P1-B-10
 Woychik, Charles P3-S-01
 Wrenn, Steve 1G-5
 Wright, Cameron 1F-5
 Wright, Oliver 5C-2, 6B-1, 6B-2
 Wright, W.M.D. P2-I-05
 Wu, Chia-Han P3-L-02
 Wu, Dawei P2-Q-08, P3-B-11
 Wu, Haodong P1-R-03, P1-T-05
 Wu, K.-T. 4B-3, 5H-5
 Wu, Kuang-Chong 4H-6, 4J-3
 Wu, Nan 5E-5, P1-Q-03
 Wu, Sean 4C-2, 5G-5
 Wu, Shih-Yen P1-B-05
 Wu, Shih-Ying P3-D-04
 Wu, W.J. 4I-3

Wu, Wen-Jong 4J-3
 Wurpts, Wiebold P3-N-07
 Wygant, Ira P2-Q-03

X

Xeridat, Olivier P3-L-04
 Xiang, Ji P2-A-04
 Xianyi, Li P3-Q-04
 Xie, Hua 1I-5
 Xie, Yuan 5C-1
 Xu, Canxing P3-B-14
 Xu, Haiyan 3G-5
 Xu, Kailiang P2-F-05, P2-F-14
 Xu, Leiting P2-F-08
 Xu, Sheng 1I-5
 Xu, Tiantian P1-F-03
 Xu, Yuan P2-M-08
 Xu, Zhen 1F-1, 1F-4, 2B-5, 2C-1, 2C-4,
 P-S-1

Y

Yahiaoui, Réda P3-I-14
 Yamada, Ken P3-I-06
 Yamaguchi, Masatsune ... 5A-1, 5F-5, P1-Q-01,
 P1-Q-03, P-S-17
 Yamaguchi, Tadashi P3-B-06
 Yamakawa, Makoto P1-G-05, P3-B-04,
 P3-D-10, P3-F-01
 Yamakoshi, Yoshiaki P1-B-04
 Yamamoto, Yutaro P3-I-07
 Yamamoto, Kansho P3-Q-03
 Yamamoto, Kazufumi 3J-4, P2-F-09
 Yamamoto, Ken P1-L-01
 Yamamoto, Seiji P1-J-10
 Yamamoto, Yutaro P3-I-05
 Yamamoto, Yuya P2-G-02
 Yamanaka, Kazushi 4E-4, P1-T-02,
 P1-U-01, P3-I-05
 Yamaner, F. Yalcin P2-Q-04
 Yamanouchi, Kazuhiko P3-Q-01
 Yan, Jize 4D-3, 4I-4, 6J-4, P2-O-04
 Yan, Ping 1J-3
 Yanagida, Hirotaka P2-Q-01, P2-R-03
 Yanagihara, Eugene 1C-3
 Yanagisawa, Takayuki P1-T-02
 Yanagitani, Takahiko 6D-1, P2-O-08
 Yang, Che-Hua 4B-4, 6K-5, P3-L-02
 Yang, Jinwei P-S-13
 Yang, Ken 3A-5
 Yang, Kun 1G-1, 2D-5
 Yantchev, Ventsislav 4A-6, 5D-2, 5G-3,
 P2-P-05
 Yao, Jorge 3G-1
 Yaoi, Yuichiro P2-F-09
 Yaoi, Zong-Jian P1-L-04
 Yasuda, Noriyuki 4A-1

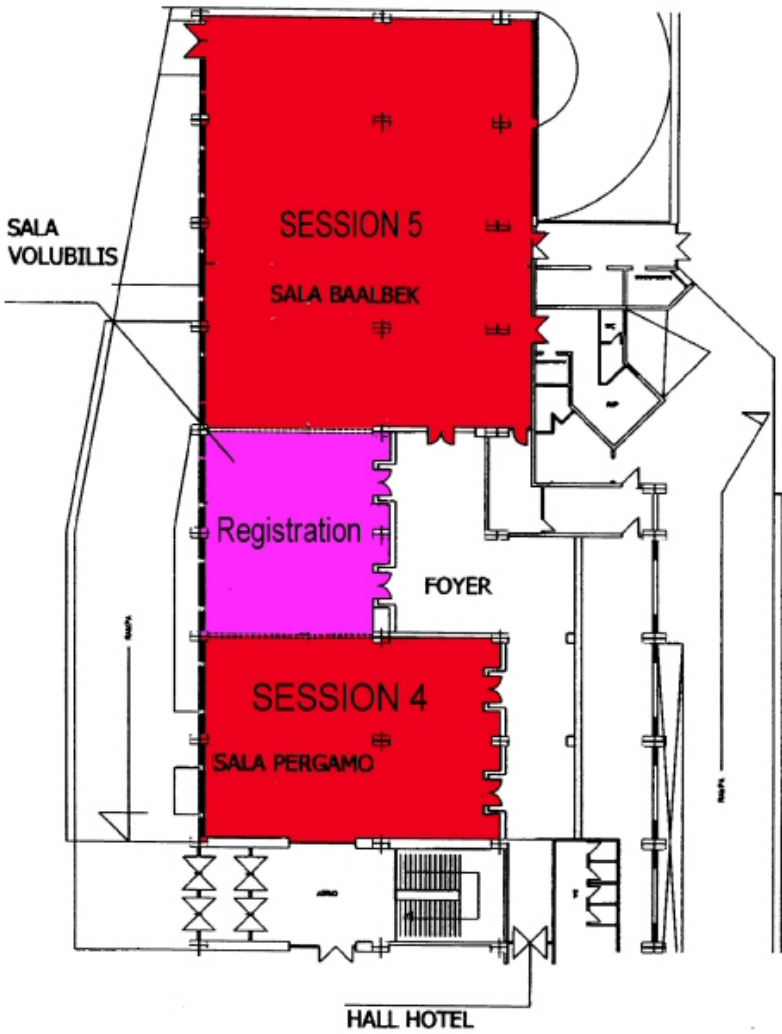
Yasumo, Yoshinobu	P1-U-06	Zahiri Azar, Reza	P3-D-11
Yazhu, Chen	P2-A-04	Zahnd, Guillaume	P1-D-07
Ye, Guoliang	4I-4	Zahorian, Jaime	5J-4, P-S-8
Ye, Jing Yong	1G-1	Zaitsev, Boris	P1-J-03, P2-J-05
Ye, Shen	5C-1	Zalalutdinov, Maxim	6J-3
Yeh, Cheng-Hung	4B-4	Zapf, Michael	P2-I-02, P3-B-01
Yeh, Chih-Kuang	P1-A-05, P1-N-05, P2-B-03, P3-H-06	Zderic, Vesna	P1-B-07
Yen, Jesse	3K-3, P2-D-06	Zduniak, Maciej	P1-M-02
Yeo, Leslie	4A-2, 4A-3, 4J-6, 5A-4	Zhai, Liang	3G-2
Yeow, John	5J-3	Zhang, Chao	4C-6, P2-J-08, P3-I-08
Yevstafiyev, Oleksandr	P2-M-07	Zhang, Chuazeng	6A-2, 6F-5, P1-L-02
Yin, Ching-Chung	5A-5	Zhang, De	P1-T-03
Yin, Jianhua	5K-1, P3-T-05	Zhang, Fuxing	3I-2, P3-H-03
Yin, Xin	P3-L-07	Zhang, Haiyan	P2-F-11, P2-H-01
Yiu, Billy Y. S.	P1-F-04, P2-D-02	Zhang, Shujun	5I-4
Yokoyama, Tsuyoshi	5C-5	Zhang, Xiaoming	2A-1, 3E-2, P3-G-03
Yong, Yonk-Kong	P2-J-06	Zhang, Zhitian	4C-6, P3-I-08
Yong, Yook-Kong	6D-2, 6D-5, P3-L-07	Zhao, Gang	P2-J-08
Yoo, Yang Mo	P1-E-05, P1-E-08, P2-D-03	Zhao, L.	4B-3
Yoon, Ra-Young	P1-D-08	Zhao, Su	4J-5
Yoon, Seok-Jin	4I-2, 6E-3, 6E-4, 6E-5	Zheng, Hairong	P1-L-03
Yorgov, Meriem	P1-H-03	Zheng, Xinliang	2B-3, P2-A-03
Yoshida, Kenji	P2-B-06, P2-L-02	Zheng, Yong-Ping	P2-F-04, P3-A-11, P3-B-07
Yoshida, Sachiko	P1-J-10	Zhgoon, Sergei	P3-P-06
Yoshida, Sho	4K-6, 6I-4	Zhou, Qifa	P1-C-03, P1-U-03, P1-U-19, P2-Q-07, P2-Q-08, P3-B-11
Yoshikawa, Taisuke	P2-L-02	Zhou, Xiao-Zhou	6A-2
Yoshizawa, Makoto	P3-A-03	Zhou, Yong-Jin	P3-B-07
Yoshizawa, Shin	1G-3	Zhou, Yun	1G-1, 2D-5
Yoshizumi, Natsuki	P3-S-05	Zhu, Benpeng	P1-U-03, P1-U-19, P2-Q-07
Young, Roger	6I-3	Zhu, Hongtu	P2-E-04
Yu, Alfred C. H.	2J-4, P1-F-04, P2-D-02	Zhu, Jie	P2-O-07
Yu, Cunjiang	P2-O-07	Zhu, Yongyuan	P2-J-08
Yu, François T. H.	2G-4	Zhuang, Xuefeng	5J-5, P2-Q-02
Yu, Gui-Lan	P1-L-04	Zinn, Kurt	2E-4
Yu, Hongyu	P2-O-07	Zipser, Lothar	P1-N-10, P3-M-07
Yu, Jaesok	P1-E-05	Zolotova, Olga	P3-L-01
Yu, Z.	P1-D-06	Zozulya, Oleg	P2-J-04
Yuhas, Donald E.	4D-5	Zuniga, Chiara	4G-2, P3-K-04
Yushkov, Konstantin	P3-M-01	Zuo, Chengjie	6J-5
		Zyryanova, Anna	6I-1

Z

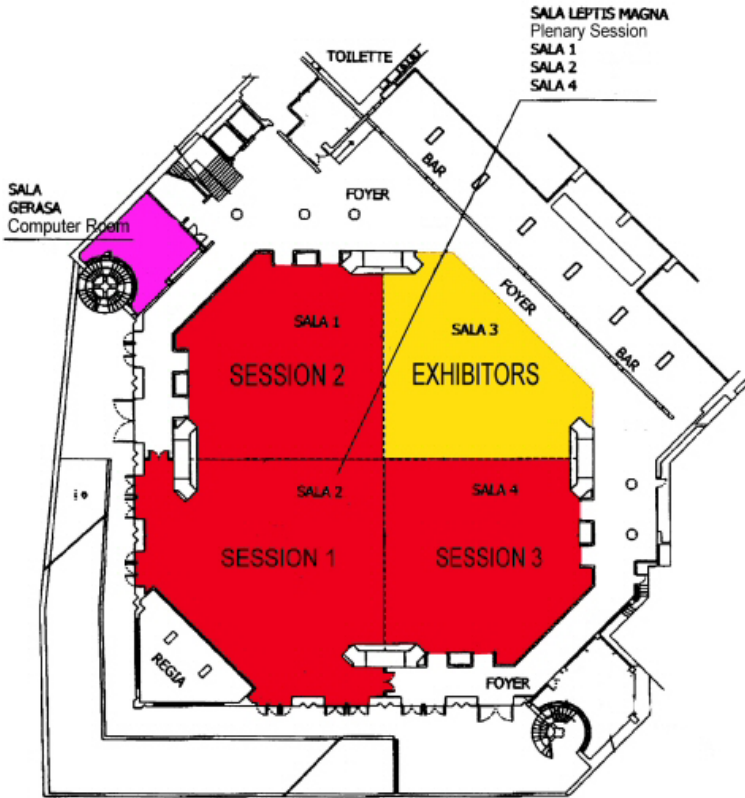
Zagrodsky, Vladimir	P2-G-03
Zagzebski, James	1I-3, 2G-6, P2-G-06

Floor Plans

Ground Floor



2nd Floor Underground



Condensed Program of 2009 IEEE International Ultrasonics Symposium

Rome, Italy, September 20-23, 2009

Room Names:	Sala 1: Oral Sessions Sala 2: Oral Sessions Sala 4: Oral Sessions	Tarragona: Oral Sess. Pergamo: Oral Sessions Baalbek: Oral Sessions	Hama: Short Course Efeso: Short Course Merida: Short Course	Pola: Short Course Cesarea: Short Course Spalato: Short Course	Sala 3: Exhibitors Sala Orange: Posters Gerasa: Computer Rm	Leptis Magna (Sala 1+2+4): Plenary Session Volubilis: Registration
Invited Talks:	(1I): 1 st Time Slot	(3I): 3 rd Time Slot	(5I): 5 th Time Slot			
Color Codes:	<u>Group I: Pink</u> Medical Ultrasonics	<u>Group II: Purple</u> Sensor, NDE, Industrial Applications	<u>Group III: Green</u> Physical Acoustics	<u>Group IV: Orange</u> Microacoustics – SAW, FBAR, MEMS	<u>Group V: Blue</u> Transducers & Transducer Materials	
SATURDAY, Sep. 19	Condensed Program --- 2009 IEEE International Ultrasonics Symposium, Rome, Italy, September 20-23, 2009					
	Symposium Registration (Volubilis), 6:00 p.m. – 9:00 p.m.					
SUNDAY, Sep. 20	Short Courses (Refreshments in Galleria Expo at breaks)					
	Symposium Registration (Volubilis), 7:00 a.m. – 6:00 p.m.					
	Short Courses (8:00 a.m. – 12:00 p.m.):		Short Courses (1:00 p.m. – 5:00 p.m.):		Short Courses (6:00 p.m. – 9:00 p.m.):	
	1A: Film Bulk Acoustic Resonator (FBAR) (Hama)		1B: SAW Modeling Techniques (Hama)		1C: Time Reversal Acoustics (Merida)	
	2A: Materials for Acoustic Wave Devices (Efeso)		2B: Piezoelectric Ultrasound Transducer Fundamentals - Materials, Structure, Behavior, and Analysis (Spalato)		2C: Ultrasound Contrast Agents: Theory and Experiment (Spalato)	
	3A: Microwave Acoustic Sensors (Merida)		3B: Quantitative Acoustic Microscopy - Fundamentals and New Applications from Cells to Airplanes (Merida)		3C: Zooming into the Near Field (Efeso)	
	4A: Therapeutic Ultrasound (Pola)		4B: Ultrasound Imaging Systems: from Principles to Implementation (Pola)		4C: CMUTs: Theory, Technology, and Applications (Pola)	
	5A: Ultrasonic NDE and Industrial Process Diagnostics at High Temperatures (Cesarea)		5B: Passive UHF RFID Tags, Systems & Applications (Efeso)		5C: Guided SH-SAW Devices for Liquid-Phase Biochemical Sensors (Hama)	
	6A: Estimation and Imaging of Blood Flow Velocity (Spalato)		6B: Ultrasonic Signal Processing for Detection, Estimation & Imaging (Cesarea)		6C: Elasticity Imaging: Dynamic Approaches (Cesarea)	

MONDAY, Sep. 21	Sala 1	Sala 2	Sala 4	Tarragona	Pergamo	Baalbek
	Symposium Registration (Volubilis), 7:00 a.m. – 6:00 p.m.			Exhibitors (Sala 3), 8:30 a.m. – 5:00 p.m.		
8:00 a.m. – 9:30 a.m.	Plenary Session (Leptis Magna – For All Attendees)					
9:30 a.m. – 10:00 a.m.	Refreshments (Foyer Leptis Magna)					
	Posters (Sala Orange)					
10:00 a.m. – 11:30 a.m.	PS. Student Finalists P1A. Contrast Agents: Behavior and Imaging P1B. Contrast Agents Appl. P1-C. Therapeutic Appl.	P1-D. Beamforming Sys'ts & Hardware P1-E. Blood Flow I P1-F. Blood Flow II P1-G. Myocardial Imaging	P1-H. Quanty. Elasticity Methods P1-I. Acoustic Imaging P1-J. Guided Wave & Micros. P1-K. Sig. Process. & Imag.	P1-L. Phononic Crystals-Band Structure & Propag. P1-M. Materials Charac. P1-N. Physical Acoustics: Modeling & Simulation	P1-O. Thin Films-Growth & Charac. P1-P. Actuators & Pumps P1-Q. Measurement & Yields P1-R. Device Modeling	P1-S. High Temp. Matls & Prop. P1-T. Tags and Sensors P1-U. Transducer Materials and Characterization
11:30 a.m. – 1:00 p.m.	1A. Targeted Contrast Agents (11)	2A. Ultrasound Systems and Devices	3A. Ferroelectrets & Other Transducer Matls (31)	4A. Microfluidic Manipulation	5A. SAW Applications	6A. Phononic Crystals-Fundamentals (51)
1:00 p.m. – 2:30 p.m.	Lunch					
2:30 p.m. – 4:00 p.m.	1B. Contrast Agents and Sonoporation (51)	2B. Therapy Monitoring, Control, and Quality Assurance	3B. Transducers & Ultrasound Modeling	4B. Advances in NDE (11)	5B. SAW Modeling	6B. Visualization Interferometry (31)
4:00 p.m. – 4:30 p.m.	Refreshments (Leptis Magna Foyer, Baalbek Foyer and Tarragona Foyer)					
4:30 p.m. – 6:00 p.m.	1C. New Methods & High Freq. Ultrasound for Tissue Charac. (11)	2C. Therapeutic In-Vivo Studies	3C. CMUT Modeling (51)	4C. Acoustic Wave Sensors	5C. BAW I (31)	6C. Novel Ultrasonic Motors I
8:00 p.m. – 11:00 p.m.	Gala Dinner Awards Reception (Le Quattro Stagioni Restaurant & Space by the Pool)					

TUESDAY, Sep. 22	Sala 1	Sala 2	Sala 4	Tarragona	Pergamo	Baalbek
	Symposium Registration (Volubilis), 7:00 a.m. – 6:00 p.m.			Exhibitors (Sala 3), 8:30 a.m. – 5:00 p.m.		
8:00 a.m. – 9:30 a.m.	1D. Clinical Ultrasound (1)(3)(5)	2D. High Freq Ultrasound & its Applications	3D. Elastography	4D. Flow Sensing	5D. Oscillators & Temp. Compensation (1)	6D. Bulk Wave Effects and Devices
9:30 a.m. – 10:00 a.m.	Refreshments (Leptis Magna Foyer, Baalbek Foyer and Tarragona Foyer)					
	Posters (Sala Orange)					
10:00 a.m. – 11:30 a.m.	P2-A. Therapy: Monitoring, Control, Quality Assurance P2-B. Therapy Microbubbles P2-C. Contrast Agents: Charac. & Modeling	P2-D. Ultrasound Systems & Devices P2-E. Acoustic Radiation Force Imaging P2-F. Hard Tissue & Bone	P2-G. Cardiac, Vascular & General Tissue Charac. P2-H. Wave Propagation and Energy Harvesting P2-I. Ultrasonic Signal Proc.	P2-J. Bulk Wave Effects P2-K. Laser Interactions P2-L. Bubbles & Beads P2-M. High Intensity Ultrasound Application	P2-N. Device Modeling P2-O. MEMS & Sensors P2-P. BAW Materials P2-Q. Sensors, High Freq., CMUTs & Micromachining	P2-R. Various Transducer Topics
11:30 a.m. – 1:00 p.m.	7E. Therapeutic Arrays	2E. Microbubbles: Characterization & Modeling	3E. Elastography Methods	4E. Array Imaging (3)	5E. BAW II	6E. Ultrasonic Linear Motors (1)
1:00 p.m. – 2:30 p.m.	Lunch					
2:30 p.m. – 4:00 p.m.	1F. Therapeutic Applications	2F. Contrast Agent Imaging	3F. Cardiac Imaging	4F. NDE Signal Processing	5F. SAW Device Design (1)	6F. Phononic Crystals- Propagation
4:00 p.m. – 4:30 p.m.	Refreshments (Leptis Magna Foyer, Baalbek Foyer and Tarragona Foyer)					
4:30 p.m. – 6:00 p.m.	1G. Therapy Microbubbles (3)	2G. Tissue Characterization	3G. Cancer Imaging	4G. Nanoscale Acoustic Sensing (1)	5G. Novel SAW Materials & Structures	6G. High Frequency Transducers & Arrays

WEDNESDAY, Sep. 23	Sala 1	Sala 2	Sala 4	Tarragona	Pergamo	Baalbek
Symposium Registration (Volubilis), 7:00 a.m. – 1:00 p.m.						
Exhibitors (Sala 3), 8:30 a.m. – 1:00 p.m.						
8:00 a.m. – 9:30 a.m.	1H. Optical & Photoacoustic Imaging (5l)	2H. Medical Imaging	3H. Bone I	4H. Acoustic Imaging and Characterization	5H. Novel Devices & Systems (1l)	6H. Phononic Crystals-Devices, Filters, Couplers
9:30 a.m. – 10:00 a.m.	Refreshments (Leptis Magna Foyer, Baalbek Foyer and Tarragona Foyer)					
Posters and Refreshments (Sala Orange)						
10:00 a.m. – 11:30 a.m.	P3-A. Tissue Charact P3-B. Imaging Methods P3-C. Beamforming P3-D. Signal Processing	P3-E. Elasticity Methods: Clinical Applications P3-F. Motion Tracking and Elasticity Imaging	P3-G. Vascular Elastography P3-H. Ultrasound Segmentation P3-I. Acoustic Sensors	P3-J. Defects & Charac. P3-K. Thin Films-Charac. P3-L. Lamb Waves P3-M. Optical Interactions	P3-N. Novel Ultrason. Motors P3-O. Air-Coupled Ultrason. P3-P. Acoustic Materials & Structures P3-Q. Device Design	P3-R. Device Modeling (SAW) P3-S. Medial Imaging Transducers P3-T. Transducer Modeling
11:30 a.m. – 1:00 p.m.	1I. Elasticity and Thermal Effects	2I. Beamforming	3I. New Developments in Blood Flow Imaging	4I. Energy Harvesting (1I)	5I. Piezoelectric Transducer Materials (3I)	6I. Acoustic Propagation (5I)
1:00 p.m. – 2:30 p.m.	Lunch					
2:30 p.m. – 4:00 p.m.	1J. Cardiovascular Elastography (5I)	2J. Bioeffects	3J. Bone II	4J. Ultrasound in Air	5J. Micromachined Ultrasonic Transducers	6J. RF MEMS (1I)
4:00 p.m. – 4:30 p.m.	Refreshments (Leptis Magna Foyer, Baalbek Foyer and Tarragona Foyer)					
4:30 p.m. – 6:00 p.m.	1K. Dynamic Elastography	2K. Signal Processing	3K. Surgical Automation	4K. Material and Defect Characterization	5K. Medical Imaging and Therapeutic Transducers	6K. Industrial Ultrasonics

Notes

Notes